Missile Guidance and Control Systems

GEORGE M. SIOURIS

Missile Guidance and Control Systems

Springer
New York
Berlin
Heidelberg
Hong Kong
London
Milan
Paris
Tokyo

George M. Siouris

Missile Guidance and Control Systems

Springer

George M. Siouris
Consultant
Avionics and Weapon Systems
Formerly
Adjunct Professor
Air Force Institute of Technology
Department of Electrical and Computer Engineering
Wright-Patterson AFB, OH 45433
USA
GSiouris@worldnet.att.net

Cover illustration: Typical phases of a ballistic missile trajectory.

Library of Congress Cataloging-in-Publication Data

Siouris, George M.
Missile guidance and control systems / George M. Siouris.
p. cm.
Includes bibliographical references and index.
ISBN 0-387-00726-1 (hc. : alk. paper)
1. Flight control. 2. Guidance systems (Flight) 3. Automatic pilot (Airplanes) I. Title.

TL589.4.S5144 2003
629.132′6–dc21

2003044592

ISBN 0-387-00726-1 Printed on acid-free paper.

Printed in the United States of America. TES/SBA

9 8 7 6 5 4 3 2 1 SPIN 109/8951

Springer-Verlag is a part of *Springer Science+Business Media*

springeronline.com

To Karin

This page intentionally left blank

Preface

In every department of physical science there is only so much science, properly so-called, as there is mathematics.

Immanuel Kant

Most air defense systems in use or under development today, employ homing guidance to effect intercept of the target. By virtue of the use of onboard data gathering, the homing guidance system provides continually improving quality of target information right up to the intercept point. More than any single device, the guided missile has shaped the aerospace forces of the world today. Combat aircraft, for example, are fitted with airborne weapons that can be launched against enemy aircraft, ground forces, or strategic targets deep inside enemy territory. Also, the guided missile can be employed as a diversionary weapon to confuse ground and air forces. Ground-based missile systems have various range capabilities from a few miles to several thousand miles. These ground-based missiles are ballistic or nonballistic types, depending on their mission requirements. The design of a guided weapon (i.e., a missile) is a large undertaking, requiring the team effort of many engineers having expertise in the areas of aerodynamics, flight controls, structures, and propulsion, among others. The different design groups must work together to produce the most efficient weapon in terms of high accuracy and low cost.

The intent of this book is to present the fundamental concepts of guided missiles, both tactical, and strategic and the guidance, control, and instrumentation needed to acquire a target. In essence, this book is about the mathematics of guided flight. This book differs from similar books on the subject in that it presents a detailed account of missile aerodynamic forces and moments, the missile mathematical model, weapon delivery, *GPS* (global positioning system) and *TERCOM* (terrain contour matching) guidance, cruise missile mechanization equations, and a detailed analysis of ballistic guidance laws. Moreover, an attempt has been made to give each subject proper emphasis, while at the same time special effort has been put forth to obtain simplicity, both from the logical and pedagogical standpoint. Typical examples are provided, where necessary, to illustrate the principles involved. Numerous figures give the maximum value of visual aids by showing important relations at a glance and motivating the various topics. Finally, this book will be

of benefit to engineers engaged in the design and development of guided missiles and to aeronautical engineering students, as well as serving as a convenient reference for researchers in weapon system design.

The aerospace engineering field and its disciplines are undergoing a revolutionary change, albeit one that is difficult to secure great perspective on at the time of this writing. The author has done his best to present the state of the art in weapons systems. To this end, all criticism and suggestions for future improvement of the book are welcomed.

The book consists of seven chapters and several appendices. Chapter 1 presents a historical background of past and present guided missile systems and the evolution of modern weapons. Chapter 2 discusses the generalized missile equations of motion. Among the topics discussed are generalized coordinate systems, rigid body equations of motion, D'Alembert's principle, and Lagrange's equations for rotating coordinate systems. Chapter 3 covers aerodynamic forces and coefficients. Of interest here is the extensive treatment of aerodynamic forces and moments, the various types of missile seekers and their function in the guidance loop, autopilots, and control surface actuators. Chapter 4 treats the important subject of the various types of tactical guidance laws and/or techniques. The types of guidance laws discussed in some detail are homing guidance, command guidance, proportional navigation, augmented proportional navigation, and guidance laws using modern control and estimation theory. Chapter 5 deals with weapon delivery systems and techniques. Here the reader will find many topics not found in similar books. Among the numerous topics treated are weapon delivery requirements, the navigation/weapon delivery system, the fire control computer, accuracies in weapon delivery, and modern topics such as situational awareness/situation assessment. Chapter 6 is devoted to strategic missiles, including the classical two-body problem and Lambert's theorem, the spherical Earth hit equation, explicit and implicit guidance techniques, atmospheric reentry, and ballistic missile intercept. Chapter 7 focuses on cruise missile theory and design. Much of the material in this chapter centers on the concepts of cruise missile navigation, the terrain contour matching concept, and the global positioning system. Each chapter contains references for further research and study. Several appendices provide added useful information for the reader. Appendix A lists several fundamental constants, Appendix B presents a glossary of terms found in technical publications and books, Appendix C gives a list of acronyms, Appendix D discusses the standard atmosphere, Appendix E presents the missile classification, Appendix F lists past and present missile systems, Appendix G summarizes the properties of conics that are useful in understanding the material of Chapter 6, Appendix H is a list of radar frequencies, and Appendix I presents a list of the most commonly needed conversion factors.

Such is the process of learning that it is never possible for anyone to say exactly how he acquired any given body of knowledge. My own knowledge was acquired from many people from academia, industry, and the government. Specifically, my knowledge in guided weapons and control systems was acquired and nurtured during my many years of association with the Department of the Air Force's Aeronautical Systems Center, Wright-Patterson AFB, Ohio, while participating in the theory,

design, operation, and testing (i.e., from concept to fly-out) the air-launched cruise missile (*ALCM*), *SRAM II*, *Minuteman III*, the *AIM-9 Sidewinder*, and other programs too numerous to list.

Obviously, as anyone who has attempted it knows, writing a book is hardly a solitary activity. In writing this book, I owe thanks and acknowledgment to various people. For obvious reasons, I cannot acknowledge my indebtedness to all these people, and so I must necessarily limit my thanks to those who helped me directly in the preparation and checking of the material in this book. Therefore, I would like to acknowledge the advice and encouragement that I received from my good friend Dr. Guanrong Chen, formerly Professor of Electrical and Computer Engineering, University of Houston, Houston, Texas, and currently Chair Professor, Department of Electronic Engineering, City University of Hong Kong. In particular, I am thankful to Professor Chen for suggesting this book to Springer-Verlag New York and working hard to see that it received equitable consideration. Also, I would like to thank my good friend Dr. Victor A. Skormin, Professor, Department of Electrical Engineering, Thomas J. Watson School of Engineering and Applied Science, Binghamton University (SUNY), Binghamton, New York, for his encouragement in this effort. To Dr. Pravas R. Mahapatra, Professor, Department of Aerospace Engineering, Indian Institute of Science, Bangalore, India, I express my sincere thanks for his commitment and painstaking effort in reviewing Chapters 2–4. His criticism and suggestions have been of great service to me. Much care has been devoted to the writing and proofreading of the book, but for any errors that remain I assume responsibility, and I will be grateful to hear of these.

The author would like to express his appreciation to the editorial and production staff of Springer-Verlag New York, for their courteous cooperation in the production of this book and for the high standards of publishing, which they have set and maintained.

Finally, but perhaps most importantly, I would like to thank my family for their forbearance, encouragement, and support in this endeavor.

Dayton, Ohio
November, 2003

George M. Siouris

This page intentionally left blank

Contents

1 Introduction 1
References 13

2 The Generalized Missile Equations of Motion 15
2.1 Coordinate Systems 15
2.1.1 Transformation Properties of Vectors 15
2.1.2 Linear Vector Functions 16
2.1.3 Tensors 17
2.1.4 Coordinate Transformations 18
2.2 Rigid-Body Equations of Motion 22
2.3 D'Alembert's Principle 45
2.4 Lagrange's Equations for Rotating Coordinate Systems 46
References 51

3 Aerodynamic Forces and Coefficients 53
3.1 Aerodynamic Forces Relative to the Wind Axis System 53
3.2 Aerodynamic Moment Representation 62
3.2.1 Airframe Characteristics and Criteria 77
3.3 System Design and Missile Mathematical Model 85
3.3.1 System Design 85
3.3.2 The Missile Mathematical Model 91
3.4 The Missile Guidance System Model 99
3.4.1 The Missile Seeker Subsystem 102
3.4.2 Missile Noise Inputs 113
3.4.3 Radar Target Tracking Signal 119
3.4.4 Infrared Tracking Systems 125
3.5 Autopilots 129
3.5.1 Control Surfaces and Actuators 144
3.6 English Bias 151
References 153

4 Tactical Missile Guidance Laws 155
4.1 Introduction 155
4.2 Tactical Guidance Intercept Techniques 158
4.2.1 Homing Guidance 158
4.2.2 Command and Other Types of Guidance 162
4.3 Missile Equations of Motion 174
4.4 Derivation of the Fundamental Guidance Equations 181
4.5 Proportional Navigation 194
4.6 Augmented Proportional Navigation 225
4.7 Three-Dimensional Proportional Navigation 228
4.8 Application of Optimal Control of Linear Feedback Systems with Quadratic Performance Criteria in Missile Guidance 235
4.8.1 Introduction 235
4.8.2 Optimal Filtering 237
4.8.3 Optimal Control of Linear Feedback Systems with Quadratic Performance Criteria 242
4.8.4 Optimal Control for Intercept Guidance 248
4.9 End Game 256
References 266

5 Weapon Delivery Systems 269
5.1 Introduction 269
5.2 Definitions and Acronyms Used in Weapon Delivery 270
5.2.1 Definitions 271
5.2.2 Acronyms 279
5.3 Weapon Delivery Requirements 284
5.3.1 Tactics and Maneuvers 286
5.3.2 Aircraft Sensors 289
5.4 The Navigation/Weapon Delivery System 290
5.4.1 The Fire Control Computer 292
5.5 Factors Influencing Weapon Delivery Accuracy 293
5.5.1 Error Sensitivities 294
5.5.2 Aircraft Delivery Modes 297
5.6 Unguided Weapons 299
5.6.1 Types of Weapon Delivery 300
5.6.2 Unguided Free-Fall Weapon Delivery 302
5.6.3 Release Point Computation for Unguided Bombs 304
5.7 The Bombing Problem 305
5.7.1 Conversion of Ground Plane Miss Distance into Aiming Plane Miss Distance 308
5.7.2 Multiple Impacts 312
5.7.3 Relationship Among *REP*, *DEP*, and *CEP* 314
5.8 Equations of Motion 314
5.9 Covariance Analysis 320

5.10 Three-Degree-of-Freedom Trajectory Equations and Error Analysis . . . 323
5.10.1 Error Analysis . . . 326
5.11 Guided Weapons . . . 328
5.12 Integrated Flight Control in Weapon Delivery . . . 332
5.12.1 Situational Awareness/Situation Assessment (*SA/SA*) . . . 334
5.12.2 Weapon Delivery Targeting Systems . . . 336
5.13 Air-to-Ground Attack Component . . . 339
5.14 Bomb Steering . . . 344
5.15 Earth Curvature . . . 351
5.16 Missile Launch Envelope . . . 353
5.17 Mathematical Considerations Pertaining to the Accuracy of Weapon Delivery Computations . . . 360
References . . . 364

6 Strategic Missiles . . . 365
6.1 Introduction . . . 365
6.2 The Two-Body Problem . . . 366
6.3 Lambert's Theorem . . . 382
6.4 First-Order Motion of a Ballistic Missile . . . 389
6.4.1 Application of the Newtonian Inverse-Square Field Solution to Ballistic Missile Flight . . . 389
6.4.2 The Spherical *Hit Equation* . . . 392
6.4.3 Ballistic Error Coefficients . . . 418
6.4.4 Effect of the Rotation of the Earth . . . 440
6.5 The Correlated Velocity and Velocity-to-Be-Gained Concepts . . . 443
6.5.1 Correlated Velocity . . . 443
6.5.2 Velocity-to-Be-Gained . . . 449
6.5.3 The Missile Control System . . . 457
6.5.4 Control During the Atmospheric Phase . . . 462
6.5.5 Guidance Techniques . . . 466
6.6 Derivation of the Force Equation for Ballistic Missiles . . . 472
6.6.1 Equations of Motion . . . 477
6.6.2 Missile Dynamics . . . 480
6.7 Atmospheric Reentry . . . 482
6.8 Missile Flight Model . . . 490
6.9 Ballistic Missile Intercept . . . 504
6.9.1 Introduction . . . 504
6.9.2 Missile Tracking Equations of Motion . . . 515
References . . . 519

7 Cruise Missiles . . . 521
7.1 Introduction . . . 521
7.2 System Description . . . 527
7.2.1 System Functional Operation and Requirements . . . 532
7.2.2 Missile Navigation System Description . . . 534
7.3 Cruise Missile Navigation System Error Analysis . . . 543
7.3.1 Navigation Coordinate System . . . 548
7.4 Terrain Contour Matching *(TERCOM)* . . . 551
7.4.1 Introduction . . . 551
7.4.2 Definitions . . . 555
7.4.3 The Terrain-Contour Matching (TERCOM) Concept . . . 557
7.4.4 Data Correlation Techniques . . . 563
7.4.5 Terrain Roughness Characteristics . . . 568
7.4.6 *TERCOM* System Error Sources . . . 570
7.4.7 *TERCOM* Position Updating . . . 571
7.5 The NAVSTAR/GPS Navigation System . . . 576
7.5.1 *GPS/INS* Integration . . . 583
References . . . 587

A Fundamental Constants . . . 589

B Glossary of Terms . . . 591

C List of Acronyms . . . 595

D The Standard Atmospheric Model . . . 605
References . . . 609

E Missile Classification . . . 611

F Past and Present Tactical/Strategic Missile Systems . . . 625
F.1 Historical Background . . . 625
F.2 Unpowered Precision-Guided Munitions (*PGM*) . . . 644
References . . . 650

G Properties of Conics . . . 651
G.1 Preliminaries . . . 651
G.2 General Conic Trajectories . . . 653
References . . . 657

H Radar Frequency Bands . . . 659

I Selected Conversion Factors . . . 661

Index . . . 663

1

Introduction

Rockets have been used as early as A.D. 1232, when the Chinese employed them as unguided missiles to repel the Mongol besiegers of the city of Pein-King (Peiping). Also, in the fifteenth century, Korea developed the *sinkijon** (or *Sin-Gi-Jeon*) rocket. Manufactured from the early fifteenth to mid-sixteenth century, the *sinkijon* was actively deployed in the northern frontiers, playing a pivotal role in fending off invasions on numerous occasions. Once out of the rocket launcher, the fire-arrows were set to detonate automatically near the target area. Also, the high-powered firearm was utilized in the southern provinces to thwart the Japanese marauders. The main body of the *sinkijon*'s rocket launcher was five to six meters long, the largest of its kind at that time**. A *sinkijon* was capable of firing as many as one hundred fire-arrows or explosive grenades. The fire-arrow contained a device equipped with gunpowder and shrapnel, timed to explode near the target. The introduction of gunpowder made possible the use of cannon and muskets that could fire projectiles great distances and with high velocities. It was desirable – in so far as the study of cannon fire is desirable – to learn the paths of these projectiles, their range, the heights they could reach, and the effect of muzzle velocity. Several years later, the *sinkijon* went through another significant upgrade, which enabled it to hurl a fire-arrow made up of small warheads and programmed to detonate and shower multiple explosions around the enemy. In 1451, King Munjong ordered a drastic upgrade of the hwacha (a rocket launcher on a cartwheel). This improvement allowed as many as one hundred *sinkijon*s to be mounted on the hwacha, boosting the overall firepower and mobility of the rocket.

Since those early times and in one form or another, rockets have been used as weapons and machines of war, for amusement through their colorful aerial bursts, as life-saving equipment, and for communications or signals. The lack of suitable guidance and control systems may have accounted for the rocket's slow improvement over the years. Strangely enough, it was the airplane rather than the rocket that stimulated the development of a guided missile as it is known today.

**Sinkijon* means "ghost-like arrow machine."

**The author would like to thank Dr. Jang Gyu Lee, Professor and Director of the Automatic Control Research Center, Seoul National University, Seoul, Korea, for providing the information on *sinkijon*.

In the twentieth century, the idea of using guided missiles came during World War I. Specifically, and as stated above, the use of the airplane as a military weapon gave rise to the idea of using remote-controlled aircraft to bomb targets. As early as 1913, René Lorin, a French engineer, proposed and patented the idea for a ramjet powerplant. In 1924, funds were allocated in the United States to develop a missile using radio control. Many moderately successful flights were made during the 1920s with this control, but by 1932 the project was closed because of luck of funds. Radio-controlled target planes were the first airborne remote-controlled aircraft used by the Army and Navy.

Dr. Robert H. Goddard was largely responsible for the interest in rockets back in the 1920s. Early in his experiments he found that solid-propellant rockets would not give him the high power or duration of power needed for a dependable supersonic motor capable of extreme altitudes. On March 16, 1926, Dr. Goddard successfully fired the first liquid-propellant rocket, which attained an altitude of 184 ft (56 m) and a speed of 60 mph (97 km/hr). Later, Dr. Goddard was the first to fire a rocket that reached a speed faster than the speed of sound. Moreover, he was the first to develop a gyroscopic steering apparatus for rockets, first to use vanes in the jet stream for rocket stabilization during the initial phase of a rocket in flight, and the first to patent the idea of step rockets.

The first flight of a liquid-propellant rocket in Europe occurred in Germany on 14 March 1931. In 1932 Captain Walter Dornberger (later a general) of the German Army obtained the necessary approval to develop liquid-propellant rockets for military purposes [1]. Subsequently, by 1936 Germany decided to make research and development of guided missiles a major project, known as the "Peenemünde Project," at Peenemünde, Germany. The German developments in the field of guided missiles during World War II were the most advanced of their time. Their most widely known missiles were the *V-1* and *V-2* surface-to-air missiles (note that the designation *V1* and/or *V2* is also found in the literature). As early as the spring of 1942, the original *V-1* had been developed and flight-tested at Peenemünde.

In essence, then, modern weapon (missile) guidance technology can be said to have originated during World War II in Germany with the development of the *V-1* and *V-2* (German: *A-4*; the *A-4* stands for *Aggregat-4*, or fourth model in the development type series; the *V* stands for *Vergeltungswaffe*, or retaliation weapon, while some authors claim that initially, it stood for *Versuchsmuster* or experimental model) surface-to-surface missiles by a group of engineers and scientists at Peenemünde. It should be noted that static firing of rockets, notably the *A-3*, was performed as early as in the spring of 1936 at the Experimental Station, Kummersdorf West (about 17 miles south of Berlin). In the spring of 1942 the original *V-1* (also known by various names such as *buzz bomb, robot bomb, flying bomb, air torpedo*, or *Fieseler Fi-103*) had been developed and flight-tested at Peenemünde. Thus, the *V-1* and *V-2* ushered in a new type of warfare employing remote bombing by pilotless weapons launched over a hundred miles away through all kinds of weather, day and night [1], [3].

The *V-1* was a small, midwing, pilotless monoplane, lacking ailerons but using conventional airframe and tail construction, having an overall length of 7.9 m (25.9 ft) and a wingspan of 5.3 m (17.3 ft). It weighed 2,180 kg (4,806 lb), including gasoline fuel and an 850 kg (1,874 lb) warhead. Powered by a pulsejet engine and launched

from an inclined concrete ramp 45.72 m (150 ft) long and 4.88 m (16 ft) above the ground at the highest end, the *V-1* flew a preset distance, and then switched on a release system, which deflected the elevators, diving the missile straight into the ground. The engine was capable of propelling the *V-1* 724 km/hr (450 mph). A speed of 322 km/hr (200 mph) had to be reached before the *V-1* propulsion unit could maintain the missile in flight. The range of the *V-1* was 370 km (230 miles). Guidance was accomplished by an autopilot along a preset path. Specifically, the plane's (or missile's) course stabilization was maintained by a magnetically controlled gyroscope that directed a tail rudder. When the predetermined distance was reached, as mentioned above, a servomechanism depressed the elevators, sending the plane into a steep dive. The *V-1* was not accurate, and it was susceptible to destruction by antiaircraft fire and aircraft. Several versions of the *V-1* were developed in Germany at that time. One version was designed for launch from the air. The missile could be carried under the left wing of a *Heinkel He-111* aircraft. A *manned V-1* version was also developed, called the *Reichenberg*, flown first by Willy Fiedler, followed by Hanna Reitch. This version was planned for suicide missions. Three versions were built.

The *V-2* (*A-4*) rocket was one of the most fearsome weapons of *WWII*. Successor to the *V-1 buzz bomb*, the *V-2* inflicted death, destruction, and psychological fear on the citizens of Great Britain. In essence, the *V-2* was the first long-range rocket-propelled missile to be put into combat. Moreover, the *V-2* was a liquid-propellant, 14 m (45.9 ft) rocket that was developed between 1938 and 1942 under the technical direction of Dr. Werner von Braun and Dr. Walter Dornberger, Commanding General of the Peenemünde Rocket Research Institute. In addition to Great Britain, the *V-2* was used to bomb other countries. However, although the first successful *V-2* test occurred on October 3, 1942, Adolf Hitler authorized full-scale development on July 27, 1943. The *V-2* had movable vanes on the outer tips of its fins. These fins were used for guidance and control when the missile was in the atmosphere, which would be for most of its flight when used as a ballistic weapon. It also had movable solid carbon vanes projecting into the rocket blast for the same purpose when it was in rarified atmosphere. The first *V-2,* which landed in England in September 1944, was a supersonic rocket-propelled missile launched vertically and then automatically tilted to a 41°–47° angle a short time after launch. Furthermore, the *V-2* had a liftoff weight of 12,873 kg (28,380 lb), developing a thrust of 27,125 kg (59,800 lb), a maximum acceleration of 6.4 g, reaching a maximum speed of about 5,705 km/h (3,545 mph), an effective range of about 354 km (220 miles), carrying a warhead of 998 kg (2,201 lb). In addition, the powered flight lasted 70 sec, reaching a speed of about 6,000 ft/sec at burnout, with a burnout angle of about 45° measured from the horizontal. A flat-Earth model was assumed. Like the *V-1*, the *V-2* was not known for its accuracy. For instance, the *V-2* had a dispersion at the target of 10 miles (16 km) over a range of 200 miles (322 km). Active countermeasures against the *V-2* were impossible at that time. Except for its initial programmed turn, it operated as a free projectile at extremely high velocity. The *V-2* consisted of two main parts: (1) a directional reference made up of a gyroscopic assembly to control the attitude of the missile and a clock-driven pitch programmer, and (2) an integrating accelerometer in order to sense accelerations along the thrust axis of the missile, thereby determining velocity, and to cut off the engine upon reaching a predetermined velocity. In essence,

the *V-2* system was the first primitive example of inertial guidance, making use of gyroscopes and accelerometers [3].

Several other German missiles were also highly developed during World War II and were in various stages of test. One of these, the *Rheinbote* (Rhein Messenger), was also a surface-to-surface missile. This rocket was a three-stage device with booster-assisted takeoff. Its range was 217 km (135 miles), with the third stage reaching over 5,150 km/hr (3200 mph) in about 25 seconds after launch. The overall length of the rocket was about 11.3 m (37 ft). After having dropped a rearward section at the end of each of the first and second stages, it had a length of only 3.96 m (13 ft). The 3.96 m (13 ft) section of the third stage carried a 40 kg (88 lb) high-explosive warhead. An antiaircraft or surface-to-air missile, the *Wasserfall* (Waterfall), was a remote radio-controlled supersonic rocket, similar to the *V-2* in general principles of operation (e.g., both were launched vertically). When fully loaded, it had a weight of slightly less than 4,907 kg (5.4 tons). Its length was 7.62 m (25 ft). Designed for intercepting aircraft, the missile had specifications that called for a maximum altitude of 19,812 m (65,000 ft), a speed of 2,172 km/hr (1,350 mph), and a range of 48.3 km (30 miles). Its 90.7 kg (200 lb) warhead could be detonated by radio after the missile had been command-controlled to its target by radio signals. It also had an infrared proximity fuze and homing device for control on final approach to the target and for detonating the warhead at the most advantageous point in the approach. Propulsion was to be obtained from a liquid-propellant power plant, with nitrogen-pressurized tanks. Another surface-to-air missile, the *Schmetterling* (Butterfly), designated *HS-117*, was still in the development stage at the close of the war. All metal in construction, it was 3.96 m (13 ft) long and had a wingspan of 1.98 m (6.5 ft). Its effective range against low-altitude targets was 16 km (10 miles). It traveled at subsonic speed of about 869 km/hr (540 mph) at altitudes up to 10,668 m (35,000 ft). A proximity fuze would set off its 24.95 kg (55 lb) warhead. Propulsion was obtained from a liquid-propellant rocket motor with additional help from two booster rockets during takeoff. Launching was to be accomplished from a platform, which could be inclined and rotated toward the target. The *Schmetterling* was developed at the Henschel Aircraft Works.

The *Enzian* was another German surface-to-air missile (SAM). Designed to carry payloads of explosives up to 1000 pounds (453.6 kg), it was intended to be used against heavy-bomber formations. The *Enzian* was about 12 ft (3.657 m) long, had a wingspan of approximately 14 ft (4.267 m), and weighed a little over 2 tons (1,814.36 kg). Propelled by a liquid-propellant rocket, it was assisted during takeoff by four solid-propellant rocket boosters. The range of the *Enzian* was 16 miles (25.74 km), with a speed of 560 mph (901.21 km/hr), reaching an maximum altitude of 48,000 ft (14,630 m). In addition to the SAMs Germany had developed an air-to-air missile, designated the *X-4*. The *X-4* was designed to be launched from fighter aircraft. Propelled by a liquid-propellant rocket, it was stabilized by four fins placed symmetrically. Its length was about 6.5 ft (1.98 m) and span about 2.5 ft (0.762 m). Its range was slightly over 1.5 miles (2.414 km), and its speed was 560 mph (901.21 km/hr) at an altitude of 21,000 ft (6,401 m). Guidance was accomplished by electrical impulses transmitted through a pair of fine wires from the fighter aircraft. This missile was claimed to have been flown, but it was never used in combat.

The *V*-weapons, as mentioned earlier, were used to bombard London and southeastern England from launch sites near Calais, France, and the Netherlands. However, as the German armies were withdrawing from the Netherlands in March 1945, the *V-1*s were launched from aircraft. Over 9,300 *V-1*s had been fired against England. By August 1944, approximately 1,500 *V-1*s had been shot down over England. Also, 4,300 *V-2*s had been launched in all, with about 1,500 against England and the remaining against Antwerp harbor and other targets.

A project for developing missiles in the U.S.A. during World War II was started in 1941. In that year the Army Air Corps asked the National Defense Research Committee to undertake a project for the development of a vertical, controllable bomb. The committee initiated a glide-bomb program, which resulted in standardization of a preset glide bomb attached to a 2,000 lb (907.2 kg) demolition bomb. The *Azon*, a vertical bomb controlled in azimuth only, went on the production line in 1943. *Project Razon*, a bomb controlled in both azimuth and range, was started in 1942. By 1944, these glide bombs used remote television control. The Navy had a number of guided missile projects under development by the end of World War II. The *Loon*, a modification of the *V-1*, was to be used from ship to shore and to test guided-missile components. Another Navy missile, known as *Gorgon IIC*, used a ramjet engine with radar tracking and radio control.

At the close of World War II the Americans obtained sufficient components to assemble two to three hundred *V-2*s from the underground factory, the *Mittelwerk*, near Nordhausen, Germany. The purpose of this was to use these *V-2*s as upper-atmosphere research vehicles carrying scientific experiments from *JPL* (Jet Propulsion Laboratory), Johns Hopkins, and other organizations.

In essence, the ballistic missile program in this country culminated with the development of the *Atlas ICBM* (intercontinental ballistic missile) (see Appendix F, Table F-1). In October 1953, and under a study contract from the U.S. Air Force, the Ramo-Woolridge Corporation (later Thomson-Ramo-Woolridge, or *TRW*) began work on a new *ICBM*. Within a year the program passed from top Air Force priority to top national priority. The first successful flight of a *Series A Atlas ICBM* took place on December 17, 1957, four months after the Soviet Union had announced that it had an ICBM. By the mid-1959, more than eighty thousand engineers and technicians had participated in this program.

Strictly speaking, missiles can be divided into two categories: (1) *guided missiles* (also called *guided munitions*), or *tactical missiles*, and (2) *unguided missiles*, or *strategic missiles*. Guided and unguided missiles can be defined as follows:

Guided Missile: In the guided class of missiles belong the aerodynamic guided missiles. That is, those missiles that use aerodynamic lift to control its direction of flight. An aerodynamic guided missile can be defined as an aerospace vehicle, with varying guidance* capabilities, that is self-propelled through the atmosphere for the purpose of inflicting damage on a designated target. Stated another way, an aerodynamic guided missile is one that has a winged configuration and is usually

*Guidance is defined here as the means by which a missile steers to, or is steered to, a target. In guided missiles, missile guidance occurs after launch.

fired in a direction approximately towards a designated target and subsequently receives steering commands from the ground guidance system (or its own, onboard guidance, system) to improve its accuracy.

Guided missiles may either home to the target, or follow a nonhoming preset course. Homing missiles maybe *active*, *semiactive*, or *passive*. Nonhoming guided missiles are either inertially guided or preprogrammed [3]. (For more information, see Chapter 4.)

Unguided Missiles: Unguided missiles, which includes ballistic missiles, follow the natural laws of motion under gravity to establish a ballistic trajectory. Examples of unguided missiles are *Honest John*, *Little John*, and many artillery-type rockets. Note that an unguided missile is usually called a *rocket* and is normally not a threat to airborne aircraft. (See also Chapter 6 for more details.)

Typically, guided missiles are *homing* missiles, which include the following: (1) a propulsion system, (2) a warhead section, (3) a guidance system, and (4) one or more sensors (e.g., radar, sinfrared, electrooptical, lasers). Movable control surfaces are deflected by commands from the guidance system in order to direct the missile in flight; that is, the guidance system will place the missile on the proper trajectory to intercept the target.

As stated above, homing guidance may be of the *active*, *semiactive*, or *passive* type. Active guidance missiles are able to guide themselves independently after launch to the target. These missiles are of the so-called *launch-and-leave* class. For instance, air superiority fighters such as the *F/A-22 Raptor* that are designed with low-observable, advanced avionics and supercruise technologies are being developed to counter lethal threats posed by advanced surface-to-air missile systems (e.g., the U.S. *HAWK MIM-23*, *Patriot MIM-104*, *Patriot Advanced Capability PAC-3*, and the Russian *SA-10* and *SA-12 SAM*s) and next-generation fighters equipped with *launch-and-leave* missiles. Therefore, an active guided missile carries the radiation source on board the missile. The radiation from the interceptor missile is radiated, strikes the target, and is reflected back to the missile. Thus, the missile guides itself on this reflected radiation. Consequently, a missile using active guidance will, as a rule, be heavier than semiactive or passive missiles.

A semiactive missile uses a combination of active and passive guidance. A source of radiation is part of the system, but is not carried in the missile; that is, it is dependent on off-board equipment for guidance commands. More specifically, in semiactive missiles the source of radiation, which is usually at the launch point, radiates energy to the target, whereby the energy is reflected back to the missile. As a result, the missile senses the reflected radiation and homes on it. A passive missile utilizes radiation originated by the target, or by some other source not part of the overall weapon system. Typically, this radiation is in the infrared region (e.g., *Sidewinder*-type missiles) or the visible region (e.g., *Maverick*), but may also occur in the microwave region (e.g., *Shrike*). Nonhoming guided missiles, as we shall presently discuss, are either inertially guided or preprogrammed. From the above discussion, we note that missile guidance can occur after launch. By guiding after launch, the effect of prelaunch aiming errors can be considerably minimized. Hence, the primary purpose of postlaunch guidance is to relax prelaunch aiming requirements.

Two common types of missiles that pose a threat to aircraft are the *air-to-air* (*AA*), or *air-intercept, missile* (*AIM*), and the *surface-to-air* missile (*SAM*) mentioned earlier. The *AA* and *SAM* missiles belong to the *tactical* and *defense* missile class, and are launched from interceptor fighter aircraft, employing various guidance techniques. *Surface-to-air* missiles can be launched from land- or sea-based platforms. They too have varying guidance and propulsion capabilities that influence their launch envelopes relative to the target. Furthermore, these missiles employ sophisticated electronic countermeasure (*ECM*) schemes to enhance their effectiveness. It should be pointed out that since weight is not much of a problem, these missiles are often larger than their air-to-air counterparts, and they can have larger warheads and longer ranges.

In attempting to intercept a moving target with a missile, a desired trajectory will be needed in which the missile velocity leads the line of sight (*LOS*) by the proper angle so that for a constant-velocity target the missile flies a straight-line path to collision. In homing systems, for example, the target tracker is in the missile, and in such a case it is the relative movement of target and missile that is relevant. The two-dimensional end-game geometry of an ideal *collision course* will be discussed later in this book. Typically, an aerodynamic missile is controlled by an autopilot, which receives lateral acceleration commands from the guidance system and causes aerodynamic surfaces to move so as to attain these commanded accelerations. Since in general, there are two lateral missile coordinate axes, the general three-dimensional attack geometry can be resolved into these two directions.

Ballistic missiles belong to the *strategic* missile class, and are characterized by their trajectory. A ballistic missile trajectory is composed of three parts (for more details, see Chapter 6). These are (1) the *powered flight* portion, which lasts from launch to thrust cutoff (or burnout); (2) the *free-flight* portion, which constitutes most of the trajectory, and (3) the *reentry* portion, which begins at some point (not defined precisely) where the atmospheric drag becomes a significant force in determining the missile's path and lasts until impact on the surface of the Earth (i.e., a target). Typically, ballistic missiles rely on one or more boosters and an initial steering vector. Once in flight, they maintain this vector with the aid of gyroscopes. Therefore, a ballistic missile may be defined as a missile that is guided during the powered portion of the flight by deflecting the thrust vector, becoming a *free-falling* body after engine cutoff. However, as already noted, in ballistic missiles part of the guidance occurs before launch. Hence, prelaunch errors translate directly into miss distance. One important feature of these missiles is that they are roll stabilized, resulting in simplification of the analysis, since there is no coupling between the longitudinal and the lateral modes. Ballistic missiles are the type least likely to be intercepted. A ballistic missile can have surprising accuracy. Ballistic missiles can be classified according to their range. That is, short range (e.g., up to 300 nm (nautical miles) or 556 km), intermediate range (e.g., 2500 nm or 4632.5 km), and long range (over 2500 nm or 4632.5 km). Examples of these classes are as follows: (1) short range – *Pershing*, *Sergeant*, and *Hawk* class; (2) intermediate range – *Thor*, *Jupiter*, and *Polaris/Poseidon/Trident*, and (3) long range – *Minuteman I–III*, the *MX*, and *Titan* missiles. Note that ballistic missiles capable of attaining very long ranges (e.g., over 5000 nm) or intercontinental range,

are given the *ICBM* designator [2], [4]. Recently, the U.S. Air Force formulated plans for a new *ICBM*, likely to be named *Minuteman IV*. A possible start development date is for the year(s) 2004–2005. Among the enhancements being examined are communications upgrades, an additional postboost vehicle that could maneuver the warhead after separation from the missile, and a new rocket motor.

In common use today are the following abbreviations, which use the term *ballistic missile* in the sense that the type of missile and its capacity are indicated (for a detailed list of acronyms, see Appendix C):

IRBM: Intermediate Range Ballistic Missile
ICBM: Intercontinental Ballistic Missile
AICBM: Anti-Intercontinental Ballistic Missile
SLBM: Submarine-Launched Ballistic Missile (or *FBM* – Fleet Ballistic Missile)
ALBM: Air-Launched Ballistic Missile
MMRBM: Mobile Mid-Range Ballistic Missile.

The range has much to do with using this kind of missile designator, which like the *point-to-point* designator, is used with the vehicle's popular name. It should be noted at this point that essentially, the difference between the ballistic and aerodynamic missiles lies in the fact that the former does not rely upon aerodynamic surfaces to produce lift and consequently follows a ballistic trajectory when thrust is terminated. Aerodynamic missiles, as stated earlier, have a winged configuration.

Ballistic missiles use inertial guidance, sometimes aided with star trackers and/or with the Global Positioning System (*GPS*). More specifically, inertial guidance is used for a ballistic trajectory only during the very early part of the flight (i.e., up to fuel cut-off) in order to establish proper velocity for a hit by free fall. In ballistic missiles, the intent is to hit a given map reference, as opposed to aerodynamic missiles, whose intent is to intercept a moving and at times highly maneuverable target. Long-range intercontinental ballistic missiles are categorized as surface-to-surface. As stated above, ballistic missiles use inertial guidance to hit a target. The modern inertial navigation and guidance system is the only self-contained single source of all navigation data. Self-contained inertial navigation depends on the integration of acceleration with respect to a Newtonian reference frame. That is, inertial navigation depends on integration of acceleration to obtain velocity and position. The inertial navigation system (*INS*) provides a reliable all-weather, worldwide navigation capability that is independent of ground-based navigation aids. The system develops navigational data from self-contained inertial sensors (i.e., gyroscopes and accelerometers), consisting of a vertical accelerometer, two horizontal accelerometers, and three single-degree-of-freedom gyroscopes (or 2 two-degree-of-freedom gyroscopes). In addition to the conventional mechanical gyroscopes, there is a new generation of inertial sensors such as the *RLG* (Ring Laser Gyro), the *FOG* (Fiber-Optic Gyro), and the *MEMS* (Micro Electro-Mechanical Sensor), which functions as both a gyro and an accelerometer. Note that the *MEMS* devices are fundamentally different from the *RLG* and *FOG* optical sensors. The design of *MEMS* allows a single chip to function as both a gyro and an accelerometer. The sensing elements are mounted in a four-gimbal, gyro-stabilized inertial platform. The accelerometers are the primary source of information. They are maintained in a known reference frame by the gyroscopes. That is, the precision

gyro-stabilized platform is used for reference. Attitude and heading information is obtained from synchro devices mounted between the platform gimbals. Therefore, the heart of the inertial navigation system is the inertial platform. The platform has four gimbals for all-attitude operation, with the outermost gimbal being the outer roll, which has unlimited freedom. Proceeding inward, the next gimbal is pitch, which is normally limited to $\pm 105^\circ$ of freedom. The next inward gimbal is inner roll, which is redundant with the outer roll axis but is required in order to eliminate what is called *gimbal lock* and is limited to $\pm 15^\circ$ angular freedom. All inertial sensors are mounted on the azimuth gimbal, the innermost gimbal. The gyroscopes are mounted such that the vertical gyroscope is mounted with its spin axis parallel to the azimuth gimbal rotational axis and positioned to coincide with the local vertical when the platform is erected to X and Y (level) accelerometer nulls. The X and Y axis accelerometers, mounted on the azimuth structure, are aligned to sense horizontal accelerations along the gyro X and Y axes, respectively, while the Z, or vertical, accelerometer senses accelerations along the azimuth axis. After being supplied with initial position information, the *INS* is capable of continuously updating extremely accurate displays of position, ground speed, attitude, and heading. In addition, it provides guidance or steering information for autopilot and flight instruments (in the case of aircraft).

Note that the above discussion was for gimbaled inertial navigation systems. There is also a class of *strapdown INS*s in which the inertial sensors are mounted directly on the host vehicle frame. In this way, the gimbal structure is eliminated. In the strapdown version of the *INS*, wherein sensors are mounted directly on the vehicle, the transformation from the sensor to inertial reference is "computed" rather than mechanized. Specifically, the strapdown system differs from the gimbaled system in that the specific force is measured in the body frame, and the attitude transformation to the navigation specific force is computed from the gyro data, because the strapdown sensors are fixed to the vehicle frame. Regardless of mechanization (i.e., gimbaled or strapdown), alignment of an inertial navigation system is of paramount importance. In alignment, the accelerometers must be leveled (i.e., indicating zero output), and the platform must be oriented to true north. This process is normally called *gyrocompassing*.

In ballistic missiles (in particular *ICBM*s), rocket propulsion is employed to accelerate the missile to a position of high altitude and speed. This places it on a trajectory that meets certain guidance specifications in order to carry a warhead, or other payload, to a preselected target. An operational ballistic missile may acquire speeds up to 15,000 mph (24,140 km/hr) or better at heights of several hundred miles. After boost burnout (*BBO*), or engine shutoff, the missile payload travels along a free-fall trajectory to its destination; its motion follows, approximately, the laws of *Keplerian* motion. A special type of onboard navigation/guidance computer is used in ballistic missiles in which the platform (e.g., in gimbaled systems) maintains its alignment in space for the few minutes during which the inertial system is operating to launch the warhead. The computer is fed the velocity and position that the warhead ought to achieve when the motors are cut off. Consequently, the actual positions and velocities are recorded from the information taken from the inertial platform, and by comparing the two, a correction may be passed to the control system of the missile. Thus, the correction ensures that the motors are cut off when the warhead is traveling at a velocity and from a position that will enable it to hit the same target as if it had

followed exactly a planned (or programmed) flight path or trajectory. The planned path takes into account the change of gravity due to the forward movement of the missile, the change in the force of gravity due to upward movement of the missile, and the Earth's tilt, rotation, and *Coriolis* acceleration. However, the planned path may involve a good deal of calculation, and as a result it may not be easy to alter the aiming point by more than a small amount without a completely new plan. It was mentioned earlier that part of the guidance of a ballistic missile occurs before launch. Moreover, during the powered portion of the flight, the objective of the guidance system is to place the missile on a trajectory with flight conditions that are appropriate for the desired target. This is equivalent to steering the missile to a burn-out point that is uniquely related to the velocity and flight-path angle for the specified target range.

Another type of strategic missile is the now canceled USAF's *SRAM II* missile. The *SRAM* (Short-Range Attack Missile) *II* was a *standoff*, air-launched, inertially guided strategic missile. As designed, the missile had the capability to cover a large target accessibility footprint when launched with a wide range of initial conditions. The missile was designed to be powered by a two-pulse solid-fuel rocket motor with a variable intervening coast time. The guidance algorithm was based on modern control linear quadratic regulator (*LQR*) theory, with the current missile state (a vector consisting of position, velocity, and other parameters) provided by a strapdown inertial navigation system. The *SRAM II* trajectory was dependent on the relative locations of the launch point and target, as well as the flight envelope characteristics of the carrier (i.e., aircraft).

Still another class of strategic missiles is the nuclear *ALCM* (Air-Launched Cruise Missile) designated as *AGM-86B*. The *ALCM* uses an inertial navigation system together with terrain contour matching (*TERCOM*) for its guidance. A later version of the *ALCM*, known as the *CALCM* (Conventionally Armed Air-Launched Cruise Missile) and designated *AGM-86C*, uses an *INS* integrated with the *GPS* and/or *TERCOM* (for more information, see Chapter 7).

It should be pointed out that there is still another class of missiles, namely, *radiation* missiles. In radiation missiles, radiation energy is transmitted as either particles or waves through space at the speed of light. Radiation is capable of inflicting damage when it is transmitted toward the target either in a continuous beam or as one or more high-intensity, short-duration pulses. Weapons utilizing radiation are referred to as *directed high-energy weapons* (*DHEW*). These are as follows:

1. Coherent Electromagnetic Flux: The coherent electromagnetic flux is produced by a high-energy laser (*HEL*). The *HEL* generates and focuses electromagnetic energy into an intense concentration or beam of coherent waves that is pointed at the target. This beam of energy is then held on the target until the absorbed energy causes sufficient damage to the target, resulting in eventual destruction. On the other hand, radiation from a laser that is delivered in a very short period of time with a high intensity is referred to as a pulse-laser beam. (For more details on high-energy weapons see Section 6.9.)
2. Noncoherent Electromagnetic Pulse (*EMP*): The noncoherent electromagnetic pulse consists of an intense electronic signal of very short duration that travels

through space just as a radio signal does. When an *EMP* strikes an aircraft, the electronic devices in the aircraft can be totally disabled or destroyed.

3. Charged Nuclear Particles: The charged-particle-beam weapon is the newest of the developing threats that utilizes radiation in the form of accelerated subatomic particles. These particles, or bunches of particles, may be focused on the target by means of magnetic fields. Thus, considerable damage can result. This type of weapon has the advantage that it will propagate through visible moisture, which tends to absorb energy generated by the *HEL*.

Regardless of the type of missile, a development cycle must be formulated that takes into account several phases of design and analysis. The missile development cycle commences with concept formulation, where one or more guidance methods are postulated and examined for feasibility and compatibility with the total system objectives and constraints. Surviving candidates are then compared quantitatively, and a baseline concept is adopted. Specific subsystem and component requirements are generated via extensive tradeoff and parametric studies. Factors such as missile capability (e.g., acceleration and response time), sensor function (e.g., tracking, illumination), accuracy (signal to noise, waveforms), and weapons control (e.g., fire control logic, guidance software) are established by means of both analytical and simulation techniques. After iteration of the concept/requirements phase and attainment of a set of feasible system requirements, the analytical design is initiated. During this stage, the guidance law is refined and detailed, a missile autopilot and the accompanying control actuator are designed, and an onboard sensor tracking and stabilization system is devised. This design phase entails the extensive use of feedback control theory and the analysis of nonlinear, nonstationary dynamic systems subjected to deterministic and random inputs. Finally, determination of the sources of error and their propagation through the system are of fundamental importance in setting design specifications and achieving a well-balanced design.

From the above discussion, one can safely say that of vital interest in missile design is the development of advanced guidance and control concepts. For example, in the design of a guidance law for a homing missile, a continued effort should be the study of homing guidance and the means to optimize its performance in various intercept situations. The classical approach to missile guidance involves the use of a low-pass filter for estimating the line-of-sight angular rate along with a proportional guidance law. In addition to the classical methods, we will discuss the use of optimized digital guidance and control laws for highly dynamic engagements associated with air-to-air missiles, where the classical approaches often fail to achieve acceptable performance. Conventional proportional navigation systems, as will be discussed later in this book, have been improved with time-variable filtering, and the design process has been refined with automatic computer methods. Advanced guidance systems having superior performance have been designed with on-line Kalman estimation for filtering noisy radar data and with optimal control gains expressed in closed form. For instance, trajectory estimators are designed routinely using Kalman filtering theory and provide minimum variance estimates of key guidance variables based upon a linearized model of the trajectory. The guidance laws are commonly designed to

yield as small a *miss distance* as possible, consistent, of course, with the missile's acceleration capability. This is accomplished by mathematically requiring the commanded acceleration to minimize an appropriate performance index (or cost function) involving both the miss distance and the missile acceleration level. Today, the concept of optimized guidance laws is well understood in applications where information concerning the target range and line-of-sight angle is available. This is the case when the homing sensor is an active or semiactive radar (*RF*) or laser range finder. Moreover, considerable attention has been given to developing advanced guidance concepts for the situation in which direct measurements of range are unavailable, as with passive infrared or electro-optical sensors.

Synthesis of sample data homing and command guidance systems is also of particular importance, as will be discussed later. Classical servo theory has been used to design both hydraulic and electric seeker servos that are compatible with requirements for gyro-stabilization and fast response. Furthermore, pitch, yaw, and roll autopilots have been designed to meet such problems as Mach variation, altitude variation, induced roll moments, instrument lags, body-bending modes, guidance response, and guidance stability. Although classical theory is still applicable to autopilots, research efforts are continually made to apply modern control theory to conventional autopilot design and adaptive autopilot design.

Optimal control and estimation theory is commonly used in the design of advanced guidance systems. Specifically, since the late 1960s and early 1970s, considerable research has been devoted to applying modern optimal control and estimation theory in the development of optimized advanced tactical and strategic missile guidance systems. In particular, this technology has been used to develop tracking algorithms that extract the maximum amount of information about a target trajectory from homing sensor data and to derive guidance and control laws that optimize the use of this information in directing the missile toward the selected target. Performance improvements attainable with optimized systems over conventional guidance and control techniques are most significant against airborne maneuverable targets, where target acceleration information and rapid guidance system response time are required to achieve acceptable accuracy, in minimum time. Historically, surface-to-air missiles were among the first missiles to implement digital guidance systems. Such missiles may employ command guidance whereby all digital computation is done on the ground with guidance commands telemetered to the missile. Today, the ease of availability of microprocessors makes digital processing increasingly attractive for small, lightweight air-to-air missiles. Recently developed neural network algorithms and fuzzy logic theory serve as possible approaches to solving highly nonlinear flight control problems. Thus, the use of fuzzy logic control is motivated by the need to deal with nonlinear flight control and performance robustness problems.

It was noted earlier that prior to beginning an engineering development program for a digital guidance and control system, it is desirable to perform a detailed computer-aided feasibility study within the context of a realistic missile–target engagement model. In order to accomplish these, guidance and control laws that have been developed and evaluated for simplified missile–target engagement scenarios must be extended and adapted to the air-to-air missile situation and then implemented in a complete three-dimensional engagement model.

Finally, microprocessor technology will allow future application of more sophisticated guidance and control laws that consider the effects of uncertain system parameters than have heretofore been considered for tactical missiles. System miniaturization is becoming more and more common in weapon systems. For example, a miniaturized system that can integrate *GPS* and inertial guidance to increase accuracy of Army and Navy artillery shells has already been developed. These systems can be placed on a circuit board and are small enough to fit into the nose of an artillery shell. Above all, a single processor placed on the board can be used to handle *GPS* and inertial data from *MEMS*. The Army's *XM-982* and the Navy's Extended Range Guided Munition (*ERGM*) will use the *GPS* system (see also Appendix F). Missile guidance systems are advancing on several fronts as *GPS* spreads into old and new systems, automatic target recognition moves toward deployment, and ballistic missile defense programs improve the state of the art in data fusion and infrared sensors. Missile systems presently under research and development will evolve into smaller, more accurate missiles.

A revolutionary new generation of miniature loitering *smart* weapons (or submunition) is the U.S. Air Force's *LOCAAS* (Low-Cost Autonomous Attack System) missile that was designed and flight-tested in the 1990s as a gliding weapon for armored targets only. *LOCAAS* can be air launched singly or in a self-synchronizing swarm that will deconflict targets so only one *LOCAAS* pursues each target. This futuristic *smart* weapon has a mind of its own. Scanning the land below, these weapons can identify and destroy mobile launchers. The key here is that they can distinguish between different targets and then shape their warheads to inflict maximum damage. Nose to tail, these $40,000, 31-inch (0.787 meter) long air-to-surface weapons will be anything but small in performance. The current production version calls for a five-pound turbojet engine with thirty pounds of thrust to fly 100 m/sec (328 ft/sec) while hunting for fast-moving missile launchers over a large target area. The size of a soup bowl, the warhead uses a shaped charge to transform a copper plate into fragments, a shuttlecock-shaped slug, or a rod that can penetrate several inches of high-carbon steel. That is, its warhead can explode into fragments, a long-rod penetrator, or a slug, depending on the type of target it detects. Without designating a specific target, flight crews will leave the thinking to the missile's three-dimensional imaging ladar (or laser radar) and use its target recognition system in its nose to continuously scan target areas. That is, the *LOCAAS* seeker uses advanced target recognition algorithms to detect, prioritize, reject, and select targets. As many as two hundred of these flying smart weapons can be swooping down on an enemy battlefield.

References

1. Dornberger, W.: *V-2*, The Viking Press, New York, NY, 1954.
2. Laur, T.M. and Llanso, S.L. (edited by W.J. Boyne): *Encyclopedia of Modern U.S. Military Weapons*, Berkley Books, New York, NY, 1995.
3. Pitman, G.R., Jr. (ed.): *Inertial Guidance*, John Wiley & Sons, Inc., New York, NY, 1962.
4. *Airman*, Magazine of America's Air Force, September 1995.

This page intentionally left blank

2

The Generalized Missile Equations of Motion

2.1 Coordinate Systems

2.1.1 Transformation Properties of Vectors

In a rectangular system of coordinates, a vector can be completely specified by its components. These components depend, of course, upon the orientation of the coordinate system, and the same vector may be described by many different triplets of components, each of which refers to a particular system of axes. The three components that represent a vector in one set of axes, will be related to the components along another set of axes, as are the coordinates of a point in the two systems. In fact, the components of a vector may be regarded as the coordinates of the end of the vector drawn from the origin. This fact is expressed by saying that the scalar components of a vector transform as do the coordinates of a point. It is possible to concentrate attention entirely on the three components of a vector and to ignore its geometrical aspect. A vector would then be defined as a set of three numbers that transform as do the coordinates of a point when the system of axes is rotated. It is often convenient to designate the coordinate axes by numbers instead of letters x, y, z so that the components of a vector will be a_1, a_2, and a_3. The designation for the whole vector is a_i, where it is understood that the subscript i can take on the value 1, 2, or 3. A vector equation is then written in the form

$$a_i = b_i. \tag{2.1}$$

This represents three equations, one for each value of the subscript i. The rotation of a system of coordinates about the origin may be represented by nine quantities $\gamma_{ij'}$, where $\gamma_{ij'}$ is the cosine of the angle between the i-axis in one position of the coordinates and the j-axis in the other position. These nine quantities give the angles made by each of the axes in one position with each of the axes in the other. They are also the coefficients in the expression for the transformation of the coordinates of a

point. The cosines can be conveniently kept in order by writing them in the form of a matrix:

$$\begin{bmatrix} \gamma_{11'} & \gamma_{12'} & \gamma_{13'} \\ \gamma_{21'} & \gamma_{22'} & \gamma_{23'} \\ \gamma_{31'} & \gamma_{32'} & \gamma_{33'} \end{bmatrix}. \tag{2.2}$$

Of the nine quantities, only three are independent, since there are six independent relations between them. Since $\gamma_{ij'}$ can be considered as the component along the j'-axis in one coordinate system of a unit vector along the i-axis in the other, then

$$\gamma_{i1'}^2 + \gamma_{i2'}^2 + \gamma_{i3'}^2 = \sum_{j'} \gamma_{ij'}^2 = 1. \tag{2.3a}$$

This will be true for every value of i. Similarly,

$$\sum_{i'} \gamma_{ij'}^2 = 1. \tag{2.3b}$$

The components of a vector, or the coordinates of a point, can be transformed from one system of coordinates to the other by

$$a_i = \gamma_{i1'} a_{1'} + \gamma_{i2'} a_{2'} + \gamma_{i3'} a_{3'} = \gamma_{ij'} a_{j'}. \tag{2.4}$$

Here $a_{j'}$ represents the components of the vector a in one system of coordinates, and a_i the components in the other. The summation sign is omitted in the last term, since it is to be understood that a sum is to be carried out over all three values of any index that is repeated.

2.1.2 Linear Vector Functions

If a vector is a function of a single scalar variable, such as time, each component of the vector is independently a function of this variable. If the vector is a linear function of time, then each component is proportional to the time. A vector may also be a function of another vector. In general, this implies that each component of the function depends on each component of the independent vector. Moreover, a vector is a linear function of another vector if each component of the first is a linear function of the three components of the second. This requires nine independent coefficients of proportionality. The statement that a is a linear function of b means that

$$\begin{aligned} a_1 &= C_{11} b_1 + C_{12} b_2 + C_{13} b_3, \\ a_2 &= C_{21} b_1 + C_{22} b_2 + C_{23} b_3, \\ a_3 &= C_{31} b_1 + C_{32} b_2 + C_{33} b_3. \end{aligned} \tag{2.5}$$

Using the summation convention as in (2.4), this becomes

$$a_i = C_{ij} b_j. \tag{2.6}$$

A relationship such as that in (2.6) must be independent of the coordinate system in spite of the fact that the notation is clearly based on specific coordinates. The components a_i and b_i are with reference to a particular coordinate system. The constants C_{ij} also have reference to specific axes, but they must so transform with a rotation of axes that a given vector b always leads to the same vector a.

If the coordinate system is rotated about the origin, the vector components will change so that

$$a_i = \gamma_{ij'} a_{j'} = C_{ij} \gamma_{jk'} b_{k'}. \tag{2.7}$$

If both sides of this equation are multiplied by $\gamma_{l'i}$ and the equations for the three values of i are added, the result is

$$\gamma_{l'i} \gamma_{ij'} a_{j'} = a_{l'} = (\gamma_{l'i} C_{ij} \gamma_{jk'}) b_{k'}. \tag{2.8}$$

If the quantity $\gamma_{l'i} C_{ij} \gamma_{jk'}$ is called $C_{l'k'}$, then

$$a_{i'} = C_{l'k'} b_{k'}. \tag{2.9}$$

This relationship between the components in this system of coordinates is the same vector relationship as was expressed by the C_{ik} in the original system of coordinates.

2.1.3 Tensors

Tensor is a general name given to quantities that transform in prescribed ways when the coordinate system is rotated. A *scalar* is a tensor of rank 0, for it is independent of the coordinate system. A *vector* is a tensor of rank 1. Its components transform as do the coordinates of a point. A *tensor* of rank 2 has components that transform as do the quantities C_{ij}. Put another way, a scalar is a quantity whose specification (in any coordinate system) requires just one number. On the other hand, a vector (originally defined as a directed line segment) is a quantity whose specification requires three numbers, namely, its components with respect to some basis. In essence, scalars and vectors are both special cases of a more general object called a *tensor of order n*, whose specification in any given coordinate system require 3^n numbers, again called the *components* of the tensor. In fact,

scalars are tensors of order 0, with $3^0 = 1$ components,
vectors are tensors of order 1, with $3^1 = 3$ components.

Tensors can be added or subtracted by adding or subtracting their corresponding components. They can also be multiplied in various ways by multiplying components in various combinations. These and other possible operations with tensors will not be described here.

A tensor of the second rank is said to be symmetric if $C_{ij} = C_{ji}$ and to be antisymmetric if $C_{ij} = -C_{ji}$. An antisymmetric tensor has its diagonal components equal to

zero. Any tensor may be regarded as the sum of a symmetric and an antisymmetric part for

$$C_{ij} = \tfrac{1}{2}[C_{ij} + C_{ji}] + \tfrac{1}{2}[C_{ij} - C_{ji}] \tag{2.10a}$$

and

$$\tfrac{1}{2}[C_{ij} + C_{ji}] = S_{ij} \quad \tfrac{1}{2}[C_{ij} - C_{ji}] = A_{ij}, \tag{2.10b}$$

where S_{ij} is symmetric and A_{ij} is antisymmetric. Numerous physical quantities have the properties of tensors of the second rank, so that the inertial properties of a rigid body can be described by the symmetric tensor of inertia. By way of illustration, consider that we are given two vectors A and B. There are nine products of a component of A with a component of B. Thus,

$$A_i B_i (i, k = 1, 2, 3).$$

Suppose we transform to a new coordinate system K', in which A and B have components A'_i and B'_k. Then the transformation of a coordinate system can be expressed as

$$A_i = \alpha_{i'} A_k,$$

where A_k, A'_i are the components of the vector in the old and new coordinate systems K and K', respectively, and $\alpha_{i'k}$ is the cosine of the angle between the ith axis of K' and the kth axis of K. Thus,

$$A'_i = \alpha_{i'k} A_i, \; B'_k = \alpha_{k'm} B_m,$$

and hence

$$A'_i B'_k = \alpha_{i'l} \alpha_{k'm} A_l B_m.$$

Therefore, $A_i B_k$ is a second-order tensor.

2.1.4 Coordinate Transformations

There are three commonly used methods of expressing the orientation of one three-axis coordinate system with respect to another. The three methods are (1) *Euler* angles, (2) *direction cosines*, and (3) *quaternions*. The Euler angle method, which is the conventional designation relating a moving-axis system to a fixed-axis system, is used frequently in missile and aircraft mechanizations and/or simulations. The common designations of the Euler angles are roll (ϕ), pitch (θ), and yaw (ψ). Its strengths lie in a relatively simple mechanization in digital computer simulation of vehicle (i.e., missile or aircraft) dynamics. Another beneficial aspect of this technique is that the Euler angle rates and the Euler angles have an easily interpreted physical significance. The negative attribute to the Euler angle coordinate transformation method is the mathematical singularity that exists when the pitch angle θ approaches 90°. The direction cosine method yields the direction cosine matrix (*DCM*), which defines the transformation between a fixed frame, say frame a, and a rotating frame, say frame b,

such as the vehicle body axes. Specifically, the *DCM* is an array of direction cosines expressed in the form

$$C_a^b = \begin{bmatrix} c_{11} & c_{12} & c_{13} \\ c_{21} & c_{22} & c_{23} \\ c_{31} & c_{32} & c_{33} \end{bmatrix},$$

where c_{jk} is the direction cosine between the jth axis in the a frame and the kth axis in the b frame. Since each axis system has three unit vectors, there are nine direction cosines. Direction cosines have the advantage of being free of any singularities such as arise in the Euler angle formulation at 90° pitch angle. The main disadvantage of this method is the number of equations that must be solved due to the constraint equations. (Note that by constraint equations we mean $c_{11} = c_{22}c_{33} - c_{23}c_{32}$, $c_{21} = c_{13}c_{32} - c_{12}c_{33}$, etc.)

In order to resolve the ambiguity resulting from the singularity in the Euler angle representation of rotations about the three axes, a four-parameter system was first developed by Euler in 1776. Subsequently, Hamilton modified it in 1843, and he named this system the quaternion system. Therefore, a quaternion [Q] is a quadruple of real numbers, which can be written as a three-dimensional vector. Hamilton adopted a vector notation in the form

$$[Q] = q_0 + \mathbf{i}q_1 + \mathbf{j}q_2 + \mathbf{k}q_3 = (q_0, q_1, q_2, q_3) = (q_0, \mathbf{q}), \tag{2.11}$$

where q_0, q_1, q_2, q_3 are real numbers and the set $\{\mathbf{i}, \mathbf{j}, \mathbf{k}\}$ forms a basis for a quaternion vector space. From the orthogonality property of quaternions, we have

$$q_0^2 + q_1^2 + q_2^2 + q_3^2 = 1. \tag{2.12}$$

In terms of the Euler angles ϕ, θ, ψ, we have

$$\begin{aligned} q_0 &= \cos(\psi/2)\cos(\theta/2)\cos(\phi/2) - \sin(\psi/2)\sin(\theta/2)\sin(\phi/2), \\ q_1 &= \sin(\theta/2)\sin(\phi/2)\cos(\psi/2) + \sin(\psi/2)\cos(\theta/2)\cos(\phi/2), \\ q_2 &= \sin(\theta/2)\cos(\psi/2)\cos(\phi/2) - \sin(\psi/2)\sin(\phi/2)\cos(\theta/2), \\ q_3 &= \sin(\phi/2)\cos(\psi/2)\cos(\theta/2) + \sin(\psi/2)\sin(\theta/2)\cos(\phi/2). \end{aligned}$$

Suppose now that we wish to transform any vector, say $\mathbf{V}$, from body coordinates $\mathbf{V}^b$ into the navigational coordinates $\mathbf{V}^n$. This transformation can be expressed as follows:

$$\mathbf{V}^n = C_b^n \mathbf{V}^b,$$

where C_b^n is the direction cosine matrix, or equivalently, using quaternions,

$$\mathbf{V}^n = q\mathbf{V}^b q^*,$$

where q^* is the conjugate of q. Then [7]

$$C_b^n = \begin{bmatrix} q_0^2 + q_1^2 - q_2^2 - q_3^2 & 2(q_1q_2 - q_0q_3) & 2(q_1q_3 + q_0q_2) \\ 2(q_1q_2 + q_0q_3) & q_0^2 - q_1^2 + q_2^2 - q_3^2 & 2(q_2q_3 - q_0q_1) \\ 2(q_1q_3 - q_0q_2) & 2(q_2q_3 + q_0q_1) & q_0^2 - q_1^2 - q_2^2 + q_3^2 \end{bmatrix}.$$

For more details on the quaternion and its properties, the reader is referred to [7].

The coordinate system that will be adopted in the present discussion is a right-handed system with the positive x-axis along the missile's longitudinal axis, the y-axis positive to the right (or aircraft right wing), and the z-axis positive down (i.e., the z-axis is defined by the cross product of the x- and y-axis). This coordinate system is also known as *north-east-down* (*NED*) in reference to the inertial north-east-down sign convention [5], [7]. It should be noted here that the coordinate system used in the present development is the same one used in aircraft. Four orthogonal-axes systems are usually defined to develop the appropriate equations of vehicle (aircraft or missile) motion. They are as follows:

1. The *inertial* frame, which is fixed in space, and for which Newton's Laws of Motion are valid.
2. An *Earth-centered* frame that rotates with the Earth.
3. An *Earth-surface* frame that is parallel to the Earth's surface, and whose origin is at the vehicle's center of gravity (cg) defined in north, east, and down directions.
4. The conventional *body* axes are selected to represent the vehicle. The center of this frame is at the cg of the vehicle, and its components are forward, out of the right wing, and down.

In ballistic missiles, two other common coordinate systems are used. These coordinate systems are

1. *Launch Centered Inertial:* This system is inertially fixed and is centered at launch site at the instant of launch. In this system, the x-axis is commonly taken to be in the horizontal plane and in the direction of launch, the positive z-axis vertical, and the y-axis completing the right-handed coordinate system.
2. *Launch Centered Earth-Fixed:* This is an Earth-fixed coordinate system, having the same orientation as the inertial coordinate system (1). This system is advantageous in gimbaled inertial platforms in that it is not necessary to remove the Earth rate torquing signal from the gyroscopes at launch.

Figure 2.1 illustrates two posible methods for defining the missile body axes with respect to the Earth and/or inertial reference axes. These coordinate frames will be used to define the missile's position and angular orientation in space.

Referring to Figure 2.1, we will denote the Earth-fixed coordinate system by (X_e, Y_e, Z_e). In this right-handed coordinate system, the $X_e - Y_e$ lie in the horizontal plane, and the Z_e-axis points down vertically in the direction of gravity. (Note that the position of the missile's center of gravity at any instant of time is given in this coordinate system). The second coordinate system, the body axis system, denoted by (X_b, Y_b, Z_b), is fixed with respect to the missile, and thus moves with the missile. This is the missile body coordinate system. The positive X_b-axis coincides with the missile's center line (or longitudinal axis) or forward direction. The positive Y_b-axis is to the right of the X_b-axis in the horizontal plane and is designated as the pitch axis. The positive Z_b-axis is the yaw axis and points down. This coordinate system is similar to the *NED* system. The Euler angles (ψ, θ, ϕ) are commonly used to define the missile's attitude

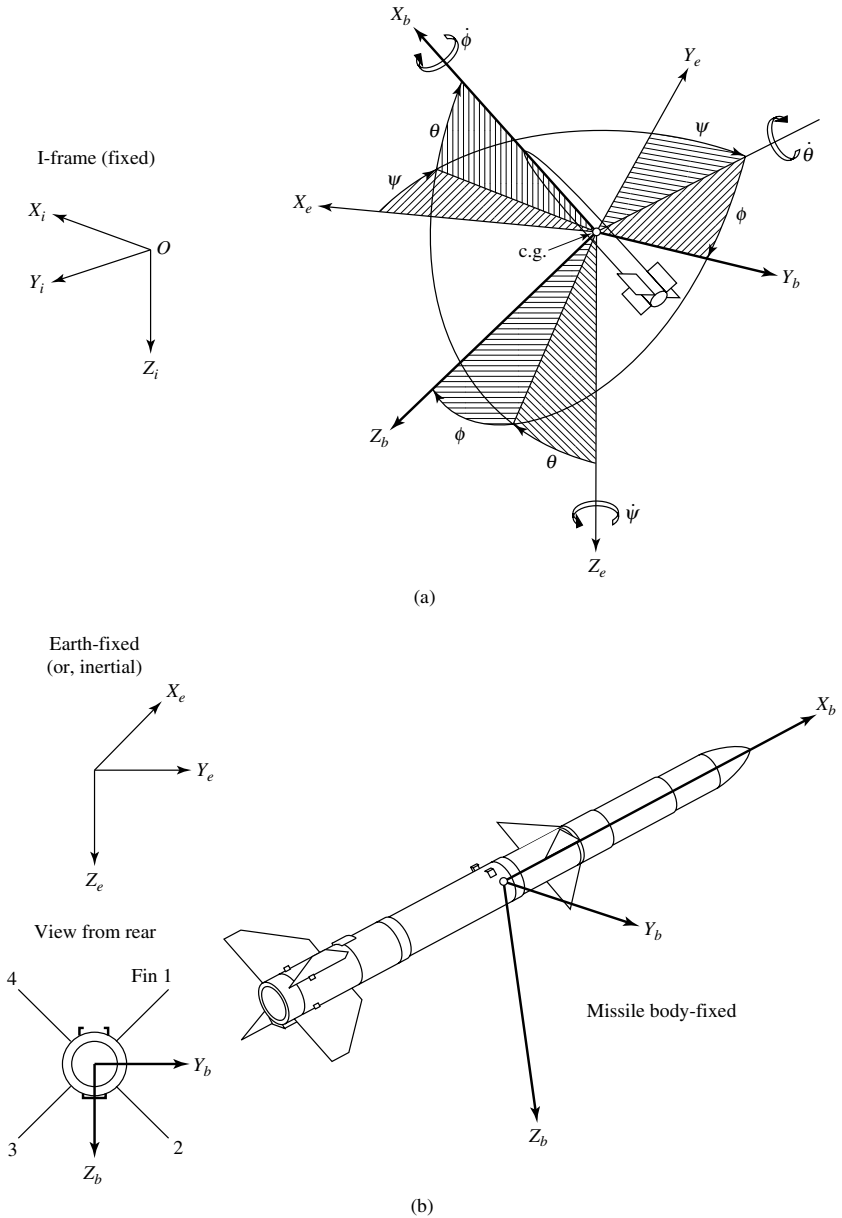

Fig. 2.1. Orientation of the missile axes with respect to the Earth-fixed axes.

with respect to the Earth-fixed axes. These Euler angles are illustrated in Figure 2.1, whereby the order of rotation of the missile axes is *yaw*, *pitch*, and *roll*. This figure also illustrates the angular rates of the Euler angles. The transformation C_e^b from the Earth-fixed axes coordinate system to the missile body-axes frame is achieved by a

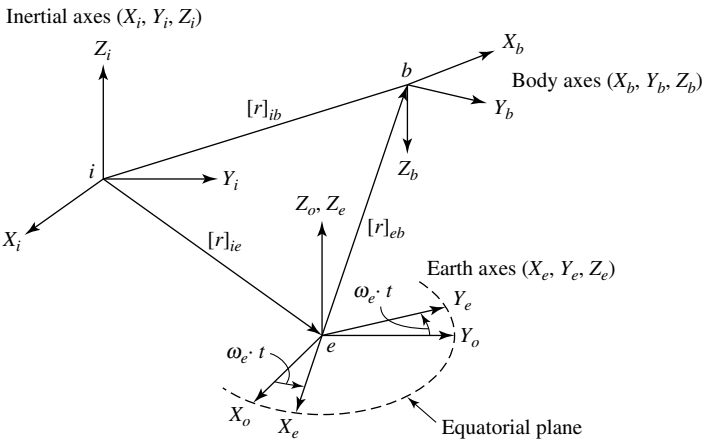

Fig. 2.2. Representation of the inertial coordinate system (inertial, Earth, and body coordinate systems).

yaw, pitch, and roll rotation about the longitudinal, lateral, and normal (i.e., vertical) axes, respectively. The resultant transformation matrix C_e^b is [2], [7]

$$C_e^b = \begin{bmatrix} 1 & 0 & 0 \\ 0 & \cos\phi & \sin\phi \\ 0 & -\sin\phi & \cos\phi \end{bmatrix} \begin{bmatrix} \cos\theta & 0 & -\sin\theta \\ 0 & 1 & 0 \\ \sin\theta & 0 & \cos\theta \end{bmatrix} \begin{bmatrix} \cos\psi & \sin\psi & 0 \\ -\sin\psi & \cos\psi & 0 \\ 0 & 0 & 1 \end{bmatrix}$$

$$= \begin{bmatrix} \cos\theta\cos\psi & \cos\theta\sin\psi & -\sin\theta \\ \sin\phi\sin\theta\cos\psi - \cos\phi\sin\psi & \sin\phi\sin\theta\sin\psi + \cos\phi\cos\psi & \sin\phi\cos\theta \\ \cos\phi\sin\theta\cos\psi + \sin\phi\sin\psi & \cos\phi\sin\theta\sin\psi - \sin\phi\cos\psi & \cos\phi\cos\theta \end{bmatrix}.$$

It should be noted here that ambiguities (or singularities) can result from using the above transformation (i.e., as $\theta, \phi, \psi \to 90°$). Therefore, in order to avoid these ambiguities, the ranges of the Euler angles (ϕ, θ, ψ) are limited as follows:

$$\begin{aligned} -\pi \le \phi < \pi \quad &\text{or} \quad 0 \le \phi < 2\pi, \\ -\pi \le \psi < \pi, & \\ -\pi/2 \le \theta \le \pi/2 \quad &\text{or} \quad 0 \le \psi < 2\pi. \end{aligned}$$

The inertial coordinate system described above is shown in Figure 2.2.

2.2 Rigid-Body Equations of Motion

In this section we will consider a typical missile and derive the equations of motion according to Newton's laws. In deriving the rigid-body equations of motion, the following assumptions will be made:

1. **Rigid Body:** A rigid body is an idealized system of particles. Furthermore, it will be assumed that the body does not undergo any change in size or shape.

Translation of the body results in that every line in the body remains parallel to its original position at all times. Consequently, the rigid body can be treated as a particle whose mass is that of the body and is concentrated at the center of mass. In assuming a rigid body, the aeroelastic effects are not included in the equations. With this assumption, the forces acting between individual elements of mass are eliminated. Furthermore, it allows the airframe motion to be described completely by a translation of the center of gravity and by a rotation about this point. In addition, the airframe is assumed to have a plane of symmetry coinciding with the vertical plane of reference. The vertical plane of reference is the plane defined by the missile X_b- and Z_b-axes as shown in Figure 2.1. The Y_b-axis, which is perpendicular to this plane of symmetry, is the principal axis, and the products of inertia I_{XY} and I_{YZ} vanish.

2. **Aerodynamic Symmetry in Roll:** The aerodynamic forces and moments acting on the vehicle are assumed to be invariant with the roll position of the missile relative to the free-stream velocity vector. Consequently, this assumption greatly simplifies the equations of motion by eliminating the aerodynamic cross-coupling terms between the roll motion and the pitch and yaw motions. In addition, a different set of aerodynamic characteristics for the pitch and yaw is not required.
3. **Mass:** A constant mass will be assumed, that is, $dm/dt \cong 0$.

In addition, the following assumptions are commonly made:

4. The missile equations of motion are written in the body-axes coordinate frame.
5. A spherical Earth rotating at a constant angular velocity is assumed.
6. The vehicle aerodynamics are nonlinear.
7. The undisturbed atmosphere rotates with the Earth.
8. The winds are defined with respect to the Earth.
9. An inverse-square gravitational law is used for the spherical Earth model.
10. The gradients of the low-frequency winds are small enough to be neglected.

Furthermore, in the present development, it will be assumed that the missile has *six degrees of freedom* (6-DOF). The six degrees of freedom consist of (1) three translations, and (2) three rotations, along and about the missile (X_b, Y_b, Z_b) axes. These motions are illustrated in Figure 2.3, the translations being (u, v, w) and the rotations (P, Q, R). In compact form, the traslation and rotation of a rigid body may be expressed mathematically by the following equations:

$$Translation: \sum \mathbf{F} = m\mathbf{a}, \tag{2.13}$$

$$Rotation: \sum \tau = \frac{d}{dt}(\boldsymbol{r} \times m\mathbf{V}) \tag{2.14}$$

where $\sum\tau$ is the net torque on the system.

Aerodynamic forces and moments are assumed to be functions of the *Mach** number (M) and nonlinear with flow incidence angle. Furthermore, the introduction

*The Mach number is expressed as $M = V_M/V_s$, where V_M is the velocity of the missile and V_s is the local velocity of sound, a piecewise linear function of the missile's altitude.

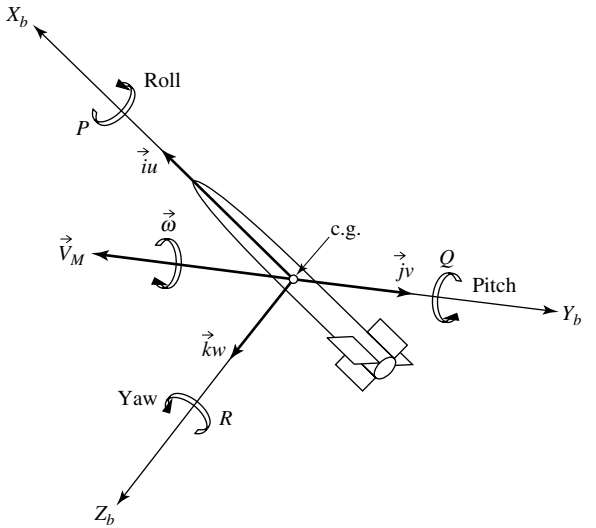

Fig. 2.3. Representation of the missile's six degrees of freedom.

of surface winds in a trajectory during launch can create flow incidence angles that are very large, on the order of 90°. Nonlinear aerodynamic characteristics with respect to flow incidence angle must be assumed to simulate the launch motion under the effect of wind. Since Mach number varies considerably in a missile trajectory, it is necessary to assume that the aerodynamic characteristics vary with Mach number.

The linear velocity of the missile **V** can be broken up into components u, v, and w along the missile (X_b, Y_b, Z_b) body axes, respectively. Mathematically, we can write the missile vector velocity, V_M, in terms of the components as

$$\mathbf{V}_M = u\mathbf{i} + v\mathbf{j} + w\mathbf{k},$$

where (**i**, **j**, **k**) are the unit vectors along the respective missile body axes. The magnitude of the missile velocity is given by

$$|\mathbf{V}_M| = V_M = (u^2 + v^2 + w^2)^{1/2}.$$

These components are illustrated in Figure 2.3.

In a similar manner, the missile's angular velocity vector **ω** can be broken up into the components P, Q, and R about the (X_b, Y_b , Z_b) axes, respectively, as follows:

$$\boldsymbol{\omega} = P\mathbf{i} + Q\mathbf{j} + R\mathbf{k},$$

where P is the roll rate, Q is the pitch rate, and R is the yaw rate. Note that some authors use lowercase letters for roll, pitch, and yaw rates instead of uppercase letters. Therefore, these linear and rotational velocity components constitute the 6-*DOF* of the missile. As stated in the beginning of this section, the rigid-body equations of

motion are obtained from Newton's second law, which states that the summation of all external *forces* acting on a body is equal to the time rate of the momentum of the body, and the summation of the external *moments* acting on the body is equal to the time rate of change of *moment of momentum* (angular momentum). Specifically, Newton's laws of motion were formulated for a single particle. Assuming that the mass m of the particle is multiplied by its velocity $\mathbf{V}$, then the product

$$\mathbf{p} = m\mathbf{V} \tag{2.15}$$

is called the *linear momentum*. Thus, the linear momentum is a vector quantity having the same direction and sense as $\mathbf{V}$. For a system of n particles, the linear momentum is the summation of the linear momenta of all particles in the system. Thus [8],

$$\mathbf{p} = \sum_{i=1}^{n} (m_i \mathbf{V}_i) = m_1\mathbf{V}_1 + m_2\mathbf{V}_2 + \cdots + m_n\mathbf{V}_n, \tag{2.16}$$

where i denotes the ith particle, and n denotes the number of particles in the system. Note that the time rates of change of linear and angular momentum are referred to an absolute or inertial reference frame. For many problems of interest in airplane and missile dynamics, an axis system fixed to the Earth can be used as an inertial reference frame (see Figure 2.1). Mathematically, Newton's second law can be expressed in terms of conservation of both linear and angular momentum by the following vector equations [1], [8], [11]:

$$\sum \mathbf{F} = \frac{d(m\mathbf{V}_M)}{dt}\Bigg]_I, \tag{2.17a}$$

$$\sum \mathbf{M} = \frac{d\mathbf{H}}{dt}\Bigg]_I, \tag{2.17b}$$

where m is the mass, $\mathbf{H}$ the angular momentum, and the symbol $]_I$ indicates the time rate of change of the vector with respect to inertial space. Note that (2.17a) is simply

$$\mathbf{F} = \frac{d\mathbf{p}}{dt}, \tag{2.18a}$$

or

$$\mathbf{F} = m\left(\frac{d\mathbf{V}}{dt}\right) = m\mathbf{a}. \tag{2.18b}$$

Equations (2.17a) and (2.17b) can be rewritten in scalar form, consisting of three force equations and three moment equations as follows:

$$F_x = \frac{d(mu)}{dt},\ F_y = \frac{d(mv)}{dt},\ F_z = \frac{d(mw)}{dt}, \tag{2.19}$$

where F_x, F_y, F_z and u, v, w are the components of the force and velocity along the missile's X_b, Y_b, and Z_b axes, respectively. Normally, these force components are composed of contributions due to (1) aerodynamic, (2) propulsive, and (3) gravitational forces acting on the missile. In a similar manner, the moment equations can be expressed as follows [6]:

$$L = \frac{dH_x}{dt}, \quad M = \frac{dH_y}{dt}, \quad N = \frac{dH_z}{dt}, \tag{2.20}$$

where L, M, N are the roll moment, pitch moment, and yaw moment, respectively, and H_x, H_y, H_z are the components of the moment of momentum along the body X, Y, and Z axes, respectively.

At this point, let us summarize the various forces, moments, and axes used in developing the missile 6-*DOF* equations of motion.

Force:

$$\mathbf{F} = F_x\mathbf{i} + F_y\mathbf{j} + F_z\mathbf{k},$$

where F_x, F_y, F_z are the (x, y, z) components of the force.

Velocity:

$$\mathbf{V} = u\mathbf{i} + v\mathbf{j} + w\mathbf{k},$$

where u, v, w are the velocity components along the (x, y, z) axes, respectively.

Moment of External Forces:

$$\sum \Delta\mathbf{M} = L\mathbf{i} + M\mathbf{j} + N\mathbf{k},$$

where L is the rolling moment, M is the pitching moment, and N is the yawing moment.

Angular Momentum:

$$\mathbf{H} = H_x\mathbf{i} + H_y\mathbf{j} + H_z\mathbf{k},$$

where H_x, H_y, H_z are the components of the angular momentum along the x, y, z axes, respectively.

Angular Velocity:

$$\boldsymbol{\omega} = \omega_x\mathbf{i} + \omega_y\mathbf{j} + \omega_z\mathbf{k} = P\mathbf{i} + Q\mathbf{j} + R\mathbf{k},$$

where P is the roll rate, Q is the pitch rate, and R is the yaw rate. ($\mathbf{i}$ = unit vector along the x-axis, $\mathbf{j}$ = unit vector along the y-axis, and $\mathbf{k}$ = unit vector along the z-axis).

We now wish to develop an expression for the time rate of change of the velocity vector with respect to the Earth. Before we do this, we note that in general, a vector $\mathbf{A}$ can be transformed from a fixed (e.g., inertial) to a rotating coordinate system by the relation [6], [7]

$$\left(\frac{d\mathbf{A}}{dt}\right)_{\text{fixed}(X',Y',Z')} = \left[\frac{d\mathbf{A}}{dt}\right]_{\text{rot.}(X,Y,Z)} + \boldsymbol{\omega} \times \mathbf{A}, \tag{2.21a}$$

Table 2.1. Axis and Moment Nomenclature

(a) Axis Definition

Axis	Direction	Name	Linear Velocity	Angular Displacement	Angular Rates
OX	Forward	Roll	u	ϕ	P
OY	Right Wing	Pitch	v	θ	Q
OZ	Downward	Yaw	w	ψ	R

(b) Moment Designation

Axis	Moment of Inertia	Product of Inertia	Force	Moment
OX	I_x	$I_{xy} = 0$	F_x	L
OY	I_y	$I_{yx} = 0$	F_y	M
OZ	I_z	$I_{zx} \neq 0$	F_z	N

or

$$\left(\frac{d\mathbf{A}}{dt}\right)_{\text{inertial}} = \left[\frac{d\mathbf{A}}{dt}\right]_{\text{body}} + \boldsymbol{\omega} \times \mathbf{V}_M, \tag{2.21b}$$

where $\boldsymbol{\omega}$ is the angular velocity of the missile body coordinate system (X, Y, Z) relative to the fixed (inertial) system (X', Y', Z'), and $\times$ denotes the vector cross product. Normally, the missile's linear velocity V_M is expressed in the Earth-fixed axis system, so that (2.21a) can be written in the form

$$\left(\frac{d\mathbf{V}_M}{dt}\right)_E = \left(\frac{d\mathbf{V}_M}{dt}\right)_{\text{rot.coord.}} + \boldsymbol{\omega} \times \mathbf{V}_M, \tag{2.22}$$

where ω is the total angular velocity vector of the missile with respect to the Earth. In terms of the body axes, we can write the force equation in the form

$$\mathbf{F} = m\left[\frac{d\mathbf{V}_M}{dt}\right]_{\text{body}} + m(\boldsymbol{\omega} \times \mathbf{V}_M). \tag{2.23}$$

The first part on the right-hand side of (2.22) can be written as

$$\left(\frac{d\mathbf{V}_M}{dt}\right)_{\text{rot.coord.}} = \left(\frac{du}{dt}\right)\mathbf{i} + \left(\frac{dv}{dt}\right)\mathbf{j} + \left(\frac{dw}{dt}\right)\mathbf{k}, \tag{2.24}$$

where

$$(du/dt) = \text{forward (or longitudinal) acceleration},$$
$$(dv/dt) = \text{right wing (or lateral) acceleration},$$
$$(dw/dt) = \text{downward (or vertical) acceleration},$$

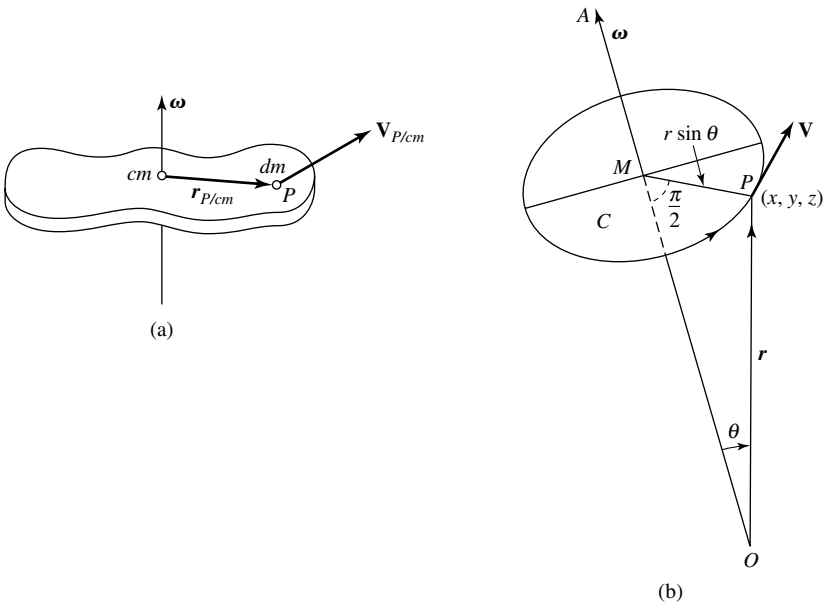

Fig. 2.4. General rigid body with angular velocity vector **ω** about its center of mass.

and the vector cross product as

$$\boldsymbol{\omega} \times \mathbf{V}_M = \begin{bmatrix} \mathbf{i} & \mathbf{j} & \mathbf{k} \\ P & Q & R \\ u & v & w \end{bmatrix} = (wQ - vR)\mathbf{i} + (uR - wP)\mathbf{j} + (vP - uQ)\mathbf{k}. \tag{2.25}$$

Next, from (2.17a) we can write the sum of the forces as

$$\sum \Delta \mathbf{F} = \sum \Delta F_x \mathbf{i} + \sum \Delta F_y \mathbf{j} + \sum \Delta F_z \mathbf{k}. \tag{2.26}$$

Equating the components of (2.24), (2.25), and (2.26) yields the missile's *linear equations of motion*. Thus, for a missile with an $X_b - Z_b$ plane of symmetry (see rigid-body assumption #1) we have

$$\sum \Delta F_x = m(\dot{u} + wQ - vR), \tag{2.27a}$$

$$\sum \Delta F_y = m(\dot{v} + uR - wP), \tag{2.27b}$$

$$\sum \Delta F_z = m(\dot{w} + vP - uQ). \tag{2.27c}$$

From (2.17b) we can obtain in a similar manner the equations of angular motion. However, before we develop these equations, an expression for **H** is needed. To this end, consider Figure 2.4.

Now let dm be an element of mass of the missile, $\mathbf{V}$ the velocity of the elemental mass relative to the inertial frame, and $\delta\mathbf{F}$ the resulting force acting on the elemental mass.

First of all, and with reference to Figure 2.4(a), the position vector of any particle of the rigid body in a Newtonian frame of reference is the vector sum of the position vector of the center of the mass and the position vector of the particle with respect to the center of mass. Mathematically,

$$\boldsymbol{r}_p = \boldsymbol{r}_{cm} + \boldsymbol{r}_{p/cm},$$

where

$$\begin{aligned} \boldsymbol{r}_p &= \text{the position vector of the particle,} \\ \boldsymbol{r}_{cm} &= \text{position vector of the center of mass of the particle,} \\ \boldsymbol{r}_{p/cm} &= \text{position vector of the particle with respect to the} \\ &\quad \text{center of mass.} \end{aligned}$$

Note that if this equation is differentiated, we obtain

$$\frac{d\boldsymbol{r}_p}{dt} = \frac{d\boldsymbol{r}_{cm}}{dt} + \frac{d\boldsymbol{r}_{p/cm}}{dt}.$$

Also, from Figure 2.4(a) we can write the velocity of the point p in the form

$$\mathbf{V}_p = \frac{d(\boldsymbol{r}_{cm})}{dt} + \boldsymbol{\omega} \times \boldsymbol{r}_{p/cm},$$

or

$$\mathbf{V}_p = \mathbf{V}_{cm} + \mathbf{V}_{p/cm}.$$

Then, from Newton's second law we have

$$\delta\mathbf{F} = dm\left(\frac{d\mathbf{V}}{dt}\right). \tag{2.28}$$

The total external force acting on the missile is found by summing all the elements of the missile. Therefore,

$$\sum \delta\mathbf{F} = \mathbf{F}. \tag{2.29}$$

The velocity of the differential mass dm is

$$\mathbf{V} = \mathbf{V}_{cm} + \left(\frac{d\mathbf{r}}{dt}\right), \tag{2.30}$$

where $\mathbf{V}_{cm}$ is the velocity of the center of mass (cm) of the missile, and $d\mathbf{r}/dt$ is the velocity of the element relative to the center of mass. Substituting (2.30) for the velocity into (2.29) results in

$$\sum \delta\mathbf{F} = \mathbf{F} = \left(\frac{d}{dt}\right) \sum \left[\mathbf{V}_{cm} + \left(\frac{d\mathbf{r}}{dt}\right)\right] dm. \tag{2.31}$$

Assuming that the mass of the missile is constant, (2.31) can be written in the form

$$\mathbf{F} = m\left(\frac{d\mathbf{V}_{cm}}{dt}\right) + \left(\frac{d}{dt}\right)\sum\left(\frac{d\mathbf{r}}{dt}\right)dm, \tag{2.32a}$$

or

$$\mathbf{F} = m\left(\frac{d\mathbf{V}_{cm}}{dt}\right) + \left(\frac{d^2}{dt^2}\right)\sum \mathbf{r}dm. \tag{2.32b}$$

Since $\mathbf{r}$ is measured from the center of the mass, the summation $\sum \mathbf{r}dm$ is equal to 0. Thus, the force equation becomes simply

$$\mathbf{F} = m\left(\frac{d\mathbf{V}_{cm}}{dt}\right), \tag{2.33}$$

which relates the external force on the missile to the motion of the vehicle's center of mass. Similarly, we can develop the moment equation referred to a moving center of mass. For the differential element of mass, dm, the moment equation can then be written as

$$\delta\mathbf{M} = d\left(\frac{\delta\mathbf{H}}{dt}\right) = \left(\frac{d}{dt}\right)(\mathbf{r}\times\mathbf{V})dm. \tag{2.34}$$

The velocity of the mass element can be expressed in terms of the velocity of the center of mass and the relative velocity of the mass element to the center of mass. Therefore,

$$\mathbf{V}_p = \mathbf{V}_{cm} + \left(\frac{d\boldsymbol{r}_{p/cm}}{dt}\right) = \mathbf{V}_{cm} + \boldsymbol{\omega}\times\mathbf{r}, \tag{2.35}$$

where $\boldsymbol{\omega}$ is the angular velocity vector of the vehicle and $\mathbf{r}$ is the position of the mass element measured from the center of mass (see Figure (2.4a)). In relation to (2.35) and Figure 2.4(a), we can write the equation

$$\left(\frac{d\mathbf{r}}{dt}\right)_{\text{inertial}} = \left[\frac{d\mathbf{r}}{dt}\right]_{\text{rel. to coord.}} + \boldsymbol{\omega}\times\mathbf{r}.$$

The reader will note that this is the well-known *Coriolis* equation, which is important in dynamics where body axes are used. Furthermore, it will be noted that the term $\boldsymbol{\omega}\times\mathbf{r}$ occurs in addition to the vector change relative to the coordinate system, so that the total derivative relative to the inertial axes is expressed by this equation. The rigid-body assumption implies that $d\mathbf{r}_{p/cm}/dt = 0$. Therefore, we can write the linear velocity of the point p in the simple form

$$\mathbf{V}_p = \boldsymbol{\omega}\times\mathbf{r}_{p/cm}.$$

In general, the moment about an arbitrary point O of the momentum $\mathbf{p} = m\mathbf{V}$ (2.15) of a particle is

$$\mathbf{H} = \mathbf{r}\times m\mathbf{V} = m\mathbf{r}\times(\boldsymbol{\omega}\times\mathbf{r}).$$

Referring to Figure (2.4(b)), it will be observed that this vector is perpendicular to both $\mathbf{r}$ and $\mathbf{V}$. Furthermore, this vector lies along MP and is directed toward M. The *moment of momentum* (or *angular momentum*) of the entire body about O is therefore

$$\mathbf{H} = \sum \mathbf{r} \times m\mathbf{V} = \sum m\mathbf{r} \times (\boldsymbol{\omega} \times \mathbf{r}) = \sum m[\boldsymbol{\omega}(\mathbf{r} \cdot \mathbf{r}) - \mathbf{r}(\mathbf{r} \cdot \boldsymbol{\omega})]$$

(note that this result was obtained using the formula $\mathbf{a} \times (\mathbf{b} \times \mathbf{c}) = (\mathbf{a} \cdot \mathbf{c})\mathbf{b} - (\mathbf{a} \cdot \mathbf{b})\mathbf{c}$). This equation can also be written as

$$\mathbf{H} = \left(\sum mr^2\right)\boldsymbol{\omega} - \sum m\mathbf{r}(\mathbf{r} \cdot \boldsymbol{\omega}).$$

From Figure (2.4(a)), the total moment of momentum can be written as

$$\mathbf{H} = \sum \delta\mathbf{H} = \sum (\mathbf{r} \times \mathbf{V}_{cm})dm + \sum [\mathbf{r} \times (\boldsymbol{\omega} \times \mathbf{r})]dm. \tag{2.36}$$

Note that the velocity $\mathbf{V}_{cm}$ is constant with respect to the summation and can be taken outside the summation sign. Thus [1], [3]

$$\mathbf{H} = \sum \mathbf{r}dm \times \mathbf{V}_{cm} + \sum [\mathbf{r} \times (\boldsymbol{\omega} \times \mathbf{r})]dm. \tag{2.37a}$$

As stated above, the first term on the right-hand side of (2.37a) is zero. Therefore, we have simply

$$\delta\mathbf{H} = \sum [\mathbf{r} \times (\boldsymbol{\omega} \times \mathbf{r})]dm \tag{2.37b}$$

and

$$\mathbf{H} = \int \mathbf{r} \times (\boldsymbol{\omega} \times \mathbf{r})dm. \tag{2.37c}$$

Performing the vector operations in (2.37c) and noting that

$$\boldsymbol{\omega} = \omega_x\mathbf{i} + \omega_y\mathbf{j} + \omega_z\mathbf{k} = P\mathbf{i} + Q\mathbf{j} + R\mathbf{k},$$
$$\mathbf{r} = x\mathbf{i} + y\mathbf{j} + z\mathbf{k},$$

we have

$$\begin{aligned} \boldsymbol{\omega} \times \mathbf{r} &= \begin{bmatrix} \mathbf{i} & \mathbf{j} & \mathbf{k} \\ P & Q & R \\ x & y & z \end{bmatrix} \\ &= (zQ - yR)\mathbf{i} + (xR - zP)\mathbf{j} + (yP - xQ)\mathbf{k}. \end{aligned} \tag{2.38a}$$

Finally,

$$\begin{aligned} \mathbf{r} \times (\boldsymbol{\omega} \times \mathbf{r}) &= \begin{bmatrix} \mathbf{i} & \mathbf{j} & \mathbf{k} \\ x & y & z \\ (zQ - yR) & (xR - zP) & (yP - xQ) \end{bmatrix} \\ &= \mathbf{i}[(y^2 + z^2)P - xyQ - xzR] + \mathbf{j}[(z^2 + x^2)Q - yzR - xyP] \\ &\quad + \mathbf{k}[(x^2 + y^2)R - xzP - yzQ]. \end{aligned} \tag{2.38b}$$

Substituting (2.38b) into (2.37c), we have

$$\mathbf{H} = \int \mathbf{i}[(y^2+z^2)P - xyQ - xzR]dm + \int \mathbf{j}[(z^2+x^2)Q - yzR - xyP]dm + \int \mathbf{k}[(x^2+y^2)R - xzP - yzQ]dm, \tag{2.38c}$$

where the $\int (y^2+z^2)$ is defined as the moment of inertia, I_x, and $\int xydm$ is defined as the product of inertia, I_{xy}. The remaining integrals in (2.38c) are similarly defined. By proper positioning of the body axis system, one can make the products of inertia $I_{xy} = I_{yz}$ equal to 0. This will be true if we can assume that the x-y plane is a plane of symmetry of the missile. Consequently, (2.38c) can be rewritten in component form as follows:

$$H_x = P\int (y^2+z^2)dm - R\int xzdm = PI_x - RI_{xz}, \tag{2.39a}$$

$$H_y = Q\int (x^2+z^2)dm = QI_y, \tag{2.39b}$$

$$H_z = R\int (x^2+y^2)dm - P\int xzdm = RI_z - PI_{xz}. \tag{2.39c}$$

From (2.17b), we note that the time rate of $\mathbf{H}$ is required. Now, since $\mathbf{H}$ can change in magnitude and direction, (2.17b) can be written as [1]

$$\sum \Delta\mathbf{M} = 1_H\left(\frac{d\mathbf{H}}{dt}\right) + \boldsymbol{\omega}\times\mathbf{H}. \tag{2.40}$$

Next, the components of $1_H(d\mathbf{H}/dt)$ assume the form

$$\frac{dH_x}{dt} = \left(\frac{dP}{dt}\right)I_x - \left(\frac{dR}{dt}\right)I_{xz}, \tag{2.41a}$$

$$\frac{dH_y}{dt} = \left(\frac{dQ}{dt}\right)I_y, \tag{2.41b}$$

$$\frac{dH_z}{dt} = \left(\frac{dR}{dt}\right)I_z - \left(\frac{dP}{dt}\right)I_{xz}. \tag{2.41c}$$

Since initially we assumed a rigid body with constant mass, the time rates of change of the moments and products of inertia are zero. The vector cross product in (2.40) is

$$\boldsymbol{\omega}\times\mathbf{H} = \begin{bmatrix} \mathbf{i} & \mathbf{j} & \mathbf{k} \\ P & Q & R \\ H_x & H_y & H_z \end{bmatrix}$$

$$= (QH_z - RH_y)\mathbf{i} + (RH_x - PH_z)\mathbf{j} + (PH_y - QH_x)\mathbf{k}. \tag{2.42}$$

Similar to (2.26), we can write an equation for the summation of all moments in the form

$$\sum \Delta \mathbf{M} = \mathbf{i} \sum \Delta L + \mathbf{j} \sum \Delta M + \mathbf{k} \sum \Delta N. \tag{2.43}$$

Equating the components of (2.41), (2.42), and (2.43) and substituting for H_x, H_y, and H_z from (2.39) yields the *angular momentum equations*. Thus [1], [5],

$$\sum \Delta L = \dot{P} I_x - \dot{R} I_{xz} + QR(I_z - I_y) - PQ I_{xz}, \tag{2.44a}$$

$$\sum \Delta M = \dot{Q} I_y + PR(I_x - I_z) + (P^2 - R^2) I_{xz}, \tag{2.44b}$$

$$\sum \Delta N = \dot{R} I_z - \dot{P} I_{xz} + PQ(I_y - I_x) + QR I_{xz}, \tag{2.44c}$$

or

$$\sum \Delta L = \dot{P} I_x + (I_z - I_y) QR - (\dot{R} + PQ) I_{xz}, \tag{2.44d}$$

$$\sum \Delta M = \dot{Q} I_y + (I_x - I_z) PR + (P^2 - R^2) I_{xz}, \tag{2.44e}$$

$$\sum \Delta N = \dot{R} I_z + (I_y - I_x) PQ - (\dot{P} - QR) I_{xz}, \tag{2.44f}$$

where dP/dt is the roll acceleration, dQ/dt is the pitch acceleration, and dR/dt is the yaw acceleration. The set of equations (2.27a)–(2.27c) and (2.44d)–(2.44f) or (2.44a)–(2.44c) represents the complete 6-*DOF* missile equations of motion. Specifically, equations (2.27) describe the translation, and equations (2.44) describe the rotation of a body. The set of equations (2.27) and (2.44) are six simultaneous nonlinear equations of motion, with six variables u, v, w, P, Q, and R, which completely describe the behavior of a rigid body. Moreover, these equations can be solved with a digital computer using numerical integration techniques. An analytical solution of sufficient accuracy can be obtained by linearizing these equations. These equations are also known as *Euler's equations*. Note that I_x, I_y, I_{xz} are constant for a given rigid body because of our choice of coordinate axes. Due to the usual symmetry of the aircraft (or missile) about the x-y plane, the products of inertia that involve y are usually omitted, and the moment equations may be rewritten as follows (note that for cruciform missiles with rotational symmetry, $I_y = I_z$ and $I_{xz} = 0$):

$$\Delta L = \dot{P} I_x + QR(I_z - I_y), \tag{2.45a}$$

$$\Delta M = \dot{Q} I_y + (I_x - I_z) PR, \tag{2.45b}$$

$$\Delta N = \dot{R} I_z + (I_y - I_x) PQ. \tag{2.45c}$$

It should be noted that the L and N equations indicate that a rolling or yawing moment excites angular velocities about all three axes. Therefore, except for certain cases,

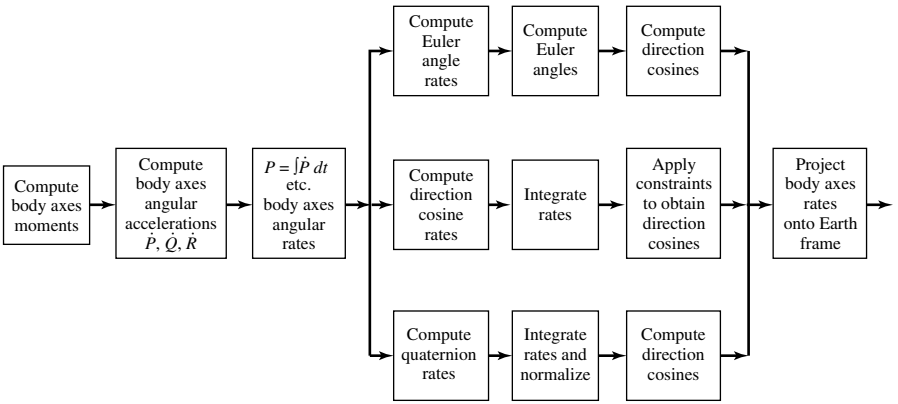

Fig. 2.5. Rotational dynamics of a rigid body.

these equations cannot be decoupled. Solving (2.45a)–(2.45c) for dP/dt, dQ/dt, and dR/dt, we obtain the *rotation* accelerations as follows:

$$\frac{dP}{dt} = QR[(I_y - I_z)/I_x] + (L/I_x), \tag{2.46a}$$

$$\frac{dQ}{dt} = PR[(I_z - I_x)/I_y] + (M/I_y), \tag{2.46b}$$

$$\frac{dR}{dt} = PQ[(I_x - I_y)/I_z] + (N/I_z). \tag{2.46c}$$

The relationship of the three coordinate systems discussed in Section 2.1 can be described in terms of the body dynamics. Figure 2.5 illustrates the manner in which these three methods are integrated into computational sequence of representing the vehicle dynamics.

The equations for the angular velocities ($d\psi/dt$, $d\phi/dt$, $d\theta/dt$) in terms of the Euler angles (ψ, ϕ, θ) and the rates (P, Q, R) can be written from Figure 2.1 as follows [1]:

$$\frac{d\psi}{dt} = (Q \sin\phi + R \cos\phi)/\cos\theta, \tag{2.47a}$$

$$\frac{d\phi}{dt} = P + \left(\frac{d\psi}{dt}\right) \sin\theta, \tag{2.47b}$$

$$\frac{d\theta}{dt} = Q \cos\phi - R \sin\phi, \tag{2.47c}$$

where P is the roll rate, Q is the pitch rate, and R is the yaw rate. The values of (ψ, ϕ, θ) can be obtained by integrating (2.47a)–(2.47c). Thus,

$$\psi = \psi_0 + \int_0^t \left(\frac{d\psi}{dt}\right) dt, \tag{2.48a}$$

$$\phi = \phi_0 + \int_0^t \left(\frac{d\phi}{dt}\right) dt, \tag{2.48b}$$

$$\theta = \theta_0 + \int_0^t \left(\frac{d\theta}{dt}\right) dt. \tag{2.48c}$$

From the transformation matrix C_e^b of Section 2.1, the components of the missile velocity $dX_e/dt, dY_e/dt, dZ_e/dt$ in the Earth-fixed coordinate system (X_e, Y_e, Z_e) in terms of (u, v, w) and (ψ, ϕ, θ) are given as follows:

$$\begin{aligned}
\frac{dX_e}{dt} &= (\cos\theta\cos\psi)u + (\cos\psi\sin\phi\sin\theta - \sin\psi\cos\phi)v \\
&\quad + (\cos\psi\cos\phi\sin\theta + \sin\psi\sin\phi)w, \\
\frac{dY_e}{dt} &= (\cos\theta\sin\psi)u + (\sin\psi\sin\phi\sin\theta + \cos\psi\cos\phi)v \\
&\quad + (\sin\psi\cos\phi\sin\theta - \cos\psi\sin\phi)w, \\
\frac{dZ_e}{dt} &= -(\sin\theta)u + (\sin\phi\cos\theta)v + (\cos\theta\cos\phi)w,
\end{aligned}$$

or in matrix form,

$$\frac{d}{dt}\begin{bmatrix} X_e \\ Y_e \\ Z_e \end{bmatrix} = C_e^b \begin{bmatrix} u \\ v \\ w \end{bmatrix}. \tag{2.49}$$

From (2.49) we can obtain the equations for (X_e, Y_e, Z_e) in the form

$$X_e = X_{e,0} + \int_0^t \left(\frac{dX_e}{dt}\right) dt, \tag{2.50a}$$

$$Y_e = Y_{e,0} + \int_0^t \left(\frac{dY_e}{dt}\right) dt, \tag{2.50b}$$

$$Z_e = Z_{e,0} + \int_0^t \left(\frac{dZ_e}{dt}\right) dt, \tag{2.50c}$$

and the altitude is

$$h = -Z_e. \tag{2.50d}$$

In the foregoing discussion, only the missile velocities relative to the ground or inertial velocities have been mentioned. If wind is being considered, the missile velocities relative to the wind must be computed, since these velocities are needed in computing the aerodynamic forces and moments (see Chapter 3).

It should be noted here that stability and control for fixed-wing aircraft are assessed through six rigid-body degrees of freedom models. Rotorcraft models provide three more degrees of freedom for the main flapping plus a rotational degree of freedom. Additional degrees of freedom for structural modes and other dynamic components

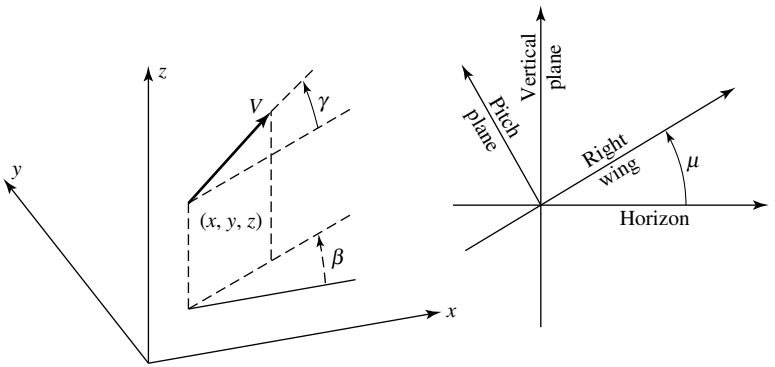

Fig. 2.6. Coordinate system

(e.g., transmissions) can be added as necessary. The aircraft models are based on aerodynamic coefficient representations of the major aircraft components, including the wing, fuselage, vertical tail, and horizontal tail. Mass distribution is represented by the center-of-gravity location and mass moments of inertia for the aircraft. A stability analysis is performed by trimming the forces and moments on the aircraft model for each flight condition. Force and moment derivatives are obtained through perturbations from trim in the state and control variables. These derivatives are used to represent the rigid-body motion of the aircraft as a set of linear first-order differential equations. The matrix representation of the aircraft motion is then used in the linear analysis package MATLAB* to assess stability and to investigate feedback control design. Aircraft dynamics and control system conceptual designs are typically analyzed with respect to dynamic performance, stability, and pilot/vehicle interface.

Example 1. In this example, we will consider an aircraft whose equations of motion can be represented as a point mass, based on five variables (i.e., 5-*DOF*). The coordinate system for this example is illustrated in Figure 2.6.

Furthermore, the variables are defined as follows:

$$
\begin{aligned}
\text{Let } x,\ y,\ z &= \text{position variables,}\\
\mathbf{V} &= \text{velocity vector,}\\
\alpha &= \text{angle-of-attack } (AOA),\\
\beta &= \text{velocity heading angle,}\\
\gamma &= \text{velocity elevation angle,}\\
\mu &= \text{orientation angle of the aircraft body axes relative}\\
&\quad\ \text{to the velocity vector.}
\end{aligned}
$$

From the definition of the above variables, the orientation of the velocity vector $\mathbf{V}$ is through the angles β and γ, while the orientation of the aircraft body axes relative

* MATLAB is a commercially available software package for use on a personal computer.

to the velocity vector is through the angle μ and the *AOA* α in the pitch plane. The yaw of the aircraft about the velocity vector, **V**, is assumed to be zero (i.e., sufficient control power exists that all maneuvers are *coordinated*). For this 5-*DOF* (x, y, z, α, μ) point mass model, the equations of motion are as follows:

$$
\begin{aligned}
\dot{x} &= V\cos\gamma\cos\beta,\\
\dot{y} &= V\cos\gamma\sin\beta,\\
\dot{z} &= V\sin\gamma,\\
\dot{V} &= \frac{1}{m}[T\cos\alpha - D] - g\sin\gamma,\\
\dot{\beta} &= \frac{1}{mV}[T\sin\alpha + L](\sin\mu/\cos\gamma),\\
\dot{\gamma} &= \frac{1}{mV}[T\sin\alpha + L]\cos\mu - (g/V)\cos\gamma,\\
\dot{m} &= \dot{m}(M, z, n),\\
\dot{n} &= \dot{n}(\alpha, V_{IAS}),\\
\dot{\alpha} &= \dot{\alpha}(\alpha, V_{IAS}),\\
\dot{\mu} &= \dot{\mu}(\alpha, V_{IAS}),
\end{aligned}
$$

where

$$
\begin{aligned}
M &= \text{Mach number},\\
g &= \text{acceleration of gravity},\\
m &= \text{mass},\\
n &= \text{throttle setting},\\
V_{IAS} &= \text{indicated airspeed},\\
T &= \text{Thrust} = T(M, z, n),\\
D &= \text{drag} = \tfrac{1}{2}\rho V^2 S C_D \text{ (see Section 3.1)},\\
L &= \text{lift} = \tfrac{1}{2}\rho V^2 S C_L \text{ (see Section 3.1)},\\
\rho &= \text{atmospheric density} = \rho(z)\\
&\quad \text{(i.e., a function of altitude)},\\
S &= \text{aerodynamic reference area},\\
C_D &= \text{coefficient of drag},\\
C_L &= \text{coefficient of lift}.
\end{aligned}
$$

Several approximations can be made in the above model. These are:

1. The $d\beta/dt$ equation of motion becomes undefined for vertical (i.e., $\gamma = \pm 90°$) flight.
2. The dn/dt, $d\alpha/dt$, $d\mu/dt$ equations are at best first-order approximations to actual aircraft control response.

From the above results and discussion, a 6-*DOF* model can be implemented that approximates an actual 6-*DOF* control response with a standard transfer function/filter whose input constants can be selected by the designer to more accurately match actual aircraft/missile control response. The roll, pitch, and yaw transfer functions are then as follows:

$$\textit{Roll:} \quad \frac{P_{\text{stab}}(s)}{P_{\text{stab}_{\text{cmd}}}(s)} = \frac{1}{\tau s + 1}$$

$$\textit{Pitch:} \quad \frac{n_z(s)}{n_{z_{\text{cmd}}}(s)} = \frac{\omega^2(\tau s + 1)}{s^2 + 2\zeta\omega s + \omega^2}$$

$$\textit{Yaw:} \quad \frac{n_y(s)}{n_{y_{\text{cmd}}}(s)} = \frac{\omega^2}{s^2 + 2\zeta\omega s + \omega^2}$$

where τ is the time constant, s is the Laplace operator, and ω is the frequency.

Under 6-*DOF* modeling, the $d\mu/dt$, $d\gamma/dt$, and $d\beta/dt$ kinematic relationships are

$$\begin{aligned}
\frac{d\mu}{dt} &= P + \tan\gamma(Q\sin\mu + R\cos\mu),\\
\frac{d\gamma}{dt} &= Q\cos\mu - R\sin\mu,\\
\frac{d\beta}{dt} &= \sec\gamma(Q\sin\mu + R\cos\mu),
\end{aligned}$$

where

$$\begin{aligned}
P &= \text{body axes roll rate},\\
Q &= \text{body axes pitch rate},\\
R &= \text{body axes yaw rate}.
\end{aligned}$$

Next, in order to eliminate the $d\beta/dt$ equations anomaly at $\gamma = \pm 90°$, the quaternion system of coordinates will be used; the kinematic rate equations are [7]

$$\begin{aligned}
\frac{de_1}{dt} &= (-e_4 P - e_3 Q - e_2 R)/2,\\
\frac{de_2}{dt} &= (-e_3 P - e_4 Q - e_1 R)/2,\\
\frac{de_3}{dt} &= (-e_2 P + e_1 Q - e_4 R)/2,\\
\frac{de_4}{dt} &= (-e_1 P - e_2 Q + e_3 R)/2,
\end{aligned}$$

and the Earth-to-body direction cosine matrix is, as before,

$$C_e^b = \begin{bmatrix} C_{11} & C_{12} & C_{13} \\ C_{21} & C_{22} & C_{23} \\ C_{31} & C_{32} & C_{33} \end{bmatrix},$$

where

$$
\begin{aligned}
C_{11} &= e_1^2 - e_2^2 - e_3^2 + e_4^2, \\
C_{12} &= 2(e_3 e_4 + e_1 e_2), \\
C_{13} &= 2(e_2 e_4 - e_1 e_3), \\
C_{21} &= 2(e_3 e_4 - e_1 e_2), \\
C_{22} &= e_1^2 - e_2^2 + e_3^2 - e_4^2, \\
C_{23} &= 2(e_2 e_3 + e_1 e_4), \\
C_{31} &= 2(e_1 e_3 + e_2 e_4), \\
C_{32} &= 2(e_2 e_3 - e_1 e_4), \\
C_{33} &= e_1^2 + e_2^2 - e_3^2 - e_4^2,
\end{aligned}
$$

and

$$
\begin{aligned}
\beta &= \tan^{-1}(C_{12}/C_{11}), \\
\gamma &= -\sin^{-1}(C_{13}), \\
\mu &= \tan^{-1}(C_{23}/C_{33}).
\end{aligned}
$$

Finally, we note that the same 6-*DOF* equations of motion can be used to model both aircraft and missiles.

Example 2. Based on the discussion thus far, let us now consider in this example a 6-*DOF* aerodynamic model. Furthermore, let us assume an *NED* coordinate system, in which all units are metric. This model is designed for a generic aircraft. A quaternion fast-processing technique will be employed to simulate aircraft navigation. This technique avoids not only time-consuming trigonometric computations in the fast-rate direction cosine updating, but also singularities in aircraft attitude determination [7].

6-*DOF* Initialization

Before processing begins, these initialization functions must be performed. Compute the initialized Earth reference velocity:

$$
\begin{aligned}
U_e &= V * \cos(\theta) * \cos(\psi), \\
V_e &= V * \cos(\phi) * \sin(\psi), \\
W_e &= -V * \sin(\theta),
\end{aligned}
$$

where

$$
\begin{aligned}
U_e &= \text{Earth } X\text{-velocity}, \\
V_e &= \text{Earth } Y\text{-velocity}, \\
W_e &= \text{Earth } Z\text{-velocity}, \\
\theta &= \text{pitch angle}, \\
\phi &= \text{roll angle}, \\
\psi &= \text{yaw angle}, \\
V &= \text{airspeed}.
\end{aligned}
$$

Compute Initialized Quaternions

$$A = [\sin(\psi/2) * \sin(\theta/2) * \cos(\phi/2)] - [\cos(\psi/2) * \cos(\theta/2) * \sin(\phi/2)],$$
$$B = -1 * [\cos(\psi/2) * \sin(\theta/2) * \cos(\phi/2)] - [\sin(\psi/2) * \cos(\theta/2) * \sin(\phi/2)],$$
$$C = -1 * [\sin(\psi/2) * \cos(\theta/2) * \cos(\phi/2)] + [\cos(\psi/2) * \sin(\theta/2) * \sin(\phi/2)],$$
$$D = -1 * [\cos(\psi/2) * \cos(\theta/2) * \cos(\phi/2)] - [\sin(\psi/2) * \sin(\theta/2) * \sin(\phi/2)],$$

where $A, B, C, D =$ quaternion parameters of the direction cosine matrix.

Now compute the initialized direction cosine matrix:

$$Cm(1,1) = A^2 - B^2 - C^2 + D^2,$$
$$Cm(1,2) = 2 * (A * B - C * D),$$
$$Cm(1,3) = 2 * (A * C + B * D),$$
$$Cm(2,1) = 2 * (A * B + C * D),$$
$$Cm(2,2) = -1 * A^2 + B^2 - C^2 + D^2,$$
$$Cm(2,3) = 2 * (B * C - A * D),$$
$$Cm(3,1) = 2 * (A * C - B * D),$$
$$Cm(3,2) = 2 * (B * C + A * D),$$
$$Cm(3,3) = -1 * A^2 - B^2 + C^2 + D^2,$$

where Cm direction cosine matrix.

Compute the initial body velocity

$$U_b = Cm(1,1) * U_e + Cm(2,1) * V_e + Cm(3,1) * W_e,$$
$$V_b = Cm(1,2) * U_e + Cm(2,2) * V_e + Cm(3,2) * W_e,$$
$$W_b = Cm(1,3) * U_e + Cm(2,3) * V_e + Cm(3,3) * W_e,$$

where

$$U_b = \text{body } X\text{-velocity},$$
$$V_b = \text{body } Y\text{-velocity},$$
$$W_b = \text{body } Z\text{-velocity}.$$

6-*DOF* Processing

The following computations are performed at every simulation cycle.

Compute the dynamic pressure

$$q = \tfrac{1}{2}\rho V^2,$$

where

$$q = \text{dynamic pressure},$$
$$\rho = \text{pressure in standard atmosphere},$$
$$V = \text{airspeed}.$$

Compute the wing lift

$$L = C_L * q * S,$$

where

$$\begin{aligned} L &= \text{lift}, \\ C_L &= \text{coefficient of lift}, \\ S &= \text{surface area of the wing}. \end{aligned}$$

Compute the wing drag

$$D = C_D * q * S,$$

where C_D = coefficient of drag.

Compute the lift acceleration

$$L_a = L/w,$$

where w = weight of the airplane.

Compute the drag acceleration

$$D_a = D/w.$$

Compute the thrust acceleration

$$T_a = T/m,$$

where

$$\begin{aligned} m &= \text{mass of the airplane}, \\ T &= \text{thrust}. \end{aligned}$$

Compute the body accelerations

$$\begin{aligned} X_{ba} &= T_a * L_a * \sin(\alpha) - D_a * \cos(\alpha) + Cm(3,1) * g + R * V_b - Q * W_b, \\ Y_{ba} &= Cm(3,2) * g - R * U_b + P * W_b, \\ Z_{ba} &= -1 * L_a * \cos(\alpha) - D_a * \sin(\alpha) + Cm(3,3) * g + Q * X_b - P * V_b, \end{aligned}$$

where

$$\begin{aligned} X_{ba} &= X\text{-axis body acceleration}, \\ Y_{ba} &= Y\text{-axis body acceleration}, \\ Z_{ba} &= Z\text{-axis body acceleration}, \\ P &= \text{roll rate}, \\ Q &= \text{pitch rate}, \\ R &= \text{yaw rate}, \\ g &= \text{acceleration due to gravity}, \\ \alpha &= \text{angle of attack}. \end{aligned}$$

Compute the Earth accelerations

$$\begin{aligned} X_{ea} &= Cm(1,1) * X_{ba} + Cm(1,2) * Y_{ba} + Cm(1,3) * Z_{ba}, \\ Y_{ea} &= Cm(2,1) * X_{ba} + Cm(2,2) * Y_{ba} + Cm(2,3) * Z_{ba}, \\ Z_{ea} &= Cm(3,1) * X_{ba} + Cm(3,2) * Y_{ba} + Cm(3,3) * Z_{ba}, \end{aligned}$$

where

$$\begin{aligned} X_{ea} &= X\text{-axis Earth acceleration}, \\ Y_{ea} &= Y\text{-axis Earth acceleration}, \\ Z_{ea} &= Z\text{-axis Earth acceleration}. \end{aligned}$$

Compute the angular deltas

$$\begin{aligned} \Delta\theta &= Q * t_i, \\ \Delta\phi &= P * t_i, \\ \Delta\psi &= R * t_i, \end{aligned}$$

where

$$\begin{aligned} \Delta\theta &= \text{pitch delta}, \\ \Delta\phi &= \text{roll delta}, \\ \Delta\psi &= \text{yaw delta}, \\ t_i &= \text{simulation cycle time}. \end{aligned}$$

Compute Cn and Sn

$$\begin{aligned} Cn &= 1.0 - (\Delta\theta^2 + \Delta\phi^2 + \Delta\psi^2)/8 + (\Delta\theta^4 + \Delta\phi^4 + \Delta\psi^4)/384, \\ Sn &= 0.5 - (\Delta\theta^2 + \Delta\phi^2 + \Delta\psi^2)/48, \end{aligned}$$

where

$$\begin{aligned} Cn &= n\text{th-order Maclaurin Series of } \cos(\Delta\theta/2), \\ Sn &= n\text{th-order Maclaurin Series of } \sin(\Delta\theta/2), \\ \Delta\theta &= \text{total body angle increment in } t_i. \end{aligned}$$

Compute the Quaternions

$$\begin{aligned} A' &= A * Cn + B * Sn * \Delta\psi + C * -1 * Sn * \Delta\theta + D * Sn * \Delta\phi, \\ B' &= A * -1 * Sn * \Delta\psi + B * Cn + C * Sn * \Delta\phi + D * Sn * \Delta\theta, \\ C' &= A * Sn * \Delta\theta + B * -1 * Sn * \Delta\phi + C * Cn + D * Sn * \Delta\psi, \\ D' &= A * -1 * Sn * \Delta\phi + B * -1 * Sn * \Delta\theta + C * -1 * Sn * \Delta\psi, \\ A &= A', \\ B &= B', \\ C &= C', \\ D &= D'. \end{aligned}$$

Renormalize the Quaternions

$$\begin{aligned}
\text{Normalizer} &= 0.5 * (3.0 - A^2 - B^2 - C^2 - D^2),\\
A &= A * \text{Normalizer},\\
B &= B * \text{Normalizer},\\
C &= C * \text{Normalizer},\\
D &= D * \text{Normalizer}.
\end{aligned}$$

Compute the direction cosine matrix

$$\begin{aligned}
Cm(1,1) &= A^2 - B^2 - C^2 + D^2,\\
Cm(1,2) &= 2 * (A * B - C * D),\\
Cm(1,3) &= 2 * (A * C + B * D),\\
Cm(2,1) &= 2 * (A * B + C * D),\\
Cm(2,2) &= -1 * A^2 + B^2 - C^2 + D^2,\\
Cm(2,3) &= 2 * (B * C - A * D),\\
Cm(3,1) &= 2 * (A * C - B * D),\\
Cm(3,2) &= 2 * (B * C + A * D),\\
Cm(3,3) &= -1 * A^2 - B^2 + C^2 + D^2.
\end{aligned}$$

Compute the Earth velocities

$$\begin{aligned}
U_e &= U_e + X_{ea} * t_i,\\
V_e &= V_e + Y_{ea} * t_i,\\
W_e &= W_e + Z_{ea} * t_i.
\end{aligned}$$

Compute the body velocities

$$\begin{aligned}
U_b &= Cm(1,1) * U_e + Cm(2,1) * V_e + Cm(3,1) * W_e,\\
V_b &= Cm(1,2) * U_e + Cm(2,2) * V_e + Cm(3,2) * W_e,\\
W_e &= Cm(1,3) * U_e + Cm(2,3) * V_e + Cm(3,3) * W_e.
\end{aligned}$$

Compute the airspeed

$$V = (U_e^2 + V_e^2 + W_e^2)^{1/2}.$$

Compute the Earth referenced position

$$\begin{aligned}
U_e &= U_e * t_i,\\
V_e &= V_e * t_i,\\
W_e &= W_e * t_i.
\end{aligned}$$

Compute the angle of attack

$$\alpha = A\tan 2(W_b/U_b).$$

Compute the attitudes

$$\begin{aligned}\theta &= A\sin(-1*Cm(3,1)),\\ \phi &= A\tan 2(Cm(3,2)/Cm(3,3)),\\ \psi &= A\tan 2(Cm(2,1)/Cm(1,1)).\end{aligned}$$

Compute the sideslip angle

$$\beta = A\tan 2(V_b/U_b),$$

where β is the sideslip angle.

Compute the flightpath angle

$$\gamma = A\tan 2((-1*W_e)/(U_e^2+V_e^2)^{1/2}),$$

where γ is the flightpath angle.

Earlier in this section, the equations of motion for a missile were discussed assuming the missile to be a rigid body. However, all materials exhibit deformation under the action of forces: *elasticity* when a given force produces a definite deformation, which vanishes if the force is removed; *plasticity* if the removal of the force leaves permanent deformation; *flow* if the deformation continually increases without limit under the action of forces, however small.

A "fluid" is material that flows. Actual fluids fall into two categories, namely, gases and liquids. A "gas" will ultimately fill any closed space to which it has access and is therefore classified as a (highly) *compressive fluid*. A "liquid" at constant temperature and pressure has a definite volume and when placed in an open vessel will take under the action of gravity the form of the lower part of the vessel and will be bounded above by a horizontal free surface. All known liquids are to some extent compressible. For most purposes it is, however, sufficient to regard liquids as *incompressible fluids*. It should be pointed out that for speeds that are not comparable with that of sound, the effect of compressibility on atmospheric air can be neglected, and in many experiments that are carried out in wind tunnels the air is considered to be a liquid, in the above sense, which may conveniently be called *incompressible air*.

All liquids (and gases) in common with solids exhibit *viscosity* arising from internal friction in the substance. For those readers interested in pursuing more thoroughly the area of incompressible air and/or fluid flow, the *Navier–Stokes* equation is a good start. The *Euler* and *Navier–Stokes* equations describe the motion of a fluid in $\mathbf{R}^n$ ($n=2$ or 3). These equations are to be solved for an unknown velocity vector $\mathbf{u}(\boldsymbol{x},t)=(\mathbf{u}_i(\boldsymbol{x},t))_{1\le i\le n}\in\mathbf{R}^n$ and pressure $p(\boldsymbol{x},t)\in\mathbf{R}$, defined for position $\boldsymbol{x}\in\mathbf{R}^n$ and time $t\ge 0$. We restrict attention here to incompressible fluids filling all of $\mathbf{R}^n$. The *Navier–Stokes* equations are then given by

$$(\partial/\partial t)u_i+\sum_{j=1}^{n}u_j(\partial u_i/\partial x_j)=\nu\Delta u_i-(\partial p/\partial x_i)+f_i(x,t)\quad(\boldsymbol{x}\in\mathbf{R}^n,t\ge 0),\tag{2.51}$$

$$\operatorname{div} u = \sum_{i=1}^{n} (\partial u_i / \partial x_i) = 0 \quad (\boldsymbol{x} \in \mathbf{R}^n, t \geq 0), \tag{2.52}$$

with initial conditions

$$\mathbf{u}(\boldsymbol{x}, 0) = \mathbf{u}^0(\boldsymbol{x}), \quad \boldsymbol{x} \in \mathbf{R}^n, \tag{2.53}$$

where

$$\Delta = \sum_{i=1}^{n} (\partial^2 / \partial x_i^2)$$

is the Laplacian in the space variables.

Here, $\boldsymbol{u}^0(\boldsymbol{x})$ is a given $\boldsymbol{C}^\infty$ divergence-free vector field on $\mathbf{R}^n$, $f_i(x, t)$ are the components of a given externally applied force (e.g., gravity), and ν is a positive coefficient (the viscosity). Equation (2.51) is just Newton's law $\boldsymbol{f} = m\boldsymbol{a}$ for a fluid element subject to the external force $\boldsymbol{f} = (f_i(x, t))_{1 \leq i \leq n}$ and to the force arising from pressure and friction. Equation (2.52) just says that the fluid is *incompressible*. For physically reasonable solutions, we want to make sure that $\boldsymbol{u}(\boldsymbol{x}, t)$ does not grow large as $|\boldsymbol{x}| \to \infty$. Moreover, we accept a solution of equations (2.51)–(2.53) as physically reasonable only if it satisfies

$$p, \boldsymbol{u} \in \boldsymbol{C}^\infty(\mathbf{R}^n \times [0, \infty))$$

and

$$\int_{\mathbf{R}^n} |\boldsymbol{u}(\mathbf{x}, t)|^2 dx < \boldsymbol{C} \quad \forall t \geq 0 \text{ (bounded energy)}.$$

2.3 D'Alembert's Principle

In Section 2.2 we discussed the rigid-body equations of motion. Specifically, we discussed Newton's second law as given by (2.17b) and (2.18b). In the fundamental equation (2.18b), $\mathbf{F} = m\mathbf{a}$, the quantity $m(-\mathbf{a})$ is called the *reversed effective force* or *inertia force*. D'Alembert's principle is based on Newton's second and third laws of motion and states that 'the inertia force is in equilibrium with the external applied force,' or

$$\mathbf{F} + m(-\mathbf{a}) = 0. \tag{2.54}$$

This principle has the effect of reducing a dynamical problem to a problem in statics and may thus make it easier to solve. Based on the principle of *virtual work,* * which was established for the case of static equilibrium, we can proceed as follows: Let $\mathbf{p}$ be the momentum of a particle in the system, and separate the forces acting on it into an

* Consider a particle acted upon by several forces. If the particle is in equilibrium, the resultant $\mathbf{R}$ of the forces must vanish, and the work done by the forces is a virtual displacement $\delta\mathbf{r}$ is zero. Thus, $\mathbf{R} \cdot \delta\mathbf{r} = 0$.

applied force $\mathbf{F}$ and a constraint force $\mathbf{f}$. Then the equation of motion of the particle can be written as [9]

$$\mathbf{F}+\mathbf{f}-\left(\frac{d\mathbf{p}}{dt}\right)=0.$$

The quantity $(d\mathbf{p}/dt)$ is usually referred to as the *reverse effective force* discussed above. Note that the virtual work of the constraint force is zero, since $\mathbf{f}$ and $\delta\mathbf{r}$ are mutually perpendicular. The virtual work of the forces acting on the particle is

$$\left[\mathbf{F}_i-\left(\frac{d\mathbf{p}_i}{dt}\right)\right]\cdot\delta\mathbf{r}_i=0\quad(i=1,2,\ldots,N),$$

and for a system of N particles,

$$\sum_{i=1}^{N}\left[\mathbf{F}_i-\left(\frac{d\mathbf{p}_i}{dt}\right)\right]\cdot\delta\mathbf{r}_i=0\quad(i=1,2,\ldots,N).$$

Another way of writing this equation is

$$\sum_{i=1}^{N}\left[\mathbf{F}_i-m_i\left(\frac{d^2\mathbf{r}_i}{dt^2}\right)\right]\cdot\delta\mathbf{r}_i=0\quad(i=1,2,\ldots,N),$$

where $\mathbf{r}_i$ is the position vector of the particle. The term $-m_i(d^2\mathbf{r}_i/dt^2)$ has the dimensions of force and is known as the *inertia force* acting on the ith particle (see also discussion above). This is the *Lagrangian* form of d'Alembert's principle and is one of the most important equations of classical dynamics.

2.4 Lagrange's Equations for Rotating Coordinate Systems

The missiles considered thus far were assumed to obey the laws of rigid bodies. However, in analyzing the dynamics of flexible missiles, such as intermediate-range ballistic missiles or intercontinental ballistic missiles, it is convenient to use a set of coordinates moving with the missile. In this case, the missile can be considered as a system of particles whose position relative to the moving axes can be defined by generalized coordinates q_i. Specifically, we will consider the motion of a *holonomic** system with n degrees of freedom. Let $(q_1, q_2, \ldots, q_n)$ be the coordinates that specify the configuration of the system at time t. Furthermore, we will consider a mechanical system of n particles whose coordinates are $(x_1, y_1, z_1, x_2, y_2, z_2, \ldots, x_n, y_n, z_n)$. The motion of the system is known when the value of every coordinate is known as a function of time. Suppose now that the system moves from a certain configuration given by $(x_1', \ldots, z_n')$ at time t_1 to another configuration given by $(x_1'', y_1'', \ldots, z_n'')$ at

*A dynamical system for which a displacement represented by arbitrary infinitesimal changes in the coordinates is, in general, a possible displacement is said to be *holonomic*. When this condition is not satisfied, the system is said to be *nonholonomic*.

time t_2. During all of the motion between these two configurations, the Newtonian equations of motion will be followed, and the acceleration of each particle will be given by the total force acting on it. Moreover, this motion can be described by expressing each coordinate as a function of time.

There are then $3n$ dependent variables depending on the one independent variable t. These functions can be written in the form

$$x_1 = x_1(t),\ y_1 = y_1(t),\ \ldots,\ z_n = z_n(t). \tag{2.55}$$

In deriving the equations of motion, it is common practice to start the derivation using the concepts of kinetic and potential energies of the system using Lagrange's equation. As will be noted, however, these equations differ from the usual Lagrange equations for fixed coordinates. Now consider some other way in which the system might have moved from the initial configuration to the final configuration in the same amount of time, $t_2 - t_1$. This new motion is to be one that satisfies the geometric conditions, or the constraints of the problem. If this new motion is just slightly different from the original motion, the coordinates, as functions of time, can be written as follows:

$$x_1(t) + \delta x_1(t),\ y_1(t) + \delta y_1(t),\ \ldots,\ z_n(t) + \delta z_n(t).$$

The variation of a coordinate x is a function of time and is the difference between the x coordinate of the comparison path and that of the true path. It is also assumed that the true path is a continuous function with continuous first derivatives satisfying Newton's equations. The same ideas apply to the comparison path. Therefore,

$$\delta x_1(t_1) = \delta x_1(t_2) = \delta y_1(t_1) = \delta y_1(t_2) = \cdots = \delta z_n(t_2) = 0. \tag{2.56}$$

The true path was originally defined in terms of the Newtonian equations of motion. For the true path there are $3n$ equations of the form

$$m_i \left(\frac{d^2 x_i}{dt^2} \right) = X_i, \tag{2.57}$$

where m_i typifies the mass of one of the particles of the system. The quantity X_i may be a function of the coordinates, of the time explicitly, or of both. It may be considered, however, as a function of time only, since the dependence on the coordinates is a dependence upon the positions of the particles, and these are uniquely determined by the time along any path that may be considered. In general, the coordinates of the individual particles (referenced to some fixed set of rectangular coordinates) are known functions of the coordinates $(q_1, q_2, \ldots, q_n)$ of the system, and possibly of t also. Let this dependence be expressed by the equations [11]

$$\begin{aligned} x_i &= f_i(q_1, q_2, \ldots, q_n, t), \\ y_i &= g_i(q_1, q_2, \ldots, q_n, t), \\ z_i &= h_i(q_1, q_2, \ldots, q_n, t). \end{aligned} \tag{2.58}$$

Furthermore, let (X_i, Y_i, Z_i) be the components of the total force (external) acting on the particle m_i. Then, the equations of motion of this particle are

$$m_j\left(\frac{d^2x_j}{dt^2}\right)=X_i,\quad m_j\left(\frac{d^2y_j}{dt^2}\right)=Y_i,\quad m_j\left(\frac{d^2z_j}{dt^2}\right)=Z_i. \tag{2.59}$$

If each component of the force X_i is now multiplied by the variation of path in the direction of the force and all the resulting equations are added together, the result is [4], [11]

$$\begin{aligned}\delta U &= \sum_i (X_i\delta x_i + Y_i\delta y_i + Z_i\delta z_i),\\ &= \sum_i m_i\left(\frac{d^2x_i}{dt^2}\delta x_i + \frac{d^2y_i}{dt^2}\delta y_i + \frac{d^2z_i}{dt^2}\delta z_i\right)\\ &= \sum_i m_i\left[\frac{d}{dt}(\dot{x}_i\delta x_i + \dot{y}_i\delta y_i + \dot{z}_i\delta z_i) - \dot{x}_i\delta\dot{x}_i - \dot{y}_i\delta\dot{y}_i - \dot{z}_i\delta\dot{z}_i\right]\end{aligned} \tag{2.60}$$

where the symbol $\sum$ denotes summation over all the particles of the system; this can be either an integration (if the particles are united into rigid bodies) or a summation over a discrete aggregate of particles. The quantity δU is defined by the first equality in (2.60). It is the work done by the forces of the system during the infinitesimal displacement $(\delta x_i, \ldots, \delta z_n)$ and is a function of the time and the independent coordinates of the system. If the forces do not depend explicitly on the time, δU can be expressed as a function of the coordinates only. The last part of (2.60) represents the variation of the kinetic energy δT. Hence the equation can be written as [3]

$$\delta T + \delta U = \sum\nolimits_i m_i\frac{d}{dt}(x_i\delta x_i + y_i\delta y_i + z_i\delta z_i). \tag{2.61}$$

It should be noted that in the above expressions t is the independent variable. Now, if both sides of (2.61) are integrated with respect to this independent variable between the limits t_1 and t_2, the result is

$$\int_{t_1}^{t_2}(\delta T + \delta U)dt = \delta\int_{t_1}^{t_2} T\,dt + \int_{t_1}^{t_2}\delta U\,dt = 0. \tag{2.62}$$

In this equation, we note that the right-hand side is zero because all of the variations are zero at both limits. Therefore, (2.62) is a property of the path that satisfies the equations of motion, and this property furnishes a way of defining the true path of the system. In the special case in which the forces are conservative, that is, when they can be derived from the potential energy, δU is the negative of the variation of the potential energy. Consequently, we have

$$\delta\int_{t_1}^{t_2}(T-U)dt = \delta\int_{t_1}^{t_2} L\,dt = 0, \tag{2.63}$$

where T is the kinetic energy and U is the potential energy.

Commonly, the quantity $(T-U)$ is denoted by L and is called the *Lagrangian function* or the kinetic potential of the system, or $L=T-U$. The function L, defined as the excess of kinetic energy over potential energy, is the most fundamental quantity in the mathematical analysis of mechanical problems. The Lagrangian function can be expressed in any convenient coordinate system, and the variation principle will still apply. Thus, if we introduce a new function L of the variables $(q_1, q_2, \ldots, q_n, \dot{q}_1, \dot{q}_2, \ldots, \dot{q}_n, t)$, defined by the equation

$$L = T - U,$$

then Lagrange's equations can be written in the form [11]

$$\frac{d}{dt}\left(\frac{\partial L}{\partial \dot{q}_i}\right) - \frac{\partial L}{\partial q_i} = 0 \qquad i = 1, 2, \ldots, n, \quad t_1 \le t \le t_2. \tag{2.64}$$

Hamilton's principle for the motion of a mechanical system states that

$$\delta \int_{t_1}^{t_2} L(q_1, q_2, \ldots, q_n, \dot{q}_1, \dot{q}_2, \ldots, \dot{q}_n, t)dt. \tag{2.65}$$

In (2.65) the q's represent the coordinates necessary to specify the configuration of the system. Note that the time appears explicitly in the Lagrangian function only in case the forces are explicit functions of time, or the coordinates used are in motion. In the simple conservative cases the Lagrangian function depends upon the coordinates and their first derivatives only. If, as has been assumed, the coordinates are all independent, then the path can be described by the set of differential equations (2.64).

The Euler–Lagrange equations for Hamilton's principle (2.64) are usually called simply Lagrange's equations. They contain nothing more than was contained in the Newtonian equations, but they have the decided advantage that the coordinates may be of any kind whatever. It is necessary only to write the potential and kinetic energies in the desired coordinates to obtain the equations of motion by simple differentiation. This is usually much simpler than transforming the differential equations themselves. Finally, we note here that Lagrange's equations and Newton's equations are entirely equivalent.

Now, if the $(x\text{-}y)$ plane is rotated by an angle θ, the coordinate axes in plane motion will have three degrees of freedom, namely, x_0, y_0, and θ, which can be varied independently. In this case, the Lagrange equations can be written in the form [4], [9]

$$\frac{d}{dt}\frac{\partial T}{\partial \dot{x}_0} - \dot{\theta}\frac{\partial T}{\partial \dot{y}_0} = \sum F_x \tag{2.66a}$$

$$\frac{d}{dt}\frac{\partial T}{\partial \dot{y}_0} + \dot{\theta}\frac{\partial T}{\partial \dot{x}_0} = \sum F_y \tag{2.66b}$$

$$\frac{d}{dt}\frac{\partial T}{\partial \dot{\theta}} + \dot{x}_0\frac{\partial T}{\partial \dot{y}_0} - \dot{y}_0\frac{\partial T}{\partial \dot{x}_0} = \sum M_0 \tag{2.66c}$$

where the equation for the q_i remains unaltered. In accounting for the terms in these equations, the partials $\partial T/\partial \dot{x}_0$ and $\partial T/\partial \dot{y}_0$ will be recognized as the general momenta, and $\partial T/\partial \dot{\theta}$ as the generalized angular momentum. The linear momentum can then be represented by the expression

$$\boldsymbol{p} = (\partial T/\partial \dot{x}_0)\mathbf{i} + (\partial T/\partial \dot{y}_0)\mathbf{j}. \tag{2.67}$$

Since the force equation is the rate of change of the linear momentum, we have

$$\boldsymbol{F} = [d\boldsymbol{p}/dt] + \boldsymbol{\omega} \times \boldsymbol{p}. \tag{2.68}$$

The terms of (2.66a) and (2.66b) are immediately accounted for. Moreover, the terms of (2.66c) can be identified from the expression

$$\mathbf{M}_0 = \left(\frac{d\boldsymbol{h}_0}{dt}\right) + \left(\frac{d\boldsymbol{R}_0}{dt}\right) \times \sum m_i \left(\frac{d\boldsymbol{r}_i}{dt}\right). \tag{2.69}$$

The term $\partial T/\partial \dot{\theta}$ is the angular momentum $\boldsymbol{h}_0$, and the remaining two terms are equal to $(d\boldsymbol{R}_0/dt) \times \sum m_i (d\boldsymbol{r}_i/dt)$, where $d\boldsymbol{R}_0/dt = (dx_0/dt)\mathbf{i} + (dy_0/dt)\mathbf{j}$.

Example 3. A typical example illustrating the above principles will now be given. Specifically, we will work out Problem 2, p. 118, of reference [4]. Consider a particle moving in a plane attracted toward the origin of coordinates with a force inversely proportional to the square of the distance from it. In plane polar coordinates (r, θ) one has

$$U = -\left(\frac{k}{r}\right) \quad \text{and} \quad T = \left(\frac{m}{2}\right)\left[\left(\frac{dr}{dt}\right)^2 + r^2\left(\frac{d\theta}{dt}\right)^2\right].$$

From these expressions, we form the *Lagrangian function* as follows:

$$L = T - U = \left(\frac{m}{2}\right)\left[\left(\frac{dr}{dt}\right)^2 + r^2\left(\frac{d\theta}{dt}\right)^2\right] + \left(\frac{k}{r}\right).$$

Furthermore, using (2.64), we obtain the derivatives as

$$\frac{\partial L}{\partial \dot{r}} = m\left(\frac{dr}{dt}\right) \quad \text{and} \quad \frac{\partial L}{\partial r} = mr\left(\frac{d\theta}{dt}\right)^2 - \left(\frac{k}{r^2}\right),$$

which give for this equation of motion

$$m\left(\frac{d^2r}{dt^2}\right) - mr\left(\frac{d\theta}{dt}\right)^2 + \left(\frac{k}{r^2}\right) = 0.$$

For the other equation in the variable θ, we have

$$\frac{\partial L}{\partial \dot{\theta}} = mr^2\left(\frac{d\theta}{dt}\right) \quad \text{and} \quad \frac{\partial L}{\partial \theta} = 0,$$

so that this equation of motion is

$$m\left(\frac{d}{dt}\right)\left[r^2\left(\frac{d\theta}{dt}\right)\right]=0.$$

Note that since θ is not explicitly present in L, the derivative of L with respect to $d\theta/dt$ is a constant.

References

1. Blakelock, J.H.: *Automatic Control of Aircraft and Missiles*, John Wiley & Sons, Inc., New York, NY, second edition, 1991.
2. Etkin, B.: *Dynamics of Atmospheric Flight*, John Wiley & Sons, Inc., New York, NY, 1972.
3. Goldstein, H.: *Classical Mechanics*, Addison-Wesley, Reading, MA., 1950.
4. Lanczos, C.: *The Variational Principles of Mechanics*, University of Toronto Press, second edition, Toronto, Canada, 1960.
5. Nicolai, L.M.: *Fundamentals of Aircraft Design*, METS, Inc., San Jose, CA., 1984.
6. Roskam, J.: *Airplane Flight Dynamics and Automatic Flight Control*, Part I, Roskam Aviation and Engineering Corporation, Ottawa, Kansas, second printing, 1982.
7. Siouris, G.M.: *Aerospace Avionics Systems*: *A Modern Synthesis*, Academic Press, Inc., San Diego, CA., 1993.
8. Synge, J.L. and Griffith, B.A.: *Principles of Mechanics*, third edition, McGraw-Hill Book Co., New York, 1959.
9. Thomson, W.T.: *Introduction to Space Dynamics*, John Wiley & Sons, Inc., second printing, New York, NY, 1963.
10. Timoshenko, S. and Young, D.H.: *Advanced Dynamics*, McGraw-Hill Book Co., New York, 1948.
11. Whittaker, E.T.: *A Treatise on the Analytical Dynamics of Particles and Rigid Bodies*, Cambridge University Press, fourth edition, Cambridge, U.K., 1964.

This page intentionally left blank

3

Aerodynamic Forces and Coefficients

3.1 Aerodynamic Forces Relative to the Wind Axis System

In this section we will discuss briefly the aerodynamic forces acting on a missile. In particular, and unless otherwise specified, we will assume a *skid-to-turn* missile because this technique is used in the majority of both surface-to-air and air-to-air missile applications (for more details see Section 3.3.2). However, the reader should be cautioned that both the aerodynamics and rigid-body dynamics are highly nonlinear. For a more in-depth discussion of these forces the reader is referred to [2], [6], and [8]. Generally, the magnitude of the forces and moments that act on an air vehicle depend on the combined effects of many different variables. Briefly, the parameters that govern the magnitude of aerodynamic forces and moments include the following: (1) configuration geometry, (2) angle of attack, (3) vehicle size, (4) free-stream velocity, (5) density of the undisturbed air, (6) Reynolds number (i.e., as it relates to viscous effects), and (7) Mach number (i.e., as it relates to compressibility effects). In order to correlate the data for various stream conditions and configurations, the measurements are usually presented in dimensionless form. In practice, however, flow phenomena such as boundary-layer separation, shock-wave/boundary-layer interaction, and compressibility effects limit the range of flow conditions over which the dimensionless force and moment coefficients remain constant. In essence, the motion of the air around an aircraft or missile produces pressure and velocity variations, which produce the aerodynamic forces and moments. As discussed in Section 2.2, the forces acting on a missile in flight consist of aerodynamic, propulsive (i.e., thrust), and gravitational forces. These forces can be resolved along the missile's body-axis system (X_b, Y_b, Z_b) and fixed to the missile's center of gravity (cg). The reference axis system standardized in guided weapons is centered on the cg and fixed in the body. Thus, any set of axes fixed in a rigid body is a *body-fixed* reference frame. Before we proceed with the present discussion, some of the fundamental concepts and definitions of aerodynamics will be reviewed. These definitions and nomenclature will be given with reference to Figure 3.1.

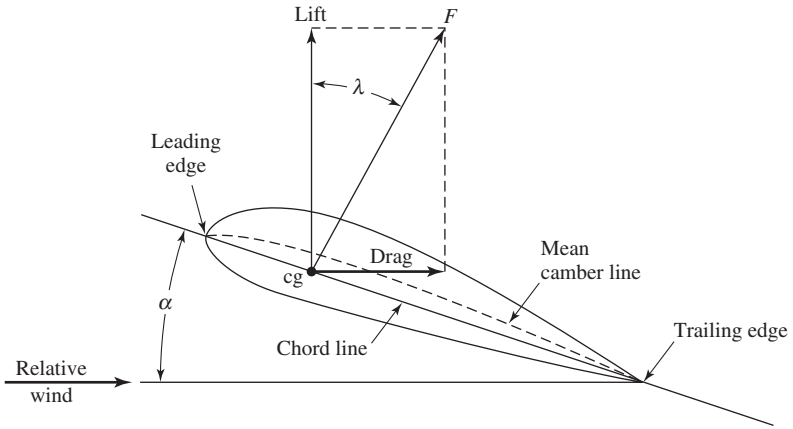

Fig. 3.1. Nomenclature and definitions.

Angle of Attack (α)*:* The angle between the relative wind and the chord line.

Aerodynamic Center: The point on the chord of an airfoil about which the moment coefficient is practically constant for all angles of attack. Moreover, the aerodynamic center is that point along the chord where all changes in lift effectively takes place. Since the moment about the aerodynamic center is the product of a force (the lift acts at the center of pressure) and a lever arm (the distance from the aerodynamic center to the center of pressure), the center of pressure must move toward the aerodynamic center as the lift increases.

Center of Gravity: The forces due to gravity are always present in an aircraft (or missile) and act at the center of gravity (cg). Since the centers of mass and gravity in an aircraft practically coincide, there is no external moment produced by gravity about the cg. The gravitational force acting upon an aircraft is commonly expressed in terms of the Earth axes (see also Section 3.2.1).

*Center of Pressure:** The point on the chord of an airfoil through which all of the aerodynamic forces act. The center of pressure (cp) in general will not be located at the center of gravity of the airfoil; thus a moment will be produced.

Dynamic Pressure: The aerodynamic pressure appears frequently in the derivation of aerodynamic formulas. Dynamic pressure, denoted by the symbol q, is given by the expression $q = \frac{1}{2}\rho V^2$, where ρ is the air density, and V is the free-stream velocity.

Center of Mass: The origin of the body axes is usually the mass center (cm).

Relative Wind: Refers to the motion of air relative to an airfoil and is equal and opposite to the forward velocity of the air vehicle.

Resultant Aerodynamic Force: The vector summation of all of the aerodynamic forces acting on the airfoil. Its point of application is at the center of pressure.

*Note that in aircraft design, aerodynamicists call the center of pressure (cp) the aerodynamic center (ac). Therefore, cp and ac will be assumed here to denote the same thing.

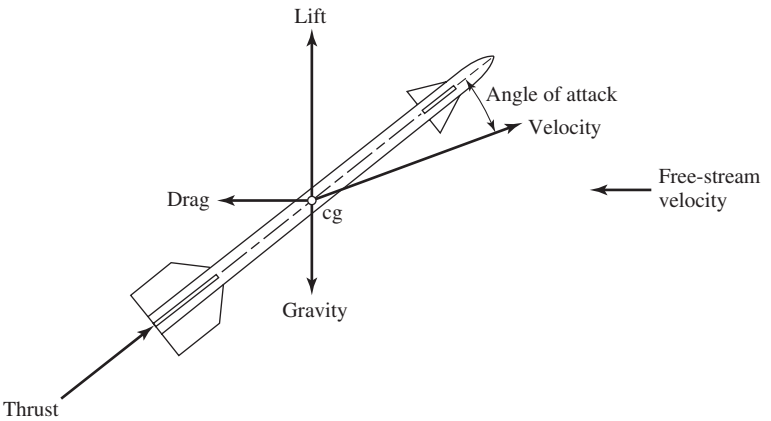

Fig. 3.2. Aerodynamic forces and thrust acting on a missile.

It is conventional in aerodynamics to resolve the sum of the normal (or pressure) forces and the tangential (or viscous shear) forces that act on the surface due to the fluid motion around a vehicle into three components along axes parallel and perpendicular to the free-stream direction. These forces are *lift* (L), *drag* (D), and *side force* (Y). The relation of the lift and the drag forces to the free-stream velocity is shown in Figure 3.2. It should be noted from this figure that if an angle of attack is generated, the lift vector acting at the center of pressure (cp) has a destabilizing effect and must be controlled.

We will now define these forces in some detail.

Lift–Lift is the component of the resultant aerodynamic force that is perpendicular (i.e., upward) to the relative wind (direction of flight) or to the undisturbed free-stream velocity. The aerodynamic lift is produced primarily by the pressure forces acting on the vehicle surface. Also, the lift force is perpendicular to the missile's velocity vector in the vertical plane.

Drag–Drag is the component of the resultant aerodynamic force that is parallel to the relative wind. In other words, it is net aerodynamic force acting in the same direction as the undisturbed free-stream velocity. The aerodynamic drag is produced by the pressure forces and by skin friction forces that act on the surface. The drag force is measured along the velocity vector, but in the opposite direction.

Side Force–Side force is the component of force in a direction perpendicular to both the lift and the drag and is measured in the horizontal plane. The side force is positive when acting toward the starboard wing, provided that the bank angle is zero. If the bank angle is not zero, L and Y will be rotated by a negative angle about the velocity vector.

The definitions of the aerodynamic forces, moments, and velocity components in the body-fixed coordinate system, which will be used in this chapter, are summarized in Table 3.1.

Table 3.1. Missile Aerodynamic Moments, Coordinates, and Velocity Components

	Roll Body Axis (X_b)	Pitch Body Axis (Y_b)	Yaw Body Axis (Z_b)
Angular Rates	P	Q	R
Velocity Components	u	v	w
Aerodynamic Force Components	F_X	F_Y	F_Z
Aerodynamic Force Coefficients	C_D	C_Y	C_L
Aerodynamic Moment Coefficients	C_l	C_m	C_n

The basic aerodynamic forces are commonly defined in terms of dimensionless coefficients, the flight dynamic pressure, and a reference area. For missiles that *skid* (yaw) *to turn* (see Section 3.3.2 for more details), the basic aerodynamic forces are illustrated in Figure 3.2 and are calculated as follows [2], [6]:

$$\text{Drag:} \quad D = C_D q S, \tag{3.1}$$

$$\text{Lift:} \quad L = C_L q S, \tag{3.2}$$

$$\text{Side Force:} \quad F_Y = C_Y q S, \tag{3.3}$$

where

C_D = Coefficient of drag in the wind axis system,
C_L = Coefficient of lift in the wind axis system,
C_Y = Side force coefficient,
q = Free-stream dynamic pressure at a point far from the airfoil = $\frac{1}{2}\rho V^2$,
S = Reference area, usually the area of one of the airfoils,
V = Free-stream velocity,
ρ = Atmospheric density = 2.3769×10^{-3}lb-sec^2-ft^{-4} at sea level (see also Appendix D).

For missiles that *roll* to turn, drag is the same as in (3.1), but the lift and side force are as follows:

$$\text{Lift} = C_{LT}(\cos\,\phi) q S, \tag{3.4}$$

$$\text{Side Force} = C_{LT}(\sin\,\phi) q S, \tag{3.5}$$

where

C_{LT} = Total lift coefficient in the maneuver plane = $(C_L^2 + C_Y^2)^{1/2}$,
ϕ = Roll angle.

For the purposes of the discussion in this book, the three most important aerodynamic force coefficients are commonly defined as*

$$C_L = L/qS,$$
$$C_D = D/qS,$$
$$C_M = M/qSd,$$

where M is the moment and d is the mean missile diameter from a body cross-section. Figure 3.3 illustrates the aerodynamic forces relative to the wind-axis system.

The aerodynamic forces may also be expressed in the form

$$\textit{Axial Force (Drag):} \quad F_X = q(V,h)SC_D(V,h,\alpha,\beta), \tag{3.6}$$

$$\textit{Side Force:} \quad F_Y = q(V,h)SC_Y(V,h,\alpha,\beta), \tag{3.7}$$

$$\textit{Normal Force (Lift):} \quad F_Z = q(V,h)SC_L(V,h,\alpha,\beta), \tag{3.8}$$

showing the dependence on the angle of attack (α), sideslip angle (β), and altitude h. On occasion, it may be convenient to measure the aerodynamic forces in the body axis coordinate system. In this case, we have the normal force (F_Z) along the Z_b-axis, side force (F_Y) along the Y_b-axis, and the axial force (F_X) along the X_b-axis. The specification of forces in the body-axis system is similar to that in the wind-axis system. That is,

$$F_{Xb} = qSC_D,$$
$$F_{Yb} = qSC_Y,$$
$$F_{Zb} = qSC_L.$$

The aerodynamic force coefficients C_L, C_D, and C_Y are commonly expressed in the wind-axis system oriented relative to the free-stream. Since the aerodynamic force components of the equations of motion (see Section 2.2) are required to be in the body-fixed coordinate system, one must express these coefficients in terms of the angle of attack and sideslip angle. The aerodynamic force coefficients can be determined in the wind tunnel in the body-fixed axis system, designated as C_{Xb}, C_{Yb}, and C_{Zb}. Thus,

$$C_{Xb} = -C_D \cos\alpha \cos\beta - C_Y \cos\alpha \sin\beta + C_L \sin\alpha, \tag{3.9}$$

$$C_{Yb} = -C_D \sin\beta + C_Y \cos\beta, \tag{3.10}$$

$$C_{Zb} = -C_D \sin\alpha \cos\beta - C_Y \sin\alpha \sin\beta - C_L \cos\alpha. \tag{3.11}$$

Figure 3.4 illustrates these coefficients.

For a simple point mass case, relative to the airstream, the aerodynamic force coefficients C_D, C_L, and C_Y will be assumed to be functions of one or more of the following:

*Note that here we assume that the specification of forces in the *body-axis* system is similar to that in the *wind-axis* system.

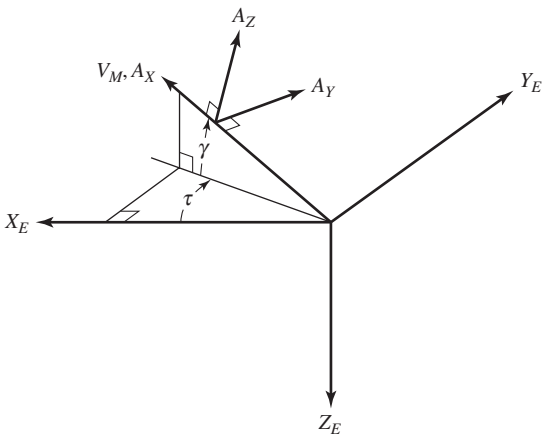

Earth axis system

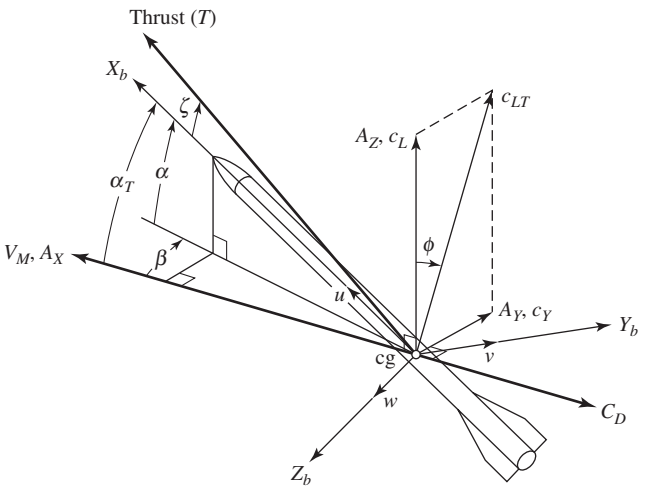

Wind axis system

Fig. 3.3. Aerodynamic forces: wind axes.

(1) Angle of attack and sideslip angle.
(2) Lift and/or side force.
(3) Mach number and/or Reynolds number (plays a role only in the drag force).
(4) Center of gravity location.
(5) Altitude.

As mentioned above, all the aerodynamic force coefficients are, in general, functions of the state variables and the control variables, so that one can write, for example,

$$C_D = C_D(\alpha, \beta, M, q, \dots).$$

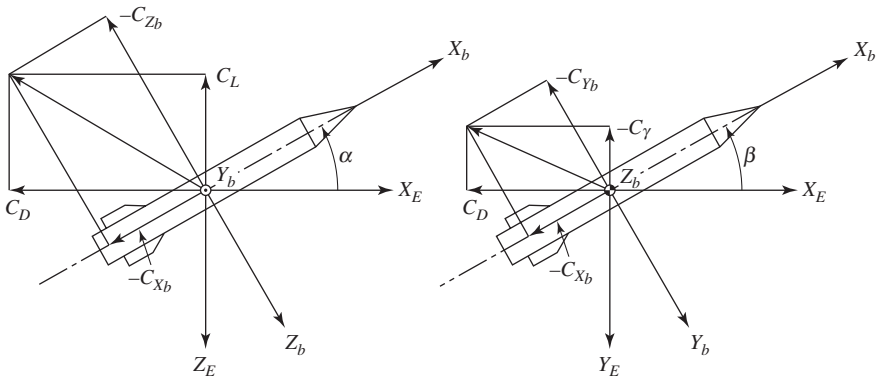

Fig. 3.4. Wind tunnel representation of the aerodynamic coefficients.

By taking the partial derivatives, we have

$$dC_D = (\partial C_D/\partial\alpha)d\alpha + (\partial C_D/\partial\beta)d\beta + (\partial C_D/\partial M)dM + (\partial C_D/\partial q)dq + \cdots .$$

Therefore, the aerodynamic force coefficients C_D, C_L, and C_Y may be expressed in terms of the aerodynamic derivatives as follows:

$$C_D = C_{D0} + C_{D\alpha}|\alpha| + C_{D\alpha^2}\alpha^2 + C_{D\beta}|\beta| + C_{D\beta^2}\beta^2 + C_{D\alpha\beta}|\alpha||\beta|, \quad (3.12)$$

$$C_L = C_{L0} + C_{L\alpha}|\alpha| + C_{L\alpha^2}\alpha^2 + C_{L\beta}|\beta| + C_{L\beta^2}\beta^2 + C_{L\alpha\beta}|\alpha||\beta|, \quad (3.13)$$

$$C_Y = C_{Y0} + C_{Y\alpha}|\alpha| + C_{Y\alpha^2}\alpha^2 + C_{Y\beta}|\beta| + C_{Y\beta^2}\beta^2 + C_{Y\alpha\beta}|\alpha||\beta|, \quad (3.14)$$

where $C_{D0} = (\partial C_D/\partial\alpha)|_{\alpha=0}$ (i.e., evaluated at $\alpha = 0$), $C_{D\alpha} = \partial C_D/\partial\alpha$, etc. For our purposes, the functional dependence of the aerodynamic force coefficients will be assumed to take the simpler form as follows [6], [8]:

Drag Coefficient (C_D)

$$C_D = C_{D0} + C_{D\alpha}\alpha, \quad (3.15a)$$

where

C_{D0} = total drag coefficient evaluated at $\alpha = 0$ (or close to it) $= (\partial C_D/\partial\alpha)|_{\alpha=0}$,
$C_{D\alpha}$ = total drag coefficient variation with angle of attack $= \partial C_D/\partial\alpha$,
α = angle of attack (in radians).

The derivatives are evaluated at constant Mach number and Reynold's number. The *drag polar* is written in the form [4]

$$C_D = C_{D0} + KC_L^2, \quad (3.15b)$$

where

C_{D0} = zero lift drag coefficient,
K = drag due to lift factor (also called the separation drag due to lift factor)
$= dC_D/dC_L^2$,
C_L = lift coefficient.

Equation (3.15b) states that the total drag may be written as the sum of (1) the drag that exists when the configuration generates zero lift (C_{D0}), and (2) the induced drag associated with lift (KC_L^2).

Lift Coefficient C_L

$$C_L = C_{L0} + C_{L\alpha}\alpha, \tag{3.16a}$$

where

C_{L0} = total lift coefficient evaluated at $\alpha = 0$
$= (\partial C_L/\partial\alpha)|_{\alpha=0}$,
$C_{L\alpha}$ = total lift-curve slope.

The derivatives here are evaluated at constant Mach number. The lift coefficient can also be written as

$$C_L = (\partial C_L/\partial\alpha)|_{\alpha=0}\alpha + C_l\alpha^2, \tag{3.16b}$$

where C_l is a nonlinear factor.

Side Force Coefficient (C_Y)

The functional dependence of the side force coefficient on sideslip angle, β, aileron angle, δ_A, etc., is expressed as

$$C_Y = C_{Yo} + C_{Y\beta}\beta + C_{Y\delta}\delta_A, \tag{3.17}$$

where

C_{Yo} = side force coefficient for zero sideslip and zero control deflection
$= (\partial C_Y/\partial\beta)|_{\beta=0}$,
$C_{Y\beta}$ = change in side force coefficient due to a unit sideslip angle
$= \partial C_Y/\partial\beta$,
β = sideslip angle (in radians).

The derivatives here are evaluated at constant Mach number and constant angle of attack.

The components of the normalized instantaneous accelerations in the wind-axis system are calculated as follows (see Figure 3.3):

$$A_X = (T\cos(\alpha+\zeta)\cos\beta - C_D q S)/W, \tag{3.18a}$$

$$A_Y = (T\cos(\alpha+\zeta)\sin\beta + C_Y qS)/W, \tag{3.18b}$$

$$A_Z = (T\sin(\alpha+\zeta) + C_L qS)/W, \tag{3.18c}$$

where

W = the missile weight,
T = the thrust,
α = angle of attack in the pitch plane,
β = sideslip angle,
θ = missile pitch reference angle $= \alpha + \gamma$,
ψ = missile yaw reference angle $= \beta + \tau$,
γ = flight path angle in the vertical plane,
ζ = thrust inclination relative to the missile body axis in the pitch plane,
τ = flight path angle in the horizontal (X_E, Y_E) plane.

The instantaneous accelerations in the Earth-axis system (see Figure 3.3) are obtained through the following transformation [6]:

$$\frac{d^2X_E}{dt^2} = (A_X\cos\gamma\cos\tau - A_Y\sin\tau - A_Z\sin\gamma\cos\tau)g, \tag{3.19a}$$

$$\frac{d^2Y_E}{dt^2} = (A_X\cos\gamma\sin\tau + A_Y\cos\tau - A_Z\sin\gamma\sin\tau)g, \tag{3.19b}$$

$$\frac{d^2Z_E}{dt^2} = (1 - A_X\sin\gamma - A_Z\cos\gamma)g, \tag{3.19c}$$

where g is the gravitational acceleration and γ is the flight path angle in the vertical plane. Integration of (3.19a)–(3.19c) yield the velocities dX_E/dt, dY_E/dt, and dZ_E/dt. The velocities can then be integrated to obtain the missile position coordinates X_E, Y_E, and Z_E. The angle of attack (α) and sideslip (β) can be defined in terms of the velocity components as shown in Figure 3.3. Mathematically, the equations for these angles are given in the form

$$\alpha = \tan^{-1}(w/u), \tag{3.20a}$$

$$\beta = \sin^{-1}(v/V_M), \tag{3.20b}$$

where $V_M = (u^2 + v^2 + w^2)^{1/2}$. If the angle of attack and sideslip are small, say, $< 15°$, then (3.20a) and (3.20b) assume the simpler form

$$\alpha = w/u, \tag{3.21a}$$

$$\beta = v/u, \tag{3.21b}$$

where α and β are given in radians. Angle of attack and sideslip completely define the attitude of the vehicle with respect to the velocity vector. These angles can also be

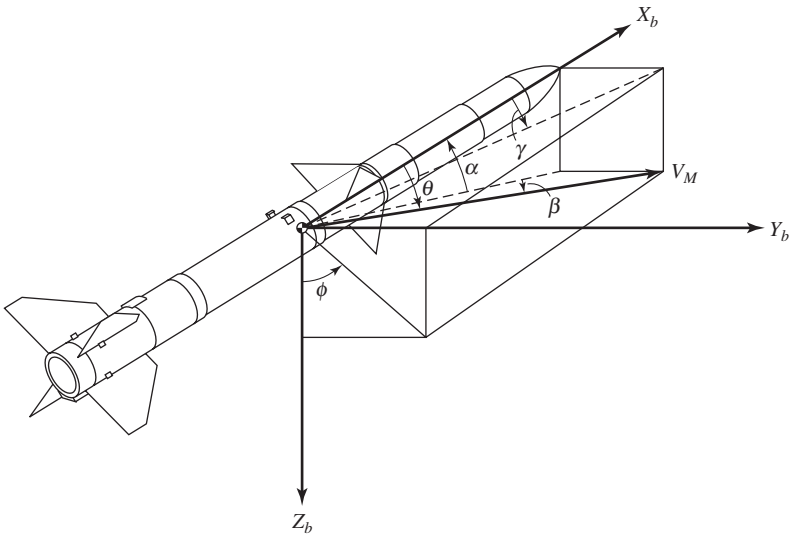

Fig. 3.5. Missile angular relationships.

expressed in terms of the other angles indicated in Figure 3.5 (see also Figure 2.1(b)) as follows:

$$\tan\alpha = \tan\theta\cos\phi, \tag{3.22a}$$

$$\tan\gamma = \tan\theta\sin\phi, \tag{3.22b}$$

$$\sin\beta = \sin\theta\sin\phi, \tag{3.22c}$$

$$\cos\theta = \cos\alpha\cos\beta = (\tan^2\alpha + \tan^2\beta)^{1/2}, \tag{3.22d}$$

$$\tan\phi = \cot\alpha\tan\gamma = \tan\beta/\sin\alpha. \tag{3.22e}$$

3.2 Aerodynamic Moment Representation

In a similar manner to the aerodynamic forces of the previous section, the moments on the missile can be divided into moments created by the aerodynamic load distribution and the thrust force not acting through the center of gravity. Specifically, the moment due to the resultant force acting at a distance from the origin may be divided into three components, referring to the missile's body reference axes. The three moment components are the *pitching moment*, the *rolling moment*, and the *yawing moment*. These moments will now be defined more closely:

Pitching Moment: The pitching moment is the moment about the missile's lateral axis (i.e., the Y_b-axis). The pitching moment is the result of the lift and the drag forces acting on the vehicle. A positive moment is in the nose-up direction.

Rolling Moment: This is the moment about the longitudinal axis of the missile (i.e., the X_b-axis). A rolling moment is often created by a differential lift, generated by some type of aileron. A positive rolling moment causes the right or starboard wingtip to move downward.

Yawing Moment: The moment about the vertical axis of the missile (i.e., the Z_b-axis) is the yawing moment. A positive yawing moment tends to rotate the nose to the right.

It should be pointed out here that the calculation of the aerodynamic forces and moments acting on a vehicle often requires that the engineer be able to relate data obtained at other flow conditions to the conditions of interest. For example, the engineer often uses data from the wind tunnel, where scale models are exposed to flow conditions that simulate the design environment or data from flight tests at other flow conditions. In order that one can correlate the data for various stream conditions and configuration scales, the measurements are usually presented in dimensionless form. The procedure used to nondimensionalize the moments created by the aerodynamic forces is similar to that used to nondimensionalize the lift. Thus, the components of the aerodynamic moment can be expressed in terms of dimensionless coefficients, flight dynamic pressure, reference area, and a characteristic length as follows [6]:

$$\textit{Rolling Moment}\,(L): \quad L = C_l q S l, \tag{3.23a}$$

$$\textit{Pitching Moment}\,(M): \quad M = C_m q S l, \tag{3.23b}$$

$$\textit{Yawing Moment}\,(N): \quad N = C_n q S l, \tag{3.23c}$$

where C_l, C_m, and C_n are the aerodynamic moment coefficients in roll, pitch, and yaw, respectively. Note that in missiles, the reference area S is usually taken as the maximum cross-sectional area, and the characteristic length l is taken as the mean diameter, whereas in aircraft [2], [6],

$$L = C_l q S b, \tag{3.24a}$$

$$M = C_m q S c, \tag{3.24b}$$

$$N = C_n q S b, \tag{3.24c}$$

where b is the wingspan, c is the aerodynamic chord, and S is the wing planform area used to nondimensionalize the aerodynamic forces. In general, and as stated earlier, the standard six-degree-of-freedom aerodynamic coefficients C_L, C_D, C_Y, C_l, C_m, and C_n are primarily a function of center-of-gravity location, altitude, *Mach* number, *Reynolds** number, angle of attack (α), and sideslip angle (β), and are secondary functions of the time rate of change of angle of attack and sideslip, and the angular velocity of the missile. (The pitching moment coefficient C_m is independent of the Reynolds number). We will now develop the aerodynamic moments and their associated coefficients in terms of measured quantities.

*The Reynolds number is a nondimensional number defined as $R = (\rho V l)/\mu = (V l)/\nu$, where ρ is the density of the fluid, μ is the coefficient of absolute viscosity of the fluid, v is the velocity, l is the characteristic length, and v is the kinematic viscosity ($\nu = \mu/\rho$).

(a) Aerodynamic Rolling Moment

We begin the development of the moments by noting that the rolling moment L is a function of α_p, α_y, and δ_a, where

α_p = angle of attack in the pitch plane; in the present development, the angle of attack will be taken to be the acute angle between the X_b-axis of the missile and the line of relative airflow or the missile velocity;
α_y = angle of attack in the yaw plane (this angle is identified as the *sideslip* β);
δ_a = deflection angle of the aileron (this angle controls the roll of the missile).

The moments L, M, and N can be linearized using the Maclaurin series for three-variable functions. The Maclaurin series is a type of Taylor series, and so a function in three variables can be approximated by the sum of the first three terms of the series. As a result, the rolling moment L can be approximated as follows:

$$L \cong [(\partial L/\partial \alpha_p)|_{\alpha_p=0}]\alpha_p + [(\partial L/\partial \alpha_y)|_{\alpha_y=0}]\alpha_y + [(\partial L/\partial \delta_a)|_{\delta_\alpha=0}]\delta_a = 0. \quad (3.25)$$

Let us now define the following coefficients:

$[(\partial L/\partial \alpha_p)|_{\alpha_p=0}] \equiv L_{\alpha_p}$ = the rate of change of the rolling moment due to a change in angle of attack in pitch,

$[(\partial L/\partial \alpha_y)|_{\alpha_y=0}] \equiv L_{\alpha_y}$ = the rate of change of the rolling moment due to a change in angle of attack in yaw,

$[(\partial L/\partial \alpha_y)|_{\delta_\alpha=0}] \equiv L_{\delta_\alpha}$ = the rate of change of the rolling moment due to a change in aileron deflection angle.

In order to simplify equations and calculations, the above coefficients can be non-dimensionalized so that they become *normalized* moments:

$L_{\alpha_p}/qSl_{ref} = C_{l_{\alpha_p}}$ = rolling moment coefficient due to angle of attack in pitch,
$L_{\alpha_y}/qSl_{ref} = C_{l_{\alpha_y}}$ = rolling moment coefficient due to angle of attack in yaw,
$L_{\delta_\alpha}/qSl_{ref} = C_{l_{\delta_\alpha}}$ = rolling moment coefficient due to aileron deflection angle,

where

q = free-stream dynamic pressure at a point far from the airfoil,
S = reference area, usually the area of one of the airfoils,
l_{ref} = reference length, usually the mean missile diameter from a body cross-section.

Figure 3.6 illustrates the angles under discussion.

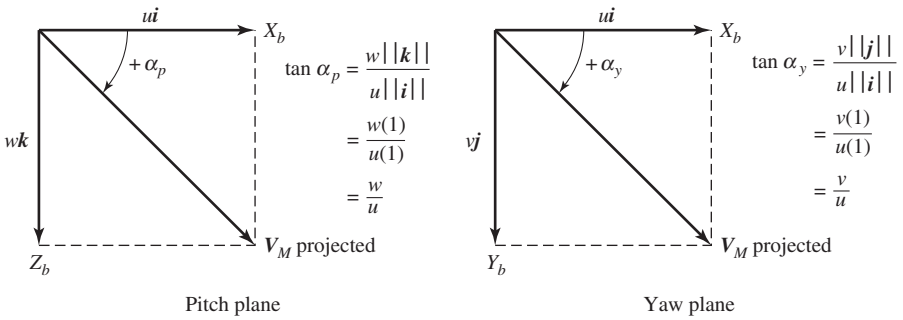

Fig. 3.6. Missile angle representation.

The rolling moment L can now be rewritten using the above-introduced coefficients and definitions:

$$\begin{aligned} L &= [(\partial L/\partial\alpha_p)|_{\alpha_p=0}]\alpha_p + [(\partial L/\partial\alpha_y)|_{\alpha_y=0}]\alpha_y + [(\partial L/\partial\delta_a)|_{\delta_\alpha=0}]\delta_a \\ &= (L_{\alpha_p})\alpha_p + (L_{\alpha_y})\alpha_y + (L_{\delta_\alpha})\delta_a \\ &= qSl_{ref}(C_{l_{\alpha_p}})\alpha_p + qSl_{ref}(C_{l_{\alpha_y}})\alpha_y + qSl_{ref}(C_{l_{\delta_\alpha}})\alpha_p \\ &= qSl_{ref}[(C_{l_{\alpha_p}})\alpha_p + (C_{l_{\alpha_y}})\alpha_y + (C_{l_{\delta_\alpha}})\delta_a]. \end{aligned} \tag{3.26}$$

Solving (2.29a) for dP/dt, we can now write the rotational acceleration equation for roll in the form

$$\frac{dP}{dt} = QR[(I_y - I_z)/I_x] + (qSl_{ref}/I_x)[(C_{l_{\alpha_p}})\alpha_p + (C_{l_{\alpha_y}})\alpha_y + (C_{l_{\delta_\alpha}})\delta_\alpha]. \tag{3.27}$$

Before we proceed with the derivation of the aerodynamic pitching and yawing moments, it will be necessary to develop the nondimensionalized *aerodynamic normal force coefficients*, as well as the nondimensionalized pitching and yawing moment coefficients. We begin by noting that when an inclined surface moves through the air, there is a force perpendicular to that surface, caused by the deflecting stream. This force is called the aerodynamic normal force, and is normal (perpendicular) to the X_b-body axis. Now let us define the following quantities:

F_Y = component of the aerodynamic normal force (*side*) along the Y_b-body axis, being positive from the origin in the direction of the negative Y_b-axis,

F_N = component of the aerodynamic normal force (*normal*) along the Z_b-body axis, positive from the origin in the direction of the negative Z_b-axis.

These two components of the aerodynamic normal force can be non-dimensionalized as follows:

$$C_Y = F_Y/qS, \tag{3.28a}$$

$$C_N = F_N/qS, \tag{3.28b}$$

where C_Y is called the *lateral force coefficient*, and C_N is called the *normal force coefficient*. The components C_Y and C_N are usually defined as positive for positive angles of attack and zero control surface deflection (see Figure 3.7). These aerodynamic normal force coefficients are extremely nonlinear and usually cannot be accurately linearized, as could the rolling moment coefficient. The aerodynamic normal force coefficients are functions of *Mach* number (M), α_p or α_y, and δ_p or δ_y, and are commonly written in the form

$$C_Y(M, \alpha_y, \delta_y),$$
$$C_N(M, \alpha_p, \delta_p),$$

where δ_p is the control surface deflection in pitch, and δ_y is the control surface deflection in yaw.

(b) Aerodynamic Pitching Moment

The aerodynamic pitching moment M is a function of the pitch rate Q as well as α_p and δ_p. Define now the components of the pitching moment as

$$M = M_o + M_q, \tag{3.29}$$

where

M_o = moment contribution from the *AOA* (angle of attack) in pitch (α_p) and pitch control surface deflection (δ_p),

M_q = pitching moment rate.

These two components are commonly described in the following manner:

$$M_o = C_m q S l_{ref}, \tag{3.30a}$$

$$M_q = (C_M Q q S (l_{ref})^2)/2V_M, \tag{3.30b}$$

where

C_m = pitching moment coefficient, which is a function of Mach number, α_p, and δ_p,

C_M = coefficient of moment due to pitch rate, or rate of change of pitching moment,

V_M = total velocity of the missile.

(c) Aerodynamic Yawing Moment

The aerodynamic yawing moment N is a function of yaw rate R as well as α_y and δ_y. Now, define the components of the yawing moment as follows:

$$N = N_o + N_r, \tag{3.31}$$

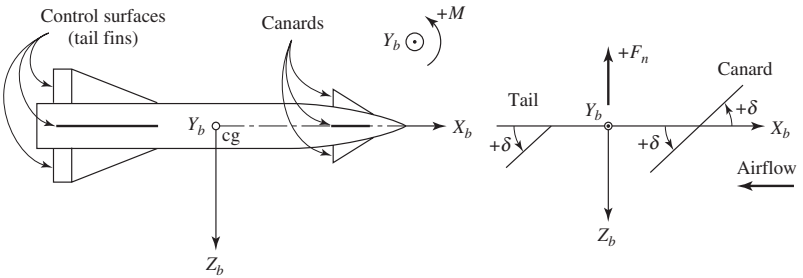

δ = Positive deflection of control surface, measured with respect to X_b-axis; positive for anti-clockwise sense of rotation about the hinge looking into the Y_b-axis towards the missile body.

Tail - Positive deflection as shown is producing:
1) *Negative Pitching Moment* (Ð*M*) about the cg.
2) *Positive Normal Force* (+F_N).

Canard - Positive deflection as shown producing:
1) *Positive Pitching Moment* (+*M*) about the cg.
2) *Positive Normal force* (+F_N).

(a) *X-Z* (pitch) plane.

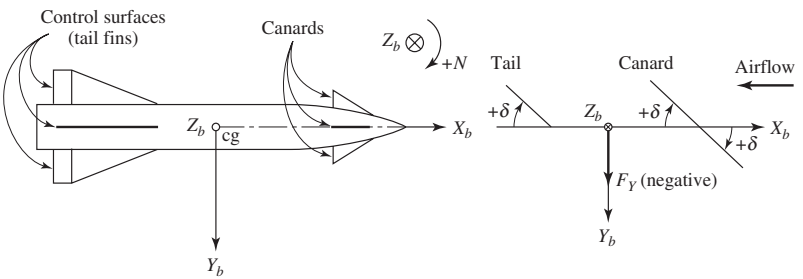

δ = Positive for clockwise sense of rotation about the hinge looking down the Y_b-axis away from the missile body.

Tail - Positive deflection as shown is producing:
1) *Negative Yawing Moment* (Ð*N*) about the cg.
2) *Negative Lateral Force* (ÐF_Y).

Canard - Positive deflection as shown producing:
1) *Positive Yawing Moment* (+*N*) about the cg.
2) *Negative Lateral force* (ÐF_Y).

(b) *X-Y* (yaw) plane.

Fig. 3.7. Control surface deflections.

where

N_o = the moment contribution from the *AOA* in yaw (α_y) and yaw plane control surface deflection (δ_y),

N_r = yawing moment rate.

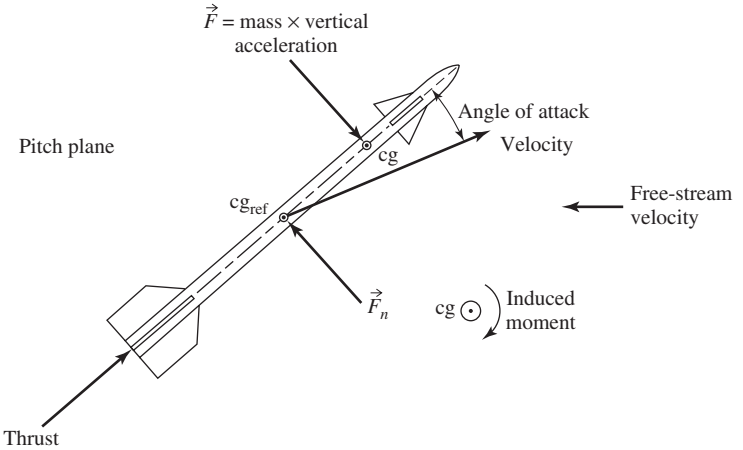

Fig. 3.8. Forces acting on a missile in the pitch plane.

These two components are usually described in the following manner:

$$N_o = C_n q S l_{ref}, \tag{3.32a}$$

$$N_r = (C_N R q S (l_{ref})^2)/2V_M, \tag{3.32b}$$

where

C_n = yawing moment coefficient, which is a function of Mach number, α_y, and δ_y,

C_N = coefficient of moment due to yaw rate.

In missiles, the center of gravity (cg) normally shifts due to the burning off of fuel. Consequently, a new moment is produced. Therefore, M_o and N_o are evaluated at a reference center of gravity at launch. Also, the actual center of gravity moves when the missile begins to move. However, the referenced center of gravity remains in the original position. Thus, applying this concept of a referenced center of gravity, the moment contributions due to the movement of the actual center of gravity can be evaluated. A simple free-body diagram that shows the forces and moments acting on the missile in the pitch plane is illustrated in Figure 3.8.

When the moment coefficients are evaluated, the vector normal force $\mathbf{F}_N$ is assumed to act through the referenced center of gravity (cg_{ref}). Moreover, the missile vertical acceleration vector ($\mathbf{F}/m$) acts through the same point, which corresponds to the momentary center of gravity at launch. As the real center of gravity moves, the acceleration vector stays at the same location, but an additional moment arises due to the motion of the center of gravity. Since the force is taken to be applied through the reference center of gravity, the induced moment is clockwise about the actual center of gravity, is negative, and is equal to

$$(-)M_{cg} = F_N(d_{cg-ref} - d_{cg}), \tag{3.33}$$

where M_{cg} is the moment of $\mathbf{F}_N$ about the actual center of gravity and $(d_{cg-ref} - d_{cg})$ is the distance between the actual center of gravity and cg (note that d is usually measured from the nose of the missile). Equation (3.33) can also be written in the form

$$M_{cg} = F_N(d_{cg} - d_{cg-ref}) = C_N q S(d_{cg} - d_{cg-ref}). \tag{3.34}$$

It should be pointed out that the force $\mathbf{F}$ would produce no moment about the center of gravity, since it acts through that point. An induced moment will similarly be produced in the yaw plane with $\mathbf{F}_Y$ and lateral acceleration. A positive aerodynamic force will produce a positive moment:

$$N_{cg} = F_Y(d_{cg-ref} - d_{cg}), \tag{3.35a}$$

or

$$N_{cg} = -F_Y(d_{cg} - d_{cg}) = -C_Y q S(d_{cg} - d_{cg-ref}). \tag{3.35b}$$

The above equations for the pitching moment and yawing moment must be rewritten in order to include the change in the center of gravity position. Thus,

$$\begin{aligned} \textit{PitchingMoment}: &\quad M = M_o + M_q + M_{cg}, \\ \textit{YawingMoment}: &\quad N = N_o + N_r + N_{cg}. \end{aligned}$$

From these expressions, we can now obtain the pitching moment (M) and yawing moment (N) by substitution as follows:

$$\begin{aligned} M &= C_m q S l_{ref} + C_M Q q S(l_{ref})^2)/2V_M + C_N q S(d_{cg} - d_{cg-ref}) \\ &= q S l_{ref}\{C_m + C_M((Q l_{ref})/2V_M) + C_M[(d_{cg} - d_{cg-ref})/l_{ref}]\}, \end{aligned} \tag{3.36}$$

$$\begin{aligned} N &= C_n q S l_{ref} + C_N R q S(l_{ref})^2/2V_M - C_Y q S(d_{cg} - d_{cg-ref}) \\ &= q S l_{ref}\{C_n + C_N((R l_{ref})/2V_M) - C_Y[(d_{cg} - d_{cg-ref})/l_{ref}]\}. \end{aligned} \tag{3.37}$$

Substituting (3.25) and (3.26) into (2.30b) and (2.30c), we obtain

$$\begin{aligned} \frac{dQ}{dt} &= ((I_z - I_x)/I_y)PR + (q S l_{ref}/I_{yy})\{C_M + C_N((d_{cg} - d_{cg-ref})/l_{ref}) \\ &\quad + C_M(Q l_{ref}/2V_M)\} \end{aligned} \tag{3.38}$$

$$\begin{aligned} \frac{dR}{dt} &= ((I_x - I_y)/I_z)PQ + (q S l_{ref}/I_{yy})\{C_N - C_Y((d_{cg} - d_{cg-ref})/l_{ref}) \\ &\quad + C_N(R l_{ref}/2V_M)\}. \end{aligned} \tag{3.39}$$

Equations (3.38) and (3.39) are the rotational accelerations for pitch and yaw, respectively. The following definitions from second-order differential equations should also be noted:

$$\begin{aligned} \textit{PitchDampingMoment}: &\quad C_M = \partial C_M/\partial(Q l_{ref}/2V_M), \\ \textit{YawDampingMoment}: &\quad C_N = \partial C_N/\partial(R l_{ref}/2V_M). \end{aligned}$$

These damping moments are important to the missile designer, in that they are necessary to keep the missile from oscillating. The rotational rates P, Q, and R can be obtained by integrating the equations for dP/dt, dQ/dt, and dR/dt. Thus,

$$\textit{Roll Rate: } P = \int_0^t \left(\frac{dP}{dt}\right) dt, \tag{3.40a}$$

$$\textit{Pitch Rate: } Q = \int_0^t \left(\frac{dQ}{dt}\right) dt, \tag{3.40b}$$

$$\textit{Yaw Rate: } R = \int_0^t \left(\frac{dR}{dt}\right) dt. \tag{3.40c}$$

In terms of the Euler angles ϕ (roll), θ(pitch), and ψ(yaw), the rotational rates P, Q, and R (assuming that the missile X_b-axis is along the longitudinal axis, the Y_b-axis out to the right, and the Z_b-axis down) can be expressed in the form [1]

$$P = \frac{d\phi}{dt} - \left(\frac{d\psi}{dt}\right) \sin\theta, \tag{3.41d}$$

$$Q = \left(\frac{d\theta}{dt}\right) \cos\phi + \left(\frac{d\psi}{dt}\right) \cos\theta \sin\phi, \tag{3.41e}$$

$$R = \left(\frac{d\psi}{dt}\right) \cos\theta \cos\phi - \left(\frac{d\theta}{dt}\right) \sin\phi, \tag{3.41f}$$

or in matrix form,

$$\begin{bmatrix} P \\ Q \\ R \end{bmatrix} = \begin{bmatrix} 1 & 0 & -\sin\theta \\ 0 & \cos\phi & \cos\theta \sin\phi \\ 0 & -\sin\phi & \cos\theta \cos\phi \end{bmatrix} \begin{bmatrix} \dot{\phi} \\ \dot{\theta} \\ \dot{\psi} \end{bmatrix}.$$

(d) Derivation of the Translation Equations (X_b-Body Axis)

The translational equations of motion can be derived from (2.11). Therefore, rearranging (2.11), we have

$$\frac{du}{dt} = Rv - Qw + (F_x/m), \tag{3.42a}$$

$$\frac{dv}{dt} = Pw - Ru + (F_y/m), \tag{3.42b}$$

$$\frac{dw}{dt} = Qu - Pv + (F_z/m). \tag{3.42c}$$

Next, we must determine the forces acting along each of the body axes. Assume now that a flat surface moves through a mass of air at some angle of attack. Friction acting between the mass of air and the inclined surface, resulting in a force that tends to move

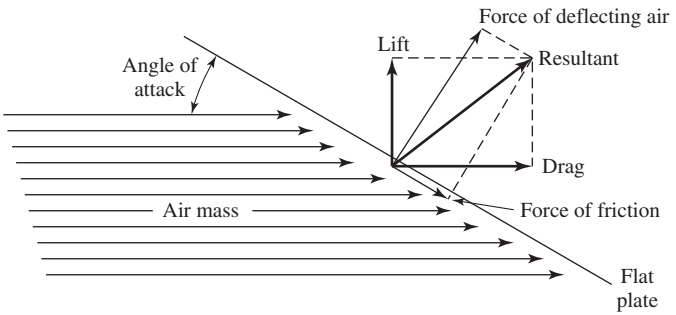

Fig. 3.9. Forces acting on a missile airfoil.

the surface parallel to itself. There is also a force perpendicular to the surface, caused by the pressure difference across the plate. These combined forces give a resultant force backward in the direction of the moving air mass. Resolving this resultant force into components, we have one force with its vector perpendicular to the moving mass of air, called the *lift*, and another force parallel to the mass of air, called the *drag*. Figure 3.9 illustrates these forces.

This figure refers to one panel of the missile airfoil.* However, the concept can be extended to illustrate the effects on a full airfoil. At each panel there is a pressure force acting normal to the panel and a friction force acting parallel to the panel. By summing these forces and taking the component parallel to the velocity vector and component perpendicular to the velocity vector, the lift and drag can be obtained. Drag acts along the total velocity vector, but the largest component is along the X_b-axis. The X_b-component of drag is referred to as the *axial force* F_A, and as is customary in aerodynamics, this force is described in terms of a nondimensionalized coefficient C_A. Thus,

$$F_A = qSC_A, \tag{3.43}$$

where C_A is the axial force coefficient, which is a function of Mach number, δ_p, δ_y, and altitude (with respect to the earth) of the missile body. The other primary force acting along the X_b-body axis is the thrust. Thrust is defined as the forward force produced by the propulsion system to sustain the aircraft in flight. Sometimes, thrust is expressed in the same manner as drag and other aerodynamic forces. However, it is not usually convenient to do so, since the thrust is often constant or is some unknown function of altitude, whereas the other aerodynamic forces are not. Typically, a missile has two modes of thrusting: (1) the boost phase, and (2) the sustain phase (a boost–sustain mode is also used. See Sections 3.3.1 and 4.5 (Table 4.5)). The boost phase is the first stage of missile flight. During this phase, the missile is propelled from rest to slightly supersonic speeds by a high-powered rocket engine. The sustain phase is the

*An airfoil is a streamlined body that when set at a suitable angle of attack, produces more lift than drag.

second stage of missile propulsion, which begins when the missile is traveling close to the speed of sound (i.e., Mach 1). The missile booster is an auxiliary propulsion system that imparts thrust to the missile during the initial phase of flight. It generally consists of a solid rocket motor and an attaching device. A solid rocket motor is best suited for this purpose because of its simple construction and operation and its ability to develop a high thrust in a short time. The missile sustainer, on the other hand, is usually a ramjet engine, which allows a greater missile range than would a rocket engine. Often, the booster and sustainer burn simultaneously for a short time prior to jettison of the booster, in order to ensure a reasonably smooth transition to the sustain phase.

Prior to the sustain phase, the missile sustainer is open, allowing airflow that will exert a negative thrust (i.e., an axial drag force of $(-C_A q S)$, since $F_A = C_A q S$). Typically, the total thrust is expressed as

$$T = T_{\text{boost}} + T_{\text{sust}}, \tag{3.44}$$

where T is the total thrust, T_{boost} is the thrust from the booster, and T_{sust} is the thrust from the sustainer. The remaining force acting along the X_b-axis of the missile is the X-component of weight due to gravity. Referring to Figure 3.10, we note that the missile body and inertial Earth axes will show that the weight component of the missile along the X_b-axis is

$$x_{mg} = mg \sin\theta, \tag{3.45}$$

where

x_{mg} = weight component along the X_b-axis,

z_{mg} = weight component along the Z_b-axis,

g = acceleration due to gravity,

θ = angle between the body axes and Earth axes (pitch angle), defined as positive for the counterclockwise sense of rotation in the $X - Z$ plane.

Summing all the force components along the X_b-axis, we have

$$\begin{aligned} F_x &= T_{\text{boost}} + T_{\text{sust}} - x_{mg} - F_A \\ &= T_{\text{boost}} + T_{\text{sust}} - mg \sin\theta - C_A q S. \end{aligned} \tag{3.46}$$

(e) Derivation of Translation Equations (Y_b-Body Axis)

The forces acting along the Y_b-body axis of a missile consist of the Y_b-components of weight and aerodynamic normal force. Recall that the Y_b-component of the aerodynamic normal force is

$$F_Y = C_Y q S.$$

Figure 3.11 illustrates the weight component of the missile along the Y_b-axis in three dimensions with respect to the missile-body axes and inertial Earth axes.

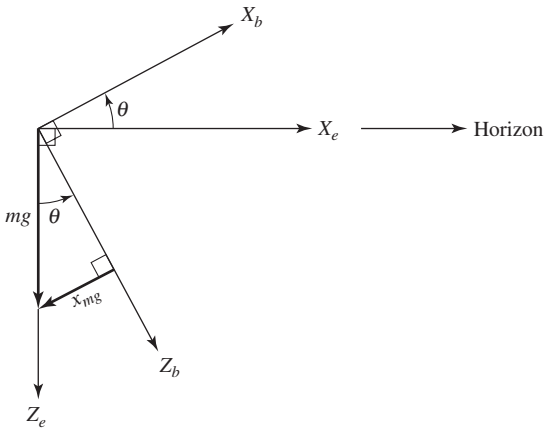

Fig. 3.10. Missile body and Earth-fixed axes.

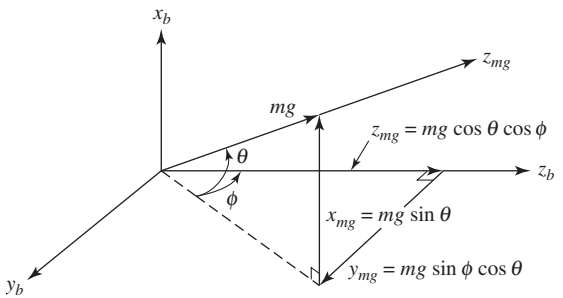

Fig. 3.11. Three-dimensional view of the missile weight components.

The weight component of the missile along the Y_b-axis is

$$y_{mg} = mg \sin\phi \cos\theta, \tag{3.47}$$

where

$$y_{mg} = \text{weight component along the } Y_b\text{-axis},$$

ϕ = angle between the projection of the weight vector onto the $Y_b - Z_b$ plane and the Z_b-axis; this is the roll angle and is defined to be positive for the counterclockwise sense of rotation in the $Y_b - Z_b$.

Note that the weight vector is directed along the Z_E-axis. If we project this vector onto the $Y_b - Z_b$ plane by dropping a perpendicular, we obtain the vector $mg \cos\theta$. Next, we drop a perpendicular from this vector onto the Z_b-axis, thus obtaining the Z_b-component of the weight:

$$z_{mg} = mg \cos\theta \cos\phi. \tag{3.48}$$

The third side of this vector triangle is parallel to the Y_b-axis, and so is the Y_b-component of the weight. This vector is positive because of its orientation with respect to the Y_b-axis. Now we can sum the force components along the Y_b-axis:

$$F_y = y_{mg} - F_Y = mg \sin\phi \cos\theta - C_Y qS. \tag{3.49}$$

(f) Derivation of Translation Equations (Z_b-Body Axis)

The forces acting along the Z_b-body axis of a missile consist of the Z_b-component of weight and the Z_b-component of the aerodynamic normal force. We have noted earlier that the Z_b-component of the aerodynamic normal force is

$$F_N = C_N qS$$

and that the Z_b-component of the weight is

$$z_{mg} = mg \cos\phi \cos\theta.$$

Summing the force components along the Z_b-axis, we have

$$F_z = z_{mg} - F_N = mg \cos\phi \cos\theta - C_N qS. \tag{3.50}$$

Substituting the above results into (3.42) results in the following equations:

$$\frac{du}{dt} = Rv - Qw + (F_x/m) = Rv - Qw + [(T_{\text{boost}} - T_{\text{sust}})/m] - g\sin\theta - (C_A qS/m), \tag{3.51a}$$

$$\frac{dv}{dt} = Pw - Ru + (F_y/m) = Pw - Ru + g\cos\theta \sin\phi - (C_Y qS/m), \tag{3.51b}$$

$$\frac{dw}{dt} = Qu - Pv + (F_z/m) = Qu - Pv + g\cos\phi\cos\theta - (C_N qS/m). \tag{3.51c}$$

Finally, in order to obtain the translational velocity components u, v, and w, (3.51) must be integrated. Thus,

Longitudinal Component of Velocity

$$u = \int_0^t \left(\frac{du}{dt}\right) dt. \tag{3.52a}$$

Lateral Component of Velocity

$$v = \int_0^t \left(\frac{dv}{dt}\right) dt. \tag{3.52b}$$

Vertical Component of Velocity

$$w = \int_0^t \left(\frac{dw}{dt}\right) dt. \tag{3.52c}$$

We will now summarize the translational and rotational equations of motion of a missile in terms of the body axes:

Translation Equations

(1) Longitudinal Acceleration

$$\frac{du}{dt} = Rv - Qw + (T_{\text{boost}} - T_{\text{sust}})/m - g\sin\theta - (C_A q S)/m. \tag{3.53a}$$

(2) Lateral Acceleration

$$\frac{dv}{dt} = Pw - Ru + g\cos\theta\sin\phi - (C_Y q S)/m. \tag{3.53b}$$

(3) Vertical Acceleration

$$\frac{dw}{dt} = Qu - Pv + g\cos\theta\cos\phi - (C_N q S)/m. \tag{3.53c}$$

Rotation Equations

(4) Roll Acceleration

$$\frac{dP}{dt} = (q S l_{ref}/I_x)[C_L(\delta_a) + C_L(\alpha_p) + C_L(\alpha_y)] + QR[(I_y - I_z)/I_x]. \tag{3.53d}$$

(5) Pitch Acceleration

$$\begin{aligned}\frac{dQ}{dt} &= (q S l_{ref}/I_y)[C_M + C_N((d_{cg} - d_{cg-ref})/l_{ref}) + C_M(Q l_{ref}/2V_M)] \\ &\quad + PR[(I_z - I_x)/I_y].\end{aligned} \tag{3.53e}$$

(6) Yaw Acceleration

$$\begin{aligned}\frac{dR}{dt} &= (q S l_{ref}/I_z)[C_N - C_Y((d_{cg} - d_{cg-ref})/l_{ref}) + C_N(R l_{ref}/2V_M)] \\ &\quad + PQ[(I_x - I_y)/I_z].\end{aligned} \tag{3.53f}$$

Example 1. In Section 2.1, the transformation matrix from the Earth to body axes was developed. Consider now the free-flight dynamic model of a missile. The mathematical model describing the missile motion consists of six rigid-body degrees of freedom (i.e., three body inertial position coordinates and three Euler-angle body attitudes). In this example, we will use the Earth's surface (or ground) as the inertial reference frame. The body frame is defined in the conventional manner, and the dynamic equations are written with respect to this coordinate system [9]. The missile's translation and rotation kinematic and dynamic equations are given by

$$\begin{bmatrix}\dot{x}\\ \dot{y}\\ \dot{z}\end{bmatrix} = \begin{bmatrix} c_\theta c_\psi & s_\phi s_\theta c_\psi - c_\phi s_\psi & c_\phi s_\theta c_\psi + s_\phi s_\psi \\ c_\theta s_\psi & s_\phi s_\theta s_\psi + c_\phi c_\psi & c_\phi s_\theta s_\psi - s_\phi c_\psi \\ -s_\theta & s_\phi c_\theta & c_\phi c_\theta \end{bmatrix} \begin{bmatrix} u \\ v \\ w \end{bmatrix}, \tag{1}$$

$$\begin{bmatrix} \dot{\phi} \\ \dot{\theta} \\ \dot{\psi} \end{bmatrix} = \begin{bmatrix} 1 & s_\phi t_\theta & c_\phi t_\theta \\ 0 & c_\theta & -s_\phi \\ 0 & s_\phi / c_\theta & c_\phi / c_\theta \end{bmatrix} \begin{bmatrix} P \\ Q \\ R \end{bmatrix}, \tag{2}$$

$$\begin{bmatrix} \dot{u} \\ \dot{v} \\ \dot{w} \end{bmatrix} = \begin{bmatrix} X/m \\ Y/m \\ Z/m \end{bmatrix} - \begin{bmatrix} 0 & -R & Q \\ R & 0 & -P \\ -Q & P & 0 \end{bmatrix} \begin{bmatrix} u \\ v \\ w \end{bmatrix}, \tag{3}$$

$$\begin{bmatrix} \dot{P} \\ \dot{Q} \\ \dot{R} \end{bmatrix} = [I]^{-1} \left[\begin{bmatrix} L \\ M \\ N \end{bmatrix} - \begin{bmatrix} 0 & -R & Q \\ R & 0 & -P \\ -Q & P & 0 \end{bmatrix} [I] \begin{bmatrix} P \\ Q \\ R \end{bmatrix} \right], \tag{4}$$

where

c = cos,
s = sin,
t = tan,
m = mass of the missile,
L = rolling moment,
M = pitching moment,
N = yawing moment,
P = roll rate,
Q = pitch rate,
R = yaw rate,
ϕ = roll angle,
θ = pitch angle,
ψ = yaw angle,
u, v, w = components of velocity of the center of mass relative to the atmosphere.

The total applied force is composed of the weight W and body aerodynamic force A terms. The weight portion of the external loads is given by

$$\begin{bmatrix} X_W \\ Y_W \\ Z_W \end{bmatrix} = mg \begin{bmatrix} -s_\theta \\ s_\phi c_\theta \\ c_\phi c_\theta \end{bmatrix}, \tag{5}$$

where g is the gravitational acceleration. The aerodynamic force contribution is given by

$$\begin{bmatrix} X_A \\ Y_A \\ Z_A \end{bmatrix} = -q_\alpha \begin{bmatrix} C_{XO} + (\alpha^2 + \beta^2) \\ C_{NA}\beta \\ C_{NA}\alpha \end{bmatrix}, \tag{6}$$

where

$$\alpha = \tan^{-1}(w/v),\ -\pi \leq \alpha \leq \pi, \tag{7a}$$

$$\beta = \tan^{-1}(v/u),\ -\pi \leq \alpha \leq \pi, \tag{7b}$$

$$q_a = \tfrac{1}{8}\rho(u^2 + v^2 + w^2)\pi D^2, \tag{8}$$

where D is the drag. The right-hand side of the rotation kinematic equations contains the externally applied moments. Note that the external moment components contain contributions from steady and unsteady body aerodynamics. The steady-body aerodynamic moment is computed by a cross product between the distance vector from the center of gravity to the center of pressure and the steady-body aerodynamic force vector given above. As in the case of the aerodynamic coefficients, the center of pressure location is dependent on the local Mach number and is computed by linear interpolation.

In Section 3.1 we discussed briefly the role of the airfoil. The airfoil used in modern airplanes has a profile of the "fish" type, as illustrated in Figure 3.1. Such an airfoil has a blunt *leading edge* and a sharp *trailing edge*. The projection of the profile on the double tangent, as shown in the diagram, is the *chord*. The ratio of the span to the chord is the *aspect ratio*. The *camber line* of a profile is the locus of the point midway between the points in which an ordinate perpendicular to the chord meets the profile. The *camber* is the ratio of the maximum ordinate of the camber line to the chord. From the theory of the flow around such an airfoil, the following assumptions apply:

(1) That the air behaves as an *incompressible* inviscid fluid (see also Section 2.2).
(2) That the airfoil is a cylinder whose cross-section is a curve of the above type.
(3) That the flow is two-dimensional irrotational cyclic motion.

The above assumptions are, of course, only approximations to the actual state of affairs, but by making these simplifications, it is possible to arrive at a general understanding of the principles involved.

3.2.1 Airframe Characteristics and Criteria

In this section we will examine the general airframe features and stability from the point of view of the guidance designer. Commonly, the airframe is symmetrically cruciform, with four fixed wings and four movable control surfaces. The cruciform configuration permits lateral maneuvering in any direction without first rolling (i.e., banking to turn, as required of an airplane). In a wing-controlled airframe with movable wings slightly forward of the center of gravity (cg) and fixed stabilizing tail surfaces, variable downwash from the control surfaces impinges on the fixed surfaces and may induce undesirable roll moments, etc. On the other hand, in this type of airframe, the normal force on the control surface is in the direction of the desired maneuver, so that this feature aids the overall response of the guidance system.

• Wing control (e.g., Sparrow III AIM-7F):

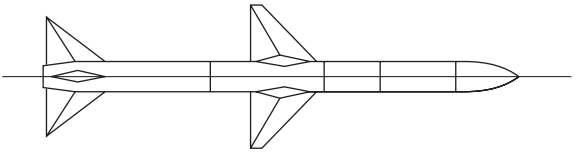

• Tail control (e.g., Phoenix AIM-54A):

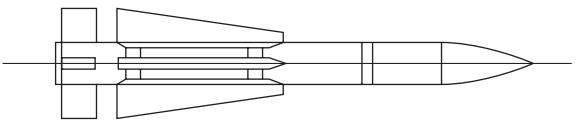

• Canard* (e.g., Sidewinder AIM-9):

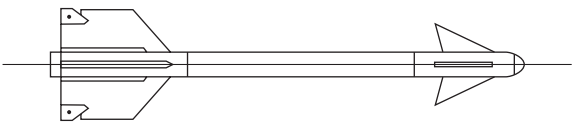

Fig. 3.12. Airframe types.

Similar generalities hold true for a canard airframe with control surfaces far forward of the cg. There are three typical types of airframes used in aerodynamically guided missiles (or munitions). Figure 3.12 illustrates these types.

Each of these types has its own advantages and disadvantages, and the missile system designer must exploit these advantages and disadvantages for the given threat and operating environment. Also, the selected airframe must be able to deliver the required aerodynamic performance (see also Section 3.3.1).

From Figure 3.12, we note that the typical *Sparrow* missile uses wing control with tail fins for stability and aerodynamics. The *Phoenix* (or *Falcon*) missile uses tail control, via fins with fixed wings. The typical *Sidewinder* uses fixed tail wings, with movable nose fins (or canards). We note here that the type and size of airframe is strongly dependent on the guidance characteristics, motor size, and warhead size. It should be noted that situations do arise, however, in which some of these choices are dictated: for example, to use a motor existing in the inventory, or to use an existing airframe. Since typically these items were designed for some other threat, and with other system considerations, the system design problem focuses on obtaining the most out of these designs.

The present discussion will be restricted to the tail-controlled configuration, which has no downwash interference from the control surfaces. If the autopilot pitch and yaw axes are each 45° from the planes of adjacent control surfaces, then all four

*Canards are forward control surfaces, placed far forward of the center of gravity. An advantage of using canards is that the downwash from canards onto the main lifting body can, in certain configurations, nullify any attempt to control the missile in roll.

control surfaces are deflected equally by the pitch (or yaw) autopilot. However, in some applications it is preferable to put the autopilot axes in the planes of the control surfaces, so that only two surfaces are deflected by the pitch autopilot and two by the yaw autopilot. It is apparent that the tail-controlled airframe has a tail normal force opposite to the direction of the desired maneuver acceleration, which causes a small initial airframe acceleration in the wrong direction. Analytically, this effect manifests as a right-half-plane zero in the transfer function from the control surface deflection, δ, to a lateral (i.e., normal to the missile's longitudinal axis) acceleration a_n at the missile cg, thus tending to limit the speed of response of the guidance system. However, it is very desirable to have the roll autopilot command all four surfaces, so that the induced roll moments from "shadowing" of the control surfaces at high angles of attack will be minimized. In most cases, the control surfaces exert only aerodynamic forces, although it is possible to augment these at high altitudes by reaction jets embedded in the control surfaces.

In Section 3.2 the various forces and moments acting on a missile were developed. In this section, we will discuss the stability conditions in terms of the airframe dynamics. Specifically, in an aerodynamically maneuvering missile, the function of the control surfaces is to exert a moment so that the missile can develop an angle of attack (*AOA*), and thereby achieve lift from the body and wings (if any). (Note that in some applications, a wingless airframe relying only on body-lift is preferred.) As will be discussed further in the autopilot section, the pitching of the airframe causes the seeker to develop a spurious component of the measured line-of-sight (*LOS*) angular rate $d\lambda/dt$, which results in a *parasitic attitude loop.** An important measure of the necessary pitching of the airframe is the *alpha over gamma dot* $(\alpha/\dot{\gamma})$ time constant, τ, of the linearized airframe response, defined by the following relation:

$$\tau = \alpha/\dot{\gamma} = \frac{2M}{\rho V_m S}\left[\frac{\dfrac{\partial C_m}{\partial \delta}}{\dfrac{\partial C_L}{\partial \alpha}\left(\dfrac{\partial C_m}{\partial \delta}\right) - \dfrac{\partial C_L}{\partial \delta}\left(\dfrac{\partial C_m}{\partial \alpha}\right)}\right],$$

where

M = mass of the missile,
V_m = missile speed,
S = missile reference area,
α = angle of attack,
γ = flight path angle,
ρ = air (or atmospheric) density,

*A parasitic attitude loop is defined as a control loop that interferes with the guidance stability, resulting in a larger miss distance.

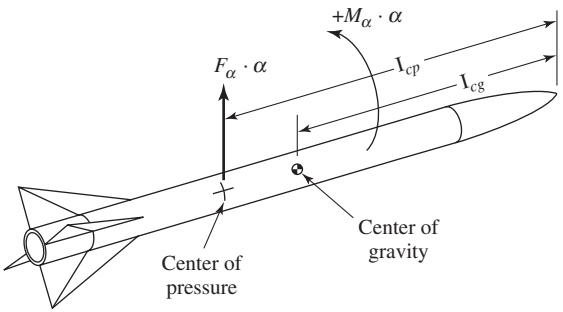

(a) Stable condition: $M_\alpha < 0$

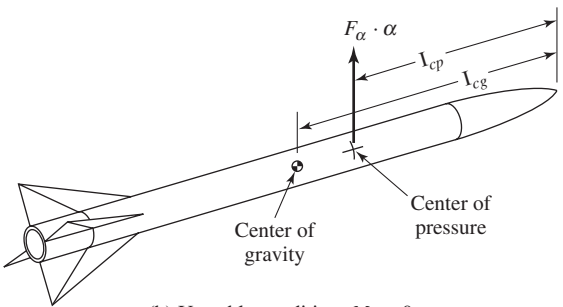

(b) Unstable condition: $M_\alpha > 0$

$$M_\alpha = \frac{F_\alpha(I_{cg} - I_{cp})}{I_{pitch}} = \frac{qSdC_{m_\alpha}}{I_{pitch}}$$

(d = diameter ot the missile)

Fig. 3.13. Aerodynamic missile stability conditions.

and the aerodynamic derivatives are conventionally defined. Here, it is assumed that thrust and drag are negligible. The $(\alpha/\dot{\gamma})$ term in the above equation is the angle of attack required to achieve a given flight path rate, and therefore represents the gimbal angle change in achieving a given missile maneuver. At high altitudes, it is necessary for the airframe to have a relatively large angle of attack in order to develop 1 g of lateral acceleration. The ratio $\alpha/\dot{\gamma}$ can be reduced, if it becomes large, by using movable wings near the cg, so that very little body pitching is required to develop lateral acceleration. However, a practical difficulty with this scheme is that the body cg moves appreciably as the booster (and sustainer, if used) motor burns.

Based on the discussion of this section, the stability condition for an aerodynamic missile is illustrated in Figure 3.13 (see also Sections 3.1 and 3.3.2 for a discussion of the center of pressure (cp)).

The quantity M_α is a measure of responsiveness of the airframe to pitch-moment changes with alpha. A small positive M_α and slightly unstable airframe can be tolerated, but a highly negative M_α is preferable for stability of the autopilot and attitude loop. It appears that a zero or slightly negative M_α (fairly stable airframe) is the best total compromise that the guidance designer could ask for. In words, the conditions

depicted in Figure 3.13 can be stated as follows: (a) If the center of pressure (cp) is ahead of the center of gravity (cg), the missile is said to be statically unstable; (b) if the cp is behind the cg, the missile is said to be statically stable; and (c) if the cp and cg coincide, then the missile is said to be neutrally stable. Note that the distance between the cp and cg is called the "static margin." A summary of some of the important airframe characteristics is given below:

$$\begin{aligned} G_{pr} &= \text{pitch rate } \theta_m / \text{surface angle } \delta \\ &= K_{pr}(1+\tau s)/(1+b_{11}s+b_{12}s^2) \\ &\cong M_\delta[1+(1/s)]/[s^2+(b_{11}/b_{12})s-M_\alpha], \end{aligned}$$

$$M_\delta = \frac{1}{2}\rho V_m^2 \frac{Sd}{I_{yy}} C_{m_\delta}|_{cg},$$

$$M_\alpha = \frac{1}{2}\rho V_m^2 \frac{Sd}{I_{yy}} C_{m_\alpha}|_{cg} \quad \begin{matrix} \text{Stable if } M_\alpha < 0, \\ \text{Unstable if } M_\alpha > 0, \end{matrix}$$

$$\tau = \alpha/\dot{\gamma}|_{s.s},$$

$$\begin{aligned} G_{la} &= \text{lateral accel. } n_l / \text{surface angle } \delta \\ &= K_{la}(1+a_{11}s+a_{12}s^2)/(1+b_{11}s+b_{12}s^2) \end{aligned}$$

$$K_\delta = \frac{1}{2}\rho V_m^2 \frac{Sd}{I_{xx}} C_{l_{\delta_a}},$$

$$\frac{M_\delta}{K_\delta} = \frac{I_{xx}}{I_{yy}} \frac{C_{m_\delta}}{C_{l_\delta}}\bigg|_{cg},$$

where

$$\begin{aligned} M_\delta &= \text{Surface pitch effectiveness}, \\ K_\delta &= \text{Surface roll effectiveness}, \\ s.s &= \text{steady-state (subscript)}. \end{aligned}$$

Note that instabilities can be eliminated by means of a suitable feedback control system. Finally, it is noted that the majority of tactical missiles have fixed main lifting surfaces (often called wings) with their cp somewhere near the missile cg, and rear control surfaces. In subsonic missiles, it may be more efficient to use control surfaces as flaps immediately behind the wings, since the flaps control the circulation over the entire surface. In supersonic flow, the control surface cannot affect the flow ahead of itself, and therefore it is placed as far to the rear as possible in order to exert the maximum moment on the missile. Rear control surfaces often make for a convenient placement and/or arrangement of components [2].

For those readers interested in aerodynamics, it should be mentioned that an experimental flexible-wing jet made its first flight in November 2002, from *NASA*'s Dryden Flight Research Center at Edwards AFB, California. During an hour-long

test, the modified *F/A-18* took off, climbed to 30,000 ft., and flew over a test range northeast of Edwards AFB. The first flight followed a three-year period of modification and ground tests at the *NASA* facility. Officials from AF Research Laboratory, Boeing's Phantom Works, and *NASA* Dryden collaborated on the research effort, called the Active Aeroelastic Wing (*AAW*) program. The project intends to demonstrate improved aircraft roll control through aerodynamically induced wing twist on a full-scale manned supersonic aircraft. The new wing technology is important to the AF because it represents a new approach to designing wings that are more, structurally and aerodynamically from a control effectiveness standpoint. With *AAW*, leading and trailing edge control surfaces are deflected, which causes a change in the aerodynamic pressure distribution on the wing's surface, causing it to warp or twist. The surfaces are deflected such that the wing twists into a shape that helps the wing perform better than it would if it did not twist at all.

Moreover, *AAW* is applicable to a wide variety of future air vehicle concepts that are under study and not only to supersonic flight. While the technology was conceived during a supersonic fighter aircraft design study, aircraft that fly subsonically can also experience a high degree of wing deformation, and therefore could benefit from the *AAW* design approach. Since *AAW* exploits wing flexibility, it also is viewed as a first step toward future "morphing" wings that can sense their environment and adapt their shape to perform optimally in a wide range of flight conditions.

The test-bed aircraft was modified with additional actuators, a split leading edge flap actuation system, and thinner skins on a portion of the upper wing surface that will allow the outer wing panels to twist up to 5°. With the first flight completed, the modified aircraft will undergo 30 to 40 flights over a three to four month period. *NASA* expects the second phase of the research flights with new control software to begin in mid to late 2003.

Example 2. In this example we will apply the most important results of Sections 3.1 and 3.2. Consider an air-to-air missile represented in Figure 3.14.

The problem will be formulated as follows:

Missile Dynamics

$$\frac{du}{dt} = \{[-C(\alpha, M, h, t) + T(t)]/m(t)\} - qw, \tag{1}$$

$$\frac{dw}{dt} = \{-N(\alpha, M, \delta_z)/m(t)\} + qu, \tag{2}$$

$$\frac{dq}{dt} = \left\{[M_y(\alpha, M, \delta_z, X_{cg} - X_{cp}, t] - q\left(\frac{dI_y(t)}{dt}\right)\right\}/I_y(t), \tag{3}$$

where

u = longitudinal velocity component,
C = axial force,
M = Mach number = V_m/V_s,
V_m = missile speed,
V_s = speed of sound,
α = angle of attack = $\tan^{-1}(u/w)$,

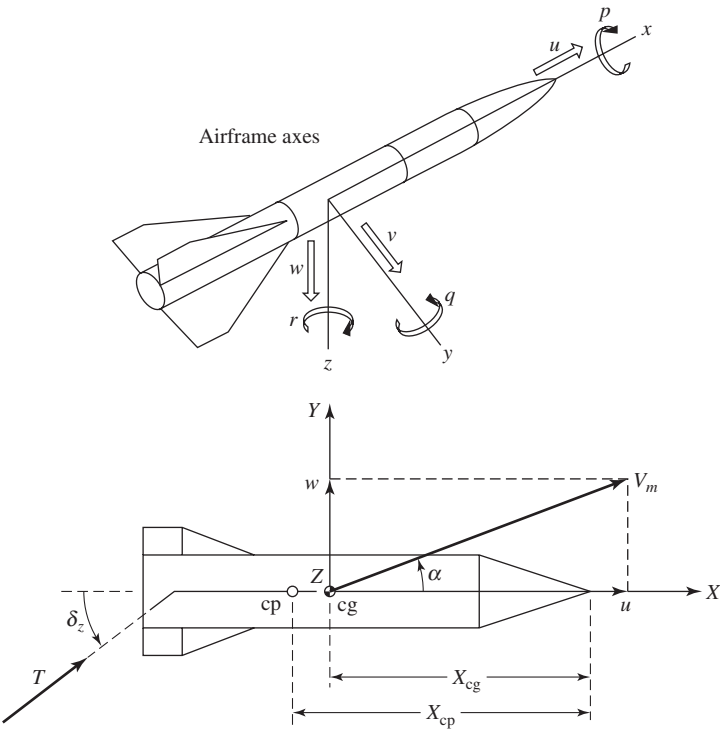

Fig. 3.14. Representation of the missile in the local reference frame *XYZ*.

h = flight altitude,
t = time,
m = mass of missile,
w = normal velocity component,
q = pitch rate,
T = rocket motor thrust,
N = normal force (yawing moment),
δ_z = thrust deflection (or tail fin) angle,
M = pitching moment,
X_{cg}, X_{cp} = center of gravity and center of aerodynamic pressure, respectively,
I_y = missile's moment of inertia about the Y-axis.

The aerodynamic forces with respect to the local reference frame XYZ are as follows:

Axial Force

$$C = \tilde{q} C_c(\alpha, M, h, t), \tag{4}$$

$$C_c = F_{fr}(M)\{[(h - 6.096)/3.048] + F_{afc}(\alpha, M) + F_b(M, t)[1 - (A_e/A_b)]. \quad (5)$$

Normal Force

$$N = \tilde{q} C_n(\alpha, M, \delta_z), \quad (6)$$

$$C_n = F_{nfc}(\alpha, M)\alpha - F_{tnf}(M)\delta_z, \quad (7)$$

where

F_{nfc} = normal force coefficient,
F_{tnf} = trim normal force effectiveness,
F_b = base drag coefficient,
F_{fr} = friction drag coefficient,
F_{afc} = axial force coefficient.

Aerodynamic Couple

$$M_y = \tilde{q} L_r C_m(\alpha, M, \delta_z, q, t), \quad (8)$$

$$C_m = C_{ma}\alpha + C_{m\delta z}\delta_z + C_{mq} q, \quad (9)$$

$$C_{m\alpha} = F_{nfc}(\alpha, M)\{[X_{cg}(t) - X_{cp}(\alpha, M)]/L_r\}, \quad (10)$$

$$C_{m\delta z} = F_{tpm}(M) - F_{tnf}(M)\{[X_{cg}(t) - X_{cgb}]/L_r\}, \quad (11)$$

$$C_{mq} = -F_{pdm}(M)]500 L_r / V_m, \quad (12)$$

where

$\tilde{q}$ = dynamic force = $S_r \hat{q}$,
S_r = reference area,
$\hat{q}$ = dynamic pressure = $\frac{1}{2}\rho_o(h) V_m^2$,
ρ_o = volumic air mass,
A_b = base area,
A_e = nozzle exit area,
L_r = reference length,
X_{cgb} = center of gravity location at burnout.

The aerodynamic forces as given in the above equations are functions of aerodynamic coefficients, which depend on the angle of attack α and on the Mach number M. Values of these coefficients for various α and M are available in tabular form, which are obtained from wind tunnel experiments [2], [8]. Note also that numerical values for $\rho_o(h)$, V_s, $T(t)$, and $X_{cp}(t)$ are tabulated along with the analytical expressions of the functions $m(t)$, $X_{cg}(t)$, and $I_y(t)$.

3.3 System Design and Missile Mathematical Model

3.3.1 System Design

In general, a missile can be defined as an aerospace vehicle with varying guidance capabilities that is self-propelled through space for the purpose of inflicting damage on a designated target (see also Chapter 1). These vehicles are fabricated for air-to-air, surface-to-air, or surface-to-surface roles. They contain a propulsion system, warhead section, guidance systems, and control surfaces, although hypervelocity missiles do not use warheads or control surfaces. The guidance capabilities of the different missiles vary from self-guided to complete dependence on the launch equipment for guidance signals.

Specifically, a guided missile is typically divided into four subsystems: (1) the airframe, (2) guidance, (3) motor (or propulsion), and (4) warhead. These subsystems will now be examined in more detail:

1. **Airframe:** The type and size of airframe is strongly dependent on guidance characteristics, motor size, and warhead size (see also Section 3.2.1).
2. **Guidance:** The type of guidance that can be used is also dependent on the motor, warhead, and threat. More specifically, the type of guidance chosen is dependent on the overall weapon system in which the missile will be used, on the type of threat the missile will be used against, the characteristics of the threat target, and other factors. Guidance, as we have seen earlier, is the means by which a missile steers or is steered to a target.
3. **Motor:** The motor characteristics are dependent on guidance requirements, the threat, and the airframe characteristics.
4. **Warhead:** The warhead is dependent on the threat and type of guidance. Commonly, the procedure is to size the guidance requirements (e.g., accuracy, response time, range capability) from the threat, select an airframe that can deliver the required aerodynamic performance, size the motor based on threat and airframe considerations, and size the warhead from guidance and airframe considerations.

Figure 3.15 illustrates the above missile characteristics for an aerodynamic air-to-air missile.

In addition to the above considerations, there are other basic factors that affect the design of any weapon system. These are (1) the threat, (2) the operating environment, (3) cost, and (4) state of the art. Typically, the threat and operating environment are known or are given. Also, the state of the art is known. Therefore, the design effort of any missile centers on meeting the threat in the environment with the state of the art, at minimum cost. Consequently, three of these four factors are specified, with the fourth being either minimized (i.e., cost, state of the art) or maximized.

In Section 3.2 the boost and sustain motor thrusting methods were discussed. However, in certain applications, missiles are designed to be of the boost–sustain type. Consequently, a major consideration in any missile design is the motor (or propulsion system) type selection. The important factors in selecting a motor type are (1) aerodynamic heating due to the incremental missile velocity, (2) aerodynamic drag, which decreases missile velocity, (3) maximum altitude at which the missile

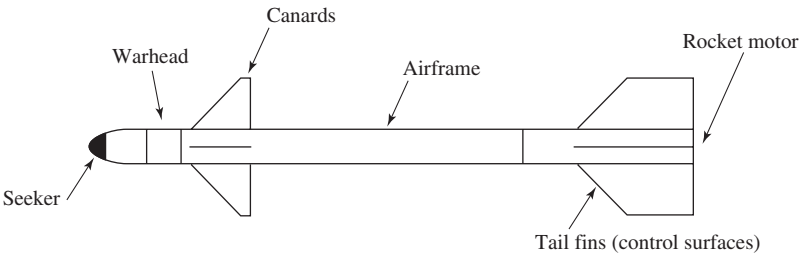

1 Radome
2 Planar array active radar antenna
3 Proximity fuze antenna (one of four spaced at 90°)
4 Warhead
5 Fuzing unit
6 Fixed wings
7 Umbilical connector
8 Moving control fins
9 Nozzle
10 Rear detection antenna
11 Hydraulic power unit
12 Autopilot
13 Electric converter
14 Rocket motor
15 Guidance section

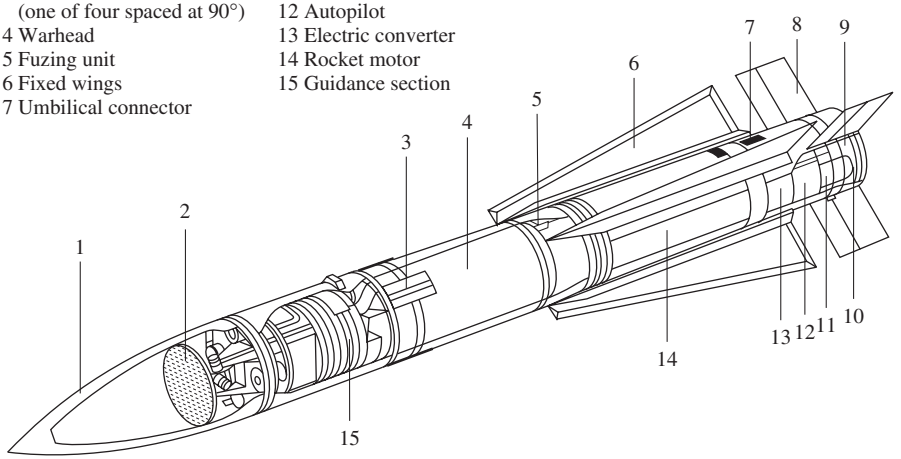

Fig. 3.15. Basic weapon construction.

must perform, and (4) maximum and minimum intercept ranges required. For the reader's convenience, these missile motor types are summarized below:

All-Boost: An all-boost motor typically will make the missile accelerate rapidly, causing high peak velocities. However, this causes high missile drag, high aerodynamic heating, and short time of flight, for a given range. This motor is suitable for a rear hemisphere, tail chase encounter.

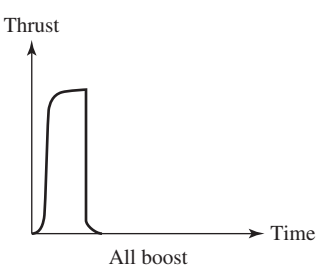

All-Sustain: The all-sustain motor has low missile acceleration, resulting in lower aerodynamic drag and longer time of flight, for a given range. Since the motor burns for a long period of time, the motor can be used to overcome gravity in a look-up engagement, and to provide sufficient velocity for maneuvering at high altitude. This motor is suitable for head-on engagements, or in look-up engagements at high altitudes.

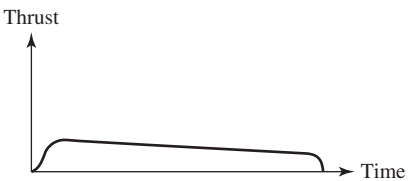

All sustain

Boost–Sustain: The boost–sustain motor represents an attempt to combine the best features of the all-boost and the all-sustain designs.

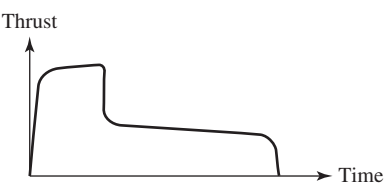

Boost sustain

The warhead is typically an input to the system design. Since almost all warheads for missiles are *GFE* (government furnished equipment), we see that the role of the system designer is to design a system to deliver a given warhead to a given point in space, within a given accuracy, and to fuze it at the appropriate time.

The threat typically describes what the target can do, in terms of performance, which translates into what the missile has to do, in terms of performance. These important threat factors are:

1. The rate of closure: This is the combination of interceptor velocity and target velocity.
2. Engagement altitude: This is the altitude regime over which the target can be expected.
3. The engagement range: This is the limit over which the missile can be launched.

All of these factors reflect missile requirements or constraints.

In addition to solid and/or liquid fuel missile engines (or motor), there is another class, namely the *ramjet*. The ramjet is the simplest (in terms of moving parts) of all air-breathing engines, in which the compression is produced by the *ram*, or forward velocity pressure in the intake; combustion downstream of the intake thus gives the high-velocity jet. Thus, the ram effect can be defined as the pressure increase obtained in an air-breathing engine intake by virtue of its forward motion.

Ramjet propulsion is a key ingredient of new antiradar missile technology. With a Mach 3 or more capability, ram rocket propulsion will have increased range and reduced time to target. Research is also being conducted into the so-called *scramjet* engines. These engines would have the power to hurtle through the air at Mach 6 or more. The engines initially will be installed in cruise missiles, making them hypersonic, meaning that they move faster than five times the speed of sound, and more deadly. Cruise missiles, which are launched from aircraft, now travel slower than the speed of sound. The scramjet engine should enable cruise missiles to strike targets such as transportable Scud missile launchers or fixed targets that must be taken out quickly. It also could be used to hit deeply buried targets. A 1996 study conducted at Maxwell Air Force Base in Alabama showed that hypersonic cruise missiles could have a range of more than 1,000 miles, allowing the aircraft from which they are launched to stay out of harm's way.

Unlike conventional jet engines, the scramjet does not require rotating fans and compressors. Instead, it relies on the forward motion of the vehicle to compress the air. Once inside the engine, the air mixes with the injected fuel and is burned. The hot gas exits the rear of the engine and provides thrust by pushing against a nozzle-like surface. The biggest hurdle for researchers is dealing with the high speed of the wind as it enters the engine. The main issue is to get the fuel and the air mixed well enough so that fuel and air can burn in the very limited time available.

A European development of a new beyond-visual-range air-to-air missile (*BVRAAM*) would employ a Mach 3 ram-rocket propulsion system for increased range and reduced time to target. The ram-rocket motor would feature four inlets in the center of the missile body and high boron content in the sustainer propellant for high specific impulse with low volume. After being boosted to the required operating speed, the air-breathing ramjet sustainer would take over for the rest of the flight, mixing fuel-rich gas from a boron gas generator. The Raytheon Company also is offering a next-generation version of the *AIM-120 AMRAAM*, dubbed the future medium-range air-to-air missile (*FMRAAM*). Raytheon's *FMRAAM* design employs a liquid fuel ramjet developed by Aerospatiale Missiles. Still another European concept is to employ a solid fuel, variable flow ducted ramjet developed by Germany's DASA subsidiary Bayern-Chemie. The Russian *Kh-31*, which has an active or passive *RF* seeker for antiship or antiradiation missions; is one of the few operational ramjet missiles; it flies at Mach 2.7 while sea-skimming. The Defense Advanced Research Projects Agency's (*DARPA*) Affordable Rapid Response Missile Demonstration (*ARRMD*) is examining two different concepts: one from the Air Force's HyTech program and the other from the Office of Naval Research's Hypersonic Weapon Technology Program. The Aerojet Corporation, which builds the dual combustion ramjet (*DCR*), proposes

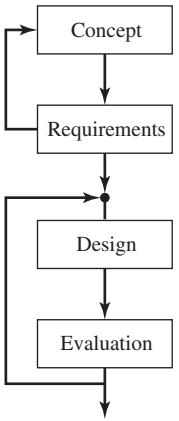

Fig. 3.16. Missile development phases.

a central subsonic ramjet combustor that feeds fuel-rich exhaust into the surrounding supersonic scramjet stream, where combustion is completed. Before we leave this topic, it should be pointed out that there is another type of propellant, namely, the *hypergolic** propellant. This is a rocket propellant that ignites spontaneously upon contact with an oxidizer.

In the development of missile systems, a broad spectrum of engineering disciplines is employed with primary emphasis placed on the guidance and control subsystems. A comprehensive systems-oriented approach is applied throughout the system development. Specifically, there are four basic phases in the development of a missile. These are:

1. Concept formulation and/or definition;
2. Requirements;
3. Design;
4. Evaluation.

In diagram form, these four phases are shown in Figure 3.16.

Consequently, the development cycle for a missile system commences with the concept formulation, where one or more guidance methods are postulated and examined for feasibility and compatibility with the total system objectives and constraints. Surviving candidates are compared quantitatively and a baseline concept adopted. Specific subsystem and component requirements are generated via extensive tradeoff and parametric studies. In particular, such factors as missile capability (e.g., acceleration and response time), sensor function (e.g., tracking, illumination), accuracy (i.e,

Hypergolic is a coined word, the element *golic* being obtained from a German code word *Gols*, used to refer to a series of rocket propellants containing methylaniline, organic amine, and certain other compounds.

SNR and waveforms), and weapons control (e.g., fire control logic, guidance software) are established by means of both analytical and simulation techniques. After iteration of the concept/requirements phases, the analytical design is initiated. The guidance law is refined and detailed, a missile autopilot and the accompanying control actuator are designed, and an onboard sensor tracking and stabilization system devised. This design phase entails the extensive use of feedback control theory and the analysis of nonlinear, nonstationary dynamic systems subjected to deterministic and random inputs. Determination of the sources of error and their propagation through the system are of fundamental importance in setting design specifications and achieving a well-balanced design. Finally, overall evaluation is conducted using numerous simulation techniques and test facilities to verify the design, predict performance, define zones of effectiveness, and analyze post-flight results.

As stated above, classical servomechanism theory has been used extensively to design both hydraulic and electric seeker servos that are compatible with requirements for gyro-stabilization and fast response. Pitch, yaw, and roll autopilots have been designed to meet problems of Mach variation, altitude variation, induced roll moments, instrumentation lags, body-bending modes, guidance response, and stability. Although classical theory presently is most applicable to autopilots and airframe stability, research efforts are continually made to apply modern control and estimation theory to conventional as well as adaptive autopilot design. Modern advanced guidance and control systems having superior performance have been designed with on-line Kalman filter estimation for filtering noisy radar data and with optimal control gains expressed in closed form. Synthesis of sampled data homing and command guidance systems are being used extensively today. For example, a vital point in the development of advanced homing guidance and control systems is to optimize the performance of the missile under design for various intercept situations and target maneuvers. Furthermore, trends in operational requirements indicate that future air-to-air or air-to ground missiles will have to have a high probability of kill under total sphere launch engagement conditions and a launch and leave capability (such as the *AGM-154* Joint Standoff Weapon (*JSOW*)) when employed against a wide variety of highly maneuverable intelligent targets. In order to satisfy these requirements, future air-to-air missiles will require complex guidance algorithms. Additionally, in order to implement these complex guidance algorithms, more information about the missile and target dynamic states will have to be accurately measured or estimated on board the missile. The very nature of this problem lends itself to the use of modern control theory to derive the advanced guidance laws and modern estimation theory to develop techniques to process the available information and estimate the unavailable information. The key to a successful problem formulation is a translation of the mission requirements into a mathematical performance index (P.I.). No matter what theoretical techniques are used to develop the optimal control strategy, they will always be based on the minimization (or maximization) of some performance index. Hence, the optimal control strategy will be no better than our selection of the critical performance drivers and our translation of these into concise mathematical terms. In addition to the performance index, two other formulations will impact the optimal control strategy, namely, the mathematical model of the system and the additional

equality and inequality constraints to be placed on the system. In general, a more detailed system model results in a more accurate control strategy, but this is achieved at the expense of additional complexity in both the derivation and resulting algorithms. The selection of appropriate equality/inequality constraints can be based upon either actual system parameters or trajectory properties that we want the optimal solution to possess. Some of the modern control techniques that have been investigated and/or applied are (1) reachable set theory, (2) singular perturbation theory, (3) differential game theory, and (4) adaptive control theory.

The performance index (also known as cost functional) study is a fundamental but extremely complex problem. To be sure, the mission objectives influence the choice of the parameters/states that are included in the performance index. However, there are many other factors that must be considered in the construction of the performance index. These additional factors are due to the interrelationships of the steps involved in the modern control problem formulation. Specifically, for every different performance index or cost functional there is a different optimal guidance law. In essence, the measure of performance for any guidance law will be the ability of the missile to hit the target (e.g., minimum terminal miss distance) in various engagement scenarios. Additional measures of performance involve (1) launch envelope (full 360° launch aspect angle, minimum inner launch boundary), (2) fuel considerations, (3) time considerations, and (4) maneuver capability.

3.3.2 The Missile Mathematical Model

Guided tactical missiles are sometimes referred to according to their airspeed relative to the speed of sound and their type of propulsion system. Generally, the highest rate of airspeed that can be reached safely and still ensure correct operation is considered as that missile's classification. In essence, the general means of classification of a missile's airspeed is related to the speed of sound (or *Mach 1*), which varies with respect to the ambient temperature. Commonly, there are four groups that are considered in classifying a particular missile. These are:

1. **Subsonic:** Airspeeds less than *Mach 1*.
2. **Sonic:** Airspeeds equal to *Mach 1*.
3. **Supersonic:** Airspeeds ranging between *Mach 1 and Mach 5*.
4. **Hypersonic:** Airspeeds exceeding *Mach 5*.

Practically all *AIM* and *SAM* missiles can be placed in the supersonic classification, since modern military aircraft are capable of attaining *Mach 1* speed.

A commonly used missile mathematical model in the analysis and design of surface-to-air and air-to-air weapon systems is the *skid-to-turn* (*STT*) missile, in which both the pitch and yaw plane systems have identical response behavior. As discussed in Section 3.1, the main reason for using the skid-to-turn design is that the inertial cross coupling between roll, pitch, and yaw is negligible. For this reason, we will assume that our missile mathematical model is of the skid-to-turn type. However, as noted earlier, in this technique both aerodynamics (the aerodynamics cannot be described in closed form, but are available in look-up table form) and rigid-body dynamics are highly

Table 3.2. Comparison of Weapon System Characteristics

Feature	Sparrow-type weapon	Bank-to-turn weapon
Guidance Mode	Skid-to-Turn	Bank-to-Turn
Control Surfaces	Wing Control	Tail Control
Autopilot Sensors	Accelerometers/Rate Gyros	Accelerometers/Rate Gyros
Maximum Acceleration	45g's (32 g's per axis)	100 g's in pitch, 10 g's in yaw
Guidance Delay	0.75 seconds	0.40 seconds
Launch Speed	0.5–2.0 Mach	0.5–2.0 Mach
Speed Range	0.5–3.0 Mach	0.5–4.0 Mach
Maximum Roll Rate	Not Applicable	$\pm 600^\circ$/sec

nonlinear (see Chapter 2). The highly nonlinear aerodynamic effects occur at high Mach numbers. Also, the skid-to-turn missile will experience difficulty when attacking high-g targets. The *Sparrow* weapon is a skid-to-turn type missile. At this point it should be mentioned that another missile configuration is the *bank-to-turn* (*BTT*) type.

This configuration is suitable for highly maneuverable ramjet missiles. However, the asymmetrical airframe of this missile design requires rolling the missile to maintain target motion in the missile pitch plane. Another drawback of this design is that the bank angle causes a coupling between the pitch and yaw channel dynamics, which can vary considerably even for a short period of time. Table 3.2 summarizes the skid-to-turn and bank-to-turn missile characteristics.

Specifically, the pitch/yaw plane rotational responses behave like a spring–mass damper system. Mathematically, this system response can be expressed in the form

$$\frac{d^2y}{dt^2} + 2\zeta\omega\left(\frac{dy}{dt}\right) + \omega^2 y = \omega^2 u(t). \tag{3.54}$$

Equation (3.54) can also be written in the usual frequency domain as follows:

$$y(s)/u(s) = \omega^2/(s^2 + 2\zeta\omega s + \omega^2), \tag{3.55}$$

where

$$\begin{aligned} y(s) &= \text{output},\\ u(s) &= \text{input},\\ \zeta &= \text{damping ratio (dimensionless)},\\ \omega &= \text{frequency (rad/sec)},\\ s &= \text{Laplace operator (rad/sec)}. \end{aligned}$$

The above continuous system can be constructed in a simulation as a feedback network that represents a load factor command system in both pitch/yaw planes (see also Section 3.5). Figure 3.17 represents a typical pitch/yaw network.

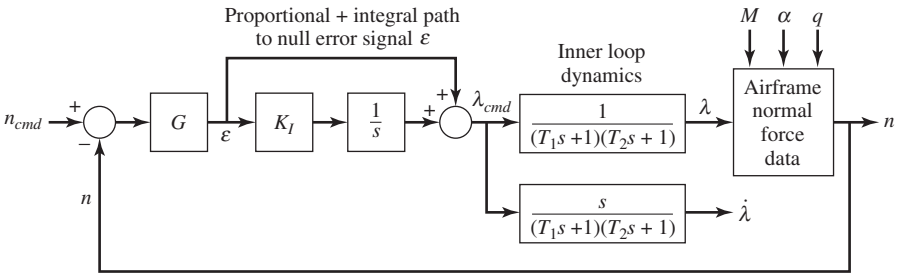

Fig. 3.17. Pitch-yaw feedback network.

Let us now digress for a moment and return to (3.1). In (3.1) the drag was given simply as a function of the coefficient of drag, dynamic pressure, and reference area. However, drag is a nonlinear function of velocity. For the purposes of control design, drag can be modeled by the parabolic drag form

$$D = qSC_D + (KL^2)/qS, \tag{3.56}$$

where K is defined as in (3.15b). In the present analysis, we will consider lift as the control. Lift is chosen subject to the constraint

$$L \leq Wg_m(v), \tag{3.57}$$

where W is the weight and $g_m(v)$ represents the load factor limit, which may arise due to a structural limit, control surface actuator, or autopilot stability considerations. In general, lift is a function of missile speed. From the above discussion, the load factor is simply expressed by the equation

$$g_m(v) = \eta = L/W = \tfrac{1}{2}\rho V^2 SC_L/W. \tag{3.58}$$

The dynamics for the angle of attack (AOA), α, as well as $d\alpha/dt$, load factor n_z, and pitch rate, are commonly modeled after the short-period approximations of longitudinal motion. The short-period approximation for the angle of attack is given by the following transfer function:

$$\frac{\alpha(S)}{\alpha_{\text{cmd}}(s)} = \frac{\omega^2(T_\alpha s + 1)}{s^2 + 2\zeta\omega s + \omega^2}, \tag{3.59a}$$

where

$$\begin{aligned} T_\alpha &= AOA \text{ time constant (sec)},\\ \zeta &= \text{short-period damping ratio}\\ &\quad\ \text{(dimensionless)},\\ \omega &= \text{short-period frequency (rad/sec)},\\ s &= \text{Laplace transform operator (rad/sec)}. \end{aligned}$$

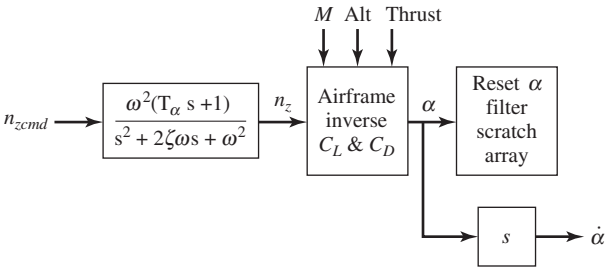

Fig. 3.18. Load factor command system.

This transfer function is expressed in the frequency domain and represents the lower-order equivalent system of the full closed-loop system. We note that the load factor and angle-of-attack transfer functions are identical in form. Specifically, the dynamics for the load factor in the pitch plane, n_z, can be modeled by the following transfer function:

$$\frac{n_z(s)}{n_{\text{zcmd}}(s)} = \frac{\omega^2(T_\alpha s+1)}{s^2+2\zeta\omega s+\omega^2}, \tag{3.59b}$$

where

$$\begin{aligned} n_{zc} &= \text{commanded load factor in the pitch plane,} \\ T_\alpha &= AOA \text{ time constant (sec),} \end{aligned}$$

and ω, ζ, and s are defined as in (3.59a). The parameters ω, ζ, and T_α can be found by linear analysis of the entire closed-loop system. The above transfer function is valid, provided that the load factor being modeled is located at the center of pressure (cp), that is, the point ahead of the center of gravity (cg) where the effect of pitch acceleration and horizontal tail force cancel. Moreover, load factor measured at the center of pressure will reflect forces mostly due to angle of attack, which is why it has the same transfer function form. This assumption eliminates having to deal with a pair of complex second-order zeros in the numerator for an n_z accelerometer located away from the cp. Figure 3.18 illustrates the load factor command system.

We have seen that in terms of the continuous system (3.55), a feedback network for the purposes of simulation that represents the load factor command system in both the pitch/yaw planes was shown in Figure 3.17. The load factor control system can be reduced to have an identical response to that of (3.55) with $y = n$ and $u = n_{\text{cmd}}$. Specifically, this is done by properly computing the inner-loop parameters. This can be done by linearizing the airframe normal forces in the pitch and yaw planes to obtain the slopes $n_{z\alpha}$ and $n_{y\beta}$. Since both the pitch and yaw use the same aerodynamic data, let $n_{y\beta} = -n_{z\alpha}$ or $n_{z\alpha} = n_\lambda$, where λ is either α or β (the sideslip angle). Then compute the slope at each frame. The linearization of the feedback network (see Figure 3.17), reduces to that shown in Figure 3.19.

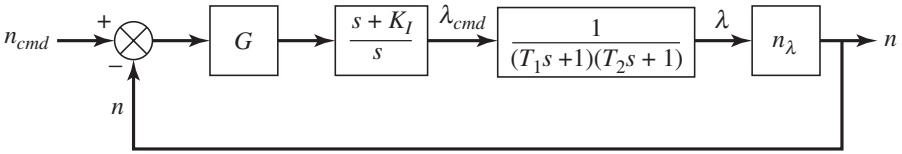

Fig. 3.19. Linearized load factor control system.

In Figure 3.19, K_I is an integrator gain and G is a gain whose function is to force the response of the reduced-order system to behave like the original system. Note that this system is identical to that of a digital aircraft yaw axis system.

Using the methods of classical feedback control theory, the inner-loop parameters are as follows:

$$\frac{1}{T_1} = \frac{2\zeta\omega + K_1}{2} + \frac{1}{2}\sqrt{4\zeta^2\omega^2 - 4\zeta\omega K_1 + K_1^2}, \tag{3.60a}$$

$$\frac{1}{T_2} = \frac{2\zeta\omega + K_1}{2} - \frac{1}{2}\sqrt{4\zeta^2\omega^2 - 4\zeta\omega K_1 + K_1^2}, \tag{3.60b}$$

$$G = \frac{\omega^2 T_1 T_2}{n_\lambda}, \tag{3.60c}$$

$$K_1 = 2\zeta\omega. \tag{3.60d}$$

Next, we need the expressions for ζ and ω. In order to solve for these two parameters, we first write the second-order differential equation for the angle-of-attack response at launch with a forcing function of order 0. Thus,

$$\frac{d^2\alpha}{dt^2} + 2\zeta\omega\left(\frac{d\alpha}{dt}\right) + \omega^2\alpha = 0. \tag{3.61}$$

It is well known that the response in α for this system will be a damped oscillatory motion that decays to zero. Equation (3.61) has the solution $\alpha = re^{\lambda t}$. Substituting results in

$$\lambda^2 + 2\zeta\omega\lambda + \omega^2 = 0. \tag{3.62}$$

Solving for the eigenvalue λ yields two solutions as follows:

$$\lambda_{1,2} = -\zeta\omega \pm j\omega\sqrt{1-\zeta^2}, \tag{3.63}$$

where j is a complex number. Now let

$$r_1 = a - jb \quad \text{for } \lambda_1,$$
$$r_2 = a + jb \quad \text{for } \lambda_2.$$

Substitute both solutions into (3.61) and add the equations to obtain the result for $\alpha(t)$. Thus,

$$\alpha(t) = e^{-\zeta\omega t}\left(a\cos\omega t\sqrt{1-\zeta^2} + b\sin\omega t\sqrt{1-\zeta^2}\right). \tag{3.64}$$

Differentiating $\alpha(t)$, we obtain

$$\begin{aligned}\frac{d\alpha(t)}{dt} = e^{-\zeta\omega t}\Bigg[&\left(b\omega\sqrt{1-\zeta^2} - a\zeta\omega\right)\cos\omega t\sqrt{1-\zeta^2} \\ &- \left(a\omega\sqrt{1-\zeta^2} + b\zeta\omega\right)\sin\omega t\sqrt{1-\zeta^2}\Bigg].\end{aligned} \tag{3.65}$$

Given the initial conditions α_0 and $d\alpha_0/dt$, a and b can be solved for by setting $t = 0$. Thus,

$$a = \alpha_0,$$
$$b = \frac{\dot{\alpha}_0 + \zeta\omega\alpha_0}{\omega\sqrt{1-\zeta^2}}.$$

Therefore, the time responses for $\alpha(t)$ and $d\alpha(t)/dt$ become

$$\alpha(t) = \alpha_0 e^{-\zeta\omega t}\left(\cos\omega t\sqrt{1-\zeta^2} + \frac{\zeta}{\sqrt{1-\zeta^2}}\sin\omega t\sqrt{1-\zeta^2}\right) \tag{3.66}$$

$$\begin{aligned}\frac{d\alpha(t)}{dt} = \dot{\alpha}_0 e^{-\zeta\omega t}&\left(\cos\omega t\sqrt{1-\zeta^2} - \frac{\zeta}{\sqrt{1-\zeta^2}}\sin\omega t\sqrt{1-\zeta^2}\right) \\ &- \alpha_0\frac{\omega}{\sqrt{1-\zeta^2}}e^{-\zeta\omega t}\sin\omega t\sqrt{1-\zeta^2}.\end{aligned} \tag{3.67}$$

Next, if a tip-off behavior exists at launch, we can solve for the peaks by setting $d\alpha(t)/dt = 0$:

$$0 = -\alpha_0\frac{\omega}{\sqrt{1-\zeta^2}}e^{-\zeta\omega t}\sin\omega t\sqrt{1-\zeta^2}.$$

We note that peaks are periodic according to the sine wave function. Therefore, time to peaks are given by

$$n\pi = \omega t_{\text{peak}}\sqrt{1-\zeta^2} \Rightarrow t_{\text{peak}} = \left.\frac{n\pi}{\omega\sqrt{1-\zeta^2}}\right|_{n=0,1,2,\ldots,\infty} \tag{3.68}$$

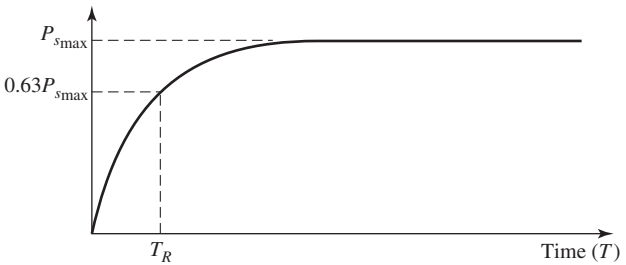

Fig. 3.20. Roll rate response.

The time of the first overshoot (i.e., $n = 1$) is the largest overshoot. Next, we solve for the peak overshoot at t_{peak} for $n = 1$:

$$\alpha_{\text{peak}} = -\alpha_0 e^{-\frac{\zeta\pi}{\sqrt{1-\zeta^2}}}. \tag{3.69}$$

Finally, we can solve for ζ from (3.69), giving

$$\zeta = \frac{|ln(-\frac{\alpha_{\text{peak}}}{\alpha_0})|}{\sqrt{\pi^2 + [ln(-\frac{\alpha_{\text{peak}}}{\alpha_0})]^2}}, \tag{3.70}$$

and for ω from (3.68), yielding

$$\omega = \frac{\pi}{t_{\text{peak}}\sqrt{1-\zeta^2}}. \tag{3.71}$$

A few words about the roll axis model are in order. The missile roll dynamics for stability axis roll rate, P, can be modeled after the roll approximation of lateral/directional motion. This approximation ignores the coupling effects in the rotary cross terms and in sideslip angle β. The roll approximation for roll rate is given by the following simple transfer function:

$$\frac{P_{\text{stab}}(s)}{P_{\text{stab}_{\text{cmd}}}(s)} = \frac{1}{T_R s + 1}, \tag{3.72}$$

where T_R is the augmented roll mode time constant with units of seconds. It should be noted that this represents the lower-order equivalent system of the full closed-loop airframe. The filter time constant may be found from linear analysis of the entire closed-loop system or by computing it with the augmented stability derivatives. From classical control theory, we note that the roll rate response for a step input command is as illustrated in Figure 3.20.

In Figure 3.20 we note that the time constant T_R corresponds to the time at which the roll rate response reaches 63% of its final value.

Example 3. Assume for simplicity that the missile's motion is constrained in the vertical plane. Furthermore, we will assume that the missile can be modeled as a point mass. Therefore, from the missile's balanced forces shown in the diagram below, we can write the equations of motion as follows (see also Example 1 in Chapter 2):

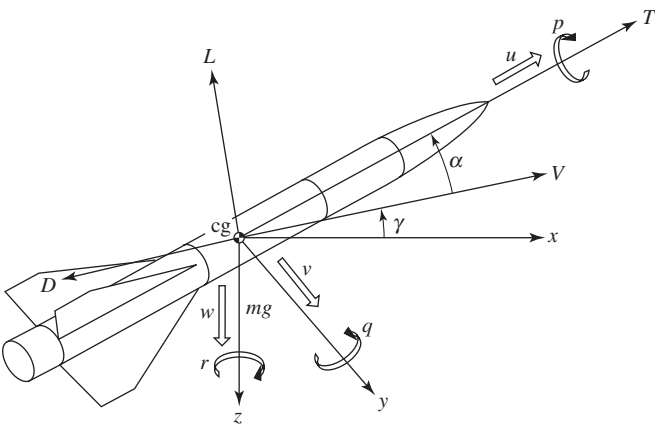

Fig. 3.21.

Equations of Motion

$$\frac{dV}{dt} = (1/m)[T\cos\alpha - D] - g\sin\gamma,$$
$$\frac{d\gamma}{dt} = (1/mV)[L + T\sin\alpha] - (g/V)\cos\gamma,$$

$$\frac{dx}{dt} = V\cos\gamma,$$
$$\frac{dh}{dt} = V\sin\gamma.$$

Aerodynamic Derivative Coefficients

$$L = \tfrac{1}{2}\rho V^2 S C_L,$$
$$D = \tfrac{1}{2}\rho V^2 S C_D,$$
$$C_L = C_{L\alpha}(\alpha - \alpha_0),$$
$$C_D = C_{D0} + kC_L^2,$$

where

$$
\begin{aligned}
g &= \text{acceleration of gravity,}\\
h &= \text{altitude,}\\
k &= \text{induced drag coefficient,}\\
m &= \text{mass,}\\
D &= \text{drag,}\\
L &= \text{lift,}\\
M &= \text{Mach number,}\\
S &= \text{reference area,}\\
T &= \text{thrust,}\\
V &= \text{velocity,}\\
C_D, C_L &= \text{drag and lift coefficients,}\\
&\quad\ \text{respectively,}\\
C_{D0} &= \text{zero-lift drag coefficient,}\\
C_{L_\alpha} &= \partial C_L/\partial\alpha.
\end{aligned}
$$

The aerodynamic derivative coefficients C_{L_α}, C_{D0}, and k are functions of the Mach number as follows:

$$
\begin{aligned}
C_{L\alpha} &= C_{L\alpha}(M),\\
C_{D0} &= C_{D0}(M),\\
M &= M(V,h),\\
k &= k(M),\\
\rho &= \rho(h).
\end{aligned}
$$

Moreover, the missile mass and the thrust are functions of time; that is,

$$m = m(t) \quad \text{and} \quad T = T(t).$$

Note that the *AOA* can be treated as a control variable (if used in connection with an optimization case) that satisfies the inequality constraint

$$\alpha_{min} \le \alpha \le \alpha_{max}.$$

3.4 The Missile Guidance System Model

This section briefly describes the basic subsystems that form a missile's guidance system. Guidance is the means by which a missile steers, or is steered, to a target. A guided missile is guided according to a certain guidance law. In this chapter we consider homing guidance systems. A meaningful comparison of homing guidance

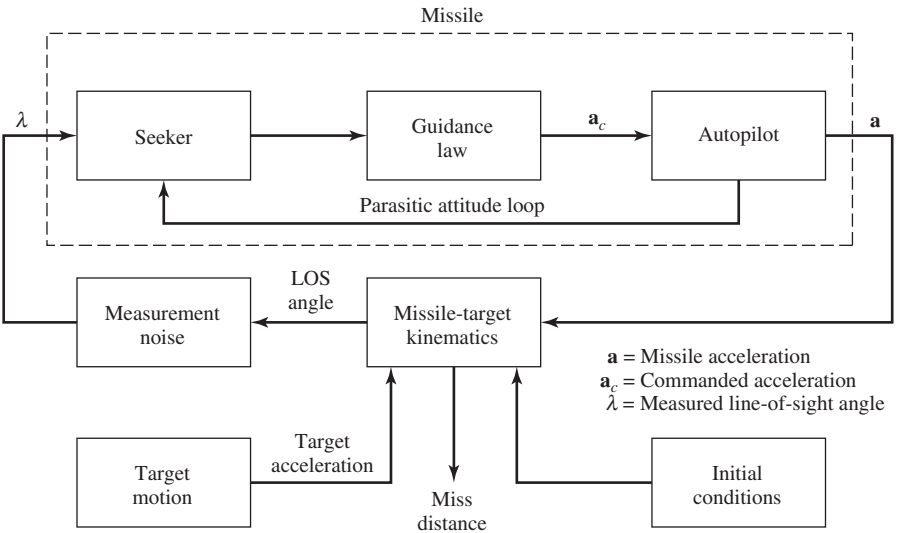

Fig. 3.22. Major subsystems of a missile guidance system.

systems for missiles requires realistic models for the missile and its target engagement geometry model in order for terminal *miss distance* to be accurately evaluated. This model should include the important dynamics and system nonlinearities that influence performance, and yet be representative of missiles in general. In the simplest form, the principal elements that make up a missile guidance system are illustrated in Figure 3.22.

For a missile, the inputs are target location and missile-to-target separation. The desired output is that the missile have the same location as the target. The missile does this by using a certain guidance system and flying according to a certain guidance law. As stated in Chapter 1, the type of guidance system chosen is dependent on the overall weapon system in which the missile can be used, on the type of threat the missile will be used against, and the characteristics of the threat among other factors. The various subsystems indicated in Figure 3.22 will be discussed in the subsequent sections. It should be noted at the outset that the model developed herein assumes that the target and missile motions are constrained to a plane. Consequently, development of the missile and guidance models is limited to a single channel.

A more detailed block diagram for a controlled missile guidance model than the one illustrated in Figure 3.22, which includes the equations of motion and aerodynamics, is given in Figure 3.23. Note that this model is for a *roll-stabilized* missile.

Listed below are the three main problems that the guidance system designer must face in the design of a guidance system.

General Problems of Guidance System Design

1. Help to maximize the single-shot kill probability *(SSKP)* by minimizing the miss distance.

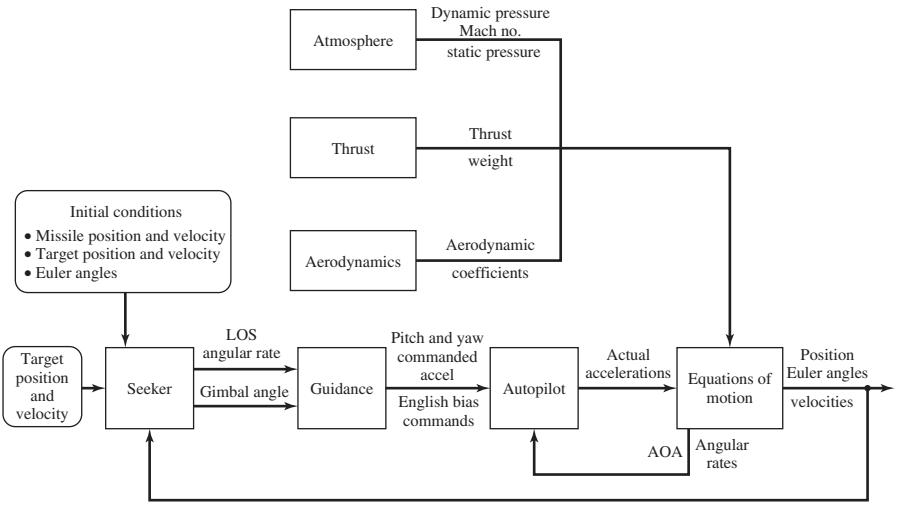

Fig. 3.23. A typical roll-stabilized missile guidance/kinematic loop.

Sources of Miss Distance

(1) Initial heading error.
(2) Acceleration bias.
(3) Gyro drifts (if gyros are used in seeker stabilization).
(4) Glint (scintillation noise).
(5) Receiver noise.
(6) Fading noise (except for monopulse).
(7) Angle noise (due to varying refraction with frequency diversity).

Noise components of miss depend on guidance-system response and thus $\alpha/\dot{\gamma}$ and refraction slope R.

2. Preserve stability of the *parasitic attitude loop* (to be discussed in Section 3.5). (In maneuvers, missile pitching affects seeker boresight-error measurement.)
3. Filtering.

(1) Limit power consumption and saturation of the actuators.
(2) Prevent noise from excessive hitting of dynamic-range limits, such as autopilot g-limits.

A more detailed discussion of the above problems is in order. First, in order to maximize the single-shot kill probability, the main problem of the guidance designer is to minimize the miss distance enumerated above under problem 1. The seven sources of miss distance listed above are statistical in nature. Both the *alpha over gamma dot* of the airframe and the statistically varying radome-refraction slope R affect the speed of response of the guidance system and thereby affect the components of miss due to noise. Evaluation and partial optimization of total *rss* (root-sum-squares) miss distance can be performed rapidly and efficiently with a digital computer program.

The second major problem of the guidance designer is to preserve the stability of the *parasitic attitude loop* (for a discussion see Section 3.5). The third problem states that some filtering must be used to limit noise perturbations of the seeker and actuators, so that power consumption, saturation, g-limiting, etc., will not be excessive. A successful guidance design requires a compromise that meets all three major problems listed above.

3.4.1 The Missile Seeker Subsystem

In this subsection we discuss missile seekers and the role they play in guidance systems. The discussion herein is by no means exhaustive, and is intended to stimulate further research. Missile seeker and radome error analysis has been carried out extensively. Basically, the main function of the missile seeker (also known as *homing eye*) subsystem is to:

(1) Provide the measurements of target motion required to mechanize the guidance law.
(2) Track the target with the antenna or other energy-receiving device (e.g., radar, infrared (*IR*), laser, or optical). We note here that the antenna refers to any type of energy-collecting device.
(3) Track the target continuously after acquisition.
(4) Measure the *LOS* (line-of-sight) angular rate $d\lambda/dt$.
(5) Stabilize the seeker against a missile pitching rate $d\theta_m/dt$ (also, yawing rate) that may be much larger than the *LOS* rate $d\lambda/dt$ to be measured.
(6) Measure the closing velocity V_c (note that this is possible with some radars but difficult with infrared seekers).

The typical classical seeker hardware consists of two or three gimbals on which are mounted gyroscopes (either conventional spinning mass or laser gyros) and an antenna. Most seekers of the gimballing variety have two gimbal axes, namely, yaw (or azimuth) and pitch (or elevation), which are orthogonal to the longitudinal axis, relying on the missile roll autopilot for roll stabilization. Space stabilization about the instrument axes is necessary, although a slow roll rate about the *LOS* itself is tolerable. Numerous gimbal configurations have been used in the past. Occasionally, a special application may justify a roll gimbal to roll-stabilize the whole seeker. In an active radio frequency (RF) seeker or passive *IR* seeker, two gimbals are commonly used, namely, one for azimuth and one for elevation measurement. However, only one gimbal and its associated dynamics are required for a planar-motion model. Associated with each gimbal is a servomechanism, whose function is to adjust its angular orientation in response to the tracking error signal measured by, say, a radar receiver. (Note that here we will assume that the seeker consists of a radar receiver, unless otherwise specified.) In addition to the gimbaled systems, there are also body-mounted antenna systems (i.e., in a strapdown configuration), which do not use moveable gimbals in order to position the antenna. Moreover, these systems use either a fixed antenna position relative to the missile or electronic beam steering by means of a phased-array radar antenna. It is important to emphasize here that the use of electronic beam

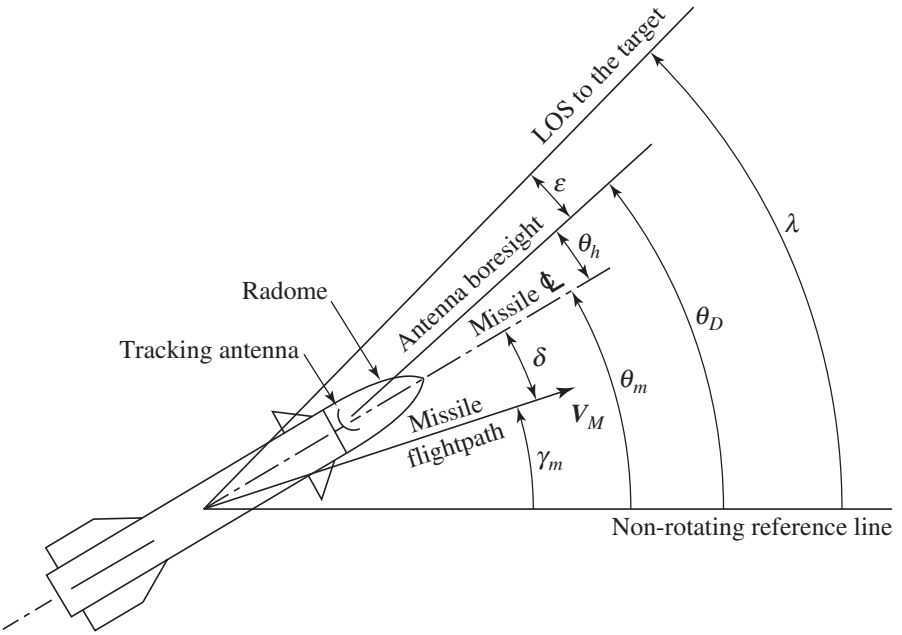

Fig. 3.24. Missile seeker showing angular geometry.

steering is in many ways analogous to the gimbaled system as far as the guidance system operation is concerned. The fundamental measurement obtained from a homing sensor receiver is assumed to be the indicated angular position of the target relative to the antenna centerline or boresight. Figure 3.24 illustrates a typical missile radar seeker.

The line of sight (*LOS*), λ, is defined as the angle between a line from the center of the seeker antenna to the target, and some arbitrary nonrotating (e.g., inertial) reference line. Commonly, it is convenient to select this reference equal to the *LOS* position at the beginning of the homing guidance phase. Consequently, $\lambda(t)$ at time t is the total change in the angular position of the *LOS* relative to the initial *LOS*. Referring to Figure 3.24, we note that the angular position of the missile body centerline, θ_m, is measured relative to the initial *LOS*. (Note that θ_m is identified as the pitch angle.) Furthermore, the angular position of the antenna centerline is defined by the gimbal angle, θ_h. Therefore, the *LOS* angle λ is given by

$$\lambda = \theta_m + \theta_h + \varepsilon, \tag{3.73a}$$

where ε is the true boresight error, that is, the error between antenna center line and line of sight to the target. Alternatively, by writing (3.73a) as

$$\varepsilon = \lambda - \theta_m - \theta_h, \tag{3.73b}$$

we obtain the expression for the true boresight error. It is important to note that the boresight error is a function of both the missile attitude relative to inertial space and the angular position of the antenna relative to the missile centerline. Since λ or $d\lambda/dt$ is the desired measurement for guidance purposes, it is necessary to remove the missile motion from the *LOS* measurement data. One requirement on the seeker subsystem is to keep the antenna pointed at the target, so that the error ε is always much smaller than the beam width of the received energy. Furthermore, in the region of small ε, the seeker receiver measurement of indicated boresight error is nearly linear. However, if ε cannot be considered small relative to the antenna beamwidth, the receiver boresight error processor operation may become nonlinear. Specifically, if ε is allowed to approach the half beamwidth of the antenna, the receiver detection circuitry will at some point lose lock, and all guidance information will be lost. Therefore, the seeker must track the tracker sufficiently closely so that large boresight errors do not occur. Otherwise, the nonlinearity of the boresight error position should be considered as an important system nonlinearity. The actual form of the boresight error processor nonlinearity is strongly dependent on the specific beamwidth, processing scheme (i.e., monopulse radar, *CW* radar, etc.), and detector characteristics of individual systems. In the present discussion, it will be assumed that the beamwidth and tracking response of the seeker are adequate to keep the boresight error processor in its linear region.

The radome forms the nosepiece of a missile and covers the *RF* head assembly of the target seeker. More specifically, the radome forms an important part of the external contour of the missile and becomes a vital link in the electromagnetic path of *RF* energy reflected from the target to the missile antenna. The same reasoning applies to an infrared seeker. In either case, aerodynamic, structural, and electrical requirements must be adjusted in order to produce optimum performance.

Because of the presence of lags in the seeker tracking loop and radome refraction effects, the seeker will not point directly at the actual target. Instead, the seeker will point to the apparent target. The reader should be cautioned that radar reflectivity from a target is affected by the frequency of the radar. An aircraft design that is invisible to high-frequency fire-control radar may be plainly obvious to low-frequency search radar. The half-wave-length phenomena can be a factor. Parts of an aircraft that equal one-half of radar's wavelength create a resonance that greatly increases radar reflectivity. The *aberration* (or *refraction*) angle error is the result of nonlinear distortions in the received energy as it passes through the protective covering (e.g., radome in the case of a radar homing sensor) over the antenna. This distortion produces a false boresight error signal, ε' which is interpreted as an error in the angular position and motion of the target by the guidance system. Referring to Figure 3.25, we note that the indicated boresight error ε' in the presence of radome aberration or refraction angle error θ_r is given by the expression [3], [5], [12]

$$\varepsilon' = \lambda + \theta_r - \theta_m - \theta_h, \tag{3.73c}$$

where the radome aberration angle error θ_r is in general not constant, but is a function of the gimbal angle θ_h; that is, the radome angle error is a nonlinear function of the gimbal angle θ_h. Mathematically, this can be expressed by the relation $\theta_r = f(\theta_h)$. It should be noted here that the size of the measurement error, that is, the angle θ_r,

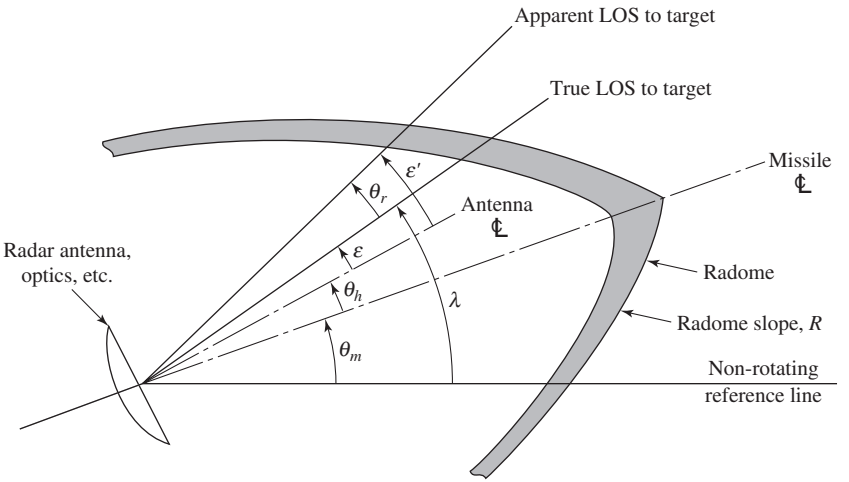

Fig. 3.25. Effect of radome aberration error.

depends on the orientation of the antenna with respect to the radome (antenna cover), which is fixed to the missile airframe.

Furthermore, the dependency of θ_r on θ_m couples body motion into the boresight error signal, thus forming what is commonly called the *parasitic attitude loop* (for a discussion of the parasitic attitude loop see Section 3.5). This loop can drastically alter missile response characteristics and in turn increase the miss distance. This is particularly true at high altitudes, where the missile body motion tends to be greatest. The aberration (or refraction) angle error is normally a nonlinear function of the following factors: (a) the angle between the missile center line and the line of sight to the target (also known as the look angle, which is defined as $(\lambda - \theta_m)$); (b) the radome thickness distribution; (c) material; (d) radome shape; (e) manufacturing tolerances; (f) temperature; and (g) erosion of the surface during flight. In addition, the nonlinearity arises from such optical and electrical properties as frequency, standing waves inside the radome, and polarization of the received signal. Consequently, an accurate model may require a nonlinear, time-varying statistical characterization of the radome. From the above discussion, it can be said that the radome error magnitude can neither be precisely measured nor predicted. However, since these characteristics tend to vary over rather wide limits depending on the particular application and missile configuration, a constant refraction error slope model is used to capture the important body-coupling effect.

From the above discussion, we note that radome aberration error is one of the errors contributing to the overall miss distance of a radar-guided homing missile. Figure 3.26 illustrates the aberration angle as a function of look angle [3].

The derivation of the radome model can be obtained as follows. Let λ be the true *LOS* and λ_m the measured *LOS*. Then,

$$\lambda_m = \lambda + \theta_r, \tag{3.74a}$$

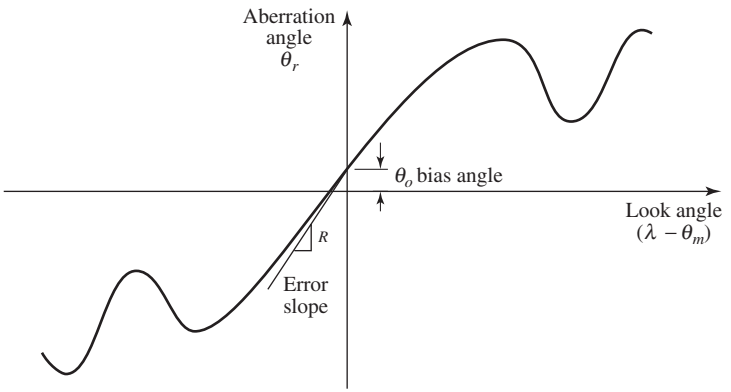

Fig. 3.26. Aberration angle error as a function of look angle.

where $\theta_r = f(\theta_h)$. Taking the derivative of (3.74a), we have

$$\frac{d\lambda_m}{dt} = \frac{d\lambda}{dt} + \frac{d\theta_r}{dt}. \tag{3.74b}$$

Now, since $\theta_r = f(\theta_h)$,

$$d\theta_r = \left(\frac{\partial \theta_r}{\partial \theta_h}\right) d\theta_h,$$

where $(\partial\theta_r/\partial\theta_h)$ is the radome error slope; that is,

$$R = \frac{\partial \theta_r}{\partial \theta_h}. \tag{3.75}$$

Also, the following relation holds:

$$\frac{d\theta_r}{dt} = \left(\frac{\partial \theta_r}{\partial \theta_h}\right)\left(\frac{d\theta_h}{dt}\right) \Rightarrow \frac{d\theta_r}{dt} = \left(\frac{\partial \theta_r}{\partial \theta_h}\right)\left(\frac{d\theta_h}{dt}\right).$$

The gimbal angle, θ_h, can be obtained from Figure 3.23 as follows:

$$\theta_h = (\lambda - \theta_m) - \varepsilon,$$

or

$$\theta_h = \lambda - (\theta_m + \varepsilon), \tag{3.76}$$

where $(\lambda - \theta_m)$ is the look angle, and

$$\frac{d\theta_h}{dt} = \frac{d\lambda}{dt} - \frac{d\theta_m}{dt} - \frac{d\varepsilon}{dt}. \tag{3.77}$$

Therefore, from (3.74a) and (3.74b) we have

$$\begin{aligned}\frac{d\lambda_m}{dt} &= \frac{d\lambda}{dt} + \frac{d\theta_r}{dt} = \frac{d\lambda}{dt} + \left(\frac{\partial\theta_r}{\partial\theta_h}\right) d\theta_h \\ &= \frac{d\lambda}{dt} + \left(\frac{\partial\theta_r}{\partial\theta_h}\right)\left[\left(\frac{d\lambda}{dt}\right) - \left(\frac{d\theta_m}{dt}\right) - \left(\frac{d\varepsilon}{dt}\right)\right] \\ &= \frac{d\lambda}{dt} + \left(\frac{\partial\theta_r}{\partial\theta_h}\right)\left(\frac{d\lambda}{dt}\right) - \left(\frac{\partial\theta_r}{\partial\theta_h}\right)\left(\frac{d\theta_m}{dt}\right) - \left(\frac{\partial\theta_r}{\partial\theta_h}\right)\left(\frac{d\varepsilon}{dt}\right) \\ &= \left[1 + \left(\frac{\partial\theta_r}{\partial\theta_h}\right)\right]\frac{d\lambda}{dt} - \left(\frac{\partial\theta_r}{\partial\theta_h}\right)\left(\frac{d\theta_m}{dt}\right) \\ &= [1+R]\left(\frac{d\lambda}{dt}\right) - R\left(\frac{d\theta_m}{dt}\right). \end{aligned} \tag{3.78}$$

Note that in (3.78) it has been assumed that the bias angle θ_0 is zero. The $(1 + R)$ term in (3.78) is therefore the radome model; it shows how the actual *LOS* is perturbed. Moreover, this equation shows that the measured *LOS*, λ_m, is corrupted by the radome error slope.

A linear model for the general aberration angle can be obtained using a Taylor series approximation of the form

$$\theta_r = \theta_0 + (\lambda - \theta_m)R, \tag{3.79}$$

where θ_0 is a bias angle and R is the radome error slope. Substituting (3.79) into (3.73c) and solving for ε' yields [5], [12]

$$\varepsilon' \cong (1+R)(\lambda - \theta_m) + \theta_0 - \theta_h. \tag{3.80}$$

The radome error slope, R, which varies from radome to radome, is the main parameter in the homing loop. Mathematically, the radome local slope can be expressed as

$$R = \partial\theta_r/\partial(\lambda - \theta_m).$$

The radome characteristics have a predominant effect on missile performance at high altitude. This occurs because the radome introduces an angular change between the actual *LOS* and the apparent *LOS* to the target. The effect of this angular change is an erroneous radar-tracking error signal, which will command false missile maneuvering and can result in large miss distances (see Figure 3.27).

Normally, the boresight error is assumed to be negligible as compared to other system errors. Also, there is a possible contribution of the refraction error to measurement noise, when the frequency of the received signal is varied in a pseudorandom manner in order to reduce the effect of a potential enemy jammer (for example, when the seeker is an active or semiactive radar). This noise can be treated as a contributor to range-independent noise. The various noises (to be discussed in Section 3.4.2) associated with the seeker must also be considered in the design of a missile. As discussed earlier, the *LOS* angle is the fundamental quantity measured by the seeker. These measurements will generally be corrupted by various types of noise, which can

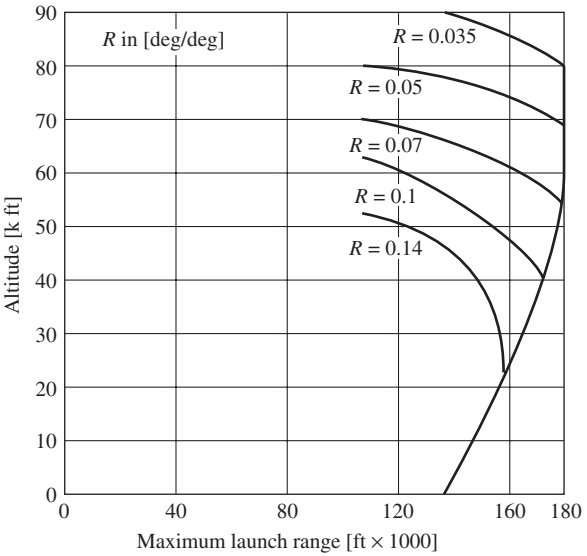

Fig. 3.27. Radome error slope (R) limitations on maximum launch range.

be categorized according to the dependency of their rms (root-mean-square) levels on the missile-to-target range. The actual noise levels and bandwidths are dependent on the exact form of the measurement signal processor, target configuration and characteristics, environmental conditions, and a number of other system effects. In block diagram form, the seeker can be represented as shown in Figure 3.28. It should be pointed out that here we consider a single channel; an actual seeker system will require the implementation of two or three channels in order to account for motion in three dimensions.

Commonly, the stabilization dynamics comprise the gimbal servo and rate gyro, mounted on the antenna. Typically, the stabilization dynamics have a very wide bandwidth, in excess of 100 rad/sec. Moreover, the track loop model can be represented by simple first-order dynamics, commanding a gimbal rate proportional to the measured boresight error. In essence, the loop attempts to drive the boresight error to zero, thereby causing the antenna to track the target [5].

Using classical feedback control theory, it is easily shown that the linear transfer function from $d\lambda/dt$ to ε' (assuming unity gain for the radome, the signal processor, and the stabilization dynamics) is given by the following first-order transfer function [3], [12]:

$$\frac{\varepsilon'}{\dot{\lambda}} = \frac{\tau}{(1+s\tau)}. \tag{3.81}$$

Note that at low frequencies (i.e., $\omega < 1/\tau$), the indicated boresight error is proportional to the *LOS* rate. That is, the indicated boresight error ε' is scaled by $1/\tau$, which forms the desired rate command to the stabilization loop. As we shall see

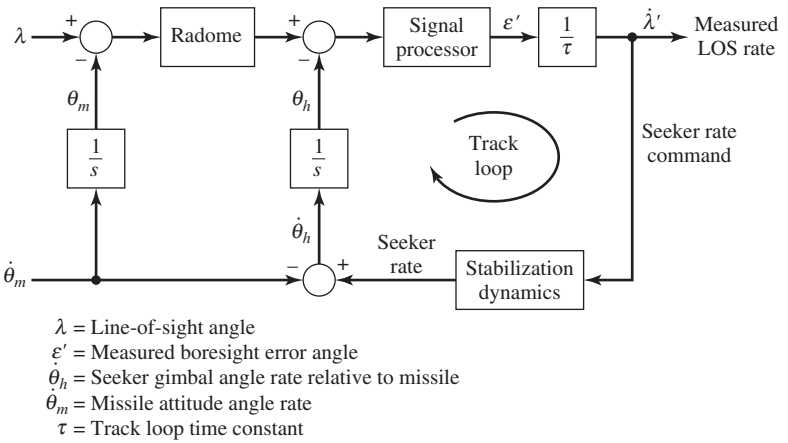

Fig. 3.28. Typical block diagram of a seeker subsystem.

later, this is the desired measurement for classical proportional navigation guidance, which commands a missile's lateral acceleration proportional to the *LOS* rate. Equation (3.81) provides an indication of the important region of boresight error linearity. Now, using the fact that ε' is proportional to $d\lambda/dt$ in the steady state for constant $d\lambda/dt$, we obtain the following expression for ε'_{max}:

$$\varepsilon'_{max} = \tau \left(\frac{d\lambda}{dt} \right)_{max}. \tag{3.82}$$

Assuming that τ is sufficiently small, ε'_{max} can be held within the linear range of the received beamwidth. Figure 3.29 illustrates the resulting seeker block diagram with a linear refraction error model.

From Figure 3.29 it can be seen that the transfer function relating θ_m to λ' is given by [3]

$$\lambda'/\theta_m = -R/(1 + s\tau), \tag{3.83}$$

where λ' is the measured *LOS* angle. Thus, the measured *LOS* rate is corrupted by a term proportional to the body rate. Furthermore, since body rate is a result of commanded acceleration, a loop is formed that can have a destabilizing effect on missile attitude, resulting in an increase in miss distance. When R is zero, the contributions from the body angular rate input (see Figure 3.29) cancel, producing no effect on ε'. It is well known that most missiles use some form of proportional navigation as the guidance law. Although classical proportional navigation guidance uses measurements of *LOS* rate, it is more convenient to use measurements of *LOS* angle in guidance laws that utilize a Kalman filter. In such a case, let us define the measured *LOS* angle λ' as follows (see (3.78)):

$$\lambda' = (1 + R)\lambda - R\theta_m. \tag{3.84}$$

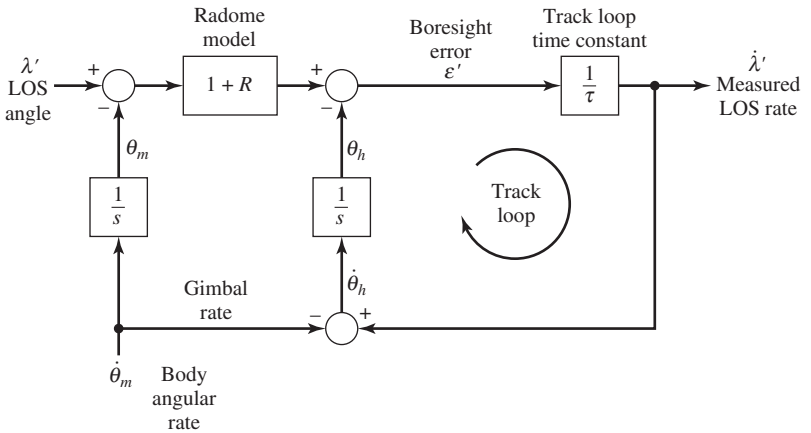

Fig. 3.29. Block diagram of the seeker model with track loop.

From Figure 3.29 it follows that

$$\varepsilon' = \tau s \lambda' / (1 + s\tau). \tag{3.85}$$

Now, since the boresight error is an observable quantity, (3.85) can be inverted, yielding

$$\lambda' = [(1 + s\tau)/s\tau]\varepsilon'. \tag{3.86}$$

That is, λ' can be recovered from the measured seeker boresight error. We can summarize the above discussion by noting that a typical classical seeker model consists of (1) the antenna pointing dynamics, and (2) the parasitic coupling of the missile airframe dynamics into the *LOS* direction as perceived by the seeker.

Earlier in this subsection we discussed the refraction error and the various errors caused by the radome's nonlinear nature. Furthermore, we noticed that a radome (or *irdome* in the case of infrared seekers) is required in order to protect the seeker sensor and to transmit the reflected radar (or infrared energy, as the case may be) energy from the target. Regardless of the nature of the seeker sensor used, the requirements for the protective dome that the guidance designer must consider are as follows:

1. It must transmit the energy with a minimum loss.
2. It must have minimum aerodynamic drag.
3. It must transmit the energy with minimum distortion. Specifically, a change of angular distortion with seeker position causes a severe guidance problem with the parasitic attitude loop.
4. It must have satisfactory mechanical properties, such as (a) sufficient strength, (b) resistance to thermal shock (e.g., from rapid aerodynamic heating), (c) resistance to rain erosion at high speeds, and (d) minimum water absorption.

Figure 3.30 illustrates three conceivable shapes for a radome.

1) Ideal aerodynamic with (L/D) ≅ 5.

2) Ideal electromagnetically with (L/D) ≅ 1/2.

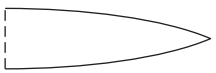

3) Compromise radome with (L/D) ≅ 3.

Fig. 3.30. Three conceivable radome shapes.

For minimum angular distortion, a hemispherical shape (e.g., a hyperhemispherical shape as in ground-based radar) would be ideal from an electromagnetic design point of view. However, the drag of such a shape would be excessive. The aerodynamicist, on the other hand, would prefer the first shape shown in Figure 3.30, because this shape minimizes drag. This design shape tends to have rather high peak values of radome error slope R. A typical compromise is the so-called *tangent-ogive* shape with a length-to-diameter (L/D) ratio of about 3. Some missiles use much blunter domes despite the drag penalty.

The modeling, evaluation, and compensation for dome error angle effects are among the most difficult problems of the guidance designer. For instance, each radome from a production run has a different characteristic, which varies with plane of examination (defined by the longitudinal axis and the seeker boresight axis), frequency, and possibly environmental factors. Preliminary analytical models utilize fixed values of radome error slope R, which may be positive or negative. These slopes usually lie within the range from -0.1 to $+0.1$ degree/degree.

In addition to the conventional and electronically steered (or scanned) array (*ESA*) tracking radar seekers, the following seekers are used extensively in various guided missiles (see also Section 3.4.4):

- *E*lectro-*O*ptical (*EO*) *TV*.
- *LADAR* (*L*Aser *D*etecting *A*nd *R*anging, or Laser Radar).
- *SAR* (*S*ynthetic *A*perture *R*adar), as well as Semiactive *SAR*.
- Dual Mode *LADAR/MMW* (*M*illimeter *W*ave).
- *IIR* (Imaging Infrared); also seen as I^2R.
- *TWS* (Track-While Scan) multiple-target tracking radar.

Conformal *RF* antennas built into missile nosecones will give better combined *RF*/*Electro-optical* performance, due in part to removing the mechanical antenna gimbal. Next-generation missile seekers will most likely use *ESA*s. However, electronically steered antennas will see application if the cost becomes low enough. More

efficient solid-state transmitters, low-probability-of-intercept waveforms, and shorter wavelengths such as the 94–130 GHz *W*-band are other potential *RF* changes. In addition, future seekers using these new technologies will offer high-resolution air-to-air and air-to-ground modes, outstanding tracking performance, sophisticated *ECCM*, and high reliability. Visual and infrared seekers will be upgraded to true imaging as focal plane arrays and processing chips become cheaper. Improvements over pseudo-imaging include better target recognition and clutter/countermeasures rejection. Automatic target recognition (*ATR*) may change the rules of engagement for *BVR* air-to-air shots. Instead of requiring positive identification before launch, good *ATR* would make the *friend-or-foe* decision itself.

New seeker technology is evolving with a new generation of advanced missile systems. For example, the *AIM-9X Sidewinder II* design features a high-resolution *rotate-to-view* seeker. In this design, the outer seeker casing, slightly larger in diameter than the missile body, rotates 360° to provide a clear viewing path for the seeker, which is mounted on a two-axis gimbal fixed to the body. The seeker head can be slaved to a helmet-mounted sight, with the seeker window rotating to view what the pilot is looking at. It has an off-boresight capability of more than 90°.

We conclude this section by noting that a new generation of radar is the *AESA* (active electronically scanned arrays). This radar allows tracking of fast, stealthy, cruise-missile-size flying targets at hundreds of miles. The *AESA* will be used to upgrade the *Joint-STARS* airborne ground-surveillance radar. An *AESA* radar uses hundreds or even thousands of small transmitter–receiver (*T/R*) elements (or modules) that allow it to conduct widely diversified tasks simultaneously, including surveillance, communications, and jamming. These *T/R* elements are used to update a radar's computer several times a second, so that target data are much more accurate. For example, each array in the *AESA* radar is made up of about 1,000 transmitter–receiver elements on the *F/A-22 Raptor* and several hundred in the *JSF*. The number of elements dictates the power output and range of the radar, which equates to about 125 miles on the *F/A-22* and 90 miles on the *JSF*. Other aircraft that will use the *AESA* technology are the *F/A-18E/F* and *F-15C* interceptors. Some of the new combined-technology radars may first be used operationally in the *Global Hawk UAV*. So far, *Global Hawk*'s mission has been that of supplying *E/O* and *IR* digital photos and *SAR/GMTI* data of vehicles (see also Appendix F). However, *HAWK*'s new payload will not be a fully developed new-technology radar system, but rather an existing air-to-air radar scaled down with *AESA* technology. In some applications the *ASARS-2* (Advanced Synthetic Aperture Radar System) is used to track and observe ground targets. *ASARS-2* offers a resolution of 1 ft over a 1 sq mile *FOV* from a range of more than 108 nm (200 km) and an altitude of more than 65,000 ft when observing ground targets.

Recently, the Navy tested a combination millimeter-wave radar/*RF*-homing seeker for a follow-on to the current *HARM* radar-killing missile called the Advanced Anti-Radiation Guided Missile. In addition, the USAF is investigating the possibility of developing a *next-generation HARM*-like missile that fits in the *F/A-22*'s weapons bays.

3.4.2 Missile Noise Inputs

We have heretofore assumed that the *LOS* rate, $d\lambda/dt$, can be accurately measured by the radar on board the missile. In fact, however, noise within the radar and on the target signal limits the accuracy to which $d\lambda/dt$ can be measured, and significantly affects the miss distance. In either radar or an infrared system, noise tends to be a problem because it increases miss distance. In a radar system, the guidance designer would like to have high illuminating power on the target, in order to reduce the receiver gain and internally generated noise. The antenna size is made a maximum within the constraint of missile body diameter, so as to maximize power reception and to minimize the angular beamwidth. Furthermore, a passive infrared seeker is also designed to have a maximum aperture to maximize incoming power, and may utilize special optical modulation of the incoming radiation in order to amplify without drift the weak electrical signal of the infrared detector. Thus, in order to maximize the incoming infrared power, a tail attack against a jet aircraft tail pipe is preferred, as are moderate ranges and good weather. A small wavelength in a radar reduces the angular beamwidth, but the choice of wavelength is limited by problems of power generation and environmental absorption, etc. Consequently, a missile radar antenna usually has a relatively broad beamwidth, and so it is unable to resolve two closely spaced targets by their angular separation until the last moments of intercept. This classic problem may lead to a bad miss distance. Therefore, because of its much higher ratio of aperture diameter to wavelength, an infrared seeker has a narrower beamwidth and much higher angular resolution. Radar illumination may be continuous-wave (CW) or pulsed, depending on which factor of application is governing. In a simple CW radar, the closing velocity V_c is obtained from Doppler measurements.

The fundamental effect of noise is to mask or hide the true value of $d\lambda/dt$. Noise can occur due to target effects or receiver (missile) effects. As we saw in the previous subsection, the radome contributes a bias error due to the diffraction effects of the radome, which is called boresight error. Receiver noise is generated within the missile receiver, and the target signal must compete with it. This noise has increased angular amplitude at longer ranges, where the signal-to-noise ratio* (*SNR*) of the target is the lowest. Receiver noise consists primarily of thermal noise generated by the antenna and receiver electronics on board the missile. The effective amplitude of this noise increases with increasing range, because of the corresponding decreasing *SNR*. There are, in general, three types of missile receivers that can be considered. These are:

Passive: The target supplies the radiated signal.
Semiactive: The target is illuminated by a source that is not on board the missile.
Active: The target is illuminated by a source on board the missile.

Specifically, the receiver will generally include some type of automatic gain control, which attempts to keep the receiver signal power nearly constant. As a result, the

*The *SNR* is defined as $10 \log_{10}(A^2/\sigma^2)$, where A is the signal amplitude and σ^2 is the variance of the noise.

effective noise level will change with received signal power relative to some reference level. Commonly, a normalized angular measurement noise model is defined that uses the variance (or power spectral density) of the indicated boresight error, measured at a range that yields an *SNR* of unity as the reference level.

In addition to the receiver noise, there are four other basic types of noise associated with the design of a missile guidance system. These are:

Glint: Glint, or angle noise, is the phenomenon in which interference by two or more sources causes a distortion in the shape of the propagating wavefront. The effect of this distortion is to change the apparent angle of arrival of the wavefront. This appears to the tracking system as a wander of the apparent target location from its true location. Thus, glint is a target-induced error term that introduces an angular error in the target tracker. The apparent center of the target moves along the length of the target and can occasionally exceed the target dimension. Furthermore, the apparent location of the target may lie outside of the target a significant amount of time. (Note that the phenomenon of glint is also known as the radar *bright spot* wander.) Since glint is a distance error along the target, the equivalent angular error varies as $1/R_{mt}$, where R_{mt} is the total missile-to-target range. Glint is usually described as a Gaussian random variable whose main value is at the center of the target and whose standard deviation (σ) depends on the target span, perpendicular to the *LOS* angle. A typical value for the standard deviation of correlated glint for an aircraft is

$$\sigma = 0.25S/R_{mt}, \tag{3.87a}$$

where S is a characteristic length (or effective target length). The correlation coefficient is computed by

$$\rho = \exp(-\omega_g \cdot \Delta T), \tag{3.87b}$$

where

$$\begin{aligned} \omega_g &= \text{the glint half-power frequency,} \\ \Delta T &= \text{magnitude of time since last call.} \end{aligned}$$

The standard deviation of the correlated glint error is then computed by the following relation:

$$\sigma_c = \sigma \cdot (1 - \rho^2)^{1/2}. \tag{3.87c}$$

The spectral density of glint error is maximum at zero hertz and decreases with upward concavity as frequency increases. The glint spectral density is commonly approximated with a Lorentzian lineshape as follows:

$$\Phi_g(\omega) = \Phi_0[\omega_g^2/(\omega^2 + \omega_g^2)], \quad -\infty < \omega < \infty, \tag{3.87d}$$

where

$$\begin{aligned} \Phi_g(\omega) &= \text{spectral density,} \\ \Phi_0 &= \text{zero-frequency value of the spectral density,} \\ \omega_g &= \text{glint half-power frequency.} \end{aligned}$$

The glint half-power frequency is given by

$$\omega_g = 4\pi\Omega S/\lambda,$$

where

$$\begin{aligned}\omega_g &= \text{glint half-power frequency,}\\ \Omega &= \text{rotation rate of target,}\\ S &= \text{target characteristic length (or span),}\\ \lambda &= \text{radar wavelength.}\end{aligned}$$

The variance of the glint error is given by the integral of the spectral density (3.87d). Thus,

$$\sigma_g^2 = \int \Phi_g(\omega)d\omega,$$

which yields, after defining $z = \omega/\omega_g$ and $dz = d\omega/\omega_g$,

$$\sigma_g^2 = \int dz/(1+z^2) = \pi\Phi_0\omega_g. \tag{3.87e}$$

A frequency analysis of the time record of glint from an aircraft target often suggests that its spectrum approximates white noise passed through a first-order lag of the form [3]

$$\Phi_g = (K_g^2)/(1+\omega_g^2 T_g^2) \quad \text{in units of m}^2\text{/rad/sec}, \tag{3.87f}$$

where T_g is the guidance time constant (typically in the range 0.1 to 0.25 sec), and L_g^2 is the mean-square value of the glint and is given by $L_g^2 = \pi K_g^2/2T_g$ (if T_g and L_g are known approximately, then K_g^2 can be evaluated).

Range-Independent Noise (*RIN*): This noise, also known as *fading noise*, has a constant angular amplitude, and is caused by amplitude fluctuations of the target occurring at the information frequency in the missile receiver, for example, at the conical scan frequency of a conical scanning missile seeker. Range-independent noise σ_f is inherent in the missile receiver. The noise can be modeled as $\sigma_f \approx N(0, r_f)$, that is, zero mean and variance, with equivalent white noise power spectral density Φ given by

$$\Phi = 2\tau_f r_f$$

where τ_f is the correlation time constant and r_f is the variance. Also, *RIN* may be caused by the seeker servo system. (Another type of noise commonly encountered in connection with a missile radar seeker noise is *range-dependent* noise. However, this is strictly a ground-tracking radar noise, used in command guidance systems.)

Scintillation Noise: Scintillation is a phenomenon similar to glint, in that reflections from various parts of the aircraft (e.g., target) interfere. In the case of scintillation, this affects the amplitude of the received signal. Typically, an aircraft is composed of many individual conducting surfaces, or scatterers, each with different scattering

properties that vary as the viewing or striking angle changes. In addition, multiple or sequential reflections of the radiated signal may occur between the various scatterers. These features can strongly affect the resultant value of the target aircraft's radar cross section (*RCS*)* signature. The large-amplitude fluctuation of an *RCS* signature with respect to small changes in the viewing angle is referred to as *scintillation*. In general, the amount of scintillation decreases as the wavelength increases. The presence of interference in the returned signal causes a modulation of the returned signal amplitude. In conical scan systems, any component of amplitude scintillation at or near the system scan frequency will be interpreted by the system as a signal resulting from an off-axis target. For this reason, frequency components of amplitude scintillation near the scan frequency will drive the radar off target. Note, however, that this effect is absent from monopulse radar systems, which do not extract information from modulation frequencies. Scintillation errors can be modeled in the same manner as glint errors, with the exception of the form of the standard deviation. For scintillation, the standard deviation is given by

$$\sigma_s = \frac{B\sqrt{W(\omega_g)B_n}}{E}, \tag{3.87g}$$

where

B = beamwidth,

B_n = equivalent bandwidth for the noise of the tracking loop,

E = error slope,

$$W(\omega_g) = \frac{1}{2\pi}\frac{\omega_g}{\omega_g^2 + \omega_s^2}.$$

In the above equation, ω_g is the glint half-power frequency, and ω_s is the scan frequency. As for the glint error, the correlation coefficient is given by

$$\rho = \exp(-\omega_g \cdot \Delta T),$$

and the standard deviation of the correlated output by the relation

$$\sigma_c = \sigma(1 - \rho^2)^{1/2}.$$

The reflection characteristics of an aircraft determine both the *RCS* level and the amount of *RCS* scintillation and target glint, all of which affect tracking accuracy. The angular scintillation noise can also be expressed as

$$\sigma_s^2 = \sigma_{wd}^2 / R_{mt}^2, \tag{3.87h}$$

*The *RCS*, σ, is a measure of the size of the body as seen by the radar. The *RCS* is an area and is usually measured in square meters or decibels, with 1 m^2 reference level, and, except for the sphere, is aspect-angle dependent. Specifically, σ is 4π times the ratio of the signal power per unit solid angle (i.e., one unit solid angle is the s*teradian*, and there are 4π steradians in a sphere) scattered in the direction of the receiver to the signal per unit area (the signal power density) that strikes the body.

where σ_{wd}^2 is the variance of the apparent wander distance and R_{mt} is defined as before. This equation states that although the magnitude of the wander is essentially range independent, the equivalent noise on the *LOS* angle measurements increases as range decreases.

As previously noted, receiver- and range-independent noise are generally assumed to be wide-band relative to the guidance system bandwidth. Angular scintillation noise is, in general, a narrow-band source and is often modeled as white noise through a low-pass filter with a time constant that depends primarily on the target motion spectrum.

Scintillation can be an important factor in various parts of an engagement. For instance, during acquisition, target fades, or periods of low aircraft return, can inhibit detection of the aircraft and therefore cause a lengthening of the prelaunch time of an engagement. Similarly, a surge in return strength can make an otherwise undetectable aircraft visible to a radar. Scintillation is usually less important once radar tracking has been established, since a lower signal level is needed to maintain track. However, in some cases, particularly in marginal detection circumstances, an aircraft fade can cause a radar loss of track.

In the application of modern optimal control and estimation theory to modeling of the seeker and missile/target dynamics, glint and scintillation errors are commonly modeled using filtered Gaussian white noise input in order to produce correlated noise output. The new noise treatment replaces the fourth-order Runge–Kutta approximation with the method of conditional probability density function (*pdf*). This new technique allows random draws of correlated errors to be made directly, thus eliminating the need to make white noise input draws and to filter this input before output draws are made. The probability density function of the correlated output error is found in closed form in terms of the previous value of the correlated output and the correlation coefficient. The new method provides accurate statistics and satisfies the necessary correlation properties. Its computational simplicity translates into substantial savings in computer processing time. The correlated output terms for glint and scintillation are computed using the same form of the conditional probability density function. The pdf is derived from the spectral density and autocorrelation function and is given by the expression

$$p(g_2|g_1) = \frac{1}{\sqrt{2\pi(1-\rho^2)\cdot\sigma_c^2}} \cdot \exp\left(-\frac{1}{2\sigma_c^2\cdot(1-\rho^2)}(g_2-\rho g_1)^2\right) \tag{3.88}$$

where

$$\begin{aligned} g_1 &= \text{previous value of the error term,} \\ g_2 &= \text{current value of the error term,} \\ \sigma_c &= \text{standard deviation of correlated noise,} \\ \rho &= \text{correlation coefficient.} \end{aligned}$$

This is a Gaussian density with mean ρ and variance $\sigma_c^2\ (1-\rho^2)$. Error terms are computed using the radar error covariance function RADEV(σ_c), which returns a

normally distributed random number with zero mean and standard deviation σ_c. The expression for computing the glint and scintillation is

$$g_2 = \rho \cdot g_1 + \text{RADEV}(\sigma_c), \tag{3.89}$$

where appropriate statistics are substituted into the above expression for glint or scintillation.

Thermal Noise: Thermal noise appears as random signals within the system bandpass. Thermal noise is usually viewed as white Gaussian noise, that is, noise with a power density equal across all frequencies and with an instantaneous value given by a Gaussian probability density function. The signal energy the radar tries to track is contained within the pulse repetition interval (*PRI*) lines within the system bandpass. Thermal noise contained within the bandpass is also passed through the signal processing elements and competes with the true signal. Since the thermal noise voltage is a random process, it tends to drive the radar off the true target return. The direction of this thermal-noise-induced track error changes continuously with time, since the noise instantaneous value is continuously changing. If the target return is much larger than the thermal noise return (e.g., if the signal lines within the bandpass are much larger than the noise level), then the thermal noise will have a relatively small impact, and system tracking will not be significantly disturbed. However, if the target return is small or if the noise level is large, then the energy contained in the noise can swamp the energy return of the target, and the system will drift far off the true target position.

The total measurement noise variance is the sum of the variances of the individual uncorrelated noise components

$$\sigma_t^2 = \sigma_f^2 + \sigma_c^2 + \sigma_s^2 + \sigma_{th}^2, \tag{3.90}$$

where σ_{th}^2 is the thermal noise variance.

Other typical error sources of a guidance system are *multipath* and *clutter* effects. Multipath and clutter occur naturally in the low-angle track situation, and each is capable of degrading radar-tracking performance. More specifically, multipath and clutter are types of noise signals caused by reflections from terrain surface features. Multipath and clutter effects will tend to degrade radar performance is, for example, tracking low-altitude targets. Multipath is a result of multiple paths the radar signal makes from the radar site to the target and return. Both the specular multipath, which is that governed by Snell's law–type reflections from a flat surface, and diffuse multipath (or random scatter from rough surfaces) reflection components are considered in radar tracking error analysis. The apparent range caused by multipath effects is

$$\textbf{\textit{Range}} = (|\mathbf{R}_{TS}| + |\mathbf{R}_{TSP}| + |\mathbf{R}_{SPS}|)/2,$$

where $\boldsymbol{R}_{TS}$ is the target-to-site vector, $\boldsymbol{R}_{TSP}$ is the target-to-specular-point vector, and $\boldsymbol{R}_{SPS}$ is the specular-point-to-site vector. The diffuse multipath, which is a random scattering of the radar energy from rough surfaces, can be implemented using Monte Carlo techniques. Clutter, which is the radar energy return that has been backscattered from the terrain surrounding the target, provides a competition signal to the target

return depending on the following: (a) general terrain type, (b) depression angle, (c) geometry, (d) surface roughness, and (e) radar characteristics. Specifically, the term *clutter* can be defined as any undesired radar echo, and is descriptive of the fact that such echoes can "clutter" the radar output and make detection of targets difficult. Reflectivity, a term associated with clutter, refers to the intensity of the reflection from clutter and is typically denoted by σ_0 (also termed the *incremental backscattering coefficient*). It is the cross-section per unit area:

$$\sigma_0 = \sigma_c / A_c,$$

where σ_c is the radar cross section (*RCS*) from the area A_c. Reflectivity σ_0 varies with the angle of incidence, frequency, and polarization of the transmitted wave, electrical characteristics of the surface, and roughness of the terrain. It is commonly expressed in dB (m^2/m^2). The power received from a clutter patch with *RCS* σ_c is [10]

$$P_c = P_t G_t^2 \sigma_c \lambda^2 F_c^4 / (4\pi)^3 R^4 L_c,$$

where

$$\begin{aligned} P_t &= \text{transmitted power,} \\ G_t &= \text{antenna gain,} \\ R &= \text{target slant range,} \\ F_c^4 &= \text{clutter pattern propagation factor,} \\ L_c &= \text{clutter transmission and beamshape losses.} \end{aligned}$$

3.4.3 Radar Target Tracking Signal

For missiles using radar as the target tracking sensor, the signal-to-noise ratio (*SNR*) and power requirements play an important role in the proper design of a guidance system. For example, in surface-to-air missiles (*SAM*s), the target's radar return signal strength is used for three purposes: (1) unless the *SNR* is above a given threshold, the missile will not be fired by the *SAM* system; (2) if the *SNR* drops below a given threshold, the target track will be lost by the system; this will result in a cessation of missile guidance; and (3) in an electronic countermeasures (*ECM*) environment, the *SNR* will be compared to the jammer-to-signal ratio (J/S) in simulations utilizing jammers to determine whether jamming is effective. Based on the discussion of Section 3.4.2, the radar sensor tracking errors of concern are the following:

(1) **Target glint.**
(2) **Instrumentation.**
(3) **Thermal noise.**
(4) **Ground clutter.**
(5) **Multipath.**

(6) **Knife edge diffraction:** In many low-angle tracking cases, there is a hill or tree line that masks the target at long range and that blocks the paths to the specular reflection point and to much of the diffuse glistening surface. Reflected multipath is then replaced by a diffraction component arriving from the top of the mask.

Each of these errors affects both the target elevation and target azimuth angle measurement channels. The instrumentation errors can be modeled as a fixed value nominally set at 0.5 mils and distributed about the true target elevation and azimuth angles with a Gaussian distribution standard deviation of 0.0005 mils.

In this section, the background methodology used to calculate radar and jamming *SNR* in surface-to-air missiles will be briefly described. We begin this section by developing the radar range equation. The basic relationship that determines the effectiveness of a radar is known as the *radar range equation*. This equation defines the maximum range at which a given radar can detect a given target. In essence, the radar range equation provides the most useful mathematical relationship available to the engineer in assessing both the need for, and the resulting effectiveness of, efforts to reduce radar target cross-section. In its complete form, the radar equation accounts for the following: (1) radar system parameters, (2) target parameters, (3) background effects (e.g., clutter and noise), (4) propagation effects (e.g., refraction and diffraction, and (5) propagation medium (absorption and scatter).

Assume now that a radar transmitter has a power output of P_t watts. If the power of the radar is radiated into space omnidirectionally, the power will be distributed evenly over the surface of a sphere whose center is located concentrically with the source of the power. Thus, at any range from the radar r, the surface area of the sphere is $4\pi r^2$. Dividing the total signal power by the surface area gives the power density at r for the omnidirectional antenna. Therefore, the power density of the signal at the target, located at a distance R from the radar, is simply [10]

$$\text{Power density at the target} = P_t G_t/(4\pi)R^2 \quad [\text{watts/m}^2], \tag{3.91}$$

where G_t is the peak gain of the antenna. Next, we note that the transmitted signal illuminates the target representing an area A_t, creating power at the target. The portion of the signal that is scattered in the direction of the radar receiver will either amplify or degrade this power by the gain factor G_t. Consequently, the product $A_t G_t$ represents the radar cross-section σ in units of m^2. In other words, σ is defined as the projected area that would be required to intercept and radiate isotropically the same power as the target radiates toward the radar receiver. Thus, we can treat the problem as though the target intercepts the power,

$$\text{Power intercepted} = P_t G_t \sigma/(4\pi)R^2 \quad [\text{watts}], \tag{3.92}$$

and radiates it isotropically, so that the power density at the receiving antenna (which for simplicity is assumed to be collocated with the transmitting antenna) is [10]

$$\text{Power density} = P_t G_t \sigma/(4\pi)^2 R^4 \quad [\text{watts/m}^2]. \tag{3.93}$$

The power received by the radar antenna is simply the power density at the antenna, multiplied by the effective capture area A_c of the antenna, but it is usually more convenient to work with antenna gain, where the gain and capture area are given by

$$A_c = G_r \lambda^2/(4\pi) \quad [\text{m}^2], \tag{3.94}$$

where λ is the signal wavelength in meters.

Finally, if we assume that the same antenna is used for both transmission and reception, so that $G_t = G_r = G$, then the received power P_r is [10]

$$P_r = (P_t G^2 \lambda^2 \sigma)/(4\pi)^3 R^4 \quad [\text{watts}], \tag{3.95}$$

where all the symbols have been defined. This is the simplest, most basic, radar equation. However, this equation ignores a number of effects that can be critical in detailed radar performance analysis. Nevertheless, it is invaluable for rough performance calculations. Equation (3.95) is sometimes presented in decibel form as follows:

$$\text{dBP}_r = 10 \log_{10} P_r \quad [\text{dBw}].$$

For detection range estimates, it is convenient to rewrite the radar equation in a slightly different form. Specifically, in the simple case of detection of a target in receiver noise, a required minimum *SNR* can be defined based on required detection probability, target statistics, and radar characteristics. However, because receiver noise can be considered to be a constant, the minimum *SNR* defines the maximum detection range by defining a minimum level of received signal, P_{min}, that can be tolerated. Therefore, the maximum detection range is given by

$$R_{max} = [P_t G^2 \lambda^2 \sigma/(4\pi)^3 P_{min}]^{1/4} \quad [\text{m}]. \tag{3.96}$$

The target radar cross-section (σ) coordinate system is commonly site oriented with zero azimuth defined at the tail of an aircraft (the target) and 180° at the nose. Next, we note that in many systems, $G_t = G_r$, since the same antenna is used for both transmitting and receiving. Equation (3.91) is sometimes presented in decibel form as follows:

$$\text{dBS} = 10 \log_{10} S \quad [\text{dBw}].$$

We will now discuss briefly the radar noise statistics. For a typical radar receiver, the thermal noise power that is generated by the random thermal motion of conduction electrons in the input stages limits the signal that can be detected. The available thermal noise power is a function of the temperature T and the bandwidth B_n of the receiver, and is commonly expressed in the form [10]

$$P_n = kTB_n \quad [\text{watts}], \tag{3.97}$$

where

$$k = \text{Boltzmann's constant} = 1.38054 \times 10^{-25}\ J/K,$$
$$T = 290\ K, \text{ reference (or room) temperature.}$$

(At room temperature, $P_n = -114$ dBm; dB relative to a milliwatt for a receiver with a 1-MHz bandwidth.)

An ideal receiver would add no noise to the signal to be amplified, so that the input and output *SNR* would be the same. However, actual receivers add some noise of their own, and the noise figure F, defined for a linear system as

$$F = (S_{in}/N_{in})/(S_{out}/N_{out}), \tag{3.98}$$

is a measure of how much the receiver degrades the input *SNR*. Additional losses, such as scanning, beam shape, integration, and collapsing in the radar system can be defined that further degrade the received signal power. If we lump all losses together and designate them by L, then the radar equation can be expressed in terms of the *SNR* as follows:

$$SNR = (P_t G^2 \lambda^2 \sigma)/(4\pi)^3 R^4 k T B_n F L. \tag{3.99}$$

The *SNR* plays a major role in the detection and tracking capabilities of a radar system. For instance, during the operation of any radar system, the goal of the radar operator is to be able to distinguish target (e.g., aircraft) echoes from the noise.

Another important area in missile guidance is electronic countermeasures (*ECM*). *ECM* relies on a number of techniques, such as creating saturation of the radar screen to hide the desired target by using a stand-off jammer, thus creating false targets with chaff, or using a deception jammer to break radar track on the target. In the case of chaff, the idea is to force the tracking radar off the target. Specifically, in order to avoid *SAM*s headed at them, jet aircraft fighter pilots frequently eject chaff and flares that disrupt the missile's homing system. If that does not work, they may have to wait until seconds before a *SAM* is about to catch up to them and then do an evasive maneuver. Also, in order to slip away from a *SAM*, which is faster than a fighter jet, pilots often have to jettison the external fuel tanks that hang under each wing. (Note that a rising *SAM* looks like a doughnut to a pilot, that is, it appears as a ring of fire with a hole in the middle and is probably on a trajectory aimed directly at the plane.

Deception jammers are generally carried on the jamming vehicle (i.e., aircraft or missile). Thus, spatial separation of the jammer and target cannot be used to break track, as can be done with chaff. In addition, most modern missiles have a *home-on-jam* mode; thus simple barrage jamming will also be unsuccessful. (Barrage or broadband jamming consists in jamming a spectrum of frequencies much wider than the operating bandwidth of the radar. Barrage jamming is normally used when the radar frequency is either unknown or changing, or to cover the operating frequencies of more than one radar.) For this reason, deception jammers must produce a signal that appears to the radar to come from somewhere other than the target. One successful jamming technique is to produce a jamming signal amplitude modulated at the conical scan frequency. If sufficiently strong, such a signal will mask the signal from the target and produce a false error signal likely to cause a loss of track. It should be pointed out that monopulse systems are immune to amplitude modulation jamming because they produce an error signal based on each pulse. All jamming methods require that

the jamming signal overcome the skin return from the target. Three common types of jamming models are the following:

1. Noise jamming, which is assumed to be continuous in time (CW).
2. Track break jamming, a responsive technique that denies acquisition.
3. Deceptive countermeasures ($DECM$), which cause errors in range or angle measurement.

All three types of these jamming models are characterized by the effective radiated power and jammer bandwidth.

Since the effective radiated power includes the jammer's antenna gain, it is input as a function of the aspect angles (i.e., azimuth and elevation) of the target.

One of the most important parameters affecting the effectiveness of noise jamming is the jam-to-signal or (J/S) ratio. This is the ratio of the power of the noise J to the power of the echo S. Thus, for a jammer with an output power P_j and an antenna gain G_j , the power received by a radar with antenna gain G is given by

$$J = (P_j G_j G\lambda^2)/(4\pi)^2 R^2 \quad \text{[watts]}. \tag{3.100}$$

The skin return is simply given by the radar equation, (3.95); therefore,

$$J/S = (4\pi P_j G_j R^2)/P_t G\sigma. \tag{3.101}$$

This equation is sometimes written in the form

$$J/S = [P_j G_j / P_t G][4\pi/\sigma][R^2].$$

As with P_r, J can also be written in decibel form as follows:

$$dBJ = 10\log_{10} J \quad \text{[dBw]}.$$

At this point, let us examine the radar *range-tracking* loop. Typically, tracking radars are closed-loop systems that attempt to keep the selected target centered within the beam scan pattern and provide tracking data to a fire-control system. The primary output of most radar tracking systems is the target location determined by the pointing angles of the antenna beam and the positions of the range-tracking gates [10]. The tracking data is used by a fire-control computer to predict the future position of the target so as to achieve an intercept. In pulsed systems, target range is determined by measuring the time delay between transmission of an RF pulse and the reception of the pulse echo from the target. Range tracking provides an important means of multiple-target discrimination by eliminating signal returns other than those of the intended target. This is accomplished by receiver gating. That is, the receiver-input channel is opened for an interval when a pulse return is expected, and closed the remainder of the time. The range-tracking circuitry is used to keep an open gate centered on the desired target return.

A simple range-tracking loop is illustrated in Figure 3.31. This range-tracking loop has two major components: (1) the range discriminator, and (2) the servo that repositions the range gate. In Figure 3.31, R_t is the true range to the target, and R_g is the measured range to the target.

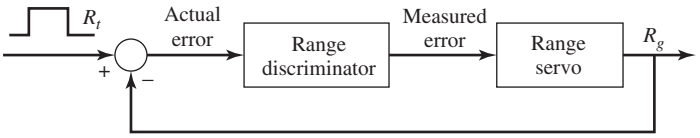

Fig. 3.31. Range-track loop.

We conclude this section by noting that in aircraft survivability design and/or analysis, one commonly distinguishes between onboard and standoff (or offboard) active electronic equipment to degrade the effectiveness of the various nonterminal threat elements. Onboard radiation emission equipment for defensive electronic countermeasures is usually referred to as a self-screening or self-protection jammer, such as the Navy's airborne self-protection jammer. Offboard equipment can be carried either by a drone (e.g., an unmanned aerial vehicle (*UAV*)) or by a special-purpose *ECM* support aircraft, such as the Navy's *EA-6* and the Air Force's *EF-111* aircraft.

The Block 5 *HARM AGM-88C* missile uses a new *home-on-jam* capability to lock onto a jammer. Specifically, this missile has the capability to attack a *GPS* jammer; that is, it has the capability to attack the last known geographic location if a threat radar goes off the air, and improved capability against advanced radar waveforms. A new, *smarter* version of the *AGM-88 HARM* antiradar missile is under development at the present time, which is designed as a substitute for the existing models. Development of the *smarter* control/guidance section of the new *HARM*, which will include both *GPS* and inertial guidance. The development of this new *HARM* missile is a joint effort of Germany, Italy, and the United States, and is called the International *HARM* Upgrade Program. The enhanced version of the U.S. *AGM-88C* will be designated as the *AGM-88D*, while the German and Italian versions as *AGM-88B+*. The original *HARM* concept, developed more than two decades ago, was designed to home on signals emitted by threat radars. Thus, if a *HARM* missile were launched against a specific threat radar that suddenly stopped transmitting, the *HARM* guidance system could "look" for and attack another radar in the vicinity. The new *HARM*s equipped with both *GPS* and inertial guidance will be able to accurately determine "no-attack" geographic areas, that is, cases where the threat radars may be intentionally located near hospitals or other populated areas. If the geographic coordinates of a threat radar have been determined by photographic or electromagnetic reconnaissance, its location can be programmed into the upgraded *HARM*'s guidance system. This will enable the missile to continue its attack even if the threat radar shuts down. To this end, an even *smarter* antiradar guidance system with such capability is being developed under an advanced technology demonstration program called *Advanced Anti-Radiation Guided Missile* (*AARGM*). The dual-mode guidance technique is designed to enable a further upgrade of *HARM* missiles. As the *AARGM* approaches the vicinity of its intended target (e.g., if the radar has shut down), the missile's millimeter-wave radar will activate to search for strong echoes from the target's radar antenna and/or its launcher of antiaircraft missiles.

3.4.4 Infrared Tracking Systems

In addition to the radar target-tracking seekers described in the previous section, a number of other target-tracking sensors are used in tactical missile guidance. In general, sensors used as seekers that depend on their operating wavelength are typically characterized (depending on the sensor's operating wavelength) as (1) optical sensor, (2) infrared (*IR*) sensor, (3) synthetic aperture radar* (*SAR*), (4) laser radar (also known as *ladar*), (5) television (*TV*)/video, (6) microwave, (7) millimeter wave (*MMW*), and (8) acoustic sensors. In this section we will discuss the *IR* sensor. An obvious advantage of the *IR* sensor is that it is capable of operating during the day as well as at night, in conditions of rain or smoke, and capable of hot-spot detection. A word of caution, however, is in order here. An *IR* missile cannot be used in bad weather or at low altitude, where most targets are to be found. However, new types of seekers today offer greater sensitivity and the ability to distinguish between real and false targets by using advanced designs such as Cassegrain optics. A sensor that is worth mentioning is the *IRSS* sensor. The *IRSS* was designed to thwart heat-seeking missiles. Moreover, the *IRSS* is like an extra cowling that hides the heat-seeking signature of the engines from observers below. The system was first installed in the Vietnam-era *AC-130H Spectre* gunships.

For many years, a great deal of attention was paid to the infrared end of the spectrum (e.g., in surveillance systems and missile guidance), and this in turn stimulated the development of infrared materials. Specifically, infrared detection and tracking systems are often used in the guidance of tactical missiles, either by command, semiactive, or passive homing. For example, missiles using command guidance may carry an *IR* beacon in the tail. The beacon is passively tracked by an *IR* sensor in the tracking device while the operator attempts to track the target, usually with the aid of either direct-view optics or electrooptics (*EO*). In other words, the tracking system notes the difference in the target and missile positions and generates the necessary commands to direct the missile to an intercept. The command-to-*LOS* (*CLOS*) navigation technique is usually used when the target range information is not available.

In order to have a better understanding of the infrared tracking systems, a brief discussion of the physics of infrared will now be given. The infrared band lies within the optical region and extends roughly from 3×10^{11} Hz up to about 4×10^{14} Hz. The renowned astronomer Sir William Herschel first detected this region in 1800. The infrared band is often divided into four subbands as follows: (1) the *near* infrared, i.e., near the visible band (780–3000 nm**), (2) the *intermediate* infrared band (3000–6000 nm), (3) the *far* infrared band (6000–15,000 nm), and (4) the *extreme* infrared band (15,000 nm–1.0 nm). This is a rather loose division, and there is no universality in the nomenclature. Any body that has a temperature above absolute zero emits electromagnetic radiation in the IR band. As the temperature of a body increases above absolute zero, the molecules start to rotate. Furthermore, as the temperature increase continues, atomic vibrations become important, and further

*A synthetic aperture radar (*SAR*) uses the aircraft's own flight path to simulate the curve of a radar dish several hundred meters long.

**1 nanometer (nm) $= 1 \times 10^{-9}$m.

increases in the temperature can cause electron transition radiation. Therefore, the total amounts of thermal power radiated by a body and the distribution of the power over the wavelength spectrum are functions of the body material and temperature. For solids, the power is smoothly distributed over a relatively broad band of wavelengths, whereas in hot gaseous mixtures, such as engine exhaust plumes, the power is radiated within very small bandwidths centered at discrete wavelengths. *IR* missiles are limited to attack from the rear in order that the seeker can lock onto the hot jetpipes of the target aircraft. Thus, infrared hot-spot guidance has applications in short-range air intercept using as *IR* sources the target aircraft exhaust pipe, the exhaust plume, and for high-speed targets the aerodynamically heated leading edges. Radiant energy at the long wavelength extreme can be generated using either microwave oscillators or incandescent sources, i.e., molecular oscillators. Indeed, any material will radiate and absorb *IR* via thermal agitation of its constituent molecules. In addition to the continuous spectra emitted by dense gases, liquids, and solids, thermally excited isolated molecules may emit *IR* in specific narrow ranges. The need for warning devices from *IR* missiles is obvious. For example, and as mentioned above, if *IR* homing missiles are expected to approach the target (e.g., aircraft) from the rear only, the launch warning system will be installed in the tail of the aircraft. Therefore, a warning that a missile is actually approaching the aircraft can be provided by an active missile approach device that uses an active transmitter and receiver to track the missile. Note that the warning device must discriminate between actual target and background clutter; therefore, the system must be so designed as to ensure a low level of false alarm.

A recent development in *IR* sensors is the *AN/AAQ-24*(*V*) directed infrared counter-measures (*DIRCM*). This sensor is designed to detect and track an incoming *IR* missile fired at an aircraft, and to focus high-power arc-lamp countermeasures at the missile seeker to confuse it. It is the optical assemblies that transmit the high-powered arc-lamp beam with its *IR* countermeasures. An industrial team consisting of Northrop Grumman and BAE Systems jointly developed *DIRCM* for the U.S. Special Operations Command and for the U.K. Ministry of Defence to protect aircraft and helicopters from shoulder-fired heat-seeking missiles, such as the *Stinger* (*FIM-92*). Figure 3.32 illustrates a generic *IR* seeker.

The *IR* seeker (or tracker) typically consists of the following components: (1) a gimbaled platform that contains the optical components for collecting and focusing the target radiation, (2) an *IR* sensor that converts the incident radiation into one or more electrical signals, (3) the electronics for processing the sensor output signals and converting them to guidance commands, (4) a servo and stabilization system to control the position of the tracking platform, (5) *IR* cooling system, and (6) a protective covering, the dome (also known as *irdome*). The infrared radiation incident on the seeker dome passes through the dome and strikes the primary mirror, which in turn redirects the incident radiation to the secondary mirror. This mirror then focuses the radiation on a spinning reticule or chopper. The reticle periodically interrupts or modulates the incoming radiation or signal for the purpose of target discrimination and tracking. The *IR image processor* (item 3 above) is needed to provide a two-dimensional image with target and background. The image processor consists of a head assembly, scanners, *IR* optics, detector, cryogenic system, preamplifier/amplifier,

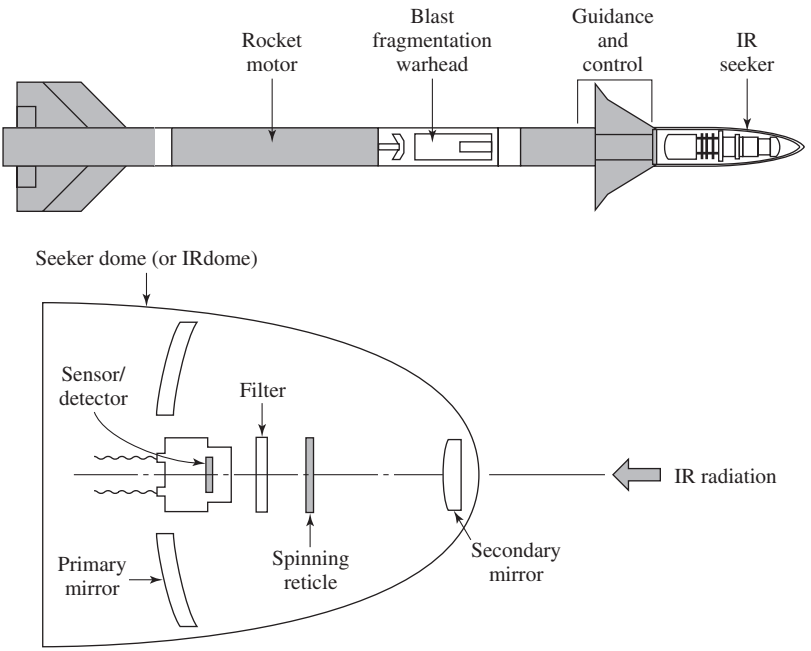

Fig. 3.32. Example of a generic *IR* seeker and its location on a missile.

and display. An infrared guided missile, such as the Sidewinder, is similar in many respects to other aerodynamic tactical missiles, except for the seeker. These seekers are self-contained and need no specialized carrier (or launch) aircraft equipment (with the exception, perhaps, of the cooling system), resulting in a lower missile cost. Some passive *IR* systems may use more than one detector element to cover different portions of the infrared band, thus enhancing the tracking capability; these are referred to as multiple color systems. When detection occurs, the tracking process is initiated, provided that the tracking platform is uncaged. Therefore, if the tracker is continuously and automatically tracking the target, the seeker is said to be locked on. It should be pointed out that when the guidance system is in the *IR* detection mode, the signal detected by the *IR* detector may be contaminated by disturbance noise; this should be considered in designing the system. Once the missile seeker locks onto the target, the range can be computed. This range will depend on the minimum signal-to-noise ratio required by the sensor for target lock-on. Mathematically, the range can be expressed in the form

$$R_{LO} = [I/(L\xi_{min}\psi_n)]^{1/2}, \tag{3.102}$$

where

I = target aircraft radiant intensity [w/steradian],

L = atmospheric loss or attenuation of the signature as it propagates over the distance R_{LO} ($R \geq 1$),

ξ_{min} = minimum *SNR* required by the *IR* sensor for target lock-on,

ψ_n = noise equivalent flux density $[w/m^2]$.

As was the case with the radar *SNR*, the *IR* seeker also exhibits an *SNR*. For *IR* seekers, the *SNR* depends upon several effects: (1) the aspect of the target aircraft in the seeker field of view (*FOV*), (2) the distance from the aircraft to the seeker, (3) the off-boresight angle of the aircraft in the seeker *FOV*, and (4) the reflection of sunlight off the target body.

Future smart air-to-air and surface-to-air missiles will carry advanced multimode infrared seekers and new countermeasure systems that will reduce considerably the effectiveness of conventional self-protection systems. In particular, the future joint air-to-surface standoff missile (*JASSM*) seekers will most likely be designed with imaging infrared (I^2R) and the use of *SAR*. For instance, the *AIM-9X* air-to-air missile guidance system has been designed with an advanced imaging infrared focal plane array detector, and high off-boresight seeker and helmet-mounted display capability (see also Appendix F). A later version of the *AIM-9X Sidewinder II*, the *AIM-9X Evolved Sidewinder* heat-seeking missile development, has been delayed because of problems with the missile's control actuation system: The mechanism that unlocks the control fins failed. This problem was corrected by redesigning the fin lock. The fin lock holds the control surfaces in place until a few moments after the missile has separated from the aircraft. Another type of passive infrared system is the forward-looking infrared (*FLIR*) imaging sensor, which provides a different mode of target detection and recognition. The *FLIR* is commonly used in fire-control systems for initial target acquisition. Furthermore, *FLIRS*s may use a two-dimensional planar array of individual infrared detectors, so that the output is a two-dimensional infrared picture of the target. A video tracker microprocessor *FLIR* consists of sensors and ancillary electronics as well as video processing.

An advanced threat infrared countermeasures (*ATIRCM*) system has been developed for U.S. Army helicopters. In addition, a common missile warning system that is part of *ATIRCM* will serve as a stand-alone system without the jammer in many Air Force and Navy fighters and transports. *ATIRCM* will use a laser system mounted in a turret to direct a beam of jamming energy into the eye of the seeker of an incoming *IR* missile. The object is to provide deceptive signals or to overload the seeker with excessive radiation. The directed-energy approach is needed to provide enough intensity to defeat the new types of seekers that will key on the image of an aircraft rather than just a hot spot. Current omnidirectional *CM* systems would require too much aircraft electrical power to radiate at that required intensity. (Note that missiles with imaging *IR* seekers are already in operational service). *ATIRCM* is designed to work with a variety of other systems such as advanced-threat radar jammers. It also ties together missile warning, jamming, and *CM* dispensing functions. A common missile warning system also is being designed for Block 50 *F-16*s along with the *F-15E* and *C* and the *A-10*. In addition, the *MH-53J* special operations helicopter and the *CV-22* are candidates to receive the full system including missile warning and jamming. The common warning system will be compatible for use in Navy fighters including the *F/A-18C*, *D*, and *E*/*F* as well as the *F-14A*, *B*, and *D*. An Air

Force version of the *ATIRCM* is undergoing testing. Known as the *LAIRCM* (Large Aircraft Infrared Countermeasure), this laser-based *CM* system is designed to protect large aircraft such as the *C-17A Globemaster III* and the *C-130*s from man-portable, heat-seeking* missiles like the *Stinger* (*FIM-92*). The *LAIRCM* system, designed by Northrop-Grumman, underwent live-missile-fire testing. Testing of the system was completed successfully on July 3, 2002, putting the program on track to deliver the first laser-protected transport to Air Mobility Command (*AMC*) by the year 2004. Because of its importance, we will now go into some more detail of the *LAIRCM* system.

***LAIRCM*:** *LAIRCM*, which autonomously detects, tracks, and then jams *IR* threat missiles, successfully completed tests conducted at the White Sands Missile Range, NM, aerial cable facility. During the tests, missiles were fired at a carrier, holding the *LAIRCM* system and four heat sources in an orientation emulating a *C-17* during takeoff. The live-missile-fire tests follow extensive laser tests conducted earlier in the year 2002 at the AF Electronic Warfare Evaluation Simulator at Fort Worth, Texas. According to a 1999 U.S. Transportation Command report to Congress, the vulnerability of its large, slow-flying aircraft to the increasing shoulder-fired surface-to-air missile (i.e., the *Stinger*) capability is their number-one force-protection concern. Consequently, high on their priority list is fielding a large-aircraft *IRCM* system that can counter this threat. It is estimated that more than 500,000 shoulder-fired surface-to-air missiles exist and are available on the worldwide market. *AMC* flies more than 10,000 missions a year into locations where groups armed with these types of weapons could pose a significant risk. Therefore, the need for such a system is obvious.

Transport aircraft are especially vulnerable because they present a slow, predictable target that can be easily "seen" and tracked by an *IR* missile's sensor. That means that an *IR* missile can go after a larger aircraft with its corresponding larger engines more easily and from a longer range. To counter this threat, large aircraft have to put out a jamming energy that is larger than the aircraft signature; that is, it has to present a brighter target in order to blind and confuse the missile's *IR* seeker. *LAIRCM* is an active countermeasure that defeats the threat missile guidance system by directing a high-intensity modulated laser beam into the missile seeker. In addition, the *LAIRCM* system automatically counters advanced *IR* missile systems with no action required by the crew. The pilot will simply be informed that a threat missile was detected and jammed.

3.5 Autopilots

This section considers the design of autopilots utilizing the discussion of Section 3.2.1 on airframe transfer functions. As can be seen from Figures 3.22 and 3.23, an autopilot is a closed-loop system inside the main guidance subsystem that ensures that the missile achieves accelerations as commanded and maintains stability; the control system consists of a roll autopilot and, as will be discussed below,

*Heat-seeking missiles guide on the radiated energy created by an aircraft's engines.

two essentially identical pitch and yaw autopilots. The function of the autopilot is to stabilize and guide the missile by requesting fin deflections, which cause the missile body to rotate and hence translate. Its basic job changes at the target acquisition phase from nulling the seeker gimbal angles (if used) to satisfying acceleration commands. The fin servos respond to the commands ordered by the autopilot, and the actual fin deflection is computed by the balance between servo torque and aerodynamic hinge moment. These fin deflections then act to force the airframe dynamic model. Historically, autopilots were developed for aircraft flight control systems. As a result, and because the transient response of an aircraft varies considerably with changes in airspeed and altitude, the gains of all autopilots were scheduled as a function of Mach number or dynamic pressure. The autopilot requirements and limitations are closely related to the overall design of the guidance subsystem. The aerodynamic characteristics of the missile airframe are an integral part of the autopilot design and operation. Therefore, the autopilot refers to the missile airframe dynamics and associated stability augmentation system, which is designed so that the missile lateral acceleration follows the autopilot acceleration commands as closely as possible. The design of an autopilot must be tailored to each individual missile airframe configuration and its associated aerodynamic characteristics, which are nonlinear functions of missile velocity, angle of attack, control surface deflection, and altitude. Therefore, a properly designed autopilot provides a nearly linear response characteristic if changes in these parameters about their nominal design values are small. It should be pointed out, however, that there are some missile designs that do not require an autopilot. The most important nonlinear characteristic associated with the airframe is acceleration saturation, which occurs when the missile attempts to pull a large angle of attack. It is desirable to avoid a large angle of attack, since the associated drag results in a rapid loss of missile velocity. Furthermore, the airframe structural limit must not be exceeded. It is common practice in missile design to limit the commanded lateral acceleration in order to prevent both angle-of-attack saturation and structural failure. Therefore, autopilot command limiting is assumed to be the dominant nonlinear effect, and all other nonlinear characteristics, such as actuator angle and angle rate limiting, aerodynamic nonlinearities, and instrumentation nonlinearities, are assumed to be secondary or equivalently represented as acceleration-limiting, or as changes in autopilot dynamics. The resulting model is therefore simple and generally applicable to a wide range of missile systems, and captures what is known to be a dominant nonlinear system characteristic and an important factor in miss distance: lateral acceleration.

Note that it is standard practice in the design of missile autopilots to utilize a linearized second-order airframe model. The airframe acceleration command must be limited in an actual missile in order to prevent structural failure or an excessively large angle of attack, which causes increased missile drag and loss of lateral (note that in missiles, lateral movement usually means up–down or left–right) acceleration capability, often referred to as airframe acceleration saturation. Therefore, we can define the function of the autopilot subsystem as follows: (1) provide the required missile lateral acceleration response characteristics, (2) stabilize or damp the bare airframe, and (3) reduce the missile performance sensitivity to disturbance inputs over

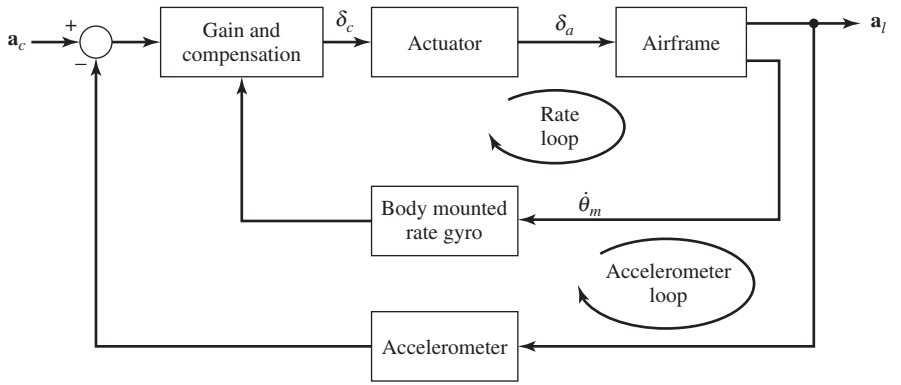

Fig. 3.33. Typical missile autopilot configuration.

the missile's flight envelope. Autopilots are commonly classified as either controlling the motion in the pitch/yaw planes, in which case they are called lateral autopilots, or controlling the motion about the fore-and-aft axis, in which case they are called roll autopilots (or longitudinal autopilots). Note that in aircraft design, the autopilot nomenclature is somewhat different from that of missile autopilots. Specifically, in aircraft nomenclature, autopilots designed to control the motion in the pitch plane are called longitudinal autopilots, while those designed to control motion in the yaw plane are called lateral autopilots.

Strictly speaking, a typical interceptor missile has three separate autopilots for control of roll, pitch, and yaw. The pitch and yaw autopilots control the lateral acceleration of the missile in accordance with some guidance law, such as the proportional navigation guidance law. Although the roll autopilot is not used directly in homing, nevertheless it is designed to enable maximum homing performance in the other two axes.

A realistic autopilot can be designed that requires knowledge of very few specific aerodynamic parameters, yet its response characteristics are easily related to the important missile aerodynamic properties. Figure 3.33 illustrates a block diagram of a generic autopilot, which uses accelerometer feedback in order to control the lateral acceleration of the missile [1], [3], [11].

Using a linearized airframe model, the closed-loop transfer function for the general autopilot configuration of Figure 3.33 can be developed for specific gains and compensation. Commonly, and as we shall see later, lateral acceleration control is used in accordance with the proportional navigation guidance law, which requires a missile lateral acceleration proportional to the measured missile-to-target line-of-sight (*LOS*) rotation rate $(d\lambda/dt)$. Furthermore, the body-mounted rate gyroscope senses the body-attitude rate, $d\theta_m/dt$, which is used by the autopilot to increase the effective damping ratio of the airframe's short-period poles. The missile motion in space is completely defined by the acceleration normal to the velocity vector and the rate of change of the velocity magnitude. The commanded normal acceleration is the input

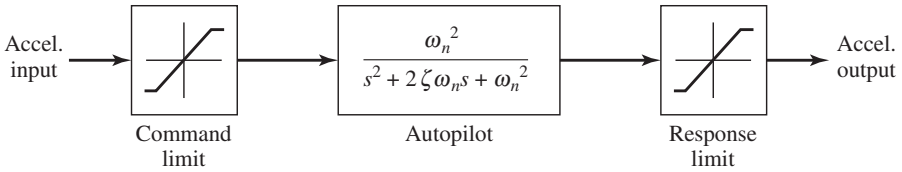

Fig. 3.34. Control system/aerodynamic response transfer function.

to a combination of limiters and transfer functions that simulate the autopilot, control system, and aerodynamics, yielding realized accelerations as the output. Specifically, the commanded acceleration is passed to the autopilot in a body frame sense. For example, for a tail-controlled missile, the autopilot/control system generates an output fin deflection, which rotates the missile, causing an angle of attack and thereby altering lift and drag. Aerodynamic linearization techniques, empirical data, and assumptions as to nominal velocity magnitude allow the missile designer to predict lateral acceleration as a function of commanded control fin deflection (and time). The primary source of commanded acceleration in tactical homing missiles is, as stated above, some form of proportional guidance. The proportional guidance law uses seeker information to generate acceleration commands.

Another effect of importance to a real missile arises if the missile is rolling and the pitch/yaw autopilots fail to compensate for the roll. This effect, which manifests itself as roll cross-coupling, causes the lateral acceleration calculated in one plane to be executed, due to system lags, in another plane. For this reason, missiles are often fitted with roll-attitude hold autopilots. The autopilot also assumes that the missile roll rate is either zero, or known and compensated for. Indicated in Figure 3.34 is the flow of commanded and output normal accelerations through the missile control system.

In Figure 3.34, ω_n is the system natural frequency, ζ is the system-damping ratio, and s is the Laplace operator. Before passing into the autopilot, the commanded accelerations are checked to ensure that they do not exceed structural or aerodynamic limits. That is, the inputs to the autopilot block transfer function are restricted to some maximum value if limits are exceeded. The autopilot block transfer function can be represented either as a first- or second-order lag with inputs of commanded acceleration and outputs of realized output acceleration. The roll, pitch, and yaw autopilots will now be discussed in more detail.

Roll Autopilot: The basic function of the roll autopilot is to roll-rate stabilize the missile, that is, to provide missile stabilization of roll attitude about the longitudinal axis. This is accomplished by sensing roll rate, and using the signal to deflect the fins (or wings) by an amount sufficient to counteract roll disturbances. Moreover, the response of the system must be sufficiently fast to prevent the accumulation of significant roll angles. When mounted on an aircraft, the missiles may be mounted at some angle other than their correct flight orientation. In order to align the polarization of the illuminator and the missile front antenna, the missile must be rolled to its umbilical up position (with respect to the attitude of the launching aircraft) after launch. To produce this required roll, a fixed dc voltage is supplied to the missile. At

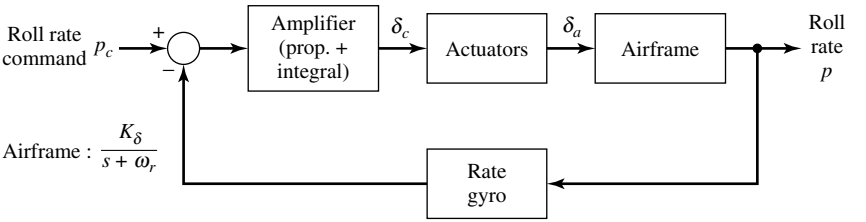

Fig. 3.35. Block diagram of a roll autopilot.

shorter ranges, the roll command is not necessary and may be removed to improve the effectiveness of the missile at shorter ranges. Roll in a missile can be caused by (1) asymmetric loading of the lifting and control surfaces in supersonic flight, which occurs when pitch and yaw incidences (i.e., angles) occur simultaneously and are not equal, and (2) atmospheric disturbances, especially if the missile is flying close to the ground. Some missiles are deliberately designed to have a high roll rate, with appropriately timed periodic lateral acceleration so as to null the *LOS* rotation rate. However, high roll rates can cause cross-coupling between the symmetric pitch and yaw autopilot channels, thereby tending to destabilize the system. In still other missile designs, the roll autopilot is designed to hold the roll attitude of the missile nearly constant for two major reasons: (1) Because of the lags in the guidance system, rolling at moderate or high frequencies may cause a lateral corrective acceleration to occur out of the proper plane, thereby causing an increase in the miss distance; (2) severe continuous rolling may cause loss of tracking the target or loss of aerodynamic control.

One common type of roll autopilot utilizes a spring-restrained rate gyroscope for measurement of roll rate, in conjunction with proportional-plus-integral (*PI*) compensation in the autopilot amplifier, in order to give the approximate equivalent of roll-rate plus roll-angle feedback. Other roll autopilot designs utilize a free vertical gyroscope as an attitude reference. That is, in order to maintain a desired roll angle, an attitude reference must be used. A block diagram of the roll autopilot is shown in Figure 3.35.

A more elaborate missile design has utilized a full-fledged stable platform, however, for other reasons as well as roll control. The function of the amplifier in the roll autopilot is to send aileron-command signals to either two diametrically opposite fin (or wing) servos or to all four. The airframe transfer function can be represented simply by

$$p/\delta_a = K_\delta/(s+\omega_{cr}),$$

where p is the roll rate, δ_a is the commanded aileron deflection, K_δ is the surface effectiveness, s is the Laplace operator, and ω_{cr} is the maximum gain-crossover frequency. As indicated in Figure 3.35, roll stabilization is obtained by sensing the roll rate with a rate gyroscope. The gyro output is amplified and applied to a phase-sensitive comparator. This output is then electronically integrated, and the resulting

signal is used, as stated above, to deflect fins 2 and 4 differentially (the fin order and nomenclature will be discussed in Section 3.5.1). In other words, the required rolling moment can be achieved by differential movement of the control surfaces. The variation in stabilization-loop bandwidth is a function of aerodynamic pressure, which is dependent upon missile altitude and velocity. Electronic gain in the loop also is a factor affecting bandwidth. Some missiles use altitude *band-switching*.

Basically, band-switching is used to maintain within appropriate limits the product of surface roll effectiveness K_δ and the electronic gains. In general, the criterion (such as M_δ) for band-switching in pitch would govern the band-switching in roll. This requires some minor measurement and computation in the carrier aircraft, which sets the proper band in the missile prior to launch. If the missile changes altitude radi-cally as in a *snap-up* attack or otherwise changes drastically its value of M_δ, then some compromise in stability and/or speed of guidance response may be necessary. In general, it is not considered practical for the missile to make measurements of air data and to compute M_δ for autonomous band-switching. Instead, a better solution is an *adaptive* autopilot system. Altitude band-switching compensates for the effects of altitude. (Note that this band-switching can be eliminated by designing adaptive autopilots.) Bandwidth variations at a given altitude are compensated for by making the electronics portion of the loop gain a function of velocity. The bandwidth of the roll autopilot may need to be about twice that of the pitch autopilot, in order to suppress high-frequency induced roll moments that are caused by the guidance system noise. Furthermore, in order to minimize the effects of aerodynamic cross-coupling, the roll autopilot should have a gain-crossover frequency (bandwidth) appreciably greater than that of the pitch or yaw autopilots. As stated above, a roll autopilot is typically compensated for changes in altitude and Mach number by band-switching the amplifier gain, and if the application warrants adaptive autopilots, the adaptive measurement may advantageously be made in the relatively noise-free roll channel and then used in all three autopilots. In addition, the roll autopilot has velocity compensation to further increase its effectiveness over the operational envelope.

Variation of dynamic pressure with flight conditions alters the autopilot characteristics from one of fast response with minimum stability at high dynamic pressures to one of relatively slow response with maximum stability at low dynamic pressures. In addition, the roll autopilot has velocity compensation to further increase the roll autopilot effectiveness over the operational envelope. Another function of the roll autopilot, say in air-to-air engagements, is to roll the missile in response to command signals initiated by the launching aircraft. In other words, and as stated above, a commanded rotation of the missile is necessary to achieve proper umbilical-up missile orientation when the configuration of the launching aircraft makes it impractical to launch the missile with this orientation. The aircraft roll command is delayed from being applied to the autopilot until the missile has cleared the aircraft, at approximately 0.5 seconds.

The missile velocity for controlling roll autopilot gain during flight is accomplished by electronically integrating the output of the longitudinal accelerometer and using this integrator output to control roll gain. In the prelaunch condition, the true

air speed (*TAS*) signal at 1-volt peak-to-peak of 400 Hz signal per 100 ft/sec from the launching aircraft is converted and stored on a capacitor. The initial velocity of the missile is the true airspeed of the carrier aircraft at the time of launch. Note that air-to-air missiles use *TAS* at launch, in conjunction with missile acceleration, to enable better control of corrective missile maneuvers through the use of velocity compensation in the autopilot. Maximum fin deflection is limited by the missile velocity and the altitude band in which the missile is flying.

We conclude the discussion of the roll autopilot by noting that in designing the roll loop, one must know the maximum anticipated induced rolling moment and the desired roll-position accuracy. It is estimated that the largest rolling moments will occur at about $M = 2.8$ due to unequal incidence in pitch and yaw. Rolling moments are obtained from the following four sources and converted into acceleration about the missile longitudinal axis:

1. *Induced Roll:* The four fins on the missile produce a rolling moment when the wind direction is not symmetric.
2. *Fin Blanking:* When the fins are displaced, asymmetric air flow causes differential lift on either side of the body. The rolling moment induced will depend on the angle of attack and Mach number; therefore, to modify these effects, a modifying function is commonly used.
3. *Aileron Moment:* The effective aileron deflection δ_a, obtained by differential fin commands, is used to calculate a rolling moment (assumed to vary linearly with δ_a, but with a slope varying with Mach number.
4. *Roll Damping:* The roll damping moment is assumed proportional to roll rate, and the coefficient C_l is looked up as a function Mach number alone.

Pitch/Yaw Autopilot: Basically, the pitch/yaw autopilots (also known as *lateral* autopilots) each consist of a major accelerometer feedback loop that provides the desired conversion of commanded acceleration to missile acceleration, and a minor rate feedback loop that provides the necessary damping of missile pitch or yaw rates. Therefore, because the pitch and yaw autopilots must control the lateral (lateral movement means up–down or left–right) acceleration of the missile in accordance with the proportional navigation guidance law, each autopilot must have feedback from an accelerometer. Additionally, one or usually two inner loops with feedback from a spring-restrained rate gyro are required for compensating the poles of the airframe response. (These two loops could also be mechanized with an integrating gyro, but at a higher cost than the improvement in drift performance would warrant.) For a symmetric cruciform missile, the pitch and yaw autopilot channels are identical. Therefore, only one will be discussed.

Variation of dynamic pressure with flight conditions also alters the pitch/yaw autopilot characteristics, as in the roll autopilot, from the one extreme of fast response with minimum stability at high dynamic pressures to the other extreme of relatively slow response with maximum stability at low dynamic pressures. This effect can be minimized by providing altitude gain switching, which permits a prelaunch selection of the proper launch logic as a function of launch altitude and target altitude. This

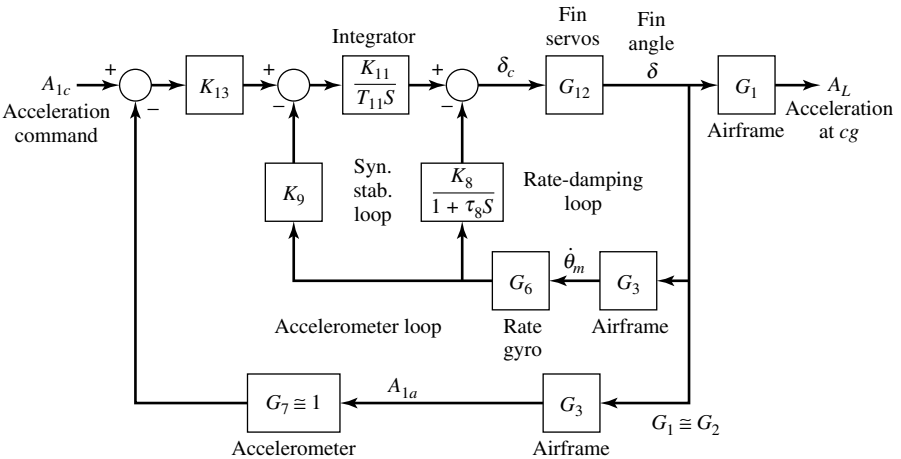

Fig. 3.36. The pitch/yaw autopilot.

launch logic is used to determine the proper in-flight switching, which occurs as the missile goes from midcourse to terminal phase. In addition, an in-flight course correction command called *English bias* (for a discussion of English bias, see Section 3.6) is processed by the pitch/yaw autopilot to correct for a missile launch at other than the desired lead angle. Because missile acceleration and slowdown during the boost and glide phases of flight affect the missile lead angle for proper intercept, axial compensation provides lateral commands to the pitch/yaw autopilot in order to adjust the lead angle. From the time the flight control pressure (e.g., hydraulic) is up, pitch or yaw stabilization is obtained by sensing pitch or yaw rates with the pitch or yaw rate gyros, respectively. A block diagram mechanization of a conventional pitch/yaw autopilot is shown in Figure 3.36.

The yaw stabilization loop senses yaw rates, which are amplified and applied to a phase-sensitive comparator. The comparator output is then amplified within the damping circuit, which has been set to the proper altitude band gain. The damping circuit also contains suitable structural filtering, which provides suitable frequency-response shaping.

The transfer function G_1 for lateral acceleration of the cg has the same poles as those of G_3, plus high-frequency zeros that depend on the tail forces. (Note that the transfer functions G_1 and G_3 correspond to the transfer functions G_{la} and G_{pr} of Section 3.2.1, respectively, and K_1 corresponds to K_{la} of the same section.) Furthermore, K_1 diminishes with increasing altitude. At intercept, the missile needs an acceleration capability of at least 4 g's. Hence, another requirement is that at the maximum altitude and minimum velocity, the available acceleration must be at least 4 g's at an angle of attack (α) of, say, 25° or 30°. Generally, the largest value of the time constant $\tau(\tau = \alpha/\dot{\gamma}$; see also Section 3.2.1) may be related to this condition. The transfer function G_2 for acceleration at the accelerometer is quite similar to G_1. Referring to Figure 3.36, we note that there are three feedback loops, the four

actuator servos being represented by a single closed-loop transfer function G_{12}. Since control of acceleration is required, the outermost loop is closed by an accelerometer. Commonly, the accelerometer is placed well forward of the cg, probably about half to two-thirds of the distance from the cg to the nose of the missile. Its sensitive axis is in the direction of pitch axis (i.e., out the right wing). If the accelerometer is placed at a distance d ahead of the cg, the total acceleration it sees is equal to the acceleration of the cg plus the angular acceleration (i.e., dR/dt, where R is the yaw rate) times this distance d. Therefore, it is clear that if d is positive (that is, the accelerometer is ahead of the cg), we have from the two instruments (rate gyro and accelerometer) some feedback. The outer accelerometer loop has the lowest bandwidth of the three loops. The innermost rate-damping loop is required to damp the response of the bare airframe, which has an underdamped resonance in the stable case (i.e., positive static margin). In addition, the innermost rate-damping loop has a wide bandwidth for damping the poles of the airframe. The *synthetic stability loop* improves the high-frequency poles of the autopilot if the airframe is stable, and enables the autopilot to tolerate some instability (i.e., positive M_α) of the airframe. Furthermore, the synthetic stability loop in Figure 3.36 effectively feeds incremental pitch angle back to the fin servos, thereby moving the autopilot closed-loop poles, corresponding to the bare airframe poles given by the transfer function G_{pr} (see Section 3.2.1), further from the origin of the complex plane. Summarized below are the design methods for a band-switched pitch autopilot.

Design Method for Pitch Autopilot (Band-Switched)

Preliminary:

1. The airframe must meet broad criteria as discussed in Section 3.2.1.
2. Divide altitude-Mach envelope into bands of M_δ contours.
3. Select a design point and obtain airframe transfer functions.
4. Utilize pessimistic transfer functions for the gyroscope and actuators.

For stable Airframe:

5. From the gain margin, find the maximum ω_{cr} and the "integral break frequency ω_i"
$$(\omega_i = K_9 K_{11}/K_8 T_{11}).$$
6. Discard the lags of the gyroscope, actuator, etc. Use a cubic autopilot model of the form
$$\frac{A_L}{A_{lc}} = \frac{K_a(1 + a_{11}s + a_{12}s^2)}{1 + b_1 s + b_2 s^2 + b_3 s^3} = \frac{K_a(1 + a_{11}s + a_{12}s^2)}{\left[1 + \frac{s}{\omega_1}\right]\left[1 + 2\zeta_2\left(\frac{s}{\omega_2}\right) + \left(\frac{s}{\omega_2}\right)^2\right]}.$$
7. Fix the parameters of the rate-damping and synthetic stability loops.
8. Calculate the accelerometer loop, which meets the specifications on the dominant frequency ω_1.

9. Check by calculating the coefficients b_1, b_2, and b_3 and factoring into poles. A digital-computer program can perform Steps 5–9.
10. Check the structural stability on a digital frequency-response program.

For Unstable Airframe:

11. Find the maximum tolerable M_α (body stability parameter) from the formula involving autopilot parameters.
12. If this is not acceptable, reduce the autopilot lags or redesign the airframe for better static margin.

At high frequencies, the rate-damping loop has the most gain, while at low frequencies the accelerometer loop has the most gain. Assuming that the bare airframe meets the criteria discussed in Section 3.2.1, the altitude-Mach envelope is divided into bands by M_δ contours. The reason for this is that the transfer function G_3 (or G_{pr}) is approximately (M_δ/s) at high frequencies, and consequently the product of M_δ and the electronic gains of the rate-damping loop must be lower than an unstable value and higher than an ineffective value. Band-switching on lines of constant altitude rather than constant M_δ may be adequate if the range of Mach number is not too great. Next, a particular design point is selected, typically on the lower boundary of a given band. Then, realistic airframe transfer functions and pessimistic (i.e., worst temperature case) transfer functions for the gyro and actuators are obtained. From design speci-fications and/or requirements, the gain margin and realistic transfer functions, the maximum gain-crossover frequency ω_{cr}, and the "integral break frequency $\omega_i = K_9 K_{11}/K_8 T_{11}$" of the synthetic stability loop can be determined. These parameters tend to be limited mainly by the actuator lags. Therefore, the lags listed in step 6 above are then discarded, so that a simplified *cubic* autopilot model may be used for algebraic synthesis. In general, it is well to keep the integral break frequency ω_i somewhere between $0.2\omega_{cr}$ and $0.4\omega_{cr}$. Application of classical control theory, in particular the Routh criterion, has led to analytic limits on the positive value of M_α. As a rule of thumb, the approximate limit for the tolerable M_α is

$$\text{Tolerable } M_\alpha \cong \frac{1}{2}\omega_i \omega_{cr}.$$

Both ω_{cr} and ω_i are limited by the high-frequency lags, particularly in the actuator, which shows the need for fast actuator response.

One free gain parameter in each of the two inner loops is then calculated. A specification on the dominant break frequency ω_1, obtained from analyses of miss distance and attitude-loop stability, is then used to calculate a free gain parameter of the accelerometer loop. Finally, as a check, the coefficients b_1, b_2, and b_3 are then calculated, and the cubic polynomial is factored in order to check the autopilot poles. The design method discussed above achieves the required dominant break frequency ω_1 and maximizes ω_2 and ζ_2 within stability constraints.

As discussed earlier, each autopilot must have feedback from an accelerometer. The rate-damping loop must have a wide bandwidth for damping the poles of the

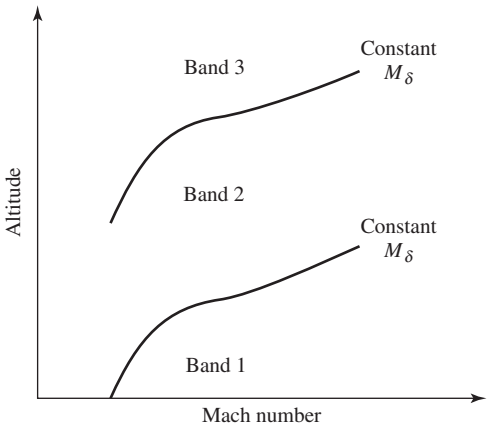

Fig. 3.37. Curves of constant M_δ for band-switching of autopilot gains.

airframe, while the synthetic stability loop stabilizes the poles of an unstable bare frame. In reference to Figure 3.36, some other useful transfer functions are as follows:

$$
\begin{aligned}
G_1 &= A_L/\delta = K_1(1 + a_{11}s + a_{12}s^2)/(1 + b_{11}s + b_{12}s^2),\\
G_1 &\cong G_2,\\
G_3 &= (1/\delta)[K_3(1 + A_{31}s)]/(1 + b_{11}s + b_{12}s^2)\\
&\cong M_\delta[s + (1/A_{31})]/[s^2 + (b_{11}/b_{12})s - M_\alpha].
\end{aligned}
$$

(Note that $A_{31} \equiv \tau$ as in $\tau = \alpha/\dot{\gamma}$).

Figure 3.37 shows the typical contours of constant M_δ for band-switching on the plane of altitude versus Mach number for a hypothetical missile. As a final step in the design process, the effects of high-frequency structural modes on autopilot stability are checked by a digital computer frequency-response program. It should be pointed out that the autopilot can tolerate some bare-airframe instability (i.e., some maximum positive value of M_α). This parameter M_α tends to be most troublesome at sea level (i.e., low altitude and corresponding low angles of attack) and maximum Mach number.

In the designing of missile autopilots, it is a common practice to utilize a linearized second-order airframe model. The required stability derivatives are obtained from the nonlinear moment and force coefficients by making the following assumptions: (1) constant missile velocity, (2) body lift force is a linear function of the change in the angle of attack α about some trim condition α_0, (3) constant altitude, (4) constant center of pressure, (5) fixed missile mass inertia, and (6) control surface lift force is a linear function of control surface deflection angle δ and independent of α. Although these assumptions appear to be rather restrictive, nevertheless, they simplify the autopilot design task considerably. Practical experience has shown that the resulting autopilot response characteristics with the nonlinear airframe are closely approximated

by the linearized response characteristics near the given nominal conditions for a properly designed autopilot.

Up to now we have discussed the conventional and/or band-switched autopilot design. The design of *adaptive* autopilots follows as an extension. In a January 1949 symposium held at Wright-Patterson AFB, Ohio, initiated by the former Air Research and Development Command (*ARDC*) and published in the form of a Western Area Development Command (*WADC*) technical report, a self-adaptive system is defined as one "which has the capability of changing its parameters through an internal process of measurement, evaluation, and adjustment to adapt to a changing environment, either external or internal, to the vehicle under control." Or, in the definition by the Air Force, a self-adaptive autopilot measures its own performance, compares it to a standard, and adjusts one or more parameters until its performance meets the standard. There are self-adaptive autopilot design models. Historically, among the best known are the Sperry self-adaptive control system, the Minneapolis-Honeywell self-adaptive control system, and the *M.I.T.* self-adaptive autopilot. The Sperry self-adaptive control system was designed to keep the damping ratio of the servo poles between 0.11 and 0.23. The Sperry system demonstrated the practicality of the self-adaptive control system utilizing a maximum forward gain controlled by a self-contained process of measurement, evaluation, and adjustment. The Minneapolis-Honeywell self-adaptive control system uses a reference model as an input filter ahead of the summer. The dynamics of the model can be adjusted to yield an optimum response. A variant of this design is the *MH-90* adaptive control system, which maintains the forward loop gain at a sufficient level so as to keep the complex servo poles on the imaginary axis. The *MH-90* flight control system was developed specifically for the *F-101* fighter aircraft. The *M.I.T.* system also uses a model. In this design, the output of the model is compared to the output of the system, and the gains of the system are adjusted as a function of the system error. That is, the gains are not kept at the highest possible level consistent with a certain stability level, but are adjusted so that certain error criteria are satisfied. For more details on these designs the reader is referred to [1], [4], [7], [11], [13], [14], and [15].

Figure 3.38 illustrates an adaptive roll autopilot, which is quite similar to a conventional roll autopilot. The function of the added adaptive loop is to maintain constant the gain product $K_m\ K_\delta$ (K_m is the gain setting constant) by holding constant the gain-crossover frequency (i.e., the frequency of the unity loop gain) in the main autopilot loop.

Note that in Figure 3.38, a dither oscillator with an appropriate fixed frequency below 12 *cps* inserts a small sine-wave dither into the main loop. As a result, the dither propagates around the main roll loop, causing only a minimal disturbance (e.g., about 0.1° peak angle per surface). The peak roll rates at the dither frequency are never large enough to affect guidance. Moreover, the dither output signal is processed in the adaptive elements, which adjusts the gain K_m until the in-phase component of the dither output signal is minus one-half the dither input signal. It can be shown that this results in unity gain of the main loop at the dither frequency; that is, the gain-crossover frequency and the product $K_m\ K_\delta$ are constant. In designing an adaptive roll autopilot, the designer must make certain that the system is not sensitive to phase changes in

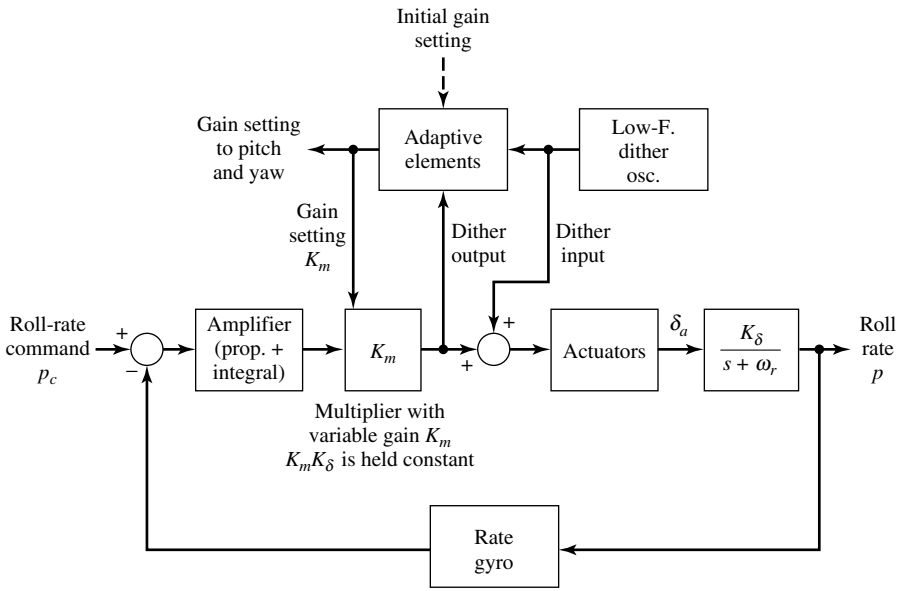

Fig. 3.38. Typical self-adaptive roll autopilot.

the main roll loop and is not sensitive to noise, partly because the dither processing involves cross-correlation of the dither output and input signals. Initial performance after launch is improved if the carrier (or parent) aircraft makes an approximate initial gain setting.

The discussion above showed that the adaptive roll autopilot maintains constant the product $K_m\ K_\delta$. Moreover, in Section 3.2.1 it was shown that the ratio M_δ / K_δ of surface pitch effectiveness to surface roll effectiveness is nearly constant in a tail-controlled missile, fundamentally because the two moment arms are nearly constant. Consequently, the gain setting K_m in roll can be used as the variable gain K_{22} in pitch, so that the product $K_{22}\ M_\delta$ and the gain-crossover frequency of the pitch-rate damping loop are nearly constant. Consequently, the gain setting K_m in roll can be used as the variable gain K_{22} in pitch, so that the product $K_{22}\ M_\delta$ and the gain-crossover frequency of the pitch-rate damping loop are nearly constant. Figure 3.39 shows the location of the variable gains in the pitch/yaw autopilot.

Also, the gain setting K_m can be used for autonomous band-switching of the pitch gain K_{69} so as to control the dominant break frequency ω_1. The self-adaptive system results in good stability and desirable high-frequency poles of the pitch autopilot, with further benefits of excellent stability in the attitude loop. The feasibility of self-adaptive autopilots has been amply demonstrated by flight simulations and with realistic radar noise. Also, the state of the art in microminiaturization and cost-reduction techniques indicate that self-adaptive autopilot systems for air-to-air interceptor missiles may well be preferred over band-switched autopilots. Future missiles will have larger altitude-Mach envelopes and possibly larger excursions of M_δ relative to the launch value, so that adaptive autopilots appear to be attractive.

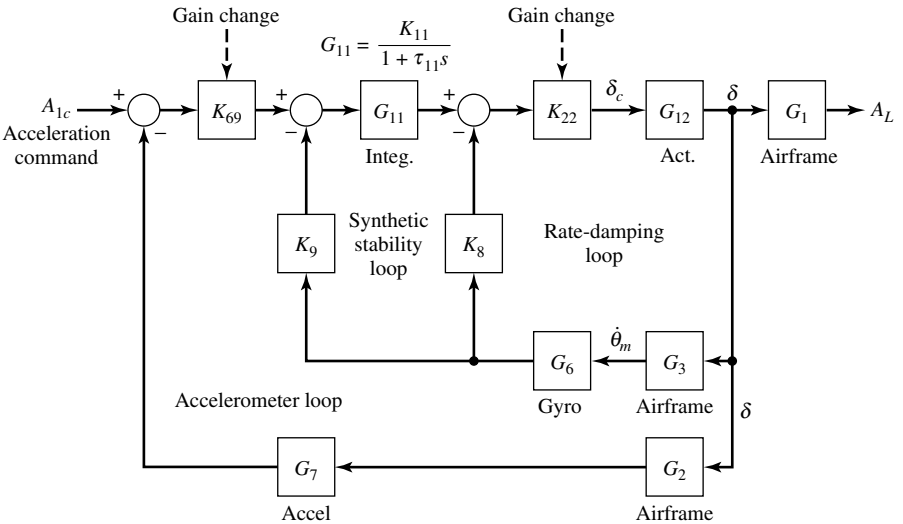

Fig. 3.39. Pitch/yaw autopilot for self-adaptation.

At this point, it is appropriate to discuss briefly the function of the *parasitic attitude loop* (for more details the reader is referred to [3], [5], and [12]). In Section 3.4 it was mentioned that one problem the guidance designer faces is to preserve the stability of the parasitic attitude loop. The parasitic, or unwanted, attitude loop arises because the guidance system's measurement of the line-of-sight (*LOS*) rate calls for corrective missile lateral acceleration, which is accompanied by a missile pitching that disturbs the measurement of *LOS* rate. More specifically, one of the most serious parasitic feedback paths in tactical radar homing missiles is created by the radome. As discussed in Section 3.4.1, the radome causes a refraction (i.e., bending) of the incoming radar wave, creating a false indication of the target's location. In essence, body rate and body acceleration are parasitic feedback loops, owing to the fact that an aerodynamic missile must pitch to an angle of attack in order to be able to maneuver. As a result of radome refraction, the autopilot and seeker dynamics are coupled through the missile body rate signal. Another type of parasitic feedback loop may arise due to body bending effects. This effect is simply a high-frequency autopilot instability in which body bending is detected by the autopilot as a missile motion. Parasitic feedback paths arising within the guidance or homing loop will work in the direction of larger time constants and smaller effective navigation ratios in order to obtain acceptable performance. In particular, at high altitudes, the parasitic feedback is appreciable, and the guidance subsystem may become unstable, resulting in a flight failure. Stability may be achieved merely by low-pass filtering in the guidance subsystem, but this may make it sluggish and cause a bad miss.

Figure 3.40 depicts the guidance subsystem as having an input *LOS* rate $d\lambda/dt$, an output corrective acceleration A_L, and a parasitic attitude loop. The direct path from $d\lambda/dt$ to A_L shows the mechanization of the proportional navigation law (indicated by

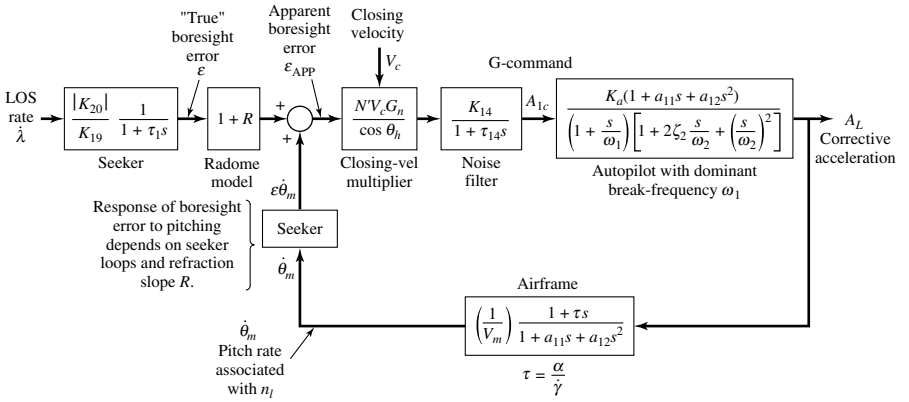

Fig. 3.40. The parasitic attitude loop (inside guidance kinematic loop).

the "closing velocity multiplier" block), with a low-pass noise filter in order to reduce the high-frequency noise, chiefly for the sake of the fin servos inside the autopilot. If only this direct path from $d\lambda/dt$ to A_L existed, then the guidance design would be much easier than it actually is. In the feedback path of Figure 3.40, the airframe transfer function relates the pitch rate to the lateral acceleration of the cg.

The *alpha over gamma dot* time constant τ may be a fraction of a second at low altitude and may exceed 10 seconds at high altitude. Neglecting the feedback for a moment, it is seen that the *LOS* rate $d\lambda/dt$ causes the seeker to develop a boresight error signal that is multiplied by the closing velocity V_c and suitably filtered to form a g-command A_{lc} for the autopilot. The feedback arises because the missile must develop a pitch rate $d\theta_m/dt$, and this disturbs the gyro-stabilized seeker (if such is used) a finite amount, thus changing the boresight error ε_{app}. Also, during pitching motion the seeker must look through a different part of the radome with a different refraction, and this too affects the boresight error signal.

From the airframe transfer function in Figure 3.40, it is apparent that at high altitudes and low velocities the time constant $\tau(\tau = \alpha/\dot{\gamma}, \alpha =$ angle of attack, $\gamma =$ flight-path angle; the equation for τ is given in Section 3.2.1) increases and thereby increases the loop gain of the parasitic attitude loop. In other words, the time constant increases with increasing missile altitude and decreasing missile velocity. Hence, the stability problems of the attitude loop increase with increasing altitude. Analysis of Figure 3.40 shows that stability considerations at high altitude make it desirable for the response of the autopilot to have a single dominant break frequency ω_1 and a fairly well damped pole pair with a much higher frequency ω_2. The simplified transfer function for the autopilot also contains constants a_{11} and a_{12}, which are characteristics of the bare airframe.

In the critical period of homing guidance, the tendency of portions of the guidance system to saturate must be kept low in order to avoid a bad miss distance. An exception occurs just before intercept, when the *LOS* angle suddenly changes by almost 90°

even for a small distance, thereby saturating the seeker servo and the autopilot. From Figure 3.40 for the parasitic attitude loop and Figure 3.36 for the pitch/yaw autopilot, it is apparent that the *LOS*-angle noise undergoes appreciable frequency-dependent ampli-fication before entering the fin servos. The fin servos may have a high probability of saturating in angle δ or rate $d\delta/dt$ on this noise, particularly the receiver-noise component at a long illuminator-to-target range and missile-to-target range. The saturation itself tends to increase miss distance more than linear theory would indicate for the miss due to noise, perhaps because the effective fin-servo gain for the actual homing data on the *LOS* rate (i.e., $d\lambda/dt$) is reduced by the saturation. Indeed, saturation can even cause a catastrophic loss of control. Obviously, a remedy for just the saturation problem per se would be to increase the low-pass filtering in Figure 3.40. However, as we shall see later, it is desirable to keep the guidance system fast in order to minimize miss distance. The following types of remedies may be helpful for the noise saturation problem: (1) Design efficient filtering in the parasitic attitude loop, to reduce high-frequency noise, maintain stability, and minimize miss distance; (2) choose sufficiently high power in the radar illuminator so that the receiver *SNR* is high and receiver noise is low; and (3) if possible, choose airframe design with sufficiently large tails, that is, sufficiently large M_δ at high altitudes.

We summarize the discussion of the parasitic attitude loop by noting that stability of the attitude loop can always be achieved by increasing certain major filtering time constants, but at the cost of making the guidance system slow. This increases most of the components of miss distance. Therefore, the design of the parasitic attitude loop is crucial. Considering that factors of Mach number, altitude, radome modeling, design of the autopilot, and design of the seeker all enter into the parasitic attitude loop, it is perhaps not surprising that different design approaches are utilized by each guidance designer.

3.5.1 Control Surfaces and Actuators

The function of a guided missile's control system, which is an integral part of the guidance system, is to make certain that the missile follows the prescribed trajectory, that is, to detect whether the missile is flying too high or low, or too far to the right or left. The guidance system measures these errors and sends signals to the control system to reduce these errors to zero. For the purposes of the present discussion, it will be assumed that the missile is tail-controlled by four fins, which have no downwash interference from the control surfaces. At this point, it is appropriate to define the terms *elevators*, *rudders*, and *ailerons*. Commonly, aerodynamically guided missiles have two axes of symmetry, that is, arranged in a cruciform configuration. If the missile has four control surfaces as shown in Figure 3.41a, then we will define surfaces 2 and 4 as elevators, and 1 and 3 as rudders.

Referring to Figure 3.41a, if 2 and 4 are mechanically linked, then a servo must impart the same rotation to both these surfaces and call elevators. The same argument applies to surfaces 1 and 3, which we call rudders. Furthermore, if surfaces 2 and 4 each have their own servo, they can act as ailerons (i.e., one can move clockwise

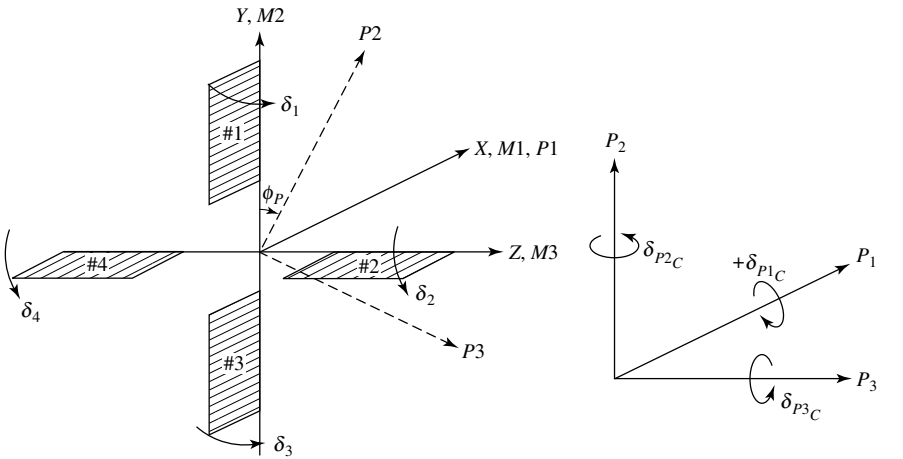

(a) Fin deflection convention (b) autopilot requested fin commands

Fig. 3.41. Control surfaces and autopilot commands.

while the other can move counterclockwise) [3], [5]. (Note that if the autopilot pitch and yaw axes are each 45° from the planes of adjacent control surfaces, then all four control surfaces are deflected equally by the pitch (or yaw) autopilot.) From the above discussion, we note that the majority of tactical missiles are designed in a cruciform configuration, thus enabling them to maneuver with ease horizontally and vertically. In a cruciform configuration, the two horizontal lifting surfaces are deflected equally by the fin control actuation system. The same concept applies to the vertical surfaces.

In essence, the actuator consists of the control surfaces (or fins) and associated servomechanisms, and is used to change the missile's attitude and trajectory or flight path. Therefore, the function of the four fin actuators is to move the control surfaces in accordance with commands from the three autopilots. The autopilot outputs are virtual fin deflection commands shown in Figure 3.41b. In Figure 3.41b, the roll autopilot is along the P_1 axis, while the pitch and yaw axes are along the P_3 and P_2 axes, respectively; the corresponding positive fin deflection commands are indicated by the corresponding δ_P's. The four real fins are located in the missile or M-frame, which is shown in Figure 3.41a and is rotated from the autopilot axis system (P) by an angle ϕ_P. In order to obtain equivalent effects, the autopilot commands must be transformed through $-\phi_P$. The roll command is affected by a differential deflection, and the sign is such that a positive roll command is accomplished by negative deflection of fins 1 and 2 and a positive deflection of fins 3 and 4. Note that this is not the only fin convention and/or arrangement available to the missile designer. Reference [3] gives a somewhat different fin convention. In some applications it is preferable to put the autopilot axes in the plane of the control surfaces, and so

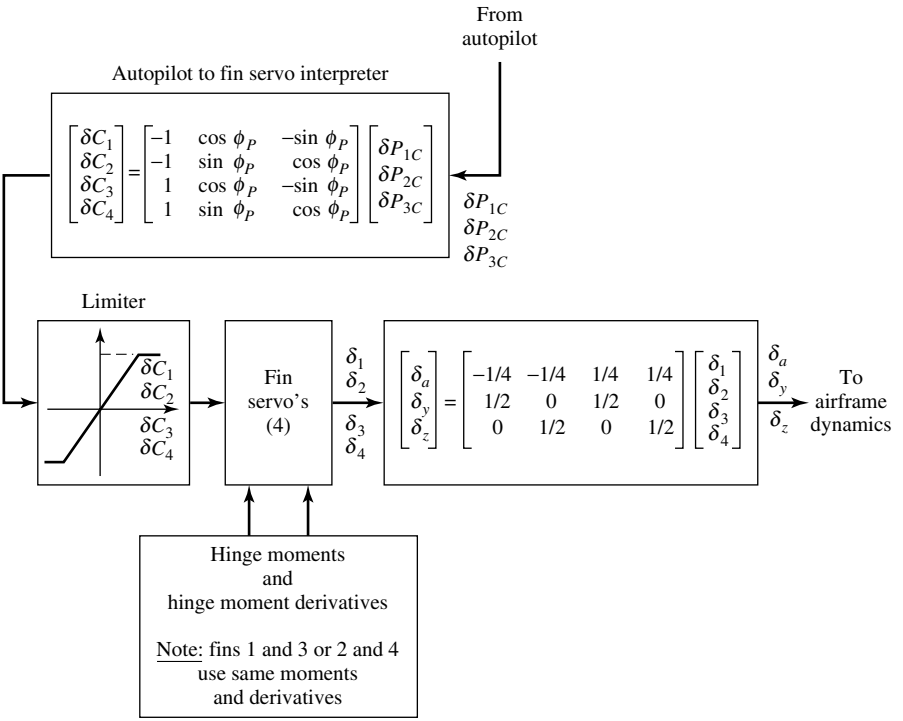

Fig. 3.42. Autopilot to fin servo to airframe dynamics flow.

only two surfaces are deflected by the pitch autopilot and two are deflected by the yaw autopilot. The resulting fin deflections from the actuator models are recombined into equivalent deflections used in the computation of airframe forces and moments. Thus,

$$\begin{aligned}\delta_a &= \tfrac{1}{4}(-\delta_1 - \delta_2 + \delta_3 + \delta_4),\\ \delta_Y &= \tfrac{1}{2}(\delta_1 + \delta_3),\\ \delta_Z &= \tfrac{1}{2}(\delta_2 + \delta_4).\end{aligned}$$

The effective aileron deflection δ_a is obtained by differential fin commands and is used to calculate a rolling moment, assumed to vary linearly with δ_a, but with a slope varying with Mach number. Figure 3.42 shows the rotation and further limiting required to calculate the four individual commands to the fin servos.

An alternative way of expressing the fin deflections is to consider Figure 3.43. Here we use a coordinate system with the X-axis (roll) pointing along the missile's longitudinal axis, the Y-axis (pitch) pointing to the right, and the Z-axis (yaw) pointing down.

The corresponding equations of motion can be written as follows [1], [3], [12]:

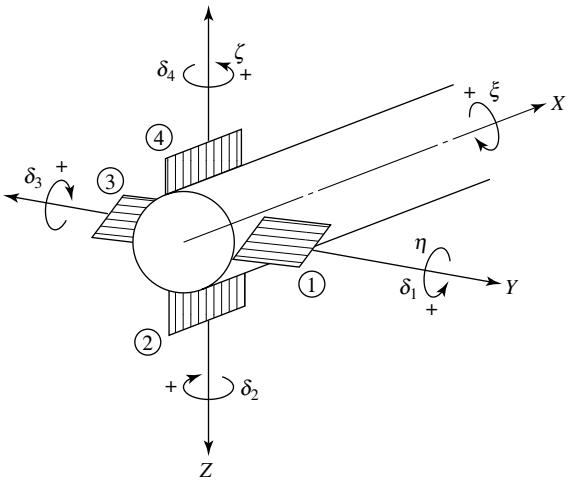

Fig. 3.43. Fin (control surface) deflections.

Pitch rudder angle:

$$\eta = \tfrac{1}{2}(\delta_1 - \delta_3).$$

Yaw rudder angle:

$$\zeta = \tfrac{1}{2}(\delta_2 - \delta_4).$$

Roll rudder angle:

$$\xi = \tfrac{1}{4}(\delta_1 + \delta_2 + \delta_3 + \delta_4).$$

The equations of motion can now be written as follows:

Longitudinal Equations:

$$\Sigma \mathrm{X}: m(u - rv + qw) = \tfrac{1}{2}\rho V^2 S C_X + F_X + mg_X,$$

$$\Sigma \mathrm{Z}: m(w - qu + pv) = \tfrac{1}{2}\rho V^2 S C_Z + F_Z + mg_Z + F_\eta \cdot \eta,$$

$$\Sigma \mathrm{M}: I_Z \left(\frac{dq}{dt}\right) = \tfrac{1}{2}\rho V^2 S d C_M + (I_Y - I_X)rp + (mX_G^2 - I_Y)q + x_s F_\eta \cdot \eta.$$

Yaw (Lateral) Equations:

$$\Sigma \mathrm{Y}: \; m(v - pw + ru) = \tfrac{1}{2}\rho V^2 S C_Y + F_Y + mg_Y + F_\eta \cdot \zeta,$$

$$\Sigma \mathrm{N}: \; I_Z \left(\frac{dr}{dt}\right) = \tfrac{1}{2}\rho V^2 S d C_N + (I_Y - I_X)qp + (mX_G^2 - I_Z)r + x_s F_\eta \cdot \xi.$$

Roll Equations:

$$I_X\left(\frac{dp}{dt}\right) = \tfrac{1}{2}\rho V^2 S d C_L + y_s F_\xi \cdot \xi$$
$$(F_\xi = F_\eta = 0;\ P_k = 0).$$

(Assumptions: $q = 0$, $V =$ constant, $u = V$, $p = 0$),
where

$x, y, z =$ body (missile fixed axes),
X, Y, Z = Forces (air),
$p, q, r =$ angular velocities roll, pitch, yaw),

$u, v, w =$ velocity components about x, y, z,
$\xi, \eta, \zeta =$ fin angular deflection (in roll, pitch, and yaw),
$L, M, N =$ aerodynamic moments (in roll, pitch, and yaw),
$P =$ thrust (lbs),
$P_k =$ air stream deviation force (roll displacement),
$X_G =$ distance (i.e., aileron cg),
$C_X, C_Y, C_Z =$ force coefficients about X, Y, Z,
$C_L, C_M, C_N =$ aerodynamic coefficients,
$g_X, g_Y, g_Z =$ gravitational components,
$S =$ reference area,
$d =$ missile diameter,
$\rho =$ air density.

A remarkable variety of actuators and fin servomechanisms have been employed in the past. One type is a bistable-clutch actuator in a simple limit-cycling adaptive roll autopilot. Servomechanisms may be of the hydraulic, pneumatic, or electric type, depending on the maximum hinge moment of the control surface. Other missiles have used fin servos with rate commands, while still others have utilized force-balanced fin servos in an adaptive autopilot that is approximately compensated for changes in dynamic pressure. As an example, the pitch/yaw autopilot of Figure 3.36 utilizes positional fin servos with angle feedback. The fin servo is a critical part of the missile, and it limits the performance of the autopilot and indeed the performance of the entire guidance system. The detailed requirements for the fin servo are developed from various considerations in the guidance system, such as:

(a) The frequency response of the fin servos must be high enough so that adequate bandwidth can be achieved in the pitch autopilot for stabilizing an unstable bare airframe, so that the roll autopilot can be fast enough to suppress induced roll moments at high frequency.

(b) The no-load angular rate should be high enough so that saturation on radar noise does not appreciably reduce the average actuator gain for guidance signals.
(c) The stall torque should appreciably exceed any possible hinge moment, particularly if it is decentering (i.e., with the fin *cp* ahead of the hinge line).
(d) The fin servo should be very stiff to load torques so that the performance of it and the autopilot will not be degraded by unwanted feedback from fin angle or angle of attack.

The selection and design requirements for actuators turns out to be a very complex question, because it depends on the following: (1) the bare airframe, (2) flight conditions, (3) the guidance system, and (4) the inevitable radar noise therein (if a radar seeker is used). For example, for a missile of limited flight duration, a hydraulic system has very attractive performance, weight, and volume, as shown from experience with the Sparrow and Hawk missiles. For flights longer than about one minute, a closed hydraulic system with a pump would probably be lighter. Hydraulic systems have problems after long storage (dirt, deterioration of seals, etc.). Other types of actuators, such as cold-gas, and magnetic-particle clutches (with proportional control), have problems with packaging and efficiency. On the other hand, a d-c torquer appears to be a strong contender for air-to-air missiles, assuming both a suitable airframe design for limited hinge moment and good packaging. It should be pointed out however, that d-c torquers may not have enough dynamic torque stiffness to be satisfactory for decentering hinge moments. Although a particular actuator application would require a careful study, some useful generalizations can be made. The general criteria for the actuators are summarized below:

1. Good frequency response, that is, less than 20° phase lag at 10 *cps*. Use proportional, not switched, operation.
2. Sufficient angular travel, perhaps ± 30°.
3. Sufficient maximum angular rate, for example, ± 300°/sec.
4. Sufficient hinge moment based on static trip and acceleration.
5. Static and dynamic stiffness under hinge-moment load.
6. Reliability after a long storage.
7. Efficiency, light weight, and volume.
8. Economy.

As discussed in the previous section, good frequency response is necessary for good performance in the autopilot and attitude loop, particularly if the bare airframe is unstable. Proportional operation is usually preferred. The actual angular travel depends on the bare airframe, and may be low if the airframe is nearly neutrally stable. At high altitudes, the angular rates due to noise propagation tend to be high, but hinge moments may be low because of the low q, while at sea level the opposite may be true. Clearly, good stiffness under load is necessary.

Another design, in addition to the conventional fin control actuation systems, is the *thrust vector control*, whereby steering of the missile is accomplished by altering the direction of the efflux from the propulsion motor. In this design, a thrust vector

controller is used to follow the thrust vector command. More specifically, the fire control system can command the thrust generator to generate the thrust amplitude and direction commands. Consequently, the thrust amplitude obtained by controlling the exhaust mass flow rate and the thrust direction generated by controlling the thrust vector control servo are combined to construct a thrust vector control. As in the conventional fin control actuation systems, a servo control system can be used. In such a case, an autopilot can be used to follow the trajectory shaping and optimization commands and to stabilize the missile during flight. The advantage of this method is that it does not depend on the dynamic pressure of the atmosphere. On the other hand, a missile using the thrust vector control method becomes inoperative after motor burnout. Therefore, in such a design a boost-coast velocity profile must be generated during the design/simulation phase of the weapon.

Many of the modern (e.g., air-to-air) missiles use deflector vanes in their rocket motor exhaust in order to execute sharp turns in either direction (i.e., left or right) off the aircraft's nose. Missiles using thrust-vectoring control, thrust-vectoring augment canards in controlling pitch and yaw, and tail ailerons control roll. Finally, we end this section by noting that thrust vector control finds extensive application in short-range air-to-air missiles, and vertically launched intercontinental ballistic missiles (*ICBM*s) as well as submarine-launched missiles such as the *Trident*, where early boost course corrections are required. Ballistic missiles will be discussed in more detail in Chapter 6.

In Section 3.3.1 the *ramjet*/*scramjet* concepts were briefly described, while in Section 3.3.2 we discussed the various missile airspeed classifications. The Defense Advanced Research Projects Agency (*DARPA*) and the Office of Naval Research (*ONR*) initiated a four-year HyFly (Hypersonic Flight) demonstrator project. As a result, *DARPA* and the U.S. Navy plan to air-launch a powered prototype hypersonic missile in late 2004 as part of a technology development and validation effort that eventually could lead to the procurement of a production version of the weapon later in the decade. The proposed Mach 6–6.5 missile would be carried by surface ships, submarines, and aircraft (e.g., under the wings of the *F*/*A-18*) initially to combat highly mobile, time-sensitive surface targets like mobile *Scud* launchers. Eventually, the weapon also could be used against hardened, buried, and heavily defended targets. The Mach 6-class weapon could have a range of 400–600 nm. In July 2002 a series of free-jet wind tunnel tests exercised the proposed weapon's hydrocarbon-fueled dual combustion ramjet (*DCR*) at hypersonic speeds. The tests were conducted at NASA Langley Research Center's 8-ft high-speed wind tunnel under simulated speeds of Mach 6–6.5 and angles of attack 0° and 5°.

The *DCR* concept was invented by the Johns Hopkins University Applied Physics Laboratory (*APL*) in the early 1970s. The *DCR* differs significantly from both a pure ramjet and a supersonic combustion ramjet of the type being jointly pursued by Pratt & Whitney, the U.S. Air Force, and NASA. Ramjets typically operate in the Mach 3–3.5 flight regime. In flight, the air entering the power plant is compressed by the engine inlet and slowed to subsonic speeds to raise the pressure and temperature so that combustion can occur. Fuel is added to this subsonic air, and the mixture is ignited. Combustion products are then allowed to accelerate through a converging/diverging

nozzle at supersonic speeds, generating thrust. Above Mach 5, the inefficiencies associated with slowing the air for mixing and combustion are large and result in a loss of net positive thrust. In contrast, a supersonic combustion ramjet, or scramjet, begins at flight speeds of around Mach 4–4.5 and, theoretically, can continue to operate up to about Mach 25. In this power plant, supersonic air entering the engine inlet is mixed with fuel under supersonic conditions, ignited, and expanded to create thrust. However, getting the fuel–air mixture to ignite when mixing time is less than 1 millisec is extremely difficult. Early scramjet researchers used highly reactive fuel additives to enhance the mixing and combustion process. However, these chemicals cannot be used on board ships or submarines because the materials are highly toxic. Pratt & Whitney, working with the Air Force and NASA, is developing a scramjet powered by conventional, unadulterated liquid hydrocarbon fuels such as *JP7*. In order to accomplish this, they direct the liquid fuel through the scramjet's walls and use the heat generated by supersonic and hypersonic flight to crack the *JP7* into lighter, more volatile components. These gaseous components are then introduced into the supersonic airstream and ignited, producing thrust. *APL*'s dual combustion ramjet is yet another way to obtain hypersonic speeds. In this power plant, supersonic air ingested through one inlet is slowed to subsonic speeds, mixed with a conventional hydrocarbon fuel in a fuel-rich environment, and ignited, as in a ramjet. To break through the ramjet's operating speed limitations, though, the expanding combustion products are then mixed with supersonic air entering through a second inlet and are more completely burned in a supersonic combustor. The *DCR* has an operating threshold of about Mach 3, and a maximum operating speed of about Mach 6.5.

Guidance for the proposed hypersonic missile will be *GPS*-based. Future weapons also may carry a communications link so they can be retargeted in flight.

3.6 English Bias

In order to compensate any aircraft steering error (i.e., a missile aiming error) that exists at launch, an *English bias* (or lead angle error) signal is provided that will command the missile to turn after launch. The fundamental idea of this command is to provide the means of correcting missile heading error prior to lock-on to the target and thereby minimize the time required after speedgate* lock to solve the guidance problem and effect a satisfactory intercept. At launch, the computer supplies the interceptor missile with English bias commands, which simply are voltage analogues of the gimbal angles the missile should have in order to be on a collision course with the target. Each of these signals is compared correspondingly with its existing antenna gimbal angle during the boost phase to produce error signals, which in turn are used to direct the missile body axis to a collision course orientation.

*The speedgate acquires and tracks the Doppler signal, using automatic gain control (*AGC*) to adjust the signal to a constant level, so that AM directional information can be extracted at a known scale factor. (Note: 10% modulation is equal to 1° of directional error off antenna boresight).

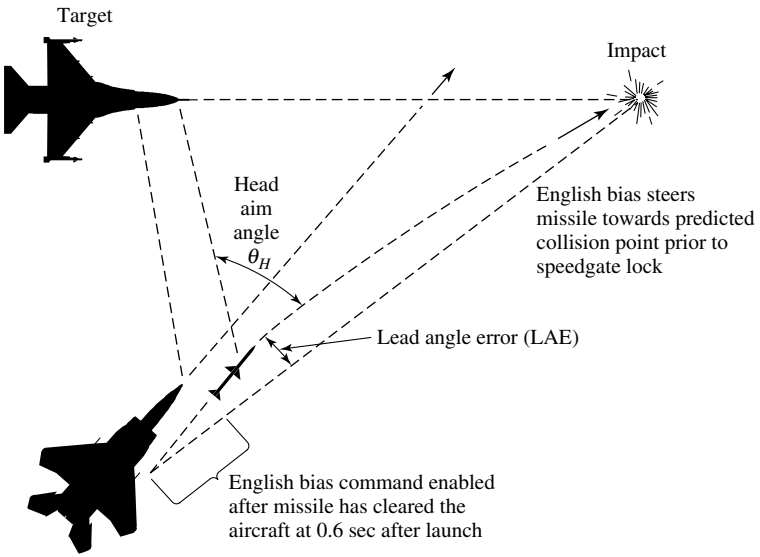

Fig. 3.44. Effect of English bias commands.

More specifically, English bias commands guide the missile to the proper course as computed by the launching aircraft computer as shown in Figure 3.44. If the missile is to be launched at other than the desired lead angle, in-flight course correction commands, that is, English bias, are applied to the pitch/yaw autopilot. English bias has the ability to correct up to 25° of lead angle error. For example, upon missile speedgate lock on target video, t_{go}^{**} = Lock + 0.5 s, pre-t_{go} = Launch + 3 s, English bias is switched out and axial compensation and homing guidance commands derived from target video are applied to the pitch/yaw autopilot (t_{go} is the time remaining before intercepting the target).

A g-bias is included in the pitch/yaw autopilot to eliminate the bias affects of the aircraft pitch and yaw accelerometer instruments' sensing of Earth's gravitational pull of one g. The g-bias is enabled at approximately 0.6 s after launch. English bias commands are stored on capacitors by the aircraft prior to launch (1 volt *dc* per degree of angle error) and allowed to be processed in the pitch and yaw autopilots 0.6s after launch at a g-command conversion of 0.45 g's per degree commanded. This g-command is summed and integrated and then converted to degrees of wing by the servo amplifier and wing hydraulics (assuming that hydraulic actuators are used). As the missile translates laterally, its lateral accelerometer instruments sense g's responded. This g response is amplified, sense compared, and applied to the same summing point to null out the commanded g's. As this process takes place, the missile is turning to correct for lead angle error, but the missile head is space

**Mathematically, t_{go} is defined as $t_{go} = R/V_c$, where R is the range between missile (or pursuer) and the target, and V_c is the missile's closing velocity.

stabilized. Therefore, while the missile is turning, it is also rotating about the headspace stabilized attitude. If, for example, 5° of English bias were commanded, the missile would increase or decrease the original head aim by 5°, therefore nulling the commanded g's.

As previously discussed (see Section 3.5), the autopilot is basically a tight acceleration feedback loop designed so that guidance signal commands cause the missile to accelerate laterally. Rate gyroscopes can be used to achieve proper pitch, yaw, and roll damping. The pitch and yaw rate gyros are also used for synthetic stability, that is, to stabilize the missile against parasitic feedback caused by radome refractions and imperfect head stabilization. Immediately before launch, the antenna in the head of the missile is positioned by "head aim" signals to a position where the target is predicted to be located a short time after launch. The autopilot stabilizes the missile at all speeds throughout its altitude and range envelope. In each channel (i.e., pitch and yaw), the command signal is fed to the amplifiers of the wing servo system in that channel. When the speedgate is locked and starts tracking Doppler video, for example, a command is generated to the autopilot that switches the English bias command out of the acceleration command processor and switches in axial compensation if this has not already been accomplished by the launch plus 3 s command. At speedgate lock, radar error commands that have been amplified and adjusted by closing velocity in the error multiplier command the pitch or yaw autopilot to process lateral g's (A_L).

References

1. Blakelock, J.H.: *Automatic Control of Aircraft and Missiles*, John Wiley & Sons, Inc., New York, NY, second edition, 1991.
2. Etkin, B.: *Dynamics of Atmospheric Flight*, John Wiley & Sons, Inc., New York, 1972.
3. Garnell, P.: *Guided Weapon Control Systems*, Pergamon Press, Oxford, New York, second edition, 1980.
4. Li, Y.T. and Whitaker, H.P.: *Performance Characterization for Adaptive Control Systems*, paper presented at the Symposium on Self-Adjusting System Theory sponsored by the International Federation of Automatic Control and the Italian Commission on Automation, Rome, Italy, April 1962.
5. Lin, C.F.: *Modern Navigation, Guidance, and Control Processing*, Vol. II, Prentice Hall, Englewood Cliffs, New Jersey, 1991.
6. Nicolai, L.M.: *Fundamentals* of *Aircraft Design*, METS, Inc., San Jose, CA., 1984.
7. Osborn, P., Whitaker, H.P., and Kezer, A.: *New Developments in the Design of Model Reference Adaptive Control Systems*, Institute of Aeronautical Sciences, paper No. 61-39, presented at the IAS 29^{th} annual meeting, January 1961.
8. Roskam, J.: *Airplane Flight Dynamics and Automatic Flight Control*, Part I, Roskam Aviation and Engineering Corporation, Ottawa, Kansas, second printing, 1982.
9. Siouris, G.M.: *Aerospace Avionics Systems: A Modern Synthesis*, Academic Press, Inc., San Diego, CA., 1993.
10. Skolnik, M.I.: *Introduction to Radar Systems*, McGraw-Hill, New York, second ed., 1980.
11. Whitaker, H.P., Yarmon, J., and Kezer, A.: *Design of Model-Reference Adaptive Control Systems for Aircraft*, Instrumentation Laboratory, M.I.T., Report R-164, September 1958.

12. Zarchan, P.: *Tactical and Strategic Missile Guidance*, "Progress In Astronautics and Aeronautics," Published by the American Institute of Aeronautics and Astronautics, Inc., third edition, 1998.
13. *A Study to Determine an Automatic Flight Control Configuration to Provide a Stability Augmentation Capability for a High-Performance Supersonic Aircraft*, Minneapolis-Honeywell Regulator Company, Aeronautical Division, WADC-TR-349 (Final), May 1958.
14. *Final Technical Report Feasibility Study Automatic Optimizing Stabilization System*, Part 1, Sperry Gyroscope Company, WADC-TR-243, June 1958.
15. Proceedings of the Self-Adaptive Flight Control Systems Symposium, WADC-TR-59-49, March 1959.

4

Tactical Missile Guidance Laws

4.1 Introduction

This chapter presents a discussion and overview of missile guidance and control laws as well as the basic equations that are used in intercepting a given target. Theoretically, the missile–target dynamics are highly nonlinear. This is due to the fact that the equations of motion are best described in an inertial coordinate system, whereas aerodynamic forces and moments are conveniently represented in the missile and target body axis system. In addition, and if optimal control theory is used to model and/or formulate the plant (or system), unmodeled dynamics or parametric perturbations usually remain in the plant modeling procedure. Furthermore, speed plays an important role in determining interceptor missile aerodynamic maneuverability. Two basic guidance concepts will be discussed: (a) the *homing* guidance system, which guides the interceptor missile to the target by means of a target seeker and an onboard computer; homing guidance can be modeled as *active*, *semiactive*, and *passive*; and (b) *command* guidance, which relies on missile guidance commands calculated at the ground launching (controlling) site and transmitted to the missile. In addition to these guidance systems, two other forms of missile guidance have been used in the past or are being used presently: (a) inertial guidance (used mostly in ballistic missiles, and which will be discussed in detail in a later chapter), and (b) position-fixing guidance. Some guided missiles may contain combinations of the above systems. One such missile, the *Bomarc* (developed in the 1950s), had a command guidance system that controlled the weapon from the ground to the approximate altitude and general area of the target aircraft, whereupon the *Bomarc's* own homing guidance system took over. Again, a combined inertial and position-fixing guidance system may be used. The latter may occasionally refer to a map, chart, or star to check the missile trajectory. Examples of this type are the Air Force's nuclear *ALCM* (*a*ir-*l*aunched *c*ruise *m*issile), the *AGM-86B*, which uses both inertial guidance and *TERCOM* (*te*rrain *co*ntour *m*atching), and the Navy's *Trident IRBM*, which uses a star tracker for position fixing after launch. (Note that a *conventional* version of the air-launched cruise missile (*CALCM*) using the global positioning system (*GPS*) instead of *TERCOM* to update the inertial navigation system was developed in the mid-1980s, and was

successfully used in *Operation Desert Storm* in 1991 (see also Section 7.1). Still a later version, the *AGM-86C* air-launched cruise missile, which has greater accuracy, uses *GPS* navigation in addition to *TERCOM*. Infrared seekers and radar homing devices are employed in guidance systems for many *AIM*s (air-interceptor missiles) such as the *Falcon*, *Sidewinder*, and *Sparrow*.

Guided missile (also known as *guided munition*) systems contain a guidance package that attempts to keep the missile on a course that will eventually lead to an intercept with the target. Most guidance and control laws used in the current tactical air-to-air missiles (*AA*) or *AIM*s, air-to-ground missiles (*AGM*s), and surface-to-air missiles (*SAM*s) or air defense systems employ either homing or command guidance in order to intercept the target. At this point it is appropriate to note that short-range, shoulder-fired *SAM*s using *IR* guidance have been developed by various nations. Examples of these missiles are (a) the Hughes *Stinger*, which has an all-aspect firing capability and a maximum altitude of 14,000 ft (4,267.2 m); note that the Block 2 *Stinger* missile includes a focal plane array and 10 to 100 times more processing power; (b) the Matra *Mistral*; its all-aspect capability allows it to be fired at an approaching aircraft or from the side, has a maximum altitude of 14,000 ft (4,267.2 m), and the missile and launcher weigh 47 lbs including a 6.6 lb high-explosive (*HE*) warhead; and (c) the Russian *SA-7, -14, -16, and -18*; the first two weigh more, have a maximum altitude of 12,000 ft (3,657.6 m), and are effective only when shooting at the rear of an aircraft, while the *SA-16*, and *-18* with their improved sensing devices allow them to hit a target head-on or from the side.

The Russian *Igla* (*9M342*) man-portable shoulder-launched *SAM* is now in production. This missile, while externally similar to the basic *9M39 Igla*, is claimed to have significantly enhanced performance; the latest version can be used effectively to engage cruise missiles and *UAV*s. The *Igla* missile family, including the basic *9M39* (*SA-18 Gimlet*) and the improved *9M313* (*SA-16 Grouse*) missiles, have been widely exported. The latest *Igla* version is dubbed *Igla-S* (Super), and has a warhead weighing 2.5 kg (5.5 lb) compared with 1.2 kg for the basic *Igla*. Lethality has also been improved by fitting the missile with a laser proximity fuze having a guaranteed detection radius of 1.5 m (4.9 ft). A five-meter false detection gate limit has also been set. In terms of range, control modifications to reduce missile drag have resulted in the maximum slant range of the missile being increased to 6,000 meters, versus 5,200 meters for the basic design. The *SA-18 Gimlet* (*9M39 Igla*) was used by Yugoslav ground forces during the Kosovo conflict.

Matra BAe Dynamics upgraded and improved the performance of the *Mistral* surface-to-air missile, which is now designated *Mistral 2*. The "fire and forget" *Mistral 2* has a 6-km (3.7-mi) range and can fly at Mach 3 at a 6,600-ft maximum altitude. It has a solid rocket booster and a passive *IR* guidance system, weighs 44 lb, and carries a 6.6-lb warhead. In addition to the portable version, the company has developed a twin launcher mounted on wheeled and tracked armored vehicles, an air-to-air derivative for attack helicopters, and a naval surface-to-air antiaircraft/antimissile version.

Another way to classify homing systems is by the frequency spectrum to which the system is sensitive (i.e., the wavelength it seeks out). Moving through the spectrum from low to high frequency, *sound* has had some use in seeker systems. Naval

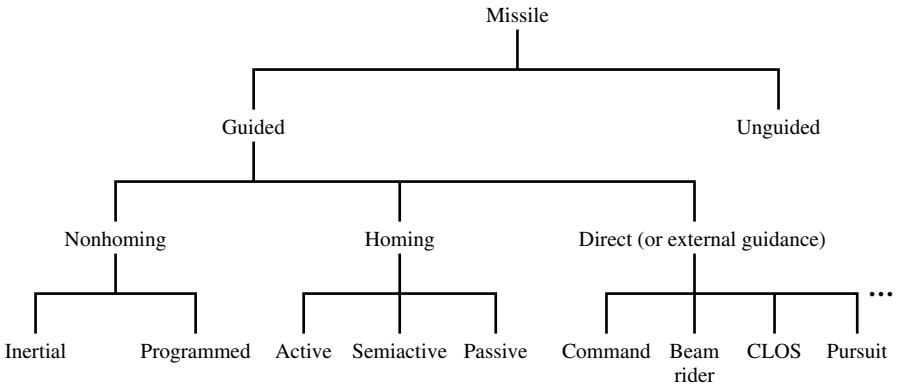

Fig. 4.1. Missile types and classification.

torpedoes have been developed as passive sound seekers, but such seekers have certain drawbacks. The sound-seeking missile is limited in range and utility because it must be shielded or built so that its own motor noises and sound from the launching platform will not affect the seeker head. Electromagnetic radiation is the most popular form of energy detected by homing systems. Radar can be the primary sensor for any of the three classes of homing guidance systems, but it is best suited for semiactive and active homing. Currently, the use of electromagnetic radiation via radar in a target seeker is foremost in effectiveness. Radar is little restricted by weather or visibility, but is susceptible to enemy jamming. Heat (infrared radiation) is best used with a passive seeker. It is difficult to mislead or decoy heat-seeking systems when they are used against aerial targets because the heat emitted by engines and rockets of the aerial targets is difficult to shield. With a sufficiently sensitive detector, the infrared system is very effective. Light is also useful in a passive seeker system. However, both weather and visibility restrict its use. Such a system is quite susceptible to countermeasure techniques.

Various flight paths or trajectories may be deployed with respect to fixed targets, but for moving targets special requirements must be met. In homing systems, sensing elements must be sharply directional to perceive small angular displacements between a missile and its target. Figure 4.1 illustrates a possible classification of the various missile types by their guidance method. The scheme of classification is not unique. Nevertheless, this figure is presented here as a starting point for further discussion and to establish a standard in this diversified field.

Fighter aircraft entering service in the early twenty-first century will be equipped with helmet-mounted display systems fully integrated with all of the aircraft's avionics systems that will give pilots the ability to fire up to 90° to the left and right of the aircraft during air-to-air engagements. Consequently, advanced medium-range air-to-air missiles using helmet-mounted display systems will have a $50\,g/90°$-turn capability for off-boresight targets. Even today, close-in engagements (up to 5 km in range) involving helmet-mounted display systems can direct infrared missiles to their target.

For instance, the present Russian *R-73* (*NATO* code: *AA-11 Archer*) air-to-air missile has a passive infrared seeker and uses helmet-mounted display technology, which can acquire targets up to 60° left or right; that is, it can be used to point to the target by the helmet system. Thus, a pilot can engage an enemy aircraft simply by turning his head without turning the nose of the aircraft (for more details, see Section 5.12.1).

Air-to-air weapons vary in size, weight, and guidance package. The weapons or other stores must be compatible for carriage on U.S. and other allied military aircraft. For this reason, U.S. Air Force and U.S. Navy organizations are involved in ensuring that stores will fit on different aircraft. Specifically, a computational fluid dynamics program is under development by the Air Force. This program is supposed to model airflow around stores and the impact on them in order to conduct flow separation and cavitation analysis.

4.2 Tactical Guidance Intercept Techniques

4.2.1 Homing Guidance

The expression *homing guidance* is used to describe a missile system that can sense the target by some means, and then guide itself to the target by sending commands to its own control surfaces. Homing is useful in tactical missiles where considerations such as autonomous (or *fire-and-forget*) operation usually require sensing of target motion to be done from the interceptor missile (or pursuer) itself. Consequently, in such cases the sensor limitations generally restrict the sensed target motion parameters to the set consisting of the direction of the line of sight and its rates of various orders.

Homing is used not only for the terminal guidance of missiles, but also for the entire flight in some cases, particularly for short-range missiles. The various homing guidance schemes were briefly discussed in Chapter 1. In this section, we will discuss these guidance techniques in more detail. At this point it is appropriate to define the expression *homing guidance*. Homing guidance is a term used to describe a guidance process that can determine the position (or certain position parameters) of the target (e.g., an aircraft, ship, or tank) with respect to the pursuer and can formulate its own commands to guide itself to the target. More specifically, a homing system is a specialized form of guidance, which entails selecting, identifying, and following (*chasing*) a target through some distinguishing characteristic of the target. Such identifying characteristics as heat or sound from a factory, light from a city, or reflections of radar waves from a ship or aircraft are used as the source of intelligence to direct the missile to the target.

Homing systems may be classified in three general groups as follows [6], [11]:

- *Active*
- *Semiactive*
- *Passive*

In an active homing system, the target is illuminated and tracked by equipment on board the missile itself (Figure 4.2, top). That is, the missile carries the source of radiation on board in addition to the radiation sensor. In an active radar homing

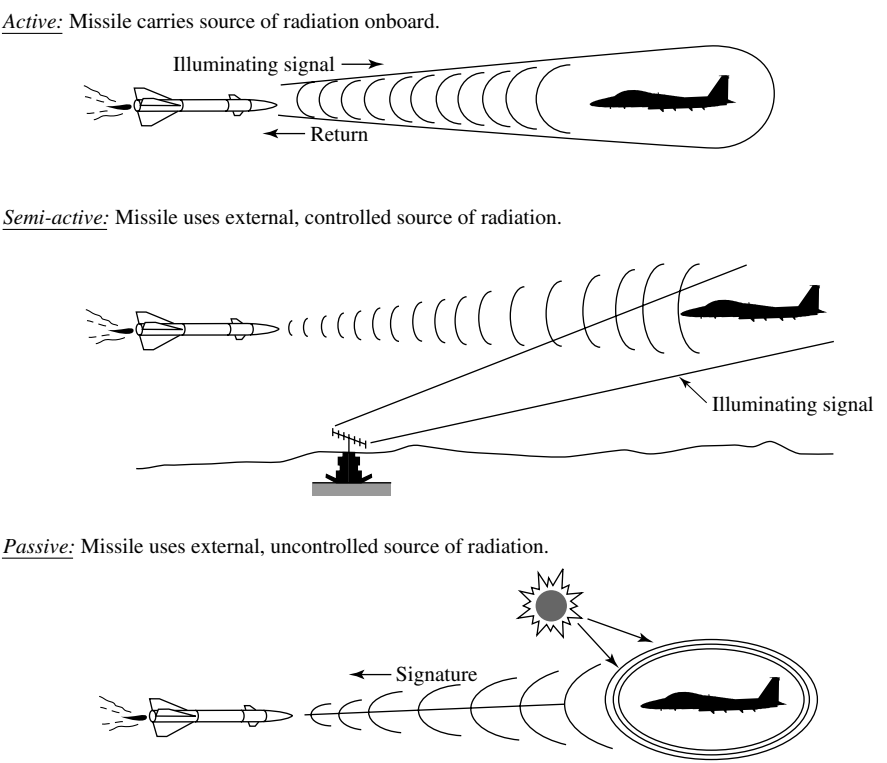

Fig. 4.2. Homing missile guidance types. (Originally published in *The Fundamentals of Aircraft Combat Survivability Analysis and Design*, R.E. Ball, AIAA Education Series, copyright © 1985. Reprinted with permission.)

system, for example, both the radar transmitter and the receiver are contained within the missile. Actively guided missiles have the advantage of *launch-and-leave*; i.e., they can be launched and forgotten. Disadvantages of the active homing system are additional weight, higher cost, and susceptibility to jamming, since the radiation it emits can reveal its presence. An example of an active homing missile system is the European *Meteor* active radar-guided *AAM*.

A semiactive homing system is one that selects and chases a target by following the energy from an external source, such as a tracking radar, reflecting from the target (Figure 4.2, middle). This *illuminating* radar may be ground-based, ship-borne, or airborne. Semiactive homing requires the target to be continuously illuminated by the external radar at all times during the flight of the missile. The illuminating energy may be supplied by the target-tracking radar itself or by a separate transmitter collimated with it. The radar energy reflected by the target is picked up by a tracking receiver (the seeker) in the nose of the missile and is used by the missile's guidance system. Equipment used in the semiactive homing systems is more complex and bulky than that used in passive systems. It provides homing guidance over much greater ranges

and with fewer external limitations in its application. An example of semiactive missile guidance is found in the supersonic *Sparrow III* (model *AIM-7F*), while the *Phoenix* missile uses both active and semiactive homing guidance.

A passive homing system (Figure 4.2, bottom), one that is designed to detect the target by means of natural emanations or radiation such as heat waves, light waves, and sound waves. Thus, passive homing guidance systems are based on the use of the characteristic radiation from the target itself as a means of attracting the missile, for example, as in infrared homing systems. In other words, the target acts as a lure. Regardless of the type of intercept guidance technique used, the missile must have sufficient maneuver capability (pull sufficient *g*'s) to intercept the target within the lethal distance of the warhead. At lower altitudes, the airframe capability is not a limiting factor because it can generally execute *g*'s in excess of the autopilot limit, say 25 *g*'s. At higher altitudes, especially in a snap-up attack, the airframe maneuver limit is usually the parameter that determines the launch boundary and/or terminal accuracy.

The *Sidewinder* is an example of a passive infrared homing guided missile. The infrared (*IR*) homing devices are suitable for use against such targets as mills, factories, bridges, railroad yards, jet aircraft, troop concentrations, ships, or any other targets that present large temperature differentials with respect to their surroundings (see also Section 3.4.4). The actual temperature of the target is not important, but the difference in temperature between the target and its surroundings is the factor that enables the heat seeker to identify the target against the background. It is important to keep in mind, however, that all homing systems are subject to limitations in use. For example, the heat seeker requires a clear, relatively moisture-free atmosphere, and could be led astray by countermeasures such as fires set to guide it away from its intended target. The components of homing guidance systems are essentially the same in all types of homing, but there are differences in location and methods of using the components. Figure 4.2 illustrates the various forms of missile homing guidance.

A fundamental requirement of any homing system is that the scanning sensor (or seeker) be accurately aligned with respect to the longitudinal axis of the missile in which it is installed. The controls are actuated so that its longitudinal axis is always in line with the target.

With the exception of the passive infrared missiles, radar is the most commonly used sensor for target tracking in the homing context. In radar target tracking systems, antennas radiate and receive energy in all directions; however, for pencil beam antennas, the greater portion of the energy is concentrated in a more or less conical region about the central axis (i.e., the boresight axis). This region is referred to as the main lobe; it is surrounded by weaker side lobes. The transmitter may be located at a surface installation, on an aircraft, or in the nose of the chasing missile itself. The missile launcher may be in close proximity to the transmitter, but not necessarily so. Throughout its flight, the missile is between the target and the radar that illuminates the target. It will receive radiation from the launching station, as well as reflections from the target. The missile must therefore have some means for distinguishing between the two signals, so that it can home on the target rather than on the launching station. This can be done in several ways. For example, a highly directional antenna may be mounted in the nose of the missile. Or the Doppler principle may be used to

distinguish between the transmitter signal and the target echoes. Since the missile is receding from the transmitter and approaching the target, the echo signals will be of a higher frequency than the direct signal.

Onboard missile receivers generally include some type of automatic gain control, which attempts to keep the receiver output signal power nearly constant. As a result, the effective noise level will change with received signal power relative to some reference level. A meaningful comparison of homing guidance systems for tactical missiles requires realistic models for the missile and the target engagement geometry, in order to accurately evaluate the terminal miss distance. This model should include the system dynamics and system nonlinearities, which influence the missile's performance. By virtue of the use of onboard data gathering, the homing guidance system provides continually improving quality-of-target information almost up to the intercept point. This permits the achievement of an accuracy that is unmatched by any other form of missile guidance. The modern short-range air-to-air missile engagement is the most demanding tactical weapon scenario from the viewpoint of the guidance law, due to a number of factors. These factors include short engagement times (nominally 2–3 seconds) and rapid, drastic changes in the kinematics of the scenario. Homing missiles of all three types are used because there are many variables in the military requirements. Among these are speed, altitude, and expected maneuvers of the target; the number and type(s) of targets that must be engaged and/or destroyed in rapid succession; the area to be defended (which influences the possible courses of the target); the permissible complexity of the system; and the permissible cost of the missiles.

All homing systems in use today employ some form of *proportional navigation* (*PN*) for the guidance law (for more details on *PN* see Section 4.5). There are several reasons why proportional navigation has been used extensively in past and present homing systems. First, proportional navigation is very effective in guiding missiles to intercept low-maneuvering aircraft under restricted launch conditions. Second, proportional navigation is relatively easy to implement using simple off-the-shelf hardware. Third, even though the specific guidance and control law may vary from one missile to another, all of these laws work fairly well against stationary and constant-velocity targets. However, these control laws must be modified when used against highly maneuverable targets. Section 4.1.3 presents a survey of the overall performance of proportional navigation systems based on linearized theory. Linearization reduces the complexity of design, without compromising the realism of the resulting analysis. Therefore, a major task of the missile designer is to ensure that significant nonlinearities do not occur. Finally, the advantage of using homing guidance is that the measurement accuracy continually improves because the interceptor missile, and its seeker, get closer to the target as the flight progresses.

A typical military requirement might be for a surface-to-air missile that will engage and destroy targets of the following characteristics: (1) A speed of up to 2,000 ft/sec, (2) high maneuverability, (3) low altitude, and (4) minimum ground station to target range of about 1,500 ft. At such close range a line-of-sight missile would have to make a very sharp turn at high speed to engage the target, particularly if the target's course was not directed toward the ground station. It would be difficult or impossible to construct a missile that would withstand the resulting accelerations

without going out of control. Therefore, the situation requires a guidance system capable of minimizing missile maneuver, one in which the missile *leads* the target to a collision at an anticipated position. A semiactive homing missile with proportional navigation is particularly suited to a problem of this kind.

From a performance perspective, an interceptor with 10 g acceleration and a top speed of 10 km/sec (6.2 miles/sec) would have a range of about 400 km (248.5 miles) to reach a target that requires 90 sec to accelerate. A higher acceleration interceptor, capable of 20 g, could cover an 800 km (497 mile) range.

4.2.2 Command and Other Types of Guidance

As discussed in Section 4.1.1, homing missiles may home on the target using a variety of techniques. Each technique entails a certain mathematical law and/or constraint. The majority of the guidance systems that we will discuss in this section are of the line-of-sight type; i.e., the primary source of guidance information is the direction of the line from the missile to the target (and its rates). In Chapter 1, guidance was defined as the means by which a missile steers or is steered to a target. Missile guidance is generally divided into three distinct phases: (1) *boost* or *launch*, (2) *midcourse*, and (3) *terminal*. The boost phase lasts from the time the missile leaves the launcher until the booster burns all of its fuel. The missile may or may not be actively guided during this phase. The midcourse phase, when it has a distinct existence, is usually the longest in terms of both distance and time. During this phase, guidance may or may not be explicitly required to bring the missile onto the desired course and to make certain it stays on course until it enters a zone (in parametric space) from which terminal guidance can successfully take over. The terminal phase is the last phase of guidance and must have high accuracy and fast reaction in order to ensure an intercept with the target. In this phase, the guidance seeker (if one is used) is *locked* onto the target, permitting the missile to be guided all the way to the target. Therefore, proper functioning of the guidance system during the terminal phase, when the missile is approaching its target, is of critical importance. A great deal of work has been done to develop extremely accurate equipment for use in terminal-phase guidance.

There are several guided systems that fall into this category. The most common ones are the short-range homing systems and some type of inertial system. These terminal systems may also be the only guidance systems used in short-range missiles. Furthermore, it was mentioned in Chapter 1 that prelaunch aiming errors must be minimized because these errors tend to translate directly into miss distance. The prelaunch requirements are given in Table 4.1 Subsequent to launch, the missile has certain requirements. First, the missile needs a target signal. For example, in the case of a semiactive guided missile, the target signal is the result of energy reflected from the target. The source of this energy is the interceptor, which in turn receives energy from the illuminator. Thus, subsequent to launch, the missile requires that the target be continuously illuminated. Target illumination, by itself, does not require that the interceptor track the target, although this may occur. In addition, the missile requires the presence of certain modulations on the target return, which are conveniently

Table 4.1. Prelaunch Requirements

Activation	Three-Phase Power
	Rear *RF* Reference
Target Location	Angle and Angle Rate
	Range and Range Rate
	Head Aim, English Bias
	Range at Launch, True Air Speed
	Simulated Doppler, Sweep Control
Conditioning Signals	Autopilot Commands
	Sweep Select
Commitment	Battery/Hydraulic (or other) Activate
	Battery Up
Postlaunch Requirements: (a) Target	Missile tracks target return
(b) Missile	Missile generates guidance commands from tracking data
(c) Interceptor	Interceptor illuminates target to provide signal for missile to track

impressed on the illuminating signal itself. Typically, this is an 85 Hz *FM* ranging signal, which the missile uses to select the target from clutter or noise.
Command guidance techniques as well as other command/homing methods, which are part of the postlaunch phase, can be effected in a number of ways, the more prominent of which are listed below:

Command Guidance: Command guided missiles are missiles whose guidance instructions or commands come from sources outside the missile. In this type of guidance, a tracking system that is separated from the missile is used to track both the missile and the target. Therefore, a missile seeker is not required in command guidance. The tracking system may consist of two separate tracking units, one for the missile and one for the target aircraft, or it may consist of one tracking unit that tracks both vehicles. The tracking can be accomplished using radar, optical, laser, or infrared systems. A radar beacon or infrared flare on the tail of the missile can be used to provide information to the tracking system on the location of the missile. The target and missile ranges, elevations, and bearings are fed to a computer. Consequently, using the position and position rate information (i.e., range and range rate), the computer determines the flight path the interceptor missile should take that will result in a collision with the target. That is, a computer at the launch point determines whether the interceptor missile is on the proper trajectory to intercept the target. If it is not, steering commands are generated by the ground computer and transmitted to the in-flight missile. Furthermore, the computer compares this computed flight path with the predicted flight path of the missile based on current tracking information, and determines the correction signals required to move the missile control surfaces to change the current flight path to the new one. These signals are the command guidance and are sent to the missile receiver via either the missile tracking system or a separate command link, such as radio. In addition

to the steering instructions, the command link may be required to transfer other instructions to the missile, such as fuse arming, receiver gain setting, and warhead detonation. Finally, in command guidance, the launch point *commands* the missile. Command guidance all the way to the target is used mostly with short-range missile systems because of the relatively large tracking errors that occur at long range. The *NIKE* family uses this type of guidance. Also, the Army's *PATRIOT MIM-104* air-defense missile uses a modified version of command guidance, in which only one radar is needed. A disadvantage of command guidance is that the external energy source must illuminate the target often enough (i.e., high data rate) to make guidance effective. The target may thus get alerted of the illuminating radar's presence and operation, and may resort to evasive action.

Beam Rider: Beam riding is another form of command guidance. Specifically, in this type of guidance, the aircraft (target) is tracked by means of an electromagnetic beam, which may be transmitted by a ground (or ship or airborne) radar or a laser tracking system (e.g., a ladar (*laser detection and ranging*), or *la*ser ra*dar*). In order to follow or ride the beam, the interceptor missile's onboard guidance equipment includes a rearward-facing antenna, which senses the target-tracking beam. By utilizing the modulation properties of the beam, steering signals that are a function of the position of the missile with respect to the center (or the scanning axis) of the target-tracking beam are computed on board and sent to the control surfaces. These correction signals produce control surface movements intended to keep the missile as nearly as possible in the center of the target-tracking beam (or scanning axis). For this reason, the interceptor missile is said to ride the beam. Either the beam that the missile rides can track the target directly, or a computer can be used to predict the direction the missile beam should be pointing in order to effect an eventual collision of the interceptor missile with the target. In this case, a separate tracker is required to track the target. Some ground-tracking systems use a *V*-shaped beam to track the target. In such a case, the interceptor missile *rides* in the bottom of the V. If the missile moves out of the V bottom, sensing circuits in the missile cause the missile to return to the bottom of the V. As long as the launch point continues to track the target, and the missile continues to ride the radar beam, the missile will intercept the target. As in any system, there are advantages and disadvantages in using one method versus another. The advantage of the beam-riding guidance technique is that it permits the launching of a large number of missiles into the same control or target-tracking beam, since all of the guidance equipment is carried in the missile. A disadvantage of this guidance technique is that the tracking beam must be reasonably narrow to ensure intercept, thus increasing the chance of the interceptor missile losing track of the target, particularly if the target undergoes evasive maneuvers. The problem of large tracking error for long-range targets usually restricts the use of this guidance technique to short ranges.

Command to Line of Sight (CLOS): A particular type of command guidance and navigation where the missile is always to *commanded* lie on the line of sight (*LOS*) between the tracking unit and the aircraft is known as *command to line of sight* (*CLOS*) or three-point guidance. That is, the missile is controlled to stay as close as possible on the *LOS* to the target after missile capture. In *CLOS* guidance an up-link

is used to transmit guidance signals from a ground controller to the missile. More specifically, if the beam acceleration is taken into account and added to the nominal acceleration generated by the beam-rider equations, then *CLOS* guidance results. Thus, the beam rider acceleration command is modified to include an extra term. The beam-riding performance described above can thus be significantly improved by taking the beam motion into account. *CLOS* guidance is used mostly in short-range air defense and antitank systems.

The following target intercept rules are possible within command/homing guidance strategies.

Pursuit: In the pursuit trajectory, the interceptor missile flies directly toward the target at all times. Thus, the heading of the missile is maintained essentially along the *LOS* between the missile and the target by the guidance system. The missile is constantly turning during an attack. Missiles flying a pursuit course usually end up in a tail-chase situation, similar to a dog chasing a rabbit (or hound-and-hare course). Pursuit guidance is considered impractical as a homing guidance law against moving targets because of the difficult maneuvers that are required to end the attack in a tail chase. That is, the maneuvers required of the missile become increasingly hard during the last, critical, stages of the flight. Another disadvantage of this guidance method is that the missile speed must be considerably greater than that of the target. The sharpest curvature of the missile flight path usually occurs at the end of the flight, so that at this time the missile must overtake the target. If the target attempts to evade, the last-minute angular acceleration requirements placed on the missile could exceed the aerodynamic capability, thereby causing a large miss distance. Furthermore, near the end of the flight, the missile is usually coasting because the booster (and sustainer) motor thrusts last for only a short part of the flight. The result is that more energy is required on the part of the missile to make short-radius, high-speed turns at a time when the missile is losing speed and has the least turning capability. The most favorable application of the pursuit course guidance law is against slow-moving aircraft, or head on toward an incoming aircraft.

Deviated Pursuit: The interceptor missile tracks the target and produces guidance commands. This guidance law is similar to *pure pursuit*, except that the missile heading *leads* the *LOS* by a fixed angle. When the fixed lead angle is zero, deviated pursuit becomes pure pursuit. No missile is designed to fly deviated pursuit; however, random errors and unwanted bias lines often result in a deviated pursuit course.

Lead Pursuit: A lead pursuit course is flown by an interceptor (i.e., a missile) directing its velocity vector at an angle from the target so that projectiles launched from any point on the course will impact on the target if it is within the range of the weapon. Note that the interceptor in conjunction with the missile trajectory flies lead pursuit.

Lead Collision: Lead collision is a straight-line course flown by an interceptor such that the interceptor will achieve a single given firing position. Specifically, in lead collision homing, if the target speed and heading remain constant, a constant-speed

missile will fly a straight-line path to the target–missile collision. The target and missile flight paths form a single triangle with the line of sight (*LOS*) from the missile to the target. This relationship is shown in Figure 4.3. An obvious advantage of collision homing is that the missile is subjected to a minimum of maneuvers since the flight path approximates a straight line. The time of flight of the weapon is a constant.

Pure Collision: Pure collision is a straight-line course flown by an interceptor or weapon such that it will collide with the target.

Constant Load Factor: A constant load factor course is flown by an interceptor or missile so that a constant-g load factor load on the interceptor will result in collision with the target. No missiles presently fly constant load factors. Normal acceleration is constant in this course.

Proportional Navigation: Proportional navigation (also referred to as *collision homing*) is flown in such a manner as to change the lead angle at a rate proportional to the angular rate of the line of sight to the target. The missile measures the rotation of the *LOS* and turns at a rate proportional to it. Specifically, the classical proportional navigation guidance law tries to null the heading error for intercepting the target. The constant of proportionality between the turn rate and line-of-sight rate is called the *navigation constant* (N). In essence, the trajectory flown by the missile is heavily influenced by its navigation constant. This constant is maintained between the missile lateral acceleration (a_n) and the product of the line-of-sight rate ($d\lambda/dt$) and closing velocity V_c. Mathematically, proportional navigation can be expressed as

$$a_n = N V_c \left(\frac{d\lambda}{dt} \right).$$

For more details on proportional navigation, the reader is referred to Section 4.5 and Figures 4.3 and 4.11.

Three-Point: In three-point guidance, the missile is constantly being steered to lie between the target tracker and target. This type of trajectory is typically used only in short-range missile systems employing command-to-line-of-sight (*CLOS*) or beam-rider guidance. Thus, three-point guidance refers to the ground tracker, missile, and target. Three-point guidance is also known in the literature as *constant bearing guidance* [17]. Note that as we shall see later, constant bearing guidance is a specialized case of proportional navigation; that is, constant-bearing guidance is obtained in the limit as $N' \to \infty$.

Hyperbolic Guidance: The guidance or control of a guided missile or the like in which the difference in the time of delay of radio signals transmitted simultaneously from two ground stations, arriving at the missile at different time intervals, controls the position of the missile. This system is based upon the geometric theorem that the locus of all points of fixed difference in distance from two base points is a hyperbola.

Another type of guidance technique is the *retransmission guidance*. This type of guidance, also known as *track via missile* (*TVM*), is the latest technique to be used to direct missiles toward air targets. Typically, in this case a ground radar tracking

system tracks both the target and the missile, as in command guidance. However, in *TVM* the target-tracking beam also serves as a target illuminator, and a receiver on the missile detects the reflected illumination, as in semiactive homing guidance. The ground computer generates commands and returns them to the missile to both guide and control the radar target tracker. It should be pointed out that the data link in this guidance technique must be secure in order to prevent jamming.

Weapons utilizing radiation as the destructive agent (in contrast to the explosive warhead) are referred to as directed high-energy weapons (*DHEW*). Commonly, there are three types of radiation that are propagated by the *DHEW*. These are (a) coherent electromagnetic flux, (b) noncoherent electromagnetic pulse (*EMP*), and (c) charged nuclear particles. The coherent electromagnetic flux is produced by the high-energy laser (*HEL*). The *HEL* generates and focuses electromagnetic energy into an intense concentration or beam of coherent waves that is pointed at the target. This beam of energy is then held on the target until the absorbed energy causes sufficient damage to the target, resulting in its destruction.

Radiation from a laser that is delivered in a very short period of time with a high intensity is referred to as a pulse-laser beam. The noncoherent electromagnetic pulse consists of an intense electronic signal of very short duration that is radiated through space like a radio signal. When an *EMP* strikes an aircraft, the electronic devices in the aircraft can be totally disabled or destroyed. The charged-particle-beam weapon produces radiation in the form of accelerated subatomic particles. A laser beam (of relatively low power) can also be used to guide a weapon. Laser-guided weapons home on energy reflected from the target. Typically, a forward air observer designates a target, and a spot of laser light is shined on the target. The homing weapon detects the reflected laser light from the target, and its autopilot steers a course to impact on the laser spot. A device known as a *laser target designator* produces the laser beam. These target designators are normally carried on board a forward air observer aircraft (e.g., the *O-1*, *O-2*, *OV-10*). It is essential that there exist a direct line of sight between the designator and the target, and the laser must operate during the entire terminal guidance phase of the weapon's flight.

Laser-guided munitions provide the pinpoint accuracy required to minimize collateral damage at a relatively low unit cost, and since fewer rounds are needed per kill, they provide a low cost per kill. In addition, laser-guided munitions are not susceptible to *GPS* or other radio jamming. An Electrooptical (*EO*) targeting system with long-range laser designation capability could be mounted on an unmanned aerial vehicle (*UAV*) to provide target designation for semiactive laser (*SAL*) guided munitions from a safe altitude with no risk to human life. Hands-off targeting by the shooter and initial weapons guidance would be ensured by providing the target *GPS* coordinates to the *UAV*. *SAL* guided munitions that are currently available include *AGM-114 Hellfire* and *AGM-65E Maverick* missiles, the 155 mm *Copperhead* artillery round, the *GBU-15*, the *GBU-28*, and *Paveway II* and *III* laser guided bombs (see Appendix F for more details on these weapons).

Another concept of current interest is the "all-weather precision strike of multiple targets." This concept is realized by employing a wide-area scanner, high-resolution synthetic aperture radar (*SAR*) with ground moving-target

indicator/tracking* (*GMTI/T*) mode, *GPS/INS* reference system augmented with automatic target recognition (*ATR*), a high-resolution targeting forward-looking infrared radar (*FLIR*), and a data-link connectivity to a helmet-mounted cueing system (*HMCS*). In order to reduce *GPS* errors, *GPS* relative targeting is used. By utilizing newly developed targeting algorithms and employing radar modes for measuring the aircraft's height above the target, the system will be able to generate precise *GPS* target coordinates. By using a relative mode of *GPS*, some of the absolute *GPS* errors will cancel out, greatly increasing weapon accuracy.

At this point, a few remarks regarding the "Precision Airborne Target Locator for *GPS/INS AG* Weapons" are in order. The Precision Airborne Target Locator combines a low-cost active (gated) *TV* with a laser rangefinder/designator to provide positive identification and precision location of fixed and movable targets at five times the range of today's targeting *FLIR* systems. This system will yield accuracies on the order of 3 meters, which is compatible with the lethality *CEP* (circular error probable) of *INS/GPS* guided munitions, at ranges out to 25 nm (46.3 km).

Whatever the intended application, there is a wide choice of guidance types. Typically, the homing scheme is described by two terms, which indicate where the target-homing energy comes from, and what portion of the electromagnetic spectrum is being used. Examples are *RF*-active, *RF*-semiactive, and *IR*-passive. Nine combinations are common, though the great majority of air-to-air missiles use either radar or infrared (*IR*) as the radiation for homing. The various guidance sensor types for homing missiles can be categorized based on the type of radiation used for guidance. These are (see also Sections 3.4.3 and 3.4.4):

1. Radio/radar frequency (*RF*).
2. Infrared (*IR*).
3. Visible (Optical).

It should be noted that radiation, as defined here, is energy transmitted as either particles or waves through space at the speed of light. Radiation is capable of inflicting damage when it is transmitted toward the target either in a continuous beam or as one of high-intensity, short-duration pulses. The interceptor missile may also require direct illumination from the ground tracking system to use in the processing of the reflected signal from the target. With this type of guidance, and if the target is an aircraft, the aircraft may know it is being tracked, but it does not know whether a missile is on the way. With this homing technique, several targets can be illuminated and tracked on a time-share basis. Passive homing systems use electromagnetic emissions or natural reflections from the target itself for guidance. An example of passive homing is an infrared-type missile. As discussed in Chapter 3, an infrared guided missile homes in (i.e., closes) on the heat generated by the target (e.g., the tail exhaust of an aircraft). Another type of passive homing is the antiradiation missile. These missiles home in on radar navigation systems, fire-control signals, or on jamming signals from electronic countermeasure equipment on an aircraft. The most recent of these antiradiation missiles is the *AARGM* (advanced antiradiation guided missile). The *AARGM*s, which are based on the *AGM-88 HARM* airframe and use a combination

*A moving-target indicator (*MTI*) is a radar enhancement that filters out fixed objects (scatterers) on the ground and displays (or registers in database) only the moving objects.

of *INS/GPS* midcourse navigation, together with passive antiradiation homing and active millimeter-wave radar terminal guidance, are intended destroy emitters rather than merely disabling them. Figure 4.3 summarizes the various guidance techniques discussed above.

In order to intercept high-speed targets such as supersonic fighter aircraft or missiles, a semiactive homing missile must follow a lead (collision) course. If the target flies a straight-line constant-velocity course, the missile can also follow a straight-line collision course if its velocity does not change. In actual situations, there usually are variations in missile speed, changes in its path, maneuvers of the target, etc. The missile has to adjust its direction to maintain a constant bearing with the target. The components in the missile must be able to sense the changes and make the necessary adjustments in its course to the target. The missile velocity is seldom constant. Boost-glide or boost-sustain-glide thrust schemes result in nonuniform speeds. Irregular propellant burning changes thrust and therefore affects speed. Wind gusts and/or air density variations can change the speed and path of the missile. The same factors can also influence the target trajectory. As we will see later, the missile must use proportional navigation in order to achieve target intercept. If the missile path is changed at the same rate as the target bearing, the missile will have to turn at an increasing rate, and will end up chasing the target. This flight path follows a pursuit curve, and the missile cannot maintain a constant bearing with the target. It is just keeping up with changes in target bearing and may not be able to catch up with the target. Figure 4.4 illustrates a general pursuit course.

Early missiles used a pursuit form of navigation in which steering commands are generated to drive the look angle to zero. The missile then tries to head in the direction of the current target position. The control strategy is optimal for stationary targets and leads to tail chases for moving targets. In an extension of this approach, called proportional navigation (mentioned above), the line-of-sight (*LOS*) rate is driven to zero by using lateral acceleration commands proportional to the *LOS* rates. Proportional navigation and its variants form the basis of guidance laws used in all tactical air-to-air and surface-to-air missiles today. In developing the concepts of proportional navigation, the purely geometrical relationships are first examined, and the concept of navigation gain established. Then the effects of time lags in the missile control system are examined. Next, the effects of stochastic inputs into the control system are examined, specifically those of the three types of noise associated with the homing problem [29]. The miss distance performance under these various conditions is examined and requirements established for the control system response. Also, the significance of the most important nonlinearity in the system, that of saturation of the missile's maneuvering capability, is examined.

An important figure of merit for all missiles is the *probability of kill* (for more details see Section 4.7), defined as the overall probability that the expected target will be destroyed by the system. This probability depends mainly on the following individual probabilities:

1. *Reliability:* What is the probability that the ground system (e.g., a *SAM* site) will be operating when a target comes within range? When a missile is launched, what is the probability that it will operate correctly?

(a) Command guidance: (All guidance and tracking is done outside the interceptor missile)

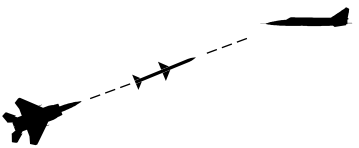

(b) Beam rider:

PURSUIT

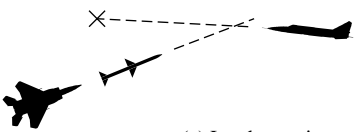

(c) Lead pursuit:

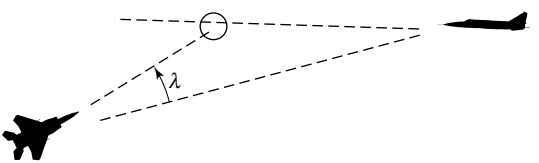

(d) Deviated pursuit:

COLLISION

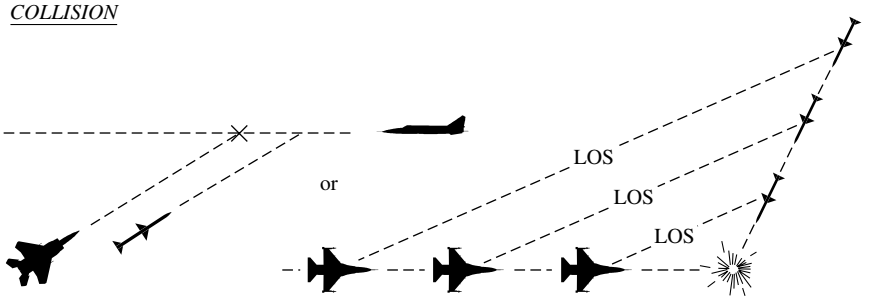

(e) Lead collision:

Fig. 4.3. Types of guidance. (Originally published in *The Fundamentals of Aircraft Combat Survivability Analysis and Design*, R.E. Ball, AIAA Education Series, copyright © 1985. Reprinted with permission.)

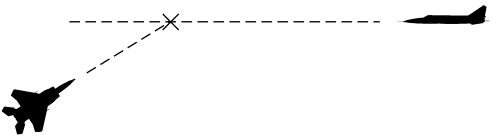

(f) Pure collision:

OTHER

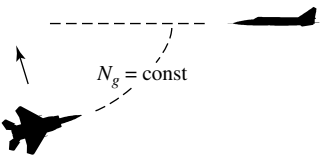

(g) Constant load factor:

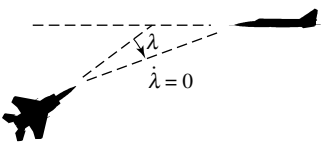

(h) Proportional navigation:

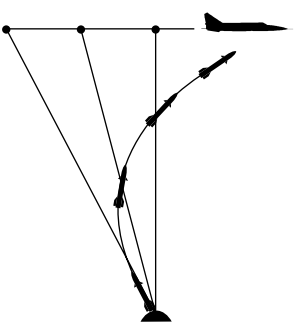

(i) Three-point:

Fig. 4.3. continued

2. *Probability of Detection:* For a given target at a given range, what is the probability that the target will be detected?
3. *Single-Shot Kill Probability:* Given an operable missile launched against a known target, what is the probability that it will destroy the target?

The overall weapon system effectiveness, or probability of kill, is the product of these probabilities. Note that unless otherwise specified, it will be assumed that the interceptor missile uses radar as its onboard sensing/tracking system.

The guidance systems discussed in this section are summarized in Table 4.2. Listed with each type of guidance system are the possible methods of navigation, the

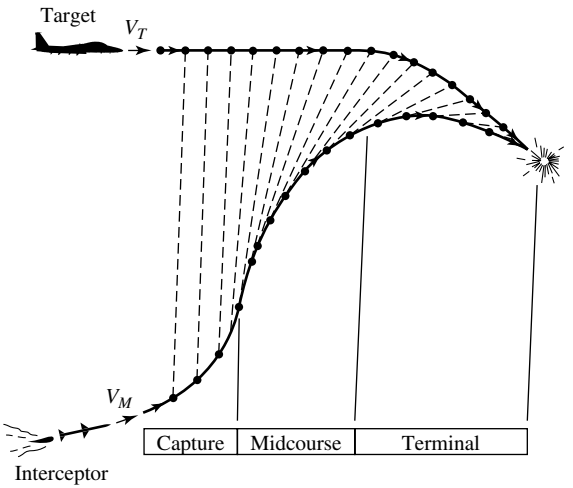

Fig. 4.4. General pursuit guidance course.

sensing devices that may be used to locate and/or track the target, and some important characteristics that make each type suitable for certain situations.

Finally, it should be noted that no one type of guidance is best suited for all applications. Consequently, many missile systems use more than one type of guidance, with each one operating during a certain phase of the interceptor missile's trajectory. For example, a system may use beam-rider guidance or semiactive homing from launch until midcourse, at which time the guidance mode switches to active or passive homing for more accurate tracking and guidance during the terminal phase. An advantage of this technique is that this combination allows the launching aircraft to break away from the engagement earlier than otherwise possible. Such systems are commonly referred to as *composite guidance* systems. Several types of guidance may also be used simultaneously to avoid countermeasures employed by the aircraft, such as the use of a decoy flare to draw an infrared homing missile off the radiation from the aircraft. However, if an active homing system is used in conjunction with a passive one, the missile may reject the flare and continue on toward the target aircraft.

Of particular significance, from the point of view of defensive weapons, is the surface-to-air missile. A surface-to-air missile is launched from the ground or from the surface of the sea against an airborne target. It is generally a *defensive* weapon, since its function is to intercept an enemy aircraft or an incoming missile that is approaching the point or area to be defended. In synthesizing a surface-to-air air-defense missile system the designer must make two basic decisions: (1) the method of guiding the missile, and (2) the type of path over which it travels to the target. The homing, beam-rider (or *CLOS*), and command types of guidance are all applicable to surface-to-air missiles.

Before a surface-to-air missile system can go into action against any hostile airborne target, the system radar must detect the target. Detection must take place at a range long enough to take advantage of the range of the missile, for the following reasons: (1) It may be necessary to launch a number of missiles to destroy all the

Table 4.2. Types of Guidance Systems

Type	Methods of Navigation	Sensing Devices	Characteristics
Active Homing	1. Proportional Navigation 2. Pure Pursuit 3. Deviated Pursuit	1. Radar 2. Infrared 3. Imaging Infrared 4. Laser 5. TV	Ground System Not Committed to Single Target. Very Expensive Missile.
Semiactive Homing	1. Proportional Navigation 2. Pure Pursuit 3. Deviated Pursuit	1. Radar 2. Infrared 3. Imaging Infrared 4. TV 5. Laser	Ground System Committed to Single Target Until Intercept Takes Place.
Passive Homing	1. Proportional Navigation 2. Pure Pursuit 3. Deviated Pursuit	1. Infrared 2. Visible Light 3. Electro magnetic Energy	Ground System Not Committed to Single Target. All Sensing Devices Have Limited Capability Compared with Radar.
Command	Any Method	1. Radar 2. Infrared 3. Visible Light	Ground System Committed To Single Target. Missile Dynamically Linked to Ground System. Ground Computer Required for Programmed Flight. Low-Cost Missile.
Beam Rider (or *CLOS*)	1. Line-of-Sight 2. Programmed	1. Radar 2. Infrared 3. Visible Light	Same as Command

targets in a group detected one at a time; (2) it is obviously desirable to destroy the target before it comes close to the point being defended; and (3) with many types of missile guidance, excessive accelerations are required of the missile to engage the target at close ranges. The system radar must also be capable of acquiring and tracking a target of the specified radar cross section (*RCS*), and may be required to do this at low altitudes in the presence of ground or sea clutter return. Finally, there must be a high probability that a target will be detected *if and only if* a target exists. Closely associated with the early detection requirement is the system *reaction time*, defined as

Table 4.3. Guidance Methods for Surface-to-Air Missiles.*

Command	Beam Rider	Homing Semiactive	Homing Passive
Spartan	Seaslug	Sea sparrow	Chaparral
Sprint	RBS 70	Standard, MR	Redeye
Crotale	Talos (+*SAH*)	Standard, ER	Stinger
Rapier (*CLOS*)	Terier (+*SAH*)	Tartar	Redtop
Seawolf (*CLOS*)		Masurca	Tan-sam
Blowpipe (*CLOS*)		Bloodhound	SA-7
Indigo		Aspide	SA-9
Roland (*CLOS*)		Seadart	
Patriot (+*SAH*)		SA-6	
SA-8		Thunderbird	
		Hawk	

*Originally published in *The Fundamentals of Aircraft Combat Survivability Analysis and Design*, R.E. Ball, AIAA Education Series, copyright © 1985. Reprinted with permission.

the time elapsing between detection of a target and the launching of a missile toward it. If this time is long, then the target would need to be detected correspondingly early during its approach.

A final comment on pursuit guidance is in order. For pursuit against a nonmaneuvering target, the collision course exhibits a constant bearing property, whereby the *LOS* maintains a fixed direction in space; that is, the *LOS* moves parallel to itself in space during the engagement. Consequently, the pursuer will appear to be coming in straight at the target, though pointed off by the lead angle. If a *constant-bearing* guidance law is adopted against a maneuvering target, the resulting pursuer trajectory no longer remains a straight line; however, it still has the desirable property that the demanded pursuer lateral acceleration is at most equal to that of the target. From a theoretical point of view, a constant-bearing guidance law would be a desirable one against both maneuvering and nonmaneuvering targets. However, a constant-bearing law is difficult to implement, especially for the general case of maneuvering targets, since it requires the pursuer to be able to detect the component of target motion perpendicular to the *LOS*, and to adjust its own motion instantaneously, in such a way that its velocity component perpendicular to the *LOS* equals that of the target.

Tables 4.3 and 4.4 present a sample of typical guidance systems used by some of the past and current missiles (see also Appendix F) [14]:

4.3 Missile Equations of Motion

A point-mass model will be assumed for the missile's flight dynamics, which include aerodynamic, gravitational, rocket thrust forces, a time-varying mass, and up to four stages (for more details on the missile dynamics the reader is referred to Chapters 2 and 3). In simplified form, this particular model will require the following input parameters to describe the missile:

Table 4.4. Guidance Methods for Air-to-Air Missiles*

Semiactive Homing	Active Homing	Passive Homing
Falcon	Meteor	Sidewinder
Sparrow	Sidewinder II AIM-9X	Mica
Skyflash	AMRAAM AIM-120A	Magic 2
Aspide	Patriot MIM-104	Shafrir
Phoenix (+ *Active*)	Harpoon AGM-84G	SAAB 327
AA-1 Through AA-7		ASRAAM (British Aerospace)
		Super R530
		R-73 (NATO Code: *AA-11 ARCHER*)
		Shrike
		Standard Arm
		Harm
		Aerospatiale (*AS-30L*)-Laser Guided

*Originally published in *The Fundamentals of Aircraft Combat Survivability Analysis and Design*, R.E. Ball, AIAA Education Series, copyright © 1985. Reprinted with permission.

1. Initial vacuum thrust T_o
2. Initial weight W_o
3. Final weight W_f
4. Burn time t_b
5. Nozzle exit area A_e
6. Aerodynamic reference area A
7. Either:
   (a) Cone angle θ_c and induced axial force coefficient C_{x2} to compute the axial force coefficient C_x by a functional expression, or
   (b) A table for powered flight and, if applicable, for coasting flight, or C_x as a function of Mach number M and angle of attack α.
8. Either:
   (a) Normal force coefficients C_{N1} and C_{N2} to compute the normal force C_N as a quadratic expression in α, or
   (b) A table of C_N as a function of M and α.
9. Coast time before ignition and after burnout.
10. Maximum permissible normal acceleration loading a_{Nmax} .
11. Maximum angle of attack α_{max}.

Figure 4.5 shows the aerodynamic and thrust acceleration vectors that will be used for this model.

The missile's equations of motion are

$$\frac{d\mathbf{r}}{dt} = \mathbf{v}, \tag{4.1a}$$

$$\frac{d\mathbf{v}}{dt} = \mathbf{a} = a_v \mathbf{1}_v + a_L \mathbf{1}_L + \mathbf{g}. \tag{4.1b}$$

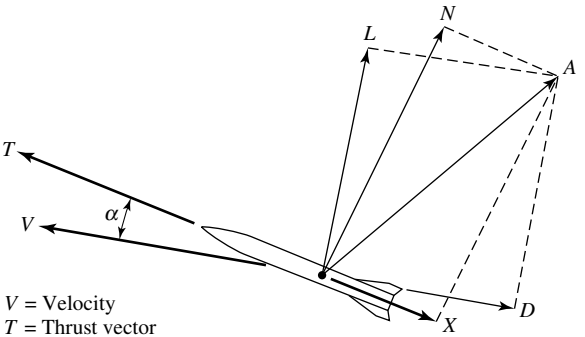

Fig. 4.5. Definition of aerodynamic and thrust acceleration vectors.

In these equations, **r**, **v**, and **a** are the missile's position, velocity, and acceleration vectors, respectively; $\mathbf{1}_v$ and $\mathbf{1}_L$ are unit vectors in the velocity and lift directions; a_v and a_L are the corresponding components of thrust and aerodynamic acceleration; and **g** is the gravitational acceleration. The gravity term is assumed to be constant (i.e., Earth-surface value). The acceleration terms a_v and a_L are given as follows:

$$a_v = (1/m)[(T - C_x QA)\cos\alpha - C_N QA \sin\alpha], \tag{4.2a}$$

$$a_L = (1/m)[(T - C_x QA)\sin\alpha + C_N QA \cos\alpha], \tag{4.2b}$$

where

T = delivered thrust,
m = current mass of the missile,
Q = dynamic pressure = $\frac{1}{2}\rho \mathbf{v}\cdot\mathbf{v}$,
ρ = atmospheric density, computed as a piecewise exponential function of the missile's altitude,
C_x = axial aerodynamic force coefficient,
C_N = normal aerodynamic force coefficient.

Two alternative models for the thrust profile are available to the designer. The first assumes a constant vacuum thrust for the duration of the stage burn time,

$$T_{\text{vac}} = T_o, \tag{4.3a}$$

while the second model assumes a decreasing vacuum thrust shaped to yield constant axial acceleration and is given by

$$T_{\text{vac}} = T_o[W_f / W_o]^{(t-t_1)/t_b}, \tag{4.3b}$$

where t_I is the ignition time of the current stage. The delivered thrust is then obtained from the vacuum thrust by the expression

$$T = T_{\text{vac}} - pA_e, \tag{4.3c}$$

where

$$\begin{aligned} p &= \text{ambient atmospheric pressure (i.e., corresponding to the missile's altitude)} \\ &= \rho g c^2/\gamma [N/m^2], \\ c &= \text{local velocity of sound [m/sec]}, \\ \gamma &= \text{gas ratio of specific heat [1.401]}, \\ g &= \text{gravitational constant [m/sec}^2\text{]}. \end{aligned}$$

During coasting periods, $T = 0$. Note that missile thrust comes from rocket engines, ramjet engines, or both in combination. The rocket engines use either solid or liquid propellant. Mass and inertial characteristics are commonly defined in terms of launch and burnout conditions, and equivalent sea-level impulse. The missile's mass, m, is computed according to one of two equations, depending on which form of thrust calculation is being used. For the constant-thrust model, mass decreases linearly with time and is given by [2]

$$m = (1/g)\{W_o - (W_o - W_f)[(t - t_1)/t_b]\}, \tag{4.4a}$$

and for the variable thrust model,

$$m = (W_o/g)[W_f/W_o]^{(t-t_1)/t_b}. \tag{4.4b}$$

During coasting, m remains constant at W_o/g or W_f/g for preignition or postburnout coasts, respectively. The aerodynamic coefficients C_x and C_N are generally expressed as functions of M and α, where the Mach number M is obtained from the missile's velocity by the relation $M = |\mathbf{v}|/c$. Either or both of these functions may be input to the program in tabular form. Alternatively, functional expressions must be employed. The total mass can also be expressed as

$$m(t) = m_L + C_m \int_0^t T_{SL}(t)dt, \tag{4.4c}$$

where

$$\begin{aligned} m_L &= \text{missile mass at launch}, \\ m_{BO} &= \text{missile mass at motor burnout}, \\ T_{SL}(t) &= \text{motor sea-level thrust history}, \end{aligned}$$

and

$$C_m = (m_{BO} - m_L) / \int_0^t T_{SL}(t)dt.$$

The expression for C_x represents a simplified theoretical model for the axial force coefficient of a cone:

$$C_x = \begin{cases} 2\sin^2\theta_c + C_{x2}\alpha^2, & M \le 0.5, \\ 2\sin^2\theta_c\{1.0 + [((k_1 + k_2\sin\theta_c)/(k_3 + k_4\sin\theta_c)) - 1.0 \\ \quad + (k_5\kappa/2\sin^2\theta_c)(M - 0.5)\} + C_{x2}\alpha^2, & 0.5 \le M \le 0.5, \\ 2\sin^2\theta_c[(k_6 + \sqrt{M^2-1}\sin\theta_c)/(k_7 + \sqrt{M^2-1}\sin\theta_c)] \\ \quad + \kappa/M^2 + C_{x2}\alpha^2, & M \ge 1.5, \end{cases}$$

where $k_1, \ldots, k_7$ represent design values depending on the missile configuration, and $\kappa = 0$ during powered flight, and $\kappa = 1$ during coasting flight. The expression for C_N is a quadratic in α as follows:

$$C_N = C_{N1}\alpha + C_{N2}\alpha^2.$$

The angle-of-attack α is taken to be the smallest of the following three quantities:

1. Commanded angle of attack α_c,
2. Limiting angle of attack $\alpha_{\max}$,
3. Angle of attack $\alpha_{N\max}$, yielding limiting normal acceleration $a_{N\max}$, as computed by iteratively solving the implicit equation

$$a_{N\max} = C_N(M, \alpha_{N\max})QA/m$$

for $\alpha_{N\max}$.

The commanded angle of attack is obtained by iteratively solving the equation

$$a_{LA} = (QA/m)[C_N(M, \alpha_c)\cos\alpha_c - C_x(M, \alpha_c)\sin\alpha_c] \tag{4.5}$$

for α_c. Here, a_{LA} is the desired aerodynamic lift acceleration. It is computed from the desired total lift acceleration a_{Ld} by

$$a_{LA} = a_{Ld} - I_g\mathbf{g}\cdot\mathbf{1}_L, \tag{4.6}$$

where a_{Ld} is computed by the guidance algorithm and I_g is zero if the input guidance parameter is zero or negative, and I_g equals one otherwise. The guidance algorithm also computes the unit lift vector $\mathbf{1}_L$.

Next, (4.1a) and (4.1b) can be numerically integrated using the fourth-order Runge–Kutta integration scheme with a specified time step. Integration is terminated at each dynamic discontinuity (e.g., staging, burnout, or target closest approach), and if necessary, restarted after the discontinuity.

The missile trajectory is integrated in conjunction with the target trajectory. For the state vector at discrete instant i, the following quantities related to the missile motion are computed and saved:

$$\text{time } t_i, \text{ position } \mathbf{r}(t_i), \text{ velocity } \mathbf{v}(t_i), \text{ acceleration } \mathbf{a}(t_i),$$

$$\mathbf{f}(t_i) = (10\sigma_i - 4\Delta_i\mu_i + 0.5\Delta_i^2 v_i)/\Delta_i^3, \tag{4.7a}$$

$$\mathbf{g}(t_i) = (-15\sigma_i + 7\Delta_i\mu_i - \Delta_i^2 v_i)/\Delta_i^4, \tag{4.7b}$$

$$\mathbf{h}(t_i) = (6\sigma_i - 3\Delta_i\mu_i + 0.5\Delta_i^2 v_i)/\Delta_i^5, \tag{4.7c}$$

where

$$\begin{aligned}\sigma_i &= \mathbf{r}_{i+1} - \mathbf{r}_i - \Delta_i\mathbf{v}_i - 0.5\Delta_i^2\mathbf{a}_i,\\ \mu_i &= \mathbf{v}_{i+1} - \mathbf{v}_i - \Delta_i\mathbf{a}_i,\\ v_i &= \mathbf{a}_{i+1} - \mathbf{a}_i,\\ \Delta_i &= t_{i+1} - t_i.\end{aligned}$$

The vector functions $\mathbf{f}(t_i)$, $\mathbf{g}(t_i)$, and $\mathbf{h}(t_i)$ are calculated as in (4.7a,b,c) so as to satisfy the Taylor series expansion in $(t - t_i)$ for $\mathbf{r}$, $\mathbf{v}$, and t over the time interval $t_i \le t < t_{i+1}$. Then, using (4.2c,d,e) as stored quantities, we can compute $\mathbf{r}(t)$, $\mathbf{v}(t)$, and $\mathbf{a}(t)$ as follows:

$$\begin{aligned}\mathbf{r}(t) = \mathbf{r}(t_i) + \mathbf{v}(t_i)(t-t_i) + 0.5\mathbf{a}(t_i)(t-t_i)^2 + \mathbf{f}(t_i)(t-t_i)^3\\ + \mathbf{g}(t_i)(t-t_i)^4 + \mathbf{h}(t_i)(t-t_i)^5,\end{aligned} \tag{4.8a}$$

$$\mathbf{v}(t) = \mathbf{v}(t_i) + \mathbf{a}(t-t_i) + 3\mathbf{f}(t_i)(t-t_i)^2 + 4\mathbf{g}(t_i)(t-t_i)^3 + 5\mathbf{h}(t_i)(t-t_i)^4, \tag{4.8b}$$

$$\mathbf{a}(t) = \mathbf{a}(t_i) + 6\mathbf{f}(t_i)(t-t_i) + 12\mathbf{g}(t_i)(t-t_i)^2 + 20\mathbf{h}(t_i)(t-t_i)^3. \tag{4.8c}$$

We will now discuss the target motion model. The target aircraft trajectory is described by its initial conditions (position and velocity) and a maneuver start time. Maneuver direction will be defined as follows: A plane, which we shall call the "lift plane," is perpendicular to the instantaneous velocity vector. The unit lift vector $\mathbf{1}_L$ will lie in this plane and will be in the direction as shown in Figure 4.6, given the roll direction angle ϕ. The lift magnitude a_L is computed as

$$a_L = \omega_v|\mathbf{v}_T|, \tag{4.9}$$

where ω_v is the input velocity vector turn rate and $\mathbf{v}_T$ is the instantaneous target velocity vector.

In general, the target equations of motion can be written as follows [2]:

$$\frac{d\mathbf{r}_T}{dt} = \mathbf{v}_T, \tag{4.10a}$$

$$\frac{d\mathbf{v}_T}{dt} = \mathbf{a}_T = a_v\mathbf{1}_v + a_L\mathbf{1}_L, \tag{4.10b}$$

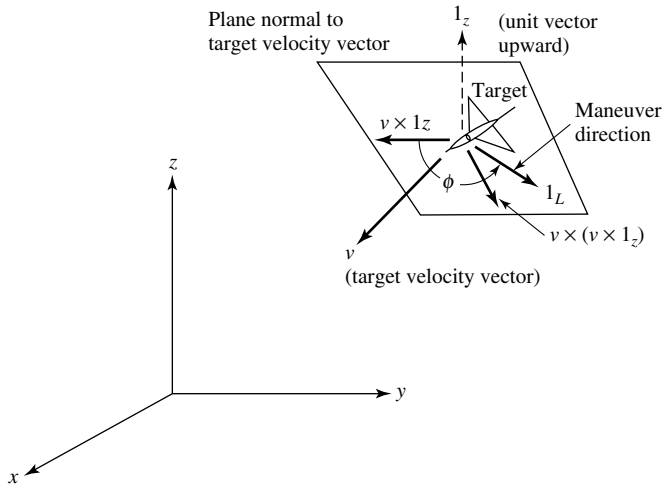

(a) Coordinate system for specifying target maneuver direction

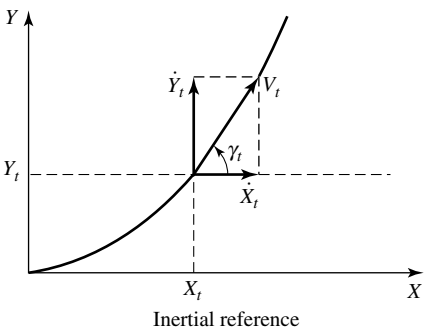

(b) Target flight trajectory

Fig. 4.6. Planar target maneuver and trajectory.

where $\mathbf{r}_T$, $\mathbf{v}_T$, and $\mathbf{a}_T$ are the target's position, velocity, and acceleration vectors, and $\mathbf{1}_v$ and $\mathbf{1}_L$ are unit vectors in the velocity and lift directions. Assuming that the target trajectory is divided into segments with and without maneuver, ω_v is nonzero during maneuver segments of the flight, so that these equations can be numerically integrated using a fourth-order Runge–Kutta integration, typically with a 1-second step. Integration is terminated at the end of each maneuver segment and restarted with the next segment. For segments that have $\omega_v = 0$ (i.e., no turning), the numerical integration is bypassed, since the closed-loop solutions

$$\mathbf{r}(t_{i+1}) = \mathbf{r}(t_i) + \mathbf{v}(t_i)\Delta_i + 0.5\mathbf{a}(t_i)\Delta_i^2, \tag{4.10c}$$

$$\mathbf{v}(t_{i+1}) = \mathbf{v}(t_i) + \mathbf{a}(t_i)\Delta_i, \tag{4.10d}$$

$$\mathbf{a}(t_{i+1}) = \mathbf{a}(t_i), \tag{4.10e}$$

where $\Delta_i = t_{i+1} - t_i$, can be used when the acceleration (if any) is only along the velocity vector.

Let us now assume that the target is considered to be a point mass following an evasive circular trajectory beginning at the origin of the inertial reference frame at a constant speed v_T in the same evolution plane as that of the missile (see Figure 4.6(b)). An evasive maneuver is determined by the absolute acceleration a_T of the target. Under these assumptions, the movement of the target with respect to the inertial reference frame XY is defined by the following equations of motion:

$$\frac{dx_T}{dt} = v_T \cos(\omega_T t + \gamma_{T_o}), \tag{4.10f}$$

$$\frac{dy_T}{dt} = v_T \sin(\omega_T t + \gamma_{T_o}), \tag{4.10g}$$

$$\frac{d\omega_T}{dt} = \frac{d\gamma_{T_o}}{dt} = [g(a_T^2 - 1)^{1/2}]/v_T, \tag{4.10h}$$

where

x_T = target position [m],
y_T = target position ordinate [m],
a_T = target absolute acceleration [g],
v_T = target velocity [m/sec],
g = acceleration due to gravity [m/sec^2],
γ_{T_o} = initial target flight-path angle [rad],
γ_T = target flight-path angle [rad],
ω_T = target angular speed [rad/sec].

4.4 Derivation of the Fundamental Guidance Equations

In order to guide itself to a successful target intercept, the missile must obtain information about the target. Both prelaunch and postlaunch information must be gathered. Before a missile is launched, that is, during the prelaunch phase, the missile needs to know where to go. It knows that it is supposed to go to the target, but it must be told where the target is. The missile is told where the target is by electrical signals entering through the umbilical from the launcher. These signals are *head aim* (to point the missile head at the target), *English bias* (to point the missile to the intercept point), and an estimate of true target Doppler on the simulated Doppler line. The missile then flies according to the proportional navigation guidance law; that is, it senses a change in the line-of-sight angle between the missile velocity vector and the target. In addition, the missile is given certain conditioning signals, which let the missile adjust for variations. These conditioning signals are the autopilot commands to adjust autopilot responses, and auxiliary Doppler positioning signals. Furthermore, though

the missile is designed to guide to impact, an actual impact may not occur, and the missile may miss the target by some finite distance. Specific circuits in the missile give an indication of closest missile approach to the target. These circuits then cause the warhead to be triggered so as to explode as close to the target as possible. In addition, other circuits in the missile are designed to provide indications of a total miss. All of this logic and information is built into the missile, so that the missile *knows* what to do before it is launched.

Guidance systems can use any one of several methods or laws to navigate a missile along a trajectory or flight-path to intercept a target (e.g., an aircraft). The specific target flight path information required by the guidance package depends on which law is used. In this section we will discuss the three types of pursuit courses, namely, *pure pursuit*, *deviated pursuit*, and *pure collision*, and develop the respective differential equations. The homing trajectory that a missile flies depends in the type of guidance law employed. The guidance law depends on the mathematical requirements or constraints of the engagement. Figure 4.7 will be used as the basis to derive these equations. In particular, the kinematics of an attack course, as illustrated in Figure 4.7, are based on the relationships between the interceptor (or missile) velocity V_I, the target velocity V_T, the interceptor lead angle λ, the target aspect angle α, and the interceptor to target range R.

The basic differential equations can be derived from considerations of the geometry. Referring to Figure 4.7, the range rate can be written in the form

$$\frac{dR}{dt} = V_I \cos\lambda + V_T \cos(180 - \alpha) = V_I \cos\lambda - V_T \cos\alpha, \tag{4.11}$$

where the angle reference is the interceptor-to-target range vector. The velocity components orthogonal to R consist of two parts: (1) the translational component, and (2) the tangential (or turning) component. Selecting the interceptor as the reference point for the tangential component, and taking $d\lambda/dt$ positive in the same sense as λ (i.e., increasing λ implies increasing $d\lambda/dt$), the equations can be written as follows:

$$R\left(\frac{d\lambda}{dt}\right) = V_I \sin\lambda - V_T \sin(180 - \alpha) = V_I \sin\lambda - V_T \sin\alpha. \tag{4.12}$$

The conditions for the various types of trajectories result from holding constant one of the parameters in the equations.

Pure Pursuit

In the pure pursuit trajectory, the interceptor missile flies directly toward the target at all times. Thus, the heading of the missile is maintained essentially along the line of sight between the missile and the target by the guidance system. Missiles flying a pure pursuit course usually end up in a tail-chase situation, similar to a dog chasing a rabbit. Furthermore, in pure pursuit the nose of the interceptor missile (note that the term interceptor is used to denote missiles as well as fighter aircraft) is pointed at the target aircraft. The interceptor missile directing its velocity vector toward the target

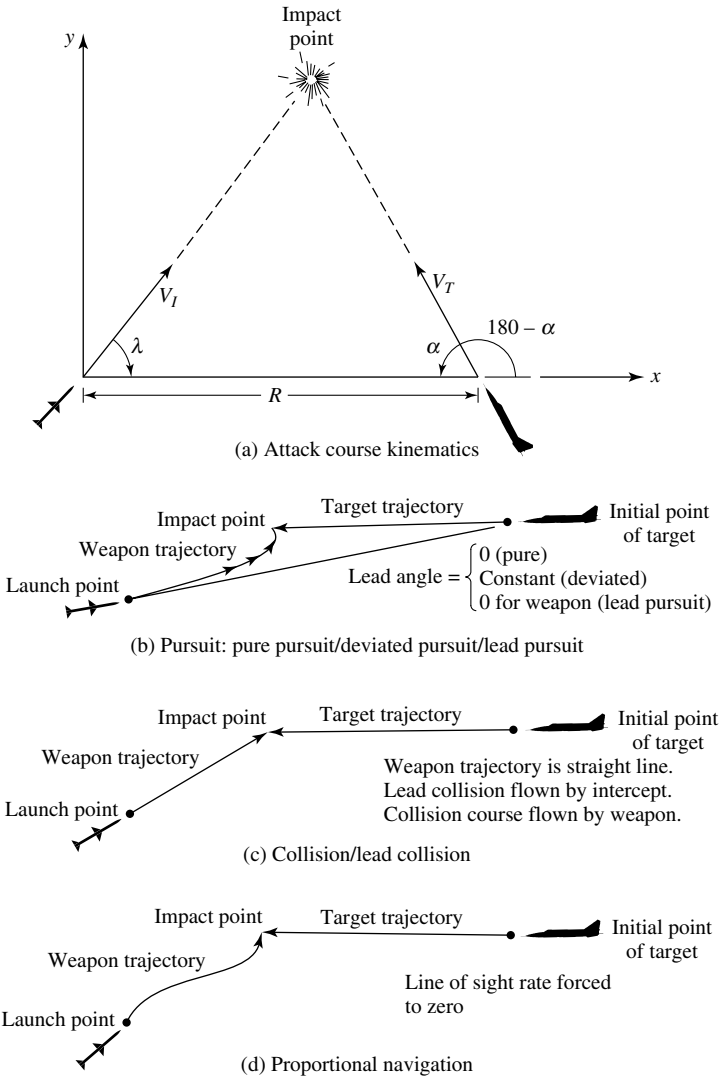

Fig. 4.7. Derivation of the guidance equations.

flies a pure pursuit attack course. In such a case the interceptor's lead angle is zero. Consider now Figure 4.8.

The decomposition of the velocity vector components along and perpendicular to $\boldsymbol{R}$ yields the following equations:

$$\frac{dR}{dt} = V_M - V_T \sin\theta, \tag{4.13a}$$

$$R\left(\frac{d\theta}{dt}\right) = -V_T \cos\theta, \tag{4.13b}$$

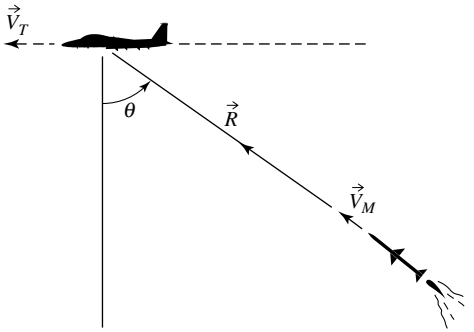

Fig. 4.8. Pure pursuit guidance geometry.

where R is the range magnitude, θ is the orientation of the line of sight to the target, V_M is the interceptor missile velocity component, and V_T is the target's velocity. For the special but nontrivial cases of a stationary target or head/tail chase ($\theta = \pm\ 90°$), we have

$$\left(\frac{dR}{dt}\right)/R = \{(1/\cos\theta)(V_M/V_T) + \tan\theta\}\left(\frac{d\theta}{dt}\right) = \{(\kappa/\cos\theta) + \tan\theta\}\left(\frac{d\theta}{dt}\right), \tag{4.14}$$

where $\kappa = V_M/V_T$. For a constant speed ratio κ, the following expression results:

$$\int (dR/R) = \int \tan\theta d\theta + \kappa \int (d\theta/\cos\theta). \tag{4.15}$$

Letting C be the constant of integration, the general solution of (4.15) assumes the form

$$ln(R/C) = -ln\cos\theta + (\kappa/2)ln[(1+\sin\theta)/(1-\sin\theta)].$$

Therefore,

$$R/C = (1/\cos\theta)[(1+\sin\theta)/(1-\sin\theta)]^{\kappa/2}.$$

From the identity

$$1/\cos\theta = 1/(1+\sin\theta)^{1/2}(1-\sin\theta)^{1/2}$$

we have

$$R/C = \rho = [(1+\sin\theta)^{(\kappa-1)/2}]/[(1-\sin\theta)^{(\kappa+1)/2}]. \tag{4.16}$$

The integration constant C can be determined from the initial conditions R_0 and $\theta_0 = \pm\ 90°$. Thus from (4.16) we obtain

$$\lim_{\theta \to 90°} R = \infty,$$

$$\theta = 0, \quad \rho = 1, \quad R = C,$$

$$\lim_{\theta \to -90^\circ} R = \begin{cases} 0, & \text{when } \kappa > 1, \\ R/2, & \text{when } \kappa = 1, \\ \infty, & \text{when } \kappa < 1. \end{cases}$$

From the above analysis, we note that the missile will intercept the target if its velocity is greater than that of the target. From (4.16), $\rho(\theta)$ can be plotted for different values of the parameter κ (i.e., $\kappa = 0.5, 1.0, 1.5, 2.0, 3.0$).

We will now consider the concept of pursuit guidance using vectorial representation. First, the relative position and velocity vectors are computed as follows:

$$\mathbf{R}_r = \mathbf{R}_T - \mathbf{R}_M,$$
$$\mathbf{V}_r = \mathbf{V}_T - \mathbf{V}_M,$$

where $\mathbf{R}_T$ and $\mathbf{R}_M$ are the position vectors of the target and missile, respectively, and $\mathbf{V}_T$ and $\mathbf{V}_M$ are their velocity vectors. The estimated time-to-go for the closest approach is then

$$t_{go} = -(\mathbf{R}_r \cdot \mathbf{V}_r)/(\mathbf{V}_r \cdot \mathbf{V}_r).$$

Next, compute

$$\mathbf{u} = (\mathbf{R}_r/|\mathbf{R}_r|) \times \mathbf{V}_M)$$

and the pursuer's *lateral* velocity

$$\mathbf{V}_{ML} = |\mathbf{u}|.$$

The unit lift vector's (see Figure 4.5) direction is then

$$\mathbf{1}_L = (\mathbf{V}_M \times \mathbf{u})/(\mathbf{V}_M \times \mathbf{u}),$$

and the desired lift acceleration magnitude is computed as

$$a_{Ld} = (G_1 \mathbf{V}_{ML})/\max(t_{go}, 1),$$

where G_1 is an input guidance gain. Note that the minimum value of the denominator is held at unity to avoid a singularity in a_{Ld} as $t_{go} \to 0$ at impact.

There are two basic disadvantages of the pure pursuit method. First, the maneuvers required of the missile become increasingly hard during the last, and critical, stages of flight. Second, the missile's speed must be considerably greater than the target's speed. The sharpest curvature of the missile flight path usually occurs near the end of the flight; at this point in time, the missile must overtake the target. If the target attempts to evade, the last-minute angular acceleration requirements placed on the missile could exceed its aerodynamic capability, thereby causing a large miss distance. Moreover, near the end of the flight, the missile is usually coasting because the booster (and sustainer) motor thrusts last for only a short part of the flight. The most favorable application of the pursuit course is against slow-moving aircraft, or for missiles launched from a point directly to the rear of the aircraft or head-on toward an incoming aircraft.

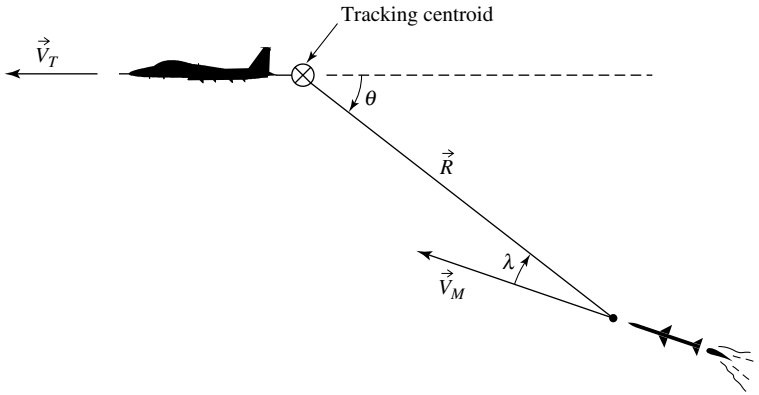

Fig. 4.9. Deviated pursuit geometry.

Deviated Pursuit

Deviated pursuit points the nose of the intercepting missile (or aircraft) by a fixed angle in front of the target (see Figure 4.7). In other words, an interceptor directing its velocity vector at a constant angle ahead of the target flies a deviated pursuit attack course. Since the interceptor lead angle is constant for deviated pursuit, $\lambda = \lambda_o$. Therefore, from (4.11) and (4.12) we have the differential equations

$$\frac{dR}{dt} = V_I \cos\lambda_o - V_T \cos\alpha, \tag{4.17a}$$

$$R\left(\frac{d\lambda}{dt}\right) = V_I \cos\lambda_o - V_T \cos\alpha. \tag{4.17b}$$

In order to obtain the deviated pursuit algebraic equations, we will use Figure 4.9.

The differential equations for the deviated pursuit case are

$$\frac{dR}{dt} = -V_M \cos\lambda + V_T \cos\theta, \tag{4.18a}$$

$$R\left(\frac{d\theta}{dt}\right) = V_M \sin\lambda - V_T \sin\theta, \tag{4.18b}$$

with

$$\lambda = \text{constant}.$$

Solution of the differential equations for R and θ requires a given V_M and V_T as well as initial values of R and θ. The normal acceleration for the deviated pursuit is obtained as

$$a_n = -V_M\theta/g = (V_M/gR)[V_T \sin\theta - V_M]. \tag{4.19}$$

The angle off the target tail, at which θ is maximum, is obtained from the expression

$$\theta(\max g) = \cos^{-1}[V_M/2V_T], \tag{4.20}$$

where $V_M > 2V_T$; note that a maximum does not occur on the course. The time required to intercept the target can be obtained from the expression

$$t = (1/V_T)\int R d\theta/[(V_M/V_T)\sin\lambda - \sin\theta]. \tag{4.21}$$

Pure Collision

A pure collision course is a straight-line course flown by an interceptor so as to collide with the target. Referring to Figure 4.9, the differential equation assumes the form

$$\frac{dR}{dt} = -V_M\cos\lambda + V_T\cos\theta, \tag{4.22a}$$

$$\theta = \text{constant},$$

$$\lambda = \sin^{-1}(V_T\sin\theta/V_M), \tag{4.22b}$$

$$R = R_o + \left(\frac{dR}{dt}\right)t. \tag{4.22c}$$

This course is obviously very simple to generate.

In addition to the three guidance courses just discussed, another course of interest is the *lead collision* course. A lead collision course is a straight-line course flown by the interceptor such that it will attain a single given firing position. For lead collision, the time of flight (a derived parameter) is constant. Generation of this course is begun by specifying V_M, V_o, V_T, t_f, and the initial angle θ_o. The differential equations for lead collision can be obtained in a straightforward manner from Figure 4.9 as

$$\frac{dR}{dt} = -V_M\cos\lambda + V_T\cos\theta, \tag{4.23a}$$

$$R\left(\frac{d\theta}{dt}\right) = V_M\sin\lambda - V_T\sin\theta, \tag{4.23b}$$

where

$$\lambda = \sin^{-1}\left\{-R\left(\frac{d\theta}{dt}\right)t_g/V_o t_f\right\}, \tag{4.23c}$$

$$t_g = (-R + V_o t_f\cos\lambda)/\left(\frac{dR}{dt}\right), \quad t_f = \text{constant}. \tag{4.23d}$$

Note that collision courses are flown so as to cause the interceptor missile or aircraft to collide with the target.

From the guidance techniques discussed above, the two most popular techniques are pure pursuit and proportional navigation. However, proportional navigation is more complicated to mechanize in terms of hardware, whereas pure pursuit causes higher aerodynamic loading on the airframe. The basic difference between the two is that pursuit guidance causes the interceptor missile to home on the target itself, while proportional navigation guidance causes the missile to home on the expected impact point. No matter which method is selected by the missile designer, in order to achieve a target kill the missile must be able to pull sufficient g's to intercept the target within the lethal distance of the warhead. At lower altitudes, the airframe is not a limiting factor because the available g's are in excess of the autopilot limit (e.g., 25 g). At higher altitudes, especially in a snap-up attack, available g's are usually the parameter that determines the launch boundary.

The maximum possible missile turn rate is a limiting factor at minimum range. This is because in a minimum-range situation, an air-to-air missile is usually required to turn rapidly to intercept the target within the short flight times. The maximum turn rate of the missile is limited by two factors: (1) autopilot saturation, and (2) maximum wing deflection. The pitch or yaw autopilot will saturate when the corresponding commanded lateral acceleration exceeds, say, 25 g's. This is predominant at low altitudes, where the missile maneuver is not aerodynamically limited. At high altitudes, the wing deflection required for turning increases, and its maximum value becomes the limiting parameter. When either type of limiting occurs, miss distance increases very rapidly.

Another factor influencing maximum turn rate is the roll orientation of the missile with respect to the maneuver plane. If the direction of the turn is perpendicular to either the pitch or yaw plane, then the turn will be confined only to that plane, and the maximum acceleration will be limited by the autopilot to 25 g's. If the direction of the turn is halfway between the two planes, both autopilots will contribute, and the allowable turning acceleration is as high as $25\sqrt{2}$, i.e., about 35 g's. Note that the time for which the missile locks on the target can vary from about 0.6 to 1.0 second. Increased lock time can have a significant affect because of the rapidly changing geometry, and usually results in increased missile flight times to attain a successful intercept. Because lock time is an uncontrollable factor, a degree of uncertainty is introduced to the minimum-range zone.

At this point, simple interception model dynamics will be developed. Assuming that the target and the missile motions evolve in the same horizontal plane, the geometry of the interception process is shown in Figure 4.10(b). The interception is characterized by two variables, namely, the target range and the LOS angle. The kinematic equations are expressed by the following relations:

$$\frac{dr}{dt} = V_t \cos(\lambda - \gamma_t) - u\cos(\lambda - \theta) - w\sin(\lambda - \theta),$$

$$\frac{d\lambda}{dt} = -[V_t \sin(\lambda - \gamma_t) + u\sin(\lambda - \theta) - w\cos(\lambda - \theta)]/r,$$

where

r = missile–target range,
λ = *LOS* angle,
θ = pitch angle (or missile axis angle),
u = longitudinal velocity component of the missile,
w = normal velocity component of the missile.

The rate of variation of the *LOS*, $d\lambda/dt$, is measured by the seeker, and the tracking error related to the system of measurement is neglected. In other words, the axis of the seeker is assumed to lie always along the *LOS*. The seeker head will be limited to a cone with a maximum half-angle equal to 45°, which imposes the saturation constraint $|\lambda - \theta| \leq 45°$. The variable q is by definition the pitch rate $d\theta/dt$ of the longitudinal axis of the missile about the OY' axis. Therefore, the kinematic equations can be grouped together, forming an eighth-order nonlinear system represented by the deterministic state space equation (see Section 4.8),

$$\frac{dx}{dt} = f(\boldsymbol{x}),$$

with the state vector represented by

$$\boldsymbol{x} = [u \quad w \quad q \quad \theta \quad \delta_z \quad \delta_{zd} \quad r \quad \lambda]^T$$

and the control vector

$$\boldsymbol{u} = [\delta_{zel}],$$

where

δ_z = tail fin (or thrust) deflection angle,
δ_{zd} = gyroscopic feedback,
δ_{zel} = steering fin actuator signal.

Figure 4.10 shows the interceptor missile maneuver capability and geometry for a hypothetical air-to-air interceptor missile.

We conclude this section by presenting some additional mathematical expressions and algorithms of the following guidance laws: (1) pure pursuit, (2) collision course interception, and (3) line-of-sight (*LOS*) interception.

Pure Pursuit

Description

Pure pursuit strives to keep the vehicle's (i.e., missile's) heading always pointing to the target, in order to achieve the maximum killing capability:

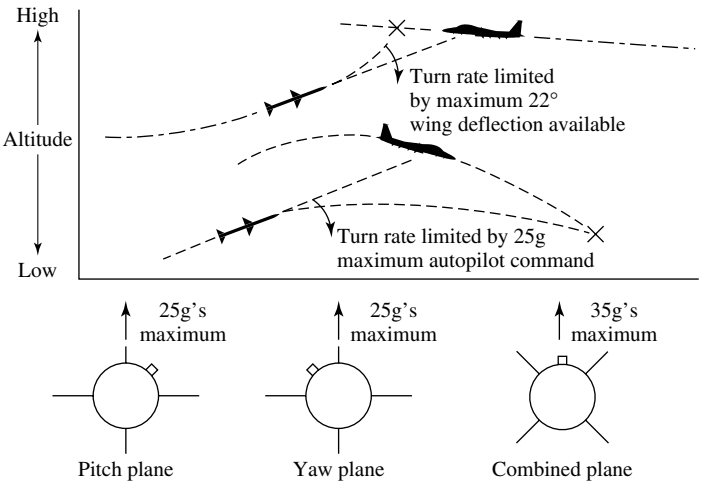

(a) Maximum maneuver capability.

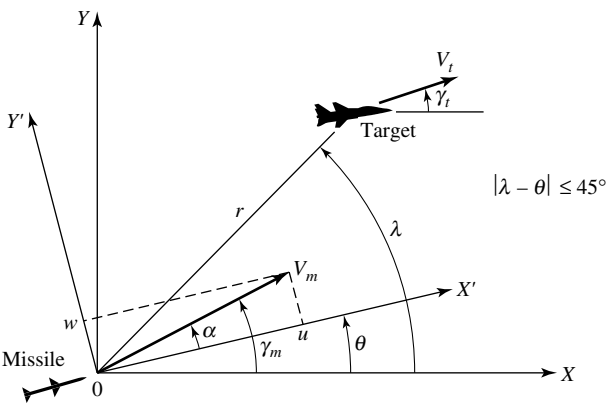

(b) Geometry of the interception process.

Fig. 4.10. Target interception maneuver capability and geometry.

Input

Aspect angle θ, antenna train angle χ, LOS vector $\mathbf{R}$, missile altitude h_1, velocity v_1, flight path angle γ_1, target altitude h_2, velocity v_2, and flight path angle γ_2.

Method

The desired heading-angle turn-rate for pure pursuit is given by

$$\frac{d\Psi_1}{dt} = -K_p \chi, \tag{P.1}$$

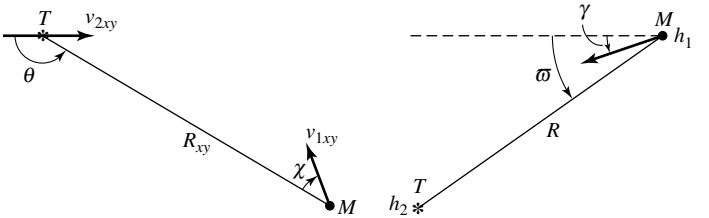

God's-view (or top view) Missile v-γ plane

where K_p is a design proportionality constant. The desired pure pursuit flight path angle is computed from the relation

$$\varpi = \sin^{-1}[(h_2 - h_1)/R]. \tag{P.2}$$

The desired flight path angle rate of change for the pure pursuit case is determined from the relation

$$\frac{d\gamma_1}{dt} = K_\gamma(\varpi - \gamma), \tag{P.3}$$

where K_γ is a design constant.

Algorithm

(a) Compute ϖ by (P.2), (b) $d\Psi/dt$ and $d\gamma/dt$ by (P.1) and (P.3).

Collision Course Interception

Collision course interception strives to fly the missile along a predicted collision course with the target commanding a turn rate proportional to the angle between the collision course and the current heading of the missile.

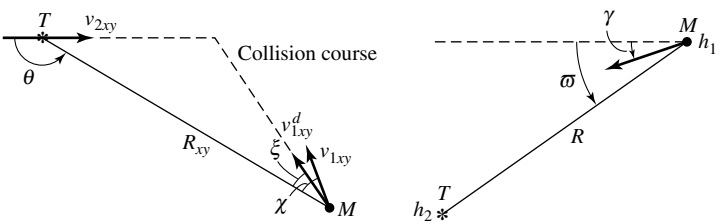

God's-view Missile v-γ plane

Input

Aspect angle θ, antenna train angle χ, LOS vector $\mathbf{R}$, missile altitude h_1, velocity v_1, flight path angle γ_1, target altitude h_2, velocity v_2, and flight path angle γ_2.

Method

Suppose that the target flies straight and level. A collision course will lead the missile to collide with the target, provided that the missile also flies straight and level along the course. The collision course (*CC*) interception strategy is to turn the missile's heading to coincide with the predicted collision course by commanding a turn rate proportional to the angle between the collision and the current heading of the interceptor missile. If the missile is on the collision course, then from the triangular law we have

$$v_{2xy}\tau/\sin\xi = v_{1xy}\tau/\sin(180^\circ - \theta), \tag{C.1}$$

where τ is the interception time. Consequently, the collision antenna train angle ($CATA$) ξ can be determined from the relation

$$\xi = \sin^{-1}(v_{2xy}\sin\theta/v_{1xy}). \tag{C.2}$$

The degree to turn for the collision course interception in the xy-plane is $(\chi - \xi)$. The desired heading-angle turn rate for the collision course interception is taken as

$$\frac{d\Psi}{dt} = K_c(\chi - \xi), \tag{C.3}$$

where K_c is a design factor given by

$$K_c = 6v_1/R. \tag{C.4}$$

Moreover, from the triangular law, we have the following expression:

$$\tau = \begin{cases} -R_{xy}/2v_{2xy}\cos\theta & \text{if} \quad v_{1xy} = v_{2xy}, \\ v_{2xy}\cos\theta \pm [(2v_{2xy}\cos\theta)^2 & \\ \quad +(v_{1xy}^2 - v_{2xy}^2)]^{1/2}/R_{xy}(v_{1xy}^2 - v_{2xy}^2) & \text{if} \quad v_{1xy} \neq v_{2xy}. \end{cases} \tag{C.6}$$

If $\tau < 0$, the interception is then impossible. To reach altitude h_2 after time t, The missile needs a flight path angle ϖ. Thus,

$$\varpi = \sin^{-1}[(h_2 - h_1)/v\tau]. \tag{C.7}$$

Consequently, the desired flight path angle change rate for the *LOS* interception is taken as

$$\frac{d\gamma}{dt} = K_\gamma(\varpi - \gamma), \tag{C.8}$$

where K_γ is determined by the missile's aero-characteristics.

Algorithm

Compute v_{1xy}, v_{2xy} by the equation $v_{xy} = v\cos\gamma$.
Compute *CATA* ξ by (C.2).
Compute the interception time τ by (C.6).
Compute the desired flight path angle by (C.7).
Compute the desired heading and flight path angle change rates $d\Psi/dt$ and $d\gamma/dt$ by (C.3) and (C.8).

Line-of-Sight (*LOS*) Interception

Description

The *LOS* interception turns the heading of the missile toward the *LOS* direction by commanding an acceleration proportional to the angular rate of the direction.

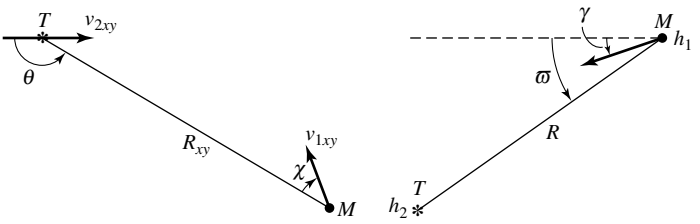

Input

Aspect angle θ, antenna train angle χ, *LOS* vector $\mathbf{R}$, missile altitude h_1, velocity v_1, flight path angle γ_1, target altitude h_2, velocity v_2, flight path angle γ_2. The estimated target heading angle turn rate and flight path angle variation rate $d\Psi_2/dt$ and $d\gamma_2/dt$.

Method

Compute the *LOS* turn rate by the following expression:

$$\frac{d\sigma}{dt} = (\mathbf{R}_{xy} \times \mathbf{v}_{xy})/R_{xy}^2 = (v_{2xy} \sin\theta - v_{1xy} \sin\chi)/R_{xy}, \tag{L.1}$$

and the closure rate

$$\frac{dR}{dt} = (\mathbf{R}_{xy} \bullet \mathbf{v}_{1xy} + \mathbf{R}_{xy} \bullet \mathbf{v}_{2xy})/R_{xy} = v_{2xy} \cos\theta + v_{1xy} \cos\chi. \tag{L.2}$$

The desired heading angle turn rate for the *LOS* interception is given by

$$\frac{d\Psi_1}{dt} = -K_L \left[\left(\frac{d\sigma}{dt} \right) \left(\frac{dR}{dt} \right) + 0.5 \left(\frac{d\Psi_2}{dt} \right) \right]. \tag{L.3}$$

On the other hand, if the missile keeps flying with a flight path angle determined by the horizontal plane and the *LOS* vector, the missile will reach the same altitude with the target at the interception point. Moreover, if the altitude of the vehicle is initially higher than that of the target, the missile will approach the target from above, and vice versa. The *LOS* flight path angle can be computed as follows:

$$\varpi = \sin^{-1}[(h_2 - h_1)/R]. \tag{L.4}$$

The angle change rate for the *LOS* interception is then taken as

$$\frac{d\gamma_1}{dt} = K_\gamma(\varpi - \gamma) - \left(\frac{d\gamma_2}{dt} \right). \tag{L.5}$$

Algorithm

Compute the *LOS* turn rate $(d\sigma/dt)$ by (L.1).
Compute the *LOS* closing rate (dR/dt) by (L.2).
Compute the *LOS* flight path angle ϖ by (L.4).
Compute the desired heading and flight path angle change rates $(d\Psi/dt)$ and $(d\gamma/dt)$ by (L.3) and (L.5).

4.5 Proportional Navigation

Perhaps the most widely known and used guidance law for short- to medium-range homing missiles is *proportional navigation* (*PN*), because of its inherent simplicity and ease of implementation. Simply stated, classical proportional navigation guidance is based on recognition of the fact that if two bodies are closing on each other, they will eventually intercept if the line of sight (*LOS*) between the two does not rotate relative to the inertial space. More specifically, the *PN* guidance law seeks to null the *LOS* rate against nonmaneuvering targets by making the interceptor missile heading proportional to the *LOS* rate. For instance, in flying a proportional navigation course, the missile attempts to null out any line-of-sight rate that may be developing. The missile does this by commanding wing deflections to the control surfaces. Consequently, these deflections cause the missile to execute accelerations normal to its instantaneous velocity vector. Thus, the missile commands g's to null out measured *LOS* rate. As will be developed in the discussion that follows, this relation can be expressed as follows:

$$a_n = NV_c\left(\frac{d\lambda}{dt}\right), \tag{4.24}$$

where

a_n = the commanded normal (or lateral) acceleration [ft/sec^2] or [m/sec^2],
N = the *navigation constant* (also known as *navigation ratio*, *effective navigation ratio*, and *navigation gain*), a positive real number [dimensionless],
V_c = the closing velocity [ft/sec] or [m/sec],
$\frac{d\lambda}{dt}$ = the *LOS* rate measured by the missile seeker [rad/sec].

The proportionality factor consists of the navigation constant, closing velocity multiplier, and a geometric gain factor that accounts for the fact that the orientation of the missile velocity is not necessarily along the instantaneous *LOS*. The *navigation constant* (N) is based on the missile's acceleration requirements and will vary depending on target maneuvers and other system-induced tracking-error sources. In order to minimize the missile acceleration requirement, values of N between 3 and

5 are usually used to obtain an acceptable miss distance intercept. Note that for most applications, the effective navigation ratio is restricted to integer values.

Basically, the proportional navigation equations are easy to derive. However, exact analytical solutions are possible only for highly restrictive and special conditions. In the absence of exact general solutions for the *PN* equations, several approaches have been taken in the past to study the proportional navigation problem [1], [7], [9, 8], [18], [34]. In certain designs, such as active homing guidance (see Section 4.2.1), the *PN* equations must be solved on board the interceptor (or pursuer) missile. For instance, in certain optimal guidance laws where the time-to-go (t_{go}) estimate is required, the corresponding time for *PN* pursuit provides one alternative for such an estimate. Furthermore, in some variants of *PN*, certain parameters must be determined on board the pursuer based on such sensed target parameters as maneuvers. As a rule, closed-form solutions provide a distinct advantage, since the parameters can be evaluated even on the simple processors/computers on board such missiles [9].

In proportional navigation, the rate of rotation of the line-of-sight angle is measured with respect to fixed space coordinates by an onboard seeker, and a lateral (or normal) acceleration of the missile is commanded proportional to that line-of-sight rate. The lateral acceleration is desired to be normal to the *LOS*. For aerodynamically maneuvered vehicles, this acceleration occurs normal to the instantaneous velocity vector of the interceptor missile. This difference normally has little practical significance for reasonable values of lead angle (i.e., as defined earlier, the angle between the velocity vector and the line of sight). However, it should be noted at the outset that from a practical point of view, even though proportional navigation performs reasonably well in a wide range of engagement conditions, its performance degrades sharply in the presence of rapidly maneuvering targets and large off-boresight angle launches. Moreover, the neglected aerodynamic drag affects the missile maneuverability and velocity, resulting in a loss of performance at higher altitudes and in the case of retreating targets. Maneuvering targets are commonly treated and modeled based on optimal control theory and differential game-theoretic approaches. Proportional navigation and its variants have been treated extensively in the literature. In particular, the following variations should be mentioned:

Pure Proportional Navigation (PPN): The commanded acceleration is applied in the direction normal to the pursuer's velocity, and its magnitude is proportional to the angular rate of the *LOS* between pursuer and its target. For stationary targets, solutions are available in closed form in terms of range-to-go and for general values of N, while explicit solutions as a function of time are available only for $N = 2$. By explicit solutions we mean trajectory-dependent parameters obtained as explicit expressions from analytical treatment and that are more readily computable than numerical methods. For nonmaneuvering targets, partial exact solutions exist only for the specific case $N = 1$ (this corresponds to the pure/deviated pursuit case).

Biased Proportional Navigation (BPN): Biased *PN* is another variant that has been suggested in order to improve the efficiency of the *PPN*. Because of the introduction of an extra parameter (i.e., rate bias), such a biased *PN* may be made to achieve a given intercept with less control effort. This is an important advantage

for operations outside the atmosphere where lateral control forces are generated by the operation of control rockets, and the total control effort (i.e., integrated lateral force) determines the fuel requirement of the control engine(s). The linear theory is extended to the treatment of the *BPN* case, and the performance of *BPN* is optimized to obtain the optimum bias value. In its simplest form, the lateral commanded acceleration a_n of the pursuer under *BPN* is obtained as [12], [24]

$$a_n = NV_m\left[\left(\frac{d\lambda}{dt}\right) - \left(\frac{d\lambda_b}{dt}\right)\right],$$

where $d\lambda_b/dt$ is the rate bias on the *LOS* turn rate. Note that the *BPN* guidance law reduces to the standard *PN* (i.e., (4.24) when $d\lambda_b/dt = 0$).

True Proportional Navigation (TPN): In traditional *TPN*, the commanded acceleration is applied in a direction normal to the *LOS*, and its magnitude proportional to the *LOS* rate. A modified *TPN* has also been suggested, in which the commanded acceleration is applied in a direction normal to the *LOS* and its magnitude is proportional to the product of *LOS* rate and the closing speed between pursuer and target. For nonmaneuvering targets, a closed-form solution is available for the general value of N. Moreover, in this case the intercept is restricted to situations where the launch conditions are within the circle of capture.

Generalized Proportional Navigation (GPN): Here the commanded acceleration is applied in a direction with a fixed bias angle in the direction normal to the *LOS* and normal to the relative velocity between pursuer and target [23].

Augmented Proportional Navigation (APN): This guidance law, which can be used for maneuvering targets, includes a term proportional to the estimate of the target acceleration in the commanded missile acceleration. Augmented proportional navigation is treated in more detail in Section 4.6.

Ideal Proportional Navigation (IPN): Is similar to *GPN*.

Figure 4.11 shows the geometry from which the equations representing proportional navigation can be derived. In the derivation of the proportional navigation equations, it will be assumed that the missile speed and target speed remain constant during the time of flight of the missile; this is normally a good assumption.

From the engagement geometry of Figure 4.11, we note that the range between the missile and the target has a value R, and the line of sight has rotated through an angle λ from the initial value. The rate of rotation of the line of sight at any time is given by the difference in the normal components of velocity of the target and missile, divided by the range. This can be expressed by the equation

$$R\left(\frac{d\lambda}{dt}\right) = v_t \sin(\gamma_t - \lambda) - v_m \sin(\gamma_m - \lambda), \tag{4.25a}$$

while the velocity component along the line of sight is given by the equation

$$\frac{dR}{dt} = v_t \cos(\gamma_t - \lambda) - v_m \cos(\gamma_m - \lambda), \tag{4.25b}$$

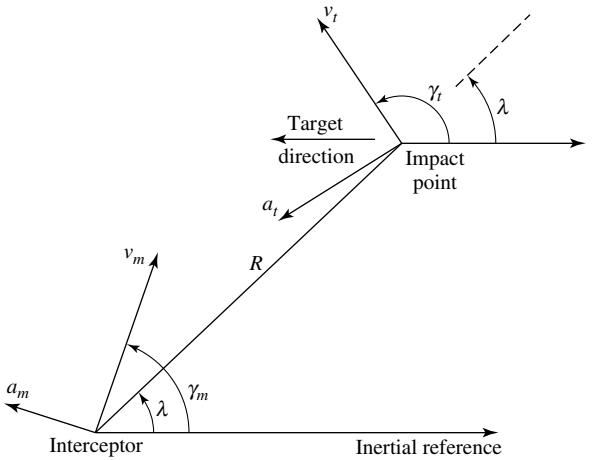

Fig. 4.11. Geometry for derivation of proportional navigation.

where

$$
\begin{aligned}
R &= \text{range between missile and target,}\\
v_m &= \text{interceptor missile velocity,}\\
v_t &= \text{velocity of the target,}\\
\lambda &= \text{line-of-sight } (LOS) \text{ angle,}\\
\gamma_m &= \text{missile flight path (or heading) angle,}\\
&\quad \text{that is, angle between the missile velocity}\\
&\quad \text{vector and inertial reference,}\\
\gamma_t &= \text{target flight path angle.}
\end{aligned}
$$

The proportional navigation guidance law states that the rate of change of the missile heading (γ_m) is directly proportional to the rate of change of the line-of-sight angle (λ) from the missile to the target. Therefore, the basic differential equation for this case is given by

$$\frac{d\gamma_m}{dt} = N\left(\frac{d\lambda}{dt}\right), \tag{4.26}$$

where N is the navigation constant (see also (4.24)). Equations (4.25a), (4.25b), and (4.26) represent the complete equations of motion for the system. The dependent variables are R, γ_m, and λ; the velocities v_m, v_t and the target's flight path angle γ_t must be known or assumed. The usual means of implementing a proportional navigation guidance system is to use the target tracker (or seeker) to measure the line-of-sight rate ($d\lambda/dt$).

We will now develop the general proportional navigation guidance equation. In order to do this, we begin by differentiating (4.25a), yielding

$$\dot{R}\dot{\lambda} + R\ddot{\lambda} = (\dot{\gamma}_t - \dot{\lambda})v_t \cos(\gamma_t - \lambda) - (\dot{\gamma}_m - \dot{\lambda})v_m \cos(\gamma_m - \lambda), \tag{4.27a}$$

$$\begin{aligned}\dot{R}\dot{\lambda} + R\ddot{\lambda} = {} & \gamma_t v_t \cos(\gamma_t - \lambda) - \dot{\gamma}_m v_m \cos(\gamma_m - \lambda) - \dot{\lambda}[v_t \cos(\gamma_t - \lambda) \\ & - v_m \cos(\gamma_m - \lambda)].\end{aligned} \tag{4.27b}$$

Substituting (4.25b) and (4.26) into (4.27b), we obtain

$$2\dot{R}\dot{\lambda} + R\ddot{\lambda} = \dot{\gamma}_t \cos(\gamma_t - \lambda) - N\dot{\lambda}v_m \cos(\gamma_m - \lambda),$$

or

$$\frac{d^2\lambda}{dt^2} + (\dot{\lambda}/R)[2\dot{R} + N v_m \cos(\gamma_m - \lambda)] = (1/R)\dot{\gamma}_t v_t \cos(\gamma_t - \lambda). \tag{4.28}$$

In the above derivation, we note that the equation system consisting of (4.25b), (4.26), and (4.28) constitutes the proportional navigation guidance in the plane. We will now investigate the case whereby the target flies a straight-line course. For a straight-line course, the target's flight path angle rate in (4.28) is zero; that is, $d\gamma_t/dt = 0$. Therefore, with this condition we have a homogeneous differential equation for $d\lambda/dt$. Now, in order for $d\lambda/dt$ to approximate the zero line, $d\lambda/dt$ and $d^2\lambda/dt^2$ must have different signs. Thus, we have the inequality

$$2\left(\frac{dR}{dt}\right) + N v_m \cos(\gamma_m - \lambda) > 0, \tag{4.29}$$

since by definition $R > 0$. From (4.29), we obtain the navigation ratio N as

$$N > \left\{-2\left(\frac{dR}{dt}\right)/(v_m \cos(\gamma_m - \lambda))\right\} \quad \text{for} \quad \cos(\gamma_m - \lambda) > 0. \tag{4.30}$$

The condition $\cos(\gamma_m - \lambda)$ means that the missile's direction of flight forms an angle with the *LOS* to the target. Substituting dR/dt from (4.25b) into (4.30), one obtains

$$N > 2\{1 - [\cos(\gamma_t - \lambda)/(\kappa\cos(\gamma_m - \lambda))]\}, \tag{4.31}$$

where we have substituted $\kappa = v_m/v_t$. We can now write (4.31) as [17]

$$\begin{aligned}N &= N'\{1 - [\cos(\gamma_t - \lambda)/(\kappa\cos(\gamma_m - \lambda))]\} \\ &= -N'\left\{\left(\frac{dR}{dt}\right)/(v_m \cos(\gamma_m - \lambda))\right\},\end{aligned} \tag{4.32a}$$

or

$$N' = -N\left\{(v_m \cos(\gamma_m - \lambda))/\left(\frac{dR}{dt}\right)\right\}, \tag{4.32b}$$

where N' ($N' > 2$) is commonly called the *effective navigation ratio*, and $-dR/dt$ is the missile's closing velocity (i.e., $-(dR/dt) = v_c$). We note from (4.28) that when $d^2\lambda/dt^2$ remains finite, then as $R \to 0$, $(d\lambda/dt) \to 0$ also.

Since the missile velocity vector cannot be controlled directly, the missile normal acceleration a_n is defined as

$$a_n = v_m \left(\frac{d\gamma_m}{dt} \right), \tag{4.33}$$

where $d\gamma_m/dt$ is the missile's turning rate. Substituting (4.26) into (4.33), we have

$$a_n = v_m \left(\frac{d\gamma_m}{dt} \right) = v_m N \left(\frac{d\lambda}{dt} \right). \tag{4.34}$$

Furthermore, substituting (4.32) into (4.34) results in

$$a_n = \{-N\dot{R}v_m/(v_m \cos(\gamma_m - \lambda))\} \left(\frac{d\lambda}{dt} \right) = \{N v_c/(\cos(\gamma_m - \lambda))\} \left(\frac{d\lambda}{dt} \right), \tag{4.35}$$

where the closing v_c is equal to $-(dR/dt)$, and N is given in terms of (4.32). Equation (4.35) is the well-known general classical proportional navigation guidance equation and is similar to (4.24). This equation is used to generate the guidance commands, with the missile velocity expressed in terms of the closing velocity v_c (between the missile and the target) and the seeker gimbal angle $(\gamma_m - \lambda)$. Note that sometimes, the gimbal angle is simply written as θ_h (assuming that a gimbaled seeker is used). Equation (4.35) appears in the literature in many variations.

At this point, let us consider the special case of a nonmaneuvering target. Specifically, we will investigate the *LOS* rate $d\lambda/dt$. Furthermore, we will introduce the range R in (4.28) as the independent variable. Thus, we can form the operator

$$\frac{d}{dt} = \left(\frac{d}{dR} \right) \left(\frac{dR}{dt} \right). \tag{4.36}$$

With this operator, (4.28) becomes

$$R \left(\frac{dR}{dt} \right) \left(\frac{d\dot{\lambda}}{dR} \right) + \dot{\lambda}[2\dot{R} + N v_m \cos(\gamma_m - \lambda)] = \dot{\gamma}_t v_t \cos(\gamma_t - \lambda). \tag{4.37}$$

From (4.32) we have

$$N v_m \cos(\gamma_m - \lambda) = -N' \left(\frac{dR}{dt} \right), \tag{4.38}$$

so that (4.37) takes the form

$$\begin{aligned} R \left(\frac{dR}{dt} \right) \left(\frac{d\dot{\lambda}}{dt} \right) + \dot{\lambda}[2R - N'R] &= \gamma_t v_t \cos(\gamma_t - \lambda), \\ R \left(\frac{d\dot{\lambda}}{dt} \right) + \dot{\lambda}(2 - N') &= \dot{\gamma}_t (v_t/R) \cos(\gamma_t - \lambda). \end{aligned} \tag{4.39}$$

Substituting

$$\xi = \ln(R_o/R) = -\ln(R/R_o) \tag{4.40}$$

with

$R = R_o$ (launch) corresponding to $\xi = 0$,
$R = 0$ (intercept) corresponding to $\xi = \infty$,

from (4.40) one obtains

$$d\xi = -(R_o/R)(dR/R_o), \tag{4.41a}$$

$$d/dR = -(1/R)(d/d\xi). \tag{4.41b}$$

Therefore, (4.39) becomes*

$$d\dot{\lambda}/d\xi + \dot{\lambda}(N' - 2) = -\dot{\gamma}_t(v_t/\dot{R})\cos(\gamma_t - \lambda). \tag{4.42}$$

If we assume that the target is flying a straight-line course, then $d\gamma_t/dt = 0$, and the solution of homogeneous differential equation takes the form

$$\dot{\lambda}(\xi) = \dot{\lambda}_o e^{(2-N')\xi}. \tag{4.43}$$

The initial condition λ_o can be computed from (4.25a). Substitution of (4.40) into (4.43) yields [17]

$$\dot{\lambda}(R/R_o) = \dot{\lambda}_o(R/R_o)e^{(N'-2)}. \tag{4.44}$$

The solution of this differential equation tends to zero for the interceptor–target closing; that is, $(dR(t)/dt) < 0$. When $N' = 2$, a constant target maneuver is required, and $d\lambda/dt$ is constant during the flight. For values of N' greater than 2, the acceleration required at intercept reduces to zero. This is a highly desirable situation, since this early correction of the heading error preserves the full maneuvering capabilities of the missile at intercept to overcome the effects of a late target maneuver or of target noise. Furthermore, (4.44) shows that $d\lambda/dt$ is maximum at the beginning of the flight, decreases linearly to zero for $N' = 3$, and approaches the value of zero asymptotically for $N' > 3$. The collision course condition $d\lambda(t)/dt = 0$ is satisfied at the final (or intercept) point $R = 0$, with a vanishing turning rate $d\gamma_m/dt = 0$. Figure 4.12 shows a plot of $(\dot{\lambda}/\dot{\lambda}_o)$ vs. (R/R_o), wherein the target is assumed to fly from left to right.

Consider now a maneuvering target. For simplicity, we will assume that in the estimation of the *LOS* rate $d\lambda/dt$, the target maneuvers so that the right-hand side of (4.42) remains constant. Exact computations show that in proportional navigation, dR/dt varies very little during flight. The solution of (4.42) is now given by

$$\frac{d\lambda}{dt} = (\dot{\gamma}_t v_t \cos(\gamma_t - \lambda))/\dot{R}(2 - N')\{1 - e^{-(N'-2)\xi}\}. \tag{4.45}$$

* Note that from this point on, we will use N and N' interchangeably. Under certain conditions (e.g., $\gamma_m = \lambda$ and $v_m = v_c$) these two constants are equal, as evidenced from (4.32) and (4.38).

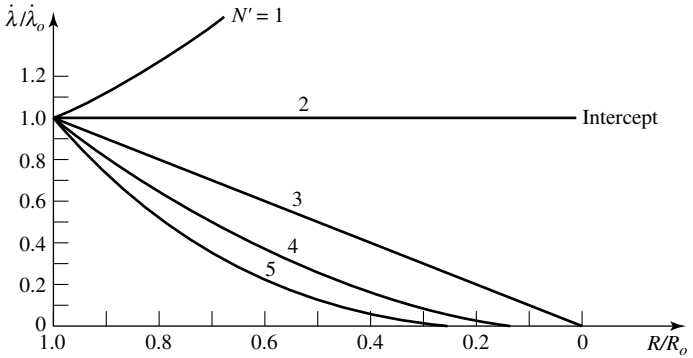

Fig. 4.12. Plot of $(\dot{\lambda}/\dot{\lambda}_o)$ vs. (R/R_o) with N' as parameter for a nonmaneuvering target.

Eliminating ξ from (4.45) by using (4.40), one obtains

$$\frac{d\lambda}{dt} = ((\dot{\gamma}_t v_t \cos(\gamma_t - \lambda))/\dot{R}(2 - N'))\{1 - (R/R_o)^{N'-2}\}. \tag{4.46}$$

The ratio of the interceptor missile's lateral (or normal) acceleration to the target's lateral acceleration is given by the expression

$$|a_{nm}/a_{nt}| = |v_m \dot{\gamma}_m / v_t \dot{\gamma}_t| = (v_m/v_t) N(\dot{\lambda}/\dot{\gamma}_t), \tag{4.47}$$

where we have substituted (4.26), and a_{nm} and a_{nt} are the interceptor missile and target lateral (or normal) accelerations, respectively. Using the ratio κ (see (4.31), (4.32), and (4.46)), we have

$$|a_{nm}/a_{nt}| = (N'/(N' - 2))|\cos(\gamma_t - \lambda)/\cos(\gamma_m - \lambda)|\{1 - (R/R_o)^{N'-2}\}. \tag{4.48}$$

Regardless of the direction of approach to the target (i.e., head-on or from the rear), and making use of the approximation $|cos(\gamma_t - \lambda)/\cos(\gamma_m - \lambda)| \approx 1$, we obtain the expression

$$|a_{nm}/a_{nt}| \approx (N'/(N' - 2))\{1 - (R/R_o)^{N'-2}\}. \tag{4.49}$$

Figure 4.13 shows the variation of the ratio $|a_{nm}/a_{nt}|$ for a maneuvering target with respect to the relative distance to the target (R/R_o) with N' as the parameter for a maneuvering target.

With reference to Figure 4.13, we note that the missile course is from left to right. Also, we note that the largest accelerations appear at the end of the flight. If the interceptor missile's maximum lateral acceleration is three times the acceleration of the target, then one must choose $N' \geq 3$. This figure also shows that for $N' = 2$, a_{nm} grows beyond all limits. In order to evaluate (4.49) for $N' = 2$, the following transformation will be used: Substituting the expression $(R/R_o)^{N'-2}$ into the series

$$a^x = 1 + \frac{\ln a}{1!}x + \frac{(\ln a)^2}{2!}x^2 + \cdots,$$

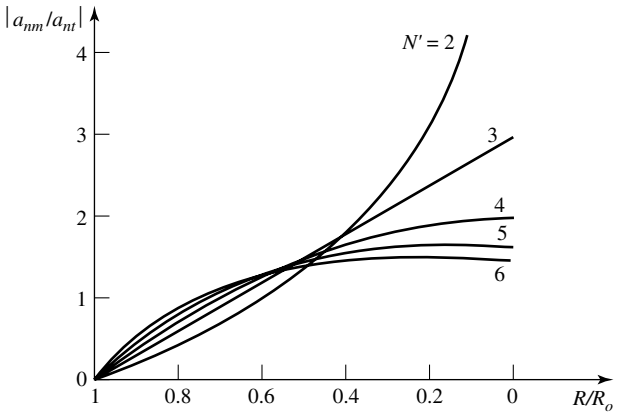

Fig. 4.13. $|a_{nm}/a_{nt}|$ vs. target (R/R_o) for a maneuvering target.

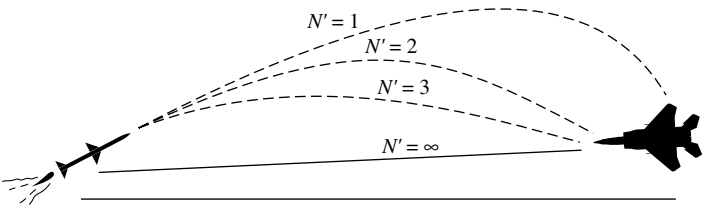

Fig. 4.14. Effect of N' on missile flight.

we obtain (4.49) in the form

$$|a_{nm}/a_{nt}| = N' \left\{ -(\ln(R/R_o)/1!) - \frac{[\ln(R/R_o)]^2}{2!}(N'-2) - \dots \right\},$$

or for $N' = 2$,

$$|a_{nm}/a_{nt}| \approx -2\ln(R/R_o). \tag{4.50}$$

It is easy to see that for a nonzero maneuver a_{nt}, the missile lateral acceleration satisfies $a_{nm} \to \infty$ as $R \to 0$ (intercept).

We summarize the above analysis by noting that a correction of the launch heading error by means of proportional navigation requires a minimum value of two for the effective navigation ratio (i.e., $N' = 2$). Moreover, we note that when $N' \leq 2$, the missile requires an ever-increasing maneuver as it approaches the target. For $N' > 3$, the collision course errors are corrected earlier in flight so that missile maneuvers during the terminal portion of the flight are at reasonable levels. Figure 4.14 shows a family of homing missile trajectories for various values of effective navigation ratios and a fixed launching error.

Finally, we note that as the effective navigation ratio N' increases, the following events occur: (1) The heading error decreases; (2) the missile requires higher initial

acceleration; and (3) the terminal-phase acceleration required to intercept the target is reduced.

As in pursuit guidance, we will now discuss briefly a vector representation of proportional navigation guidance. Let the relative position and velocity vectors be computed as

$$\mathbf{R}_r = \mathbf{R}_T - \mathbf{R}_M,$$
$$\mathbf{V}_r = \mathbf{V}_T - \mathbf{V}_M.$$

The line-of-sight angular rate is then

$$\boldsymbol{\omega} = (\mathbf{R}_r \times \mathbf{V}_r)/(\mathbf{R}_r \cdot \mathbf{R}_r),$$

the unit lift vector is

$$\mathbf{1}_L = (\boldsymbol{\omega} \times \mathbf{V}_M)/|\boldsymbol{\omega} \times \mathbf{V}_M|,$$

and the desired lift acceleration magnitude is

$$a_{Ld} = G_1 |\boldsymbol{\omega} \times \mathbf{V}_M|.$$

The basic proportional navigation trajectory is sensitive to variations in certain parameters. The degree of sensitivity reflects the impact of the parameter on the proportional navigation equation and on the mechanization considerations. The following parameters are considered significant (but they are by no means exhaustive):

1. ***Missile Time Constant***: The pursuit time constant T_p is the time required for the missile to respond to a measured $d\lambda/dt$. If the missile is executing normal acceleration a_{nm}, then in T_p seconds the missile will travel $\frac{1}{2}a_{nm}\ T_p^2$ feet before corrections are applied. Thus, reducing T_p tends to reduce *overshoot* or *undershoot*. However, reducing T_p increases the missile bandwidth, thus making the missile more susceptible to guidance noise.
2. ***Effective Navigation Ratio*** N': As the effective navigation ratio is increased, smaller values of $d\lambda/dt$ will produce given amounts of commanded g's. However, as N' is increased, the effects of guidance noise associated with $d\lambda/dt$ become more significant.
3. ***Heading Error***: The effect of heading error is strongly dependent on N'. The higher N', the greater the allowable heading error that can be successfully guided against.
4. ***Target Maneuver***: As N' is increased, the greater is the amount of target maneuver that can be allowed while still permitting successful intercept of the target. However, since unwanted bias levels are indistinguishable from target maneuvers, increasing N' aggravates the effect of bias errors.
5. ***Noise***: The fundamental effect of noise is to mask (or hide) the true value of $d\lambda/dt$. Noise can occur due to target effects or receiver (missile) effects. Target effects are fading and scintillation noise. In addition, the radome contributes a bias error (known as boresight error) due to refraction effects.

The boresight angle error ε, discussed in Section 3.4.1, is measured by the missile antenna gimbal (if a gimbaled system is used) system, and closing velocity v_c is

determined from the target Doppler signal. The effective navigation ratio (N') is based on the missile's acceleration requirements and will vary depending on target maneuvers and other system-induced tracking-error sources. As stated earlier, in order to minimize missile acceleration requirement, values of N' in the range $3 \leq N' \leq 5$ are usually used to obtain an acceptable miss distance at intercept. From Figure 3.21 it can be seen that the boresight angle ε can be expressed as

$$\varepsilon = \lambda - \theta_m - \theta_h + r, \tag{4.51}$$

where r is an error in the *LOS* measurement due to the radome (see also (3.73b). This error, in general, is not a constant, but it is a function of the gimbal angle. In an actual tracking system, the seeker does not respond instantaneously, and the radar antenna boresight will lag behind the *LOS* of the tracker (seeker). The magnitude of this lag depends upon the tracker time constant τ and is proportional to the line-of-sight rate. A simplified tracker can be represented by a first-order transfer function as follows:

$$\varepsilon = \left(\frac{d\lambda}{dt}\right) \cdot [\tau/(1 + s\tau)]. \tag{4.52}$$

The input to the tracker is the target position λ, and the output is ε. The denominator acts as a low-pass filter that will tend to damp out large disturbance rates. Additional error sources such as internal receiver noise and target-induced angular glint discussed in Section 3.4.2 must be included in order to accurately represent the overall performance of the missile guidance system. A schematic showing the functional characteristics of a typical guidance system is given in Figure 4.15. (Note that there are two similar control systems of this type used to stabilize the missile system about the pitch and yaw axes.)

Figure 4.15(b) shows how proportional navigation guidance enters into the guidance loop. In this figure, y_m and y_t are the missile and target positions, respectively. The error sources and the tracker lag terms have been omitted in order to simplify the system. The incorporation of a seeker into the missile system provides some important advantages. The seeker and radar receiver are used to measure the *LOS* rate ($d\lambda/dt$) and the closing velocity v_c. This eliminates the need to measure the missile to target range R_{mt} and the *LOS* angle λ that are needed in a command-guided system. However, one can note from Figure 4.15b that the gain of the system is inversely proportional to the time-to-go t_{go} (time-to-go is defined as the time remaining to intercept; mathematically, $t_{go} = T - t$, where T is the final time and t is the present time; also, time-to-go can be expressed as $t_{go} = R/v_c$). This coupled with the seeker lag term and other external error sources tends to make the guidance system unstable as R_{mt} approaches zero.

As pointed out in Section 3.5, the primary function of the autopilot is to convert commanded lateral acceleration (a_n), which is proportional to the *LOS* rate, into actual missile lateral acceleration. Basically, the autopilot is a tight acceleration feedback loop designed so that guidance signal commands cause the missile to accelerate laterally (see Figure 4.15). Moreover, as mentioned in Section 3.5, rate gyroscopes are used to achieve proper pitch, yaw, and roll damping. The pitch and yaw gyros

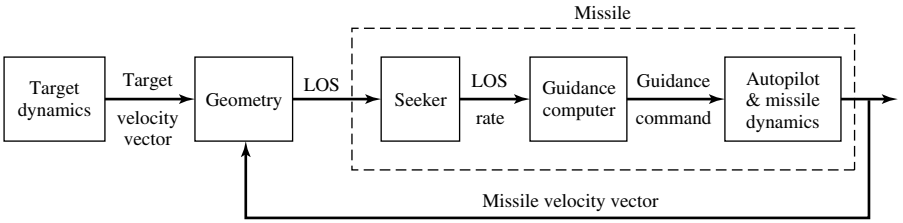

(a) Block diagram for proportional navigation

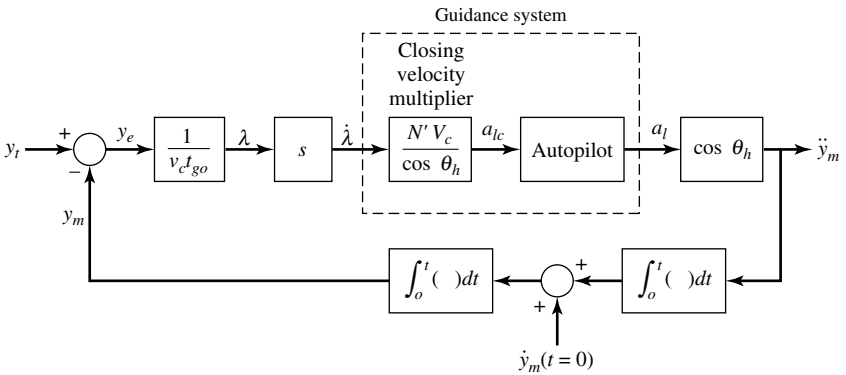

(b) Guidance kinematics loop

Fig. 4.15. Schematic of a typical guidance system.

are also used for synthetic stability, that is, to stabilize the missile against parasitic feedback caused by radome refraction and imperfect seeker head stabilization. The autopilot stabilizes the missile at all speeds throughout its altitude and range envelope. In each channel (pitch and yaw), the command signal is fed to the amplifiers of the wing hydraulic servo system in that channel.

When the speedgate (to be discussed later in this section) is locked and starts tracking the Doppler video signal, a command is generated and fed to the autopilot, which switches the *English bias* command out of the acceleration command processor and switches in axial compensation if this has not already been accomplished by the launch plus 3 sec command. At speedgate lock, radar error commands, which have been amplified and adjusted by closing velocity in the error multiplier, command the pitch or yaw autopilot to process lateral g's (a_{nc}). These lateral (or normal) g's are integrated with an integrator that has been set to the proper altitude band gain. The output of this integrator is a wing command in degrees/sec, which is applied to the appropriate wing hydraulic servo system. As the missile responds to these g commands, the appropriate accelerometer senses these lateral g's and hence generates a signal, which is amplified and synchronously detected for direction by a comparator and is then summed with the original g command to close the accelerometer loop.

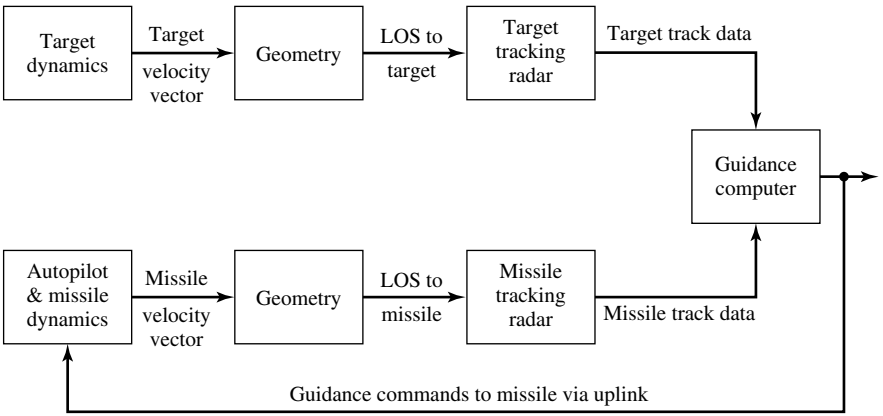

Fig. 4.16. System block diagram for command guidance.

Command Guidance

In Section 4.2.2 the concept of command guidance was discussed. Here we will present some of the mathematical aspects of command guidance. A command guidance scheme, shown in Figure 4.16, consists of missile guidance commands calculated at the launch (or ground) site and transmitted to the missile.

The *Patriot MIM-104* surface-to-air missile (*SAM*) is an example of a radar-command-guided system using a multifunction phased array (i.e., electronically scanning) radar. The Patriot's accuracy is due to its *TVM* terminal guidance method. Targets are selected by the system and illuminated by its ground or *ECS* (engagement control station) phased-array radars. A lateral error command guidance scheme is used for many of the *SAM* systems. In a command guidance system, the ground site tracks the target and missile and transmits acceleration commands to the missile, which are proportional to the lateral displacement error from the desired course. Several variations of this scheme that have been implemented in various *SAM* programs are described below. Figure 4.17 illustrates the lateral error components in the elevation plane for command guidance.

Assuming small-angle approximations, the lateral displacement from the missile to the desired course, λ_ε, and the displacement from the site to the target, D_ε, can be expressed as

$$D_\varepsilon = R_m(\theta_D - \theta_t), \tag{4.53a}$$

$$\lambda_\varepsilon + D_\varepsilon = R_m(\theta_m - \theta_t). \tag{4.53b}$$

Subtracting these equations gives the missile's lateral error from the desired course:

$$\lambda_\varepsilon = R_m(\theta_m - \theta_t) - R_m(\theta_D - \theta_t). \tag{4.54}$$

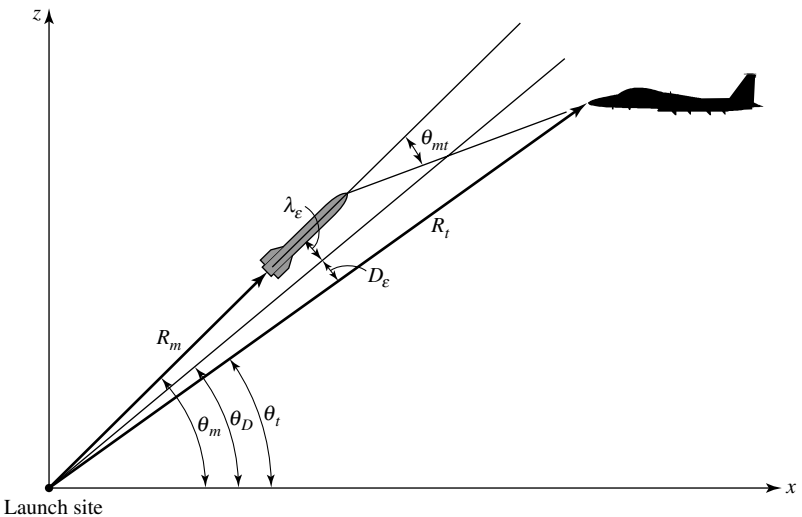

Fig. 4.17. Command guidance geometry.

In order to achieve an intercept, the missile and target range must be the same when the time-to-go t_{go} is zero. This condition can exist only if

$$\theta_D = \theta_t + \left(\frac{d\theta_t}{dt}\right) t_{go}, \tag{4.55}$$

where

$$t_{go} = (R_t - R_m)/(\dot{R}_m - \dot{R}_t). \tag{4.56}$$

Substituting these values in (4.54) gives the basic equation for the lateral elevation error:

$$\lambda_E = R_m(\theta_m - \theta_t) - K_G R_m \left(\frac{d\theta_t}{dt}\right) \{(R_t - R_m)/(\dot{R}_m - \dot{R}_t)\}, \tag{4.57}$$

where K_G is a proportionality constant used to tune the guidance system. Similarly, it can be shown that the lateral error for the azimuth plane is given by

$$\lambda_A = R_m(\psi_m - \psi_t)\cos\theta_t - K_G R_m \left(\frac{d\theta_t}{dt}\right) \{(R_t - R_m)/(\dot{R}_m - \dot{R}_t)\}\cos\theta_t. \tag{4.58}$$

Note that in both these equations, the second term goes to zero as the missile approaches the target. Furthermore, the proportionality constant K_G can assume the following values:

If

$K_G = 1$, the intercept is a constant-bearing collision course.

$K_G = \frac{1}{2}$ represents the half-rectified lead angle guidance mode.

$K_G = 0$ represents the 3-point guidance mode (see Section 4.2.2 for definition).

In order to follow a proportional navigation course, the missile must be able to measure changes in the line of sight. Usually, this is accomplished, among other methods, by a conical scanning method. Here the received signal is amplitude modulated as a function of the angular position of the target from the antenna boresight reference. Scan information is retained throughout the mixing process in the missile circuits. It is extracted in the missile speedgate and coupled back to the front antenna drive as a tracking command. In the head control, the error command (ε), derived from the percentage of modulation, is summed with the output of the head gyro feedback circuit to establish proportionality between the error and the head rate. Under steady-state conditions,

$$\varepsilon = \tau_1 \left(\frac{d\lambda}{dt} \right),$$

where τ_1 is the head tracking time constant (typically 0.1 second for an air-to-air missile during the terminal phase, and 0.2 second during the preterminal guidance phase). An approximate knowledge of closing velocity is necessary for the optimum solution of the navigation problem because the optimum value of the acceleration command to the autopilot is proportional to the closing velocity. The Doppler frequency, representing closing velocity, is used to control the multiplication of the error signal, which is proportional to the line-of-sight rate. In the actual mechanization, the acceleration command to the autopilot (a_c) is generated as a constant (K) multiplied by the product of radar error (ε) and closing velocity V_c:

$$a_c = K \varepsilon V_c.$$

In this manner, the missile trajectory is optimized as a function of missile and target velocity variations.

In terms of their contribution to proportional navigation, the principal functions of the major circuits in the guidance and control system are as follows:

RF and Microwave Section: The front antenna is typically a flat-plate slotted array antenna. Directional information for the missile flight is obtained by conical scanning the target's reflected energy using ferrite phase shifters. The radar antenna that receives RF energy from the launching aircraft is used for automatic frequency controlling.

Rear Receiver: The rear receiver acquires and tracks illuminator transmission for use as a reference for extracting the Doppler signal.

Front Receiver and Video Amplifier: The front receiver and video amplifier amplify and AGC (automatic gain control) the front signal to a level compatible with the dynamic range of the speedgate.

Speedgate: The speedgate acquires and tracks the Doppler signal, using *AGC* to adjust the signal to a constant level, so that *AM* directional information (ε) can be extracted at a known scale factor (10% modulation is equal to 1° of direction error off antenna boresight (see also Section 3.6)).

Head Control: The head control establishes proportionality between antenna error (ε) and line-of-sight rate ($d\lambda/dt$). Whenever error is not equal to the tracking time

constant (τ_1) multiplied by the head rate in space $[(d\lambda/dt) + (d\varepsilon/dt)]$, the head servo must adjust the head rate and position.

Error Multiplier: The error multiplier generates an acceleration command proportional to the product of head error (ε) and closing velocity V_c. The scale factor (K) of the acceleration command is 0.023 g's per degree (ε) per foot per second V_c, that is, 0.023 g/ε.

Autopilot: The autopilot ensures that the missile achieves accelerations as commanded and maintains stability. The control system consists of a roll autopilot and two essentially identical pitch and yaw autopilots (see Section 3.5).

In order to get better insight into the navigation constant discussed earlier, consider now the problem of designing an advanced angle-tracking system for an air-to-air missile with all-aspect, all-altitude, and all-weather tactical capabilities, such as the *ERAAM* + (extended range air-to-air missile +), which is a more advanced extended-range *AIM-120A AMRAAM* powered by a dual-pulse rocket motor. The *AMRAAM* is able to engage a target throughout the *FOV* of the fighter's radar, including about 70° off boresight. After the *AMRAAM* is launched, the aircraft tracking radar would continue to provide updates, which would be relayed to the missile through the side and back lobes of the radar on the fighter that fired the missile. Another advanced missile using the above capabilities is the *AIM-9X Sidewinder II*.

Let us now return to (4.32). The missile steers a proportional navigation course against a maneuvering target. In the usual classical implementation, the measured error ε_m is processed through a transfer function (which encompasses the filter dynamics and controller) to generate a commanded radar-antenna rate ω_c proportional to ε_m. The optimal Kalman filtering approach (see also Section 4.8.2) enables the missile designer to systematically and more effectively remove noise from ε_m and to obtain estimates of the radar antenna pointing (or tracking) error ε and the *LOS* rate ω_{LOS} to form ω_c. (Note that here we consider a conventional radar antenna, not an *ESA*.) The advantages of having an estimate of ω_{LOS} available as a result of optimal filtering are that it can be used as (1) a rate-aiding term to improve the tracking performance, and (2) a signal for missile steering that is statistically more accurate than the signal from the classical loop.

For the proposed tracker, the system equations are

$$\frac{d\varepsilon}{dt} = \omega_{LOS} - \omega_a, \tag{4.59a}$$

$$\frac{d\omega_{LOS}}{dt} = -\left(\frac{1}{\tau}\right)\omega_{LOS} + \left(\frac{1}{\tau}\right)n(t), \tag{4.59b}$$

where

$$\begin{aligned} \varepsilon &= \text{antenna pointing or tracking error,} \\ \omega_a &= \text{radar antenna angular rate,} \\ n(t) &= \text{zero-mean Gaussian white noise process,} \\ \tau &= \text{correlation time constant.} \end{aligned}$$

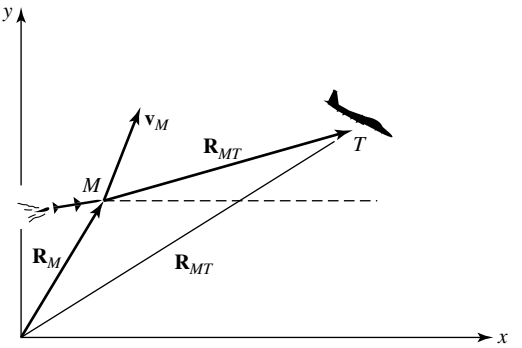

(a) Missile-target geometry

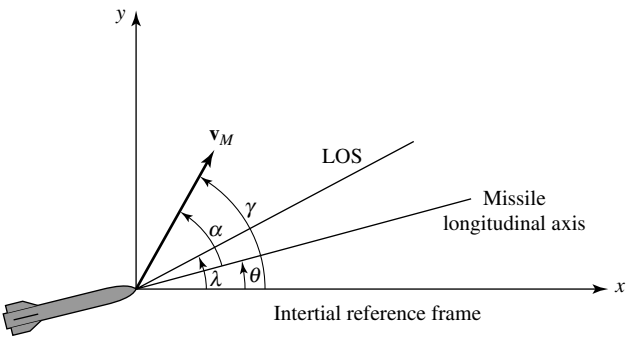

(b) Missile angular orientation

Fig. 4.18. Target Geometry and Orientation.

Equation (4.59b) is based on the assumption that anticipated *LOS* rate histories can be considered as sample functions of a process generated by white noise through a first-order lag, $1/(\tau s + 1)$. Notice that in order to guarantee best performance in all tactical environments, the effects of angular scintillation, radome error, cross coupling (receiver, dynamical), any gyro errors (i.e., drift, offset), and antenna servo dynamics should be considered. The missile–target geometry is illustrated in Figure 4.18.

The missile velocity vector $\mathbf{v}_m$ can be resolved into components along and normal to the *LOS* as follows:

$$\mathbf{v}_m = v_m \cos(\gamma - \lambda)\mathbf{1}_{LOS} + v_m \sin(\gamma - \lambda)\mathbf{1}_n, \tag{4.60}$$

where

$$\begin{aligned} v_m &= |\mathbf{v}_m|, \\ \mathbf{1}_{LOS} &= \text{unit vector along the } LOS, \\ \mathbf{1}_n &= \text{unit vector normal to the } LOS, \\ \gamma &= \text{angle between missile velocity vector and inertial reference}, \\ \lambda &= \text{missile–target } LOS \text{ angle}. \end{aligned}$$

Taking the derivative of (4.60) results in

$$\frac{d\mathbf{v}_m}{dt} = v_m \left(\frac{d\gamma}{dt}\right) \cos(\gamma - \lambda)\mathbf{1}_n - v_m \left(\frac{d\gamma}{dt}\right) \sin(\gamma - \lambda)\mathbf{1}_{LOS}, \tag{4.61}$$

where it is assumed that the missile has constant speed (i.e., $dv_m/dt = 0$). If the angle of attack α is equal to 0, then the missile acceleration normal to the longitudinal axis a_{mn} is given by the expression

$$a_{mn} = v_m \left(\frac{d\gamma}{dt}\right). \tag{4.62}$$

From (4.60),

$$a_{mn} = v_m \left(\frac{d\gamma}{dt}\right) \cos(\gamma - \lambda). \tag{4.63}$$

Now, from Figure 4.18(a) we obtain the following relationship:

$$\mathbf{R}_{MT} = R_{MT}\mathbf{1}_{LOS}, \tag{4.64}$$

where

$$\begin{aligned} R_{MT} &= |\mathbf{R}_{MT}| = \text{missile–target distance}, \\ \mathbf{1}_{LOS} &= \text{unit vector along the } \textit{LOS}. \end{aligned}$$

Taking the derivative of (4.64) yields

$$\frac{d\mathbf{R}_{MT}}{dt} = \left(\frac{dR_{MT}}{dt}\right)\mathbf{1}_{LOS} + R_{MT}\left(\frac{d\mathbf{1}_{LOS}}{dt}\right) = \left(\frac{dR_{MT}}{dt}\right)\mathbf{1}_{LOS} + R_{MT}\left(\frac{d\lambda}{dt}\right)\mathbf{1}_n, \tag{4.65}$$

where $\mathbf{1}_n$ is a unit vector normal to $\mathbf{R}_{MT}$ and $d\mathbf{R}_{MT}/dt$ is the range rate. After taking the second derivative of (4.65), we have the following relations:

$$\begin{aligned} \mathbf{R}_{MT} &= \mathbf{R}_{OT} - \mathbf{R}_{OM}, \\ \mathbf{a}_{MT} &= \mathbf{a}_{OT} - \mathbf{a}_{OM}, \end{aligned}$$

where $\mathbf{a}_{OT}$ and $\mathbf{a}_{OM}$ are the target and missile accelerations relative to the inertial frame (x, y). Now $\mathbf{a}_{OT}$ and $\mathbf{a}_{OM}$ can be resolved into components along $\mathbf{1}_{LOS}$ and $\mathbf{1}_n$, resulting in

$$a_{T-LOS} - a_{M-LOS} = \frac{d^2R_{MT}}{dt^2} - R_{MT}\left(\frac{d\lambda}{dt}\right)^2, \tag{4.66a}$$

$$a_{T-n} - a_{M-n} = 2\left(\frac{dR_{MT}}{dt}\right) - \left(\frac{d\lambda}{dt}\right), \tag{4.66b}$$

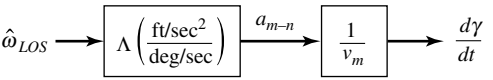

Fig. 4.19. Generation of missile turning rate.

where a_{T-LOS} and a_{M-LOS} are the target and missile accelerations along the *LOS*, and a_{T-n} and a_{M-n} are the accelerations normal to the *LOS*. From (4.66b) we obtain

$$\frac{d\omega_{LOS}}{dt} = \left[-2\left(\frac{dR_{MT}}{dt}\right)\omega_{LOS}\right]/R_{MT} + (a_{T-n} - a_{M-n})/R_{MT}, \tag{4.67}$$

where $\omega_{LOS} = d\lambda/dt$. Finally, from (4.60) we can write $(d\omega_{LOS}/dt)$ in the form

$$\begin{aligned}\frac{d\omega_{LOS}}{dt} = &-\left[2\left(\frac{dR_{MT}}{dt}\right)/R_{MT}\right]\omega_{LOS} + (a_{T-n}/R_{MT}) \\ &-\left[\left(\frac{d\gamma}{dt}\right)v_M\cos(\gamma-\lambda)\right]/R_{MT},\end{aligned} \tag{4.68a}$$

or

$$\begin{aligned}\frac{d\omega_{LOS}}{dt} = &-\left[2\left(\frac{dR_{MT}}{dt}\right)/R_{MT}\right]\omega_{LOS} + (a_{T-n}/R_{MT})(180/\pi) \\ &-\left[\left(\frac{d\gamma}{dt}\right)v_M\cos(\gamma-\lambda)\right]/R_{MT}\end{aligned} \tag{4.68b}$$

and

$$\frac{d\gamma}{dt} = (\Lambda/v_M)(180/\pi)\hat{\omega}_{LOS}, \tag{4.68c}$$

where

$$\begin{aligned}\hat{\omega}_{LOS} &= \text{estimate of the } LOS\,[\text{deg/sec}], \\ \Lambda &= a_{M-n}/\hat{\omega}_{LOS}[(\text{ft/sec}^2)/\text{deg/sec}], \\ v_M &= \text{missile velocity}\,[\text{ft/sec}].\end{aligned}$$

As we discussed earlier, in proportional navigation the missile turning rate $(d\gamma/dt)$ is made proportional to the best estimate of the *LOS* rate available. That is, proportional navigation implies that for a no-time-lag missile,

$$\frac{d\gamma}{dt} = \xi\hat{\omega}_{LOS}, \tag{4.69}$$

where $\xi = \Lambda/v_M$. The blocks representing (4.69) are shown in Figure 4.19.

Finally, we note that the missile effective navigation ratio N' is given by the relation

$$N' = \left\{[K_T\Lambda\cos(\gamma-\lambda)]/\left|\frac{dR_{MT}}{dt}\right|\right\}(180/\pi), \tag{4.70}$$

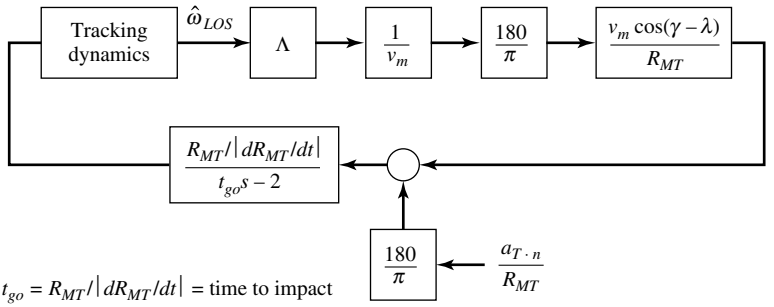

Fig. 4.20. Closed-loop configuration for the angle tracker.

where $K_T = \hat{\omega}_{LOS}/\omega_{LOS}$ in the steady state and ω_{LOS} is a unit step input. (Compare this equation with (4.32)). Assuming that $\Lambda = 480\,[(\text{ft/sec}^2)/(\text{deg/sec})]$, $|dR_{MT}/dt| = 4000\,\text{ft/sec}$, $K_T \cong 1$, and $(\gamma - \lambda) = 0$, then $N' \cong 6.8$. A possible closed loop for this angle-tracking system is shown in Figure 4.20.

A few final remarks about the navigation constant N are in order. As mentioned earlier, the proportional navigation constant appears in the literature under different form(s) and/or nomenclature. Specifically, let us examine three versions for this constant as given in the literature.

(1) In [12], the navigation constant for the "biased proportional navigation" case is given as

$$N > 1 + [\rho/\sqrt{1-(\rho+\beta)^2}],$$

where $\rho = v_t/v_m$ (where it is assumed that $v_m > v_t$). From geometrical considerations between pursuer and evader (i.e., target), we have

$$|\rho \sin\theta_t(t) - \sin\theta_m(t)| < \beta, \quad t_0 \le t \le t_1,$$
$$|\sin\theta_m(t_o)| < \pi/2,$$

with

$$\sin\theta_m(t) = \gamma_t - \lambda,$$
$$\sin\theta_m(t) = \gamma_m - \lambda,$$

where

γ_m, γ_t = interceptor and target body attitude angles, respectively,
λ = line of sight.

(2) In [23], the navigation constant is given in terms of the effective navigation constant N' as

$$N = N'(V_{Li}/V_m \cos\phi_c),$$

where

$$V_{Li} = \text{initial value of the relative velocity along the } LOS,$$
$$\phi_i = \phi_c + \Delta\phi_i,$$

where ϕ_c is the perturbation heading angle of the pursuer and $\Delta\phi_i$ is the initial missile heading error.

(3) In [19], the navigation constant is given as

$$N = 3T^3/(T^3 - t_{go}^3),$$

where T is the intercept time and $t_{go} = T - t$. Here we note that the navigation constant N of proportional navigation is such that the maximum value of the commanded acceleration in proportional navigation is the same as the maximum acceleration commanded by the optimal guidance law (see also Section 4.8). Compare this navigation constant with the effective navigation constant given in [3],

$$K = 3/[1 - (C_e/C_p)],$$

where C_e and C_p are constants relating the energies of the evader and pursuer, respectively.

Table 4.5 attempts to summarize what has been discussed in Sections 3.2, 3.2.1, 3.3.1, and 4.2–4.5 with the exception of the warhead (compare also with Figure 4.12). Three U.S. Navy air-to-air missiles, *Sparrow*, *Phoenix*, and *Sidewinder*, have been selected for illustration. We can add a fourth, the *Advanced Sparrow* (*AIM-7F*), which is a wing control proportional navigation boost–sustain missile. (Note that externally, the *Advanced Sparrow* is identical to the *Sparrow 7E*.)

As an illustration of a rocket motor, consider the *MK-58* boost–sustain type, which uses a solid propellant and internal burning powder grain enclosed in a thin-walled cylindrical chamber. An igniter and safe/arm assembly are located in the forward end of the motor. The igniter ignites the motor propellant when the missile is launched. The safe/arm switch permits arming the igniter just prior to aircraft takeoff and ensures safe handling of the motor or assembled missile. The motor firing is completed by means of a connection between the motor and launching aircraft. The motor fire connector used to accomplish this purpose maintains contact with the aircraft until the missile is launched. Figure 4.21 shows the typical *MK-58* motor thrust and velocity profiles.

Before we leave this section, a few words about the mid-course phase missile axial compensation is in order. The missile's acceleration and deceleration have an effect on the line-of-sight rate. Therefore, the missile is mechanized to compensate for this. As the missile accelerates, proportional navigation would dictate that the missile turn into the target. On the other hand, as the missile slows down, proportional navigation would dictate that the missile turn away from the target. Air-to-air interceptor missiles are commonly mechanized with axial compensation in order to increase the system performance due to acceleration and slowdown. Figure 4.22 is a functional diagram of the axial compensation command generator.

Table 4.5. General Missile Types

Airframe	Guidance	Rocket motor
Missile		
Wing control		
	Pursuit	
		Boost
		Sustain
		Boost–Sustain
	Proportional nav	
		Boost (Sparrow *AIM*-7*E*)
		Sustain
		Boost–Sustain (*AIM*-7*F*)
Tail control		
	Pursuit	
		Boost
		Sustain
		Boost–Sustain
	Proportional nav	
		Boost
		Sustain (Phoenix *AIM*-54)
		Boost–Sustain
Canard		
	Pursuit	
		Boost (Sidewinder *AIM*-9)
		Sustain
		Boost–Sustain
	Proportional nav	
		Boost
		Sustain
		Boost–Sustain

Summary

Because of the important role that proportional navigation (*PN*) plays in missile guidance, we will summarize here for the reader some of the most important concepts.

Intercept Geometry

Figure 4.23 will be used to summarize the concepts of proportional navigation.

Classical PN Equation (Normal Interceptor Acceleration)

$$a_n = N v_c \left(\frac{d\lambda}{dt} \right) \tag{4.24}$$

or

$$a_n = (N/t_{go}^2)[\mathbf{R}(t) + \mathbf{v}_m(t) t_{go}],$$

where $\mathbf{R}(t)$ is the missile–target range vector, and the term in brackets is the *zero effort* miss.

Closing Velocity

$$v_c = -\frac{dR}{dt},$$

where R is the range (or distance) between interceptor missile and target ($R \cong v_c t_{go}$).

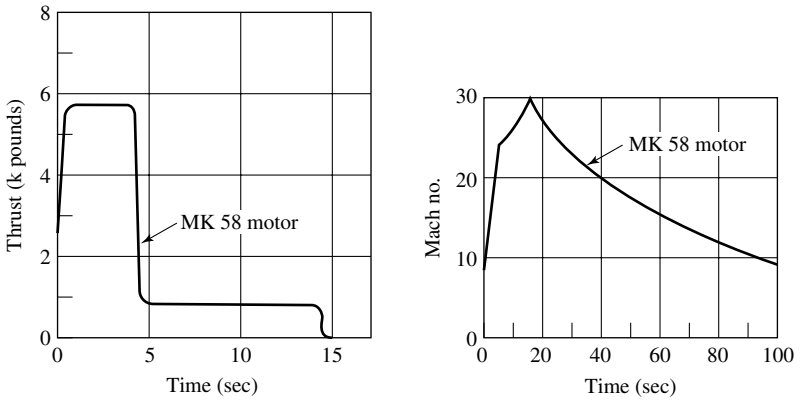

(a) Thrust profile
(sea level thrust variation with time)

(b) Velocity profile
(Note: $M_{launch} = M_T$
$h = 40{,}000$ ft)

Fig. 4.21. *MK-58* motor characteristics.

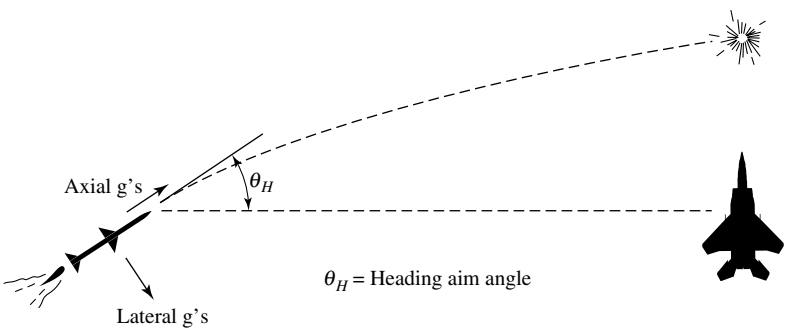

Fig. 4.22. Missile axial compensation diagram.

Navigation Constant, N

$$N = -N' \left[\left(\frac{dR}{dt} \right) / v_m \cos(\gamma_m - \lambda) \right] = N'[v_c / v_m \cos(\gamma_m - \lambda)]. \tag{4.32a}$$

Effective Navigation Constant, N′

$$N' = N \left[v_m \cos(\gamma_m - \lambda) / \left(\frac{dR}{dt} \right) \right]. \tag{4.32b}$$

Equation of Motion

$$\frac{dy_m}{dt} = v_m \sin\gamma,$$

$$\frac{d^2 y_m}{dt^2} = N'[s/(1+\tau s)][(y_t - y_m)/t_{go}],$$

where γ is the missile heading or attitude angle. (Note: *Heading* and *attitude* may not be the same, unless the angle of attack is neglected, that is, assumed to be zero.)

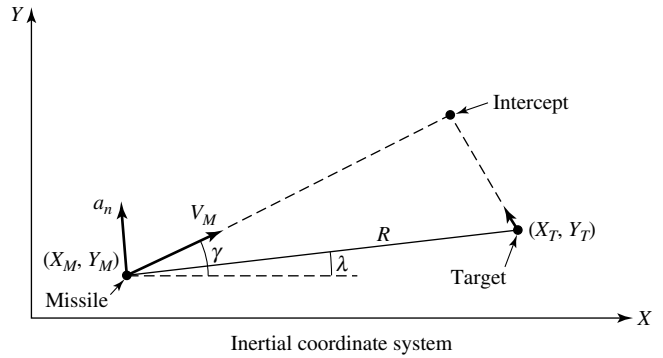

Fig. 4.23. Missile–target intercept geometry.

Rate of Change of Missile Heading or Body Angle ($d\gamma_m/dt$)

$$\frac{d\gamma_m}{dt} = N\left(\frac{d\lambda}{dt}\right). \tag{4.26}$$

Guidance Law

$$\frac{d\gamma}{dt} = [N/(1+\tau s)]\left(\frac{d\lambda}{dt}\right) = \left(\frac{d^2 y_m}{dt^2}\right)(1/v_m \cos\gamma),$$

where γ is the body angle, τ is the time constant, and s is the Laplace operator.

Line of Sight (LOS), λ

$$\lambda = (y_t - y_m)/R.$$

Time-to-Go, t_{go}

$$t_{go} = T - t = R/v_c = (R_t - R_m)/\left[\left(\frac{dR_m}{dt}\right) - \left(\frac{dR_m}{dt}\right)\right]. \tag{4.56}$$

Missile-Target Geometry Loop (see Figure 4.24)

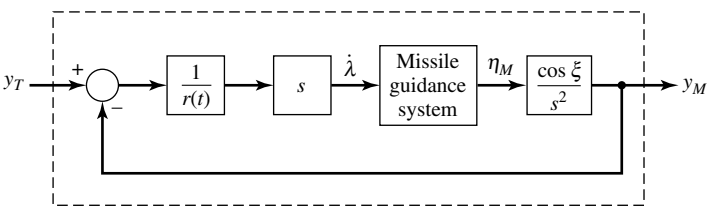

Fig. 4.24. ξ = lead angle (i.e., angle between missile velocity vector and the *LOS*)

Typical missile–target geometry loop.

Generation of Target Displacement from White Noise (see Figure 4.25)

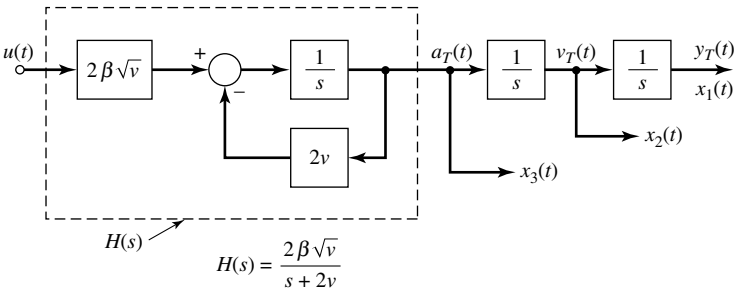

Fig. 4.25. Diagram for the generation of target displacement from white noise.

An Example.
This example summarizes the concept of proportional navigation guidance and how it relates to the work presented thus far in this book. In particular, the example will deal with a semiactive homing missile. Although some of the equations are a repetition of the equations already derived in this section, nevertheless, a set of new equations will be developed that may be used as the basis for further research by the interested reader. Consider the geometry of the interception problem for a homing missile as shown in Figure 4.26.

From this figure, the equations of motion can be written as follows (see also (4.25a,b)):

$$\frac{dR_{MT}}{dt} = -V_M \cos(\gamma - \sigma) - V_T \cos(\sigma - \gamma_T), \tag{1}$$

$$R_{MT}\left(\frac{d\sigma}{dt}\right) = -V_M \sin(\gamma - \sigma) + V_T \sin(\sigma - \gamma_T), \tag{2}$$

where

R_{MT} = distance from missile to target,
V_M = missile velocity,
V_T = target velocity,
γ = missile velocity vector angle with respect to space coordinates,
γ_T = target velocity vector angle with respect to space coordinates,
σ = angle of missile-to-target sight line with respect to space coordinates.

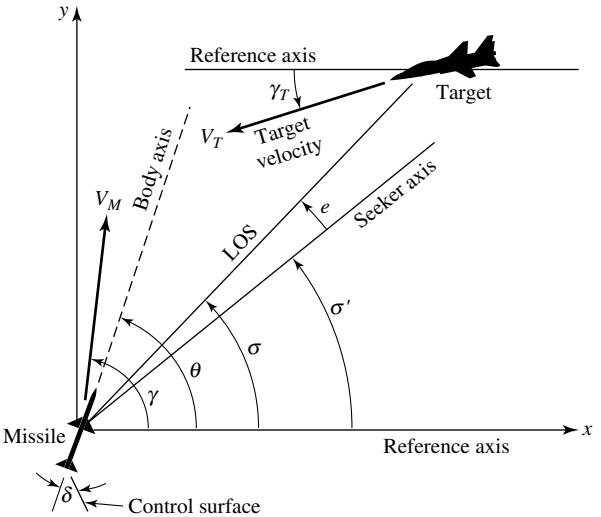

Fig. 4.26. Geometrical relationship between a homing missile and its target.

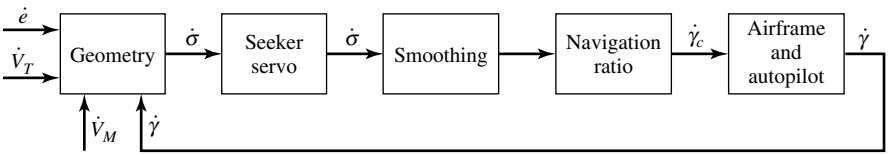

Fig. 4.27. Homing action feedback loop.

As before, differentiation of (2) with no restraints gives

$$\begin{aligned}\dot{R}_{MT}\dot{\sigma} + R_{MT}\ddot{\sigma} = &-\dot{V}_M \sin(\gamma-\sigma) - V_M \cos(\gamma-\sigma)(\dot{\gamma}-\dot{\sigma}) \\ &+ \dot{V}_T \sin(\sigma-\gamma_T) + V_T \cos(\sigma-\gamma_T)(\dot{\sigma}-\dot{\gamma}_T).\end{aligned} \tag{3}$$

Expanding (3) and substituting (2) into (3) yields the following equation:

$$\begin{aligned}2\dot{R}_{MT}\dot{\sigma} + R_{MT}\ddot{\sigma} = &-\dot{V}_M \sin(\gamma-\sigma) - V_M \cos(\gamma-\sigma)\dot{\gamma} \\ &+ \dot{V}_T \sin(\sigma-\gamma_T) - V_T \cos(\sigma-\gamma_T)\dot{\gamma}_T.\end{aligned} \tag{4}$$

The four terms on the right-hand side of (4) denote accelerations due to both the missile and the target. For the missile, dV_M/dt is the longitudinal acceleration and $V_M\dot{\gamma}$ is the lateral maneuver. For the target, dV_T/dt and $V_T\dot{\gamma}_T$ are the corresponding accelerations. Figure 4.27 shows how the homing action is represented as a feedback loop that keeps constant the direction in space of the line joining the missile and the target.

Note that (4) corresponds to the block labeled *geometry* in Figure 4.27, showing the kinematic coupling between missile and target velocities, accelerations, and the

resultant motion of the line of sight. Taking the Laplace transform of (4) results in the following equation:

$$\frac{d\sigma}{dt} = \frac{\begin{bmatrix} -\dot{V}_M \sin(\gamma - \sigma) - V_M \dot{\gamma} \cos(\gamma - \sigma) \\ +V_T \sin(\gamma - \gamma_T) - V_T \dot{\gamma}_T \cos(\sigma - \gamma_T) \end{bmatrix}}{2\dot{R}_{MT}(1 + \frac{R_{MT}}{2\dot{R}_{MT}} s)} \tag{5}$$

where s is the Laplace operator. Later in this example (5) will be used to represent the dynamic relation between target and missile in closing the guidance loop. It should be pointed out, however, that the coefficients of (5) are not constant and that therefore taking the Laplace transform is not rigorously accurate. However, the closed-loop behavior can be evaluated at discrete times along the trajectory at which the coefficients are assumed constant.

As already discussed in Section 3.4.1, the function of the seeker in the missile is to generate a measure of the *LOS* space rate (i.e., the rate of turning in space of the line joining the missile and the target). A rate gyro mounted on the seeker stabilizes the servo loop and provides an output voltage proportional to the sight line space rate. Because the response of the seeker antenna control loop may be made fast in comparison with the airframe response, it is necessary to smooth the seeker output signal to prevent noise signals from causing excessive missile gyrations. Moreover, since the smoothing time constant must usually be long in comparison with the other time constants in the seeker assembly, the seeker transfer function may be written in the form (see also *guidance law* equation in summary)

$$\frac{d\sigma'}{dt} = \left(\frac{d\sigma}{dt}\right) / (1 + t_s s), \tag{6}$$

where

t_s = smoothing time constant,
σ' = angle of the seeker antenna axis with respect to space coordinates.

Based on the material presented in Chapters 2 and 3, and Figure 4.26, the following equations can be written:

1. Summation of forces perpendicular to the velocity vector:

$$-V_{M\dot{\gamma}} = \frac{Z_\alpha - T}{m}\alpha + \frac{Z_\delta}{m}\delta$$

2. Summation of moments about the center of gravity of the missile:

$$\ddot{\theta} = \frac{M_\alpha}{I}\alpha + \frac{M_\delta}{I}\delta + \frac{M_\theta}{I}\dot{\theta}$$

3. The angle-of-attack equation:

$$\theta = \alpha + \gamma,$$

where

γ = angle of missile velocity vector in space
θ = attitude angle of missile body in space
α = angle of attack
δ = wing or control surface deflection
m = mass of missile
I = moment of inertia of missile
M_α, M_δ = moments due to α and δ
Z_α, Z_δ = forces due to α and δ
M_θ = moment due to viscous damping about θ axis
T = thrust

The first two equations are differential equations with nonconstant coefficients. These coefficients are primarily functions of the air density, the velocity, and the missile design. In Figure 4.27, the block labeled navigation ratio will be discussed next. An equation similar to (4.26) that expresses the idea of proportional navigation in this example is

$$\frac{d\gamma}{dt} = N\left(\frac{d\sigma}{dt}\right), \tag{7}$$

where N is the navigation constant between the *LOS* turning rate and the missile velocity vector turning rate. In this example N will be given by

$$N = N'\left(\frac{dR_{MT}}{dt}\right)/(V_m\cos(\gamma-\sigma)), \tag{8}$$

where N' is the effective navigation ratio and may be chosen as required (see also (4.32)). Substituting (8) into (7) leads to the following navigational equation, the combined seeker and autopilot transfer function in the over-all guidance loop:

$$\frac{d\gamma}{dt} = N'\{N\dot{R}_{MT}\dot{\sigma}'/(V_M\cos(\gamma-\sigma))\}. \tag{9}$$

The primary reason for using the ratio given in (8) is that with it, the dynamic response of the system remains constant no matter what the angle of approach between the missile and target velocity vectors.

The three equations required in closing the loop in Figure 4.27 are (5), representing the geometry; (6), representing the smoothing in the seeker; and (9), representing the navigation ratio. If (6) and (9) are substituted into (5), a closed-loop expression is obtained that expresses the lateral acceleration of the missile (a_M) as a function of the input disturbances V_M, V_T, and $V_T(d\gamma_T/dt)$:

$$a_M = V_M\left(\frac{d\gamma_T}{dt}\right) = \frac{N/(N-2)}{\left[\frac{t_g t_s}{N-2}p^2 + \frac{t_g-2t_s}{N-2}p + 1\right]}\left[-\dot{V}_M\tan(\gamma-\sigma)\right.$$
$$\left. + \dot{V}_T\frac{\sin(\sigma-\gamma_T)}{\cos(\gamma-\sigma)} + V_T\dot{\theta}_T\frac{\cos(\sigma-\gamma_r)}{\cos(\gamma-\sigma)}\right] \tag{10}$$

where t_g (time-to-go until intercept) equals $R_{MT}/(dR_{MT}/dt)$, and s is the Laplace operator. Several qualitative statements can be made about (10):

1. The characteristic equation is independent of the missile–target approach angle. This is because of the definition of the navigation ratio.
2. As N' is increased, the required missile acceleration for any input target acceleration decreases. Further, the system becomes more responsive.
3. $N' > 2$ in order to obtain a stable system.
4. A region of instability occurs when $t_g < 2t_s$, the smoothing time constant. This implies that the missile control loop is no longer fast enough to solve the geometry.
5. No missile maneuver is required if the missile speed is constant ($dV_M/dt = 0$) and the target flies a constant-speed straight-line course ($dV_T/dt = V_T(d\gamma/dt) = 0$).

All of the above certainly indicates that if only the dynamics are considered, N' should be made as large as possible and t_s as small as possible. Unfortunately, the system must also contend with noise. In a homing system such as this, the type of noise that predominates is glint noise, which is present because the seeker is not tracking a point source but wanders randomly over the target's cross section. As the range from the missile to target decreases, the angular magnitude of this wander increases.

The above results will now be a extended to a *line-of-sight command* missile. A line-of-sight missile could be of the beam-rider type, which automatically keeps itself centered in a radar beam transmitted by the ground station. However, in the command guidance system, the ground station tracks both the missile and the target, sending command signals to the missile to cause it to correct any deflection from the *LOS* path. To determine the acceleration requirements for the missile, an equation must be obtained that describes the acceleration as a function of target motion. As seen in Figure 4.28, the effect of θ_M, the angle of the *LOS* to the interceptor missile, on the missile velocity vector angle γ must first be determined.

The equations of motion of the missile with respect to the tracking radar are

$$R_{OM}\left(\frac{d\theta_M}{dt}\right) = V_M \sin(\gamma - \theta_M), \tag{11}$$

$$\frac{dR_{OM}}{dt} = V_M \cos(\gamma - \theta_M), \tag{12}$$

where

R_{OM} = distance from missile to ground station,
V_M = missile velocity,
γ = missile velocity vector angle with respect to the reference axis,
θ_M = angle of sight line from ground station to the missile.

Differentiating (11) with the assumption that V_M remains constant yields

$$\dot{R}_{OM}\dot{\theta}_M + R_{OM}\ddot{\theta}_M = V_M \cos(\gamma - \theta_M)(\dot{\gamma} - \dot{\theta}_M). \tag{13}$$

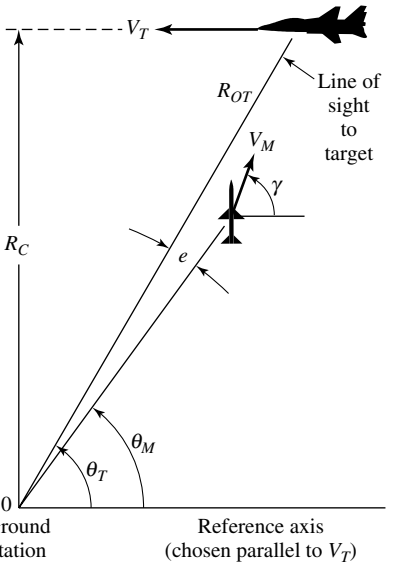

Fig. 4.28. Geometric relationship for a line-of-sight command system.

Substituting (12) into (13) and dividing by (dR_{OM}/dt) yields

$$\dot{\gamma} = 2\dot{\theta}_M + \frac{R_{OM}}{\dot{R}_{OM}}\ddot{\theta}_M,$$

and since the missile lateral acceleration is equal to $V_M(d\gamma/dt)$,

$$a_M = 2V_M\dot{\theta}_M + \frac{R_{OM}V_M}{\dot{R}_{OM}}\ddot{\theta}_M.$$

If it is assumed that there are no errors in the system, then $\theta_M = \theta_T$ and

$$a_M = 2V_M\dot{\theta}_T + \frac{R_{OM}V_M}{\dot{R}_{OM}}\ddot{\theta}_T. \tag{14}$$

This equation yields missile acceleration as a function of motion of the target tracking line. Now, if the reference axis is chosen as parallel to the target velocity vector, the equations of motion of the target are

$$R_{OT}\left(\frac{d\theta_T}{dt}\right) = V_T \sin\theta_T, \tag{15}$$

$$\frac{dR_{OT}}{dt} = -V_T \cos\theta_T, \tag{16}$$

where R_{OT} is the distance from the ground station to the target and V_T is the velocity of the target. From the geometry,

$$\sin\theta_T = R_C/R_{OT}, \tag{17}$$

where R_C is the crossover range, or the perpendicular distance from the ground station to the line of the target velocity vector. Substituting (17) into (15) gives

$$R_{OT}^2\left(\frac{d\theta_T}{dt}\right) = V_T R_C. \tag{18}$$

For a target flying a constant-speed straight-line course, $V_T R_C$ is constant. Realizing this and differentiating (18), we obtain

$$\frac{d^2\theta_T}{dt^2} = -(2\dot{R}_{OT}/R_{OT})\theta_T. \tag{19}$$

Substituting (16) and (19) into (14), we obtain

$$a_M = 2V_M\dot{\theta}_T\left[1+\frac{\dot{R}_{OM}V_T\cos\theta_T}{\dot{R}_{OM}R_{OT}}\right]. \tag{20}$$

The most important result to be obtained from (20) is the maximum value of acceleration required for any given target course. It is seen that the maximum acceleration occurs when $R_{OM} = R_{OT}$, or at intercept. Furthermore, if we make the approximation that $V_M \approx d R_{OM}/dt$, the equation for maximum required missile acceleration for any given target course is

$$a_M = 2V_M\left(\frac{d\theta_T}{dt}\right)[1+\kappa\cos\theta_T], \tag{21}$$

where $\kappa = V_T/V_M$, the ratio of the target to missile velocity. In order to obtain an expression for a_M in terms of ground-station-to-target range, crossover range, target velocity, and missile velocity, (17) and (18) may be substituted into (21), yielding the following expression:

$$a_M = \frac{2V_M V_T R_c}{R_{OT}^2}\left[1+\frac{V_T}{V_M}\sqrt{1+\left(\frac{R_C}{R_{OT}}\right)^2}\right]. \tag{22}$$

With today's technological advances, controlled missile lateral accelerations of more than 30 g's can be attained. Unfortunately, however, when missile velocity is increased, drag increases rapidly, requiring increased thrust. In this event, a larger rocket motor must be used, increasing the missile weight or decreasing the payload by a large amount for a small increase in speed. Furthermore, as the speed is increased, aerodynamic heating may become a problem not only to the aerodynamicist, but also to the designer of the electronic equipment within the missile.

4.6 Augmented Proportional Navigation

We have seen in the previous section that the basic proportional navigation law is expressed as

$$a_n = NV_c\left(\frac{d\lambda}{dt}\right), \tag{4.24}$$

where N is the navigation constant, V_c is the interceptor missile's closing velocity, and $d\lambda/dt$ is the line-of-sight angle rate measured by the onboard radar or other sensor. The missile's lateral (or normal) acceleration a_n (note that here we use the subscript n instead of l to indicate the missile's lateral or normal acceleration) history is in general invariant. This lateral acceleration is desired to be normal to the LOS. For aerodynamically maneuvering missiles, this acceleration occurs normal to the instantaneous velocity vector. Moreover, the effective navigation ratio takes several values. For instance, for $N \geq 3$, a nearly straight-line missile trajectory results. Guidance accuracy decreases as N increases. Next, we note that the line of sight is given by

$$\lambda = y/R_{MT} = y/V_c(t_f - t), \tag{4.71}$$

where y is the relative missile–target separation, R_{MT} is the range from the missile to the target, t_f is the final intercept time, and t is the present time (note that as discussed earlier in this chapter, $t_f - t = t_{go}$). Taking the derivative of (4.71) results in [17], [35]

$$\frac{d\lambda}{dt} = (1/V_c t_{go}^2)[y + \dot{y}t_{go}]. \tag{4.72}$$

Making use of (4.72), (4.24) can now be written in the form

$$a_n = NV_c\left(\frac{d\lambda}{dt}\right) = (N/t_{go}^2)\left[y + \left(\frac{dy}{dt}\right)t_{go}\right], \tag{4.73}$$

where the navigation constant N is given by (4.32a).

The expression in the brackets represents the miss distance that would occur, assuming no target maneuver and if the missile underwent no further corrective acceleration. This miss distance is called *zero effort miss* and is perpendicular to the *LOS*. However, if the target undergoes, say, a constant maneuver, the zero effort miss term in (4.72) or (4.73) must be augmented by an additional term as follows [35]:

$$a_n = (N/t_{go}^2)\left[y + \left(\frac{dy}{dt}\right)t_{go} + (1/2)a_T t_{go}^2\right], \tag{4.74}$$

where a_T represents the additional term due to the target maneuver. Thus, in the presence of target maneuver, and using (4.73), we have

$$a_n = NV_c\left(\frac{d\lambda}{dt}\right) + (1/2)a_T t_{go}^2. \tag{4.75}$$

Equation (4.75) is known as the *augmented proportional navigation* (*APN*) guidance law [17], [26], [35]. Note that since the target acceleration is not known a priori, if *APN* is chosen as the guidance law, then the target acceleration must be estimated continuously during the flight.

The acceleration required by a missile using the *APN* guidance law to intercept a step-maneuvering target is given by [17]

$$a_n = \tfrac{1}{2}N' a_T[1 - (t/t_f)]^{N'-2}. \tag{4.76}$$

Equation (4.76) arises from a zero-lag homing loop. Furthermore, we see from (4.76) that as time increases, the intercept missile's acceleration required to intercept a maneuvering target decreases. As a result, we see from (4.76) that the maximum required acceleration using the *APN* guidance law at the initial time is expressed as

$$(a_n)_{\max} = \tfrac{1}{2}N' a_T, \tag{4.77}$$

indicating that only half as much acceleration is required by the missile with *APN* than missiles employing the conventional *PN* guidance law with $N' = 3$.

The concept of augmented proportional navigation will now be discussed from a different perspective. Consider a linearized version of the guidance law given by

$$y(t) = w(t) * [(y_T - y)/(T - t)] + v(t) * y_T(t), \tag{4.78}$$

where

$y(t)$ = missile perturbation from a collision course normal to the nominal *LOS* [ft],
$y_T(t)$ = corresponding target perturbation [ft],
t = time from the start of the engagement [sec],
T = total time of engagement [sec].

The asterisk ($*$) in (4.78) denotes convolution. Furthermore, $v(t)$ is a low-pass filter, and $w(t)$ corresponds to a pure integrator followed by a low-pass filter. When $v(t)$ is zero, (4.78) will be recognized as the usual proportional navigation. Historically, *APN* has been used for command guidance. Potential exists also for application to systems that detect the target with an onboard interceptor sensor.

In modeling *PN*, the transforms of $v(t)$ and $w(t)$, $V(s)$ and $W(s)$, respectively, are idealized to

$$\begin{aligned} V(s) &= 0, \\ W(s) &= N'/s, \end{aligned} \tag{4.79}$$

where as before, N' is the effective navigation ratio. The solution for interceptor terminal maneuver for *PN* is

$$a_M/a_T = N'/(N' - 1), \tag{4.80}$$

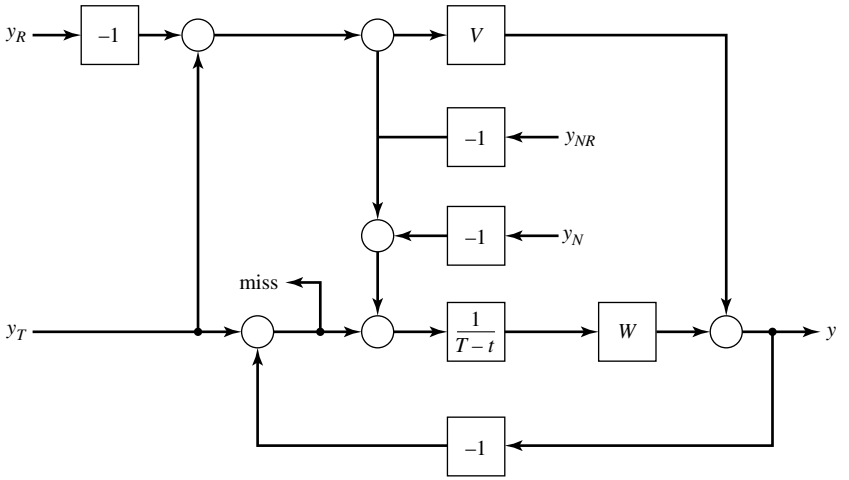

Fig. 4.29. Block diagram for *APN*.

where a_M is the interceptor missile acceleration, a_T is the target acceleration, and the *APN* infinite bandwidth is given by

$$\begin{aligned} V(s) &= 1.0, \\ W(s) &= N'/s. \end{aligned} \tag{4.81}$$

In this case, the interceptor maneuver is equal to the target maneuver for all values $N'(a_M/a_T = 1.0)$. The block diagram corresponding to *APN* is shown in Figure 4.29. In practice, the second derivative of y_T would be estimated and added directly as an acceleration command to the missile guidance system.

The solution given for (4.78) corresponds to the case where the augmentation command y_T has either the same error as the *PN* term or an entirely independent error. That is, y_R is the error on the sensed y_T in the augmentation, and y_N the error on $y_T - y$ in the *PN* portion of the system. Noise impulse responses for the common sensor mechanization are denoted by y_{NR}, and for two sensors by y_N and y_R.

The key feature of the guidance law pursued herein (*APN*) is the reduced g requirement relative to *PN*, associated with a given level of miss effectiveness against target maneuver. Thus, the interceptor g requirements to satisfy the guidance law are solved for the case of infinite bandwidth, that is, with guidance time lags neglected. The infinite bandwidth acceleration solutions for *PN* and *APN* are plotted for several cases in Figure 4.30.

In certain command guidance applications the target tracking data, as opposed to missile tracking data, is the dominant source of command guidance noise. Also, noise within the radar and on the target signal limits the accuracy to which $d\lambda/dt$ can be measured and significantly affects the miss distance. Specifically, augmented proportional navigation offers a reduction in the interceptor terminal acceleration requirement relative to proportional navigation for the same miss distance. However,

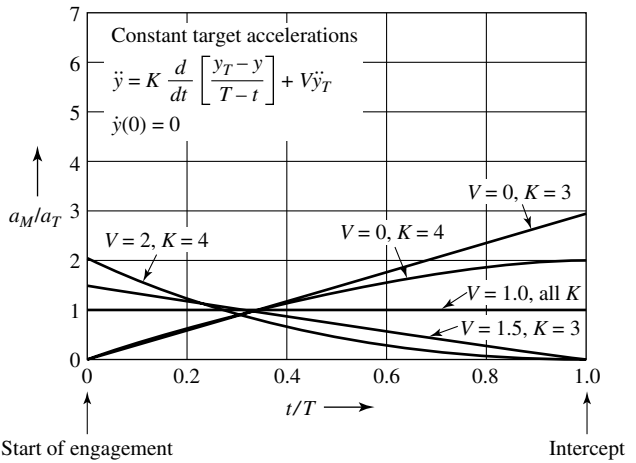

Fig. 4.30. Infinite-bandwidth acceleration histories.

the terminal noise level g's increase when *APN* is used. For more discussion on the application of *APN*, the reader is referred to [17], [26], and [35].

4.7 Three-Dimensional Proportional Navigation

In the previous sections we discussed two-dimensional (or navigation in the plane) proportional navigation (*PN*) guidance laws and homing systems used in intercepting airborne targets. Other modified forms of proportional navigation such as pure proportional navigation (*PPN*), true proportional navigation (*TPN*), and generalized true proportional navigation (*GTPN*) have been discussed in the literature. These analyses were based on two-dimensional models. However, even though actual pursuit–evasion dynamics occur in three-dimensional space, the extension from two-dimensional guidance laws to the three-dimensional case is not immediately obvious. Therefore, in this section we will briefly discuss a possible approach to the three-dimensional true proportional navigation. For more details, the reader is referred to [13], [21], [22], [34], and [34].

The proportional navigation law in three dimensions shows that is necessary to measure the *LOS* angular rate $d\lambda/dt$ in two seeker-instrument axes that are orthogonal to the seeker boresight axis (which is virtually coincident with the *LOS* to the target). Space-stabilization about these two instrument axes is necessary, although a slow roll rate about the *LOS* itself is tolerable. Specifically, in three-dimensional proportional navigation the seeker measurements are in spherical coordinates. That is, one must consider three parameters: (1) range, and (2) two angles (i.e., azimuth and elevation). These three parameters (or measurements) are a nonlinear function of the states in a Cartesian coordinate system. However, the nonlinear transformation of the states can be avoided if the guidance laws were formulated in spherical coordinates.

Only the equations for target motion estimation will be given here. Moreover, it is felt that the models assumed for generation of the target maneuver are realistic enough to provide satisfactory estimation accuracy in most situations. The target position equations can be combined with the pursuer equations to yield relative position equations. However, the target and pursuer velocity and acceleration equations cannot be combined, because estimates of target absolute velocity and acceleration are required for generating some of the equation coefficients.

Assuming a point-mass model for the missile, the three-dimensional equations can be stated as follows [13]:

$$\frac{dx}{dt} = V \cos\gamma \cos\psi, \tag{4.82a}$$

$$\frac{dy}{dt} = V \cos\gamma \sin\psi, \tag{4.82b}$$

$$\frac{dh}{dt} = V_m \sin\gamma, \tag{4.82c}$$

$$\frac{dE}{dt} = [T - D(h, M, n](V/W), \tag{4.82d}$$

$$\frac{d\gamma}{dt} = (n_v - \cos\gamma)(g/V), \tag{4.82e}$$

$$\frac{d\psi}{dt} = (n_h/\cos\gamma)(g/V), \tag{4.82f}$$

where

x = downrange displacement of the missile,
y = cross-range displacement of the missile,
h = altitude of the missile,
g = gravitational acceleration,
γ = flight path angle,
V_m = velocity of the missile = $(2g\,(E - h))^{1/2}$,
E = specific energy,
M = Mach number,
T = thrust,
D = aerodynamic drag,
W = weight of the missile,
n_h, n_v = horizontal and vertical load factors, respectively,
$n = \sqrt{(n_h^2 + n_v^2)}$ = resultant load factor.

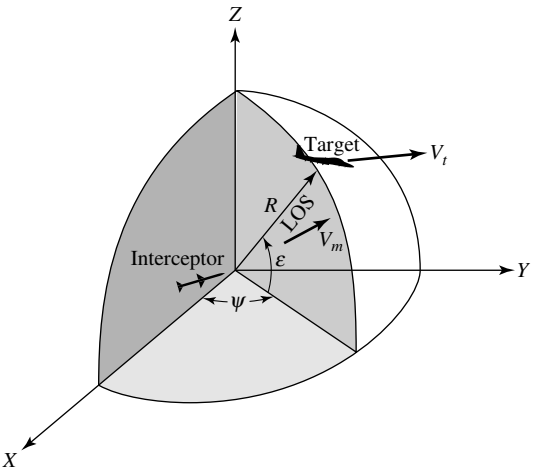

Fig. 4.31. Three-dimensional pursuit–evasion geometry.

In the above set of equations, the variation of drag with altitude, Mach number, and load factor is given by the expression [13]

$$D/W(h, M, n) = D_o + D_i n^k, \tag{4.83a}$$

$$D_o = (qA/W)C_{Do}(h, M), \tag{4.83b}$$

$$D_i = (qA/W)^{i-k} C_{Di}(M), \tag{4.83c}$$

$$Q = \tfrac{1}{2}\rho(h)V^2, \tag{4.83d}$$

where

$$\begin{aligned} A &= \text{reference area,} \\ C_{Do} &= \text{zero-lift drag coefficient,} \\ C_{Di} &= \text{induced drag coefficient,} \\ \rho(h) &= \text{air density,} \\ q &= \text{dynamic pressure.} \end{aligned}$$

The assumptions on these equations are (1) pursuer and evader are considered as constant-speed mass points, (2) the pursuer is a homing missile launched against an initially nonmaneuvering evader (i.e., target), (3) pursuer and evader have perfect information on their relative state with respect to the other, and (4) gravity can be neglected.

Referring to Figure 4.31, one can write the three second-order differential equations as follows [34]:

$$a_r = a_{Tr} - a_{Mr} = \frac{d^2r}{dt^2} - r\left(\frac{d\varepsilon}{dt}\right)^2 - r\left(\frac{d\psi}{dt}\right)^2 \cos^2\varepsilon, \tag{4.84a}$$

$$a_\psi = a_{T\psi} - a_{M\psi} = r\left(\frac{d^2\psi}{dt^2}\right)\cos\varepsilon + 2\left(\frac{dr}{dt}\right)\left(\frac{d\psi}{dt}\right) - 2r\left(\frac{d\varepsilon}{dt}\right)\left(\frac{d\psi}{dt}\right)\sin\varepsilon, \tag{4.84b}$$

$$a_\varepsilon = a_{T\varepsilon} - a_{M\varepsilon} = r\left(\frac{d^2\varepsilon}{dt^2}\right) + 2\left(\frac{dr}{dt}\right)\left(\frac{d\varepsilon}{dt}\right) + r\left(\frac{d\psi}{d}\right)^2\cos\varepsilon\sin\varepsilon, \tag{4.84c}$$

where

$$\begin{aligned} a_{Mr}, a_{M\psi}, a_{M\varepsilon} &= \text{components of missile acceleration,} \\ a_{Tr}, a_{T\psi}, a_{T\varepsilon} &= \text{coupled components of target acceleration,} \\ r &= \text{radial distance between missile and target,} \\ \varepsilon &= \text{elevation angle,} \\ \psi &= \text{azimuth angle.} \end{aligned}$$

These are coupled nonlinear equations, and they can be solved using the concept of unit angular momentum. Specifically, the unit angular momentum vector $\mathbf{h}$ for the missile–target relative motion is defined as

$$\mathbf{h} = \mathbf{r} \times \left(\frac{d\mathbf{r}}{dt}\right). \tag{4.85}$$

Next, we note that the relative displacement along the *LOS* is given by

$$\mathbf{r} = r\mathbf{e}_r \tag{4.86}$$

and the relative velocity by

$$\frac{d\mathbf{r}}{dt} = \left(\frac{dr}{dt}\right)\mathbf{e}_r + r\left(\frac{d\psi}{dt}\right)\cos\varepsilon\,\mathbf{e}_\psi + r\left(\frac{d\varepsilon}{dt}\right)\mathbf{e}_\varepsilon, \tag{4.87}$$

where $\mathbf{e}_r, \mathbf{e}_\psi, \mathbf{e}_\varepsilon$ are unit vectors along the directions indicated. By analogy to the two-dimensional true proportional navigation form (i.e., (4.24)), the three-dimensional true proportional navigation equation can be written in vector form as

$$\mathbf{a}_m = N\left(\frac{dr_o}{dt}\right)\mathbf{e}_r \times (\mathbf{h}/r^2), \tag{4.88}$$

where N is the navigation constant and $r_0 = r(0)$. In [21] the interceptor missile's acceleration is given in terms of pitch and yaw accelerations as follows:

$$a_{ym} = -NV_m\left(\frac{d\lambda_y}{dt}\right)\sin\theta_m + NV_m\lambda_z\cos\theta_m, \tag{4.89a}$$

$$a_{zm} = -NV_m\left(\frac{d\lambda}{dt}\right)\cos\psi_m, \tag{4.89b}$$

where

$$\begin{aligned} N &= \text{navigation constant,} \\ V_m &= \text{missile's velocity,} \\ (d\lambda_y/dt) &= y\text{-component of } LOS \text{ rate,} \\ \theta_m, \psi_m &= \text{Euler angles from } LOS \text{ to target body coordinate system} \\ &\quad (\theta \text{ corresponds to the elevation or pitch angle and } \psi \\ &\quad \text{to the azimuth angle).} \end{aligned}$$

In the discussion that follows, we will briefly discuss the target maneuver model, target equations, perturbation equations, and white noise roll rate. Note that target maneuver has been modeled in many different ways. For instance, in tracking a highly maneuvering target, the target can be modeled as a *jerk model** [5], [10], [20].

Target Maneuver Model

Assume that three random processes are involved in the target maneuver description: (1) the normal force F_n (perpendicular to the velocity vector $\mathbf{v}$), (2) the longitudinal force F_v along $\mathbf{v}$ (which models the thrust and drag variations, and (3) the roll rate ω. Assume now that all three processes are exponentially correlated, and generated by the following differential equations (see also Sections 4.3–4.5). Thus,

$$\frac{dF_n}{dt} = -(F_n/\tau_n) + w_n, \tag{4.90a}$$

$$\frac{dF_v}{dt} = -(F_v/\tau_v) + w_v, \tag{4.90b}$$

$$\frac{d\omega}{dt} = -(\omega/\tau_\omega) + w_\omega, \tag{4.90c}$$

where the w's are white noises. The roll rate parameter ω is essentially a rate of change in the acceleration, and as such will probably never be estimated with any great accuracy. For this reason, an assumption of a white noise ω may yield results that are just as good as those resulting from the above model. However, it is probably essential that rolling be modeled in some fashion, in order to acknowledge the possibility of nonplanar target maneuvers. Otherwise, one could not expect the estimator to accurately track a maneuver such as a barrel roll (which, incidentally, would probably be an excellent maneuver against which to test different intercept schemes). If we define roll angle as the integral of ω, the above model allows the rms roll angle to increase without limit. This is a desirable property for the model, since it is quite possible for the target aircraft to roll through many revolutions in one direction without ever returning to zero roll angle. This fact would not be properly accounted for if the

*The term *jerk model* refers to the inclusion of the acceleration rate of the target motion (or the third derivative of the target position) in the description of the target motion.

roll angle itself were assumed to be a zero-mean process. The target jerk model mentioned above can be represented by an autocorrelation function such as [20]

$$r_j(\tau) = E\{j(t)\,j(t+\tau)\} = \sigma_j^2 e^{-\alpha|\tau|},$$

where σ_j^2 is the variance of the target jerk and α is the reciprocal of the jerk time constant.

Target Equations

Referring to Figure 4.32, the total acceleration $\mathbf{a}$ is the sum of two vectors, namely, $\mathbf{F}_n$ and $\mathbf{F}_v$, where

$$\mathbf{F}_v = F_v \mathbf{e}_v = (F_v/v)\mathbf{v}, \tag{4.91}$$

where

$$\begin{aligned}
\mathbf{a} &= \text{acceleration vector,}\\
\mathbf{F}_v &= \text{force vector along the velocity vector,}\\
\mathbf{F}_n &= \text{force vector along the normal,}\\
\mathbf{v} &= \text{velocity vector,}\\
\mathbf{e}_v &= \text{unit vector along the velocity vector } \mathbf{v},\\
\mathbf{e}_n &= \text{unit vector along } \mathbf{F}_n.
\end{aligned}$$

The coordinate system defined by the vectors $\mathbf{v}$ and $\mathbf{F}_n$ rotates at a rate

$$\omega_c = \omega \mathbf{e}_v + (F_n/v)\mathbf{e}(\mathbf{v}\times\mathbf{a}) = (\omega/v)\mathbf{v} + (1/v^2)(\mathbf{v}\times\mathbf{a}). \tag{4.92}$$

Hence, we can write the rate of change of $\mathbf{a}$ as follows:

$$\begin{aligned}
d\mathbf{a}/dt &= \left(\frac{d\mathbf{F}_n}{dt}\right)\mathbf{e}_n + \left(\frac{d\mathbf{F}_v}{dt}\right)\mathbf{e}_v + \boldsymbol{\omega}_c\times\mathbf{a}\\
&= (1/F_n)\left(\frac{dF_n}{dt}\right)[\mathbf{a} - (F_v/v)\mathbf{v}] + (1/v)\left(\frac{dF_v}{dt}\right) + (\omega/v)(\mathbf{v}\times\mathbf{a})\\
&\quad + (1/v^2)(\mathbf{v}\times\mathbf{a})\times\mathbf{a}\\
&= [(-1/\tau) + (w_n/F_n)][\mathbf{a} - (F_v/v)\mathbf{v}] + \{(-F_v/v\tau_f) + (w_f/v)\}\mathbf{v}\\
&\quad + (\omega/v)(\mathbf{v}\times\mathbf{a}) + (1/v^2)[vF_v\mathbf{a} - a^2\mathbf{v}]\\
&= (\omega/v)(\mathbf{v}\times\mathbf{a}) + [(F_v/v) - (1/\tau_n)]\mathbf{a} - k\mathbf{v} + w_n\mathbf{e}_n + w_f\mathbf{e}_v,
\end{aligned} \tag{4.93}$$

where

$$k = (a/v)^2 + (F_v/v)[(1/\tau_f) - (1/\tau_n)]. \tag{4.94}$$

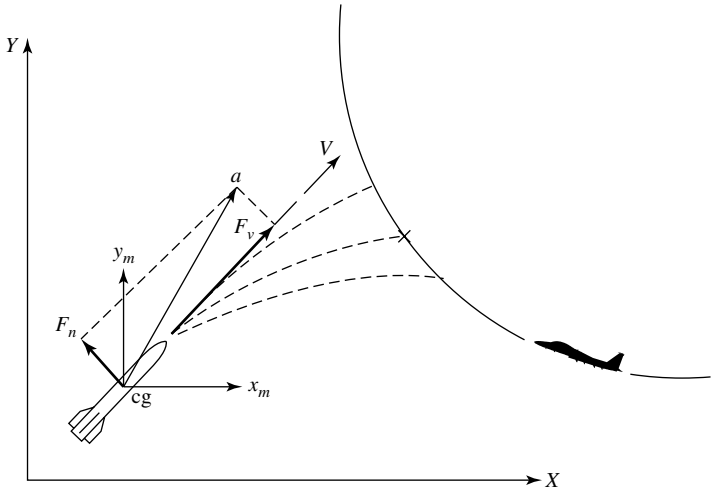

Fig. 4.32. Coordinate system for target equations.

Equations (4.90) and (4.93), together with equations

$$\frac{d\mathbf{x}}{dt} = \mathbf{v}, \tag{4.95a}$$

$$\frac{d\mathbf{v}}{dt} = \mathbf{a}, \tag{4.95b}$$

where $\mathbf{x}$ is the position vector, $\mathbf{a}$ the acceleration vector, and $\mathbf{v}$ the velocity vector, represent the equations that describe the behavior of the target. The equations by which the estimates are propagated are identical, except that the w's are set to zero and estimated values are used for all other quantities (except the τ's, which are assumed known). It is understood that a, v, and F_n are the magnitudes of $\mathbf{a}$, $\mathbf{v}$, and $\mathbf{F}_n$, and F_v and $\mathbf{F}_n$ are determined from the relations

$$F_v = (1/v)(\mathbf{a} \cdot \mathbf{v}), \tag{4.96a}$$

$$\mathbf{F}_n = \mathbf{a} - F_v \mathbf{e}_v. \tag{4.96b}$$

Perturbation Equations

For purposes of propagating the covariance matrix in the intervals between measurements (see the discussion in Section 4.8) it is necessary to linearize (4.93) by perturbing around the present best estimate. In the perturbation equation, the scalars a, v, and F_v are treated by using the relations

$$\delta v = \mathbf{e}_v \delta \mathbf{v} = (1/v)\mathbf{v}^T \delta \mathbf{v}, \tag{4.97a}$$

$$\delta a = (1/a)\mathbf{a}^T \delta \mathbf{a}, \tag{4.97b}$$

and from (4.96a),

$$\begin{aligned}\delta F_v &= (-1/v^2)\mathbf{v}^T\mathbf{a}\delta v + (1/v)[\mathbf{a}^T\delta\mathbf{v} + \mathbf{v}^T\delta\mathbf{a}] \\ &= (-1/v^2)(v\mathbf{a} - F_v\mathbf{v})^T\delta v + (1/v)\mathbf{v}^T\delta\mathbf{a}. \end{aligned} \tag{4.98}$$

Note that the terms containing the w's in (4.93) are not differentiated, since the w's themselves are assumed to be small. Equations (4.97) and (4.98) can be cast in the usual form (see Section 4.8, (4.100)):

$$\frac{d\mathbf{x}(t)}{dt} = F\mathbf{x}(t) + G\mathbf{w}(t).$$

The matrices F and G are used in the propagation of the covariance matrix from one measurement time to the next, as is the 3×3 spectral-density matrix Q of the white noise vector $\mathbf{w}$. Also, the white noise vector $\mathbf{w}(t)$ consists of the three noises in (4.90), that is, $\mathbf{w}^T(t) = [w_n\ w_v\ w_\omega]$.

White Noise Roll Rate

The above formulation involves the use of a total of ten state variables (i.e., 3 positions, 3 velocities, 3 accelerations, and one roll rate). However, it may be reasonable to use a model in which the roll rate is assumed to be white noise; that is, (4.90c) is replaced by

$$\omega = w_\omega. \tag{4.99}$$

In this case the number of state variables is reduced to nine. Thus, if we simply omit the roll-rate noise w_ω, the estimator will exclude any random out-of-plane maneuvers.

The scheme described above is believed to provide a reasonable approach to the three-dimensional target maneuver estimation problem. Although the derivation is relatively complex, the final result does not appear unreasonable computationally, especially in view of the fact that it is probably difficult to achieve good three-dimensional tracking with fewer than nine state variables. It could prove necessary to introduce more state variables if one wished to estimate such rates as gyro drift rates, etc. Finally, it is recommended that such a scheme be simulated and tested against realistic maneuvers.

4.8 Application of Optimal Control of Linear Feedback Systems with Quadratic Performance Criteria in Missile Guidance

4.8.1 Introduction

The classical techniques of using low-pass filtering to attenuate the noise inherent in the guidance signal and using proportional navigation to steer a missile toward the target were well developed before the advent of modern control and estimation

theory. They have become firmly entrenched in guided missile designs because they have worked well in the rather benign environment of past air-to-air engagements and were easily implemented with analog circuitry. Because of such an approach, missile designers have often tried to satisfy the increased performance requirements of modern-day air-to-air missiles by increasing the complexity of associated hardware such as airframes, seekers, gyroscopes, accelerometers, and engines. Such approaches in many cases have improved performance, but the resulting cost has often been so high that the systems were never developed for operational use or were purchased in small quantities.

During the late 1960s and early 1970s a few missile designers did take a cursory look at applying the modern control theory developed during the late 1950s and early 1960s to tactical missiles. Basically, such an approach would replace the low-pass filter with an optimal estimator, such as the Kalman filter. In theory, this would allow one to optimally separate the signal from the noise by using information about the missile dynamics and noise covariances rather than filtering based only on frequency content. In addition, missile/target states other than *LOS* rate could be estimated, even if not measured, provided they were mathematically observable. This, in turn, would allow one to design more advanced guidance laws based upon optimal control theory, because such theory usually requires complete information concerning the missile states.

Since the early 1970s technology has advanced drastically. That is, using optimal control and estimation theory, one could perform more calculations, more often, at less cost, and in a smaller volume than anyone would have imagined just a few years ago. Bryson and Ho [3] used optimal control theory to show that proportional navigation (*PN*) is the optimal control law that minimizes the terminal miss distance. In their derivation, many assumptions were made both implicitly in the problem formulation and explicitly in the derivation. These assumptions were necessary in order for the solution to result in proportional navigation. The optimality of proportional navigation is therefore dependent on the deviation from the real-world implementation, application of the guidance law from the model and assumptions used in deriving *PN*, and the sensitivity of the guidance law performance to those deviations. In order to explicitly state all the assumptions involved in claiming that *PN* is the optimal control law that minimizes the terminal miss distance, an optimal feedback guidance law will be derived using linear quadratic theory. Once the guidance law is derived, several further assumptions will be made in order to arrive at the optimality of the proportional navigation guidance law. The form and performance of optimal guidance law, say, for air-to-air missiles, are dependent on a performance index, control constraints, terminal constraints, assumptions on the availability of target acceleration information, and system dynamics used in the derivation of the guidance law. The aim of any missile guidance system design is to minimize the terminal miss distance. An optimal guidance law that minimizes terminal miss distance will be derived using optimal control theory. Once derived, it is shown that by making several simplifying assumptions the optimal guidance law reduces to proportional navigation. It is determined by realistic simulation and analysis that these simplifying assumptions substantially reduce the

performance capability of short-range air-to-air missiles employing proportional navigation.

Generally speaking, a missile's guidance law is thought of as two cascaded functions: (1) state estimation (also known as *Kalman filtering* or *optimal filtering*), and (2) control. The function of the former is to obtain estimates of those variables needed to mechanize the control law. The latter prescribes the acceleration command according to a policy that will direct the missile trajectory to intercept the target.

4.8.2 Optimal Filtering

(a) Continuous-Time Kalman Filtering

We begin with a brief discussion of filtering theory as applied to the design of optimal homing missile guidance systems. In particular, we will develop the covariance equations that are used in the design of these homing guidance systems. The principal advantage of the covariance technique is that it circumvents Monte Carlo simulations, thereby achieving substantial savings in computer running time. Furthermore, this application of filtering theory yields a simple method for determining the smallest possible *rms* miss distance that can be obtained with the "optimal missile" for an arbitrary specification of noise and target statistics, and parameters such as nominal closing velocity, initial range, and initial errors at the launch time of the missile. Knowledge of the best theoretically possible performance is always important in determining whether further improvement can be obtained in a guidance system that has been designed via another, perhaps trial and error, design method. It also helps in estimating the performance shortfall (with respect to ideal) while using a heuristic and/or suboptimal scheme.

Consider now the dynamics of a stable, nth-order, time-invariant, linear, continuous stochastic system that can be represented by a first-order vector–matrix differential equation of the form [25]

$$\frac{d\mathbf{x}(t)}{dt} = F(t)\mathbf{x}(t) + G(t)\mathbf{u}(t), \tag{4.100}$$

where

$$\begin{aligned}
\mathbf{x}(t) &= \text{state vector of dimension } n \times 1,\\
F(t) &= \text{a matrix that describes the system dynamics}\\
&\quad\ (n \times n),\\
G(t) &= \text{noise gain matrix}(n \times r),\\
\mathbf{u}(t) &= \text{zero-mean white Gaussian noise}(r \times 1).
\end{aligned}$$

The continuous available measurements are modeled by a process defined by

$$\mathbf{z}(t) = H(t)\mathbf{x}(t) + \mathbf{v}(t), \tag{4.101}$$

where

$$\begin{aligned}\mathbf{z}(t) &= \text{measurement (or observation) vector}(m \times 1),\\ H(t) &= \text{observation matrix}(m \times n),\\ \mathbf{v}(t) &= \text{zero-mean white Gaussian noise}(m \times 1).\end{aligned}$$

The system prior statistics can be represented by

$$E\{\mathbf{u}(t)\mathbf{u}^T(\tau)\} = Q(t)\delta(t-\tau),\ E\{\mathbf{u}(t)\} = \mathbf{0}, \tag{4.102a}$$

$$E\{\mathbf{v}(t)\mathbf{v}^T(\tau)\} = R(t)\delta(t-\tau), \qquad E\{\mathbf{v}(t)\} = \mathbf{0}, \tag{4.102b}$$

$$E\{\mathbf{x}(t_o)\} = 0, \tag{4.102c}$$

$$E\{\mathbf{x}(t_o)\mathbf{x}^T(t_o)\} = P(t_o);\ P(0) = P_o, \tag{4.102d}$$

$$E\{\mathbf{u}(t)\mathbf{v}^T(\tau)\} = \begin{cases} C(t)\delta(t-\tau) & \text{if the process and measurement noises are correlated,} \\ 0 & \text{if the process and measurement noises are uncorrelated,} \end{cases} \tag{4.102e}$$

where $\delta(t-\tau)$ is the Dirac function, $Q(t)$ and $R(t)$ are the respective noise covariance matrices, $C(t)$ is the correlation covariance matrix, and the symbol E{ ... }* denotes ensemble expectation or average value. Under the above conditions, the random state can be described in terms of its covariance matrix $P(t)$ as follows:

$$P(t) \triangleq E\{\mathbf{x}(t)\mathbf{x}^T(t)\}. \tag{4.103}$$

The equation for the propagation of the covariance matrix for the system described by (4.100) is [3], [25]

$$\frac{dP(t)}{dt} = F(t)P(t) + P(t)F^T(t) + G(t)Q(t)G^T(t) - P(t)H^T(t)R^{-1}(t)H(t)P(t) \tag{4.104a}$$

if $R^{-1}(t)$ exists. The superscript T denotes the transpose of a vector or matrix, and the superscript (–1) denotes the inverse of a matrix. This equation is nonlinear in P and is referred to in the literature as the *matrix Riccati equation*. In the absence of measurements (4.104a) takes the simple form

$$\frac{dP(t)}{dt} = F(t)P(t) + P(t)F^T(t) + G(t)Q(t)G^T(t). \tag{4.104b}$$

Note that $G(t)Q(t)G^T(t)$ accounts for the increase of uncertainty due to process noise, while the term $-P(t)H^T(t)R^{-1}(t)H(t)P(t)$ accounts for the decrease of uncertainty as a result of measurements.

*Note that instead of writing, for example, $E\{\mathbf{u}(t)\mathbf{v}^T(\tau)\} = C(t)\delta(t-\tau)$, we can write also $\text{Cov}\{\mathbf{w}(t), \mathbf{v}(\tau)\} = C(t)\delta(t-\tau)$.

The diagonal elements of $P(t)$ are the mean-square values of the state variables, while the off-diagonal elements represent the amount of correlation between the different state variables. Equation (4.104) provides a direct method for analyzing the statistical properties of $\mathbf{x}(t)$. This is to be contrasted with the Monte Carlo method, where many sample trajectories of $\mathbf{x}(t)$ are calculated from computer-generated random noise, or random numbers in the case of a digital computer. In using the latter technique, m such trajectories are generated using (4.100), each denoted by $\mathbf{x}_k(t)$, $k = 1, 2, \ldots, m$. Consequently, $P(t)$ can be approximated by the expression

$$P(t) \cong \hat{P}(t) \triangleq (1/m) \sum_{k=1}^{m} \mathbf{x}_k(t) \mathbf{x}_k^T(t). \tag{4.105}$$

Note that in the limit, as $m \to \infty$, we have

$$\lim_{m \to \infty} \hat{P}(t) = P(t). \tag{4.106}$$

Kalman and Bucy showed that the optimal filter (which is independent of the weightings given to each of the error components) is a linear dynamic system described by

$$\frac{d\hat{\mathbf{x}}(t)}{dt} = [F(t) - R(t)H(t)]\hat{\mathbf{x}}(t) + R(t)\mathbf{z}(t), \tag{4.107}$$

where $\hat{\mathbf{x}}(t)$ is the best linear estimate of $\mathbf{x}(t)$. In other words, the form of the optimal filter is specified by the form of the *message process*. The time-varying gain matrix (also known as *Kalman gain matrix*) $K(t)$ is of the form

$$K(t) = P(t)H^T(t)R^{-1}(t). \tag{4.108}$$

By way of illustrating the error covariance matrix $P(t)$, let y_M be the missile displacement and y_T the target displacement. In particular, let $\hat{\mathbf{x}}_1(t)$ be the best linear estimate of the target displacement, $\hat{\mathbf{x}}_2(t)$ be the best linear estimate of the target velocity, and $\hat{\mathbf{x}}_3(t)$ the best linear estimate of target acceleration. The filter state variables can be formulated as follows:

$$\begin{aligned}
\hat{\mathbf{x}}_1(t) &= \text{best linear estimate of } y_T(t), \\
\hat{\mathbf{x}}_2(t) &= \text{best linear estimate of } v_T(t), \\
\hat{\mathbf{x}}_3(t) &= \text{best linear estimate of } a_T(t).
\end{aligned}$$

For the error in the estimate, that is, $\tilde{\mathbf{x}}(t) = \mathbf{x}(t) - \hat{\mathbf{x}}(t)$, the error covariance matrix takes the form

$$P(t) = E\{(\mathbf{x}(t) - \hat{\mathbf{x}}(t))(\mathbf{x}(t) - \hat{\mathbf{x}}(t))^T\} = \begin{bmatrix} P_{11} & P_{12} & P_{13} \\ P_{21} & P_{22} & P_{23} \\ P_{31} & P_{32} & P_{33} \end{bmatrix}$$

In order to compute the solution for the matrix $P(t)$, initial conditions must be specified for $P_{11}(0)$, $P_{12}(0)$, $P_{13}(0)$, $P_{22}(0)$, $P_{23}(0)$, and $P_{33}(0)$. One of the assumptions

of the Kalman–Bucy filter theory is that the filter output at $t = 0$ is zero. Since the matrix $P(t)$ is the error covariance matrix, the diagonal elements have the following significance:

$$\begin{aligned} P_{11}(t) &= E\{y_T(t) - y_M(t)\}^2, \\ P_{22}(t) &= E\{v_T(t) - \hat{x}_2(t)\}^2, \\ P_{33}(t) &= E\{a_T(t) - \hat{x}_3(t)\}^2. \end{aligned}$$

The mean-square miss distance is given by $P_{11}(T)$, where T is the final or intercept time ($t_{go} = T - t$). At this point it should be pointed out, in general, that the variances of the separate components of $\mathbf{x}$ are along the diagonal:

$$P_{ii} \triangleq E\{(x_i - m_i)^2\},$$

where m_i is the mean value and is given by $m_i = E\{x_i\}$. Therefore, the square root of a variance P_{ii} is termed the *standard deviation* of $\mathbf{x}_i$, and is denoted by σ_i. Thus, the diagonal terms can be expressed as

$$P_{ii} \triangleq \sigma_i^2.$$

(b) Discrete-Time Kalman Filtering

Consider the linear stochastic system given in state-space description [4], [25]:

$$\mathbf{x}(k+1) = A(k)\mathbf{x}(k) + B(k)\mathbf{w}(k), \tag{4.109}$$

$$\mathbf{z}(k) = H(k)\mathbf{x}(k) + \mathbf{v}(k), \tag{4.110}$$

$$\text{with initial state } \mathbf{x}(k) = 0,\ k = 0, 1, 2, \ldots,$$

where $A(k)$, $B(k)$, $H(k)$ are known $n \times n$, $n \times p$, and $q \times n$ constant matrices, respectively, with $1 \leq p, q \leq n$, and k identified as time (i.e., kth instant). Furthermore, $\{\mathbf{w}\}$ and $\{\mathbf{v}\}$ are zero-mean Gaussian white noise sequences with prior statistics [30]

$$\begin{aligned} E\{\mathbf{w}(k)\mathbf{w}^T(k)\} &= Q(k)\delta_{kl}, \\ E\{\mathbf{v}(k)\mathbf{v}^T(k)\} &= R(k)\delta_{kl}, \\ E\{\mathbf{w}(k)\mathbf{v}^T(k)\} &= \mathbf{0}, \\ \forall\, k, l &= 0, 1, \ldots, \\ \delta_{kl} &= \begin{cases} 1 \text{ if } k = l, \\ 0 \text{ if } k \neq l, \end{cases} \end{aligned}$$

where $Q(k)$ and $R(k)$ are known $p \times p$ and $q \times q$ nonnegative and positive symmetric matrices, respectively, independent of k. The vector $\mathbf{z}(k)$ is called, as before, the measurement or observation vector and is of dimension $q \times 1$.

Now let $\hat{\mathbf{x}}(k \mid j)$ be the (optimal) least-squares estimate of $\mathbf{x}(k)$ when all measurements up to the jth sample are available. Then,

for $j = k$, $\hat{\mathbf{x}}(k) = \hat{\mathbf{x}}(k \mid k)$: that is, the estimation process is called a digital *filtering process;*

$j < k, \hat{\mathbf{x}}(k \mid j)$: the process is called *optimal prediction* of $\mathbf{x}$(k);

$j > k, \hat{\mathbf{x}}(k \mid j)$: this is called a *smoothing estimate* of $\mathbf{x}$(k), and the process a *digital smoothing process*.

In order to compute $\hat{\mathbf{x}}(k)$ in real time, the following recursive equations are needed:

$$\hat{\mathbf{x}}(k \mid k-1) = A(k-1)\hat{\mathbf{x}}(k-1), \tag{4.111}$$

$$\hat{\mathbf{x}}(k \mid k) = \hat{\mathbf{x}}(k \mid k-1) + K(k)[\mathbf{z}(k) - H(k)\hat{\mathbf{x}}(k \mid k-1)], \tag{4.112a}$$

or

$$\hat{\mathbf{x}}(k \mid k) = A(k-1)\hat{\mathbf{x}}(k-1) + K(k)[\mathbf{z}(k) - H(k)A(k-1)\hat{\mathbf{x}}(k-1)], \tag{4.112b}$$

$$\hat{\mathbf{x}}(0) = E\{\mathbf{x}(0)\},$$

where $K(k)$ is known as the *Kalman gain* matrix and $E\{\mathbf{x}(0)\}$ is the mean vector of the initial state. Here we will discuss only digital filtering. However, since $\hat{\mathbf{x}}(k) = \hat{\mathbf{x}}(k \mid k)$ is determined by using *all* data $\mathbf{z}(0), \ldots, \mathbf{z}(k)$, the process is not practical for real-time problems for very large values of k, since the need for storage of data and the computational requirements grow with time. Therefore, we will present only the recursive algorithm that gives $\hat{\mathbf{x}}(k) = \hat{\mathbf{x}}(k \mid k)$ from the prediction $\hat{\mathbf{x}}(k \mid k-1)$, and $\hat{\mathbf{x}}(k \mid k-1)$ from the estimate $\hat{\mathbf{x}}(k-1) = \hat{\mathbf{x}}(k-1 \mid k-1)$. Thus, the discrete-time *Kalman filtering algorithm* can be summarized as follows [4], [25]:

Coprocess

$$P(0,0) = Var\{\mathbf{x}(0)\} \quad \text{(given)}, \tag{4.113}$$

$$P(k,k-1) = A(k-1)P(k-1,k-1)A^T(k-1) + B(k-1)Q(k-1)B^T(k-1), \tag{4.114}$$

$$K(k) = P(k,k-1)H^T(k)[H(k)P(k,k-1)H^T(k) + R(k)]^{-1}, \tag{4.115}$$

$$P(k,k) = [I - K(k)H(k)]P(k,k-1), \tag{4.116}$$

Main Process

$$\hat{\mathbf{x}}(0|0) = E\{\mathbf{x}(0)\} \quad \text{(given)}, \tag{4.117}$$

$$\hat{\mathbf{x}}(k \mid k-1) = A(k-1)\hat{\mathbf{x}}(k-1 \mid k-1), \tag{4.118}$$

$$\hat{\mathbf{x}}(k \mid k) = \hat{\mathbf{x}}(k \mid k-1) + K(k)[\mathbf{z}(k) - H(k)\hat{\mathbf{x}}(k \mid k-1)], \tag{4.119}$$

where $P(k)$ is known as the *error covariance matrix*. Note that in the above Kalman filter algorithm, the starting point is the initial estimate $\hat{\mathbf{x}}(0) = \hat{\mathbf{x}}(0|0)$. Since $\hat{\mathbf{x}}(0)$ is an *unbiased* estimate of the initial state $\hat{\mathbf{x}}(0)$, we could use $\hat{\mathbf{x}}(0) = \mathrm{E}\{\hat{\mathbf{x}}(0)\}$, which is

a constant vector. Also, the Kalman gain $K(k)$ must be computed recursively. Note that if we use the Kalman filtering scheme for the linear system given by (4.111) and (4.112) with non-Gaussian noise sequences, the resulting filtering performance can be very unsatisfactory. Hence, in this case, *suboptimal*, or robust, Kalman filtering becomes necessary. We will not treat the suboptimal Kalman filtering here. For more details on this subject, the reader is referred to [3], [4].

Finally, we note that in the Kalman filtering algorithm given above, it is necessary to invert a matrix at every instant to obtain the Kalman gain matrix $K(k)$ (i.e., before prediction–correction can be carried out in the main process (4.117)–(4.119)). The application of linear, time-varying filter theory has resulted in this new method for designing optimal homing-missile guidance systems, which, unlike the classical techniques, helps in achieving the minimum *rms* miss distance that is theoretically attainable. However, before this approach is applied to practical guidance systems, a considerable amount of work must be done by the missile designer. Some of the areas that must be addressed are as follows:

1. Investigation of the tendency of the guidance system to demand more lateral acceleration than the missile is capable of providing. Since the missile is constantly trying to reduce the distance (i.e., error) between itself and the target, it may be desirable to allow the guidance system to drive the missile acceleration to its maximum possible magnitude as opposed to imposing an artificial mathematical constraint on the mean-square value of acceleration.
2. Development of general methods for the determination of the dynamic system (i.e., differential equation) that generates a signal having a specified autocorrelation function from a white noise input. This is of importance in the determination of the F, G, and Q matrices.
3. Study of the instrumentation requirements for this type of guidance system. Since the time-varying multiplier gains are instantaneous functions of the components of the $P(t)$-matrix and the range $r(t)$ (i.e., $r(t) = v_c(T - t)$), they may be determined in-flight by solving the variance equations by the onboard computer. The range along the *LOS* between target and missile, $r(t)$, must then be fed into the missile's computer in order to compute $P(t)$. When this is done, it is not necessary to make estimates of the total time of flight, since T does not enter into computation of multiplier gains. A satisfactory performance may be obtained with a predetermined program of multiplier gains stored in the missile prior to launching.

4.8.3 Optimal Control of Linear Feedback Systems with Quadratic Performance Criteria

The application of optimal linear regulator theory in missile guidance and analysis is, as stated in the introduction, not a new idea. Specifically, there have been investigations dealing with subsystem decomposition, partial state feedback, and the constraining of the time-varying structure of feedback gains. It is well known that the optimal control law of the form $\mathbf{u}^*(t) = -K^*(t)\mathbf{x}(t)$, where the elements of $K^*(t)$ are time-varying

feedback gains, is computed from the solution of a nonlinear matrix Riccati differential equation. The guidance algorithm (or law) that will be developed here is a linear quadratic regulator (*LQR*) (or specifically, a linear quadratic tracker with terminal controller) derived from modern control theory. Designed for implementation in an onboard digital computer, the algorithm will calculate the motor ignition times and the missile steering angles during powered and unpowered flight using full missile state feedback. The current missile state will be provided by a ring laser gyro strapdown inertial navigation system. The algorithm must calculate commands for complex maneuvers, respond to in-flight perturbations, adapt to varying mission requirements, interface with other software subsystems, and fit within the resources of the onboard computer. Real-time implementation of a guidance law requires bridging the gap that exists between theory and flight code. This means solving numerous difficult problems that are not apparent until the missile hardware and software subsystems, together with the operational missions, are well defined.

Consider now the linear dynamical system characterized by the canonical equation

$$\frac{d\mathbf{x}(t)}{dt} = \mathbf{A}\mathbf{x}(t) + \mathbf{B}\mathbf{u}(t), \tag{4.120}$$

$$\begin{gathered}\mathbf{x}_o \triangleq \mathbf{x}(t_0),\\ \mathbf{u}(t) \in U,\\ 0 \leq t \leq T,\end{gathered}$$

where $\mathbf{x}(t)$ is the n-dimensional state vector, $\mathbf{u}(t)$ is the r-dimensional unconstrained control input, $\mathbf{A}$ and $\mathbf{B}$ are constant $n \times n$ and $n \times r$ matrices, respectively, and U is a convex subset of the r-dimensional Euclidean space. Here we will assume that the initial time t_0 is given and that the terminal (or final) time $T\,(T > t_0)$, is also known. It should be noted that the terminal time $T > t_0$ may be a fixed finite number, or alternatively, one may consider the limiting case $T \to \infty$. The essence of the optimal regulator problem is to determine the control law $\mathbf{u}(t)$ on $[t_0, T]$ of a class of piecewise continuous functions that minimizes the quadratic performance index (or cost functional)

$$J(\mathbf{x}_0, t_0, \mathbf{u}(\cdot)) = \frac{1}{2}\mathbf{x}^T(T)\mathbf{S}\mathbf{x}(T) + \frac{1}{2}\int_{t_0}^{T} [\mathbf{x}^T(t)\mathbf{Q}\mathbf{x}(t) + \mathbf{u}^T(t)\mathbf{R}\mathbf{u}(t)]dt, \tag{4.121}$$

where the terminal state $\mathbf{x}(T)$ is unconstrained, $\mathbf{S}$ is a constant positive semidefinite matrix (so as to guarantee a unique minimum), and $\mathbf{Q}$ and $\mathbf{R}$ are constant nonnegative symmetric $n \times n$ and $r \times r$ matrices, respectively. (Note that the matrices $\mathbf{A}$, $\mathbf{B}$, and $\mathbf{Q}$ need not be constant.) Mathematically speaking, the performance index J depends on the entire history $\mathbf{x}(t)$ and $\mathbf{u}(t)$ over $t_0 < t < T$. The performance index defined by (4.121) allows the missile analyst/designer to specify the importance attached to each of the factors that characterize the trajectory of a guided missile. From the point of view of design rationale, the quadratic term $\mathbf{x}^T(t)\mathbf{Q}\mathbf{x}(t)$ in (4.121) is chosen so as to penalize deviations of the regulated state $\mathbf{x}(t)$ from the desired equilibrium condition (or nominal trajectory) $\mathbf{x}(t) \equiv 0$, while the term $\mathbf{u}^T(t)\mathbf{R}\mathbf{u}(t)$ discourages the use of

large control effort. The term $\mathbf{x}^T(t)\mathbf{S}\mathbf{x}(t)$ is a penalty for deviations from the terminal state (e.g., in missile guidance it is desired that this term approach zero, signifying zero miss distance).

The above is a problem of the Bolza type. In the present derivation, we will use the Bellman equation [3], [25]

$$-\left(\frac{\partial J^*}{\partial t}\right) = \min_{u(t)\epsilon\mathcal{U}}\left[L(\mathbf{x}(\mathbf{u},t),\mathbf{u},t) + \left(\frac{\partial J^*}{\partial \mathbf{x}}\right)^T f(\mathbf{x},\mathbf{u},t)\right] \tag{4.122}$$

because it provides a necessary condition for optimality (note that we will use the asterisk to denote optimality). The Bellman equation assumes a system of the form

$$\frac{d\mathbf{x}}{dt} = f(\mathbf{x},\mathbf{u},t) \tag{4.123}$$

starting from an initial state $\mathbf{x}(t_0) = t_0$. Then, one wishes to find an input $\mathbf{u}(t)$, defined over $[t_0, T]$, that minimizes a performance index of the form

$$J = \int_{t_0}^{T} L(\mathbf{x},\mathbf{u},t)dt, \tag{4.124}$$

where the function $L(\mathbf{x},\mathbf{u},t)$ is assumed to be continuous with respect to t. Thus, the Bellman equation for (4.121) is

$$-\frac{\partial J^*}{\partial t} = \left[\frac{1}{2}\mathbf{x}^T(t)\mathbf{Q}(t)\mathbf{x}(t) + \frac{1}{2}\mathbf{u}^{*T}(t)\mathbf{R}(t)\mathbf{u}^*(t) + \left(\frac{\partial J^*}{\partial \mathbf{x}}\right)^T(\mathbf{A}(t)\mathbf{x} + \mathbf{B}(t)\mathbf{u}^*)\right]. \tag{4.125}$$

The boundary condition is

$$\lim_{t\to T} J^*(\mathbf{x},t) = \tfrac{1}{2}\mathbf{x}^T(T)\mathbf{S}\mathbf{x}(T). \tag{4.126}$$

The minimization procedure results in

$$\left.\frac{\partial L}{\partial \mathbf{u}}\right|_{\mathbf{u}=\mathbf{u}^*} + \frac{\partial}{\partial \mathbf{u}}\left[\left(\frac{\partial J^*}{\partial \mathbf{x}}\right)^T(\mathbf{A}(t)\mathbf{x} + \mathbf{B}(t)\mathbf{u})\right]\Bigg|_{\mathbf{u}=\mathbf{u}^*} = 0, \tag{4.127}$$

where L is the integrand in (4.121). This yields

$$\mathbf{u}^*(t) = -\mathbf{R}^{-1}(t)\mathbf{B}^T(t)(\partial J^*/\partial \mathbf{x}). \tag{4.128}$$

If we wish to have a linear feedback control, J^* should be of the quadratic form

$$J^*(\mathbf{x},t) = \tfrac{1}{2}\mathbf{x}^T\mathbf{P}(t)\mathbf{x} \tag{4.129}$$

with $\mathbf{P}(t)$ an $n \times n$ symmetric matrix. Now, substituting (4.128) and (4.129) into the Bellman equation (i.e., (4.122)), we obtain a *matrix Riccati equation* [25]

$$-\frac{d\mathbf{P}(t)}{dt} = -\mathbf{P}(t)\mathbf{B}(t)\mathbf{R}^{-1}(t)\mathbf{B}^T(t)\mathbf{P}(t) + \mathbf{P}(t)\mathbf{A}(t) + \mathbf{A}^T(t)\mathbf{P}(t) + \mathbf{Q}(t) \quad (4.130)$$

satisfying the boundary condition at the terminal time $t = T$,

$$\mathbf{P}(T) = \mathbf{S}. \quad (4.131)$$

The matrix $\mathbf{P}(t)$ can in theory be found by integrating (4.130) *backward* (or *sweep* method) from the final condition (4.131). When $\mathbf{P}(t)$ has been found, since it is symmetric, using (4.128), and (4.129) we obtain [3], [25]

$$\mathbf{u}^*(\mathbf{x}, t) = -\mathbf{R}^{-1}(t)\mathbf{B}^T(t)\mathbf{P}(t)\mathbf{x}(t). \quad (4.132)$$

Thus, there will be a unique absolute minimum of (4.122) only if the matrix Riccati equation, (4.130), has a unique solution. Equation (4.132) can also be written in the form

$$\mathbf{u}^*(\mathbf{x}, t) \triangleq -\mathbf{K}^*(t)\mathbf{x}(t), \quad (4.133)$$

where $\mathbf{K}^*(t)$ is a matrix of feedback gains, also known as control gain. When $T \to \infty$, Kalman has shown that for a linear time-invariant system that is completely controllable and with a performance index that is of the form

$$J = (1/2)\int_{t_0}^{T} (\mathbf{x}^T(\tau)\mathbf{Q}\mathbf{x}(\tau) + \mathbf{u}^T(\tau)\mathbf{R}\mathbf{u}(\tau))d\tau \quad (4.134)$$

with $\mathbf{Q}$ and $\mathbf{R}$ both symmetric positive definite matrices, so that the condition

$$\lim_{T\to\infty}\left(\frac{d\mathbf{P}(t)}{dt}\right) = 0 \quad (4.135)$$

holds, the matrix Riccati equation (4.130) is reduced to a nonlinear matrix algebraic equation of the form

$$-\mathbf{P}\mathbf{B}\mathbf{R}^{-1}\mathbf{B}^T\mathbf{P} + \mathbf{P}\mathbf{A} + \mathbf{A}^T\mathbf{P} + \mathbf{Q} = 0. \quad (4.136)$$

The solution of this equation will yield a constant matrix $\mathbf{P}$, which is the matrix for the optimal feedback function $\mathbf{u}^*(\mathbf{x}, t) = -\mathbf{R}^{-1}\mathbf{B}^T\mathbf{P}\mathbf{x}$. Equation (4.136) is a neat way to indicate the usual relations that must be satisfied by the feedback matrix $\mathbf{K}$. Note that the form $\mathbf{u}^*(\mathbf{x}, t) = -\mathbf{R}^{-1}\mathbf{B}^T\mathbf{P}\mathbf{x}$ indicates that in general all states are to be fed back. This implies that up to the $(n-1)$th derivative of the system, the output must be measured accurately. However, this is usually a difficult undertaking. The solution for $\mathbf{u}^*(t)$, that is, (4.132), has several attractive properties. The most important ones for our application are as follows:

(1) The solutions for $\mathbf{u}^*(\mathbf{x}, t)$ and $\mathbf{P}(t)$ are independent of $\mathbf{x}_o$ and $\mathbf{x}_T$. This is extremely important, because it means that the problem need be solved only once (off-line), and this solution will be valid for all initial and final conditions.
(2) $\mathbf{u}^*(\mathbf{x}, t)$ is a function of the system state $\mathbf{x}(t)$. The fact that $\mathbf{u}^*(\mathbf{x}, t)$ is a feedback control law means that it is less sensitive to noise, external disturbances, and modeling errors. Such a property is called *robustness*.
(3) From (4.133) we note that all the information needed to determine $\mathbf{K}^*(t)$ can be computed off-line and stored in the missile's onboard computer. Furthermore, if $\mathbf{A}$, $\mathbf{B}$, $\mathbf{Q}$, and $\mathbf{R}$ are constant and the final time $T \to \infty$, the matrix $\mathbf{K}$ becomes a constant. However, we must realize that the true missile system is nonlinear. If we use the on-line linearization technique discussed previously, we must compute a new $\mathbf{K}$ for each new value of $\mathbf{A}$, $\mathbf{B}$, $\mathbf{Q}$, and $\mathbf{R}$.

From the above discussion we note that minimizing the performance index J results in the generation of a matrix of feedback gains $\mathbf{K}$ that when used by the *LQR* algorithm optimally translates the mission requirements into missile guidance commands. For example, in the case of a maximum-range missile flight, conserving energy is the dominant factor in the performance index, reflected in guidance commands that minimize induced drag. Furthermore, an in-flight perturbation that causes a departure from the nominal path will be allowed by the guidance system, maneuvers that slow the missile will be avoided, and final miss distance will be constrained. On the other hand, shorter-range flights require staying close to the nominal path, without regard for the wasted energy. This will be achieved by increasing the relative weight of the $\mathbf{Q}$ matrix on the nominal path deviations in the performance index.

As noted earlier, the control system objective, which is an essential element of the optimal control problem formulation, specifies the desired output of the system, defining the particular task to be performed and methods to be used. Typical control system objectives are minimum time, minimum fuel, minimum energy, terminal control, tracking control, and regulation. In practice, the input signals to the system are given by devices that provide limited amount of energy. As a result, the controls generated by these devices are constrained. The control history, which satisfies the control constraints during the interval $[t_0, t_f]$, is termed an admissible or feasible control. If U represents the set of admissible controls, then an admissible control history of u is denoted by $u \in U$. Similarly, the corresponding state history or trajectory is admissible if it satisfies the state constraints, that is, $x \in X$, where X represents the set of admissible states. The controls described above are given below. For more details see [25].

Minimum Time: This entails the transferring of an arbitrary initial state $x(t_0) = x_o$ to a specified target set as fast as possible. For the minimum-time problem the performance measure takes the form

$$J(u) = t_f - t_0 = \int_{t_0}^{t_f} dt, \tag{4.137}$$

where t_f is the first time that $x(t)$ intersects the target set.

Minimum Fuel: This entails the transferring of an arbitrary initial state $x(t_o) = x_o$ to a specified target set in a specified amount of time while minimizing some linear combination of the absolute value of the controls. For the minimum-fuel problem,

$$J(u) = \int_{t_0}^{t_f} \left[\sum_{i=1}^{m} c_i |u_i(t)| \right] dt, \tag{4.138}$$

where c_i is a proportionality constant, $c_i > 0$.

Minimum Energy: This entails the transferring of an arbitrary initial state $x(t_0) = x_o$ to a specified target set in a specified amount of time while minimizing some weighted combination of the squares of the controls. For the minimum-energy problem,

$$J(u) = \int_{t_0}^{t_f} [u^T(t) R u(t)] dt \tag{4.139}$$

which is the norm of the control with weighting positive definite matrix R. A matrix R is positive definite, denoted by $R > 0$, if $y^T R y > 0$ for all $y \neq 0$, and positive semidefinite denoted by $R \geq 0$, if $y^T R y \geq 0$ for all y.

Terminal Control: This entails the minimization of the deviations (weighted if so desired) of the final system state values from some desired values. For the terminal control problem,

$$J(u) = [x(t_f) - d(t_f)]^T H [x(t_f) - d(t_f)], \tag{4.140}$$

where $d(t_f)$ is the desired final value of the states and the weighting matrix H is positive semidefinite (i.e., $H \geq 0$).

Tracking Control: This entails minimization of the deviations (weighted if so desired) of the system state values from some desired values throughout the interval of operation. For the tracking-control problem,

$$J(u) = \int_{t_0}^{t_f} [x(t) - d(t)]^T Q [x(t) - d(t)] dt. \tag{4.141a}$$

For bounded controls;

$$J(u) = \int_{t_0}^{t_f} ([x(t) - d(t)]^T Q [x(t) - d(t)] + u^T(t) R u(t)) dt. \tag{4.141b}$$

For unbounded (unconstrained) controls, the desired state value $d(t)$ is defined throughout the interval $[t_0, t_f]$ while the weighing matrices Q and R (possibly time varying) are $Q \geq 0$ and $R > 0$.

Regulating Control: This is a special case of the tracking control where the desired state values are zero. For the regulating-control problem where the desired state value is zero throughout the interval $[t_0, t_f]$, the performance measure is

$$J(u) = \int_{t_0}^{t_f} [x^T(t)Qx(t) + u^T(t)Ru(t)]dt, \qquad Q \geq 0, \qquad R > 0. \quad (4.142)$$

A general representative mathematical expression for the performance measure of a control system objective covering all the above cases is

$$J(u) = h[x(t_f), t_f] + \int_{t_0}^{t_f} g[x(t), u(t), t]dt, \quad (4.143)$$

where t_0 is the initial time, t_f is the final time, h is a scalar-valued function of terminal time and the states, and g is a scalar-valued function of the states, controls, and time defined in the entire interval $[t_0, t_f]$. The performance measure for a missile control problem is (4.137), or it may take the form

$$J(u) = [x(t_f) - d(t_f)]^T H[x(t_f) - d(t_f)] + \int_{t_0}^{t_f} dt, \quad (4.144)$$

with $d(t_f)$ representing the specified target point. Then in the above objective function (4.144), the first quadratic term indicates the weighted deviations of the final states of the missile from the target (i.e., miss distance), and the second integral indicates the time of flight. The elements of the positive semidefinite weighting matrix H can be selected so as to reflect the relative importance between the two terms ($H = 0$ gives a strict minimal-time optimal control problem).

4.8.4 Optimal Control for Intercept Guidance

Linear quadratic theory is a subset of the general nonlinear optimal control theory. The key elements in the formulation are the same; that is, (1) a dynamical system model, (2) a performance index (or cost functional), and (3) appropriate constraints. The difference in formulation lies in the fact that for linear quadratic theory to be valid, the dynamical system model must be linear, the cost functional must be quadratic in nature, and only a limited set of constraints is allowed. The linearity assumption is the most severe for air-to-air missiles. Nonlinear aerodynamics, nonlinear equations of motion, and nonlinear kinematics are prevalent in air-to-air missiles.

We will now show that the optimal control law that minimizes the terminal miss distance turns out to be the proportional navigation guidance law. To this end, we will follow the works of [3], [4], and [17]. Before we proceed, certain assumptions

are in order. First of all, it will be assumed that the engagement takes place in a plane. Second, we will assume that the target acceleration is zero; that is, $a_T = 0$ (this assumption implies constant target velocity; note this is not true in an actual air-to-air engagement). The last assumption is that the control vector is the missile's inertial acceleration ($\mathbf{u}\Delta\mathbf{a}_M$). In effect, this last assumption says that we have complete and immediate control over all three acceleration components (i.e., a_x, a_y, a_z) of the missile. The missile acceleration component along its centerline equals the thrust minus its axial drag, divided by the missile's instantaneous mass. Here we note that the thrust is usually designed to maximize missile velocity early in the flight so that the time for the target evasive maneuvers is minimized. The nature of the above assumptions will become more obvious as we work a simplified example below.

The control input to be determined is the commanded missile lateral acceleration. Continuous control will be assumed in deriving the guidance laws, and it is desired to minimize the expected mean square of the miss distance subject to a penalty function on the total control energy. Therefore, the performance index to be minimized will be assumed to be given by [19],

$$J = y_d^2(T) + \gamma \int_0^T u_c^2(t)dt, \tag{4.145}$$

where $y_d = y_T - y_M$ is terminal miss distance at the intercept time T, $\gamma(\gamma \geq 0)$ is the weighting on the control effort, and $u_c(t)$ is the commanded control. That is, this equation states that the optimal control consists in minimizing the terminal mean-square miss distance plus the weighted integral-square missile acceleration normal to the line of sight (*LOS*). In general, the missile commanded acceleration normal to the *LOS* is constrained by $|u| \leq u_{\max}$.

In order to illustrate the above theory, consider the following simple two-dimensional intercept case, illustrated in Figure 4.33. Let $\mathbf{R}_M$, $\mathbf{v}_M$, and $\mathbf{a}_M$ be the interceptor missile's position, velocity, and acceleration vectors relative to an inertial reference frame. Furthermore, let $\mathbf{R}_T$, $\mathbf{v}_T$, and $\mathbf{a}_T$ be the target's corresponding position, velocity, and acceleration vectors relative also to the inertial reference frame. Assume now that the time-to-go t_{go} is known and can be computed separately (e.g., as an initial guess, $t_{go} = R_{MT}/v_c$, where v_c is the missile's closing velocity). We will assume t_{go} to be independent of the future control, that is, the missile's corrective lateral acceleration. Moreover, it will be assumed that gravity compensation is used in the missile guidance law to negate the effect of gravity on the missile performance. From Figure 4.33 the closing velocity v_c is defined as the relative velocity measured along the *LOS*. Mathematically, the closing velocity is given by the expression

$$v_c = v_M \cos(\theta_l + \theta_{he} - \lambda) + v_T \cos(\theta_a + \lambda), \tag{4.146}$$

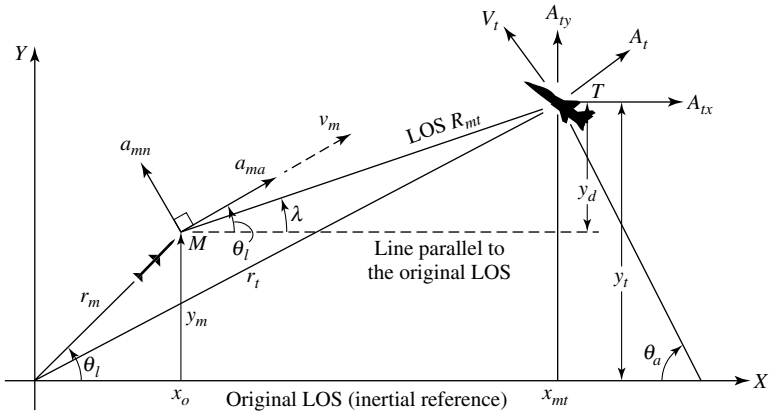

Fig. 4.33. Intercept geometry.

where

$$\begin{aligned}
\theta_l &= \text{the missile lead angle (note: the instantaneous} \\
&\quad \text{lead angle is } (\theta_l - \lambda)), \\
\theta_{he} &= \text{missile heading error,} \\
\theta_a &= \text{target aspect angle,} \\
\lambda &= \text{line of sight (}LOS\text{),} \\
v_M &= \text{missile velocity,} \\
v_T &= \text{target velocity.}
\end{aligned}$$

The missile lead angle and target aspect angle define the orientation of the respective missile and target velocity vectors relative to the original *LOS*. The heading error θ_{he} is the angular error in the collision-course triangle defined at the initiation of the terminal phase. For a given target aspect angle, the *collision-course* missile lead angle is given by

$$\theta_{lc} = \sin^{-1}[(v_T/v_M)\sin\theta_a], \tag{4.147}$$

where $\theta_{he} = \theta_{lc} - \theta_l$. From (4.147) we note that if the orientation and magnitude of the velocity vectors were to remain fixed for the remainder of the terminal phase, the two vehicles would collide. However, it should be pointed out that it is not possible to achieve the collision-course lead angle. For missile systems having a midcourse guidance phase preceding the terminal phase, the heading error tends to be small (i.e., having an *rms* (root mean square) value of a few degrees or less).

Before we develop the optimal guidance law, certain relationships will be defined. Referring to Figure 4.33, we note first of all that the *LOS* angle λ is given by

$$\lambda = \tan^{-1}(y_d/x_{TM}), \tag{4.148}$$

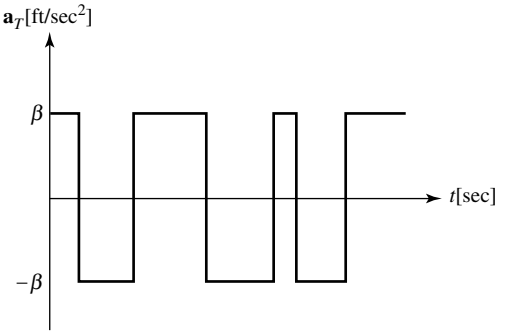

Fig. 4.34. Poisson target acceleration maneuver.

where y_d is the miss distance and x_{TM} is the missile-to-target range measured along the original *LOS*. For modeling purposes, accurate computation of λ is not required during the period it becomes large, thus allowing small-angle approximation, eliminating the nonlinear $\tan^{-1}$ operation. Therefore,

$$\lambda \cong y_d / x_{TM} \quad \text{[radians]}. \tag{4.149}$$

Next, we will consider the target model. It will be assumed that the target may have random changes in its acceleration normal to its velocity vector. The assumed acceleration time history model is a randomly reversing Poisson square wave, as shown in Figure 4.34, with an average of v zero-crossings per second and an *rms* level (or amplitude) of $\pm\beta$ ft/sec^2 (that is, the square wave switches between $\pm\beta$).

The autocorrelation function for the observation times t_1 and t_2 is given by [25]

$$\phi(t_1 - t_2) = \beta^2 \exp(-2v|t_1 - t_2|). \tag{4.150}$$

If $v \to 0$, the target acceleration $\mathbf{a}_T$ approaches a constant level. That is, the mean-squared value of $\mathbf{a}_T$ is β^2. The power spectral density of this Poisson wave, associated with $\mathbf{a}_T$, is

$$\Phi(\omega) = (\beta^2 / 2\pi v)[1/(1 + (\omega/2v)^2]. \tag{4.151}$$

Note that since the Kalman filter is based on minimizing the mean-squared error of the state estimate, it is justifiable to replace the Poisson wave model of target maneuver with one that has the same mean and autocorrelation function, so as to obtain the same quality of estimate with a mathematically more convenient model.

The control input to be determined is the commanded missile lateral (or normal) acceleration. Continuous control will be assumed in developing the guidance laws. To this end, it is desired to minimize the expected square of the miss distance y_d subject to a penalty function on the total control energy. Consequently, the performance index to be minimized is given by (4.152) [3], [17], [19],

$$J = y_d^2(T) + \gamma \int_0^T u_c^2 dt, \tag{4.152}$$

where, as before, $y_d(T)$ and γ are respectively the terminal miss distance at the intercept time T and the weighting on the control effort u_c, subject to

$$\frac{d\mathbf{x}(t)}{dt} = A\mathbf{x}(t) + B\mathbf{u}(t). \tag{4.120}$$

The model of the target maneuver and the system states $y_d, \dot{y}_d, a_T$ can be written in the usual state-space notation

$$\begin{bmatrix} \dot{y}_d \\ \ddot{y}_d \\ \dot{a}_T \end{bmatrix} = \begin{bmatrix} 0 & 1 & 0 \\ 0 & 0 & 1 \\ 0 & 0 & -2v \end{bmatrix} \begin{bmatrix} y_d \\ \dot{y}_d \\ a_T \end{bmatrix} + \begin{bmatrix} 0 \\ -1 \\ 0 \end{bmatrix} u_c + \begin{bmatrix} 0 \\ 0 \\ 2vw \end{bmatrix}, \tag{4.153}$$

where w is a white process noise, and u_c is the corrective missile acceleration. Equation (4.145) corresponds to (4.121) of Section 4.8.3 with

$$S = \begin{bmatrix} 1 & 0 & 0 \\ 0 & 0 & 0 \\ 0 & 0 & 0 \end{bmatrix}, Q = \begin{bmatrix} 0 & 0 & 0 \\ 0 & 0 & 0 \\ 0 & 0 & 0 \end{bmatrix}, R = \gamma,$$

while in (4.120) of Section 4.8.3,

$$B = \begin{bmatrix} 0 \\ -1 \\ 0 \end{bmatrix}, u_c = \frac{d^2 y_M}{dt^2}.$$

From the foregoing equations, the solution for the three control gains is given by [31]

$$C_1 = 3(t_i - t)/[3\gamma + (t_i - t)^3], \tag{4.154a}$$

$$C_2 = (t_i - t)C_1, \tag{4.154b}$$

$$C_3 = (3(t_i - t)/4v^2)\{[\exp(-2v(t_i - t)) + 2v(t_i - t) - 1]/(3\gamma + (t_i - t)^3)\}. \tag{4.154c}$$

The missile corrective acceleration normal to the *LOS* is

$$\frac{d^2 Y_d}{dt^2} = u_c = C_1 y_d + C_2 \dot{y}_d + C_3 a_T. \tag{4.155}$$

Inserting the C-values, making use of

$$\frac{d\lambda}{dt} = 1/v_c t_{go}^2,$$

we have

$$\frac{d^2 y_M}{dt^2} = N' v_c \left(\frac{d\lambda}{dt}\right) + N'\{[\exp(-2vt_{go}) + 2vt_{go} - 1]/4v^2 t_{go}^2\} a_T, \tag{4.156}$$

where $t_{go} = t_i - t$ and the effective navigation ratio N' is

$$N' = 3t_{go}^3/(3\gamma + t_{go}^3). \tag{4.157}$$

From (4.157) we note that for large values of t_{go}, N' is asymptotically 3, and the bracketed term in (4.156) is asymptotically zero. Furthermore, if t_{go} or v goes to zero, the bracketed term becomes 1/2, by double application of L'Hospital's rule. Also, if the constraint on the applied acceleration is removed by setting $\gamma = 0$, then $N' = 3$ for all values of t_{go}. Equation (4.156) indicates that the solution of the optimal control problem, for the simple case of a zero-lag autopilot, is a form of augmented proportional navigation. If γ and v are zero, then the optimal control is pure augmented proportional navigation with $N' = 3$ and an autopilot bias term equal to $N'a_T/2$ (see also Section 4.5).

We will now discuss the above results from a different point of view. Consider the missile/target kinematic relationships in state-space notation:

$$\begin{aligned} \dot{x}_1 &= x_3, \\ \dot{x}_2 &= x_4, \\ \dot{x}_3 &= a_{Tx} - a_{Mx}, \\ \dot{x}_4 &= a_{Ty} - a_{My}, \end{aligned} \tag{4.158}$$

where

$$\begin{aligned} x_1 &= r_{Tx} - r_{Mx}, \\ x_2 &= r_{Ty} - r_{My}, \\ x_3 &= \text{missile/target relative velocity in the } x\text{-direction}, \\ x_4 &= \text{missile/target relative velocity in the } y\text{-direction}. \end{aligned}$$

In Chapter 3 we saw that for aerodynamic control, the airframe must undergo rotations in order to produce the proper angle of attack, which in turn results in normal forces, the magnitude of which are controlled through a feedback loop using accelerometers that measure the actual normal accelerations. However, in the present model under discussion, the rotational and translational inertial properties of the missile have been neglected. Furthermore, we have assumed a perfect control loop. Equation (4.158) can now be written in the form

$$\begin{aligned} \dot{x}_1 &= x_3, \\ \dot{x}_2 &= x_4, \\ \dot{x}_3 &= u_1 = -a_{Mx}, \\ \dot{x}_4 &= u_2 = -a_{My}. \end{aligned} \tag{4.159}$$

These equations can be put in the canonical equation (4.120) as follows:

$$\begin{aligned} \frac{d\mathbf{x}}{dt} &= \mathbf{A}\mathbf{x} + \mathbf{B}\mathbf{u} \\ &= \left[\begin{array}{c|c|c} 0 & | & I \\ - & + & - \\ I & | & 0 \end{array}\right] \mathbf{x} + \begin{bmatrix} 0 \\ I \end{bmatrix} \mathbf{u}, \end{aligned} \tag{4.160}$$

where I is the 2×2 identity matrix. Writing the performance index as in (4.121), we have

$$J = \mathbf{x}^T(T)\mathbf{S}\mathbf{x}(T) + \frac{1}{2}\int_{t_0}^{T} \mathbf{u}^T(t)\mathbf{R}\mathbf{u}(t)dt, \tag{4.161}$$

where

$$\boldsymbol{S} = \begin{bmatrix} I & | & 0 \\ - & + & - \\ 0 & | & 0 \end{bmatrix} \text{ and } \mathbf{R} = \begin{bmatrix} b & | & 0 \\ - & + & - \\ 0 & | & b \end{bmatrix}$$

where b is an element of the positive definite matrix $\mathbf{R}$.

Now the performance index reduces to

$$J = x_1^2(T) + x_2^2(T) + \frac{1}{2}\int_{t_0}^{T} (u_1^2 + u_2^2)dt. \tag{4.162}$$

In Section 4.8.3 we noted in connection with (4.121) that the term $\mathbf{u}^T(t)\mathbf{R}\mathbf{u}(t)$ discourages the use of excessive large control effort. In a similar manner, we can say that if the term b is chosen to be small, the missile designer is willing to expend whatever acceleration is required to minimize the terminal miss distance (assuming, of course, that the missile is capable of producing and sustaining such accelerations). On the other hand, if b is chosen to be large, the magnitude of the acceleration available will be limited in achieving small miss distance. Using (4.132), we have

$$\mathbf{u}^*(\mathbf{x}, t) = -\mathbf{R}^{-1}\mathbf{B}^T\mathbf{P}(t)\mathbf{x}(t) = -(1/b)[0 \vdots \mathrm{I}]\mathbf{P}(t)\mathbf{x}(t), \tag{4.163}$$

and from (4.130),

$$-\frac{d\mathbf{P}(t)}{dt} = \mathbf{P}\begin{bmatrix} 0 & | & I \\ - & + & - \\ 0 & | & 0 \end{bmatrix} + \begin{bmatrix} 0 & | & 0 \\ - & + & - \\ I & | & 0 \end{bmatrix}\mathbf{P} - \mathbf{P}\begin{bmatrix} 0 \\ -- \\ I \end{bmatrix}(1/b)[0 \vdots \mathrm{I}]\boldsymbol{P}. \tag{4.164}$$

Equations (4.163) and (4.164) can be solved analytically yielding the control law as follows:

$$\begin{aligned} u_t &= \begin{bmatrix} u_1(t) \\ \\ u_2(t) \end{bmatrix} \\ &= \begin{bmatrix} -3t_{go}/(3b + t_{go}^3) & 0 & -3t_{go}^2/(3b + t_{go}^3) & 0 \\ 0 & -3t_{go}/(3b + t_{go}^3) & 0 & -3t_{go}^2/(3b + t_{go}^3) \end{bmatrix}, \end{aligned} \tag{4.165}$$

where $t_{go} = T - t = -R/(dR/dt)$ (note that T and t_{go} are design parameters). If we assume $b = 0$, then (4.165) becomes

$$u_1(t) = -(3/t_{go}^2)x_1 - (3/t_{go})x_3, \tag{4.166a}$$

$$u_2(t) = -(3/t_{go}^2)x_2 - (3/t_{go})x_4, \tag{4.166b}$$

where $u_1(t)$ is the control along the x-axis and $u_2(t)$ along the y-axis. Here we note that the assumption $b=0$ implies that we have a missile that can exert unlimited control, as evidenced from (4.166). If we assume that the *LOS* angle is small, then the control $u_1(t)$ is 0, implying that this component is along the thrust. After some algebra, the final guidance law reduces to

$$\mathbf{u}(t)=u_2(t)=3\left(\frac{dR}{dt}\right)\left(\frac{d\lambda}{dt}\right), \tag{4.167}$$

where dR/dt is the missile closing velocity (i.e., v_c). This is the desired result, and it will be recognized as the proportional navigation guidance law with the effective navigation ratio $N'=3$. In practice, navigation ratios of 4 and 5 are commonly used, based on classical control theory analysis.

In general, the missile commanded acceleration normal to the reference *LOS* is constrained by the inequality

$$|u_c|\leq u_{\max}. \tag{4.168}$$

The above discussion can be extended for the case in which one wishes to compute the *minimum time* in intercepting the target. This leads to a nonlinear, two-point boundary value problem (*TPBVP*) in the calculus of variations and Pontryagin's minimum time principle. For more details the reader is referred to [27].

The most important nonlinear characteristic associated with the airframe is acceleration saturation, which occurs when the missile attempts to pull a large angle of attack. As discussed in Chapter 3, it is desirable to avoid a large angle of attack, since the associated drag results in a rapid loss of missile velocity. Moreover, there is also the airframe structural limit, which must not be exceeded. Consequently, it is a common practice by missile designers to limit the commanded lateral acceleration, in order to prevent both angle-of-attack saturation and structural failure. Autopilot command limiting is assumed to be the dominant nonlinear effect, while all other nonlinear characteristics such as actuator angle and angle rate limiting, and aerodynamic nonlinearities are assumed to be secondary. Therefore, the resulting model is simple and generally applicable to a wide range of missile systems, and captures what is known to be a dominant nonlinear system characteristic and an important factor in miss distance performance, that is, lateral acceleration saturation.

We conclude this section by noting that the optimal guidance laws produce the best missile performance, as measured by miss distance, when heavy penalties are imposed in the performance index for nonzero values of predicted miss throughout the flight relative to the penalty on control energy. However, including seeker noise in the simulations can be expected to degrade the performance of these guidance laws due to the resulting high gains. Knowledge of the present (and future) target acceleration for use by the guidance laws generally improves the missile performance. The laws based on a first-order airframe/autopilot response appear to be sensitive to errors in time-to-go estimates. More research is needed in the following areas: (1) a matrix Riccati method to numerically generate guidance gains, which will allow investigation of a broader class of performance index/constraint combinations, (2) the incorporation of very accurate time-to-go estimates in the guidance laws, and

(3) accounting for the variable velocity profile of the missile during its flight. The latter two areas are expected to improve the performance of the laws based on the performance index/constraint combinations, especially those laws based on a first-order airframe/autopilot response.

Finally, the basic requirements for a high-performance missile are:

1. Maneuverability in the sense of fast response to large commands.
2. Stability or recoverability of the missile from the effects not only of large commands, but also from large disturbances.
3. Insensitivity of the large signal behavior with respect to aerodynamic and environmental variation (e.g., large variation in the dynamic pressure q).
4. For a near-optimal design, as many state variables as it is physically possible to measure should be utilized.
5. Simplicity of design.

4.9 End Game

The guidance techniques discussed in Sections 4.2 and 4.4, that is, command guidance, semiactive homing, and ground-aided semiactive guidance, can be simulated based on threat characteristics. For the end game concept, we will consider a surface-to-air missile (*SAM*) interceptor. Regardless of the mission, however, all guided missiles, whether tactical or strategic, carry some kind of warhead. In this section, we will discuss briefly the concept of end game. End game consists of two parts: (1) determination of fuzing, and (2) warhead detonation or explosion effects. The type of ordnance package carried by the missile is determined by the threat it is designed to counter. A typical ordnance package consists of the warhead and possibly a fuze. The purpose of the warhead is to provide or generate the damage mechanisms and the different types of warheads can be described in terms of their configuration and ingredients. In conventional weapons such as projectiles and missiles, the warhead consists of a core or filler and a casing. A fuze package is included when a high-explosive (*HE*) core is employed. Some high-explosive warheads may contain incendiary materials that are ignited upon warhead impact or detonation. High-explosive warheads may be further subdivided into (a) blast or pressure warheads, (b) fragmentation warheads, (c) continuous-rod warheads, and (d) shaped-charge warheads. For example, the *AGM-88C HARM* missile uses a 140-lb class blast/fragmentation warhead to destroy *SAM* systems and their radars, while the *AIM-120C AMRAAM* employs a 40-lb class blast/fragmentation warhead designed for defeating aircraft. Blast fragmentation warheads can maximize the effect on a large area. The counterpart of the conventional warhead for directed energy (*DE*) weapons is the delivered energy distribution (*DED*). It should be mentioned here that *DE* weapons for use in combat situations have drawn considerable interest in the U.S., Russia, and China. Specifically, the effects of radio-frequency weapons, a class of *DE* systems that generate high-power electromagnetic pulses to disrupt or destroy the electronics of an enemy's hardware, have drawn high-level interest in the mentioned countries. While *EMP* effects are generally associated with a nuclear detonation, some *RF* weapons act in a similar way, even if at different frequencies and lesser intensity. Particularly,

ultra-wide-band *RF* weapons try to emulate the effects of a nuclear blast. It should be pointed out that weapons of this type are far from being fielded. One problem, in particular, is packaging the systems, because these devices are large and operationally not suitable.

In Section 4.1 we discussed the various techniques used in guided missile homing and the vulnerability of these missiles to jamming. In particular, the guided missiles (*AAM*, *SAM*, etc.) discussed in this chapter are vulnerable to a new laser-based infrared countermeasures (*IRCM*) system, designed to protect large aircraft (e.g., *C-17 Globemaster*) from heat-seeking missiles. The system has successfully used a laser beam to scan the inner workings (e.g., guidance system) and outer shape of an attacking weapon, precisely identify it, and finally provide the correct jamming signal to lead it off course. As a result, laser technology, in particular the rapidly advance of directed-energy weapons (*DEW*) mentioned earlier in this section, could supplant the traditional air-to-air and antiaircraft missiles. Specifically, the system will use a multiband laser to identify an approaching weapon by the sensor it carries and other characteristics. A closed-loop infrared countermeasures (*CLIRCM*) capability enables the system to assess the characteristics of the incoming missile and then return a complex synchronized jam code that causes the missile to make a high-g turn away from the aircraft (to chase a cluster of false targets), break lock, and miss by a great distance. The system phases the generation of false targets so that the incoming missile tracks away in one direction. Older open-loop, laser-based self-defense systems degrade the guidance system by producing random false targets that make the missile wobble in flight, but not necessarily break lock on the target.

While effective defenses against radar-guided missiles have been developed, the ability to defeat *IR* missiles has not been as effective. Aircraft like the *C-17* produce huge heat signatures. As a result, they are threatened by the hundreds of thousands of cheap, very mobile *SA-14/-16/-18*-type missiles on the world market that could be operated clandestinely within a few miles of an airfield. About half of the aircraft lost in combat over the last two decades have been lost to heat-seeking missiles. Because the U.S. has been so effective in foiling radar-guided missiles, foreign manufacturers are modifying their radar missiles with *EO* and *IR* sensors to avoid detection. The new technology is expected to aid in the development of future self-defense systems for both manned and unmanned aircraft. Today, all the *IR* countermeasure systems are open-loop, which means they only transmit. A closed-loop system, on the other hand, both transmits and receives laser signals. It uses the laser in a radar-like function as the heart of a closed-loop operation capable of defending against a variety of missiles. Like many other new weapons and sensors, a key technology is an onboard processor capable of performing billions of operations per second. Such speed is critical, given a *SAM*'s flight time of a few seconds when the aircraft are at low altitude.

Typically, warheads come in two basic categories: (1) fuzed, and (2) nonfuzed. Fuzed warheads contain a high-explosive charge and are detonated at or in the vicinity of the target. The fuze package consists of a safety and arming device to keep the weapon safe until it is deployed and clear of friendly forces, a detonator to initiate the *HE* charge detonation, a device that senses the presence of a target, known as the target detection device (*TDD*), and a logic circuit that initiates detonation at the proper time.

Fuzing or charge detonation may be accomplished by several methods. The simplest of these methods uses the time- and contact-fuzed warheads normally associated with light *AAA*. Time-fuzed warheads are set to detonate at a predetermined elapsed time after launch. Contact fuzes may detonate the charge either instantaneously upon target contact or after a short delay, depending upon whether the detonation is desired on the external surface or within the target. Proximity fuzing (sometimes referred to as variable-time (*VT*) fuzing) is normally used in conjunction with heavy *AAA* and missile warheads. With proximity fuzing, the warhead is detonated at some distance from the aircraft based upon the fuze logic and the relative location and motion of the target. The fuze *TDD* may be active, semiactive, or passive. The active *TDD* radiates an electromagnetic signal, a portion of which is reflected by the target and detected by the *TDD*. A semiactive *TDD* detects electromagnetic energy reflected from a target that is being illuminated by another source. A passive *TDD* detects electromagnetic energy radiated from the aircraft itself. Some missile warheads can be command detonated by radio signals from the missile controller when the nonterminal tracking and guidance equipment displays indicate sufficient proximity to the target.

Nonfuzed warheads are referred to as *penetrator* warheads or *kinetic energy* penetrators and cause damage only when direct contact is made with the target. Penetrator warheads are optimized to attack deeply buried and hardened targets. The penetrator class of warheads includes (a) armor-piercing projectiles, and (b) armor-piercing incendiary projectiles. Fuzing may be analyzed with a simple glitter* point methodology or in a highly detailed manner including a physically extended target, antenna patterns, fuze processing, and seeker/guidance impacts. As is the case for any design, a simulation method must be used to model the end game. For example, the model must simulate sensor lock-on and tracking, missile aerodynamics, propulsion, guidance, and control. Furthermore, the model must compute the probability of kill (P_k), miss distance, range of intercept, terminal approach angles, and missile time of flight for, say, a specified surface-to-air missile system against a single airborne target. When the missile warhead detonates, the simulation models the distribution and speed of warhead fragments and determines kill probability based on target attitude, vulnerable area, and blast. The simulation model inputs include missile and radar type, target/aircraft signature, target vulnerability, target flight-path, clutter/multipath data, and terrain. Furthermore, the model for target/threat system combinations, as dictated by different scenarios, generates *IR* threat probability of kill data.

Commonly, and as mentioned above, the end game simulation models the target vulnerability used to compute probability of kill and the missile warhead subsystem. However, before the P_k evaluation is made, the warhead detonation point must be determined. This point is found by examining the target's glitter points until one of the glitter points satisfies the criteria for fuzing the warhead. Once this occurs, there is a short delay followed by the warhead explosion and P_k evaluation. Two different methods are available for P_k evaluation: (1) The method by which detailed blast/fragmentation computes the fuzing based on target glitter points and evaluates

*Glitter points are points on a target that are good radar energy reflectors such as sharp corners, wing roots and tips, and engine inlets.

P_k on the basis of fragment and blast effects, and (2) the method based on target vulnerability. The P_k table method, if used, determines fuzing and evaluates the P_k based on miss distance and aspect angle. Target vulnerability points normally consist of the following: pilot, left and right stabilizer controls, left and right engine, left and right fuel tanks, and hydraulic pumps and auxiliary power system. With regard to fuzing, the missiles modeled in the simulation can be armed with either proximity fuzes or contact fuzes (see discussion above). Fuzing of the warhead is accomplished by examining target glitter points for their proximity to the missile warhead fuze cone (i.e., the warhead detonation forms a cone). The glitter points can be located on a coordinate system, for example, the ith glitter points in the target body reference system.

The success of a guided missile depends to a large degree on the successful operation of the fuzing system. In order to achieve the required fuzing capability, the fuzing circuitry must be able to:

1. Operate on the illumination energy for missile guidance.
2. Perform in either the skin-track (i.e., Doppler) or *ECM* mode and maintain this performance under mode-switching conditions.
3. Maintain high-angle accuracy.
4. Prevent premature activation.
5. Discriminate against clutter when operating against targets at low altitudes.
6. Operate without degradation in accuracy or kill probability in the presence of interference from turbines or propellers on the target.
7. Operate in conjunction with other circuits to avoid overkill.
8. Maintain effectiveness for all missile–target approach attitudes.

The fuzing system consists of a special antenna that has a narrow fan-beam angled forward of the plane perpendicular to the longitudinal axis of the antenna and the missile. Two antennas are positioned on opposite sides of the missile to produce an almost flat cone of acceptance with fuzing initiated when the cone intercepts a source of energy. The fuze operates either on illuminator-derived signals reflected from the target or by comparison of signal levels received from jammers aboard the target. Since the strength of the source may vary over wide limits, means must be incorporated into the system to adjust the sensitivity of the detector in order that the energy source will initiate action when it is closest to the peak of the antenna beam. The means chosen consist of a broad-beam antenna system, which detects the source, adjusts the system sensitivity, and provides a signal for a differential detector used to trigger the fuze.

Each antenna is connected to an amplifier to increase the signal level to a value sufficient to operate a differential detector. To maintain signal level, the gain of the amplifiers is controlled by an *AGC* (automatic gain control) loop functioning from the broad-beam antenna signal, which will be larger than the narrow-beam in all directions except when the target is precisely in the narrow beam. This mechanization provides the required relationship between the two antennas over all possible directions. Provisions are usually made to prevent fuzing on direct illuminator radiation into the fuze antennas by using a rear signal of the guidance receiver to convert

the fuze channel signals into a Doppler frequency spectrum. Illuminator leakage into the fuze channels is converted to a zero-frequency Doppler band signal.

Fuzing can also be represented in terms of the active radar fuze power by using a form of the radar range equation and the target radar cross-section (*RCS*). The fuze power received (P_{fz}) in dB is calculated by the following equation:

$$P_{fz} = \sigma_{mgk} - 4R_{mgk} - K_{fuz}, \tag{4.169}$$

where

$$\begin{aligned}
\sigma_{mgk} &= RCS \text{ at target glitter point [dB]},\\
R_{mgk} &= \text{Range from missile to target glitter point [dB]},\\
K_{fuz} &= \text{Fuze sensitivity factor [dB]}.
\end{aligned}$$

The power seen by the fuze is then compared to the power level required. When the fuzing criteria are met, the warhead detonates after a programmed time delay (t_{fd}). For low-altitude *SAM* systems, there is a possibility that the warhead could fuze prematurely off of ground clutter. If the missile flight time t_m is greater than or equal to 3 seconds and the time-to-go t_{go} is less than or equal to 1 second, a check is made to see whether the height of the missile over the terrain is less than a specified altitude. If the missile is lower than this altitude, the warhead fuzes immediately.

Typically, the fragmentation warhead sends out pellets in a circular band centered at the point of explosion (blast point). More specifically, the band would be circular if the missile were motionless at the time of the blast. Since the missile has a velocity of its own, a pellet's total velocity is the vector sum of the missile and the velocity provided by the warhead detonation. Hence, the pellets in different parts of the spray will have different velocities, in both direction and magnitude. The factors considered in determining the total P_k are blast kill and a system reliability factor (P_k computation). Blast kill depends solely upon the location of the blast point relative to the target at the time of the blast. Fragment kill depends upon several factors: (1) look angles from blast point to component, (2) striking velocity, (3) fragment density, and (4) percentage of the component inside the pellet spray. In an actual warhead explosion, some pellets bump into each other, while others break up; nevertheless, it is felt that the above adequately models the situation. Therefore, a number of pellets, say K, are ejected from the blast point. Assume now that each pellet is subject to atmospheric drag proportional to the square of its velocity magnitude and in direct opposition to the velocity. Therefore, the equation of motion for the pellet with position vector $\mathbf{r}_p$ may be expressed as

$$\mathbf{r}_p = \mathbf{r}_p(t)$$

or

$$m\left(\frac{d^2\mathbf{r}_p}{dt^2}\right) = -k|\dot{\mathbf{r}}_p|\dot{\mathbf{r}}_p, \tag{4.170a}$$

where k is the drag term, and is computed from the relation

$$k = C_d \rho_a A_{ref}/2, \tag{4.170b}$$

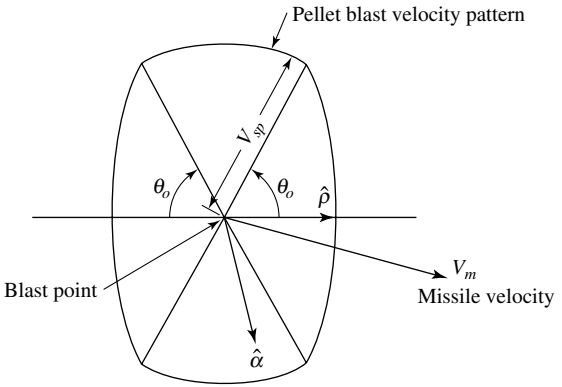

Fig. 4.35. Pellet spray pattern.

where

$$\begin{aligned} A_{ref} &= \text{reference area,} \\ C_d &= \text{coefficient of drag,} \\ \rho_a &= \text{atmospheric density.} \end{aligned}$$

Figure 4.35 illustrates a typical pellet spray pattern. As discussed above, the pellets are ejected from the blast point in a ring-shaped surface* about the missile roll axis with blast velocity V_{sp}. Thus, the effect of the warhead explosion is to impart to a number of pellets the blast velocity V_{sp} in a symmetric surface about the missile roll axis. This symmetric surface is defined by the angle θ_o, as shown in Figure 4.35. Moreover, all the pellets lie on a surface, which expands with time. This surface would be exactly an expanding ring-shaped surface if the missile velocity were zero. Since the missile velocity is not zero, pellets in different parts of the spray do not have the same initial velocity magnitude. Therefore, integrating (4.170a), we find that the pellet has the initial velocity

$$V_o = |\mathbf{V}_o| = V_{sp}\hat{\alpha} + \mathbf{V}_m, \tag{4.171}$$

where

$$\begin{aligned} \hat{\alpha} &= \text{unit vector,} \\ V_{sp} &= \text{pellet blast velocity,} \\ V_m &= \text{missile velocity at the blast point.} \end{aligned}$$

The position vector of the pellet is given by

$$\mathbf{r}_p(t) = S(t)(\mathbf{V}_o / V_o), \tag{4.172}$$

*This surface is obtained by rotating a circular arc about the missile roll axis.

where $S(t)$ is the distance traveled by the pellet (i.e., from the blast point). Mathematically, $S(t)$ is given by the expression

$$S(t) = (m/k)\ln[(V_o k/m)t + 1], \tag{4.173}$$

where m is the pellet mass and $V_o = |\mathbf{V}_o|$. Equation (4.172) is the desired parametric representation of the solution surface. At any time t after blast, $\mathbf{r}_p(t)$, given by (4.172), traces out the solution surface as $\hat{\alpha}$ traces out the unit sphere.

From (4.172) and (4.173) we obtain the pellet velocity vector:

$$\frac{d\mathbf{r}_p(t)}{dt} = \mathbf{V}_p(t)$$

or

$$\mathbf{V}_p(t) = (\mathbf{V}_o/V_o)\left(\frac{dS(t)}{dt}\right) = V_o/[(V_o k/m)t + 1]. \tag{4.174}$$

There are several models used to evaluate and/or assess the performance of end game. One of these models is the enhanced surface-to-air missile simulation (*ESAMS*). The *ESAMS* model is used to simulate the interaction between a single airborne target and a specified *SAM* fired from a designated location. The model simulates sensor lock-on and tracking, missile aerodynamics, propulsion, guidance, and control. More specifically, *ESAMS* computes the probability of kill, miss distance, range of intercept, terminal approach angles, and missile time of flight for a specified *SAM* system against a single airborne target. The postlaunch flyout in *ESAMS* is modeled in *5-DOF*, with boost/sustain/glide phases simulated if the threat has such capability. *ESAMS* inputs include missile and radar type, target/aircraft signature, target vulnerability, target flight path, multipath/clutter data, and terrain.

It was mentioned earlier that blast fragmentation warheads could maximize the effect on a large area. However, one must also consider *mission-responsive ordnance*. Mission-responsive ordnance is an important step in using advanced precision to avoid collateral damage. It can be described as follows:

Mission-Responsive Ordnance: Mission-responsive ordnance refers to weapons that change their blast and fragmentation pattern depending on the target. Computer-controlled microminituarized detonators integrated into the explosive material can control its timing, magnitude, shape, and lethal area. The mission-responsive ordnance concept makes a single relatively small warhead capable of attacking a very wide range of targets, such as a fuse box in an office building, a tank on a city street, or an entire section of a building. The flexibility of mission-responsive ordnance allows explosives to be tailored for constrained environments and may mean fewer weapons in inventory.

Some other types of warheads are the *particle beam* and *nuclear* warheads.

Particle Beam: The warhead descriptors for the particle beam weapon are the particle type (i.e., charge and mass) and the particle velocity (i.e., potential). These two parameters define the kinetic energy, and thus the ionizing ability of the particles. A third important factor is the particle density in the beam. Therefore, accelerated particles are merely a directed-energy form of radiation.

Table 4.6. Nuclear Warheads

Warhead	Nuclear Missile
W-56	Minuteman *II ICBM*
W-62	Minuteman *III ICBM* (Mk 12)
W-70	Lance *SRBM*
W-76	Trident *C-4 SLBM*
W-78	Minuteman *III ICBM* (Mk 12A)
W-80	Air Launched Cruise Missile *AGM-86B*
W-87	Peacekeeper *ICBM*
W-88	Trident *D-5 SLBM*

Nuclear Warheads: These warheads are of the thermonuclear type or the *W-70* enhanced radiation (neutron bomb). Table 4.6 lists some of the nuclear warheads and the missile system used.

The older warhead, the *W53*, was a high-yield thermonuclear warhead carried on a *Titan II ICBM* (see also Appendix F-2, Table F-7). A megaton-class weapon, it was stockpiled by the U.S. from 1962 until 1987. One of the warheads that is attracting attention is the certifiable *W88* deployed on the Navy's *Trident* submarine-launched ballistic missiles.

Next, we will discuss briefly the concept of *probability of kill*. The probability of kill, P_k, is theoretically the limit of the number of times during a radar missile system engagement against an enemy target that the target is destroyed, divided by the number of missiles fired at the target as the number of fired missiles is increased to infinity. In order to determine P_k in a practical situation, firing a large number of missiles under a controlled test situation usually produces a sufficient accuracy. If the killing of a target can occur in S different ways, and can fail in F different ways, where all these ways are equally likely, then P_k for a single missile shot can be expressed mathematically as

$$P_k = S/(S+F), \tag{4.175a}$$

and the probability of the single missile shot failing as

$$P_f = F/(S+F). \tag{4.175b}$$

Therefore,

$$P_k + P_f = 1, \tag{4.176a}$$

$$P_k = 1 - P_f, \tag{4.176b}$$

and

$$P_f = 1 - P_k. \tag{4.176c}$$

In the situation where many missiles are fired at a single target, each having a kill probability of P_k, the cumulative fail probability, P_{fcum}, is

$$P_{fcum} = (1 - P_k)^n, \tag{4.177a}$$

where n is the number of missiles fired. The cumulative kill probability, P_{kcum}, is then

$$P_{kcum} = 1 - (1 - P_k)^n. \tag{4.177b}$$

In order to get a feeling of the above concepts, consider a missile with a single-shot kill probability of 0.7. Then for a salvo of two missiles the cumulative kill probability can be calculated as follows:

$$P_{kcum} = 1 - (1 - 0.7)^2 = 0.91.$$

For a salvo of three missiles (i.e., $n = 3$), the $P_{kcum} = 0.973$; and so on.

For the case of fragments or pellets, the cumulative probability that at least one fragment or pellet has hit the target can be calculated by the expression

$$P_{cum} = 1 - \prod_{i=1}^{n} (1 - P_{Hi}), \tag{4.178}$$

where P_{Hi} is the ith pellet or fragment hit probability and n is the number of pellets. For instance, in *AAA* cases, the probability of a projectile hitting the target has many interrelated factors, including the following: (1) aim errors, (2) ballistic dispersion, (3) target size, and (4) relative position of the target and projectile. On the other hand, the probability that an aircraft will be killed by a single exposure to the burst of a specific internally detonated round, given a particular set of encounter conditions, will now be examined. For a specific warhead and set of encounter conditions, P_{ke} can be obtained by means of the expression

$$P_{ke} = 1 - \exp(-E_k) = 1 - \exp(-pA_v), \tag{4.179}$$

where

$$\begin{aligned} E_k &= \text{the expected number of lethal hits,} \\ A_v &= \text{the aircraft vulnerable area at aspect} \\ &\quad \text{under consideration,} \\ P &= \text{the average number of fragments} \\ &\quad \text{per unit area incident on } A_v. \end{aligned}$$

Figure 4.36 illustrates a possible endgame scenario. In particular, the figure demonstrates the interaction between an airborne target and *SAM* air defense system, and provides a one-on-one framework in which to evaluate air vehicle survivability and tactics optimization. The probability of kill can be enhanced to include probability of kill due to blast and probability of kill due to fragments.

The single-shot kill probability P_k for gun projectiles and guided missiles can also be expressed in terms of a two-dimensional equation in the intercept plane as

$$P_k = \int_{-\infty}^{\infty} \int_{-\infty}^{\infty} \rho(x, y) P_f(x, y) V(x, y) dx\, dy, \tag{4.180}$$

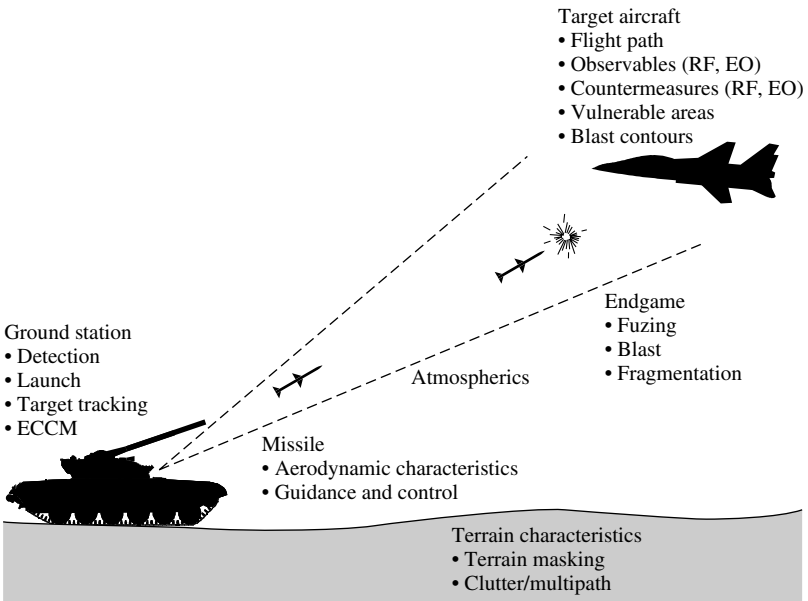

Fig. 4.36. Interaction between an airborne target and a *SAM* air defense system.

where

$$\begin{aligned}
\rho(x, y) &= \text{the miss distance} \\
V(x, y) &= \text{kill function that defines the probability that} \\
&\quad \text{the target is killed due to a propagator (i.e., missile)} \\
&\quad \text{whose trajectory intersects the intercept plane} \\
&\quad \text{at } x, y, \\
P_f(x, y) &= \text{probability of fuzing.}
\end{aligned}$$

In typical tactical homing missile cases, the single-shot kill probability is not a function of range, because as long as all parts of the radar missile system are operating within their designed dynamic range, the distance from the missile launch site to the target is unimportant. In the command guidance or gunfire situation this is not the case, so that the single-shot probability is a function of target range, and the cumulative P_k equations must be modified accordingly. In the actual case, P_{kcum} can be only approximated by the above mathematics because the shots of a salvo are not mutually independent. Each shot uses the same radar information, computer, launcher, etc. Also, the first missile may not kill the target but only damage it and therefore would not be classified as a success. However, the killing job for the succeeding missiles is made easier. The P_k of a radar missile system is dependent on many factors in the chain of events that occur from target detection to interception.

References

1. Becker, K.: *Closed-Form Solution of Pure Proportional Navigation, IEEE Transactions on Aerospace and Electronic Systems*, Vol. 26, No. 3, May 1990, pp. 526–533.
2. Blakelock, J.H.: *Automatic Control of Aircraft and Missiles*, John Wiley & Sons, Inc., New York, NY, second edition, 1991.
3. Bryson, A.E. Jr. and Ho, Y.C.: *Applied Optimal Control*, Revised Printing, Hemisphere Publishing Corporation, A Halsted Press Book, Washington, D.C., 1975.
4. Chui, C.K. and Chen G.: *Kalman Filtering with Real-Time Applications*, third edition, Springer-Verlag, Berlin, New York, NY, 1999.
5. Garber, V.: *Optimum Intercept Laws for Accelerating Targets, AIAA Journal*, Vol. 6, No. 11, November 1968.
6. Garnell, P.: *Guided Weapon Control Systems*, second edition, Pergamon Press, Oxford, New York, NY, 1980.
7. Ghose, D.: *On the Generalization of True Proportional Navigation, IEEE Transactions on Aerospace and Electronic Systems*, Vol. 30, No. 2, pp. 545–555.
8. Guelman, M.: *Proportional Navigation with a Maneuvering Target, IEEE Transactions on Aerospace and Electronic Systems*, Vol. 8, No. 3, May 1972, pp. 364–371.
9. Guelman, M.: *The Closed Form Solution of True Proportional Navigation, IEEE Transactions on Aerospace and Electronic Systems*, Vol. 12, No. 4, July 1976, pp. 472–482.
10. Ha, I.J., Hur, J.S., Ko, M.S., and Song, T.L.: *Performance Analysis of PNG Laws for Randomly Maneuvering Targets, IEEE Transactions on Aerospace and Electronic Systems*, Vol. 26, No. 5, September 1990, pp. 713–721.
11. James, J.P.: *Homing Guidance*, A-62-1732.3-68, Aerospace Corporation, September 14, 1962.
12. Kim, B.S., Lee, J.G., and Han, H.S.: *Biased PNG Law Impact with Angular Constraint, IEEE Transactions on Aerospace and Electronic Systems*, Vol. 34, No. 1, January 1998, pp. 277–288.
13. Kumar, R.R., Seywald, H., Cliff, E.M., and Kelley, H.T.: *Three-Dimensional Air-to-Air Missile Trajectory Shaping, Journal of Guidance, Control, and Dynamics*, Vol. 18, No. 3, May–June 1995, pp. 449–464.
14. Lauer, T.M. and Llanso, S.L.: *Encyclopedia of Modern U.S. Military Weapons*, edited by W.J. Boyne, Berkley Books, New York, NY, 1995.
15. Lee, R.G., Garland-Collins, T.K., Johnson, D.E., Archer, E., Sparkes, C., Moss, G.M., and Mowat, A.W.: *Guided Weapons*, third edition, Brassey's London, Washington, 1998.
16. Lee, G.T. and Lee, J.G.: *Improved Command to Line-of-Sight for Homing Guidance, IEEE Transactions on Aerospace and Electronic Systems*, Vol. 31, No. 1, January 1995, pp. 506–510.
17. Lin, C.F.: *Modern Navigation, Guidance, and Control Processing*, Vol. II, Prentice Hall, Englewood Cliffs, New Jersey, 1991.
18. Locke, A.S.: *Guidance*, D. Van Nostrand Company, Princeton, New Jersey, 1956.
19. Massoumnia, M.A.: *Optimal Midcourse Guidance Law for Fixed-Interval Propulsive Maneuvers, Journal of Guidance, Control, and Dynamics*, Vol. 18, No. 3, May–June 1995, pp. 465–470.
20. Mehrotra, K. and Mahapatra, P.R.: *A Jerk Model for Tracking Highly Maneuvering Targets, IEEE Transactions on Aerospace and Electronic Systems*, Vol. 33, No. 4, October 1997, pp. 1094–1105.
21. Oh, J.H. and Ha, I.J.: *Capturability of the 3-Dimensional Pure PNG Laws, IEEE Transactions on Aerospace and Electronic Systems*, Vol. 35, No. 2, April 1999, pp. 491–503.

22. Shinar, J., Rotszein, Y., and Bezner, E.: *Analysis of Three-Dimensional Optimal Evasion with Linearized Kinematics, Journal of Guidance and Control*, September–October 1979, pp. 353–360.
23. Shukla, U.S. and Mahapatra, P.R.: *A Generalized Linear Solution of Proportional Navigation, IEEE Transactions on Aerospace and Electronic Systems*, Vol. AES-24, No. 3, May 1988, pp. 231–238.
24. Shukla, U.S. and Mahapatra, P.R.: *Optimization of Biased Proportional Navigation, IEEE Transactions on Aerospace and Electronic Systems*, Vol. AES-25, No. 1, January 1989, pp. 73–80.
25. Siouris, G. M.: *An Engineering Approach to Optimal Control and Estimation Theory*, John Wiley & Sons, Inc., New York, NY, 1996.
26. Siouris, G.M.: *Comparison Between Proportional and Augmented Proportional Navigation, Nachrichtentechnische Zeitschrift* (*NTZ*-Communications Journal), 27. Jahrgang, Heft 7, July 1974, pp. 278–280.
27. Siouris, G.M. and Leros, A.P.: *Minimum-Time Intercept Guidance for Tactical Missiles, Journal of Control-Theory and Advanced Technology* (C-TAT), Vol. 4, No. 2, published by the MITA Press, Tokyo, Japan, June 1988, pp. 251–263.
28. Song, T.L.: *Target Adaptive Guidance for Passive Homing Missiles, IEEE Transactions on Aerospace and Electronic Systems*, Vol. 33, No. 1, January 1997, pp. 312–315.
29. Song, T.L. and Um, T.Y.: *CLOS + IRTH Composite Guidance, IEEE Transactions on Aerospace and Electronic Systems*, Vol. 33, No. 4, October 1997, pp. 1339–1344.
30. Warren, R.S., Price, C.F., Gelb, A., and Vander Velde, W.E.: *Direct Statistical Evaluation of Nonlinear Guidance Systems*, AIAA Guidance and Control Conference, Key Biscayne, FL, August 20–22, 1973, AIAA Paper No.73-836.
31. Willems, G.: *Optimal Controllers for Homing Missiles*, Report No. RE-TR-68-15, U.S. Army Missile Command, Redstone Arsenal, Alabama, September 1968.
32. Yang, C.D. and Yang, C.C.: *Analytical Solution of 3D Realistic True Proportional Navigation, Journal of Guidance, Control, and Dynamics*, Vol. 19, No. 3, May–June 1996.
33. Yang, C.D., Yeh, F.B., and Chen, J.H.: *The Closed Form Solution of Generalized Proportional Navigation, Journal of Guidance, Control and Dynamics*, Vol. 10, No. 2, March–April 1987, pp. 216–218.
34. Yang, C.D., Yeh, F.B., and Hsiao, F.B.: *Generalized Guidance Law for Homing Missiles, IEEE Transactions on Aerospace and Electronic Systems*, Vol. AES-25, No. 2, March 1989, pp. 197–212.
35. Zarchan, P.: *Tactical and Strategic Missile Guidance*, third edition, Vol. 157, Progress in Astronautics and Aeronautics, American Institute of Aeronautics and Astronautics, Inc., Washington, D.C., 1998.

This page intentionally left blank

5

Weapon Delivery Systems

5.1 Introduction

The primary purpose of this chapter is to provide a general overview of weapon delivery systems and estimates of combat delivery accuracy for computing effectiveness of air-to-ground (or surface) weapons delivered from fixed-wing aircraft. Weapon delivery includes bombing, air-to-air and air-to-ground (or surface) gunnery, and missile launching. More specifically, weapon delivery is divided into three phases and includes the following: (a) target acquisition, (b) maneuvering to weapon release, and (c) postrelease egress maneuver. The weapon delivery function can improve both survivability and delivery accuracy. Although conventional, wings-level dive bomb delivery can achieve acceptable accuracy (especially when assisted by a dive-toss or other automatic bomb release system), an aircraft is vulnerable during this phase. Survivability can be enhanced without sacrificing accuracy by flying a maneuvering delivery profile in which the bomb is released from a continuous turn. The delivery maneuvers can be flown manually, using steering cues generated by the system, or automatically, with the system controlling the aircraft.

The performance and flexibility of the maneuvering weapon delivery system makes it ideal for use with advanced weapons. For example, the tactical flight management (*TFM*) system will set up toss deliveries for standoff weapons and provide controlled postrelease maneuvering to allow target designation for laser-guided bombs. It also allows delivery of multiple bombs in a string along a specific ground track not aligned with the release heading. This feature is needed for tossing multiple dispenser munitions against linear targets, such as vehicle columns or runways.

In order to achieve acceptable accuracy, especially against small mobile targets, target position must be known precisely. Medium-range sensors such as high-resolution *SAR* and imaging *FLIR* can be used to update target position, but they must have a clear line of sight to the target. When terrain-following penetration is used, an acquisition maneuver must be flown to get the sensor above the intervening terrain. This is a dangerous maneuver because the aircraft is exposed during the pop-up. Note

that the *TFM* can compute and fly a continuously accelerating acquisition maneuver to maximize survivability.

Present-day state-of-the-art avionics technology has enhanced the air-to-ground and air-to-air (*AA*) weapon delivery capabilities of fighter and/or attack aircraft. Modern fighter avionics systems support all-weather air-to-ground attack and air-to-air combat missions. The weapon delivery system enables the pilot to deliver guided weapons, unguided bombs, laser-guided bombs and cluster bombs over a large delivery envelope with a high degree of accuracy. The system utilizes a digital computer for computation of the automatic release signal in conjunction with an inertial navigation system (*INS*); in modern fighter aircraft, a global positioning system (*GPS*) user set is also used, which is integrated with the *INS* for enhanced accuracy. Certain military missions, such as tactical and strategic intelligence, require precise navigation in order to provide real-time ground target positioning. Sensor control for pointing and mode management can be done only in conjunction with very tight and accurate navigation control, including velocity control for image motion compensation.

The weapon delivery system provides the capability to attack either preplanned or in-flight designated surface targets. If in-flight designation of the target is desired, a radar must be available for interfacing with the digital computer to provide the relative position of the target. Moreover, the weapon delivery system permits the pilot to attack a target at any dive angle, velocity, and attitude within the delivery envelopes of most attack aircraft. The heart of the weapon delivery design lies in the ballistic trajectory computation, which takes into account ballistic corrections for aircraft velocity, position, winds, Coriolis, gravitational variations, bomb separation effects, and centroid offset for multiple and ripple bombing. The accuracy of the predicted impact point of the bomb is ensured by providing extremely accurate position and velocity estimates from a *GPS* user set, if available. In a highly dynamic vehicle environment such as a fighter aircraft (e.g., *F-15*, *F-16*, *F-18*, and *F-22**), the *GPS* user set is augmented by an *INS* in order to maintain weapon delivery accuracy during high-acceleration maneuvers. When the predicted impact point approaches the target position, automatic ordnance release occurs under computer control.

5.2 Definitions and Acronyms Used in Weapon Delivery

Before we discuss the problem of weapon delivery, it is appropriate to define at this point some of the most common terms and acronyms that the reader will encounter in dealing with the concept of weapon delivery.

*On September 17, 2002, the *F-22 Raptor* was redesignated as *F/A-22 Raptor*, using the *A* (or attack) prefix to emphasize the multiple roles of the *Raptor*. The change is meant to more accurately reflect the aircraft's multimission roles and capabilities in contemporary strategic environments.

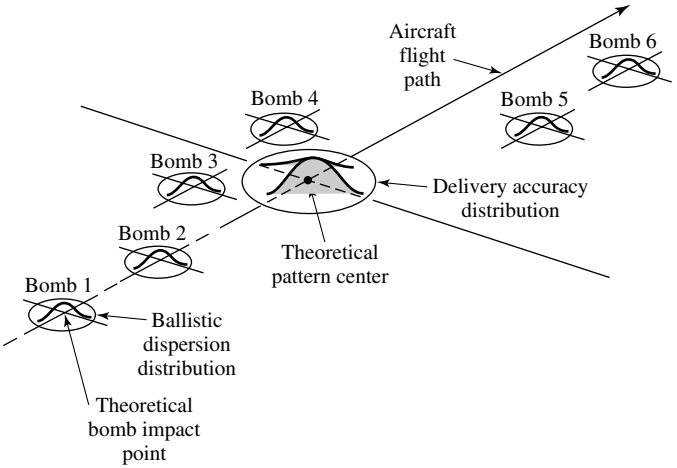

Fig. 5.1. Ballistic dispersion.

5.2.1 Definitions

Aim Point: A preselected position on the target at which a *HEL* (high energy laser) beam is to be directed.

Aiming Error: Aiming error is a measure of the pilot's ability to place the pipper on the *DMPI* (desired mean point of impact). In other words, it is the variation between the actual aiming point and the *DMPI*. Aiming errors are used to represent those errors involved in pointing or positioning a device such as a weapon or weapon platform at a desired point as computed from a fire control system.

Ballistic Dispersion: Ballistic dispersion is the round-to-round (weapon-to-weapon) variation in the flight path of a weapon, which is attributed to several random errors, notably, manufacturing tolerances or accidental misalignments occurring during assembly and handling of the weapon. As illustrated in Figure 5.1, each weapon in the stick has a theoretical impact point based on where the weapon was located on the aircraft, the type of rack, the position on the rack if the rack was a multiple-carriage-type rack, the sequencing of weapons off the aircraft, the interval between weapons, release conditions (e.g., angle, altitude, airspeed, and g's), and any peculiar airflow effects as the weapon is ejected off the aircraft. Figure 5.1 illustrates a stick of six bombs, with the theoretical bomb impact points for each of the six bombs and a ballistic dispersion distribution centered at each of the points. Centered on each theoretical impact point is a ballistic dispersion distribution. The actual bomb impact should occur somewhere near the theoretical impact point; the probability that the actual bomb impact occurs in any given area is a function of the shape and spread of this distribution. Ballistic dispersion is a characteristic of the weapon type.

Barrage Fire: Fire that is designed to fill a volume of space or area rather than aimed specifically at a given target. Barrage fire has been used by defenses

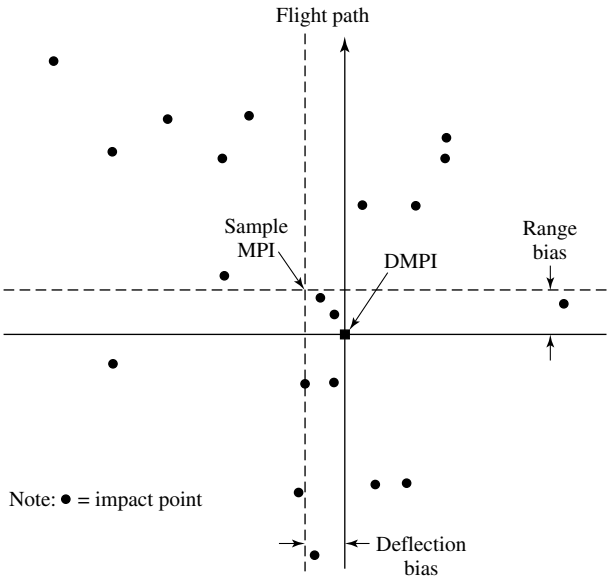

Fig. 5.2. Sample bias.

when (1) insufficient time is available to establish a tracking solution, (2) aircraft penetration tactics or *ECM* environment prohibits use of "fire-while-track" mode, or (3) the penetrating aircraft flight path or penetration corridor is known such that the defense can optimize its effectiveness by massing threats in a localized area.

Bias: Bias is the distance from the target to the middle of a sample of independent weapon impacts. This bias may be in range (along the direction of aircraft travel) and/or in deflection (across the direction of aircraft travel). Usually, bias occurs in the range direction and is found during testing of operational flight programs (*FOP*s), that is, computer software found in embedded aircraft computers. Subsequent to testing, the *FOP*s are usually modified to remove, or at least minimize the impact of, any significant biases. In this chapter, it will be assumed that in the weapon delivery accuracy estimates the biases have been removed. Figure 5.2 shows a typical bias.

Bivariate Normal Distribution: A two-dimensional distribution where the distribution in one of the directions is different from the distribution in the other directions is called a bivariate normal distribution. For delivery accuracy purposes, the two directions are range (i.e., the direction along the track of the aircraft at the time of release) and deflection (i.e., the direction perpendicular to the track).

Bombing Accuracy: Bombing accuracy is the combination of delivery accuracy and ballistic dispersion. The most common statistical measure for bombing accuracy is the *circular error probable* (*CEP*), which is the radius of a circle that should contain one-half (or 50%) of the total number of bomb impacts in a sample. Note that the *CEP* is applicable only when the distribution is equally proportioned in range and

deflection, which is usually not the case when working in the ground plane. The plane where the distribution is equally proportioned is in a plane perpendicular to the bomb trajectory at the time of impact. For most cases, especially level or dive deliveries, the plane perpendicular to the line of sight (i.e., from the aircraft at the time of release to the center of impact) is an adequate approximation to the flight path normal plane to ensure that the distribution is equally proportioned. The ballistic dispersion distribution is circular in roughly the same plane. Now, if it is ascertained that both the delivery accuracy and ballistic dispersion distributions are circular in the same plane, their standard deviations can be used to determine the standard deviation for delivery accuracy σ_D. Mathematically,

$$\sigma_D = (\sigma_A^2 - \sigma_B^2)^{1/2},$$

where

$$\sigma_A = \text{standard deviation for bombing accuracy distribution,}$$
$$\sigma_B = \text{standard deviation for ballistic dispersion.}$$

For some weapons, such as unretarded general-purpose bombs, ballistic dispersion is relatively small; therefore, bombing accuracy and delivery accuracy are nearly the same.

Circular Error Probable: As mentioned above, *CEP* is a measure of delivery accuracy and bombing accuracy. Its value is equal to the radius of a circle that is centered on the target (i.e., aimpoint) and that should contain one-half of the impact points in a sample. *CEP* is associated with the circular normal distribution, where *CEP* is equal to 1.1774 times the standard deviation σ of the distribution ($CEP = 1.1774\sigma$) [7]. In terms of the *DEP* (deflection error probable) and *REP* (range error probable), the *CEP* can be computed by the relation (see also (5.17))

$$CEP = 0.875(REP + DEP).$$

Figure 5.3 illustrates the *CEP*.

Circular Normal Distribution: Circular normal distribution is a special case of the bivariate normal distribution (range and deflection component distributions are equal).

Deflection Error Probable (*DEP*): *DEP* is one of two measures for delivery accuracy used when the distribution is bivariate normal (i.e., when the circular normal distribution cannot be used). Its value is equal to one-half of the distance between two lines that are equidistant from the target (aimpoint) and parallel to the aircraft track at time of release, and which should contain one-half of the impact points in a sample. Thus, $DEP = 0.6745\sigma_D$ (see also Section 5.7.3). Figure 5.4 illustrates the *DEP*.

Delivery Accuracy: Delivery accuracy is the ability of a weapon system to place the theoretical center of a stick* of weapons on a designated target/aimpoint on the

*A number of bombs arranged for release from a bombing plane in a series across a target (Webster's New Collegiate Dictionary, G. & C. Merriam Company, 1997).

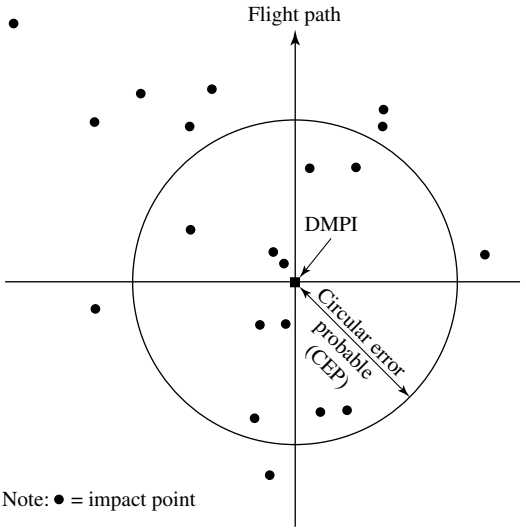

Fig. 5.3. Sample *CEP*.

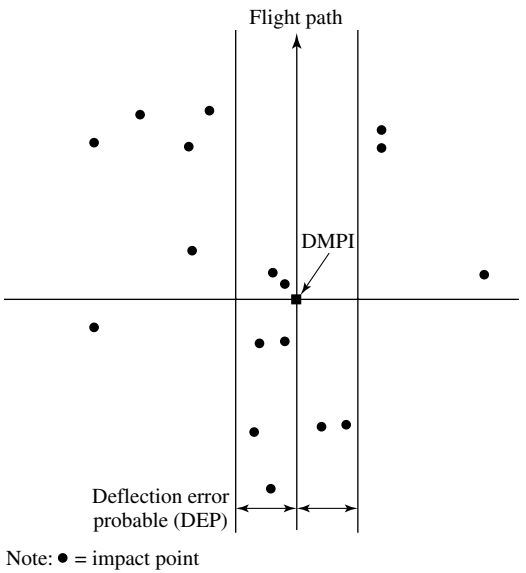

Fig. 5.4. Sample *DEP*.

ground. Also, delivery accuracy can be defined as a measure of the aircrew's ability to put the weapon-impact-pattern center on the target when ballistic dispersion is not a factor. This is expressed in terms of the standard deviation in the actual points of impact stemming from the combined errors in sight alignments, dive

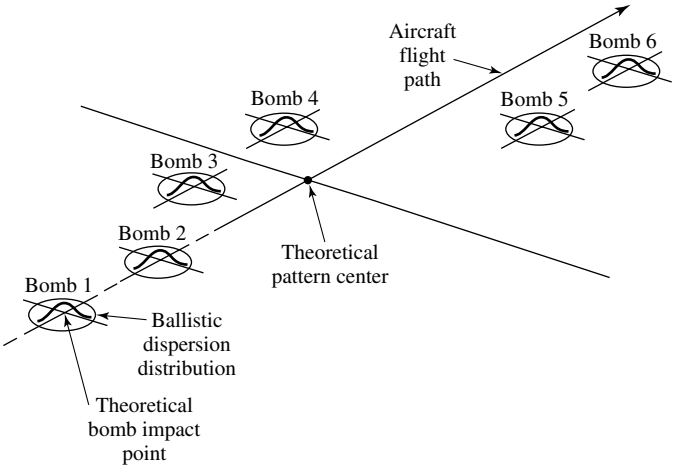

Fig. 5.5. Delivery accuracy.

angle, airspeed, altitude, and aircraft attitude at release. It is important to note that ballistic dispersion affecting each of the weapons in the stick is excluded as one of the factors affecting weapon accuracy. Effectiveness computations consider delivery accuracy and ballistic dispersion as two separate entities. Therefore, in order to fully understand the meaning of delivery accuracy, it is necessary to think in terms of a generic weapons delivery, i.e., a stick of bombs. For example, a drop of a single bomb or the firing of a single missile can be thought of as a stick of one. Figure 5.5 shows the concept of delivery accuracy.

Note that Figure 5.5 is similar to Figure 5.1; also, note that in Figure 5.5 the delivery accuracy distribution is centered.

Desired Mean Point of Impact (*DMPI*): *DMPI* is the planned, or intended, aimpoint used by the pilot during a weapon delivery.

Dive Toss: A weapon-delivery maneuver in which the aircraft is dived to a predetermined altitude point in space, pulled up, and the weapon released in such a way that it is tossed onto the target.

Doppler/Doppler Effect: A frequency shift due to velocity on a reflected signal. Used for velocity measurement and moving-target detection/tracking.

Firing/Launch Envelope: A locus of points that represent the position of an aircraft target when a missile or other projectile can be fired/launched with the expectation of achieving an intercept on the aircraft. When considering ground-based (or sea-based) threats, the launch envelope is generally depicted relative to the location of the threat. Conversely, the launch envelope is normally shown relative to the target aircraft in the consideration of airborne threats. This envelope considers the tracking time required before a launch can feasibly be accomplished.

Gravity Drop: A measure of the deviation in the flight path of a projectile attributable to gravitational force. *Gravity drop* is used to describe the displacement in the ideal trajectory of a projectile due to gravity. The gravity drop is proportional to the time

of flight and has been approximated as $\frac{1}{2}gt^2$, where g is the gravitational force and t is the time of flight (MIL-STD-2089).

Ground Plane: The plane that the target rests upon, which is parallel to level ground.

Hit Distribution: A mathematical representation that defines the results of a firing pass on an aircraft in terms of the probability of n hits.

Infrared Signature: The amplitude, bandwidth, and modulation of a signal emitting or reflecting energy in the 0.7 to 300 micron band. This includes radiation from hot engine parts, gas exhaust, ram air temperature rise, and other aircraft hot spots. It also includes solar reflections.

Jinking: Aircraft maneuvers (i.e., random changes on flight path, altitude, speed, etc.) designed to induce miss-producing effects on enemy-launched weapons.

Kill Levels: Measures of the degree to which a target element suffers performance degradation due to damage processes.

Lead Angle Prediction: The process used to establish desired weapon positioning or aiming information. All weapons employing ballistic projectiles must be provided with some means of solving the fire control problem. From measurement of current target position and velocity, future target position must be established, weapon air angles (e.g., azimuth and elevation) determined, and the weapon positioned and fired so that the projectiles and target will arrive at the same point simultaneously. This process is referred to as "lead angle prediction."

Lock-On: Signifies that a tracking or target-seeking system is continuously and automatically tracking a target in one or more coordinates (e.g., range, bearing, elevation).

Masking: The use of terrain to block the line-of-sight path between a sensor (usually aboard an aircraft) and a target.

Maximum Effective Range: The maximum distance at which a weapon may be expected to fire accurately to achieve the desired result. This also refers to the maximum distance at which the delivered energy density of a *HEL* (high-energy laser) beam is sufficient to cause damage to the target after an appropriate time interval is considered. This measure does not consider the effects of such operational considerations as tracking time, projectile/missile time of flight, and probability of hit.

Mean Point of Impact (*MPI*): *MPI* is the point that has as its range deflection coordinates, the arithmetic means of the range, and deflection coordinates of the impact points of a sample. *MPI* is a typical measure of bias, discussed earlier.

Median: The median is the halfway point in a rank-ordered list of values. For example, for a sample of 23 bombs, it is the 12th value on the rank-ordered list; for a sample of 22 bombs, it is halfway between the 11th and 12th values on the rank-ordered list. In weapon delivery, the median can be defined as the halfway point in miss distance (circular, range, or deflection only) when impacts are arranged in order of size.

Mil: Mil is a measure of delivery accuracy as a function of slant range (1 foot at 1,000 feet equates to 1 mil). To obtain a mil *CEP*, divide the *CEP*, in feet, in the normal plane (defined below) by slant range in thousands of feet. For example, if the *CEP* in the normal plane is 75 ft for a release made at 5,000 ft slant range, the mil *CEP* is 75/5, or 12.5. Mils expand with distance or slant range.

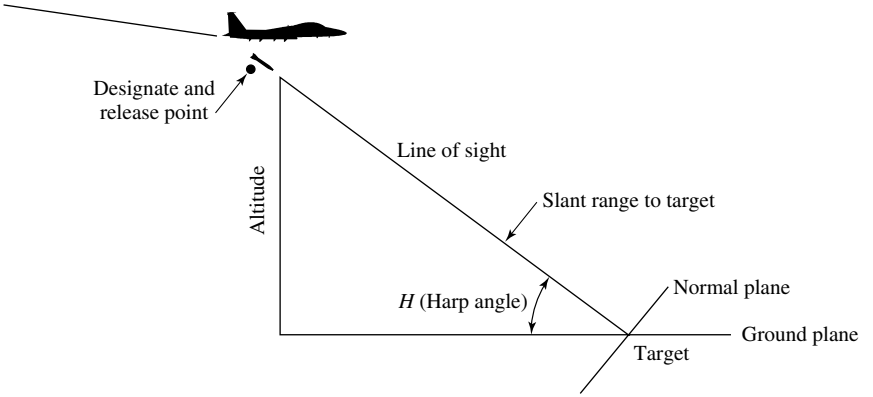

Fig. 5.6. Normal plane.

Miss Distance: The difference in the location of the target and a threat missile/projectile fired at the target at missile/projectile detonation or at closest point of proximity to the target.

Normal Plane: The normal plane is an imaginary plane perpendicular to the line of sight (*LOS*) between the release point and the target. A circular normal distribution in the normal plane is bivariate normal in the ground plane. If the ratio of the standard deviations for the bivariate normal distribution (σ_R in range and σ_D in deflection) is less than 5:1 ($\sigma_R < 5\sigma_D$), the *CEP* in the normal plane (CEP_N) and the *CEP* in the ground plane (CEP_G) are related by the following equation:

$$CEP_G = [(1 + \sin H)/2 \sin H]CEP_N,$$

where H is the *harp angle* (defined in Figure 5.6).

Observables: Detectable emissions from an aircraft, such as radar, infrared, smoke, acoustical, optical, and ultraviolet characteristics (MIL-STD-2089).

Pattern Center: Pattern center is the center of impact points resulting from a drop of multiple weapons on a single pass. Two commonly used measures of pattern center are the mean (or *MPI*) and median. Pattern center for a stick of bombs is illustrated in Figure 5.7.

Range Error Probable (*REP*): *REP* is the second of two measures for delivery accuracy used when the distribution is bivariate normal. Its value is equal to one-half of the distance between two lines that are equidistant from the target (aimpoint) and perpendicular to the aircraft track at time of release, and should contain one-half of the impact points in a sample. Mathematically, the *REP* can be expressed as

$$REP = 0.6745\sigma_R.$$

The *REP* is illustrated in Figure 5.8.

Shaped Charge: A charge shaped so as to concentrate its explosive force in a particular direction. In general, there are two types of shaped charges: (1) spherical, which

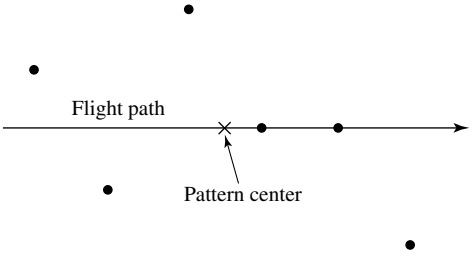

Fig. 5.7. Pattern center for a stick of bombs.

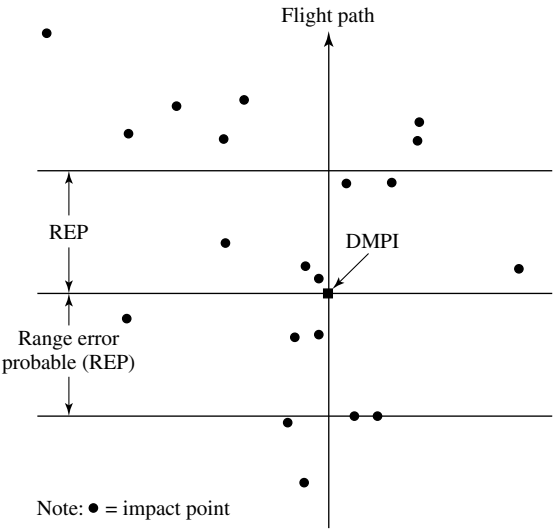

Fig. 5.8. Sample *REP*.

focuses energy to a selected point in the warhead, and (2) linear, which focuses the energy in a desired array around the warhead.

Single-Shot Probability of a Hit (P_{SSH})**:** The probability of hitting an aircraft given a single firing from a threat. The single-shot probability of a hit can be computed in many ways. An example of one procedure application to *AAA* is shown below. (This example assumes that the distribution of hits is circular normal.)

$$P_{SSH} = (A_p/2\pi\sigma^2)\ \exp(-b^2/2\sigma^2),$$

where

A_p = presented area,
b = bias error or distance between the centroid of the trajectory distribution and the aim point on the target (fire control error),
σ = Total weapon system dispersion (ballistic error).

Stick: A series of weapons released sequentially at predetermined intervals from a single aircraft (see also footnote discussed under *Deliver Accuracy*).

Stick Bombing: Stick bombing is synonymous with ripple bombing or train bombing and is used to denote the pattern resulting from the sequential release of unguided weapons during a single pass on the target. The individual weapon releases are spaced along the flight path through the use of an intervalometer in the aircraft. In addition to spacing of weapon impacts in the direction of aircraft travel (i.e., the range direction), the weapons may also be spaced perpendicular to the flight path because of lateral separation of bomb racks on the aircraft and because of side-ejection forces if the weapons are carried on the shoulder positions of multiple-carriage racks.

Target Angle Off: An angle between the velocity vector of the aircraft and the *LOS* between the target and threat.

Target Offset: The minimum horizontal separation distance from the aircraft to a ground- or sea-based threat site when the aircraft flight path is projected beyond the threat site.

Threats: The elements of a manmade environment designed to reduce the ability of an aircraft to perform mission-related functions by inflicting damaging effects, forcing undesirable maneuvers or degrading the system's effectiveness.

Warhead: The part of a missile, projectile, torpedo, rocket, or other munitions that contains either the nuclear or thermonuclear system, high-explosive system, chemical or biological agents, or inert materials intended to inflict damage. (For more details, see Section 4.9).

Warhead Fuze: The element of a warhead that initiates the detonation of the explosive charge. Proximity fuzing (i.e., initiation on impact) is normally used for *AAA* projectiles and may be delayed or instantaneous.

Workload/Stress: Workload/stress is a subjective measure of a pilot's condition at time of weapon release. The four levels of workload/stress considered are training, low, medium, and high. No precise definition of each level is given; it is up to the user to select the workload/stress level suitable for the particular scenario being considered. Factors causing increased stress are unfamiliar terrain, increasing levels of ground defenses, night or deteriorating weather, and deteriorating aircraft systems. Training, the lowest level of stress, might be experienced by a pilot about to complete a training mission on a familiar range. The highest level of stress might be faced by a new pilot on his first mission into an unfamiliar and heavily defended environment. Thus, on any given mission, four pilots could conceivably have four different stress levels.

5.2.2 Acronyms

This section contains an alphabetical listing of acronyms and abbreviations commonly used in connection with weapon delivery systems. They are presented here for the benefit of the reader (see Appendix C for a more general list of acronyms).

AA Antiaircraft (Note: *AA* also refers to "air-to-air")
AAA Antiaircraft Artillery

ADC Air Data Computer. Aircraft measuring equipment for pressure altitude, temperature, calibrated air speed, and/or true airspeed data.
AEP Avionics Evaluation Program.
AGL Above Ground Level.
AGM Air-to-Ground Missile.
AGR Air-to-Ground Ranging.
AH Aircraft Heading. Angle in the horizontal plane measured clockwise from a specific reference point to the fuselage reference line.
AH_m Aircraft magnetic Heading. The angle in the horizontal plane measured clockwise from *magnetic north* to the aircraft fuselage reference line.
AHRS Attitude and Heading Reference System.
AH_t Aircraft true Heading. The angle in the horizontal plane measured clockwise from *true north* to the fuselage reference line.
AMTI Airborne Moving Target Indicator.
ARBS Angle Rate Bombing System.
ARM Antiradiation Missile. A missile that homes passively on a radiation source.
ARS Attitude Reference System.
ASL Azimuth Steering Line.
AT Aircraft Track. The path of the aircraft over ground. Also, the angle measured from a specific reference point to the aircraft ground path. The angle is measured clockwise through 360°.
AT_m Aircraft magnetic Track.
AT_t Aircraft true Track.
ATC; ATR Automatic Target Cueing; Automatic Target Recognizer. Improved cuers, recognizers and processors will provide enhanced target discrimination capability, robustness against partially obscured/signature reduced targets, improved area search capability and reduced false alarm rates and flexibility to rapidly add new targets.
AZ Azimuth Angle. The angle measured in the horizontal plane from a specific reference point to a reference line.
AZ_m *Magnetic* Azimuth Angle.
AZ_t *True* Azimuth Angle.
B_d Ballistic deflection error of the weapon(s) in the ground plane. Distance in deflection from the desired mean point of impact (*DMPI*) due to manufacturing tolerances and weapon stability characteristics.
BARO Barometric altitude (pressure altitude).
BDA Bombing Damage Assessment.
BEI Bridge Effectiveness Index. An empirically derived constant developed for a particular weapon against a particular bridge type.
BFL Bomb Fall Line. The predicted vertical path of a weapon as displayed on the head-up display (*HUD*).
BOC Bomb on Coordinates.
B_r Ballistic range error. The distance in range from the *DMPI* due to manufacturing tolerances and weapon stability factors.

BR Bomb Range. The horizontal distance traveled by the bomb during the ballistic trajectory.

BW Beam Width. The angle either side of the center of a radar beam to the *half-power point*.

CAINS Carrier Aircraft Inertial Navigation System. (Also, Carrier-Aligned INS).

CAS Close Air Support.

CCIP Continuously Computed Impact Point. A visual sighting mechanization that displays the projected weapon impact point on the *HUD*.

CCRP Continuously Computed Release Point. A bombing problem solution that displays turn requirements and release cue(s) to reach one or more point(s) in space from which the weapon ballistic trajectory will cause the weapon to impact the target.

CEP Circular Error Probable. A statistical measure of delivery accuracy reflecting a circle within which 50% of the mean points of impact (*MPS*s) should fall.

CEP$_N$ Circular Error Probable in the normal plane. Expressed in mils or feet, the circle perpendicular to the line of sight passing through the target statistically containing half the *MPI*s.

CT Crosstail. The crosswind effect on a ballistic trajectory that causes a weapon to be blown further downwind than the path of the delivery aircraft. The crosstail distance is equal to the sine of the drift angle times the trail.

DA Drift Angle. The angle between the aircraft heading and the aircraft track. The angle is measured from heading to track; that is, a heading of $90^{\mathbf{o}}$ and track of $85^{\mathbf{o}}$ would indicate a $5^{\mathbf{o}}$ left drift.

DBS Doppler Beam Sharpening.

DDC Digital Data Computer.

DDI Digital Display Indicator.

DEP Deflection Error Probable. The deflection distance either side of the target within which statistically half the *MPI*s should occur.

DLIR Down-Looking Infrared.

DME Distance Measuring Equipment.

DMPI Desired Mean Point of Impact. The point on the ground about which it is desired to center the weapon impacts.

DMT Dual-Mode Tracker.

DPI Desired Point of Impact.

DTED Digital Terrain Elevation Data.

DVST Direct View Storage Tube.

EO Electro-Optical. Television and infrared sensors; the term often is used to mean visible spectrum (*TV*) only.

FAC Forward Air Controller. An officer (pilot) member of the tactical air control party who, from a forward ground or airborne position, controls aircraft engaged in close air support of ground troops.

FAE Fuel–Air Explosive. Munitions whose effects result from an explosive mixture of atmospheric oxygen and a selected fuel.

FFAR Folding-Fin Aerial Rocket.

FLIR Forward-Looking Infrared. An infrared device that generates an image based on temperature differentials of the viewed scene.

FLR Forward-Looking Radar

FOV Field of View

FRL Fuselage Reference Line.

FTT Fixed Target Track.

g Acceleration due to gravity.

GMTI Ground Moving Target Indicator (see also **MTI**)

GP General-Purpose (bomb).

GR Ground Range. The distance in the ground plane traveled by a bomb from release to impact.

H Harp Angle. The angle with sine equal to the quotient of the release altitude divided by the slant range (Y/SR).

$\frac{d\mathbf{h}}{dt}$ Vertical velocity or rate of change of altitude ($\frac{d^2\mathbf{h}}{dt^2}$ is vertical acceleration).

$\mathbf{H}_T$ Target height.

HARM High-Speed Anti-Radiation Missile (*AGM*-88); also described as "High-Speed Antiradar Missile." This missile has *home-on-jam* capability, that is, it can lock onto jamming radars.

HUD Head-Up Display. A means for displaying data in the pilot's normal wind screen field-of-view to minimize distractions during critical maneuvers; often employs a transparent combining glass onto which other imagery is projected.

I Impact angle. The angle between the longitudinal axis of the bomb and the horizontal plane at weapon impact.

ICNIA Integrated Communications Navigation Identification Avionics.

IMS Inertial Measurement Set. A device that measures acceleration in three dimensions, using these measurements to provide altitude, position, and velocity data.

IMU Inertial Measurement Unit.

INS Inertial Navigation System. An *IMS* coupled with a computer to generate accurate acceleration, velocity, position, altitude, and attitude data.

I/WAC Interface/Weapon Aiming Computer.

K_D Coefficient of drag. A measure of weapon drag versus velocity (usually expressed in units of Mach). Related by a constant of proportionality to C_D, the aerodynamic drag coefficient.

$\mathbf{k}_e$ East–west offset component. Horizontal distance in the east–west direction measured from the target to the offset aiming point (*OAP*).

$\mathbf{K}_g$ Gravitational correction for altitude.

$\mathbf{k}_n$ North–south offset component. The horizontal distance in the north–south direction from the target to the offset aiming point.

kn Knot. A speed of one nautical mile per hour (1.688 ft/sec).

KTAS Knots True Air Speed.

LABS Low-Altitude Bombing System.

LASER Light Amplification by Stimulated Emission of Radiation. A highly focused, narrow beam of monochromatic light. A pulsed light beam may be used for accurately measuring distance and velocity as well as illuminating targets for electromagnetic seekers.

LLLGB Low-Level Laser Guided Bomb.

LORAN Long Range Navigation. A hyperbolic navigation system using time difference measurements from three precisely timed ground transmitters, pulsing at regular intervals. LORAN C and D are accurate systems that may be used for weapons delivery.

LSDR Laser Spot Designator and Receiver.

LSR Laser Spot Receiver.

LST Laser Spot Tracker.

MPI Mean Point of Impact. The geometric center of a pattern of weapons or submunitions.

MRE Mean Radial Error.

MSD Multisensor Display.

MTD Moving Target Detector. A radar that employs differential Doppler shift to eliminate stationary terrestrial returns and detect or display moving targets.

MTI Moving-Target Indicator. A radar presentation that shows only targets that are in motion.

MTT Moving-Target Tracker. A range and angle change detector mechanized for following a moving target.

MWS Missile Warning System.

NM *or* nm Nautical Mile(s). 1 nm = 6, 076.412 feet (or 1852 meters).

NWDS Navigation/Weapon Delivery System.

OAP - Offset Aim point. A detectable feature (or distinct radar return) of known vector distance from a target that is used to cue a bombing system.

PA Pressure Altitude.

Pave Tack Pod combining a FLIR and LSDR.

$\mathbf{P}_H$ Probability of a hit. ($\mathbf{P}_k$ Probability of kill).

$\mathbf{P}_{NM}$ Probability of a near miss. Hit distribution probability for guided weapons.

PW Pulse Width. The duration of a radar pulse (also called pulse length) that causes radar returns to be extended in range beyond their physical length.

RALT Radar Altitude.

$\mathbf{REP}_N$ Range Error Probable in the normal plane.

RHAW Radar Homing and Warning. Aircraft electromagnetic receiving equipment used to indicate direction and range-to-radar signals sufficient for targeting with antiradiation or hard munitions.

SAR Synthetic Aperture Radar.

SR Slant Range. The *LOS* distance from the computed release point to the aiming point. For stick releases, the distance from release of the first weapon to the center of the stick on the ground.

TAS True Air Speed.

TF/TA^2/OA Terrain Following/Terrain Avoidance/Threat Avoidance/Obstacle Avoidance.

TD Target Designator.

TDD Target Detection Device.

$\mathbf{T}_f$ Time of flight. The time in seconds from weapon release to impact.

TRAM Target Recognition Attack Multisensor.

UAV Unmanned Aerial Vehicle.
VSD Vertical Situation Display.
WDC Weapons Data Computer.
WDS Weapon Delivery System.
WRCS Weapon Release Computer System.

5.3 Weapon Delivery Requirements

The need for precision tactical weapon delivery systems providing day/night all-weather, low- and high-altitude capability against targets at ranges to 300 nm can be met by self-contained fail-safe and fault-tolerant guidance aids and advanced kinematic bombing subsystems. To support these, continued development and use of *GPS*, time-of-arrival (*TOA*) measurement, distance measuring equipment (*DME*), down-looking infrared (*DLIR*), forward-looking infrared (*FLIR*), moving target indication (*MTI*) radar, digital land mass data, and *SAR* is required. Research directed toward increasing the bandwidth, quantum efficiency, antijam tolerance, and low-power signal handling ability of these devices can provide the desired capability.

Development of techniques for accurate position, velocity, attitude, and time fixing; threat and obstacle detection; low-aircraft observable terrain following and terrain avoidance (*T F / T A*); and optimum use of land-mass multisensor data for route optimization, control of aircraft observables,* and control of radar probability of intercept are important to achieve survivability through covertness and stealth in severe defensive threat environments. Of the stealthy technologies, bistatic synthetic aperture radar and its associated need for radio frequency (*RF*) signal coherency by maintaining timing and phase synchronization between the illuminator and receiver frequency reference is one of the most technically challenging requirements for future navigation, motion compensation, and timing systems. This problem is greatly compounded by severe operational environments, which will include severe jamming and air defenses, terrain masking, weather and atmospheric turbulence, and the penetrator aircraft employment of high-g, minimum exposure, pop-up maneuvers to improve survivability. Strategic weapon delivery systems operating at significantly longer ranges need autonomous navigation systems, which can respond automatically to unplanned mission events. Development of sensors and data processors for accurate position fixing, target damage assessment/retargeting, threat and obstacle detection, and route optimization are important for vehicle survivability in severe defensive threat environments.

Close air support (*CAS*) requires weapon terminal guidance techniques compatible with moving-target-indicating radars and forward-looking infrared systems. Counter air requires self-contained integrated flight and fire control systems for air superiority fighters. All tactical mission aircraft including remotely manned vehicles need integrated reference and flight control systems to provide more accurate weapon delivery and greater aircraft performance options. Tactical air-to-air missiles employing

*Observables refers to detectable emissions from an aircraft, such as radar, infrared, smoke, acoustical, optical, and ultraviolet characteristics (MIL-STD-2089).

semiactive guidance systems are hindered by radar clutter. Mathematical analysis of acquisition and tracking in mono and bistatic clutter and receiver performance in main lobe clutter must be further researched. Medium-range tactical air-to-air missiles need midcourse guidance with a low-cost, wide-angle, and fixed *FOV* terminal sensor. Sensor elements and arrays, sensor tracking logic, and rapid handover techniques (*FCS* to missile) for such concepts must also be researched.

Navigation, guidance, and control are functions that demand highly specialized supporting technologies. Navigation is the process of determining position and velocity of a vehicle. Engineering investigations and analyses reveal that technology has advanced sufficiently to permit multiple usage of inertial navigation systems. Guidance, the process of using vehicle position, velocity, attitude, and mission data to compute thrust and steering commands, is the process between navigation and control and includes space, intercontinental ballistic missiles (*ICBM*), antiballistic missiles (*ABM*), and air-to-ground missile applications. Control is the process of causing a dynamical system to behave in a desired manner.

Associated with weapon delivery is the problem of survivability. Survivability will be enhanced through the use of emerging technologies that will allow single-pilot night-in-weather operations at altitudes and speeds that are impossible to attain with current systems or their derivatives. The principal concept used to ensure a high degree of survivability and mission success is passive operation. During penetration, terrain following/terrain avoidance/threat avoidance (TF/TA^2) will be employed at low altitudes (150–200 ft; 46–61 m). Target location is to be provided by mission planning or forward air controller (*FAC*) in common coordinate system directly to passive onboard navigation. In the target area and in weather described for this scenario, passive *IR* target detection and identification will be used in order to maintain the element of surprise and a high probability of survival. During attack, the navigation/forward-looking infrared (*NAV/FLIR*) is correlated to a targeting *FLIR* where three line-pairs are required to provide target identification.

Very low level penetration can be selected for a mission after considering the alternatives of high or medium altitudes. High altitude offers low threat density and good target view but does not provide for a surgical weapon delivery. In a forward base concept of operation, climbing to medium or high altitude allows exposure to early warning (*EW*) radars and *IR* weapons. Low altitude with *GPS* navigation offers both survival benefits and close-in attack. Target acquisition and identification with very high speed correlation, when coupled to new multikill weapons, can produce orders-of-magnitude improvement in lethality.

Mission equipment must be modularized to satisfy worldwide operational requirements. A basic core avionics suite includes comm-nav (*ICNIA*), data processors (MIL-STD-1553B bus and MIL-STD-1750A architecture), and the controls and displays (including head-out visor display and system health monitors). The modular attack subsystem includes offensive and defensive quick-change modules. For passive operations, the attack subsystem must rely primarily on *NAV/FLIR*, targeting *FLIR*, *INS*, *GPS*, and *DTED*. Timely application of artificial intelligence is foreseen to provide automation for mission planning, missile evasion, target data processing, and sensor fusion to result in a simple pilot task of point, shoot, and pull (*g*'s).

Future force effectiveness will be characterized by the following:

1. **Lethality** Weapon kill load, accuracy, launch rate, target acquisition, and weapon suitability.
2. **Survivability** Defense suppression, observability, and $TF/TA^2/OA$.
3. **Availability** Response time, radius/loiter, night' in-weather, high reliability, and mission suitability.

Essential for weapon delivery requirements is the establishment of air-to-ground requirements. Typical air-to-ground missions include:

(1) Close air support (*CAS*) of surface forces. The *CAS* mission often requires visual target acquisition and positive visual target identification under the duress created by terrain, vegetation, camouflage, smoke, dust, heavy antiair defenses, and nearby presence of friendly troops. The high-speed attack aids survivability of target acquisition. For example, at 500 knots the pilot will not have time to see and engage on the same pass.
(2) Battlefield interdiction to interfere with enemy movements and cut lines of communication.
(3) Suppression of enemy defenses to clear a path through the enemy's surface-to-air missile (*SAM*) and antiaircraft artillery (*AAA*) belts.
(4) Deep strike against fixed targets, such as airfields and bridges; relocatable targets, such as garrison areas; and moving targets, such as ships or tanks.

Critical mission phases include timely launch, safe ingress, timely and accurate target attack, lethal self-defense, safe egress, and reliable recovery. Typical mission tasks consist of takeoff and landing, flight control, navigation, fuel, weapons and expendables management, sensor control, and weapons delivery. A survey of Southeast Asia combat losses of jet attack fighters indicates the critical threats of our most recent large-scale conflict. Eighty-eight percent (88%) were downed by ground fire, 9% fell to *SAM*s, while only 3% were *MiG* victims. Air-to-ground technologies of the future must satisfy three critical technology needs. These are (1) low observables, (2) standoff air-to-ground missiles, and (3) thrust vectoring/thrust reversing exhaust nozzles. Multifunction nozzles will contribute heavily to both low observables and survivable standoff weapons launch, as well as of the thrust vectoring and thrust reversing. More specifically, the thrust vectoring, low observable multifunction nozzles will allow supercruise point designed (i.e., high supersonic lift-to-drag ratio at the expense of low-speed, high angle-of-attack aerodynamic stability and control) tailless, small aircraft. High-altitude supersonic cruise will allow deep strike fighters to avoid just about all of the *AAA* threats and most of the *SAM* threats during ingress/egress.

5.3.1 Tactics and Maneuvers

The bombing problem is dynamic, constantly changing as the aircraft moves through space, causing both ballistic and sighting solutions to vary from moment to moment. Velocity and acceleration, the active ingredients in this dynamic process, must be

measured and controlled to obtain a simultaneous matching solution at the time of weapon release. In any tactical situation, the effects of tactical maneuvering on delivery accuracy must be taken into account. Defining the correct release point is a three-dimensional problem. Measurement and/or calculation of release parameters, as well as target identification and accuracy of target designation/aiming index placement, may be affected significantly by the flight path of the aircraft approaching the target. For example, a low-altitude, high subsonic $TF/TA^2/OA$ dash of the close air support and battlefield interdiction requires efficient, highly maneuverable flight.

At this point, a more detailed account of tactics and maneuvers will be given. These are as follows:

Approach and Entry Tactics. The approach and entry into a dive delivery are usually dictated by (a) enemy defenses, (b) weather conditions, and (c) aircraft maneuvering abilities. Relatively low levels of enemy defenses and good visibility will permit medium- to high-altitude approaches with controlled roll-in point/attack axis selection and flight spacing. Multiple passes by each delivery aircraft may be possible, with adjustments in aiming to account for observed errors and target damage. The capability of an aircraft to maneuver over a target varies with aircraft type. A pilot facing an identical target and defenses, with other factors equal, will experience a higher stress/workload (see Section 5.2.1) level in a less-capable aircraft. Enemy defenses may necessitate a low-altitude approach to the target area with a popup to dive maneuver. Such maneuvers not only increase delivery errors due to increased pilot/aircrew workload/stress, but also increase the possibility of target misidentification and gross delivery errors. Combinations of weather and enemy defenses may require a low-altitude approach with a shallow dive entry from low altitude. Finally, terrain masking can be used as an aid in hiding from target defenses, but this can increase target acquisition problems.

High-Angle Dive Delivery. Dive deliveries greater than or equal to 25°, generally result in ballistic trajectories that are shorter than those in low-angle deliveries of unretarded weapons. Specifically, the reduced slant range results in smaller delivery errors in the ground plane.

Low-Angle Dive Delivery. Dive deliveries at angles less than 25° are usually performed from lower altitudes. However, this decrease in delivery may cause the aircraft to approach the fragmentation envelope of the detonating weapons. Therefore, in order to avoid this condition, weapon retardation devices and/or aircraft escape maneuvers are employed. For example, retarded bombs such as the Mk82 *Snakeye* (see also Section 5.6) slow the weapon to increase safe separation, shorten the ballistic range, and thereby lessen sighting errors. However, ballistic dispersion errors are increased due to the variability in retarder opening and the perturbed trajectory.

Accelerated (Dive Toss)/Unaccelerated Deliveries. Manual dive deliveries using depressed-reticle optical sights require meeting preplanned dive angle, airspeed, and altitude parameters to match the computed ballistic range and sight-depression angle. This results in an unaccelerated approach to the release point along the desired dive angle, as shown in Figure 5.9. It is evident that such a maneuver

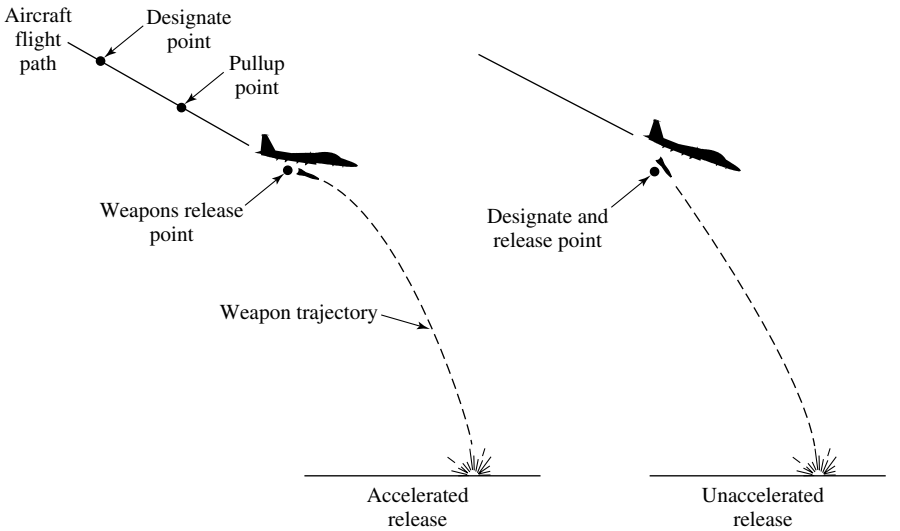

Fig. 5.9. Dive delivery profiles.

becomes more difficult if the entry (roll-in) is complicated by a popup or a *jinking* path to avoid enemy defenses. Maintaining a relatively straight flight path during the dive approach to the release point simplifies the enemy gunner's lead problem and reduces aircraft probability of survival. However, the advent of computer-aided visual deliveries has reduced the restrictions on the approach to release. Systems that provide dynamic ballistic solutions usually permit or require an accelerated flight path in the approach (see Figure 5.9). Initially, these systems employed wings-level pull-up through the correct release angle, with automated release during the maneuver. However, for aircraft equipped with improved stable platforms and computing devices, other approaches are possible with minimal degradation of delivery accuracy. Finally, when executing an accelerated delivery, at some point the dive becomes a pullout.

Level Deliveries. Low-altitude level visual deliveries, as with low-angle dive deliveries, often employ retarded weapons to avoid the fragmentation envelope of the weapons. Since retarded weapons have a shorter ballistic range, optical sight-depression angles are large and in some cases cannot be displayed on the combining glass. This restriction also affects presentation of computer-aided systems. Therefore, low radar-grazing angles and high angular velocity can reduce system accuracy. There are three classes of altitude deliveries: (1) *Low-altitude* radar deliveries are often accomplished during the night and/or during periods of restricted visibility. Besides the short target acquisition range and aircraft altitude uncertainties, radar target identification at low grazing angles can present significant problems. (2) *Medium-altitude* level deliveries offer increased acquisition time at attack airspeeds, but increased ballistic range and time of fall decrease accuracy. Typically, low-drag weapons are delivered, and the defense environment is usually

benign. (3) *High-altitude* level releases suffer from the increased release ranges and weapon time of fall with little, if any, improvement in target acquisition.

Lateral Toss Deliveries. Lateral toss deliveries are made during high-g turning maneuvers at low altitude. The maneuver typically is initiated at altitudes of 100–200 ft *AGL*, evolving into a slight climb to 700–1000 ft *AGL*, with weapon release occurring in a shallow dive (5°–10°) at 600–700 ft *AGL*, and ending in a descent to low egress. Because of the rapidity of the delivery, only a few bombs are normally released in a stick (note that long sticks of bombs require seeing the desired point of impact earlier than for a single release).

Loft deliveries. Loft deliveries involve releasing the weapon in a climbing attitude. In this case, delivery accuracy is relatively poor compared with level and dive release, due to sighting difficulties, increased ballistic range, and longer time of fall. However, the standoff range obtained permits weapon delivery without overflight of the target area. This delivery profile significantly increases the weapon ballistic range up to a critical angle near 45°. Three methods are used to accomplish this maneuver: (a) mechanical timer, (b) aircraft pitch attitude angle, and (c) onboard computer.

Angle Release. Angle release loft maneuvers are initiated in much the same manner as timer release. In many cases, the pull-up timer is used to cue the maneuver; however, release is effected when the aircraft reaches the prescribed pitch angle value.

Computer Aided. Computer-aided loft deliveries permit target tracking with an aiming sensor such as the attack radar. A pull-up indicator cues initiation of the maneuver when at the proper distance from the target. The g-profile is followed to establish the desired acceleration rate, and release is automatically accomplished when range to target equals ballistic range.

5.3.2 Aircraft Sensors

A variety of devices are available for onboard measurement of elements of the bombing problem. These devices, or sensors, can measure range, angle, velocity, or acceleration. A critical input to most methods of solving the ballistic trajectory is range to the target. Typical instruments measure range using radar or laser beams, or estimate range by using barometric pressure. The accuracies of these devices affect the total system bombing accuracy and are a significant input to the accuracy model used to develop estimates. Sighting angles are a critical input to target designation. Angle rate systems use this quantity to replace range in the bombing solution.

One means of controlling the release involves a display of the ballistic solution on a sighting device. The displayed solution may be a static *canned* one, valid for only a specific set of conditions, or it may be dynamic, changing to reflect current delivery aircraft altitude, range, and velocity data. This display of the predicted impact point on the sighting device permits steering the delivery aircraft to obtain coincidence, just as a marksman places the crosshairs of a rifle's sight on a target. If the displayed ballistic solution is dynamic, it provides a *CCIP*. This technique has significant advantages for

tactical maneuvering to enhance delivery aircraft survival while providing improved accuracy over fixed-sight canned solutions.

A second means of providing control information involves the display of the difference, or *delta*, between existing sighting and ballistic solutions. Display methods vary from cockpit steering and time-to-go meters/indicators to sophisticated *HUD* steering and release cue symbology. This solution technique provides direction from the present position to the release point where the *delta* signal will be zero. The ballistic and sighting values are dynamic, and the display provides direction for this *CCRP*. The *CCRP* technique is particularly well suited for deliveries where the sighting device(s) is separated from steering data, as for radar deliveries, or for loft maneuvers, where sighting may be discontinued before release is effected. In some computing systems, *CCRP* steering may involve established values at a designated point and performing a prescribed maneuver (such as a wings-level pull-up) to obtain release.

5.4 The Navigation/Weapon Delivery System

The navigation/weapon delivery system (*NWDS*) is the heart of a fighter and/or attack aircraft. Attack aircraft are specifically designed for close air support and interdiction missions. They have been designed to incorporate a continuous solution navigation and weapon delivery system for increased bombing accuracy. The *NWDS* continuously performs the vital computations required for greatly increased delivery accuracy, and for maneuvering freedom throughout the navigation to a target and the attack, air-to-ground (or surface) and air-to-air weapon release, pull-up, and safe return phases of the mission. For example, in order to perform a successful tactical mission, the fighter must have accurate reference information for controlling the vehicle, navigating over the surface of the Earth, and providing inertial inputs to the weapon delivery system.

Moreover, the navigation and weapon delivery system not only provides the pilot with an impressive number of options during weapon delivery, but also relieves him during an attack run from a compulsory straight-path approach to the target (precalculated dive angle, airspeed, altitude, and pipper-on-target), which considerably reduces vulnerability to enemy fire. The system permits a highly flexible attack envelope, augmenting the pilot's ability to find targets, maneuver when necessary, and reattack promptly when required. The aforementioned flexibility is made possible through the *NWDC* digital fire control computer (*FCC*) in conjunction with the projected multifunction displays, the wide-angle head-up display (*HUD*), forward-looking radar and/or fire-control radar, stores (i.e., weapons) management, inertial navigation system, radar altimeter, and projected map, if available. The multimode fire control radar provides multiple (e.g., 10) target track-while-scan information as well as single-target search, providing tracking capability in both lookdown and look-up encounters.

The navigation weapon delivery computer (*NWDC*) is an indispensable central element in the weapon delivery function or process, integrating the displays, sensors, controls, and pilot's commands. In particular, its most important role is to solve ballistic prediction problems in real time, which permits an unconstrained selection of flight path and altitude during weapons pass. During navigation, the *NWDC* continuously

derives and displays present position and destination guidance data. Specifically, using a control panel in the cockpit, the pilot can *converse* with the *NWDC*, prestoring more than twenty destinations that can be called up during the flight.

Commonly, the *NWDC* provides several variations of both continuously computed release point (*CCRP*) and continuous computation of impact (i.e., target) point (*CCIP*) modes. (The *CCIP* is the point on the ground where the weapon would impact if released at that instant.) The *HUD* is driven by the *NWDC* through a MIL-STD-1553B MUX interface, allowing the pilot to acquire and attack targets with more *heads up* time. If available, as mentioned above, the *NWDC* also can drive the projected map display, which provides a continuous display of aircraft geographical position. A range indicator shows distance from present position to the selected destination. The forward-looking infrared (*FLIR*) *POD* (e.g., *AAR-45*) turns night target scenes into day; the *FLIR* permits detection, classification, and identification of targets, at sufficient range for a first pass attack if the target proves to be hostile. At night with the *FLIR* activated, an attack aircraft can deliver the same ordnance with the same accuracy as during daytime.

The sensitivity of weapon delivery accuracy to some release point error sources varies with the mode, weapon type, delivery condition, and configuration option. Navigation system parameters for which sensitivity analyses must be conducted are (a) the horizontal velocity components, (b) vertical velocity components, and (c) pitch and roll. Therefore, the sensitivity of weapon delivery accuracy to errors in the navigation system parameters is considered to be the release-point error sources. In addition to the release conditions and weapon delivery configuration specification, inputs to an error analysis program must include the sensor errors, pilot errors, and other miscellaneous errors. These input quantities are release point errors, which are converted by means of the error analysis equations into impact point errors (i.e., on the ground). The impact point errors are combined into a single statistical measure of weapon delivery accuracy, the impact *CEP* (circular error probable), which is the distance from the mean impact point (which is assumed to be unbiased) within which 50% of the weapons will impact [7]. The values of the sensor error sources (except for the navigation system parameters) are normally obtained from sensor performance specifications.

Extensive computer runs must usually be conducted in order to perform the necessary sensitivity analyses. The method most frequently used to determine the sensitivity of weapon delivery accuracy to a particular error source can be stated as follows: Keeping all other error sources fixed at their nominal value, the error source in question is varied from zero to a value that is usually five to ten times as large as its nominal value. Furthermore, the *CEP* is computed for each value of the error source, and a graph may be constructed showing *CEP* versus the value of that particular error source. Consequently, the effect of a single error source on the overall weapon delivery accuracy may be demonstrated in this way.

In summary, the fire control system works in conjunction with the communication, navigation, and identification (*CNI*), and survivability avionics to penetrate defenses and locate, acquire, and deliver air-to-ground and air-to-air weapons. The key elements of the navigation/weapon delivery system are (a) fire control radar, (b) wide-angle

HUD, (c) control panel, (d) multifunction display, (e) inertial navigation system, (f) fire control computer, (g) stores management set, (h) radar altimeter, and (i) data transfer equipment.

5.4.1 The Fire Control Computer

The fire control computer (*FCC*) can be considered an integral part of the navigation weapon/delivery system. Typically, the *FCC* is a MIL-STD-1750A, modular, general-purpose, microprogrammed, parallel, high-speed digital computer. As mentioned in the previous section, the *FCC* is the principal component of the weapons control subsystem, and provides real-time computations for the following functions: (a) automatic air-to-surface weapon deliveries, (b) air-to-air missile algorithms, (c) navigation-related data, (d) stores data select, (e) display control, (f) self-test, (g) fix taking, and (h) energy management information. The most important function of the fire control computer is to serve as the primary bus controller for the serial digital buses (avionics multiplex buses (*AMUX*) and the display multiplex buses (*DMUX*)). (Note that by multiplex we mean *time-sharing*.) Normally, data transmitted on both the *AMUX* and *DMUX* is in serial digital form and is coded in the Manchester biphase format. Data on the *MUX* buses is transmitted and received at a 1 MHz rate. The *FCC* also provides storage for centralized fault gathering and reporting of weapons' control terminals' self-test information.

The central processing unit (*CPU*) of the fire control computer can use 16-, 32-, and 48-bit data words for single- and double-precision fixed-point, and single- and extended-precision floating-point calculations. The *CPU* also performs single-precision addition, subtraction, and loading in 1.3 microseconds, multiplication in 2.9 microseconds, and division in 7.5 microseconds. The *FCC* has six major addressing modes that enable it to address 64 K words of memory, and it uses a 16-register general register file to accomplish this function. The input/output (*I/O*) system is the means by which the *FCC* communicates with external sources.

The subsystems listed above include provisions for the low-altitude navigational and targeting infrared for night (*LANTIRN*) targeting and navigation pods; the pods are considered part of the avionics system. Both visual and blind all-weather, air-to-ground weapon delivery modes are available for conventional unguided and guided weapons. With the *LANTIRN* navigation pod, a fighter aircraft can penetrate at low altitude in all-weather conditions by the use of terrain following/terrain avoidance (*TF/TA*) radar and the navigation pod *FLIR* video on a wide-angle *HUD* (see also Section 5.12.2).

In April 2002 the Air Force began testing an advanced targeting pod for the *F-16 Sniper* program. The *Sniper XR* targeting pod is a multipurpose targeting and navigation system that provides tactical aircraft with 24-hour precision strike capability against land- and sea-based targets. The pod is a self-contained sensor and laser designator (see also Section 5.5.2 on laser systems) that allows improved target detection and recognition. Among the pod's capabilities are an *IR* camera for thermal imaging and an additional camera that adjusts for daylight and low thermal contrast conditions. Using the *Sniper XR*, pilots can identify tactical targets at greatly improved standoff

ranges compared to current systems. The *Sniper* pod also has an *IR* pointer compatible with night-vision goggles. Initially, the pods will be installed on the *F-16CJ* aircraft and some Air National Guard *F-16*s. Other strike aircraft, such as the *F-15E Strike Eagle*, may also take part in testing.

5.5 Factors Influencing Weapon Delivery Accuracy

Before we discuss the various factors that influence weapon delivery accuracy, it is appropriate to briefly state the weapon delivery modes. The common weapon delivery modes are as follows:

- Continuous computation of impact (i.e., target) point (*CCIP*); that is, compute the point on the ground where the weapon would impact if released at that instant.
- Continuous computation of release point (*CCRP*).
- Time-to-go weapon release.
- Computer-generated release signal.
- Limitation of roll command steering (i.e., number of degrees of roll is limited).

In general, data under real combat conditions are difficult to collect because the environment is uncontrolled and all variables are continuously changing. Thus, data from unfamiliar ranges with realistic terrain are used as a measure of combat accuracy. Resources are too limited to test all aircraft in all release conditions for a wide spectrum of pilots and aircrews. Detailed analysis of the factors influencing delivery accuracy has allowed a reasonable simulation of aircraft system performance. Knowing the significant parameters in the delivery problem allows aircrews to improve accuracy under some conditions. It is important to note that error sources are different for guided and unguided free-fall weapons. The factors influencing weapon delivery accuracy that will be discussed here are (a) workload/stress, (b) aircraft performance, (c) target acquisition, and (d) accuracy relationships.

Workload/Stress. As discussed in Section 5.2.1, the human being is a primary element in the weapon delivery process. Judgment, motor response, and perception all contribute to accuracy. Tactical maneuvers dictated by weather conditions and/or enemy defenses may limit time allocated to perform required tasks. The accuracy data discussed here are expressed in terms of four levels of workload/stress: training, low, medium, and high. No precise definition for conditions generating low, medium, or high workload/stress is practical. Targets attacked in daylight and clear weather may represent a low workload/stress level, while the same target attacked in late afternoon, with haze and broken clouds, may produce medium to high workload/stress. Properly designed tactics can reduce workload/stress.

Aircraft Performance. Aircraft performance, or lack thereof, does not seriously affect delivery accuracy except when the roll-in maneuver or popup technique to the roll-in maneuver is used. To be a good weapon delivery platform, an aircraft must have adequate damping, maneuverability, and controllability to permit the

pilot to effectively place the aircraft in a predetermined position (altitude and slant range) in space for accurate manual/visual bombing. Automatic fire-control systems compensate for most aircraft characteristics.

Target Acquisition. Target acquisition plays a major role in mission accomplishment. More specifically, target acquisition can be accomplished, in addition to visual means, by such techniques as radar, forward-looking infrared (*FLIR*), laser systems, and helmet-mounted display systems. Acquisition system errors are included in an analysis used to generate the accuracy estimates. Target acquisition and workload/stress are interrelated in a manner difficult to quantify. Late target acquisition can raise the workload/stress level.

Accuracy Relationships. For single releases from a large number of individual passes and corresponding aiming operations, the delivery accuracy is a measure of the variation of the impact point about the intended aimpoint. For example, for salvo and stick releases, delivery accuracy is a measure of the variations of the centers of impact (pattern centers) about the aimpoint. Delivery accuracy may be expressed in several ways. In this book, accuracies are expressed in mils (milliradians) perpendicular to the line of sight (*LOS*) for most cases. For weapons systems or tactics that have accuracies dependent on slant range (mil accuracy not constant), accuracy estimates in the ground plane are generally used. Terminally guided weapons require additional parameters to adequately describe the system accuracy.

5.5.1 Error Sensitivities

In this section a discussion of the error sensitivities and interaction is given. A complete error sensitivity analysis requires an error budget approach with the resultant analytical answers compared with the test data. Therefore, in this section we will consider the following error-impacting error sensitivity: (1) dive deliveries, (2) dive-angle errors, (3) altitude errors, (4) airspeed errors, and (5) level radar delivery errors.

Dive Deliveries. Dive deliveries shorten the ballistic trajectory by increasing the downward vertical component of velocity. In general, this permits a closer approach to the target and reduces wind effects by reducing time of fall. These deliveries are further characterized by the approach and entry maneuver and aircraft acceleration condition during weapon release. The primary factors affecting dive delivery accuracy are (a) dive angle, (b) slant range, (c) airspeed, (d) coordinated flight, (e) target motion, and (f) wind.

Dive Angle, Slant Range, and Airspeed Are Independent. Quite often, delivery accuracy tables assume normal g-loading for a given dive angle that can be obtained only when a wings-level, coordinated flightpath is maintained prior to release. To achieve this, the pipper of a fixed sight should be allowed to walk toward the target or aimpoint and should arrive when the aircraft is at the correct release altitude and airspeed. The depressed-reticle sight is used, in conjunction with the altimeter, to determine the release point. Wind effect can be divided into range-wind and crosswind if attack heading is known. Several factors must be considered when determining an indicated release altitude: altitude loss during pullout, minimum

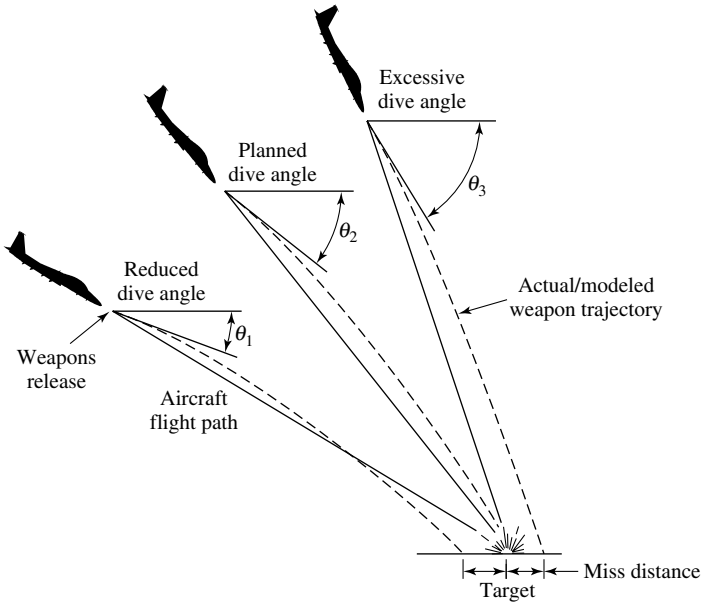

Fig. 5.10. Dive-angle error effect (constant airspeed and slant range; varying altitude).

aircraft ground clearance for bomb fragments, time of fall for fuze arming, altimeter lag, and target elevation.

Dive-Angle Errors. For free-fall bombs, errors in dive angle have a greater effect on weapon delivery accuracy than do proportionate errors in airspeed and slant range. Since sight angle is computed for specified release conditions, accurate delivery can be obtained only if these conditions are achieved, or corrected for, at release. Considering that a weapon was released at the proper airspeed and slant range, variations in dive angle have the following effect: Too steep a dive angle will result in a long hit, and too shallow a dive angle will result in a short hit. Note that dive angle is the most difficult parameter to correct for after a roll-in. Figure 5.10 illustrates the effect of dive-angle errors.

Altitude Errors. Delivery accuracy is affected by the slant range at release, particularly for retarded bombs. If release is at a too short a slant range, the weapon will overshoot the target; if the slant range is long, the weapon will undershoot. In manual fixed-sight deliveries, a pilot has no direct indication of slant range. Dive angle release height above the target must be used to determine the release slant range. Thus, slant-range error translates into altitude error if dive angle and airspeed are correct. Figure 5.11 illustrates a low-altitude low-dive-angle weapon delivery.

Airspeed Errors. Deviation from the airspeed used in determining sight angle will cause two cumulative errors in delivery accuracy: (1) The first of these errors results from a flattening of the weapon trajectory as speed is increased. Thus,

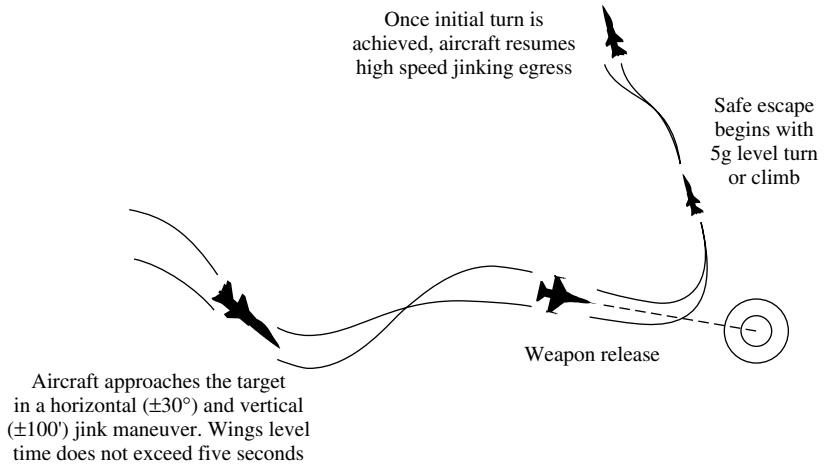

Fig. 5.11. Typical low-altitude/low angle delivery.

too slow a speed results in a short hit, and too high a speed results in a long hit. (2) The second error results from the relation between airspeed and angle of attack. As airspeed increases, angle of attack decreases. This, in effect, alters the sight angle. Therefore, a release airspeed greater than planned causes a late sight picture, which in turn results in a long hit. Deviations in release airspeed particularly affect free-fall bombs. Also, a gross weight change (i.e., as bombs are dropped and fuel is used) also affects the aircraft angle of attack.

Level Radar Delivery Errors. Most of the world's fighter aircraft today use fully integrated radar delivery systems. Since the radar crosshairs are generated based on slant range, they will move off the target as the range to target decreases. For an aircraft higher than the system altitude, the slant range computed to track the target from the previous position will be too small; thus, the crosshairs will move short of the target. If the weapons officer applies correction to reposition the crosshairs, the resulting increase in computer range will cause the release to be delayed, and the weapon will hit long, due to induced slant-range error. For an error in true airspeed with fully operational digital bombing solution and the correct inertial ground speed, the effect is opposite that of the manual system. Finally, a steering error will cause the weapon to be misdirected during its trajectory by the erroneous steering angle.

With regard to airspeed errors, the Department of Defense has approved the production of a wind-corrected munitions dispenser (*WCMD*). The program was started in 1994 as one of four selected Air Force "lead" programs. In essence, the *WCMD* is an inertial guidance tail kit that can be installed on existing "dumb" cluster munitions to transform them into "smart," accurate, adverse-weather weapons. The tail kits will be used on the *CBU-87* combined effects munition, the *CBU-89 Gator Mine System,* and the *CBU-97* sensor fused weapon. These weapons will be integrated on

the *F-16 Fighting Falcon*, *F-15E Strike Eagle*, *B-1B Lancer*, *A-10 Thunderbolt II*, *F-117 Nighthawk*, *B-52H Stratofortress*, *JSF*, and perhaps the *F/A-22 Raptor*. The *WCMD* gives combat crews a significant new capability. With existing "dumb" cluster weapons to be effective, aircrews will need to deliver the munitions from low altitudes, making the aircrews extremely vulnerable to enemy air defenses. During *Desert Storm*, when aircrews tried launching these cluster weapons from high altitudes, the munitions were blown off course by winds or wandered off course due to launch alignment or ballistic errors. Using an inertial navigation unit, *WCMD* solves the problem by allowing very high altitude delivery. Specifically, altitudes of up to 45,000 ft (13,716 m) have been demonstrated. The Air Force is also pursuing the development of a 250-lb-class weapon, the Small-Diameter Bomb (*SDB*) program. Moreover, the Air Force would like to mount a *GPS/INS* guidance kit on 250-kg bombs, which would increase the number of targets that could be engaged by platforms like the *B-52H* bomber.

5.5.2 Aircraft Delivery Modes

As aircraft delivery system technology has developed, different terms have been used for the same phenomenon. Terminology has been standardized to reduce some of the confusion in comparing aircraft. In this book, we will use the term *mode* to denote the sensor the system is using for data input to the fire control computer, and *mechanization* to denote the way the information is processed and displayed to the pilot. In this section, we will discuss radar, electrooptical sensors, and laser systems.

Radar. Level radar deliveries usually employ radar calibration of the pressure altimeter, and slant-range measurement to the target radar echo. With these two sides determined, the remaining side and angles are easily computed. There are four major functions associated with air-to-ground radars: (1) range measurement, (2) ground map, (3) terrain following/terrain avoidance (TF/TA), and (4) Doppler/moving target. Off-boresight ranging to target means that the target need not be directly ahead of the aircraft to have its range measured (i.e., slewable radar dish). Radar altimeters can be classed with these range-only systems; however, the radar beam of radar altimeters is not focused forward, but is broadcast in the lower aircraft hemisphere to obtain an echo from the Earth. Ground target mapping provides a map-like presentation of the returning radar echoes to permit target identification and aiming. Sophisticated ground-map bombing radars provide automatic sweep expansion as the range to the target decreases. Terrain following/terrain avoidance radars are focused into narrow cones that sweep at precisely controlled elevation angles to provide a picture of the vertical aspects of the radar echoes. Ground-map radars and terrain-following radars are at opposite ends of the spectrum. That is, one set of radar characteristics cannot do both jobs well. In state-of-the-art terrain-following systems, multiple radar antennas are employed, and a variety of computer-enhanced presentations are used to present data to the pilot/aircrew or automatically control the flight path. Doppler radar and automatic moving-target indicator (*AMTI*) are two names for the same type

of system. As radar technology has improved, frequency-stable transmitters have been developed that permit use of the *Doppler effect*. The Doppler effect causes a frequency shift in the radar echo that is proportional to the relative velocity between the transmitter and the surface reflecting the signal. Specifically, in the case of airborne radars, the Earth's surface is a moving target. Measurement of the frequency shift of the ground echo may be used to provide ground speed and drift information.

Electrooptical Sensors. Electrooptical (*EO*) systems provide sighting enhancement through amplification of received electromagnetic radiation and display of this information for use in the sighting problem. Television cameras receive visible light and display it on a cathode ray tube (*CRT*). Since *TV* tubes can be made very small, they can be placed on the inner ring of a gimbal system. Thus, the angle rate bombing system (*ARBS*) uses a *TV* sensor. Forward-looking infrared (*FLIR*) systems use cooled solid-state detectors to spot blackbody radiation. An object need not necessarily be hot to be perceived by this detector; it is the contrast with the surrounding territory that is significant. The *FLIR* pictures resemble *TV* except for some odd shading.

Laser Systems. Laser systems are semiactive. One party, the forward air controller (*FAC*), illuminates a desired target with laser energy while the attacking aircraft receives the signal. The aircraft avionics incorporates the direction information into the bombing problem and displays the information to the pilot executing the attack. A laser spot tracker (*LST*) is a four-quadrant detector similar to the seeker of the laser-guided bomb. An *LST* is a receiver only. A laser designator is a laser aboard the aircraft used to designate targets for other aircraft or to guide weapons with laser seekers. A laser ranger obtains range to target because of the shorter wavelength of the laser signal. However, lasers do not penetrate weather as well as radar. Laser systems are small, light, relatively cheap, and are popular in a podded configuration to increase the capability for close air support in daylight. An example is the Pave Penny pod used on the *A-10* attack aircraft, while the *GBU-24* is an example of a laser-guided bomb (see also Appendix F). Laser systems provide a partial answer to the target acquisition problem.

With regard to radar discussed above, it should be pointed out that current radars have an inherent problem *seeing* through trees and vegetation that provide cover to vehicles traveling along roads. Consequently, the problem with maintaining surveillance on vehicles under these conditions is that they are able to maneuver in ways that are unpredictable, such as stopping for periods of time or changing directions. Because of this limitation, the Air Force is doing research on integrated sensors to enhance the radar detection of ground targets obscured by foliage (see also Section 7.4.6). The objective of the integrated sensors is to investigate radars that are capable of seeing through foliage and use this information to fuse with existing systems leading to a capability to track vehicles through move–stop–move conditions within the foliage cover. Two primary modes of radar will be investigated. *SAR* develops radar images of the area for detection of fixed targets, such as vehicles that are not moving, while ground-moving target-indication radar (e.g., *ISAR*) develops radar detections

of moving targets or vehicles. Moreover, integrated sensor research will be devoted to developing algorithms that will fuse these two types of radar into a composite picture that maintains a track of the vehicle through the foliage.

5.6 Unguided Weapons

Unguided weapons (e.g., bombs) can be considered as low-drag or high-drag (for guided bombs, see Appendix F). Examples of low-drag and high-drag weapons are the following:

(1) Low Drag General Purpose (*LDGP*) Mk 82, 83, and 84. (Note: the Mk 83 and 84 are also designated as *Mk 83/BLU-110* and *Mk 84/BLU-109*, respectively.) In addition to these bombs, there is the Mk 80 *iron bomb*.
(2) High-Drag Mk 82 *Snakeye*.

Some more details on these bombs are presented here.

***Mk 82*:**
Primary Function. 500-pound gravity (i.e., free-fall), general-purpose weapon.
Dimensions. Length: 5 ft, 6.2 in; Diameter: 10.75 in.
Range. Varies by method of employment.
Mk 83:
Primary Function. 1,000-pound gravity (i.e., free-fall), general-purpose weapon.
Dimensions. Length: 9 ft., 10 in; Diameter: 14 in.
Range. Varies by method of employment.
***Mk 84*:**
Primary Function. 2,000-pound gravity (i.e., free-fall), general-purpose weapon.
Dimensions. Length: 10 ft., 10 in; Diameter: 18 in.
Range. Varies by method of employment.

The above weapons can function in either *CCIP* (continuously computing intercept point) or the *CCRP* (continuously computing release point) mode. For a given release altitude the airspeed may be on the order of 834 km/hr (450 nm/hr), dive angles between 0° and 60°, and ejection velocity on the order of 3.048 m/sec (10 ft/sec). Two weapon delivery configuration options can be considered. These are (1) the *vertical velocity* option, which represents a three-axis navigation system and in which the aircraft dive angle is computed from the aircraft velocity components, and (2) the *angle-of-attack* (*LOS*) option, which represents a two-axis navigation system (i.e., only horizontal velocity components are considered), where the dive angle is computed from the sum of the pitch angle and angle of attack.

Another bomb, in addition to the ones mentioned above, is the *BLU-82* that was used in Afghanistan. The *BLU-82*, also known as *Daisy Cutter,** is a 15,000-lb (6,804-kg) conventional weapon. It is the most powerful conventional weapon in the U.S. arsenal. The bomb is generally dropped in low areas surrounded by mountains.

Daisy Cutter refers to a type of fuse extender and is not the name of the bomb.

Upon release from the aircraft, such as the *MC-130* (e.g., *MC-130E/H Combat Talon I* and *II*), a stabilizing parachute opens to help guide it to its target. Moreover, because of the enormous blast, the bomb must be dropped from at least 6,000 ft (1,829 m) above the ground. The bomb, which incinerates everything within 600 yards (549 meters) of its blast, explodes 3 ft (0.914 m) above ground, cutting a wide swath of destruction without digging a crater (for other *BLU*s, see Appendix F-3).

With regard to unguided weapons, the parameters that play a major role are the *horizontal* and *vertical* velocities, and *pitch* and *roll*.

Horizontal Velocity: Bombing accuracy is moderately sensitive to errors in the horizontal velocity components, particularly for high-drag weapons, for *CCRP*, and for the vertical velocity option, all under certain release conditions. Gunnery accuracy is almost totally insensitive (within limits) to horizontal velocity errors. Bombing accuracy sensitivity dictates an accuracy requirement of approximately 0.6098 m/sec (2.0 ft/sec) per axis (both along- and cross-range).

Vertical Velocity: Weapon delivery accuracy exhibits a high sensitivity to errors in the vertical velocity component for shallow dive angle releases. Gunnery accuracy and bombing accuracy at shallow dive angle releases dictate that the accuracy requirement for the vertical velocity component be about 0.6098 m/sec, equivalent to the accuracy obtainable by a good-quality *INS*. It should be noted that even a vertical velocity accuracy of about 1.83 m/sec (6.0 ft/sec) could keep the overall *CEP* under 30.48 m (100.0 ft).

Pitch and Roll: Weapon delivery accuracy sensitivity to pitch and roll exhibits a wide variation in magnitude, from extremely low to very high. For bombing, the vertical velocity option displays a higher sensitivity than the angle-of-attack option; for gunnery, the opposite is true. Furthermore, for the low-drag bomb, the *CCRP* displays a higher sensitivity than the *CCIP*. For the most sensitive case, the accuracy requirements for pitch and roll should be approximately 0.25°.

5.6.1 Types of Weapon Delivery

For single low-drag weapon deliveries, such as illustrated in Figure 5.12, the interpretation of the variables time of fall T, slant range SR, harp angle H, and pitch angle θ is clear. For other types of deliveries the interpretation is not apparent.

Therefore, four additional types of weapon delivery that encompass the entire spectrum will be discussed. These are (1) stick bombing, (2) high-drag, (3) cluster, and (4) dispenser weapons.

(1) **Stick Bombing:** Figure 5.13 illustrates a typical unaccelerated delivery. N bombs are released with a constant interval of time between individual releases. For this type of delivery, T is the average time of fall of the bombs; SR is the slant range from the release of the first bomb to the center or other point in the impact pattern being aimed; and H is computed as $\sin^{-1}(Y/SR)$, where Y is the release height of the first bomb. It is a common tactic to pull recovery maneuvers during weapon release, particularly for long sticks. Modern bombing systems are equipped to compute appropriate weapon spacing during an accelerated release.

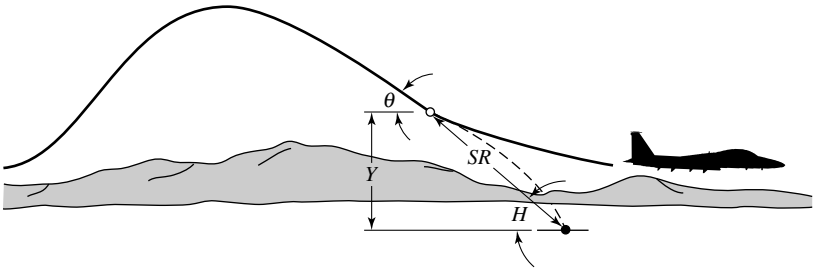

Fig. 5.12. Single-weapon delivery.

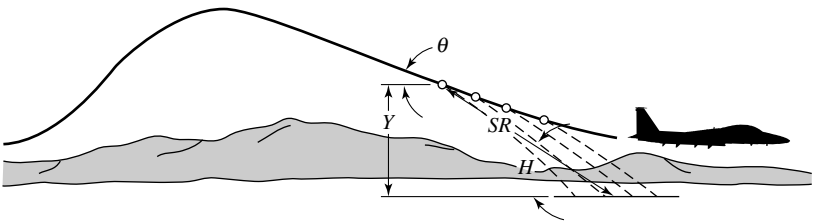

Fig. 5.13. Stick bomb delivery.

(2) **High-Drag Munitions:** High-drag munitions (or weapons) offer special accuracy estimation problems for two reasons: (a) They are usually released level or at shallow dive angles at low altitude, and (b) They can have a two-phase trajectory or a three-phase trajectory (low drag/retarded/terminal booster). Level low-altitude release presents the greatest problem for the bombing system to solve accurately. High-drag munitions with significant times of fall are most affected by variations in the velocity vector due to winds in the target area. In addition, the ballistic dispersion of high-drag munitions is larger than that of low-drag or slick munitions. However, due to much shorter slant range, impacts are sometimes closer to the target center than those for low-drag munitions. The representative high-drag munition is the Mk82 *Snakeye*.

Low-drag munitions, on the other hand, are the most frequently used free-fall weapons. The Mk82, 83, and 84 bombs are representative of this type of ordnance. Deliveries are from relatively high altitude because of the long down-range distances of the trajectories and the requirement for the releasing aircraft to remain clear of the bomb fragment envelope.

(3) **Cluster Weapons:** Figure 5.14 illustrates delivery where a canister is dropped from an aircraft, falls for T_1 seconds, and then opens. A cargo of munitions in the canister then falls another average time T_2 before impacting. For this type of delivery, T is the sum of T_1 and T_2; SR is the slant range from release to the center or other point of the impact pattern being aimed; and as before, H is computed as $\sin^{-1}(Y/SR)$, where Y is the release height of the first munitions.

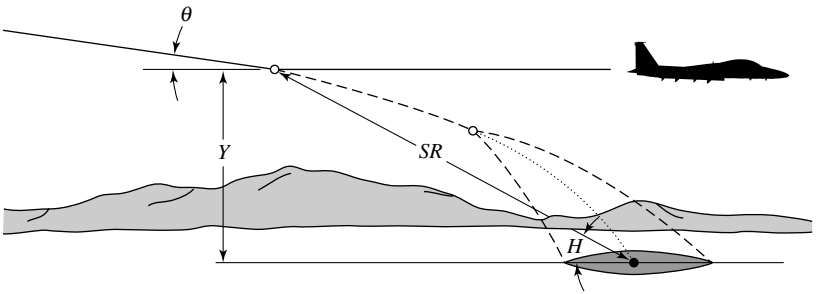

Fig. 5.14. Cluster weapon delivery.

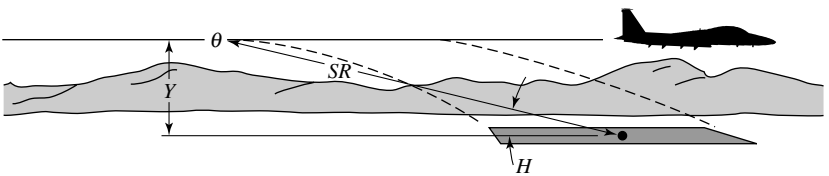

Fig. 5.15. Dispenser weapon delivery.

(4) **Dispenser Weapons:** Figure 5.15 illustrates this delivery, where a dispenser remains on the aircraft and only the munitions contained in the dispenser are released. For this delivery, T is the average time of fall of the munitions; SR is the slant range from the point where the first munition is released to the center or other point of the impact pattern being aimed; and H is computed from $\sin^{-1}(Y/SR)$, where Y is the release height of the first munitions.

5.6.2 Unguided Free-Fall Weapon Delivery

For unguided weapons (see also Section 5.6), such as free-fall bombs, delivery accuracy is affected by two categories of error sources: human errors and aircraft system errors. Their relationship is illustrated in Table 5.1. As shown, aircraft off-parameters error and aiming errors are both human-related, while platform error and weapon separation error are aircraft related. For computed deliveries, the aircraft off-parameters error is absent.

If the weapon is a free-fall bomb, a flat Earth approximation can be used to compute the time from launch to impact. The initial velocity of the weapon is assumed to be the velocity of the aircraft at launch of the bomb. The time required for the weapon to fall to the target's altitude is computed based on the initial velocity and the force of gravity acting on the weapon. If the weapon is unable to traverse the distance in the horizontal plane to the target in the time required for the weapon to impact the target in the vertical plane, the weapon will fall short of the target. Once the weapon will at least reach the target, the launch will occur. The launch action will be performed on the target.

Table 5.1. Sources of Delivery Accuracy Errors

Delivery	Human Errors		Aircraft Errors	
Manual	Aircraft Off-Parameters	Aiming	Platform	Weapon Separation
Computed		Aiming	Platform	Weapon Separation

The time of impact with the target is computed as the time required for the weapon to traverse the distance to the target along a straight-line path. The velocity specified for the weapon is oriented directly along the straight-line path and is assumed constant. The intercept phase is scheduled at the computed intercept time.

In reference to Table 5.1, the various errors will now be discussed in some more detail. *Aircraft off-parameters* error results when the aircraft is not at the planned airspeed, altitude, and dive angle at the time of weapon release. This is because the bombing reticle has been set by the pilot based on the ballistics of the weapon for the planned release conditions; thus, these conditions must be met for the bomb to hit the desired point of impact. Variations in altitude, dive angle, and airspeed cause different errors. Pilot *aiming* error is a measure of the pilot's ability to place the aircraft cockpit aiming symbology on the desired aimpoint at the correct time. *Aircraft platform* error is a measure of the aircraft's ability to determine weapon release conditions and aircraft position in relation to the target. This error has continued to decrease as sensor, computer capacity, and navigation improvements have been fielded. *Weapon separation* error results from turbulent airflow around the aircraft. This error is a function of aircraft type, pylon and rack configuration, weapon type, and release conditions. Efforts to minimize, or at least predict, this error offer a great opportunity for improving delivery accuracy for unguided weapons.

We summarize this section by noting that weapon system error applies to the mean point of impact of a stick of weapons, while ballistic dispersion acts on the individual weapon impact points. Ballistic dispersion is the deviation from the mean ballistic trajectory due to manufacturing tolerances and other munition variances. Ballistic dispersion is circular normal in the normal plane and is given as a standard deviation (sigma). The delivery accuracy problem may be subdivided into three parts: (1) the ballistic problem, determining the weapon ballistic trajectory for existing position and velocity vectors; (2) the sighting problem, measurement of the delivery aircraft position and velocity vectors relative to the target; and (3) the control problem, the inclusion of problem dynamics as the delivery aircraft approaches the release point, changing position and/or velocity to simultaneously satisfy the ballistic and sighting problem. Finally, the effect of the wind on the bombing problem can be significant and difficult to measure with onboard sensors. In addition, wind shears between the target and the aircraft are, in essence, unmeasurable and can contribute to bombing errors, especially for high-drag weapons. In dive deliveries, headwinds tend to shallow the dive path and reduce bomb range, while tailwinds tend to steepen the dive path. Correction is made by adjusting the horizontal distance from target entry. Conversely,

tailwinds increase bomb range, increasing the slant range, thus decreasing the sight angle. The wind effect on the bomb after release can be corrected by establishing an aimpoint upwind of the target (see also Section 5.5.1 for details on these effects).

5.6.3 Release Point Computation for Unguided Bombs

In Section 5.5.2 aircraft delivery modes were discussed using radar and electrooptical sensors. In this section we will discuss briefly radar-aided and *EO*-aided bombing. The most stringent *IRS* (inertial reference system) requirements occur with unguided weapons. Therefore, the approach is to establish unguided weapon error budgets in which velocity errors are commensurate with other system errors. Based upon these budgets, the most stringent *IRS* velocity requirement is 0.5 ft/sec during bomb delivery.

Radar-Aided Bombing: An error budget is dependent upon flight conditions at the time of launch. For example, a fighter aircraft with automatic bomb delivery mode using *SAR* (synthetic aperture radar) target designation can have as many as 14 error budget sources (e.g., slant range, azimuth angle, altitude, *IRS* ground speed, *IRS* vertical velocity, true airspeed, time delay, ejection velocity, pilot steering, heading-induced sideslip, bomb dispersion, air-to-ground radar elevation position, air-to-ground slant range, and ballistic fit computation) including both error magnitudes and their contribution to weapon *CEP*. In this mode, the *IRS* velocity error contributes to the *CEP* from time of target designation to bomb release to bomb impact. The horizontal velocity error is 0.5 ft/sec in this budget, which results in an along-track error contribution of more than 30 ft (1 σ). Doubling the velocity error would make this the largest term in the error budget, but eliminating it would not reduce the *CEP* significantly. Therefore, 0.5 ft/sec is a reasonable choice for *IRS* velocity accuracy.

EO-Sensor Aided Bombing: An error budget for a fighter aircraft with automatic mode bomb delivery using an *EO* sensor target designation will have the same error budget as the radar-aided bombing. In this mode, the *IRS* velocity error contribution to the bomb *CEP* accrues only from bomb release time to impact. For example, during diving deliveries, the target is designated continuously through the weapon release point, so that the vertical velocity errors have greater error contribution than horizontal velocity errors. A vertical velocity error of 1.5 ft/sec (corresponds to a 0.5 ft/sec horizontal velocity error) is commensurate with other errors in the budget. Decreasing it does not reduce the *CEP* significantly; increasing it makes it the largest error. Therefore, 0.5 ft/sec horizontal velocity error and 1.5 ft/sec vertical velocity error are reasonable budget values.

The elevation angle error is based upon a 0.1° attitude error. Reducing the attitude error to 0.05° reduces the elevation angle error to the same level as other avionics and *IRS* errors.

Air-to-ground studies have shown that assuming a pilot aim error of 3 mils (1 σ) and total dispersion errors of 3.6 mils (1 σ), the fire control system was capable of estimating target acceleration with a 1 σ error of 10 ft/sec^2 and target velocity with a 1 σ error of 6 ft/sec in order to achieve a reasonable kill level.

Finally, and in reference to the use of an *IRS*, an analysis of current technology accelerometers indicates that their signal output is not a significant contributor to system error compared to a typical target maneuver estimation uncertainty during a gun firing pass. Similarly, a current technology rate gyroscope was evaluated to determine whether its signal output was accurate enough to achieve the 6-ft/sec target velocity estimation error. Analysis of gyroscope error sources indicates that only the rate scale factor error might be significant. The principal effect of the rate gyroscope bias error is to cause a corresponding bias error in the estimated *LOS* rate. This does not affect the pointing error due to the closed-loop action of the angle tracking filter/electrooptical sensor interface. Also, its effect on estimated acceleration normal to the *LOS* is negligible. However, it does affect the estimated velocity normal to the *LOS* through the cross product of the error in *LOS* rate with range. Thus, the sensitivity of estimated normal velocity to rate gyro bias is the target range.

5.7 The Bombing Problem

At release, the weapon is imparted an initial velocity vector $\mathbf{V}_o$. It is the vector sum (or resultant vector) of three vectors: the true airspeed $\mathbf{V}_{TAS}$, the ejection velocity $\mathbf{V}_e$, and the wind effect vector at the instant of release $\mathbf{V}_w$. These three velocity vectors are three-dimensional, as are the position vectors that describe the relative locations of the weapons and target. For purposes of the present discussion, the frame of reference shall be defined as a mutually orthogonal, three-dimensional, right-handed Cartesian coordinate system as shown in Figure 5.16. The x-axis is horizontal, representing the projection of the weapon longitudinal axis onto the xy-plane, with the positive direction along the weapon trajectory; the y-axis is vertical, positive up; the z-axis is mutually perpendicular to both x- and y-axes, with the positive axis to the right when facing down the x-axis [7]. The origin is chosen as the point in the target plane directly beneath the weapon at release. Three-plane views will be used to discuss the weapon's path through space, the ballistic trajectory.

The ballistic problem in the xy-plane will be discussed next. Figure 5.17 shows a view of the ballistic trajectory in the xy-plane in the absence of wind. This no-wind ballistic trajectory can be described by solving for two values, the downrange distance by the bomb and the time from release to impact (time of fall, T_f).

The weapon velocity vector $\boldsymbol{V}_o$ is the resultant of the delivery true airspeed $\boldsymbol{V}_{TAS}$ and the ejection velocity $\boldsymbol{V}_e$. In the xy-plane, only the vertical component will be described in the xz-plane.

Next we will discuss the sighting angle problem. Visual deliveries such as dive and level, usually involve measurement of the sighting angle β. Methods vary in complexity and accuracy from the depressed-reticle iron sights to sophisticated *EO* devices, such as *FLIR* and *TV*. From Figure 5.18 we see that the angle β is the algebraic sum of three angles in the xy-plane. That is,

$$\beta = \theta' - \alpha + \varepsilon, \tag{5.1}$$

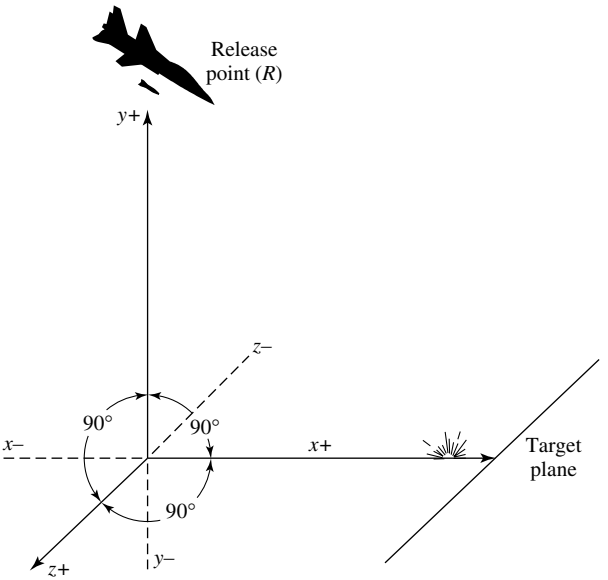

Fig. 5.16. Cartesian coordinate system.

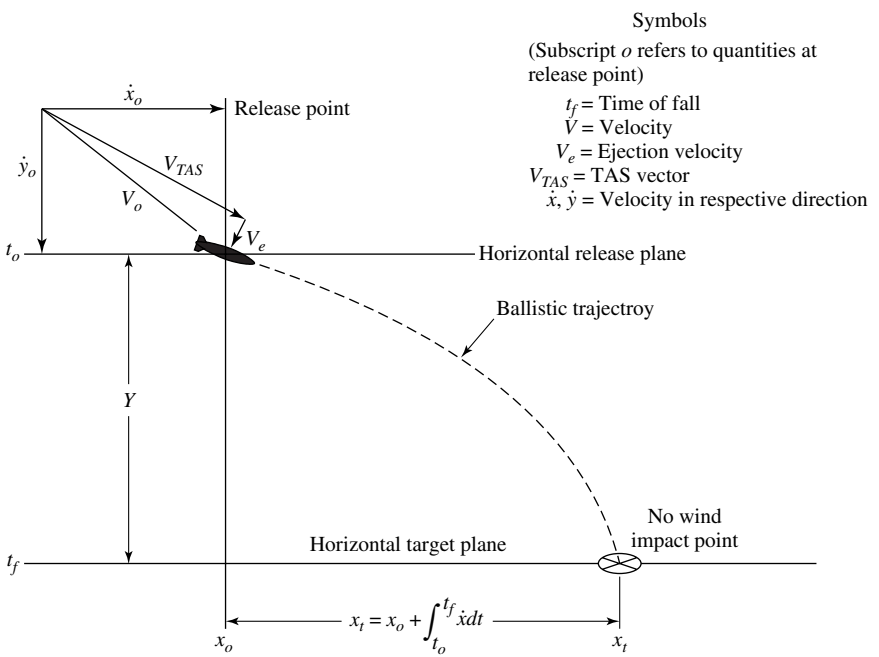

Fig. 5.17. The ballistic problem in the xy-plane.

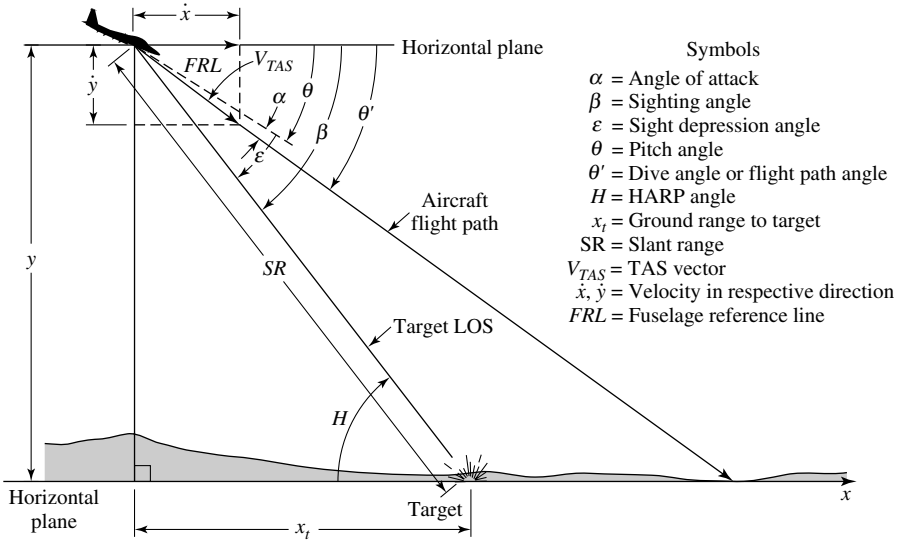

Fig. 5.18. The sighting problem in the xy-plane.

and

$$|\beta| = H = \tan^{-1}(y_t/x_t), \tag{5.2}$$

where

$|\beta|$ = absolute value of the sighting angle,
θ' = angle from the horizontal to the aircraft line of flight,
α = angle of attack between *FRL* and the line of flight,
ε = sight depression angle from the *FRL* to the target *LOS*,
H = harp angle,
x_t = distance to the target in the x-direction at time t,
y_t = distance to the target in the y-direction at time t.

It should be noted that β and ε are negative angles. θ' is negative for dive deliveries, nominally zero for level releases, and positive for loft or toss deliveries. The angle of attack α is positive for normal conditions where the *FRL* (fuselage reference line) is above the flight path.

Consider now the problem of parallax. Since the sighting device is not generally collocated with the ordnance, an additional factor, parallax, must be considered. The separation from the weapon to the sighting location will be considered

positive XP if the sight is forward of the weapon, and positive YP if the sight is above the weapon. The sight depression angle ε for a specific location (XP, YP) in the xy-plane becomes

$$\varepsilon = \tan^{-1}\left[\frac{Y + \cos\theta(YP) - \sin\theta(XP)}{X - \cos\theta(XP) - \sin\theta(YP)}\right] + \theta \tag{5.3}$$

5.7.1 Conversion of Ground Plane Miss Distance into Aiming Plane Miss Distance

Consider now Figure 5.19. This figure illustrates the relationship between the ground and aiming planes when examined in the vertical plane. The point I_Y is the projection of the *hole-in-the-ground* on the heading axis of the bombing run. What needs to be determined is the miss angle Y_M at the release point.

From Figure 5.19(a), the following equations are obtained:

$$H_T = \sin^{-1}(A/SR_T), \tag{5.4}$$

$$H_{IY} = \tan^{-1}[A/(Y + SR_T \cos H_T)], \tag{5.5}$$

$$Y_M = \sin^{-1}(Y \sin H_{IY}/SR_T). \tag{5.6}$$

Next, we note that Figure 5.19(b) illustrates the geometry in the deflection direction in the ground plane. The deflection in mils is

$$X_M = \tan^{-1}(X/SR_T). \tag{5.7}$$

The total error in range and deflection in mils, called the *radial error*, is thus

$$RE = (X_M^2 + Y_M^2)^{1/2}. \tag{5.8}$$

At this point, a more detailed description of miss distance is in order. In essence, the miss distance can also be defined as the measure of the threat system's ability to position a bomb or other warhead within the vicinity of a target, that is, the closest point of approach of the missile or bomb with respect to the target (note that although the discussion in this chapter deals with delivering bombs to a target, the concept of miss distance is equally applicable to delivering guided missiles). The miss distance is basically an error, and consequently, it can be expressed by a distribution function of the same form as the tracking error. In general, the miss distance is a function of the three spatial coordinates (x, y, z) whose origin is centered at aim point on the target. However, in most evaluations, the problem is usually simplified to two spatial dimensions (x, y).

Miss distance can be related to the probability that a threat (i.e., a missile, bomb, or even an aircraft) will arrive at a specific (x, y, z) location in space relative to the target. This probability depends upon the ability of the threat system to guide or fire a

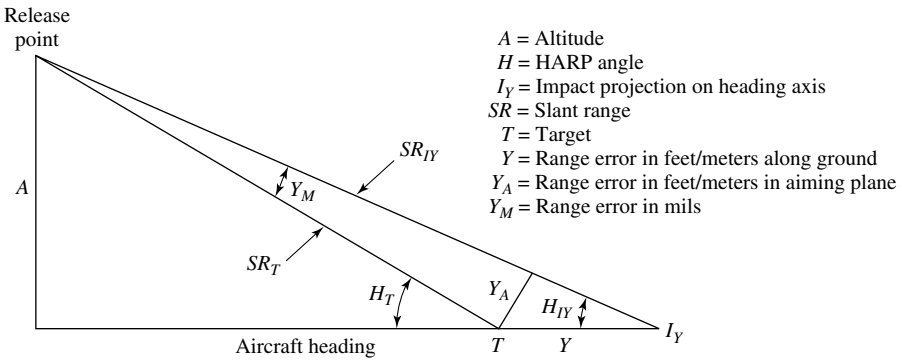

(a) Side view of the impact geometry (range miss distance)

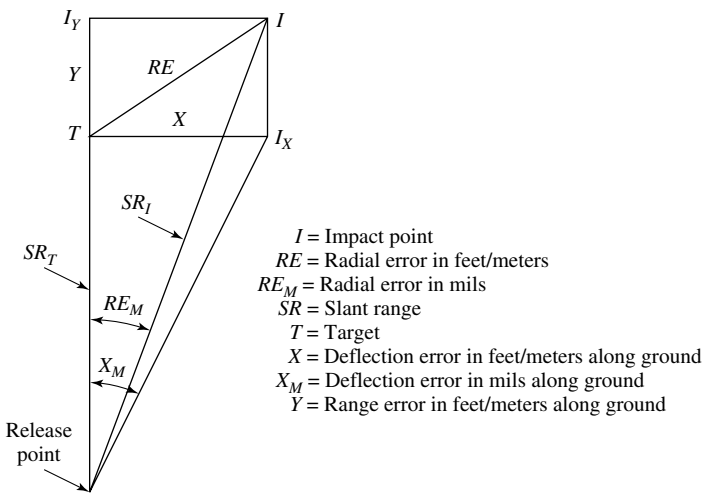

(b) Top view of the impact geometry (deflection miss distance)

Fig. 5.19. Geometry for the conversion of ground plane miss distance into aiming plane miss distance.

missile toward an intercept with the target. There are certain factors that influence the miss distance. For instance, the miss distance for ballistic projectiles is affected by (1) the accuracy of the tracking system, (2) the logic and operation of the fire control system, (3) the forces acting on the missile or bomb as it approaches the target, and (4) the flight path of the aircraft (see also Section 5.5). For guided missiles, there are several important factors relating to the design of the missile that influence the miss distance. One of these factors is the missile *response time*, which defines the relative ability of the missile to rapidly change direction. Specifically, missiles that have a relatively short response time are highly maneuverable, whereas missiles that have relatively a long response time are slow to respond and may continually oscillate about the desired flight path. The missile energy in the terminal phase of the encounter

is also an important factor. The missile's maximum turning rate also affects the miss distance. This rate is directly proportional to the maximum load factor of the missile and inversely proportional to the velocity. For example, a missile traveling at Mach 3 requires a 27-g maneuver capability to have the same turning rate as a target aircraft pulling 9-g's at Mach 1.

The guidance and control laws that navigate many of today's missiles are usually approximations to the proportional navigation law (see Chapter 4). These approximations can have a significant effect on the miss distance, particularly for maneuvering targets. The measurement of all of the target coordinates, such as position and velocity, allows the use of more sophisticated navigation laws. When radar tracking is used, internal thermal noise and external noise, target glint, and scintillation will cause errors in the measured target coordinates that will contribute to the miss distance. For example, at the beginning of an engagement, the thermal and external noise can seriously degrade a missile's performance by causing erroneous maneuvers that unnecessarily add to the drag on the missile, thus slowing it down. When the signal-to-noise ratio is low, the missile can literally chase the noise. Target glint can also be a serious problem, particularly when the missile gets close to the target, because of the fact that it is inversely proportional to the relative range. Target scintillation is another contributor to the tracking error, and hence the miss distance. This error is independent of range and may be smaller than the larger of the noise and glint errors. Passive *IR* homing missiles also have angular tracking errors.

In many weapon delivery cases, one calculates the miss distance frequency distribution. In order to do this, we need to define the intercept plane. The intercept plane (see Section 5.1, Figure 5.6, and Section 5.9, Figures 5.23 and 5.24) is the plane that contains the miss distance vector from the target aim point to the closest point of approach (*CPA*) and is normal to the bomb or missile path (relative to a stationary aircraft). Let the distance from the aircraft aim point (i.e., the origin of the coordinate system and normally the aircraft centroid) to any (x, y) pair be the miss distance for that particular launch (or bomb throw), and the distances x and y be the coordinate errors. If there is no correlation between the x and y components of the miss distances, the frequency distribution of the miss distance $\rho(x, y)$ can be expressed by the bivariate normal distribution

$$\rho(x, y) = \frac{1}{2\pi\sigma_x\sigma_y} \exp\{[-(x-\mu_x)^2/2\sigma_x^2] - [(y-\mu_y)^2/2\sigma_y^2]\},$$

where the sample means μ_x and μ_y and the standard deviations σ_x and σ_y are related to the sample means M and variances σ^2 by

$$\mu = M \quad \text{and} \quad \sigma^2 = [N/(N-1)]S^2$$

(note that σ^2 is sometimes set equal to S^2, particularly when N is large compared to unity). The sample means M_x and M_y are given by

$$M_x = \frac{1}{N}\sum_{i=1}^{N} x_i \quad \text{and} \quad M_y = \frac{1}{N}\sum_{i=1}^{N} y_i,$$

where x_i and y_i denote the x and y locations of the miss distance for the ith launch, and the sample variances S_x^2 and S_y^2 are computed using

$$S_x^2 = \frac{1}{N}\sum_{i=1}^{N}(x_i - M_x)^2 \quad \text{and} \quad S_y^2 = \frac{1}{N}\sum_{i=1}^{N}(y_i - M_y)^2.$$

If the two means are found or assumed to be equal to zero, and if the two standard deviations are found or assumed to be equal, the bivariate distribution simplifies to the circular normal distribution given by

$$\rho(r) = \frac{1}{2\pi\sigma_r^2}\exp[-r^2/2\sigma_r^2],$$

where r is the radial miss distance from the target aim point, and σ_r is the circular standard deviation, which is equal to both σ_x and σ_y. The circular miss distance within which 50% of the shots fall (the *CEP*) is given by [7]

$$CEP = 1.177\sigma_r.$$

As stated earlier, the miss distance is dependent upon both the tracking accuracy and the fire control/guidance accuracy of the system. From a total error point of view, the total miss distance standard deviation σ_m is related to the tracking error variance σ_t^2 and the fire control/guidance miss distance variance σ_g^2 by the *rss* relationship when the two errors are independent. Thus,

$$\sigma_m = (\sigma_t^2 + \sigma_g^2)^{1/2}.$$

Note that the expression for σ_m given above can be used to estimate the total *rms* miss distance based upon the contributions of the individual errors. The tracking error standard deviation is given by

$$\varepsilon_t = [\varepsilon_R^2 + R^2(\varepsilon_{d1}^2 + \varepsilon_{d2}^2)]^{1/2},$$

where

$$\begin{aligned} \varepsilon_t &= \text{total tracking error,} \\ R &= \text{slant range,} \\ \varepsilon_R &= \text{range error,} \\ \varepsilon_{d1}, \varepsilon_{d2} &= \text{orthogonal angular errors (given in radians).} \end{aligned}$$

The error associated with each one of these features can be represented by a normal distribution with a specific variance. The aircraft flight path also affects the miss distance. Finally, if both the angular tracking errors and the fire control/guidance errors are circular symmetric, and if the range tracking error is neglected, then the total radial miss distance standard deviation σ_t is given by the simpler equation

$$\sigma_m = \sigma_t = (R^2\sigma_a^2 + \sigma_g^2)^{1/2},$$

where σ_a is the standard deviation of the angular tracking error in radians.

5.7.2 Multiple Impacts

Using the geometry of Figure 5.19, the following procedure may be used to calculate the *CEP* for multiple impacts.

(1) Convert the alongtrack and crosstrack misses for each weapon impact into mils in the normal plane alongtrack and crosstrack using the following equations:

$$\text{Crosstrack: } X_M = \tan^{-1}(X/SR_T), \tag{5.7}$$

$$\text{Alongtrack: } Y_M = \tan^{-1}(Y \sin H_{IY}/SR_T), \tag{5.6}$$

where $1^\circ = 17.4533$ mils.

(2) Compute the alongtrack and crosstrack mean point of impact as follows:

$$\bar{X}_M = (X_{M1} + X_{M2} + \cdots + X_{Mn})/n, \tag{5.9a}$$

$$\bar{Y}_M = (Y_{M1} + Y_{M2} + \cdots + Y_{Mn})/n. \tag{5.9b}$$

(3) Compute the alongtrack and crosstrack standard deviations about their mean points of impact:

$$S_{X_M} = [(\bar{X}_M - X_{M_1})^2 + (\bar{X}_M - X_{M_2})^2 + \cdots + (\bar{X}_M - X_{M_n})^2/(n-1)]^{1/2} \tag{5.10a}$$

$$S_{Y_M} = [(\bar{Y}_M - Y_{M_1})^2 + (\bar{Y}_M - Y_{M_2})^2 + \cdots + (\bar{Y}_M - Y_{M_n})^2/(n-1)]^{1/2} \tag{5.10b}$$

(4) Subtract the alongtrack and crosstrack ballistic dispersions (in mils) from the alongtrack and crosstrack standard deviations by the root-sum-square method. When working in mils or in the normal plane the standard deviation of the ballistic dispersion is equal in the alongtrack and crosstrack directions:

$$S_X = (S_{X_M}^2 - S_B^2)^{1/2}, \tag{5.11a}$$

$$S_Y = (S_{Y_M}^2 - S_B^2)^{1/2}. \tag{5.11b}$$

(5) Compute the *CEP* (in mils about the mean point of impact) using one of the following methods:

(a) If $\sigma_S/\sigma_L \geq 0.28$,
where

$$\sigma_S = \text{smaller of } \sigma_X \text{ or } \sigma_Y,$$
$$\sigma_L = \text{larger of } \sigma_X \text{ or } \sigma_Y,$$

then

$$CEP = 0.589(\sigma_X + \sigma_L). \tag{5.12}$$

Table 5.2. Value of K Corresponding to Probability P

$\frac{\sigma_S}{\sigma_L}$	Impact Angle (degrees)	Probability					
		0.30	0.50	0.75	0.90	0.95	0.99
0.00	0.0	0.3853	0.6745	1.1504	1.6449	1.9600	2.5758
0.05	2.9	0.3886	0.6764	1.1514	1.6456	1.9606	2.5763
0.10	5.7	0.3987	0.6820	1.1547	1.6479	1.9625	2.5778
0.15	8.6	0.4169	0.6916	1.1603	1.6518	1.9658	2.5803
0.20	11.5	0.4421	0.7059	1.1683	1.6573	1.9704	2.5838
0.25	14.5	0.4705	0.7254	1.1788	1.6646	1.9765	2.5884
0.30	17.5	0.4997	0.7499	1.1925	1.6738	1.9842	2.5942
0.35	20.5	0.5285	0.7779	1.2097	1.6852	1.9937	2.6013
0.40	23.6	0.5568	0.8079	1.2310	1.6992	2.0051	2.6100
0.45	26.7	0.5842	0.8389	1.2564	1.7163	2.0190	2.6203
0.50	30.0	0.6109	0.8704	1.2853	1.7371	2.0359	2.6326
0.55	33.4	0.6369	0.9021	1.3172	1.7621	2.0564	2.6474
0.60	36.9	0.6621	0.9337	1.3514	1.7915	2.0813	2.6653
0.65	40.5	0.6867	0.9651	1.3874	1.8251	2.1111	2.6875
0.70	44.4	0.7107	0.9962	1.4247	1.8625	2.1460	2.7151
0.75	48.6	0.7342	1.0271	1.4631	1.9034	2.1858	2.7492
0.80	53.1	0.7571	1.0577	1.5023	1.9472	2.2303	2.7907
0.85	58.2	0.7796	1.0880	1.5422	1.9936	2.2791	2.8401
0.90	64.2	0.8017	1.1181	1.5827	2.0424	2.3318	2.8974
0.95	71.8	0.8233	1.1479	1.6237	2.0932	2.3881	2.9625
1.00	90.0	0.8446	1.1774	1.6651	2.1460	2.4478	3.0349

(b) If $\sigma_S/\sigma_L < 0.28$,
then

$$CEP = 0.9263(\sigma_S/\sigma_L)^{2.09} + 0.6745\sigma_L. \tag{5.13}$$

(c) Using Table 5.2, select K from the 0.5 probability column for the current ratio of (σ_S/σ_L); then compute

$$CEP = K\sigma_L. \tag{5.14}$$

Because most users are interested only in the weapon delivery accuracy about the target, an estimation of sigma may be made by root-sum-square addition of the along-track and crosstrack standard deviations with their respective mean points of impact. Then, the *CEP* may be computed as indicated in paragraph (5), above. This estimation is fairly accurate if the mean point of impact is a small distance from the target center (i.e., less than 25% of the standard deviation). If the *MPI* is a large distance from the target center, the system has a bias that should be corrected. Thus,

$$\sigma_{X_T} \approx (\sigma_X^2 + \bar{X}_M^2)^{1/2}, \tag{5.15a}$$

$$\sigma_{Y_T} \approx (\sigma_Y^2 + \bar{Y}_M^2)^{1/2}. \tag{5.15b}$$

5.7.3 Relationship Among *REP*, *DEP*, and *CEP*

When the *REP* and *DEP* are approximately equal, the bivariate normal distribution approaches circular normal, where $\sigma_R = \sigma_D = \sigma$. Thus, since $CEP = 1.1774\sigma$,

$$CEP = 1.1774(\sigma_R + \sigma_D)/2, \tag{5.16}$$

$$REP = 0.6745\sigma_R,$$

$$DEP = 0.6745\sigma_D.$$

Therefore,

$$CEP = 0.873(REP + DEP). \tag{5.17}$$

When *REP* and *DEP* are not equal, this relationship can also be used to approximate *CEP* even when *REP* and *DEP* differ by a factor as much as two. Beyond this range, the approximation is increasingly poor, and the values given in Table 5.2 should be used.

5.8 Equations of Motion

We begin our analysis by defining three coordinate systems that are necessary to describe the bomb dynamics. These coordinate systems are [1], [5], [7]:

1. **Inertial Coordinate System:** This is a right-handed coordinate frame ($\mathbf{i}_X$,$\mathbf{i}_Y$,$\mathbf{i}_Z$), whose origin is at the center of the Earth, but nonrotating with respect to the Earth, has the $\mathbf{i}_X$-axis pointing toward the first point of *Aries*, the $\mathbf{i}_Z$-axis along the Earth's spin axis, and the $\mathbf{i}_Y$-axis located 90° to the right of the $\mathbf{i}_X$-axis, completing a right-handed coordinate system.
2. **Earth-Centered Earth-Fixed (*ECEF*) Coordinate System:** As the inertial coordinate system, the *ECEF* coordinate system (X_e, Y_e, Z_e) is a right-handed system that is located at the center of the Earth, and rotating with the Earth. The X_e-axis points toward the intersection of the Greenwich Meridian and the equatorial plane, the Z_e-axis points along the Earth's spin axis, and the Y_e-axis completes the right-handed coordinate system.
3. **Target Coordinate System:** This coordinate system (X_t, Y_t, Z_t) is located at the target, with the X_t-axis pointing east, the Y_t-axis north, and the Z_t-axis up.

The above three coordinate frames are illustrated in Figure 5.20.

The simplest case is that of the equation of motion of a bomb whose position with respect to the target at any time t is $\mathbf{R}(t)$. It will be derived under the following assumptions: (1) The bomb (or projectile) is a point mass; (2) the bomb is not powered and has a constant mass; (3) the Earth is flat; (4) the gravitational attraction is constant; and (5) the effect of winds on the weapon delivery system are neglected. From the aforementioned assumptions, the differential equations of motion can be written in the following form [7]:

$$\frac{d\mathbf{V}}{dt} = \mathbf{f} - \mathbf{g} - 2\Omega \times \mathbf{V}, \tag{5.18}$$

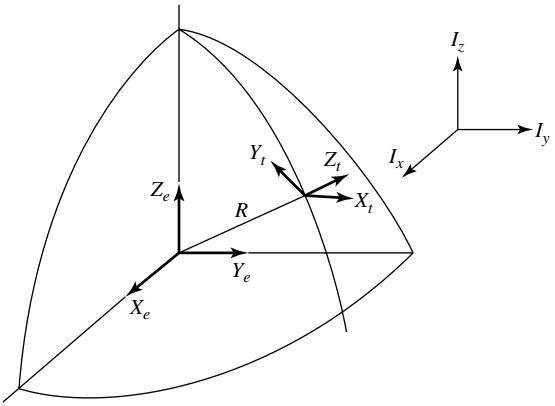

Fig. 5.20. Coordinate systems.

where

$\mathbf{V}$ = velocity vector of the bomb with respect to the target and is equal to d$\mathbf{R}$/dt,
$\mathbf{f}$ = specific force acting on the bomb,
$\mathbf{g}$ = acceleration due to gravity with components [0 0 g],
Ω = Earth rate vector ($= 7.291151 \times 10^{-5}$rad/sec $\approx$ 15 deg/hr).

This is the fundamental equation of motion, which specifies the position and velocity of the bomb at any time t. The position and velocity initial conditions must be provided to the *FCC*. Now let the initial position and velocity of the bomb at the time of release, $t = 0$, be $\mathbf{R}_r$ and $\mathbf{V}_r$. Integrating (5.18), we obtain the following equation:

$$\mathbf{V}(t) = \mathbf{V}_r + \int_0^t (\mathbf{f} - \mathbf{g} - 2\Omega \times \mathbf{V}) d\tau. \tag{5.19}$$

In order to find the position of the bomb at any time t, (5.19) must be integrated. Thus,

$$\mathbf{R}(t) = \mathbf{R}_r + \mathbf{V}_r t + \int_0^t \int_0^\tau (\mathbf{f} - \mathbf{g} - 2\Omega \times \mathbf{V}) d\tau_1 d\tau, \tag{5.20}$$

$$0 \le \tau_1 \le \tau,$$

$$0 \le \tau \le t.$$

In (5.20), if we wish to compute the bomb's position at the time of impact (i.e., from the time of release to the final impact time), then we must substitute $t = t_f$ and $\mathbf{R}(t) = \mathbf{R}(t_f)$. The external forces acting on the bomb must be included in the above analysis. These forces are:

W The weight of the bomb, which acts at the center of gravity. The weight has no x-y components in the horizontal plane. Therefore, its components are [0 0 mg].

D The drag. This force originates at the center of pressure, and its direction is parallel but opposite to the direction of motion.
L This force also originates at the center of pressure, and is directed perpendicular to the direction of motion.

Assuming no other forces except that the weight and drag are acting on the bomb, the drag force is given by the equation

$$\mathbf{D} = -C_d \left(\tfrac{1}{2}\rho V_a^2\right) S[\mathbf{V}_a / V_a], \tag{5.21}$$

where

$$\begin{aligned} C_d &= \text{the coefficient of drag,} \\ \rho &= \text{the density of air,} \\ \mathbf{V}_a &= \text{the true air velocity vector,} \\ S &= \text{the cross-sectional area of the bomb} = \pi d^2/4, \\ V_a &= |\mathbf{V}_a|. \end{aligned}$$

Consequently, the deceleration to the bomb is subjected is

$$\mathbf{f} = \mathbf{D}/m. \tag{5.22}$$

Figure 5.21 shows the nomenclature of a lightweight fighter attacking a ground target. The steady state (terminal velocity) along the flight path during the dive delivery occurs when the aircraft and nozzle aerodynamic drag equals the weight times the sine of the dive angle plus the gross thrust of the engine(s) minus the air engine air ram drag.

It should be pointed out that survivability is an important aspect of a given mission. Survivability is related to the amount of time that the aircraft spends inside a designated lethal envelope [3]. With regard to bomb launch and/or delivery, the *F/A-22 Raptor*, for example, is expected to close, without being detected, to within 15 mi of the current generation of radar that controls the Russian-built *S-300* family (designated *SA-10/12/20* by *NATO*) of *SAM*s, which have a range of 85–120 mi, while the *S-400* generation of *SAM*s will have a range of 250 mi. The problem is that 15 mi is the extreme range of the *F/A-22*'s standard air-to-ground weapon, the 1,000-lb *JDAM*, when launched from about 40,000 ft. Both the new Navy-developed *JSOW* glide bomb and the Air Force-developed *JASSM* standoff missile provide the necessary standoff range for survivability. Accuracy is quantified as bomb miss distance per degree error in dive angle at bomb release. From Figure 5.21 we can now define the various forces acting on the bomb. The target state data and weapon delivery capability, as specified by the weapon delivery computer, are the basic inputs for computation of aircraft commands by application of the appropriate control laws that cause the flight control system to maneuver the aircraft to an effective weapon release point. The weapon delivery computation will likely be based on data stored in the weapon delivery computer memory in tabular form, characterized as functions of

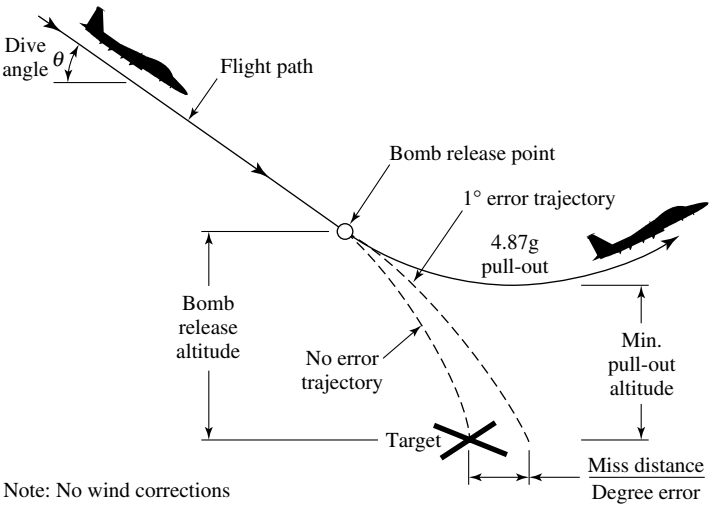

Fig. 5.21. Dive-bomb definitions.

aircraft altitude and airspeed. Target state data, derived from such sensors as radar and *EO* sensors, are subjected to errors. Primary error sources for the target state sensors are the following: boresight misalignment, target signature variations, measurement accuracy, tracking lags and biases, and airframe flexibility. Figure 5.22 illustrates the forces acting on the bomb.

Navigation error at weapon release is only one contributor to the accuracy of unguided bombs. As mentioned in Section 5.1, with the *GPS* as in input, the contribution of navigation error to impact error becomes small. Finally, we note that in fighter aircraft weapon delivery systems bombing accuracy is highly sensitive to altitude error. In this case, the system designer must consider using a *nonstandard day* altitude derived from the central air data computer (*CADC*).

When the bomb is in free fall, and assuming that there is no air resistance, then $\mathbf{f} = 0$. Furthermore, assuming that the impact point and velocity vectors are given by

$$\mathbf{R}^T = [X_i \quad Y_i \quad Z_i],$$

$$\mathbf{V}^T = [V_{xi} \quad V_{yi} \quad V_{zi}],$$

then we have from the vacuum trajectory the impact points $(X_i,\ Y_i,\ Z_i)$ as follows [1]:

$$X_i = X_r + V_{xr} t_f + \omega_{xc}, \tag{5.23a}$$

$$Y_i = Y_r + V_{yr} t_f + \omega_{yc}, \tag{5.23b}$$

$$Z_i = Z_r + V_{zr} t_f + \int_0^{t_f} \int_0^t (f_z - g) d\tau \; dt + \omega_{zc}, \tag{5.23c}$$

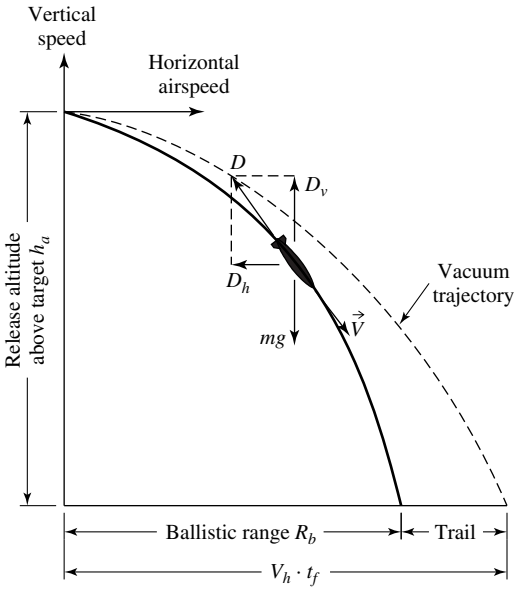

Fig. 5.22. External forces acting on the bomb.

where $\omega_{xc}, \omega_{yc}, \omega_{zc}$ are the components of the Coriolis correction vector ω_c,

$$\omega_c = -\int_0^{t_f} \int_0^t (2\Omega \times \mathbf{V}) d\tau \; dt. \tag{5.24}$$

The apparent Coriolis acceleration is given by the expression

$$\mathbf{A}_c = -2\Omega \times \mathbf{V}, \tag{5.25}$$

where Ω is the Earth rate and $\mathbf{V}$ is the bomb velocity vector with respect to the Earth. After performing the vector cross-product operation, the Coriolis equation in component form becomes

$$A_{cx} = 2(\Omega_z V_y - \Omega_y V_z), \tag{5.26a}$$

$$A_{cy} = 2(\Omega_x V_z - \Omega_z V_x), \tag{5.26b}$$

$$A_{cz} = 2(\Omega_y V_x - \Omega_x V_y). \tag{5.26c}$$

If the x-axis points east, the y-axis north, and the z-axis up, the Earth rate components become

$$\Omega_x = 0, \tag{5.27a}$$

$$\Omega_y = |\Omega| \cos \phi, \tag{5.27b}$$

$$\Omega_z = |\Omega| \sin \phi, \tag{5.27c}$$

where ϕ is the latitude of the target. The velocity components are

$$V_x = V_{xr}, \tag{5.28a}$$
$$V_y = V_{yr}, \tag{5.28b}$$
$$V_z = V_{zr} - gt. \tag{5.28c}$$

Substituting the above components into (5.26), we have

$$A_{cx} = 2\Omega_z V_{yr} - 2\Omega_y (V_{zr} - gt), \tag{5.29a}$$
$$A_{cy} = -2\Omega_z V_{xr}, \tag{5.29b}$$
$$A_{cz} = 2\Omega_y V_{xr}. \tag{5.29c}$$

When (5.29) is substituted into (5.24), one obtains the Coriolis correction components. We conclude this section by developing the impact point prediction, represented by (X_{ip}, Y_{ip}) coordinates in the target plane. In order to obtain the impact point prediction equations, we need the time-of-fall and trail relationships. These equations are given in terms of a Taylor series expansion in the form

$$t_{f_i} = t_f + \frac{\partial t_f}{\partial Z}(Z_i - Z_r) + \frac{\partial t_f}{\partial V_z}(V_{z_i} - V_{z_r}) + \frac{\partial t_f}{\partial V_h}(V_{h_i} - V_{h_r}) \tag{5.30a}$$

$$T_{r_i} = T_r + \frac{\partial T_r}{\partial Z}(Z_i - Z_r) + \frac{\partial T_r}{\partial V_z}(V_{z_i} - V_{z_r}) + \frac{\partial T_r}{\partial V_h}(V_{h_i} - V_{h_r}) \tag{5.30b}$$

where t_f and T_r are the time-of-fall and trail output from integrating the trajectory for the reference and release conditions Z_r, V_{hr}, V_{zr}. Once t_{fi} and T_{ri} have been obtained, the bomb impact point prediction equations can be expressed by the following equations:

$$X_{ip} = X_i + V_{xi} t_{fi} - T_{ri} \sin\psi + \omega_{xc}, \tag{5.31a}$$

$$Y_{ip} = Y_i + V_{yi} t_{fi} - T_{ri} \cos\psi + \omega_{yc}, \tag{5.31b}$$

where

X_{ip}, Y_{ip} = impact coordinates in the target plane,
X_i, Y_i = horizontal coordinates of the bomb's position at the potential release time in target coordinates,
V_{xi}, V_{yi} = horizontal coordinates of the bomb's ground velocity at the potential release time in target coordinates,
ψ = angle between the Y-axis and projection of the airspeed vector into the horizontal plane,
ω_{xc}, ω_{yc} = Coriolis and bomb spin correction components.

Typical error sources associated with the error values (i.e., error budget) are given in Table 5.3. It should be pointed out, however, that these error values are for weapon delivery under benign conditions. Requirements and/or specifications for more realistic combat conditions must be determined by tests, design, and evaluation.

Table 5.3. Navigation System Accuracy Requirements

Error Sources:	Horizontal Velocity (Along- and Crosstrack)	0.762 m/sec
	Vertical Velocity (3-axis system option)	0.762 m/sec
	Pitch and Roll	0.2° m/sec
Sensor Errors:	Horizontal Velocity (Along- and Crosstrack)	1.219 m/sec
	Vertical Velocity (3-axis option)	0.609 m/sec
	Airspeed	1.852 km/hr(1-kt)
	Angle of Attack (2-axis system option)	0.25°
	Pitch and Roll	0.25°
	Range	15.2 m max (0.5% slant range)
	Display Unit (Azimuth and Elevation)	1.33 mils
Miscellaneous Errors:	Release Time	0.1 sec (*CCIP*)
		0.02 sec (*CCRP*)
	Ejection Velocity (Bombs)	0.609 m/sec
	Weapon Ballistic Dispersion - *Mk 82 LDGP*	3.0 mils
	Mk 82 Snakeye	5.0 mils
Pilot Errors:	Pipper Position (azimuth and elevation)	2.5 mils
	Azimuth Steering (*CCRP* only)	3.0 mils

(All error sources given above are $1-\sigma$ values)

5.9 Covariance Analysis

An important tool in determining the target impact errors is the *covariance analysis* technique. Specifically, and as we have discussed in Section 4.8, a Kalman filter is often employed for estimating the position, velocity, and acceleration of a target. When the target motion and measurement models are linear and the measurement and motion modeling error processes are Gaussian, the Kalman filter provides the minimum mean-square error estimate of the target state. The dynamics model commonly assumed for a target in track is given by* [4]

$$X_{k+1} = F_k X_k + G_k w_k, \tag{5.32}$$

where $w_k \sim N(0, Q_k)$ is the process noise and F_k defines a linear constraint on the dynamics. The target state vector X_k contains the position, velocity, and acceleration of the target at time k. The linear measurement model is given by

$$Y_k = H_k X_k + n_k, \tag{5.33}$$

where Y_k is normally the target position measurement with statistics $n_k \sim N(0, R_k)$. The Kalman filter equations associated with the dynamics model, (5.32), and the measurement model in (5.33) are given by the following equations [8]:

*The reader will notice here different symbol designations from those given in Section 4.8. Since there is no uniformity among authors, this was done intentionally to bring to the reader's attention the different notations found in the literature.

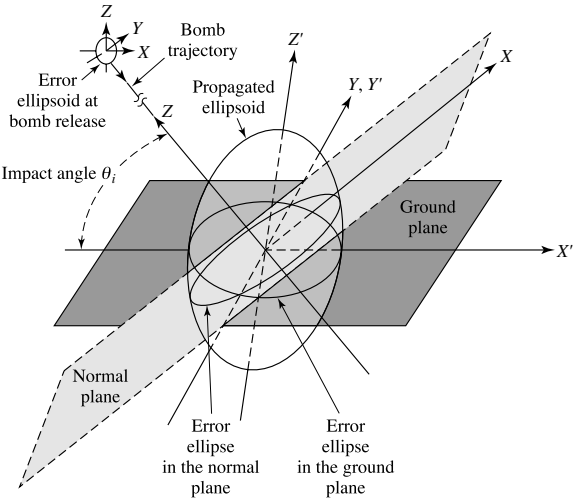

Fig. 5.23. The propagated error ellipsoid.

Time Update:

$$X_{k|k-1} = F_{k-1} X_{k-1|k-1} \tag{5.34}$$

$$P_{k|k-1} = F_{k-1} P_{k-1|k-1} F_{k-1}^T + G_{k-1} Q_{k-1} G_{k-1}^T \tag{5.35}$$

Measurement Update:

$$K_k = P_{k|k-1} H_k^T [H_k P_{k|k-1} H_k^T + R_k]^{-1} \tag{5.36}$$

$$X_{k|k} = X_{k|k-1} + K_k [Y_k - H_k X_{k|k-1}] \tag{5.37}$$

$$P_{k|k} = [I - K_k H_k] P_{k|k-1} \tag{5.38}$$

where $X_o \sim N(\bar{X}_0, P_0)$ denotes the mean and error covariance of the state estimate, respectively.

As discussed earlier, we will consider the covariance matrices at the point of impact due to the errors at bomb release. Other error sources, such as those due to ballistic dispersion and pilot azimuth error, are statistically independent of errors at release and can therefore be treated separately. Furthermore, in establishing a simulation program, the initial covariance matrix at release is commonly determined by the Kalman filter and propagated to the ground plane (i.e., target impact point) where the resulting error ellipsoid is aligned with the target coordinates (X_t, Y_t, Z_t). Therefore, the covariance matrix of the propagated ellipsoid is obtained in the (X_t, Y_t, Z_t) coordinate frame as illustrated in Figure 5.23.

In order to obtain the X-Y covariance matrix in the normal plane, which is required for computing the *CEP* radii, we must transform the propagated covariance matrix

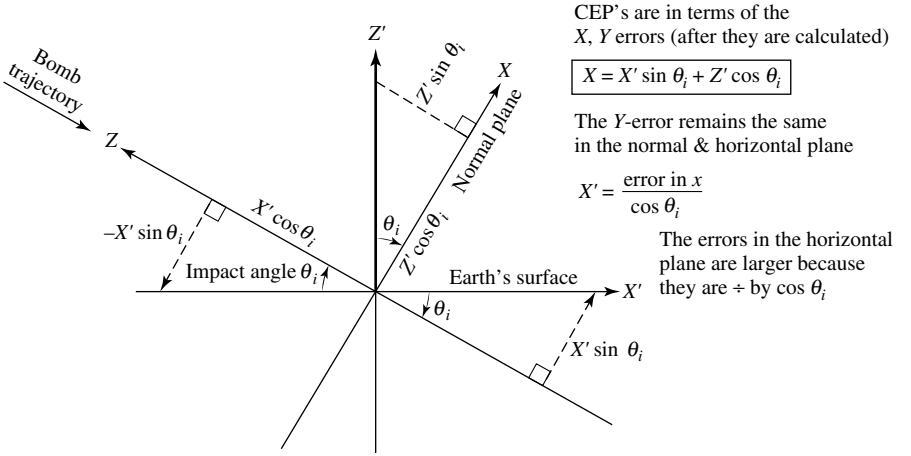

Fig. 5.24. Transformation from the X_t-Z_t frame into the X-axis and/or transformation from the X'-Z' frame into the X-axis.

into the (X, Y, Z) coordinate frame. Now, since the error ellipsoids are almost aligned with the X_t-axis, we have

$$Y \cong Y_t$$

and

$$\langle X, Y \rangle \cong \langle X_t, Y_t \rangle \cong 0$$

where $\langle \cdots \rangle$ denotes the cross-correlation components of the covariance matrix. Consequently, given the fact that $Y \cong Y_t$, we have

$$\sigma_Y^2 = \sigma_{Y_t}^2.$$

The transformation from the X_t-Y_t plane to the X-Y plane is obtained from Figure 5.24 and is simply given by the equation

$$X = X_t \sin\theta_i + Z_t \cos\theta_i, \tag{5.39}$$

where θ_i is the target impact angle. Therefore,

$$\begin{aligned}\sigma_X^2 = E\{X^2\} &= E\{(X_t \sin\theta_i + Z_t \cos\theta_i)^2\} \\ &= [\sin^2\theta_i]\sigma_{Xt}^2 + [\sin 2\theta_i]\langle X_t, Y_t \rangle + [\cos^2\theta_i]\sigma_{Zt}^2.\end{aligned} \tag{5.40}$$

Next, we note that σ_X^2 is dependent on the variance of the altitude error z_t^2, which can be large. The value of the cross-correlation $\langle X_t, Z_t \rangle$ is relatively small. The normalized *CEP* radius, R_{CEP}, can be obtained in terms of σ_Y from the following relation:

$$(R_{CEP}/\sigma_Y) = (0.562/K) + 0.615 \quad \text{for} \quad K \geq 0.3, \tag{5.41}$$

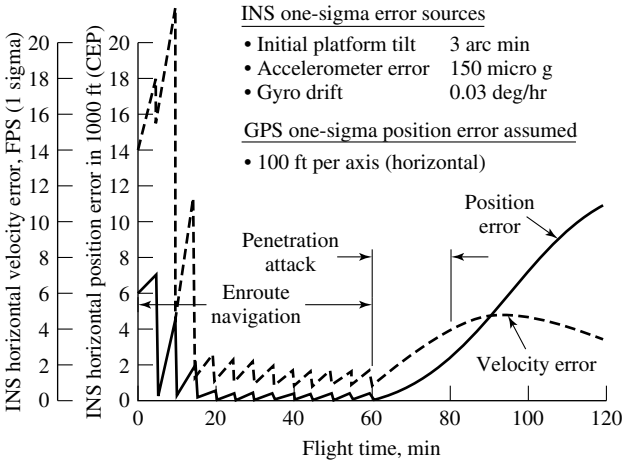

Fig. 5.25. *INS* performance with *GPS* update and after loss of *GPS* signal.

where

$$K \equiv (\sigma_Y^2/\sigma_X^2)^{1/2}.$$

Covariance simulation is used to derive weapon delivery aircraft navigation accuracies as a function of their trajectories to the target. Figure 5.25 shows the horizontal position and velocity errors of a typical *INS* using *GPS* updates, obtained from a covariance analysis simulation.

5.10 Three-Degree-of-Freedom Trajectory Equations and Error Analysis

In this section we present the equations that can be used to generate a point mass, three-degree-of-freedom (3*DOF*) trajectory and the accompanied error analysis of an unguided weapon (bomb) from an attack aircraft to impact a target on the ground. A computer program that generates the trajectory of the weapon in 3*DOF* from a set of given initial conditions can also perform a sensitivity analysis of impact errors for a given error covariance analysis at weapon release. The 3*DOF* trajectory equations are obtained from *Lagrange's* equations of motion (see also Section 2.3) of a *holonomic* system (a dynamical system for which a displacement represented by arbitrary infinitesimal changes in the coordinates is in general a possible displacement is said to be *holonomic*) for a nonthrusting object in the Earth's atmosphere. Sensitivity differential equations are obtained from the 3*DOF* equations and are used to propagate the initial condition error covariance matrix to impact where an analytical error analysis is performed to obtain the radial probability distribution of impact errors about the targeted aim point [11]. (Note that a *Monte Carlo* error analysis of initial condition errors can also be performed for comparison.)

Lagrange's equations of motion of a holonomic system with n degrees of freedom can be stated as follows: Let m_i represent the mass of one of the particles of the system, and let (x_i, y_i, z_i) be its coordinates, referred to some fixed set of rectangular axes. More specifically, these coordinates of individual particles are known functions of the coordinates $q_1, q_2, \ldots, q_n$ of the system at time t (see also Section 2.3). Therefore, this dependence can be expressed by the equations [12]

$$\begin{aligned} x_i &= f_i(q_1, q_2, \ldots, q_n), \\ y_i &= \varphi_i(q_1, q_2, \ldots, q_n), \\ z_i &= \psi_i(q_1, q_2, \ldots, q_n). \end{aligned}$$

Furthermore, let (X_i, Y_i, Z_i) be the components of the total force acting on the particle m_i. Thus, the equations of motion of this particle are [6], [11], [12]

$$m_i \left(\frac{d^2 x_i}{dt^2} \right) = X_i, \tag{5.42a}$$

$$m_i \left(\frac{d^2 y_i}{dt^2} \right) = Y_i, \tag{5.42b}$$

$$m_i \left(\frac{d^2 z_i}{dt^2} \right) = Z_i. \tag{5.42c}$$

The trajectory equation error model includes the following:

(1) A spherical rotating Earth with Coriolis (Ω-terms) and centripetal accelerations (Ω^2-terms).
(2) Altitude-varying air density $\rho(h)$ from tables.
(3) Meteorological winds $\mathbf{W}(x, y, h) \equiv [w_x \; w_y \; w_h]$ as a function of position (from tables).
(4) Altitude-varying gravity (central force field, γ-terms).
(5) Drag, lift, and side forces (drag coefficient C_D versus *Mach* Number tables).

Consider an (x, y, z) right-handed *Cartesian* coordinate system of the weapon with positive (x, y, z)-axes pointing north, east, and up, respectively. Let θ be the colatitude of the origin (0, 0, 0) attached to and rotating with the Earth ($\Omega = 7.29211 \times 10^{-5}$ rad/sec), of local radius R_e. From Lagrange's equations of motion, the point-mass trajectory equations upon which the trajectory and error analysis results will be based can be written as follows:

$$\begin{aligned} \ddot{x} = {} & -2\Omega_y \dot{z} + 2\Omega_z \dot{y} + (\Omega^2 - \gamma_o/R^3)x - \rho V_a/2\{(\dot{x} - W_x)(B_D + B_L \tan\Gamma) \\ & -[(\dot{y} - W_y)/\cos\Gamma]B_s\}, \end{aligned} \tag{5.43a}$$

$$\begin{aligned} \ddot{y} = {} & -2\Omega_z \dot{x} - \Omega_z[(z + R_e)\Omega_y - \Omega_z y] - \gamma_o y/R^3 - \rho V_a/2\{(\dot{y} - W_y) \\ & (B_D + B_L \tan\Gamma) + [(\dot{x} - W_y)/\cos\Gamma]B_s\}, \end{aligned} \tag{5.43b}$$

$$\begin{aligned} \ddot{z} = {} & 2\Omega_y \dot{x} + \Omega_y[(z + R_e)\Omega_y - \Omega_z y] - \gamma_o(z + R_e)/R^3 - \rho V_a\{(\dot{z} - W_z)B_D \\ & -(V_a \cos\Gamma)B_L\}, \end{aligned} \tag{5.43c}$$

where

$$
\begin{aligned}
R_e &= \text{local radius of the Earth},\\
h &= R - R_e,\\
\mathbf{V}_a &= \mathbf{V} - \mathbf{W}(x, y, h),\\
V &= (\dot{x}^2 + \dot{y}^2 + \dot{z}^2)^{1/2},\\
V_a &\equiv \{(\dot{x} - W_x)^2 + (\dot{y} - W_y)^2 + (\dot{z} - W_z)^2\}^{1/2},\\
R &= \{x^2 + y^2 + (z + R_e)^2\}^{1/2},\\
\Omega_z &= \Omega\cos\theta, \quad \Omega_y = \Omega\sin\theta,\\
\gamma_o &\equiv g_o R_e^2 \cong 32.174 R_e^2,\\
\cos\Gamma &= 1/V_a[(\dot{x} - W_x)^2 + (\dot{y} - W_y)^2]^{1/2}, \quad \sin\Gamma \equiv (\dot{z} - W_z)/V_a,\\
B_D(t) &\equiv C_D A_{\text{ref}}/\text{mg}_o = B_D(\xi, \alpha, V_a, h) \quad \text{Drag coefficient},\\
B_L(t) &\equiv C_L A_{\text{ref}}/\text{mg}_o = B_L(\xi, \alpha, V_a, h) \quad \text{Lift coefficient},\\
B_s(t) &\equiv C_s A_{\text{ref}}/\text{mg}_o = B_s(\xi, \alpha, V_a, h) \quad \text{Side force},\\
&\quad (\xi \equiv \text{total angle of attack}; \alpha \equiv \text{azimuth of } \xi).
\end{aligned}
$$

For an unguided weapon, the Coriolis and centripetal acceleration terms are negligible, but are retained nevertheless for completeness. The γ_0-terms represent the components of gravity, which vary with altitude h. The wind vector **W**(x, y, h) varies with position; V_a is the airspeed, which in the absence of winds equals the velocity of the weapon relative to an observer on the rotating Earth at (0, 0, 0); ρ(h) is the air density (lb/ft^3) at altitude h (published tables, e.g., 1966 *ARDC* standard atmosphere), and B_D, B_L, and B_s (ft^2/lb) are the reciprocal of the ballistic drag, lift, and side force coefficients, respectively. In general, these are functions of the total angle of attack ξ, azimuth of ξ, namely α, *Mach* number, *Reynold's* Number $\equiv \rho(\mathrm{h})\mathrm{V}_a\mathrm{L}_{ref}/\mu$, where μ is the dynamic viscosity, weapon attitude, and attitude rates. For axially symmetric weapons at zero or small angles of attack, we can assume that $\mathrm{B}_L \cong \mathrm{B}_s \cong 0$. (We can also assume that B_D is a function of *Mach* number only, whereby input consists of a table of C_D versus *Mach* number).

For application in real time, (5.43a), (5.43b), and (5.43c) can be accurately approximated by the following equations:

$$\frac{d^2x}{dt^2} = -\rho(h)V_a B_D/2\left[\left(\frac{dx}{dt}\right) - W_x\right], \tag{5.44a}$$

$$\frac{d^2y}{dt^2} = -\rho(h)V_a B_D/2\left[\left(\frac{dy}{dt}\right) - W_y\right], \tag{5.44b}$$

$$\frac{d^2z}{dt^2} = -\rho(h)V_a B_D/2\left[\left(\frac{dz}{dt}\right) - W_z\right] - g_o, \tag{5.44c}$$

$$h \cong z + \{(x^2 + y^2)/2(z + R_e)\}. \tag{5.45}$$

Note that for a flat Earth approximation, $h = z$. This is a satisfactory approximation when the origin is selected close to the target, for example, $x, y \leq 100$ miles (160.93 km).

5.10.1 Error Analysis

Equations (5.43a), (5.43b), and (5.43c) can be written symbolically for a 3*DOF* trajectory in the form

$$\frac{d^2\mathbf{r}}{dt^2} = \mathbf{f}(t, \mathbf{r}, \dot{\mathbf{r}}, \mathbf{p}), \tag{5.46}$$

where

$$\begin{aligned}\mathbf{r}^T &\equiv [x\ y\ z],\\ \mathbf{f}^T &\equiv [f_x\ f_y\ f_z],\\ \mathbf{p}^T &\equiv [\mathbf{r}_o^T\ \dot{\mathbf{r}}_o^T\ t_o\ \mathbf{D}^T\ \mathbf{W}^T].\end{aligned}$$

The first seven parameters of the $3 \times M$ vector $\mathbf{p}$ are the initial conditions and initial time. The drag ($\mathbf{D}$) and wind ($\mathbf{W}$) parameters occur in the input tables for C_D (*Mach* number) and $\mathbf{W}(x, y, h)$. The t_o parameter allows the error analysis to include a sensitivity for *release error time*.

Letting $p (p = 1, \ldots, M)$ denote any member of the set $\mathbf{p}^T$ above, the sensitivity $3 \times M$ vector may be defined as

$$\mathbf{S}(t) \equiv (\partial\mathbf{r}/\partial p),\ \frac{d\mathbf{S}(t)}{dt} \equiv (\partial\dot{\mathbf{r}}/\partial p) = \left(\frac{d}{dt}\right)(\partial\mathbf{r}/\partial p).$$

Differentiating (5.31) partially with respect to p and interchanging the order of d/dt and $\partial/\partial p$ (since p is a constant), results in a 3×1 sensitivity differential equation of the form

$$\frac{d^2\mathbf{S}(t)}{dt^2} = \mathbf{A}(t) + B(t)\mathbf{S} + C(t)\left(\frac{d\mathbf{S}(t)}{dt}\right), \tag{5.47}$$

where

$$\mathbf{A} \equiv (\partial\mathbf{f}/\partial p),\ B \equiv (\partial\mathbf{f}/\partial\mathbf{r}^T),\ C \equiv (\partial\mathbf{f}/\partial\mathbf{r}^T).$$

(Note that $\mathbf{A} \equiv 0$ for $p = x_0, y_0, z_0, (dx_0/dt), (dy_0/dt), (dz_0/dt), t_o$ and is nonzero for the $\mathbf{D}$ and $\mathbf{W}$ parameters, that is, holding $\mathbf{r}$ and $d\mathbf{r}/dt$ constant in differentiating $\mathbf{f}$ partially with respect to *explicit* dependence on p.)

Since there are three sensitivity linear differential equations (5.47) for each parameter p of M, there are $3 \times M$ sensitivity differential equations in total. For the eighteen sensitivity differential equations associated with $\mathbf{r}_0$, we have (dx_0/dt), $\mathbf{A} \equiv 0$. The (3×3) B and C matrices apply to any of the p's. The initial conditions required for integrating (5.46) for the $\mathbf{p}_0^T \equiv [\mathbf{r}_0\ \dot{\mathbf{r}}_0^T]$ sensitivities, are

$$\partial/\partial\mathbf{p}_0^T\left[\mathbf{r}/\left(\frac{d\mathbf{r}}{dt}\right)\right] = \mathbf{I}_{6\times6} \quad \text{(i.e., } 6 \times 6 \text{ identity matrix).}$$

Equations (5.46) and (5.47) are integrated concurrently from t_0 (weapon release time) to t_f (impact time). That is, for real-time implementation, (5.46) and (5.47) should be integrated in parallel because of the commonality of quantities and expressions in these equations. To recapitulate, given an estimate of the state $\mathbf{r}_0, \mathbf{r}_0$ at $t = t_0$ (launch point), and the associated error covariance matrix, the sensitivities given by (5.46), may be numerically integrated to impact (i.e., target at the ground). That is, (5.46) and (5.47) constitute the expressions relevant to generating the trajectory of the unguided weapon and performing the error analysis. Assuming a Gaussian bivariate distribution for the x, y (ground) impact errors, the elements of the impact error covariance matrix can be obtained by integrating the sensitivities, (5.47). The elements of the impact error covariance matrix are obtained from the integrated sensitivities of (5.47) as

$$\sigma_{\alpha,\beta}(h) = \sum_{i=1}^{6}\sum_{k=1}^{6}\{[S_{\alpha,k} + (\chi_\alpha/h)(\partial h/\partial p_k)]\sigma_{k,l,o}[S_{\beta,l} + (\chi_\beta/h)(\partial p_l)]\},$$
$$\alpha, \beta = 1, \ldots, 6, \quad k, l = 1, \ldots, 6, \tag{5.48}$$

$$S_{\alpha,k} \equiv \partial\chi_\alpha/\partial p_k, \quad \partial h/\partial p_k = (1/h + R_e)[x_1 S_{1,k} + x_2 S_{2,k} + (x_3 + R_e)S_{3,k}],$$

where $\chi_\alpha(\alpha = 1, \ldots, 6)$ has been defined as $x, y, z, (dx/dt), (dy/dt), (dz/dt)$, respectively, $\sigma_{k,l}$ is the k, l element of the input covariance matrix $P(t_0)$, and $S_{\alpha,k}$ are known from integration of (5.47) to impact. Equation (5.48) considers only the initial system errors. Ballistic and/or wind table parameter errors would require extension of the k, l summation limits in (5.48) to include the associated ballistic and/or wind sensitivities, and appropriate augmentation of $\sigma_{k,l}$. Finally, (5.48) applies for "small" errors, and the reference trajectory is assumed to impact the target, giving a zero mean dispersion.

Statistical air-to-ground weapon delivery error analysis employing an ensemble of events indicates that the horizontal velocity errors from the *INS* are the dominant error sources among those present, including sensor, computer, pilot, and weapon related error sources. Simulation program outputs indicate system performance in terms of horizontal position accuracy, *CEP*, where the *CEP* can be approximated by (see also Section 5.7.2, (5.12))

$$CEP \cong 0.589(\sigma_x + \sigma_y), \tag{5.49}$$

and horizontal velocity accuracy σ_v, where

$$\sigma_v = (\sigma_{vx}^2 + \sigma_{vy}^2)^{1/2}. \tag{5.50}$$

The one-sigma ensemble statistics of the velocity error applied to weapon delivery analysis are given by the expression

$$\sigma_{vs} = \sqrt{(1/T)\int_0^t \sigma_v^2(t)dt}, \tag{5.51}$$

which is equivalent to the root-mean-square *(rms)* value of the time-dependent, one-sigma statistics from the Kalman covariance analysis for a given expected penetration time span T.

Of the various roles an *INS* plays in a tactical fighter mission, such as en route navigation, supplying information for weapon delivery, flight control, sensor stabilization, and transfer alignment, the first two are considered to be the most important. It is well known that any moderately accurate *INS*, when periodically updated by the *GPS*, will provide a navigation accuracy far exceeding that generally required by tactical fighters for en route navigation [7]. Therefore, the accuracy requirement of an *INS* is determined by the required accuracy of the information it supplies for weapon delivery, that is, horizontal and vertical velocities, pitch, and roll information. Note that the time-dependent, one-sigma velocity error from the Kalman covariance analysis must be converted into one-sigma ensemble statistics before it can be applied to the weapon delivery performance trade-off.

5.11 Guided Weapons

In this section we will briefly discuss guided weapons, with particular emphasis on guidance techniques (see also Section 4.8, and Appendices E and F). Specifically, we will address the problem of optimal control theory that supports highly sophisticated weapon delivery system requirements. These guided weapons (or missiles) are capable of covering a large target accessibility footprint when launched with a wide range of initial conditions. In guided missiles, a guidance algorithm is commonly programmed into the missile's onboard digital computer, which computes steering angles and motor ignition times during the powered phase of the flight. Specifically, the function of the guidance algorithm is to guarantee that in the presence of perturbations and model approximations, the missile still satisfies all mission requirements, especially terminal accuracy. The main advantage of using modern control theory is the flexibility in designing an optimal guidance law that minimizes a performance or cost index. Among the guidance laws the missile analyst has at his disposal are proportional navigation (*PN*), the method of singular perturbation technique (*SPT*), and Kalman filter trackers. In proportional navigation, the missile launched from an aircraft is made to hit a target by pointing the relative velocity vector at the target at every point in the flight path. Also, the line-of-sight (*LOS*) rate is driven to zero by lateral acceleration commands proportional to the *LOS*. In *standoff* weapon delivery cases for ranges, perhaps up to 277.8 km (150 nm) a missile will require precise guidance and in-flight missile updates to reduce the system errors and terminal miss distance in minimum time. That is, the objective of minimum time is to transfer a system from an arbitrary initial state $\mathbf{x}_0$ at time $t = 0$ to a final state $\mathbf{x}(T)$ in minimum time. For a more detailed discussion of minimum time, see [10]. The performance index can be selected to reflect the requirements of a given or desired mission. For example, the guidance algorithm used in the *SRAM II* (short-range attack missile) is a linear quadratic regulator (*LQR*) with a terminal controller derived from modern control theory. A *regulator* is designed to keep a stationary system

within an acceptable deviation from a reference condition using acceptable amounts of control. Above all, *LQR* designs have desirable robustness (i.e., the ability to cope with adverse environments and input conditions) properties with guaranteed gain margins of at least 6 dB to ∞ and guaranteed phase margins of at least $\pm 60°$. The *LQR* is sometimes referred to as linear quadratic Gaussian (*LQG*) when Gaussian seeker noise is a significant part of the problem. In stochastic interception and rendezvous problems, one models uncertainties associated with the dynamic behavior of the target and interceptor by means of Gaussian white noise, which acts as a forcing function to the state differential equations. Designed for implementation in an onboard computer, the algorithm can use full missile-state feedback provided by an inertial navigation system (e.g., a strapdown *INS*). Furthermore, the algorithm must perform the following tasks: (1) calculate commands for complex maneuvers, (2) respond to in-flight perturbations, (3) adapt to varying mission requirements, (4) manage missile energy efficiently, and (5) interface with other software subsystems.

Normally, a guided missile is aerodynamically controlled by three or four fins. Additional control is provided by adjusting the ignition timing of the solid rocket motor. Missile launch, that is, delivery, can occur at any altitude within the carrier envelope, provided that adequate distance is available for safe launch recovery. The trajectory may include maneuvers, such as turns to orient itself to the proper target bearing. Constraints must be imposed on the path of the missile in order to satisfy conditions related to attitude stability, collision avoidance, and terminal attitude and position. Moreover, trajectories are designed to extremize certain flight parameters, such as terminal velocity, range, or time of flight to improve the probability of mission success. The general regulator problem can be formulated as follows. Consider the continuous-time linear deterministic system (or plant) expressed by

$$\frac{d\mathbf{x}(t)}{dt} = A(t)\mathbf{x}(t) + B(t)\mathbf{u}(t), \qquad \mathbf{x}(t_0) = \mathbf{x}_0, \tag{5.52}$$

where $\mathbf{x}(t)$ is the n-dimensional state vector that represents components of position, velocity, and any other modeling parameters, while $\mathbf{u}(t)$ is the r-dimensional plant control input vector. $A(t)$ and $B(t)$ are $n \times n$ and $n \times r$ matrices, respectively. The optimal linear regulator problem for a linear dynamic system entails the determination of the optimal control $\mathbf{u}(t)$, $t \in [t_0, T]$, that minimizes the quadratic performance index [2]

$$J(\mathbf{x}_0, t_0, T, \mathbf{u}(t)) = \frac{1}{2}[\mathbf{x}^T(T)S\mathbf{x}(T)] + \frac{1}{2}\int_{t_0}^{T} [\mathbf{x}^T(t)Q(t)\mathbf{x}(t) + \mathbf{u}^T(t)R(t)\mathbf{u}(t)]dt, \tag{5.53}$$

where the superscript T denotes vector or matrix transpose, S and $Q(t)$ are real symmetric positive semidefinite (i.e., nonzero) $n \times n$ matrices, $R(t)$ is a real symmetric positive definite $r \times r$ matrix, and T is the terminal time, which may be either fixed *a priori* or unspecified ($T > t_0$). The weighting matrices $R(t)$ and $Q(t)$ are selected by the control system designer to place bounds on the trajectory and control, respectively, while S and the terminal penalty cost $\mathbf{x}^T(T)S\mathbf{x}(T)$ are included in order to

ensure that $\mathbf{x}(t)$ stays close to zero near the terminal time. The term $\mathbf{x}^T(t)\,Q(t)\mathbf{x}(t)$ is chosen to penalize deviations of the regulated state $\mathbf{x}(t)$ from the desired equilibrium condition $\mathbf{x}(t) = 0$, while the term $\mathbf{u}^T(t)R(t)\mathbf{u}(t)$ discourages the use of excessively large control effort. For example, if in (5.53) $R(t) = 0$, we do not penalize the system for its control-energy expenditure. The optimal control in this case will try to bring the state to zero as fast as possible. With the aid of the *minimum* (or *maximum*) *principle*, the optimal control function that minimizes (5.53) is given by [8]

$$\mathbf{u}(t) = -R^{-1}B^T S\mathbf{x}(t), \tag{5.54}$$

where S satisfies the time-varying matrix *Riccati* equation

$$\frac{dS}{dt} = -SA - A^T S + SBR^{-1}S - Q. \tag{5.55}$$

A possible control law for the linear quadratic regulator problem may be expressed as follows:

$$\mathbf{u}(t) = \mathbf{u}_n(t) - R^{-1}(t)B^T(t)S(t)[\mathbf{x}(t) - \mathbf{x}_n(t)], \tag{5.56}$$

where

$$\begin{aligned}
\mathbf{x}(t) &= \text{measured state vector,}\\
\mathbf{x}_n(t) &= \text{nominal state vector,}\\
\mathbf{u}(t) &= \text{commanded control vector,}\\
\mathbf{u}_n(t) &= \text{nominal control vector.}
\end{aligned}$$

The discussion of the *LQR* presented above is the classical one. Finally, we note that the strength of the *LQR* lies in its ability to adapt to local disturbances without diminishing global performance.

Earlier in this section it was mentioned that the *SRAM II* uses *LQR* theory as the guidance law (or algorithm), which is an application of modern control theory, capable of intercepting and destroying moving as well as hardened targets and *SAM* sites. Even though the *SRAM II* program was canceled by the United States Congress, nevertheless, it is worth discussing some of its unique weapon delivery properties.

Designed in the early 1980s, the *SRAM II* is a supersonic standoff air-launched inertially guided strategic missile. The missile has the capability to cover a large target accessibility footprint when launched with a wide range of initial conditions. It is powered by a two-pulse solid rocket motor with a variable intervening coast time. The missile was required to fly trajectories that vary, depending on the particular mission objectives, from lofted (reaching to high altitude where path control is very limited), to low altitude (where path control is critical). Constraints may be imposed on the path of the missile in order to ensure satisfying conditions related to attitude stability, heating, collision avoidance, terminal attitude, and other mission requirements. It is also necessary to extremize certain flight parameters, such as terminal velocity, in order to enhance the probability of mission success.

As stated above, the guidance algorithm planned for *SRAM II* is an *LQR* (or specifically, a linear quadratic tracker with terminal controller) derived from modern control theory. Designed for implementation in an onboard computer, the algorithm calculates the motor ignition times and the missile steering angles during powered and unpowered flight using full missile state feedback. The current missile state is provided by an *RLG* (or other sensor) strapdown inertial navigation system. The algorithm must calculate commands for complex maneuvers, respond to in-flight perturbations, adapt to varying mission requirements, interface with other software subsystems, and fit within the resources of the onboard computer. Real-time implementation of a guidance law requires bridging the gap that exists between theory and flight code. This means solving numerous difficult problems that are not apparent until the missile hardware and software subsystems, together with the operational missions, are well defined.

Missile System

The *SRAM II* missile is designed to be carried aboard the *B-1B*. The missile system contains an *INS* and an *AVC* (air vehicle computer). For propulsion, a two-pulse solid rocket motor is used to provide thrust in free flight. The missile is aerodynamically controlled by three fins. Ignition timing of the two motor pulses can provide additional control.

Mission Description

The *SRAM II* mission starts during captive carry of the missile before launch (see also Chapter 7). While the missile is on board the carrier (note that at this point the missile will undergo an in-air alignment using *GPS* signals) the relative positions of candidate targets are calculated to determine whether they are within range. After the target is selected and assigned to the missile, the coordinates of the target are transferred to the *AVC*. The nominal trajectory that the missile will actually fly is then calculated from a database stored in the *AVC*. This trajectory must accurately represent the preflight-designed flight path and match the boundary conditions of prescribed launch point and the desired target. At the launch point, calculations are made for weapon delivery to ensure a safe release of the missile. A safe launch is dependent on the atmospheric flow field that the missile must travel through to clear the carrier, and on having sufficient carrier altitude for the missile to recover from its initial sink rate before impacting the ground. On command from the carrier crew the missile is released, and upon crossing the carrier safe-clearance boundary, the rocket motor ignites. Just after release, the missile undergoes a launch recovery maneuver to stabilize the missile and arrest the initial sink rate. The missile passes through a transition phase from launch recovery, to gradually transition into free flight. At this time, closed-loop guidance is initiated and continues to process and issue steering commands for the remainder of the flight. During powered flight, two solid-rocket motor pulses propel the missile. A nonpowered coast period follows burnout of the first motor pulse prior to second pulse ignition. After the rocket motor burns out, the missile continues to coast to the target.

Missile Trajectories

To satisfy a wide range of mission requirements, *SRAM II* is required to fly a variety of trajectories. The missile trajectory will depend on the relative locations of the carrier and target, as well as the characteristics of the carrier's flight envelope. Typically, the nominal trajectory will start with launch from the carrier and end at the target. Missile launch can occur at any altitude within the carrier envelope, provided that adequate distance is available for safe launch recovery. Trajectory shape may vary from a relatively flat trajectory to a semiballistic trajectory. The trajectory may include other maneuvers, such as turns to orient to the proper target bearing or a skip glide to increase range. The optimal trajectory (defined in terms of extremizing some trajectory parameter) is designed with constraints on initial and final position, inequality constraints on initial and final position, and inequality constraints on dynamic pressure, heating, steering angles, angular rates, and terminal flight path angles.

Guidance Problem

As in the air-launched cruise missile, the mission planners design the nominal flight trajectory to satisfy mission requirements using nominal performance data for the missile and expected environmental conditions. If the models used to derive the nominal guidance command time history represented the flight system behavior and expected flight environment, all information necessary to follow the nominal path would be contained in this time history. In practice, of course, such a situation never occurs. A missile in flight is subject to a variety of unpredictable perturbations that will affect its trajectory. The function of the guidance algorithm is to guarantee that in the presence of in-flight perturbations the missile still satisfies all mission requirements including terminal accuracy. The in-flight perturbations are caused by dispersions in initial position and velocity, rocket motor thrust, atmospheric density, winds, vehicle aerodynamic uncertainty, and steering lags.

5.12 Integrated Flight Control in Weapon Delivery

In the previous sections, we have treated weapon delivery from a mathematical perspective but did not discuss the human aspect, that is, the pilot, in this process. In any weapon delivery situation, control integration exerts a major influence on aircraft design, air combat effectiveness, and aircraft survivability. Specifically, flight control functions as the information manager and nerve center between the pilot and the vehicle optimizing the aircraft's controllability, performance, safety, and mission effectiveness during weapon delivery. In effect, we have a *man-in-the-loop* flight control system. The pilot is the *center* for this design integration process. To this end, the Boeing Aerospace Company developed the Man-In-the-Loop Air-to-Air Simulation Performance Evaluation Model (*MIL-AASPEM*) program.

The principal function of *MIL-AASPEM* is to simulate air-to-air combat at the many-on-many ($m \times n$) level. Originally, *MIL-AASPEM* was created to model many versus many beyond visual range (*BVR*) air-to-air engagements in *real time*. A later version of *MIL-AASPEM* incorporated surface-to-air and air-to-ground engagements of the air combat environment. *MIL-AASPEM* allows the most realistic simulation of futuristic aircraft, avionics, weapons, and tactics in a wide variety of scenarios.

Recognition of the human's psychological capabilities and limitations establishes the foundation for (a) crew station design, (b) task-oriented flying qualities, and (c) automation selection for workload reduction and mission task precision exceeding human capabilities. Specifically, significant synergistic benefits result from technology integration centered on the pilot and the flight control *neuromuscular* network interfaced with the airframe, avionics, weapons, propulsion, and C^3I systems [9]. In an intensive threat and target environment, trajectory controls generation for tasks such as low-level penetration threat avoidance/evasion and integrated flight/weapon control becomes a flight-critical function. In the future, fail-operational redundancy management will be extended to the mission trajectory generation avionics architecture. Since, as mentioned above, the pilot is the center of the design integration process, situational awareness/situation assessment (*SA/SA*) will be incorporated into future designs; that is, situational awareness will be provided in future aircraft with a new pilot–vehicle interface. In this case, a pilot model will be required. The pilot model provides for explicit representation of the pilot's behavior in information processing, situational assessment, and decision making during weapon delivery, using three key technologies: (1) modern estimation theory to represent the pilot's initial information processors of the sensory cues available to the pilot, (2) belief networks to model the pilot's ongoing assessment of the tactical situation, and (3) expert system production rules to represent situation-driven decision-making behavior. Situational awareness demands strict requirements for efficient information management within the cockpit to ensure that the pilot is fully cognizant of events and other combatant positions within his environment. Furthermore, knowledge of the current state allows the pilot to accurately predict future events, thereby enhancing his ability to effectively counter threat systems (e.g., air-to-ground) and achieve maximum lethality. Capability for decision making, automatic weapon preparation, autonomous and/or remote weapon control, and display alternatives are new computer functions that are required.

Efforts are underway to develop new avionics suites that will improve the flow of information in an aircraft while aiding the pilot's situational awareness (*SA*). Its terrain awareness and warning system (*TAWS*) is designed to help prevent controlled flight into terrain. It provides three views of current and predicted aircraft positions: (1) plan, (2) profile, and (3) $3D$ perspective. Each view includes the flight-plan and flight-path intent in conjunction with a detailed display of the surrounding terrain, relying on data from the flight management system, air data computer, radio altimeter, and instrument landing system. *TAWS* compares aircraft position with a worldwide terrain database stored in flash memory that contains 30-arcsec elevation data with up to 6-arcsec data near mountainous air bases.

5.12.1 Situational Awareness/Situation Assessment (*SA/SA*)

As mentioned above, air combat and/or weapon delivery demands that the pilot make dynamic decisions under high uncertainty and high time pressure. Numerous studies have shown that the most critical component of decision-making is situational awareness (*SA*), obtained via the rapid construction of tactical mental models that best capture or explain the accumulating evidence collected through continual observation of the tactical environment.

Many new technologies and subsystems are thus being considered to enhance the pilot situational awareness and situation assessment. These include advanced sensor systems and flight controls, state-of-the-art data fusion systems, onboard data link (e.g., C^3I) systems, helmet-mounted virtual reality (*VR*) displays, and novel multimodality interface technologies [13], [14]. A variety of *SA/SA* models have been hypothesized and developed by psychologists and human factors researchers, primarily through empirical studies in the field. Because of *SA/SA*'s critical role in air combat, the U.S. Air Force has taken the lead in studying the measurement and trainability of *SA/SA*. Situational assessment based on onboard information is realistic at the effects level: (a) man-machine interface (*MMI*), and (b) specific platform (e.g., *F-15*, *F/A-22*) *MMI*. Thus, optimized man–machine interfaces will provide excellent situational awareness.

Because of its importance in modern air combat, we will briefly discuss helmet-mounted displays (*HMD*) and the role they play in significantly aiding the pilot during air combat and weapon delivery. Flight tests conducted at Edwards AFB, California, in February 2000 in *F-15* fighters indicate that the helmet system, in combination with the high off-boresight (*HOB*) *AIM-9X* missile, can increase the lethality of the *F-15* by a factor of two or three. Together, the *AIM-9X* and the helmet-mounted cueing system will reestablish a first-shot, first-kill capability. Since 1998, the helmet has accumulated about 110 flight hours in *F-15 C*'s and *D*'s and about 174 flight hours in *F/A-18 C*'s and *D*'s. Known as the joint helmet-mounted cueing system (*JHMCS*), the helmet will change the nature of fighter aircraft combat and weapon delivery for pilots. For example, a pilot can use the helmet to update his navigation system if it has drifted simply by looking at known landmarks. The *JHMCS* is a revolutionary *look-and-shoot* tool worn by Air Force and Navy pilots seeking airborne and ground-based targets, and it is giving pilots a critical edge in combat. *JHMCS* displays such key information as (1) altitude, (2) airspeed, and (3) aircraft heading and target information on a visor attached to the helmet. This information is normally displayed on the *HUD*, located at the front of the cockpit. As a result, a pilot equipped with *JHMCS* will have the information available without the need to look inside the cockpit or through the *HUD* [9]. In other words, the *JHMCS* is a *HUD* on the head. Therefore, the *JHMCS* will offer U.S. pilots the ability to *look*, *lock*, and *launch* current and future generations of missiles at adversaries in the air and on the ground. The *JHMCS* initial production contract calls for 36 systems to support the *F/A-18E/F Super Hornet* (Lot 24) strike fighter.

A pilot can adjust the helmet's display to go blank when he is looking either at the *HUD* or down into the cockpit. He can also program it to go blank for both areas.

It should be noted that the *JHMCS* is not being developed to replace the *HUD*. The system augments the *HUD* by providing the pilot information outside the *HUD FOV*. The display capabilities of *JHMCS* are less important than its *cueing** capabilities. The helmet is being developed to work together with the aircraft's radar and the *AIM-9X Sidewinder* supersonic heat-seeking air-to-air missile, which is also under development at the present time. The cueing ability will allow pilots to aim and fire an *AIM-9X* missile at an enemy at a high angle off the aircraft's heading. For example, if a pilot sees an enemy aircraft off his left side, he will be able to cue his radar on the target and/or fire a missile at it without repositioning his plane to face the target. *JHMCS* will also verify that the *AIM-9X* is locked onto the correct target. Thus, the *JHMCS* will open up the weapon's employment zone, giving pilots more flexibility in combat.

Testers are initially developing *JHMCS* on an *F-15*. However, and as mentioned above, simultaneous development is also being conducted on the Navy's *F-18* at the Naval Air Warfare Center, Weapons Division, China Lake, California. Once the system is developed on these aircraft, it will be integrated into the *F-16*, the *F/A-22*, and possibly the joint strike fighter (*JSF*). In summary, the advantages of the *JHCMS* are many. Because it dramatically improves a pilot's situational awareness, the *JHCMS* represents a major increase in lethality. A pilot can now simply point his head to direct and launch advanced weapons like the *AIM-9X* high off-boresight, short-range missile. Therefore, specific benefits of the *JHCMS* include the following: (1) simultaneous cueing and display of aircraft sensor and weapon information, (2) display of threat locations through *GPS* data, navigation coordinates, and way-points, (3) the ability to cue and verify that a pilot is locked on the target (and not on his wingman) before deploying current and next-generation missiles, (4) a 20° field of view with full spherical coverage and day/night operability, and (5) easy boresight (aligning pilot's targeting optics with weapons/sensors), and video record–playback capability.

Other countries are also engaged in the development of *HMD*s. For instance, Sextant Avionique *HMD* systems are used by French pilots to engage medium-range targets up to 50 miles (80 km) with the *IR*-guided Matra *Magic 2* and advanced *Mica AIM*s. These *IR*-guided missiles have 50 g/90° turn capability for off-boresight (in either direction off the aircraft nose) shots using the *HMD*. The helmet-mounted display is fully integrated with the aircraft's (i.e., the *Rafale* and Dassault *Mirage 2000-5*s) avionics systems. Russian *AIM*s such as the *R-73E* (*NATO* code *AA-11 Archer*) and *AAM-AE* (*NATO* code *AA-12 Adder*) also use high off-boresight and *HMD* technology.

Nevertheless, the *JSF* radar's versatility in providing tracking, jamming, communications, and several other functions at virtually the same time is made possible by the *AESA* radar. The advanced *AESA* radar can spot air-to-air targets at 90 miles. The *JSF* will have no *HUD*. Instead, data will be projected on a pilot's helmet visor. In addition, the radar already has a moving-target-indicator mode that is expected to locate ground targets at about 50 mi. (*JSF*'s basic mission is air-to-ground strikes).

*Cueing refers to the ability of the helmet to cue—or point—sensors and weapons in the direction the pilot is looking.

Finally, we note that the electronic imaging system (*EIS*) plays an important role in the *HMD*. The *EIS* design uses a synthetic vision approach to expand the pilot's visual capability and situation awareness (*SA*) beyond the limits of current aircraft windows and *HUDs*. *EIS* provides an external image on the *HUD* that corresponds to the pilot's direction of view.

Recently, other advances in enhancing situational awareness and improving weapon delivery have been developed. For instance, in the summer of 2002, flight tests were conducted at Edwards AFB, California, to assess the performance of an integrated avionics suite for the *F/A-22 Raptor*. The suite is equipped with *integrated sensor fusion* capabilities that encompass electronic warfare and radar systems as well as *CNI* (communication, navigation, and identification) capabilities. With the *Raptor's* sensor-fused suite, all of the aircraft's sensors and displays work together to provide pilots with a single, integrated picture of their tactical situation. In order to evaluate the integrated suite, the test force must simulate enemy threats against the *Raptor*. Specifically, the suite will allow *F/A-22* operational pilots to focus more on tactics and less on sensor management and interpretation. Moreover, the suite complements the stealth capability of the *Raptor*, which is designated to reduce the aircraft's vulnerability to radar and *IR* threats. The stealthiness of the *Raptor* works to keep enemy forces in the dark, while its avionics suite works to provide *Raptor* pilots with the ultimate in situational awareness.

5.12.2 Weapon Delivery Targeting Systems

During *Operation Allied Force*, the U.S. Navy *F-14 Tomcats* used a new system to relay targeting information and improve the aircraft's ability to drop bombs and conduct battlefield reconnaissance. Currently, the U.S. Navy is upgrading the *F-14*s to improve the strike and reconnaissance system for air war. Specifically, the Navy has been expanding the *F-14*'s bombing capability with the introduction of the *LANTIRN* (low-altitude navigation and targeting infrared for night) *FLIR*-targeting system and its reconnaissance capability provided by the *Tarps* (targeting and positioning system) imaging pod. Moreover, *F-14* pilots will be able to use exact coordinates from the aircraft's *LANTIRN* system to accurately aim all-weather, *GPS*-guided weapons. To improve the *F-14*'s role in targeting weapons, pilots will be able to use their *LANTIRN* system to determine the exact *GPS* coordinates of a target. Those coordinates usually have a small error caused by inaccuracies in the intelligence systems that locate the target. Using different components of the *LANTIRN* system, *F-14*s will be able to reduce that error. The result is a several-foot improvement in accuracy of *GPS*-guided weapons.

Note also that the *F-15E* dual-role air-to-air/air-to-ground all-weather deep interdiction fighter carries *LANTIRN* targeting and navigation pods. In addition, the *F-15E* has an *APG-70* multimode *X*-band radar that includes *MTI* and *SAR* operating modes (*SAR* performance ranges from 10-ft low-resolution to 3-ft high-resolution, and 1-ft resolution in spot mode, while the *ASARS-2* offers a resolution of 1 ft. (0.3048 m) over a 1-sq-mi-*FOV* from a range of more than 108 nm (200 km) and an altitude of more than 65,000 ft (19,812 m) when observing ground targets). On the

other hand, the *F-16C* Block 40/50 fighter is equipped with an *APG-68* multimode radar and *LANTIRN*. The radar has a low-resolution beam mode with a *GMTI* capability.

LANTIRN pods get targeting information because the system has its own *GPS* receiver. That eliminates boresight errors that might otherwise occur between the pod and the aircraft. In essence, the system cross-cues the *GPS* data with information from the laser range finder to determine the precise location of the target. Those coordinates are then shown on the *LANTIRN* display. Through a second upgrade, *F-14*s will be able to share those target coordinates with other users. Two *F-14* squadrons in *Operation Allied Force* have been equipped with the fast tactical imagery (*FTI*) system, which allows cockpit video from the television zoom camera, *HUD*, or *LANTIRN* targeting system to be transmitted from the aircraft. Specifically, it takes about 15 sec for the *FTI* to capture and transmit the image. Moreover, the system has only *LOS* capability. However, data can be relayed via several *F-14*s so that imagery can be received on a carrier several hundred miles away. The information is processed at the same terminal where digital imagery from the *Tarps* reconnaissance pod is displayed. From there it can be sent to other locations on the ship. *FTI* is expected to be used more frequently once the *F-14*'s ability to update *GPS* coordinates is fielded. The target coordinates could be transmitted to other strike aircraft, like *F-15*s, which would then plug the data into their *GPS* weapons.

Another step in upgrading the *F-14*'s bombing capability is the newly planned integration of *GPS*-guided bombs. These are, for example, the 2,000-lb. laser-guided *GBU-24*s (see Appendix F). The enhanced *GBU-24*s are being fitted with a *GPS* receiver so they can still strike with near-precision even when cloud cover prevents laser targeting. The next *GPS*-guided weapon to become operational would be the 2,000-lb *GBU-32 JDAM*. The *F-14* upgrades also will use a *LANTIRN* upgrade so the laser designator can be used from 40,000 ft (12,192 m). At the present time, the system is cleared to operate only from 25,000 ft (7,620 m). Finally, the *JSF*'s electrooptical targeting system will be able to locate targets with enough acuity to identify a target such as a tank at more than 6.5 miles.

At this point, a more detailed description of the *JDAM* (joint direct attack munitions) is in order. The *JDAM* is a multiservice effort, with the Air Force as the lead service, for a strap-on *GPS/INS* guidance kit to improve the accuracy of the existing 1,000-lb and 2,000-lb general-purpose bombs in all-weather conditions. The *JDAM* looks much like most bombs, except for the added fins. It starts as a 1,000-pound or 2,000-pound dumb. *JDAM* is a state-of-the-art upgrade kit that turns free-falling "dumb" bombs into "smart" ones using inertial navigation and global positioning systems. A tail section, bolted onto the bomb, makes up most of the kit. Inside is a guidance control unit with inertial navigation and global positioning systems. A connection runs to a small electric motor that controls the tail's three movable fins. Strapped to the bomb are strakes, like fins. They help give it lift. From the guidance unit, an umbilical cord of wires plugs the bomb into the aircraft's computers. Because of the bomb's satellite-aided guidance system, the aircraft (e.g., *B-52H*s) can loiter in an area until they receive target identification, instead of waiting at the home base. With cruise missiles or laser-guided bombs, the aircraft has a long standoff fighting

range. That means facing fewer enemy defenses. The *JDAM* conversion kit weighs 100 pounds and costs $18,000 (in 2001 dollars).

JDAM is a true force multiplier that allows a single aircraft to attack multiple targets from a single release point and has been proven in recent operations in both Iraq and Kosovo. (A *JDAM* launched from a *B-2* bomber struck the People's Republic of China embassy in Belgrade during *Operation Allied Force*, indicating the critical need for more accurate intelligence and targeting for such high-precision weapons.) As a result, a product improvement program is underway to assess the utility of improvements such as an autonomous seeker, improved *GPS*, and a range extension to the *JDAM* unit. Moreover, the *B-1B Lancer* Block D (second upgrade) aircraft can perform near-precision attacks against targets deep into enemy airspace by employing up to 24 *JDAM*s (the *B-52H*s carry 12 *JDAM*s, 6 on each wing). To this end, the Block D modifications include installation of a MIL-STD-1760 weapons interface, *GPS* capability (for both aircraft and weapon navigation), and an upgraded aircraft communications package. Future *B-1B* upgrades, that is, Block E, are currently under development. The final block upgrade currently planned is Block F, or the defensive systems upgrade program. As the ground-to-air threat continues to grow and become more lethal, the *B-1B*'s defensive capability must be improved to enhance survivability. This program replaces the existing defensive system with an upgraded radar-warning receiver and the *RF CM* portion of the Navy's Integrated Defensive Electronic *CM* Program, which includes a fiber-optic towed decoy. These new systems will significantly improve aircrew situational awareness (*SA*) and survivability against emerging threats. For more details on weapon warheads, the reader is referred to Section 4.9.

In addition to the targeting methods discussed above, the Air Force is accelerating the *Link 16* implementation in the *F-15E Strike Eagle* fighters, thus improving the pilot's ability to successfully strike time-sensitive targets such as moving convoys, mobile weapons, and even inhabited caves (as in the Afghanistan conflict). Specifically, *Link 16* is a wide-band tactical data link that delivers critical information faster via a computer link, which provides significant improvements to response time. When fully operational, *Link 16* will provide real-time target data to strike aircraft. The *Link 16*-equipped *F-15*s will work with the *E-8C Joint STARS* and other intelligence gathering assets to accomplish their mission (see also Section 6.9.1). By the year 2010, the Air Force expects to field more than 4,000 tactical data links.

Precision Weapons

With no new platforms on the drawing board (except some modifications to the *B-2*) the Air Force is redefining its priorities on a variety of conventional weapons upgrades for use in theater war. One of these, the most prominent, is the *JDAM*, another star of the Afghan war. As stated earlier, the *JDAM* is a low-cost tail kit, which when linked to the *GPS* navigation signals transforms a standard 1,000-lb or 2,000-lb iron bomb into an all-weather, day-or-night, near-precision weapon (note: All three USAF bomber types—*B-52H*, *B-1B*, and *B-2*—now can carry the 2,000-lb *JDAM*).

We will now summarize some of the most important Air Force precision munitions systems discussed in this chapter:

Joint Air-to-Surface Standoff Missile (*JASSM*). This is a precise, stealthy cruise missile built to hit hardened, heavily defended, fixed, and relocatable targets from outside of area defenses.

Joint Standoff Weapon (*JSOW*). The *JSOW* is an accurate, all-weather, unpowered glide munition, capable of destroying armored targets at ranges exceeding 40 nautical miles.

Wind-Corrected Munitions Dispenser (*WCMD*). This is an inertial-guided tail kit that gives greater accuracy to the combined effects munition, sensor fuzed weapon, and the gator mine dispenser from medium to high altitude in adverse weather.

Small Diameter Bomb (*SDB*) or Small Diameter Munition (*SDM*). Under development for the *F/A-22*, the *SDB* will offer standoff capabilities against the most difficult surface-to-air threats. The *F/A-22* will carry up to eight *SDB*s internally.

5.13 Air-to-Ground Attack Component

This section supplements and summarizes the discussion of Sections 5.5, 5.6, and 5.7. Another important aspect in weapon delivery is the air-to-ground attack component. In essence, this component determines weapon trajectories, miss distance, time-to-go to weapon release, and attack steering signals. Moreover, the air-to-ground attack component provides the conditions, logic, and control functions required to deliver weapons using visual or "blind" attack techniques against planned or in-flight designated ground targets. These are implemented in a set of five separate weapon delivery modes. The computations (depending on the mode) include the following: (1) automatic ballistics, (2) course-to-release point, (3) time delay (for "under-the-nose" weapon releases), (4) time-to-go, and (5) toss-maneuver maximum range. When conditions are satisfied for weapon impact on the designated target, a weapon release command is generated if pilot consent is present. These delivery computations are used to position the *HUD* reticle and radar antenna to the impact point of any selected weapon when the stores management set (*SMS*) is commanding an air-to-ground visual delivery mode. In addition, computations are included to determine miss distance, time-to-go, and attack steering signals when a computed release point delivery mode is selected. Other functions (or components) relating to weapon delivery will now be discussed.

Mechanization. This component uses a trajectory integration technique as the basic mathematical tool to predict weapon impact points. The trajectory integration, which runs approximately 10 times a second, provides a reference solution that is augmented by a bomb-range extrapolation scheme, which runs 50 times a second, to provide accurate, timely impact-point prediction. With this prediction and the knowledge of target location, time-to-go and steering for weapon delivery are computed. An overview of the weapon delivery solution is found in Figure 5.26.

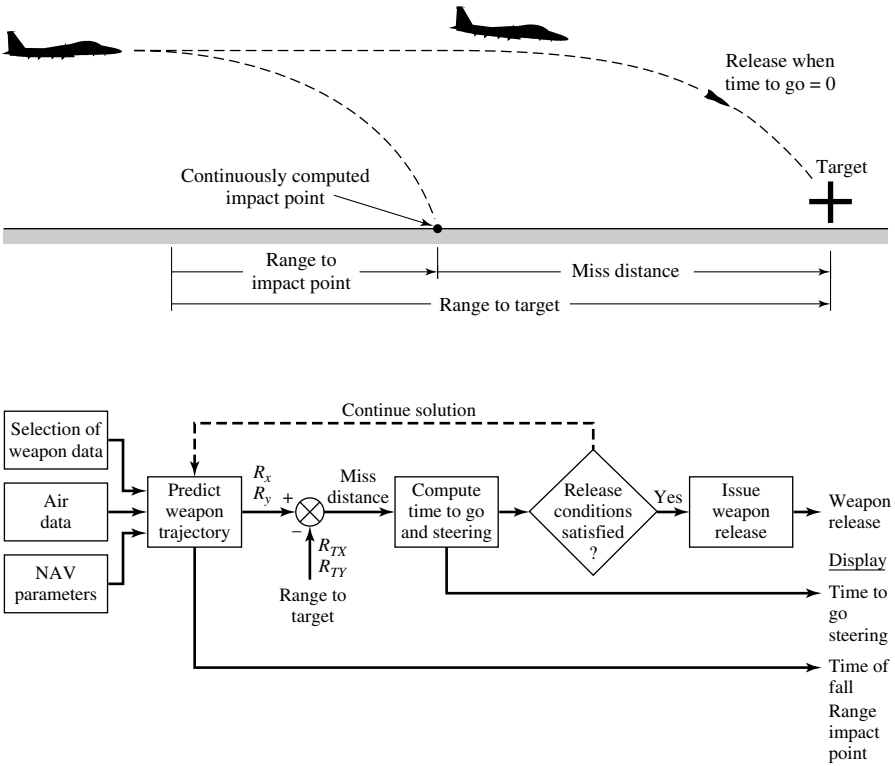

Fig. 5.26. Overview of weapon delivery solution.

Current Aircraft Condition Initialization for Weapon Trajectory Integration. Current aircraft conditions are used as inputs to the weapon delivery trajectory integration. This input is then adjusted to compensate for (1) data age, and (2) time delay between release command and actual release of the weapon. Then the data are predicted ahead 1.5 times the time between trajectory solutions to minimize bias of the reference solution during the time period it will be used. A coordinate transformation is required before doing the trajectory integration.

Weapon Trajectory Integration. The weapon trajectory integration computes the path of the bomb from release point to the burst altitude. This integration is accomplished in a reference coordinate system in which the X-axis is along the aircraft ground track, the Z-axis is up, and the Y-axis is such as to make a right-hand coordinate system. A recurrent third-order Runge–Kutta technique is the numerical integration algorithm used for the weapon trajectory integration. The weapon trajectory integration includes the effects of (1) weapon ballistics, (2) lateral and vertical offset and roll rate, (3) nonstandard atmosphere, (4) weapon separation effects, (5) measured and predicted wind structure, (6) *Coriolis* accelerations, and (7) gravitational variation. Furthermore, the results of the integration provide

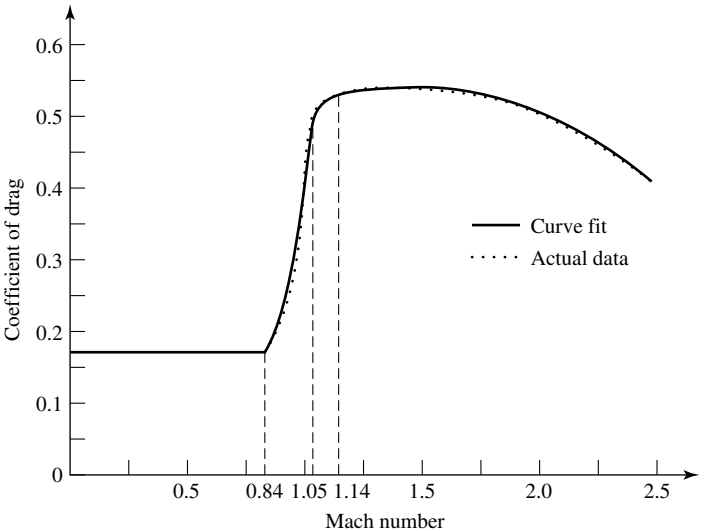

Fig. 5.27. Coefficient of drag versus Mach number for Mk 82.

(a) horizontal bomb range components in the reference coordinate system, and (b) the partial derivatives of bomb range with respect to variation in flight parameters.

Weapon Ballistics. The weapon ballistics data consist of coefficient of drag C_D, weapon weight (a constant), and weapon frontal area. The frontal area is a constant value dependent upon the selected weapon. Frontal area, weight, and weight variation are stored as constants in the operational flight program (*OFP*). Coefficients of drag are stored in three ways, depending on weapon: (1) a curve relating the coefficient of drag C_D to Mach number, (2) a step function relating C_D to time, wherein C_D changes at specific time events and is constant between, or (3) a combination of 1 and 2. The functional relationship of C_D versus Mach number is determined by a curve fit to a set of empirical data points. This curve fit consists of four second-order polynomials of the form (see also Section 3.1):

$$C_D = K_0 + K_1 M + K_2 M^2, \tag{5.57}$$

where

$$K_0 K_1, K_2 = \text{curve fit coefficients},$$
$$M = \text{Mach number}.$$

This technique is illustrated in Figure 5.27 for an *Mk 82* weapon. Note that the coefficients of the curve fit and the values of the Mach numbers separating the four polynomials vary for each weapon. The values of these coefficients, time events, and constants are inputs.

Atmospheric Equations. The atmosphere algorithm predicts the air density and speed of sound at weapon location throughout its trajectory. Inputs include measured air data at aircraft, weapon speed, and weapon altitude for each trajectory integration. The atmosphere equations are separated into two groups: (1) initialization equations, and (2) prediction equations. The initialization equations compute the parameters of the nonstandard atmosphere based on the current aircraft location. These computations lie outside the integration loop and are performed at a slow rate. The prediction equations use the parameters computed by the initialization equations, weapon speed, and weapon altitude to compute the air density and the Mach number at each trajectory integration level. These computations lie inside the integration loop and are performed once for each point in the trajectory integration (for more details on the standard atmosphere, see Appendix D).

Weapon Separation Effects. Weapon separation effects are defined to be changes in free-fall ballistics due to the interaction between aircraft and weapon. These effects are unique for each aircraft/weapon combination, and tend to vary with the release conditions. The separation effects equations can be derived empirically from flight-test results. The need for separation effects corrections depends on (1) weapon, (2) dynamic pressure, (3) Mach number, (4) bomb rack position, and (5) normal acceleration. Dynamic pressure has a secondary effect for subsonic releases. The separation effects equation for velocity correction for both along the flight path and cross-track (i.e., special release bombing only) is of the form

$$V = K_0 + K_1 M, \tag{5.58}$$

while the form for velocity correction normal to the flight path is

$$V = K_0 + K_1 M + K_2 a_n, \tag{5.59}$$

where a_n is the normal acceleration and the constants are as defined previously. These equations are implemented with separation effects coefficients set to zero.

Wind Equations. The method used for wind prediction is a straight-line approximation using the values of wind speed at aircraft altitude. The equation has a slope that represents the expected decrease of wind velocity with altitude. Factors are computed to modify the equation for prediction of both along-track and cross-track winds. The assumed wind direction is constant, in the direction of wind velocity at aircraft altitude.

Coriolis and Centripetal Accelerations. The acceleration forces on the weapon include forces due to *Coriolis* and centripetal accelerations generated by Earth rotation and aircraft velocity [7].

Gravitational Variations. The acceleration due to gravity varies as a function of both altitude and latitude. The variation of gravity at sea level due to altitude is as follows [7]:

$$g_o = 32.0882 + 0.16969 \sin^2 \phi - 1.887 \times 10^{-4} \sin^2(2\phi), \tag{5.60}$$

where

$$g_o = \text{gravitational acceleration at sea level,}$$
$$\phi = \text{latitude (i.e., present position).}$$

The variation of gravity due to altitude can be simplified as follows:

$$g_h = g_o/[1 + (h/R_E)]^2, \tag{5.61}$$

where

$$g_h = \text{gravitational acceleration at altitude } h,$$
$$h = \text{altitude above the Earth,}$$
$$R_E = \text{radius of the Earth.}$$

The value of the gravitational acceleration at aircraft altitude is input. In order to include the effects of gravitational variation with weapon altitude, a simple weighted-average gravity is computed for the weapon delivery solution. That is,

$$\bar{g} = g_h + K_1 h, \tag{5.62}$$

where

$$\bar{g} = \text{weighted average gravitational acceleration,}$$
$$g_h = \text{gravitational attraction at altitude } h,$$
$$K_1 = \text{weighting constant } (= 5.8 \times 10^{-7} \text{ seconds}^{-2}).$$

This computation takes place outside the integration loop as an initialization.

Manual Ballistics. Manual ballistics are used in lieu of automatic ballistics when the pilot enters values for weapon time of fall and weapon range via the fire control computer.

Predict Ahead Trajectory Integration. In order to display the 45° toss and level toss cues, predicted impact points are continuously computed in some modes. By predicting these release points and computing a weapon trajectory, the bomb range resulting from these predicted release points is known. Thus, the cues can be displayed when the target is within range.

Bomb Range Extrapolation and Weapon Release. The current bomb range is computed in platform coordinates by transformation and extrapolation of the bomb range components obtained from the trajectory integration. The bomb range extrapolation also computes velocity components of the impact point relative to the ground. The bomb range extrapolation requires calculating the partial derivatives of the along-track and cross-track ranges with respect to the release velocities and release altitude. In the *CCIP* mode, when the depression angle to the *CCIP* exceeds the lower elevation limit of the *HUD* aiming reticle, the reticle is positioned near its lower limit and an appropriate time delay is computed to delay the issuing of the weapon release command. Calculations are made to determine the

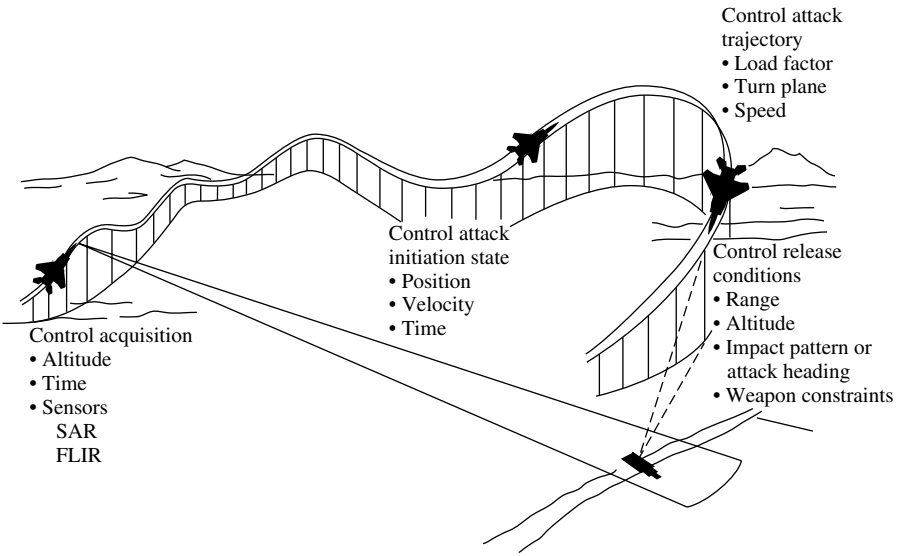

Fig. 5.28. The weapon delivery concept.

along-track and the cross-track components of miss distance in the target designate modes. These components are computed by differencing range-to-target (obtained from the fixtaking component) and bomb range. The cross-track component of miss distance is used to calculate a lateral steering signal. Also, the along-track component of miss distance is used to compute the time-to-go to weapon release. These computations are also made in the *CCIP* mode after target designation for a delayed release. In addition, horizontal bomb range and weapon time-of-fall are computed. Finally, these data are provided for display on the fire control/navigation panel. In all modes, a pull-up anticipation and breakaway computation is made.

Programming. The air-to-ground attack component has been structured into twelve segments comprising both main loop and timeslice tasks. The main loop routines provide a set of ballistic values to be used by the timeslice routines. Ballistic values (i.e., time-of-fall and bomb range) are computed by the main loop trajectory integration routine, or these values may be entered manually. The timeslice routines update (extrapolate) ballistic values to the current release conditions, issue the weapon release command, and compute values for display to the pilot.

Figure 5.28 illustrates the overall weapon delivery concept.

5.14 Bomb Steering

We begin this section by defining the aircraft navigational steering requirements. This function includes the computation of the desired track angle and path, track angle and crosstrack errors, a steering command to the automatic flight control system

(*FCS*), and related variables for display. Navigation steering operates under several modes determined in the system management control. The steering modes to be mechanized are:

Direct (Great Circle) Mode. The aircraft flight path includes many intermediate reference points that form a sequence of destinations. When it is time to turn and/or pass a given reference point, it is necessary to sequence the reference points used actively in the guidance equations. These active reference points are known as "previous destination," "current destination," and "next destination." The "current destination" is the reference point near which the next sequencing will occur and is often the point toward which the aircraft is directed. After sequencing, the former "current destination" becomes the "previous destination," and the former "next generation" becomes the "current destination." Each reference point is specified by its latitude and longitude. In FLY-TO crosshairs, the crosshairs location becomes the "current destination." In direct mode, a great circle course (desired track angle) is continuously computed based on current position and destination. In this mode, the steering command is proportional to the track angle error.

Centerline Recovery Mode. In the centerline recovery mode, the aircraft is steered to follow a great circle ground track path, directed from one point to another, spaced by at least 6,000 feet. These two points, for example, may be previous and current destinations. The steering command is a function of both track angle error and crosstrack position error. The crosstrack position and azimuth errors are calculated from the desired track for use by the steering law. By definition, since the desired track is from the current aircraft position to the destination, the crosstrack position error is zero in the direct mode.

The system must provide the capability for a smooth transition from one course to another and to fly directly over a destination. The smooth transition from one course to another is called "turn short," and the ability to fly directly over a destination is called overfly. Turn short is accomplished in minimum time. For gravity weapons release, the impact point cross-range miss distance is used to generate steering commands to the bomb release point. The bomb steering mode will be flagged via system management control. Bomb steering is accomplished by using the basic navigation steering. Overfly is automatically set when the bomb mode is initiated. The navigation steering mode used for bomb steering corresponds to the mode selected for navigation steering. If operating in the direct mode with overfly, the system automatically switches to centerline recovery when the range to go becomes less than a given value (e.g., 6,000 feet) in either navigation or bomb steering. The inputs to navigation steering include:

a. Prime data set from either the *INS* or alternative navigation.
b. Steer point and tracking data from system management control.
c. Computed gravity weapon crossrange drift from weapon delivery.
d. Mode control flags from system management and control logic.

The prime data set inputs include the aircraft latitude, longitude, inertial coordinates, ground speed, and course, as well as the Earth radius and prime data validity. Steer

point data include latitudes and longitudes of previous, current, and next destinations. The tracking data are crosshair corrections. The navigation steering outputs are:

a. Range-to-go to current destination.
b. Range from current destination to next destination
c. Time-to-go to current destination (or turn point in turn short).
d. Estimated time from current destination to the next destination.
e. Track angle error.
f. Crosstrack error.
g. Steering command to the automatic *FCS*.
h. Flag for time to sequence between current and next destination.
i. Ground track angle between current and next destination.

If there is insufficient data for steering outputs:

1. Set a flag for insufficient data. This flag is to be used by system management control.
2. Set all steering outputs to zero.

The navigation/bomb steering algorithm is designed for both general navigation and for weapon delivery. However, the effective destination in the steering equation is modified according to the predicted crosstrack drift, CI (computed bomb drift, to be discussed later), of the impact prediction algorithm. We will now discuss the inclusion of the CI term into the steering during weapon delivery.

The direct mode is the primary mode for gravity weapon delivery and is entered upon the selection of bomb mode. Direct mode provides the shortest route to the target and the fastest elimination of the predicted impact errors. Centerline recovery mode steering is also available and provides weapon delivery along a specific path. Before proceeding to the minor modifications to the basic steering law for bomb steering, a simple explanation of the processing of the radar data will be given. The geometry is presented first, followed by simplified equations for processing the radar data into the steering.

Assume now that an offset aim point (*OAP*) is being used and the latitude and longitude of the *OAP* and the target are known. The basic assumption is that the relative latitude and longitude between the target and the *OAP* is not in error. Secondly, if the relative position is in error, there is no way to correct this during flight. The geometry of a typical situation before a tracking handle correction is shown in Figure 5.29.

Aircraft latitude and longitude are modified for use in bomb steering based on target position fix. This update is not applied to the prime data set values or the navigation filter. The ΔN and ΔE in the tracking handle buffer are converted to $\Delta\lambda$ and $\Delta\phi$ by

$$\Delta\lambda = (\Delta N/R_E)(180/\pi), \tag{5.63a}$$

$$\Delta\phi = (\Delta E/R_E \cos\lambda)(180/\pi), \tag{5.63b}$$

$$\lambda R_{A/C} = \lambda_{A/C} - \Delta\lambda, \tag{5.64a}$$

$$\phi R_{A/C} = \phi_{A/C} - \Delta\phi, \tag{5.64b}$$

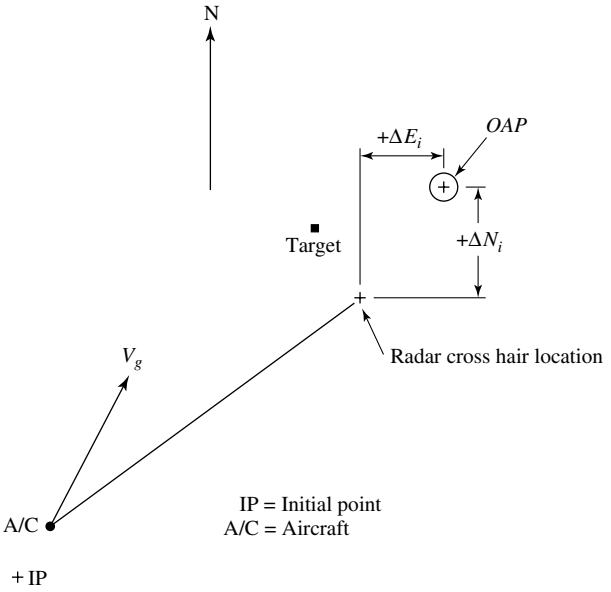

Fig. 5.29. Geometry before tracking handle movement.

where

$$\begin{aligned}
\phi &= \text{longitude},\\
\lambda &= \text{latitude},\\
\lambda_{OAP} &= \text{latitude of } OAP,\\
\phi_{OAP} &= \text{longitude of } OAP,\\
\lambda_{A/C} &= \text{latitude of aircraft from the } INS \text{ or alternative navigation},\\
\phi_{A/C} &= \text{longitude of aircraft from the } INS \text{ or alternative navigation},\\
\lambda R_{A/C} &= \text{modified latitude of aircraft},\\
\phi R_{A/C} &= \text{modified longitude of aircraft},\\
R_E &= \text{radius of the Earth}.
\end{aligned}$$

The current aircraft position $\mathbf{P}_o$ is computed using $\lambda R_{A/C}$ and $\phi R_{A/C}$ during the bomb run. If a position update is taken, the tracking handle buffer is set to zero, and $\lambda_{A/C}$ and $\phi_{A/C}$ are updated in the autopilot, and as a result, $\Delta\lambda$ and $\Delta\phi$ are zero until the tracking is moved again. The target is used as the destination in the great circle equations.

The manner in which an update to the aircraft position vector $\mathbf{P}_o$ is accomplished during a bomb run depends on whether alternative navigation or inertial navigation is used. When using alternative navigation, the direction cosines of the aircraft position vector are

$$C_{31} = \cos\phi\cos\lambda, \tag{5.65a}$$

$$C_{32} = \sin\phi \cos\lambda, \tag{5.65b}$$

$$C_{33} = \sin\lambda. \tag{5.65c}$$

These equations are updated relative to the target as follows:

$$C'_{31} = \cos(\phi - \Delta\phi)\cos(\lambda - \Delta\lambda), \tag{5.66a}$$

$$C'_{32} = \sin(\phi - \Delta\phi)\cos(\lambda - \Delta\lambda), \tag{5.66b}$$

$$C'_{33} = \sin(\lambda - \Delta\lambda), \tag{5.66c}$$

where C'_{31}, C'_{32}, and C'_{33} are the newer direction cosines that define the aircraft position relative to the target, and $\Delta\lambda$ and $\Delta\phi$ are the relative latitude and longitude increments resulting from a tracking handle correction. With inertial navigation, (5.65a)–(5.65c) are applied. Consequently, $\mathbf{P}_o$ is modified to account for radar updates by (5.67a)–(5.67c). Note that

$$\Delta\phi = \Delta E / R_E \cos\lambda,$$

$$\Delta\lambda = \Delta N / R_E,$$

where

$$\Delta E = \text{easterly component of the update},$$

$$\Delta N = \text{northerly component of the update}.$$

Then

$$C'_{31} = C_{31} + [(C_{33}C_{31}\Delta N + C_{32}\Delta E)/R_E \cos\lambda], \tag{5.67a}$$

$$C'_{32} = C_{32} + [(C_{33}C_{32}\Delta N - C_{31}\Delta E)/R_E \cos\lambda], \tag{5.67b}$$

$$C'_{33} = C_{32} - [(\cos\lambda \cdot \Delta N)/R_E]. \tag{5.67c}$$

Summarizing, (5.66a)–(5.66c) are exact and apply during the dead reckoning mode of navigation. Equations (5.67a)–(5.67c) are approximate and apply with inertial navigation.

It is noted here that the great circle path in the centerline recovery mode is continuous. Therefore, the approach or overfly of a destination is not a problem. In the direct mode, the desired path is always to the destination, thus presenting a potential problem when a destination is to be overflown. As stated previously, the predicted crosstrack drift of the bomb, CI, must be considered to deliver a weapon on target. The crosstrack error Y_e computed in the navigation equations is modified by CI as follows:

$$Y'_e = Y_e + CI, \tag{5.68}$$

Y_e is negative, as shown in Figure 5.30, and CI is positive when the predicted bomb drift is to the left. The steering equation uses Y'_e when in the bomb mode instead of Y_e. If there is no crosstrack drift of the bomb, then $Y'_e = Y_e$.

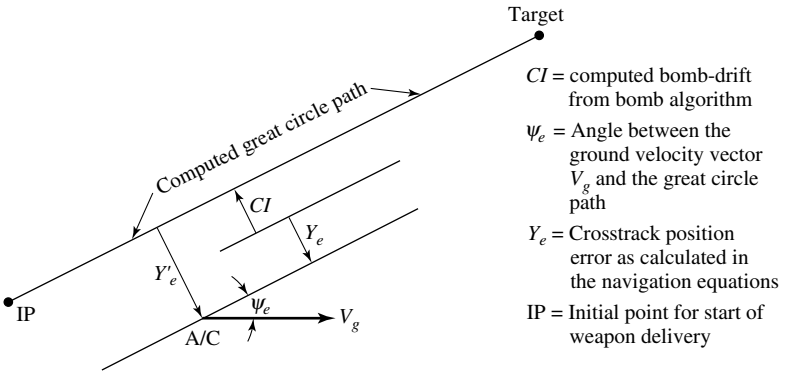

Fig. 5.30. Centerline recovery mode geometry.

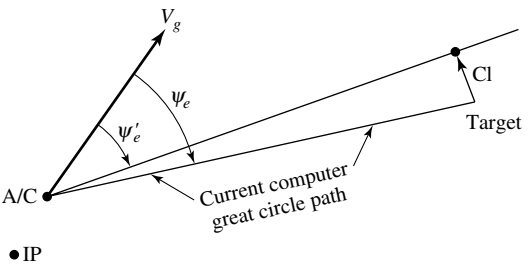

Fig. 5.31. Direct mode geometry.

In order to account for the crosstrack drift CI of the bomb, the track angle error ψ_e of the basic navigation equation is modified as follows:

$$\psi'_e = \psi_e + \sin^{-1}(CI/D_o), \tag{5.69}$$

where

D_o = distance from the aircraft to the target,
ψ_e = track angle error,
ψ'_e = modified track angle error.

Figure 5.31 illustrates the direct mode.

When the aircraft approaches the target in the direct mode, the system establishes a track just as it does in the navigation mode. Steering cycles automatically to the centerline recovery mode when $D_o \leq 6{,}000$ feet. However, the track angle and crosstrack errors are modified to eliminate transients upon entering the new mode. The modified track angle error equation for ψ'_e for automatic entry of the centerline recovery mode from the direct mode when $D_o \leq 6{,}000$ feet is given by

$$\psi'_e = \psi_e + \sin^{-1}(CI/6000). \tag{5.70}$$

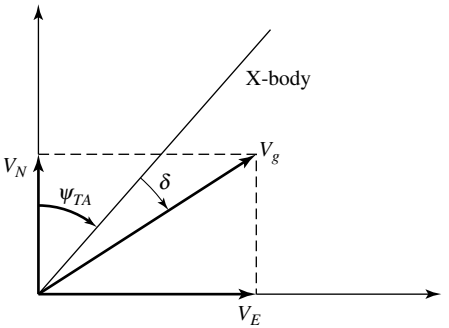

Fig. 5.32. Wind velocity transformation.

In the discussion of Section 5.7, the bombing problem was treated without any wind present. Here we will briefly discuss the role the wind plays in the navigation process and subsequent accuracy of bombing. The navigation processing function is responsible for wind computations using prime ground speed (i.e., *INS*, Doppler, etc.). If *INS* or Doppler data are selected as prime, the winds can be computed as follows:

$$W_N = -V_{N/TAS} + V_N, \tag{5.71a}$$

$$W_E = -V_{E/TAS} + V_E, \tag{5.71b}$$

$$V_N = V_g \cos(\psi_{TA} + \delta), \tag{5.71c}$$

$$V_E = V_g \sin(\psi_{TA} + \delta), \tag{5.71d}$$

$$\psi_g = \psi_{TA} + \delta, \tag{5.71e}$$

where

$V_{N/TAS}$ = north component of the true airspeed (TAS),
$V_{E/TAS}$ = east component of the true airspeed,
V_g = ground speed,
δ = drift angle,
ψ_{TA} = true heading angle,
ψ_g = ground track angle.

If the *INS* or Doppler data are unavailable, corrections to wind estimates will be input from the system management and control function. The various relationships are illustrated in Figure 5.32.

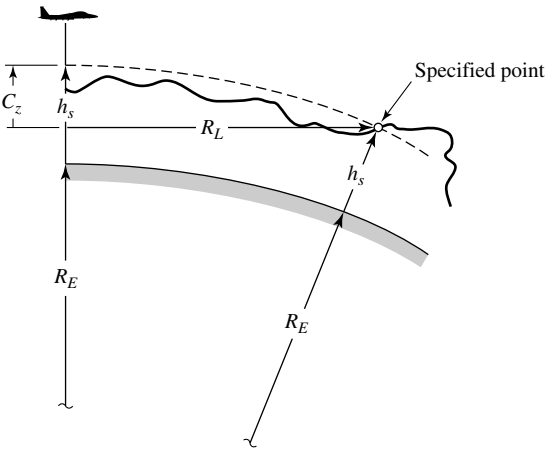

Fig. 5.33. Earth curvature definition.

5.15 Earth Curvature

As mentioned in Sections 5.8 and 5.12, sometimes it becomes necessary to release ordnance from a greater distance than usual and assume a flat Earth in the computation of a target's distance. In such cases, the weapon delivery system and/or the fire control computer must consider the Earth's curvature. Figure 5.33 illustrates the derivation of the Earth curvature equation.

The Earth's curvature to the specified point is computed as follows:

$$\begin{aligned} C_Z &= (R_E + h_S) - [(R_E + h_S)^2 - R_L^2]^{1/2} \\ &= (R_E + h_S)[1 - (1 - R_L^2/(R_E + h_S)^2)^{1/2}] \\ &= (R_E + h_S)[1 - (1 - R_L^2/2(R_E + h_S)^2)] \\ &= R_L^2/2(R_E + h_S) \\ &\cong R_L^2/2R_E, \end{aligned} \tag{5.72}$$

where

h_S = mean sea-level elevation of the specified point,
R_L = horizontal component of range to the specified point,
R_E = radius of the Earth.

Figure 5.34 illustrates the definition of the Earth curvature limit window.

The depression angle to the Earth's curvature, that is, the limit window, can be calculated from the following expression:

$$\tan^2 \theta_{DLIM} = (|h_T| + C_{LIM})/R_{ECLIM}^2, \tag{5.73}$$

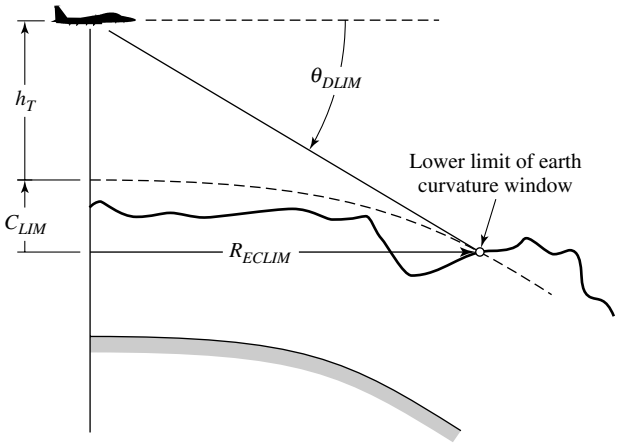

Fig. 5.34. Definition of the Earth curvature limit window.

where

h_T = height above the terrain,
C_{LIM} = limit on Earth's curvature (6076.12 ft),
R_{ECLIM} = horizontal range to Earth curvature limit (504,275.8 ft),
θ_{DLIM} = depression angle to each curvature limit.

In weapon delivery, fixtaking of a specific target plays an important role. The primary fixtaking task is to calculate the range-to-target vector and associated display information. This vector is continuously computed in all modes, and in the air-to-ground weapon delivery modes (except *EO*) serves to define the location of the target. The range-to-target vector may be defined (1) by a latitude, longitude, and elevation, (2) as an offset from such, or (3) by the pilot visually designating the target. Fixtaking also converts radar-ranging measurements to a terrain elevation measurement when valid air-to-ground ranging data are available. The data are then used to correct the calculation of the vertical component of the range-to-target vector on a continuous (i.e., as long as data are valid) basis.

The most important fixtaking tasks are to calculate the range from present aircraft position to target and sighting point. Often, these calculations involve simple arithmetic operations on the proper data. Fixtaking employs a data table and uses pointers to select the proper set of data to be executed upon a set of "standard" equations. The vertical component of the range-to-target vector is the sum of the height above terrain, the vertical cursor associated with the basic range (which is zero unless the *HUD* target designator box is in the Earth curvature limit window), and the Earth's curvature based on the horizontal components of the range-to-target vector. Note that the fundamental quantity involved in the calculation of the horizontal components of the range-to-target vector and range-to-sighting-point vector is the basic range. Finally, fixtaking computes the distance from the aircraft to the steerpoint using an

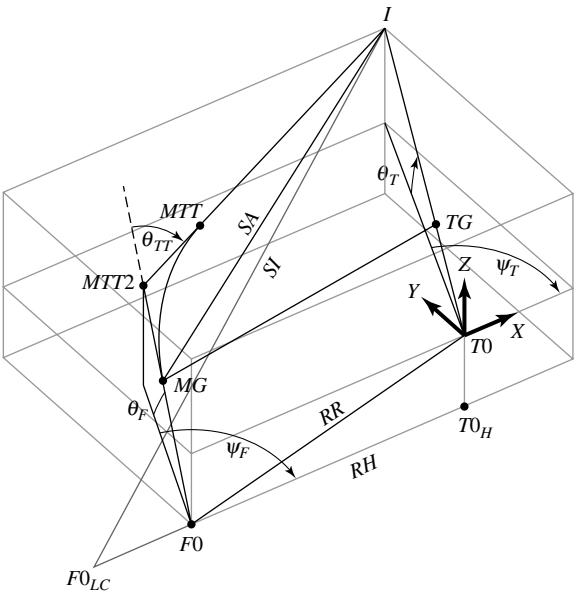

Fig. 5.35. Missile launch geometry.

Earth-fixed coordinate system. The key to these calculations is the determination of aircraft present position in this Earth-fixed coordinate system. This determination uses a nine-element direction cosine matrix, which relates the inertial platform to an Earth-fixed coordinate system [7].

5.16 Missile Launch Envelope

This section describes briefly the general principles involved in determining the launch envelope of a missile. The launch envelope calculations are based on the performance of the missile in a straight-line flyout.

Geometry

There is an idealized flight-path, termed a *lead-collision* trajectory (see Section 4.4.2 for details), in which the missile does not have to maneuver to intercept the target. This flight-path is shown in Figure 5.35 for a launch platform at the position FO_{LC}, and for which it is assumed that the launch aircraft is pointing in the correct direction.

If the minimum and maximum launch ranges for the straight-line flight of the missile are known, then the position FO_{LC} for minimum and maximum ranges can be calculated. This can be done in the following way. First, a coordinate system is chosen that is centered at the position of the target (TO) at missile launch and in which the x-axis is aligned with the horizontal *LOS* from the launch aircraft to the

target, the y-axis is to port, and the z-axis is up, forming a right-handed set of axes. If the time-of-flight t_f is known, then the target position at intercept (TI) is calculated. The target is assumed to fly on a constant heading and at constant speed. The angle between the horizontal *LOS* and the projection of the target's flight-path onto the horizontal plane is the relative azimuth heading angle (ψ_T) and the angle between the target's flight-path and the horizontal plane is the actual pitch heading (θ_T). The total missile flight-path to intercept (SI) is known, and the position of the launch aircraft when the missile is released can be found from geometry, since it must be on the x-axis (i.e., the horizontal *LOS* at launch).

However, in general, the launch aircraft will not be pointed in a direction to generate a lead-collision trajectory for the missile, but will have an azimuth heading of ψ_F relative to the horizontal component of the *LOS* and a pitch heading of θ_F. This means that the missile will have to maneuver during its flight to the target. Initially, we will assume that the missile will travel the same total distance in the same time as if it were flying the lead-collision course (note that in reality it will not fly as far in the same time because of the drag penalty associated with maneuvering). Furthermore, we can consider the missile trajectory to be made up of three idealized portions. The first part is a straight-line flyout on the launch heading from the launch position (FO) to the point where the missile guidance is enabled (MG). The second part is a turn through an angle (θ_{TT}) between the point where guidance is enabled (MG) to the point where the turn is complete (MTT). This is then assumed that the missile in placed onto a lead-collision course for the remainder of the flight to intercept at point (I). The launch aircraft must lie somewhere (FO) along the x-axis (the initial horizontal component of the *LOS*). The point (FO) represents the launch aircraft for the minimum or maximum range shot. The horizontal component of the launch range (RH) is the distance between (FO) and the projection of the initial position of the target onto the same horizontal plane (position TO_H). The total launch range is the distance (RR) between the initial positions of the launch aircraft (FO) and the target (TO). The initial position of the launch aircraft (FO) can be found from a knowledge of the total flight-path length (SI), the distance traveled during the time to guidance enable (FO to MG), and the size of the turn (θ_{TT}) and the same time spent in the turn (which gives the path length traveled during the turn). Note that the rate of turn will depend on the maneuvering capabilities of the missile and the guidance commands it generates. The maneuvering capabilities of the missile are represented by the aerodynamic characteristics, the mass properties, and the structural limitations of the missile. The guidance commands will depend on the guidance law, for which simple proportional navigation is assumed in which the guidance command will be equal to the product of the navigation constant and the inertial *LOS* rate.

The following algorithms solve this geometric problem. This solution also takes into consideration the fact that the missile will be maneuvering in both the vertical and horizontal planes and must also make an allowance for the decreased speed of the missile due to the induced drag (drag due to lift) during the maneuver. For a missile flight in a straight line it is possible to develop equations that describe the position and speed of the missile at any given time, provided that some assumptions are made about the nature of the propulsion and drag forces.

Missile Flight During Motor Burn

Here we will assume that the thrust is constant during motor burn and that the drag coefficient, air density, and missile mass are also constant. The missile drag D is given by the expression

$$D = 0.5\rho V^2 S C_D, \tag{5.74}$$

where

$$\begin{aligned} \rho &= \text{density of air,} \\ V &= \text{speed,} \\ S &= \text{reference area,} \\ C_D &= \text{coefficient of drag.} \end{aligned}$$

The acceleration due to drag, A_D, is given by

$$A_D = -V^2[(0.5\rho S C_D)/M], \tag{5.75a}$$

where M is the mass of the missile. Since we have assumed that the drag coefficient, air density, and missile mass are constant, the parameter $(0.5\rho V^2 S C_D)/M$ is also a constant. Denoting this quantity by D_p, then the acceleration due to the drag is given by

$$A_D = -D_p V^2. \tag{5.75b}$$

If the thrust T is constant, then the net acceleration A is given as follows:

$$A = T - D_p V^2. \tag{5.76}$$

Therefore, we can write

$$\frac{ds}{dt} = V, \tag{5.77a}$$

$$\frac{dV}{dt} = T - D_p V^2. \tag{5.77b}$$

Given the initial conditions t_o, s_o, V_o, if we set

$$u = \exp\left[D_p \int_{t_0}^{t} V\,dt\right] = \exp[D_p(s - s_o)], \tag{5.78}$$

then we can write

$$\frac{du}{dt} = D_p u V, \tag{5.79a}$$

$$\frac{d^2u}{dt^2} = D_p\left[u\left(\frac{dV}{dt}\right) + V\left(\frac{du}{dt}\right)\right], \tag{5.79b}$$

or

$$\frac{d^2u}{dt^2} = D_p[u(T - D_pV^2) + D_puV^2] = TD_pu. \tag{5.79c}$$

The general solution is given by

$$u = a\exp[T^{1/2}D_p^{1/2}(t - t_o)] + b\exp[-T^{1/2}D_p^{1/2}(t - t_o)]. \tag{5.80}$$

Substituting the initial conditions, we obtain

$$u(t_o) = 1, \left[\frac{du}{dt}\right]_t = D_pV_o, \tag{5.81a}$$

$$a = [1 + V_o(D_p/T)^{1/2}]/2, \tag{5.81b}$$

$$b = [1 - V_o(D_p/T)^{1/2}]/2. \tag{5.81c}$$

This yields the particular solution

$$u = \cos h[(T/D_p)^{1/2}(t - t_o)] + V_o(D_p/T)\sin h[(T/D_p)^{1/2}(t - t_o)] \tag{5.82}$$

and

$$\begin{aligned} s - s_o &= (1/D_p)\ln(u) \\ &= (1/D_p)\ln\{\cos h[(T/D_p)^{1/2}(t - t_o)] + V_o(D_p/T) \\ &\quad \sin h[(T/D_p)^{1/2}(t - t_o)]\}, \end{aligned} \tag{5.83}$$

$$\begin{aligned} V &= \left(\frac{du}{dt}\right)/D_pu \\ &= \{V_o + (T/D_p)^{1/2}\tan h[(T/D_p)^{1/2}(t - t_o)]\}/\{1 + V_o(D_p/T)^{1/2} \\ &\quad \tan h[(T/D_p)^{1/2}(t - t_o)]\}. \end{aligned} \tag{5.84}$$

This enables the missile position(s) and speed V to be calculated, given the initial conditions. While the assumptions of constant thrust (T) and constant drag parameter (D_p) appear to be gross simplifications, this does lead to the closed-form solutions given above. Furthermore, if the motor burn time is subdivided into several intervals, then these assumptions will be more valid when applied to the individual time intervals rather than being applied over the complete duration of the motor burn.

Missile Flight After Motor Burnout

Once the motor has burned out, the missile will enter a "coast" phase in which the change in the missile's velocity along the flight-path will be due entirely to the aerodynamic drag. For this period of the missile flight, the missile mass (M) will be constant, and it will also be assumed that the air density is also constant. It will be assumed that the product of the drag coefficient and the velocity raised to a power

(β) is also constant. Note that the case $\beta = 0$ corresponds to constant drag coefficient (as was assumed during motor burn).

The missile drag (D) is given by the expression

$$D = 0.5\rho V^2 S C_D, \tag{5.74}$$

while the acceleration due to drag (A_D) is given by $-(D/M)$; that is,

$$A_D = -V^2[(0.5\rho S C_D)/M]. \tag{5.75a}$$

Since we have assumed that the air density and missile mass are constant, and that $C_D V^\beta$ is also a constant, then the parameter $(0.5 C_D V^\beta \rho S)/M$ is also constant. If this is denoted by D_C, then the acceleration due to drag is given by

$$A_D = -D_C V^{2-\beta}. \tag{5.85}$$

Therefore, we can write

$$\frac{ds}{dt} = V, \tag{5.86a}$$

$$\frac{dV}{dt} = -D_p V^{2-\beta}. \tag{5.86b}$$

For the missile distance traveled we need to solve

$$ds = V dt - (V^{\beta-1} dV / D_C), \tag{5.87a}$$

$$\int_{s_0}^{s} ds = -\int_{V_0}^{V} (V^{\beta-1}/D_C) dV. \tag{5.87b}$$

Here we will assume two solutions as follows:

If $0 < \beta < 1$,

$$s = s_o + [(V_o^\beta - V^\beta)/\beta D_C]. \tag{5.88a}$$

If $\beta = 0$,

$$s = s_o + [\ln(V_o/V)/D_C]. \tag{5.88b}$$

For the missile speed we need to solve

$$-(V^{\beta-2} dV / D_C) = dt, \tag{5.89a}$$

$$-\int_{V_0}^{V} (V^{\beta-2}/D_C) dV = \int_{t_0}^{t} dt. \tag{5.89b}$$

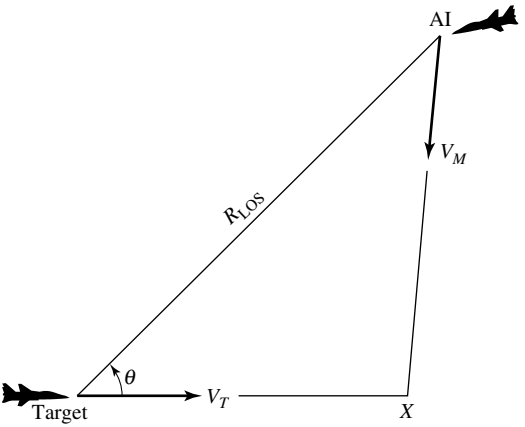

Fig. 5.36. Geometry for impact point calculations.

From the above, we obtain two solutions as follows:

If $1 < \beta < 1$,

$$t = t_o + [(V_o^{\beta-1} - V^{\beta-1})/(D_C(\beta - 1))]. \tag{5.90a}$$

If $\beta = 0$,

$$t = t_o + [\ln(V_o/V)/D_C]. \tag{5.90b}$$

An examination of typical values of the drag coefficient as a function of Mach number indicates that it is not possible to use one value of β to cover the complete range of speeds that the missile will experience during a typical flyout. However, it is possible to approximate the variation of the coefficient of drag with speed by producing fits to three distinct regions of the drag curve. The first region is from low Mach number up to the drag rise Mach number (usually somewhere around Mach 0.8) for which the drag coefficient is reasonably constant ($\beta = 0$). The second region is from the drag rise Mach number up to the Mach number where the maximum drag coefficient is obtained (usually somewhere around Mach 1.2). The third region is from the Mach number for maximum drag coefficient up to the maximum Mach number of the data (usually around Mach 5.0). A subroutine must be written that calculates the value of β for each of these three regions to provide the best fit to the tabular drag data.

The launch envelope imposes many constraints on the times when the missile launches are possible. The constraints vary according to the type of missile and which track mode (i.e., normal radar, track-on-jam, etc.) is being employed. During normal radar track, a predicted impact point is calculated using the average missile velocity and the current target position and velocity. Figure 5.36 depicts the geometry used to calculate the impact point.

Let X be the distance ahead of the target to the impact point, V_M the average missile velocity, and R_{LOS} the range from the airborne interceptor (AI) to the target. We can write an expression for X based on the law of cosines:

$$X = R_{LOS}\{[-\cos\theta \pm (\cos^2\theta + (\rho^2 - 1))^{1/2}]/(\rho^2 - 1)\}, \tag{5.91}$$

where $\rho = V_M / V_T$. The negative root is of no interest (it corresponds to negative flight time). In most cases, the missile velocity is not constant. For this reason, a two-step iteration is normally used to refine the estimate of average velocity. The first step uses the AI velocity to calculate an impact point (earliest collision point on target path that AI can reach). The range from the AI to this point is used to estimate the average missile speed. This speed is then used to find a second impact point, which is used to calculate the range to impact and the heading error (angle between the AI velocity vector and the *LOS* vector to the impact point).

The following checks are made to determine whether a missile launch is possible:

- The range to impact must be greater than the input minimum range and less than the maximum range.
- The heading error must be less than the input maximum.
- The velocity to impact must be greater than the target velocity.
- The current AI acceleration must be less than the input maximum g-limit.

Additional criteria are imposed depending on the type of missile:

- *IR* missiles must be within the aspect-dependent lock-on range.
- Semiactive missiles must have seeker lock-on.
- No additional checks are made for active missiles, but they must achieve lock-on during flight before an input time limit prior to impact.

Seeker lock-on for all types of missiles includes gimbal (if used) limit checks. *RF* missiles (both active and semiactive) require the signal-to-interference ratio to be greater than an input threshold. *RF* missiles can be launched only if the AI radar is tracking on noise jamming. In this mode, no impact predictions are made, since the radar is presumed to have no range or range rate data. Only three checks are made:

- The heading error (which in this case is the angle between the AI velocity vector and the jam strobe) is less than the allowed heading error.
- The current AI acceleration is less than the maximum allowed.
- The missile (either active or semiactive *RF*) has a home-on-jam capability, and the *J/N* ratio exceeds an input threshold level.

Since no checks are made on range or velocity, it is quite possible for missiles to be launched that have no chance of reaching the target.

On November 22, 2002, the Air Force completed the flight tests of the *F/A-22* with the successful launching of a guided *AIM-9 Sidewinder* missile over the White Sands Missile Range. The mission demonstrated the aircraft's ability to fire an *AIM-9* at Mach speed using an unmanned, full-scale *QF-4 Phantom II* aircraft as a target. During the test, the *F/A-22* was flying at 1.4 Mach at 24,000 ft, while the target was traveling at 1.0 Mach at 14,000 ft.

5.17 Mathematical Considerations Pertaining to the Accuracy of Weapon Delivery Computations

In Sections 5.7.1–5.7.3 we discussed the CEP for calculating the miss distance for aiming a weapon at a target during a bombing run. Error analyses, which are part of any proposed weapon system, usually contain a study of dispersion of data. This section presents briefly an analysis of dispersion in a plane. How to determine the probability of an impact occurring within a circle of given radius is an important question.

In many missile system designs, system accuracies can be related to payload effectiveness in terms of the circle size, which will contain a given fraction of the impacts. The probability P that a launched warhead or payload falls within a region of the xy-plane is calculated by integration of this probability density function. Before we begin with the computation of the *CEP* (circle of equal probability or circular error probable), let us define *CEP* [7]:

Definition:

The probability of a warhead impacting within a circle centered at the target of radius *CEP* is 50%.

Figure 5.37 shows the scatter plot of the points of impact of n objects (e.g., ordnance) dropped from the aircraft. Furthermore, here we will assume that the coordinate system is target centered, where R_I is the radial miss distance from the target.

In order to maintain meaningful statistics, it is assumed that:

1. All objects dropped were of the same type.
2. The nominal values of the vectors were the same for all objects.
3. The atmospheric conditions were the same during all object drops.

For unbiased errors, the objects at impact will be scattered on the ground around some mean point O. Each object will then have an offset from point O defined by x_{CR}, y_{DR}.

In terms of the means x, y the correlation coefficient is given by

$$\rho = \frac{\sum_{i=1}^{n}(x_i - \bar{x}) \cdot (y_i - \bar{y})}{\sqrt{\sum_{i=1}^{n}(x_i - \bar{x})^2 \cdot \sum_{i=1}^{n}(y_i - \bar{y})^2}} \tag{5.92}$$

Consider now computing the CEP. From Figure 5.38 we can compute the CEP as follows:

***CEP* Computation**

Compute the covariances at the target for each of the n error sources:

$$\sigma_{DR}^2 = \sum_{i}^{n} \delta DR_i^2, \tag{5.93a}$$

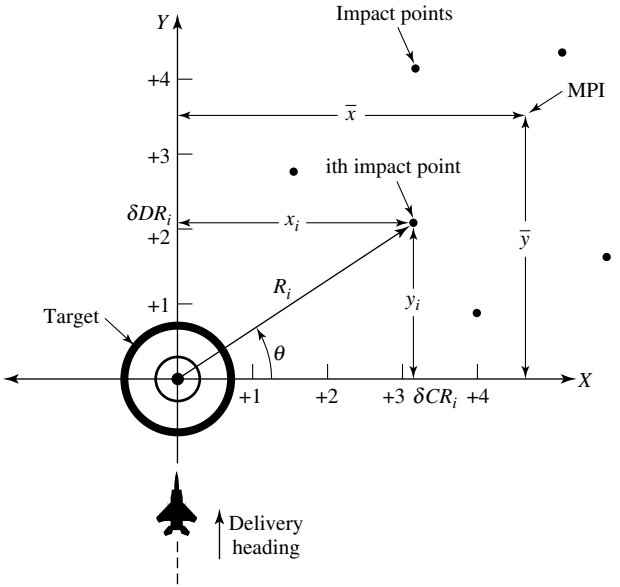

Fig. 5.37. Coordinate system for data measurement.

$$\sigma_{CR}^2 = \sum_i^n \delta CR_i^2, \tag{5.93b}$$

$$\sigma_{DR,CR}^2 = \sum_i^n \delta CR_i \delta DR_i. \tag{5.93c}$$

In general, the contours of equal probability will be ellipses for which the major and minor axes are *DR*, *CR*.

From Figure 5.38 we have the transformation of variables

$$x = x_{CR}\cos\theta + y_{DR}\sin\theta,$$
$$y = -x_{CR}\sin\theta + y_{DR}\cos\theta,$$

where

x = cross-range miss distance,
y = down-range (azimuth) miss distance,
θ = angle measured counterclockwise from weapon delivery heading,
R = radial miss distance from target.

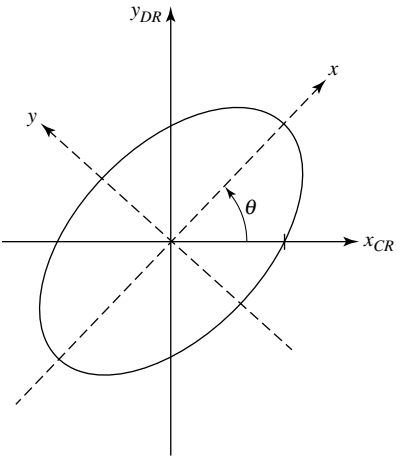

Fig. 5.38. Coordinate rotation geometry.

In matrix form,

$$\begin{bmatrix} x \\ y \end{bmatrix} = \begin{bmatrix} \cos\theta & \sin\theta \\ -\sin\theta & \cos\theta \end{bmatrix} \begin{bmatrix} x_{CR} \\ y_{DR} \end{bmatrix}. \tag{5.94}$$

Taking the covariance matrix of (5.94) (using the expectation operator E) and after some algebra, we obtain

$$\text{cov} \begin{bmatrix} x \\ y \end{bmatrix} = E \left\{ \begin{bmatrix} x \\ y \end{bmatrix} \begin{bmatrix} x \\ y \end{bmatrix}^T \right\} = \begin{bmatrix} \sigma_x^2 & 0 \\ 0 & \sigma_y^2 \end{bmatrix}. \tag{5.95}$$

The *CEP* is determined from the position error covariance matrix, denoted by

$$P = \begin{bmatrix} p_{11} & p_{12} \\ p_{21} & p_{22} \end{bmatrix}.$$

The elements of the position error covariance matrix indicate the standard deviations of and correlation between the north (or down-range) and east (or cross-range) position errors. They are given by

$$\begin{aligned} p_{11} &= \sigma_{DR}^2, \\ p_{22} &= \sigma_{DR}^2, \\ p_{12} &= p_{21} = \rho_{CR,DR}\sigma_{CR}\sigma_{DR}, \end{aligned}$$

or

$$P = \begin{bmatrix} \sigma_{DR}^2 & \rho_{CR,DR}\sigma_{CR}\sigma_{DR} \\ \rho_{CR,DR}\sigma_{CR}\sigma_{DR} & \sigma_{CR}^2 \end{bmatrix}, \tag{5.96}$$

where the statistical correlation coefficient $\rho_{CR,DR}$ is given in terms of the cross-range and down-range position errors by

$$E\{x_{CR}y_{DR}\}/\sigma_{CR}\sigma_{DR} = E\{x_{CR}y_{DR}\}/\sigma_{x_{CR}}\sigma_{y_{DR}}. \tag{5.97}$$

The position error covariance matrix is a tensor that defines an ellipse of constant probability indicating the variances and covariances of the down-range and cross-range position errors as shown in Figure 5.38.

Define now

$$h \triangleq [(\sigma_{y_{DR}}^2 - \sigma_{x_{CR}}^2)^2 + 4A^2]^{1/2}, \tag{5.98a}$$

where $A = \rho\sigma_x\sigma_y = \rho\sigma_{x_{CR}}\sigma_{y_{DR}}$. After some algebra we obtain the covariances in the form

$$\sigma_{x_{CR}}^2 = \frac{1}{2}(\sigma_{x_{CR}}^2 + \sigma_{y_{DR}}^2 + h), \tag{5.98b}$$

$$\sigma_{x_{CR}}^2 = \frac{1}{2}(\sigma_{x_{CR}}^2 + \sigma_{y_{DR}}^2 - h), \tag{5.98c}$$

and

$$\theta = \frac{1}{2}\tan^{-1}[2\rho_{CR,DR}\,\sigma_{x_{CR}}\sigma_{y_{DR}}/(\sigma_{DR}^2 - \sigma_{CR}^2)]. \tag{5.98d}$$

The radius of the circle of 50% equivalent probability is obtained as follows:

For $\sigma_y^2/\sigma_x^2 \geq 0.9$,

$$R_{CEP} = 0.562\sigma_x + 0.615\sigma_y. \tag{5.99a}$$

For $\sigma_y^2/\sigma_x^2 \leq 0.9$,

$$R_{CEP} = \sigma_y[0.675 + 0.835(\sigma_y^2/\sigma_x^2)]. \tag{5.99b}$$

Another way to compute the *CEP* is as follows. Assume that, by the central limit theorem, the probability density function describing target miss distance will be normal. Then,

$$f(x, y) = (1/2\pi\sigma_x\sigma_y)\exp\{-1/2[(x/\sigma_x)^2 + (y/\sigma_y)^2]\}. \tag{5.100}$$

When this function is integrated over the ellipse (see Figure 5.38) whose major axis is $CEP \bullet \sigma_x$ and set equal to $\frac{1}{2}$, the major axis becomes $1.1774\sigma_x$, and the minor axis becomes $1.1774\sigma_y$. When these are averaged, the familiar formula results:

$$CEP = 0.5887(\sigma_x + \sigma_y). \tag{5.101}$$

References

1. Aggarwal, A.K: *Weapon Delivery Systems Using GPS, Proceedings of the NAECON'81*, 19–21 May 1981, Dayton, Ohio, pages 258–267.
2. Athans, M. and Falb, P. L.: *Optimal Control: An Introduction to the Theory and Its Applications*, McGraw-Hill Book Company, New York, 1966.
3. Ball, R.E.: *The Fundamentals of Aircraft Combat Survivability Analysis and Design*, AIAA Educational Series, American Institute of Aeronautics and Astronautics, Inc., New York, 1985.
4. Chui, C.K. and Chen, G.: *Kalman Filtering with Real-Time Applications*, third edition, Springer-Verlag, Berlin, Heidelberg, New York, 1999.
5. Duke, A.A., Brown, T.H., Burke, K.W., and Seely, R.B.: *A Ballistic Trajectory Algorithm for Digital Airborne Fire Control*, Naval Weapons Center, China Lake, California, Report TP 5416.
6. Lanczos, C.: *The Variational Principles of Mechanics*, second edition, The University of Toronto Press, Toronto, Canada, 1962.
7. Siouris, G.M.: *Aerospace Avionics Systems: A Modern Synthesis*, Academic Press, Inc., San Diego, New York, 1993.
8. Siouris, G.M.: *An Engineering Approach to Optimal Control and Estimation Theory*, John Wiley & Sons, Inc., New York, 1996.
9. Siouris, G.M.: *Flight Control Technology*: *An Overview*, paper presented at the 14th *IFAC* Symposium on Automatic Control in Aerospace, Seoul, Korea, August 24–28, 1998.
10. Siouris, G.M. and Leros, A.P.: *Minimum-Time Intercept Guidance for Tactical Missiles*, Control-Theory and Advanced Technology, Vol. 4, No. 2, June 1988, pp. 251–263.
11. Thomson, W.T.: *Introduction to Space Dynamics*, John Wiley & Sons, Inc., New York, 1961.
12. Whittaker, E.T.: *A Treatise on the Analytical Dynamics of Particles and Rigid Bodies*, fourth edition, Cambridge University Press, London, UK, 1964.
13. Zacharias, G.L., Miao, A., Illgen, C., and Yara, J.M.: *SAMPLE-Situation Awareness Model for Pilot-in-the-Loop Evaluation*, Charles River Analytics, Inc., Final Report No. *R95192*.
14. Zacharias, G.L., Miao, A., and Riley: *Passive Sensor Altitude and Terrain Awareness System*, Charles River Analytics, Inc., Final Report No. *R91071*.

6

Strategic Missiles

6.1 Introduction

In Chapters 2 through 4 we discussed short-range tactical missiles. These missiles are of the surface-to-air, air-to-air, and air-to-ground (or surface) variety. Combat aircraft, for example, are fitted with airborne weapons, which can be launched against enemy aircraft, enemy ground forces, or strategic targets deep inside enemy territory. Ground-based missile systems have various range capabilities from a few miles to several thousand miles. These ground-based missiles are ballistic or nonballistic types, depending on their mission requirements. The short-range guided missiles discussed in Chapters 2 through 4 are usually mobile so that they may be transported easily and quickly to locations where they are most needed.

Very long range guided missiles require large fuel supplies and extremely complex guidance and control systems. These missiles are usually stored within specific and specially designed areas. Later-generation ballistic missiles are designed for underground hardened-site storage to be launched as retaliatory measures in the event of attack by missiles from an unfriendly nation. Certain of these larger ballistic missiles have been integrated with space vehicle systems. In these cases, the guided missile has been used for the booster and sustainer stages to carry vehicles into outer space. The guided missile possesses many, if not all, of the desirable characteristics that are predominant in aerospace forces. These are as follows: (1) range, (2) mobility, (3) speed, (4) firepower delivery, (5) penetration, and (6) flexibility.

This chapter presents various methods of missile guidance for long-range strategic missiles. These guidance systems include inertial, celestial navigation, and terrestrial reference and magnetic systems. Of the many types of automatic guidance systems, the most important developments pertain to the inertial navigation and guidance system. All inertial guidance systems are similar in basic operation. In its simplest terms, inertial guidance can be described as a type of guidance that is complete within itself. It needs no exterior energy or radiation source to determine its course. It emits no signal, and it does not depend on ground equipment to operate it once the missile is launched [11]. Inertial guidance is especially advantageous for ballistic missiles, because it sends no signal and receives no signal, and cannot be jammed. Also, it is

almost impossible to detect or intercept. It is not influenced by weather conditions. Missiles can be launched and guided accurately to the target with all corrections for winds, atmospheric conditions, and other factors automatically made in flight. The inertial system is presently considered the best guidance system for use against stationary targets. During flight, the system computes its present position, altitude, and velocity, and it applies various compensations to its computer. These corrections minimize the errors introduced into the system by gravity, Coriolis, gyro unbalances, accelerometer bias and scale factor errors, and the nonspherical shape of the Earth. Specifically, the powered portion of the flight (i.e., from launch to burnout) is the most critical part of the flight. Therefore, during this critical phase of the flight, the path is determined by the inertial navigation and guidance system. On the other hand, during the free-flight phase, the trajectory is part of a conic section, almost always an ellipse. Reentry, as we shall see later, involves the dissipation of energy by friction with the atmosphere.

An inertial navigation and guidance system makes use of Newton's second law of motion, which states, "An unbalanced force acting on a body causes the body to accelerate in the direction of the force, and the acceleration is directly proportional to the unbalanced force and inversely proportional to the mass of the body." The three basic elements of any inertial system relating to a specific flight problem are accelerometers, gyroscopes, and memory devices. Even the most sophisticated of inertial guidance systems (i.e., systems using ring laser gyros, fiber-optic gyros, and microelectromechanical sensors or systems (*MEMS*)) today have some counterpart to these basic elements. At the present time, there is very little that can be done to divert or destroy ballistic missiles, which are capable of traveling over intercontinental distances and at hypersonic speeds. Technological developments are in progress. Such developments are, for example, energy weapons (e.g., laser beams) that can be used to intercept and destroy such missiles (for more details see Section 6.9). The *ABM* (antiballistic missile) is designed to provide limited protection in this area.

In addition to the United States, other nations are developing ballistic missiles. Specifically, China is developing a multiple-warhead system that could be deployed on its *Dong Feng DF-41 ICBM*, with a range goal of up to 12,000 km (7,456.8 miles). Also, China's *DF-31*, which has been successfully test-fired, has a single-warhead capacity and a range of about 8,000 km (4,971.2 miles). China is continuing the improvement of the medium-range (600 km, 372.8 miles) *M-9* and short-range (300 km, 186.4 miles) *M-11* ballistic missiles.

6.2 The Two-Body Problem

In Chapter 1 it was mentioned that a ballistic missile's trajectory is composed of three segments. Because of their importance, we will repeat them here in more detail for the reader's convenience. These segments are:

1. **Powered Flight:** The portion, which lasts from the time of launch to missile motor thrust cutoff or burnout and exit from the atmosphere (depending on cutoff altitude).

The terms cutoff and burnout, as used in this book, define the conditions at the beginning of the free-fall, that is, the termination of powered flight. Therefore, they denote the initial conditions necessary to solve the differential equations of motion. More specifically, this is the flight through the atmosphere and extending into free space where the aerodynamic forces may be neglected. During this portion of the flight, the greatest force acting on the vehicle is the thrust, which is derived from a rocket engine. The acceleration of the missile from this thrust is usually about 1.1 to 1.5 *g*'s at liftoff; it increases as the mass of the vehicle decreases with fuel consumption and staging, until a final value in the range of 5 to 10 *g*'s will be reached. At the time of cut-off (or burnout), the vehicle will have attained an altitude such that aerodynamic forces are no longer of major importance to the trajectory. However, the velocity and position of the vehicle must be controlled along the trajectory so as to limit the aerodynamic loading of the structure and to place the vehicle on a free-fall trajectory, which will carry it to its target. It should be pointed out that the guidance of a ballistic missile occurs entirely during this powered portion (or phase) of the flight; consequently, its objective is to place the missile on a trajectory with flight conditions that are appropriate for the desired target. This is equivalent to steering the missile to a burnout point that is uniquely related, as stated above, to the velocity and flight path angle for the specified target range. If there were no restrictions on the maneuvers that the missile can make during the powered flight, the guidance and control would be relatively simple, and the only major problem would be that of precision guidance. Structural limitations and flight performance requirements will combine to restrict the ascent trajectory such that only limited correction maneuvers may be employed. Typically, an *ICBM* will burn out at about 264.4 nm (490 km) altitude and 420.9 nm (780 km) downrange from its target.

2. **Free-Flight (or Free-Fall):** The portion that constitutes most of the trajectory. The free-flight trajectory is a conic section (i.e., an ellipse). This is also called "vacuum flight." For this phase of the flight, the initial conditions determine the parameters of the orbit; in other words, these parameters establish the trajectory to be followed. After the termination of powered flight, the missile is in a free-fall condition under the influence of gravitation alone. Above the thrust termination point (or cut-off point) the atmosphere is, in general, almost nonexistent for missiles capable of attaining ranges on the order of 5,000 to 6,000 nautical miles (9,260 to 11,112 kilometers). As the missile converges on the target, it will reenter the atmosphere. The missile is then no longer in the free-fall condition; this, as we shall see below, is the reentry phase of the missile trajectory. Many effects influence the free-flight trajectory. The main effects are those arising from the assumption that the Earth is a homogeneous rotating sphere. This gives rise to an elliptical trajectory passing through the cut-off point and target with one focus at the center of the Earth. All the other factors that affect the free-flight trajectory can be considered to cause only perturbations of the elliptic orbit. As in the powered flight trajectory, there is also a broad selection of free-flight trajectories to choose from, for a given range. The choice must be based on both technical and strategic factors. It should be noted that the entry of a ballistic missile into its free-fall trajectory occurs abruptly

upon the event of thrust cut-off, but the termination of the free-fall trajectory is not similarly well defined. For the definition of free-fall, it will be convenient to adopt the convention of a "reference sphere." The reference sphere is defined as the sphere with the center at the center of the Earth having the thrust termination (i.e., burnout) point on its surface. The free flight will be assumed to terminate when the missile returns to the reference sphere (see Figure 6.1). This same convention may be employed to define the initial point for reentry. Consequently, the flight conditions that obtain at the time of initiation of the free-fall phase of the flight have the greatest influence on the impact point of the missile. The powered flight is designed to place the vehicle in an appropriate trajectory so that upon thrust termination the missile will begin a free-fall orbit to the target. As stated above, under powered flight, no guidance need be employed during this free-fall, since the trajectory will be fully predictable.

3. **Reentry:** The portion that begins at some point where the atmospheric drag becomes a significant force in determining the missile's path and lasts until impact (i.e., target on the surface of the Earth). The reentry trajectory is determined to a great extent by the conditions of flight that obtain as the missile approaches the effective atmosphere of the Earth. Frequently, it is convenient to treat the reentry phase as terminal perturbation acting on the free-fall trajectory. The reentry phase of the trajectory should begin at an altitude of about 100,000 ft (30,480 m), where the dynamic pressure starts to significantly affect the motion of the missile. The computation of this trajectory phase involves knowledge of aerodynamic stability derivatives of the missile. It can be shown that the effects of reentry constitute only a perturbation to the free-flight trajectory. The importance of this phase of flight to navigation and guidance arises from the high accelerations that are experienced by the missile on reentry. In particular, the extremely high heating rates that are obtained during this flight limit the reentry trajectories that are permissible for any given missile configuration. While the transition from powered flight to free-fall is abrupt, the transition from free-fall to reentry flight is more gradual as a result of the builtup of air density as the missile penetrates the atmosphere. It should be noted here that the reentry point is not defined precisely.

These three phases of a ballistic missile's flight are illustrated in Figure 6.1 [2].

In this section we will discuss certain geometric properties of elliptic motion under a central attraction force and the two-body problem. The discussion presented in this section is useful in the development of Lambert's theorem, which will be discussed in Section 6.3. Specifically, we will begin our discussion with the development of the polar equation of a *conic section* (for more details on conic sections, see Appendix G).

Definition. A *conic section* is the locus of points so situated that the ratio of the distance of each point from a fixed point to its distance from a fixed line not through the fixed point is a constant.

The fixed point is called the *focus* of the conic, the fixed line is called its *directrix*, and the constant ratio, generally denoted by e, is called its *eccentricity*. Figure 6.2 illustrates the conic sections. Note that the directrix has no physical significance as

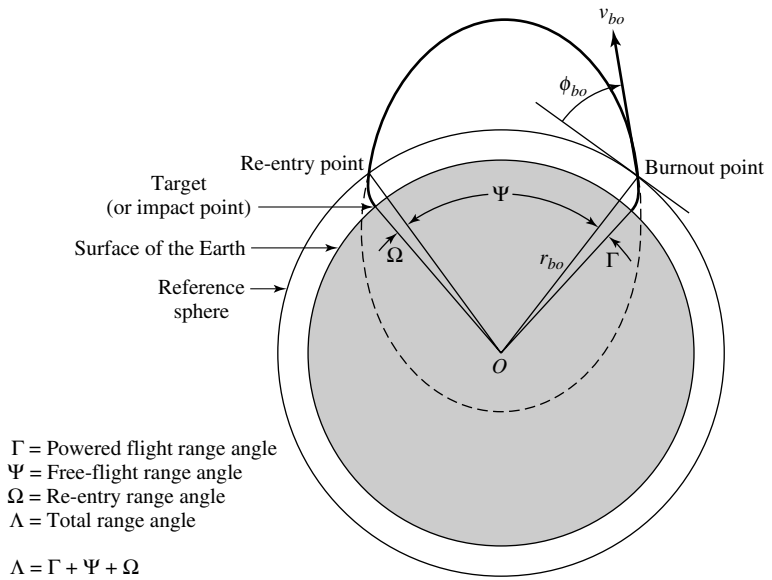

Fig. 6.1. Geometry of a ballistic missile's trajectory. Originally published in *Fundamentals of Astrodynamics*, R. R. Bate, D. D. Mueller, and J. E. White, Dover Publications, Inc., Copyright ©1971. Reprinted with permission.

far as orbits are concerned. However, the focus and eccentricity are indispensable concepts in the understanding of orbital motion.

From Figure 6.2 we note that the family of curves called *conic sections* (i.e., circle, ellipse, hyperbola, and parabola) represent the only possible paths for an orbiting object in the two-body problem. The focus of the conic orbit must be located at the center of the central body [10].

The most important types of curves (i.e., conic sections) can be represented by the general equation of the second degree in two variables as follows [7]:

$$Ax^2 + Bxy + Cy^2 + Dx + Ey + F = 0. \tag{6.1}$$

An equation of this type may represent an ellipse (or circle), a parabola, or a hyperbola. The ancient Greeks studied these curves as plane sections of a cone. However, for our purposes, it will be more convenient to represent the equation of the conic sections in polar coordinates. The polar equation of a conic section is given by the equation [2]

$$r = p/(1 + e\cos\nu), \tag{6.2}$$

where p is a geometric constant of the conic called the *parameter* or *semilatus rectum*, e is called the *eccentricity*, which determines the type of conic section represented by (6.2), and ν is the polar angle known as the *true anomaly*, which is the angle between r and the point on the conic nearest the focus. Consequently, (6.2) is the expression for the polar conic sections (i.e., the equation of all curves formed by the intersection of a complete conic surface and a plane, as shown in Figure 6.2). It is the trajectory

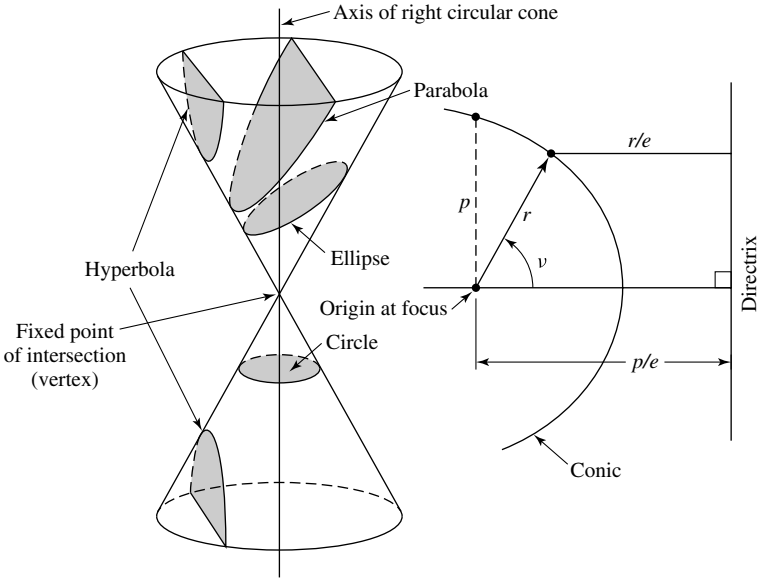

Fig. 6.2. The conic sections.

equation of a body expressed in polar coordinates. Equation (6.2) is also known as a *Keplerian ellipse*.

The exact nature of the resulting curves depends only upon the absolute value of the constant e, that is, the eccentricity. The origin of the r, ν coordinate system is located at the "primary focus" of the conic sections. The following relations define the various paths (see also Appendix G):

$$
\begin{aligned}
|e| &> 1 \quad \text{hyperbola,} \\
|e| &= 1 \quad \text{parabola,} \\
|e| &< 1 \quad \text{ellipse,} \\
|e| &= 0 \quad \text{circle.}
\end{aligned}
$$

These values may be verified by investigating (6.2) directly or by transforming this expression into rectangular Cartesian coordinates and recognizing that the general quadratic equation results. For example, when $|e| \geq 1$, it is possible for the denominator of (6.2) to vanish, and hence the path cannot be closed in this case. Moreover, we will see that if we let $e \to 0$, the parameter p is constant, so that a circular path results for $e = 0$.

Our next step is to develop the trajectory equation in polar coordinates for a small body (e.g., a planet) orbiting a large central body (e.g., the Sun). For the present discussion, we will assume that the two-body problem is applicable. In the two-body problem where one of the masses is very large compared to the other, the motion of the smaller mass takes place about the larger mass, whose gravitational attraction is

an inverse-square central force. For example, for an artificial satellite moving around the Earth as its focal center, the gravitational attraction is

$$F = -\frac{GMm}{r^2}, \tag{6.3}$$

where M and m are the masses of the Earth and satellite, G is the universal constant, and r is the distance of m from the center of the Earth. Equation (6.3) also applies to the Earth–Sun, the Moon–Earth, and the Earth–missile systems. From the above discussion, consider again the motion of a particle of small mass (e.g., the missile) m that is attracted by a particle of large mass (the Earth) M. The force of gravitational attraction between the masses is along the line joining them, so that the resulting motion is called *motion under a central force.* The acceleration of M is much smaller than that of m, so that without making too great an error we may consider M to be at rest, with m moving about it. Any motion under a central force takes place in a plane. From the above discussion, we can make the following assumptions:

(1) Assume an inverse square law of force between the missile and the Earth.
(2) Assume that the gravitational acceleration is a constant.
(3) Assume that the missile follows a path described by a conic section. This implies:
   (a) The dissipative forces of the system are negligible. This means that the system is conservative and the sum of the kinetic and potential energies is constant.
   (b) The only forces acting on the missile after engine cut-off is that of gravity (i.e., no guidance forces).
   (c) The path of the missile is in a single vertical plane.

In vector form, the equation of motion for the two-body problem is

$$\frac{d^2\mathbf{r}}{dt^2} = -\left(\frac{\mu}{r^3}\right)\mathbf{r}, \tag{6.4}$$

where $\mu = G(M+m) \approx GM$, G is the universal gravitational constant, M is the mass of the central body, and m is the mass of the orbiting body. (Note that μ is called the *gravitational constant* or *parameter*). In order to derive the trajectory (or orbit) equation, we will use scalar notation instead of vector notation given by (6.4). Figure 6.3 shows an ellipse where S (Sun) and F (focus) are two foci, C is the center, and AB is the major axis.

Kepler's first law states that the path, or orbit, of a planet around the Sun is an ellipse, the position of the Sun being at one focus of the ellipse. Kepler's first law is illustrated in Figure 6.3. Furthermore, Kepler's second law states that the radius vector SP sweeps out equal areas in equal times. Now, from Figure 6.3 we let (x, y) be the coordinates of the planet referenced from these axes. Therefore, using (6.4), the equations of motion in the orbital plane of the planet are [10]

$$\frac{d^2x}{dt^2} + \mu\left(\frac{x}{r^3}\right) = 0, \tag{6.5a}$$

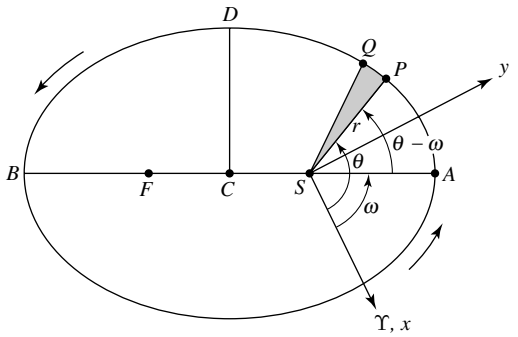

Fig. 6.3. The elliptical orbit.

$$\frac{d^2y}{dt^2} + \mu\left(\frac{y}{r^3}\right) = 0, \tag{6.5b}$$

where $r = (x^2 + y^2)^{1/2}$. We wish now to transform these equations given in rectangular coordinates (x, y) into polar coordinates (r, θ). Let

$$x = r\cos\theta \quad \text{and} \quad y = r\sin\theta.$$

Taking the first and second derivatives of these equations, we have

$$\frac{dx}{dt} = \dot{r}\cos\theta - r\dot{\theta}\sin\theta, \tag{6.6a}$$

$$\begin{aligned}\frac{d^2x}{dt^2} &= \ddot{r}\cos\theta - \dot{r}\dot{\theta}\sin\theta - \dot{r}\dot{\theta}\sin\theta - r\dot{\theta}^2\cos\theta - r\ddot{\theta}\sin\theta \\ &= \ddot{r}\cos\theta - 2\dot{r}\dot{\theta}\sin\theta - r\dot{\theta}^2\cos\theta - r\ddot{\theta}\sin\theta.\end{aligned} \tag{6.6b}$$

Similarly,

$$\frac{dy}{dt} = \dot{r}\sin\theta + r\dot{\theta}\cos\theta, \tag{6.7a}$$

$$\begin{aligned}\frac{d^2y}{dt^2} &= \ddot{r}\sin\theta + \dot{r}\dot{\theta}\cos\theta + \dot{r}\dot{\theta}\cos\theta - r\dot{\theta}^2\sin\theta + r\ddot{\theta}\cos\theta \\ &= \ddot{r}\sin\theta + 2\dot{r}\dot{\theta}\cos\theta - r\dot{\theta}^2\sin\theta - r\ddot{\theta}\cos\theta.\end{aligned} \tag{6.7b}$$

Substituting (6.6) and (6.7) into (6.5) results in

$$[\ddot{r} - r\dot{\theta}^2 + (\mu/r^2)]\cos\theta - (2\dot{r}\dot{\theta} + r\ddot{\theta})\sin\theta = 0, \tag{6.8a}$$

$$[\ddot{r} - r\dot{\theta}^2 + (\mu/r^2)]\sin\theta + (2\dot{r}\dot{\theta} - r\ddot{\theta})\cos\theta = 0. \tag{6.8b}$$

Since (6.8) must hold for all values of θ, then a planet's motion is governed by the following equations of force:

$$m(\ddot{r} - r\dot{\theta}^2) = -m(\mu/r^2),$$

$$m(2\dot{r}\dot{\theta} + r\ddot{\theta}) = 0,$$

or

Radial force:

$$\frac{d^2r}{dt^2} - r\left(\frac{d\theta}{dt}\right)^2 = -(\mu/r^2); \tag{6.9a}$$

Transverse force:

$$r\ddot{\theta} + 2\dot{r}\dot{\theta} = (1/r)\left(\frac{d}{dt}\right)(r^2\dot{\theta}) = 0. \tag{6.9b}$$

The second equation, (6.9b), leads to the statement of conservation of moment of momentum per unit mass $r^2(d\theta/dt) = h$. These are the polar equations of motion. Since

$$\left(\frac{d}{dt}\right)(r^2\dot{\theta}) = (2\dot{r}\dot{\theta} + r\ddot{\theta})r,$$

the function

$$r^2\left(\frac{d\theta}{dt}\right) = h \tag{6.10}$$

satisfies (6.9b), where h is the constant of integration (h is also called the *angular momentum*). Equation (6.10) is simply the mathematical expression of Kepler's second law. Now let us introduce the variable

$$u = 1/r. \tag{6.11}$$

From (6.10) we have

$$\frac{d\theta}{dt} = h/r^2 = hu^{\cdot 2}. \tag{6.12}$$

Taking the derivative of (6.11) yields

$$\frac{dr}{dt} = -u^{-2}\left(\frac{du}{dt}\right) = -(1/u^2)\left(\frac{du}{d\theta}\right)\left(\frac{d\theta}{dt}\right), \tag{6.13}$$

and from (6.10) and (6.11),

$$\frac{d\theta}{dt} = hu^2. \tag{6.14}$$

Hence, (6.13) may be written as follows:

$$\frac{dr}{dt} = -u^{-2}(du/d\theta)hu^2 = -h(du/d\theta). \tag{6.15}$$

Taking the second derivative of (6.15), we have

$$\frac{d^2r}{dt^2} = -h\left(\frac{d}{dt}\right)(du/d\theta) = -h\left(\frac{d^2u}{dt^2}\right)\left(\frac{d\theta}{dt}\right). \tag{6.16}$$

Again from (6.10) we have

$$\frac{d^2r}{dt^2} = -h^2(d^2u/d\theta^2)u^2. \tag{6.17}$$

Substituting (6.10) into (6.9a), results in

$$-(1/h^2u^2)[-h^2(d^2u/d\theta^2)u^2 - (1/u)h^2u^4 = -\mu u^2],$$

or

$$\frac{d^2u}{d\theta^2} + u = \frac{\mu}{h^2}. \tag{6.18}$$

The differential equation represented by (6.18) is called the *harmonic equation*; its solution is well known. The complementary solution of (6.18) is the general solution of

$$d^2u/d\theta^2 + u = 0.$$

That is,

$$u_c = A\sin\theta + B\cos\theta,$$

or

$$u_c = C_1\cos(\theta - C_2), \tag{6.19}$$

where C_1 and C_2 are constants of integration. The particular solution is readily found to be $u_p = \mu/h^2$.

Then the complete solution of (6.18) is

$$u = u_c + u_p = C_1\cos(\theta - C_2) + \mu/h^2 = (\mu/h^2)/[1 + C_1\cos(\theta - C_2)],$$

or

$$r = (h^2/\mu)/[1 + C_1\cos(\theta - C_2)]. \tag{6.20}$$

This is the polar form of an ellipse with origin at one focus. In terms of Figure 6.3, the constant C_1 is identified with the eccentricity e, and the constant C_2 identified with ω. Therefore, we can write (6.20) as

$$r = (h^2/\mu)/[1 + e\cos(\theta - \omega)], \tag{6.21}$$

where e and ω are constants of integration. The initial conditions on the motion are the burnout conditions of the ballistic missile or orbital vehicle (or the burnout conditions of the retrorocket in the case of reentry). These conditions must, of course, exist at a point of zero aerodynamic forces. A statement of the initial conditions that appears natural from an engineering point of view is

$$\begin{aligned} \text{at t} = 0: \qquad \theta &= 0, \\ \frac{d\theta}{dt} &= \frac{d\theta_i}{dt}, \\ r &= r_i, \\ \frac{dr}{dt} &= \frac{dr_i}{dt}. \end{aligned}$$

Note that the polar angle θ has been set equal to zero at the initial conditions. This puts no restrictions on the solution, since the effect of having $\theta = \theta_i$ rather than $\theta = 0$ is simply to rotate the reference for measurement of the polar angle. The astronomical solution uses a slightly different choice of θ_i.

From Figure 6.3 we note that the semilatus rectum p is given by

$$p = b^2/a = a(1 - e^2), \tag{6.22a}$$

or we can write

$$p = h^2/\mu, \tag{6.22b}$$

so that $h^2 = p\mu = \mu a(1 - e^2)$. Again, we remark in reference to (6.21) that this is the general equation of a conic section, which may be (see also Appendix G)

(i) an ellipse if $e < 1$,
(ii) a parabola if $e = 1$,
(iii) a hyperbola, if $e > 1$.

Although case (i) is that with which we are closely concerned here, the extension of the possibilities concerning the motion of a body under the gravitational attraction of the Sun should be noted.

It is convenient to interpret the initial conditions in terms of r_i, V_i, and γ_i, rather than in terms of r_i, dr_i/dt, and $d\theta_i/dt$. Here γ_i is the initial missile flight-path elevation angle, measured, of course, in the plane of motion, and V_i is the magnitude of the initial velocity vector in inertial space, or relative to the nonrotating Earth. From Figure 6.4, we have

$$\frac{dr_i}{dt} = V_i \sin \gamma_i, \tag{6.23a}$$

$$r_i \left(\frac{d\theta_i}{dt} \right) = V_i \cos \gamma_i. \tag{6.23b}$$

It is now convenient to introduce a parameter Δ_o defined by the relationship

$$\Delta_o \equiv r_i V_i^2/\mu. \tag{6.24}$$

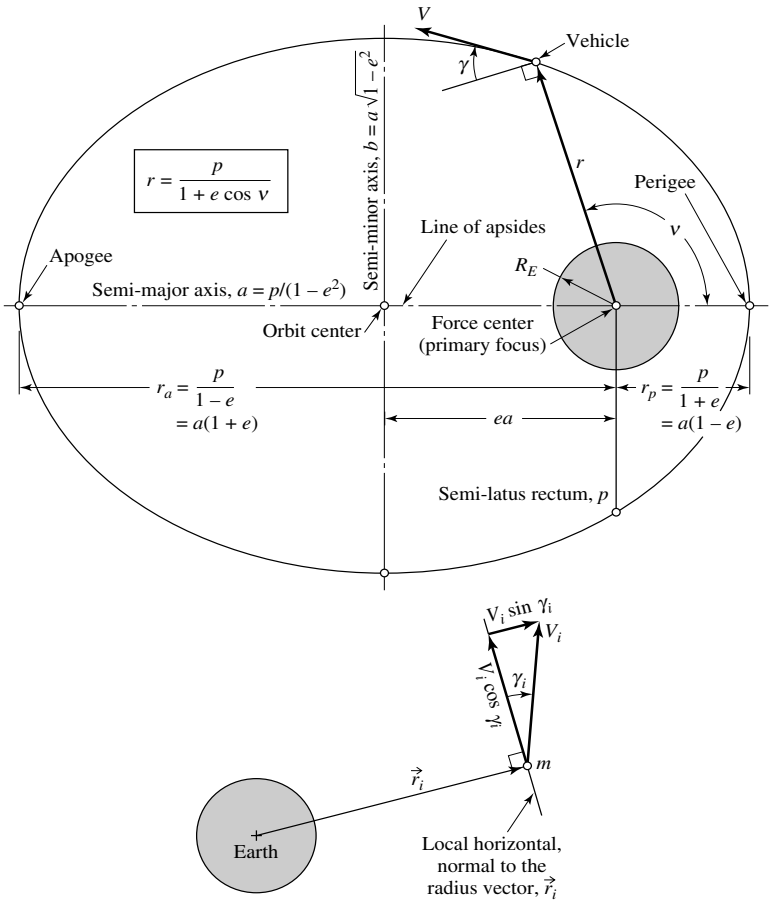

Fig. 6.4. Geometry of the ellipse.

This parameter is termed the *initial condition parameter*, and it can be interpreted as the ratio of twice the particle's initial kinetic energy to its initial potential energy.* We can now obtain expressions for h_i in terms of r_i, Δ_o, and γ_i. From (6.10) and (6.23) we obtain

$$h_i = r_i^2 \left(\frac{d\theta_i}{dt} \right) = r_i V_i \cos \gamma_i . \tag{6.25}$$

Squaring and introducing (6.24), we have

$$h_i^2 / \mu = r_i \Delta_o \cos^2 \gamma_i . \tag{6.26}$$

Figure 6.4 illustrates the geometry of the ellipse applicable to an elliptical orbit.

*For a body at heights beyond the influence of the atmosphere, the system is conservative, and the total energy $E = T + U$ of any orbit is a constant. In this equation it is convenient to consider the energies as those associated with a unit mass.

It can be verified that the equation of motion (6.2) reduces to the statement $r = r_i =$ [constant] by using (6.25) and (6.22b) to write

$$r = p/(1 + e\cos\nu) = (h_i^2/\mu)/(1 + e\cos\nu) = (r_i \Delta_o \cos^2\gamma_i)/(1 + e\cos\nu)$$

for the circular orbit $\gamma_i = 0$, $e = 0$, and $\Delta_o \equiv 1$, and hence $r = r_i$. The discussion of the complete elliptical orbit best proceeds by considering first the maximum and minimum values of r, as given by (6.2), taking the derivative of r with respect to ν and setting the result equal to zero. Thus,

$$dr/d\nu = (pe\sin\nu)/(1 + e\cos\nu)^2 = (r^2 e\sin\nu)/p = 0.$$

But $p = \infty$ and $er^2 = 0$ are trivial solutions to this equation, and so it follows that

$$\sin\nu = 0, \quad \text{for} \quad \nu = 0, \pi, 2\pi, \ldots,$$

gives the extreme values for r. These values are

Minimum (perigee) radius occurs for $\nu = 0$:

$$r_p = p/(1 + e); \tag{6.27a}$$

Maximum (apogee) radius occurs for $\nu = \pi$:

$$r_a = p/(1 - e). \tag{6.27b}$$

Dividing (6.27b) by (6.27a) gives the expression for e in terms of r_a and r_p:

$$e = (r_a - r_p)/(r_a + r_p). \tag{6.28}$$

Now introduce a, the semimajor axis of the ellipse (often called the *mean distance*, not to be confused with the mean equatorial radius a_E) defined by

$$a = (r_a + r_p)/2. \tag{6.29}$$

We can now add the two equations (6.27a) and (6.27b) and solve for p, which, as we saw earlier, is often called the *parameter* of the motion:

$$r_a + r_p = 2a = p[(1/(1 + e)) + (1/(1 - e))] = p\{(1 - e + 1 + e)/(1 - e^2)\},$$

or

$$p = a(1 - e^2), \tag{6.30}$$

which allows the equation of motion to be written in the simple form

$$r = a(1 - e^2)/(1 + e\ \cos\ \nu), \qquad |e| < 1. \tag{6.31}$$

This is the equation of the elliptical orbit that is usually encountered in the astronomical literature [5], [10]. The pertinent geometric relationships are shown in Figure 6.4. As stated earlier, the angle ν is usually referred to as the *true anomaly* of the ellipse. In as much as *initial conditions* are generally unknown in the astronomical problem, the polar angle θ is not given a name in this analysis. Note that once the perigee and apogee radii are known, the equation of motion is completely specified, since (6.28) and (6.29) determine a and e. In fact, any two of the six purely kinematic or geometric elements (r_a, r_p, a, e, p, b) completely define the ellipse and allow the remaining four elements to be determined. The relationships for the parameter p and the semiminor axis b may be readily found from (6.27) through (6.31) as

$$p = 2[r_a r_p/(r_a + r_p)] = a(1 - e^2) \tag{6.32}$$

and

$$b = (r_a r_p)^{1/2} = a(1 - e^2)^{1/2}. \tag{6.33}$$

Numerous other relationships between these kinematic elements may be derived by manipulation. In general, the mean distance a and the eccentricity e are considered basic in astronomy. The dynamic elements of the elliptical orbit are those that change with position, and include the radial distance r from the force center, the velocity V, the flight-path angle γ, and the period P, among others. In general, the dynamic elements all depend upon the gravitational constant μ. The radius vector has already been considered at some length and is given as a function of the true anomaly ν by (6.31).

The orbital period P is an important dynamic parameter of the orbit, which relates time to the motion in a somewhat gross way. The period is, of course, the time interval between successive passages of the body through any fixed point in its orbit. The law of conservation of angular momentum affords a rapid way to compute the period, since from (6.25), (6.26), and (6.22b) one may obtain

$$r^2\left(\frac{d\theta}{dt}\right) = r^2\left(\frac{d\nu}{dt}\right) = h_i = \sqrt{\mu p},$$

which may be rearranged and integrated (i.e., integrating over a complete orbit) to yield

$$\int_0^P dt = P = (1/\sqrt{\mu p}) \int_0^{2\pi} r^2 d\nu. \tag{6.34}$$

But we observe that the area enclosed by an ellipse is simply

$$A = \int_0^{2\pi} \int_0^r r dr d\nu = \frac{1}{2} \int_0^{2\pi} r^2 d\nu = \pi ab. \tag{6.35}$$

Comparing (6.34) and (6.35) readily shows that

$$P = (2\pi/\sqrt{\mu})(ab/\sqrt{p}).$$

Substituting b from (6.33) and the semiparameter p from (6.30), we have

$$P = (2\pi/\sqrt{\mu})[(a^2\sqrt{1-e^2})/(\sqrt{a(1-e^2)})],$$

or

$$P = (2\pi/\sqrt{\mu})\, a^{3/2} = 2\pi\sqrt{a^3/\mu}. \tag{6.36}$$

This result is basically a statement of Kepler's *third law*, which states that *the squares of the planetary periods are proportional to the cubes of their mean distances from the sun*. Actually, Kepler's third law stated in this way is completely correct only if the masses of the planets are negligible in comparison to the mass of the Sun. Otherwise, the squares of the periods are also inversely proportional to the planetary masses. Note that in astronomy, the quantity $2\pi/P$, which is the *mean angular velocity* of the particle in orbit (rad/sec), is defined to be the *mean angular motion* [5], [10]. Thus, the mean angular motion of a planet n is given by

$$n \equiv 2\pi/P. \tag{6.37a}$$

From (6.36) it is clear that

$$a^3n^2 = \mu \equiv G(M+m),$$

or

$$n = \sqrt{\mu/a^3}.$$

Now, as we saw from (6.35), the entire area of an ellipse is πab, and this is described in the interval defined by the period P. Hence,

$$P = (2/h) \times \text{ Area of ellipse}, \quad \text{or} \quad 2\pi ab/P = h, \tag{6.37b}$$

or making use of the relation $b^2 = a^2(1-e^2)$,

$$h = [2\pi a^2(1-e^2)^{1/2}]/P. \tag{6.37c}$$

Equation (6.34) also affords a way to relate the true anomaly ν to time. Substituting r from (6.31), p from (6.30), and integrating from the *time of perigee passage* (often called the *epoch* of perigee) T at any time t, we obtain

$$t - T = (a^2(1-e^2)^2)/(\sqrt{\mu a(1-e^2)}) \int_0^{\nu} d\nu/(1+e\cos\nu)^2.$$

This expression may be integrated with the help of integral tables (for example, see integrals 308 and 300 in [8]). The result is

$$t - T = \frac{2\pi a^{3/2}}{\sqrt{\mu}} \left\{ \frac{1}{\pi} \tan^{-1}\left[\sqrt{\frac{1-e}{1+e}} \tan\left(\frac{\nu}{2}\right) \right] - \frac{e\sqrt{1-e^2}\sin\nu}{2\pi(1+e\cos\nu)} \right\} \tag{6.38a}$$

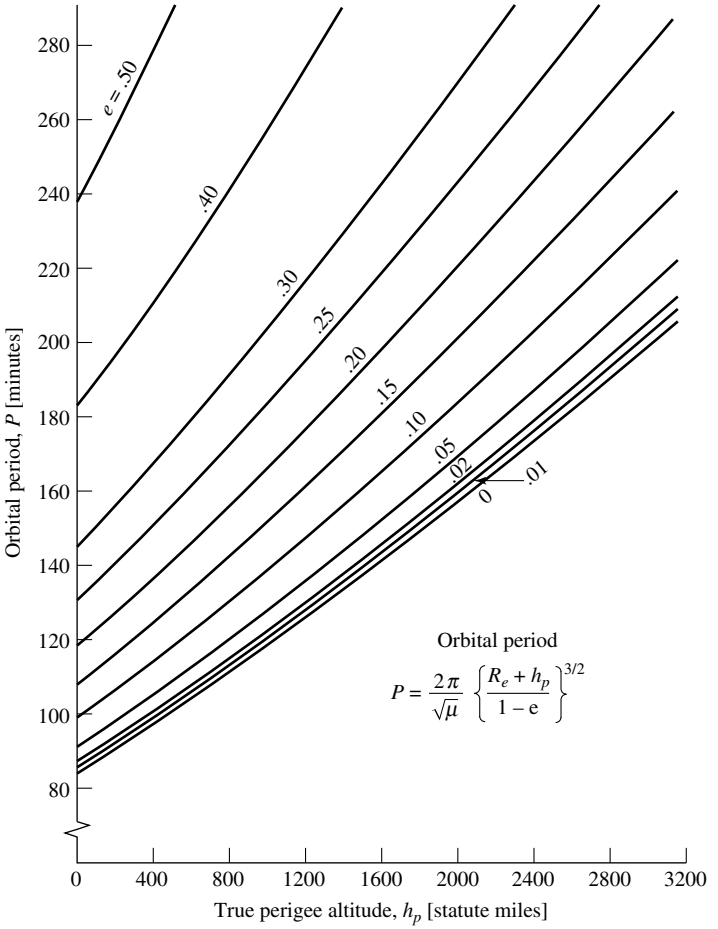

Fig. 6.5. Orbital period plotted in terms of different values of eccentricity e.

or

$$t - T = \frac{a^{3/2}}{\sqrt{\mu}} \left[2 \tan^{-1} \left(\sqrt{\frac{1-e}{1+e}} \tan \frac{1}{2}\theta \right) - \frac{e\sqrt{1-e^2} \sin\theta}{1 + e\cos\theta} \right] \tag{6.38b}$$

($e < 1$) for elliptic orbits. Thus, from (6.38) one can compute the time elapsed during travel along an elliptical orbit. Note that the coefficient of the term in brackets is simply the Keplerian period $= P$, and that the only kinematic element involved is the eccentricity e. This relation is presented graphically in Figure 6.5, since the solution for ν corresponding to a given value of t can be obtained only in this way. It should be pointed out that (6.37) may be inverted through the use of a series expansion in the small parameter e for nearly circular orbits (say, $e < 0.30$).

Another dynamic element of considerable importance for the elliptical orbit is the magnitude of the velocity vector at each point. From the sum of the squares of the radial and tangential velocity components, we have

$$V^2 = \dot{r}^2 + r^2\dot{\nu}^2. \tag{6.39}$$

The term $\dot{r}^2$ may be found by differentiating (6.2) and squaring. Thus,

$$\dot{r}^2 = r^4\dot{\nu}^2 e^2(\sin^2 \nu/p^2). \tag{6.40}$$

The term $d\nu/dt$ is found from the conservation of angular momentum, as before. The result for V^2 is therefore

$$V^2 = (\mu/p)[e^2 \sin^2 \nu + (1 + e\cos \nu)^2].$$

It should be noted that this result is not restricted to the elliptical orbit, since e and p are defined for all of the conic sections. However, for the elliptical orbit, this may be rearranged with the help of (6.30) in the form

$$V = \sqrt{\frac{\mu}{a}}\left[\sqrt{\left(\frac{1+e^2}{1-e^2}\right) + \left(\frac{2e}{1-e^2}\right)\cos \nu}\right]. \tag{6.41}$$

Note further that the *mean velocity* of the orbit is defined as that for a circular orbit at the *mean distance* a. Therefore,

$$V_m \equiv (\mu/a)^{1/2}.$$

The velocities at perigee and apogee may be readily found from this result, since

At perigee, $\nu = 0$*:*

$$V_p = V_m[(1+e)/(1-e)]^{1/2}; \tag{6.42a}$$

At apogee, $\nu = \pi$*:*

$$V_a = V_m[(1-e)/(1+e)]^{1/2}. \tag{6.42b}$$

It is interesting to note that the ratio of the perigee and apogee velocities is simply

$$V_p/V_a = (1+e)/(1-e) = r_a/r_p, \tag{6.43}$$

or

$$r_p V_p = r_a V_a.$$

Note that we may solve (6.43) for e in terms of V_a and V_p:

$$e = (V_p - V_a)/(V_p + V_a).$$

These results could have been deduced directly from the law of conservation of angular momentum, since at perigee and apogee the velocity vector is perpendicular to the radius vector, and so the product $r_a V_a$ or $r_p V_p$ is merely the angular rate (per unit mass) at these points. Finally, note that the quantity $(\mu/a)^{1/2}$ is the circular orbit velocity for an orbit at a distance a from the force center. Thus, for an elliptical orbit, $V_a < V_m$ and $V_p > V_m$.

The final dynamic element that we consider here is the so-called *flight path angle* γ, which is the angle of inclination between the instantaneous velocity vector and a line perpendicular to the instantaneous radius vector, as shown in Figure 6.4. By definition,

$$\tan\gamma \equiv \left(\frac{dr}{dt}\right) \Big/ r\left(\frac{d\nu}{dt}\right),$$

or, from (6.2) and (6.40), choosing the principal value,

$$\tan\gamma = e\sin\nu/(1+e\cos\nu). \tag{6.44}$$

This result is not restricted to the elliptical (or closed) paths; however, for $|e| < 1$, it is noted that $|\gamma| < \pi/2$. The maximum and minimum values of γ are found by differentiating (6.44) with respect to ν and setting the result to zero. We find that the only physically reasonable solution is that $\cos\nu = -e$, which gives the extreme value of γ as

$$|\tan\gamma_{\max}| = e/(1-e^2)^{1/2}. \tag{6.45}$$

Note that since $\cos\nu$ is negative, the maximum (and minimum) values of γ occur near apogee. Moreover, (6.44) shows that γ has the same algebraic sign over one-half of the orbit between perigee and apogee and the opposite sign over the remaining half. Therefore, according to our definition, γ is positive when the particle recedes from perigee. Figure 6.6 is a plot of (6.44), that is, the variation of the flight path angle γ versus the true anomaly ν. Table 6.2 summarizes the various parameters of an elliptical orbit.

6.3 Lambert's Theorem

With the preliminaries complete, we will now discuss Lambert's theorem. The German mathematician Johann Heinrich Lambert (1728–1777) showed in the eighteenth century (in 1761) that in elliptic motion under Newtonian law, the time required in describing any arc depends only on the major axis, the sum of the distances from the center of force to the *initial* and *final* points, and the length of the chord joining these points. Therefore, if these elements are given, the time can be determined regardless of the form of the ellipse.

Consider now Figure 6.7. Let E_1 and E_2 be the eccentric anomalies of two points P_1 and P_2 in an elliptic orbit such that $E_2 > E_1$. Next, define $2G = E_1 + E_2$ and $2g = E_2 - E_1 > 0$. Then the radii of the ellipse are given by [2], [3]

$$r_1 = a(1 - e\cos E_1), \tag{6.46a}$$

$$r_2 = a(1 - e\cos E_2). \tag{6.46b}$$

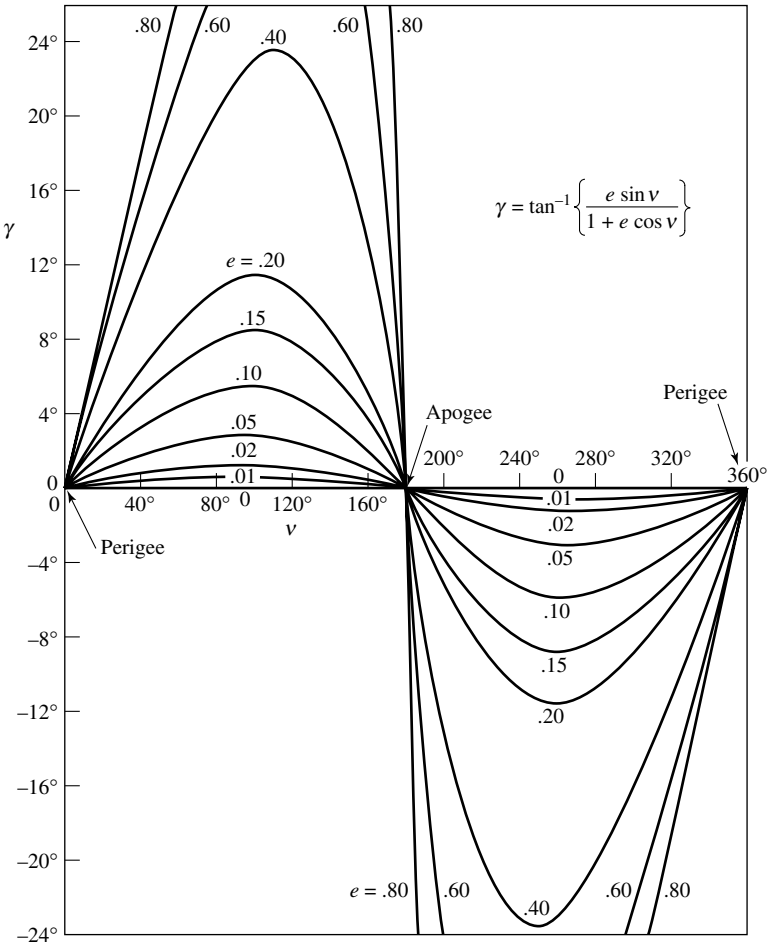

Fig. 6.6. Variation of the flight path angle γ with position along the orbit.

Adding the two radii r_1 and r_2 results in

$$r_1 + r_2 = a[2 - e(\cos E_1 + \cos E_2)],$$

or

$$r_1 + r_2 = 2a(1 - e \cos G \cos g), \tag{6.47}$$

since

$$\begin{aligned} \cos E_1 + \cos E_2 &= 2\cos((E_1 + E_2)/2)\cos((E_2 - E_1)/2) \\ &= 2\cos G \cos g. \end{aligned}$$

Table 6.1. Parameters of an Elliptical Orbit

		Known Elements				
Symb.	Quantity	a, e	p, e	r_p, e	r_a, e	r_a, r_p
a	Semi-major axis	a	$\frac{p}{1-e^2}$	$\frac{r_p}{1-e}$	$\frac{r_a}{1+e}$	$\frac{1}{2}(r_a + r_p)$
b	Semi-minor axis	$a\sqrt{1-e^2}$	$\frac{p}{\sqrt{1-e^2}}$	$r_p\sqrt{\frac{1+e}{1-e}}$	$r_a\sqrt{\frac{1-e}{1+e}}$	$\sqrt{r_a r_p}$
p	Semi-latus rectum	$a(1-e^2)$	p	$r_p(1+e)$	$r_a(1-e)$	$\frac{2r_a r_p}{r_a + r_p}$
e	Eccentricity	e	e	e	e	$\frac{r_a - r_p}{r_a + r_p}$
r_a	Apogee distance	$a(1+e)$	$\frac{p}{1-e}$	$r_p\left(\frac{1+e}{1-e}\right)$	r_a	r_a
r_p	Perigee distance	$a(1-e)$	$\frac{p}{1+e}$	r_p	$r_a\left(\frac{1-e}{1+e}\right)$	r_p

Let the chord P_1P_2 be denoted by c and let the coordinates of P_1 be (x_1, y_1):

$$x_1 = a\cos E_1,$$
$$y_1 = b\sin E_1 = a(1-e^2)^{1/2}\sin E_1.$$

Furthermore, let the coordinates of P_2 be (x_2, y_2):

$$x_2 = a\cos E_2,$$
$$y_2 = a(1-e^2)^{1/2}\sin E_2.$$

Hence, the length of P_1P_2 is given by

$$P_1P_2 = c = [(x_1 - x_2)^2 + (y_1 - y_2)^2],$$

or

$$c^2 = a^2(\cos E_2 - \cos E_1)^2 + a^2(1-e^2)(\sin E_2 - \sin E_1)^2.$$

Making use of trigonometric identities for $(\cos E_2 - \cos E_1)$ and $(\sin E_2 - \sin E_1)$, we can also write c^2 as follows:

$$c^2 = 4a^2\sin^2 G\sin^2 g + 4a^2(1-e^2)\cos^2 G\sin^2 g.$$

Now define the relationship $e\cos G \triangleq \cos j$, so that

$$c^2 = 4a^2\sin^2 g(1-\cos^2 j),$$

making $c = 2a\sin g\sin j$. Using (6.47), we can also write

$$r_1 + r_2 = 2a(1 - e\cos G\cos g) = 2a(1 - \cos g\cos j). \tag{6.48}$$

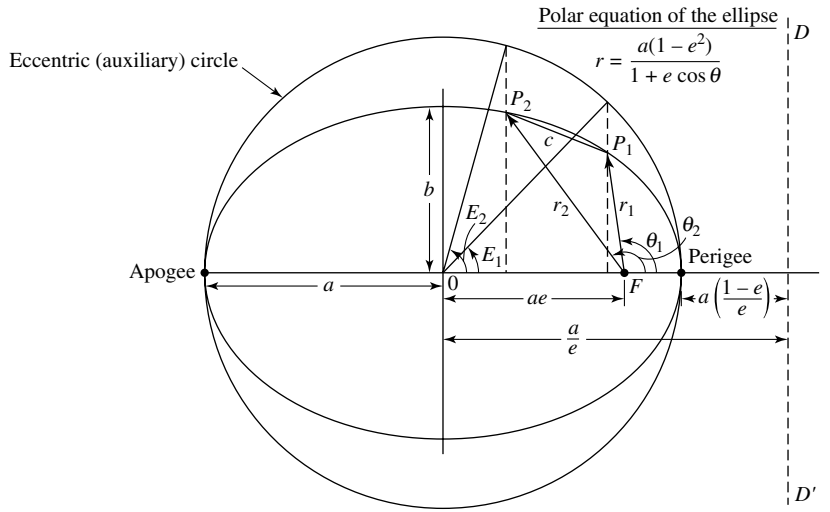

a = Semi-major axis
b = Semi-minor axis
e = eccentricity = $[(a^2 - b^2)/a^2]^{1/2}$
F = Focus = ae units from 0
DD' = directrix = a/e units from 0
θ = angle in polar equation of the ellipse known as *true anomaly*
c = chord
θ_1, θ_2 = true anomalies
E_1, E_2 = eccentric anomalies
t = time required to describe the arc P_1P_2
nt = mean anomaly
P = orbital period

Fig. 6.7. Geometry of the elliptic motion for deriving Lambert's theorem.

If we now define $\varepsilon \triangleq j + g$ and $\delta \triangleq j - g$, then

$$\begin{aligned} r_1 + r_2 + c &= 2a(1 - \cos g \cos j) + 2a \sin g \sin j \\ &= 2a(1 - \cos g \cos j \sin g \sin j) \\ &= 2a[1 - \cos(g + j)] \\ &= 4a \sin^2(\varepsilon/2). \end{aligned} \tag{6.49a}$$

Similarly,

$$r_1 + r_2 - c = 2a[1 - \cos(g - j)] = 4a \sin^2(\delta/2). \tag{6.49b}$$

If t_{ff} is the time of free fall in the ellipse between points P_1 and P_2, then $t_{ff} = t_2 - t_1$, so that

$$\begin{aligned} n \times \text{ the required time } &= n(t_2 - t_1) = E_2 - e \sin E_2 - (E_1 - \sin E_1) \\ &= (E_2 - E_1) - e(\sin E_2 - \sin E_1), \end{aligned} \tag{6.50}$$

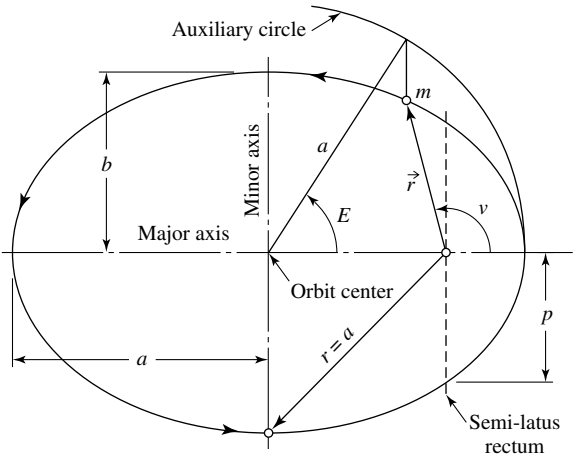

Fig. 6.8. Geometry of the ellipse.

where as was shown by (6.37), n is the *mean motion*; that is,

$$n = 2\pi/P = \sqrt{\mu/a^3},$$

where n is given in radians per unit time and P is the period of orbit (or period of revolution in the ellipse). If P is expressed in mean solar days, then n is called the *mean daily motion*.

From (6.43) we can also write

$$\begin{aligned} nt_{ff} &= (E_2 - E_1) - e(\sin E_2 - \sin E_1) \\ &= (\varepsilon - \delta) - 2\sin\left(\frac{\varepsilon - \delta}{2}\right)\cos\left(\frac{\varepsilon + \delta}{2}\right), \end{aligned}$$

or

$$nt_{ff} = (\varepsilon - \delta) - (\sin\varepsilon - \sin\delta). \tag{6.51}$$

The angles ε and δ are given by (6.49a) and (6.49b) in terms of $(r_1 + r_2)$, c, and a. Equations (6.50) and (6.51) constitute Lambert's theorem for elliptic motion [10], [17].

Consider again the geometry of the ellipse, given in Figure 6.8 (see also Appendix G).

Several additional kinematic elements and definitions that are frequently encountered in the astronomical literature deserve brief mention [5], [10]. For example, it is not difficult to show that the length of the radius vector from the force center to the point where the minor axis intersects the orbit exactly equals the length of the semimajor axis a. Another angle that was first introduced by Kepler is the *eccentric anomaly* E, which is measured from the center of the ellipse rather than from the force center. Geometric considerations show that the equation of motion may be written very simply in terms of the eccentric anomaly. That is,

$$r = a(1 - e\cos E).$$

It may be shown that

$$\cos \nu = (\cos E - e)/(1 - e \cos E), \quad \sin \nu = (1 - e^2)^{1/2} \sin E/(1 - e \cos E),$$

while the inverse relations are readily found to be

$$\cos E = (\cos \nu + e)/(1 - e \cos \nu), \quad \sin E = (1 - e^2)^{1/2} \sin \nu/(1 + e \cos \nu).$$

This form is useful in computing the relationship between time and position in orbit. For example, in terms of E, (6.38) may be written in the simple form

$$t - T = (1/n)[E - e \sin E],$$

or

$$n(t - T) = E - e \sin E,$$

where n is the previously defined *mean motion* $2\pi/P$. This leads to the Keplerian equation for the motion

$$n(t - T) = M = E - e \sin E, \tag{6.52}$$

where T is a constant of integration, also called the time of perihelion passage; E is the eccentric anomaly; e is the eccentricity; and M is defined as the *mean anomaly* [5]. The mean anomaly is the angle through which the vehicle would move at the uniform speed n, measured from the perigee. The quantity $n(t - T)$ is the angle that would have been described by the radius vector if it had moved uniformly with the average rate. Equation (6.52) is known as *Kepler's equation*. It is transcendental in E, and the solution for this quantity cannot be expressed in a finite number of terms. Equation (6.52) is also written in the form

$$t - T = (\sqrt{a^3/\mu})[E - e \sin E], \tag{6.53}$$

where we see that T is the constant of integration, and as stated above, it is the time of perihelion passage.

It is of interest now to express the total mechanical energy E in terms of the orbit elements (the reader should not confuse the use of the symbol E for energy with E for the eccentric anomaly). As stated earlier, in Section 6.2, the total energy is the sum of the kinetic and potential energies (by definition) and has the form

$$E = T + U = \frac{1}{2} m V^2 - m(\mu/r) \tag{6.54}$$

(again, here the reader should not confuse the kinetic energy T with the time of perihelion passage T). Here the potential energy is taken to be negative (by convention) and is zero at infinity. This expression may be written as

$$E = (m\mu/2r)\{[V^2/(\mu/r)] - 2\}, \tag{6.55}$$

and since the total energy must remain constant (in a conservative force field and without dissipative influences such as drag), it follows that

$$E = (m\mu/2r_i)\{\Delta_o - 2\}. \tag{6.56}$$

Thus, the initial condition parameter of (6.24), Δ_o, is recognized as the ratio of twice the initial kinetic energy to the initial potential energy of the particle. Substituting now the value of V from (6.41) and from (6.2), there is found, after some simplification,

$$E = (m\mu/2p)[e^2 - 1], \tag{6.57}$$

which, of course, applies to any path, open or closed. For the closed path $|e| < 1$, (6.30) reduces this equation to the simple form

$$E = -m\mu/2a, \qquad |e| < 1, \tag{6.58}$$

which may be interpreted as stating that the total mechanical energy depends only upon the semimajor axis of the ellipse, and all paths with the same semimajor axis have the same total energy irrespective of their eccentricity or "shape." Stated another way, this expression tells us that a body traveling on a long, slender ellipse of high eccentricity may have the same total energy as a body of the same mass traveling a circular path of eccentricity zero, provided that the mean distance, a, is the same for each path. The negative sign on the total energy is to be expected, since the sign convention on the potential energy results in a negative energy for all of the closed paths, as shown in the above discussion. Considering the above results, along with (6.36), it becomes evident the all orbits of the same energy have the same period and the same semimajor axis. This fact is often quite useful; for example, the period of a satellite in an elliptical orbit may be found by finding the period of a satellite in a circular orbit of radius equal to the semimajor axis of the elliptical orbit. No discussion of energy relative to orbit computations would be complete without some mention of the *vis viva** (or *energy integral*). Combining (6.55) and (6.58), one obtains [3], [5]

$$V^2 = \mu[(2/r) - (1/a)], \tag{6.59}$$

which permits the velocity at any point on the orbit to be found in terms of that at any other point, through the relation

$$V_1^2 - V_2^2 = 2\mu[(1/r_1) - (1/r_2)]. \tag{6.60}$$

Thus, (6.59) is the energy equation for an elliptic orbit. That (6.59) represents a true integral of the equations of motion may be demonstrated starting with Newton's second law in the form of (6.4):

$$\frac{d^2\mathbf{r}}{dt^2} = -(\mu/r^2)\mathbf{e}_r, \tag{6.61}$$

*The name *vis viva*, the Latin words meaning *living force*, was given by the German mathematician Gottfried Wilhelm Leibniz (1646–1716) in the year 1695.

where $\mathbf{e}_r$ is a unit vector in the radial direction, and $\mathbf{r}$ is the radius vector to the point in question. (Note that throughout the book, we will use boldface notation to denote vectors.) Performing the dot product on both sides of this equation results in

$$\dot{\mathbf{r}} \cdot \ddot{\mathbf{r}} = \frac{1}{2}\left(\frac{d}{dt}\right)(\mathbf{r} \cdot \mathbf{r}) = -(\mu/r^2)(\mathbf{r} \cdot \mathbf{e}_r) = -(\mu/r^2)\left(\frac{dr}{dt}\right),$$

and integrating yields

$$\left(\frac{d\mathbf{r}}{dt}\right) \cdot \left(\frac{d\mathbf{r}}{dt}\right) = V^2 = (2\mu/r) + \text{constant}, \tag{6.62}$$

which applies to all motion in an inverse-square force field. The *vis viva* equation is given in textbooks on celestial mechanics in a slightly different form. We will make use of one such reference [4]. Using (6.56) and (6.10), we can write the equations of motion in the orbital plane as [5]

$$\frac{d^2x}{dt^2} = -\mu(x/r^3), \qquad \frac{d^2y}{dt^2} = -\mu(y/r^3) \tag{6.63}$$

with

$$r^2 = x^2 + y^2.$$

Now introduce polar coordinates by

$$x = r\cos\theta,\ y = r\sin\theta.$$

Then

$$\left(\frac{dx}{dt}\right)^2 + \left(\frac{dy}{dt}\right)^2 = \left(\frac{dr}{dt}\right)^2 + r^2\left(\frac{d\theta}{dt}\right)^2.$$

Consequently, the integral of area and the *vis viva* integral may be written as

$$r^2\left(\frac{d\theta}{dt}\right) = h, \tag{6.64a}$$

$$\left(\frac{dr}{dt}\right)^2 + r^2\left(\frac{d\theta}{dt}\right)^2 = 2[(\mu/r) + C]. \tag{6.64b}$$

These equations are a system of the second order, but the presence of two constants of integration renders them fully equivalent to the system (6.63), which is of the fourth order.

6.4 First-Order Motion of a Ballistic Missile

6.4.1 Application of the Newtonian Inverse-Square Field Solution to Ballistic Missile Flight

As indicated in Sections 6.2 and 6.3, the solution for the equations of motion of a particle under the influence of a Newtonian inverse-square attracting force field about

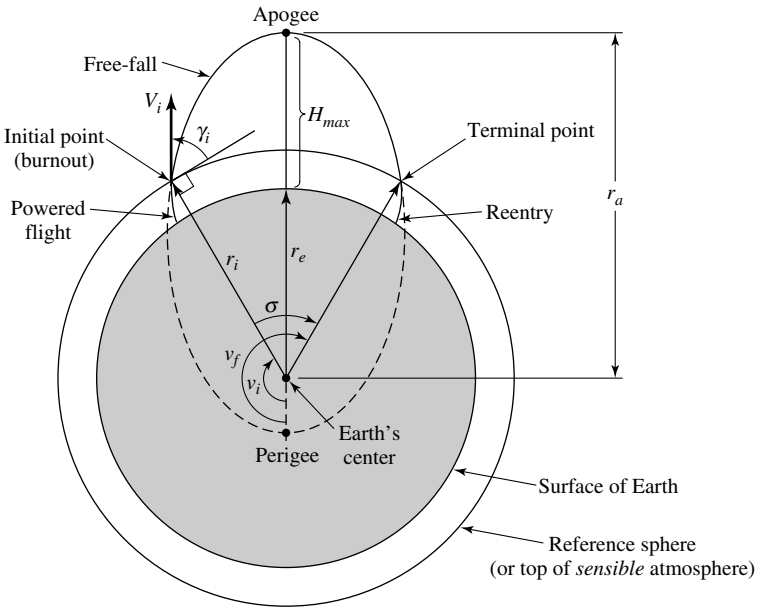

Fig. 6.9. Typical ballistic missile orbit.

a nonrotating spherical Earth constitutes a very good approximation for the study of ballistic missile trajectories. Therefore, the force field is a central field, and the trajectory plane will contain the burnout point, the mass center of the Earth, and the target, if the initial velocity vector is properly aligned in azimuth. In particular, the solution is virtually exact for the portion of the trajectory that is above the sensible atmosphere, say, above an altitude of 300,000 ft (91,440 m). The small perturbations due to Earth oblateness and atmospheric drag, while not altogether negligible, will be considered later, since their influence does not materially change such design parameters as takeoff weight, time of flight, and range.

Since the shortest distance between two points on the surface of a sphere is along a great circle, ballistic trajectories are also considered in the great circle plane. Figure 6.9 shows the pertinent geometry of a ballistic trajectory, which is an ellipse with the center of the Earth as one focus. Perigee is then inside the Earth, while the point of maximum height coincides with the apogee. For the present purpose a ballistic missile shall be considered any unmanned vehicle that for one reason or another cannot completely traverse its orbit. Of course, in the most important case, the reason is that a portion of the orbit actually lies below the Earth's surface, as shown in Figure 6.9. This corresponds to the ballistic missile situation. Other cases of interest include intercept paths, which may be portions of elliptical orbits, or launch trajectories, which are generated by continual application of thrust and/or control.

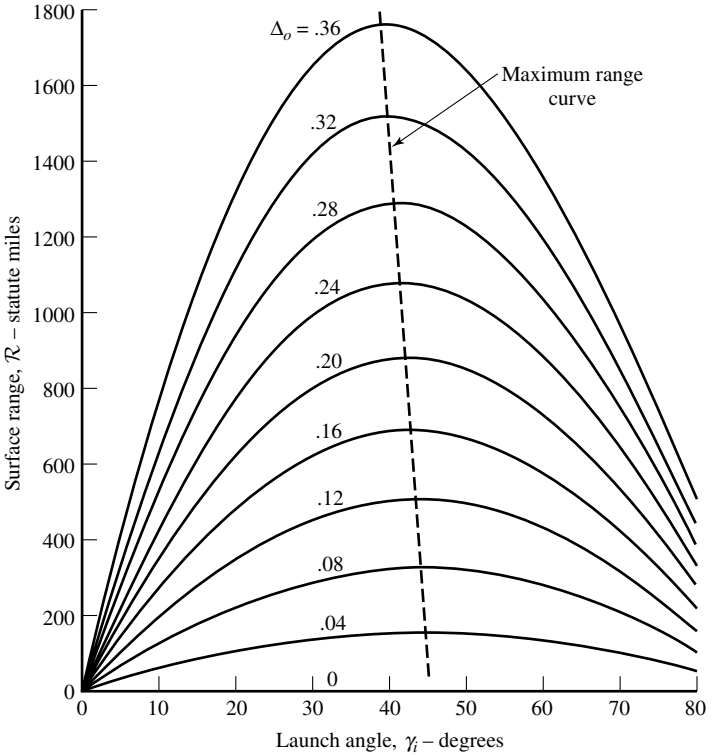

Fig. 6.10. Range vs. launch angle γ_i.

As we shall see shortly, the range R along the Earth's surface between two points of constant altitude can be written in the form

$$R = 2r_e(\pi - \delta_i).$$

The term $(\pi - \delta_i)$ can be interpreted as one-half the angle included between the radii to these points. After some trigonometric manipulation, the angle δ_i turns out to be $\nu_I = \delta_i$, and the maximum flight path angle γ_{im} is

$$\gamma_{im} = \sin^{-1}[(1 - \Delta_o)/(2 - \Delta_o)]^{1/2},$$

where $\Delta_o \equiv r_i V_i^2/\mu$. Figure 6.10 shows a plot of R versus the launch angle γ_i for various values of the initial condition parameter Δ_o, for short ranges.

Also, Figure 6.10 shows that the value of γ_i for maximum range continuously decreases for 45° as Δ_o increases from zero.

It must be noted that if the flight path intersects the Earth at all, it may intersect only twice. This may be seen by noting that the Earth's center must lie at the primary focus, and since from (6.2) the equation of the path is

$$r = p/(1 + e\cos\nu), \tag{6.2}$$

then there are at most two values of ν that correspond to each $r = r_e = e \neq 0$, where r_e is the radius of the Earth. It follows that if a closed path intersects the Earth, the perigee must be interior to the Earth, as shown in Figure 6.9. One of the most significant design parameters of a ballistic missile is the range covered over the surface of the Earth. From Figure 6.9, it is clear that this quantity, from the initial instant to any other time, is simply

$$R = r_e(\nu - \nu_i), \tag{6.65}$$

where the true anomaly ν is related to the time t through (6.38). Using (6.22b) and (6.26), we have $(\nu - \nu_i) = \theta$, and so

$$R = r_e\theta. \tag{6.66}$$

The angle θ may be obtained by solving (6.21). Or in terms of Figure 6.9, the range is $r_e\sigma$. Therefore, of interest here is the determination of the range $r_e\sigma$, the height H_{max}, and the time $t = T$ as a function of the initial conditions, which are $r_i = r_e$, V_i, and γ_i. The eccentricity is determined from the equation

$$e^2 = [(RV_i^2/\mu) - 1]^2 \cos^2\gamma_i + \sin^2\gamma_i.$$

Consequently, the range of the missile in free flight, that is, the range as it travels from the initial point (or burnout) on the reference sphere to the apogee and back to the reference sphere (at the terminal or reentry point) can be defined in terms of the geocentric angle σ by the expression

$$\sigma = 2(\pi - \nu), \tag{6.67}$$

where ν is the true anomaly. Using the orbit equation (6.21), the range may be related to the orbit parameters as follows:

$$r_i = (h^2/\mu)/(1 + e\cos\nu) = (h^2/\mu)[1 + e\cos(\pi - (\sigma/2))]. \tag{6.68}$$

From Figure 6.9, the altitude at the apogee, that is, H_{max}, is given by the expression

$$H_{max} = r_a - r_e = (h^2/\mu)(1 - e) - r_e.$$

6.4.2 The Spherical *Hit Equation*

From the discussion of Sections 6.2 and 6.3, we note that there are many trajectories that can be formed from the equation of an ellipse (e.g., (6.2)). It is now necessary to determine which of the many possible trajectories will actually impact at some predetermined target. Specifically, we will develop the equation for the velocity required to impact a target, and the *hit equation*, which is an equation that expresses the relation among the burnout parameters r_i, V_i, and γ_i. Let us now return to (6.9a) and (6.9b):

$$\frac{d^2r}{dt^2} - \left(\frac{d\theta}{dt}\right)^2 r = -\mu/r^2, \tag{6.9a}$$

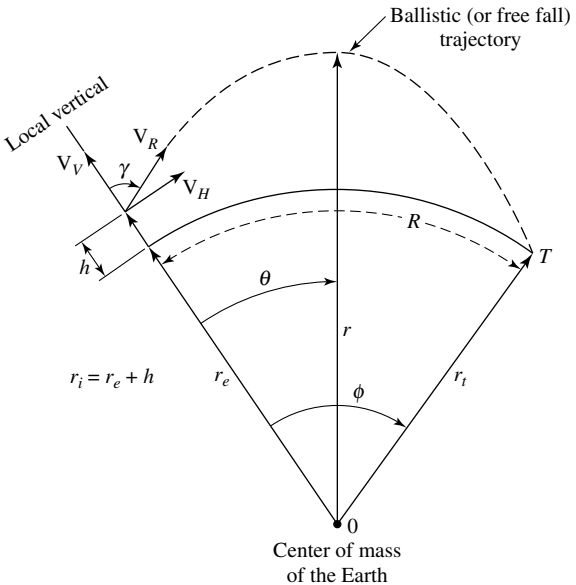

Fig. 6.11. Planar geometry for a typical ballistic trajectory.

$$\left(\frac{d}{dt}\right)\left[r^2\left(\frac{d\theta}{dt}\right)\right] = 0. \tag{6.9b}$$

As stated in Section 6.2, equation (6.9b) expresses the conservation of angular momentum h for the motion of the vehicle in a central force field. Now, integrating (6.9b), we obtain (6.25), that is,

$$r^2\left(\frac{d\theta}{dt}\right) = h = r_i V_i \sin\gamma_i. \tag{6.25}$$

Note that here in (6.25) we use $\sin\gamma$ instead of $\cos\gamma$ because the flight path angle γ has been defined differently; that is, here we measure γ from the local vertical instead of from the horizontal.

The geometry used to describe the elliptical free flight path of the vehicle is shown in Figure 6.11. Here note that r and θ are the in-plane polar coordinates, γ the burnout flight path angle, ϕ the in-plane range angle, r_e the equatorial radius of the Earth (we assume here a spherical Earth), V the in-plane burnout velocity of the vehicle, R the great circle linear range, r_t the distance from the center of the mass of the Earth to the target, and h the burnout altitude of the vehicle. Then, the burnout radius is $r_i = r_e + h$ (note that here h is the height above the Earth, and should not be confused with the definition of the angular momentum).

The angular momentum integral given by (6.25) allows us, as before, to express time derivatives in terms of θ derivatives. Thus,

$$\frac{d}{dt} \equiv \left(\frac{d\theta}{dt}\right)\left(\frac{d}{d\theta}\right) = (h/r^2)\left(\frac{d}{d\theta}\right). \tag{6.69a}$$

This relationship will facilitate writing the solution to (6.9a) so as to obtain the geometric relation between r and θ. First, let us define (see also Section 6.2)

$$u(\theta) = 1/r(\theta) \tag{6.69b}$$

and

$$\lambda = r_i V_R^2/\mu. \tag{6.70}$$

The parameter λ (identified with the parameter Δ_o; see also (6.24) and Sections 6.3 and 6.4.1) is the dimensionless ratio of twice the kinetic energy at burnout to the potential energy at burnout [18]. For elliptic orbits, λ varies between zero and two and has a value of two at escape velocity. Specifically, the parameter λ gives the following conics:

$$\begin{aligned} &\lambda < 2, \quad \text{elliptic trajectory,} \\ &\lambda = 2, \quad \text{parabolic trajectory,} \\ &\lambda > 2, \quad \text{hyperbolic trajectory.} \end{aligned}$$

Using (6.69a), (6.69b), and (6.70) in (6.9a), one obtains for the transformed equation of motion the following expression:

$$d^2u/d\theta^2 + u = \mu/h^2 = 1/(\lambda r_i \sin^2\gamma). \tag{6.71}$$

This is (6.18). From Figure 6.11, letting $t = 0$ corresponds to $\theta = 0$, so that the appropriate initial conditions are

$$u(0) = 1/r_i, \tag{6.72a}$$

$$du/d\theta|_{\theta=0} = -(1/r_i)\cot\gamma. \tag{6.72b}$$

Therefore, the complete solution to the differential equation (6.71) is

$$\begin{aligned} r_i u(\theta) &= r_i/r(\theta) = [(1-\cos\theta)/(\lambda\sin^2\gamma)] + [\sin(\gamma-\theta)/\sin\gamma] \\ &= [\mu(1-\cos\theta)/r_i V^2 \sin^2\gamma] + [\sin(\gamma-\theta)/\sin\gamma]. \end{aligned} \tag{6.73}$$

It should be noted that the solution has been written in terms of the burnout variables, since these are the quantities that are actually controlled by a guidance system. Given the above development, we can now proceed to write the hit equation. The conditions necessary that the vehicle impact the target are

$$r = r_t, \tag{6.74a}$$

when

$$\theta = \phi. \tag{6.74b}$$

Substituting (6.74) into (6.73) we obtain the spherical Earth *hit equation* [9], [16]:

$$r_i/r_t = [(1-\cos\phi)/\lambda\sin^2\gamma] + [\sin(\gamma-\phi)/\sin\gamma], \tag{6.75}$$

Solving (6.75) for λ results in the following expression:

$$\lambda = (1 - \cos\phi)/[(r_i/r_t)\sin^2\gamma + \sin(\phi - \gamma)\sin\gamma]. \tag{6.76}$$

Again, the reader should note the slight difference between (6.75) and the *hit equation* given in [18]; this difference is due to the way we defined the flight path angle γ.

Equation (6.75) expresses the relation between the burnout parameters V, γ, $h = r_i - r_e$, and the target conditions r_t and ϕ. Even for a specified burnout altitude, there are many combinations of burnout velocity and flight path angle that satisfy (6.75). In order to uniquely determine V and γ, one must satisfy the time of free flight, which will be developed shortly. Doing this also uniquely determines the free flight trajectory of the vehicle. This can most readily be shown by writing the geometric equation for an ellipse and evaluating the parameters of the conic in terms of the burnout variables. From the definition of the ellipse, (6.31), we have

$$r = a(1 - e^2)/(1 + e\cos\theta), \tag{6.31}$$

where r and θ are the polar coordinates for the ellipse (note: at the perigee $\theta = 0$), a is the length of the semimajor axis, and e is the eccentricity of the ellipse. One can easily show that [3], [9]

$$a = (r_i/2)\{1 + [r_t(1 - \cos\phi)/(r_i(1 - \cos 2\gamma) + r_t(\cos(2\gamma - \phi) - 1))]\} \tag{6.77}$$

and that

$$e^2 = (\lambda - 1)^2\sin^2\gamma + \cos^2\gamma. \tag{6.78}$$

Equation (6.77) then contains the missile and target positions and is tangent to the required velocity vector $\mathbf{V}_r$ (see Figure 6.11). If we substitute (6.77) and (6.78) into (6.31), the analytic formulation of the free flight conic is completely specified in terms of the burnout and target parameters.

Next, we wish to develop the required (also known as *correlated*) velocity to impact a target. For a spherical Earth model, the component of velocity normal to the trajectory must be zero. Therefore, only the in-plane velocity V needs to be determined. Again, consider (6.18), where the general solution is

$$u = (\mu/h^2) + A\cos\phi + B\sin\phi. \tag{6.79}$$

(Note that in the present analysis, we will assume the general case of (r, ϕ) in deriving the equation for the required velocity, and substitute $r \equiv r_i$ shown in Figure 6.11.) Differentiating (6.79) we obtain

$$\frac{du}{dt} = -\dot{\phi}A\sin\phi + \dot{\phi}B\cos\phi. \tag{6.80}$$

In order to have the trajectory pass through the general point (r, ϕ), we must have

$$\phi = \phi \quad \text{when} \quad u = 1/r,$$
$$\frac{du}{dt} = -\left(\frac{dr}{dt}\right)/r^2 \quad \text{when} \quad \frac{d\phi}{dt} = h/r^2.$$

Substituting these equations into (6.79) and (6.80) gives the simultaneous equations

$$A\cos\phi + B\sin\phi = (1/r)(\mu/r^2), \tag{6.81a}$$
$$A\sin\phi - B\cos\phi = r/h^2. \tag{6.81b}$$

The solution of (6.81a) and (6.81b) is

$$A = [(1/r) - (\mu/h^2)]\cos\phi + (\dot{r}/h)\sin\phi, \tag{6.82a}$$
$$B = [(1/r) - (\mu/h^2)]\sin\phi - (\dot{r}/h)\cos\phi. \tag{6.82b}$$

Furthermore, we need to have the trajectory pass through the target, that is, $r = r_t$ when $\phi = 0$. Hence (6.79) becomes

$$1/r_t = (\mu/h^2) + A. \tag{6.83}$$

Substituting (6.82a) into (6.83) results in

$$1/r_t = (\mu/h^2) + [(1/r) - (\mu/h^2)]\cos\phi + (\dot{r}/h)\sin\phi. \tag{6.84}$$

From (6.84) we will now develop an expression for the velocity required at any point (r, ϕ) to have the missile impact at the target in the free-fall. In order to do this, we note from Figure 6.11 that

$$U_H = V_R\sin\gamma,$$
$$U_V = V_R\cos\gamma,$$

where V_R is the required velocity and γ is the flight path (or pitch) angle from the local vertical. Since the angular momentum h is constant, the product of r and U_H at any point must equal h, because the horizontal component of velocity is the only one that contributes to the angular momentum. Furthermore, it must equal negative h, since positive h tends to open up the range angle, whereas we want to close the range angle. The vertical component is simply the radial velocity dr/dt. Thus,

$$rU_H = -h, \quad \text{implying} \quad h = -rV_R\sin\gamma; \tag{6.85a}$$
$$U_V = \frac{dr}{dt}, \quad \text{implying} \quad \left(\frac{dr}{dt}\right) = V_R\cos\gamma. \tag{6.85b}$$

Substituting (6.85) into (6.84), we obtain

$$1/r_t = [\mu(1-\cos\phi)/r^2V_R^2\sin^2\gamma] + (\cos\phi/r) - (V_R\cos\gamma/rV_R\sin\gamma)\sin\phi. \tag{6.86}$$

Multiplying (6.86) through by $r^2 sin^2\gamma$ and rearranging, we have

$$\mu(1-\cos\phi)/V_R^2 = r^2\sin^2\gamma[(1/r_t) - (\cos\phi/r) + (\cos\gamma\sin\phi/r\sin\gamma)], \tag{6.87a}$$

or

$$V_R^2 = \mu(1-\cos\phi)/\{(r^2/r_t)\sin^2\gamma - r\sin^2\gamma\cos\phi + r\sin\gamma\cos\gamma\sin\phi\}. \tag{6.87b}$$

After some algebra, (6.87b) can be written in the final form [3], [9], [16]

$$V_R^2=(2\mu/r)\{(1-\cos\phi)/[(r/r_t)-\cos\phi-(r/r_t)\cos 2\gamma+\cos(2\gamma-\phi)]). \quad (6.88)$$

This is the expression for the velocity required for impacting a point or a target in *inertial space* as a function of r, ϕ, and γ. In terms of (6.10), we can substitute r with r_i. Thus,

$$V_R^2 = (2\mu/r_i)\{(1-\cos\phi)/[(r_i/r_t)-\cos\phi-(r_i/r_t)\cos 2\gamma + \cos(2\gamma-\phi)]\}. \quad (6.89a)$$

$$V_R^2 = \left(\frac{2\mu}{r_i}\right)\left[\frac{(1-\cos\phi)}{\left(\frac{r_i}{r_t}\right)(1-\cos 2\gamma)-\cos\phi+\cos(2\gamma-\phi)}\right]. \quad (6.89b)$$

In realistic cases, however, $\mathbf{V}_R$ must be obtained for oblate spheroids. Another method of solving for the spherical Earth correlated velocity follows directly from the *vis viva* integral, (6.58) [3], [5], [9]:

$$V^2=\mu[(2/r)-(1/a)]. \quad (6.59)$$

If we set $r=r_i$ and substitute (6.77) into (6.59), we obtain again (6.89b). Thus,

$$V_R^2=(2\mu/r_i)\{(1-\cos\phi)/[(r_i/r_t)(1-\cos 2\gamma)-\cos\phi+\cos(2\gamma-\phi)]\}.$$

The spherical *hit equation* can also be written in the form

$$r/r_t=[(1-\cos\phi)/(rV_R^2/\mu)](1+\cot^2\gamma)+\cos\phi-\cot\gamma\sin\phi.$$

We note here that $\mathbf{V}_R$ has either two or three components, depending on the number of guidance constraints to be satisfied. The implicit dependence on choosing a time of flight in order to obtain the one-parameter family of V_R and γ may be avoided if it is more desirable to obtain a flight path angle such that one obtains a given range for a minimum burnout velocity. The flight path angle that satisfies this condition is the optimum burnout angle γ^*, obtained by differentiating (6.89) with respect to γ and equating the resulting expression to zero. Performing this, one obtains the optimum burnout angle in the form

$$\gamma^*=\frac{1}{2}\tan^{-1}[\sin\phi/(\cos\phi-(r_i/r_t))]. \quad (6.90)$$

Equation (6.90) gives the well-known *minimum energy* trajectory. Therefore, once the target is chosen and the vehicle's position is determined, the required spherical Earth velocity may be computed and processed to provide input information for the autopilot. Finally, we need to compute the spherical-Earth time of flight. The time of flight for a ballistic trajectory, besides determining V_R and γ uniquely, serves certain tactical purposes for an *ICBM* mission. It specifies the location of the target at the time of arrival when inertial coordinates are used, thus taking into account the effect of the Earth's rotation (see Section 6.4.3.1).

The time of flight to reach the target can be derived in a similar manner as was done in the derivation of Lambert's theorem, in Section 6.3. If we assume that E_v is the eccentric anomaly of the vehicle, and E_t the eccentric anomaly of the target, then

$$E_v = \cos^{-1}[(1/e)(1-(r_i/a))], \tag{6.91a}$$
$$E_t = \cos^{-1}[(1/e)(1-(r_t/a))], \tag{6.91b}$$

where

$$e = \{[(r_i V_R \cos\gamma)^2/\mu a] + (1-(r_i/a)^2)\}^{1/2}.$$

Substituting these equations into (6.50), we have

$$t_{ff} = (\sqrt{a^3/\mu})[(E_t - E_v) - e(\sin E_t - \sin E_v)]. \tag{6.92}$$

Therefore, (6.92) permits us to compute the time of free-flight for a ballistic trajectory as a function of the range-constrained burnout variables. Note that in (6.92) we mean the time of flight to impact the target. It should be further noted that (6.91a) and (6.91b) are valid for the boost phase (i.e., below apogee), since $\cos^{-1}$ is positive in the range from 0 to π (i.e., in the first and second quadrants). In order to circumvent this singularity, use of

$$2\pi - E_v = \cos^{-1}(\ldots),$$
$$2\pi - E_t = \cos^{-1}(\ldots),$$

should be made. A closed-form solution for the time of free-flight is necessary for three important reasons:

(1) To specify the target position vector in inertial space at the time of arrival.
(2) To uniquely specify the flight path angle and correlated velocity.
(3) To fulfill particular mission requirements.

The guidance laws for free-fall phases discussed previously are based on unperturbed Keplerian motion. The assumptions implicit in Kepler's Laws are (a) an inverse-square force field, (b) no attraction from bodies other than the central mass, and (c) no other forces acting on the body in motion. In real life, of course, there are many other forces that must be considered if accuracy is needed. The more important ones from the standpoint of near-Earth operations are:

(1) Asphericity (or oblateness) of the Earth.
(2) Atmospheric drag.
(3) Attraction of Sun and Moon.

The oblateness effects will be discussed next, while the effect of atmospheric drag will be deferred and/or briefly discussed in Section 6.4.2.1. Below an altitude of ten Earth radii, the effects of the Sun, Moon, and other celestial bodies are small compared to the effect of the Earth's oblateness and can be neglected. Specifically, the effect of the Sun's and Moon's gravitational fields on a typical ballistic missile flight is to perturb the trajectory by less than 10 ft in each case; therefore, these effects will be neglected.

6.4.2.1 Oblateness Effects The spherical Earth *hit equation* and other relations developed thus far must be modified to account for the oblateness effects of the Earth. Specifically, the powered and free flight trajectory of a ballistic missile will undergo perturbations due to local gravitational field anomalies. The Earth's gravitational field is known to depart from a true central force field, since the Earth is nonspherical in shape and inhomogeneous in its mass distribution. These perturbations are most important in the effects they have on the portion of the missile trajectory that is closest to the Earth. The effects of atmospheric drag and those due to gravitational anomalies both diminish at increasing altitudes above the Earth. Consequently, because of the Earth's flattening at the poles and bulging at the equator, there is a latitude variation of mass distribution. By assuming the Earth an oblate spheroid with the axis of symmetry the polar axis, a latitude-dependent potential in terms of spherical harmonics and certain constants may be determined from satellite and geophysical measurements. Therefore, the Earth's oblateness can be expressed in terms of a latitude-dependent potential function $V(r, \sigma)$ as follows [11]:

$$V(r,\sigma) = -(GMm/r)\{(R/r) + J(R^3/r^3)(1-\cos\sigma) + \left(\frac{8}{35}\right) D(R^5/r^5)[\left(\frac{1}{8}\right)(35\cos^4\sigma - 30\cos^2\sigma + 3)] + \cdots\}, \quad (6.93a)$$

where

G = universal gravitational constant,
M = mass of the central body,
m = mass of the orbiting body,
r = orbital radius (or distance to the vehicle from the center of the Earth,
R = radius of the Earth,
σ = colatitude of the vehicle,
J = dimensionless constant $\approx 1.637 \times 10^{-3}$,
D = dimensionless constant $\approx 1.07 \times 10^{-5}$.

Thus, this equation represents the Earth's actual gravity potential function at a distance r from the geocenter. The errors incurred in flying a vehicle over the oblate Earth requires the need for a more complete analysis to account for the oblateness-induced effects. However, here we will not pursue further the oblateness effects of the Earth. Suffice it to say that the equations of motion, that is, (6.9), must be modified to account for oblateness effects. A complete analysis of these effects must begin by considering the first-order effects of the oblate gravitational field given above. Since the D term in the potential equation is approximately of order J^2, the truncated potential can be written as

$$V(r,\sigma) = -(GMm/r)\{(R/r) + J(R^3/r^3)[(1/3) - \cos^2\sigma]\}. \quad (6.93b)$$

The perturbation expansion, in the small coupling constant J, is most efficiently performed about the nominal trajectory plane. This is an adequate procedure when

one is interested only in the cumulative perturbation for a time less than the period of the free-flight ellipse. The computation is most conveniently performed by separating the effects of downrange and crossrange components. Finally, we note that the force of gravitational attraction and hence the acceleration due to gravity may be derived from the potential

$$\mathbf{g} = (1/m)[-\text{grad}\, V(r,\sigma)] = -(GM/r^2)\left\{1 + J(R^2/r^2)\left[\left(\frac{1}{3}\right) - \cos^2\sigma\right]\right\}.$$

Consequently, in order to get a feel for the consequences of neglecting the oblateness (or nonspherical) terms, a simple example is in order. For ballistic missile altitudes, the nonspherical acceleration terms shown will have magnitudes that are always less than, say, C_1, as follows:

$$C_1 \leq \frac{4}{3}(JR^2/r^2)g = 0.068\ \text{ft/sec}^2.$$

Thus, it is noted that the effect of gravity moments can be neglected only under special flight conditions, or where extreme precision is not required. For more information on oblateness effects, the reader is referred to Wheelon [16]. We will now propose a gravitation model suitable for real-time position and velocity indication in a missile-borne computer.

Gravitation Models for Missile Navigation There are several deterministic (as opposed to statistical) gravitation models from which to choose for real-time navigation in a missile computer. Among these deterministic models are [11] (a) zonal (or spherical) harmonics, (b) ellipsoidal harmonics, (c) tesseral harmonics, (d) point mass, (e) Chebychev polynomial, and (f) finite-element. Here we will choose the zonal harmonics model. Specifically, we will make use of only the second zonal harmonic (J) and the fourth zonal harmonic (D) terms of the gravitational field, in which the international ellipsoid (1924) is treated as an equipotential surface for the gravitational field. Although gravitation generated by the other models mentioned above might have a significant effect relative to mission accuracy requirements, it is believed that these effects are best computed in the ground-based fire control computer, and then compensated by presets in the missile computer. It would also be desirable to determine whether the J and D terms could be likewise compensated. If so, the missile gravitation model reduces to the inverse square law, in which case it may be in the range amenable to solution on an airborne computer. A further benefit from the inverse square model is that it is not tied to the Earth's polar axis. Gravitation can then be computed in accelerometer coordinates, thus eliminating an otherwise necessary coordinate conversion. This gravitation model computes and integrates gravitation explicitly in the computation cycle. For computation cycles up to $\frac{1}{2}$ second, the integration error is smaller than 4×10^{-3} ft/sec (through boost). Integration is performed directly on the gravitation vector in order to dimensionally match the output of the integrating accelerometers. The total inertial velocity change over the computation cycle is then the sum of the integrated gravitation and the accelerometer outputs.

Definitions: Position and velocity are expressed in an Earth-centered coordinate system, the third coordinate of which coincides with the Earth's polar axis:

a = equatorial radius of the Earth,
ψ = the latitude of the missile,
g = intermediate variable,
$\mathbf{g}$ = gravitation vector at the cycle midpoint,
μ = Earth's mass multiplied by the universal gravitation constant,
$R = |\mathbf{R}|$,
$\mathbf{R}_j^H$ = approximate midpoint position for this cycle,
$\mathbf{R}_{j-1}$ = position at the end of the preceding cycle,
$\mathbf{V}_{j-1}$ = velocity at the end of the preceding cycle,
$\Delta\mathbf{V}_g$ = estimated time integral of gravitation across the computation cycle,
J = coefficient of the second zonal harmonic in the expansion of the gravitational field,
D = coefficient of the fourth zonal harmonic in the expansion of the gravitational field,
Δt = computation cycle time.

Equations:

$$\mathbf{R}_j^H = \mathbf{R}_{j-1} + (\Delta t/2)\mathbf{V}_{j-1}, \tag{1}$$

$$(R^2) = (\mathbf{R}_j^H \cdot \mathbf{R}_j^H), \tag{2}$$

$$(1/R)_j = (1/R)_{j-1}[1.5 - 0.5(R^2)(1/R)_{j-1}^2], \tag{3}$$

$$(a^2/R^2) = [(a)(1/R)_j]^2, \tag{4}$$

$$(\sin^2\psi) = [(R_{3j}^H)(1/R)_j]^2, \tag{5}$$

$$\begin{aligned} g = {} & \mu\,(1/R_j^3)[1 + J(a^2/R^2)\{1 - 5(\sin^2\psi)\} \\ & + 3D(a^2/R^2)^2\{(1/7) - (\sin^2\psi)\}\{2 - 3(\sin^2\psi)\}], \end{aligned} \tag{6}$$

$$g_1 = -R_1^H g, \tag{7}$$

$$g_2 = -R_2^H g, \tag{8}$$

$$g_3 = -R_3^H (g + 2\mu(1/R)^3)(a^2/R^2)[J + 2D(a^2/R^2)((3/7) - \sin^2\psi)], \tag{9}$$

$$\Delta\mathbf{V}_{gj} = \Delta t\,\mathbf{g} \tag{10}$$

(see also the example in Section 6.8; in that example, $J_2 = J$ and $J_4 = D$).

Integration Errors: For a given missile path during the computation cycle, gravitation may be expressed as a function of time only. Now, expanding $\boldsymbol{g}$ about the cycle midpoint time gives

$$\mathbf{g}(t) = \mathbf{g}_H + \frac{d\mathbf{g}_H(t - t_H)}{dt} + (1/2)\left(\frac{d^2\mathbf{g}(t - t_H)}{dt^2}\right) + \ldots.$$

Integrating $\mathbf{g}(t)$ between $(t_H - (\Delta t/2))$ and $(t_H + (\Delta t/2))$ gives

$$\Delta \mathbf{V}_g = \int_0^t \mathbf{g}(t)dt = \Delta t \mathbf{g}_H + (\Delta t^3/24)) \left(\frac{d^2\mathbf{g}(t_H)}{dt^2} \right) + \text{higher (even) derivatives.}$$

Since the equations use $\Delta \mathbf{V}_g \cong \Delta t \mathbf{g}_H$, the error (for the jth computation cycle) is

$$\varepsilon(\Delta \mathbf{V}_g)_j \cong (\Delta t^3/24)) \left(\frac{d^2\mathbf{g}(t_H)}{dt^2} \right)_j .$$

If these errors are summed to time T, the total velocity error is

$$\begin{aligned} \varepsilon \Delta \mathbf{V}_g &= \sum \varepsilon(\Delta \mathbf{V}_g)_j \cong \sum (\Delta t^3/24) \left(\frac{d^2\mathbf{g}(t_H)}{dt^2} \right)_j \\ &= (\Delta t^2/24) \sum \left(\frac{d^2\mathbf{g}(t_H)}{dt^2} \right)_j \Delta t \cong (\Delta t^2/24) \int_0^t \left(\frac{d^2\mathbf{g}(t_H)}{dt^2} \right)_j dt \\ &= (\Delta t^2/24) \left[\left(\frac{d\mathbf{g}(T)}{dt} \right) - \left(\frac{d\mathbf{g}(0)}{dt} \right) \right] \cong (\Delta t^2/24) \left(\frac{d\mathbf{g}(T)}{dt} \right). \end{aligned}$$

Now, since $\mathbf{g}(t)$ is close to the inverse square law, we have

$$\mathbf{g}(t) \cong -\mu \mathbf{R}/R^3.$$

Then its derivative is about

$$\frac{d\mathbf{g}(t)}{dt} \cong -\mu[R\mathbf{V} - 3\left(\frac{dr}{dt} \right) \mathbf{R}]/R^4,$$

from which it is easily shown that $|d\mathbf{g}(t)/dt| \leq 2\mu V/R^3$. Therefore, the velocity error at T is bounded by

$$|\varepsilon \mathbf{V}_g| \leq \mu(\Delta t^2/12)(V/R^3).$$

This error is usually largest near boost cut-off. Substituting typical values $V = 2 \times 10^4$ ft/sec, $R = 2.2 \times 10^7$ ft, $\mu = 1.4 \times 10^{16}/\text{sec}^2$, we have

$$|\varepsilon \mathbf{V}_g| \cong (3 \times 10^{-3} \Delta t^2)\text{ft/sec},$$

where Δt is expressed in seconds. The other integration error source is in the midpoint position estimate $\mathbf{R}_j^H$. Since this is obtained by an extrapolation through the velocity at the end of the preceding cycle, it is in error by the amount of the missing acceleration term:

$$\varepsilon(\mathbf{R}_j^H) \cong \frac{1}{2} \mathbf{A}_H (\Delta t/2)^2 = \mathbf{A}_{j-1}(\Delta t^2/8).$$

Approximating $\mathbf{g}$ by the inverse square law, the gravitation gradient between adjacent points is approximately

$$\Delta \mathbf{g} \cong -(\mu/R^3)[\Delta \mathbf{R} - 3\mathbf{R}(\Delta R/R)],$$

and its magnitude is bounded by

$$|\Delta \mathbf{g}| \leq 2\mu \Delta R/R^3 \cong 2\mu(A\Delta t^2/8)/R^3.$$

The velocity error in the jth cycle is therefore

$$(|\varepsilon \mathbf{V}_g|)_j = |\Delta g|_j \Delta t \leq \mu A_j \Delta t^3/4R_j^3.$$

Summing the velocity error up to time T gives

$$\varepsilon \mathbf{V} = \sum \varepsilon \mathbf{V}_j \leq \sum \mu A_j \Delta t^3/4R_j^3 < (\mu \Delta t^2/4R_{\min}^3) \sum A_j \Delta t$$
$$\cong (\mu \Delta t^2/4R_{\min}^3) \int_0^t A_j dt = (\mu \Delta t^2/4R_{\min}^3)(\Delta V)_{total},$$

where $R_{\min}$ is the smallest R (at the Earth's surface), and ΔV is the total velocity change over the time period. This function is maximum at cut-off, and with a typical value of $\Delta V = 2 \times 10^4$ ft/sec, it becomes

$$\varepsilon \mathbf{V} < 1.2 \times 10^{-2} \Delta t^2 \text{ft/sec}.$$

If these velocity errors were in effect during a 2,000-second flight, the position error would be on the order of

$$\Delta R \approx (2000)(1.5 \times 10^{-2} \Delta t^2) = 30 \Delta t^2 \text{ft}.$$

6.4.2.2 Minimum Energy Trajectories For any range that the free-flight trajectory must traverse, there is always a cut-off condition that will allow the trajectory to traverse this range with the least amount of energy imparted on the missile. The condition of minimum energy may be conceived as the condition of maximum range for a given cut-off velocity. There are many useful interrelations among the eccentricity, cut-off velocity, initial flight-path angle, and geocentric range angle for the minimum energy case. Before we proceed with the derivation of the minimum energy equations, we will develop the symmetric free-flight trajectory of a ballistic missile. The discussion here, to some extent, complements the work thus far. At this point, let us define what we mean by a symmetric trajectory. A symmetric trajectory is one in which the cut-off point and the target are the same distance from the center of the Earth. This oversimplified case is included in order that the basic properties of ballistic trajectories may be understood before we proceed to the more complicated general case.

Specifically, the symmetric free-flight trajectory of a ballistic missile will be derived on the assumption that the Earth is a perfect nonrotating sphere. Furthermore, it is presumed that the powered flight is terminated on a reference sphere of radius r_o, measured from the center of the Earth. In general, the target will not be located on the reference sphere just defined. It will, however, be located at a distance from the center of the Earth that differs only slightly from that of the cut-off point. In the simplified theory that follows, it will be assumed that both the cut-off point and the target lie on the reference sphere.

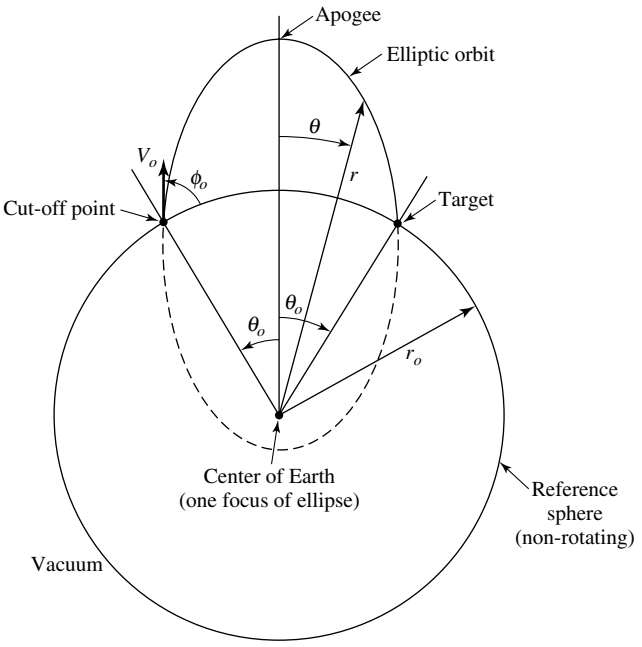

Fig. 6.12. Definition of terms used for symmetric trajectory analysis.

Figure 6.12 presents the basic geometry of the problem. In the presence of the radial gravitational field, it will be shown that the trajectory of a missile has the general form of a conic in which one focus coincides with the center of the radial field. In the case of interest, the conic can be shown to be an ellipse, which will be symmetric about the apogee (i.e., the point on the trajectory at maximum distance from the center of the Earth) when the initial and terminal points lie on the same reference sphere.

Consider now the general problem of a body moving in the presence of a gravitational field. If no forces are applied to the body, then the sum of the potential and kinetic energies must remain fixed. In the case of a ballistic missile, the sum of the potential and kinetic energies of the missile immediately after thrust cut-off must remain the same for all subsequent time during which no forces are exerted on the missile. This implies that the motion takes place in a vacuum, so that no aerodynamic forces exist. This is practically true for motion above a reference sphere that is at least 100,000 ft above sea level. That is, the greatest (or, as discussed earlier, the *sensible* part of the atmosphere is at an altitude of about 100,000 ft (see also Section 6.7)).

Using the notation of Figure 6.12, the potential energy can be expressed as

$$\text{potential energy per unit mass} = \mu[(1/r_o) - (1/r)], \tag{6.94}$$

where $\mu = GM_e$. The potential energy is defined herein to be zero on the reference sphere, so that the potential energy becomes a maximum at an infinite distance from the center of the reference sphere. The kinetic energy is given by the expression

$$\text{kinetic energy per unit mass} = \frac{1}{2}\left[\dot{r}^2 + r^2\left(\frac{d\theta}{dt}\right)^2\right]. \tag{6.95a}$$

Consequently, the total energy per unit mass above the reference sphere is

$$\text{total energy per unit mass} = \mu[(1/r_o) - (1/r)] + \frac{1}{2}\left[\dot{r}^2 + r^2\left(\frac{d\theta}{dt}\right)^2\right]. \tag{6.95b}$$

It should be pointed out here that this equation is frequently called the Lagrangian. The Lagrangian is written as

$$L = (m/2)\left[\dot{r}^2 + r^2\left(\frac{d\theta}{dt}\right)^2\right] + (GMm/r),$$

where $GM = 1.4077 \times 10^{16}$ ft^3/sec^2.

However, the total energy must equal the energy of the missile immediately after cut-off. Thus,

$$\text{energy per unit mass immediately after cut-off} = \tfrac{1}{2}V_o^2, \tag{6.95c}$$

where V_o is the cut-off velocity. (Note that V_o is the same as the required velocity discussed in Section 6.4.2.) The potential energy is defined to be zero on the reference sphere. Hence, by the law of conservation of energy,

$$\mu[(1/r_o) - (1/r)] + \frac{1}{2}\left[\dot{r}^2 + r^2\left(\frac{d\theta}{dt}\right)^2\right] = \frac{1}{2}V_o^2. \tag{6.95d}$$

For motion in a central force field, angular momentum must be conserved (Kepler's second law), since all the force is directed toward the center. As a result, the angular momentum at any time above the reference sphere must equal the angular momentum (6.25) immediately after cut-off:

$$h = r^2\left(\frac{d\theta}{dt}\right) = r_o V_o \cos\phi_o. \tag{6.96}$$

Equations (6.95d) and (6.96) represent the conservation of energy and angular momentum, respectively. If time is eliminated from (6.95d) and (6.96), and the subsequent expression is solved for $(dr/d\theta)^2$, the following expression results:

$$(dr/d\theta)^2 = (r^4/r_o^2 V_o^2 \cos^2\phi_o)\{V_o^2 - 2\mu[(1/r_o) - (1/r)]\} - (h^2/r^2). \tag{6.97}$$

An explicit expression for the trajectory will result from integrating (6.97), the result of which may be written as follows:

$$d\theta = \frac{-d\left(\frac{r_o V_o \cos\phi_o}{r}\right)}{\sqrt{V_o^2 - 2\mu\left(\frac{1}{r_o} - \frac{1}{r}\right) - \frac{r_o^2 V_o^2 \cos^2\phi_o}{r^2}}}. \tag{6.98}$$

Now let

$$x = r_o V_o \cos\phi_o / r. \tag{6.99a}$$

Then

$$\begin{aligned} 2\mu/r &= [(r_o V_o \cos\phi_o)/r][2\mu/(r_o V_o \cos\phi_o)] \\ &= [2\mu/r_o V_o \cos\phi_o]\, x. \end{aligned} \tag{6.99b}$$

Now let

$$a = -1, \quad b = 2\mu/r_o V_o \cos\phi_o, \quad c = V_o^2 - (2\mu/r_o). \tag{6.99c}$$

Then (6.98) may be written in the form

$$d\theta = -[dx/(ax^2 + bx + c)^{1/2}]. \tag{6.100}$$

From integral tables [8] we have

$$\theta = -(1/\sqrt{-a}) \sin^{-1}\{(-2ax - b)/\sqrt{b^2 - 4ac}\} + \kappa, \tag{6.101}$$

where κ is the constant of integration. Substituting the values for a, b, c, and x from (6.99a) and (6.99c), we obtain r in the form

$$\begin{aligned} r = {} & [r_o^2 V_o^2 \cos^2\phi_o/\mu]/\{1 - [(r_o V_o \cos_o)/\mu][V_o^2 - (2\mu/r_o) \\ & + (\mu^2/(r_o^2 V_o^2 \cos^2\phi_o)]^{1/2} \cos\theta\}. \end{aligned} \tag{6.102}$$

Equation (6.102), like (6.2) and (6.21), is the equation of a conic in polar coordinates (r, θ), whose eccentricity is

$$e = [(r_o V_o \cos_o)/\mu]\{V_o^2 - (2\mu/r_o) + (\mu^2/(r_o^2 V_o^2 \cos^2\phi_o)\}^{1/2}. \tag{6.103a}$$

Then

$$r = [r_o^2 V_o^2 \cos^2\phi_o/\mu]/(1 - e\cos\theta). \tag{6.103b}$$

As before, the value of the eccentricity determines which type of conic the trajectory is. That is,

$$\begin{aligned} 0 < e < 1, &\quad \text{ellipse,} \\ e = 1, &\quad \text{parabola,} \\ e > 1, &\quad \text{hyperbola.} \end{aligned}$$

If the conic is an ellipse, the trajectory either returns to the Earth or moves as a satellite about the Earth.

Let us now return to (6.103b). Here we note that when $r = r_o$ and $\theta = \theta_o$, the following expression results:

$$r_o = [r_o^2 V_o^2 \cos^2\phi_o/\mu]/(1 - e\cos\theta_o). \tag{6.103c}$$

This expression may be rearranged to yield

$$\theta_o = \cos^{-1}\{(\mu - r_o V_o^2 \cos^2\phi_o)/\{r_o V_o \cos\phi_o[V_o^2 - (2\mu/r_o) + (\mu^2/(r_o^2 V_o^2 \cos^2\phi_o))]^{1/2}\}, \tag{6.104a}$$

$$\theta_o = \sin^{-1}\{V_o \sin\phi_o/[V_o^2 - (2\mu/r_o) + (\mu^2/(r_o^2 V_o^2 \cos^2\phi_o))]^{1/2}\}, \tag{6.104b}$$

$$\theta_o = \tan^{-1}\{r_o V_o^2 \cos\phi_o \sin\phi_o/(\mu - r_o V_o^2 \cos^2\phi_o)\}. \tag{6.104c}$$

Equations (6.104) present the symmetric trajectory relationships, which are valid in a vacuum above a spherical nonrotating Earth.

We can summarize the discussion of this subsection by noting that the basic equations of motion of a ballistic missile moving in a vacuum in the immediate neighborhood of the Earth may be derived from the conservation of energy and momentum. The resulting trajectory is shown to be a conic (6.103b), with one focus at the center of the Earth. The eccentricity of the conic determines its type. If the initial velocity is sufficiently large, the conic becomes a hyperbola, and the missile will escape the Earth's gravitational field entirely. Based on the foregoing discussion, we will now develop the equation for achieving a minimum-energy trajectory.

If a ballistic missile is required to traverse a given range, the question may naturally arise as to what minimum cut-off velocity is necessary. Or conversely, given a particular cut-off velocity magnitude, in which direction should the velocity vector point in order to achieve a maximum range? There is a particular class of trajectories that possess this minimum-energy or maximum-range property. It is well known that for very short (artillery) ranges, maximum-range is achieved when the velocity vector is elevated 45° above the horizontal, in the absence of air resistance. It will be shown that this maximum-range, initial-velocity elevation angle linearly decreases from 45° to zero as the range increases from zero to halfway around the Earth. The conditions for minimum energy may be derived from (6.103a) and (6.103c). From (6.103a), we have

$$\cos^2\phi_o = \{(1 - e^2)/[2(r_o V_o^2/\mu) - (r_o^2 V_o^4/\mu^2)], \tag{6.105a}$$

but from (6.103c),

$$\cos^2\phi_o = (\mu/r_o V_o^2)(1 - e\cos\theta_o) = (1 - e^2)/[2(r_o V_o^2/\mu) - (r_o^2 V_o^4/\mu^2)], \tag{6.105b}$$

or

$$V_o^2 = (2\mu/r_o) - \{[(1 - e^2)/(1 - e\cos\theta_o)](\mu/r_o)\}. \tag{6.106}$$

For a given range, the minimum energy condition may be expressed as

$$dV_o^2/de = 0. \tag{6.107}$$

Consequently,

$$(1 - e\cos\theta_o)2e - (1 - e^2)\cos\theta_o = 0,$$

or

$$e^2 - (2/\cos\theta_o)e + 1 = 0,$$

whence

$$e = (1 \pm \sin\theta_o)/\cos\theta_o.$$

If V_o^2 is to be a minimum, the minus sign must be used. This may be shown by requiring that the second derivative of V_o^2 with respect to e be positive at this value of e. As a result,

$$e_{ME} = (1 - \sin\theta_o)/\cos\theta_o. \tag{6.108}$$

The cut-off velocity may now be expressed as a function of range and reference sphere radius for the minimum-energy trajectory. An expression for V_o may be obtained by substituting (6.108) into (6.106):

$$V_{oME}^2 = (2\mu/r_o)[\sin\theta_o/(1 + \sin\theta_o)]. \tag{6.109}$$

Note that $V_{oME} = V_c^*$ when $\theta_o = 90°$. Hence, the minimum-energy trajectory degenerates to the circular satellite radius r_o for a range that is halfway around the Earth. The initial flight path angle ϕ_{oME} may be found from (6.103c) and (6.108). Thus

$$\cos^2\phi_{oME} = (\mu/r_o V_{oME}^2)\sin\theta_o \tag{6.110a}$$

$$= \sin\theta_o/2[1 - ((1 - \sin\theta_o)/\cos^2\theta_o)] \tag{6.110b}$$

$$= (1 + \sin\theta_o)/2. \tag{6.110c}$$

Consequently,

$$[1 + \sin((\pi/2) - 2\phi_{oME})]/2 = (1 + \sin\theta_o)/2.$$

Thus

$$\theta_o = (\pi/2) - 2\phi_{oME}. \tag{6.111}$$

A further quantity of interest is the maximum altitude above the reference sphere (apogee condition). This can be found from (6.103b) by setting $\theta = 0$. Thus,

$$r_{\max ME} - r_o = r_o[(\sin\theta_o/(1 - e_{ME})) - 1]. \tag{6.112a}$$

If (6.108) is applied to the above, then the maximum altitude may be expressed as

$$r_{\max ME} - r_o = r_o\{[(1 - \sin\theta_o)\sin(\theta_o/2)]/[\cos(\theta_o/2) - \sin(\theta_o/2)]\}. \tag{6.112b}$$

---

* V_c is the circular velocity and is given by $V_c = \sqrt{\mu/r}$.

There are a number of other relationships among the trajectory parameters for the minimum-energy case. They may be found from (6.103c) and (6.108). The more important relationships are summarized below:

$$\tan\phi_{oME} = e_{ME}, \tag{6.113a}$$

$$\sin\phi_{oME} = e_{ME}\Big/\sqrt{1+e_{ME}^2}, \tag{6.113b}$$

$$\cos\phi_{oME} = 1\Big/\sqrt{1+e_{ME}^2}, \tag{6.113c}$$

$$\tan\theta_o = (1-e_{ME}^2)/2e_{ME}, \tag{6.113d}$$

$$\sin\theta_o = (1-e_{ME}^2)/(1+e_{ME}^2), \tag{6.113e}$$

$$\cos\theta_o = 2e_{ME}/(1+e_{ME}^2). \tag{6.113f}$$

The general equation for the minimum-energy trajectory can be shown to be

$$r = (r_o \sin\theta_o)/(1 - e_{ME}\cos\theta_o). \tag{6.114}$$

Equation (6.114) is the polar expression for an ellipse of eccentricity e_{ME} and semi-latus rectum $r_o \sin\theta_o$. An examination of Figure 6.12 will indicate that for a minimum-energy ellipse, one focus must lie in the mid-position of the chord intersecting the target and cut-off point for a symmetric trajectory, since the other focus coincides with the center of the Earth. It can also be shown that the energy ratio (ER) is given by

$$(ER)_{ME} = (r_o V_{oME}^2)/\mu = 1 - \tan\phi_{oME}^2. \tag{6.115a}$$

The energy ratio appears explicitly in all symmetric trajectory equations. Furthermore, it can be shown to be twice the ratio of kinetic energy to gravitational potential. That is,

$$\begin{aligned} 2 \times [\text{kinetic energy/gravitational potential}] &= [(V_o^2)/(\mu/r_o)] \\ &= (r_o V_o^2/\mu) = ER. \end{aligned} \tag{6.115b}$$

The initial flight path angle ϕ_{oME}, cut-off velocity V_{oME}, and maximum altitude for minimum energy trajectories are plotted in Figure 6.13 as a function of geocentric semirange, θ_o.

The discussion of Sections 6.4.2 and 6.4.2.1 will now be summarized by means of an example. In this example, it will be assumed that the total time of flight is fixed. In essence, as will be defined in Section 6.5.5, the development in this example constitutes a missile-explicit guidance technique.

Example. Consider the missile/target relationship illustrated in the following diagram. More specifically, this figure shows vector positions of the target and the ballistic missile at any time t. A spherical Earth gravitational model will be assumed. If the target is fixed to the Earth's surface, then

$$\mathbf{r}_t(t) = \mathbf{r}_t(t_o) + \int_{t_0}^{t_1} \dot{\mathbf{r}}_t dt, \tag{1}$$

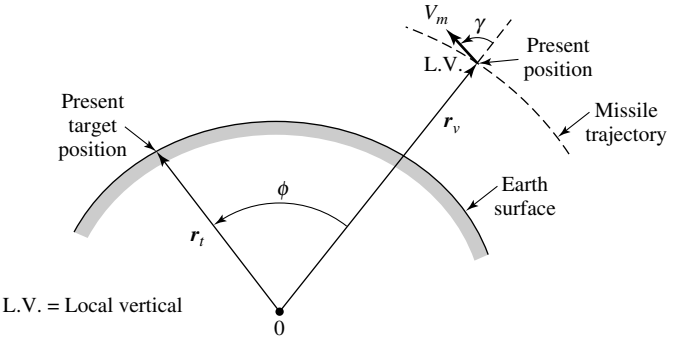

Missile and target vectors.

where

$$\frac{d\mathbf{r}_t}{dt} = \boldsymbol{\Omega}_e \times \mathbf{r}_t(t) \tag{2}$$

(here, t_o is any arbitrary time, and $\boldsymbol{\Omega}_e$ is the Earth's angular rate vector). If the vehicle is in unpowered flight, the only significant forces acting upon it will be gravitational

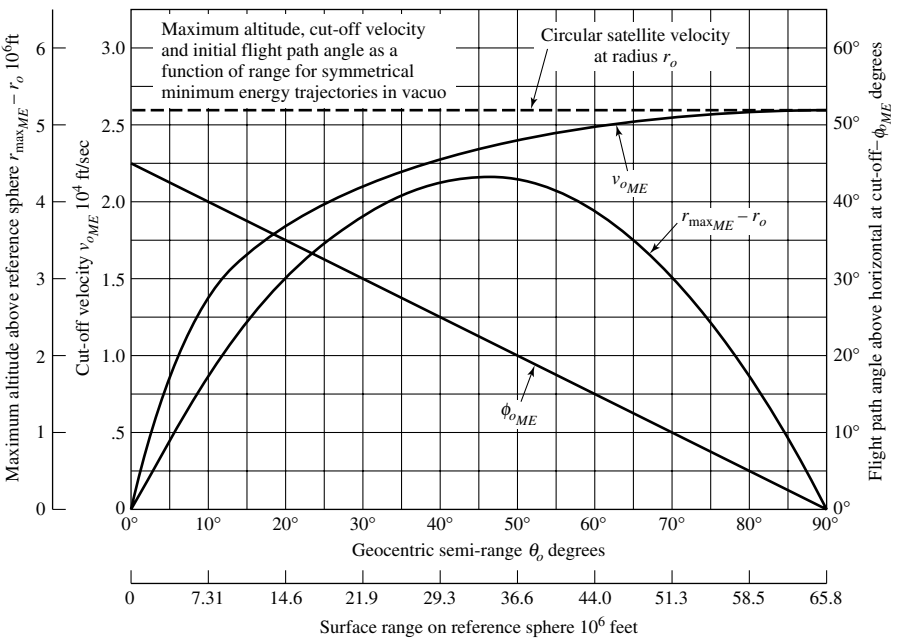

Fig. 6.13. Maximum altitude, cut-off velocity, and initial flight path angle as a function of range for symmetric minimum-energy trajectories in vacuum (Reference sphere radius $= r_o =$ 21.1×10^6 ft).

and aerodynamic forces. These forces per unit mass will be denoted by the symbol **f**. The acceleration on the vehicle is thus

$$\mathbf{a}_v = \mathbf{f}. \tag{3}$$

Equation (3) may be integrated to give the vehicle velocity as

$$\mathbf{V}_v(t) = \mathbf{V}_v(t_o) + \int_{t_0}^{t} \mathbf{f}\, dt, \tag{4}$$

where $\mathbf{V}_v(\mathrm{t}_o)$ is the vehicle velocity vector at time t_o. Integrating (4) gives the vehicle position as

$$\begin{aligned} \mathbf{r}_v(t) &= \mathbf{r}_v(t_o) + \int_{t_0}^{t} \mathbf{V}_v(t)dt \\ &= \mathbf{r}_v(t_o) + \int_{t_0}^{t} \mathbf{V}_v(t_o)dt + \int_{t_0}^{t}\int_{t_0}^{t} \mathbf{f}\, dt\, dt \\ &= \mathbf{r}_v(t_o) + \mathbf{V}_v(t_o)(t - t_o) + \int_{t_0}^{t}\int_{t_0}^{t} \mathbf{f}\, dt\, dt \end{aligned} \tag{5}$$

where $\mathbf{r}_v(\mathrm{t}_o)$ is the vehicle position at time t_o. Now, in order for the vehicle to impact the target at some time t_I, it is necessary that

$$\mathbf{r}_t(t_i) = \mathbf{r}_v(t_i). \tag{6}$$

Substituting (1) and (5) into (6) yields

$$\mathbf{r}_t(t_o) + \int_{t_0}^{t} \left(\frac{d\mathbf{r}_t}{dt}\right) dt = \mathbf{r}_v(t_o) + \mathbf{V}_v(t_o)(t - t_o) + \int_{t_0}^{t}\int_{t_0}^{t} \mathbf{f}\, dt\, dt. \tag{7}$$

Equation (7) is the generalized form of the *hit equation* discussed earlier. If we let time (t_o) be the thrust cut-off time for the ballistic missile under consideration, we see that (7) can be satisfied if we control both vehicle position and velocity.

Long-range ballistic missiles, however, use exclusively forms of velocity control. Two primary reasons are (1) the complexity of the guidance if both position and velocity are controlled, and (2) the fact that impulsive corrections can be made to velocity, which is not true of position. Therefore, all long-range ballistic missile guidance systems effect guidance by determining and obtaining the correct $\mathbf{V}_v(t_o)$ in (7) for the position $\mathbf{r}_v(t_o)$. The following are several of the possible "required velocity" schemes of guidance.

(1) *Required Velocity*: *Amplitude and Directional Control Scheme* From (7) we see that there are seven variables on the right-hand side of the equation. These are (a) 3 position variables, (b) 3 required velocity variables, and (c) the time of flight $(t_{ff} = t_i - t_o)$. Since we wish to effect guidance as a function of vehicle position, it is therefore necessary to apply a constraint to (7) in order to reduce the dependent variables to three. For the scheme to be described in this section, the following constraint is used:

(a) First, the missile velocity is constrained to lie in the plane formed by the present missile position, the center of the Earth, and the target position at the time of impact. This is accomplished by using a yaw steering error signal of the form

$$\varepsilon_{yaw} = [\mathbf{r}_v(t_o) \times \mathbf{r}_t(t_i)] \cdot \mathbf{V}_m(t_o). \tag{8}$$

(b) Secondly, the required velocity to impact is constrained to lie along the missile velocity vector $\mathbf{V}_m(t_o)$. Thus, whenever the amplitudes of $\mathbf{V}_m(t_o)$ and $\mathbf{V}_v(t_o)$ are equal, the thrust will be terminated. The value obtained in using a guidance scheme of this type is that an arbitrary pitch program can be used. The scheme is, however, complicated by the fact that a variable total time of flight results, necessitating the consideration of a moving target.* The development of this guidance scheme will begin with a spherical Earth model and a nonmoving target, and then be expanded to take into account effects of target motion due to the Earth's angular rate.

(2) *Spherical Earth Case*: *Nonmoving Target* For the spherical Earth case, (4) is often written in the form

$$\mathbf{a}_v = -(\mu/\mathbf{r}_v^3)\mathbf{r}_v, \tag{9}$$

and it can be shown that the required velocity with a nonmoving target is given by the *vis viva* integral (6.59)

$$V_R^2 = \mu[(2/r_v) - (1/a)], \tag{10}$$

where a is the semimajor axis of the resulting elliptical trajectory between the missile's present position and the target's position, and is given as (see (6.77))

$$a = (r_v/2)\{1 + [r_t(1 - \cos\phi)/(r_v - r_t - r_v\cos 2\gamma + r_t\cos(2\gamma - \phi))]\}, \tag{11}$$

where $\gamma = \cos^{-1}(\mathbf{r}_v \cdot \mathbf{V}_{vm}/r_v r_t)$, the angle between the missile local vertical (L.V.) and the velocity heading

$$\phi = \cos^{-1}(\mathbf{r}_v \cdot \mathbf{r}_t/r_v r_t),$$

the angle between the missile position and target position.

Substituting (11) into (10) gives (see (6.89))

$$V_R^2 = (2\mu/r)\{(1 - \cos\phi)/((r_v/r_t)(1 - \cos 2\gamma)) - \cos\phi + \cos(2\gamma - \phi)\}. \tag{12}$$

(3) *Spherical Earth Case*: *Earth Fixed target* For an Earth fixed target, we note from (1) and (2) that the target position becomes a function of the free-flight time $t_{ff} = t - t_o$. The free-flight time, however, is a function of the required velocity, and the required velocity is in turn a function of the target position. Thus, to effect a solution, it is necessary to perform an iterative computation procedure, such as the following:

*A pitch control scheme with a fixed total time of flight eliminates the need to consider a moving target.

(a) Estimate future position of the target.
(b) Compute the required velocity from (12).
(c) Compute the time of free flight.
(d) Compute the new target position from the time of free flight.
(e) The procedure is repeated until it converges.

The time of free flight $t_{ff} = t - t_o$ can be shown to be (see (6.92))

$$t_{ff} = (\sqrt{a^3/\mu})[(E_t - E_v) - e(\sin E_t - E_v)], \tag{13}$$

where

$$\begin{aligned} E_t &= \text{eccentric anomaly of the target position,} \\ E_v &= \text{eccentric anomaly of the missile position,} \\ e &= \text{trajectory eccentricity.} \end{aligned}$$

An examination of the equations presented in this section shows that we are forcing a solution to the problem of impacting the target for a given flight path angle γ. Thus, for a given vehicle position and flight path angle γ, there is a unique solution to the problem. If the flight path angle were to have a different value, the time of flight to impact the target would be different, and the required azimuth heading would be different, by the control (8).

(4) *Required Velocity*: *Fixed Time-of-Flight Schemes* A sufficient constraint in (7) to reduce the dependent variables to (3) and therefore to effect a unique solution is to constrain the total time of flight of the missile from launch to impact. For this scheme, the target becomes an inertially fixed target, the position of which is given as

$$\mathbf{r}_t = \mathbf{r}_t(t_L) + \int_{t_L}^{T} \left(\frac{d\mathbf{r}_t}{dt} \right) dt \tag{14}$$

where

$$\begin{aligned} t_L &= \text{launch time,} \\ T &= \text{constrained time of missile arrival at the target,} \\ \frac{d\mathbf{r}_t}{dt} &= \text{velocity of the target given by (2).} \end{aligned}$$

As before, the discussion of this guidance scheme will begin with a spherical Earth gravitational model.

(4.1) *Velocity Required*: *Spherical Earth Case* For the spherical Earth case, the required velocity can be formulated in many different ways. The following represents three possibilities.

(4.1.1) *Formulation* (I)

$$
\begin{aligned}
V_R &= \text{required missile velocity},\\
V_r &= \text{radial component of velocity} = dr_v/dt,\\
V_\theta &= \text{tangential component of velocity}
\end{aligned}
$$

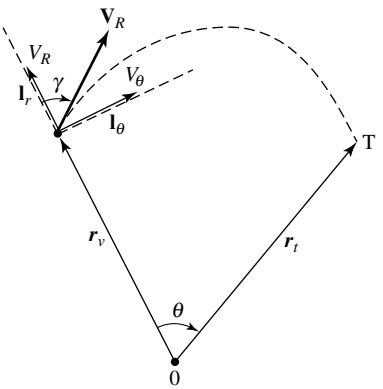

Required velocity geometry.

From the above figure, we obtain

$$\mathbf{V}_R = V_r \mathbf{1}_r + V_\theta \mathbf{1}_\theta,$$

and the unit vectors $\mathbf{1}_r$, $\mathbf{1}_\theta$, and $\mathbf{1}_n$ are the radial, tangential, and normal unit vectors, respectively, and are given by the expressions

$$
\begin{aligned}
\mathbf{1}_r &= \mathbf{r}_v/|\mathbf{r}_v| = (X/r_v)\mathbf{1}_x + (Y/r_v)\mathbf{1}_y + (Z/r_v)\mathbf{1}_z,\\
\mathbf{1}_\theta &= \mathbf{1}_n \times \mathbf{1}_r,\\
\mathbf{1}_n &= (\mathbf{r}_v \times \mathbf{r}_t)/|\mathbf{r}_v \times \mathbf{r}_t|.
\end{aligned}
$$

Therefore,

$$\mathbf{V}_R = V_r \mathbf{1}_r + V_\theta \mathbf{1}_\theta = V_r(\mathbf{r}_v/r_v) + \{[V_\theta(\mathbf{r}_v \times \mathbf{r}_t) \times \mathbf{r}_v]/[|\mathbf{r}_v| \cdot |\mathbf{r}_v \times \mathbf{r}_t|]\}, \tag{15}$$

where

$$V_R^2 = 2\mu\left[(1/r_v) - \left(\frac{1}{2a}\right)\right] - V_\theta^2, \tag{16}$$

$$V_\theta^2 = h^2/r_v^2 = (\mu a/r_v^2)(1 - e^2). \tag{17}$$

The quantity $(1 - e^2)$ is given as

$$1 - e^2 = [4(s - r_v)(s - r_t)/c^2]\sin^2((\alpha - \beta)/2) \tag{18}$$

if

$$t_{ff} > \left(\sqrt{a^3/\mu}\right)[\pi - (\beta - \sin\beta)],$$
$$\alpha = \pi,$$
$$a = s/2,$$

or

$$1 - e^2 = [4(s - r_v)(s - r_t)/c^2]\sin^2((\alpha + \beta)/2) \tag{19}$$

if

$$t_{ff} < \left(\sqrt{a^3/\mu}\right)[\pi - (\beta - \sin\beta)],$$
$$\alpha = \pi,$$
$$a = s/2,$$

and

$$s = \frac{1}{2}(r_v + r_t + c), \tag{20}$$

$$c = |\mathbf{r}_t - \mathbf{r}_v|, \tag{21}$$

$$\sin(\alpha/2) = \sqrt{s/2a} = ((r_v + r_t + c)/4a)^{1/2}, \quad \alpha \leq \pi, \tag{22}$$

$$\sin(\beta/2) = \sqrt{(s - c)/2a} = ((r_v + r_t - c)/4a)^{1/2}, \quad \beta \leq \alpha \leq \pi. \tag{23}$$

The semimajor axis a is determined by the constraint of a required time-of-flight $(T - t_o)$ and is determined by the methods that will be presented in Section (5).

(4.1.2) *Formulation* (*II*) The required velocity can also be expressed as follows:

$$\mathbf{V}_R = (\sqrt{\mu/2})\{([A(c - r_v) - B(c + r_v)]/cr_v)\cdot\mathbf{r}_v + [(A + B)/c]\mathbf{r}_t\}, \tag{24}$$

where

$$A = \begin{cases} \{(1/(s - c)) - (1/2a)\}^{1/2} & \text{if} \quad \cos\theta = \mathbf{r}_v\cdot\mathbf{r}_t/\mathbf{r}_v\mathbf{r}_t < 180°, \\ -\{(1/(s - c)) - (1/2a)\}^{1/2} & \text{if} \quad \cos\theta > 180°, \end{cases} \tag{25}$$

and

$$B = \begin{cases} -\{(1/s) - (1/2a)\}^{1/2} & \text{if} \quad t_{ff} > t_{ff(m)}, \\ \{(1/s) - (1/2a)\}^{1/2} & \text{if} \quad t_{ff} < t_{ff(m)}, \end{cases} \tag{26}$$

where $t_{ff(m)}$ is the time of flight for the minimum-energy trajectory, and is given by the right side of the inequality presented with (18). That is, for the special case of minimum-energy trajectory, $\alpha = \pi$ and (18) and (19) are identical. Again, the semimajor axis a will be determined by the constraint on a required time of flight $(T - t_o)$ as determined by the methods that will be presented in Section (5).

(4.1.3) *Formulation (III)* Here we will take the required velocity to be

$$\mathbf{V}_R = \frac{\sqrt{\mu}}{r_v r_t \sin\theta}\{\mathbf{r}_t - [1-(r_t/p)(1-\cos\theta)]\mathbf{r}_v\}, \tag{27}$$

where

$$r_v r_t \sin\theta = |\mathbf{r}_v \times \mathbf{r}_t|. \tag{28}$$

The semilatus rectum p will be determined by the constraint on a required time-of-flight $(T - t_o)$ as determined by the methods presented in Section 5.

(5) *Solution for Trajectory Parameter*: *Spherical Earth Case* We see from the previous section that the required velocity is expressible in terms of the geometry defined by $\mathbf{r}_v$ and $\mathbf{r}_t$ and in terms of one or more trajectory parameters, as yet undetermined. These parameters are uniquely determined for a spherical Earth model by the requirement of a fixed total time of flight, such that the time of flight remaining, $t_{ff} = T - t_o$, is determined.

Now it is possible to write an equation for the time of flight t_{ff} explicitly in terms of the geometry defined by $\mathbf{r}_v$ and $\mathbf{r}_t$ and in terms of one or more of the trajectory parameters. It is not, however, possible to obtain one of the trajectories as an explicit function of t_{ff}, and the geometry defined by $\mathbf{r}_v$ and $\mathbf{r}_t$, due to the transcendental nature of the explicit function for t_{ff}. Thus, although the solution is unique, it is necessary to perform a numerical iteration to determine the trajectory parameters. Once the parameters are determined, the required velocity can be computed by the methods presented in the previous section. In this section, three possible iteration methods will be outlined. The following sections will consider some of the more detailed aspects of the iteration processes.

(5.1) *Iteration on the Semimajor Axis* (a) The time of flight can be given by the equations

$$t_{ff} = \begin{cases} (\sqrt{a^3/\mu})[2\pi - (\alpha - \sin\alpha) - (\beta - \sin\beta)] & \text{if} \quad t_{ff} > t_{ff(m)}, \qquad (29) \\ (\sqrt{a^3/\mu})[(\alpha - \sin\alpha) - (\beta - \sin\beta)], & \text{if} \quad t_{ff} \le t_{ff(m)}, \qquad (30) \end{cases}$$

where $t_{ff(m)}$, the required time for the minimum energy trajectory, is given by

$$t_{ff(m)} = \left(\sqrt{a^3/\mu}\right)[\pi - (\beta - \sin\beta)], \tag{31}$$

where

$$\alpha = \pi,$$
$$a = s/2,$$

and s, α, and β in these equations are determined as functions of the parameter a and the geometry by (20), (22), and (23), respectively. The iteration procedure may then be outlined as follows

(1) A value of a is chosen and t_{ff} computed by (29) or (30).
(2) The difference between the required time of flight $t_{ff} = T - t_o$ and that computed in (1) is used to compute a corrected value of a.

(3) Step (1) is repeated using this new value of a.
(4) This procedure is repeated until a sufficiently small difference between the required time of flight and that computed is obtained.

The value of a obtained may then be used to compute the required velocity by the equations described in Sections (4.1.1) and (4.1.2). For the method described in Section (4.1.3) it will be necessary to first compute the parameter p, which is given as (see (6.30))

$$p = a(1 - e^2), \tag{32}$$

where $(1 - e^2)$ may be computed from (18) or (19).

At this point it should be noted that the iteration process on the semimajor axis a will have a serious convergence problem as a approaches the value of a corresponding to a minimum energy trajectory. Specifically, the derivative of t_{ff} with respect to a goes to infinity for a corresponding to the minimum energy trajectory. This difficulty may be overcome by defining an auxiliary variable for which the derivative does not possess this discontinuity. Such a procedure will be described in the next section.

(5.2) *Iteration on the Auxiliary Parameter* λ The equation for the time of flight can be written in the form

$$t_{ff} = (1/\sqrt{\mu})[s/(1 - \cos\lambda)]^{3/2}\{\lambda - \sin\lambda - (\beta - \sin\beta)\}, \tag{33}$$
$$0 \le \beta \le \pi \le \lambda \le 2\pi$$
$$0 \le \beta \le \lambda,$$
$$0 \le \beta \le \pi,$$

where

$$\lambda = r_i V_R^2/\mu \quad (6.70),$$
$$\beta = \cos^{-1}\{(1/s)[c + (s - c)\cos\lambda]\}, \quad s \ne c.$$

Here, s and c are again determined from (20) and (21), respectively. The semimajor axis a is computed from the equation

$$a = s/(1 - \cos\lambda). \tag{34}$$

The iteration process for the solution will be the same as that described in Section (5.1), except that the iterations will be with respect to λ. When λ is finally determined, the semimajor axis a is computed from (34). The velocity required may then be computed by the equations described in Section (4.1). For he required velocity formulation in Section (4.1.3) (18), (19), and (32) will be needed to compute the trajectory parameter p.

(5.3) *Iteration on the Trajectory Parameter p* The time of flight can be given by the equation

$$t_{ff} = \left(\sqrt{a^3/\mu}\right)[-E_v + e\sin E_v + (E_t - e\sin E_t)] \tag{35}$$

where

$$a = p/(1-e^2), \tag{36}$$

$$e = [(|\mathbf{r}_v \times \mathbf{r}_t|)^2(r_v - p)^2 + \{(r_t - p)^2 r_v^2 - (r_v - p)\mathbf{r}_v \cdot \mathbf{r}_t\}^2]^{1/2}/r_v|\mathbf{r}_v \times \mathbf{r}_t|, \tag{37}$$

$$\sin E_v = [(r_t - p)r_v^2 - (r_v - p)\mathbf{r}_v \cdot \mathbf{r}_t]/[(ea\sqrt{1-e^2})(|\mathbf{r}_v \times \mathbf{r}_t|], \tag{38}$$

$$\sin E_t = [(r_t - p)\mathbf{r}_v \cdot \mathbf{r}_t - (r_v - p)r_t^2]/[(ea\sqrt{1-e^2})(|\mathbf{r}_v \times \mathbf{r}_t|)], \tag{39}$$

$$E_v = \begin{cases} \sin^{-1}\{\sin E_v\} & \text{if } \cos E_v \geq 0, \\ \pi - \sin^{-1}\{\sin E_v\} & \text{if } \cos E_v < 0, \end{cases} \tag{40}$$

$$E_t = \begin{cases} \sin^{-1}\{\sin E_t\} & \text{if } \cos E_t \geq 0, \\ \pi - \sin^{-1}\{\sin E_t\} & \text{if } \cos E_t < 0, \end{cases} \tag{41}$$

where

$$\cos E_v = -[e - ((r_v - p)/e)], \tag{42}$$

$$\cos E_t = -[e - ((r_t - p)/e)]. \tag{43}$$

The iteration process for the solution will be the same as that described in Section (5.1), except that the iterations will be with respect to p. When p is finally determined, the velocity required may be computed from the equations described in Section (4.1).

6.4.3 Ballistic Error Coefficients

An important aspect of ballistic missile guidance is the determination of the error coefficients at the burnout or thrust termination. The propagation of burnout errors is a very important aspect of ballistic missile design. Burnout errors that are critical in the design are the velocity (V), flight path angle (γ), and burnout altitude (h). These variables control the missile's flight in achieving the burnout condition. The burnout errors δV, $\delta\gamma$, δh, etc.,* are commonly described in terms of *error coefficients*. Furthermore, the propagation of burnout errors into impact errors as the vehicle

*The symbol δ will be used throughout this work to denote a small variation of the quantity it prefixes.

travels over the perturbed free-flight trajectory is significant in two areas: It permits one (1) to evaluate the effects of measurement and control errors of the guidance system, and (2) to determine the types of trajectories that would be less sensitive to burnout errors than others. Therefore, in this section we will derive closed-form mathematical expressions that can be used to calculate the changes in the position and velocity vectors from their nominal values at any given time along a free-fall trajectory that arise from perturbations in the nominal position and velocity vectors at the initial (or thrust termination) time. The assumptions upon which this development rests are summarized as follows:

1. The free-fall trajectory takes place in a simple inverse-square central gravitational field.
2. The only force acting is that of gravity; that is, the trajectory occurs in a vacuum where no aerodynamic forces are present.
3. The time of flight is constant.

Specifically, we will develop in this section the in-plane and out-of-plane error coefficients. However, before we proceed with the above development of the error coefficients, we will briefly discuss the *cross-range* and *down-range* errors. To begin with, note that variations in position, velocity, and launch direction of the missile at thrust cut-off will produce errors at the target (or impact point). These errors are of two types: (1) errors in the intended plane, which cause either a long or short hit, and (2) out-of-plane errors, which cause the missile to hit to the right or left of the target. Commonly, the errors in the intended plane are designated as *down-range* errors, and the out-of-plane errors are designated as *cross-range* errors.

Cross-Range Errors: Assume that the thrust cut-off point is displaced by an amount $\delta\chi$ perpendicular to the intended (or nominal) plane of the trajectory. From Figure 6.14, we can determine by spherical trigonometry the cross-range error δC at the impact point or target as follows [2]:

$$\cos\delta C = \sin^2\psi + \cos^2\psi\cos\delta\chi, \tag{6.116a}$$

where ψ is the free-flight range angle. For small angles (i.e., $\delta\chi$ and δC),

$$\delta C \approx \delta\chi\cos\psi. \tag{6.116b}$$

From Figure 6.14 one can see that the cross-range error is zero when the free-flight range approaches 90°.

The propagation of navigation errors (e.g., initial alignment, initial position, and initial velocity) has a considerable effect on cross-range and down-range errors. These effects are illustrated in Figure 6.15.

Figure 6.16 illustrates the effect of initial velocity error on the cross-range and down-range errors, while Figure 6.17 illustrates the effects of position errors.

In Figure 6.17 we note that because the North Pole is not, in general, normal to the launch position, longitude must be propagated in two ways. During free-fall, the sensitivity matrices are analytic functions of the cut-off and impact conditions. Thus,

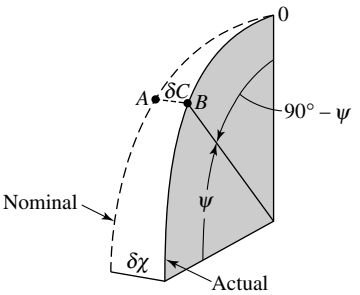

Fig. 6.14. Lateral displacement of burnout point.

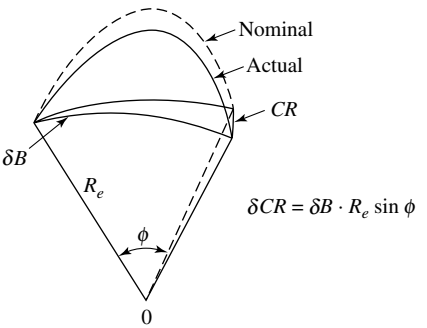

(a) Initial alignment

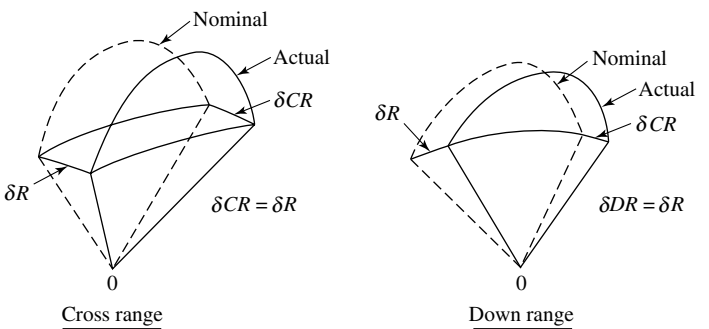

(b) Initial position

Fig. 6.15. Effect of initial alignment and position on cross-range and down-range errors.

the down-range and cross-range errors, in terms of the sensitivity matrices, are as follows:

$$\delta DR = (\partial DR/\partial \mathbf{V})\,\delta \mathbf{V} + (\partial DR/\partial \mathbf{R})\,\delta \mathbf{R}, \tag{6.117a}$$

$$\delta CR = (\partial CR/\partial \mathbf{V})\,\delta \mathbf{V} + (\partial CR/\partial \mathbf{R})\,\delta \mathbf{R}. \tag{6.117b}$$

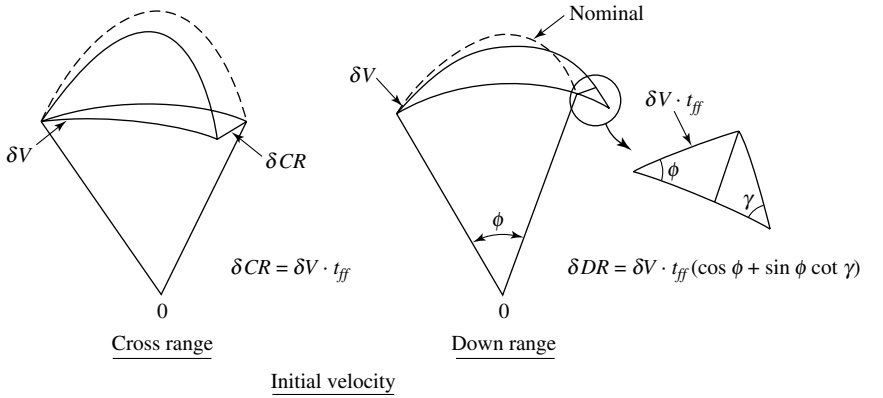

Fig. 6.16. Effect of initial velocity error on cross-range and down-range errors.

In the next two subsections we will treat the in-plane and out-of-plane error coefficients in more detail.

It should be emphasized that there are other methods for determining the ballistic error coefficients; the method presented here is only to stimulate an interest for further study.

6.4.3.1 In-Plane Error Coefficients

In the guidance problem of ballistic missiles, it is important to know how, for example, the range and velocity are dependent upon the other variables affecting the problem. The purpose of this section is to derive the partial derivatives of range and velocity with respect to the other variables. The total set of error coefficients consists of two independent subsets: (1) the coefficients that generate position and velocity changes in the plane of the free-fall trajectory, and (2) those that generate changes normal to the plane of the free-fall trajectory. The derivation of the in-plane coefficients involves time explicitly. The normal-to-plane coefficients, on the other hand, are derived solely on the basis of trajectory geometry and do not involve time explicitly. The coordinate system and geometry upon which the in-plane coefficients are based are shown in Figure 6.18.

We will formulate the problem in polar coordinates, using a rotating radial–transverse coordinate system with unit vectors $\hat{\mathbf{r}}$ and $\hat{\boldsymbol{\theta}}$. In this coordinate system, the position and velocity vectors are given by

$$\mathbf{r} = r\hat{\mathbf{r}} \tag{6.118}$$

and

$$\mathbf{V} = \frac{d\mathbf{r}}{dt} = \left(\frac{dr}{dt}\right)\hat{\mathbf{r}} + r\left(\frac{d\theta}{dt}\right)\hat{\boldsymbol{\theta}} = V_r\hat{\mathbf{r}} + V_\theta\hat{\boldsymbol{\theta}}, \tag{6.119}$$

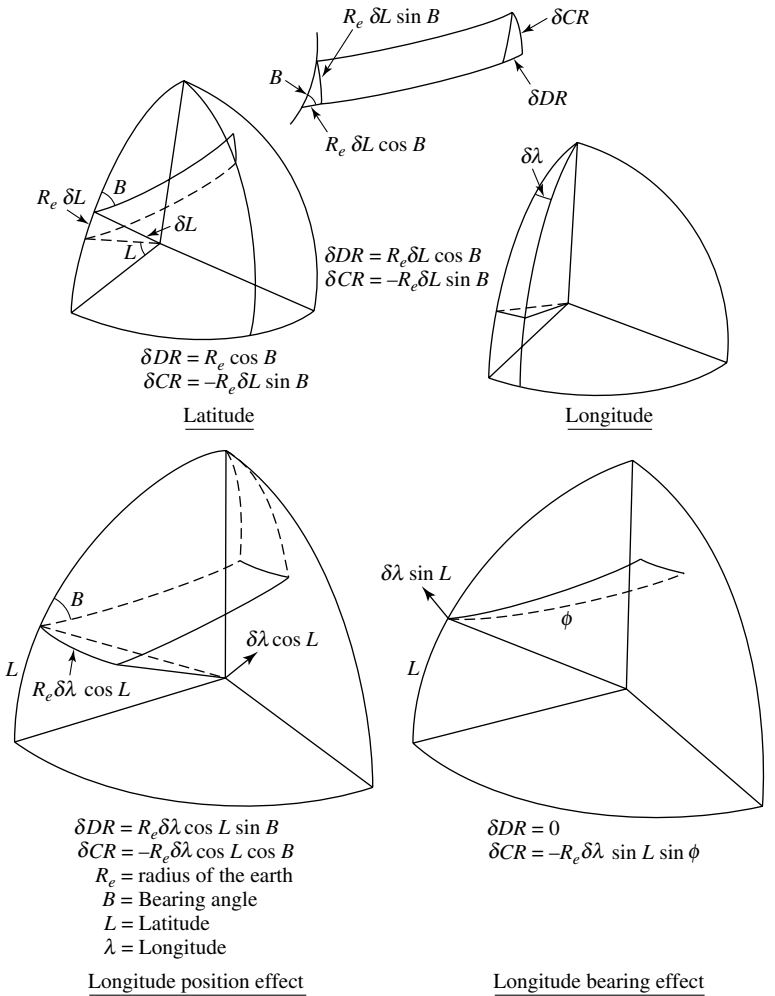

Fig. 6.17. Relation of latitude and longitude to position errors.

where

$$V_r \cong \frac{dr}{dt}, \tag{6.120a}$$

and

$$V_\theta \cong r\left(\frac{d\theta}{dt}\right). \tag{6.120b}$$

Again, referring to Figure 6.18, the four initial conditions at burnout that determine the subsequent free-fall trajectory are V, γ, h, and θ_o. Perturbations in any one of these burnout variables cause position and velocity changes at the endpoint of the

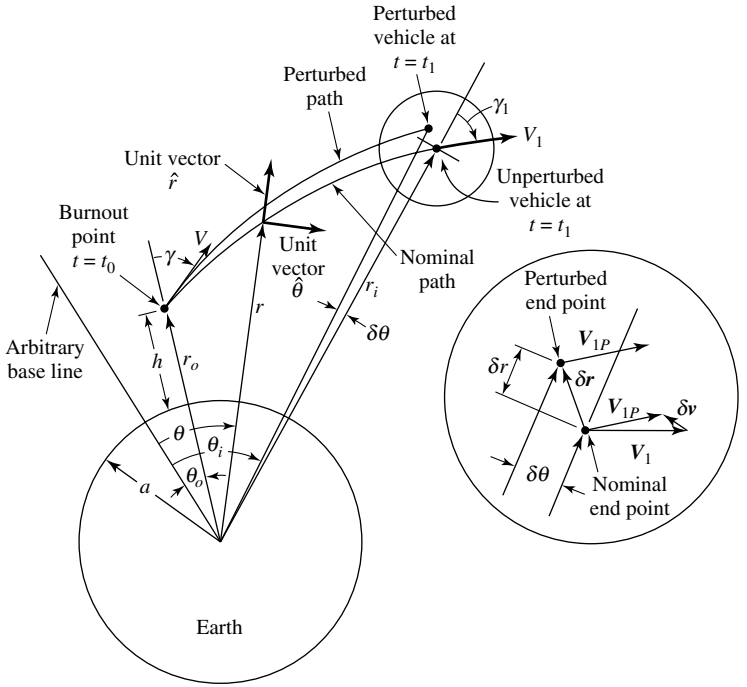

Fig. 6.18. In-plane geometry.

trajectory. (Note that here we will drop the subscript(s) from the required velocity vector $\mathbf{V}$ in order not to confuse it with the components of V_r and V_θ.)

6.4.3.1.1. Velocity Errors The velocity errors are first derived by differentiating (119) with respect to any of the four burnout variables, which we will symbolize by the letter b.

$$\begin{aligned}\partial\mathbf{V}/\partial b &= (\partial/\partial b)(\dot{r}\hat{\mathbf{r}}) + (\partial/\partial b)(r\dot{\theta}\hat{\boldsymbol{\theta}}) \\ &= (\partial\dot{r}/\partial b)\hat{\mathbf{r}} + \dot{r}(\partial\hat{\mathbf{r}}/\partial b) + (\partial/\partial b)(r\dot{\theta})\hat{\boldsymbol{\theta}} + r\dot{\theta}(\partial\hat{\boldsymbol{\theta}}/\partial b). \qquad (6.121)\end{aligned}$$

Since $\hat{\boldsymbol{\theta}}$ and $\hat{\mathbf{r}}$ are functions of θ only, then

$$\partial\hat{\mathbf{r}}/\partial b = (\partial\hat{\mathbf{r}}/\partial\theta)(\partial\theta/\partial b) \quad \text{and} \quad (\partial\hat{\boldsymbol{\theta}}/\partial b) = (\partial\hat{\boldsymbol{\theta}}/\partial\theta)(\partial\theta/\partial b). \qquad (6.122a)$$

Now, using

$$\partial\hat{\mathbf{r}}/\partial\theta = d\hat{\mathbf{r}}/d\theta \quad \text{and} \quad d\hat{\mathbf{r}}/d\theta = \hat{\boldsymbol{\theta}}, \qquad (6.122b)$$

(6.122a) becomes

$$\partial\hat{\mathbf{r}}/\partial b = (\partial\hat{\boldsymbol{\theta}}/\partial b)\hat{\boldsymbol{\theta}}. \qquad (6.122c)$$

Similarly,

$$\partial\hat{\boldsymbol{\theta}}/\partial b = (d\hat{\boldsymbol{\theta}}/d\theta)(\partial\theta/\partial b) \quad \text{and} \quad d\hat{\boldsymbol{\theta}}/d\theta = -\hat{\mathbf{r}},$$

so that

$$\partial\hat{\boldsymbol{\theta}}/\partial b = (-\partial\theta/\partial b)\hat{\mathbf{r}}. \tag{6.123}$$

Substituting (6.122c) and (6.123) into (6.121), we obtain

$$\begin{aligned}\partial\mathbf{V}/\partial b &= (\partial\dot{\mathbf{r}}/\partial b)\hat{\mathbf{r}} + \dot{\mathbf{r}}(\partial\theta/\partial b)\hat{\boldsymbol{\theta}} + \hat{\boldsymbol{\theta}}(\partial/\partial b)(r\dot{\theta}) + (r\dot{\theta})(-\partial\theta/\partial b)\hat{\mathbf{r}} \\ &= [(\partial\dot{r}/\partial b) - (r\dot{\theta})(\partial\theta/\partial b)]\hat{\mathbf{r}} + [(\partial/\partial b)(r\dot{\theta}) + \dot{r}(\partial\theta/\partial b)]\hat{\boldsymbol{\theta}}, \end{aligned} \tag{6.124a}$$

and using the definitions (6.120a) and (6.120b) yields

$$\partial\mathbf{V}/\partial b = [(\partial V_r/\partial b) - V_\theta(\partial\theta/\partial b)]\hat{\mathbf{r}} + [(\partial V_\theta/\partial b) + V_r(\partial\theta/\partial b)]\hat{\boldsymbol{\theta}}. \tag{6.124b}$$

This equation describes the change in the velocity vector $\mathbf{V}$ arising from perturbations in any of the four burnout variables V, γ, h, and θ_o, which, in turn, take the role of b in (6.124b). Now, letting $\mathbf{V}_P$ be the perturbed velocity vector at $t = t_1$, and $\mathbf{V}_I$ the unperturbed velocity vector, the following expression results:

$$\mathbf{V}_P = \mathbf{V}_I + \delta\mathbf{V}, \tag{6.125}$$

where

$$\delta\mathbf{V} = (\partial\mathbf{V}/\partial b)\delta b. \tag{6.126}$$

Thus, the error in velocity at the endpoint is

$$(\partial\mathbf{V}/\partial b)\delta = \mathbf{V}_P - \mathbf{V}_I. \tag{6.127}$$

From (6.124b), the radial component of $\delta\mathbf{V}$, $\delta V_{\hat{\mathbf{r}}}$ is

$$\delta V_{\hat{\mathbf{r}}} = [(\partial V_r/\partial b) - V_\theta(\partial\theta/\partial b)]\delta b. \tag{6.128a}$$

and the traverse component is

$$\delta V_{\hat{\boldsymbol{\theta}}} = [(\partial V_\theta/\partial b) + V_r(\partial\theta/\partial b)]\delta b. \tag{6.128b}$$

Equations (6.128a) and (6.128b) embody the terms that are the sought-after in-plane velocity error coefficients. Therefore, if we write

$$\delta\mathbf{V} = (\partial\mathbf{V}/\partial b)_{\hat{\mathbf{r}}}\delta b\hat{\mathbf{r}} + (\partial\mathbf{V}/\partial b)_{\hat{\boldsymbol{\theta}}}\delta b\hat{\boldsymbol{\theta}}, \tag{6.129}$$

then the in-plane radial and transverse velocity error coefficients are the bracketed terms of (6.128a) and (6.128b) and are given in the defining equations

$$(\partial\mathbf{V}/\partial b)_{\hat{\mathbf{r}}} = [(\partial V_r/\partial b) - V_\theta(\partial\theta/\partial b)] \tag{6.130a}$$

and

$$(\partial\mathbf{V}/\partial b)_{\hat{\boldsymbol{\theta}}} = [(\partial V_\theta/\partial b) + V_r(\partial\theta/\partial b)]. \tag{6.130b}$$

Since b encompasses four burnout variables (i.e., V, γ, h, and θ_o), (6.130a) will yield four radial velocity error coefficients, and (6.130b) four transverse velocity error coefficients, making a total of eight in-plane velocity error coefficients.

6.4.3.1.2 *Position Errors* The derivation of the vector error in position follows the same pattern as that used above for the velocity. The position error vector is defined by

$$\mathbf{r}_P = \mathbf{r}_1 + \delta\mathbf{r}, \tag{6.131}$$

or

$$\delta\mathbf{r} = \mathbf{r}_P - \mathbf{r}_1, \tag{6.132}$$

where

$$\delta\mathbf{r} = (\partial\mathbf{r}/\partial b)\delta b. \tag{6.133a}$$

This last equation is expressed in component form to yield

$$\delta\mathbf{r} = (\partial\mathbf{r}/\partial b)_{\hat{\mathbf{r}}}\delta b\hat{\mathbf{r}} + (\partial\mathbf{r}/\partial b)_{\hat{\boldsymbol{\theta}}}\delta b\hat{\boldsymbol{\theta}}, \tag{6.133b}$$

where $(\partial\mathbf{r}/\partial \mathrm{b})_{\hat{\mathbf{r}}}\delta \mathrm{b}$ and $(\partial\mathbf{r}/\partial \mathrm{b})_{\hat{\boldsymbol{\theta}}}\delta \mathrm{b}$ are the radial and transverse scalar components of position error, and at the same time are the coefficients of interest. The expressions for the error coefficients are obtained by differentiating (6.118), and thus

$$\partial\mathbf{r}/\partial b = (\partial r/\partial b)\hat{\mathbf{r}} + r(\partial\hat{\mathbf{r}}/\partial b), \tag{6.134a}$$

which, by use of (6.122c) becomes

$$\partial\mathbf{r}/\partial b = (\partial r/\partial b)\hat{\mathbf{r}} + (\partial\theta/\partial b)\hat{\boldsymbol{\theta}}. \tag{6.134b}$$

Now combining (6.133a) and (6.133b) yields

$$\partial\mathbf{r}/\partial b = (\partial\mathbf{r}/\partial b)_{\hat{\mathbf{r}}}\hat{\mathbf{r}} + (\partial\mathbf{r}/\partial b)_{\hat{\boldsymbol{\theta}}}\hat{\boldsymbol{\theta}}. \tag{6.134c}$$

When the components of the right-hand side of (6.134c) are equated with the corresponding components of (6.134b), the two error coefficient equations are obtained as follows:

$$(\partial\mathbf{r}/\partial b)_{\hat{\mathbf{r}}} = \partial r/\partial b \tag{6.135a}$$

and

$$(\partial\mathbf{r}/\partial b)_{\hat{\boldsymbol{\theta}}} = r(\partial\theta/\partial b). \tag{6.135b}$$

As before, b encompasses the four burnout variables V, γ, h, and θ_o, and there are four radial and four transverse, or a total of eight, in-plane position error coefficients. The four equations (6.130a), (6.130b), (6.135a), and (6.135b) form the basic equations for generating the 16 in-plane error coefficients.

6.4.3.1.3 *Error Partials* The next part of the development is concerned with the derivation of the error partials, which is the term applied to the mathematical functions

$$\partial r/\partial b,\ \partial\theta/\partial b,\ \partial V_r/\partial b, \quad \text{and } \partial V_\theta/\partial b,$$

which are needed to calculate the error coefficients

$$(\partial \mathbf{r}/\partial b)_{\hat{\mathbf{r}}}, (\partial \mathbf{r}/\partial b)_{\hat{\boldsymbol{\theta}}}, (\partial \mathbf{V}/\partial b)_{\hat{\mathbf{r}}}, (\partial \mathbf{V}/\partial b)_{\hat{\boldsymbol{\theta}}}.$$

There are two equations, the geometric trajectory equation and the time equation, which form the basis for the derivation of the error partials. These equations are derived in [16]. These equations are (see also Section 6.4.2)

$$r_o/r = [(1-\cos(\theta-\theta_o))/\lambda \sin^2\gamma] + [\{\sin(\gamma-(\theta-\theta_o))\}/\sin\gamma], \tag{6.136}$$

or

$$r = f_1(V, \gamma, h, \theta_o, \theta) = f_1(b, \theta),$$

and

$$t = \frac{r_o}{V\sin\gamma}\left\{\frac{\cot\gamma[1-\cos(\theta-\theta_o)] + (1-\lambda)\sin(\theta-\theta_o)}{(2-\lambda)\left[\frac{1-\cos(\theta-\theta_o)}{\lambda\sin^2\gamma} + \frac{\sin[\gamma-(\theta-\theta_o)]}{\sin\gamma}\right]}\right.$$

$$\left. + \frac{2\sin\gamma}{\lambda(\frac{2}{\lambda}-1)^{\frac{3}{2}}}\tan^{-1}\left[\frac{\sqrt{(\frac{2}{\lambda})-1}}{\sin\gamma\cot(\frac{\theta-\theta_o}{2})-\cos\gamma}\right]\right\} \tag{6.137}$$

or

$$t = f_2(V, \gamma, h, \theta_o, \theta) = f_2(b, \theta),$$

where

$$\lambda = r_o V^2/\mu \quad \text{and} \quad r_o = a + h,$$

as shown in Figure 6.18. Rewriting the defining equations (6.120a) and (6.120b), we have

$$V_r = \frac{dr}{dt} = \left(\frac{dr}{d\theta}\right)\left(\frac{d\theta}{dt}\right) \tag{6.138a}$$

and

$$V_\theta = r\left(\frac{d\theta}{dt}\right). \tag{6.138b}$$

In (6.138a), dr/dt can be obtained by differentiating (6.136), while holding the burnout variables constant. Similarly, $d\theta/dt$ can be obtained directly from the angular momentum conservation equation $p = r^2(d\theta/dt) = r_o V\sin\gamma$ (note that here we use p for the angular momentum instead of h as in (6.25) so that it will not be confused with altitude). Thus V_r can be formed to give

$$V_r = f_3(V, \gamma, h, \theta_o, \theta) = f_3(b, \theta). \tag{6.139a}$$

In the same way, V_θ can be formed using (6.136) and the differentiation of (6.137) to yield

$$V_\theta = f_4(V, \gamma, h, \theta_o, \theta) = f_4(b, \theta). \tag{6.139b}$$

The error partials that are sought could be obtained from a set of equations of the following form by direct differentiation, if such a set were available. Thus,

$$r = u_1(h, V, \gamma, \theta_o, t) = u_1(b, t), \tag{6.140a}$$
$$\theta = u_2(h, V, \gamma, \theta_o, t) = u_2(b, t), \tag{6.140b}$$
$$V_r = u_3(h, V, \gamma, \theta_o, t) = u_3(b, t), \tag{6.140c}$$
$$V_\theta = u_4(h, V, \gamma, \theta_o, t) = u_4(b, t). \tag{6.140d}$$

That is, expressions like the following could be obtained:

$$\left(\frac{\partial r}{\partial h}\right)\Big|_{V,\gamma,\theta_o,t} = (\partial u_1/\partial h),\ (\partial V_o/\partial \gamma)\Big|_{h,V,\theta_o,t} = \partial u_4/\partial \gamma.$$

The set of equations (6.140a)–(6.140d) is not available. Equations that are available are of the form

$$r = f_1(b, \theta), \tag{6.136}$$
$$t = f_2(b, \theta), \tag{6.137}$$
$$V_r = f_3(b, \theta) = V[-(\sin\theta'/\lambda \sin\gamma) + \cos(\gamma - \theta')] = f_3, \tag{6.139a}$$
$$V_\theta = f_4(b, \theta) = V[((1 - \cos\theta')/\lambda \sin\gamma) + \sin(\gamma - \theta')], \tag{6.139b}$$

where $\theta' = \theta - \theta_o$. We can rewrite these last four equations in the form

$$r - f_1 = 0, \quad \text{where} \quad r - f_1 = g_1(h, V, \gamma, \theta_o, \theta, r), \tag{6.140a}$$
$$t - f_2 = 0, \quad \text{where} \quad t - f_2 = g_2(h, V, \gamma, \theta_o, \theta, t), \tag{6.140b}$$
$$V_r - f_3 = 0, \quad \text{where} \quad V_r - f_3 = g_3(h, V, \gamma, \theta_o, \theta, V_r), \tag{6.140c}$$
$$V_\theta - f_4 = 0, \quad \text{where} \quad V_\theta - f_4 = g_4(h, V, \gamma, \theta_o, \theta, V_\theta). \tag{6.140d}$$

Thus, we have four sets of four equations involving, in general, nine variables of which the four dependent ones are chosen to be r, θ, V_r, and V_θ, and the independent variables h, V, γ, θ_o, and t. In effect, then, equations (6.140a) through (6.140d) can be expressed as

$$g_1(h, V, \gamma, \theta_o, t, \text{ and } r, \theta, V_r, V_\theta) = 0, \tag{6.141a}$$
$$g_2(h, V, \gamma, \theta_o, t, \text{ and } r, \theta, V_r, V_\theta) = 0, \tag{6.141b}$$
$$g_3(h, V, \gamma, \theta_o, t, \text{ and } r, \theta, V_r, V_\theta) = 0, \tag{6.141c}$$
$$g_4(h, V, \gamma, \theta_o, t, \text{ and } r, \theta, V_r, V_\theta) = 0. \tag{6.141d}$$

By following implicit differentiation of the four g_i functions, the error partials are obtained

$$\frac{\partial g_1}{\partial b}+\frac{\partial g_1}{\partial r}\frac{\partial r}{\partial b}+\frac{\partial g_1}{\partial \theta}\frac{\partial \theta}{\partial b}+\frac{\partial g_1}{\partial V_r}\frac{\partial V_r}{\partial b}+\frac{\partial g_1}{\partial V_\theta}\frac{\partial V_\theta}{\partial b}=0 \tag{6.142a}$$

$$\frac{\partial g_2}{\partial b}+\frac{\partial g_2}{\partial r}\frac{\partial r}{\partial b}+\frac{\partial g_2}{\partial \theta}\frac{\partial \theta}{\partial b}+\frac{\partial g_2}{\partial V_r}\frac{\partial V_r}{\partial b}+\frac{\partial g_2}{\partial V_\theta}\frac{\partial V_\theta}{\partial b}=0 \tag{6.142b}$$

$$\frac{\partial g_3}{\partial b}+\frac{\partial g_3}{\partial r}\frac{\partial r}{\partial b}+\cdots=0 \tag{6.142c}$$

$$\frac{\partial g_4}{\partial b}+\frac{\partial g_4}{\partial r}\frac{\partial r}{\partial b}+\cdots=0 \tag{6.142d}$$

This set of four equations contains the four unknowns

$$\partial r/\partial b,\ \partial\theta/\partial b,\ \partial V_r/\partial b,\ V_\theta/\partial b,$$

which can be solved for after one obtains the values for their coefficients,

$$(\partial g_1/\partial r,\ \partial g_1/\partial\theta,\ \partial g_1/\partial V_r,\ \partial g_1/\partial V_\theta,\ \partial g_2/\partial r,\ \text{etc.}),$$

by differentiation of the g functions. As before, V, γ, h, and θ_o are substituted in the place of b in (6.142a)–(6.142d) to produce four sets of equations, each set of which is solved for its four error partials. Finally, the following equations form the basic set from which the 16 in-plane error partials are computed:

$$\partial r/\partial b=[(\partial f_1/\partial b)(\partial f_2/\partial\theta)-(\partial f_1/\partial\theta)(\partial f_2/\partial b)]/(\partial f_2/\partial\theta), \tag{6.143a}$$

$$\partial\theta/\partial b=(\partial f_2/\partial b)/(\partial f_2/\partial\theta), \tag{6.143b}$$

$$\partial V_r/\partial b=[(\partial f_2/\partial\theta)(\partial f_3/\partial b)-(\partial f_2/\partial b)(\partial f_3/\partial\theta)]/(\partial f_2/\partial\theta), \tag{6.144a}$$

$$\partial V_\theta/\partial b=[(\partial f_2/\partial\theta)(\partial f_4/\partial b)-(\partial f_2/\partial b)(\partial f_4/\partial\theta)]/(\partial f_2/\partial\theta). \tag{6.144b}$$

We will now compute the in-plane error equations by implicitly differentiating the spherical Earth *hit equation* (6.75) with respect to the central angle ϕ and each of the burnout variables. This gives, after some trigonometric substitutions [16],

$$\begin{aligned}\delta\phi[((\sin\phi)/\lambda\sin^2\gamma))-(\cos(\gamma-\phi)/\sin\gamma)]&=(2\delta V_r/V_r)[(1-\cos\phi)/(\lambda\sin^2\gamma)]\\&+(\delta h/r_t)\{1+(r_t/r_i)[(1-\cos\phi)/(\lambda\sin^2\gamma)]\}\\&+(\delta\gamma)[2(r_t/r_i)\cot\gamma-(\sin(2\gamma-\phi)/\sin^2\gamma)].\end{aligned} \tag{6.145}$$

From Figure 6.11, the range error is given by

$$\delta R=r_t\delta\phi, \tag{6.146}$$

where R is the range, thus related to each of the burnout errors through (6.145).

The analysis of the burnout errors will be performed assuming independent variations of each, even though they are actually interdependent. That is, to study the range error due to a specific burnout error, it will be assumed that all other burnout

variables are controlled perfectly. In a similar manner, we can write the required (or correlated) velocity perturbed equation as follows:

$$\delta V_R = (\partial \mathbf{V}_R/\partial \mathbf{r}_t)\delta \mathbf{r}_t + (\partial \mathbf{V}_R/\partial t_{ff})\delta t_{ff}. \tag{6.147}$$

A variation in the burnout speed will modify the trajectory profile and impact point, since either more or less energy has been imparted to the vehicle at burnout. The error equation is obtained from (6.145) and (6.146) as [16]

$$\frac{\delta R}{\delta V_R} = \left(\frac{2r_t}{V_R}\right)\left[\frac{1-\cos\phi}{\sin\phi - \lambda \sin\gamma\cos(\gamma-\phi)}\right], \tag{6.148}$$

and using (6.76), we obtain

$$\frac{\delta R}{\delta V_R} = \left(\frac{2r_t}{V_R}\right)\left\{\frac{(1-\cos\phi)[((\frac{r_i}{r_t}) - \cos\phi)\tan\gamma + \sin\phi]}{(1-\cos\phi) + ((\frac{r_i}{r_t}) - 1)\tan\gamma\sin\phi}\right\}. \tag{6.149}$$

We may obtain a first-order approximation for (6.149) by letting

$$r_i/r_t \cong 1, \tag{6.150}$$

resulting in

$$\frac{\delta R}{\delta V_R} = \left(\frac{2r_t}{V_R}\right)[\tan\gamma(1-\cos\phi) + \sin\phi]. \tag{6.151a}$$

The range error due to an error in controlling and/or measuring the flight-path angle in the trajectory plane may be computed from (6.145) and (6.146), and after making use of (6.15), we obtain, to a first-order approximation, the equation

$$\frac{\delta R}{\delta \gamma} = 2r_t\left[1 + \frac{\sin(\phi - 2\gamma)}{\sin 2\gamma}\right]. \tag{6.151b}$$

Note that at a burnout flight-path angle of γ^* (a *minimum-energy* trajectory; for more details on minimum energy see Section 6.4.2.1), one may readily show by substituting (6.90) into (6.151b) that $\partial R/\partial\gamma = 0$. Thus, if the mission does not otherwise require, the flight-path angle should be near γ^* at burnout, so as to minimize the range error that results from $\delta\gamma$.

Next, we consider the variation of impact range with errors in burnout altitude about the nominal design point. The variation about the nominal point can also be inferred from (6.145) and (6.146) as follows:

$$\frac{\delta R}{\delta h} = \frac{1 + (\frac{r_t}{r_i})(\frac{1-\cos\phi}{\lambda\sin^2\gamma})}{\frac{\sin\phi}{\lambda\sin^2\gamma} - \frac{\cos(\gamma-\phi)}{\sin\gamma}}, \tag{6.152a}$$

and using (6.76) for λ,

$$\frac{\delta R}{\delta h} = \frac{1 + (\frac{r_t}{r_i})[(\frac{r_i}{r_t}) - \frac{\sin(\gamma-\phi)}{\sin\gamma}]}{\{(\frac{\sin\phi}{1-\cos\phi})[(\frac{r_i}{r_t}) - \frac{\sin(\gamma-\phi)}{\sin\gamma}] - \frac{\cos(\gamma-\phi)}{\sin\gamma}\}}. \tag{6.152b}$$

To first order, use (6.150) in (6.152b) to obtain the simplified expression [16]

$$\frac{\delta R}{\delta h} = 2\tan\gamma - \frac{\sin(\gamma - \phi)}{\sin\gamma}. \tag{6.152c}$$

Consequently, since the primary effect of burnout altitude errors is to change the potential energy of the trajectory, the general form of (6.152c) should be, and is, similar to that of Eq. (6.151a), which also represents an energy change of the free-flight ellipse.

6.4.3.2 Out-of-Plane Error Coefficients

The perturbations at the initial point normal to the plane of the nominal trajectory propagate at the endpoint of the trajectory into errors in position and velocity that are also normal to the plane. As in the case of the in-plane perturbations, which produced only in-plane errors, the out-of-plane perturbations produce only out-of-plane errors. Here it is important to note that there is no cross coupling between in-plane and out-of-plane perturbations to first order. The derivations of the out-of-plane coefficients are somewhat simpler than the derivations of the in-plane coefficients because the former are treated geometrically, whereas the latter become complicated due to the necessity of including the effects of time.

The justification for handling the out-of-plane errors geometrically hinges upon the fact that first-order small perturbations in travel time along the trajectory (i.e., arising from burnout perturbations) create first-order small errors in in-plane position and velocity, whereas the same type of first-order small perturbations in travel time along the trajectory create only second-order errors in the out-of-plane position and velocity. Hence, the time perturbation in the out-of-plane travel time along the trajectory creates only second-order errors in the out-of-plane position and velocity. Therefore, the time perturbation in the out-of-plane case can be neglected. There can be two perturbations at the initial point normal to the plane of the nominal trajectory. These are δn, the position perturbation, and δV_n, the velocity perturbation normal to the plane. Each of these gives rise to errors at the end time t_1 in lateral position L and lateral velocity V_L. Hence, there are four out-of-plane error coefficients, which when written in a notation consistent with the in-plane case are as follows:

$$(\partial \mathbf{L}/\partial n)_{\hat{n}},\ (\partial \mathbf{L}/\partial V_n)_{\hat{n}},\ \text{and}\ (\partial \mathbf{V}_L/\partial n)_{\hat{n}},\ (\partial \mathbf{V}_L/\partial V_n)_{\hat{n}},$$

where $\hat{n}$ is a unit vector normal in a right-hand sense to the trajectory plane.

Because of the simplifications inherent in the out-of-plane case, the notation used in the in-plane case, where a distinction must be made between error coefficients and error partials, is redundant, and the above four error coefficients are identical to their error partials. That is,

$$(\partial \mathbf{L}/\partial n)_{\hat{n}} = \partial L/\partial n, \quad (\partial \mathbf{L}/\partial V_n)_{\hat{n}} = \partial L/\partial V_n,$$

and

$$(\partial \mathbf{V}_L/\partial n)_{\hat{n}} = \partial V_L/\partial n, \quad (\partial \mathbf{V}_L/\partial V_n)_{\hat{n}} = \partial V_L/\partial V_n. \tag{6.153}$$

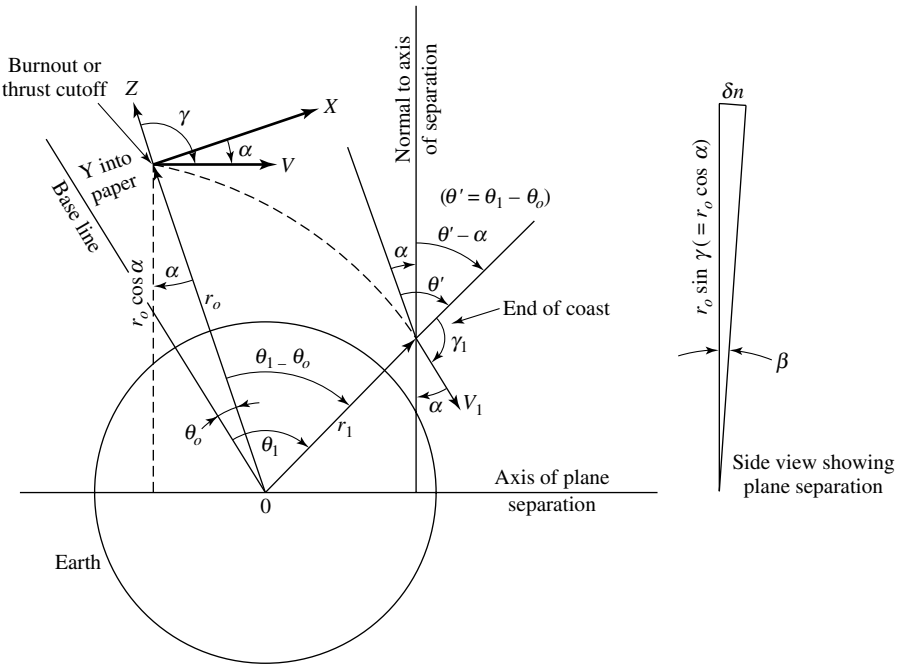

Fig. 6.19. Geometry for $(\partial V_L/\partial n)$ and $(\partial L/\partial n)$.

The equations for generating $\delta\mathbf{L}$, the lateral vector position error, and $\delta\mathbf{V}_L$, the lateral vector velocity error, are thus

$$\delta\mathbf{L} = (\partial\mathbf{L}/\partial b_n)_{\hat{n}}\delta b_n\hat{n} = (\partial L/\partial b_n)\delta b_n\hat{n} \tag{6.154}$$

and

$$\delta\mathbf{V}_L = (\partial\mathbf{V}_L/\partial b_n)_{\hat{n}}\delta b_n\hat{n} = (\partial V_L/\partial b_n)\delta b_n\hat{n}, \tag{6.155}$$

where b_n includes n and V_n the burnout variables normal to the plane of the nominal trajectory. Equation (6.153) involves two coefficients: $(\partial L/\partial n)$ and $(\partial L/\partial V_n)$. The first of these is derived with reference to Figure 6.19 (which is also used later for the derivation of ∂V_L).

The key to the geometry of a perturbation δn is the fact that the axis of separation of the two trajectory planes must be parallel to the initial velocity vector. The plane separation angle β is thus

$$\beta = \delta n/r_o\cos\alpha.$$

From Figure 6.19 it is evident that

$$\delta L = \beta r_o \sin(90^\circ + \alpha - \theta').$$

Substituting for β yields

$$\delta L = (\delta n/(r_o\cos\alpha))r_1\sin(90^\circ + \alpha - \theta'),$$

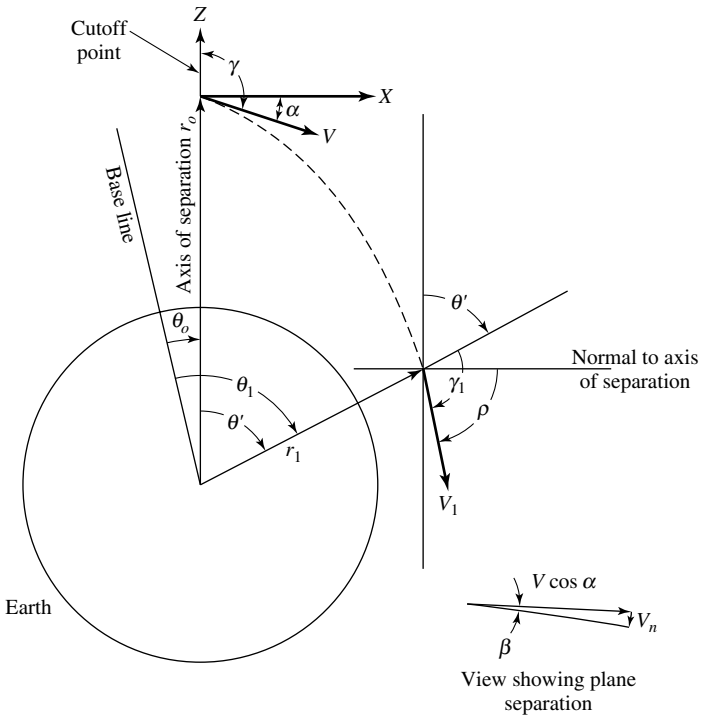

Fig. 6.20. Geometry for $(\partial L/\partial V_n)$ and $(\partial V_L/\partial V_n)$.

or

$$\partial L/\partial n = [r_1 \sin(90^\circ + \alpha - \theta')]/r_o \cos\alpha.$$

Now, using $\gamma - 90^\circ = \alpha$, the last equation becomes

$$\partial L/\partial n = r_1 \sin(\gamma - \theta')/r_o \sin\gamma,$$

or

$$\partial L/\partial n = r_1 \sin[\gamma - (\theta - \theta_o)]/r_o \sin\gamma. \tag{6.156}$$

The second partial, $\partial L/\partial V_n$, is derived with reference to Figure 6.20.

In this case, the plane separation axis is along r_o, and the angle of the plane separation β is

$$\beta = \delta V_n / V \cos\alpha = \delta V_n / V \sin\gamma.$$

The lateral error in position is (see Figure 6.20)

$$\delta L = \beta r_1 \sin\theta',$$

or

$$\delta L = (\delta V_n / V \sin\gamma) r_1 \sin\theta',$$

and

$$\partial L/\partial V_n = r_1 \sin\theta' / V \sin\gamma = r_1 \sin(\theta_1 - \theta_o)/V \sin\gamma. \tag{6.157}$$

The remaining two out-of-plane coefficients $(\partial V_L/\partial n)$ and $(\partial V_L/\partial V_n)$ are derived by means of the following requirements. First, $(\partial V_L/\partial n)$ is considered. Figure 6.19 shows the geometry involved. The out-of-plane position perturbation δn is taken along the positive y axis. Similarly, positive velocity perturbations are in the direction of the positive y axis. By displacing the cut-off position a distance δn along y from the nominal value, a new trajectory plane is formed that intersects the original plane along the line labeled "axis of separation." The small separation angle β between the two planes is given by the expression

$$\beta = \delta n/r_o \cos\alpha = \delta n/r_o \sin\gamma, \tag{6.158}$$

since $\gamma = 90^\circ + \alpha$. The error in velocity δV_L at the end of the coast, point (r_1, θ_1), is equal to

$$\delta V_L = -V_1 \times (\text{angle between } V_1 \text{ and } \Delta V_1 \text{ (i.e., } V_1\text{-perturbed)}), \tag{6.159}$$

which assumes a small angle (a valid assumption) between V_1 and ΔV_1.

Next, the angle between V_1 and ΔV_1 is $\beta \cos\rho$, where β is the plane separation angle and ρ is the angle measured from V_1 to the line normal to the axis of separation. Note that if V_1 were along the normal to the axis of separation, the angle between V_1 and ΔV_1 would simply be β. The farther that V_1 is from the normal (i.e., ρ grows toward 90°), the smaller the angle between V_1 and ΔV_1 becomes.

Now it is necessary to express ρ in terms of known angles $\rho = 90^\circ + \gamma - \gamma_1 - \theta'$. Substituting this angle in

$$\delta V_L = -V_1 \beta \cos\rho, \tag{6.160a}$$

we obtain

$$\delta V_L = -V_1(\delta n/r_o \sin\gamma)\cos[90^\circ + (\gamma - \gamma_1 - \theta')], \tag{6.160b}$$

where

$$\theta' = \theta - \theta_o, \tag{6.161}$$

which reduces to

$$\delta V_L = V_1(\delta n/r_o \sin\gamma)\sin(\gamma - \gamma_1 - \theta'), \tag{6.162}$$

and thus the desired error coefficient is

$$\delta V_L = V_1 \sin(\gamma - \gamma_1 - \theta')/r_o \sin\gamma.$$

Upon substitution from (6.139a), and (6.139b), we have

$$V_r = V[-(\sin\theta'/\lambda \sin\gamma) + \cos(\gamma - \theta')]$$

and

$$V_\theta = V[((1 - \cos\theta')/(\lambda \sin\gamma)) + \sin(\gamma - \theta')],$$

and we obtain

$$\partial V_L/\partial n = (-V/r_o)[(\cos(\gamma - \theta') - \cos\gamma)/\lambda \sin^2\gamma]. \tag{6.163}$$

The last error coefficient to be derived is $(\partial V_L / V_n)$, which relates the out-of-plane or lateral velocity (δV_L) at the end-of-coast point (r_1, θ_1) to the out-of-plane velocity perturbation (δV_n) at cutoff. The geometry for this case is illustrated in Figure 6.20. The development is similar to that for $\partial V_L / \partial n$. The plane separation angle β is

$$\beta = (1/\cos\alpha)(\delta V_n / V) = (1/\sin\gamma)(\delta V_n / V). \tag{6.164}$$

As was discussed earlier, the angle between V_1 and ΔV_1 is equal to $\beta \cos\rho$. However, ρ is simply $\rho = \gamma_1 + \theta' - 90°$. Hence,

$$\text{angle between } V_1 \text{ and } \Delta V_1 = (1/\sin\gamma)(\delta V_n / V)\cos(\gamma_1 + \theta' - 90°), \tag{6.165a}$$

which by trigonometric expansion reduces to

$$(1/\sin\gamma)(\delta V_n / V)\sin(\gamma_1 + \theta'). \tag{6.165b}$$

Now, $\delta V_L = V_1 \times$ angle between V_1 and ΔV_1 for small angles (which is the case here). Thus,

$$\delta V_L = V_1[(1/\sin\gamma)(\delta V_n / V)\sin(\gamma_1 + \theta')]. \tag{6.166}$$

Finally, the ballistic error coefficient is

$$\partial V_L / \partial V_n = V_1 \sin(\gamma_1 + \theta')/V \sin\gamma = 1 - [(1 - \cos\theta')/\lambda \sin^2\gamma]. \tag{6.167}$$

In summary, for the out-of-plane case, there are four error coefficients that complete this case. These error coefficients are given by the equations (6.156), (6.157), (6.163), and (6.167).

Verification in downrange burnout position simply translates into an equivalent downrange error at impact. This is clear, since the effect is simply to rotate the free-flight ellipse about the mass center of the Earth. If the burnout point is laterally (i.e., out-of-plane) displaced by an amount δn from the reference trajectory plane, then one may use spherical trigonometry to show that the cross-range error at impact δR_{xr} is (using (6.150))

$$\delta R_{xr} / \delta n = \cos\phi. \tag{6.168}$$

The final "error coefficient" to be considered in this section establishes the relationship between a lateral, or cross-range, velocity at burnout, δV_{xr}, and the resulting cross-range error at impact, δR_{xr}. For the spherical Earth explicit guidance scheme (to be discussed later in this chapter), this component of velocity is ideally zero, but for the case of an oblate Earth gravitational field this is not necessarily so. We will not consider the oblateness-induced effects further, although we will give the required equation here:

$$\delta R_{xr} / \delta V_{xr} = r_o \sin\phi / V \sin\gamma. \tag{6.169}$$

If one considers δV_{xr}, a burnout error for the spherical Earth case, then we may note two important features: (1) The error vanishes for a range angle of 180° and has its

maximum at a typical *ICBM* range angle of 90°, and (2) the error increases as the flight-path angle approaches zero degrees, that is, for increasingly steeper flights. This is clear from the above equation, which shows that as the flight path angle decreases, a fixed cross-range or lateral velocity component produces a greater azimuthal angular error.

For the reader's convenience, the error coefficients developed in Sections 6.4.3.1 through 6.4.3.2 will now be summarized. There are a total of twenty error coefficients needed to describe position and velocity errors both in and out of the normal trajectory plane at time t after thrust cutoff. Sixteen of these error coefficients cover the in-plane case according to (6.130a), (6.130b), (6.135a), and (6.135b). As seen in these equations, these sixteen error coefficients are made up of various combinations of sixteen error partials, which are described by (6.143a), (6.143b), (6.144a), and (6.144b). The remaining four error coefficients out of the total of twenty are associated with the out-of-plane perturbations. These four error coefficients are given in (6.154) and (6.155) and are identical to their corresponding error partials given in (6.156), (6.157), (6.163), and (6.167). These equations are summarized below.

ERROR COEFFICIENT SUMMARY

In Plane

Vector Error Equations:

$$\begin{aligned}\delta\mathbf{V} = {} & [(\partial\mathbf{V}/\partial h)_{\hat{\mathbf{r}}}\delta h + (\partial\mathbf{V}/\partial V)_{\hat{\mathbf{r}}}\delta V + (\partial\mathbf{V}/\partial\gamma)_{\hat{\mathbf{r}}}\delta\gamma \\ & + (\partial\mathbf{V}/\partial\theta_o)_{\hat{\mathbf{r}}}\delta\theta_o]\hat{\mathbf{r}} + [(\partial\mathbf{V}/\partial h)_{\hat{\boldsymbol{\theta}}}\delta h + (\partial\mathbf{V}/\partial V)_{\hat{\boldsymbol{\theta}}}\delta V + (\partial\mathbf{V}/\partial\gamma)_{\hat{\boldsymbol{\theta}}}\delta\gamma \\ & + (\partial\mathbf{V}/\partial\theta_o)_{\hat{\boldsymbol{\theta}}}\delta\theta_o]\hat{\boldsymbol{\theta}},\end{aligned}$$

$$\begin{aligned}\delta\mathbf{r} = {} & [(\partial\mathbf{r}/\partial h)_{\hat{\mathbf{r}}}\delta h + (\partial\mathbf{r}/\partial V)_{\hat{\mathbf{r}}}\delta V + (\partial\mathbf{r}/\partial\gamma)_{\hat{\mathbf{r}}}\delta\gamma \\ & + (\partial\mathbf{r}/\partial\theta_o)_{\hat{\mathbf{r}}}\delta\theta_o]\hat{\mathbf{r}} + [(\partial\mathbf{r}/\partial h)_{\hat{\boldsymbol{\theta}}}\delta h + (\partial\mathbf{r}/\partial V)_{\hat{\boldsymbol{\theta}}}\delta V \\ & + (\partial\mathbf{r}/\partial\gamma)_{\hat{\boldsymbol{\theta}}}\delta\gamma + (\partial\mathbf{r}/\partial\theta_o)_{\hat{\boldsymbol{\theta}}}\delta\theta_o]\hat{\boldsymbol{\theta}}.\end{aligned}$$

Velocity Error Coefficients:

$$\begin{aligned}(\partial\mathbf{V}/\partial h)_{\hat{\mathbf{r}}} &= [(\partial V_r/\partial h) - V_\theta(\partial\theta/\partial h)], \\ (\partial\mathbf{V}/\partial V)_{\hat{\mathbf{r}}} &= [(\partial V_r/\partial V) - V_\theta(\partial\theta/\partial V)], \\ (\partial\mathbf{V}/\partial\gamma)_{\hat{\mathbf{r}}} &= [(\partial V_r/\partial\gamma) - V_\theta(\partial\theta/\partial\gamma)], \\ (\partial\mathbf{V}/\partial\theta_o)_{\hat{\mathbf{r}}} &= [(\partial V_r/\partial\theta_o) - V_\theta(\partial\theta/\partial\theta_o)], \\ (\partial\mathbf{V}/\partial h)_{\hat{\boldsymbol{\theta}}} &= [(\partial V_\theta/\partial h) + V_r(\partial\theta/\partial b)], \\ (\partial\mathbf{V}/\partial V)_{\hat{\boldsymbol{\theta}}} &= [(\partial V_\theta/\partial V) + V_r(\partial\theta/\partial V)], \\ (\partial\mathbf{V}/\partial\gamma)_{\hat{\boldsymbol{\theta}}} &= [(\partial V_\theta/\partial\gamma) + V_r(\partial\theta/\partial\gamma)], \\ (\partial\mathbf{V}/\partial\theta_o)_{\hat{\boldsymbol{\theta}}} &= [(\partial V_\theta/\partial\theta_o) + V_r(\partial\theta/\partial\theta_o)].\end{aligned}$$

Position Error Coefficients:

$$
\begin{aligned}
(\partial \mathbf{r}/\partial h)_{\hat{\mathbf{r}}} &= \partial r/\partial h,\\
(\partial \mathbf{r}/\partial V)_{\hat{\mathbf{r}}} &= \partial r/\partial V,\\
(\partial \mathbf{r}/\partial \gamma)_{\hat{\mathbf{r}}} &= \partial r/\partial \gamma,\\
(\partial \mathbf{r}/\partial \theta_o)_{\hat{\mathbf{r}}} &= \partial r/\partial \theta_o,\\
(\partial \mathbf{r}/\partial h)_{\hat{\boldsymbol{\theta}}} &= r(\partial \theta/\partial h),\\
(\partial \mathbf{r}/\partial V)_{\hat{\boldsymbol{\theta}}} &= r(\partial \theta/\partial V),\\
(\partial \mathbf{r}/\partial \gamma)_{\hat{\boldsymbol{\theta}}} &= r(\partial \theta/\partial \gamma),\\
(\partial \mathbf{r}/\partial \theta_o)_{\hat{\boldsymbol{\theta}}} &= r(\partial \theta/\partial \theta_o).
\end{aligned}
$$

Normal to Plane

Vector Error Equations:

$$
\begin{aligned}
\delta \mathbf{V} &= [(\partial \mathbf{V}_L/\partial n)_{\hat{\mathbf{n}}}\delta n + (\partial \mathbf{V}_L/\partial V_n)_{\hat{\mathbf{n}}}\delta V_n]\hat{\mathbf{n}},\\
\delta \mathbf{L} &= [(\partial \mathbf{L}/\partial n)_{\hat{\mathbf{n}}}\delta n + (\partial \mathbf{L}/\partial V_n)_{\hat{\mathbf{n}}}\delta V_n]\hat{\mathbf{n}}.
\end{aligned}
$$

Velocity Error Coefficients:

$$
\begin{aligned}
(\partial \mathbf{V}_L/\partial n)_{\hat{\mathbf{n}}} &= \partial V_L/\partial n,\\
(\partial \mathbf{V}_L/\partial V_n)_{\hat{\mathbf{n}}} &= \partial V_L/\partial V_n.
\end{aligned}
$$

Velocity Error Partials:

$$
\begin{aligned}
\partial V_L/\partial n &= (-V/r_o)[(\cos(\gamma-\theta') - \cos\gamma)/\lambda \sin^2\gamma)],\\
\partial V_L/\partial V_n &= 1 - \{(1-\cos\theta')/\lambda \sin^2\gamma\}.
\end{aligned}
$$

Position Error Coefficients:

$$
\begin{aligned}
(\partial \mathbf{L}/\partial n)_{\hat{\mathbf{n}}} &= \partial L/\partial n,\\
(\partial \mathbf{L}/\partial V_n)_{\hat{\mathbf{n}}} &= \partial L/\partial V_n.
\end{aligned}
$$

Position Error Partials:

$$
\begin{aligned}
\partial L/\partial n &= r_1 \sin[\gamma - (\theta_1 - \theta_o)]/r_o \sin\gamma,\\
\partial L/\partial V_n &= r_1 \sin(\theta_1 - \theta_o)/V \sin\gamma.
\end{aligned}
$$

Example. In this example we will discuss the error sensitivities of the various parameters describing the motion of a ballistic missile. Specifically, we will derive the error sensitivities of the free-fall time-of-flight (t_{ff}), the semimajor axis (a), the eccentricity (e), etc. We begin the development with the free-fall time-of-flight, (6.92),

$$
\begin{aligned}
t_{ff} &= (\sqrt{a^3/\mu})[E_2 - E_1 - e(\sin E_2 - \sin E_1)]\\
&= (\sqrt{a^3/\mu})[E_2 - E_1 - e\sin E_2 + e\sin E_1],
\end{aligned}
$$

where the E's are the eccentric anomalies of the initial and final points. Now, taking the partial derivative of the free-fall time-of-flight, we have

$$\begin{aligned}
\partial t_{ff}/\partial r &= \tfrac{1}{2}(3a^2/\mu)(a^3/\mu)^{-1/2}(\partial a/\partial r)[E_2 - E_1 - e(\sin E_2 - \sin E_1)] \\
&\quad + \left(\sqrt{a^3/\mu}\right)\{(\partial E_2/\partial r) - (\partial E_1/\partial r) - e\cos E_2(\partial E_2/\partial r) - \sin E_2(\partial e/\partial r) \\
&\quad + e\cos E_1(\partial E_1/\partial r) + \sin E_1(\partial e/\partial r)\} \\
&= \left(\tfrac{3}{2}\right)(a^2/\mu)(a^3/\mu)^{-1/2}(a/a)[E_2 - E_1 - e(\sin E_2 - \sin E_1)](\partial a/\partial r) \\
&\quad + \left(\sqrt{a^3/\mu}\right)\{(1 - e\cos E_2)(\partial E_2/\partial r) - \sin E_2(\partial e/\partial r) \\
&\quad - [(1 - e\cos E_1)(\partial E_1/\partial r) - \sin E_1(\partial E_1/\partial r),
\end{aligned}$$

and since

$$\begin{aligned}
r &= a(1 - e\cos E) \text{ or } r/a = 1 - e\cos E, \\
&= \tfrac{3}{2}(1/a)(a^3/\mu)(a^3/\mu)^{-1/2}(\partial a/\partial r)[E_2 - E_1 - e(\sin E_2 - \sin E_1)] \\
&\quad + \left(\sqrt{a^3/\mu}\right)\{(r/a)(\partial E_2/\partial r) - \sin E_2(\partial e/\partial r) \\
&\quad - [(r/a)(\partial E_1/\partial r) - \sin E_1(\partial e/\partial r)]\}.
\end{aligned}$$

After rearranging and simplifying, we obtain

$$\begin{aligned}
\partial t_{ff}/\partial r = \tfrac{3}{2}(t_{ff}/a)(\partial a/\partial r) + (\sqrt{a^3/\mu})\{(r/a)[(\partial E_2/\partial r) - (\partial E_1/\partial r)] \\
-(\sin E_2 - \sin E_1)(\partial e/\partial r)\}.
\end{aligned}$$

Next, we need an expression for $\partial a/\partial$r. From the *vis viva* integral (6.59),

$$V^2 = \mu[(2/r) - (1/a)],$$

we can solve for a, yielding

$$a = 1/[(2/r) - (V^2/\mu)],$$

$$\begin{aligned}
\partial a/\partial r &= \{[(2/r) - (V^2/\mu)]\cdot 0 - 1\cdot(2/1)(d/dr)(1/r)\}/[(2/r) - (V^2/\mu)]^2 \\
&= -2(-1/r)/[(2/r) - (V^2/\mu)]^2 \\
&= (2/r^2)\{1/[(2/r) - (V^2/\mu)]^2\},
\end{aligned}$$

or

$$\partial a/\partial r = 2a^2/r^2.$$

Writing now t_{ff} in the form

$$t_{ff} = \left(\sqrt{a^3/\mu}\right)(M_2 - M_1),$$

where

$$M_1 = E_1 - e \sin E_1,$$
$$M_2 = E_2 - e \sin E_2.$$

Let $M_j = E_j - e \sin E_j$, $j = 1, 2$. Then,

$$\begin{aligned}\partial M_j/\partial r &= (\partial E_j/\partial r) - e \cos E_j(\partial E_j/\partial r) - \sin E_j(\partial e/\partial r)\\ &= (1 - e \cos E_j)(\partial E_j/\partial r) - \sin E_j(\partial e/\partial r).\end{aligned}$$

Again, making the substitution $r/a = 1 - e \cos E$, we have

$$\partial M_j/\partial r = (r/a)(\partial E_j/\partial r) - \sin E_j(\partial e/\partial r).$$

Writing the semimajor axis in the form

$$a^{-1} = [(2/r) - (V^2/\mu)],$$

we can develop the sensitivities $\partial a/\partial V_r$ and $\partial a/\partial V_\theta$, where $V^2 = V_r^2 + V_\theta^2$. Substituting this expression in the equation for a^{-1}, we obtain

$$a^{-1} = [(2/r) - (V_r^2/\mu) - (V_\theta^2/\mu)].$$

Taking the partial derivatives results in the following:

$$-a^{-2}(\partial a/\partial V_r) = -(2V_r/\mu),$$

or

$$\partial a/\partial V_r = 2V_r a^2/\mu.$$

Similarly,

$$\partial a/\partial V_\theta = 2V_\theta a^2/\mu.$$

The partial $\partial e/\partial r$ can be obtained as follows: Let the angular momentum h be given by

$$h = r^2\dot{\theta} = r\left[r\left(\frac{d\theta}{dt}\right)\right] = rV_\theta.$$

Also, we know that $h^2 = \mu a(1 - e^2)$, so that

$$a = h^2/\mu(1 - e^2) = r^2V_\theta^2/\mu(1 - e^2).$$

Therefore,

$$V^2 = V_r^2 + V_\theta^2 = \mu[(2/r) - (1/a)] = \mu[(2/r) - (\mu(1 - e^2)/r^2V_\theta^2)].$$

Multiplying through by V_θ^2, we obtain

$$\begin{aligned}V_r^2V_\theta^2 + V_\theta^4 &= (2\mu V_\theta^2/r) - (\mu^2/r^2) + (\mu^2e^2/r^2),\\ \mu^2e^2/r^2 &= (\mu^2/r^2) - (2\mu V_\theta^2/r) + V_r^2V_\theta^2 + V_\theta^4.\end{aligned}$$

After some algebra, we obtain e in the form

$$e = (r/\mu)\{[(\mu/r) - V_\theta^2]^2 + V_\theta^2 V_r^2\}^{1/2}.$$

Having e, we can now form the sensitivity partial $\partial e/\partial r$:

$$\begin{aligned}\partial e/\partial r = {} & \{[(\mu/r) - V_\theta^2]^2 + V_\theta^2 V_r^2\}^{1/2}(1/\mu) + (r/\mu)(1/2)\{[(\mu/r) - V_\theta^2]^2 \\ & + V_\theta^2 V_r^2\}^{-1/2} \cdot 2[(\mu/r) - V_\theta^2](-\mu/R).\end{aligned}$$

Again, after some algebra, the above equation reduces to

$$\partial e/\partial r = (e/r) - (1/\mu e)[(\mu/r) - V_\theta^2].$$

This equation can be further reduced as follows:

$$\partial e/\partial r = p \cos E/r^2,$$

where p is the semilatus rectum and is given by $p = a(1 - e^2)$. The remaining sensitivity partials, that is, $\partial t_{ff}/\partial V_\theta$, $\partial t_{ff}/\partial V_r$, $\partial a/\partial V_\theta$, $\partial e/\partial V_\theta$, and $\partial e/\partial V_r$, will now be developed. Beginning with the equation for the free-fall time-of-flight, we have as before

$$t_{ff} = (\sqrt{a^3/\mu})[E_2 - E_1 - e(\sin E_2 - \sin E_1)],$$

$$\begin{aligned}\partial t_{ff}/\partial V_\theta = {} & \tfrac{1}{2}(a^3/\mu)^{-1/2}(3a^2/\mu)(\partial a/\partial V_\theta)[E_2 - E_1 - e(\sin E_2 - \sin E_1)] \\ & + (\sqrt{a^3/\mu})\{(\partial E_2/\partial V_\theta) - (\partial E_1/\partial V_\theta) - e\cos E_2(\partial E_2/\partial V_\theta) \\ & - \sin E_2(\partial e/\partial V_\theta) + e\cos E_1(\partial E_1/\partial V_\theta) + \sin E_1(\partial e/\partial V_\theta)\} \\ = {} & \tfrac{3}{2}(a^2/\mu)(a^3/\mu)^{-1/2}(a/a)(\partial a/\partial V_\theta)[E_2 - E_1 - e(\sin E_2 - \sin E_1)] \\ & + (\sqrt{a^3/\mu})\{(1 - e\cos E_2)(\partial E_2/\partial V_\theta) - \sin E_2(\partial e/\partial V_\theta) \\ & - [(1 - e\cos E_2)(\partial E_1/\partial V_\theta - \sin E_1(\partial E_1/\partial V_\theta)]\},\end{aligned}$$

$$\begin{aligned}\partial t_{ff}/\partial V_\theta = {} & \tfrac{3}{2}(t_{ff}/a)(\partial a/\partial V_\theta) + (\sqrt{a^3/\mu})\{(r_2/a)(\partial E_2/\partial V_\theta) \\ & - (r_1/a)(\partial E_1/\partial V_\theta) - (\sin E_2 - \sin E_1)(\partial e/\partial V_\theta)\}.\end{aligned}$$

Similarly, the partial of $\partial t_{ff}/\partial V_r$ is formed as above:

$$t_{ff} = (\sqrt{a^3/\mu})[E_2 - E_1 - e(\sin E_2 - \sin E_1)],$$

$$\begin{aligned}\partial t_{ff}/\partial V_r = {} & \tfrac{1}{2}(a^3/\mu)^{-1/2}(3a^2/\mu)(\partial a/\partial V_\theta)[E_2 - E_1 - e(\sin E_2 - \sin E_1)] \\ & + (\sqrt{a^3/\mu})\{(\partial E_2/\partial V_r) - (\partial E_1/\partial V_r) - e\cos E_2(\partial E_2/\partial V_r) \\ & - \sin E_2(\partial e/\partial V_r) + e\cos E_1(\partial E_1/\partial V_r) \\ & + \sin E_1(\partial e/\partial V_r)\}.\end{aligned}$$

Simplifying as before,

$$\partial t_{ff}/\partial V_r = \tfrac{3}{2}(t_{ff}/a)(\partial a/\partial V_r) + (\sqrt{a^3/\mu})\{(r_2/a)(\partial E_2/\partial V_r) - (r_1/a)(\partial E_1/\partial V_r) - (\sin E_2 - \sin E_1)(\partial e/\partial V_r)\}.$$

Again, from the relation

$$V^2 = V_r^2 + V_\theta^2$$

and

$$V^2 = \mu[(2/r) - (1/a)],$$

we have

$$(2\mu/r) - (\mu/a) = V_r^2 + V_\theta^2,$$
$$(\mu/a^2)(\partial a/\partial V_\theta) = 2V_\theta,$$

or

$$(\partial a/\partial V_\theta) = 2V_\theta\, a^2/\mu.$$

From the eccentricity equation developed earlier, that is,

$$e^2 = (r^2/\mu^2)\{[(\mu/r) - V_\theta^2]^2 + V_\theta^2 V_r^2\},$$
$$2e(\partial e/\partial V_\theta) = (r^2/\mu^2)\{2[(\mu/r) - V_\theta^2]^2(-2V_\theta) + 2V_\theta V_r^2\},$$
$$(\partial e/\partial V_\theta) = (r^2/\mu^2)(V_\theta/e)[V_r^2 - 2(\mu/r) + 2V_\theta^2],$$

after some simplification, and letting $c = \frac{1}{2}V^2 - (\mu/r)$, we obtain

$$\partial e/\partial V_\theta = (p/e\mu V_\theta)[2c + V_\theta^2].$$

Now making use of the expression for e^2 as before, we have

$$e^2 = (r^2/\mu^2)\{[(\mu/r) - V_\theta^2]^2 + V_\theta^2 V_r^2\},$$

$$2e(\partial e/\partial V_r) = (r^2/\mu^2)[2V_r V_\theta^2],$$

or

$$\partial e/\partial V_r = pV_r/e\mu.$$

6.4.4 Effect of the Rotation of the Earth

In Section 6.4.2 an equation (i.e., (6.88)) was developed for the required velocity to impact a target in inertial space. Moreover, it was assumed that the missile travels around a spherical, stationary, Earth. However, since the Earth rotates, and most targets are not fixed in inertial space, but are fixed to the Earth and rotate* with it. Typically,

*The Earth rotates once in its axis in 23 hrs 56 min, producing a surface velocity at the equator of 1,524 ft/sec. The rotation is from west to east. For example, for a typical *ICBM* flight of 30 minutes and a target latitude of 45°, the target moves with respect to inertial space a distance of almost 350 nm during free fall.

the Earth-centered-inertial (*ECI*) coordinate system is used to locate targets on the surface of the Earth. Therefore, the *ECI* coordinates of an Earth-fixed target at some future time are given by the following expression [11]:

$$x_t = r_t \cos\varphi_t \cos(\lambda_t + \omega t_{ff}), \tag{6.168a}$$

$$y_t = r_t \cos\varphi_t \sin(\lambda_t + \omega t_{ff}), \tag{6.168b}$$

$$z_t = r_t \sin\varphi_t, \tag{6.168c}$$

where φ_t and λ_t are the latitude and reference longitude of the target, ω is the Earth's rate of rotation, and t_{ff} is the time of free flight. These equations show that in order to predict the position of the target at impact, the time of free flight must be known. Furthermore, the rotation of the Earth will introduce a dependence on the time of flight into errors that will appear at the terminal point of the flight. This dependence may be calculated from an analysis of the equation for the time of flight of the ballistic missile, (6.92).

When the variation of the time of flight that results from the variations in initial position and velocity is known, the contribution to the error at the terminal point (or target) due to the rotation of the Earth may be calculated. This error will be in the longitude direction, and will be given by the product of the velocity of the reentry point, which is due to the rotation of the Earth, times the variation in the time of flight as follows:

$$\Delta_t = (r_i \omega \cos\lambda)\Delta t_{ff} \tag{6.169}$$

where

Δ_t = terminal point error due to Earth's rotation,
ω = Earth rate = 7.29×10^{-5} rad/sec,
r_i = distance from the center of the Earth to burnout point (see Figure 6.9)),
λ = geographic longitude.

The sensitivity of the time of flight to errors in position and velocity in the horizontal directions is such that they will not introduce errors that must be considered in a first-order error analysis. It should be noted that the time of free flight depends on V_R, which in turn is a function of the impact position. Hence, an iterative procedure must be used to calculate the required velocity and the time of free flight. This iteration process may be thought of as follows [9]:

(1) A future target position is assumed.
(2) The corresponding required velocity V_R is computed.
(3) Compute the elements of the resulting ellipse.
(4) Compute the time of free flight.

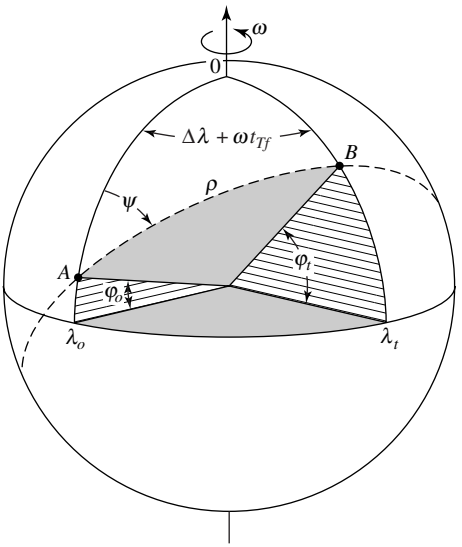

Fig. 6.21. Launch site and aiming point at the instant of launch. Originally published in *Fundamentals of Astrodynamics*, R. R. Bate, D. D. Mueller, and J. E. White, Dover Publications, Inc., Copyright ©1971. Reprinted with permission.

(5) Compute (or assume) a future target position.
(6) Repeat the above procedure.

In reference [2], the effect of the Earth's rotation is computed in terms of the range. From Figure 6.21 we can obtain the range ρ (i.e., launch point to target) using the law of cosines for spherical triangles as follows:

$$\cos\rho = \sin\varphi_o \sin\varphi_t + \cos\varphi_o \cos\varphi_t \cos(\Delta\lambda + \omega t_{Tf}),$$

where

$$\begin{aligned}
\varphi_o &= \text{launch latitude},\\
\varphi_t &= \text{target latitude},\\
\Delta\lambda &= \text{longitude differential},\\
\omega &= \text{Earth's rate of rotation},\\
t_{Tf} &= \text{total time-of-flight (i.e., launch to target intercept)}.
\end{aligned}$$

Note that here we use the total time-of-flight instead of the free-fall time-of-flight t_{ff}, since we consider the launch from the surface of the Earth to a target on the surface of the Earth.

Similarly, using the law of cosines for spherical triangles, we can obtain the launch azimuth angle ψ in terms of the range ρ as follows:

$$\cos\psi = (\sin\varphi_t - \sin\varphi_o \cos\rho)/\cos\varphi_o \sin\rho.$$

The total time-of-flight t_{Tf} can be computed, as before, by iteration. In order to do this, one must first use a reasonable time or "guess" t_{Tf}. This first guess can be used to compute an initial estimate for ρ, which in turn would allow one to get a first estimate of t_{ff}. By adding the times of powered flight and reentry (which also depend somewhat on ρ) to t_{ff}, one obtains a value of t_{Tf}, which can be used as a second "guess." The entire process is then repeated until the computed value of t_{Tf} agrees with the estimated value.

6.5 The Correlated Velocity and Velocity-to-Be-Gained Concepts

6.5.1 Correlated Velocity

In Section 6.4.2 we developed an equation (i.e., (6.89)) for the velocity required of the missile at burnout in order to hit a given target. This required velocity is also referred to as the *correlated velocity*. In this section, we shall therefore adapt the term correlated velocity. We begin our development by considering a body whose free-fall motion is governed by a central force field. Let $\mathbf{r}$ denote the current position vector, and $\mathbf{r}_t$ the target (or second position) position, and let a unique time-of-flight t_{ff} also be specified. The correlated velocity vector $\mathbf{V}_c$ is the velocity that the body must have at the position $\mathbf{r}$ such that if acted on only by the central force, it would arrive by free fall at $\mathbf{r}_t$ (the target) in t_{ff} seconds. The correlated velocity vector $\mathbf{V}_c$ constrains the total time-of-flight of the missile to be constant. As a result, this definition eliminates the bothersome problem of accounting for the motion of the target due to the Earth's rotation.

The solution for $\mathbf{V}_c$ inevitably involves an iteration to determine some parameter (e.g., time-of-flight) that leads to a value for $\mathbf{V}_c$. Several choices for the iteration parameter have been proposed, and one from the various possibilities is described in [3]. To recapitulate, then, the vector $\mathbf{V}_c$ is defined to be the velocity vector that would be required by the missile at the specified position and time in order that it might travel thereafter by free fall in vacuum into a desired condition. For the particular application considered, the "desired terminal condition" is coincidence of the missile and a target on the Earth's surface (neglecting, of course, atmospheric effects during reentry). To make the definition of $\mathbf{V}_c$ unique in this case, a further condition must be stipulated, such as the time at which the missile and target shall coincide.

In essence, the vector $\mathbf{V}_c$ provides a standard of comparison for the actual missile velocity vector $\mathbf{V}_m$ such that if equality is attained between $\mathbf{V}_m$ and $\mathbf{V}_c$, the missile may fulfill its mission without further application of thrust. It is therefore natural to define a "velocity-to-be-gained" (or "velocity-to-go") vector (to be discussed in more detail in Section 6.5.2) $\mathbf{V}_g$ as the vector difference between $\mathbf{V}_c$ and $\mathbf{V}_m$ [9]:

$$\mathbf{V}_g = \mathbf{V}_c - \mathbf{V}_m. \tag{6.170}$$

The vector $\mathbf{V}_g$, then, represents the velocity that if added instantaneously to the present missile velocity would permit thrust to be cut off at that instant. The condition

$$\mathbf{V}_g = 0 \tag{6.171}$$

is then the desired condition for cut-off of thrust. Also, we note here that engine (or motor) cut-off can be mechanized to occur when [9]

$$(V_R/V_m)^2 = 1,$$

or

$$\mathbf{V}_R - \mathbf{V}_m = 0.$$

Further, in a rough sense, the direction of $\mathbf{V}_g$ defines the direction in which the missile thrust vector should be applied in order to drive $\mathbf{V}_g$ toward zero. This vector is therefore generally suited for use as a guidance and control quantity.

These general concepts are illustrated in Figure 6.22a. The point M in the illustration represents the missile position at time t. The heavy line through M represents the powered flight path, terminating at the cut-off point (CO) in the elliptical free-fall trajectory shown as a dashed line terminating at the target position T. Tangent to the correlated velocity vector $\mathbf{V}_c$ is shown a second ellipse, which would be followed by the missile in free fall, provided that it possessed the velocity $\mathbf{V}_c$ at the point M. All quantities are shown to an exaggerated scale, in order to clarify the illustration.

Suppose now that for a given launch point and target combination on the Earth's surface, a desired total time-of-flight t_{Tf} from launch to target has been fixed upon by some process. The specification of the instant of launch then determines uniquely the location of the future target position T_F (i.e., at the desired instant of impact) with respect to a nonrotating set of coordinates. The motion of the target due to the Earth's rotation must, of course, be taken into account in the initial determination of T_F. However, this point remains stationary during the flight of the missile except insofar as the total time of flight may deviate from the predetermined value. The system considered here is an attempt to keep the total time of flight constant, so that any deviation in this time is regarded as an uncompensated error.

As a result of these considerations, at any given time t and position $\mathbf{r}$ along the flight path of the missile, the correlated velocity vector is specified uniquely, although implicitly. Let us begin the development by assuming a spherical Earth. The vector $\mathbf{V}_c$ must lie in the plane determined by the radius vectors $\mathbf{r}$ and $\mathbf{r}_t$ drawn from the center of the Earth to the present missile position and future target position, respectively. Other properties, such as that the resulting free-fall trajectory must pass through the target and that the time of free flight t_{ff} shall take on the value

$$t_{ff} = t_{Tf} - t, \tag{6.172}$$

then serve to determine $\mathbf{V}_c$ uniquely within this plane. As a result, $\mathbf{V}_c$ may be expressed mathematically at the current time t in the functional form

$$\mathbf{V}_c = \mathbf{V}_c(\mathbf{r}, t), \tag{6.173}$$

with a further implied dependence upon the launch and target sites and the assigned total time of flight t_{Tf}. In general, (6.73) can be expressed as

$$\mathbf{V}_c = \mathbf{V}_c(\mathbf{r}_m, \mathbf{r}_t, t_A, t),$$

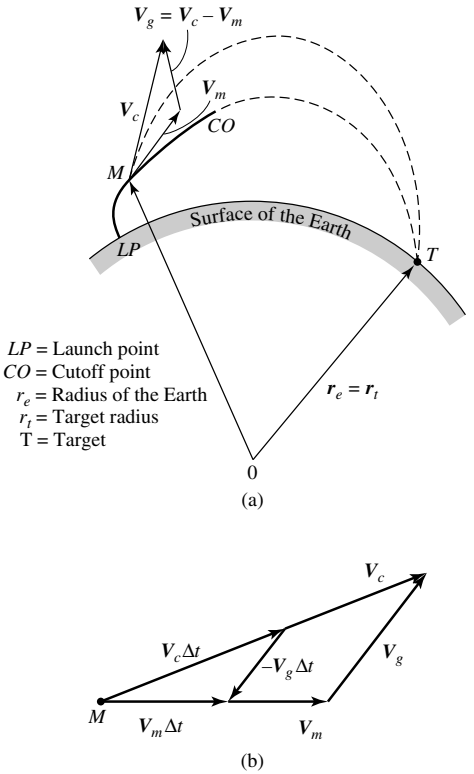

Fig. 6.22. Vector representation of correlated velocity, missile velocity, and velocity-to-be-gained vector.

where $\mathbf{r}_m$ is the inertial location of the missile, $\mathbf{r}_t$ is the inertial location of the target, t_A is the specified time of arrival at the target, and t is the current time. We now define a Q-matrix, which forms the so-called *Q-guidance*, of variable coefficients that form the heart of the systems considered here [3]. More specifically, the Q-matrix, or directional derivative, is a matrix whose elements consist of the time-of-flight-constrained correlated velocity vector $\mathbf{V}_c$. Let an arbitrary set of Earth-centered nonrotating orthogonal coordinate axes (x, y, z) be assigned, and let $\mathbf{i}$, $\mathbf{j}$, and $\mathbf{k}$ be the unit vectors along the respective axes. Writing $\mathbf{r}$ and $\mathbf{V}_c$ in the form

$$\begin{aligned} \mathbf{r} &= x\mathbf{i} + y\mathbf{j} + z\mathbf{k}, \\ \mathbf{V}_c &= u_c\mathbf{i} + v_c\mathbf{j} + w_c\mathbf{k}. \end{aligned} \tag{6.174}$$

The elements of the Q-matrix may be defined by the relations

$$\begin{array}{lll} Q_{xx} = \partial u_c/\partial x, & Q_{xy} = \partial u_c/\partial y, & Q_{xz} = \partial u_c/\partial z, \\ Q_{yx} = \partial v_c/\partial x, & Q_{yy} = \partial v_c/\partial y, & Q_{yz} = \partial v_c/\partial z, \\ Q_{zx} = \partial w_c/\partial x, & Q_{zy} = \partial w_c/\partial y, & Q_{zz} = \partial w_c/\partial z, \end{array} \tag{6.175}$$

or in matrix form,

$$Q = \begin{bmatrix} Q_{xx} & Q_{xy} & Q_{xz} \\ Q_{yx} & Q_{yy} & Q_{yz} \\ Q_{zx} & Q_{zy} & Q_{zz} \end{bmatrix}.$$

It is understood that in carrying out the indicated differentiation, the target location vector $\mathbf{r}_t$ and the total time of flight t_{Tf} are held fixed in the process, as is t itself. In an abbreviated notation, Q may be expressed in the equivalent form [3]

$$Q = \|\partial \mathbf{V}_c(\mathbf{r}, t)/\partial \mathbf{r}\|_{\mathbf{r}_t, t_{ff}}. \tag{6.176}$$

It is noted in the last expression that t_{ff} is indicated as being held fixed; this is equivalent to fixing t_{Tf} by virtue of (6.172) and the fact that t is fixed. In terms of $\mathbf{V}_c$, the Q-matrix can be written in the form

$$Q = \begin{bmatrix} \partial V_{cx}/\partial x & \partial V_{cx}/\partial y & \partial V_{cx}/\partial z \\ \partial V_{cy}/\partial x & \partial V_{cy}/\partial y & \partial V_{cy}/\partial z \\ \partial V_{cz}/\partial x & \partial V_{cz}/\partial y & \partial V_{cz}/\partial z \end{bmatrix}. \tag{6.177}$$

Thus, the Q-matrix consists of at most of nine elements, six of which are distinct. For any given present missile position, target position, and time remaining before the specified time of arrival at the target, the elements of the Q-matrix may be computed. The elegance of the Q-guidance equations lies in the fact that these equations take accelerometer output as a function of time and yield at the output the velocity-to-be-gained $\mathbf{V}_g$.

A guidance technique that is applicable for a variety of powered flight guidance phases will now be presented. Specifically, a convenient and efficient guidance law will be developed in which the direction of the thrust acceleration is such that the vector $\mathbf{V}_g$ and its derivative are parallel. Thus,

$$\left(\frac{d\mathbf{V}_g}{dt}\right) \times \mathbf{V}_g = 0.$$

Since (see also Section 6.5.2, (6.179))

$$\left(\frac{d\mathbf{V}_m}{dt}\right) = \mathbf{a}_T + \mathbf{g},$$

where $\mathbf{g}$ is the acceleration of gravity and $\mathbf{a}_T$ is the thrust acceleration vector provided by the engine (and measured by the *IMU* accelerometers), the rate of change of the velocity-to-be-gained can be expressed as

$$\frac{d\mathbf{V}_g}{dt} = \left(\frac{d\mathbf{V}_c}{dt}\right) - \mathbf{a}_T - \mathbf{g} = \mathbf{b} - \mathbf{a}_T,$$

where

$$\mathbf{b} = \left(\frac{d\mathbf{V}_c}{dt}\right) - \mathbf{g}.$$

It is evident that at cut-off, the required velocity is attained simultaneously as $\mathbf{b} \to 0$. The essential principle of steering is to point the thrust so that

$$\mathbf{a}_T \times \mathbf{V}_g = c\mathbf{b} \times \mathbf{V}_g,$$

where c is a scalar. In the absence of $\mathbf{a}_T$, the term $(\mathbf{b} \times \mathbf{V}_g)$ represents the rotational effect on $\mathbf{V}_g$. Hence, the factor c specifies the degree of rotational effect on $\mathbf{V}_g$ during powered flight. If $c = 1$, the total rotational effect is nil, and from the above equations it is evident that $\mathbf{V}_g / |\mathbf{V}_g|$ remains constant. Rearrangement of the equation

$$\mathbf{a}_T \times \mathbf{V}_g = c\mathbf{b} \times \mathbf{V}_g$$

gives

$$\left((c-1)\mathbf{b} + \left(\frac{d\mathbf{V}_g}{dt}\right)\right) \times \mathbf{V}_g = 0.$$

If $c = 1$, the above equation reduces to

$$\left(\frac{d\mathbf{V}_g}{dt}\right) \times \mathbf{V}_g = 0,$$

and if $c = 0$,

$$\mathbf{a}_T \times \mathbf{V}_g = 0.$$

It can be readily shown that this equation represents a faster rate of decrease of $|\mathbf{V}_g|$. However, in most practical applications, nonzero values (unity in particular) for c result in better fuel economy than when the thrust is aligned with $\mathbf{V}_g$.

Example. In [3], page 79, equation (3.26), a possible equation for the correlated velocity is given as

$$\mathbf{V}_c = (\sqrt{\mu p}/R_1 R_2 \sin\theta)\{\mathbf{R}_2 - [1 - (R_2/p)(1 - \cos\theta)]\mathbf{R}_1\},$$

where p is the semilatus rectum or conic parameter, $\mathbf{R}_1$ is the missile's present position vector, $\mathbf{R}_2$ is the target vector, θ is the central angle between $\mathbf{R}_1$ and $\mathbf{R}_2$, and μ is the gravitational constant as illustrated in the sketch below.

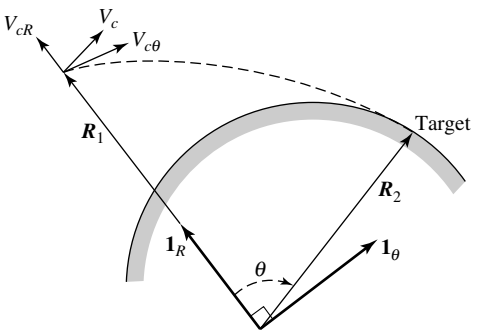

Geometry of the problem.

Since this equation is given in terms of the coordinate frame consisting of $\mathbf{R}_1$ and $\mathbf{R}_2$, it may be convenient to work in a local vertical frame. This equation, then, can be transformed as follows:

$$\begin{aligned} V_{c\theta} &= \mathbf{V}_c \cdot \mathbf{1}_\theta = (\sqrt{\mu p}/R_1 R_2 \sin\theta)[R_2 \cos((\pi/2) - \theta)] \\ &= (\sqrt{\mu p}/R_1 R_2 \sin\theta)(R_2 \sin\theta) = \sqrt{\mu}\sqrt{p}/R_1 \end{aligned}$$

$$\begin{aligned} V_{cR} &= \mathbf{V}_c \cdot \mathbf{1}_R = (\sqrt{\mu p}/R_1 R_2 \sin\theta)\{R_2 \cos\theta - [1 - (R_2/p)(1 - \cos\theta)R_1]\} \\ &= (\sqrt{\mu}\sqrt{p}/R_1 \sin\theta)[\cos\theta - (R_1/R_2) + (R_1/p)(1 - \cos\theta)]. \end{aligned}$$

In rectangular coordinates, the equation for the correlated velocity can be written as follows:

Let

$$\begin{aligned} \mathbf{R}_1 &= x_1\mathbf{i} + y_1\mathbf{j} + z_1\mathbf{k}, \\ \mathbf{R}_2 &= x_2\mathbf{i} + y_2\mathbf{j} + z_2\mathbf{k}. \end{aligned}$$

Thus,

$$\begin{aligned} \mathbf{V}_c &= (\sqrt{\mu p}/R_1 R_2 \sin\theta)\{(x_1\mathbf{i} + y_1\mathbf{j} + z_1\mathbf{k}) \\ &\qquad -[1 - (R_2/p)(1 - \cos\theta)](x_1\mathbf{i} + y_1\mathbf{j} + z_1\mathbf{k})\}, \\ V_{cx} &= (\sqrt{\mu}\sqrt{p}/R_1 R_2 \sin\theta)\{x_2 - [1 - (R_2/p)(1 - \cos\theta)]x_1\}, \\ V_{cy} &= (\sqrt{\mu}\sqrt{p}/R_1 R_2 \sin\theta)\{y_2 - [1 - (R_2/p)(1 - \cos\theta)]y_1\}, \\ V_{cz} &= (\sqrt{\mu}\sqrt{p}/R_1 R_2 \sin\theta)\{z_2 - [1 - (R_2/p)(1 - \cos\theta)]z_1\}. \end{aligned}$$

For a computer program (also for an airborne computer), the correlated velocity vector can be calculated as follows:

$$\begin{aligned} R_1 &= (x_1^2 + y_1^2 + z_1^2)^{1/2} \quad \text{position vector,} \\ R_2 &= (x_2^2 + y_2^2 + z_2^2)^{1/2} \quad \text{target vector,} \\ C_3 &= (x_1x_2 + y_1y_2 + z_1z_2)/(R_1R_2) = \cos\theta, \\ S_3 &= (1 - C_3^2)^{1/2} = (1 - \cos^2\theta)^{1/2} = \sin\theta, \\ S_1 &= \left[\tfrac{1}{2} - \tfrac{1}{2}C_3\right]^{1/2} = \left[\tfrac{1}{2} - \tfrac{1}{2}\cos\theta\right] = \sin(\theta/2), \\ C_1 &= S_3/2S_1 = \sin\theta/2\sin(\theta/2) = \cos(\theta/2), \\ U_1 &= 1/\sqrt{\mu}, \\ U_2 &= \sqrt{R_1R_2}, \\ U_3 &= U_2C_1 = \sqrt{R_1R_2}(\cos(\theta/2)), \\ B &= (R_1 + R_2)/2U_3 = (R_1 + R_2)/(2\sqrt{R_1R_2})\cos(\theta/2), \end{aligned}$$

$$
\begin{aligned}
F &= U_3\sqrt{U_3} = (\sqrt{R_1R_2})(\cos(\theta/2))[(\sqrt{R_1R_2})(\cos(\theta/2))]^{1/2},\\
F &= [(R_1R_2)^{3/2}(\cos^3(\theta/2))]^{1/2} = (R_1R_2)^{3/4}\cos^{3/2}(\theta/2),\\
C_2 &= \cos z,\\
S_2 &= \sin z,\\
U_4 &= 2(z - S_2C_2) = 2z - 2\sin z\cos z = 2z - \sin 2z,\\
U_5 &= \sqrt{B - C_2} = \sqrt{B - \cos z},\\
U_6 &= 1 + (U_5^2U_4/2S_2^3) = 1 + [(B - \cos z)(2z - \sin 2z)/2\sin^3 z],\\
T &= 2FU_5U_6U_1,\\
T &= 2(R_1R_2)^{3/4}\cos^{3/2}(\theta/2)(\sqrt{B - \cos z})\{1 + [(B - \cos z)(2z - \sin 2z)/\\
&\quad 2\sin^3 z]\}(1/\sqrt{\mu}),\\
T &= A(\sqrt{B - \cos z})\{1 + [(B - \cos z)(2z - \sin 2z)/2\sin^3 z]\},\\
A &= 2(R_1R_2)^{3/4}\cos^{3/2}(\theta/2)(1/\sqrt{\mu}),\\
P &= U_2S_1^2/U_5^2C_1 = (R_1R_2)^{1/2}\sin^2(\theta/2)/(B - \cos z)\cos(\theta/2),\\
\mathbf{V}_c &= (\sqrt{\mu p}/R_1R_2\sin\theta)\{\mathbf{R}_2 - [1 - (R_2/p)(1 - \cos\theta)]\mathbf{R}_1\}.
\end{aligned}
$$

In polar or local vertical coordinates we have

$$
\begin{aligned}
V_{c\theta} &= \sqrt{P}/U_1R_1,\\
V_{cR} &= (V_{c\theta}/S_3)[C_3 - (R_1/R_2) + (R_1/P)(1 - C_3)].
\end{aligned}
$$

Finally, in rectangular coordinates, we have

$$
\begin{aligned}
V_{cx} &= (\sqrt{P})/U_1U_2^2S_3\{x_2 - [1 - (R_2/P)(1 - C_3)]x_1\},\\
V_{cy} &= (\sqrt{P})/U_1U_2^2S_3\{y_2 - [1 - (R_2/P)(1 - C_3)]y_1\},\\
V_{cz} &= (\sqrt{P})/U_1U_2^2S_3\{z_2 - [1 - (R_2/P)(1 - C_3)]z_1\}.
\end{aligned}
$$

6.5.2 Velocity-to-Be-Gained

The velocity-to-be-gained vector $\mathbf{V}_g$ is the difference between the present missile velocity and the velocity required at that point in space and time for the missile to fall freely from that point to impact at the target at the prescribed time. This relation was expressed mathematically in Section 6.5.1 as

$$\mathbf{V}_g = \mathbf{V}_c - \mathbf{V}_m, \tag{6.170}$$

where $\mathbf{V}_c$ is the correlated velocity vector and $\mathbf{V}_m$ is the current missile velocity vector. Thus, if at any point in the powered part of the flight trajectory the velocity-to-be-gained were to vanish, the thrust of the missile could be terminated at that point, and the desired end condition would be realized. Specifically, it is the function of the guidance control system to steer the missile so that the desired cut-off condition $\mathbf{V}_g = 0$ will be achieved. Figure 6.21 illustrates these concepts.

The desired cut-off condition, that is, the vanishing of the velocity-to-be-gained vector, implies the simultaneous vanishing of all three components of that vector. A useful approach to this matter comes from noticing that if it is possible to orient the time rate of change of a vector in direct opposition to the vector itself, then the vector will maintain a fixed orientation in space and simply shrink in magnitude until at one instant the vector is zero in the sense that all of its components are simultaneously zero. In this case, we are interested in controlling $\mathbf{V}_g$; thus, we would like to control the vector $-(d\mathbf{V}_g/dt)$ so that it is oriented along $\mathbf{V}_g$. The vector $-(d\mathbf{V}_g/dt)$ can be expressed mathematically as

$$-\left(\frac{d\mathbf{V}_g}{dt}\right) = \mathbf{a}_T + Q\mathbf{V}_g,$$

or

$$\left(\frac{d\mathbf{V}_g}{dt}\right) = -\mathbf{a}_T - Q\mathbf{V}_g, \tag{6.178}$$

where

$\mathbf{a}_T$ = the thrust acceleration vector (i.e., acceleration due to nonfield forces), which is dominated by the missile thrust.

Q = matrix of partials (or directional derivatives; that is, $Q_{ij} = \partial V_{ci}/\partial r_j|_{i,j=1,2,3}$). (Note that the Q-matrix can also be designated as $\|Q\|$.)

It should be noted here that $\mathbf{a}_T$, also known as the *specific force*, accounts for aerodynamic and control forces as well. This is the quantity whose components are measured by physical accelerometers [9], [11],

$$\frac{d\mathbf{V}_m}{dt} = \mathbf{a}_T + \mathbf{g}, \tag{6.179}$$

where $\mathbf{g}$ is the gravitational acceleration vector. Figure 6.23 shows a possible indication system for (6.170) and (6.179).

The coordinate system of the missile is chosen as follows: The x-axis points downrange toward the target, the z-axis vertically, and the y-axis out of the paper, completing an orthogonal system. These axes are illustrated in Figure 6.24.

The vector for $d\mathbf{V}_g/dt$ can now be expanded into three scalar equations corresponding to the three accelerometer-input axes as follows:

$$\frac{dV_{gx}}{dt} = -a_{Tx} - Q_{xx}V_{gx} - Q_{xy}V_{gy} - Q_{xz}V_{gz}, \tag{6.180a}$$

$$\frac{dV_{gy}}{dt} = -a_{Ty} - Q_{yx}V_{gx} - Q_{yy}V_{gy} - Q_{yz}V_{gz}, \tag{6.180b}$$

$$\frac{dV_{gz}}{dt} = -a_{Tz} - Q_{zx}V_{gx} - Q_{zy}V_{gy} - Q_{zz}V_{gz}. \tag{6.180c}$$

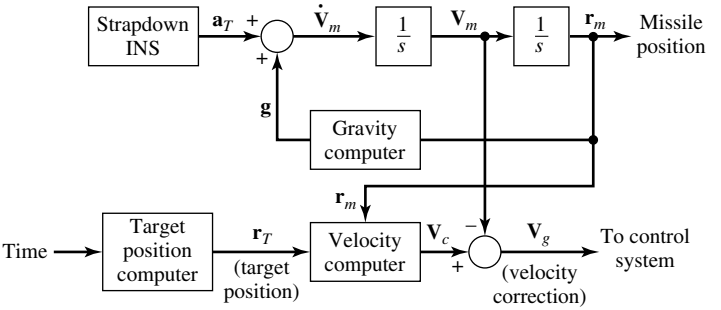

Fig. 6.23. A possible indication system.

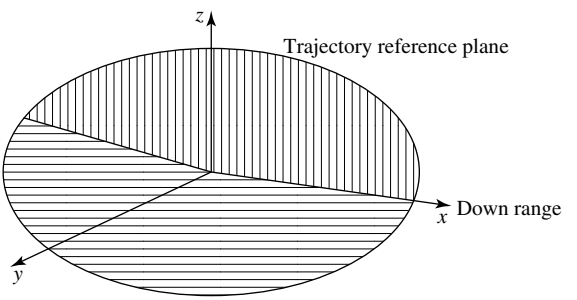

Fig. 6.24. Coordinate system.

It is possible to simplify the Q terms by making the following: assumptions

$$
\begin{aligned}
Q_{xx} &= \text{constant (a function of range)},\\
Q_{yy} &= 0 \text{ (since the } y\text{-axis is out of the trajectory plane)},\\
Q_{zx} &= \text{constant (a function of range)},\\
Q_{zz} &= Q_{xx},\\
Q_{xz} &= Q_{zx},\\
Q_{yx} &= Q_{xy} = Q_{yz} = Q_{zy} = 0.
\end{aligned}
$$

If the x-axis is mechanized to be above the horizontal in the approximate direction of the missile velocity at cut-off for maximum range, then the Q_{xx} term is the most sensitive, and not only should be a function of time explicitly, but also should be varied with deviation of the missile from the standard trajectory.

The usefulness of the Q-matrix lies in the fact that it permits the velocity-to-be-gained vector $\mathbf{V}_g$ to be expressed as the solution to the simple differential equation (6.178), that is,

$$\left(\frac{d\mathbf{V}_g}{dt}\right) = -\mathbf{a}_T - Q\mathbf{V}_g, \tag{6.178}$$

which will be derived shortly. Here, the vector $\mathbf{a}_T$ is the thrust acceleration defined previously; it represents the (vector) reading of an ideal accelerometer carried with the missile. The y-component of the product $Q\mathbf{V}_g$, for example, is the expression

$$QV_{gy} = Q_{yx}u_g + Q_{yy}v_g + Q_{yz}w_g, \tag{6.181}$$

where

$$\mathbf{V}_g = u_g\mathbf{i} + v_g\mathbf{j} + w_g\mathbf{k}. \tag{6.182}$$

Bypassing temporarily the question of mechanization of the Q-matrix, it is seen that in all other respects, the computation of $\mathbf{V}_g$ by means of (6.178) is relatively simple to instrument. Since the accelerometers give directly the time integral of $\mathbf{a}_T$, it is necessary only to determine the added contribution of the integral of $Q\mathbf{V}_g$ in order to obtain $\mathbf{V}_g$. For a typical intermediate range ballistic missile (*IRBM*), this integration may be performed by feeding back a corrective torque to the accelerometers. Therefore, the output of the accelerometers is $\mathbf{V}_g$ itself. The differential equation (6.178) lends itself to digital instrumentation. By concentrating on the direct computation of the velocity-to-be-gained, the double integration of acceleration to obtain position is avoided, as is the necessity for a **g** computer. In effect, most of the mathematical difficulties of the problem are in the determination of the Q-matrix. This is essentially a ground-based computation, however, since the resulting data can be readily approximated in a form suited to airborne instrumentation. In a sense, the computing scheme considered here suffers in presentation from the fact that the variables to be mechanized are not the familiar position and velocity of the missile with respect to some readily visualized set of coordinates. In addition, the Q-matrix, which provides the key to the system, is not a simple or readily computed expression. In fact, this scheme requires fairly elaborate precomputed data. The resultant simplicity in airborne instrumentation, however, appears to more than make up for these deficiencies.

We will now derive the fundamental equation (6.178). At a given instant of time t, let the correlated velocity vector $\mathbf{V}_c$ and the missile position vector $\mathbf{r}$ be specified. In terms of these data, the target location vector $\mathbf{r}_T$ and the time of free flight t_{ff} are uniquely determined and may be readily computed. The quantities $\mathbf{r}_T$ and t_{ff} can be expressed in the functional form

$$\mathbf{r}_T = \mathbf{r}_T(\mathbf{V}_c, \mathbf{r}), \tag{6.183}$$

$$t_{ff} = t_{ff}(\mathbf{V}_c, \mathbf{r}), \tag{6.184}$$

where it is noted that neither $\mathbf{r}_T$ nor t_{ff} depends directly upon t. Regarding $\mathbf{V}_c$ and $\mathbf{r}$ for the moment as independent variables, let independent increments $d\mathbf{V}_c$ and $d\mathbf{r}$ be applied to these variables. As a result, the quantities $\mathbf{r}_T$ and t_{ff} will experience changes given by

$$d\mathbf{r}_T = \|\partial\mathbf{r}_T/\partial\mathbf{V}_c\|d\mathbf{V}_c + \|\partial\mathbf{r}_T/\partial\mathbf{r}\|d\mathbf{r} \tag{6.185}$$

and

$$dt_{ff} = (\nabla_v t_{ff}) \cdot d\mathbf{V}_c + (\nabla_r t_{ff}) \cdot d\mathbf{r}. \tag{6.186}$$

Here, $\|\partial \mathbf{r}_T/\partial \mathbf{V}_c\|$ and $\|\partial \mathbf{r}_T/\partial \mathbf{r}\|$ are the 3×3 matrices of the partial derivatives of the components of $\mathbf{r}_T$ with respect to the components of $\mathbf{V}_c$ and of $\mathbf{r}$. Moreover, the quantities $(\nabla_v t_{ff})$ and $(\nabla_r t_{ff})$ are the gradient vectors of t_{ff} with respect to the components of $\mathbf{V}_c$ and $\mathbf{r}$. One may now ask what change in $\mathbf{V}_c$ is required, for an arbitrary differential change in $\mathbf{r}$, in order that $\mathbf{r}_T$ and t_{ff} remain unchanged. The desired relation is found by setting $d\mathbf{r}_T$ and dt_{ff} equal to zero in (6.185) and (6.186) and solving the resulting equations for the components of $d\mathbf{V}_c$ in terms of the components of $d\mathbf{r}$. It would at first appear that there are four linear equations to be solved for the three components of $d\mathbf{V}_c$ in this process. The magnitude of $\mathbf{r}_T$ is fixed, however, so that one of the three component equations in (6.185) is redundant. The resulting solution may be expressed in the symbolic form

$$d\mathbf{V}_c = \|\partial \mathbf{V}_c/\partial \mathbf{r}\|_{\mathbf{r}_T, t_{ff}} d\mathbf{r}, \tag{6.187}$$

or by comparison with the definition of (6.176), of the Q-matrix, we can write

$$d\mathbf{V}_c = Q d\mathbf{r}. \tag{6.188}$$

In other words, the Q-matrix links an arbitrary differential change in missile position to the corresponding differential change in correlated velocity required to preserve the allocation of the target and the time of free flight. The relation (6.188) could, of course, have been written more or less directly from the definition of (6.176). The intermediate operations give some clue as to how the Q-matrix can be computed in practice.

In order to derive the differential equation (6.178) for $\mathbf{V}_g$, let it now be assumed that at time t the missile is located at the point M (see Figure 6.21(b)), and that a *correlated missile* is simultaneously located at the same position. The correlated missile is assumed to move with velocity $\mathbf{V}_c$ and to be accelerated by the force of gravity only. The differential equation (6.178) is obtained by observing the changes in $\mathbf{V}_m$, $\mathbf{V}_c$, and $\mathbf{V}_g$ that occur during a small time interval Δt. It is convenient here to think of these changes as occurring in two successive steps. During the first step, the two missiles are allowed to move "naturally" for a time interval Δt, that is, under the influence of their respective velocities and accelerations. Since $\mathbf{V}_c$ and $\mathbf{V}_m$ are in general unequal, the result of the first step is a divergence in position of the two missiles (here we shall consider $\mathbf{V}_c$ and $\mathbf{V}_m$ as two missiles). In order to bring the two back into coincidence, a second step is taken in which with the time held constant, the correlated missile is realigned with the actual missile, which is held fixed during this step. Therefore, the resulting change in $\mathbf{V}_c$ is related to the corresponding positional change through the Q-matrix. A comparison of the total change in $\mathbf{V}_c$ and $\mathbf{V}_m$ for the two steps then yields the relation sought.

During the first step, the two missiles will experience change in position given by the vectors $\mathbf{V}_m \Delta t$ and $\mathbf{V}_c \Delta t$. These positional increments are shown in Figure 6.21(b) superimposed on the vectors representing the corresponding velocities. For the second step, the correlated missile is to move back into coincidence with the actual missile by giving it further positional increment as follows:

$$-\mathbf{V}_g \Delta t = \mathbf{V}_m \Delta t - \mathbf{V}_c \Delta t = d\mathbf{r}. \tag{6.189}$$

To obtain the corresponding velocity changes, it is noted that during the time interval Δt the actual missile is acted upon by the sum of the thrust acceleration vector $\mathbf{a}_T$ and gravity $\mathbf{g}$. Thus, the missile experiences a change in velocity given by

$$\Delta \mathbf{V}_m = \mathbf{a}_T \Delta t + \mathbf{g} \Delta t. \tag{6.190}$$

The corresponding change in correlated velocity is $\mathbf{g}\Delta t$ only, since the correlated missile is assumed to be in free fall. An additional change in $\mathbf{V}_c$ must be included, however, in order to accompany the displacement given by (6.189). If the target location and total time of flight are to remain fixed during this process (6.188) indicates that $\mathbf{V}_c$ must change by an amount equal to the product of the Q-matrix with the displacement (6.189). Therefore, the total change in $\mathbf{V}_c$ for the two steps is

$$\Delta \mathbf{V}_m = \mathbf{g} \Delta t + Q(-\mathbf{V}_g \Delta t). \tag{6.191}$$

The last step in the derivation consists in the computation of the change in $\mathbf{V}_g$ as the difference between $\Delta \mathbf{V}_c$ and $\Delta \mathbf{V}_m$. There results from (6.190) and (6.191) the relation

$$\mathbf{V}_g \Delta t = \Delta \mathbf{V}_c - \Delta \mathbf{V}_m = -\mathbf{a}_T \Delta t - Q \mathbf{V}_g \Delta t. \tag{6.192}$$

Dividing both sides of (6.192) by Δt yields, in the limit as $\Delta t \to 0$, the desired differential equation (6.178). The essential ingredients in this derivation are the free-fall property of $\mathbf{V}_c$ and (6.188), relating changes in $\mathbf{V}_c$ to position increments. The former property permits the cancellation of gravity in subtracting (6.190) from (6.191), while the latter allows a positional change to be translated into a corresponding change in $\mathbf{V}_g$. Any alternative definition of $\mathbf{V}_c$ that preserves these properties (with an appropriate redefinition of the Q-matrix) leaves (6.178) as a valid relation. Thus, other applications of these concepts are possible. The missile positional variation Δr_m can be approximated by

$$\Delta r_m \cong -\int_0^t \Delta \mathbf{V}_g dt. \tag{6.193}$$

In generating $\Delta \mathbf{V}_g$ to be integrated, a crude approximation to the standard time history of $\mathbf{V}_g$ can be used. Figure 6.25 illustrates the generation of $\mathbf{V}_g$.

In comparison with Figure 6.23, the above system has no gravity computation, no target position computation, and no explicit computation of the missile velocity or position or of the desired velocity. Additional integrators will be required in the $\|Q\|$ computer if position corrections are required.

In typical missile applications, the vector $Q\mathbf{V}_g$ has a magnitude less than one g at launch and decreases throughout the flight to zero at cut-off. As opposed to that, $\mathbf{a}_T$ will be greater than one g at launch, and will increase throughout each stage of the flight, usually to many g's near burnout or cut-off. Thus, $-(d\mathbf{V}_g/dt)$ is nearly equal to $\mathbf{a}_T$. This approximation becomes increasingly good toward the end of the powered flight when guidance control becomes of greatest importance. The orientation of

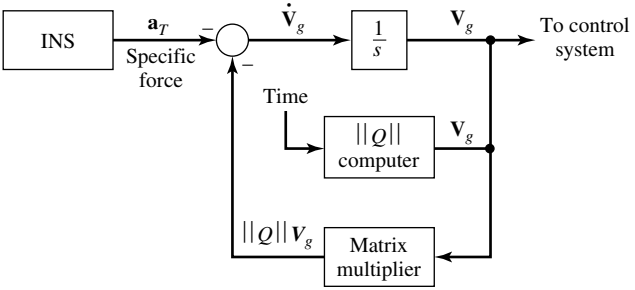

Fig. 6.25. Proposed concept for the integration of $d(\Delta \mathbf{V}_g)/dt$.

$-(d\mathbf{V}_g/dt)$ can thus be controlled by controlling the orientation of $\mathbf{a}_T$, which, especially in the latter part of powered flight when aerodynamic forces are trivial, is on average along the longitudinal axis of the missile. It is therefore clear that control over the orientation of the change of $\mathbf{V}_g$, $-(d\mathbf{V}_g/dt)$, can be exercised directly by controlling the orientation of the missile. For control purposes, $-(d\mathbf{V}_g/dt)$ can be aligned with $\mathbf{V}_g$ by commanding the missile to rotate so as to drive toward null the component of $-(d\mathbf{V}_g/dt)$ that is normal to $\mathbf{V}_g$. An indication of the component of one vector that is normal to another is given by the cross product of the two vectors. For small angles, the magnitude of the cross product of $-(d\mathbf{V}_g/dt)$ and $\mathbf{V}_g$ is proportional to the product of the magnitudes of the two vectors and the angle between them. The direction of this cross product is the axis about which $-(d\mathbf{V}_g/dt)$ must be rotated so as to turn it directly into $\mathbf{V}_g$. Thus, the cross product relation $-(d\mathbf{V}_g/dt) \times \mathbf{V}_g$ is a very useful control parameter in that it is a proportional measure of the angle that separates $-(d\mathbf{V}_g/dt)$ from $\mathbf{V}_g$ and indicates by its direction the direction of the rotation that will carry $-(d\mathbf{V}_g/dt)$ into $\mathbf{V}_g$. If the missile is commanded to take an angular velocity proportional to this control parameter, there results the familiar positional servo loop that tends to reduce the error at a rate proportional to the error.

The cross product control relation is thus stated by the vector expression

$$\omega_c = S\left[-\left(\frac{d\mathbf{V}_g}{dt}\right) \times \mathbf{V}_g\right] = S\left[\mathbf{V}_g \times \left(\frac{d\mathbf{V}_g}{dt}\right)\right], \tag{6.194}$$

where ω_c is the commanded missile angular velocity vector and S is the gain factor that sets the bandwidth of the guidance control loop. Within the accuracy of the approximation that $-(d\mathbf{V}_g/dt)$ lies along the longitudinal axis of the missile, the vector angular velocity command given by (6.194), will have zero component along the longitudinal or roll axis of the missile. In any case, only the pitch and yaw components of (6.257) would be instrumented. The roll control of the missile would consist in roll stabilization to maintain the missile axis system in proximity to the computer axis system. As mentioned above, for small angles the magnitude of the cross product of $-V_g$ and $(d\mathbf{V}_g/dt)$ is proportional to the product of the magnitudes of the two vectors and the angle between them. Another aspect to be considered is the computer coordinate system. The choice of computer axis system must be considered at this

point, since it influences the instrumentation of both the guidance control system and the Q-matrix in the target indication system. The computer axis system is the set of coordinate axes along which components of $\mathbf{V}_g$ are computed. This system may or may not coincide with the coordinate system defined by the input axes of the accelerometers. The simplest airborne computer results from computing in the same set of coordinates in which the components of $\mathbf{a}_T$ are measured. Other advantages accrue from instrumenting a matrix multiplication that transforms components of $\mathbf{a}_T$ from the accelerometer axis system into a different computer axis system. One of the most important of these is the fact that it permits a single orientation of the inertial measurement unit (*IMU*) to be used regardless of the target assignment. In either case, an orthogonal coordinate system that is nonrotating with respect to the inertial space seems appropriate.

There are two other factors to be considered in choosing the computer coordinate system. These are:

(1) The computation of command signals, such as those given by (6.194), is most simply carried out in computer coordinates, whereas, depending on the type of autopilot used, the missile may respond to commands by rotating about instantaneous missile axes. If that is the case and if a coordinate resolution between computer axes and missile axes is to be avoided, the computer axis system should be chosen so that it lies in the vicinity of the nominal missile axis system during the latter part of the powered flight. This is not a critical matter, since the commanded rates during this part of the flight are very small. Experience has shown that 20° or 30° of difference between corresponding axes in the two systems can be tolerated without noticeable difficulty.

(2) A second factor is that the azimuth orientation of the computer axis system can be chosen so that the initial $\mathbf{V}_g$ vector is contained in one of the computer coordinate planes, which we shall call the xz-plane. That is, the computer axis system can be chosen so that the initial condition on $\mathbf{V}_g$ is zero, or at least very small. In that case, $\mathbf{V}_g$ may well be maintained small throughout the flight. In fact, there is some advantage in controlling $\mathbf{V}_g$ to be null throughout the flight. For this purpose, the cross product control in yaw is not used at all; rather, a yaw rate command of the following form may be employed:

$$\frac{d\psi_c}{dt} = K_1 \mathbf{V}_g - K_2 \mathbf{a}_{Ty}, \tag{6.195}$$

where K_1 and K_2 are gain factors. This method of yaw control commands a yaw rate proportional to $\mathbf{V}_g$ in such a sense as to reduce $\mathbf{V}_g$. The purpose of the $K_2\mathbf{a}_{Ty}$ term is to provide the lead, which is required to stabilize the yaw guidance control loop.

The discussion of this section will now be summarized. At launch, initial conditions on the velocity-to-be-gained, bias, and the Q-matrix are placed into the guidance computer. From the instant of engine ignition to the initial pitchover, the command rates include $\mathbf{V}_g$ feedback, and the bias remains constant. At initiation of pitchover, the bias decreases stepwise and begins to decay exponentially. At this time, the missile

begins to pitch over. Moreover, at initiation of pitchover, lead is supplied by feedback of lateral acceleration instead of by the corresponding components of velocity-to-be-gained. The pitchover continues until a time before staging (assuming at least a two-stage missile) when the bias is reversed and/or the integrator gain is decreased slowly. After staging, the bias integrator gain continues to run to zero. After both these quantities are forced to zero, the vehicle flies a constant attitude trajectory until the burnout or cutoff condition is fulfilled. Some of the important features of the system developed in this section are:

1. The same control law and configuration can be used throughout the entire flight.
2. Attitude information is never needed explicitly; velocity is sufficient.
3. Control is exerted over velocity-to-be-gained throughout the flight.
4. Because of the Coriolis correction to velocity-to-be-gained, frame rotation is inherent in the guidance scheme.
5. The control scheme with no alteration will cause the vehicle to seek the vertical until the initiation of pitchover.
6. The bias generation is simple.
7. For some missiles, the performance of the uncompensated system becomes marginal in the presence of strong winds.
8. The proper set of initial conditions must come from outside the guidance-control package. This problem is easily solved by using a transformation computer to resolve external information into the body axis system.
9. The proper set of initial conditions must come from outside the guidance control package. This problem can be solved by using a transformation computer to resolve the external information into the body-axis system.

6.5.3 The Missile Control System

Ballistic missiles with thrust magnitude control, that is, missile engines whose thrust can be controlled, have more flexibility than those without magnitude control. By controlling the direction (i.e., steering) and the magnitude (i.e., throttling) of the thrust it is possible to match the stored profiles to an arbitrary degree, depending only on the response of the control system. Therefore, missiles with this type of control can be made to fly an exact nominal trajectory and hence can be made to burn out at a specified position, velocity, and time. The guidance computations in this case can be greatly simplified, since it is necessary only to measure the three components of thrust acceleration and to compare them or their integrals with the nominal profiles that have been stored as functions of time in the airborne computer.

There are two basic requirements that must be satisfied by the steering control system of a ballistic missile. The control system must:

1. satisfactorily control the missile during the highly critical period of high aerodynamic pressure that occurs as the missile climbs out of the atmosphere at high velocity, and
2. steer the missile to the proper cutoff condition, that is, $\mathbf{V}_g = 0$ (see Section 6.5.2).

A common solution to this dual requirement is to ignore the second problem, concentrating on the accomplishment of the ascent trajectory until the missile is out of aerodynamic danger, and then switching to another control mode for the achievement of proper terminal conditions.

For the accomplishment of the ascent trajectory, one might employ a precomputed pitch time history, which has the desirable characteristics of low angle of attack (*AOA*) during high aerodynamic pressure. For a nonperturbed ascent trajectory, that is, a trajectory that results from standard predicted values of missile thrust, weight, lift, and drag, and that experiences no wind velocity, the standard pitch program produces standard time histories of missile position and velocity as a function of time. For a perturbed missile, however, nonstandard time histories of missile velocity and position occur along each coordinate of the guidance package. That is, V_{mx}, V_{my}, and V_{mz} exhibit nonstandard time histories in the presence of missile perturbations, although the pitch and yaw angles of the missile remain essentially unperturbed because they are controlled by feedback principles. Instead of controlling the yaw angle to zero, it seems natural to control the Y velocity-to-be-gained, V_{gy}, to zero (see Section 6.5.2). In other words, instead of feeding back a signal proportional to deviations in missile yaw angle, the signal to be controlled would be V_{gy}. Then, in the presence of thrust perturbations and winds, Y velocity-to-be-gained remains nulled, while of course, missile yaw angle adjusts itself to achieve this condition.

Programmed pitch control and/or velocity steering have been the customary choices for control of a rocket vehicle during exit from the atmosphere. Commonly, steering is effected by pitch and yaw commands determined from the gravity-free accelerations and velocities-to-be-gained. Therefore, one way to control the missile is to develop a steering law, based upon velocity in missile body coordinates. In particular, it would appear that the only body velocity parameter convenient for steering is the body coordinate velocity-to-be-gained. Although this choice provides a means for meeting the specification on control of velocity-to-be-gained, it also forces the exit trajectory to be subject to the variations in velocity-to-go caused by variation of target locations. This limitation, however, can be erased by commanding the pitch rate to be proportional to the difference between velocity-to-go and a time-varying bias instead of basing the command rate solely on velocity-to-be-gained. The result is a control law of the form

$$\boldsymbol{\omega}_c = \mathbf{1}_x \times K(\mathbf{V}_g - \mathbf{B}), \tag{6.196}$$

where

$\boldsymbol{\omega}_c$ = commanded angular velocity vector of the missile,
$\mathbf{V}_g$ = velocity-to-be-gained resolved in body coordinates,
$\mathbf{B}$ = control bias,
K = control gain,
$\mathbf{1}_x$ = unit vector along the body x (or roll) axis.

The bias $\mathbf{B}$ is readily adjusted to account for variations in target and launch point parameters. It can also be shown that the bias is an exponential function of time

during the atmospheric phase of the flight. Thus, it is simple to generate in a guidance computer. By forcing the bias to zero after atmospheric exit, the control acts to null $\mathbf{V}_g$; thus, the same system configuration can be used throughout the powered flight. The analysis to follow will show that for stability purposes, it is necessary to add a lead term to the control law of (6.196). There are various ways to accomplish this, so we will select to use the lateral body acceleration. The control equation is

$$\boldsymbol{\omega}_c = \mathbf{1}_x \times \left[K_1(\mathbf{V}_g - \mathbf{B}) - K_2 \left\{ \left(\frac{d\mathbf{V}_g}{dt} \right) - \left(\frac{d\mathbf{B}}{dt} \right) \right\} \right],$$

or

$$\boldsymbol{\omega}_c = \mathbf{1}_x \times [K_1(\mathbf{V}_g - \mathbf{B}) - K_2 \mathbf{a}_B]. \tag{6.197}$$

Since the system accuracy could be degraded by a rollout maneuver at launch, the roll angle should be held at its initial value throughout the flight. In general, this will require both pitch and yaw rate commands in order to remain in the target plane. Assuming no axis coupling, the result is that (6.197) will have two components:

$$\frac{d\theta_c}{dt} = -K_1(V_{gz} - B_z) + K_2 a_{Bz}, \tag{6.198}$$

$$\frac{d\psi_c}{dt} = K_1(V_{gy} - B_y) + K_2 a_{By}. \tag{6.199}$$

The constants K_1 and K_2 in (6.198) and (6.199) are positive numbers, and the signs preceding them are chosen on the basis of the following stability considerations. It should be noted here that if acceleration occurs along the positive Z-body axis due to a disturbance force at the center of pressure, a negative-pitch angular acceleration will result. To counteract this undesirable effect, a positive pitch rate must be commanded, hence the choice of the positive sign preceding K_2 in (6.198).

In pitch, the problem is more difficult. To try to null the Z-velocity immediately would cause the missile to pitch over upon leaving the launch pad to an angle where there was no output from the Z-accelerometer. Of course, a Z-velocity programmer could also be used. However, a new approach to the problem of controlling Z-velocity appears to have great advantage over a Z-velocity programmer. This method of control, called "Z-velocity steering," uses the empirical observation that the characteristic time history of Z-velocity during a desirable ascent trajectory can be very closely approximated by an exponential function of time. Because of this, it was found that excellent ascent trajectories could be generated by commanding Z-velocity from its zero value at launch to some final (negative) value. By controlling the time constant of the closed loop that drives Z-velocity to its final value, the desired exponential time history in velocity corresponding to a desirable ascent through the atmosphere can be generated. The equation that accomplishes this characteristic is very simple. An error signal, that is, a pitch command θ_c that is to be integrated and fed to a missile autopilot that controls missile pitch attitude, can be constructed as follows [14]:

$$\frac{d\theta_c}{dt} = K(V_{Zc} - [\tau A_{TZ} + V_Z]), \tag{6.200}$$

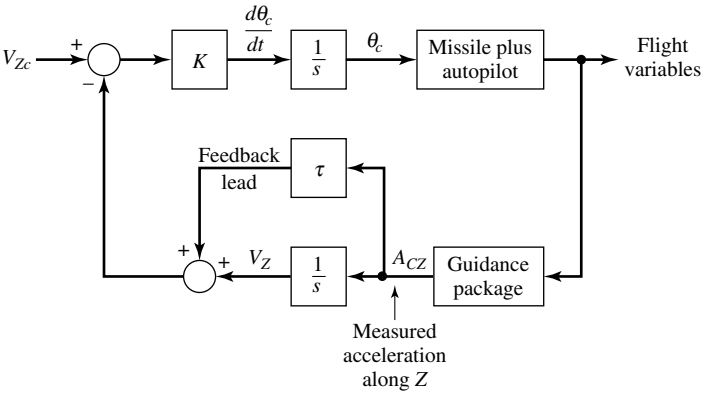

Fig. 6.26. Z-velocity steering block diagram.

where K is a gain, V_{Zc} is the commanded missile Z-velocity, A_{TZ} is the specific force acting in the Z-direction, and V_Z is the component of velocity in the Z-direction. The number τA_{TZ} must be of equal and opposite magnitude to V_Z at launch, in order that no pitch rate command occur; this condition is necessary, since the missile must leave the launch pad (or site) vertically. Finally, Z-velocity steering can therefore not only accomplish the task of guiding the missile out of the atmosphere, but can be used for the entire trajectory. Figure 6.26 presents in block diagram form a possible concept for Z-velocity steering.

Let us now return to the pitch rate command equation, (6.200). Since V_Z is the integral of A_{TZ} with a zero initial condition at launch, this equation may be simplified as follows:

$$\frac{d\theta_c}{dt} = -K[\tau A_{TZ} + V_Z], \tag{6.201}$$

where V_{Zc}, the commanded final missile Z-velocity, to be approached exponentially at the time constant of the control loop, is eliminated from the control equation by placing a bogus initial condition on V_Z at launch, equal to the negative of V_{Zc}. The time constant τ and the initial value of V_Z are used to design the ascent trajectory. In practice, however, it is probably desirable not to begin the Z-velocity steering mode until a few seconds after launch, because of this critical balance requirement on Z-acceleration at the time of launch. Figure 6.27 illustrates the characteristics of this same control concept.

Next, we must consider the problem of stability. For stability purposes, a rate autopilot, utilizing feedback of rate information, is necessary. If the dynamics of the thrust deflection mechanism are considered negligible compared to the fastest mode in the system, the pitch autopilot may be described as follows:

$$\frac{d\theta}{dt} = K_T \left[\left(\frac{d\theta_c}{dt} \right) - \left(\frac{d\theta}{dt} \right) \right], \tag{6.202}$$

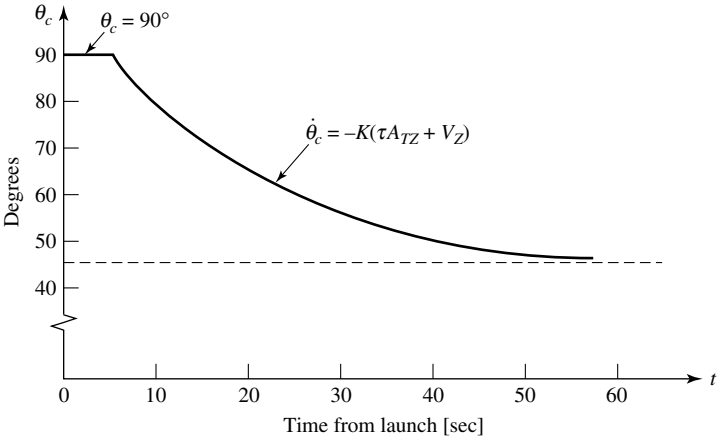

Fig. 6.27. Command pitch angle, generated by Z-velocity steering equations.

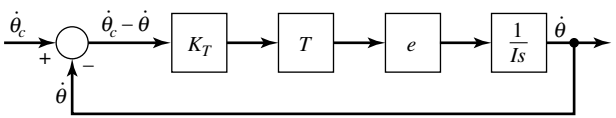

Fig. 6.28. Autopilot loop.

where K_T is the autopilot constant, $d\theta_c/dt$ is the commanded pitch rate, and $d\theta/dt$ is the pitch rate. If system stability requirements are satisfied by adjustment of other system parameters, it is possible to select the gain K_T of the autopilot loop from bandwidth considerations alone. The autopilot should have a small response time so that the system can recover quickly from perturbations and then respond to commands. This requirement can be met by making the bandwidth of the loop as large as possible.

Structural considerations require that the missile control system not excite any of the vehicle bending modes. If the bandwidth of the autopilot (i.e., the widest bandwidth loop) is sufficiently below the first bending frequency of the structure, the control system acts like a low-pass filter, and thus attenuates oscillations that would damage the vehicle. An alternative approach is to include a notch filter in the control loop in order to filter out the harmful frequencies. As a result, it is then possible to obtain a wider autopilot bandwidth. This preliminary design will proceed under the assumption that suitable system performance will be obtainable with the narrower bandwidth autopilot. Figure 6.28 illustrates this autopilot loop.

With reference to Figure 6.28, one may write the following approximate expression for the autopilot bandwidth, BW_{AP}:

$$BW_{AP} = K_T eT/I, \tag{6.203a}$$

where I is the moment of inertia and e is a stability loop parameter. Using (6.202), we can write the following equation:

$$Is\left(\frac{d\theta}{dt}\right) = K_T T e\left[\left(\frac{d\theta_c}{dt}\right) - \left(\frac{d\theta}{dt}\right)\right] = K_T T e\left(\frac{d\theta_c}{dt}\right) - K_T T e\left(\frac{d\theta}{dt}\right). \tag{6.203b}$$

Therefore,

$$\left(\frac{d\theta}{dt}\right) \Big/ \left(\frac{d\theta_c}{dt}\right) = K_T T e/(Is + K_T T e) = 1/[1 + (I/K_T T e)s], \tag{6.203c}$$

or, making use of (6.203a), we obtain

$$\left(\frac{d\theta}{dt}\right) \Big/ \left(\frac{d\theta_c}{dt}\right) = 1/[1 + (s/BW)]. \tag{6.203d}$$

An approximate value for K_T lies in the range between 0.3 and 0.5 seconds.

6.5.4 Control During the Atmospheric Phase

The powered phase of a ballistic missile is the most complex, because of the exit through the atmosphere. The trajectory begins with the missile rising vertically for a few seconds. During this time, it is usually rolled to the proper heading. Subsequently, the vehicle executes its pitch maneuver (see also Section 6.5.3). After a short transient, called transition turn, a gravity or zero lift turn (the concept of *gravity turn* will be discussed shortly) begins and continues until the missile has effectively left the atmosphere [9], [18]. After leaving the atmosphere, structural constraints can be relaxed, and a more arbitrary attitude profile can be prescribed. In Section 6.5.2 we discussed the controlling of the $\mathbf{V}_{gy}$ component of the velocity-to-be-gained vector. The null $\mathbf{V}_{gy}$ control in yaw can be initiated shortly after launch (i.e., as soon as the missile has been rolled so that its y-axis is roughly normal to the computer xz-plane) and continued without change throughout the flight. Unfortunately, the same is not true of pitch guidance control. Cross product control in pitch rotates the missile so that it lines up essentially with $\mathbf{V}_g$. If this is done too early in the flight, the missile follows an inefficiently low trajectory through the atmosphere. Therefore, guidance control in pitch is normally delayed until the missile is above the sensible atmosphere. It would be possible to instrument a more complicated pitch guidance control method that could be used throughout the flight, but such a method must be developed that would have an advantage over the use of a separate control method for the atmospheric exit trajectory. This exit phase control can be just an open loop pitch program, or it can be a simple closed loop path control system.

Studies of the atmosphere indicate that the most serious wind disturbance a missile is likely to encounter during exit is in the form of horizontal shear winds. The effect of these winds upon the missile may be linearly approximated as a ramp increase in wind velocity $V_{\omega z}$, that is, the component of the wind along the vertical z-axis. From the above discussion, we note that during the atmospheric exit phase, the steering of

the missile is mostly open loop; that is, $\mathbf{V}_g$ is not used explicitly to control the flight path. While the missile climbs through the sensible atmosphere, it experiences, among other forces, atmospheric drag acceleration. Atmospheric drag acceleration will be a function of flight altitude, flight speed, and a ballistic parameter of the specific vehicle. The drag force is given by the expression [4]

$$D = \tfrac{1}{2} C_D S \rho V^2 = (W/g) a_D, \tag{6.204a}$$

where

C_D = the drag coefficient,
a_D = drag acceleration [ft/sec^2],
S = frontal area of the missile [ft^2],
ρ = atmospheric density [slugs/ft^3],
V = velocity of the missile [ft/sec],
W = weight of the missile [lbs],
g = gravitational acceleration.

Therefore, the density of the atmosphere is a function of altitude. Rearranging the terms of (6.204a) shows that the drag acceleration can be given by

$$a_D = \tfrac{1}{2} [C_D S / W] V^2 \rho g. \tag{6.204b}$$

Note that the short-term effects of atmospheric drag are negligible at altitudes greater than approximately 150 nm. At altitudes around 100 nm, there will be a noticeable drag perturbation in orbits less than one revolution.

We will now discuss the concept of the *gravity turn*. The gravity turn is accomplished by causing the missile to thrust always along its velocity vector, thus minimizing drag effects, aerodynamic heating, and structural loading. The gravity turn is usually continued to some staging point, although this is not always the case, particularly when there is only a single stage. After thrust has been terminated, the vehicle begins its free flight, during which gravity is the only acting force. As discussed in Section 6.4, the free-flight trajectory lies completely within a plane that contains the center of the Earth, and it will be in the shape of a conic (i.e., either an ellipse, a parabola, or a hyperbola), depending on the velocity's being below or above escape velocity, the parabola being the limiting case. In the case of a ballistic missile, the ellipse intersects the Earth at the target. However, it should be noted that the Earth's oblateness causes the trajectory to be nonplanar and to differ slightly from a true ellipse (see Section 6.4.2.1).

To summarize the above discussion, the missile is steered through the atmosphere such that a gravity turn is followed. This pitch profile is alternately referred to as either a zero-lift or a zero angle-of-attack pitch program. This program is utilized in order to prevent breakage of the missile as a result of aerodynamic forces. As in Chapter 3, let the aerodynamic forces be referred to as drag **D**, and lift **L**. The drag force is directed along the roll axis, while the lift force acts normal to the missile

axis. The forces acting on the missile for flight through the atmosphere are shown in Figure 6.29. The point of application of the resultant aerodynamic force is referred to as the center of pressure (cp). The forces $\mathbf{L}$ and $\mathbf{D}$ acting at the cp are defined as

$$\mathbf{D} = -D\hat{\xi}, \tag{6.205a}$$

$$\mathbf{L} = (L/V_A)\hat{\xi} \times (\mathbf{V}_A \times \hat{\xi}), \tag{6.205b}$$

where

$$\begin{aligned}
D &= C_D S q, \\
L &= C_N(\alpha) S q, \\
\hat{\xi} &= \text{a unit vector tangent to the flight path, or direction of missile roll axis,} \\
\mathbf{V}_A &= \text{velocity of the missile with respect to the air mass,} \\
V_A &= \text{magnitude of } \mathbf{V}_A, \\
S &= \text{effective (or frontal) missile area,} \\
q &= \tfrac{1}{2}\rho V_A^2 = \text{dynamic pressure,} \\
C_D &= \text{zero-lift drag coefficient,} \\
C_N(\alpha) &= \text{coefficient of lift,} \\
\alpha &= \text{angle of attack}(V_A \cos\alpha = \mathbf{V}_A \cdot \hat{\xi}), \\
\delta &= \text{thrust deflection angle.}
\end{aligned}$$

Note that by definition, the drag force (6.205a) acts opposite to the velocity vector. The drag and lift forces are sometimes defined as acting along and normal to $\mathbf{V}_A$, rather than $\hat{\xi}$. When actual data are used, care must be taken to ensure that the definitions are consistent with the data. The axial strength of the missile is greater than the transverse strength. Hence, the normal forces (lift) must be minimized for flight through the atmosphere. Otherwise, the aerodynamic lift forces would produce bending moments that could break the long, slender missile.

Note also that when $\mathbf{L} \neq 0$, it is necessary to choose the engine thrust direction $\hat{\delta}$ to prevent the missile from rotating. The aerodynamic pitching moment is canceled by choosing

$$\mathbf{L}d = \hat{\xi} \times (\hat{\delta} \times \hat{\xi}) lT = [\hat{\delta} - \hat{\xi}(\hat{\xi} \cdot \hat{\delta})] Tl, \tag{6.206}$$

where

$$\begin{aligned}
d &= \text{distance between the } cg \text{ and the } cp, \\
l &= \text{distance between the } cg \text{ and the engine gimbal angle,} \\
T &= \text{engine thrust.}
\end{aligned}$$

When a zero-lift pitch program is not followed, the energy, required to cancel the pitching moment is wasted. Some of this wasted energy is converted to heat energy, resulting in weakening of the missile structure. Furthermore, note that $\mathbf{L}$ can be made to vanish by choosing

$$\hat{\xi} = \mathbf{V}_A / V_A. \tag{6.207}$$

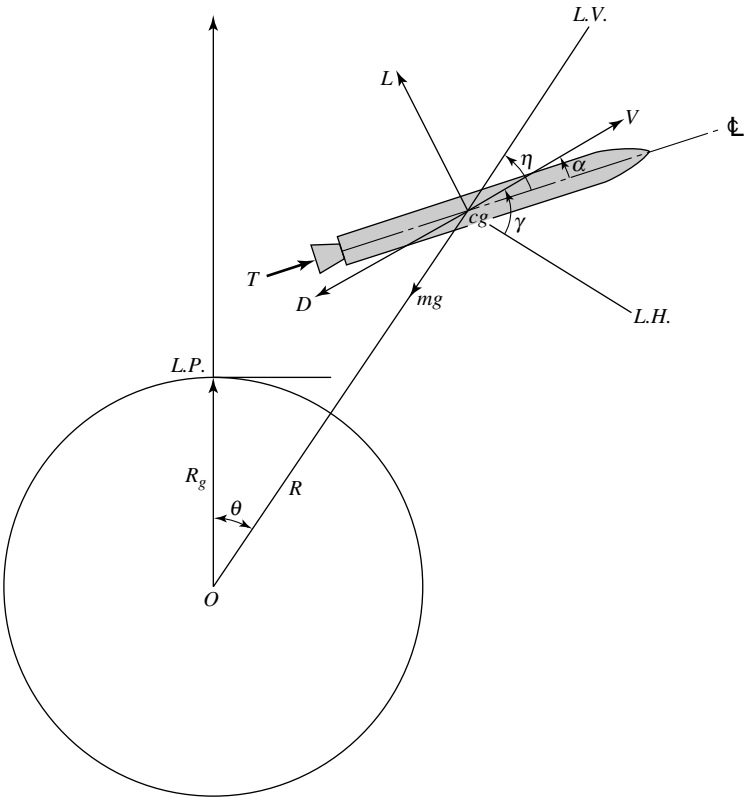

Fig. 6.29. Forces acting on a ballistic missile during flight through the atmosphere.

The quantity $\mathbf{V}_A$ is calculated as

$$\mathbf{V}_A = \left(\frac{d\mathbf{R}}{dt}\right) - \Omega_e \times \mathbf{R} + \mathbf{W}, \tag{6.208}$$

where

$\left(\frac{d\mathbf{R}}{dt}\right)$ = velocity of the missile with respect to inertial space,

$\mathbf{R}$ = missile position vector with respect to the Earth,

Ω_e = angular velocity of the Earth,

$\mathbf{W}$ = wind velocity with respect to the Earth (normally a negligible quantity).

Consequently, the missile will fly a gravity turn when (6.207) is satisfied. All the quantities required to determine the direction of $\mathbf{V}_A$ are usually calculated in standard missile simulations. Therefore, the thrust attitude $\hat{\delta}$ may be commanded as

$$\hat{\delta} = \mathbf{V}_A / V_A. \tag{6.209}$$

When a unity control system (i.e., equivalent to a point mass missile) is assumed, it follows that $\hat{\delta} = \hat{\xi}$.

Note that when a simulation is performed, the simulation will calculate the missile angular velocity $\boldsymbol{\omega} = \hat{\xi} \times (d\hat{\xi}/dt)$. This quantity may be approximated with simple functions and incorporated in a missile pitch programmer. Steering commands from the missile programmer then cause the missile to pitch over to approximate the desired gravity turn. Furthermore, note that when $\mathbf{W} \approx 0$, the initial value of $\hat{\xi} = \hat{\delta}$ is arbitrary. When the initial value $\hat{\xi} = \hat{\xi}_o$ is chosen, the resulting gravity turn is specified. In general, it is necessary to make several flights using different values for $\hat{\xi}_o$, in order to obtain the desired end conditions. These variations can be made even when $\mathbf{W} \neq 0$, since wind velocities are normally small enough to be neglected.

6.5.5 Guidance Techniques

As discussed in Section 6.5.3, the function of a ballistic missile's guidance system is to generate a sequence of command signals that will steer the vehicle and terminate its thrust in such a way that the intended mission is accomplished and all of the guidance constraints are satisfied. Once the guidance system has selected a course and calculated the initial conditions that will place the missile on this course, it is up to the flight control and propulsion systems to obtain these initial conditions with sufficient accuracy. Control errors arise through the inability of the guidance system to determine exactly when the desired position and velocity have been obtained, and to errors and dispersions in executing guidance commands. Ordinarily, the vehicle must rely solely on inertial information during the thrusting period, so that the error at cut-off is a function of the inertial system errors, cut-off control errors, and the position and velocity errors at the beginning of the thrust period. The total burnout error then propagates as a perturbation of the true path with respect to the trajectory computed in the missile, and may be evaluated at any point along the trajectory to the first order.

There are several guidance techniques of various degrees of difficulty available to the missile designer. Three of the more common types are [9]:

(1) explicit guidance,
(2) implicit guidance, and
(3) delta guidance.

These techniques are based, to some extent, on the correlated (or, required) velocity concept. These methods, as mentioned above, differ in the degree of complexity of the in-flight computations and the amount of preflight targeting or precomputation required.

Explicit Guidance: Explicit guidance is a generic term for the system of guidance equations that result from a direct solution of the equations of motion for the free-flight trajectory of a vehicle subject to specified boundary conditions. This boundary value problem may be considered a generalization of Lambert's theorem, which as we have seen, expresses the relationship for the conic path passing through the radius vector $\mathbf{r}_o$ at time t_o, and radius vector $\mathbf{r}$ at time t, for Keplerian elliptic motion.

Specifically, explicit guidance requires determination of a velocity vector at a given initial point in a simple central gravity field such that free fall to a given second point (e.g., the target) occurs in a specified interval of time. The time of flight constraint is necessitated by motion of the target. Many solutions to this problem exist. For example, there is a family of correlated velocity vectors, each of which can cause a vehicle at the initial point (e.g., engine burnout) to follow a corresponding correlated orbit through the given subsequent point. The additional constraint of time of flight is satisfied by only one of this family of velocities, or equivalently, by only one correlated orbit. The explicit guidance equations (see Sections 6.2, 6.3, and 6.4) include an accurate representation of the vehicle's environment commensurate with the mission requirements. Some of the more practical non-Keplerian effects one must examine to determine accurate ballistic missile trajectories are:

1. atmospheric forces,
2. the latitude and longitude-dependent terms necessary to describe the Earth's gravitational field,
3. local gravitational anomalies,
4. the Sun's and Moon's gravitational fields.

The only inputs required by the guidance equations are latitude, longitude, and altitude of the launch and target points and a time of flight consistent with the vehicle's propulsion capabilities. Furthermore, the guidance equations permit computation of the required quantities for the autopilot, which in turn steers the vehicle to the proper burnout conditions. Once the guidance inputs have been specified, the launch azimuth may be implemented, and no other delay is required for proper launching of the vehicle. This technique is particularly suitable for systems requiring maximum flexibility, since no prelaunch (or at least a minimum) computation or targeting is required. (Note that the time necessary to compute the launch azimuth is negligible.) In addition, the requirement of a nominal trajectory may be eliminated as a result of the complete generality and self-containment of the explicit guidance equations, but with an increase in the complexity of the mechanization of the required equations.

In the explicit guidance law, the launch portion of the trajectory is divided about equally in time into an open-loop and closed-loop phase. The open-loop phase is preprogrammed and consists of a vertical liftoff followed by a gravity turn to an approximate flight angle γ. The closed-loop phase, or guidance phase, is characterized by the computation of steering commands from the vehicle's actual location $\mathbf{r}_T$, the desired range angle, and the time-of-flight T. Moreover, the closed-loop phase of the launch trajectory is partitioned into a discrete set of control points $(t_1, t_2, \ldots, t_k, \ldots, t_{bo})$. The time duration between two neighboring points in this set is regulated by the time required for each computation cycle, which in turn produces a steering command and/or a cut-off signal. The terminal point (i.e., terminal conditions in this case) is described simply as the total range angle Λ (see Figure 6.1) and the total time of flight T, as given by (6.50) or (6.92).

Now by comparing the best estimate of the actual missile velocity $\mathbf{V}_m(t_k)$ to $\mathbf{V}_c(t_k)$, the velocity-to-be-gained vector $\mathbf{V}(t_k)$ is generated. Thus,

$$\mathbf{V}_g(t_k) = \mathbf{V}_c(t_k) - \mathbf{V}_m(t_k). \tag{6.170}$$

A simple steering philosophy is now apparent:

$$\mathbf{a}_e = \mathbf{a}_T + \mathbf{g},$$

where

$$\begin{aligned} \mathbf{a}_e &= \text{effective thrust acceleration,} \\ \mathbf{a}_T &= \text{actual thrust acceleration,} \\ \mathbf{g} &= \text{gravitational acceleration at } \mathbf{r}(t_k). \end{aligned}$$

The steering philosophy is to align the effective thrust acceleration vector with $\mathbf{V}_g$; thus

$$\mathbf{a}_e = k\mathbf{V}_g,$$

where k is an arbitrary constant. Thus, using the above relations results in

$$\mathbf{a}_T = k(\mathbf{V}_c(t_k) - \mathbf{V}_m(t_k)) - \mathbf{g},$$

as the steering law. The cut-off command is initiated when $\|\mathbf{V}_g\| = 0$. Thus, at burnout point the missile will continue on an unpowered trajectory to the terminal point. The following algorithm summarizes the computation cycle using the explicit guidance law:

(a) Measurement and generation of the best estimate of the vehicle's state at each control point $t_k(t_1, t_2, \ldots, t_k, \ldots t_{bo})$.
(b) Compute a unique velocity vector $\mathbf{V}_c$ to intersect the terminal point at the specified time. Compute the local gravitational acceleration $\mathbf{g}$, where $\mathbf{g} = -(\mu/r^3)\mathbf{r}$.
(c) Compare the calculated velocity $\mathbf{V}_c$ to the actual velocity of the missile $\mathbf{V}_m$ to produce $\mathbf{V}_g$.
(d) Produce the steering command $\mathbf{u} = (u_1, u_2)$ on the basis of $\mathbf{a}_T = k(\mathbf{V}_c - \mathbf{V}_m) - \mathbf{g}$, where:
    (1) u_1 is the angle of the thrust vector $\mathbf{a}_T$.
    (2) u_2 is t_{bo} or t such that $\|\mathbf{V}_g\| = 0$.

This algorithm, in general, requires the solution of a highly nonlinear set of differential equations at each control point for a rather simple description of the terminal conditions. If this computation is accomplished in an onboard computer, the computation cycle is usually long and complicated, since a closed-form solution of the equations of motion is not usually possible.

In summary, the explicit guidance philosophy requires the existence of closed-form or approximate closed-form guidance equations describing a set of general

terminal conditions in terms of current control and state variables such that an explicit value of control can be computed at every admissible $x \in E^n$. These guidance equations usually take the form of polynomials that are generated for each particular application. This implies that the desired terminal conditions can be easily varied or modified before actual guidance is initiated or even modified to some degree during the guidance phase.

Explicit guidance is also well suited to a mobile launcher. In this case, the missile designer wants to have the capability of being able to launch the vehicle at any geographical location and at any time. Within certain mission bounds, this type of system requirement can readily be met using an explicit guidance method.

Implicit Guidance: The implicit guidance concept tacitly assumes that the mission is completely defined before launch, that a nominal trajectory is available, and that deviations from the reference trajectory will be small, so that linear theory can be employed to generate the steering commands to fulfill the mission. The implicit guidance technique is extremely simple, since most of the difficult computations can be made before the mission on a large ground-based computer. By its very nature, the implicit guidance concept is not as flexible in modifying terminal conditions as the explicit form. This is true because this method requires large amounts of precomputed data for each set of terminal conditions. More specifically, the computation cycle of an implicit guidance law is based on a first-order expansion about each control point of the guidance phase of the launch trajectory. The terminal point is described by a reference or nominal trajectory $\mathbf{x}^*(t)$, a reference control $\mathbf{u}^*(t)$, and the partial derivatives of the control with respect to state variables in the interval $t_1 \leq t \leq t_{bo}$. As such, the terminal point is stored in many more memory locations of the computer (one set for each control point); the prelaunch computation that generates this terminal point description reduces substantially the onboard computation required. As long as the actual trajectory remains relatively close to the nominal trajectory (i.e., a few miles), the first-order terms will produce a computer velocity vector $\mathbf{V}_c$ on the basis of the control vector on the nominal trajectory $\mathbf{u}^*(t)$ and the corrected value of the control, $\delta\mathbf{u}(t)(\mathbf{u}^*(t) + \delta\mathbf{u}(t) = \mathbf{u}(t))$. The algorithm for the computational cycle of the implicit guidance law is as follows:

(a) Measurement and generation of the best estimate of the vehicle's state $\mathbf{x}(t)$ at each control point.
(b) Compare actual state $\mathbf{r}(t)$ to the nominal state $\mathbf{r}^*(t)$ to produce positional error state, $\delta\mathbf{r}(t)$. That is, $\delta\mathbf{r}(t) = \mathbf{r}(t) - \mathbf{r}^*(t)$.
(c) Computation of the desired velocity vector variation $\delta\mathbf{V}(t)$ to compensate for a deviation from the nominal state.
(d) Update the nominal velocity vector $\mathbf{V}^*(t)$ to produce a desired velocity vector $\mathbf{V}_c(t)$, $\mathbf{V}_c(t) = \mathbf{V}^*(t) + \delta\mathbf{V}(t)$.
(e) Compute cut-off signal and steering command from $\mathbf{V}_g(t)$.

This algorithm is not as flexible as the explicit guidance law; it is restricted in the number of terminal points by the capacity of the airborne computer memory.

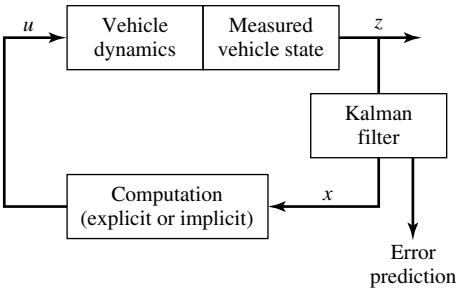

Fig. 6.30. Explicit and implicit guidance laws.

The computer program of this algorithm is also less complex, since much of the computation is accomplished before launch.

Figure 6.30 presents a simple block diagram of the explicit and implicit guidance laws.

Note that here we define a guidance law as the measurement, computation, and control synthesis required to place a space vehicle at designated terminal conditions. The measurement **z** is processed through a linear filter (estimator) to provide the best estimate of the actual position and velocity of a vehicle (i.e., vehicle's state **x**) with respect to some reference coordinate system. The computational procedure consists of the mathematical processing of internal stored information describing the desired terminal point with the measured data to generate or synthesize a control signal **u** acceptable to the control system. The mechanization of the computational block of Figure 6.30 can be accomplished in two ways, thus dividing current guidance laws into explicit and implicit philosophies. Moreover, the form in which the terminal point is stored within the computer represents the basic difference between these two philosophies. For more details on the control aspects of guidance, see Section 4.8.

Delta Guidance: As stated above, the explicit guidance equations are more complicated from the standpoint of the airborne guidance mechanization, but require a minimum of precomputation (i.e., targeting). On the other hand, the delta guidance technique requirements are the reverse of those of the explicit guidance. Specifically, the delta guidance equations are developed in terms of a power series expansion about a nominal trajectory.

In Sections 6.4.2 and 6.5 we noted that the required or correlated velocity vector $\mathbf{V}_R$ consists of two or three components. Consequently, for the general three-component case, each component, that is, each of V_{Rx}, V_{Ry}, and V_{Rz}, is a function of the four variables x, y, z, and t. Thus, they are also implicit functions of the guidance constraints themselves.

The delta guidance equations are commonly developed in terms of a power series expansion about the nominal trajectory. In essence, coefficients must be determined for each expansion point selected, and the three expansions or components of $\mathbf{V}(\mathbf{R}, t)$, that is, V_{Rx}, V_{Ry}, and V_{Rz}, would be time varying. Consider the expansion point to

be the nominal burnout point (x_o, y_o, z_o, t). We can write three expansions similar to V_{Rx} as [9]

$$V_{Rx} = \alpha_{00} + \alpha_{10}\Delta x + \alpha_{20}\Delta y + \alpha_{30}\Delta z + \alpha_{40}\Delta t + \alpha_{11}\Delta x^2 + \alpha_{12}\Delta x\Delta y + \cdots + \alpha_{44}\Delta t^2, \tag{6.210}$$

where $\alpha_{00} = V_{Rxo}$, that is, α_{00} is the nominal value of the x-component of the burnout velocity vector, and $\Delta x = (x - x_o)$, $\Delta y = (y - y_o)$, etc., are the delta quantities that give the equations their name. Similar expressions are obtained for V_{Ry} and V_{Rz}. The coefficients α_{ij} are guidance constants that must be determined. More specifically, the α_{ij} are partial derivatives given as

$$\alpha_{10} = (\partial\dot{x}/\partial x)|_{burnout}, \tag{6.211a}$$

$$\alpha_{12} = (\partial^2\dot{x}/\partial x\partial y)|_{burnout}. \tag{6.211b}$$

(Note that in terms of x, y, z, the coefficients of α_{ij} correspond to $\alpha_{10} = \alpha_{xx}$, $\alpha_{20} = \alpha_{xy}$, $\alpha_{30} = \alpha_{xz}$, $\alpha_{40} = \alpha_{xt}$, $\alpha_{11} = \alpha_{xxx}$, $\alpha_{12} = \alpha_{xxy}$, etc.) The partial derivatives are defined in terms of a two-dimensional (or more variables) Taylor series as follows:

$$f(x, y) = f(a, b) + \frac{\partial f(a, b)}{\partial x}(x - a) + \frac{\partial f(a, b)}{\partial y}(x - b) + \frac{1}{2!}\left[\frac{\partial^2 f(a, b)}{\partial^2 x}(x - a)^2 + 2\frac{\partial^2 f(a, b)}{\partial x\partial y}(x - a)(y - b) + \frac{\partial^2 f(a, b)}{\partial^2 y}(y - b)^2\right] + \ldots,$$

where x and y are the variables, and (a, b) is the point about which the series is expanded. The coefficients in (6.210) are usually obtained by a technique known as *targeting*. Specifically, targeting is the utilization of a simulation to define and verify any empirical constants that may be required by the guidance equations. For many problems, efficient use of the simulation to obtain the empirical constants requires the use of auxiliary computer programs. The word targeting is sometimes applied to operations carried out at the operational site that utilize the empirical constants obtained by the process defined above as targeting. Another technique frequently used for obtaining and/or generating the coefficients (i.e., the α_{ij}'s) is the method of least squares (or curve fitting). For more information in delta guidance, the reader is referred to [9].

Finally, two other guidance techniques, the Q-guidance and *cross-product steering*, have been discussed in Section 6.5.2.

It is appropriate at this point to list some (note that this list is by no means complete) of the ballistic missile error sources. These are:

Navigation (Correlated Output Errors):

- Position (latitude and longitude)
- Heading (azimuth)
- Velocity (north, east, vertical, relative to the Earth)
- Tilt (north, east)

Guidance (Uncorrelated Error Sources):
- Accelerometers
- Scale factor error and bias
- Nonlinearity
- Nonorthogonality

Gyroscopes:
- Bias drift
- Acceleration sensitive drift
- Acceleration squared drift

Miscellaneous Error Sources:
- Clock
- Azimuth alignment
- Velocity quantization
- Vibration
- In-flight navigation.

6.6 Derivation of the Force Equation for Ballistic Missiles

A ballistic missile (or rocket) is a variable-mass vehicle that acquires thrust by the ejection of high-speed particles. A short nonrigorous derivation of the linear force equation is given in this section. The sum of the external forces acting on any system of particles equals the rate of change of linear momentum of the system. Mathematically, this can be expressed as [14]

$$\Sigma \mathbf{F} = m\left(\frac{d\mathbf{V}}{dt}\right) + m_g \mathbf{V}_g, \tag{6.212}$$

where

$$\begin{aligned} m &= \text{mass of the missile,} \\ \mathbf{V} &= \text{velocity of the missile,} \\ m_g &= \text{mass of the escaping gas,} \\ \mathbf{V}_g &= \text{velocity of the escaping gas (this velocity should not be confused with the velocity-to-be-gained vector discussed earlier).} \end{aligned}$$

(Note that as before, the dot over a variable is used to denote differentiation with respect to time.) It will be assumed here that the only external force on the missile arises from gravitational acceleration; hence, (6.212) may be written as

$$m\mathbf{g} = m\left(\frac{d\mathbf{V}}{dt}\right) + \left(\frac{dm}{dt}\right)\mathbf{V} + m\left(\frac{d\mathbf{V}_g}{dt}\right) + \left(\frac{dm_g}{dt}\right)\mathbf{V}_g. \tag{6.213a}$$

Now, $(d\mathbf{V}_g/dt) = 0$ when the gas exits into free space, and $(dm/dt) = -(dm_g/dt)$, since the total system mass is a constant. Thus,

$$\begin{aligned} m\mathbf{g} &= m\left(\frac{d\mathbf{V}}{dt}\right) + \left(\frac{dm_g}{dt}\right)(\mathbf{V}_g - \mathbf{V}) \\ &= m\left(\frac{d\mathbf{V}}{dt}\right) + \left(\frac{dm_g}{dt}\right)\mathbf{c} = m\left(\frac{d\mathbf{V}}{dt}\right) - \mathbf{T}, \end{aligned} \tag{6.213b}$$

where

$\mathbf{c}$ = escape gas velocity (or ejection velocity) with respect to the missile; also called specific impulse,

$\mathbf{T}$ = missile thrust vector $= -\left(\dfrac{dm_g}{dt}\right)\mathbf{c}$.

Equation (6.213b) may be divided by m, resulting in [9], [11]

$$\frac{d^2\mathbf{R}}{dt^2} = \left(\frac{d\mathbf{V}}{dt}\right) = \mathbf{g} + \mathbf{a}_T, \tag{6.214}$$

where $\mathbf{a}_T$ is the thrust acceleration and is given by

$$\mathbf{a}_T = \mathbf{T}/m. \tag{6.215}$$

Figure 6.31 illustrates the forces acting on the missile.

The thrust $\mathbf{T}$ at any altitude is determined by the vacuum delivered thrust $\mathbf{T}_v$ and ambient pressure p,

$$T = T_v - pA_E, \tag{6.216}$$

where A_E is the total nozzle exit area, an input for each stage, and p is the ambient atmospheric pressure corresponding to the missile's altitude. Note that p can be represented as an exponential function of altitude (H) with

$$H = R - R_E, \tag{6.217}$$

where R_E is the radius of the Earth. The ambient atmospheric pressure p can be computed as

$$p = \rho g c^2/\gamma,$$

where ρ is the atmospheric density, g is the gravitational constant, c is the local velocity of sound, and γ the gas ratio of specific heats (1.401).

In the present discussion, we will assume that the missile engine(s) operate at constant vacuum thrust T_v and constant propellant burning rate dm/dt. Therefore, the mass flow rate can be computed from the following relation:

$$\frac{dm}{dt} = T_v/g_o I_{sp},$$

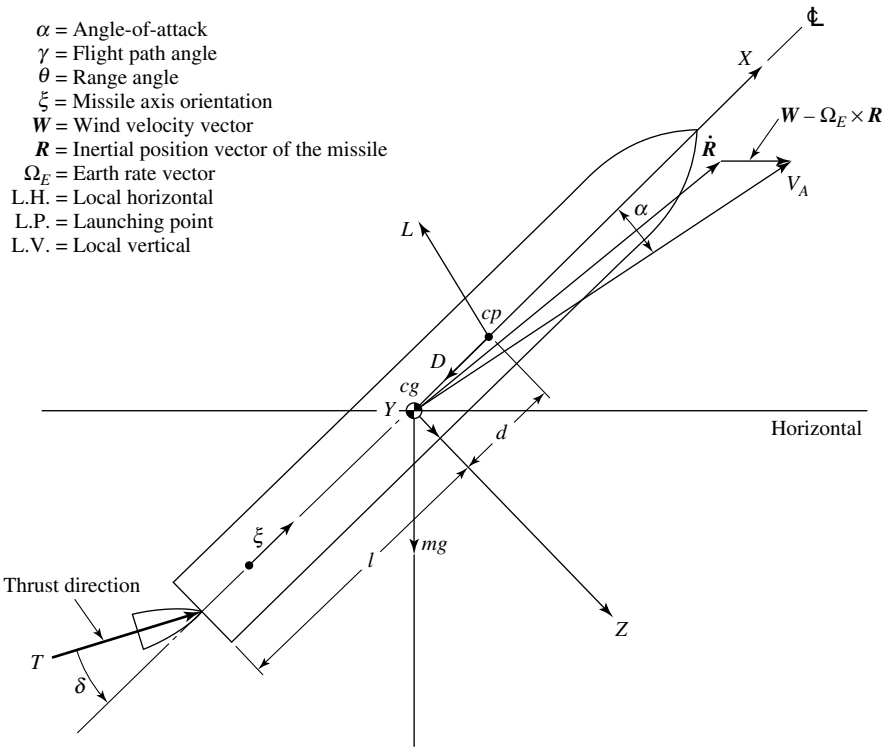

Fig. 6.31. Forces acting on the missile.

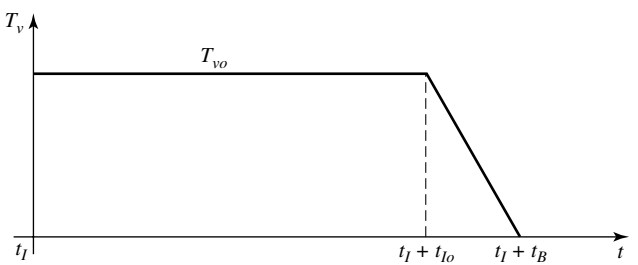

Fig. 6.32. Typical vacuum thrust profile.

where g_o is the acceleration due to gravity at sea level and I_{sp} is the specific impulse.

The vacuum-delivered thrust (i.e., the specific impulse times the weight flow rate) is assumed constant, except during thrust tailoff, as indicated in Figure 6.32.

In Figure 6.32, the values of $T_{vo}t_I$ (ignition time), t_{To} (tailoff time from ignition), t_B (burn time from ignition) are, except for second-stage ignition (t_{I2}), inputs for each

stage (t_{I2} is assumed to be the time of first-stage separation). However, these values are subject to perturbation. With constant weight flow rate, the mass (m) is a linear function of time:

$$m = m_o + \left(\frac{dm}{dt}\right)(t - t_I), \tag{6.218a}$$

$$\frac{dm}{dt} = (m_F - m_o)/t_B = \text{constant}, \tag{6.218b}$$

where $m_o = m(t_I)$ and $m_F = m(t_I + t_B)$ are inputs for each stage and are subject to perturbation. Equation (6.218b) is a realistic assumption, stating that a constant rate of fuel consumption leads to a constant thrust. Aerodynamic drag (D) is determined by the drag coefficient C_D, cross-sectional reference area S, and the dynamic pressure q:

$$D = C_D S q, \tag{6.219a}$$

where S is an input for each stage (usually identical values), and

$$q = \tfrac{1}{2}\rho V_R^2, \tag{6.219b}$$

with ρ the air density (nominally an exponential function of altitude, but subject to a perturbation that also depends on altitude), and V_R is the magnitude of the missile velocity relative to the atmosphere. Thus,

$$\mathbf{V}_R = \mathbf{V}_m + \mathbf{V}_{LP} - (\omega_{ie} \times \mathbf{R} + \mathbf{V}_W), \tag{6.220}$$

where $\mathbf{V}_{LP}$ is the launch-point velocity, $\mathbf{V}_W$ is the wind-velocity vector perturbation that depends on altitude, and $(\omega_{ie} \times \mathbf{R})$ represents the nominal ($\mathbf{V}_W = 0$) velocity of the atmosphere. Earth rate ω_{ie} in guidance axes is given by

$$\begin{aligned}
\omega_{ieX} &= \omega_{ie}(\cos\varphi_{LP}\cos\psi\cos\alpha_X + \sin\varphi_{LP}\sin\alpha_X),\\
\omega_{ieY} &= -\omega_{ie}\cos\varphi_{LP}\sin\psi,\\
\omega_{ieZ} &= \omega_{ie}(\cos\varphi_{LP}\cos\psi\sin\alpha_X - \sin\varphi_{LP}\cos\alpha_X),
\end{aligned} \tag{6.221}$$

where α_X is an angle of the X-axis above the horizontal, ψ is the launch azimuth angle, and φ_{LP} is the launch point latitude. For discussion purposes, a two-stage missile will be assumed. The drag coefficient C_D is strictly a function of both the total angle of attack and Mach number. In the present discussion, the angle-of-attack dependence is neglected, and the Mach number dependence is linearized. With a constant speed of sound ($V_S \cong$ 1,000 ft/sec), C_D becomes a function of V_R, as illustrated in Figure 6.33.

Next, an expression is needed to compute the missile's along-range and cross-range impact dispersion. Recall the differential equation for the velocity-to-be-gained, (6.178):

$$\frac{d\mathbf{V}g}{dt} = -\mathbf{a}_T - Q\mathbf{V}_g, \tag{6.178}$$

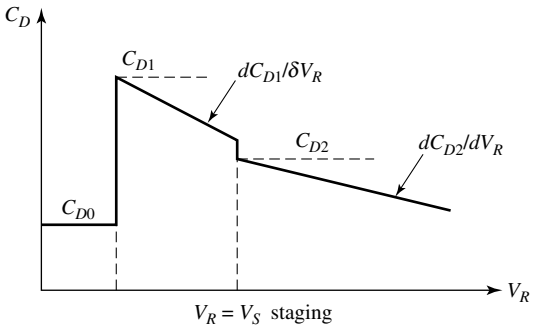

Fig. 6.33. Staging concept.

where $\mathbf{a}_T$ is the gravity-free acceleration. Now we can write this equation in component form as follows:

$$\frac{dV_{gx}}{dt} = -\frac{d^2x_T}{dt^2} - (Q_{xx} + K_q t)V_{gx} - Q_{xz}V_{gz},$$
$$\frac{dV_{gy}}{dt} = -\frac{d^2y_T}{dt^2} - Q_{yx}V_{gx},$$
$$\frac{dV_{gz}}{dt} = -\left[\left(\frac{d^2z_T}{dt^2}\right) - m_{\ddot{z}}\left(\frac{d^2z_T}{dt^2}\right)\right],$$

where

$$Q_{xx} = \text{linear function of time},$$
$$K_q = \text{a trajectory constant}.$$

The Q_{xz} term is a step function, becoming zero at a preset time, and V_{gz} is given by

$$V_{gz} = V_{gz1} + \int_0^t \left(\frac{dV_{gz}}{dt}\right) dt + V_{gz0},$$

where V_{gz1} steps from zero to a predetermined constant, and V_{gz0} is a prescribed constant. The along-range and cross-range errors ΔR and ΔC, attributed to launch and propulsion disturbances, have been found to vary linearly (i.e., to within a sufficient order of accuracy) with the Q elements. Thus,

$$\Delta R = (\partial \Delta R/\partial Q_{xx})Q_{xx} + \Delta R_o,$$

$$\Delta CR = (\partial \Delta CR/\partial Q_{xx})Q_{xx} + (\partial \Delta CR/\partial Q_{yx})Q_{yx} + \Delta CR_o.$$

The impact dispersion is just the root sum square of the along- and cross-range errors. Differentiating the dispersion function with respect to the Q parameters in question and equating this to zero affords the solution of the optimum values of Q_{xx} and Q_{yx}.

6.6.1 Equations of Motion

For long, slender ballistic missiles it is necessary to consider the actual missile dynamics. Therefore, only rigid-body dynamics will be considered here. The translational equations of rigid-body motion are solved in an inertially fixed rectangular (X, Y, Z) coordinate system with origin at the center of the Earth. This frame will be assumed here to be parallel to the (X, Y, Z) guidance axes: The Z-axis is pointing up, the Y-axis is in the local horizontal plane at launch, and the X-axis is above the horizontal by an angle α_X. Furthermore, the XZ-plane is pointed downrange (the guidance azimuth measuring the angle that the XZ-plane makes with the local north, positive clockwise). The launch latitude φ_{LP}, X erection (α_X), and the guidance azimuth (ψ) are input quantities.

In such a coordinate system, the equations of motion (XYZ components always implied) are

$$\mathbf{V} = \mathbf{V}_0 + \int_{t_0}^{t} (\mathbf{a}_T + \mathbf{g}) dt, \tag{6.222}$$

$$\mathbf{R} = \mathbf{R}_0 + \int_{t_0}^{t} \mathbf{V} dt, \tag{6.223}$$

where

$$\begin{aligned} \mathbf{a}_T &= \text{specific force vector acting on the missile,} \\ \mathbf{g} &= \text{gravitational acceleration vector due to the Earth,} \\ \mathbf{V} &= \text{inertial velocity vector of the missile,} \\ \mathbf{R} &= \text{inertial position vector of the missile,} \\ t &= \text{time measured from computer start,} \\ t_o, \mathbf{R}_o, \mathbf{V}_o &= t, \mathbf{R}, \mathbf{V} \text{ at time of nominal first-stage ignition.} \end{aligned}$$

It is convenient for output purposes to actually consider $\mathbf{V}$ to be the sum of missile velocity relative to the launch point $(\mathbf{V}_m)$ and the velocity of the launch point with respect to inertial space $(\mathbf{V}_{LP} = \text{constant})$, so that the equations of motion become

$$\mathbf{V}_m = \mathbf{V}_{mo} + \int_{t_0}^{t} (\mathbf{a}_T + \mathbf{g}) dt, \tag{6.224a}$$

$$\mathbf{R} = \mathbf{R}_o + \int_{t_0}^{t} (\mathbf{V}_m + \mathbf{V}_{LP}) dt. \tag{6.224b}$$

This constitutes what may be called the *navigation* portion of the missile motion. The computation of $\mathbf{a}_T$ and $\mathbf{g}$ will be required for the navigation process and will simulate the guidance phase. Specifically, the guidance phase of a simulation models the generalized computation of the velocity-to-be-gained and indicated Z-velocity (V_{ZI}), with

$$\mathbf{V}_g = \mathbf{V}_{go} + \int_{0}^{t} \mathbf{V}_g dt, \tag{6.225a}$$

$$V_{ZI} = V_{Zio} + \int_0^t \left(\frac{dV_{ZI}}{dt}\right) dt. \tag{6.225b}$$

Also modeled in the guidance phase of a simulation is a variety of possible pitch $(d\theta_c/dt)$ and yaw $(d\psi_c/dt)$ rate command computations. As outputs from the guidance computer, θ_c and ψ_c are intended to represent command values of pitch and yaw attitude defined as follows (where (X_M, Y_M, Z_M) are rectangular missile fixed axes of roll (X_M), pitch (Y_M), and yaw (Z_M) aligned with the (X, Y, Z) guidance axes when $\theta = \psi = 0$):

θ = pitch angle; rotation of missile X_M (roll) axis from the guidance X-axis about the guidance Y-axis;

ψ = yaw angle; subsequent rotation of missile X_M (roll) axis from the guidance XZ-plane about the pitched missile Z_M (yaw) axis.

The third Euler angle (ϕ, roll angle) is not of importance in this simulation and is always considered to be zero. It is assumed that the actual instrumentation of the autopilot will adequately approximate the above definitions of pitch and yaw.

The response of the missile to θ_c and ψ_c, which closes the guidance loop, is represented on two different ways. During launch recovery, from actual first-stage ignition to the start of guidance control, the values of θ and ψ are given as solutions to second-order differential equations as follows:

$$\frac{d^2\theta}{dt^2} = -2\zeta\omega_n\left(\frac{d\theta}{dt}\right) - \omega_n^2[\theta - (90^\circ - \alpha_X)], \tag{6.226a}$$

$$\frac{d^2\psi}{dt^2} = -2\zeta\omega_n\left(\frac{d\psi}{dt}\right) - \omega_n^2\psi, \tag{6.226b}$$

$$\left|\frac{d^2\theta}{dt^2}\right|_{max} = \left|\frac{d^2\psi}{dt^2}\right|_{max} = \kappa_{max}, \tag{6.226c}$$

where ζ is the damping ration, ω_n is the undamped natural frequency, and κ_{max} are inputs that describe the rate and proportional autopilot gains effective in this region and the physical limit on thrust vector deflection. (Note that care should be used in selecting the value of κ_{max} depending on the rollout required during launch recovery.) The vertical attitude command is represented by $\theta_c = 90^\circ - \alpha_X$ and $\psi_c = 0$ and nominally (with $\theta = 90^\circ - \alpha_X$, $d\theta/dt = 0$, $\psi = 0$, $d\psi/dt = 0$ at ignition), the missile will maintain a vertical attitude and zero attitude rate until the start of guidance control.

After the start of guidance control $(t = t_c)$ the autopilot is neglected and the command rates simply integrated to give θ and ψ as follows:

$$\theta = \theta_c(t_c) + \int_{t_c}^t \left(\frac{d\theta_c}{dt}\right) dt, \quad \theta_c(t_c) = 90 - \alpha_X, \tag{6.227a}$$

$$\psi = \psi_c(t_c) + \int_{t_c}^{t} \left(\frac{d\psi_c}{dt} \right) dt, \quad \psi_c(t_c) = 0. \tag{6.227b}$$

The missile does not instantaneously obtain $\theta = \theta_c$, $(d\theta/dt) = (d\theta_c/dt)$, $\psi = \psi_c$, $(d\psi_c/dt) = (d\psi_c/dt)$, at $t = t_c$, but assuming that the missile will have nearly completely recovered from launch at t_c, this same approximation is made in all cases and should not introduce serious error.

In terms of the values at the current time t, the missile position ($\mathbf{R}$), velocity ($\mathbf{V}$), guidance velocity-to-be-gained ($\mathbf{V}_g$), pitch angle (θ), and yaw angle (ψ), the differential equations of motion (for the powered phase of the missile) can be written in the form

$$\frac{d^2\mathbf{R}}{dt^2} = \frac{d\mathbf{V}}{dt} = \mathbf{a}_T + \mathbf{g}, \tag{6.228a}$$

$$\frac{d\mathbf{V}_g}{dt} = f(t, \mathbf{a}_T, \mathbf{V}_g), \tag{6.228b}$$

$$\frac{d\theta}{dt} = \frac{d\theta_c}{dt}, \tag{6.228c}$$

$$\frac{d\psi}{dt} = \frac{d\psi_c}{dt}. \tag{6.228d}$$

The solution of these equations will depend on the value of time (t), missile position, and yaw angle (ψ), which can be incremented by an amount based on a weighted average of the previously computed derivatives for this time step. These derivatives, in turn, depend on the current time, position, velocity, attitude, and velocity-to-be-gained. Strictly speaking, however, these functional relationships are valid only after the start of guidance control ($t = t_c$, an input). Prior to this time, the specific force ($\mathbf{a}_T$) also depends on the angular acceleration ($d^2\theta/dt^2$) and ($d^2\psi/dt^2$), which is determined by ($d\theta/dt$), θ, ($d\psi/dt$), and ψ, with θ and ψ satisfying second-order differential equations. The process of incrementing the variables and recomputing derivatives continues until a discontinuous change in any derivative is indicated. Note also that in addition to "cut-off," it is possible to terminate the powered trajectory at a selected value of time or second-stage burnout by an appropriate choice of inputs.

For any simulation process that may be used by the missile designer, initial conditions must be provided. For instance, the powered-flight simulation is started at the nominal time ($t = t_c$, an input) of first-stage motor ignition. At this time, the missile has nominally flown up the launch vertical and is at ground level (i.e., at the surface of the Earth, where $R = R_E$) with a vertical attitude, zero attitude rate, and initial vertical velocity with respect to the Earth (V_{Mvo}). That is, the nominal initial conditions are

$$\begin{aligned} X(t_o) &= R_E \sin\alpha_X, \\ Y(t_o) &= 0, \\ Z(t_o) &= -R_E \cos\alpha_X, \end{aligned} \tag{6.229a}$$

$$\begin{aligned} V_{MX}(t_o) &= V_{Mvo}\sin\alpha_X, \\ V_{MY}(t_o) &= 0, \\ V_{MZ}(t_o) &= -V_{Mvo}\cos\alpha_X, \end{aligned} \tag{6.229b}$$

$$\begin{aligned} \theta(t_o) &= 90^\circ - \alpha_X, \\ \psi(t_o) &= 0^\circ, \end{aligned} \tag{6.229c}$$

$$\begin{aligned} \frac{d\theta(t_o)}{dt} &= 0, \\ \frac{d\psi(t_o)}{dt} &= 0, \end{aligned} \tag{6.229d}$$

where R_E is the radius of the Earth and V_{Mvo} is an input. The velocity of the launch point with respect to inertial space is given by

$$\begin{aligned} V_{LPX} &= V_{LP}\sin\psi\cos\alpha_X, \\ V_{LPY} &= V_{LP}\cos\alpha_X, \\ V_{LPZ} &= V_{LP}\sin\psi\sin\alpha_X, \end{aligned} \tag{6.230}$$

where $V_{LP} = \omega_{ie} R_E \cos\varphi_{LP}$ (note that as before, φ_{LP} is the latitude of the launch point).

As discussed earlier, the nominal integration of (6.224a) and (6.224b) from computer start ($t = 0$) to ignition time ($t = t_o$) is approximated by neglecting the $\mathbf{g}$ term in $(\frac{d\mathbf{V}_M}{dt})$ and Q-terms (see also Section 6.5.2) in $\mathbf{V}_g$, so that for the guidance computations we have

$$\begin{aligned} V_{gX}(t_o) &= V_{gXo} - V_{MX}(t_o), \\ V_{gY}(t_o) &= V_{gYo} - V_{MY}(t_o), \\ V_{gZ}(t_o) &= V_{gZo} - [V_{MZ}(t_o) + SQ_{Vg}V_{MX}(t_o)], \\ V_{ZI}(t_o) &= V_{Zio} - [V_{MZ}(t_o) + SQ_{Vg}V_{MX}(t_o)], \end{aligned} \tag{6.231}$$

where V_{gXo}, V_{gYo}, V_{gZo}, and V_{Zio} are inputs that are approximations to the values at computer start, and S is the gain factor (see (6.194)). These initial conditions are subject to perturbation.

6.6.2 Missile Dynamics

This section discusses the simplified model assumed for the missile as it relates to the computation of the specific force $\mathbf{a}_T$. During launch recovery, $\mathbf{a}_T$ is given as a function of time (t), position ($\mathbf{R}$), velocity ($\mathbf{V}_M$), attitude (θ and ψ), and angular acceleration ($(d^2\theta/dt^2)$ and $(d^2\psi/dt^2)$). After the start of guidance control, $\mathbf{a}_T$ is assumed not to depend on angular acceleration. With a spherically symmetric

Earth, the gravitational acceleration ($\mathbf{g}$) is given directly as a function of missile position:

$$\mathbf{g} = -(\mu/R^3)\mathbf{R}, \tag{6.232}$$

where $\mathbf{R}$ is the position vector measured from the center of the Earth. The instantaneous thrust and aerodynamic forces that determine $\mathbf{a}_T$ are most easily computed in missile axes (X_M, Y_M, Z_M) and then transformed to the guidance axes (X, Y, Z) for use in the equations of motion as follows:

$$\begin{bmatrix} a_{TX} \\ a_{TY} \\ a_{TZ} \end{bmatrix} = \begin{bmatrix} \cos\psi\cos\theta & -\sin\psi\cos\theta & \sin\theta \\ \sin\psi & \cos\psi & 0 \\ -\cos\psi\sin\theta & \sin\psi\sin\theta & \cos\theta \end{bmatrix} \begin{bmatrix} a_{TXM} \\ a_{TYM} \\ a_{TZM} \end{bmatrix} \tag{6.233}$$

The specific force vector can then be conventionally resolved as follows:

$$\begin{aligned} a_{TXM} &= (T - D - T_D)/M, \\ a_{TYM} &= (L_{YM} + F_{YM})/M, \\ a_{TZM} &= (L_{ZM} + F_{ZM})/M, \end{aligned} \tag{6.234}$$

where

M = instantaneous missile mass,
T = total motor thrust,
T_D = total decrement in longitudinal thrust due to thrust vector deflection,
D = longitudinal aerodynamic force (drag),
L_{YM}, Z_M = normal components of aerodynamic force (lift),
F_{YM}, Z_M = normal components of thrust due to thrust vector deflection (control).

An Example: In the previous sections we developed the equations of motion for a missile (or rocket). In this example, we will state these equations in a different way. It is well known that optimal trajectories of a rocket moving with constant exhaust velocity and limited mass-flow rate in a Newtonian gravitational field may consist of arcs, such as null thrust, intermediate thrust, and maximum thrust. For such a case, the equations of motion in the Newtonian gravitational field can be written in vector form as follows:

$$\begin{aligned} \frac{d\mathbf{v}}{dt} &= (cm/M)\mathbf{u} - (\mu/r^3)\mathbf{r}, \\ \frac{d\mathbf{r}}{dt} &= \mathbf{v}, \\ \frac{dM}{dt} &= -m, \end{aligned}$$

where

$$\begin{aligned}
\mathbf{r} &= (r, 0, 0) \text{ is the radius vector,}\\
\mathbf{v} &= (v_1, v_2, v_3) \text{ is the velocity vector,}\\
\boldsymbol{u} &= (u_1, u_2, u_3) \text{ is a unit thrust vector,}\\
M &= \text{mass of the rocket,}\\
m &= \text{mass-flow rate } (0 \le m \le d^2m/dt^2),\\
c &= \text{exhaust velocity.}
\end{aligned}$$

The components of all vectors are given in a spherical coordinate system (r, θ, φ) with the origin at the attracting center. The above equations can be used as a basis for further study, depending on the needs and/or application of the user.

6.7 Atmospheric Reentry

In this section we will treat briefly the problem of reentry of a ballistic missile into the Earth's atmosphere. A complete analysis of reentry involves heat/energy transfer and/or dissipation, atmospheric models, aerodynamics, etc. Such analysis is beyond the scope of this work and will not be discussed here. Furthermore, no consideration will be given here for reentry of manned orbiting vehicles or spacecraft, since in reentry of manned spacecraft there are severe decelerations for human occupants, intense aerodynamic heating, and the tactical aspect of having control of landing location. For this reason, we will not treat manned flight reentry. Specifically, reentry is characterized by he dissipation of great quantities of kinetic and potential energy by the missile (or spacecraft). While a large fraction of this energy is transferred to the atmosphere, relatively large quantities of it will be deposited in the craft as heat. It is well known that when a ballistic missile reenters the atmosphere after having traveled a long distance, its speed will be very high and the remaining time to ground impact will be relatively short. The small displacement distance traveled by ballistic missiles after they reenter the atmosphere can be accurately modeled, to a first-order approximation, using a simplified flat-Earth constant-gravity approximation. Reentry has become a generic term for a broad function that may be accomplished by a variety of vehicle configurations in a variety of environments.

The parameters that affect the reentry problem, and are unique to ballistic missiles, are the following [1], [15]:

(1) Reentry velocity (ranging from 1000 mph to 25,000 mph for spacecraft);
(2) Approach angle in the Earth's atmosphere (e.g., grazing, shallow entry, and deep entry); and
(3) Vehicle configuration; for a ballistic missile, the vehicle configuration is designed with a lift to drag (L/D) ratio of less than 0.1 or $L/D < 0.1$, where L is the lift and D is the drag.

From atmospheric density tables, it can be seen that the greatest part of the significant aerodynamic limit is generally considered to be between 300,000 and 350,000 feet. In

order to devise an efficient method of entry for a given application, it is highly desirable that the missile designer have available relatively simple equations for computing how each variable at his disposal affects the entry trajectory, the deceleration, and the aerodynamic heating.

The atmospheric properties are different for the different planets (e.g., Mars, Venus). Two important parameters that are related to the properties of the atmosphere are (1) deceleration ($\approx \rho v^2$), and (2) heating rate ($\approx \rho v^3$), where ρ is the atmospheric density and v is the entry velocity. We will now develop the differential equations of motion in a nonrigorous way. For more details, the reader is referred to [1].

Specifically, the problem to be analyzed concerns that portion of the descent of a vehicle into planetary atmosphere wherein the decelerations and the convective aerodynamic heating are dominant. Three assumptions made at the outset are as follows:

(a) Atmosphere and planet are spherically symmetric.
(b) Variations in atmosphere temperature and molecular weight with altitude are negligible compared to the variation in density.
(c) Peripheral velocity of planet is negligible compared to the velocity of the entering vehicle.

Assumption (a) is reasonable for those planets that have only small equatorial bulges (such as the Earth, Venus, and Mars), inasmuch as the severe aerodynamic heating and decelerations occur over a length of the flight path, which is small compared to the planet's mean radius (on the order of one-tenth the planet radius for nonlifting bodies such as missiles). Assumption (b) leads to a "locally exponential" atmosphere. The atmosphere will be treated in Appendix D. Finally, assumption (c), that the peripheral velocity of the planet is negligible compared to the velocity of the entering vehicle, would not introduce significant errors for most descents into most planetary atmospheres. For descents nearly along a line of longitude, the errors in heat transfer and deceleration would, of course, be negligible. The greatest error would occur in an equatorial descent. The development of the differential equation for reentry (or descent) in a spherically symmetric atmosphere about a spherically symmetric planet would occur in a meridian plane in the absence of lateral forces. This confines the problem to one of two dimensions, for which polar coordinates (r, θ) are convenient. The velocity components are (v, u), respectively, as shown in Figure 6.34.

Referring to Figure 6.34, let $\mathbf{e}_r$ be a unit vector along the radial direction and let $\mathbf{e}_\theta$ be a tangential unit vector. Then, since

$$\mathbf{e}_r = \mathbf{r}/|\mathbf{r}| = \mathbf{r}/r, \text{ or } \mathbf{r} = r\mathbf{e}_r, \tag{6.235}$$

we obtain

$$\frac{d\mathbf{r}}{dt} = r\left(\frac{d\mathbf{e}_r}{dt}\right) + \mathbf{e}_r\left(\frac{dr}{dt}\right). \tag{6.236}$$

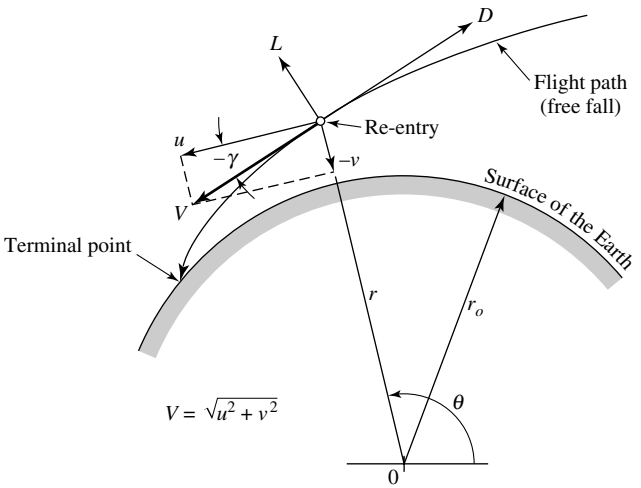

Fig. 6.34. Geometry of reentry.

Now the rate of change of the unit vectors along the r-direction and θ-direction can be interpreted as follows:

$$\frac{d\mathbf{e}_r}{dt}: \text{changing of } \mathbf{e}_r \text{ along the } \theta\text{-direction, constant along r,}$$
$$\frac{d\mathbf{e}_\theta}{dt}: \text{changing of } \mathbf{e}_\theta \text{ along the r-direction, constant along } \theta.$$

Therefore,

$$\begin{aligned}
\frac{d\mathbf{e}_r}{dt} &= \left(\frac{d\theta}{dt}\right)\mathbf{e}_\theta,\\
\frac{d\mathbf{e}_\theta}{dt} &= -\left(\frac{d\theta}{dt}\right)\mathbf{e}_r,\\
\frac{d\mathbf{r}}{dt} &= r\left(\frac{d\theta}{dt}\right)\mathbf{e}_\theta + \left(\frac{dr}{dt}\right)\mathbf{e}_r,\\
\frac{d^2\mathbf{r}}{dt^2} &= \left(\frac{dr}{dt}\right)\left(\frac{d\mathbf{e}_r}{dt}\right) + \mathbf{e}_r\left(\frac{d^2r}{dt^2}\right) + r\left(\frac{d\theta}{dt}\right)\left(\frac{d\mathbf{e}_\theta}{dt}\right)\\
&\quad + r\mathbf{e}_\theta\left(\frac{d^2\theta}{dt^2}\right) + \left(\frac{dr}{dt}\right)\left(\frac{d\theta}{dt}\right)\mathbf{e}_\theta,
\end{aligned}$$

or

$$\mathbf{a} = \frac{d^2\mathbf{r}}{dt^2} = \left[\left(\frac{d^2r}{dt^2}\right) - r\left(\frac{d\theta}{dt}\right)^2\right]\mathbf{e}_r + \left[r\left(\frac{d^2\theta}{dt^2}\right) + 2\left(\frac{dr}{dt}\right)\left(\frac{d\theta}{dt}\right)\right]\mathbf{e}_\theta. \quad (6.237)$$

The velocity components u and v are now given by

$$u = \frac{ds}{dt}, \qquad v = \frac{dr}{dt},$$

$$s = r\theta, \qquad a = \frac{dv}{dt} = \frac{d^2r}{dt^2},$$

and therefore,

$$u = r\left(\frac{d\theta}{dt}\right), \tag{6.238}$$

where r is a constant. Now let y be the altitude. Then

$$y = r_o + r,$$

where r_o is the radius of the Earth, which is constant. Next, we have

$$\frac{dy}{dt} = \frac{dr}{dt}$$

and

$$\left(\frac{d\theta}{dt}\right) = u/r, \quad \frac{d^2\theta}{dt^2} = \left[r\left(\frac{du}{dt}\right) - u\left(\frac{dr}{dt}\right)\right]/r^2.$$

Therefore,

$$\begin{aligned}
\mathbf{a} &= \left[\left(\frac{dv}{dt}\right) - r(u/r)^2\right]\mathbf{e}_r + \left\{r\left[\left(\left(\frac{du}{dt}\right) - u\left(\frac{dr}{dt}\right)\right)/r^2\right] + 2v(u/r)\right\}\mathbf{e}_\theta \\
&= \left[\left(\frac{dv}{dt}\right) - (u^2/r)\right]\mathbf{e}_r + \left[\left(\frac{du}{dt}\right) - (u/r)\left(\frac{dr}{dt}\right) + 2(uv/r)\right]\mathbf{e}_\theta \\
&= \left[\left(\frac{dv}{dt}\right) - (u^2/r)\right]\mathbf{e}_r + \left[\left(\frac{du}{dt}\right) + (uv/r)\right]\mathbf{e}_\theta.
\end{aligned} \tag{6.239}$$

Equation (6.239) is the vector acceleration in polar coordinates in terms of the unit vectors $\mathbf{e}_r$ and $\mathbf{e}_\theta$. The flight-path angle γ, which is negative for reentry, is given by the relation

$$\tan\gamma = v/u. \tag{6.240}$$

The aerodynamic force $\mathbf{F}_a$ can be obtained from Figure 6.34 as follows:

$$\mathbf{F}_a = (-mg + L\cos\gamma - D\sin\gamma)\mathbf{e}_r - (D\cos\gamma + L\sin\gamma)\mathbf{e}_\theta, \tag{6.241}$$

where L is the lift force, D is the drag, g is the acceleration of gravity, and m is the mass of the reentry vehicle. From the acceleration and aerodynamic force equations, we obtain, after dividing through by m,

$$-\left(\frac{d^2y}{dt^2}\right) = -\left(\frac{dv}{dt}\right) = g - (u^2/r) - (L/m)\cos\gamma + (D/m)\sin\gamma, \tag{6.242a}$$

$$\left(\frac{du}{dt}\right) + (uv/r) = -(D/m)[\cos\gamma + (L/D)\sin\gamma]. \tag{6.242b}$$

It should be noted that g and r are local values in these equations. This system of equations can be further simplified by neglecting the uv/r term. The omission of this term can be justified in light of the fact that during reentry, maximum deceleration and heating occur at very small reentry angles and that uv/r is on the order of 1% of du/dt. Consequently, (6.242b) reduces to

$$\frac{du}{dt} = -(D/m)\cos\gamma[1 + (L/D)\tan\gamma]. \tag{6.243}$$

Assuming now that $|(L/D)\tan\gamma| < 1$, and noting that $V = (u/\cos\gamma)$, where $V = (u^2 + v^2)^{1/2}$, we have

$$\frac{du}{dt} = -[\rho_\infty/2(m/C_D S)](u^2/\cos\gamma), \tag{6.244}$$

where

$$\begin{aligned} C_D &= \text{coefficient of drag} = C_D = \frac{D}{\frac{1}{2}\rho_\infty V^2 S}, \\ S &= \text{reference area for drag and lift,} \\ D &= \text{drag force,} \\ \rho_\infty &= \text{atmospheric density free stream (ambient atmosphere).} \end{aligned}$$

Furthermore, selecting as the independent variable the expression

$$\bar{u} \equiv u/u_c \equiv u/\sqrt{gr}, \tag{6.245}$$

where u_c is the circular orbit velocity, we obtain

$$\frac{du}{dt} = \frac{d(\sqrt{gr}\,\bar{u})}{dt} = \sqrt{gr}\left(\frac{d\bar{u}}{dt}\right). \tag{6.246}$$

Introducing now the drag coefficient in (6.242a) results in

$$\begin{aligned} -(1/g)\left(\frac{dv}{dt}\right) = -(1/g)\left(\frac{d^2y}{dt^2}\right) &= 1 - \bar{u}^2 \\ &+ (\rho_\infty/2)(C_D S r\bar{u}^2/m\cos^2\gamma)[\sin\gamma - (L/D)\cos\gamma]. \end{aligned} \tag{6.247}$$

Equation (6.247) must still be reduced in order to obtain a solution. The pair (6.244) and (6.247), representing the equations of motion, can be reduced to a single equation by transforming these equations to a new dimensionless variable. The solution is quite complicated and will not be pursued here further.

An Example: Here we will assume that the reentry trajectory is described by the translational motion of a rigid body. The equations of motion are derived for a rotating spherical Earth. The forces acting on the vehicle are gravity and the aerodynamic lift and drag. Wind will not be considered in this example. Using Newtonian two-body mechanics, the trajectory of a ballistic missile or space vehicle moving

in a conservative force field is easily developed. In essence, two dynamic variables, specific energy E and specific angular momentum H, are used to relate position and velocity to trajectory size and shape.

From the above discussion, the only aerodynamic force present is the drag force, which is directed opposite to the velocity vector of the vehicle. The magnitude of the drag force is given by

$$|\mathbf{F}_D| = \rho C_D S(v^2/2), \tag{1}$$

where

ρ = atmospheric density, a function of altitude,
v = Earth-relative speed of the vehicle,
C_D = coefficient of drag, a function of Mach number,
S = effective cross-sectional area of the vehicle.

Note that one can also use normalized lift and drag acceleration, L and D, which are related to the dynamic pressure q as follows:

$$L = qSC_L, \tag{2a}$$
$$D = qSC_D, \tag{2b}$$
$$q = \rho(v^2/2), \tag{2c}$$

with $C_L = C_{L\alpha}(\alpha - \alpha_o)$, $C_D = C_{Do} + \mu C_L^2$, α is the AOA, μ is the induced drag coefficient, and $C_{L\alpha} = \partial C_L/\partial\alpha$ (see also Chapter 3).

The load factor n_G is defined as the magnitude of the aerodynamic acceleration:

$$n_G = (L^2 + D^2)^{1/2}. \tag{3}$$

From the above discussion, we note that the total force acting on the reentry body is

$$\mathbf{F} = m\mathbf{g} + \mathbf{F}_D = -(\mu m/r^2)\mathbf{e}_r - \mathbf{F}_D\mathbf{e}_\theta = m\left(\frac{d^2\mathbf{r}}{dt^2}\right) \tag{4}$$

where

$\mathbf{e}_r$ = unit vector along the radial direction (i.e., $\mathbf{r}$),
$\mathbf{e}_\theta$ = unit vector along the tangential direction (i.e., $\mathbf{v}$),
μ = product of gravitational constant and the mass of the Earth $= GM$,
m = mass of the reentry body.

From (4) we have

$$\frac{d^2\mathbf{r}}{dt^2} = -(\mu/r^2)\mathbf{e}_r - (F_D/m)\mathbf{e}_\theta. \tag{5}$$

Next, we take the dot product of (5) with $d\mathbf{r}/dt$. Thus,

$$\left(\frac{d\mathbf{r}}{dt}\right)\cdot\left(\frac{d^2\mathbf{r}}{dt^2}\right) = \left(\frac{d\mathbf{r}}{dt}\right)\cdot[-(\mu/r^2)\mathbf{e}_r - (F_D/m)\mathbf{e}_\theta]. \tag{6}$$

Making use of the vector identity $\mathbf{v} \cdot (d\mathbf{v}/dt) = v(dv/dt)$, we have

$$v\left(\frac{dv}{dt}\right) = -(\mu/r^2)\left(\frac{dr}{dt}\right) - v(F_D/m). \tag{7}$$

Substituting (1) into (7) yields

$$\left(\frac{dv}{dt}\right) = -\left[(C_D S/m)(\rho v^2/2) + \mu\left(\frac{dr}{dt}\right)/vr^2\right]. \tag{8}$$

Next, we consider the time rate of the specific angular momentum vector $d\mathbf{H}/dt$ of the center of mass of the reentry vehicle. This is equal to the torque applied per unit mass. Thus,

$$\frac{d\mathbf{H}}{dt} = \mathbf{r} \times (\mathbf{F}/m) = -\mathbf{e}_H(F_D/m)r\cos\varphi, \tag{9}$$

where φ is the angle between the velocity vector $\mathbf{v}$ and the local horizontal, and $\mathbf{e}_H$ is the unit vector along $\mathbf{H}$. Constraining the reentry trajectory to a single plane and then combining (1) and (9) gives

$$\frac{d\mathbf{H}}{dt} = -(\rho C_D S v^2/2m)r\cos\varphi \tag{10}$$

and

$$v\cos\varphi = \left(\frac{d\sigma}{dt}\right)\rho. \tag{11}$$

Substituting (11) into (10) yields

$$H = -(C_D S/m)\left\{\left(\rho v r^2\left(\frac{d\sigma}{dt}\right)\right)\Big/2\right\}. \tag{12}$$

Now the magnitude of $\mathbf{H}$ is given by

$$H = rv\cos\varphi. \tag{13}$$

Thus, substituting (11) into (13) yields

$$\frac{d\sigma}{dt} = H/r^2. \tag{14}$$

In polar coordinates, the value of the velocity magnitude v is given by

$$v^2 = \left(\frac{dr}{dt}\right)^2 + \left(\frac{d\sigma}{dt}\right)^2 r^2 = \left(\frac{dr}{dt}\right)^2 + (H^2/r^2). \tag{15}$$

Therefore,

$$\frac{dr}{dt} = \pm[v^2 - (H^2/r^2)]^{1/2}. \tag{16}$$

Equations (8), (12), (14), and (16) define four first-order simultaneous differential equations of motion of the reentry vehicle. These equations must be solved by numerical methods, since the atmospheric density and the drag coefficient are known but are not analytic functions of r, and there is no closed-form solution to these equations.

As stated in the beginning of this example, the reentry trajectory can be described by the translational motion of a rigid body. The reentry flight model can also be described by the following dynamic equations [15]:

$$
\begin{aligned}
r &= v \sin\gamma, \\
\frac{dv}{dt} &= -D - g\sin\gamma + \omega^2 r\cos\phi[\cos\phi\sin\gamma - \sin\phi\cos\gamma\sin\psi], \\
\frac{d\gamma}{dt} &= (1/v)\{L\cos\sigma - [g - (v^2/r)]\cos\gamma + 2\omega v\cos\phi\cos\psi \\
&\quad + \omega^2 r\cos\phi[\cos\phi\cos\gamma + \sin\phi\sin\gamma\sin\psi]\}, \\
\frac{d\psi}{dt} &= (1/v)\{L(\sin\sigma/\cos\gamma) \\
&\quad - (v^2/r)\tan\phi\cos\gamma\cos\psi(\omega^2 r)(\sin\phi\cos\phi\cos\psi/\cos\gamma), \\
&\quad + 2\omega v[\cos\phi\tan\gamma\sin\psi - \sin\phi]\}, \\
\frac{d\theta}{dt} &= v\cos\gamma\cos\psi/r\cos\phi, \\
\frac{d\phi}{dt} &= v\cos\gamma\sin\psi/r,
\end{aligned}
$$

where

$$
\begin{aligned}
r &= \text{distance from the Earth's center}, \\
v &= \text{Earth-relative speed}, \\
\gamma &= \text{flight-path angle}, \\
g &= \text{acceleration of gravity}, \\
D &= \text{drag acceleration}, \\
L &= \text{lift acceleration}, \\
\theta &= \text{geodetic latitude}, \\
\phi &= \text{geodetic longitude}, \\
\sigma &= \text{bank angle}, \\
\psi &= \text{heading angle}, \\
\omega &= \text{Earth's angular velocity}.
\end{aligned}
$$

Note that in the above equations, r, v, g, D, L, ρ, and ω are normalized parameters (i.e., r is normalized by R_o, the radius of the Earth; v by $(G_o R_o)^{1/2}$; g by G_o, where G_o is the acceleration of gravity at sea level; D by G_o; L by G_o; ρ by (m/SR_o); and ω by $(G_o/R_o)^{1/2}$).

6.8 Missile Flight Model

In this section we will develop the ballistic missile flight model, summarizing the discussion of the previous sections. The development of this flight model will be treated as an example. It should be emphasized that this missile model is by no means complete, and is offered here as a guide for further study. The actual model will depend on the user requirements and missile designer/analyst. In essence, the ballistic missile model provides the capability to model multistage missiles with detailed pitch program guidance. Flight section options include the ability to set up multiple powered flight segments representing engine thrusting, unpowered segments representing ballistic flight, and missile staging events representing missile mass changes. Guidance options such as minimum energy, depressed and lofted flyouts, gravity turns, or multiple guidance phases can be used to achieve the desired flyout. Moreover, the ballistic missile model will be based on the powered flight program; the analyst can choose the *FORTRAN* (or another method such as *Ada*, *C*, or C^{++}) methodology and structure it to update multiple missiles, that is, provide the missile states to other models. The equations of the missile model have been written in a format to make it easy with regard to programming and/or coding in *FORTRAN* or on other language. The ballistic missile model is further supported by the launch iteration schemes. Specifically, the launch iteration schemes determine the correct setting of specific parameters to allow the missile to fly the desired range to the target. Furthermore, the launch iteration schemes provide the capability to model the guidance options mentioned above.

Before detailing the calculations, the various coordinate frames used in a ballistic missile model and how it references the flight section and guidance phase input data will be discussed.

Missile Coordinate Systems: The ballistic missile model uses three separate coordinate systems. These systems are (1) the Earth-centered-inertial (*ECI*) coordinate frame, (2) the east-north-up (*ENU*) frame, and (3) the missile body-axes frame. For more details on coordinate systems, the reader is referred to [11].

(a) Earth-Centered Coordinate Frame
The model is set up to perform most of the calculations in the *ECI* coordinate frame. This frame's origin is at the Earth's center, with the positive X-axis aligned with zero degrees longitude, the positive Y-axis aligned with 90° longitude, and the positive Z-axis aligned with 90° north latitude (or vertical). The *ECI* frame accounts for the velocity induced by the rotation of the Earth.

(b) East-North-Up Coordinate Frame
Calculations of missile azimuth, pitch, and flight-path angle are usually calculated in the east-north-up frame. The origin of this frame is centered at the missile's current ground track position defined by a latitude and longitude on the Earth's surface. Here, the positive X-axis points to the east, the positive Y-axis points north, and the positive Z-axis points along the local vertical. The X- and Y-axes define the local *ENU* ground plane. The missile orientation is calculated relative to this point. Note that in our model we will assume that the Earth's rotation rate has been set to zero.

(c) Missile Body-Axis Coordinate Frame
Calculations of forces acting on the missile are calculated in the body-axis coordinate frame. This frame is centered at the missile's center of gravity (cg). The positive X-axis aligns with the missile's longitudinal body-axis pointing out the nose of the missile, the positive Y-axis points in the direction perpendicular to the longitudinal body-axis and parallel to the local ENU ground plane, and the Z-axis points in the direction perpendicular to the X- and Y-axes such that a right-hand coordinate system is defined.

The rotation from the missile body-axis frame to the ECI coordinate frame will be described below. However, prior to rotation, the following quantities must be calculated for the current integration step:

$$\begin{aligned}
\mathbf{R} &= \text{missile position vector in } ECI \text{ coordinates,}\\
\mathbf{V} &= \text{missile velocity vector in } ECI \text{ coordinates,}\\
\mathbf{1}_X &= \text{unit missile velocity vector in } ECI \text{ coordinates,}\\
\mathbf{1}_Y &= \text{unit cross product of velocity and position vectors,}\\
&= (\mathbf{V} \times \mathbf{R})/(|\mathbf{V} \times \mathbf{R}|)\\
\mathbf{1}_Z &= \text{cross product of } \mathbf{1}_X \text{ and } \mathbf{1}_Y \text{ vectors} = \mathbf{1}_X \times \mathbf{1}_Y.
\end{aligned}$$

The body-axis to ECI transformation matrix T_b is then defined as

$$[T_b] = \begin{bmatrix} X_x & X_y & X_z \\ Y_x & Y_y & Y_z \\ Z_x & Z_y & Z_z \end{bmatrix},$$

and the resultant vector in ECI coordinates is

$$\mathbf{F}_{ECI} = [T_b] \times \begin{bmatrix} F_x \\ F_y \\ F_z \end{bmatrix},$$

where

$$\begin{aligned}
F_{ECI} &= \text{resultant vector in } ECI \text{ coordinates,}\\
\mathbf{F}_n &= \text{original vector in body-axis } n\text{th direction.}
\end{aligned}$$

For the special case where the missile's velocity components are zero, the rotations are performed using the missile position angles of latitude and longitude, and the orientation angles of azimuth and pitch. The missile is first rotated from its body-axis frame to the ENU frame by a positive rotation about the y-axis of 90° pitch (θ), and then a negative rotation about the z-axis of 90° azimuth (ψ). Next, the missile is rotated from the ENU frame to the ECI frame by a negative rotation about the x-axis of 90° latitude (φ), and then a negative rotation about the z-axis of 90° longitude

(λ). The transformation matrix for performing the pitch rotation about the y-axis is as follows [9]:

$$[T_p] = \begin{bmatrix} \sin\theta & 0 & -\cos\theta \\ 0 & 1 & 0 \\ \cos\theta & 0 & \sin\theta \end{bmatrix}. \tag{6.250a}$$

Next, the transformation matrix for performing the azimuth rotation about the z-axis is given by

$$[T_a] = \begin{bmatrix} \sin\psi & -\cos\psi & 0 \\ \cos\psi & \sin\psi & 0 \\ 0 & 0 & 1 \end{bmatrix}. \tag{6.250b}$$

The transformation matrix for performing the latitude rotation about the x-axis is given as follows:

$$[T_{la}] = \begin{bmatrix} 1 & 0 & 0 \\ 0 & \sin\varphi & -\cos\varphi \\ 0 & \cos\varphi & \sin\varphi \end{bmatrix}. \tag{6.250c}$$

Finally, the transformation matrix for performing the longitude rotation about the z-axis is given by

$$[T_{lo}] = \begin{bmatrix} \sin\lambda & -\cos\lambda & 0 \\ \cos\lambda & \sin\lambda & 0 \\ 0 & 0 & 1 \end{bmatrix}. \tag{6.250d}$$

(Note that all angles are given in units of radians.) Using these transformation matrices, the vector is then rotated from the missile body-axis frame to the *ECI* frame according to the transformation

$$\mathbf{F}_{ECI} = [T_{lo}] \times [T_{la}] \times [T_a] \times [T_p] \times \begin{bmatrix} F_x \\ F_y \\ F_z \end{bmatrix}. \tag{6.251}$$

Missile Flight Sections and Guidance Phases: The missile flyout is described by the use of multiple flight sections and guidance phases. The flight sections describe how the missile physically operates, while the guidance phases control the pitching characteristics of the flyout. As discussed in the previous section, all missiles are composed of one or more stages that allow them to fly to their desired target and/or range. Typically, these stages are the booster, sustainer, and reentry vehicle. It is important to remember that the staging events define both mass changes and thrust changes. Booster thrust is usually greater than sustainer thrust, while the reentry thrust is usually zero. Furthermore, some missiles vary their thrust but do not perform staging events until engine burnout. Other missiles fly without ever performing a staging event at all. The flight section methodology discussed here and used by the missile model has been developed to allow modeling of any combination of these staging events or different thrust levels.

Each flight section consists of cut-off time (sec), vacuum thrust (Newtons), fuel burn rate (kg/sec), dry mass (kg), reference area (m^2), nozzle exit area (m^2), coefficients of lift and drag as functions of Mach number, integration step size (sec), and

missile stage identifier. These important performance variables will now be defined. The cut-off time is the absolute missile flight time when the model should transition to the next flight section. The vacuum thrust is the gross amount of missile propelling force, which is produced as the motor burns the fuel. The fuel burn rate is the speed at which the fuel is burned by the motor. The dry mass is the structure mass. The fuel mass is the amount of fuel that is available for thrust production. The reference area is the missile cross-sectional area. The nozzle exit area is the total area of the thrust outlet(s) of the missile motor. The coefficients of lift and drag define the lift and drag characteristics of the missile. The integration step size is the time over which to integrate the missile position, velocity, and expended fuel. The missile stage identifier signifies to which missile stage the dry mass and fuel mass correspond. When multiple flight sections are used to model a single missile stage, then their stage identifiers are set to the same value. Only masses of the first of those sections contribute to the total mass of the missile.

At the beginning of the flyout, the dry and fuel masses of the missile are calculated as follows:

$$M_{Dt} = \Sigma M_D, \tag{6.252a}$$

$$M_{FT} = \Sigma M_F, \tag{6.252b}$$

where

M_{Dt} = total missile dry mass [kg],
M_D = individual stage dry mass [kg],
M_{FT} = total missile available fuel mass [kg],
M_F = individual stage available fuel mass [kg].

The total missile mass at liftoff is then calculated by

$$M_T = M_{Dt} + M_{FT}, \tag{6.253a}$$

where M_T is the total missile mass in [kg]. Throughout the flyout, the missile performance variables, that is, thrust, fuel burn rate, reference area, nozzle exit area, the lift/drag characteristics, and the integration step size, are all set using the parameters of the current flight section. Therefore, the total mass is updated by the following expression:

$$M_T = M_{Dt} + M_{FT} - \Delta M_F, \tag{6.253b}$$

where ΔM_F is the expended fuel mass in [kg]. When the missile time of flight exceeds the current section cut-off time, the model sets the missile performance variables using the next flight section data. If the stage identifier for a new flight section differs from the identifier of the previous stage, representing a missile stage transition, the dry and fuel masses are updated by

$$M_{Dt} = M_{Dt} - M_{DL}, \tag{6.254a}$$

$$M_{FT} = M_{FT} - M_{FL}, \tag{6.254b}$$

where

$$M_{DL} = \text{last stage dry mass [kg]},$$
$$M_{FL} = \text{last stage available fuel mass [kg]}.$$

The expended fuel ΔM_F is reset to 0.0 and the total mass M_T is then updated using (6.253b). This procedure of updating performance variables and masses based on current flight section data is repeated until the missile impacts the ground (or target).

Each missile guidance phase consists of an end time (sec), pitch angle (degrees), pitch rate (deg/sec), and a flag for performing a gravity turn. The end time tells the model when to transition to the next guidance phase. The pitch angle defines how the missile is to be aligned at the start of the phase. If it is the first guidance phase or if the gravity turn option is selected, then the pitch angle tells the model to rotate the missile body-axis to this absolute angle. Otherwise, the pitch angle is the relative number of degrees to rotate the missile from its current orientation. The pitch rate defines the speed at which the missile should pitch until the end of the current guidance phase. The gravity turn flag tells the model to limit the angle of attack, that is, the angle between the velocity vector and the missile body-axis (or missile longitudinal axis), to zero. As discussed in Section 6.5.4, thrust and drag are then aligned with the velocity vector, and so gravity is the only force that causes the missile to pitch. This multiphase capability allows for vertical flight segments, constant-attitude flight segments, thrusted and unthrusted gravity turns, as well as pitch programs whose inputs must be determined. Note that both pitch angle and rate are measured from the launch position *ENU* vertical to maintain a constant frame of reference for measuring pitch throughout the flyout. This approach simulates the constant reference frame provided by a gyroscope in the actual missile system.

Missile Integration: The ballistic missile model is a 3-*DOF* (degrees-of-freedom) model that utilizes basic equations of motion in its missile state calculations. The model calculates acceleration as a function of aerodynamic forces, gravity, and thrust. It applies this acceleration on the appropriate directions according to missile orientation and guidance. It then computes the new position, velocity, and expended fuel mass over each integration step using a fourth-order Runge–Kutta integration method.

Calculation of Aerodynamic Forces: During integration, the missile altitude is calculated by the expression

$$H = R_{\text{mag}} - R_e, \tag{6.255}$$

where

$$H = \text{missile altitude [m]},$$
$$R_{mag} = \text{missile } ECI \text{ position vector magnitude [m]},$$
$$R_e = \text{radius of the Earth}.$$

The altitude H is used to reference the speed of sound C and air density ρ from 1962 standard atmosphere tables (see Appendix D for details on the atmosphere model). Mach number is then calculated according to the equation

$$M = V_{mag}/C, \tag{6.256}$$

where

$$\begin{aligned} M &= \text{missile Mach number,} \\ V_{mag} &= \text{magnitude of missile velocity vector [m/sec],} \\ C &= \text{speed of sound [m/sec].} \end{aligned}$$

Next, we compute the dynamic pressure according to the equation

$$q = \tfrac{1}{2}\rho V_{mag}^2, \tag{6.257}$$

where,

$$\begin{aligned} q &= \text{dynamic pressure [kg/m-sec}^2\text{],} \\ \rho &= \text{air density [kg/m}^3\text{].} \end{aligned}$$

Now the coefficients of lift C_L and drag C_D must be linearly interpolated or extrapolated as functions of Mach number M. The aerodynamic forces acting on the missile body are then calculated in the body-axis frame according to the relations

$$D = -C_D q S_{ref}, \tag{6.258a}$$

$$L = C_L \alpha q S_{ref}, \tag{6.258b}$$

where

$$\begin{aligned} D &= \text{drag force in the body-axis } x\text{-direction [newtons],} \\ L &= \text{lift force in the body-axis } z\text{-direction [newtons],} \\ \alpha &= \text{angle of attack [degrees],} \\ S_{ref} &= \text{missile aerodynamic reference area [m}^2\text{].} \end{aligned}$$

The present model assumes no sideslip, so that the aerodynamic force acting in the body-axis Y direction is zero. These aerodynamic forces are then rotated from the body-axis coordinate frame to *ECI* to be used in the acceleration equations [4]

$$\begin{aligned} F_{LDx} &= L_x + D_x, \\ F_{LDy} &= L_y + D_y, \\ F_{LDz} &= L_z + D_z, \end{aligned} \tag{6.259}$$

where

$$\begin{aligned} F_{LDn} &= \text{aerodynamic force in } ECI\ n\text{-direction [newtons],} \\ L_n &= \text{lift force in } ECI\ n\text{-direction [newtons],} \\ D_n &= \text{drag force in } ECI\ n\text{-direction[newtons].} \end{aligned}$$

Acceleration due to Gravity Potential gravity is calculated by (see also (6.232))

$$g_p = -g_c / R_{mag}^3, \tag{6.260}$$

where

$$\begin{aligned} g_p &= \text{potential gravity [1/sec}^2\text{]}, \\ g_c &= \text{universal gravitational constant (also known as } \mu) \\ &= 3.986 \times 10^{14} \text{ [m}^3\text{/sec}^2\text{]}. \end{aligned}$$

Acceleration due to gravity is calculated in *ECI* coordinates according to

$$\begin{aligned} A_{gx} &= g_p R_x, \\ A_{gy} &= g_p R_y, \\ A_{gz} &= g_p R_z, \end{aligned} \tag{6.261}$$

where

$$\begin{aligned} A_{gn} &= \text{acceleration of gravity in } \textit{ECI } n\text{-direction [m/sec}^2\text{]}, \\ R_n &= \text{missile position in } \textit{ECI } n\text{-direction [m]}. \end{aligned}$$

Acceleration due to Thrust: Vacuum thrust is input as a function of the missile flight section. The ballistic missile model tracks the total amount of fuel that is available, setting the thrust to zero when all the current-stage fuel has been expended. However, if fuel is available, the total thrust is calculated from the expression

$$T = T_v - A_{NE} P, \tag{6.262}$$

where

$$\begin{aligned} T &= \text{total thrust [newtons]}, \\ T_v &= \text{vacuum thrust [newtons]}, \\ A_{NE} &= \text{nozzle exit area [m}^2\text{]}, \\ P &= \text{atmospheric pressure [newtons/m}^2\text{]}. \end{aligned}$$

The second term in (6.262) is the thrust that is canceled out by atmospheric pressure working against the vacuum thrust on the engine exit area plane. Thrust acceleration magnitude is then calculated according to (see (6.215))

$$A_T = T / M_T, \tag{6.263}$$

where

$$\begin{aligned} A_T &= \text{thrust acceleration [m/sec}^2\text{]}, \\ T &= \text{total thrust [newtons]}, \\ M_T &= \text{total missile mass [kg]}. \end{aligned}$$

Thrust Pointing Vector: In Section 6.5.4 we discussed the thrust vector control aspect for controlling the missile during the atmospheric phase. Since the thrust works along the body-axis of the missile, the missile must be rotated to a pointing vector in the desired direction in order to change the direction of flight. The model assumes that the pointing vector and the missile body-axis are the same. This pointing vector is defined by the pitch angle resulting from the guidance phases at the current time in the flyout. The guidance phases are set up from data that describe how a particular missile pitches as a function of time. Now, if the thrust T is not zero, the maximum angle of attack α is not zero, and the gravity turn option of the current guidance phase is not selected, then the desired pitch in the launch point *ENU* coordinate frame at the start of the phase is

$$\theta = \theta + \theta_A, \tag{6.264a}$$

and later in the phase,

$$\theta = \theta + \theta_R t_p, \tag{6.264b}$$

where

$$\begin{aligned} \theta &= \text{current missile pitch angle [rad]},\\ \theta_A &= \text{current guidance phase pitch angle [rad]},\\ \theta_R &= \text{current guidance phase pitch rate [rad/sec]},\\ t_p &= \text{time within the current guidance phase [sec]}. \end{aligned}$$

Azimuth is calculated in the launch *ENU* frame by rotating the current value of the pointing vector into the launch *ENU* frame as follows:

$$\psi = \tan^{-1}(R_{NTx}/R_{NTy}), \tag{6.265}$$

where

$$\begin{aligned} \psi &= \text{the current missile azimuth [rad]},\\ R_{NTn} &= \text{the current pointing vector in the } \textit{ENU } n\text{-direction}. \end{aligned}$$

The model uses pitch θ, azimuth ψ, and the launch site latitude and longitude angles to rotate a unit pointing vector in the body-axis frame into the *ECI* frame, resulting in the new pointing vector R_{NT}.

Angle-of-Attack Limits and Gravity Turns The angle of attack α is found by the expression

$$\alpha = \cos^{-1}[(\mathbf{R}_{NT} \cdot \mathbf{V})/(\mathbf{R}_{NTm} \times |\mathbf{V}|)], \tag{6.266}$$

where

$$\begin{aligned} \mathbf{R}_{NT} &= \text{current pointing vector in the } \textit{ECI} \text{ frame [m]},\\ \mathbf{R}_{NTm} &= \text{current pointing vector magnitude [m]},\\ \mathbf{V} &= \text{current velocity vector in the } \textit{ECI} \text{ [m/sec]}. \end{aligned}$$

If the angle of attack α is greater than the maximum α, then the pointing vector $\mathbf{R}_{NT}$ is recalculated so as not to exceed this maximum.

If the current phase is a gravity turn, the pitch angle θ is set to the current guidance phase angle, and the pointing vector $\mathbf{R}_{NT}$ is calculated accordingly. Pitch θ remains at that angle until the velocity vector crosses $\mathbf{R}_{NT}$; that is, the angle of attack α goes from positive to negative or vice versa. Once this crossover occurs, maximum α is set to zero, so the pointing vector $\mathbf{R}_{NT}$ is calculated according to an angle of attack of zero. This results, as indicated in Section 6.5.4, in thrust acting along the direction of the unit velocity vector, and gravity pulls the velocity vector toward the center of the Earth. Hence, a gravity turn occurs. Gravity turns also occur if the maximum α is input as zero or if the total thrust equals zero, which automatically causes the maximum α to be set to zero.

Total Acceleration: The total acceleration vector in *ECI* coordinates is then calculated as follows:

$$\begin{aligned} A_x &= A_{Gx} + A_T \times R_{NTx} + F_{LDx}/M_T, \\ A_y &= A_{Gy} + A_T \times R_{NTy} + F_{LDy}/M_T, \\ A_z &= A_{Gz} + A_T \times R_{NTz} + F_{LDz}/M_T, \end{aligned} \tag{6.267}$$

where

$$\begin{aligned} A_n &= \text{total acceleration in } \textit{ECI } n\text{-direction} \\ &\quad [\text{m/sec}^2], \\ A_{Gn} &= \text{gravity acceleration in } \textit{ECI } n\text{-direction} \\ &\quad [\text{m/sec}^2], \\ R_{NTn} &= \text{current pointing vector in} \\ &\quad \textit{ECI } n\text{-direction [m]}, \\ F_{LDn} &= \text{aerodynamic force in } \textit{ECI } n\text{-direction [newtons]}, \\ M_T &= \text{total missile mass [kg]}. \end{aligned}$$

Missile State Runge–Kutta Integration: The Runge–Kutta integration method is a fourth-order multistep integration technique that was derived from a Taylor series expansion. It allows for a high degree of accuracy while requiring an acceptable number of calculations to complete the integration. In order to perform an integration, the model sets the integration time Δt as the smaller of the flight-section-referenced integration step size and the missile-state update time interval over which to perform the integration. When integrating over the interval from time t to time $t + \Delta t$ in the missile flyout, the method calculates the state properties at the beginning of the interval, halfway through, and then at the end of the interval. Four coefficients are calculated in updating the missile state at these different points in the interval. These coefficients are calculated for each missile state parameter being integrated: time-in-flight, total missile mass, position components, and velocity components. They are then combined, and the missile's state at the end of the interval is then extracted. In

order to illustrate the Runge–Kutta technique, the missile interim state at time t is stored in temporary variables:

$$\begin{aligned} t_{RK} &= t, \\ M_{RK} &= M_T, \\ X_{RKn} &= X_n, \\ V_{RKn} &= V_n, \end{aligned} \tag{6.268}$$

where

t_{RK} = Runge–Kutta missile time of flight [sec],
t = missile time of flight [sec],
M_T = total missile mass [kg],
M_{RK} = Runge–Kutta missile mass [kg],
X_{RKn} = Runge–Kutta missile position in n-direction [m],
X_n = missile position in *ECI* n-direction [m],
V_n = missile velocity in *ECI* n-direction [m/sec],
V_{RKn} = Runge–Kutta missile velocity in n-direction [m/sec].

These interim state values are then used to calculate the acceleration A as shown above. The first of the four Runge–Kutta (RK) state coefficients is then calculated by the following relations:

$$\begin{aligned} t_{K1} &= \Delta t, \\ M_{K1} &= -B_R \times \Delta t, \\ X_{K1n} &= V_{RKn} \times \Delta t, \\ V_{K1n} &= A_n \times \Delta t, \end{aligned} \tag{6.269}$$

where

t_{K1} = Runge–Kutta coefficient 1 for missile time of flight Δ [sec],
M_{K1} = Runge–Kutta coefficient 1 for missile burned mass [kg],
B_R = missile fuel burn rate [kg/sec],
X_{K1n} = Runge–Kutta coefficient 1 for missile position Δ in n-direction [m],
A_n = total acceleration in *ECI* n-direction [m/sec^2],
Δt = integration time [sec].

The interim missile state parameters are now updated using the first Runge–Kutta coefficients:

$$\begin{aligned} t_{RK} &= t + \tfrac{1}{2} t_{K1}, \\ M_{RK} &= M_T + \tfrac{1}{2} M_{K1}, \end{aligned}$$

$$X_{RKn} = X_n + \tfrac{1}{2} X_{K1n},$$
$$V_{RKn} = V_n + \tfrac{1}{2} V_{K1n}, \tag{6.270}$$

where

$$t_{RK} = \text{Runge–Kutta missile time of flight [sec]},$$
$$t = \text{missile time of flight [sec]}.$$

The missile state at the end of the interval is then calculated using the state values at the beginning of the interval and all four of the Runge–Kutta coefficients [12]:

$$t_{RK} = t + (t_{K1} + 2t_{K2} + 2t_{K3} + t_{K4})/6.0, \tag{6.271a}$$

$$M_{RK} = M_T + (M_{K1} + 2M_{K2} + 2M_{K3} + M_{K4})/6.0, \tag{6.271b}$$

$$X_{RKn} = X_n + (X_{K1n} + 2X_{K2n} + 2X_{K3n} + X_{K4n})/6.0, \tag{6.271c}$$

$$V_{RKn} = V_n + (V_{K1n} + 2V_{K2n} + 2V_{K3n} + V_{K4n})/6.0, \tag{6.271d}$$

where all the parameters have already been defined above. This entire procedure is repeated until the missile impacts with the target. Finally, it is noted that impact is defined as having occurred when the descending missile's altitude is less than the target altitude.

In Section 6.5.3 the missile control system was discussed with particular emphasis on pitch/steering control for atmospheric exit. In some ballistic missiles, steering is effected by pitch and yaw commands determined from the gravity-free accelerations and velocities to be gained. Normally, pitch and yaw commands are issued after first-stage ignition. For the first few seconds of powered flight, steering is employed for purposes of launch recovery, in order to provide a (prescribed) given orientation to the missile axis. Steering based on the guidance equations is then dominant for the remainder of the powered trajectory.

Launch Recovery Phase A simplified simulation of the angular acceleration during the launch recovery phase can be used in order to steer the missile axis to a nominal orientation with respect to the inertial reference system. Thrust moments are included, but aerodynamic moments are neglected. The pitch command angle θ_c is computed as

$$\theta_c = \int_{t_{10}}^{t} \int_{t_{10}}^{t} \left(\frac{dq}{dt} \right) dt\, dt \tag{6.272}$$

with initial conditions

$$\theta_c(t_{10}) = \theta_{co} \quad \text{and} \quad q(t_{10}) = q_0,$$

where t_{10} is the time of first-stage ignition. The missile pitch acceleration dq/dt is given by

$$\frac{dq}{dt} = [(F_v - A_e P) k_\theta \partial\theta (L_j - L_g)]/I_{yy}, \tag{6.273}$$

where

A_e = nozzle exit area,
P = atmospheric pressure,
F_v = thrust in vacuo,
k_θ = linearization factor relating lateral thrust force and nozzle deflection angle,
$\partial\theta$ = deflection angle generated by the autopilot equation,
L_j, L_g = moment arms measured from the nose of the missile to the plane of thrust deflection and to the missile center of gravity, respectively,
I_{yy} = pitch moment of inertia.

Integrating (6.279) produces the pitch rate q.

The deflection angle $\partial\theta$ is generated by the autopilot equation and is given as

$$\partial\theta = q\delta_{\dot{\theta}} - \delta_{\theta c}[\sin((\pi/2) - \bar{\theta}_c + \bar{\theta}_t) - \sin\bar{\theta}_t], \tag{6.274}$$

where $\bar{\theta}_t$ has the value 90°. The coefficients $\delta_{\dot{\theta}}$ and $\delta_{\theta c}$ are input constants governed by missile stability characteristics. The angle $\bar{\theta}_t$ is the pitch angle with respect to the launch horizontal plane, desired to be reached by the termination of the launch recovery phase.

The yaw command angle is computed in a similar fashion. Thus,

$$\bar{\psi}_c = \int_{t_{10}}^{t}\int_{t_{10}}^{t}\left(\frac{dr}{dt}\right)dt\,dt, \tag{6.275}$$

with initial conditions

$$\bar{\psi}_c(t_{10}) = \bar{\psi}_{co} \quad \text{and} \quad r(t_{10}) = r_0.$$

The yaw acceleration is

$$\frac{dr}{dt} = [(F_v - A_e P)k_\theta \partial\psi(L_j - L_g)]/I_{yy} \tag{6.276}$$

with

$$\partial\psi = r\delta_{\dot{\psi}} - \delta_\psi\bar{\psi}_c, \tag{6.277}$$

where the symbols have been defined above.

An Example In this example we will derive the differential equations used to generate the orbital motion of a space vehicle (e.g., a missile), including gravity and drag effects.

Coordinate Systems The computations are performed in an inertial rectangular coordinate system (x, y, z), with origin at the geocenter, with the z-axis along the Earth's axis in a northerly direction. The Greenwich meridian is assumed to intersect the positive x-axis at time zero (i.e., the starting time of the orbit). A spherical coordinate system (r, θ, ϕ) will also be employed frequently (see the illustration below).

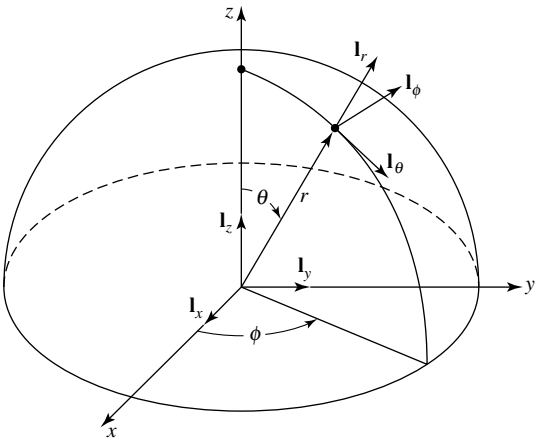

Rectangular and spherical coordinate systems.

The angle ϕ is measured counterclockwise from the positive x-axis, as seen from the North Pole. Associated with the angles θ and ϕ is a rectangular system with axes in the r, θ, and ϕ directions. The transformation matrix from the rectangular (r, θ, ϕ) system to the (x, y, z) system is [11]

$$T_{SR} = \begin{bmatrix} \sin\theta\cos\phi & \cos\theta\cos\phi & -\sin\phi \\ \sin\theta\sin\phi & \cos\theta\sin\phi & \cos\phi \\ \cos\theta & -\sin\phi & 0 \end{bmatrix} \tag{1}$$

Orbit Differential Equations The differential equations satisfied by the orbit are

$$\begin{aligned} \frac{dx}{dt} &= u, \\ \frac{dy}{dt} &= v, \\ \frac{dz}{dt} &= w, \\ \frac{du}{dt} &= g_x + D_x, \\ \frac{dv}{dt} &= g_y + D_y, \\ \frac{dw}{dt} &= g_z + D_z, \end{aligned} \tag{2}$$

or in vector form,

$$\frac{dx}{dt} = \mathbf{v}, \tag{3a}$$

$$\frac{d\mathbf{v}}{dt} = \mathbf{g} + \mathbf{D}, \tag{3b}$$

where $\mathbf{g}$ is the gravitational acceleration and $\mathbf{D}$ is the drag acceleration.

Gravitational Forces The components of gravitational acceleration are most conveniently evaluated in the (r, θ, ϕ) system and later transformed. Therefore, we use the components of $\mathbf{g}$ as follows:

$$g_r = -\left(\frac{\partial U_p}{\partial r}\right), \tag{4a}$$

$$g_\theta = -\frac{1}{r}\left(\frac{\partial U_p}{\partial \theta}\right), \tag{4b}$$

$$g_\phi = -\frac{1}{r\sin\theta}\left(\frac{\partial U_p}{\partial \phi}\right), \tag{4c}$$

where $U_p(r, \theta, \phi)$ is the gravitational potential function, assumed to be given by

$$\begin{aligned} U_p(r,\theta,\phi) = &-(\mu/r)[1 + (J_2/3)(R_e/r)^2(1 - 3\cos^2\theta) \\ &+ (J_3/5)(R_e/r)^3(3\cos\theta - 5\cos^3\theta) \\ &+ (J_4/35)(R_e/r)^4(3 - 30\cos^2\theta + 35\cos^4\theta)], \end{aligned} \tag{5}$$

where R_e is the Earth's equatorial radius. The numerical values of the parameters J_2, J_3, and J_4 are taken to be:

$$J_2 = 1.082630 \times 10^{-3}, \quad J_3 = -2.30 \times 10^{-6}, \quad J_4 = -1.80 \times 10^{-6},$$
$$\mu = 1.407645 \times 10^{16}\text{ft}^3/\text{sec}^2, \quad R_e = 20.92569 \times 10^6\text{ft}.$$

(Note: when using this equation, the reader and/or user should check for the latest values of these parameters.)

The components of the gravitational acceleration are

$$\begin{aligned} g_r = &-(\mu/r^2)[1 + (J_2/3)(R_e/r)^2(1 - 3\cos^2\theta) \\ &+(4J_3/5)(R_e/r)^3(3\cos\theta - 5\cos^3\theta) \\ &+(J_4/7)(R_e/r)^4(3 - 30\cos^2\theta + 35\cos^4\theta)], \end{aligned} \tag{6}$$

$$\begin{aligned} g_\theta = &(\mu/r^2)\sin\theta[2J_2(R_e/r)^2\cos\theta - (3J_3/5)(R_e/r)^3(1 - 5\cos^2\theta) \\ &+(4J_4/7)(R_e/r)^4(3\cos\theta - 7\cos^3\theta)], \end{aligned} \tag{7}$$

$$g_\phi = 0, \tag{8}$$

so that in the (x, y, z) system, $\mathbf{g}$ takes the form

$$\mathbf{g} = \begin{bmatrix} g_x \\ g_y \\ g_z \end{bmatrix} = T_{SR} \begin{bmatrix} g_r \\ g_\theta \\ g_\phi \end{bmatrix}. \tag{9}$$

Drag Forces The acceleration due to drag is given by

$$\mathbf{D} = -\rho\beta|\mathbf{v}_r|\mathbf{v}_r, \tag{10}$$

where ρ is the air density, β is the ballistic coefficient, and $\mathbf{v}_r$ is the velocity relative to the (rotating) atmosphere:

$$\mathbf{v}_r = \mathbf{v} - \omega_{EA}\begin{bmatrix} -y \\ x \\ 0 \end{bmatrix}, \tag{11}$$

where ω_{EA} is the angular velocity of the Earth's atmosphere. The angular velocity ω_{EA} can be made zero even if the Earth is rotating to eliminate wind effects if desired (note that the period of rotation of the atmosphere relative to the Earth is one month at a height of 500 mb and 2–3 weeks in the highest levels of the atmosphere). The density ρ is that of the 1959 *ARDC* standard atmosphere, corrupted by random perturbations. The altitude used for the density calculations is

$$h = r - R(\theta), \tag{12}$$

where

$$R(\theta) = (1-f)R_e/[(1-f)^2\sin^2\theta + \cos^2\theta]^{1/2}, \tag{13}$$

and f is the *flattening* of the Earth given by the expression

$$f = (R_e - R_p)/R_e, \tag{14}$$

where R_p is the Earth's polar radius. The air density is computed from the model atmosphere given by the symbol ρ_m, so that the true density ρ is given by

$$\rho = \rho_m \exp(n_d), \tag{15}$$

where n_d is a dimensionless "density noise." The form of the equation ensures that ρ will never be negative. When n_d is small, it represents a fractional change of the density from the nominal (i.e., model) value.

6.9 Ballistic Missile Intercept

6.9.1 Introduction

In recent years, several ballistic missile intercept concepts have been proposed as part of the overall ballistic missile defense (*BMD*) program. One such program was the midcourse concept. The missile defense technologies pursued presently include (a) the airborne laser (*ABL*), (b) the space-based laser (*SBL*), (c) the sea-based kinetic-energy kill concept, and (d) the space-based hit-to-kill experiment. The latter two are being considered to serve as hedges in case the directed-energy (*DE*) approaches fail.

Nevertheless, *DE* is considered to be the "new frontier," in that it provides military planners a new capability in warfare: to be able to fight at the speed of light. Also, the Air Force intends to put a high-power microwave (*HPM*) weapon on an advanced version of its unmanned strike aircraft by the year 2012. Moreover, the U.S. Congress wants *DE* weapons technology and the *UCAV* to make up one-third of the strike inventory by 2010. Previously, attention has been focused on airborne chemical lasers to destroy ballistic missiles. The Navy's *DD-X* ship design will use *DE* weapons that can destroy supersonic antiship missiles. However, for the near term, interest is turning to smaller, cheaper solid-state *HEL* and *HPM* weapons. A solid-state laser generates pulsed power that creates an energy buildup that damages targets made of relatively soft, easy-to-melt metals such as aluminum and other lightweight materials used in missiles. *UCAV*s equipped with *DE* weapons are also envisioned to strike air defense missiles and radar sites. Currently, the *DoD* is putting new emphasis on the boost-phase intercept (*BPI*) technology.

The interception of *ICBM*s using the *BPI* technology is considered by many experts in the field as the most promising and effective way to counter enemy ballistic missile threats. For instance, in the case of *ICBM*s, the defense has about 180–300 sec during which the target is boosting and presents a large *IR* signature to track (note that an *IR* launch warning sensor will be needed to warn of an *ICBM* launch). An obvious benefit of having a boost-phase element in a larger missile defense architecture, some experts believe, is that it makes it more difficult for an enemy to devise countermeasures. One of the greatest advantages of boost-phase systems is that they can destroy a missile regardless of its design range. Consequently, if the missile carries a nuclear, chemical, or biological warhead, in most cases, it would fall on the enemy's own territory. The greatest difficulty in using the *BPI* technology is that everything from launch to detection to intercept must be completed within a few minutes (e.g., a maximum of 5 min).

More specifically, the Missile Defense Agency (*MDA*) is working toward the deployment of an integrated, layered missile defense system that will provide limited defense against long-range threats and a robust defense against shorter-range threats. A layered defense seeks to destroy missiles in (a) the boost, (b) midcourse, and (c) terminal phases of their trajectory. That is, the system would use multiple shots in each phase. We begin this discussion by summarizing the concept of the layered missile defense system.

Boost-Phase: The boost-phase defense is the airborne laser (*ABL*). This speed-of-light laser system, as will be discussed later, would strike missiles shortly after launch. The agency is also looking at other sea-based and ground systems. It is estimated that the boost-phase system might be ready by the year 2009.

Midcourse: Midcourse defenses include the exoatmospheric kill vehicle. This *hit-to-kill* vehicle rams into incoming warheads in space. The collision, at some 15,000 miles per hour, vaporizes both. Recent tests have proved that the hit-to-kill technology is mature and effective. Another midcourse system is sea-based and has also been tested successfully. The experience with the Navy *standard missile,* 3 (*SM*-3), has been so positive that the agency will speed development.

Terminal-Phase: Terminal-phase systems are perhaps the ones the public knows most. The *PAC*-3 system is in operational testing now. Based on the *Patriot* system, the missile intercepts incoming ballistic missiles in the atmosphere. Other systems include the Theater High-Altitude Area Defense (*THAAD*) and the joint Israeli–U.S. *Arrow* system. Sea-based missile defense systems are also included in the terminal-phase plans. The recent U.S. withdrawal from the Anti-Ballistic Missile Treaty aids the U.S. missile defense effort. The withdrawal allows the United States to explore different elements of missile defense and to approach the missile defense in greater detail. It also provides for more realistic testing of these systems. Finally, the United States can now discuss the missile defense problem with allies, something the treaty forbade.

We will now discuss briefly the *SBL* and *ABL* directed-energy technology programs. A U.S. Air Force/industry consortium consisting of Boeing, Lockheed Martin, and TRW is in the early stages of defining an orbiting missile defense (or antimissile) system. A preliminary design calls for 24 satellites in low-Earth orbits of about 1,000 km (621.4 miles). This directed-energy technology, space-based missile defense program known as the space-based laser (*SBL*) program is designed to destroy intercontinental ballistic missiles shortly after launch (or boost phase). In addition to targeting ballistic missiles, the technology program is supposed to improve cruise missile defenses. In other words, the space-based laser can destroy missiles before penetration aids and multiple reentry vehicles are dispensed. The *DoD* wants the system to work in conjunction with the ground-based *NMD* system, which is already in development. Lockheed Martin is taking the lead on the space segment, and *TRW* on the payload. The payload area is further divided, with *TRW* focusing on the chemical oxygen iodine laser, Lockheed Martin on the beam control/fire control system, and Boeing on the beam director.

Unlike the ground-based midcourse intercept system (formerly known as the national missile defense (*NMD*) project), which acts as a terminal defense system and has to discriminate between real warheads and decoys, the *SBL* is intended to destroy an *ICBM* before it can deploy its warhead or decoys. *SBL* satellites will be equipped with multiple sensors, that is, passive missile detection sensors to spot launching missiles and an active laser-radar (or *ladar*) to track the missile during its boost phase. A megawatt laser will then be used to destroy the missile.

At this point, an in-orbit Air Force/Ballistic Missile Defense Organization (*BMDO*) *SBL* project is focused on an integrated flight experiment (*IFX*) planned for around the year 2012, with a major ground test of the flight-ready hardware that is supposed to go into space starting about five years earlier (note that in January 2002 the *BMDO* was elevated to agency status and redesignated as the Missile Defense Agency (*MDA*)). However, the *IFX* is serving only as a technology demonstrator, not a limited operational system. The *IFX* intercept attempt will be conducted against a modified *Minuteman III ICBM* fitted with a liquid third stage. This should be representative of *ICBM* threats. Moreover, the purpose of the *IFX* is to demonstrate the high-power laser source with regard to acquisition, tracking, and pointing. An operational system would not be ready until 2018–2020. The range requirement for the

experiment, while not yet detailed, will be far more than 100 nm (185.3 km). An operational system would have to have much greater capability. A baseline requirements review for *IFX* that assigned notional weight goals for different parts of the satellite design was recently completed. In order to fit into the constraints of a heavy-lift evolved expendable launch vehicle (*EELV*), the total spacecraft is being limited to 53 ft (16.15 m) in height and 43,400 lb (19,686.2 kg). By far the largest element will be the laser payload, which has been allotted 25,265 lb (11,460.2 kg). The beam control is being designed to 5,681 lb (2,576.9 kg), while the beam director, the mirror through which the laser will be pointed, is assigned 3,420 lb (1,551.3 kg). The mirror will measure 2.8 meters (9.19 ft) in diameter, although it would have to be 8–10 meters (26.25–32.81 ft) in an operational version.

However, the *SBL* program faces formidable technical problems. Specifically, the technically most difficult aspect of the system is likely to be the deployable optics. In order to achieve the power levels required to destroy a missile, the *SBL* has to include large optics through which the laser will propagate. But those optics will fit in a heavy-lift launcher only if they are folded. Nevertheless, the design will likely be a variant of the chemical high-frequency Alpha laser. The U.S. Air Force developed and demonstrated the feasibility of destroying missiles with a laser in the 1980s, known as the Airborne Laser Laboratory. This program served as a precursor to the airborne laser (*ABL*). There will be provisions for an operational *SBL* to be refueled in orbit. The *SBL* program is resisting some calls for use of solid-state lasers, but some argue that the technology is not mature enough.

Since its inception in 1996, the airborne laser (*ABL*), the largest program among all *BPI* efforts, is also the one with the most research and development behind it. Initially, *ABL* is designed to defeat short-range ballistic missiles, but its role can be extended for strategic missiles as well. *ABL* is a revolutionary program that is serving as a trailblazer for *SBL* technologies. Pentagon officials are inclined toward a space-based system because a large enough constellation would provide permanent global coverage, while *ABL* or most of the Pentagon's other boost-phase intercept systems would have to be deployed and positioned precisely to carry out their mission. A Russian *SS-18* (*R-36M*)-like heavy *ICBM* equipped with multiple warheads is the baseline threat against which *SBL* is being designed.

While the beam controls of the two concepts are in many respects quite similar, there are also important differences between the two *DE* systems. The *ABL* is designed to shoot down a ballistic missile during its relatively short boost phase by placing high-power energy on the missile using a megawatt-class chemical oxygen–iodine laser (*COIL*); its space-based counterpart will employ a hydrogen fluoride system. *COIL* is not suitable for space operations because its chemicals would not mix properly in a zero-*g* environment.

USAF officials hope that both directed-energy projects will do more for them than just missile defense work. *ABL* is being envisioned for potential use in destroying cruise missiles, aircraft, or even surface-to-surface missiles. *SBL*, for instance, is seen as potentially having a space-to-ground application, although that would require a laser using an atmosphere-penetrating wavelength that currently is not being pursued. *SBL* also may also be able to destroy air-breathing targets or satellites.

We will now discuss in some detail the airborne laser (*ABL*). The *ABL* is a highly modified Boeing 747-400F freighter. Rollout at the Boeing Wichita, Kansas, facility, where the aircraft is being reconfigured and the battle management system installed, was on November 10, 2001. The *ABL* made its maiden flight for airworthiness on July 18, 2002, circling over western Kansas for one hour and twenty-two minutes before returning to its takeoff location at McConnell AFB, Kansas, taking the first steps in becoming the world's first directed-energy (*DE*) combat aircraft. This successful flight is a milestone in the history of *ABL*, whose ultimate goal is that of shooting down a ballistic missile with a beam of ultrapowerful light by the end of 2004. *ABL* is scheduled to take its place as a principal member of the boost-phase segment of the Missile Defense Agency's (*MDA*) layered system, designed to protect the country and U.S. troops against enemy ballistic missiles. *ABL*'s task is to destroy the just-launched *ICBM*s by focusing its high-energy laser beam on the pressurized fuel tank, causing it to rupture and explode, in effect causing the missile to kill itself. *ABL*, now under the *MDA*'s management, is being developed, as stated earlier, by a team composed of the Boeing Co., TRW, and Lockheed Martin. Boeing supplied the aircraft and the sophisticated software system that will be the brains of the weapon system. Moreover, Boeing will develop the battle management and control system, integrating the weapon system and supplying the flying platform (i.e., the 747-400F airplane). TRW will built the megawatt-class lasers that constitute the system's kill mechanism and ground support, while Lockheed Martin built the complicated maze of mirrors and lenses used to guide the lasers to the target and the turret that will house the system's 1.5-meter telescope. A 1.8-meter in diameter turret window for the laser in the nose of the aircraft will offer 120° pointing capability. Also, Lockheed Martin is developing the beam-control/fire-control system. Once testing has been completed, the *ABL* will be turned over to the Air Force. For *ABL*, the July 18 maiden flight represents the most visible program evolution since it formally began in November 1996.

As stated above, the Boeing 747-400F underwent extensive modifications. More specifically, the nose is a 12,000-pound rotating turret, which eventually will house the *ABL*'s 5-foot telescope, the lens through which three of four onboard lasers will be fired. Besides the lethal light source, a chemical oxygen iodine laser (*COIL*) provided by TRW (see discussion above) is capable of producing from more than 200 miles away a basketball-sized spot hotter than the equivalent of 10,000 100-watt light bulbs. The aircraft also will be equipped with two solid-state kilowatt-class lasers used for tracking, aiming, and measuring the amount of atmospheric distortion between the plane and the target, a phenomenon corrected using adaptive optics. The only major laser that will not be fired through the turret will be a tracking device called the *Active Ranger System*, a CO_2 laser that sits in a teardrop-shaped pod atop the aircraft on the distinctive 747 "hump." Installed will also be 6 *IR* tracking devices, one each in the front and rear, and two on each side, to detect the heat generated by boosting missiles.

At this stage of development, the turret is made up of a rotating clamp-like device called a roll shell, and a large ball made of composite material that will simulate the housing for the five-and-a-half-foot window through which the laser beams will be fired. The turret weighs as much as the fixture that will later be installed on the aircraft

and used during testing On December 19, 2002, the aircraft, tail No. 00-0001, moved to Edwards AFB, California, for installation of the optics and laser elements and to undergo flight tests and evaluation. A two-year-long series of tests is planned. During the NMD test (*IFT-10*) on December 11, 2002, the *YAL-1A* checked its *IR* sensors by observing the launch of the target missile from 38,000 ft and 300 mi away.

Although the aircraft is generically known as *ABL*, its official name is *YAL-1A*, which in Air Force nomenclature stands for *Prototype Attack Laser*, Model *1-A* (see also Appendix E). If testing goes well, it will be followed by a so-far undetermined number of similar aircraft.

One of the most recent milestones, as stated above, was the delivery of the first two of six *IR* sensors to the Boeing Company. The sensors, derivatives of the *F-14* infrared search and track system, will be used by *ABL* to spot the boosting missile and provide 360° coverage. The sensors are being used to refine missile-tracking software. Tests will continue on fire-control elements, laser modules, and the battle-management system. Final integration and lethality tests, including a live-fire demonstration on a *Scud*-like missile, are scheduled for 2003 with final *IOC* projected in 2007.

Confidence in the emerging field of laser weapons technology was bolstered in 2000 when the U.S. Army destroyed a short-range *Katyusha* rocket with its tactical high-energy laser (*THEL*). Although *THEL* is aimed against a different set of targets from those targeted by the *ABL* or *SBL*, operating at much shorter ranges, in many respects, the *Katyusha* is a more difficult target to destroy.

The *ABL* system integrates technologies such as a modified *F-14 IR* search and track system mentioned above, *LANTIRN* targeting pods, and five lasers to locate, track, and destroy enemy ballistic missiles, similar to those used in the Gulf War. The system first looks into enemy territory to detect the launch of a missile. When it determines that the missile is a threat, it builds up laser energy and directs it at the missile through the 1,000-pound glass lens in its front turret. This causes the outside of the missile to heat up to the point that the missile ruptures. This process all takes place quickly enough to destroy the missile soon after launch, in what is called the boost phase. The *ABL* ushers in a new capability to defend troops against theater ballistic missiles. Furthermore, when it detects a launch and is able to kill the missile early, it prevents debris from falling in friendly territory; this is particularly important with chemical, nuclear, or biological weapons. In addition to the laser's ability to take out a ballistic missile directly, the battle management system on the aircraft can project a launched missile's path and pass this information on to other systems, such as the U.S. Army's *Patriot* (i.e., the *PAC-3*) missile defense system. As discussed earlier, this makes it an integral part of a layered defense system.

The U.S. Army, as mentioned above, is also pursuing a missile intercept program, known as the *THAAD* (theater high-altitude area defense) missile system, capable of both endo- and exoatmospheric missile interception. Specifically, the *THAAD* weapon system is being developed to defend against theater ballistic missiles. This mobile interceptor is designed to engage and destroy long-range strategic ballistic missiles in the highest reaches of the atmosphere. In August 1999 the Army, at the White Sands Missile Range, New Mexico, the *THAAD* successfully intercepted a *Hera* target (the

Hera target is a two-stage *RV* used to simulate a *Scud-C** configured to simulate a 310-mi range *Scud-C*. The *THAAD* is designed to have a range of 3,500 km (2,174.90 mi). The *Hera* target's apogee was about 300 km (186.4 mi.), at which point the reentry vehicle separated from the missile. Moments earlier, the *THAAD* missile had been launched. About 7 sec before the intercept, the ground-based *THAAD X*-band radar passed guidance control to the interceptor's *IIR* seeker. At a closing velocity of about 2.5 km/sec (1.55 mi/sec), the *THAAD* missile hit the target and destroyed the reentry vehicle at an altitude of about 100 km (62.4 mi). The *THAAD* was able to select an aimpoint on the reentry vehicle. The interceptor tries to hit the target as close to the warhead as possible (see also Section 4.7) to destroy any submunitions or weapons of mass destruction that may be part of the payload. When the missile seeker turned on, it required very little fuel to maneuver the interceptor toward the target. Furthermore, the seeker had no difficulty spotting the reentry vehicle, which was colder than the expended *Hera* booster that also was in its field-of-view. According to present plans, the *THAAD* program will begin flight-testing in 2003, with an operational system ready for deployment in the 2004/2005 time frame.

In a parallel effort, the Army expects to complete development tests of its *Patriot PAC-3* ballistic missile and air-defense system in 2003 and initiate operational tests. Lockheed Martin has completed development testing and will turn the system over to the Army. As of this writing (2001) the system scored 12 successes out of 13 tests. For shorter-range threats, by 2004 the Army should have fielded its short-range *PAC-3* system, which should have its first unit equipped before the end of 2003. A full-rate system production decision is planned for 2003. As stated above, the *THAAD* program, designed to counter missiles at greater range, should be in the late stages of development with a single operational system potentially ready for deployment in 2004/2005.

The USAF/*BMDO* sponsored Patriot advanced capability (*PAC-3*) *SAM* was flight tested in March 1999. This solid-rocket-motor-powered *PAC-3* missile intercepted and destroyed an incoming tactical ballistic missile. Intercept of the *RV* target occurred at an altitude of 12 km (7.5 mi) after the target had flown downrange 350 km (217 mi). The *PAC-3* flew for about 7 sec after launch and completed a nearly 90° maneuver in the final seconds prior to impact. Shortly before arriving at the point of interception, the missile's K_a-band seeker acquired the target, selected the optimal aiming point, and initiated terminal guidance (the missile uses a closed-loop homing guidance system) to impact. The *PAC-3* uses its high-speed and hit-to-kill (*HTK*) technology instead of blast/fragmentation warhead to destroy targets through direct body-to-body contact. The *PAC-3* weapon system has been selected as the next-generation *Patriot* missile; *IOC* was scheduled for 2001. Moreover, the *PAC-3* is designed to counter tactical ballistic missiles armed with biological weapons, maneuvering tactical missiles, and long-range targets such as aircraft, cruise missiles, and *UAV*s. In addition, it is capable of destroying incoming *HARM*s aimed at the *Patriot* launch sites. Technologies being examined for these systems include a high-data-rate ring laser gyro, a third-generation

*The *Scud* is a short-range surface-to-surface missile deployed on a mobile launcher. Its boost phase lasts about 60–120 seconds.

IR seeker, and advanced divert and attitude control devices using solid propellant. Note that for a *SAM* missile, such as the *PAC-3*, speed plays an important role in determining missile aerodynamic maneuverability. Decreasing the missile speed significantly decreases the missile maneuverability. The interceptor acceleration capability increases with decreasing altitude, whereas the target deceleration capability also increases with decreasing altitude. From the interceptor point of view, the ideal intercept should take place at very low altitude, where the interceptor has enormous capability and a considerable acceleration advantage over the target. However, practical considerations may require the interceptor to engage the ballistic target at much higher altitudes. For a given altitude and missile configuration, there is a minimum speed requirement such that the missile can effectively engage a responsive target.

It should be noted that from a threat perspective, the USAF is projecting a proliferation of advanced surface-to-air missiles, such as the Russian *S-300* and *S-400* class of air defense systems, with missiles that can engage a target at a range of 100 mi. The Russian counterpart of the *NMD* uses the *Galosh* antimissile system around Moscow.

The U.S. Navy is also pursuing a ballistic missile interception program. Specifically, the Navy's Standard Missile, the *SM-3* ballistic missile interceptor, is a 3-stage missile that carries an IR seeker to intercept its target. The *SM-3* is part of the Navy's *Midcourse System* (formerly known as Navy theater wide antimissile defense system). This ballistic missile defense is to be launched from the *Aegis*-type cruisers (see also Appendix F, Table F.4). The U.S. Navy's ballistic missile defense system scored a successful intercept of an *Aries* ballistic missile target on January 25, 2002, using the three-stage Standard Missile *SM-3* interceptor. The latest positive event for *MDA* came on June 13, 2002, when the sea-based midcourse system intercepted its target. The *SM-3* interceptor was fired from the USS Lake Erie *Aegis* cruiser about 6 min after the *Aries* ballistic missile target launched from the Pacific Missile Range on Kauai, Hawaii. A few minutes later, the lightweight exoatmospheric projectile (*Leap*), *SM-3*'s upper stage, intercepted the target. Note that the *Leap* (also seen as LEAP) kill vehicle uses an *IR* sensor to intercept the target.

The November 21, 2003, test (designated *FM*-4) was also successful in intercepting an *Aries* target with an *SM*-3 interceptor launched from the USS Lake Erie. This test represented the third intercept for the sea-based initiative, The next test, *FM-5*, which took place in the spring of 2003 was also an ascent-phase engagament. The primary difference from *FM-4* will be the planned upgrade to a multipulse divert and attitude control system (*DACS*) for the warhead. This gives the *Leap* upper stage more maneuvering capability to hit the target. The more capable *DACS* basically completes the core *SM*-3 missile. The next two tests, *FM-6* and *FM-7*, focus on the *Aegis* weapon system. The *FM-6* is slated for 2003, while the *FM-7* test is expected to occur in 2004. In *FM-8*, the Pentagon wants to determine the system's versatility. The final test, *FM-9*, has not been determined yet. Finally, the Navy plans to upgrade the radar of 15 *Aegis* ships in order to support missile defense engagements.

Another class of ballistic missiles for which antimissile interception techniques are under study is that of *tactical ballistic missiles* (*TBM*s). Even though *TBM*s have a short range (typically 120–1850 nm), they are nevertheless fast becoming a real threat. Tracking these missiles can be done from land or sea. Also, as stated earlier,

tracking from space with satellites can certainly be effective in identifying missiles in flight. Infrared sensors will detect missile plume. Radar tracking of *TBM*s from ships for the launch and reentry is also plausible.

The airborne laser described above has been dubbed as the "leading edge of theater ballistic missile defense systems." The *ABL* antiballistic missile program, the world's first laser-armed combat aircraft, is on track for a live-fire demonstration in the year 2004. During the preliminary design and risk reduction phase, the industry team is designing, developing, integrating, and testing the airborne laser system. The effort will culminate with the planned test destruction of *Scud*-type missiles by the airborne laser in 2003 (note the difference between this and the *IFX Minuteman III* planned intercept). Specifically, the *ABL* is scheduled to shoot down its first missile in a test over the Pacific Ocean in 2004. The ground and flight test program began in 2001 and will continue through 2003 with a series of tests against representative missiles. Finally, in actual battle, an airborne laser fleet could arrive on the scene within hours, ready to take defensive positions. Two attack lasers would be flying around the clock, orbiting at about 40,000 ft, providing defense against attacking missiles. However, it should be pointed out that the Air Force's *ABL* program and in particular the ballistic missile interception presents some difficult problems that must be dealt with in order for it to become a reality.

Another type of airborne surveillance system, although a different concept than the *ABL*, is the Air Force's *E-8C Joint STARS* (surveillance target attack radar system) aircraft (for other types of surveillance and/or reconnaissance aircraft see Appendix E). *Joint STARS* is the world's most advanced airborne surveillance and target acquisition system. *Joint STARS* provides near real-time, accurate information on surface targets and slow-moving aircraft to air, land, and naval forces. As proven battle management force multiplier, it ensures that U.S. and coalition forces will preserve the peace and win wars. In addition to the *Joint STARS* aircraft, several other special-mission aircraft are in the Air Force's inventory for carrying out surveillance, intelligence collection, and identification of moving targets. These are (a) *E-3 AWACS*, (b) *EC-130 Commando Solo*, (c) *RC-135 V/W Rivet Joint*, and (d) *EP-3E Aries III*. It should be pointed out here that another aircraft, the *E-4B* (a Boeing 747) serves as the national airborne operations center for the president and secretary of defense. In case of national emergency or destruction of ground command control centers, the aircraft provides a modern, highly survivable, command, control, and communications center to direct U.S. forces, execute emergency war orders, and coordinate actions by civil authorities (see also Section 5.12.2).

The technology associated with the task of intercepting an *ICBM* depends, to a large degree, on whether the missile-interception system has sufficient warning time, since a certain amount of time is required for the interceptor to fly thousands of miles. Another possibility is a midcourse interception. The midcourse interception option is particularly attractive because a few long-range interceptors could protect a large area, thus a very large force is required to deal with widely separated potential attackers. Similarly, terminal interceptors must be deployed around each potential missile target, which means very large numbers. It seems to be generally accepted that modern technology can build an interceptor that can be flown toward an

incoming warhead, then detect and hit it. The unanswered question is whether the same interceptor can distinguish the warhead from any decoys that might accompany it. The system currently proposed uses a midcourse interceptor boosted by an *ICBM*-size rocket. An incoming missile would be detected virtually at launch by orbiting satellites carrying *IR* sensors or the *SBL* using lasers. The orbiting satellites would cue long-range radars, which would first see the missiles as they came over the curve of the Earth. These radars would be upgraded versions of existing early warning systems. The upgrade is needed because instead of simply indicating the likely point of attack, the radar must measure the trajectory of the incoming missile so that it can be intercepted. As the missile comes closer, a ground-based radar picks it up. This high-resolution radar is the primary fire control sensor of the interception system. It tracks the incoming warhead precisely enough for the ground-based interceptor (*GBI*) to be command-guided (e.g., by up-link) into an interception "basket" from which its interceptor can home on the warhead to destroy it. Another radar also would help the system discriminate against some kinds of decoys, because it measures the behavior of the objects that separate from the incoming booster. The system as a whole can also use the space-based *IR* sensors to help discriminate between warhead and decoys.

On July 14, 2001, the sixth in a series of Air Force missile intercept flight tests (designated as *IFT-6*) took place. As in the previous tests, a ground-based national missile defense program intercepted a mock warhead during a flight test from the Kwajalein missile range. It was the second intercept in four attempts and a repeat of *IFT-5* in July 2000, when the target launcher failed to release the kill vehicle. This time, the target was launched on a Lockheed Martin-modified *Minuteman II* at 10:45 p.m. (*EDT*) from Vandenberg AFB, California. The Raytheon-built kill vehicle was launched on a surrogate booster 21 min 34 sec later, intercepting the target about 8 min from the time of launch. The kill vehicle had to pick out the warhead from a complex that included parts of the upper stage and a 1.65-meter-diameter decoy balloon, a newer version of the 1.7-meter-diameter decoy that was used in prior tests but failed to inflate during the last intercept test in 2000. In order to precisely guide the interceptor missile to the target, an *X*-band fire control radar will be used.

Another success was achieved on December 3, 2001, in intercepting a mock *ICBM* warhead. The December 3 intercept (*IFT-7*) of a dummy warhead was the second in a row for the ground-based *NMD* project. *IFT-7* began around 9:59 p.m. (EST) with the launch of the target from Vandenberg AFB, California. The interceptor fired about 20 min later from the Kwajalein missile range in the Marshall Islands. Intercept occurred 10 min later at an altitude in excess of 140 mi. The kill vehicle intercepted the target even more accurately than in the previous intercept. In the flight tests so far, only a single decoy was used. In the near future additional decoys will be added to the program. The addition of decoys in the next test (*IFT-8*) would make it the first in which the kill vehicle's target-discrimination capability would be stressed. The tests so far have focused primarily on validating the kill vehicle's ability to maneuver toward and intercept the target.

Another milestone occurred on March 15, 2002, with the successful test of the ground-based mid-course intercept system. The March 15 test (*IFT-8*) marked the fourth intercept in six attempts. It also represented a step up in complexity from

earlier tries. The mock warhead and three decoys (prior tests used only one decoy) were launched from Vandenberg AFB, California, at 9:11 p.m. (EST). The interceptor carrying the exoatmospheric kill vehicle (*EKV*) launched about 20 min later from the Kwajalein Atoll in the South Pacific. When the kill vehicle separated from its booster, it was about 870 mi (1,400 km) from the warhead. About 10 min later, the kill vehicle collided with the warhead. The *EKV* was guided to the target first through a ground-based *X*-band radar and later using its on-board visual and two *IR* sensors. The ground-based, midcourse intercept segment will be a core part of the future ballistic missile defense system. The seventh intercept for the ground-based midcourse missile defense program, the *IFT-9*, took place on October 14, 2002. As in the previous tests, the target was launched from Vandenberg AFB, California, at 10 p.m. EDT followed by launch of the interceptor 22 min later from a range in the Kwajalein Atoll. The exoatmospheric kill vehicle intercepted the mock warhead 6 min later. This was the fifth intercept in seven attempts. The test for the first time involved an *Aegis* destroyer, the USS *John Paul Jones*, tracking the engagement (i.e., gathering data on the target and interceptor) with its powerful *SPY-1* radar. The December 11, 2003, test (*IFT*-10) failed to intercept the target. Specifically, the interceptor fired from the Kwajalein Atoll in the Marshall Islands did not eject the exoatmospheric kill vehicle that intercepts the target. More tests are planned for 2003 and 2004.

The *MDA* is asking Congress to appropriate another $1.5 billion for 2003 and 2004 for certain development capabilities. These include up to 20 ground-based interceptor missiles capable of taking out *ICBM*s during midflight: 16 at Fort Greeley, Alaska, 4 at Vandenberg AFB, California and up to 20 sea-based interceptor missiles employed on existing *Aegis* destroyers.

Israel Aircraft Industries (IAI) announced that it successfully intercepted a ballistic missile target on September 14, 2000, with the *Arrow* weapon. (See also earlier discussion.) The target, including the simulated warhead, was destroyed by the *Arrow 2* antitactical ballistic missile interceptor. According to the announcement, the test was one of the most realistic and operationally oriented to date, in that it the first time the weapon system was used to intercept an incoming target headed for Israel. The test also employed for the first time the new air-launched *Black Sparrow* target, which was launched from an Israel Air Force *F-15* over the Mediterranean Sea. The *Black Sparrow*, developed by Rafael, is derived from the Israeli company's *AGM-142 Popeye* air-to-ground standoff missile, modified with a more powerful rocket motor, in order to achieve the altitude required to simulate the trajectory of the ballistic missile. *Black Sparrows* are to be used for most *Arrow* tests, which are expected to continue at a rate of two per year. Recently, certain updates and improvements on the *Arrow* antiballistic missile system were announced. These are (a) better target discrimination, (b) an expanded envelope in which the missile can strike enemy warheads, and (c) an increased probability of a hit within that envelope. Tests currently underway are aimed at ensuring adequate defense against such missiles as Iran's *Shahab 3*, which have a 600-mi range and 1,500-lb payload. *IAI*'s goal is to develop an improvement to the *Arrow* program so that it can counter Iran's latest missile, the *Shahab 4*, which is to have a 1,300-mi range and a 2,200-lb payload. This missile, with its higher

altitude capability and subsequently increased reentry speed, will be more difficult to intercept.

India's Defense Research and Development Organization (DRDO) also tested in October 2002 the guidance system of its *Akash* surface-to-air interceptor missile. The *Akash* can carry a 55-kg (121-lb) payload 25 km (15.5 mi).

6.9.2 Missile Tracking Equations of Motion

Let us assume an *ECEF* (earth-centered earth-fixed) coordinate system, in which the positive x-axis passes through the prime meridian at the equator, the positive y-axis passes through the 90° east meridian at the equator, and the positive z-axis passes through the North Pole. The target missile's equations of motion can be expressed as (assuming that only drag and gravity forces are acting on the body) [13]

$$m\mathbf{A} = m\mathbf{A}_d + m\mathbf{A}_\mathbf{g}, \tag{6.278}$$

where

$$\begin{aligned} \mathbf{A} &= \text{total acceleration of the body (i.e., target)},\\ \mathbf{A}_d &= \text{acceleration due to drag forces},\\ \mathbf{A}_g &= \text{gravitational acceleration},\\ m &= \text{mass of the body (target)}. \end{aligned}$$

The drag force will be taken to be

$$\mathbf{F}_d = m\mathbf{A}_d = -[m\rho V/2\beta]\mathbf{V}, \tag{6.279}$$

where

$$\begin{aligned} V &= \text{target velocity } (=(x^2+y^2+z^2)^{1/2}),\\ \beta &= \text{ballistic coefficient} = mC_dS, \text{ where } C_d \text{ is the coefficient of drag and}\\ &\quad S \text{ is the reference area},\\ \rho &= \text{atmospheric density at the target position } (\rho = \rho(h)). \end{aligned}$$

Note that the height h required in $\rho = \rho(h)$ is obtained as the distance between the target and the point of intersection of the reference ellipsoid and the line passing through the target and normal to the reference ellipsoid. A good approximation to this is

$$h \approx r - R_\phi = r - [a^2(1-e^2)/(1-e^2\cos^2\phi)]^{1/2},$$

where

$$\begin{aligned} r &= \text{distance from the center of the Earth to the target},\\ a &= \text{equatorial radius of the Earth},\\ e &= \text{eccentricity},\\ \phi &= \text{geodetic latitude}. \end{aligned}$$

From (6.278) the total acceleration can be written in vector form as

$$\mathbf{A} = (\rho V/2\beta)\mathbf{V} + \mathbf{A}_g; \tag{6.280}$$

$\mathbf{A}_g$ can be expressed as

$$\mathbf{A}_g = g_r \mathbf{1}_r + g_z \mathbf{1}_z, \tag{6.281}$$

where

$$g_r = -(\mu/r^2)[1 + J(a/r)^2(1 - 5\sin^2\phi)], \tag{6.282a}$$

$$g_z = (2\mu/r^2)J(a/r)^2 \sin\phi. \tag{6.282b}$$

In 6.282, the various parameters are

μ = GM ($= 3.9860322 \times 10^5 \text{km}^3/\text{sec}^2$) = universal gravitational constant,
J = dimensionless coefficient ($\approx 1.624 \times 10^{-3}$),
a = equatorial radius ($= 6,378.135$ km),
ϕ = geodetic latitude,
g_o = acceleration of gravity at the surface of the Earth $= 9.7983$ m/s^2,
r = distance from the center of the Earth to the target.

We can now write the equations of motion for the present target tracking of an incoming ballistic missile in the form

$$\frac{d^2x_r}{dt^2} = -\rho V x_r/2\beta, \tag{6.283a}$$

$$\frac{d^2y_r}{dt^2} = -\rho V y_r/2\beta, \tag{6.283b}$$

$$\frac{d^2z_r}{dt^2} = -(\rho V z_r/2\beta) - g_r. \tag{6.283c}$$

The total gravitational acceleration can also be expressed in vector form. Assuming that the Earth is modeled as an oblate aspherical planet, then its gravity vector can be approximated by expansion into spherical harmonics as follows [11]:

$$\mathbf{g} = -(\mu/R)^2 \begin{bmatrix} 1 + \frac{3}{2}J_2(a/r)^2(1 - 3\sin^2\phi) \\ 0 \\ J_2(a/r)^2 3\sin\phi\cos\phi \end{bmatrix},$$

where $J_2 = 1.08263 \times 10^{-3}$.

In the most general case of a launched *ICBM*, and taking into account the rotation of the Earth, the kinematic and dynamic equations describing the translational motion of the *ICBM* can be written in the form

$$\frac{d\mathbf{r}}{dt} = \left(\frac{d}{dt}\right)\begin{bmatrix} r \\ \lambda \\ \phi \end{bmatrix} = m \begin{bmatrix} V_r \\ (V_\lambda/r\cos\phi) - \Omega_e \\ V_\phi/r \end{bmatrix}, \tag{6.284a}$$

$$\frac{d\mathbf{V}}{dt} = \left(\frac{d}{dt}\right)\begin{bmatrix} V_r \\ V_\lambda \\ V_\phi \end{bmatrix} = (1/r)\begin{bmatrix} V_\lambda^2 + V_\phi^2 \\ V_\lambda(V_\phi \tan\phi - V_r) \\ -V_\lambda^2 \tan\phi - V_r V_\phi \end{bmatrix} + \mathbf{g} + (1/m)\Sigma\mathbf{F}, \quad (6.284b)$$

where

$$\begin{aligned} V_r, V_\lambda, V_\phi &= \text{velocity components along the indicated directions,} \\ \mathbf{V} &= \text{vehicle's inertial velocity vector,} \\ \mathbf{r} &= \text{vehicle position vector,} \\ m &= \text{mass of the vehicle,} \\ \phi &= \text{geodetic latitude,} \\ \lambda &= \text{geodetic longitude,} \\ \mathbf{g} &= \text{acceleration of gravity,} \\ \mathbf{F} &= \text{external forces (or loads),} \\ \Omega_e &= \text{angular velocity of the Earth} = 7.292115 \times 10^{-5} \text{ rad/sec.} \end{aligned}$$

The dynamic pressure in the present case is taken to be

$$Q = \tfrac{1}{2}\rho V_a^2,$$

where the airpath velocity vector $\mathbf{V}_a$ is given by

$$\mathbf{V}_a = \mathbf{V} - \Omega_e \times \mathbf{r} - \mathbf{V}_w, \quad (6.284c)$$

where $\boldsymbol{V}_w$ is the velocity of the atmosphere relative to the Earth.

The problem can be solved using the extended-interval Kalman filter (*EIKF*). This *EIKF* can be represented by the linear, discrete-time, time-varying nominal dynamic observation system [6]

$$\mathbf{x}_{k+1} = \mathbf{A}_k\mathbf{x}_\mathbf{k} + \mathbf{B}_k\xi_k, \quad (6.285a)$$

$$\mathbf{y}_k = \mathbf{C}_k\mathbf{x}_k + \eta_k \quad k = 0, 1, 2, \ldots, \quad (6.285b)$$

where $\mathbf{x}_k \in R^n$ and $\mathbf{y}_k \in R^m$ are state and output vectors, respectively, with a Gaussian initial state $\mathbf{x}_o$ of known mean $E\{\mathbf{x}_o\}$ and covariance $P_o = V\{\mathbf{x}_o\}$; $\mathbf{A}_k \in R^{nxn}$, $\mathbf{B}_k \in R^{nxp}$ and $\mathbf{C}_k \in R^{mxn}$ are known constant matrices; and $\{\xi_k\}$ and $\{\eta_k\}$ are mutually independent zero-mean Gaussian noise sequences, with known covariance matrices $\{Q_k\}$ and $\{R_k\}$, respectively, which are all independent of the initial state, namely,

$$\begin{aligned} E\{\xi_k, \xi_l\} &= Q_k\delta_{kl}, \quad E\{\eta_k, \eta_l\} = R_k\delta_{kl}, \\ E\{\xi_k, \eta_l\} &= E\{\xi_k, \mathbf{x}_o\} = E\{\eta_k, \mathbf{x}_o\} = 0 \quad \forall k, l = 0, 1, 2, \ldots, \end{aligned}$$

where $\delta_{kl} = 1$ if $k = l$ and $\delta_{kl} = 0$ otherwise. The optimal estimates are uniquely determined by the conditional expectations

$$\hat{\mathbf{x}}_k = E\{\mathbf{x}_k|\mathbf{y}_1, \ldots, \mathbf{y}_k\}. \quad (6.286)$$

It is well known that the state update at the end of the filter cycle requires $\mathbf{x}(k+1/k)$, the predicted state at $k+1$ based on the estimated state at k. This prediction uses a predictor/corrector integration of the nonlinear equations of motion implemented in range, azimuth, and elevation coordinates. Assuming the transpose of the state vector to consist of position and velocity terms, we can write the state vector as

$$\mathbf{x}^T = [r, \alpha, \varepsilon, \dot{r}, \dot{\alpha}, \dot{\varepsilon}, \beta],$$

where r is the range, α the azimuth, ε the elevation, and β the ballistic or drag coefficient. The state transition matrix Φ is computed as

$$\Phi = I + J(k) * T,$$

where I is the identity matrix, $J(k)$ is the Jacobian matrix $= df/dx|_{x=x(k/k-1)}$, and T is the filter update interval. The Jacobian matrix has the form

$$J = \begin{bmatrix} 0 & 0 & 0 & 1 & 0 & 0 & 0 \\ 0 & 0 & 0 & 0 & 1 & 0 & 0 \\ 0 & 0 & 0 & 0 & 0 & 1 & 0 \\ J_{rr} & J_{r\alpha} & J_{r\varepsilon} & J_{rr} & J_{r\alpha} & J_{r\varepsilon} & J_{r\beta} \\ J_{\alpha r} & J_{\alpha\alpha} & J_{\alpha\varepsilon} & J_{\alpha r} & J_{\alpha\alpha} & J_{\alpha\varepsilon} & J_{\alpha\beta} \\ J_{\varepsilon r} & J_{\varepsilon\alpha} & J_{\varepsilon\varepsilon} & J_{er} & J_{\varepsilon\alpha} & J_{\varepsilon\varepsilon} & J_{\varepsilon\beta} \\ 0 & 0 & 0 & 0 & 0 & 0 & 0 \end{bmatrix}, \tag{6.287}$$

where $J_{AB} = \partial A/\partial B$.

An Example Based on the discussion of this section, as well as the discussion of Section 6.7, assume now that only drag and gravity acting on the endoatmospheric ballistic target are considered. Moreover, let the target missile velocity have a velocity v_t and an initial reentry angle γ_i. The downrange of the target is x_t, and the altitude is y_t (assuming an xy coordinate system). The drag force F_D acts in the direction opposite to the velocity vector, and the gravity g always acts in a downward direction. Consequently, if the effect of drag is greater than that of gravity, the target will decelerate. The target reentry angle y_t can be computed using the two inertial xy components of the target velocity as follows (see Figure 6.34):

$$\gamma_t = \tan^{-1}(-v_{ty}/v_{tx}),$$

where v_{tx} and v_{ty} are the velocity components of $\mathbf{V}$ in the x and y directions, respectively. The acceleration components of the target in the inertial downrange and altitude directions can be expressed in terms of the ballistic coefficient β according to the following equations:

$$\frac{dv_{tx}}{dt} = (-F_D/m_t)\cos\gamma_t = (-qg/\beta)\cos\gamma_t,$$
$$\frac{dv_{ty}}{dt} = (F_D/m_t)\sin\gamma_t - g = (qg/\beta)\sin\gamma_t - g,$$

where

$$\begin{aligned} v_{tx}, v_{ty} &= \text{velocity components in the } x, y \text{ directions},\\ m_t &= \text{mass of the target missile},\\ F_D &= \text{drag force},\\ g &= \text{gravitational acceleration},\\ q &= \text{dynamic pressure},\\ \beta &= \text{ballistic coefficient},\\ \gamma_t &= \text{reentry angle}. \end{aligned}$$

Furthermore, the ballistic coefficient β is given by the expression

$$\beta = w_t / C_{tDO} S_r,$$

where w_t is the target weight and S_r is the target (missile) reference area.

The dynamic pressure q is given by

$$q = \tfrac{1}{2}\rho v_t^2,$$

where ρ is the air density and v_t is the target velocity. The air density (measured in kg/m^3) can be approximated by the expression

$$\rho = 0.12492(1 - 0.000022557 y_t)^{4.2561} g,$$

while the total target velocity is given by

$$v_t = (v_{tx}^2 + v_{ty}^2)^{1/2}.$$

Finally, since the acceleration equations are given in an inertial frame, they can be integrated directly to yield velocity and position.

References

1. Allen, H.J. and Eggers, A.J.: *A Study in the Motion and Aerodynamic Heating of Missiles Entering the Earth's Atmosphere at High Supersonic Speeds*, NACA TN 4047, 1957.
2. Bate, R.R., Mueller, D.D., and White, J.E.: *Fundamentals of Astrodynamics*, Dover Publications, Inc., New York, 1971.
3. Battin, R.H.: *Astronautical Guidance*, McGraw-Hill Book Company, New York, 1964.
4. Brouwer, D. and Clemence, G.M.: *Methods of Celestial Mechanics*, Academic Press, Inc., New York, 1961.
5. Blackelock, J.H.: *Automatic Control of Aircraft and Missiles*, John Wiley & Sons, Inc., New York, NY, Second Edition, 1991.
6. Chui, C.K. and Chen, G.: *Kalman Filtering with Real-Time Applications*, third edition Springer-Verlag, New York, 1999.
7. Kells, L.M. and Stotz, H.C.: *Analytic Geometry*, Prentice-Hall, Inc., New York, 1949.

8. Peirce, B.O.: *A Short Table of Integrals*, third revised edition, Ginn and Company, Boston, New York, 1929.
9. Pitman, G.R., Jr. (ed.): *Inertial Guidance*, John Wiley & Sons, Inc., New York, 1962.
10. Plummer, H.C.: *An Introductory Treatise on Dynamical Astronomy*, Dover Publications, Inc., 1960.
11. Siouris, G.M.: *Aerospace Avionics Systems: A Modern Synthesis*, Academic Press, Inc., New York, 1993.
12. Siouris, G.M.: *An Engineering Approach to Optimal Control and Estimation Theory*, Wiley Interscience, John Wiley & Sons, Inc., New York, 1996.
13. Siouris, G.M., Chen, G., and Wang, J.: *Tracking an Incoming Ballistic Missile Using an Extended Interval Kalman Filter, IEEE Transactions on Aerospace and Electronic Systems*, Vol. 33, No. 1, January 1997, pp. 232–240.
14. Thomson, W.T.: *Introduction to Space Dynamics*, John Wiley & Sons, Inc., New York, 1961.
15. Vinh, N.X.: *Optimal Trajectories in Atmospheric Flight*, Elsevier, New York, 1981.
16. Wheelon, A.D.: *Free Flight of a Ballistic Missile, ARS Journal*, Vol. 29, December 1959, pp. 915–926.
17. Whittaker, E.T.: *A Treatise on the Analytical Dynamics of Particles and Rigid Bodies*, Cambridge University Press, fourth edition, 1964.
18. Zarchan, P.: *Tactical and Strategic Missile Guidance*, third edition, Vol. 157, Progress in Astronautics and Aeronautics, published by the American Institute of Aeronautics and Astronautics, Inc., Washington, D.C., 1998.

7

Cruise Missiles

7.1 Introduction

A cruise missile can be defined as a dispensable, pilotless, self-guided, continuously powered, air-breathing vehicle that flies just like an airplane, supported by aerodynamic surfaces, and designed to deliver a conventional or nuclear device. Specifically, the cruise missile is powered by a small, high-efficiency turbofan engine in the 600-pound thrust class. Cruise missiles exist in three versions: (1) land-based or ground-launched cruise missiles (*GLCM*), (2) sea-based or sea-launched cruise missiles (*SLCM*), and (3) air-launched cruise missiles (*ALCM*). Unlike a ballistic missile, which is powered and hence usually guided for only a brief initial part of its flight, after which it follows a free-fall trajectory governed only by the local gravitational field, a cruise missile requires continuous guidance, since both the velocity and the direction of its flight can be unpredictably altered, for example, by local weather conditions.

In this chapter we will mainly consider the air-launched cruise missile. As described above, the air-launched cruise missile is also a strategic, subsonic, turbofan-powered, winged vehicle designed for internal and external carriage on the *B-52G/H* carrier aircraft. The *ALCM* is intended for long-range strategic missions utilizing its inherently low observables and terrain-following capabilities to penetrate enemy air defenses. Guidance is inertial with terrain correlation position update technique used to achieve high terminal accuracy. The planned operational concept for the *ALCM* uses the missile's capabilities to complement the penetrating *B-52* bomber in the strategic nuclear mission. The *B-52* system can align and launch the *ALCM*s carried on wing-mounted pylons or rotary rack carried in the bomb bay.

A ballistic missile, as we saw in Chapter 6, is guided for the first five of the twenty minutes or so it takes to travel 5,000 km; a cruise missile, which usually flies at subsonic speed, would require close to six hours of continuously guided flight to cover the same distance. Hence, guidance errors that accumulate with time would be almost 100 times larger for a cruise missile than for a ballistic missile with a comparable range. Thus, the cumulative deviation from a preassigned track over a trajectory of thousands of kilometers would be very large in the case of the cruise

missile, and therefore its accurate arrival on the target could be achieved only with continuous guidance that is updated and corrected from time to time by new location information. In order to obtain the necessary location information, a long-range cruise missile employs a device that can correlate information obtained by an onboard sensor about the terrain it is flying over with some kind of map stored in the memory of an onboard computer.

Cruise missiles are modeled with straight-line constant-velocity flight between initial location and target location. The missile is flown at constant velocity at 200 meters above ground level. A cruise missile is flown based on the missile's current position and its target's current position. The distance vector between the missile and the target is used to determine the impact and the need for terrain-following for the missile. Cruise missiles have served as warhead-delivery systems in the past, beginning with the early German *V-1 buzz bomb* developed and employed during World War II (see also Chapter 1), and continuing with such weapons as the U.S. *Matador*, *Regulus*, and *Snark* missiles, and the Russian *Shaddock* and *Kh-55* missiles.

Various types of cruise missiles are now in service or under development in the U.S.A. and other countries. In the United States, some of the cruise missile types are (1) the air-launched cruise missile (*ALCM*) designated *AGM-86B* (nuclear)* using the *W80-1* nuclear warhead, the conventional air-launched cruise missile (*CALCM*) also seen as *Calcm* designated *AGM-86C*, and the advanced cruise missile (*ACM*) designated *AGM*-129 (*A,B*) the former developed by the Boeing Aerospace Company and the latter by General Dynamics Convair Division (the program was canceled in November 1991); (2) the standoff land-attack missile (*SLAM*) designated *AGM-84E-1*; and (3) the sea-launched cruise missile (*SLCM*) such as the *Tomahawk* designated *BGM-109*. The conventional version of the *ALCM* using *GPS* navigation was secretly developed in the mid-1980s and launched successfully in *Operation Desert Storm* in 1991 against Iraqi targets. Thus, *GPS* guidance became a reality. In addition, some *SSBN*s (i.e., Tridents) are scheduled to be retired under the Strategic Arms Reduction Treaty (*START II*). President George H. W. Bush and Russian President Boris Yeltsin signed the *START II* treaty in January 1993. The treaty, to reduce nuclear arsenals to between 3,000 and 3,500, was ratified by the U.S. Senate in January 1996. The Russian parliament ratified it in 2000. It should also be pointed out here that on May 24, 2002, President George W. Bush and Russian President Vladimir Putin signed a treaty to shrink their nuclear arsenals by two-thirds. The treaty, which must be approved by the Senate, would limit the United States and Russia to 1,700 to 2,200 nuclear warheads apiece by 2012 (the United States now has about 6,000 strategic nuclear weapons, Russia about 5,500). As a result of this treaty, the nuclear-armed Trident missile boats could be converted to guided-missile submarines (*SSGN*s). Each *SSGN* would be capable of carrying 154 *Tomahawks*.

Because of its importance, some further discussion of the conventional *ALCM* is in order. As stated above, during the mid-1980s, the U.S. Air Force decided to

*Note that the deployment of strategic long-range nuclear cruise missiles has been limited by the Strategic Arms-Limitation Talks (*SALT II*) agreement between the United States and Russia.

modernize the *ALCM*, using the *GPS* integrated with an inertial navigation system (*INS*). This new cruise missile using the *GPS* and the *INS* was named the conventional air-launched cruise missile (*CALCM* or sometimes written as *Calcm*) designated *AGM-86C*. The current *Calcm*'s range is 650 miles. The advantages of *GPS/INS* integration are well known. Specifically, the long-term accuracy of the *GPS* combined with the short-term accuracy and autonomy of the *INS* results in a truly synergistic system. Two *GPS/INS* integration approaches are commonly used. These are (1) the *tightly* coupled integration approach, which yields higher accuracies; and (2) the *loosely* coupled integration approach used for short time and/or ranges, yielding lower accuracies. In the *CALCM*, the *TERCOM* guidance system was replaced with the *GPS*. As a result, the *CALCM*'s *GPS* receiver is interfaced with the *ALCM*'s altimeter, flight control system, the *INS*'s serial/digital interface, and the carrier aircraft. The navigator (i.e., dynamic navigation equations), consisting of a 15-state Kalman filter, is normally updated by the onboard navigation computer every 50 milliseconds (or a 20-Hz rate), while the *GPS* is updated at a 1-Hz rate. The *GPS* will normally consist of an 8-state Kalman filter (see Section 7.5), so that both the *INS* and *GPS* Kalman filters operate in a cascaded mode. Inertial aiding provided to the *GPS* receiver-tracking loop is at a 10-Hz rate. (Note that the *INS* is of the strapdown class. Thus, the basic strapdown *INS* algorithms that maintain the body-to-level-axis transformation matrix and transform the body-axis velocity increments to a locally level coordinate frame can be performed at a rate of 50 Hz, while the basic *INS* algorithms can be performed at an iteration rate of 10 Hz.)

In this book we will be concerned mainly with air-launched cruise missiles. However, a brief description of the *SLAM* and *SLCM* will now be given. The standoff land-attack missile (*SLAM*) is an imaging infrared (*IIR*; also seen as I^2R) seeker, man-in-the-loop, terminally guided missile that is a derivative of the *AGM-84A Harpoon* antiship missile. The *SLAM* can be launched from aircraft (e.g., *A-6E*, *F/A-18E/F Super Hornet*, *F-16C Fighting Falcon*, *P-3 Orion*, and the *B-52H Stratofortress*). The *SLAM* is capable of two modes of operation: (1) planned mission against high-value fixed or relocatable land targets, and (2) mission against ships at sea. Moreover, the *SLAM* shares common control, warhead, and sustainer sections with the *Harpoon*. Its navigational heart is the Rockwell/Collins single-channel *GPS* receiver/processor that determines the missile's three-dimensional location within 52 ft (16 m) and its velocity within 0.5 ft/sec (0.2 m/sec). *GPS* aiding of the missile's inertial navigation system (*INS*) during flight provides precise midcourse navigation accuracy. Section 7.5 discusses in more detail the *GPS* system and its role in aiding the *INS*. After launch, the *SLAM* flies automatically to the area of the target via its *GPS*-aided inertial navigation system. Consequently, at a preprogrammed point approximately one minute before target impact, the seeker turns on and, because of the *GPS*-aided navigation accuracy, should be looking directly at the target. The controller (i.e., man-in-the-loop) views the target scene and selects an aim point for the terminal phase via the *SLAM*'s data link, and the missile flies automatically to that point. That is, once the *IIR* is activated, it sends a video image to the pilot, who then selects an aim point on the target.

The *Tomahawk* is a long-range cruise missile for both surface and submarine launch against both surface ship and land targets. The *Tomahawk* was subsequently adapted for land launch as the *U.S. Gryphon* ground-launch cruise missile (*GLCM*). Navy nuclear-powered attack submarines (*SSN*s) fired 26% of the *Tomahawk* cruise missiles used against Serbia in *Operation Allied Force*. The *SSN* attack submarine can strike preemptively to prevent *WMD* deployment, or punitively and overwhelmingly in response to an enemy's use of *WMD*. Thus, the attack submarine of the future is a very credible deterrent to *WMD*. The guidance system of the *Tomahawk* consists of an inertial system updated by *TERCOM* (terrain contour matching), also known as *TERCOM*-aided inertial navigation system (*TAINS*). For more details on *TERCOM*, the reader is directed to Section 7.4. Another type of aiding used by some versions of the *Tomahawk* cruise missile is the digital scene-mapping area correlator (*DSMAC*). *DSMAC* is used as the missile nears the target. Target map updating involves relatively simple *DSMAC* reprogramming. Either *Tomahawk* version can fly preprogrammed evasive flight paths between guidance updates. Specifically, a "flex-targeting" upgrade that permits retargeting during flight has been successfully tested. The antiship *Tomahawk* is fitted with a modified *Harpoon* active radar seeker, flying a preprogrammed profile at sea-skimming height for most of its flight. Consequently, when the missile nears the target's estimated position, the active radar seeker takes over. In addition to the conventional *Tomahawk*, the Navy is pursuing development/production of the *Tactical Tomahawk* (or Block 4). After several successful flight tests, demonstrating the system's basic performance, the Navy plans full-rate production of the missile for the third quarter of 2004.

Tactical Tomahawk (or Block 4) is the latest evolution of the long-range, ship- and submarine-launched cruise missile. The main enhancement is the addition of a two-way *UHF* satellite communication link that allows operators to retarget the missile in flight and to gain imagery of the target before the missile impacts. Also, the missile uses a new Williams International *F415-WR-400* turbojet engine. The range is expected to be over 500 miles. During the flight tests, the Navy demonstrated *GPS* guidance during cruise, and refined navigation using the *DSMAC* function over land. *DSMAC*'s primary function is to determine the exact location of the missile and update the navigation system by removing guidance errors and providing greater precision than can be achieved by relying on *GPS*. Eventually, military operators should be able to change the missile's flight path, but also to simply launch the missile into a general area, have it loiter, and only then provide information on the target to be attacked, giving them an unprecedented degree of flexibility. The Navy also is preparing a development project for *Tactical Tomahawk* to carry a penetrating warhead. It would follow a Defense Threat Reduction Agency (*DTRA*)-sponsored demonstration that is to culminate in flight tests in 2003 using a *WDU-43* warhead. The Navy hopes to field *Tactical Tomahawk* in 2004.

The U.S. Navy is exploring the possibility of using a new supersonic sea-skimming target (*SSST*) to exercise ship self-protection against advanced threats. The Navy wants the new target to replicate what is widely seen as one of the greatest threats to its ships, the Russian-built *SS-N-22 Sunburn* missile. A variable-flow, solid-fuel ducted ramjet is to power the target. Among the systems to make use of the *SSST*

are the Navy's *Standard Missile* and the *Evolved Sea Sparrow Missile*. The minimum performance requirements for the *SSST* include a cruise speed of Mach 2.0 (Mach 3.0 goal) with a cruise altitude of 66 ft and 15 ft during the last phases of the flight. The target's range is supposed to be at least 45 nm, although a greater range of 55 nm capability is desired. One potential growth option for the *SSST* is equipping it with a warhead and using it as a missile.

There appears to be no observable distinction between long-range cruise missiles (that is, those capable of strategic missions) and short-range cruise missiles (that is, those suitable only for tactical missions, for example, those of the *Tomahawk* and *Harpoon* class).

In addition to the conventional weapons, the *Tomahawk* cruise missile can carry *HPMs* (also known as *E*-Bombs). As stated in Section 6.9.1, microwave weapons represent a revolutionary concept in warfare, principally because microwaves are designed to incapacitate equipment rather than humans. More specifically, *HPM*s are man-made lightning bolts crammed into cruise missiles such as the *Tomachawk*. They could be used for targeting stockpiles of biological and chemical weapons. *HPM*s fry sophisticated computers and electronic gear necessary to produce, protect, store, and deliver such agents. The powerful electromagnetic pulses can travel into deeply buried bunkers through ventilation shafts, plumbing, and antennas. *HPM*s can unleash in a flash 2 billion watts or more of electrical power.

Europe is also pursuing the development of cruise missiles. Specifically, Europe's MBDA is developing the *Scalp/Storm Shadow* cruise missile, which will be installed on the *Eurofighter*, *Rafale*, *Mirage 2000D*, *Mirage 2000-5*, *Tornado GR4*, and *Harrier GR7* aircraft. The British *Storm Shadow* variant is to enter service in 2002, the French *Scalp* version in 2003. MBDA has begun an early definition of an all-weather, day/night naval version of its *Scalp/Storm Shadow* cruise missile intended for deep strikes at land targets from submarines and surface ships. The initial definition will primarily consist of missile design, platform integration, and mission planning. The naval *Scalp/Storm Shadow* weapon could offer a more accurate alternative to the U.S. *Tomahawk* by using *GPS* navigation and terminal guidance. Provisions are also being made to ensure that the stealthy, precision-attack weapon will be compatible with the proposed European global navigation satellite system (*GNSS*). More specifically, *Scalp/Storm Shadow* is designed to employ the U.S *GPS* for midcourse updates in addition to *TERPROM* (see Section 7.4.1) terrain-following and inertial guidance systems. An imaging *IR* sensor mounted in the nose of the weapon and an autonomous target recognition system will provide terminal guidance. The naval *Scalp* cruise missile is tentatively scheduled to enter service around the year 2009.

Cruise missiles of other countries are as follows: China, *Delilah 2* and *C-802*; France, *Apache* (an earlier French cruise missile is the sea-skimming *Exocet*, which is in the inventory of several foreign countries); Israel, *Gabriel 3*, *4* and *Popeye 1, 3*; Russia, *Shaddock*, *Kh-55*, and *AFM-L Alpha*; and United Kingdom, *Centaur* and *Tomahawk*. Russia also developed the supersonic *Yakhont* (*NATO* designation *SS-N-26*) rocket/ramjet antiship cruise missile. The *Yakhont* antiship weapon carries a 440-lb warhead, has a rear rocket booster with thrust-vectoring control, and employs integral kerosene-fueled ramjet propulsion to achieve operating speeds of

Mach 2–2.6 at 45,000 ft or more over ranges up to 180 nm from airborne launches. Midcourse inertial guidance is followed by sea-skimming (33–50-ft) active/passive radar terminal homing. Other Russian antiship missiles include the *Granit* (*SS-N-19 Shipwreck*) and the *Moskit* (*SS-N-22 Sunburn*). Norway is developing a helicopter- and ship-launched antiship cruise missile known as the *NSM,* which would have about twice the range of the antiship *AGM-119 Penguin* missile, and is slated to become operational around 2004. Maritime patrol aircraft also could fire the missile. This new missile is being designed to include some low-observable (i.e., stealthy) characteristics in order to reduce the risk of being shot down by ship self-defense systems, and would carry a 120-kg (264.55-lb) warhead. The *NSM* would be capable of maneuvering during the terminal phase of the flight. During cruise, the missile will be guided using map-based terrain-following navigation. For terminal guidance it will use a passive *IIR* seeker with automatic target recognition algorithms. The missile would be powered by a *TRI40* turbojet and have a maximum operating altitude of about 6,000 meters (19,686 feet). Finally, this fire-and-forget missile would fly at subsonic speeds and at very low altitudes. For more details on these and other missiles, the reader is referred to [2], [3].

India is also developing a supersonic cruise missile, the *BrahMos*. Brahmaputra and Moscow Rivers are developing the 5,500-lb missile. The range for Mach 2.8 missile is given as 157 nm. *BrahMos* is a modified derivative of the Russian *NPO* Mashinostroenia Onix ramjet-powered antiship missile. The developers say that the missile can be launched from a submarine, surface ship, heavy vehicle, or aircraft.

In the early part of 1999, the U.S. Air Force expressed the desire for a new bomber-launched cruise missile, with six times the range of weapons currently under development (as stated earlier, the current *CALCM* range is 650 miles), to replace the aging Boeing-made *CALCM*s that once carried nuclear warheads. A possible replacement for the *CALCM* is the 14-ft-long joint air-to-surface standoff missile (*JASSM*). The *JASSM* is a joint Air Force–Navy program. *JASSM* is a stealthy, next-generation precision cruise missile designed for launch outside area defenses, which can penetrate enemy air defenses at ranges of 300 miles or more. *JASSM* is designed to destroy high-value, well-defended, fixed and moving targets. Containing an advanced *GPS/INS* guidance system, which is coupled with a terminal seeker, the *JASSM* is capable of aimpoint detection, tracking, and striking. As presently designed, the *JASSM* has only a 300-mile range. However, a study underway recommends extending the range to 1,000 miles, which should give defense planners the desired tactical flexibility. An extended-range version of the *JASSM* is also planned. Known as *JASSM-ER*, this weapon would benefit the *B-1B* bomber force. However, the *JASSM*, with its 1,000–2,000-lb-class warhead and shorter range, can be considered as complementary to the *CALCM*, with its blast/fragmentation warhead. The AF is studying the possibility of using the Lockheed Martin Advanced Unitary Penetrator (*AUP*) warhead in the *Calcm*s. Furthermore, in July 1999 the AF tested a *Calcm* with a 1,000-lb *AUP* warhead. The *AUP* is a purely kinetic energy driven warhead. Note that producing any greater ranges for the *JASSM* would likely require reduction in the warhead size to 500 lb. A replacement for the *CALCM* would optimally have a 3,000-lb warhead. Note that some of the new *CALCM*s that have been built will have penetrator warheads, while the rest will use the standard 3,000-lb-class blast/fragmentation warhead.

Future requirements for a stealthy cruise missile with a range of 1,000–2,000 nautical miles appears an attractive option. Stealth similar to *JASSM*'s all-aspect low observability will be a basic future requirement. Also, hypersonic speed will be an option. Other future cruise missile designs such as the extended-range cruise missile (*ERCM*) and the long-range cruise missile (*LRCM*) will be designed for greater survivability and fitted with a terminal-seeker, two-way data link capability to be able to retarget the missile in flight, that is, even after it has separated from the bomber (i.e., the *B-52H*), a bigger warhead (i.e., of the 3,000-lb-class), and longer range (e.g., more than 1,000 nm). It should be pointed out here that the U.S. Navy is already including in its *Tactical Tomahawk* two-way data link capability to be able to retarget the missile in flight. Moreover, the *LRCM* will be designed for increased survivability through the use of low-observable technologies or countermeasures. The possibility exists that the *LRCM* might be designed to be much smaller than *CALCM* and be able to be carried by fighters. However, to fit internally on a *JSF*, the weapon could be no larger than the current *JSOW*, which accommodates only a much smaller warhead. At this point it should be pointed out that the *JSOW* is a 1,000-lb-class launch-and-leave glide weapon with standoff capability. It will be used against a variety of targets and employs *GPS/INS* to allow day, night, and adverse weather operations. These features will also permit the *JSOW* to operate from ranges outside enemy point defenses. A *JSOW-B* is also being considered. For more details on the *JSOW*, the reader is referred to Appendix F, Table F.2. The *LRCM* would have to be even smaller to fit inside an *F/A-22 Raptor* weapons bay. (The *B-52H* can carry eight cruise missiles internally). On the *ERCM*, there are a few minor improvements that the Air Force would like to see. One is the ability to more easily reprogram the missile's target coordinates once the bomber has taken off.

During the period April 8–August 12, 1999, the U.S. Air Force conducted tests on a next-generation cruise missile, the *JASSM*, mentioned above. More recently (January 19, 2001), the Air Force successfully tested a *JASSM* using a state-of-the-art *IIR* target seeker system cruise missile. During the flight test, the *JASSM*'s *GPS* functioned flawlessly, recognizing three navigation waypoints, and completed necessary maneuvers to keep it on the preprogrammed mission attack plan. The Air Force is committed to buy up to 4,000 *JASSM*s. The U.S. Navy has also expressed interest in purchasing *JASSM*s for its *F-18 Hornets*. The stealthy missile is expected to become operational during fiscal year 2003. The *JASSM*'s cost is well below the $700,000 per unit predicted by the *DoD* at the program's offset. (The current cruise missiles cost in excess of $1 million each). Finally, unlike the current cruise missiles, the *JASSM* can be launched off the *B-1 Lancer*, *B-2 Spirit*, *B-52H Stratofortress*, and *F-16 Fighting Falcon*, and the Navy's *F/A-18E/F Hornet*. The *B-1* will carry 24 *JASSM*s, the *B-2* will carry 16, and the *B-52* will carry 12 externally under the wings. The *F-16* can carry 2 *JASSM*s.

7.2 System Description

As discussed in Section 7.1, the *AGM-86B ALCM* is a long-range, air-to-ground cruise missile originally designed to be launched by manned bombers and attack strategic

targets. The *ALCM* has many of the attributes of the earlier *Hound Dog* cruise missile, but it is slower, has a longer range, and is much more accurate. Flying at a very low altitude, the *ALCM* relies on its small radar signature and surrounding ground clutter to defeat enemy air defenses. The *ALCM*, as discussed earlier, is a conventional-(or nuclear-) warhead, turbofan-powered, strategic cruise missile that can hit a target with pinpoint accuracy at the end of a 5,000-km flight, developed specifically for air launch. It is designed to be compatible with the existing carrier aircraft (e.g., the *B-52G,H*) avionics system. The carrier aircraft avionics is part of the offensive avionics system (*OAS*) update.

Historically, the *ALCM*'s fundamental functional requirements and the resulting design originated in the *SCAD* (subsonic cruise armed decoy) program, ca. 1972. A significant characteristic of the *ALCM* is the high accuracy at long missile ranges provided by its terrain correlation updated navigation system. In order to implement a terrain correlation updated navigation system, reference terrain elevations must be stored in the missile's computer prior to launch. This elevation data must be gathered, stored in ground computers, precisely selected for each mission, stored in the carrier aircraft, and transmitted to the missile prior to launch. More specifically, the missile's navigation and guidance unit uses a terrain contour matching (*TERCOM*) system that periodically updates the missile's inertial navigation system by comparing terrain over which the missile flies with stored mapping data. The *TERCOM* data are provided by the Defense Mapping Agency-Aerospace Center (*DMAAC*). Flight-control surfaces remain stowed and the engine cold until after separation from the carrier aircraft. Surface deployment and engine startup are accomplished in two seconds. Consequently, the carrier aircraft system can align and launch *ALCM*s carried on wing-mounted pylons or a rotary rack carried in the bomb bay. The carrier aircraft avionics include a master computer, which provides initialization and alignment data to the *ALCM* and sequences the missiles through launch. The carrier aircraft *INS* can be aligned using standard operating procedures for an airborne alignment. An average of five position fixes should be taken before transfer alignment to the missile. The analysis of transfer alignment includes the time to align and the initial conditions at launch. The initial conditions are usually computed by differencing the missile position with *TSPI* (time space positioning information) data. Position updates are taken from terrain correlation maps to correct the unbounded position error growth inherent to the cruise missile guidance system.

Figure 7.1 illustrates the primary mission functions, their time sequencing, and the role the missile and carrier aircraft computers play in each part of the mission. After ground testing of the aircraft and missile systems, the *B-52* with missiles uploaded is placed on alert. Next, the mission planner selects a path for the *ALCM*, which is part of the mission data preparation system (*MDPS*), from launch to target that passes over the terrain maps. The planner has flexibility between maps, but must fly over the maps in the direction of map orientation. The distances between maps must be chosen so that there is a high probability of crossing the maps yet not so close as to unnecessarily constrain the missile flight path. The probability of map overflight is computed for each map of the mission by computing the ratio of the crosstrack and downtrack errors to one-half the map function. This function calculates

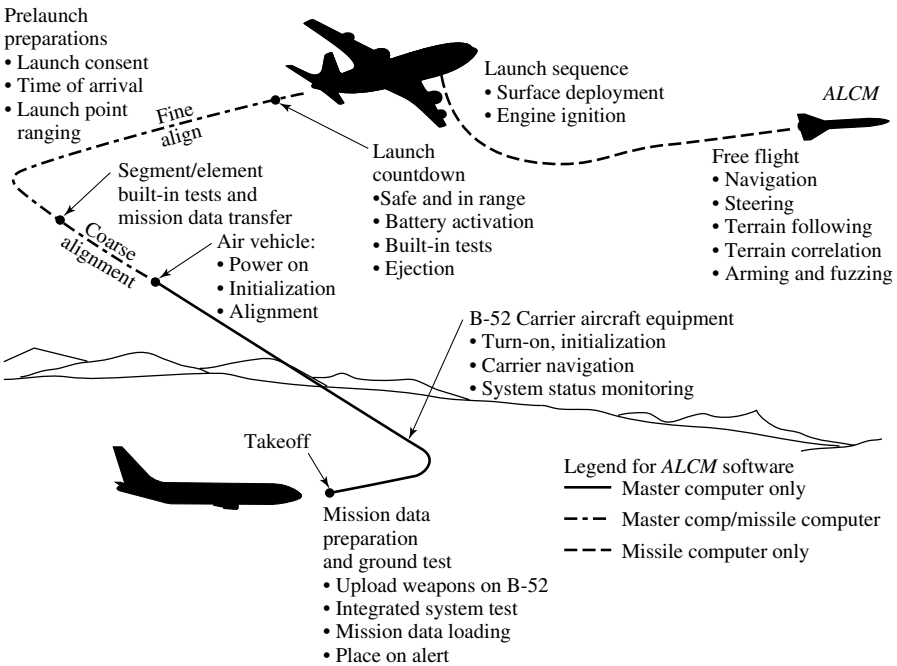

Fig. 7.1. Typical mission functions.

the probability of overflight with negligible error. Also, the mission planner selects the vertical profile based on knowledge of the terrain on the missile flight path and other trajectory requirements.

Figure 7.2 shows visually the steps involved in planning a test mission from launch point (Point 0) to the target (Point 6). The planner first selects a path from launch to the target in the horizontal plane that passes through the required maps (maps 1 and 3, in the example). In the horizontal plane selection, the mission planner takes into account the terrain over which the missile will fly, special test objectives, and distance between maps. The mission planner has two *ALCM* simulation tools (or modules) available to aid him in planning missions. These are (1) the clobber analysis module (*CAM*), and (2) the navigation accuracy module (*NAM*) (see Section 7.2.2 for more details on *NAM*).

Both these programs reside in a ground-based computer. *CAM* provides the capability to the mission planner to compute either probability of ground clobber given a specified ground clearance, or ground clearance given a specified probability of clobber. *CAM* can operate in a rapid mode or a slower mode that provides more detailed results. *NAM* predicts accuracy and map crossing probabilities along the route of the mission from launch to target. Each of the horizontal maneuvers or any missile mode or speed change requires a missile waypoint. A waypoint is defined as an action point. For more detailed discussion, see Section 7.2.1. The vertical profile is then selected. Here again, a waypoint is needed for each vertical change either in

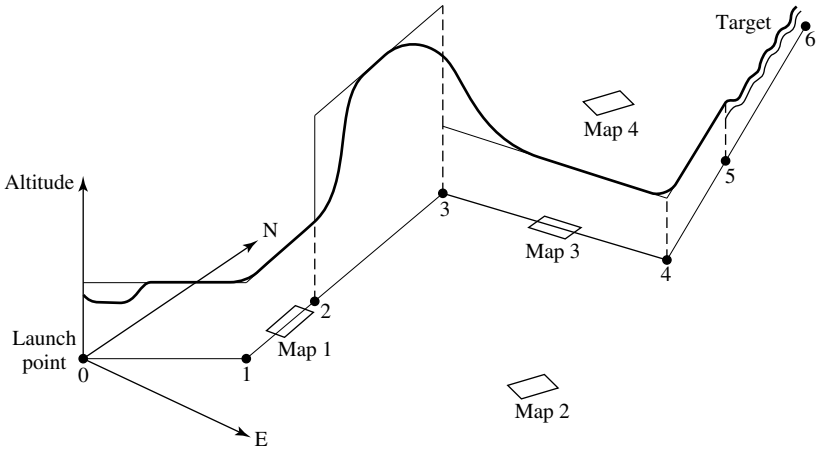

Fig. 7.2. *ALCM* mission example.

terrain following or barometric hold. Once the mission is selected and all waypoint and maps defined, the defined mission is input to the mission data preparation system.

The guidance software modules provide the command signals used by the autopilot modules to control vehicle heading, crosstrack, and altitude. The guidance modules are (1) route definition module, (2) lateral guidance module, and (3) vertical guidance module. The route definition module provides (1) launch turn control to permit launch in a direction away from the first waypoint, (2) calculation of unit vectors in a tangent plane coordinate frame for use in the lateral guidance module (which will be discussed below), (3) data control logic to sequence through profile segment data and waypoint definition data, and (4) control of logic flags that initiate turns to change from one mission segment (or leg) to the next.

The lateral guidance module calculates the bank angle commands used by the autopilot modules in controlling vehicle heading and crosstrack position. In particular, the lateral guidance module provides bank angle commands for steering to the ground track defined by waypoints. Near a waypoint, the desired path (i.e., the reference for determining lateral displacement and heading) is a circular arc transition between the two directions defined by adjacent great circle path segments, as illustrated in Figure 7.3. To recapitulate, the cruise missile is directed along the proper course between waypoints by the lateral steering system. The steering plane, that is, a plane containing the two waypoints and the Earth's center, defines the course between two waypoints. The perpendicular distance between the air vehicle position and the steering plane is the crosstrack error, and its time derivative is the crosstrack error rate.

During turns, the crosstrack error may be defined as follows. A turn center is defined (see Figure 7.3) that is the center of the circle containing the desired ground track during the turn. As a result, the crosstrack error then becomes the difference in the lengths of two vectors from the turn center. One of the vectors defines air vehicle

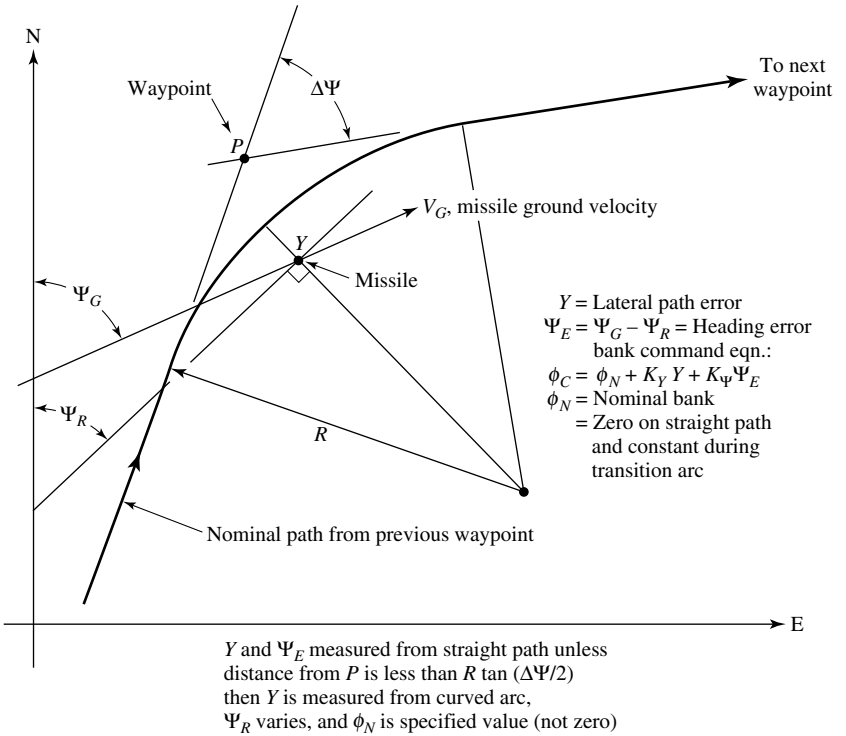

Fig. 7.3. Waypoint lateral path steering and turn control.

position, and the other, the ground velocity. The third module, the vertical guidance module, calculates the vertical acceleration commands used by the autopilot module (i.e., vertical acceleration control) to control air vehicle altitude. Specifically, the vertical guidance module commands normal accelerations based on clearance altitude error and a selected form of feedback. Note that climbing flight generally employs a clearance rate feedback, while diving flight is executed with inertial rate feedback.

The primary cruise missile avionics forming the navigation system are the onboard computer, inertial reference unit (*IRU*), radar altimeter, baro-altimeter, and temperature sensor. The radar altimeter provides absolute altitude above the terrain. Furthermore, when integrated with a navigation system, it provides altitude data for terrain following and correlation processing. The missile's computer memory has more than 65,000 16-bit words. Approximately half of the computer memory is used for storage of mission data and the other half for operational flight software. Moreover, the missile computer is the heart of the missile, controlling all missile free-flight functions including navigating and guiding the missile along its planned horizontal and vertical path. The *IRU* provides an accurate reference for cruise missile navigation functions, while the radar altimeter is used both by the flight control for terrain following and by the terrain correlator. Pressure, temperature, and inertial vertical velocity are used

for accurate vertical position determination during altitude hold flight segments and terrain correlation flight segments. The *IRU** mentioned above is part of the inertial navigation system (*INS*). Therefore, a long-range strategic cruise missile employs an inertial navigation system consisting essentially of three accelerometers mounted on a gyroscope-stabilized platform and the associated electronics to guide it along an assigned course. A practical inertial navigation system suitable for a cruise missile could allow the missile to drift about a kilometer or so off course for every hour of flight. The effects of weather and the imperfections of the jet engine that powers the missile increase the drift. After several hours of flight, the missile could be ten or more kilometers from its intended impact point. If, however, the missile could from time to time recognize where it was and compare its actual position with where it should be according to its assigned path or trajectory, then the onboard computer could instruct the autopilot to make the appropriate maneuvers to bring the missile back to the correct trajectory. Furthermore, the known difference between the actual position and the intended position is used by the computer to calibrate and reset (or update) the *INS*, a process that compensates for and reduces the missile's drift by a factor of two or three. As discussed earlier, there are several ways in which a cruise missile can determine its actual location while it is in flight. These systems are (1) the *TERCOM* and (2) the *GPS*.

7.2.1 System Functional Operation and Requirements

The guidance system performs missile computations and control for (1) prelaunch and free-flight operations, (2) interfaces with other weapon system elements during various mission phases, and (3) senses appropriate navigational information to an accuracy sufficient to meet the performance requirements specified. The guidance system stabilizes and controls the air vehicle flight along preprogrammed flight profiles between stored geographical coordinates (or waypoints).

System Functions With the appropriate operational software loaded into the guidance system, the cruise missile guidance system then is capable of performing the following functions:

(a) Program Load: The cruise missile guidance system has the capability of loading the operational program and related data into the guidance system's memory via the carrier aircraft (e.g., *B-52*) guidance system data bus. A bootstrap loader program is contained in a separate programmable read only memory (*PROM*) within the cruise missile's guidance system.
(b) Mission Profile Storage and Selection: The cruise missile guidance system accepts and stores complete mission profiles. The guidance system has the capability for target change prior to launch. Also, the guidance system is designed to be compatible with the carrier aircraft's retargeting operation.

*The *IRU* itself consists of the basic three gyroscopes and three accelerometers, as opposed to a full-fledged *INS*, which contains a navigation computer.

(c) Power Compatibility: The cruise missile guidance system will accept interruptible *DC* power to heat the inertial instruments and electronics to bring the guidance system to operating temperature within 40 minutes or less. After warm-up has occurred, the missile guidance system will require noninterruptable *DC* power for operation and continue to use interruptible *DC* power for heating as required until shortly prior to launch. The guidance system's battery is activated during the launch sequence and provides power during the launch phase. The missile's engine-driven generator provides subsequent mission power.

(d) In-Flight (Captive Carry) Alignment: The cruise missile guidance system accomplishes in-flight alignment using data available in the existing carrier aircraft.

(e) Built-In Test (*BIT*): *BIT* is incorporated in the missile guidance system and is used during prelaunch to verify that the cruise missile is ready for launch. Subsequently, the guidance system computer initiates and analyzes all specified *BIT* functions and provides *BIT* data to the carrier aircraft about the condition of the guidance set and the cruise missile airframe. The guidance system also accepts externally generated *BIT* commands.

(f) Launch Jettison: The guidance system is designed to function properly in the sequential launch mode at five-second intervals. In the event of a missile jettison command from the carrier aircraft, the guidance system will automatically erase all classified data stored in the computer prior to jettison. Moreover, the guidance system performs control functions required for safe separation whether the cruise missile is in a normal or jettisoned launch.

(g) Separation Maneuver: The guidance system issues commands to the missile flight and engine controls to maintain a vertical separation from the carrier of at least 75 feet until a lateral (forward) separation of 300 feet is reached. The missile will not be commanded to climb until this lateral separation is achieved.

(h) Stability and Control: All guidance-system-generated commands to the flight system are designed not to exceed the missile structural and aerodynamic capabilities. Thus, all software in the guidance system is constrained to turn, zoom, or dive radii that are consistent with the air vehicle's flight control equipment and strength capabilities.

(i) Air Vehicle Control Software: The software provides basic flight profile commands, which are Mach number, clearance altitude, and climb/dive rate limits for each flight segment including bank angle commands for steering to the ground track defined by the waypoints (see item "m" below) in the guidance route.

(j) Terrain Following: The guidance system performs all required terrain-following functions. In case a "breaklock" occurs due to jamming or malfunction of the radar altimeter, the guidance system will command the missile to climb to a safe altitude utilizing the backup baro/inertial altitude system. Upon reacquisition of radar altimeter data, the guidance system will command the missile back to the terrain-following mode.

(k) Terrain Correlation (*TC*): This system is used to update the navigation systems to correct drift errors and provide the navigation system with a finite position fix. This function is accomplished by averaging altitude over a waypoint, calculating

position and time, and adjustment of mean sample altitude. This system furnishes terrain altitude to the guidance computer and thus to the navigation system. The system utilizes stored map data, which are loaded prior to flight (see also Section 7.3).

(l) Navigation: The guidance system utilizes a 15-state Kalman filter navigation system using terrain correlation (*TC*) fixes. The guidance system software contains the equation for instrument compensation, velocity, and position computations. Navigation is three-dimensional with the vertical channel slaved to an external reference, barometric, or radar altimeter. The inertial navigation system determines missile position, velocity, attitude, and altitude. Moreover, the guidance system has the capability for air alignment and accepts initial conditions for navigation computation from the carrier aircraft, including retargeting.

(m) Waypoints: The cruise missile trajectory flightpath is defined by a series of geographic or action points, each of which is identified with a particular latitude, longitude, and altitude to which the cruise missile is commanded to fly. These action points, which are called waypoints, are used to define each change of state or flight mode. Each turn, change of speed, change of altitude, or any other mission-dependent parameter is performed by changing the appropriate command at the desired waypoint. The waypoints are also used in the horizontal guidance algorithms by providing the great circle track over which the air vehicle will fly. Missile commands and/or flight instructions can be made or changed only at waypoints.

7.2.2 Missile Navigation System Description

In Section 7.2 we discussed briefly the role of the inertial navigation system. A general description of the navigation system, which is part of the *NAM* (navigation accuracy module), objectives, approach, performance requirements, and input/output requirements will be discussed in this section. The navigation accuracy module is an integral part of the mission planning system (*MPS*). The *MPS* is an interactive computer system that is used to develop cruise missile routes. More specifically, the *MPS* consists of the development of a route that satisfies the cruise missile's constraints and the generation of the commands and data to be loaded into the onboard computer. The objectives of the *MPS* are:

(1) Navigation maps located to provide high probability of acquisition,
(2) Guidance and control commands achievable by the cruise missile,
(3) Achievable range, and
(4) Low probability of clobber.

Furthermore, the navigation system is designed as a self-contained, stand-alone, primary software system element for the cruise missile *MPS* that will predict mission downtrack and crosstrack errors for any action point in support of routing function to develop acceptable cruise missile route definitions. The navigation system makes use of a covariance analysis approach for generating mission navigation data to the specified accuracy and confidence levels and within computer limitations. This approach

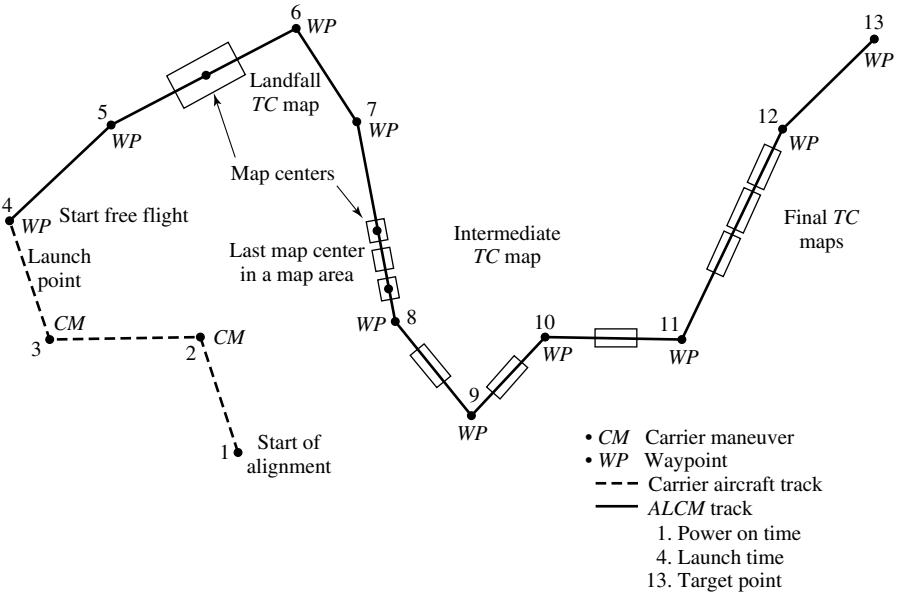

Fig. 7.4. Example flight route.

requires selecting suitable system matrices that determine the error propagation of the cruise missile navigation system between position updates. Using route definition data stored in tables established by the calling program, the navigation system produces navigation data for new mission or partial rerun of mission by performing a navigation covariance analysis time simulation and updates the tables with the processed navigation data. An example of a flight route is shown in Figure 7.4.

Navigation System Requirements As stated earlier, the navigation accuracy module (*NAM*) is designed to function as a part of the cruise missile *MPS*, which provides the following specific navigation data:

(a) Navigation error ellipse description at specified points along the route of flight.
(b) The probability of overflight of each terrain-correlation map area associated with the route of flight.
(c) The circular error probable (*CEP*) at specified points along the route of flight.
(d) The launch footprint, which allows successful acquisition of any desired terrain correlation map along the route of flight.

The functions that must be performed within the various *NAM* modules are as follows: (1) within the *NAM* data format validation, (a) evaluate buffer table data for range limits, (b) evaluate buffer record sequences, (c) evaluate waypoint locations before and after map areas, and (d) output error messages and waypoint recomputation flags as necessary; (2) within navigation matrix initialization, (a) read and load proper start navigation matrices and data, (b) build navigation matrices. Also, the following functions must be performed: (1) set matrices to alignment initialization, (2) propagate

backward from launch point to alignment initialization (power on), to establish alignment initialization position and direction cosine matrix, (3) propagate error covariance matrix forward from alignment initialization to launch point, and (4) combine carrier error covariance matrix with the alignment error covariance matrix to obtain initial free-flight error covariance matrix.

I. Within inertial computations, the following must be performed:
   1. Compare Earth relative angular velocity and propagate the direction cosine matrix (*DCM*) C.
   2. Calculate the state transition matrix Φ.
   3. Calculate the process noise matrix Q.
   4. Propagate the error covariance matrix P according to [9]:

$$P_i = \Phi_i P_{i-1} \Phi_i^T + Q_i. \tag{7.1}$$

II. Within primary TC computations, perform the following:
   (1) At the first map in a voting group save the error covariance matrix.
   (2) Calculate the accumulated state transition matrix Φ' between map centers according to

$$\Phi'_i = \Phi'_{i-1} + \Phi_i, \tag{7.2}$$

   where Φ'_i is reset to the identity matrix at step centers.
   (3) Calculate the accumulated process noise matrix Q' between map centers according to

$$Q'_i = Q'_{i-1} + Q_i, \tag{7.3}$$

   where Q'_i is reset to zero at map centers.
   (4) Save the accumulated matrices at map centers before resetting values.
   (5) Calculate and save one-sigma downtrack and crosstrack errors at map centers.

III. Within secondary TC computations, perform the following:
   (1) Perform Kalman filter update of error covariance matrix at final map center of a voting group.
   (2) Compute the time until navigation update.
   (3) Compute the time delay t_g between update time and time of completion of correction maneuvers.
   (4) Evaluate next waypoint or target for comparison with t_g and set the error message flag if map group too close.

In performing the above functions, the *NAM* system must satisfy the following accuracy and validity requirements:

(1) Within 95% confidence, the probability to successfully overfly a specified map area associated with the route of flight. The probability calculated shall be within $\pm 2\%$ of the actual probability.

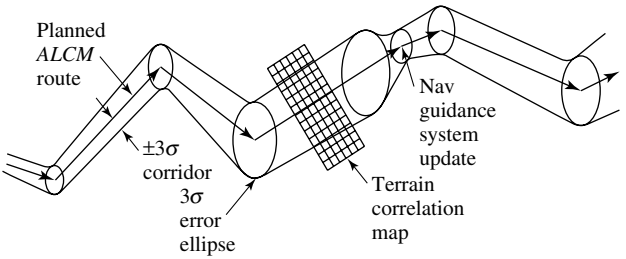

Fig. 7.5. Error ellipses.

(2) Within 90% confidence, the navigation error ellipse description at specified points along the route of flight. Ellipse dimensions shall be within ±10% of actual errors or 100 ft, whichever is greater (excluding launch platform error contribution).
(3) Within 90% confidence, the *CEP* at specified points along the route within ±10% of the actual *CEP* value at the terminal point.
(4) Within 95% confidence, the launch footprint such that the probability of successful overflight of any *TC* map satisfies the requirements of (1) above.

In addition to the above requirements, *NAM* must (a) estimate map overflight probability, (b) estimate position accuracy at the target, and (c) calculate the flight corridor widths and enroute position error ellipses. Figure 7.5 illustrates the concept of the error ellipses.

Additionally, the position error ellipse data are used to check whether adequate time is available to complete terrain-correlation processing and remove the position correction from the position update before arriving at the target. Furthermore, *NAM* also determines whether the waypoints surrounding the terrain correlation maps are correctly located. Since the terrain correlation process requires that the maps be overflown at the proper heading, this calculation can correct the waypoint preceding and following each map. More importantly, the navigation system must perform a procedure for recomputing the waypoint location. This procedure checks the location of waypoints in front of and behind each map and verifies that they form a geodesic path on the Earth ellipsoid. The geodesic path passes through the map center with the desired heading. A new waypoint is calculated, and if it is different from the input waypoint by 10 ft, the recomputed value is placed in the recomputed waypoint field of the data structure. The recomputed flag is set for the mission planner and/or system disposition. This procedure must also be performed on speed or altitude waypoints that may lie between map entries and exits.

Mathematical calculations performed within the *NAM* will produce results sufficiently accurate to ensure accuracy within the following tolerances:

Latitude and Longitude:	± 0.00001°,
Velocity:	± 1.0 m/sec,
Heading:	± 0.1°,
Map Cell Size:	± 1.0 meter,
Time:	± 1.0 second.

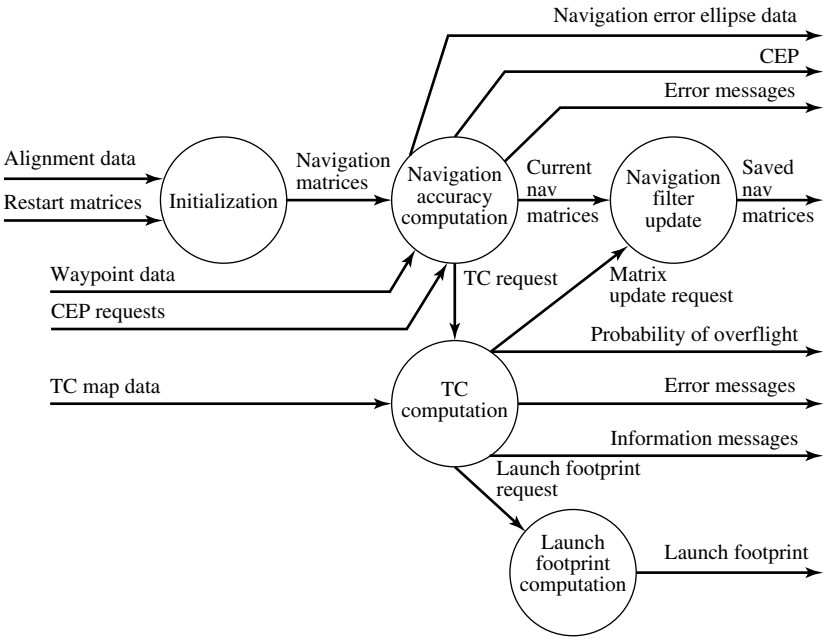

Fig. 7.6. *NAM* data flow.

Figure 7.6 illustrates the overall logical data flow for *NAM*. Input data from a record in the *IOBT* (input/output buffer table) determine a segment of the cruise missile route for which navigation errors are calculated and appropriate output data generated. These outputs are stored in the *IOBT* record. Processing of the *IOBT* data is conducted by elements as summarized in Table 7.1.

The program elements and functions of Table 7.1 will now be discussed in more detail.

NAM Inputs and Outputs The inputs and outputs of the *NAM* system are contained in *CPU*-resident buffer tables (i.e., in the *IOBT*). However, it is necessary for the calling program to execute a pre-NAM data processing function to construct these buffer tables from a database whose structure uses the joint route point table (*JRPT*). The five tables containing data required by *NAM* are (1) navigation initialization table, (2) terrain correlation table, (3) *JRPT* table, (4) error table, and (5) launch footprint table. Upon completion of *NAM* execution the required *NAM* outputs as previously described are available in the buffer tables for calling program processing/merging into the database or for use by the clobber analysis module, the operator, or the mission planning system (*MPS*).

NAM Subprogram Modules Description The major modules of the *NAM* system that are the primary candidates for testing are described below.

1. *NAM* Data Format Validation: This module checks the *IOBT* data entries for *NAM* input to ensure that the parameters are within specified boundary constraints. A

Table 7.1. Summary of *NAM* Program Elements and Functions

Elements	Features
Input/Output Buffer Table	The route definition data buffer Created via pre-*NAM* computations Existing mission for refinement Data contains: Routing data (action points, waypoints, ground speed. *TERCOM* map data (cell size, centers, group size). Carrier vehicle data (velocity, heading, position). *NAM* output data (waypoint error ellipses, update data, target *CEP*, error messages, launch footprint).
NAM Processing	
Data Format Validation	Access *IOBT* Validate data Recompute waypoints Error messages
NAV Matrix Initialization	Load restart data Back propagate in time to power-on position *FWD* propagate matrices to launch position Combine error covariance matrices.
Inertial Computations	Propagate direction cosine matrix Calculate state transition matrix Calculate process noise matrix Propagate error covariance matrix
Primary *TC* Computations	Store error covariance Accumulate intermap matrices Calculate crosstrack and downtrack error.
Secondary *TC* Computations	Update covariance matrix (Kalman filter) Calculate update time Determine whether map too close to target.
Update *NAM* Data	Output launch footprint Output *CEP* Output error ellipse Output probability of overflight Output navigation update data.

typical validation process will include verifying that (a) actual data count values are in acceptable range, (b) indices are in acceptable range, (c) alignment time values are negative, (d) heading values are in acceptable range, (e) latitude and longitude values are in acceptable range, and (f) ground-speed values are in acceptable range.

If any of these tests fail, an error message will be generated and control returned to the calling program. Validation also includes recomputation of waypoint location to ensure that a map leg between waypoints is a great circle route crossing the map center and having map heading corresponding to route heading at the map center. This is accomplished by calculating new waypoints based on map center data and the great circle track of the pre- (post-) map leg.

2. Navigation Matrix Initialization: If this is a restart program, then the *NAM* will obtain route leg and map record information from the *IOBT*. The error covariance matrix will be initialized with data stored in the *IOBT*. The direction cosine matrix (*DCM*) will be initialized using stored values of position, ground speed, and heading. Propagation will proceed from the carrier vehicle action point specified.
3. Build Navigation Matrices: For nonrestart programs, this module initializes the data and matrices for the missile alignment trajectory. The generation of the trajectory is done in two phases. The first stage initializes the *DCM* with the launch position and propagates backward using data on carrier maneuvers until missile power-on time is reached (which is the assumed beginning of fine alignment). The second stage generates the direction cosines and velocity changes using a normal forward integration at 60-second intervals for use in the computation of the state transition and process noise matrices. These are used for propagation of the error covariance matrix, as in (7.1):

$$P_i = \Phi_i P_{i-1} \Phi_i^T + Q_i, \tag{7.1}$$

where P_i is initially set to P_o, the expected navigation error state at the completion of coarse alignment; Φ_i is the state transition matrix; and Q_i is the process noise. A captive alignment measurement noise matrix R and a measurement matrix H are used for calculating the Kalman gain matrix K, according to

$$K_i = P_i H^T (H P_i H^T + R)^{-1}, \tag{7.4}$$

and the error covariance matrix is updated at each iteration or integration step as

$$P_i^+ = (I - K_i H) P_i, \tag{7.5}$$

where I is the identity matrix. At the completion of captive fine alignment the error covariance matrix corresponds to the error state relative to the carrier aircraft. Therefore, it is necessary to combine the captive alignment error covariance matrix with the carrier covariance matrix P_c at launch to obtain an error covariance matrix of navigation errors relative to an Earth reference frame.

4. Inertial Computations: This module performs the integration steps for propagation of the error covariance matrix. It is processed by three minor submodules that set iteration values, and it is composed of four submodules to perform the propagation.

5. Preparation Submodules: These modules are as follows: (a) The "get next data values" submodule indexes through the *IOBT* and extracts waypoint input data for use in other modules. In particular, it reads and saves the waypoint latitude and longitude, ground speed, heading, and indicator flags. Other pertinent data, such as map cell size, are also stored for later use as necessary; (b) The "compute time interval and mode" submodule calculates the time it will take to travel from the current waypoint (as known from the *DCM*) to the next waypoint as obtained from the *IOBT* by the "get next data values" submodule; travel is effected at the specified ground speed. Flags and internally generated condition indicators are used to set the mode (iteration time interval) to either 60 seconds or 12 seconds; (c) The "compute loop initial values" submodule calculates the number of loop iterations required for propagation to the next action point using the previously calculated time interval. This module also sets or resets flag indicators based on input data stored leg-position indicators, which keep track of current position on the route leg (i.e., whether between maps, approaching a target, etc.).
6. Compute Trajectory Parameters: This submodule uses stored values of missile velocity, iteration interval, and the direction cosine matrix to calculate Earth-relative angular rates and an intermediate matrix B. This submodule also calculates position data and velocity components at each new iteration.
7. Calculate State Transition Matrix: This submodule uses horizontal velocity components, angular rates, stored constants, and an equation set to calculate the new state transition matrix Φ_i. This matrix is used later in calculating the covariance matrix.
8. Calculate Process Noise Matrix: This submodule uses stored values of constants, horizontal velocity changes, increment time, and platform angular velocity to calculate a new process noise matrix Q_i. This matrix corresponds to noise generated by missile acceleration and angular velocity; it is used in calculating the covariance matrix.
9. Propagate Covariance Matrix: The error covariance matrix propagation consists of the propagation of a covariance matrix P of navigation errors at a fixed propagation interval of 60 seconds unless terrain correlation is in progress (i.e., between map centers) when it is 12 seconds. The navigation error state consists of fifteen elements. These are x, y position error; x, y velocity error; x, y platform tilt; platform azimuth error; x, y, z gyroscope bias drift rates; computer azimuth error; x, y gyrotorquer scale factor error; and x, y accelerometer scale factor error. The covariance matrix is updated at terrain correlation position fixes where special logic is used to accommodate the time delay in the updates due to the voting logic and characteristics of the terrain correlation process. This submodule also stores and saves elements of Q for output calculations, saves accumulated state transition and process noise matrices, and resets the temporary accumulation matrix variables.
10. Primary TC Computations: This module calculates the intermap accumulated state transition matrix Φ' and the accumulated process noise matrix Q', as in (7.2) and (7.3):

$$\Phi'_i = \Phi_i + \Phi'_{i-1}, \tag{7.2}$$

$$Q'_i = Q_i + Q'_{i-1}, \tag{7.3}$$

where the initial values of Φ' and Q' starting at a map center are

$$\Phi' = I \text{ (the identity matrix)},$$
$$Q' = 0 \text{ (zero matrix)}.$$

These propagations actually take place after calculation of Φ and Q within the "inertial computations module" but before the propagation of the covariance matrix P.

11. Secondary TC Computations:

11.1 Perform Kalman Filter Updates: This submodule uses crosstrack and downtrack one-sigma $(1-\sigma)$ error values to establish a 2×2 matrix R. Moreover, R, P, and the previously defined measurement matrix H are used to develop the Kalman gain matrix K according to

$$K = PH^T(HPH^T + R)^{-1}, \tag{7.4}$$

where K, P, and R are values established at a map center. The covariance matrix is updated at the map center according to

$$P^+ = (I - KH)P, \tag{7.5}$$

where I is the unity matrix and P^+ is the updated covariance matrix. This matrix P^+ is used with the stored accumulation matrices Φ' and Q' to propagate P to the next map center according to

$$P = \Phi' P^+ \Phi'^T + Q', \tag{7.1}$$

where Φ'^T is the transpose of Φ'. This procedure is repeated for second and third map centers of a three-map voting group, using stored values. The resulting error covariance matrix is the updated value that will later be output to the *IOBT*, enabling the mission planner to return to any map set and restart the covariance propagation. This submodule also sets and resets internal flags that indicate that the correlation process has been completed.

11.2 Compute Time Until Update: This submodule calculates the delay time for the third map of a voting group to finish correlating. (The time computation is performed on only those maps of a voting group that lie on a straight line). The delay is saved for later output to the *IOBT*. This module also calculates the time t_u at which correlation is completed. This value is saved for inertial computation to the time of update.

11.3 Compute Time Until Update Maneuver Complete: This submodule calculates the incremental time for the navigation error after update (and accounts for maximum downtrack error) to develop maneuver complete time t_g. This time is compared to the predicted time over target to verify that the missile has corrected and settled on a final heading before crossing the target. If this is not found to be the case, then an error message flag is generated to indicate that the final map group is too close to the target.

12. *NAM* Data Output: This module is composed of several submodules called upon for supplemental output calculations as necessary according to the type of *IOBT* data being processed.
    - 12.1 Output Waypoint Error Ellipse: This submodule uses position covariance elements from the error covariance matrix to calculate error ellipse semimajor axis and semiminor axis one-sigma values and the heading of the ellipse as an angle from north to the semimajor axis. Error ellipses are calculated at waypoints, and just prior to and immediately after navigation update. The error ellipse is also calculated as a preparation for *CEP*.
    - 12.2 Output Circular Error Probable *CEP*: This submodule is executed for *CEP* outputs to the *IOBT*. It accepts values of semimajor axis errors σ_u and semiminor axis error σ_v, and calculates the *CEP* according to [8]

$$CEP = 0.563\sigma_u + 0.614\sigma_v \quad \text{if } \sigma_v < 0.35\sigma_u, \tag{7.6a}$$

      and otherwise,

$$CEP = 0.674\sigma_u + 0.0786\sigma_v + 0.2753(\sigma_v^2/\sigma_u) + 1.108(\sigma_v^3/\sigma_u^2). \tag{7.6b}$$

      The value calculated for *CEP* is output to the *IOBT*; flags are reset so that further integration along the leg will continue at the 60-second rate.
    - 12.3 Output Navigation Update Data: This submodule stores update data from calculations at the final map center of a map area into the *IOBT*. These data consist of position and heading at map center, error ellipse after update, error ellipse prior to update, time at map center (update time) covariance matrix, and time delay to finish update data correlation.
    - 12.4 Output Probability of Overflight: This submodule calculates probability of overflight at each map center and outputs the value of crossstrack probability of overflight and of downtrack probability of overflight into the *IOBT*. This submodule also compares the calculated probability to the specified threshold probability allowed and sets an error flag if probability is too low.
    - 12.5 Launch Footprint Computations: For the first map on a route, the launch footprint computations submodule is invoked to determine the area within which the missile may be launched and successfully navigate to the first waypoint and then to the first map such that the probability of overflight of that map meets with specified success criteria. This computation involves determining the shape of two curves centered on the first waypoint and two azimuth angles from the first waypoint defining a "keyhole."
    - 12.6 Output Error Messages: This submodule places error messages into *IOBT* records for transfer to the main error table described above.

7.3 Cruise Missile Navigation System Error Analysis

Section 7.2 discussed briefly the function of the cruise missile inertial navigation system (*INS*). As mentioned in that section, the *INS* can be of the gimbaled or strapdown variety. (Note that because of the widespread use of ring laser or fiber optic gyros,

the present-day generation of inertial systems are of the strapdown type.) This section addresses the characteristics of the air-launched cruise missile navigation system and indicates the features that have been designed in order to achieve the missile's performance criteria. The system has successfully demonstrated all accuracy requirements. The air-launched cruise missile navigation function mechanization described herein satisfies the requirements to provide worldwide navigation following alignment and launch from the carrier aircraft and using the terrain correlation and/or the *GPS* system for periodic position updates. In essence, the navigation function for the cruise missile must satisfy three major modes of operation: (1) captive alignment, (2) free flight navigation, and (3) terrain correlation. These functions are performed by the navigation software. The alignment software can be further divided into coarse alignment and fine alignment. Coarse alignment is performed by the navigation module. The software provides a command to coarse-level the air vehicle platform to slew (assuming a gimbaled inertial platform) in azimuth even during carrier aircraft turns. It also commands the platform to the same direction as the carrier aircraft inertial platform. This slewing procedure simplifies the fine alignment mode. Fine alignment is performed by a Kalman filter. Given the requirements for fine alignment (e.g., alignment in 30 minutes or less), the best solution is to use the free flight Kalman filter for alignment. This Kalman filter resides in the carrier aircraft master computer.

Free flight navigation is performed by the navigation module. The major functional elements of the free flight navigation system are shown in Figure 7.7. The four major computational blocks of the free flight navigation system are (1) inertial navigation, (2) vertical channel (including air data), (3) terrain correlation, and (4) the free flight Kalman filter.

During free flight, the Kalman filter continues to align and calibrate the *INS* in addition to reducing the air vehicle position and velocity errors. The necessary information is provided by the terrain correlation (or *GPS*) position fixes. Velocities, angular rates, torques, and direction cosine derivatives are computed in double precision (32 bits). Moreover, the free flight Kalman filter operates radial residuals, which are defined as the difference between the missile's position determined by the terrain correlation algorithm and the inertial navigation system. Consequently, the data will be statistically combined by the filter algorithm to correct position, velocity, tilt, and gyro bias. The magnitude of the residuals decreases as the mission progresses and as the map cell size decreases, which indicates good mechanization and filter performance.

The functional diagram of the inertial navigation computations is shown in Figure 7.8. This diagram shows a standard computational sequence for a local-level wander azimuth system. The wander azimuth system gives the cruise missile worldwide navigation capability, and the local-level mechanization contributes to the simplicity of the filter design and interface with the terrain correlation system [8].

The vertical channel is mechanized by the navigation module. The vertical channel has been extensively studied and analyzed to maximize its performance for terrain-correlation usage, especially during terrain following. This altitude is used to damp a standard third-order loop whose gains are selected to minimize the errors in the vertical

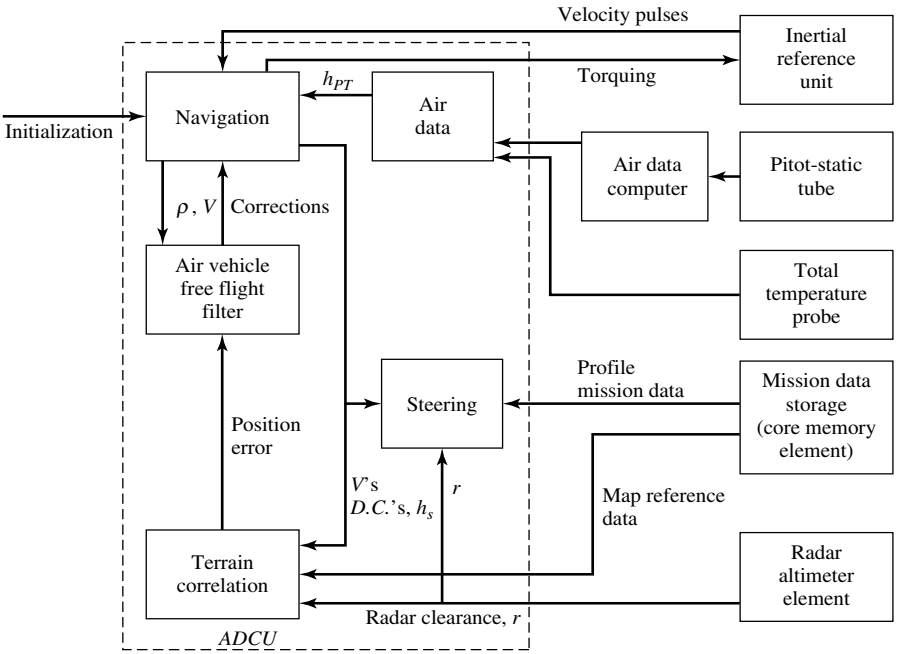

DC's = Direction cosines (i.e., C_{xx}, C_{xy}, C_{xz}, etc)
H_s = system altitude
$ADCU$ = Air data control unit

Fig. 7.7. Typical free flight navigation function.

channel during terrain following. The vertical channel thus accurately computes a reference altitude so that terrain correlation can be performed during any type of altitude changes over the maps. One additional feature of the system is the resetting of altitude h at each terrain correlation update. The system altitude h_s is reset so that no transients are introduced into the system. For more information on the vertical channel mechanization, the reader is referred to [8].

Early in the design of the cruise missile, it was decided that a Kalman filter would be the best design to improve the performance of the inertial navigation system. Therefore, the Kalman filter is provided for correcting navigation system error. The mechanization of the Kalman filter consists of four modules as follows: (1) initialization, (2) data processor, (3) propagation, and (4) update module. The Kalman filter calculations are designed for use in platform alignment and making navigation corrections based on externally supplied data (e.g., terrain correlation and/or *GPS*). These modules will now be discussed in a little more detail. The initialization module initializes the covariance matrix elements, propagation noise matrix elements, gyro error model parameters, and counters that control update and propagation periods. Execution of the Kalman calculations is controlled in part by the Kalman data processor module. The Kalman propagation module includes the covariance matrix propagation and dynamics matrix subroutines and solves the matrix Riccati differential

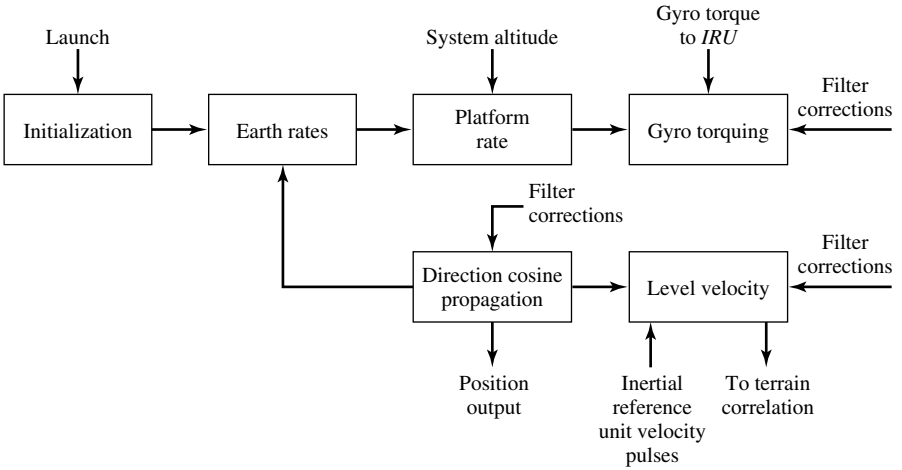

Fig. 7.8. Inertial navigation functional diagram.

equation. The Kalman update module calculates the state error vector and updates the covariance matrix.

Specifically, the benefits of the filter are to improve position and velocity of the navigation system and align and calibrate the navigation platform with each new terrain correlation update. As stated earlier in this section, the free flight is used for captive and free flight. Besides satisfying the captive align requirements, the free flight performance is improved, because the filter gets all the knowledge from captive alignment in its off-diagonal covariance matrix terms. Essentially, the *INS* Kalman filter consists of 15 dominant states. These are 2 position, 2 velocity, 2 tilt, 2 azimuth (computer and platform), 3 gyro drift, 2 gyro scale factor, and 2 accelerometer scale factor. Note that in the aided *GPS/INS* mode, additional states must be added to account for modeling the *GPS* error states. The guidance and control functions are mechanized primarily in the cruise missile's software. More specifically, the cruise missile's guidance and control system comprises sensing, computational, and actuating elements located in the *INS* and the flight control element (*FCE*). All of the computational functions except flight control gain application and filtering are performed in the air vehicle digital computer unit. These computational functions include waypoint steering, vertical screening system, terrain-following system, lateral steering, vertical steering (i.e., altitude hold and terrain following), time of arrival and Mach control, terminal maneuvers, warhead arming, and air data calculations.

The navigation system or module uses a covariance matrix to produce the position error estimates of the missile system. This covariance matrix represents the standard deviations of the errors in the navigation system at any selected point in time of the mission. Coupled with a transition matrix that propagates the covariance matrix forward along the route, the errors along the entire route can be computed. As discussed above, the covariance matrix contains the 15 dominant error states in

the navigation system. There are other types of errors that contribute to navigation accuracy, but these are the major ones. There is an additional matrix (process matrix) that is used to account for the unmodeled errors to a certain extent. By proper design of this "noise" matrix, the navigation system's covariance matrix is made to fit the true prediction of the navigation accuracy. This true prediction represents a prediction if all error sources were included. The covariance matrix is first initialized with values corresponding to the termination of coarse alignment and expected inertial instrument error parameter values. As a result, the covariance matrix is then propagated each 60 seconds during captive alignment using a state-transition matrix. The inputs to the state-transition matrix are the accelerations, velocities, and angular velocities from the planned missile route. This propagation of the covariance matrix is continued until launch, at which time the covariance matrix of the carrier aircraft navigation errors is combined with the missile's covariance matrix. The free flight propagation begins at this time and continues throughout the entire interval of missile flight. A Kalman filter process is done at each of the maps. The propagation interval of the covariance matrix in the map area is decreased to 12 seconds in order to increase the accuracy of the updating process. Note that the launch footprint calculation is made after passing over the first map set. A position error ellipse is then computed from the two level-position error covariance terms. From this position error ellipse, the navigation system output quantities may be derived. These are mainly *CEP* on target and probability of map overflight.

Summarizing the discussion of this section, we note that the navigation function includes vehicle position and velocity update and control of the platform orientation. Navigation is accomplished through the combined capabilities of the following submodules: (1) very fast navigation module, (2) fast navigation module, and (3) slow navigation module. A few words about these modules are in order. The "very fast" navigation module interfaces with the platform accelerometer interface (quantizer channels and accelerometer pulse counters) and is performed at a 32-Hz rate to preclude loss of accelerometer data. The "fast" navigation module performs the primary navigation functions of updating vehicle position and computing and controlling platform torquing rates (again, only if a gimbaled platform is used). The "slow" navigation module computes slowly varying navigation terms such as gravitational and Coriolis acceleration terms, platform wander angle, and geodetic latitude/longitude. Moreover, the slow navigation module also performs baro-inertial loop processing in order to (a) convert outside temperature, static, and pitot pressure measurements to barometric altitude, dynamic pressure, and Mach number, (b) stabilize the vertical navigation loop, and (c) estimate the baro-altitude bias. The navigation function execution rates are given below.

Task Execution Rate [Hz]

Executive Routine: 64
Very Fast Navigation: 32
Fast Navigation: 16
Slow Navigation: 2

Altitude Data Processor: 32
Kalman Data Processor: 16
Kalman Propagation: 1
Kalman Initialization: (Not regularly scheduled task; called by other program modules)
Kalman Update: (Called by other program modules)
Lateral Guidance: 8
Vertical Guidance: 16
Autopilot: 64

7.3.1 Navigation Coordinate System

The coordinate systems used for navigation computations are illustrated in Figure 7.9. The cruise missile's navigation coordinate system, designated (x, y, z), is obtained from an Earth-centered, Earth-fixed coordinate system (X, Y, Z) by successive rotations as follows [8]: (a) a positive rotation (λ-longitude) about the X-axis, (b) a positive rotation (ϕ-latitude) about the rotated Y-axis, (c) a rotation by 180° about the rotated X-axis, and (d) a positive rotation (α-wander angle) about the z-axis. The X-axis is defined by the polar axis of the Earth, the Z-axis is formed by the intersection of the plane containing the Greenwich Meridian and the equatorial plane of the Earth (positive Z intersects the Greenwich Meridian), and the Y-axis completes a right-handed coordinate system.

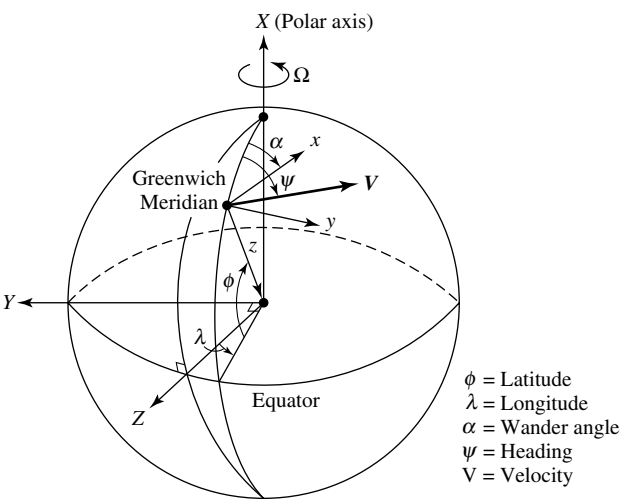

Fig. 7.9. Navigation coordinate system.

The transformation from the (X, Y, Z) system to the (x, y, z) system is obtained as follows:

$$\begin{bmatrix} x \\ y \\ z \end{bmatrix} = \begin{bmatrix} C_{xx} & C_{yx} & C_{zx} \\ C_{xy} & C_{yy} & C_{zy} \\ C_{xz} & C_{yz} & C_{zz} \end{bmatrix} \begin{bmatrix} X \\ Y \\ Z \end{bmatrix}$$

$$= \begin{bmatrix} \cos\alpha\cos\phi & \cos\alpha\sin\phi\sin\lambda - \sin\alpha\cos\lambda & -\cos\alpha\sin\phi\cos\lambda - \sin\alpha\sin\lambda \\ -\sin\alpha\cos\phi & -\sin\alpha\sin\phi\sin\lambda - \cos\alpha\cos\lambda & \sin\alpha\sin\phi\cos\lambda - \cos\alpha\sin\lambda \\ -\sin\phi & \cos\phi\sin\lambda & -\cos\phi\cos\lambda \end{bmatrix}$$

$$\begin{bmatrix} X \\ Y \\ Z \end{bmatrix} \tag{7.7}$$

Let now ψ be defined as the heading of the missile's velocity vector, measured relative to north. Also, a positive heading will correspond to a positive rotation about the z-axis. The direction cosines defining the trajectory are propagated every 60 seconds. Next, we note that the heading (ψ) and the time required to travel along a great circle path from route point (j) to the route point $(j+1)$ will be computed here for the free flight trajectory only. From the law of cosines for spherical triangles, the heading angle is obtained from the relation [8]

$$\cos\psi = \{\sin\phi_2 - \sin\phi_1\cos(\rho/a')\}/\cos\phi_1[\sin(\rho/a')], \tag{7.8}$$

where

$$\begin{aligned} a' &= \text{average radius of the Earth,} \\ \phi_1 &= \text{latitude of the initial (or present) position,} \\ \phi_2 &= \text{latitude of the target position,} \\ \rho &= \text{great circle distance (i.e., from one waypoint to the next).} \end{aligned}$$

The direction cosines at the launch position are initialized as follows:

$$\begin{aligned} C_{xx} &= \cos\phi_L, & C_{yx} &= \sin\phi_L\sin\lambda_L, \\ C_{xy} &= 0, & C_{yy} &= -\cos\lambda_L, \\ C_{xz} &= -\sin\phi_L, & C_{yz} &= \cos\phi_L\sin\lambda_L, \end{aligned}$$

where ϕ_L, λ_L are the missile launch latitude and longitude, respectively. This definition of direction cosines forces the wander angle to zero at launch. The time to reach the target can be calculated from the relation [8]

$$\delta t_T = (a'/V_j)\cos^{-1}[\sin\phi_j\sin\phi_T + \cos\phi_j\cos\phi_T\cos(\lambda_T - \lambda_j)], \tag{7.9}$$

where

$$\begin{aligned} \phi_j &= \text{latitude of the } j\text{th route point,} \\ \phi_T &= \text{latitude of the target,} \\ \lambda_j &= \text{longitude of the } j\text{th route point,} \\ \lambda_T &= \text{longitude of the target,} \\ V_j &= \text{air vehicle ground speed at the } j\text{th route point.} \end{aligned}$$

The time at which route point $(j+1)$ will be reached is given by

$$t_{j+1} = t + \delta t_j. \tag{7.10}$$

Finally, the ground velocity components of V_j for the free flight route point indices, $j = 0, 1, 2, 3, \ldots$, are given by

$$V_{xj} = (\cos\psi_j \cos\alpha + \sin\psi_j \sin\alpha) V_j, \tag{7.11a}$$

$$V_{yj} = (-\cos\psi_j \sin\alpha + \sin\psi_j \cos\alpha) V_j. \tag{7.11b}$$

For the Kaman filter discussed in Section 7.2.2, the 15 error state equations for the free flight are as follows:

$$\frac{d\delta x}{dt} = \delta v_x - V_y \phi_z, \tag{7.12a}$$

$$\frac{d\delta y}{dt} = \delta v_y + V_x \phi_z, \tag{7.12b}$$

$$\begin{aligned}\frac{d\delta v_x}{dt} = {} & g\theta_y + A_y\theta_z + A_x \delta K_x + 2\Omega_z \delta v_y - 2V_y(\Omega_y/R_e)\delta y \\ & -2V_y(\Omega_x/R_e)\delta x,\end{aligned} \tag{7.12c}$$

$$\begin{aligned}\frac{d\delta v_y}{dt} = {} & -g\theta_x - A_x\theta_z + A_y \delta K_y - 2\Omega_z \delta v_x + 2V_x(\Omega_y/R_e)\delta y \\ & +2V_x(\Omega_x/R_e)\delta y,\end{aligned} \tag{7.12d}$$

$$\frac{d\theta_x}{dt} = \varepsilon_x + \delta v_y/R_e + \Omega_z\theta_y - \omega_y\theta_z + (\Omega_z/R_e)\delta x + \Omega_y\phi_z + \omega_x \delta S_x, \tag{7.12e}$$

$$\frac{d\theta_y}{dt} = \varepsilon_y - \delta v_x/R_e - \Omega_z\theta_x + \omega_x\theta_z + (\Omega_z/R_e)\delta y - \Omega_x\phi_z + \omega_y \delta S_y, \tag{7.12f}$$

$$\frac{d\theta_z}{dt} = \varepsilon_z + \omega_y\theta_x - \omega_x\theta_y - (\Omega_y/R_e)\delta y - (\Omega_x/R_e)\delta x, \tag{7.12g}$$

$$\frac{d\phi_z}{dt} = -(V_x/R_e^2)\delta y + (V_y/R_e^2)\delta x, \tag{7.12h}$$

$$\frac{d\varepsilon_x}{dt} = 0, \tag{7.12i}$$

$$\frac{d\varepsilon_y}{dt} = 0, \tag{7.12j}$$

$$\frac{d\varepsilon_z}{dt} = 0, \tag{7.12k}$$

$$\frac{d\delta S_x}{dt} = 0, \tag{7.12l}$$

$$\frac{d\delta S_y}{dt} = 0, \tag{7.12m}$$

$$\frac{d\delta K_x}{dt} = 0, \tag{7.12n}$$

$$\frac{d\delta K_y}{dt} = 0, \tag{7.12o}$$

where

$\delta x, \delta y =$ x, y position errors,
$\delta v_x, \delta v_y =$ x, y velocity errors,
$\theta_x, \theta_y, \theta_z =$ x, y, z platform-to-true angular misalignments,
$\phi_z =$ computer-to-true azimuth misalignment,
$\varepsilon_x, \varepsilon_y, \varepsilon_z =$ x, y, z gyro bias drift rate errors,
$\delta S_x, \delta S_y =$ x, y gyrotorquer scale factor errors,
$\delta K_x, \delta K_y =$ x, y accelerometer scale factor errors,
$V_x, V_y =$ x, y Earth-relative velocity,
$A_x, A_y =$ x, y acceleration (assumed to be of the form
$A_i = \Delta V_i \delta(t_j - t_k)$ for $i = x, y$
and $\delta(t - t_k) =$ Dirac delta function, $\Delta V_i = V_{ik} - V_{i(k-i)}$),
$R_e =$ "average" radius of the Earth,
$\omega_x, \omega_y =$ x, y components of total angular velocity,
$\Omega_x, \Omega_y, \Omega_z =$ x, y, z components of Earth angular velocity.

Equations (7.12a)–(7.12o) are defined for a wander azimuth, local-level, z-down coordinate system.

7.4 Terrain Contour Matching *(TERCOM)*

7.4.1 Introduction

Terrain contour matching (*TERCOM*) can be defined as a technique for determination of the position location of an airborne vehicle with respect to the terrain over which the

vehicle is flying. More specifically, *TERCOM* is a form of correlation guidance based on a comparison between the measured and the prestored features of the profile of the ground (i.e., terrain) over which a missile or aircraft is flying. Generally, terrain height forms the basis of this comparison. Reference terrain elevation source data descriptive of the relative elevations of the terrain in the fix point areas are stored in the air vehicle's onboard computer. Obtaining the reference data requires prior measurement of the ground contours of interest. These data are in the form of a horizontally arranged matrix of digital elevation numbers. A given set of these numbers describes a terrain profile. The length of contour profile necessary for a unique fit is a function of terrain roughness, but is in the range of 6 to 10 km and can be a curved path. The *TERCOM* profile acquisition system consists of a radar terrain sensor (*RTS*) or a radar altimeter and a reference altitude sensor (*RAS*) or barometric altimeter.

As the vehicle flies over the matrix area, data describing the actual terrain profile beneath the vehicle are acquired. That is, the actual profile is acquired using a combination of radar and barometric altimeter outputs sampled at specific intervals, and when compared against the stored matrix profiles provides the position location. This type of guidance is used for updating a midcourse guidance system on a periodic basis, and has been applied to the guidance of cruise missiles, which usually fly at subsonic speeds and fairly constant altitude. With regard to midcourse guidance, it is well known that the simplest midcourse guidance is the explicit guidance method (see also Section 6.5.5). The guidance algorithm has the capability to guide the missile to a desired point in the air while controlling the approach angle and minimizing an appropriate cost function. Furthermore, the guidance gains of the explicit guidance law are usually selected to shape the trajectory for the desired conditions.

The *TERCOM* technique, first patented in 1958, relies for its operating principle on the simple fact that the altitude of the ground above sea level varies as a function of location. For example, if one were to make a rectangular map of an area 2 km $\times$ 10 km long, divide the map into squares, say, 100 meters on a side, and record in each square the average elevation of the ground in it, one would then obtain a digital map consisting of 2,000 numbers, each number corresponding to the elevation of a point of known coordinates on the ground. A set of such maps, which can be made much larger and can have squares with smaller sides if required, is stored in the memory of the missile's onboard computer. The missile is provided with a downlooking radar altimeter capable of resolving objects on the ground smaller than the map squares from a height of several kilometers. Consequently, as the missile approaches the region for which the computer memory has a map, the altimeter starts providing a stream of ground-elevation data. Furthermore, the computer, by comparing these data with the elevation data it has in its memory, can determine the actual location of the missile with an accuracy comparable to the size of the map cell. It then instructs the autopilot to take any corrective steps necessary to return the missile to its intended trajectory. More than 20 such maps can be stored in the missile's onboard computer, enabling the missile to update its location information and correct its trajectory frequently during its overland flight.

Historically, *TERCOM* has evolved from several *R&D* programs that developed certain areas of the overall process. These programs perfected the technology as

it is known today. Some of the companies that did *R&D* work on *TERCOM* are LTV-Electrosystems, the Boeing Aerospace Company, USAF Aeronautical Systems Division at Wright-Patterson AFB, Sandia Laboratories, E-Systems, and the McDonnell-Douglas Astronautics. The following list is a chronological overview of this development:

Program	Year	Objectives
Fingerprint	1958	Guidance package for *SLAM* missile *TERCOM* concept first proposed.
TERCOM	1960–1961	Feasibility study of terrain contour matching.
LACOM (Low Altitude Contour Matching)	1963–1965	Design and development of a complete fix-taking subsystem.
RACOM (Rapid Contour Matching)	1963–1966	Improve *TERCOM* computation procedures and increase accuracy.
*SAMSO** Programs (a) *TPLS* (Terminal Position Location System (b) *TERSE* (Terminal Sensing Experiment) (c) *TERF* (Terminal Fix). (d) *TSOFT* (Terminal Sensor Overland Flight Test).	1963–1971	Application of terrain correlation techniques for ballistic missiles.
Avionics Update	1972–1975	Study and define a *TERCOM*/ drone system capable of operational deployment.
TAINS (Terrain Aided *INS*) *TERCOM*	1972–1974	Feasibility study for incorporation in cruise missile and evaluation of snow coverage effects on terrain profile acquisition.
Competitive Flyoff	1975	McDonnell-Douglas Astrodynamics awarded a contract for *TERCOM* system.
RACOM (Recursive All Weather Contour Matching)	1975	Improve terrain correlation update accuracy.

**SAMSO* is an acronym for the USAF's Space and Missiles Systems Organization.

TERCOM is the only fix-taking system that can operate autonomously in a wartime environment, that has a permanent source database. In particular, the following characteristics should be noted:

- The system is self-contained and provides precision guidance/navigation for:
  (a) aircraft
  (b) drones (or *UAV*s unmanned aerial vehicles)
  (c) cruise missiles
  (d) reentry vehicles.
- *TERCOM* is applicable to both tactical and strategic systems and operates:
  (a) under *ECM* (electronic countermeasures) conditions
  (b) day/night
  (c) all weather
  (d) low altitude (terrain following)
  (e) high altitude.

TERCOM is somewhat of a misnomer, since the process does not accurately match terrain contours to determine a fit, and thus the missile's location. Rather, the "match" occurs by determining the minimum value of a summation of terrain altitude differences. The altitude for each cell of a reference strip is subtracted from cell altitudes derived from a combination of the missile's radar altimeter and air data system to obtain these differences. The map strip identified by the minimum summation locates the crosstrack position of the missile. The downtrack position of the missile is determined from the time that the minimum value occurred. Significant in this process is the fact that the reference map data are stored as a 4-bit words, limiting the number of possible altitudes to 16 quantized levels. Radar altimeter data are stored as 4-bit words. It should be noted that *TERCOM* fix accuracy degrades with increasing altitude. Above a radar altitude of 4 to 5 times the cell size, the accuracy degrades to the point that terrain correlation is not feasible.

Another terrain-aided navigation system developed in recent years is the *TERPROM* (terrain profile matching). *TERPROM* is a computer-based high-accuracy terrain profile matching navigation system using data from a radar altimeter and a digital map to determine the precise position of the air vehicle. Specifically, *TERPROM* stores terrain height for a 200,000-square-mile area and determines air vehicle position by radar altimeter measurement of the topography below. *TERPROM* has been successfully flown under simulated combat conditions in *F-16* and Panavia *Tornado* aircraft.

The heart of the system is a processor with an electronic memory that stores a terrain map in digital form. This map, together with the weapon's navigation system, is used to predict height above the ground. The processor then compares the prediction with the true height as measured by the radar altimeter. The difference is used to correct readouts from the navigation system. The following modes are commonly used:

(1) Acquisition or Single-Fix: Used to locate weapon position on the database during the early part of its flight or when reaching land after extended periods over water.

(2) Track or Continuous Fix: Fixes are taken three times per second to offer precise navigation and the confidence essential for safe, automatic, low-level terrain following.
(3) Memory: A calibrated inertial mode to improve basic navigation system performance when operating for extended periods over water or with the radar altimeter switched off for stealth reasons.

TERCOM as well as *DSMAC* (digital scene matching area correlation) have been developed for use on land-attack cruise missiles. *TERCOM* is used for midcourse and terminal guidance on conventional or nuclear-armed missiles, *DSMAC* for terminal guidance (after *TERCOM* midcourse updating) on conventionally armed cruise missiles, and *RADAG* (Radar area guidance) for *Pershing-II*–type terminal guidance. These systems, as we saw earlier, are termed map-matching, and compare a live sensor image with, a stored reference scene in the missile's computer to determine the along- and crosstrack vehicle position errors at the update location. Given the need for high-accuracy strategic missiles, it is reasonable to ask what potential operational payoffs may exist for improving these systems (and developing others). The following sections will attempt to answer this question.

7.4.2 Definitions

At this point, it is appropriate to define some of the terms that the reader will encounter in the discussion of *TERCOM*.

Cell – One terrain elevation value in a matrix of terrain elevation values.
Cell Size – The geographic distance between *TERCOM* matrix cells.
Correlation Length – The distance one has to go from a given terrain elevation profile to another parallel terrain elevation profile such that the value of the normalized autocorrelation function for the given profile is reduced to a value of $1/e$.
False Fix – A false fix has occurred when the distance between the *TERCOM* fix was position and the actual vehicle's position at the time that the *TERCOM* fix was taken exceeds the terrain correlation length.
Ground Track Signature – The shape or signature of the groundtrack profile is obtained by subtracting the *RTS* (radar terrain sensor or radar altimeter) measurement from the *RAS* (radar altimeter sensor) measurement. The subtraction removes the effects of any vertical motion of the airborne vehicle. The mean of the data is removed in the data processing, thus eliminating any requirement for absolute accuracy in the *RTS* or *RAS*.
MAD – Mean absolute difference. This is the difference between stored and acquired data, and it is expressed in terms of the difference between the measured terrain elevation and stored reference matrix.
MAD Residue – A measure of the degree of correlation between two one-dimensional sets of data. A *MAD* residue of zero represents perfect correlation (i.e., identical data). The value of the minimum *MAD* residue for a matrix represents the amount of noise present in the system.

Map Description Data – These data include the parameters that define the location, orientation, size, and other characteristics of the terrain correlation maps.

Matrix – A matrix is composed of $m \times n$ cells in which each cell is $d \times d$ feet in size. A typical cell size is 400 feet (i.e., 400 × 400 feet). Cell sizes usually increase as the area defined by the matrix increases due to storage limitations onboard the air vehicle. Cell sizes have been successful from 100 ft to 3200 ft. The number of cells in the column of the map is called the *match length*. Successful operation involves the granularity, or intrinsic resolution, with which the system attempts to measure and compare the vertical profiles. This parameter is called the matrix *cell size*. The matrix columns must be aligned to the same heading as the planned groundtrack of the vehicle for proper operation. Otherwise, large position update errors will result. Maps are normally digitized with a north–south orientation and then rotated to the desired heading. When the missile flies over a reference map area, it measures the average elevation of the terrain directly below, averaging over intervals equal to the cell size of the map.

Mean Column Elevation Data – These are the mean elevation data for each column in each terrain correlation map. They are used to update the vertical channel after each terrain correlation position fix.

Radar Terrain Sensor (*RTS*) – A radar terrain sensor is a radar altimeter system, usually pulsed, that measures air vehicle (i.e., aircraft or missile) clearance above the terrain. Military inventory radar altimeters normally meet the *TERCOM* requirement, especially for low-altitude applications. For high-altitude operations, above 20,000 ft, radar characteristics begin to take on more importance in the *TERCOM* error model, and a more careful selection must be made for the radar altimeter.

Reference Altitude Sensor (*RAS*) – The reference altitude sensor is a barometric altimeter, a vertical accelerometer, a combination of both, or the vertical channel of an inertial navigation system.

Reference Matrix – A matrix of digitized terrain elevation values that has a one-to-one correspondence to a geographical area over which a *TERCOM* fix is to be made.

Reference Terrain Data – These are the map elevation data for each terrain correlation map.

Sampling Interval – The distance between terrain elevation values that are normally measured using a radar altimeter.

Sensed Altitude – The height of the air vehicle above the terrain.

Sigma-T (σ_T) – The standard deviation of the terrain elevation values in a matrix.

Sigma-Z (σ_Z) – The standard deviation of the cell-to-cell changes in elevation in a matrix.

Source Material – Topographic charts or aerial photographs that contain terrain elevation information that can be digitized to construct the *TERCOM* matrices.

TERCOM Fix – The procedure involved in determining actual vehicle location based upon the *TERCOM* concept.

Terrain Elevation – The height of the terrain above sea level or the difference between the vehicle's height above the terrain.

Waypoint Data – These data consist of blocks of about 30 words per waypoint that define the flight profile of the air vehicle.

7.4.3 The Terrain-Contour Matching (TERCOM) Concept

As stated in the introduction of Section 7.4.1, the *TERCOM* system uses an airborne altimeter and a data processor to correlate the measured terrain contours to obtain the best estimate of position. The transmission characteristics of the airborne altimeter include an operating frequency of approximately 4.4 GHz (incidental to operation) and a transmission type that is pulsed or *CW*. As the missile flies, the radar altimeter first measures the variations in the ground's profile. These measured variations are then digitized and processed for input to a correlator for comparison with the stored data. The *TERCOM* system relies on a set of digital maps stored in the memory of the missile's onboard computer. These maps consist of rectangular arrays of numbered squares representing the variation of ground elevation above sea level as a function of location. Consequently, as the missile approaches an area for which the computer memory has a map, the onboard radar altimeter starts providing a stream of ground-elevation data. Furthermore, the computer, by comparing these data with the information it has in its memory, can accurately determine the actual trajectory of the missile and instruct the autopilot to return the missile to its planned trajectory. Four such corrective maneuvers are shown in the vertical overhead view in Figure 7.10.

From Figure 7.10, we note that there are four types of *TERCOM* maps that can be used by a cruise missile. Assuming that a cruise missile is deployed over water, these maps are as follows (1-largest, 4-smallest):

(1) landfall,
(2) en route,
(3) midcourse, and
(4) terminal.

The map types differ in length, width, and cell size. The map width determines how far that map can be spaced from either the launch site or a previous *TERCOM* map and still yield an acceptably high probability of overflight. The cell size determines, in part, the accuracy of the *TERCOM* fix. The *TERCOM* maps become smaller and are spaced closer together as the missile approaches the target. As a result, because of the decreasing cell size, the updates become more accurate. A terminal accuracy on the order of 100 meters is considered feasible for the *TERCOM* system.

The terminal guidance stage may be based on the final *TERCOM* update and a preprogrammed course relying on the inertial navigation system (*INS*), or a separate terminal homing seeker may be employed that can recognize the target and provide the final guidance commands.

The process of determining air vehicle position by the use of terrain contour matching can generally be described as consisting of three basic steps: (1) data preparation, (2) data acquisition, and (3) data correlation. Figure 7.11 illustrates this concept.

The three basic steps enumerated above will now be discussed in some more detail.

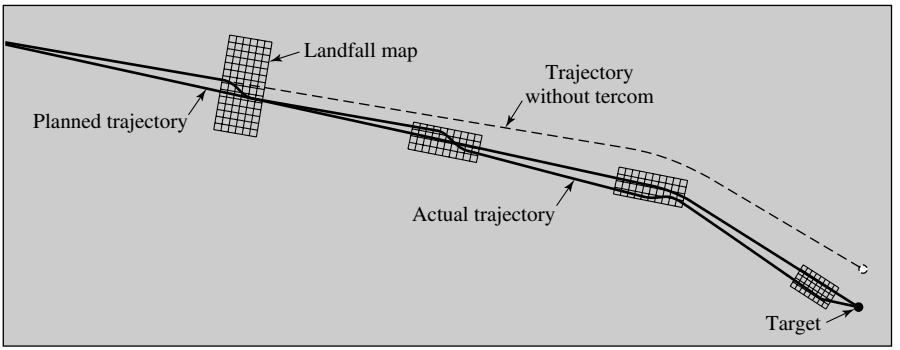

Fig. 7.10. *TERCOM* maps in use.

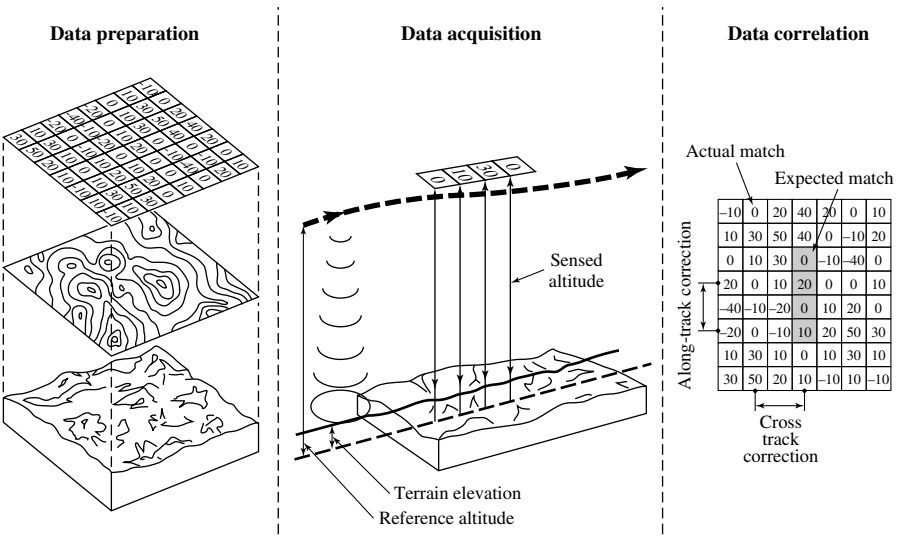

Fig. 7.11. *TERCOM* concept.

Data Preparation: Data preparation consists in selecting a fix point area large enough to accommodate the crosstrack and downtrack navigation arrival uncertainties, securing source material that contains contour information, and then digitizing the terrain elevation data into a matrix of "cells" oriented along the intended flight path. The source material is usually obtained from either topographic charts or from stereo aerial photographs of the terrain. The resulting reference matrix consists of an array of numbers that represent discrete terrain heights (e.g., above mean sea level) corresponding to a sampling interval (i.e., resolution) equal to the desired cell size. This reference matrix or map is then stored in the vehicle's onboard digital computer memory prior to the flight. One of the most important aspects of *TERCOM* data preparation is selecting the area that is to be digitized and used as

a reference matrix. The Defense Mapping Agency Aerospace Center (*DMAAC*), St. Louis AFS, Missouri, maintains a file on the type and availability of source data for all areas of the world.

Data Acquisition: As the vehicle flies over the fix point area, data are acquired by sampling the altitude of the vehicle above the terrain directly below it at an interval equal to the reference map cell size. This "sensed altitude" is measured with a radar altimeter. At the same time, the vehicle's altitude above mean sea level is measured using the combination of a barometric altimeter and a vertical accelerometer to provide the system reference altitude. The acquired terrain elevation samples are then stored in a file in the vehicle's onboard digital computer memory. This terrain elevation file represents a discrete elevation profile of the terrain along a line coincident with the vehicle's ground track. The total number of elevation samples stored in the terrain elevation file is a function of the downtrack dimension of the reference map. A typical size for the file is 64 samples, which would represent a 4.2 nm (7.78 km) strip of terrain if sampled at 400-ft (122-m) intervals.

Data Correlation: The last step in the terrain contour matching process is the correlation of the data in the terrain elevation file with each column of the reference matrix. The reference column that has the greatest correlation with the terrain elevation file is the column down which the vehicle has flown. With no navigation error, the match column would be the center column of the map, since that is the ground track the navigation system is steering along. However, with downtrack and crosstrack errors, it is probable that some column other than the center one will be flown down. In this case, the system computes the downtrack and crosstrack distance from the center of the map and uses these errors to correct the vehicle's navigation error.

In block diagram form, a generalized *TERCOM* system operation is illustrated in Figure 7.12.

The left side of the diagram describes the reference data loop. Source material in the form of survey maps or stereo-photographs of the terrain are used to collect the set of altitudes that constitute the reference matrix. The right side of the diagram describes the data acquisition loop. The radar altimeter acquires altitude estimates above terrain. As described above, the radar altimeter output is differenced with the system's reference altitude. Various arithmetic operations (e.g., mean removal and quantization) are then performed on the differenced data. Finally, the correlation between the stored and acquired data is performed with the MAD function, and a position fix is determined.

Figure 7.12 can be modified to reflect the *TERCOM* measurement process. This is done in Figure 7.13.

As the missile flies over the fix point area, data is acquired by sampling the output from the radar altimeter that is measuring the height of the vehicle above the terrain (see Figure 7.14). The radar altitude is sampled at uniform distances along the air vehicle's ground track with at least one altitude measurement being taken for each cell distance d traveled. However, several measurements are usually taken during the crossing of each matrix area cell, and the average of the measurements is stored as the measured radar (terrain clearance) altitude for that cell.

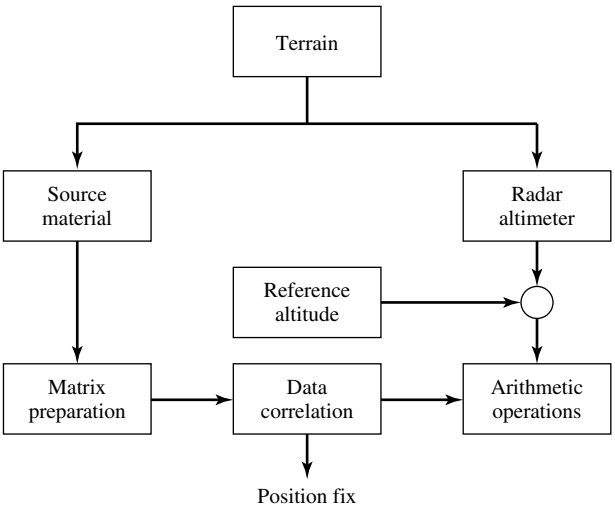

Fig. 7.12. Generalized *TERCOM* system.

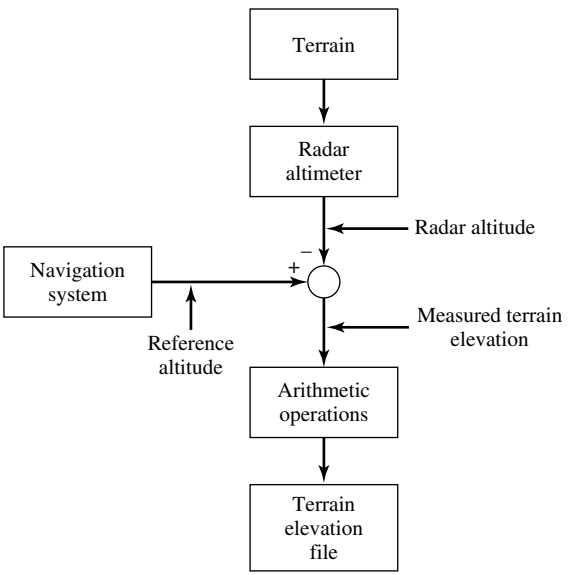

Fig. 7.13. Terrain measurement block diagram.

Note that a terrain-following (*TF*) algorithm must be designed in order to optimize the use of the vehicle acceleration in following a flight path that matches the terrain contours. The system bases its altitude reference information on a down-looking radar altimeter. This information is processed by a digital filter in the computer to reduce the effect of noise and to derive clearance altitude rate. The navigation

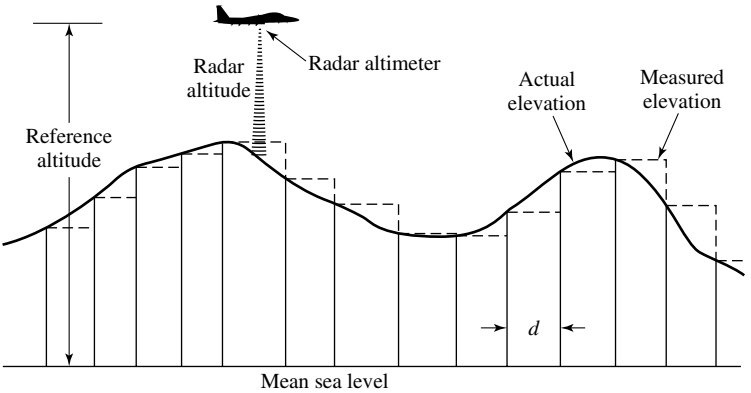

Fig. 7.14. Terrain elevation measurement.

system provides the reference altitude for the system, which is a combination of inertial (i.e., vertical accelerometer) and barometric altitudes. This reference altitude is measured with respect to the mean sea level (*MSL*), and is also averaged over the cell distance. The measured terrain elevation is computed by subtracting the measured radar altitude from the reference altitude. If necessary, the measured terrain elevation value is then scaled and manipulated to get it into the same format as the reference matrix data. The resulting value is stored in the terrain elevation file for later correlation with the reference matrix. This process is repeated for each cell along the vehicle's ground track while flying over the reference matrix area.

As discussed earlier, the *TERCOM* system yields a fix by comparison of a set of acquired data, in the form of a sequence of terrain elevation measurements, with a set of stored data in the form of a matrix of reference terrain elevations. Thus, consider Figure 7.15. The circles represent points at which the terrain altitude referred to the local mean value is determined from the contour maps or stereo-photographs.

The interstitial distance or cell size is denoted by d, and $L = Nd$ is the length of the profile used for correlation. In a typical application, $d = 800$ ft and $N = 32$, so that $L = 25{,}600$ ft. As the air vehicle approaches the fix area, *TERCOM* begins to acquire two altitude measurements during every interval d. One of the two is altitude above *MSL*, whereas the other is the altitude above the terrain. Acquisition of these measurements is continued until the vehicle is well past the fix area. Each pair is differenced, with the result that the sequence of differences yields an estimate of terrain profile along the vehicle track. There are two general approaches to *TERCOM* fix taking. One is referred to as long sample–short matrix (*LSSM*), and the other is referred to as short sample–long matrix (*SSLM*). These two concepts are illustrated in Figure 7.16.

In both cases, the matrix is made wide enough to accommodate the crosstrack arrival uncertainty. For *LSSM*, the acquired sample is long enough to accommodate the downtrack uncertainty, whereas for *SSLM* the stored matrix is long enough to

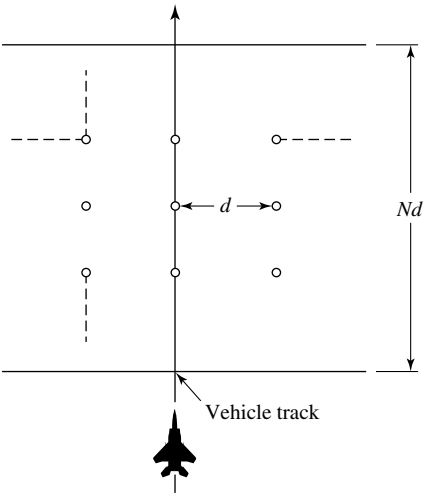

Fig. 7.15. Definition of fix area and cell size.

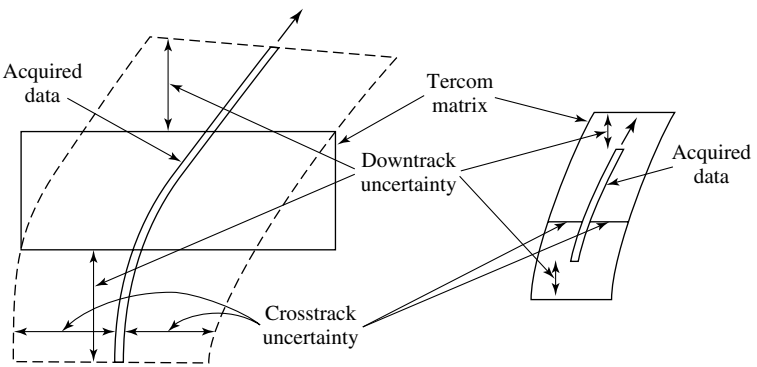

Fig. 7.16. *TERCOM* fix concepts.

accommodate the downtrack uncertainty. The *LSSM* is used whenever the vehicle arrival uncertainty is relatively large or if only small fix areas are available. The *SSLM* is also employed during a multiple fix-taking mode. In this latter mode, faster updating is achieved, provided the search area (i.e., navigation uncertainty) is kept small, and data for a longer matrix are available. The length L of the data interval is the same for either mode. For *SSLM*, only one sample set of length L is used. For *LSSM*, the first sample set is correlated, and the result (minimum residue and location) is saved. The first point that was gathered is then dropped, and another

point is collected, and the correlation process is repeated until the correlation is complete. Some of the *TERCOM* characteristics can be summarized as follows:

Precision Position Fixes: Precision terrain referenced coordinates. Absolute errors in latitude and longitude do not degrade *TERCOM* accuracies. Accuracy does not degrade with total time or distance traveled.

Repeatable Precision: *TERCOM* accuracy remains the same independent of weather, *ECM* conditions, time of day, etc., because the Earth does not change. *TERCOM* accuracy is repeatable from one *TERCOM* system to another.

Operates Under ECM Conditions: The only element subject to *ECM* is the radar altimeter. The radar altimeter has a directional antenna pointed straight down and, with the exception of some missiles, will be traveling in a random path over the Earth. This condition makes it impractical to implement effective *ECM* against *TERCOM*. If one position fix should be interrupted by passing over an *ECM* system, the *ECM* will not affect subsequent fixes.

7.4.4 Data Correlation Techniques

In Section 7.4.3 the data correlation process was briefly discussed as part of determining vehicle position. In this section we will discuss the terrain correlation technique in more detail. The *TERCOM* process involves matching the measured contour of the terrain along the ground track of the air vehicle with each downtrack column of the reference matrix that is stored in the vehicle's onboard digital computer memory prior to flight. Since the *TERCOM* system is not noiseless, the terrain profile measured during flight will probably never exactly match one of the reference matrix profiles.

A fundamental assumption of the terrain correlation process is that the geographic distance between the measured terrain elevation profile and the best-matching reference matrix column provide an excellent measure of the downtrack and crosstrack position errors of the vehicle as it flies over the reference matrix area.

There are a number of correlation algorithms (e.g., mean squared difference (*MSD*), mean absolute difference (*MAD*), the normalized *MAD*, the normalized *MSD*, and the product method) of varying complexity and accuracy that can be used to correlate the measured data with the reference data. Furthermore, the *MAD* algorithm provides the best combination of accuracy and computational efficiency for performing real-time terrain contour matching in an onboard computer environment. Therefore, here we will discuss only the *MAD* and *MSD* correlation algorithms.

Suppose now that the first N differences have been acquired. Then, these differences are removed, so that the sample profile is its mean value. Next, this profile is compared with each row of matrix data in the following manner. Let $h_n (1 \leq n \leq N)$ denote any row of matrix data and H_n the sequence of required data. Consequently, the *MAD* algorithm, which is used for correlating the measured terrain elevation file with each downtrack column of the reference matrix, is defined as follows [6]:

$$MAD_{k,m} = (1/N) \sum_{i=1}^{N} |h_{k,m} - H_{m,n}|, \tag{7.13}$$

where

$MAD_{k,m}$ = the value of the mean absolute difference between the kth terrain elevation file and the mth reference matrix column,
N = the number of samples in the measured terrain elevation file and usually it is also equal to the number of rows in the reference matrix,
M = the number of reference matrix columns,
K = the number of measured terrain elevation files used in the correlation process (for the *SSLM* technique $K = 1$),
$|\ \ |$ = the absolute value of the argument,
n, m, k = row, column, and terrain elevation file indices,
$H_{m,n}$ = the stored reference matrix data: $1 \le m \le M$, $1 \le n \le N$,
$h_{k,m}$ = the kth measured terrain elevation file: $1 \le k \le K$.

The *MSD* algorithm can be expressed in terms of the profile in question. Mathematically, the expression for *MSD* is

$$MSD_{jk} = (1/N) \sum_{i=1}^{N} (S_{ij} - S_{ik})^2, \tag{7.14}$$

where

S_j, S_k = jth and kth profiles,
N = length of each profile.

Note that for uniformity, we can also express the *MAD* algorithm as in the expression for the *MSD*. Thus,

$$MAD_{jk} = (1/N) \sum_{i=1}^{N} |S_{ij} - S_{ik}|. \tag{7.15}$$

Examination of the expressions for the *MAD* and *MSD* processors indicates that both of these correlators can be viewed as distance measures, where the dimensions of the space for which these distances are defined correspond to the number of elements in the profiles. From (7.14) and (7.15), we note that the ambiguity between any two profiles is defined as the probability (P) that sensed data corresponding to one of the profiles will be closer (in terms of the distance measure) to the other profile than to the one from which it was taken. Mathematically, the ambiguity ξ can be expressed as

$$\xi_{jk} = \begin{cases} P[C_{jk} < C_{jj}], & \text{where a minimum of } C_{jk} \text{ is sought,} \\ P[C_{jk} > C_{jj}], & \text{where a maximum of } C_{jk} \text{ is sought.} \end{cases}$$

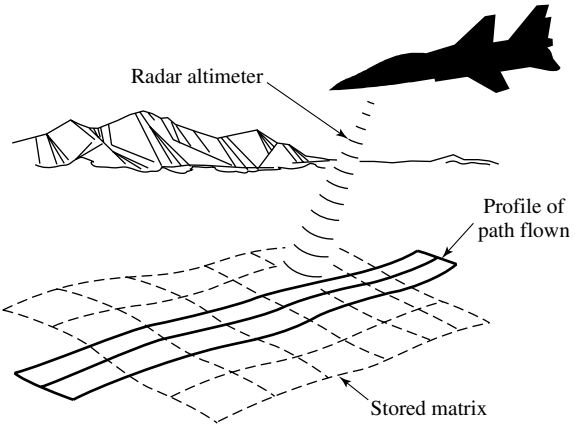

Fig. 7.17. Terrain correlation concept. Originally published in the *Proceedings of the IEEE NAECON*, 1978, article by M. D. Mobley, "Air launched Cruise Missile (ALCM) Navigation System Development Integration Test," pages 1248–1254. Reprinted with permission.

For a *MAD* processor, C_{jk} is given by the following expression:

$$C_{jk} = (1/N) \sum_{i=1}^{N} |S_{ij} - R_{ik}|,$$

where

$$S_j = j\text{th measured profile},$$
$$R_k = k\text{th reference profile}.$$

Evaluation of the ambiguity expression may be implemented on a computer. Also, computation of the ambiguity between two profiles requires a model of the measured error distribution.

The terrain correlation (*TC*) system is required to update the position of the cruise missile inertial navigation system (see also Section 7.4.7). Crosstrack errors in the inertial navigation system (*INS*) can cause the missile to cross the map at a slightly skewed angle (or to sample data too slow or fast for downtrack velocity errors). This phenomenon increases the noise in the system and therefore reduces its accuracy and correlation probability. The vertical accuracy of the *TC* update is primarily a function of the bias accuracy of the radar altimeter. For altitude update, the mean of the sensed altitude data is differenced with that of the stored column at the elevation point. Any difference in the column "means" is ascribed as an absolute error in the vertical channel. The *TC* system combines airborne and ground software, and airborne and ground hardware. It extends from the original gathering of terrain elevation data, say by the *DMA* (Defense Mapping Agency), to the in-flight updating of the *INS* by the correlator. Correlation of terrain overflown with stored map data provides navigational updates that support system accuracy. The terrain correlation concept is illustrated in Figure 7.17.

The correlating data for this system is a single string of terrain height data. This string is obtained, as discussed earlier, with measurements from the radar altimeter, which provides height of the missile above the ground level and measurements from the baro-temperature-inertial system that provides a reference height of the missile above mean sea level. The radar altimeter when used at cruising altitudes of less than 5,000 ft (1524 m) provides both the missile's height above ground and the information needed to navigate in hilly terrain. The use of the temperature probe along with the barometric and inertial vertical sensors (i.e., accelerometers) significantly increases the accuracy of the reference height measurements. These two measurements, radar altimeter and mean sea level altitude, are subtracted to obtain variation of the terrain elevation under the missile flight path. This long sample of sensed data is compared, a column at a time, with a reference column in the air vehicle's onboard computer. The computer memory contains all columns of reference terrain elevations that the missile should be flying down at that point in the mission. The matrix of reference elevations is commonly called a terrain correlation map. By computing the best possible match of the measured to stored elevation data, the navigation system estimates its position when over the map center and then updates itself. The stored maps are selected to be wide enough so that there is a very high probability of crossing the maps and also long enough so that there is a very high probability of obtaining a successful fix. Evidently, the resultant map area impacts the amount of data required to be stored in the missile. Within certain limits, the accuracy of the fix is primarily a function of the cell size of the map. That is, the smaller the cell size, the more accurate the fix. However, the smaller cell size requires more onboard storage, more processing time, and in addition, the map is more expensive to produce. This is the basic tradeoff that the systems analyst must make in selecting cell size for maps all along the mission.

A more detailed account of the terrain correlation processing for a single map is conceptually shown in Figure 7.18.

The terrain correlation process discussed here utilizes a long sample–short matrix concept (see also Section 7.4.3) and uses the mean absolute difference (*MAD*) algorithm. The terrain correlation system has several design features that give improved performance and provide mission planning flexibility. These are:

(a) There is no processing limit on map size or cell size.
(b) There is a dual-stage option for those maps with a large number of cells that might have a time limitation imposed by mission planning. The dual stage first correlates every other correlation point, thus saving a factor of 4 in processing time. The second step correlates all the nearest 24 positions to the minimum found from the first step.
(c) An altitude update is computed in addition to the horizontal position update.
(d) A residue interpolation is done on the correlation function. This improves the correlator accuracy, since the update is no longer limited to the accuracy of a cell. The residue interpolation uses the downtrack and crosstrack neighbors in the correlation residue matrix and finds a "best" smooth curve through the residue points in each direction.

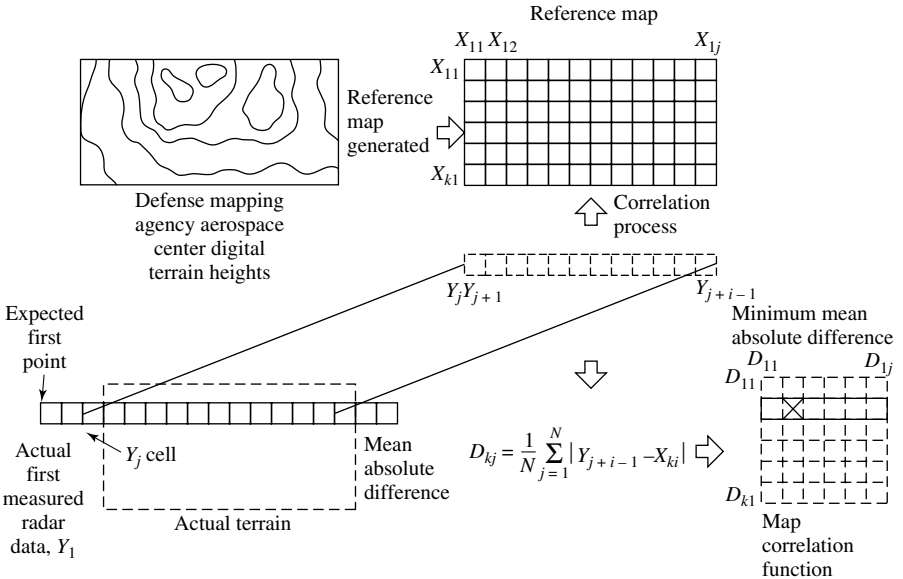

Fig. 7.18. Terrain correlation processing.

(e) The system can use either single maps or a voting group of three maps. The voting procedure normally improves the overall correlation probability of an area as compared to a single map, but for some areas, there may only be terrain of sufficient size for a single map. Even so, a single map of sufficient length can be made to have the same equivalent overall correlation probability of the shorter map set of three.

With regard to design feature "e," some more detail is in order. Specifically, some procedure to "guarantee" that a valid update has occurred is necessary to ensure mission effectiveness and safe warhead arming. One technique, which is presently used for *TERCOM* (used also in *DSMAC* (digital scene matching area correlation)), involves a voting logic with three successive fix scenes. Here, the determined fix point of two or three correlated scenes must be matched within an acceptable bound; otherwise, the fix sequence is rejected as an update. Although simple to implement and suitable for use with relatively invariant reference areas, the validity of this technique breaks down when the fix area is missed altogether, or when significant variations from the expected scene signature exist that cannot be modeled *a priori*. When coupled with the inherent modeling limitations of most sensor operating regions and modes, this technique does not provide any indication of the uncertainty in the "individual fixes" themselves. (Note that models developed should be sophisticated enough to accurately represent the *real world*, but not so much that they either require an inordinate amount of input, which may not be available even under the best of conditions, or machine processing time.)

One approach that can potentially minimize operational problems resulting from deficiencies in the present voting logic uses the correlation surface data generated by the map-matching algorithm for each in-flight fix to estimate the quality of the fix itself. If necessary, a similar voting sequence can be utilized based upon a minimum acceptable threshold associated with the probability of correct match for the number of fixes used per update. Techniques of this type use a comparison of the statistical distributions associated with the main and secondary peaks of the map-matching surface to estimate the quality of the fix itself.

The terrain correlation error parameters will now be summarized. The performance of the terrain correlation system is achieved by taking into account the uncontrollable errors in the system. They are (see also next section):

(1) Terrain mapping errors that are a function of *DMAAC* procedures and equipment.
(2) The reference map and its terrain characteristics that are a function of *DMAAC* map-selection evaluation procedures.
(3) Inertial platform errors allowed by its specification.
(4) Radar altimeter noise errors including beamwidth blurring as a function of altitude allowed by its specification.
(5) Natural errors in elevation such as snow, tree leaves, and buildings.

The remaining errors in the terrain correlation system are (a) map quantization, (b) cell-size sampling errors, (c) velocity errors, and (d) vertical reference system errors.

7.4.5 Terrain Roughness Characteristics

One of the factors that is used in selecting an update area is the roughness and uniqueness of the terrain. The variation in terrain elevation provides what can be considered as the *TERCOM* signal, and the quality of this signal increases directly with increasing amplitude, frequency, and randomness of the terrain. It should be noted that the *TERCOM* concept will not work over all types of terrain. For instance, the rougher the terrain, the better *TERCOM* works. However, good terrain must be more than just rough, it must be unique (i.e., a given profile out of the *TERCOM* map must not resemble any other map. Terrain roughness is defined as the standard deviation of the terrain elevation samples (see Figure 7.19). It is usually referred to as "sigma-T" (or σ_T).

Sigma-T is defined by the equation

$$\sigma_T = \sqrt{(1/N)\sum_{i=1}^{N}(H_i - \bar{H})^2}, \tag{7.16}$$

where $\bar{H} = (1/N)\Sigma_{i=1}^{N} H_i$.

Thus, σ_T is a measure of the variation of the terrain elevation about its average elevation. Note that the minimum value of σ_T required to support *TERCOM* operation is approximately 25 ft (7.62 m). Areas that have sigma-T values of fifty or greater are

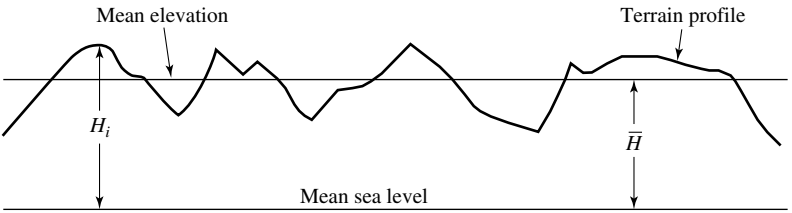

Fig. 7.19. Terrain standard deviation (σ_T).

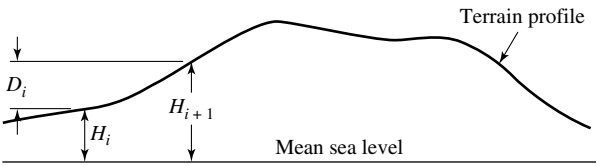

Fig. 7.20. Definition of sigma-Z.

usually considered as good candidates for *TERCOM* fix areas. Obviously, lakes and very flat or smooth areas have low values of sigma-T. Therefore, they are not suitable as fix areas. However, sigma-T is not the only criterion for determining whether a given area is suitable for *TERCOM* operation.

In particular, there are three parameters that are used to describe *TERCOM*-related terrain, and their values can give an indication of the terrain's ability to support a successful *TERCOM* fix. These parameters are (1) sigma-T, (2) sigma-Z (σ_Z), and (3) the terrain correlation length X_T. Note that the correlation length X_T represents the separation distance between two rows or columns of the terrain elevation matrix required to reduce their normalized autocorrelation function to a value of e^{-1}. It is usually assumed that parallel terrain elevation profiles that are separated by a distance greater than X_T are independent of each other.

Sigma-Z is defined as the standard deviation of the point-to-point changes in terrain elevation (i.e., the slope) as shown in Figure 7.20. Like sigma-T, the value of sigma-Z provides a direct indication of terrain roughness. Sigma-Z has also been shown to be a valid indicator of *TERCOM* performance. The expression for sigma-Z, assuming a Gaussian autocorrelation function, can be obtained from Figure 7.20. Mathematically, sigma-Z is given by the equation

$$\sigma_Z = \sqrt{[1/(N-1)]\sum_{i=1}^{N}(D_i - D)^2}, \tag{7.17}$$

where

$$D_i = H_i - H_{i+1}, \text{ and } D = (1/(N-1))\sum_{i=1}^{N-1} D_i.$$

The two parameters sigma-T and sigma-Z are related to the third parameter X_T according to the relation

$$\sigma_Z^2 = 2\sigma_T^2[1 - \exp(-d/X_T)^2], \tag{7.18}$$

where d is the cell size (or distance between elevation samples).

7.4.6 *TERCOM* System Error Sources

TERCOM system errors arise from two basic sources, according to the manner in which they influence the fix accuracy: (1) vertical measurement errors that give erroneous altitude measurements, and (2) horizontal errors that induce vertical errors by causing measurements of terrain elevation to be horizontally displaced from desired location.

The vertical errors are due to [6]:

- Inaccuracies in source data
- Radar altimeter measurement errors
- Barometric pressure measurement errors.

The horizontal errors are due to:

- Horizontal velocity and skew errors
- Vertical altitude errors
- Horizontal quantization (i.e., cell size).
  (These sources of degradation can be reduced by (1) choosing suitable terrain for fix taking, and (2) increasing the match length.)

Source data errors arise from digitization errors caused during map generation and loss of double precision in going from 32-bit to 16-bit programming. Foliage and aerial photographs are also error sources. Radar altimeter errors result from signal-to-noise ratio (*SNR*) effects, that is, the error in clearance measurement due to radar altimeter noise and the fluctuating character of the ground return. Typical values for radar altimeter noise effects are less than ± 5 ft for state-of-the-art altimeters. Barometric altimeter errors result from sensitivity to angle of attack, dynamic lag in the pressure transducer, and hysteresis errors in the sensing diaphragm. These are reduced by mixing the vertical channel of the *INS* in a second- or third-order loop. The mixing allows the fast response of the inertial system to give an accurate measure of the vehicle's short-term altitude changes with the long-term stability of the baro-altimeter used to dampen the inherent long-term stability of the *INS*'s vertical channel. Quantization is the error associated with quantization of the radar altimeter, barometric altimeter, and map elevations. Quantization can also be defined as the error induced by storing a discrete rather than continuous version of terrain, that is, quantization of the horizontal plane into cells of dimension d (see Figures 7.13 and 7.14 in Section 7.4.3).

Horizontal velocity errors in the downtrack dimension result in the measured terrain elevation data-sampling interval being either longer or shorter than the reference matrix cell size. Therefore, although it will have the right number of elevation

values, the length of the measured terrain elevation file will be either longer or shorter than it is intended to be. This distortion of the true *TERCOM* signal adds noise to the correlation process and reduces fix accuracy. Skew error occurs when the vehicle's groundtrack does not coincide with one of the reference matrix columns but crosses two or more of the columns as the vehicle flies over the matrix area. Specifically, horizontal noises include velocity and skew errors, that is, a displacement error associated with velocity and heading errors. As a result, the measured terrain elevation file is not representative of any of the reference matrix columns, and in fact, it contains measured elevations from two or more columns. Another source of vertical noise in the source data is foliage. The ideal reference data for *TERCOM* is source data based on the elevation profile of the bare terrain, and a radar altimeter that does not detect foliage. Since the radar altimeter does not see the bare Earth profile, the difference between the acquired radar profile and the photographically derived profile is system noise.

The impact of the noise, of course, depends on the foliage height relative to the terrain roughness. Also, the noise magnitude is dependent on the type of foliage coverage. For instance, jungle-type foliage with complete coverage over an area does not introduce much noise, since the tops of the foliage generally follow the terrain slopes. Moreover, isolated tall trees do not introduce much noise, since the bare ground profile can usually be identified in the photographic data. If the source data are derived from good-quality maps based on field data, so that the map elevation data do not include foliage, the noise contribution from the presence (or absence) of foliage is insignificant. That is, the radar altimeter essentially sees the ground as defined by the source data. However, if the source data are derived from aerial photographs only, the presence of foliage may introduce errors in the source data relative to the bare Earth's profile.

The effects of the increased noise due to foliage becomes important only in the smoother terrain area (e.g., $\sigma_T < 60$ ft). There should be little or no effect due to altitude changes occurring during a matrix overflight, provided the barometric reference altitude sensor is functioning properly. The purpose of the reference altitude sensor is to measure changes in altitude, not the absolute altitude above sea level. The mean is removed from the acquired profile during the *TERCOM* correlation process so that bias errors in the reference altitude sensor (or radar altimeter) have no impact on the fix accuracy. The relative change in altitude is important, and if the barometric altimeter is malfunctioning, the errors in the reference altitude enter the *TERCOM* process as noise. The impact of the noise is again dependent on the noise magnitude relative to the terrain roughness.

7.4.7 *TERCOM* Position Updating

The concept of utilizing terrain sensor data to obtain a sequence of position fixes has been under investigation since the late 1950s (see Section 7.4.1). As previously mentioned, the objective of the terrain contour matching process is to provide the vehicle's navigation system with a measured downtrack and crosstrack vehicle position error. Consequently, the navigation system then uses the measured position error

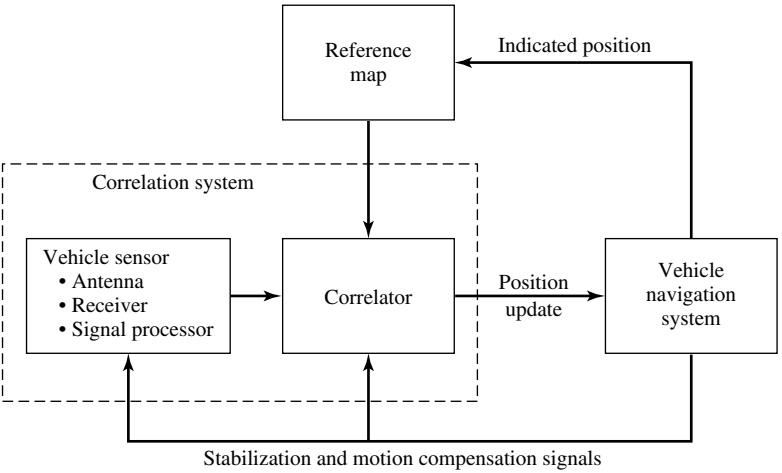

Fig. 7.21. Correlation update-aided navigation system.

to update its estimate of the vehicle's true geographic position. Usually, a Kalman filter is used to aid in reducing the navigation system's errors based on the measured vehicle position error.

TERCOM, as discussed earlier, is an Earth reference system developed for long-range cruise missiles to update periodically the *INS*. Along the preestablished missile flight path, several check areas are chosen to reinitialize the *INS*. Above the check area, a radar altimeter with a good horizontal and vertical resolution measures elevation of the terrain, resulting in a sequence of altimeter readings along the missile's track. The sequence is correlated with a stored digitized map of the check area taken from the memory unit to determine the best estimate of the actual position and subsequently to correct the *INS*. In essence, the common approach has been to obtain separate position fixes for periodically updating the *INS* by correlating a radar altimeter-derived terrain profile with a stored topographic map, taking the location of the best match to be the position of the navigation system. This correlation technique compares a sensed profile of ground signatures acquired during flight with profiles obtained from a reference map (whose position is known) prepared prior to the flight. This comparison yields the relative (fix) position of the measured profile within the reference map that is used to create a position update for the inertial navigation system onboard the missile. The method of position updating is illustrated in block diagram form in Figure 7.21. This figure shows the acquisition of a sensed data set and its interaction with the vehicle (i.e., missile) navigation system.

The ground signature used is terrain elevation, which is found by differencing the output of a pulsed radar altimeter and a barometric reference altitude maintained by the *INS*. This correlation processor is based on the mean absolute difference (*MAD*) processor discussed earlier in this chapter, with the means (i.e., mean values of altitude) removed from each profile. Using the *MAD* processor, a strip (i.e., profile) of measured ground elevations acquired along the vehicle's flight path is correlated with

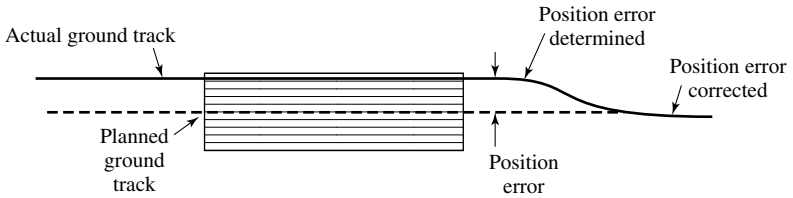

Fig. 7.22. Typical course correction after a position update.

each of the profiles within a reference map. The position of the minimum output of the *MAD* is the indicated fix position. However, it should be noted that the *MAD* indicated fix position is due to errors incurred during preparation of the reference map and measurement of the terrain profile. After the navigation system has been updated, position correction commands are sent to the flight control system, which flies the missile back into the intended course. Figure 7.22 illustrates that the planned course of the missile is down the center of the fix-taking area, and it is the planned course that the navigation system directs the missile along.

However, with errors present in the navigation system, the actual ground track of the missile will be either to the left or right of the planned course. For simplicity, the vehicle's downtrack position error will be ignored here. After the vehicle has flown over the fix-taking area and the *TERCOM* computations have been completed, the difference between the planned ground track and the actual position of the vehicle at the time the fix was made (i.e., at a map center), as determined by the correlation process, defines the downtrack and the crosstrack position errors, and these errors are sent to the navigation system for update. At the completion of navigation update, the position errors are corrected by sending course correction commands to the vehicle's flight control system, which results in the vehicle flying back into the planned course.

The vehicle receives mission data from the carrier aircraft over the carrier serial data interface and stores it in the vehicle's onboard digital computer unit memory. The carrier can target and retarget the air vehicle by sending it the desired mission data. The mission data for the air vehicle consist of the following:

- mean column elevation data
- map description data.
- reference terrain data.
- waypoint data.

As stated above, a Kalman filter is usually employed to reduce the drift rate of the vehicle's inertial navigation system. Usually implemented as part of the vehicle's real-time operational computer program, the Kalman filter software optimally estimates the internal errors in the inertial system (e.g., platform tilt angles in the case of a gimbaled system, and gyro drift rates) based upon the position error measurements that are computed from each terrain correlation position fix. The estimated internal errors are then provided to the inertial navigation system as negative feedback so that the errors in the system's present position computations can be reduced. Each time

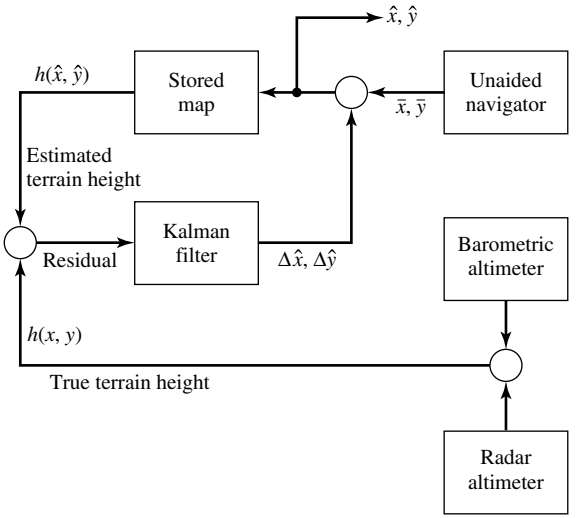

Fig. 7.23. Terrain-aided navigation concept.

a terrain correlation position fix is made, the accuracy of the Kalman filter's internal error estimate improves, with a resulting decrease in the position error growth rate [9].

Figure 7.23 illustrates the role of the Kalman filter in a terrain-aided navigation (*TAN*) system. The interpretation of this block diagram for terrain-aided navigation is as discussed earlier. That is, the terrain-aided navigation concept is based on comparing measured terrain height (i.e., the difference between barometric (or reference altitude) and radar altitudes) with terrain height at the position determined from an unaided inertial navigator. The difference between the two terrain heights is equivalent to, as stated above, the residual of Kalman filtering and can be processed to provide optimal estimates of the navigation errors. These estimates can then be used to correct the navigation system.

Note that the Kalman filter uses a dynamic model; that is, a *truth model* is used to generate the data. Finally, a simulation (e.g., covariance analysis or Monte Carlo simulation) must be carried out in which the truth model can be different from the Kalman *filter model*, so that sensitivity to modeling errors can be assessed. The terrain height $h(x, y)$ can be modeled in the form of *Gaussian hills* as follows:

$$h(x, y) = \sum_{i=1}^{N} \exp\{-c^2[(x - x_i)^2 + (y - y_i)^2]\}, \tag{7.19}$$

where the locations of the peaks (x_i, y_i) are chosen at random. In performing the aforementioned simulation, this effort would entail generating a terrain sector and obtaining its statistical characteristics (e.g., correlation function) in terms of the parameters (i.e., c^2 and N) of the model. Simultaneously, some examples of actual terrain must be analyzed for the corresponding statistical characteristics. By doing this, one can determine how to set c^2 and N to simulate different types of physical terrain. Typical

values for c^2 and N are $c^2 = 125$, $N = 25$. The smaller the value of c^2, the rougher the terrain. The *Gaussian hill* model given above matches well the statistical characteristics of some geographical region and produces terrain maps that resemble actual terrain sectors.

Another topic that must be addressed and explored in connection with terrain mapping is data storage and compression. For most geographic areas, terrain height data are available with considerably greater resolution than required for typical terrain-aided navigation (*TAN*) applications, and moreover, storage and retrieval of the data in real time imposes a severe burden on the airborne computer and/or hardware. Various techniques for data compression (e.g., finite 2-D cosine transforms) are available that are entirely adequate for this application.

We will now discuss in some detail the *TAN* concept. *TAN* is a recursive real-time algorithm designed for use on the advanced fighter technology integration (*AFTI*) *F*-16 aircraft. Developed by the Sandia National Laboratories in collaboration with the Air Force Wright Aeronautical Laboratories, Avionics Laboratory, Wright-Patterson AFB, Ohio, in the early 1980s (note that the *TAINS* system was first used in the early 1970s), *SITAN* (Sandia inertial terrain-aided navigation) as it came to be known, is a flight-computer algorithm that produces a very accurate trajectory for low-flying, high-performance aircraft by combining outputs from a radar or laser altimeter, an *INS*, and a digital terrain elevation map. Moreover, *TAN* estimates aircraft position using measurements from the *INS* and measurements of terrain variations along the aircraft's flight path. In Section 7.4.7 we discussed how *TERCOM* is used to update the *INS*. However, due to the open-loop nature of an inertial navigation system, the position error tends to increase monotonically with time. This problem can be resolved by integrating the *INS* with the *GPS* (for more details in *INS*/*GPS* integration, see Section 7.5.1), that is, resetting the *INS* periodically with *GPS* position fixes. In this particular application, we are interested in using *TAN*. Using *TAN*, the error drift in the *INS* can be mitigated by utilizing measurements of the terrain elevations along the flight path of the aircraft and matching them with an onboard digital terrain elevation database (*DTED*). Consequently, the instantaneous terrain elevation underneath the aircraft is computed as the difference between the aircraft altitude obtained by measuring the air pressure, and the distance between the aircraft and the terrain measured by an altimeter.

The state model, using the extended Kalman filter algorithm, can be formulated in the usual way as follows:

$$\begin{aligned} \delta \mathbf{x}_{k+1} &= \Phi \delta \mathbf{x}_k + w_k, \\ E\{w_k\} &= 0, \\ E\{w_k w_k^T\} &= Q_k \delta_{kj}, \end{aligned}$$

and the measurement

$$\begin{aligned} c_k = c(\mathbf{x}_k) + v_k &= z_k - h(.\,,.) + v_k, \\ E\{v_k\} &= 0, \\ E\{v_k v_k^T\} &= R_k \delta_{kj}, \end{aligned}$$

where

$\delta \mathbf{x}_k$ = *INS* error states to be estimated,
Φ = state-transition matrix for *INS* errors,
$\mathbf{x}_k$ = states of *INS* and aircraft,
c_k = ground clearance measurement,
z_k = altitude of aircraft,
h = height of terrain at position (. , .),
w_k = system driving noise,
v_k = measurement noise error,
k = subscript denoting time,
Q_k = an $r \times r$ matrix known as the covariance matrix of the state model uncertainties (or system noise strength),
R_k = an $m \times m$ matrix known as the covariance matrix of the observation noise (also called measurement noise strength).

At any time k,

$$\mathbf{x} = \mathbf{x}_{INS} + \delta \mathbf{x},$$

$$\delta \mathbf{x} = [\delta x \; \delta y \; \delta z \; \delta v_x \delta v_y]^T,$$

where δx, δy, δz, δv_x, and δv_y are the errors in the x-position, y-position, altitude, x velocity, and y velocity, respectively. (Note that other *INS* error states can also be included in $\delta \mathbf{x}$.)

We close this section by noting that *TERCOM* is also finding use in commercial aviation. More specifically, the Boeing Company recently outfitted a 737–900 with new cockpit technology that includes a situation display showing the aircraft's vertical profile compared with stored terrain data. Boeing plans to demonstrate this new technology to the airlines.

7.5 The NAVSTAR/GPS Navigation System

The most accurate way to locate the position of a cruise missile is the global positioning satellite system, which consists of 24 satellites (21 active and 3 spares) in polar orbits positioned in such a manner that any place on the Earth's surface will have at least four of the satellites in view at all times. Specifically, every four thousandth of a second, the satellites broadcast exactly synchronous coded signals that can be received by passive equipment (or receivers) on the cruise missile. By determining the difference in the arrival times of four such signals, the missile's computer can calculate the distance of the missile from each satellite. In addition, the satellites broadcast information describing their orbits around the Earth. With this information and the four different arrival times of the signals, the missile's computer can determine the true position of the missile within 10 meters in three dimensions without any other external data. From that information, it can in turn deduce its velocity at any instant.

To recapitulate, the *NAVSTAR/GPS* (navigation signal time and range/global positioning system) or simply, *GPS*, is a satellite-based system, supporting passive autonomous radio-positioning and navigation for land, sea, and air user equipment, providing 24-hour all-weather, worldwide service to military and civilian users. The system transmits signals at two L-band frequencies as follows:

L_1 : 1575.42 MHz
- *C/A* Code: Navigation data.
- P Code: Navigation data (in phase quadrature)

L_2 : 1227.60 MHz
- P Code: Navigation data (P code alone).

Using these two signals permits corrections to be made for ionospheric delays in signal propagation time. Furthermore, these signals are modulated with two codes: (1) the *C/A* or clear/access (also known as coarse/acquisition) that provides for easy lock-on to the desired signal, and (2) the P or precise code, which provides for precision measurement of time. As indicated above, the L_1 signal is modulated with both P and *C/A* pseudorandom noise (*PRN*) codes in phase quadrature, while the L_2 signal is modulated only with the P-code. Moreover, the *C/A* code is a short code operating at 1.023 Mbps, while the P-code is a long-precision code operating at 10.23 Mbps. Navigation accuracy of the *GPS* on the order of meter level for military users and decameter level for civilian users has been achieved. Superimposed on the L_1 and L_2 signals are navigation and system data including satellite ephemeris, atmospheric propagation correction data, and satellite clock bias information.

The *GPS* system is functionally divided into three segments: (1) the space segment (i.e., the satellites), (2) the control segment, and (3) user equipment (i.e., receivers). These three segments will now be discussed in more detail. As stated above, the space segment consists of a constellation of 21 satellites plus 3 active spares, operating in circular orbits at an altitude of 10,898 nm (20,183 km). The satellites are uniformly distributed in 6 orbital planes, so that 4 to 7 satellites are visible at any time on the Earth (i.e., at 5° or more above the horizon). The orbit planes are inclined at 55° with respect to the equatorial plane, with a 12-hour period. *NAVSTAR* measures the range to a set of four satellites by timing the arrival of radio signals transmitted from the satellites at precisely known times. Theoretically, a minimum of three satellites would allow a position fix to be obtained, but since three satellites may not always be in suitable positions (or view), and because timing errors in the receiving system have to be eliminated, a fourth satellite is necessary. Each satellite transmits specially coded signals that allow individual satellites to be distinguished, and the range and rate of range change (i.e., velocity) of the user to be measured. And as stated above, the signals are pseudorandom binary noise (*PRN*). The control segment consists of five monitor stations located around the world that track all satellites in view of their antennas. Data are transmitted to a master control station (*MCS*) where processing takes place to determine orbital and clock modeling parameters for each satellite. Specifically, the information from the monitor stations is processed at the *MCS* to determine satellite orbits and to update the navigation message of each satellite. This

updated information is uploaded (i.e., transmitted) to the satellites via the ground antennas. The satellites then incorporate this information into the data message.

The user segment consists of equipment designed to receive and process the satellite signals. These are commonly referred to as *UE* (user equipment). The unique codes transmitted by each satellite allow the use of common radio frequency (*RF*) carrier frequencies throughout the constellation, a process known as code division multiplexing. Measurements from four satellites are required in the general case. The *DoD* (Department of Defense) has developed two classes of receivers: (1) continuous tracking, and (2) sequential tracking. The continuous tracking receiver provides a dedicated channel for each satellite being tracked and a fifth channel that performs ancillary functions (e.g., ionospheric corrections and interchannel bias measurement). For example, in a *GPS* receiver that operates on an aircraft, there are typically four code loops (or channels) each tracking different satellites. *GPS* receivers may be designed to time multiplex channels, enabling navigation to be performed using only one or two channels and switching between satellites. However, this results in a loss of performance during maneuvers, such as in a fighter aircraft. Therefore, a five-channel receiver is commonly used; the function of the fifth channel is to scan for new satellites. (Note that recently, *GPS* receivers have been designed with as many as 12 channels.) The sequential receiver has one or two channels, for low- and medium-dynamic applications, respectively. In these receivers the channels are time shared among satellites and housekeeping chores.

GPS receivers determine a navigation solution consisting of latitude, longitude, altitude, and velocities by processing coded signals from the satellites. Specifically, *GPS* measurements are obtained by determining the relative time between transmission from the satellite to receiver. The measurement consists of a range and receiver clock bias and is referred to a *pseudorange* [5]. Pseudorange consists of four components (i.e., three positions and a clock bias). As stated above, by tracking signals from four satellites, and using information contained in the satellite broadcast, a system of equations can be solved to determine receiver position and receiver clock bias relative to *GPS* system time.

As discussed earlier, the objective of the user receiver is to take the pseudorange measurements so that the receiver can perform continuous navigation fixes. To this end, let the coordinate system be the Earth-centered Earth-fixed (*ECEF*) coordinate. Then, the user's position can be denoted by (X_u, Y_u, Z_u) and the ith satellite position by (X_{si}, Y_{si}, Z_{si}). Mathematically, the pseudorange measurement, ρ_i, to the ith satellite can be obtained as follows [5]:

$$\rho_i = R_i + \Delta B = [(X_{si} - X_u)^2 + (Y_{si} - Y_u)^2 + (Z_{si} - Z_u)^2]^{1/2} + \Delta B, \quad i = 1, 2, 3, 4, \tag{7.20}$$

where ΔB is the user's clock bias with respect to the *GPS* system time. Since the satellite position can be precomputed from the ephemeris data, the user position and clock bias can be derived by solving the above nonlinear inhomogeneous equations (i.e., ρ_i, $i = 1, 2, 3, 4$). In other words, pseudoranges are modeled as the time range between satellite and receiver, corrupted by the user equipment clock bias. A more

Table 7.2. *WGS*-84 Ellipsoid

Parameter	Value	Description
a	6,378,137.00 [meters]	Semimajor axis
b	6,356,752.3142 [meters]	Semiminor axis
f	1/298.257223563	Flattening
e	$3.4704208374 \times 10^{-3}$	Eccentricity*
Ω_E	7.292115×10^{-5} [rad/sec]	Earth's angular velocity
μ	$3986005.00 \times 10^8 [m^3/\text{sec}^2]$	Earth's gravitational constant

accurate model must include atmospheric propagation delay. Thus, (7.20) for the pseudorange can be written as

$$\begin{aligned}\rho_i &= R_i + c(\Delta t_u - \Delta t_{si}) + c\Delta t_{Ai} \\ &= [(X_{si} - X_u)^2 + (Y_{si} - Y_u)^2 + (Z_{si} - Z_u)^2]^{1/2} \\ &\quad + c(\Delta t_u - \Delta t_{si}) + c\Delta t_{Ai}, \end{aligned} \tag{7.21}$$

where

ρ_i = pseudorange to the ith satellite,
R_i = true range,
c = speed of light,
Δt_{si} = ith satellite clock offset from the *GPS* system time,
Δt_u = user clock offset from the *GPS* system time,
Δt_{Ai} = atmospheric propagation delays and other errors (note: this delay is, converted into distance along the propagation path).

The other symbols have been defined above. The value of $c\Delta t_u$ represents the range equivalent of the user clock error.

Because *GPS* position is referenced to a common grid, the World Geodetic System – 1984 (*WGS-84*), the civil and military position data can be standardized on a worldwide basis. The user equipment set (*UE Set*) is capable of converting *WGS-84* to other commonly used data when operating with other map and data products. Therefore, the *UE* coordinates are commonly expressed in the *WGS-84* frame. By reading the navigation message, the receiver can compute the coordinates of each satellite by means of the broadcast ephemeris data.

The *WGS-84* ellipsoid reference frame in which all equations are written is defined in Table 7.2 (see also Appendix A) [8], [10]:

The following *WGS*-84 ellipsoid relations are useful:

$$b = a(1 - f),$$

$$f = 1 - (b/a),$$

*Another parameter sometimes used to characterize the reference ellipsoid is the second eccentricity, e', given by the following equation $e' = [(a^2/b^2) - 1]^{1/2} = (a/b)e$. Thus, the value of $e' = 0.0820944379496$ [8]

$$e^2 = 1 - (1 - f)^2 = f(2 - f) \quad \{\text{Also}: e = [1 - (b^2/a^2)]^{1/2}\},$$
$$R_N = a/[1 - e^2 \sin^2 \phi]^{1/2},$$
$$X = (R_N + h) \cos \phi \cos \lambda,$$
$$Y = (R_N + h) \cos \phi \sin \lambda,$$
$$Z = [R_N(1 - e^2) + h] \sin \phi,$$

where

R_N = radius curvature of the prime vertical,
ϕ = latitude,
λ = longitude,
h = altitude.

The origin of the *WGS-84* coordinate system is at the center of mass of the Earth, with the (X, Y, Z) axes defined as follows:

X-axis: Intersection of the *WGS-84* reference meridian plane and the plane of the equator, corresponding to the average terrestrial pole of 1900–1905. The *WGS-84* meridian is 0.554" east of the zero meridian (near Greenwich).
Y-axis: Measured in the plane of the equator and 90° east of the X-axis.
Z-axis: Parallel to the direction of the conventional international origin, that is, coincident with the Earth's mean rotation axis 1900-1905.

GPS position accuracy is dependent on the precision with which the range to the satellite being tracked can be measured and the geometry of those specific satellites with respect to the user. A number of factors contribute to range error measurement, such as atmospheric effects, satellite signal integrity, and receiver design. In addition, position accuracy is also determined by the code (*P* or *C/A*) being used for navigation. Satellite geometry for any given user is mainly determined by the number of operational satellites in orbit, the placement of those satellites, and to a lesser extent the location of the user. The *GPS* has been defined and specified for accuracy in navigation and positioning based upon operation in the *stand-alone* mode. This stand-alone performance is remarkable, considering all the variables involved. There are users, however, that have a requirement for greater real-time accuracy.

The position, velocity, and time accuracy capabilities of the *GPS* set can now be detailed in view of correlated factors such as the response times, vehicle dynamics, and hostile threats. The accuracy values delineated herein are averaged over all points on the Earth and at all times, and are based upon the following assumptions:

(a) The *UE* set is operating in the nominal receiver operational state and navigation mode.
(b) Graceful degradation of navigational accuracy will result with fewer than 21 satellites operating properly.

The *GPS UE* set calculated position, velocity, and time accuracies quoted in the open literature are as follows:

- Position (3-dimensional, derived from the *P* code): 16 meters *SEP* (spherical error probable).
- Position (2-dimensional, derived from the *P* code): 8 meters *CEP* (circular error probable).
- Velocity (3-dimensional): ≥ 0.1 m/sec *rms* (root mean square), any axis.
- Time: 0.1 μsec (1σ).
- Position (2-dimensional, for civil users): 40 meters (*CEP*).

As discussed above, the accuracy of a navigation fix depends primarily on the geometry of the four satellites in view, which is characterized by the geometric dilution of precision (*GDOP*). The smaller the *GDOP*, the more accurate the navigation fix will be. Mathematically, the *GDOP* is expressed as [1], [7], [8]

$$GDOP = [tr(G^T G)^{-1}]^{1/2}, \tag{7.22}$$

where G is a matrix and tr denotes the trace of the matrix. The matrix G is given by

$$G = \begin{bmatrix} e_{11} & e_{12} & e_{13} \\ e_{21} & e_{22} & e_{23} \\ e_{31} & e_{32} & e_{33} \\ e_{41} & e_{42} & e_{43} \end{bmatrix} \begin{bmatrix} 1 \\ 1 \\ 1 \\ 1 \end{bmatrix} \tag{7.23}$$

The unit vector from the *GPS* receiver to each satellite is defined as

$$e_i = \begin{bmatrix} e_{i1} \\ e_{i2} \\ e_{i3} \end{bmatrix}.$$

Therefore, the elements $e_{i1}, e_{i2}, e_{i3} (i = 1, \ldots, 4)$ denote the direction cosines from the user to the satellites in question (or view). Specifically, the user will try to select the four visible satellites with minimum *GDOP* in order to reduce the error of the navigation fix induced by measurement errors. Note that by taking into account the fact that

$$e_{i1}^2 + e_{i2}^2 + e_{i3}^2 = 1,$$

a closed-form solution of (7.22) is thus possible. Furthermore, the matrix product $(G^T G)^{-1}$ can be expressed as

$$(G^T G)^{-1} = \begin{bmatrix} \sigma_{xx}^2 & \sigma_{xy}^2 & \sigma_{xz}^2 & \sigma_{xt}^2 \\ \sigma_{yx}^2 & \sigma_{yy}^2 & \sigma_{yz}^2 & \sigma_{yt}^2 \\ \sigma_{zx}^2 & \sigma_{zy}^2 & \sigma_{zz}^2 & \sigma_{zt}^2 \\ \sigma_{tx}^2 & \sigma_{ty}^2 & \sigma_{tz}^2 & \sigma_{tt}^2 \end{bmatrix}, \tag{7.24}$$

where the diagonal values (or trace) are the variances of the estimated user position in each axis and in the user time offset. Thus, the *GDOP* can be expressed in the form

$$GDOP = (\sigma_{xx}^2 + \sigma_{yy}^2 + \sigma_{zz}^2 + \sigma_{tt}^2)^{1/2}. \tag{7.25}$$

The *GDOP* is used as a figure of merit (or selection criterion) for selecting the best geometry from the satellites in view, and as stated above, the goal is to select a satellite configuration that minimizes the scalar value of *GDOP*. The *GDOP* can be further broken down into horizontal dilution of precision (*HDOP*), vertical dilution of precision (*VDOP*), position dilution of precision (*PDOP*), and time dilution of precision (*TDOP*). Mathematically, these terms are expressed in the form

$$HDOP = (\sigma_{xx}^2 + \sigma_{yy}^2)^{1/2}, \tag{7.26}$$

$$VDOP = \sigma_{zz}, \tag{7.27}$$

$$PDOP = (\sigma_{xx}^2 + \sigma_{yy}^2 + \sigma_{zz}^2)^{1/2}, \tag{7.28}$$

$$TDOP = \sigma_{tt}, \tag{7.29}$$

$$GDOP = (\sigma_{xx}^2 + \sigma_{yy}^2 + \sigma_{zz}^2 + \sigma_{tt}^2)^{1/2}. \tag{7.25}$$

Therefore, in order to determine the *GPS* user accuracy in the horizontal and vertical directions, assuming that the pseudorange accuracy is known, one simply multiplies the pseudorange accuracy by the corresponding value of *HDOP* or *VDOP*. It is clear that all *GDOP*-related performance measures indicate the error in an estimated navigation quantity "per unit of measurement noise" covariance. In terms of the pseudorange measurement error covariance matrix R, the covariance matrix P of the error in the *GDOP* can be expressed as follows:

$$P = (G^T R^{-1} G)^{-1} \tag{7.30}$$

and

$$trP = GDOP^2 = tr[(G^T R^{-1} G)^{-1}]. \tag{7.31}$$

We can summarize the *GDOP* concept by noting that all of the above *GDOP*-related measures depend solely on the geometry matrix G. Smaller *GDOP* values indicate stronger or more robust geometric solutions to the estimation problem. Finally, note that for practical navigation purposes, ships require reception of only three satellites to determine the horizontal position. Once the best *GDOP* has been selected, one must determine how good the measurement of position is. Position dilution of precision (*PDOP*) is used as a measure of position error. A "good" *PDOP* indicates that the satellites exhibit good geometry as seen by the user. A good *PDOP* is a low value, typically between 2 and 4. In the case of independent, identically distributed ranging errors to the satellites, the *rms* three-dimensional position error is equal to the *rms* ranging error multiplied by *PDOP*.

Taking advantage of *differential* methods can enhance the performance of a *GPS* receiver in a local geographic environment significantly. The differential *GPS* (*DGPS*) takes advantage of previously defined geodetic positions and stable time to determine ranging offsets relative to the received satellite (or space vehicle (*SV*)) signals. These ranging *deltas* may then be transmitted to a remote receiver, incorporated in the position solution, and thereby provide a correction to position variance associated

with the position solution. This technique will require a *GPS* set at a known (i.e., surveyed) position. That set can determine range errors or position discrepancies by comparing known position with *GPS*-derived position. The error data can then be broadcast to *GPS*-equipped users operating in the region to compensate for *GPS* system errors.

7.5.1 *GPS/INS* Integration

In many applications, *GPS/INS* integration is necessary. Specifically, this integration has proved to be a very efficient means of navigation, primarily because of the short-term accuracy achieved by the inertial navigation system (*INS*) and the long-term accuracy of the *GPS* fixes. Two versions of the *GPS/INS* integration are available. These are (1) the *tightly coupled GPS/INS*, and (2) the *loosely couple* or *modular GPS/INS*. Here we will briefly discuss the tightly coupled version, because its ability to perform optimal signal processing allows the various errors and noise sources (e.g., clock delays, atmospheric effects, inertial instrument biases) acting on both the *GPS* and *INS* units to be taken into account in a global way. Kalman filtering has been a popular tool for handling estimation problems (see also Section 4.8). However, its optimality depends on linearity. When used in nonlinear filtering (i.e., extended Kalman filter (*EKF*)), its performance relies on, and is limited by, the linearizations performed on the model in question. Moreover, implementation of nonlinear filters has been plagued so far by the difficulties inherent to their infinite-dimensional nature. Nevertheless, for the reader's convenience, the discrete form of the conventional Kalman filter will be given here [1], [4], [9].

System Model:

$$\begin{aligned} \mathbf{x}_k &= \Phi_{k-1}\mathbf{x}_{k-1} + \mathbf{w}_{k-1} \\ \mathbf{w}_k &\sim N(0, Q_k). \end{aligned}$$

Measurement Model:

$$\begin{aligned} \mathbf{z}_k &= H_k\mathbf{x}_k + \mathbf{v}_k, \\ \mathbf{v}_k &\sim N(0, R_k). \end{aligned}$$

Initial Conditions:

$$\begin{aligned} E\{\mathbf{x}(0)\} &= \hat{\mathbf{x}}_o, \\ E\{(\mathbf{x}(0) - \hat{\mathbf{x}}_o)(\mathbf{x}(0) - \hat{\mathbf{x}}_o)^T\} &= P_o. \end{aligned}$$

Other Assumptions:

$$E\{\mathbf{w}_k\mathbf{v}_\mathbf{j}^T\} = 0 \;\forall\; j, k.$$

State Estimate Extrapolation:

$$\hat{\mathbf{x}}_k(-) = \Phi_{k-1}\hat{\mathbf{x}}_{k-1}(+).$$

(Note: the $(-)$ sign denotes the time immediately *before* a discrete measurement, and $(+)$ the time immediately *after* a discrete measurement.)

Error Covariance Extrapolation:

$$P_k(-) = \Phi_{k-1} P_{k-1}(+) \Phi_{k-1}^T + Q_{k-1}.$$

State Estimate Update:

$$\hat{\mathbf{x}}_k(+) = \hat{\mathbf{x}}_k(-) + K_k[\mathbf{z}_k - H_k \hat{\mathbf{x}}_k(-)]$$

Error Covariance Update:

$$P_k(+) = [I - K_k H_k] P_k(-).$$

Kalman Gain Matrix:

$$K_k = P_k(-) H_k^T [H_k P_k(-) H_k^T + R_k]^{-1}.$$

(Note: The superscript T denotes matrix transposition.)

In Section 7.3 it was stated that the *INS* for the cruise missile can be modeled with 10 states. In integrated *GPS/INS* applications, Kalman filters of 15–24 state variables have been shown to be suitable (i.e., optimal). For the reasons mentioned earlier, tightly coupled *GPS/INS* systems are commonly used in such applications.

In a typical *GPS/INS* application, the following state variables can be chosen:

3-Axis INS Error Model:

3 Position error states,
3 Velocity error states,
3 Platform tilts,
3 Gyroscope drift rate errors,
3 Accelerometer errors (biases).

GPS Error Model:

3 User position components,
3 User velocity components,
1 User clock bias,
1 User clock bias rate.

Of course, the final selection of the appropriate state variables will depend on the mission requirements, computational load, accuracy, cost, etc. In some applications, an 11-state Kalman filter would be required. These states are:

- 3 position, 3 velocity, and 2 clock states required for navigation solution from pseudorange (pr) and delta-range (dr).
- 3 acceleration states required for propagation of velocity between measurement updates (required in a dynamic environment).

Mathematically, or in the Kalman filter notation, these states can be expressed as follows:

- States: $\mathbf{x}^T = [p_x\, p_y\, p_z\, v_x\, v_y\, v_z\, b_u\, r_u\, a_x\, a_y\, a_z]$,
- Propagation:

$$\Phi = \begin{bmatrix} I_4 & I_4 & \frac{1}{2}I_3 \\ 0 & I_4 & I_3 \\ 0 & 0 & I_3 \end{bmatrix}$$

- Pseudorange (pr) Update: $H_{pr}^T = [1_i^T\, 1\ 0^T 0^T],\ i = 1, \ldots, 4$,
- Delta-range (dr) Update: $H_{dr}^T = [0^T 1_i^T\, 1\ 0^T],\ i = 1, \ldots, 4$,
- Initial Variance: $P_o = E\{\hat{\mathbf{x}}_o \hat{\mathbf{x}}_o^T\}$,
  Initial position and time uncertainty.
  Initial velocity and clock rate uncertainty (dynamic dependent).
  Initial acceleration uncertainty (dynamic dependent).

For the Kalman measurement updates, the following facts are noted:

- Since pr and dr measurements are uncorrelated from satellite to satellite, updates can be applied independently. Therefore, 4-pr updates can be applied as independent measurements with variance ${\sigma_{pr}}^2$,

$$K = PH[H^T P H + \sigma_{pr}^2]^{-1}.$$

  (Note that no matrix inversion is necessary to calculate K.)
- Similarly, the same is true for 4-dr updates.
- This implementation significantly reduces computation.
  ($8 \times$ scalar measurement updates takes significantly less computation than 1×8-element vector update.)

Next, we need to define the state and measurement noise matrices, Q and R. These are defined as follows:

State Noise Q: State noise represents effects of unmodeled *GPS* system errors on states:

Atmospheric effects.
Ephemeris and clock errors.
Selective availability.

Measurement Noise R: Combination of receiver and user clock noise:

$$R_{pr} = 15 \text{ m (C/A code)},$$
$$R_{dr} = 1 \text{ cm}.$$

Lastly, we must consider the state propagation process. For the state propagation, the following facts are observed:

- Pr and dr updates provided every second.
- For navigation, position and velocity updates are generally required more frequently. Therefore, Pr and dr updates must propagate between seconds:

$$P(kT + \Delta t) = P(kT) + V(kT)\Delta t + A(kT)(\Delta t^2/2),$$
$$V(kT + \Delta t) = V(kT) + A(kT)\Delta t,$$

(Note: $A =$ acceleration, $V =$ velocity.)

In designing a Kalman filter for *GPS*, the following facts should be considered:

- An 11-state filter is the optimal Kalman implementation for dynamic environments.
- Reducing the number of states reduces the computational load.
- There is a trade-off between optimal implementation and computational cost.

An 8-state Kalman filter design would be sufficient in a low dynamic environment, such as land or marine navigation.

It should be noted here that in military applications, *GPS* signal acquisition must be done quickly in a high-jamming environment, using the more precise, harder to jam *GPS Y*-code. Usually, military *GPS* receivers first acquire the less-precise *CA*-code, then search for the *Y*-signal. In an integrated *GPS/INS* system, the *GPS* will pass on position data to update the inertial navigation system. If the *GPS* is jammed, the navigation computer will rely solely on the *INS*. Other precision-guided weapons are fed inertial data before launch, then use *GPS* to update the *INS* in flight. The phase stability of the *GPS* receiver's oscillator also must be high in order to acquire the satellites and accurately track the vehicle's velocity. Finally, the goal for the use of an integrated *GPS/INS* system is to bring the price below $1500.

We conclude this section by noting that the receiver clock drift δ_t can be represented by the integration of an exponentially correlated random process x_i. Therefore, for the purposes of modeling clock drifts and uncertainties, the equations that describe the clock drifts are as follows [9]:

$$\frac{dx_t}{dt} = -ax_t + w_t,$$

$$\frac{d\delta_t}{dt} = x_t,$$

where w_t is a Gaussian white noise, $a = 1/\tau$ (τ is the correlation time), and

$$E\{w(t)w(t+\tau)\} = (2\sigma_{x_t}^2/\tau)\delta(\tau).$$

References

1. Felter, S.C. and Wu, N. Eva: *A Relative Navigation System for Formation Flight, IEEE Transactions on Aerospace and Electronic Systems*, Vol. 33, No. 3, July 1997, pages 958–967.
2. Fulghum, D.A.: *Cruise Missile Threat Spurs Pentagon research, Aviation Week and Space Technology*, July 14, 1997, pages 44–46.
3. Laur, T.M. and Llanso, S.L.: *Encyclopedia of Modern U.S. Military Weapons*, edited by Walter J. Boyne, Berkley Books, New York, 1995.
4. Lin, C.F.: *Modern Navigation, Guidance, and Control Processing*, Prentice Hall, Englewood Cliffs, New Jersey, 1991.
5. Milliken, R.J. and Zoller, C.J.: *Principle of Operation of NAVSTAR and System Characteristics, Navigation, Journal of the Institute of Navigation*, Vol. 25, No. 2, Summer 1988, pages 95–106.
6. Mobley, M.D. and Brown, J.I.: *Impact of Terrain Correlation Elevation reference Data on Boeing's Air Launched Cruise Missile*, Institute of navigation National Meeting, Dayton, Ohio, March 1980, pages 108–112.
7. Parkinson, B.W. and Spilker J.J. (editors), with P. Axelrod and P. Enge (associate editors): *Global Positioning System: Theory and Applications*, Vols. I and II, AIAA, 1996.
8. Siouris, G.M.: *Aerospace Avionics Systems: A Modern Synthesis*, Academic Press, New York, 1993.
9. Siouris, G.M.: *An Engineering Approach to Optimal Control and Estimation Theory*, John Wiley & Sons, Inc., New York, 1996.
10. *Department of Defense World Geodetic System 1984: Its Definition and Relationship with Local Geodetic Systems*, DMA TR8350.2, September 30, 1987.

This page intentionally left blank

A

Fundamental Constants

The following table gives the values of some frequently used constants.

Symbol	Value	Units	Explanation
a	6,378,137.000	m	Semimajor axis of the *WGS-84* ellipsoid
b	6,356,752.314	m	Semiminor axis of the *WGS-84* ellipsoid
f	1/298.257	-	Flattening (*WGS-84*, 1987)
g_o	9.80665	m/sec^2	Gravitational acceleration at sea level
μ	3.986030×10^{14}	m^3/sec^2	Earth gravitational constant
l_c	3.2808400	ft/m	Length conversion
m_c	2.2046226	lb/kg	Mass conversion
R_E	$\sqrt{\mu/g_o}$	m	Earth radius
T_E	86164.09886	sec	Length of a sidereal day
c_o	1116.4(1/lc)	m/sec	Sea-level atmospheric sound speed
p_o	$2116.2(g_o l_c^2/m_c)$	N/m^2	Sea-level atmospheric pressure
ρ_o	1.224949119	kg/m^3	Sea-level atmospheric density
π	3.14159256		Mathematical constant
ω	$2\pi/T_E$	rad/sec	Earth sidereal rotation rate
ω_E	7.292115×10^{-5}	rad/sec	Angular velocity of the Earth
	6076.10	ft/nm	Number of feet per nautical mile

This page intentionally left blank

B

Glossary of Terms

The following celestial mechanics terms are commonly used in deriving the free flight of ballistic missiles.

Anomaly – An angle; for example, eccentric anomaly, mean anomaly, true anomaly.

- *Eccentric Anomaly* – An angle at the center of an ellipse between the line of apsides and the radius of the auxiliary circle through a point having the same apsidal distance as a given point on the ellipse.
- *Mean Anomaly* – The angle through which an object would move at the uniform average angular speed n measured from the principal focus. Commonly, the angle $n(t - t_o)$ is called the *mean anomaly*, where n is the mean motion.
- *True Anomaly* – The angle at the focus between the line of apsides and the radius vector measured in the direction of orbital motion; the angle measured in the direction in which the orbit is described, starting from perihelion.

Aphelion – The point on an elliptical orbit about the sun that is farthest from the sun.

Apoapsis – The point farthest from the principal focus of an orbit in a central force field.

Apogee – The highest point on an *Earth-centered* elliptical orbit. The point of intersection of the trajectory and its semimajor axis that lies farthest from the principal focus.

Apsides (or Line of Apsides) – In an elliptical orbit, the major axis.

Apsis – The point on a conic where the radius vector is a maximum or a minimum.

Celestial Equator – The great circle on the celestial sphere that is formed by the intersection of the celestial sphere with the plane of the Earth's equator. For solar system applications, it is formed by intersection with the ecliptic.

Celestial Horizon – The celestial horizon of an observer is the great circle of the celestial sphere that is everywhere 90° from the observer's zenith.

Celestial Sphere – A sphere of infinite radius with its center at the center of the Earth upon which the stars and other astronomical bodies appear to be projected. This sphere is fixed in space and appears to rotate counter to the diurnal rotation

of the Earth. For solar system navigation purposes, the celestial sphere may be considered to be centered at the Sun.

Colatitude – Defined as $90° - \varphi$, where φ is the latitude.

Coordinates on the Celestial Sphere – Polar coordinates are used in specifying the location of a star or other heavenly body on the celestial sphere. These are the *declination* (δ) and the *right ascension* (*R.A.*).

Declination – The declination of a star is the angular distance north or south, of the celestial equator measured on the celestial sphere.

Earth rate – The angular velocity at which the Earth rotates about its own polar axis. The Earth rate is equal to $15.041°/hr$ or 7.29215×10^{-5} rad/sec.

Ecliptic – The great circle on the celestial sphere that is formed by its intersection with the plane of the Earth's orbit.

Ellipticity – Deviation of an ellipse or a spheroid from the form of a circle or a sphere. The Earth is assumed to have an ellipticity of about 1/297.

Epoch – Arbitrary instant of time for which elements of an orbit are valid.

First Point of Aries (Υ) – Vernal equinox.

Geocentric – Pertaining to the center of the Earth as a reference.

Geocentric Coordinates – Coordinates on the celestial sphere as they would be observed from the center of the Earth.

Geodetic Latitude – Geodetic latitude is defined as the angle between the equatorial plane and the normal to the surface of the ellipsoid. It is the latitude commonly used on maps and charts.

Geodesic Line – The shortest line on the curved surface of the Earth between two points. (see also *Great Circle*).

Geographic – Pertaining to the location of a point, line, or area on the Earth's surface.

Gravity – A vertical force acting on all bodies and mass in or around the Earth. The magnitude of the force of gravity varies with location on the Earth and elevation or altitude above mean sea level. This force will cause a free body to accelerate approximately 32.16 ft/sec^2 (or 9.80665 m/sec^2). (Commonly abbreviated by the letter g.)

Great Circle – A circle on the surface of the Earth, the plane of which passes through the center of the Earth, dividing it into two equal parts. A course plotted on a great circle is the shortest distance between two points on the surface of the Earth and is called a geodesic line.

Hour Circle – A great circle of the celestial sphere that passes through the poles and a celestial body.

Hyperbolic Excess Velocity – In the two-body problem, the relative velocity of the bodies after escape from the mutual potential field.

Nadir – The *nadir* is the point of the celestial sphere 180° from the zenith.

North Celestial Pole – This is the point of intersection of the Earth's axis of rotation with the celestial sphere. In solar system navigation applications, the celestial poles form a line normal to the ecliptic plane while preserving the sense of the north–south orientation.

Orbital Elements – The orbit of a body that is attracted by an inverse-square central force can be specified unambiguously by six elements, which are constants of integration from the equations of motion. These parameters (or orbital elements) define an elliptic orbit in space and are as follows: (1) semimajor axis (a), which specifies the size; (2) eccentricity (e), specifies shape and size; (3) time of perigee passage (T), specifies path position at a given time; (4) orbit inclination angle (i), specifies the orientation of the orbital plane to the equatorial plane ($0 \leq i \leq 180°$); (5) longitude of the ascending node (Ω), specifies the angular distance between the first point of Aries (Υ) and the ascending side of the line of nodes; (6) argument of perigee (ω), an angle that specifies the orientation of the ellipse within its own plane. It should be noted that the definition of these elements may differ from those given in books on celestial mechanics. For example, in these books, the *mean longitude, epoch, mean motion*, and *longitude of perihelion* are also included.

Parameters (Orbit) – Orbital elements.

Parameters (Flight) – Descriptive quantities that define the flight conditions relative to a selected reference frame.

Periapsis – In an elliptical orbit, the apses closest to the nonvacant focus. In an open orbit, the point of closest approach to the orbit center.

Perigee – The point in the orbit of a spacecraft that is closest to the Earth when the orbit is about the Earth.

Perihelion – The point of an orbit about the Sun that is closest to the Sun.

Reference, Inertial Space – A system of coordinates that are unaccelerated with respect to the *fixed* stars.

Retrograde – Orbital motion in a direction opposite to that of the planets in the solar system, that is, clockwise as seen from the north of the ecliptic.

Right Ascension (R.A.) – The right ascension of a star is the angle, measured eastward along the celestial equator, from the vernal equinox to the great circle passing through the north celestial pole and the star under observation. Right ascension is frequently expressed in hours, minutes, and seconds of sidereal time (i.e., 1 hour is equal to 15°) because clocks are used in the terrestrial measurement of right ascension.

Sidereal Hour Angle – The sidereal hour angle of a celestial body is the angle at the pole between the hour circle of the vernal equinox and the hour circle of the body, measured westward from the hour circle of the vernal equinox from 0° to 360°.

Sidereal Day – A sidereal day is the interval of time between two successive transits of the vernal equinox over the same meridian.

$$24^h \text{ sidereal time} = 23^h\ 56^m\ 04.1^s \text{ civil time;}$$

conversely,

$$24^h \text{ civil time} = 24^h 03^m 56.6^s \text{ sidereal time.}$$

Time – In astronomical usage, time is usually expressed as universal time (*UT*). This is identical with Greenwich Civil Time and is counted from 0 to 24 hours

beginning with midnight. A decimal subdivision is often used in place of hours, minutes, and seconds. Thus, the following are all identical:
Nov 30.75 *UT*,
Nov 30; 18^h 00^m *UT*,
Nov 30; 1800 *Z*,
Nov 30; 1:00 *PM EST*.

Topocentric Coordinates – Coordinates on the celestial sphere as observed from the surface of the Earth.

Topocentric Parallax – The difference between geocentric and topocentric positions of a body in the sky.

Vernal Equinox – The point where the Sun appears to cross the celestial equator from south to north. The time of this crossing, when day and night are everywhere of equal length, occurs at about 21 March. Also known as *first point of Aries* and designated by the symbol Υ.

Zenith – The point on the celestial sphere vertically overhead (its direction can be defined by means of a plumb-line).

C

List of Acronyms

A

AA	Air-to-Air (or Anti-Aircraft)
AAA	Antiaircraft Artillery
AAAM	Air-to-Air Attack Management
AAAW	Air-launched Anti-Armor Weapon
AAM	Air-to-Air Missile
AARGM	Advanced Anti-Radiation Guided Missile
AAWS-M	Advanced Antitank Weapons System-Medium
ABICS	Ada-Based Integrated Control System
ABL	Airborne Laser
ABM	Anti-Ballistic Missile (also, Air Breathing Missile)
ABR	Agile Beam fire control Radar (used in the *F*-16's)
AC^{2}ISR	Airborne Command & Control, Intelligence, Surveillance and Reconnaissance
ADOCS	Advanced Digital Optical Control System
AESA	Active Electronically Scanned Arrays
AEW &C	Airborne Early Warning and Control
AFCS	Automatic Flight Control System
AGM	Air-to-Ground Missile (or Air-launched Surface-attack Guided Missile)
AGNC	Adaptive Guidance, Navigation, and Control
AI	Artificial Intelligence
AIM	Air-Interceptor Missile (or Air-launched Intercept-aerial Guided Missile)
ALCM	Air-Launched Cruise Missile
ALS	Advanced Launch System
AMAS	Automated Maneuvering Attack System
AMRAAM	Advanced Medium-Range Air-to-Air Missile (*AIM-120*)
APT	Acquisition, Pointing, and Tracking
ARM	Antiradiation Radar Missile (also Antiradar Missile)

ASARG Advanced Synthetic Aperture Radar Guidance
ASARS Advanced Synthetic Aperture Radar System (seen as *ASARS-2*)
ASM Air-to-Surface Missile (also, Antiship Missile)
ASRAAM Advanced Short-Range Air-to-Air Missile (*AIM-132*)
ASROC Anti-Submarine Rocket
ASW Antisubmarine Warfare
AT Aerial Target
ATA Automatic Target Acquisition
ATACMS Army Tactical Missile System
ATB Advanced Technology Bomber (e.g., *B-2*)
ATBM Anti-Tactical Ballistic Missile
ATC Automatic Target Cueing
ATCSD Assault Transport Crew System Development
ATF Advanced Tactical Fighter
ATIRCM Advanced Threat Infrared Countermeasures
ATR Automatic Target Recognition
ATT Advanced Tactical Transport
AUV Advanced Unitary Penetrator (warheads used in *CALM*s)
AVMS Advanced Vehicle Management System
AWACS Airborne Warning and Control System

B

BAI Battlefield Air Interdiction
BDA Bomb Damage Assessment
BLU Bomb, Live Unit
BMDO Ballistic Missile Defense Organization
BMEWS Ballistic Missile Early-Warning System
BOL Bearing Only Launch
BPI Boost-phase Intercept
BVR Beyond Visual Range

C

CAD Computer-Aided Design
CAINS Carrier Aircraft Inertial Navigation System
CAS Close Air Support
CASOM Conventionally Armed Stand-Off Missile
CAT Cockpit Automation Technology
CBU Cluster Bomb Unit (e.g., *CBU-97 Sensor Fuzed Weapon*)
C^3I Command, Control, Communications, and Intelligence
C^4ISR Command, Control, Communications, Computers, Intelligence, Surveillance, and Reconnaissance
CCD Charged Couple Device
CCIP Continuously Computed Impact Point
CCV Control Configured Vehicle

CEP Circular Error Probable
CEPS Control Integrated Expert Parameter System
CFD Computational Fluid Dynamics
CG Command Guidance
CLOS Command-to-Line of Sight
CM Countermeasures
CNI Communication, Navigation, and Identification
CW Continuous Wave
CWAR Continuous-Wave Acquisition Radar

D

DEW Directed-Energy Weapon
DGPS Differential Global Positioning System
DHEW Directed High-Energy Weapon
DIRCM Directed Infrared Countermeasures
DMA Defense Mapping Agency
DSMAC Digital Scene-Mapping Area Correlation

E

ECM Electronic Counter Measures
ECCM Electronic Counter-Counter Measures
EIS Electronic Imaging System
ELINT Electronic Intelligence
EMD Engineering and Manufacturing Development
EMI/EMP Electromagnetic Interference/Electromagnetic Pulse
EO Electro-Optic
EOTS Electro-Optical Targeting System
ER Extended Range
ESA Electronically Steered Antenna
ESAM Enhanced Surface-to-Air Missile Simulation
EW Electronic Warfare
ERGM Extended-Range Guided Munition (e.g., the US Navy's *EX 171*)

F

FAC Forward Air Controller
FBM Fleet Ballistic Missile
FBW Fly-By-Wire
FCS Flight Control System
FDIR Fault Detection, Identification, Recovery
FEBA Forward Edge of Battle Area
FLIR Forward-Looking Infrared
FMS Flight Management System
FOV Field of View

G

GATS/GAM	Global Positioning System-Aided Targeting System/GPS-Aided Munition
GBI	Ground-Based Interceptor
GBU	Guided Bomb Unit
GLCM	Ground-Launched Cruise Missile
GMTI	Ground Moving Target Indication
GNC	Guidance, Navigation, and Control
GNSS	Global Navigation Satellite System (the European counterpart of the U.S. *GPS*).
GPS	Global Positioning System
GNC	Guidance, Navigation, and Control
GNSS	Global Navigation Satellite System (the European counterpart of the U.S. *GPS*).
GPS	Global Positioning System

H

HAE	High Altitude, long-Endurance (used in connection with *UAV*s)
HARM	High-speed Anti-Radiation (or Antiradar) Missile
HAW	Homing All the Way
HAWK	Homing All the Way Killer (*MIM-23 SAM*)
HDD	Head-Down Display
HEAP	High-Explosive Armor-Piercing (i.e., a shaped-charge warhead)
HEL	High-Energy Laser
HMD	Helmet-Mounted Display
HMS	Helmet-Mounted Sight
HOBA	High Off-Boresight Angle
HOBS	High Off-Boresight System
HOJ	Home on Jam
HOL	Higher Order Language
HPM	High-Power Microwave
HTK	Hit-to-Kill (this high speed technology destroys targets through direct body-to-body contact)
HUD	Head-Up Display

I

ICAAS	Integrated Control and Avionics for Air Superiority
ICNIA	Integrated Communications Navigation Identification Avionics
IF	Intermediate Frequency
IFF	Identification, Friend or Foe

IFFC Integrated Flight/Fire Controls
IFPS Intra-Formation Positioning System
IFTS Internal Forward-looking infrared and Targeting System
IFWC Integrated Flight/Weapon Controls
IIR Imaging Infrared
INS Inertial Navigation System
I/O Input/Output
IOC Initial Operating Capability
IOT&E Initial Operational Test and Evaluation
IR Infrared
IRCCM Infrared Counter-Countermeasures
IRCM Infrared Countermeasures
IRLS Infrared Line Scan
IRSS Infrared Suppressor System
IRST Infrared Search and Track
IRVAT Infrared Video Automatic Tracking
ISAR Inverse Synthetic Aperture Radar (used for target motion detection)
ISR Intelligence gathering, Surveillance, and Reconnaissance
ITAG Inertial Terrain-Aided Guidance

J

JASSM Joint Air-to-Surface Standoff Missile
JAST Joint Advanced Strike Technology
JDAM Joint Direct Attack Munition
JDAM-ER Joint Direct Attack Munitions-Extended Range
JHMCS Joint Helmet-Mounted Cueing System
J/S Jamming to Signal Ratio
JSOW Joint Standoff Weapon
JSTARS Joint Surveillance Target Attack Radar System
JTIDS Joint Tactical Information Distribution System

K

KEW Kinetic Energy Weapon

L

LADAR Laser Radar, or Laser Amplitude Detection And Ranging
LAIRCM Large Aircraft Infrared Measures
LANTIRN Low Altitude Navigation and Targeting Infrared for Night
LASM Land Attack Standard Missile (a US Navy missile launched from the *DDG 51* destroyers and cruisers)
LASS Low Altitude Surveillance System
LGB Laser-Guided Bomb
LLLGB Low-Level LGB

LOBL Lock-On Before Launch (e.g., *Hellfire AGM-114*)
LOCAAS Low-Cost Autonomous Attack System (note: System is also seen as Submunition)
LOS Line-of-Sight
LOV Low Observable Vehicle
LQG Linear Quadratic Gaussian
LST Laser Spot Tracker

M

MALD Miniature Air Launched Decoy
MAP Mission Area Plan
MaRV Maneuvering Reentry Vehicle
MAWS Missile Approach Warning System
MEAD Multidisciplinary Expert-Aided Design
MEMS Micro-Electro-Mechanical Sensors
MFCRS Multi-Function Control Reference System
MIM Mobile Interceptor Missile
MIMO Multi-Input, Multi-Output
MIRV Multiple Independently targetable Reentry Vehicle
Mk Mark (General Purpose Bomb)
MLRS Multiple-Launch Rocket System
MMS Mission Management System
MMW Millimeter Wave
MR Medium Range
MTI Moving Target Indication (or Indicator)

N

NMD National Missile Defense

O

OAS Offensive Avionics System
OTH Over The Horizon

P

PA Pilot's Associate
PBW Power-By-Wire
PGM Precision-Guided Munition
PTAN Precision Terrain Aided Navigation (used in the TacTom or Tactical Tomahawk missile).
PVI Pilot Vehicle Interface

R

RADAG Radar Area Guidance
RAM Rolling Airframe Missile

RCS Radar Cross-Section
RESA Rotating Electronically Scanned Array
RF Radio Frequency
RFI Radio Frequency Interference
RHWR Radar Homing and Warning Receiver
RPV Remotely Piloted Vehicle
RV Reentry Vehicle
RWR Radar Warning Receiver
RWS Range-While-Scan

S

SACLOS Semi-Active Command to Line-of-Sight
SAH Semi-Active Homing
SAM Surface-to-Air Missile
SAR Synthetic Aperture radar
SA/SA Situational Awareness/Situation Assessment
SATCOM Satellite Communications
SCAD Subsonic Cruise Armed Decoy
SDB Small-Diameter Bomb
SDI Strategic (or Space) Defense Initiative
SEAD Suppression of Enemy Air Defenses
SFW Sensor Fuzed Weapon (i.e., this is an unguided gravity weapon)
SIGINT Signal Intelligence (also seen as *Sigint*)
SLAM Standoff Land-Attack Missile
SLAM-ER Standoff Land-Attack Missile – Expanded Response
SLBM Submarine (or Sea)-Launched Ballistic Missile
SLCM Sea-Launched Cruise Missile
SNR Signal-to-Noise Ratio
SOF Special Operations Forces
SRAM Short-Range Attack Missile
SSBXR Small Smart Bomb Extended Range (a *JDAM* spin-off)
SSGNs Nuclear-powered Guided-missile submarines
SSNs Nuclear-powered attack submarines
SSST Supersonic Sea-Skimming Target
START Strategic Arms Reduction Treaty
STOL Short Take-Off and Landing
STOVL Shorts Take-Off and Vertical Landing

T

TADS Terrain Awareness and Display System
TAINS *TERCOM*-Aided Inertial Navigation System
TAMD Theater Air and Missile Defense
TAN Terrain-Aided Navigation
TAP Technology Area Plan

TAWS	Terrain Awareness and Warning System, or Theater Airborne Warning System (this is an *IR* capability)
TBM	Theater Ballistic Missile (also called Tactical Ballistic Missile)
TERCOM	Terrain-Contour Matching
TERPROM	Terrain Profile Matching
TFLIR	Targeting Forward-Looking Infrared
TFR	Terrain-Following Radar
TF/TA^2	Terrain Following/Terrain Avoidance/Threat Avoidance
TGSM	Terminally Guided Sub-Munition
TGW	Terminally Guided Warhead
THAAD	Theater High Altitude Area Defense
TIALD	Thermal Imaging Airborne Laser Designator
TIAS	Target Identification and Acquisition System
TLAM	Tomahawk Land Attack Missile
TMD	Theater Missile Defense (also: Tactical Munitions Dispenser)
TOW	Tube-launched, Optically-tracked, Wire-guided
TRAM	Target-Recognition Attack Multisensor
TSS	Target Sight System (uses focal plane array *FLIR* and *LST*)
T-UAV	Tactical Unmanned Aerial Vehicle
TVC	Thrust Vector Control
TVM	Track-Via-Missile
TWS	Track-While-Scan (a multiple target tracking radar)

U

UAV	Unmanned Aerial (or Air) Vehicle
UCAV	Unmanned Combat Air Vehicle (also seen as "Uninhabited Combat Aerial Vehicle")
UHF	Ultra High-Frequency
URAV	Unmanned Reconnaissance Air Vehicle
URV	Unmanned Research Vehicle
USW	Undersea Warfare

V

VCATS	Visually-Coupled Acquisition and Targeting System
VHSIC	Very High Speed Integrated Circuit
VLS	Vertical Launch System
VLSI	Very Large Scale Integration
VMS	Vehicle Management System
VR	Virtual Reality
VSIM	Virtual Simulator
VSTOL	Vertical/Short Takeoff and Landing
VTAS	Visual Target Acquisition System

W

WCMD	Wind Corrected Munitions Dispenser
WGS	World Geodetic System
WMD	Weapons of Mass Destruction
WVR	Within Visual Range

This page intentionally left blank

D

The Standard Atmospheric Model

For computing drag and thrust, it is necessary to know, as functions of altitude, the Earth's atmospheric pressure, density, and speed of sound. These functions follow from the so-called *ARDC* (Air Research and Development Command, of the U.S. Air Force) model atmosphere, a more accurate model than those used previously (e.g., RAND model). The *ARDC* model assumes that the air from sea level up to an altitude of roughly 300,000 ft (91,440 m) is of constant molecular weight and consists of six concentric layers.

In this appendix, the *ICAO* (International Civil Aviation Organization) standard atmosphere model is used as the flight environment for missiles.

At Sea Level

$T_o =$ temperature (288.1667) [kelvin]
$P_o =$ static pressure (101314.628) [N/m^2]

At altitude z, an approximation to the standard atmosphere is used. The atmosphere is divided into three zones as follows:

(1) $z \leq 11,000\,m$,
(2) $1,000\,m < z \leq 25,000\,m$,
(3) $z > 25,000\,m$.

Different formulas are used to find the ambient atmospheric temperature and pressure, T_a and P_a, in each of the zones.

Zone 1: $z \leq 11,000\,m$

$$T_a = T_o - (0.006499708)z \quad [K], \tag{D.1}$$

$$P_a = P_o(1 - 2.255692257 \times 10^{-5}\, z)^{5.2561} \quad [N/m^2], \tag{D.2}$$

Zone 2: $11,000\,m < z \leq 25,000\,m$,

$$T_a = 216.66666667 \quad [K], \tag{D.3}$$

$$P_a = P_o(0.223358)\{\exp[-1.576883202 \times 10^{-4}(z - 11000)]\}\ [N/m^2]. \tag{D.4}$$

Zone 3: $z > 25,000\,m$,

$$T_a = 216.66666667 + (3.000145816 \times 10^{-3})(z - 25000) \ \ [K], \tag{D.5}$$

$$P_a = (2489.773467)\{\exp[-1.576883202 \times 10^{-4}(z - 25000)]\}\ [N/m^2]. \tag{D.6}$$

In all three zones, the ambient atmospheric density and the speed of sound are given by

$$\rho_a = P_a / RT_a \ \ [kg/m^3], \tag{D.7}$$

$$V_a = 20.037673\sqrt{T_a} \ \ [m/sec], \tag{D.8a}$$

where R is the gas constant (286.99236 [(N-m)/(K_p-K)]. Note that the speed of sound V_a, can also be calculated from the relation

$$V_a = kRT, \tag{D.8b}$$

where

$k =$ the ratio of specific heat of the gas ($= 1.4$ for air),
$R =$ gas constant ($= 286.99236$[(N-m)/(Kp -°K)]),
$T =$ absolute temperature for the standard atmosphere.

ICAO Standard Atmosphere Input/Output:

The input to the atmosphere model is

$z =$ altitude of interest $[m]$.

The output from the model is

$T_a =$ ambient atmospheric temperature at altitude z $[K]$,
$P_a =$ ambient atmospheric pressure at altitude z $[N/m^2]$,
$\rho_a =$ ambient atmospheric density at altitude z $[kg/m^3]$,
$V_a =$ speed of sound at altitude z $[m/sec]$.

While not a factor in some studies, altitude can be an important consideration. As altitude increases, density decreases, leading to a lower dynamic pressure for a given speed. This leads to lower drag, so that missile deceleration is less pronounced, but it also leads to lower moments and forces, so the missile loses some maneuverability. Also, since the speed of sound is a function of altitude, the missile Mach number for a given speed depends on altitude. Missile aerodynamic properties (e.g., drag coefficient, lift coefficient, and moment coefficient) depend on Mach number and so will change with altitude, giving different missile aerodynamic responses.

Pressure, temperature, air density, and speed of sound are calculated using pressure curve fits and temperature gradients derived from the 1962 standard atmosphere data. The input altitude and the calculated atmospheric conditions are all in

metric units. Four data tables of the 1962 U.S. standard atmosphere data are used to calculate the atmosphere parameters: temperature, temperature gradient, pressure, and corresponding reference altitudes. Table D.1 shows these four data tables combined [1]. These tables are referenced using altitudes expressed in geopotential meters. One geopotential meter is defined as the vertical distance through which a one-kilogram mass must be moved to increase its potential energy by 9.80665 joules [2]. Thus, a given input altitude h in geometric meters is converted to altitude H in geopotential meters using the expression [2]

$$H = [R_E/(R_E + h)]h, \tag{D.9}$$

where

$H =$ geopotential altitude,
$h =$ geometric altitude,
$R_E =$ radius of the Earth $= 6,356,766\,m$ corresponding to 45° latitude on a nonperfect spherical Earth model.

Table D.1. *1962 U.S. Standard Atmosphere* Data Tables

Altitude H $[m]$	Temperature T $[K]$	Temp. Gradient ΔT $[K]$	Pressure P $[N/m^2]$
0.0	288.15	− 0.0065	101325.000
11,000.0	216.65	0.0	22632.000
20,000.0	216.65	0.0010	5474.8700
32,000.0	228.65	0.0028	868.0140
47,000.0	270.65	0.0	110.9050
52,000.0	270.65	− 0.002	59.0005
61,000.0	252.65	− 0.004	18.2099
79,000.0	180.65	0.0	1.0377
90,000.0	180.65	0.003	0.16438
100,000.0	210.65	0.005	3.0075E-2
110,000.0	260.65	0.010	7.3544E-3
120,000.0	360.65	0.020	2.5217E-3
150,000.0	960.65	0.015	5.0617E-4
160,000.0	1110.65	0.010	3.6943E-4
170,000.0	1210.65	0.070	2.7926E-4
190,000.0	1350.65	0.005	1.6852E-4
230,000.0	1550.65	0.004	6.9604E-5
300,000.0	1830.65	0.0033	1.8838E-5
400,000.0	2160.65	0.0026	4.0304E-6
500,000.0	2420.65	0.0017	1.0957E-6
600,000.0	2590.65	0.0011	3.4502E-7
700,000.0	2700.65	0.0	1.1918E-7

As stated in the beginning of this appendix, the *ARDC* model atmosphere assumes that the air from sea level to roughly 300,000 ft consists of six concentric layers. Within each layer, the gradient of the absolute temperature τ with respect to the geopotential altitude H is assumed constant. From (D-9), the gradient $d\tau/dH$ within each layer is given in Table D.2.

Table D.2. Absolute Temperature Gradient for Different Layers

Layer	Gradient $(d\tau/dH)$ [$^\circ R/ft$]	Altitude Range [ft]
I	-3.566×10^{-3}	$0 < H < 36,089$
II	0	$36,089 < H < 82,021$
III	1.646×10^{-3}	$82,021 < H < 154,199$
IV	0	$154,199 < H < 173,885$
V	-2.469×10^{-3}	$173,885 < H < 259,186$
VI	0	$259,186 < H < 295,276$

The air density ρ decreases exponentially with altitude within the isothermal layers. That is,
Layers II, IV, VI:

$$\rho = C_1\, e^{-pH}. \tag{D.10}$$

Layers I, III, V:

$$\rho = C_2 \tau^{-k}, \tag{D.11}$$

where C_1, C_2, p, and k are constant within a given layer.

Table D.3 shows documented atmospheric data for a 1976 U.S. standard atmosphere in metric units [3].

Table D.3. *1976 U.S Standard Atmosphere* Data in Metric Units

Geopotential Altitude [m]	Pressure [N/m^2]	Density [kg/m^3]	Speed of Sound [m/sec]	Temperature [K]
0.0	101,325.0	1.2250	340.3	288.2
5,000.0	54,019.0	0.73612	320.5	255.7
10,000.0	26,436.0	0.41271	299.5	223.2
15,000.0	12,044.0	0.19367	295.1	216.7
20,000.0	5,475.0	0.088035	295.1	216.7

References

1. *Handbook of Chemistry and Physics*, 55th edition, Chemical Rubber Company, 1974, page F-191.
2. *Handbook of Geophysics and Space Environment*, 1985, pp.14–17.
3. *Airplane Aerodynamics and Performance*, Roskam Aviation and Engineering Corporation, 1981, page 13.

This page intentionally left blank

E

Missile Classification

In much the same manner as aircraft, missiles are typed by their general characteristic grouping. Such a grouping may show in what manner a missile is used, but it will not identify a particular missile. This general classification makes use of three items: (1) launch environment, (2) target environment (or mission), and (3) type of vehicle. These classifications will now be discussed in more detail.

Launch Environment: Launch environment may be air, ground, underground, or underwater. Thus the letters are ***A*** for air, ***G*** for ground, ***L*** for underground, and ***U*** for underwater. A more complete designation of missile launch environments is as follows:

A - Air
B - Multiple
C - Coffin
F - Individual
G - Ground
H - Silo stored
L - Silo launched
M - Mobile
P - Soft pad
R - Ship
U - Underwater.

Examples of this general classification are as follows:

AIM - Air-Interceptor Missile
AGM - Air-to-Ground (or Surface) Missile
LGM - Silo-launched Surface-to-Surface Missile
UGM - Underwater-to-Surface Missile.

A more typical example is as follows:

ADM - 20***A***,

where ***A*** implies "air," ***D*** "decoy," ***M*** "guided missile," the 20 implies the "20th design," and *A* the "A series."

Target Environment (or Mission): The second letter is used to designate the target environment or mission. This letter may be ***I*** for interceptor, ***G*** for surface target, or ***Q*** for drone. The complete mission designation symbols are as follows:

D - Decoy
E - Special electronic
G - Surface attack
I - Intercept
Q - Drone
T - Training
V - Underwater attack
W - Weather.

Type of Vehicle: The third letter designates the type vehicle as follows:

M - Guided missile
N - Probe
R - Rocket.

Status: The status designation symbols are as follows:

J - Special test, temporary
N - Special test, permanent
X - Experimental
Y - Prototype
Z - Planning.

In addition to the general designator for missile identification, additional items of information may be included as follows:

1. Status prefix
2. Launch environment
3. Primary mission
4. Vehicle type
5. Vehicle design number
6. Vehicle series
7. Manufacturer's code
8. Serial number.

More specifically, missile designators, when the occasion warrants, will have a status prefix symbol but not necessarily a launch environment symbol. For example, a typical designator is shown below for an early *Minuteman* missile (***JLGM-30BO03***). Note that it contains eight items of essential information:

J - Status prefix
L - Launch environment
G - Mission symbol
M - Vehicle type symbol
30 - Design number
B - Series symbol
BO - Manufacturer's code
03 - Serial number.

Tables E.1 through E.3 give more complete designations.

Table E.1 shows the various methods of protecting, storing, and launching a military rocket or guided missile. Rocket systems employed for line-of-sight (LOS) fire against ground targets are not included. Some typical examples of missile designators are given in this table.

Note that several missiles are designed for similar tasks; only the method of launching differs. This similarity is noted by the second symbol with the missile designator. These tasks or missions are given in Table E.2 along with their characteristic identifying letter and description.

Table E.1. Launch Environment Symbols

1st Letter	Title	Description	Example
A	Air	Launched from aircraft while in flight.	*AGM-45A* (Shrike)
B	Multiple	Capable of being launched from more than one environment.	*BQM-34A* (Firebee)
C	Coffin	Horizontally stored in a protective enclosure and launched from the ground.	*CGM-13B* (Mace)
F	Individual	Carried by one man.	*XFIM* (Redeye)
H	Silo Stored	Vertically stored below ground level and launched from the ground.	*HGM-25A* (Titan)
L	Silo Launched	Vertically stored and launched from below ground level.	*LGM-30G* (Minuteman III)
M	Mobile	Launched from a ground vehicle or movable platform.	*MIM-23A K* (Hawk)
P	Soft Pad	Partially or nonprotected in storage and launched from the ground.	*PGM-17A* (Thor)
R	Ship	Launched from a surface vessel such as a ship or barge.	*RIM-46A* (Sea Mauler)
U	Underwater	Launched from a submarine or other underwater device.	*UGM-27C* (Polaris)

Table E.3 shows the types of vehicles that have a combat-related mission. The last two items of a missile designator are the design number and series symbol. The same design number identifies each vehicle type of the same basic design. Where more than one design is present for a single vehicle type, consecutive design numbers are assigned. When major modifications are present in a vehicle type, then a sequential

Table E.2. *Mission* Symbols

2nd Letter	Title	Description	Example
D	Decoy	Vehicles designed or modified to confuse, deceive, or divert enemy defenses by simulating an attack vehicle.	*ADM-20A* (Quail)
E	Special Electronic	Vehicles designed or modified with electronic equipment for communications, countermeasures, electronic radiation sounding, or other electronic recording or relay missions.	*XFEM-43B* (Redeye)
G	Surface Attack	Vehicles designed to destroy enemy land or sea targets.	See Table E-1
I	Intercept-Aerial	Vehicles designed to intercept aerial targets in defensive or offensive roles.	*AIM-9E* (Sidewinder)
Q	Drone	Vehicles designed for target, reconnaissance, or surveillance purposes.	*BQM-34A* (Firebee)
T	Training	Vehicles designed or permanently modified for training purposes.	*ATM-12B* (Bullpup)
U	Under water Attack	Vehicles designed to destroy enemy submarines or other underwater targets.	*UUM-44A* (SUBROCK)
W	Weather	Vehicles designed to observe, record, or relay data pertaining to meteorological phenomena.	*PWN-5A*

letter (e.g., *A*, *B*) indicates each modification. For example, the latest version (as of this writing) or modification of the *Sidewinder* air interceptor missile is the *AIM-9X* (see Table F.2).

In addition to the launch environment, mission, and vehicle type, the status is also used (see also Appendix F). The status prefix designations are listed in Table E.4.

Table E.4 presents the joint electronics type designation system (*JETDS*) used in US military electronic equipment. An example for this type of designation is shown below.

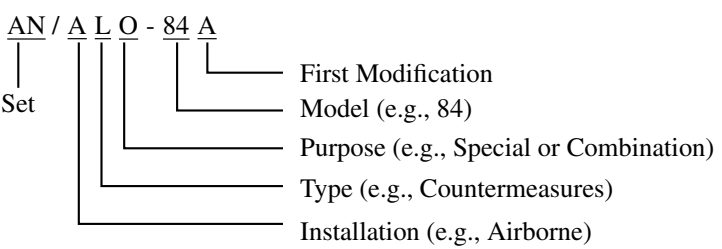

Table E.3. Vehicle Type Symbols

3rd Letter	Title	Description	Example
M	Guided Missile	As the third letter in a missile designator, it identifies an unmanned, self-propelled vehicle. Such a vehicle is designed to move in a trajectory or flight path that may be entirely or partially above the Earth's surface. While in motion, this vehicle can be controlled remotely or by homing systems, or by inertial and/or programmed guidance from within. The term "guided missile" does not include space vehicles, space boosters, or naval torpedoes, but it does include target and reconnaissance drones.	See Table E.2
N	Probe	The letter *N* is used to indicate nonorbital-instrumented vehicles that are not involved in space missions. These vehicles are used to penetrate the space environment and transmit or report back information.	None
R	Rocket	This identifies a self-propelled vehicle without installed or remote control guidance mechanism. Once launched, the trajectory or flight path of such a vehicle cannot be changed.	*AIR-2B* (Super Genie)

Aerial Targets, Drones, and Decoys:

We conclude this appendix by listing some of the better-known *aerial targets* and *decoys*.

MQM-107D/E Streaker:

This is a jet-powered recoverable, variable-speed target drone. The third-generation *D* model is a recoverable, variable-speed target drone used for *RDT&E* (research, development, test, and evaluation) and weapon system evaluation, while the fourth-generation *E* model with improved performance is now operational. The guidance and control system is either underground control or preprogrammed flight, and has high-*g* autopilot provisions. The *MQM-107D/E*'s speed is 230–594 mph, operating at an altitude of 50–40,000 ft, with an endurance of 2 hr, 15 min. The *IOC* (initial operating capability) was in 1987.

Table E.4. Status Prefix Symbols

Letter	Title	Description
J	Special Test, Temporary	Vehicles on special test programs by authorized organizations and vehicles on bailment contract having a special configuration to accommodate the test. At completion of the test, the vehicles will be either returned to their original configuration or returned to standard operational configuration. Example: *J85-GE-7* turbojet engine.
N	Special Test, Permanent	Vehicles on special test programs by authorized activities and vehicles on bailment contract whose configurations are so drastically changed that return of the vehicles to their original configurations is beyond practicable or economical limits.
X	Experimental	Vehicles in a developmental or experimental stage, but not established as standard vehicles for service use. Example: Army's *Nike Zeus XLIM-49A*.
Y	Prototype	Preproduction vehicles procured for evaluation and test of a specific design.
Z	Planning	Vehicles in the planning or predevelopment stage.

BQM-34A Firebee:

The *Firebee* is also a jet-powered, variable-speed, recoverable target drone. Initial development of the *BQM-34A* drones was in the early 1950s (*IOC* was circa 1951), and was used to support weapon system and *RDT&E* (research, development, test, and evaluation). A microprocessor flight control system provides a prelaunch and in-flight test capability. The guidance and control methods include choice of radar, radio, active seekers, and an automatic navigator. The maximum speed of the *BQM-34A* drone is 690 mph at 6,500 ft. Current *BQM-34A*s have been updated with General Electric *J85-100* engines, and are used for weapon system evaluation. The latest version of the *Firebee* is the *BQM-34 M/L*.

BQM-74C:

These target drones were used as decoys during the Persian Gulf War.

Q-4:

The *QF-4* is a converted, remotely piloted *F-4 Phantom* fighter aircraft, used for full-scale training and/or testing purposes. The *QF-4* replaces the *QF-106* as a joint

Table E.5. Joint Electronics Type Designation System

Installation	Type	Purpose
A Piloted Aircraft	*A* Invisible light, heat radiation	*B* Bombing
B Underwater mobile sub-marine	*C* Carrier	*C* Communications
D Pilotless carrier	*D* Radiac	*D* Direction finder, reconnaissance and/or surveillance
F Fixed ground	*G* Telegraph or teletype	*E* Ejection and/or release
G General purpose use	*I* Interphone and public address	*G* Fire-control or Searchlight directing
K Amphibious	*J* Electromechanical or Inertial wire covered	*H* Recording and/or Reproducing
M Mobile (ground)	*K* Telemetering	*K* Computing
P Portable	*L* Countermeasures	*M* Maintenance and/or Test assemblies
S Water	*M* Meteorological	*N* Navigation aids
T Transportable (ground)	*N* Sound in air	*Q* Special or combination of purposes
U General utility	*P* Radar	*R* Receiving, passive detecting
V Vehicular (ground)	*Q* Sonar and underwater sound	*S* Detecting and/or range and bearing
W Water surface and under water combination	*R* Radio	*T* Transmitting
Z Piloted–pilotless vehicle combination	*S* Special or combinations of types	*W* Automatic flight or Remote control
	T Telephone (wire)	*X* Identification and Recognition
	V Visual and visible light	
	W Armament	
	X Facsimile or television	
	Y Data processing	

service full-scale aerial target, and uses an improved flight control system and has a greater payload. Guidance of the *QF-4* consists of multifunction command-and-control multilateration system.

QF-106:

The *QF-106* is a converted, remotely piloted Convair *F-106A Delta Dart* fighter used for full-scale training or testing. With a service ceiling of 50–55,000 ft, the *QF-106* has a range of 575 miles. Its power plant is a 24,500 lb thrust (with afterburning) Pratt & Whitney *J75-P-17* turbojet.

In addition to the aerial targets and decoys, there are a number of *reconnaissance and surveillance* aircraft:

RQ-1A, B, L Predator:

This is a medium-altitude, long-endurance *UAV* (unmanned aerial vehicle), flown remotely and controlled from the ground. It is envisioned primarily as a reconnaissance platform. More specifically, the *Predator* is a fire-and-forget, inertial guided system designed to strike targets from 17 m (55.78 ft) to 600 m (1968.6 ft) either by direct attack or by flying over the target and shooting at the most vulnerable aspect in an attack profile, known as fly-over, shoot-down mode. Navigation is accomplished by *GPS/INS*. It cruises at 75 mph (it can reach 90 mph) an altitude of 10,000–15,000 ft (with a ceiling of 25,000 ft), and has a range of about 500 nm. Note that the *Predator* must fly as high as 25,000 ft to avoid shoulder-fired weapons. Moreover, the *Predator* can cover mobile targets from a 15,000-ft slant range for at least 24 hours. This *UAV* has already demonstrated its capability during surveillance missions over Bosnia and in Operation Allied Force in the skies above Kosovo, Yugoslavia, where it collected intelligence data and searched for targets. The *Predator* can stay in the air for 40 hours, loitering over dangerous areas, and is equipped with *EO/IR* and *SAR* sensors with a K_u-band (12–18 GHz range) satellite data link allowing real-time transmissions of video images to a ground station (i.e., it sends back real-time video images to commanders of what it is observing). In the Afghanistan conflict, live video was transferred from the *Predator* (*RQ-1B*) to *AC-130 gunships* and real-time retargeting of heavy bombers. The *Predator* can also spot buried land mines, even newer plastic versions that elude other radars. Pilots fly the aircraft remotely from vans at their base, using controls found in a normal cockpit. (Note that one problem with controllers mentioned is the limited field of view.)

More recently, the Air Force's *Predator UAV* program is beginning to evolve from a nonlethal reconnaissance asset to an armed, highly accurate tank-killer. On February 16, 2001, an inert *Hellfire-C* (for more information on the *Hellfire* missile see Table F.3) laser-guided missile using its *LOS* communication band and *IR* laser-ball was successfully launched from a *Predator UAV* at the Nellis AFB, Nevada. It aimed and struck the turret of a stationary tank from an altitude of 2,000 ft (610 meters) and a range of 3 miles (4.83 km) as part of a Phase I feasibility demonstration. On February 21, 2001, two more successful test launches were made. The *Predator* successfully aimed and launched a live *Hellfire-C* laser-guided missile that struck an unmanned stationary Army tank. General Atomics Aeronautical Systems, Inc. redesigned two of its *UAV*s as *Predator-Bs (MQ-9)* with a turboprop engine. The enhanced aircraft would be able to carry eight *Hellfire* missiles, rather than only two in the current system. It would also fly several times faster and could reach an altitude of 45,000–52,000 ft. Phase II of the program will take the *Predator–Hellfire* combination to more realistic operational altitudes and conditions, including the challenge of a moving target. The *Predator B* will also be equipped with a multispectral targeting system for its newest support role: "hunter–killer."

The *DoD* has further expanded the payload options for the *Predator*, demonstrating its ability to launch other, smaller, *UAV*s and deliver weapons just beyond the laser-guided *Hellfire* missile. More specifically, on the initiative of the Defense Threat Reduction Agency (*DTRA*) and the Naval Research Laboratory, the *Predator*

can be used as a mother ship to launch other smaller *UAV*s, namely, the *Finder* (flight inserted detector expandable for reconnaissance). The *Finder* is a 57-lb, *GPS*-guided system that can carry different sensors; the *Predator* can carry one *Finder* under each wing. During tests in August 2002 at Edwards AFB, California, the *Predator* launched one *Finder* from 10,000-ft altitude. The flight lasted 25 min, and the aircraft was monitored by the *Predator* ground station. The *Finder* can be equipped with various payloads, including an atmospheric sampling sensor or an imagery sensor to conduct reconnaissance in heavily defended areas prior to attack. The *Finder* is less expensive and harder to detect than the *Predator*, so it could more easily fly into heavily defended areas without incurring a significant loss if shot down.

Since its first flight on July 3, 1994, the *RQ-1A Predator UAV* program reached a major milestone, 50,000 flight hours, on October 26, 2002, during an operational sortie.

In addition to the RQ-1 model, that is used for reconnaissance, there is a multirole Predator designated MQ-1, that is used as an unmanned strike platform. On March 22, 2003, during Operation Iraqi Freedom, the MQ-1 Predator found and destroyed an Iraqi ZSU-23-4 radar guided mobile anti-aircraft artillery gun outside the southern Iraqi town of Al Amarah using an AGM-114K Hellfire II missile.

RQ-4A Global Hawk:

Global Hawk is a high-altitude, long-endurance, unmanned, multiple battlefield applications reconnaissance *UAV*. *Global Hawk* is designed to operate at high altitudes for long periods of time, giving battlefield commanders accurate, near-real-time high-resolution imagery of areas as large as 40,000 square miles (e.g., the size of Illinois). With a 116-foot wingspan, the 44-foot-long 15-foot-high *UAV* can range as far as 13,500 nautical miles up to 65,000 feet mean sea level (*MSL*), gathering vital battle space data. That makes *Global Hawk* the world's most advanced high-altitude, long-range remotely operated aircraft. The *UAV* is designed to have 42-hr endurance with airspeed of approximately 335 knots, and carrying a 1-ton payload, and 900-lb of dedicated communications. (Note that the *Global Hawk* can stay aloft for almost two days). Specifically, the *Global Hawk* has the capability to capture and deliver images from SAR, EO, signals intelligence (*SIGINT*), and *IR* sensors to ground controllers from 65,000 feet with its 48-in K_u-band *Satcom* antenna in all types of weather, day or night. That is, once airborne, it can be controlled from the ground and can see the movements of enemy assets and personnel with startling clarity and near-real time accuracy. The *Global Hawk*'s ground surveillance mission could be expanded to include air surveillance and targeting. Navigation is by *GPS/INS*. Once mission parameters are programmed and loaded into the mission computer, *Global Hawk* can carry out the entire mission autonomously (i.e., the vehicle flies autonomously from takeoff to landing). More specifically, the aircraft's "pilots" stay on the ground. Its flight control, navigation, and vehicle management are independent and based on a mission plan. That means that the airplane flies itself: There is no pilot on the ground with a joystick maneuvering it around. However, it does get instructions from airmen at ground stations. The launch and recovery element provides precision guidance for

takeoff and landing, using a differential global positioning system (*DGPS*). That team works from the plane's operating base. At another ground station, airmen in the mission control element tell *Global Hawk* where to go and where to point its sensors to get the best images. The *Global Hawk* is being considered to take over the duties of the manned *U-2S* aircraft. The *Global Hawk* entered *EMD* on March 6, 2001. Two production *Global Hawk* aircraft are expected to be delivered to the Air Force by the contractor (Northrop Grumman's Ryan Aeronautical Center) in fiscal 2003. The Air Force is planning a series of upgrades to turn the *Global Hawk* into a true multi-intelligence collector. Modifications will include making wing stations functional for extra payloads, including *SAR* and multispectral sensors.

Specifically, the Block 10 *Global Hawk*'s *IOC* is for the year 2009, and will include a huge array of sensors such as a sophisticated synthetic aperture radar, moving target indicator, electrooptical and infrared sensors, and high-rate satellite and line-of-sight data link systems. To use them properly and gather the best information, it must fly above 40,000 feet. That way the craft can get a good slant range.

Since its first flight in February 1998, *Global Hawk* has flown 74 times, logging a total of 884.7 hours as of April 5, 2001. Currently there are five U.S. Air Force *Global Hawks*. The USAF's *Global Hawk* made aerospace history as the first *UAV* to fly unrefueled 7,500 miles (12,067.5 km) across the Pacific Ocean from America to Australia. Departing from the AF Flight Test Center at Edwards AFB, California, April 22, a *Global Hawk* named *Southern Cross II* flew 23 hours, 20 minutes, and arrived April 23 at 8:40 P.M. local time at the RAAF Air Base Edinburgh, near Adelaide. While in Australia for six weeks, *Global Hawk* will fly 12 missions, demonstrating its ability to perform maritime and littoral surveillance for the RAAF, USAF, Canadian Navy, U.S. Navy and Marine Corps, and U.S. Coast Guard units participating in the allied exercise *Tandem Thrust 01*.

The per-unit cost of a *Global Hawk*, without sensors, is projected to range from $16 million to $20 million.

Dark Star:

The *Dark Star* is a low-observable *UAV*, intended to operate in high-threat environments at altitudes in excess of 45,000 ft for at least 8 hours, 575 miles from the base. Navigation is via *GPS/INS*. Cruise speed is 300 mph with a flight endurance of 12 hours. The vehicle flies autonomously from takeoff to landing, providing near real-time imagery information for tactical and theater commanders. Furthermore, the vehicle was designed to monitor a mission area of 18,500 square miles using a recon/optical *EO* camera or an *SAR*, transmitting primarily fixed-frame images while in flight. This program was terminated in January 1999.

UCAV:

In the spring of 2001, the Pentagon flight-tested the *UCAV* (unmanned combat air vehicle), a bomb-dropping version of the pilotless spy/reconnaissance planes that

circled over Kosovo in 1999. Expected *IOC* is for 2010, assuming that Congress allocates the necessary funds for *RDT&E*.

Unlike fighter aircraft that can pull up to 8 *g*'s, the *UCAV* can withstand only 3–5 *g*'s. It uses off-the-shelf engines, sensors, and other parts. Therefore, without a pilot, a *UCAV* would require far less protective gear, avionics, and other pilot-support systems. However, future *UCAV*s are expected to perform maneuvers, such as 18-*g* turns, that human pilots cannot withstand.

The *UCAV*'s primary mission is focused on suppressing enemy air defenses (*SEAD*), that is, take out enemy *SAM*s and other defenses, as well as conducting strike missions. Moreover, controllers, rather than pilots, will monitor as many as four *UCAV*s from a ground station. The *UCAV*s will be programmed to fly a preset flight path or to loiter over heavily defended areas looking for targets. The *UCAV* is the most advanced and futuristic application for *UAV*s that will perform high-risk combat missions. The *UCAV* could be made stealthy and autonomous using inertial guidance.

Most recently, the Air Force's *UCAV* has been redesigned. Specifically, the vehicle will be much larger and heavier than the first design. The redesign is intended to narrow the gap between initial prototypes and an operational system. The first prototype, the *X-45A UCAV* technology demonstration, completed its first flight on May 23, 2002, at Edwards AFB, California, reaching an airspeed of 195 knots at an altitude of 7,500 feet (2,286 meters). The 14-minute flight was a key step in providing a transformational combat capability for the Air Force. Moreover, this first flight successfully demonstrated the *UCAV*'s flight characteristics and the basic aspects of aircraft operations, particularly the command and control link between the aircraft and its mission-control station. A second *X-45A*, the *Red Bird*, is nearly completed and will begin flight test demonstrations in 2003. This will lead to multiaircraft (pack) flight-test demonstrations in 2003. Eventually, *UCAV*s will fly in packs, searching for enemy antiaircraft missile launchers and working together to destroy them under the supervision of a human operator, who, as stated above, could be located anywhere in the world. Beginning in the summer of 2003, into early 2004, demonstrations for weapons delivery will begin. Culminating in 2006, testing will eventually include *UCAV*s and manned aircraft operating together during an exercise. Boeing (the developer of the vehicle) and *DARPA* (Defense Advanced Research Projects Agency) updated the design to prepare for production of the more operationally representative system, the *X-45B*. The *X-45B* will be a fieldable prototype aircraft, laying the foundation for an initial operational system toward the end of this decade. Moreover, the *X-45B* will incorporate low-observable technologies and will be larger and more capable than its predecessor.

The basic concept for *UCAV* will be a four-ship pack under the command of a battle manager, who will have the situational awareness to command and control the vehicles. In the 2007–2008 time frame, the *UCAV* will begin to perform its mission, achieving the preemptive destruction of enemy air defense targets.

In order to improve the aerodynamic performance, the *X-45B*'s wing area and fuselage length have increased. For example, the wing area grew by 63%, and the fuselage, 11%. The total vehicle is now 24% larger. In addition, the redesign increases

the length of the *UCAV*'s internal weapons bay by 21 in to 168 in. This should allow the aircraft to carry six *SDB*s internally and give the *UCAV* the same size bay as the *JSF*. Changes also will be made to the propulsion system. The airframe has been expanded to accept a turbofan with a 26-in-diameter fan, versus the 24-in version presently used. The increase should boost the thrust by 7% and elevate the *UCAV* into the 7,000-lb-thrust class. *UCAV*s with early-model directed-energy weapons would target air defense missiles and radar sites.

The U.S. Navy is also exploring the possibility of using *UAV*s. However, the Navy wants a more capable *UCAV* than the Air Force. It is requesting an airborne surveillance capability, in addition to the *SEAD*/strike role. The Navy version would feature conformal apertures operating a *UHF* radar, the same frequency used by the *E-2C*. Furthermore, it would include a narrow-field-of-view *SAR/GMI* radar, which is also on the *USAF* system to refine bombing coordinates and conduct poststrike battle damage assessment. The Navy's air vehicle is expected to have an empty weight of 6,000–12,000 lb. Mission endurance may vary depending on the mission. While a strike mission may last 5–6 hr, a surveillance mission would likely last 9–12 hr. In addition, the Navy is looking into the possibility of first- and second-generation vertical takeoff unmanned aerial vehicles (*VTUAV*). The performance requirements for a first-generation *VTUAV* are modest. With a payload of 200–300 lb, the aircraft is to operate at 6,000 ft and above to provide *LOS* electrooptical data transmission and command and control links. However, the requirements stiffen for generation two, which must deliver antisurface weapons by the year 2020. Specifically, the first-generation *VTUAV*s would add precision targeting for naval surface fires, wide-area data relay, chemical or biological warfare, reconnaissance, and a search capability for combat search and rescue. Second-generation *VTUAV*s, expected to be available after 2012, would add five more capabilities: (a) strike warfare, (b) antiair warfare detection, (c) offboard mine detection, (d) long-range communications intercept, and (e) overwater search capabilities. It is expected that *VTUAV* requirements will rise rapidly after the year 2010 with increasing deliveries of *DD-21*-class destroyers.

In addition to the *UAV* efforts described above, the U.S. Navy is exploring the possibility of controlling small tactical *UAV*s from submarines for the long-term goal of using them to clandestinely find targets ashore and attack them with cruise missiles. The relatively small 12-ft (3.66-m) wingspan, 100-lb (45.36-kg) vehicle would carry a color video camera to collect imagery that can be transmitted to the submarine by a 100-nm (185.3-km)-range *UHF* data link. Toward this end, the Navy is using on an experimental basis the *Dakota* air vehicle. The *Dakota* is serving as a surrogate air vehicle for a future operational system. The Navy would like to field a submarine-launched, expendable *UAV* that could stay airborne for 12 hr. Moreover, the *Dakotas*, used primarily for reconnaissance, may deploy a network of ground sensors and act as a relay between the submarine and the sensors ashore. The *Dakota* is an autonomous air vehicle using *GPS* guidance and would not have required updates unless commanders wanted to alter the flight plan. Northrop Grumman also is developing a submarine-launched surveillance *UAV* concept. Once a mission plan

was uploaded on the *UAV*, the submarine would have been in a receive-only mode in order to avoid detection through its emissions. For a future tactical version, the payload would be refined with a limited automatic target recognition system. Rather than transmitting all video to the submarine, the *UAV* would broadcast imagery only after recognizing a target to reduce bandwidth demands. It would also use digital communications rather than the analog data link used in the demonstration. Finally, in order to preserve covertness, the Navy is willing to make the system expendable.

The U.S. Army is also studying the possibility of using its *Shadow 200* tactical unmanned aerial vehicle (*T-UAV*) for signal intelligence, or *Sigint*. In this initial stage of the program, only an *EO/IR* sensor is considered as a baseline payload. Sensors will be required to collect signals in the 20–2,000-MHz region. Operationally, the *Sigint-UAV* is intended to support brigade commanders. Locating an emitter would be the primary role for the payload. Anticipated *IOC* for the program is in the year 2007.

EADS (European Aeronautic Defense and Space Co.) is studying a design for a *URAV* in the 1,500-kg (3,307-lb) takeoff weight class. The *URAV* will be 5.5-meters (21-ft) long with a 4.1-meter (13.5-ft) wingspan and have low-observable requirements. The *URAV* would operate similarly to a recoverable cruise missile with a data link to a ground control station.

It is conceivable that future strike forces will include a mix of unmanned combat air vehicles and manned aircraft. *UCAV*s offer such strengths as persistence, expandability and stealth.

Miniature Air Launched Decoy (MALD):

DARPA (Defense Advanced Research Projects Agency) is in the process of transferring the *MALD* technology demonstration follow-on program to the Air Force's lethal *SEAD* program office. *MALD* is being developed to provide Air Combat Command with the ability to achieve air superiority by confusing enemy air defense systems. The 91-in (2.31-m) decoy is designed to fly autonomously to simulate the mission profiles of typical fighter aircraft with the ability to maneuver through high-*g* turns, climbs, and dives. *MALD* is equipped with a signature augmentation subsystem, which provides active augmentation to the vehicle's radar cross section across *VHF*, *UHF*, and microwave frequencies to replicate a tactical fighter when viewed by enemy radar systems.

A *MALD* variant (or derivative) is a supersonic miniature air-launched interceptor *(Mali)* to defeat cruse missiles. It is being built by *DARPA*, which also sponsored *MALD*'s development. *Mali* would be cued by a surveillance aircraft, such as an *E-3 AWACS*, which would provide target updates while the interceptor flies supersonically toward a target that could be as far away as 200 nm (371 km). Once close to the cruise missile, *Mali* would activate its *Stinger* seeker and engage the target from the rear at subsonic speeds. (The USAF terminated the *MALD* program in January 2002.)

Other nations are also involved in *R&D* of *UAV*s. For example, Saab Aerospace (Avionics and Dynamics Division) is conducting wind tunnel tests of a low-signature *UAV* designed for attack missions under the framework of Sweden's National

Aeronautics Research Program. Other areas being studied include (a) production engineering, (b) propulsion systems, (c) strength, (d) radar, and (e) *IR* signatures and weapons separation. Finally, *NATO* countries operate a number of *UAV*s such as the *Exdrome* and *Hunter*.

F

Past and Present Tactical/Strategic Missile Systems

F.1 Historical Background

Immediately following the closing phase of *World War II*, and in particular in 1950 with the involvement in the Korean conflict, the United States embarked on a crash program of missile research and development. Some of these missiles, in particular those developed in the years 1950–1964, are listed in Table F.1.

Most of these missiles are no longer in current inventories. They are presented here from a historical perspective. Those that still are in the inventory, for example the *Sidewinder* and *Sparrow III*, have advanced state-of-the-art guidance systems. Therefore, all of the missile programs that have come and gone have served as a basis for the constantly improving research and development programs for the current missiles.

The research program is a continuing process, not only for the production of missiles, but also for the many individual system components. The program of component research is based on realizing major aims and overcoming problems that are inherent in the development of dependable solid-rocket motors that provide reliable high-altitude, supersonic operation.

Some of the earlier (1947–1956) USAF/ARMY guided missile *popular names* are the following:

Guided Missile	*Name*
TM-61B	Matador
SM-62	Snark
GAM-63	Rascal
SM-64	Navaho
SM-65	Atlas
GAM-67	Crossbow
IM-99 (69)	Bomarc
GAR-1	Falcon
SAM-N-6	Talos (Army/Navy)
SAM-A-7	Nike (Army)
SSM-A-17	Corporal (Army).

Table F.1. Missile Development 1950–1964

Missile System and Designation	Guidance System	Propulsion System	Service
TITAN I (*HGM-25A*)	Radio–Inertial	Liquid rocket	Air Force
TITAN II (*LGM-25C*)	Inertial	Liquid rocket	Air Force
ATLAS (*CGM-16D*) (*HGM-16F)*	Radio–Inertial	Liquid rocket	Air Force
MATADOR (*MGM-1C*)	Radar–Command and Hyperbolic	Turbojet	Air Force
MACE (*MGM-13A*)	Map-matching	Turbojet	Air Force
MACE (*CGM-13B)*	Inertial	Turbojet	Air Force
MINUTEMAN (*LGM-30A, B, F*)	Inertial	Solid propellant	Air Force
BOMARC (*CIM-10A*, and *10B*)	Radar–homing	Ramjet	Air Force
FALCON (*AIM-4A, C, E, F*), (AIM-26A, 47A)	Radar and Infrared Homing	Solid propellant	Air Force
GENIE (*AIR-2A*)	Free-flight	Solid propellant	Air Force
QUAIL (*ADM-20C*)	Gyro–autopilot	Turbojet	Air Force
HOUND DOG (*AGM-28*)	Inertial	Turbojet	Air Force
DAVY CROCKET	Free-flight	Solid propellant	Army
ENTAC (*MGM-32A*)	Wire-guided	Solid propellant	Army
HONEST JOHN (*MGR-1*)	Free-flight	Solid propellant	Army
LITTLE JOHN (*MGR-3A*)	Free-flight	Solid propellant	Army
PERSHING (*MGM-31A*)	Inertial	Solid propellant	Army
HAWK (*MIM-23A*)	Radar-homing	Solid propellant	Army
SERGEANT (*MGM-29A*)	Inertial	Solid propellant	Army
SHILLELAGH (*MGM-51A*)	Command	Solid propellant	Army
NIKE-HERCULES (*MIM-14B*)	Command-tracking Radar	Solid propellant	Army
POLARIS (*UGM-27*)	Inertial	Solid propellant	Navy
REGULUS (*RGM-6*)	Inertial	Turbojet	Navy
SUBROC (*UUM-44A*)	Inertial	Solid rocket	Navy
TALOS *ARM* (*RIM-8E, RGM-8H*)	Beam-rider homing	Ramjet	Navy
TARTAR (*RIM-24B*)	Beam-rider	Solid propellant	Navy
TERRIER (*RIM-2E*)	Beam-rider homing	Solid propellant	Navy
SHRIKE (*AGM-45A*)	Radar-homing	Solid propellant	Navy
SIDEWINDER 1-C (*AIM-9D*)	IR homing	Solid propellant	Navy, AF
SPARROW III-6B (*AIM-7E*)	Homing	Solid propellant	Navy, AF
BULLPUP (*AGM-12B*)	Radio command	Solid propellant	Navy, AF
BULLPUP (*AGM-12C*)	Radio command	Liquid propellant	Navy, AF

Tables F.2 through F.7 summarize the development and classification of some of the modern U.S. tactical/strategic guided weapon systems. However, it should be noted that some of these have been phased out and replaced with more advanced state-of-the-art guidance and propulsion systems. Reliability of the guidance systems is always a primary subject for research. The major effort is for improvement of components of inertial systems, microelectronics, star trackers, and radar and infrared homing systems. The introduction of lasers, fiber optics, the global positioning system, etc., opened up a new field for highly accurate guidance systems as demonstrated in *Operation Desert Storm* in 1991, and in Yugoslavia in 1999. For more details on past and present guided weapons, the reader is referred to [2],[3],[4].

Table F.2. Air-to-Air Guided Missiles

Missile System and Designation	Guidance System	Speed	Range	Remarks
Sparrow III (*AIM-7*) Variants: *AIM-7C IOC*: 1958; *AIM-7E IOC*: 1963; *AIM-7F IOC*: l976; *AIM-7M IOC*: 1983; *AIM-7P IOC*: 1990	Radar-guided. Inverse monopulse semiactive radar homing seeker.	Mach 4^{+}	30 nm (56 km)	The *Sparrow III* is a radar-guided medium-range *AAM* with all-weather, all-altitude, and all-aspect offensive capability that has been in service for more than 40 years. The missile has been completely redesigned with new and improved guidance, warhead, and longer range.
Sidewinder (*AIM-9*) Variants: *AIM-9A, 9B, 9H, 9J, 9L/P, 9M,* and *9X*.	*IR* homing; *IIR*.	Mach 2^{+}	10 nm (18.5 km)	The *Sidewinder* is an *AAM* used by many western nations. It is used in the *F-15C, F/A-18*, and *F-14*'s. The *AIM-9X Sidewinder II* is the newest variant of the *Sidewinder* heat-seeking *AAM*; it is a replacement for the *AIM-9M*. The *AIM-9X* is a high-agility *IIR* missile that uses thrust vector control for additional maneuverability instead of tail-control. The *AIM-9X* provides *BVR* and short-range *HOBS* attack capabilities and is designed to work with the *JHMCS*.

(Continued)

Table F.2. *(Continued)*

Missile System and Designation	Guidance System	Speed	Range	Remarks
Phoenix (*AIM-54*) Variants: *AIM-54A IOC* 1974 *AIM-54B* not produced *AIM-54C IOC 1986* *AIM-54C*$^{+}$ *IOC* 1990	Semiactive radar homing for midcourse; pulse–Doppler radar for the terminal phase.	Mach 5	110 nm (204 km)	This is a U.S. Navy *AIM* that is used as part of the *F-14 Tomcat* weapon system.
AMRAAM (*AIM-120*) Variants: *AIM-120A, B*, and *C*	*TWS* multiple target tracking radar; inertial reference before launch; midcourse and terminal phase updates.	≈ Mach 4	40 nm (74.1 km)	The *AMRAAM* is an *AAM* that uses an active radar seeker. *The AIM-120C* is an improved version. An unguided *AIM-120C* missile was successfully tested and launched from an *F/A-22* for the first time on October 24, 2000, at Mach 0.9 and 15,500 ft (4,724 m). The *C* version was developed specifically for internal carriage on the *F/A-22*. Later versions are expected to carry a multispectral seeker to better spot the small radar altimeter and *IR* signatures of stealthy cruise missiles.

Table F.3. Air-to-Surface Guided Missiles

Missile System and Designation	Guidance System	Speed	Range	Remarks
Shrike (*AGM-45A*)	Semiactive radar-homing guidance.	Mach 2	10 nm (18.53 km)	The *Shrike* is an air-to-surface, anti-radar missile, based on the *AIM-7 Sparrow AA* missile. The missile was first used in combat in Vietnam in 1966, and deployed on *F-4Gs, F-16C, D, F/A-18s*, and Israeli *F-4s* and *Kfirs*. The *Shrike* is being replaced by the *AGM-88C HARM*.
Maverick (*AGM-65*) Variants: *AGM-65 A, B, D, E, F* (Navy version) *G, H,* and *K*.	Various variants of the *Maverick* use *TV*-guidance, laser guidance, and *IIR*.	Mach 1-2	3000-ft. to 12 nm (914-m to 22.2 km)	The *Maverick* is configured for antitank and antiship roles.
SRAM I (*AGM-69A*), and SRAM II (*AGM-113*)	Inertial.	Mach 2.5	100 nm at high altitude, 35 nm at low altitude (186 km – 65 km).	The *SRAM*'s payload possesses a nuclear capability. The *SRAM II* was canceled after Congress stopped funding it.
Standard Arm (*AGM-78*) Variants: *AGM-78A, B, C*, and *D*.	Passive radar homing direct and proximity fuzes.	Mach 2.5	18.4–34.8 nm (30–56 km)	This is an air-launched weapon based on the shipboard *RIM-66A SM-1* surface-to-air missile. It was developed to supplement the *AGM-45 Shrike*.

(Continued)

Table F.3. *(Continued)*

Missile System and Designation	Guidance System	Speed	Range	Remarks
Harpoon *AGM-84A/C/D/G R/UGM-84A/C/D/G* (Submarine-launched).	Uses a 3-axis *ARA* (attitude reference assembly) to monitor the missile's relation to launch platform. In addition, it uses a *BOL* when the range to the target is known. Sea-skimming cruise monitored by radar altimeter, active radar terminal homing. Uses an active radar-homing seeker.	Mach 0.85	75–80 nm (139–148 km) 150 nm (278 km for the RGM-84F)	These series of *Harpoons* are long-range sea-skimming antiship missiles; they can be launched from bombers, ships, submarines, and coastal defense platforms. Like the French (Aerospatiale) *Exocet* and the Norwegian (Kongsberg) *AGM-119 Penguin* short-range antiship missiles, the *Harpoon* is a "fire and forget" weapon. In addition to the Navy aircraft, the *Harpoon* has also been deployed from *B-52G* aircraft. (See also Table F.6).
Air-Launched Cruise Missile *(AGM-86B)*	Inertial plus *TERCOM*.	Mach 0.6	1,555 miles (2,502 km)	A small, subsonic, winged air vehicle, currently deployed on *B-52H* aircraft, which is equipped with a nuclear warhead.
Conventionally armed Air-Launched Cruise Missile (*AGM-86C/D*)	*GPS/INS*	Mach 0.6	1,600 miles (2,574 km)	A nonnuclear version of the *AGM-86B*, the *conventionally* armed *air-launched cruise missile* (*CALCM*) was first used operationally during the Persian Gulf War. The 3,150 lb. *CALCM* has a 2,000-lb high-explosive warhead that throws out a spray of metal balls,

(Continued)

Table F.3. *(Continued)*

Missile System and Designation	Guidance System	Speed	Range	Remarks
				making it most useful for soft targets such as *SAMs*, *SAsM* launchers, radar antennas, and radar command vans. Its accuracy is similar to that of the *Tomahawk*.
HARM (*AGM-88*) Variants: *AGM-88A, B*, and *C*.	All-aspect, passive radar homing. The *AGM-88C Block IV* has a more sensitive seeker.	Mach 2^+	10 nm (18.53 km)	The *HARM* was developed as a replacement for the *AGM-45 Shrike* and *AGM-78* standard antiradiation missile (*ARM*). See also Section 3.4.3. An advanced technology demonstration program, called the *AARGM*, will combine a wide-band passive antiradiation multimode seeker with an active *MMW* terminal guidance system and precision *GPS/INS* navigation. The *AARGM* is intended to hit a target after it stops radiating.
AGM-88E	*GPS/INS*	Mach 3.5–4.5	100 miles	The U.S. Navy is developing the *AGM-88E* with a dual mode *AARGM* (advanced antiradiation guided missile) seeker. This includes a *W*-band *MM* wave sensor and greater field-of-regard. The *HARM* upgrade is to include a variable-flow ducted rocket ramjet engine.

(Continued)

Table F.3. *(Continued)*

Missile System and Designation	Guidance System	Speed	Range	Remarks
Hellfire (*AGM-114*) Variants: *AGM-114A, K, L*, and *M*.	Laser-guided. Some *Hellfire* variants use *IIR, RF/IR*, and an *MM* wave seeker. The laser seeker works in conjunction with a laser target designator.	Mach 1.1	4.3 nm (8 km)	The *Hellfire* is a U.S. Army antitank air-to-ground missile launched from attack helicopters (e.g., the *AH-64A* Apaches). A later version, the *Hellfire II*, was developed in 1997 as an antiship missile. It is armed with a blast fragmentation warhead designed for attacks on ships, buildings, and bunkers. The weapon penetrates the target before detonation.
Sidearm (*AGM-122*)	Passive radar-homing with broadband seeker.	Mach 2.5	9.6 nm (17.79 km)	The *Sidearm* is a short-range antiradar missile. It is an inexpensive self-defense missile used by the U.S. Marines, and is used in fixed-wing and rotary-wing aircraft.
Advanced Cruise Missile *(AGM-129A/B)*	Inertial with *TERCOM* updates.	Mach 0.9	$\approx 2,000$ nm (3,700 km)	This is a stealthy, long-range air vehicle, with a nuclear warhead. Deployed on *B-52H* aircraft, it has improved range, accuracy, and targeting flexibility compared with the *AGM-86B*. This program was canceled in Nov. 1991. The *IOC* was scheduled for circa 1992.

(Continued)

Table F.3. *(Continued)*

Missile System and Designation	Guidance System	Speed	Range	Remarks
AGM-130 Variants: *AGM-130A* (Currently in production with an Mk 84 warhead). *AGM-130C* (Currently in production with a *BLU-109/B* penetrating warhead).	*TV* or *IIR*. Later versions include improved *TV* and *IR* seekers, and *GPS/INS* guidance that permit operation in adverse weather and target acquisition.	Subsonic	N/A	This is a rocket-powered air-to-surface missile carried by the *F-15* fighters, and is designed for high-and low-altitude strikes at standoff ranges against heavily defended hard targets. The pilot-guided *AGM-130* weapon, which was used in air strikes against Iraq and Yugoslavia, adds a radar altimeter and digital control system, providing it with triple the standoff range of the *GBU-15*. *IOC* was in 1994.
AGM-142 Have Nap	Inertial with data link, *TV*, or *IR* homing.	Subsonic	50 miles (80 km)	This is a medium-range, standoff air-to-surface guided missile carried by AF heavy bombers (*B-52H*), built by Rafael (Israel). The warhead is a high-explosive, 750-lb-class blast/fragmentation or penetrator. *IOC* was in 1992.
AGM-154 Joint Standoff Weapon (JSOW) Variants: *AGM-154A Baseline* configuration carries 145 *BLU-97A/B* cluster bombs	Tightly coupled *GPS/INS* for midcourse, *IIR* terminal guidance.	Subsonic	17 miles (27 km) from low altitudes; 40 miles (64 km) from high-altitude launch.	This is an air-to-surface guided missile. First in a joint USAF and Navy family of low-cost, highly lethal glide weapons with a standoff capability, usable against heavily defended soft targets (e.g., radar

(Continued)

Table F.3. *(Continued)*

Missile System and Designation	Guidance System	Speed	Range	Remarks
or submunitions, and is intended against relatively *soft* targets. *AGM-154B* is loaded with six *sticks* of *BLU-108/B* sensor-fuzed submunition arrays. *AGM-154C* carries the same *BLU-111/B* 500-lb unitary warhead used in the Mk 82 *iron bombs*.	Tightly coupled *GPS/INS* for midcourse, *IIR* terminal guidance.	Subsonic	17 miles (27 km) from low altitudes; 40 miles (64 km) from high-altitude launch.	antennas, launchers, and control vans). *JSOW* allows for integration of several different submunitions and unitary warheads, nonlethal payloads, various terminal sensors, and different modes of propulsion into a common glide vehicle. *IOC*: Navy 1998, USAF 2000. The *B-2* will use both the *JSOW* with bomblets and a second version with the *BLU-108* antiarmor submunition. The *JSOW* is intended for use in the *F/A-18s* and *F-16* fighters.
AGM-158 JASSM	*GPS/INS, IIR*	Mach 0.6–0.8	300 nm (556 km)	This is a conventional AF/Navy missile program. After previous failures, the missile was successfully flight tested on Nov. 20, 2001, at the Army's White Sands Missile Range. The missile was fired from an *F-16* flying about 15,000 ft at Mach 0.8. New design changes include a new *IIR* seeker, new missile control unit, and the addition of selective availability antijam GPS receiver. The first aircraft to field *JASSM* (or *Jassm*) will be the *B-52* in 2003. The Navy plans to use the missile on the *F/A-18s*.

Table F.4. Surface-to-Air Guided Missiles.

Missile System and Designation	Guidance System	Speed	Range	Remarks
Stinger (*FIM-92*) Variants: *FIM-92A, C*, and *D*.	Proportional navigation, with lead bias all aspect automatic passive *IR* homing.	Mach 1^{+}	3 miles (4.8 km)	The *Stinger* is a U.S. Army shoulder-fired short-range *SAM* with a maximum altitude of 9,840 ft (3,000 meters). *Stingers* of other countries are: The French *Mistral*, and Russian *SA*-7, -14, -16, and -18. (For more information, see Section 4.1.)
Nike Hercules (*MIM-14*)	Command guidance.	Mach 3.65	75 nm (140 km)	This is an Army *SAM* that is no longer in production.
Hawk (*MIM-23*) Variants: *MIM-23B*, and Improved (*I-HAWK*)	Proportional navigation guidance coupled with *CW* and semiactive terminal homing.	Mach 2.5	21.6 nm (40 km)	The *Hawk* is a *SAM* whose *IOC* was in August 1960. The missile can reach an altitude of 60,000 ft. The *Hawk*'s warhead is a conventional *HE* blast/fragmentation with proximity and contact fuzes. The *Hawk* is used by more than 20 foreign nations.
Chaparral (*M48*) (Also designated as *MIM-72C*)	Launched from an *M54* launcher. The launcher has a *FLIR* thermal-imaging system with automatic target tracking and *IFF*. The missile has passive *IR* homing with radar proximity fuze.	Supersonic.	3.2 nm with a maximum altitude of 9,843 ft (3,000 m).	This is a short-range *SAM* system. It is a modified *AIM-9 IR* homing missile. Target acquisition and postlaunch tracking are accomplished by the missile's *IR* seeker, giving it a *fire and forget* capability.

(Continued)

Table F.4. *(Continued)*

Missile System and Designation	Guidance System	Speed	Range	Remarks
Patriot (*MIM-104*) Variants: *PAC-1, 2, 3*	*TVM* terminal guidance; semiactive monopulse seeker.	Mach 3–4	43 nm (80 km)	The *Patriot* is a new generation of medium-to-high altitude *SAM*s developed as an area defense weapon to replace the *Nike–Hercules* missile. The *Patriot (PAC-3)* is commonly classified as an antitactical ballistic missile (*ATBM*) defense system. For more details, see Section 6.9.1.
Sea Sparrow (*RIM-7M*)	Semiactive *CW* radar homing.	Mach 2.5	12 nm (22.24 km)	This is a U.S. Navy surface-to-air missile.
Standard *SM-1*MR (*RIM-66B*)	Semiactive homing (*SAR*).	Mach 2^+	25 nm (46.3 km)	This is a Navy MR (medium range) *SAM* that can reach an altitude of 60,000 ft. It is a replacement for the *Talos*, *Terrier*, and *Tartar* missiles.
Standard *SM-2*MR (*RIM-66C*)	Inertial navigation with 2-way communication link for midcourse guidance from warships; semiactive homing radar.	Mach 2^+	Block I: 40 nm (74 km). Block II: 90 nm (167 km).	This is a Navy vertical launch system intended for the *Aegis* missile system.
Standard *SM-2*ER (*RIM-67A/B*), and *67C/D*.	Inertial navigation with 2-way communication link for midcourse guidance from warships.	Mach 2^+	75–90 nm (139–167 km).	This ER (extended range) version has improved resistance to *ECM*.

(Continued)

Table F.4. *(Continued)*

Missile System and Designation	Guidance System	Speed	Range	Remarks
Standard *SM-2*AER (*RIM-67B*)	Same as *RIM-66C*	-	-	This is the latest variant in the *Aegis Extended Range* (AER) missile program using *VLS*. The Navy is also developing the *SM-3*. This is a ballistic missile interception system as part of the *Midcourse System* (formerly known as Navy Theater Wide) ballistic missile defense program (see also Section 6.9.1).
Rolling Aiframe Missile (*RIM-116*)	The *RAM* switches to *IR* homing during the terminal phase; initially uses *RF* to home on target emissions to point its *IR* seeker at the target. (Passive dual mode *RF/IR* target acquisition.)	Supersonic	N/A	The *RAM* (rolling airframe missile) is a short-range *SAM*. It is a U.S. Navy *fire and forget* missile.

Table F.5. Antitank Guided Missiles.

Missile System and Designation	Guidance System	Speed	Range	Remarks
TOW (*BGM-71*) Variants: *TOW/BGM-71AIOC*: 1970 *ITOW/BGM-71CIOC*: 1982 *TOW2/BGM-71DIOC*: 1984 *TOW2A/BGM-71EIOC*: 1987 *TOW2B/BGM-71FIOC*: 1992	Wire-guided optical semiautomatic *CLOS* and automatic IR tracking. Also, the *TOWs* use thermal night sight and *EM*/optical/magnetic proximity sensor.	Mach 0.8–0.9	2.33 miles (3.75 km).	The *TOW* is the most widely used antitank guided missile. It is fired from rotary-wing aircraft and ground-combat vehicles. Many countries around the world use the *TOW* as a standard antitank weapon. The *ITOW* (improved *TOW*) added a telescoping standoff detonation probe. The *TOW2B* entered service in 1992. The *TOW* was used in Vietnam, *Operation Desert Storm*, and by the Iranian forces against Iraqi tanks during the 1980–1988 *Gulf War*.
Hellfire (*AGM-114A*)	Laser-guided; also using *IIR* and *RF/IR*.	Mach 1.1	4.3 nm (8 km)	See Table F.3 for details.

Table F.6. Antiship Guided Missiles.

Missile System and Designation	Guidance System	Speed	Range	Remarks
Harpoon (*AGM-84*) Variants: *AGM-84A/C/D/G*. *R/UGM-84/A/C/D/G* (Submarine-launched).	3-axis *ARA* to monitor the missile's relation to launch platform.	Mach 0.85	75–80 nm (139–148 km)	For a detailed description of the *Harpoon*, see Table F.3. The *Harpoon* is being improved under the Block 2 effort.
Slam (*AGM-84E-1*)	Variants of the *SLAM* use either single-channel *GPS* receiver, *IIR* seeker, *man-in-the-loop* terminal guidance, 3-axis *ARA*, or terminal homing *IIR* seeker. The *SLAM* navigates to the target area using a preloaded mission profile updated by real-time *GPS* data.	Mach 0.85	60 nm (111 km)	The *SLAM* is a derivative of the *Harpoon*. Used in the *A-6E, F/A-18, F-16*, and *B-52* aircraft.
Slam ER (*AGM-84H*)	Adaptive terrain following, a passive seeker, and precise aim-point control.	Mach 0.90	> 150 nm (278 km)	The air-launched *SLAM-ER*, an evolutionary upgrade to the *AGM-84E SLAM*, is designed to strike high-value fixed land targets, as well as ships at sea or in port. Moreover, the *SLAM-ER* has an improved penetrating warhead to strike its target with precision and lethality. It also has provisions for installation of automatic target recognition. The wings of the *AGM-84H* can be folded so that it can be mounted on the pylon of an *F/A-18E/F Super Hornet* strike fighter.

Table F.7. Surface-to-Surface Ballistic Missiles

Missile System and Designation	Guidance System	Speed	Range	Remarks
ATACMS (MGM-140) Variants: Block 1, 1A, and 2	*GPS/INS*	N/A	Block 1: 89 nm (165 km) Block 1A: 162 nm (300 km) Block 2: 78 nm (144.5 km)	This is a U.S. Army long-range tactical missile for deployment in modified *M270* armored vehicle-multiple rocket launchers (*AVMRL*). *ATACMS* is a semiballistic missile that uses an *M74* warhead. Launch can be as much as 30° off axis. The missile is steered aerodynamically by electrically actuated control fins during descent, modifying the flight path from a ballistic parabola.
Tomahawk (BGM-109A) Variants: *Tactical Tomahawk* (or Block 4)	Uses the global positioning system, inertial and *TERCOM* guidance. Other variants use *DSMAC*, inertial/terminal active radar homing, or inertial/*TERCOM*.	Mach 0.5–0.70	250–1350 nm (464–2500 km)	The *Tomahawk* is a long-range cruise missile that can be launched vertically from both surface ships and submarines against both ships and land targets. Initially known as *SLCM*, the *Tomahawk's* principal roles are antiship, land attack with conventional warhead (*TLAM-C*), and land attack with a nuclear warhead (*TLAM-N*).

(Continued)

Table F.7. *(Continued)*

Missile System and Designation	Guidance System	Speed	Range	Remarks
				The *Block 4 TLAMs* use *GPS* guidance and have an accuracy of 10–15 meters (32–50 feet) CEP.
Minuteman Variants: *Minuteman I (LGM-30A/B)* *Minuteman II (LGM-30F)* *Minuteman III (LGM-30G)*	Inertial guidance with post-boost control and stellar/inertial.	Speed at burnout is more than 15,000 mph at the highest point of the trajectory.	6,950 nm (12,875 km)	The *Minuteman* is a land-based, long-range *ICBM*; it consists of 2 solid-state stages while the third stage is a liquid-propellant using fuel-injection thrust vector control. The *Minuteman* was the first *ICBM* using *MIRV*. The warhead consists of 3 Mk 12/12A *MIRVs*.
Peacekeeper (*LGM-118A*)	Inertial guidance. Stellar/inertial. Advanced inertial reference sphere (*AIRS*) *IMU* developed by Rockwell Autonetics Division. The *MIRVs* are deployed on the ballistic trajectory phase.	N/A	More than 7,000 nm (11,118 km).	The *Peacekeeper* was developed to replace the *LGM-30 Minuteman ICBM*. It is also known as *MX*. This is a 4-stage solid-propellant *ICBM* using *MIRVs* in the post-boost vehicle. The payload of the *LGM-118A* consists of 10 Mk 21 *MIRVs*. The missile can be moved around to protect it from preemptive attack.

(Continued)

Table F.7. *(Continued)*

Missile System and Designation	Guidance System	Speed	Range	Remarks
				The *Peacekeeper* will be scheduled for retirement under the provisions of the *START II* treaty.
Trident I *C-4* (*UGM-96A*)	Stellar-inertial guidance.	N/A	4,000 nm (7,412 km)	The *Trident I* is an *SLBM* ballistic missile. As is the case with the *MX*, the *C-4* uses a *MIRV* payload.
Trident II *D-5* (*UGM-133A*)	Dormant stellar-inertial guidance.	N/A	More than 6,000 nm (11,118 km).	This is an advanced version of *Trident I*, having a *hard target* kill capability.
Titan II First Launch: April 1964 (*NASA's Titan II-Gemini*). *IOC*: Sept. 5, 1988 (USAF). Variants: *TITAN I* *TITAN IVA* *TITAN IVB*	Inertial guidance.	N/A	N/A	A modified *ICBM* used to launch military, classified, and *NASA* payloads into space. The *Titan* family was established in October 1955. It became known as the *Titan I*, the nation's first two-stage and first silo-based *ICBM*.

F.2 Unpowered Precision-Guided Munitions (*PGM*)

In this section we will discuss the role of the precision-guided bomb, or *GBU*-series. Historically, the unpowered *Paveway Bomb Series*, known as *Paveway I, II* and *III PGMs*, is based on the Mk 80 low-drag general-purpose unguided bomb series that was developed in the 1950s (see also Section 5.6). Specifically, the *Paveway* family (or series) consists of electronic guidance units and fin kits that attach to the nose and tail of standard 500-lb (226.8-kg), 1,000-lb (453.6-kg), and 2,000-lb (907.2-kg) conventional Mark-series bombs. The guidance unit includes a control section, computer, and laser detector. All weapons within a *Paveway* series (e.g., all *Paveway IIs*) use the same electronics package, but the wing assembly, canards, and structure are tailored to the particular bomb size. The *Paveway IIs* were designated *GBU-10E/B* (Mk 84), -12*E*/*B* (Mk 82), and -16*C*/*B* (Mk 83), and *Paveway III* as *GBU-24A/B* (Mk 84) and *GBU-27*. (Note that the *Paveway IIs* are laser-guided bombs.) The lessons learned from the *GBU-10* series and *GBU-15* precision-guided weapons systems assisted in developing the U.S. Air Force's rocket-powered *AGM-130* standoff land-attack missile [3]. (Note that the *AGM-130* is a powered version of the *GBU-15* that has been heavily used against the well-protected portions of the integrated air defense systems of both Iraq and Yugoslavia since the beginning of 1999; the *AGM-130* uses *TV* guidance and has a range of 30 miles; see also Table F.3.)

Among the best known of these *GBUs* (guided bomb unit) is the *GBU-15*. The *GBU-15* glide bomb can be fitted with two types of warheads, either the Mk 84 2,000-lb blast-fragmentation bomb or the *BLU-109* deep-penetrating bomb. The blast fragmentation warhead is used for attacks on conventional buildings, air-defense weapons, aircraft, and radar sites, while the penetrator is aimed at reinforced aircraft hangars, command and control bunkers, and other hardened targets.

During the 1990–1991 Persian Gulf *Operation Desert Storm*, the *GBU-15* glide bomb with *IR* and *TV* guidance was used with great effect by *F-111F* pilots against Iraqi targets. Specifically, during *Operation Desert Storm*, the *GBU-15s* were dropped from *F-111s* destroying targets from a standoff range of 16–20 nm. Given this standoff range, *F-15E Strike Eagle* fighters can launch these glide bombs outside the lethal envelope of most antiaircraft missiles.

Development of the *GBU-15* began in 1974, based on experience gained in Vietnam with the earlier *Pave Strike GBU-8* modular weapon program. As a result of the *Operation Allied Force* in the air war against Yugoslavia, the U.S. Air Force will modify the *GBU*-series of glide bombs to enable them to hit targets through heavy clouds. In particular, the *Enhanced GBU-15* (or *EGBU-15*) air-to-ground guided munitions, applicable to the *F-15E* aircraft, is likely to be the first in a series of inexpensive, rapid-response modifications planned by the Air Force to refit a range of weapons that will allow autonomous launch in all weather conditions. That is, as the first in a series of programs to give laser-guided bombs an adverse-weather capability, the *USAF* has begun equipping the *GBU-15* glide bombs with *GPS*-satellite guidance. The guidance kit, which is similar to those used in *JDAM* (note that the *JDAM* is a low-cost strap-on guidance kit with *GPS/INS* capability, which converts existing unguided free-fall bombs into accurately guided smart

weapons, thus improving the aerial capability for existing 1,000- and 2,000-lb bombs) gravity bombs dropped by the *B-2 Spirit* bombers, will allow the *Enhanced GBU-15* glide bomb to strike within a few feet of its aimpoint, even through a heavy layer of clouds. The system uses reference signals provided by the navigation satellites (i.e., *GPS*). The *EGBU-15* successfully completed its first Phase II program weapon drop test at the Eglin AFB range in August 2000. An *F-15E* launched the weapon at 25,000 ft at a speed of 530 knots (roughly 609 mph), 17.8 miles from the target location [1]. The weapon received a significant upgrade in its ability to attack in all weather conditions using the *GPS*. Moreover, the weapon can carry either a 2,000-lb Mk 84 blast fragmentation warhead or a *BLU-109* penetrating warhead, and can be guided by either television or an *IR* seeker. It has a nominal standoff range of 15 nautical miles, the ability to lock on after launch mode, and high precision against critical targets.

Note that the all-weather attack *GBU-32 JDAM* uses *GPS/INS* to home in on its target with a high degree of accuracy (better than 6 meters (19.68 ft)). Each *JDAM* carries a 1,000-lb or 2,000-lb warhead and can destroy or disable military targets within a 40-foot radius of its point of impact. Furthermore, *JDAMs* can be dropped from more than 15 miles from the target, with updates from *GPS* satellites guiding the bombs to their target. A *B-1B* bomber can carry 24 *JDAMs*. The 1-ton *JDAM* can be selected for air-burst, impact, or penetrating mode. A typical *B-1B* mission might involve targets such as airplane shelters, bridge revetments, or command bunkers. The *B-1B's* use of *JDAMs* became operational in 1999 (see also Section 5.12.2).

As mentioned above, the *GPS* is being applied to a broad range of weapons, such as the *GBU-32 JDAM* (see Table F.8). Specifically, the use of *GPS* will improve the overall performance and accuracy of laser-guided bombs; that is, *GPS* will improve its resistance to laser jamming or clouds interrupting the laser beam. The updated *GBUs* can conduct blind bombing against preloaded *GPS* coordinates. For example, if the laser spot disappears because of a cloud cover or is obscured because of jamming, then guidance temporarily reverts to the *GPS* coordinates. In the near future, *JDAMs* will be equipped with an *FMU-152 A/B* turbine alternator and *FZU-55 A/B* fuze mechanism. The fuze and alternator will allow pilots to reprogram the *JDAM* during a mission.

In addition to the *GBU-15*, other candidate weapons include the *GBU-24* (a 2,000-lb, laser-guided bomb used by the *F-15E* and *F-16*), *GBU-27*, and *EGBU-27* (a laser-guided bomb designed for the *F-117A Nighthawk* stealth fighter), and the *GBU-28* (a 5,000-lb bomb designed to penetrate deep bunkers). A variant of the *GBU-24* guided hard-target penetrator bomb, the *GBU-24E/B*, is used by the Navy's *F-14D Tomcats*. The *GBU-24E/B*, a 2,200-lb (998-kg) bomb, adds *GPS* guidance to the existing laser guidance of the Navy's *GBU-24B/B* baseline. Specifically, the *E/B* first heads toward a *GPS* target point, and the laser designator can refine that point or steer the bomb toward a different target. Figure F.1 illustrates a *Paveway III GBU*.

Another type of bomb is the *GAM-113*. The *GAM-113* is a near-precision, deep-penetration bomb. The 5,000-lb *GAM-113* employs a follow-on version of the *GATS/GAM* guidance package now used with *2,000-lb* bombs. The *GPS/INS* tail kit gives the weapon an all-weather, day/night, and launch-and-leave capability, plus a

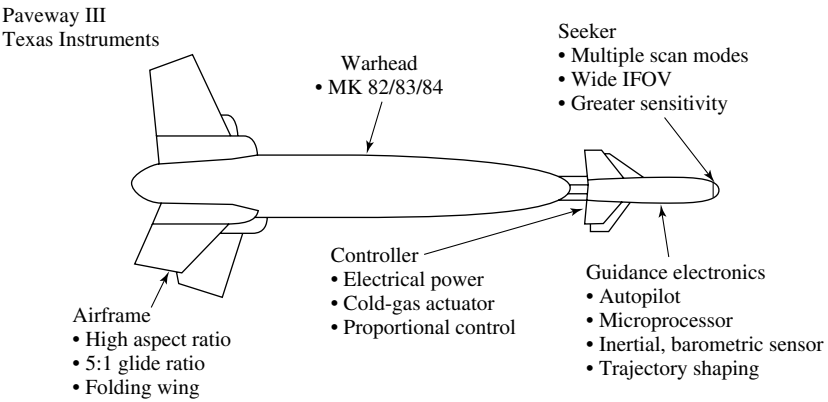

Fig. F.1. Main components of the *Paveway III GBU*.

CEP of less than 20 ft. The *B-2 Spirit* can carry up to eight *bunker-buster GAM-113s*, which are based on the *BLU-113* bomb body. The same device, when mated with a laser-guidance kit, is called the *GBU-28*. At this point, it is worth noting that the *BLU-97* submunitions (or bomblets) have three "kill" mechanisms as follows: (1) a conical charge capable of penetrating 5–7-in armor, (2) a main charge that bursts the case into about 300 fragments, and 3) an incendiary zirconium sponge ring. Table F.8 summarizes some of these guided bomb units [3].

The *Paveways*, however, are not perfect. Clouds, fog, dust, and other weather or battlefield obscurants can interfere with the laser-designation signal, precluding effective *LGB* use. Moreover, laser-guided weapons are only as accurate as the designator's boresighting. For true standoff situations, where an airborne or ground-based designator cannot get near a target, a *GPS*-guided weapon augmented by an *INS* is often better suited than an *LGB*.

At this point, it is appropriate to mention another guided glide bomb, namely, the *AGM-62* Walleye. The *AGM-62* is a *TV*-guided glide bomb designed to be used primarily against targets such as fuel tanks, tunnels, bridges, radar sites, and ammunition depots. The controlling aircraft must be equipped with an *AWW-9B* data link pod.

In addition to the *GPS/INS*-guided weapons, the *LANTIRN* system is used on the Air Force's *F-15E Strike Eagle* and *F-16C/D Fighting Falcon* fighters. The *LANTIRN* system significantly increases the combat effectiveness of these aircraft, allowing them to fly at low altitudes, at night, and under weather to attack ground targets with a variety of precision-guided and unguided weapons discussed in this appendix.

The Army and Navy are developing a 5×60-in artillery shell that will home on *GPS* jammers, besides its normal mode of attacking preloaded *GPS* coordinates. The extended-range guided munition (*ERGM*) is a five-year program that started in September 1996. It comes in two versions: (1) the 60-in-long Navy *EX-171*, which includes a solid rocket motor to boost range to 60 nautical miles, and (2) the Army

Table F.8. Guided Bombs

Bomb Series (*GBU-*)	Guidance	Remarks
Paveway II		
GBU-10E/B Mk 84 *GBU-12E/B* Mk 82 *GBU-16C/B* Mk 83	EO. More specifically, bombs of this series have a small seeker; in addition, an optical silicon detector staring array behaves analogously to a monopulse semiactive radar-homing seeker. The latest *Paveway II* series use laser guidance.	2,000-lb class (907.2 kg) 500-lb-class (226.8 kg) 1,000-lb class (453.6 kg) Note: The *GBU-16*, a laser-guided bomb, is built for the Navy by Lockheed Martin.
Paveway III		
GBU-22/B	Laser-homing.	The GBU-22 was a 500-lb class bomb.It was discontinued in the mid-1980s because of technical problems.
GBU-24A/B Mk 84 Variants: *GBU-24E/B*	The *GBU-24* is a laser-guided, low-level, wide area *LGB*. A gimbaled seeker searches for the laser spot. *GPS* and laser guidance.	2,000-lb steel-encased penetrator. Uses a *BLU-109/B* penetrator warhead. A powerful microprocessor allows for land, loft, or dive applications. This is a 2,200-lb bomb used by the Navy in the *F-14D's*.
GBU-27, 27/B	Laser-homing.	Steel-case, 2000-lb bomb delivered by the *F-117A*. Tests have shown that the bomb can penetrate 100 ft (30.5 m) of earth or more than 22 ft (6.71 m) of

(Continued)

Table F.8. *(Continued)*

Bomb Series (*GBU-*)	Guidance	Remarks
		concrete. Used during the 1990–1991 Persian Gulf War. The *GBU-27/B* is *BLU-109/B* compatible.
EGBU-27	Laser-homing and GPS/INS.	The Block 2 *F-117s* upgrade will carry the 2,000-lb *EGBU-27* bomb. The Block 2 will also provide the capability to drop 2,000-lb versions of the *JDAM* with both the penetrator *BLU-109* and the blast/fragmentation Mk 84. In the Afghan conflict the AF used the latest penetrating warhead, namely, the *BLU-118/B*. The *BLU-118/B* penetrating warhead detonates and generates high, sustained blast pressure in a confined space to make the make the munition more effective against tunnels and caves than the *BLU-109* penetrator warhead.
GBU-28A/B	Laser-homing.	This new bunker-busting weapon was developed (and successfully used) for *Operation Desert Storm*, dropped by *F-111s*. *GBU-28s* were also used in Kosovo, dropped by *F-15Es*. The *GBU-28* is a *4,700-lb* (2,131.92-kg) weapon. The warhead used is the *BLU-113/AB* blast fragmentation.
EGBU-28	Laser-homing.	This is an improved, 5,000-lb-class penetrating bomb.
GBU-28B/B	*GPS* and laser homing. It also uses auto *GPS*-aided targeting that updates and refines target information send to the weapon.	The *GBU-28B/B* is an enhanced version of the *GBU-28A/B*, designed specifically for the *B-2*. Testing of the weapon began in March 2003 first with inert and later with live *GBU-28B/B*s. The weapon is deployable in all weather conditions. The program is scheduled for completion by the end of 2004.
GBU-15	Uses *TV* or *IIR* seeker. Targeting options include *LOBL* and *LOAL*.	2,000-lb class bomb. Used against bridges, buildings, bunkers, and chemical plants. Uses a Mk 84 blast/frag or *BLU-109* penetrating warhead. The *IIR* seeker has 90% commonality with the Maverick *AGM-65D*.

Table F.8. *(Continued)*

Bomb Series (*GBU-*)	Guidance	Remarks
EGBU-15	The *EGBU-15* uses *GPS, TV*, laser, and *IR*.	The *EGBU-15* is a 2,000-lb unpowered precision-guided weapon. The *IOC* of the *GBU-15* was as follows: *GBU-15 (TV)*, 1983 *GBU-15 (IIR)*, 1987. The *EGBU-15* underwent successful Phase II tests in August 2000. Its *IOC* is for 2007.
JDAM Series of GBUs		1,000-lb or 2,000-lb class. Low-cost alternative to the cruise missiles. The 1,000-lb *JDAM* blast-fragmentation bomb is accurate to within 36 ft of the target, while the improved *JDAM* is accurate to within 9 ft.
GBU-31	*GPS/INS*	The *GBU-31* uses Mk 84 blast/frag, *BLU-109* penetrator. Standoff range is 15 nm (27.8 km).
GBU-32	*GPS/INS*	The *GBU-32* uses Mk 83 blast/frag, *BLU-110* penetrator. Standoff range is 15 nm (27.8 km).
GBU-35	*GPSINS*	The *GBU-35* uses the Mk 82 blast/frag warhead. Its standoff range is also 15 nm (27.8 km).
GBU-37	*GPS/INS* guided.	This is a 5,000-lb penetrator bomb used against hardened underground targets. It is also known as *GAM-113*. The *GBU-37* was used successfully in Afghanistan against the Taliban.

XM 172 (see also Chapter 1). The *ERGM* is a 12-caliber rocket-assisted projectile carrying a four-caliber submunitions payload to ranges of about 63 nautical miles (117 km), well beyond the range of current Navy gun ranges. The 110-lb (50-kg) aerodynamic projectile is 5 in (13 cm) in length, uses a coupled *GPS/INS* guidance system, and is armed with a submunitions warhead. The *GPS* guidance is tightly coupled to an inertial guidance system that will be immune to jamming, a feature that will enable the *ERGM* round to attack targets in a heavy *ECM* environment. The initial warhead configuration for *ERGM* will consist of 72 *EX-1* submunitions per round. The *EX-1* is a variant of the U.S. Army-developed *M80* dual-purpose conventional munition, which incorporates a shaped charge and an enhanced fragmentation case for use against materiel and personnel targets. The *ERGM*'s submunitions will be uniformly dispensed within a predetermined area that depends upon the specific target to be attacked and the altitude at which the submunitions are released. *ERGM*'s range and precise *GPS* targeting capability will improve naval surface fire support (*NSFS*) and provide near-term gunfire support for amphibious operations, the suppression and destruction of hostile antishipping weapons and air-defense systems, and naval fires support to the joint land battle. Thus, the *ERGM* will allow ships to hit enemy targets deep ashore with concentrated fire, in support of Army and Marine units. Guidance will be provided from an inertial measurement unit (*IMU*). Relying on *GPS* satellites for accuracy, the missile will be launched from shipboard guns. Upon exiting the gun barrel, the missile's' canards and tail fins deploy immediately to control it to an unjammed 20-meter *CEP* accuracy; submunitions can be dispensed at an altitude of 250–400 meters. The *ERGM*, with a short time-of-flight, has $200°/hr$ fiber optic gyros in the Navy version and micromachined silicon gyros in the Army shell.

IOC is scheduled for *FY* 2005 and is to be deployed on later versions of the *DDG-51* Arleigh Burke-class destroyer and the future *DD-21 Land Attack* destroyer equipped with the service's new 5-in/0.62 caliber gun.

References

1. *Airman*, Vol. XLIV, Number 11, November 2000.
2. Gunston, B.: *The Illustrated Encyclopedia of Aircraft Armament*, Orion Books, a division of Crown Publishers, Inc., New York, 1988. (This book is out of print.)
3. Laur, T.M. and Llanso, S.L.: *Encyclopedia of Modern U.S. Military Weapons*, edited by Walter J. Boyne, Berkley Books, New York, 1995.
4. McDaid and Oliver, D.: *Smart Weapons*, Welcome Rain, New York, 1997.

G

Properties of Conics

G.1 Preliminaries

It is well known that when a body is in motion under the action of an attractive central force that varies as the inverse square of the distance, the path described will be a conic whose focus is at the center of attraction. The particular conic (ellipse, hyperbola, or parabola) is determined solely by the velocity and the distance from the center of force. In this appendix, we will consider the purely geometric problem of determining the various conic paths that connect two fixed points and that have a focus coinciding with a fixed center of force. Specifically, in this appendix we will discuss the geometric and analytic properties as applied to ballistic missile trajectories.

There are many equivalent definitions of conics; however, we shall find the following ones most convenient for our purposes [1], [2], [3]:

Ellipse:

The locus of points the sum of whose distances from two fixed points (i.e., foci) is constant.

Hyperbola:

The locus of points the difference of whose distances from two fixed points (i.e., foci) is constant.

Parabola:

The locus of points equally distant from a fixed point (i.e., the focus) and a fixed straight line (i.e., the directrix).

The familiar elements of these conics are shown in Figures G-1, G-2, and G-3.

In Section 6.2, equation (6.1), the general equation of a conic in Cartesian coordinates was given as a second-degree equation of the form [4], [5]

$$Ax^2 + Bxy + Cy^2 + Dx + Ey + F = 0. \tag{G.1}$$

Specifically, any equation of this form with $(A, B, C) \neq (0, 0, 0)$ corresponds to a conic section and vice versa; that is, the coefficients are assumed to be real and $A^2 + B^2 + C^2 \neq 0$. Equation (G-1) can also be expressed as

$$(p^2 + q^2)[(x - \alpha)^2 + (y - \beta)^2] = e^2(px + qy + r)^2,$$

where e is the eccentricity, (α, β) the focus, and $px + qy + r$ is the equation of the directrix of the conic. In *vertex form* the equation is

$$y^2 = 2px - (1 - \epsilon^2)x^2,$$

where $2p$ is the *parameter* of the conic, that is, the length of its latus rectum, which in the ellipse and hyperbola equals b^2/a^2 (where a and b are the lengths of the semiaxes of the conic), and ε is the numerical eccentricity, e/a; there are many other equivalent descriptions. (Vertex is an expression for a conic, obtained by a suitable change of variables, in which the *vertex* is taken as the origin of the coordinate system, and the axis of the conic lies along the x-axis.)

Moreover, the type of conic section is determined by the values of the characteristic equation $B^2 - 4AC$ and the discriminant [5]

$$\begin{vmatrix} A & B/2 & D/2 \\ B/2 & C & E/2 \\ D/2 & E/2 & F \end{vmatrix}$$

of (G-1) is shown in Table G.2. The general quadratic equation is $ax^2 + bx + c = 0$ with solutions

$$x = (-b \pm \sqrt{b^2 - 4ac})/2a.$$

The vanishing of $b^2 - 4ac$, called the discriminant, is a necessary and sufficient condition for equal roots. If a, b, c are all rational numbers, then the roots are real and unequal if and only if $b^2 - 4ac > 0$. At this point, a few words about the discriminant are in order.

The discriminant is an algebraic expression, related to the coefficients of a polynomial equation (or to a number field), that gives information about the roots of the polynomial; principally, the discriminant is nonzero if and only if the roots are distinct. For example,

$$D = b^2 - 4ac$$

is the discriminant of the quadratic equation

$$ax^2 + bx + c = 0;$$

D is positive exactly when the equation has distinct real roots, and is zero exactly when it has equal real roots. More precisely, the discriminant of a polynomial p of degree n over a given field is the quantity.

$$D(p) = (-1)^{n(n-1)/2} R(p, p'),$$

where R is the *resolvent* of p and p'.

Characteristic	Discriminant	Type of Conic
0	$\neq 0$	Nondegenerate parabola.
0	0	Degenerate parabola; 2 real or imaginary parallel lines.
< 0	$\neq 0$	Nondegenerate ellipse or circle; real or imaginary.
< 0	0	Degenerate ellipse; point ellipse or circle.
> 0	$\neq 0$	Nondegenerate hyperbola.
> 0	0	Degenerate hyperbola; 2 distinct intersecting lines.

G.2 General Conic Trajectories

Preliminaries

From the geometry of the ellipse given below,

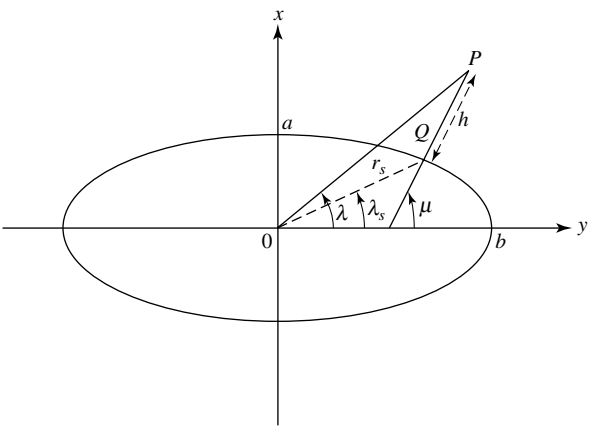

the equation for the ellipse is given as

$$(x^2/a^2) + (y^2/b^2) = 1, \quad b > a > 0,$$

where the length of the semiminor axis is given by

$$a = b(1 - f),$$

with f being the flattening. From the above figure, we can obtain for the point Q at sea level an equation in terms of the geocentric latitude λ as follows:

$$\tan \lambda_s = (1 - f)^2 \tan \mu,$$

where μ is the geodetic latitude angle. Furthermore, using the polar coordinates (r_s, λ_s) for the point Q we can readily develop an expression for the sea-level radius. Thus,

$$r_s^2 = \{r_e^2/([1 + [1/(1 - f)^2 - 1] \sin^2 \lambda_s)\},$$

where r_e is the radius of the Earth.

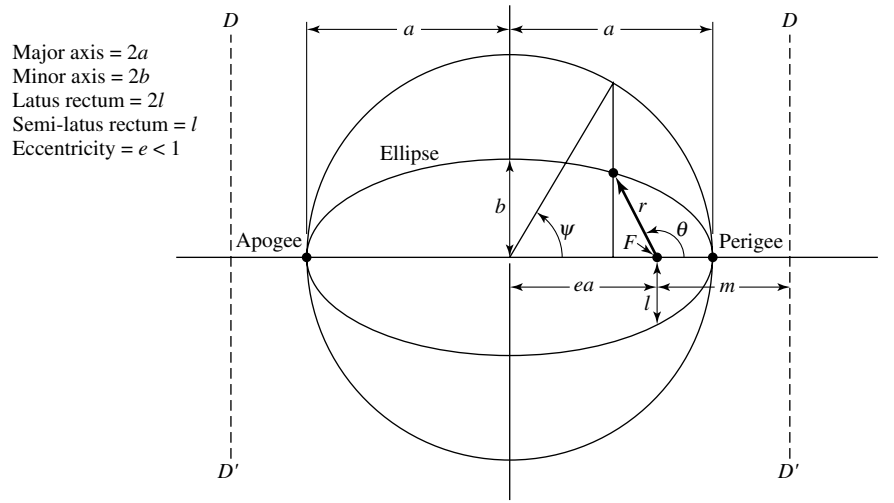

Fig. G.1. Geometry of the ellipse.

Let us now return to the discussion of conics. To recapitulate, a conic is the locus of points whose distance from a fixed point F and a fixed line DD' have a constant ratio e. The fixed point F is called the focus, the fixed line DD' the directrix, and the ratio e the eccentricity. Letting m be the distance from the focus to the directrix DD', the polar equation for the conic is

$$r = e(m - r\cos\theta),$$

or

$$r = em/(1 + e\cos\theta). \tag{G.2}$$

By letting $\theta = 0°, 90°, 180°$, and $\tan^{-1}(b/a)$, important distances are found; see Figure G.1.

Other expressions describing the geometry of the ellipse are as follows:

$$\begin{aligned} r &= l/(1 + e\cos\theta) \\ &= r_p(1 + e)/(1 + e\cos\theta) \\ &= a(1 - e^2)/(1 + e\cos\theta), \end{aligned} \tag{G.3}$$

where $me = l$ (note that in Chapter 6 the letter p was used to denote the semilatus rectum);

Eccentricity:

$$e = \sqrt{1 - (l/a)^2} = (r_a - r_p)/(r_a + r_p), \tag{G.4}$$

$$l = a(1 - e^2). \tag{G.5}$$

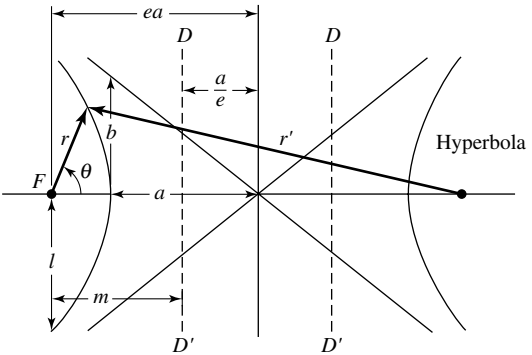

Fig. G.2. Geometry of the hyperbola.

Periapsis radius ($e < 1$):

$$r_p = a(1-e) = l/(1+e). \tag{G.6}$$

Apogee radius ($e < 1$):

$$r_a = a(1+e) = l/(1-e). \tag{G.7}$$

Major axis ($e < 1$):

$$2a = r_a + r_p = 2l/(1-e^2). \tag{G.8}$$

Semiminor axis:

$$b = a\sqrt{1-e^2} = l/\sqrt{1-e^2}. \tag{G.9}$$

Expressions describing the geometry of the hyperbola are as follows:

$$\begin{aligned} r &= l/(1+e\cos\theta) \\ &= r_p(1+e)/(1+e\cos\theta) \\ &= a(e^2-1)/(1+e\cos\theta), \end{aligned} \tag{G.10}$$

where

$$me = l, \tag{G.11}$$

$$r_p = a(e-1), \tag{G.12}$$

$$2a = r' - r, \tag{G.13}$$

$$e = \sqrt{1+(b/a)^2}, \tag{G.14}$$

$$l = a(e^2-1). \tag{G.15}$$

Figure G-2 illustrates the geometry of the hyperbola.

The mathematical expressions describing the geometry of the parabola are as follows:

$$r = m/(1+\cos\theta) = 2r_p/(1+\cos\theta), \tag{G.15}$$

$$m = l, \tag{G.16}$$

$$r_p = l/2. \tag{G.17}$$

Figure G-3 illustrates the geometry of the parabola.

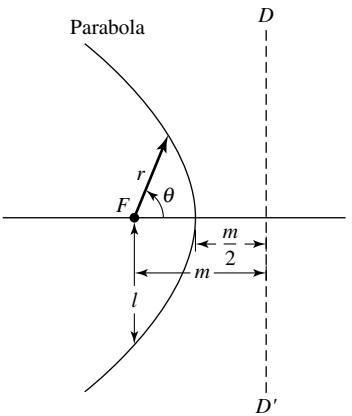

Fig. G.3. Geometry of the parabola.

If $P(r,\theta)$ is any point (or position) on a conic of a planet in its orbit, the radius vector r and the angle θ (measured in the direction of the planet motion) is given by (see (6.2) and (6.21))

$$\begin{aligned} r &= l/(1+e\cos\theta) \\ &= a(1-e^2)/(1+e\cos\theta) \\ &= (h^2/\mu)/(1+e\cos\theta), \end{aligned}$$

where l is the *parameter or semilatus rectum* (that is, l determines the size of the conic), e is the eccentricity (which determines the shape of the conic), μ is the gravitational parameter ($= 1.407654 \times 10^{16}\,\text{ft}^3/\text{sec}^2$; note that in Appendix A the value of μ was given in the metric system), and h is the specific angular momentum given by $h^2 = \mu a(1-e^2)$. Therefore, for motion under the inverse-square control force, the numerical value of e is as follows:

Hyperbola: if $e > 1$,
Parabola: if $e = 1$,
Ellipse: if $0 < e < 1$ (perigee corresponding to $\theta = 0$),
Circle: if $e = 0$,
Subcircular Ellipse: if $-1 < e < 0$ (apogee=point of maximum distance from the origin of r corresponding to $\theta = 0$).

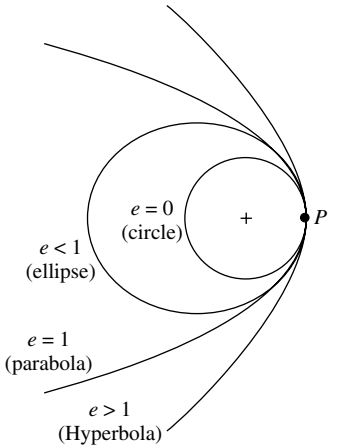

Fig. G.4. Conic sections as gravitational trajectories.

Figure G-4 illustrates the conic sections as simple gravitational trajectories, and as stated earlier, the dimensionless eccentricity e determines the character of the conic section in question. For more information, see Section 6.2.

References

1. Battin, R.H.: *Astronautical Guidance*, McGraw-Hill Book Company, New York, 1964.
2. Brouwer, D. and Clemence, G.M.: *Methods of Celestial Mechanics*, Academic Press, Inc., New York, 1961.
3. Danby, J.M.A.: *Fundamentals of Celestial Mechanics*, The Macmillan Company, New York, 1962.
4. Kells, L.M. and Stotz, H.C.: *Analytic Geometry*, Prentice-Hall, Inc., New York, 1949.
5. Pearson, C.E. (ed): *Handbook of Applied Mathematics*, Van Nostrand Reinhold Company, New York, Cincinnati, 1974.

This page intentionally left blank

H

Radar Frequency Bands

Band Designation	Frequency Range	Typical Usage
VHF	50–330 MHz	Very long-range surveillance.
UHF	300–1,000 MHz	Very long-range surveillance.
L	1–2 GHz	Long-range surveillance, enroute traffic control.
S	2–4 GHz	Moderate-range surveillance, terminal traffic control, long-range weather.
C	4–8 GHz	Long-range tracking, airborne weather.
X	8–12 GHz	Short-range tracking, missile guidance, mapping, marine radar, airborne intercept.
K_u	12–18 GHz	High-resolution mapping, satellite altimetry.
K	18–27 GHz	Little used (H_2O absorption)
K_a	27–40 GHz	Very high-resolution mapping, airport surveillance.
mm	$40–100^+$ GHz	Experimental.

Source: AIAA (American Institute of Aeronautics and Astronautics)

This page intentionally left blank

I

Selected Conversion Factors

Length:

$1\ \text{m} = 100\ \text{cm} = 1000\ \text{mm}$
$1\ \text{km} = 1000\ \text{m} = 0.6214$ statute miles
$1\ \text{m} = 39.37\ \text{in};\ 1\ \text{cm} = 0.3937\ \text{in}$
$1\ \text{ft} = 30.48\ \text{cm};\ 1\ \text{in} = 2.540\ \text{cm}$
1 statute mile $= 5,280\ \text{ft} = 1.609\ \text{km}$
1 nautical mile (nm) $= 1852\ \text{m} = 1.852\ \text{km}$
1Å (angstrom) $= 1 \times 10^{-8}$ cm; 1μ (micron) $= 1 \times 10^{-4}$ cm
1 nanometer (nm) $= 1 \times 10^{-9}$ m

Area:

$1\ \text{cm}^2 = 0.155\ \text{in}^2;\ 1\ \text{m}^2 = 104\ \text{cm}^2 = 10.76\ \text{ft}^2$
$1\ \text{in}^2 = 6.452\ \text{cm}^2;\ 1\ \text{ft}^2 = 144\ \text{in}^2 = 0.0929\ \text{m}^2$

Volume:

1 liter $= 1000\ \text{cm}^3 = 10^{-3}\ \text{m}^3 = 0.0351\ \text{ft}^3 = 61\ \text{in}^3$
$1\ \text{ft}^3 = 0.0283\ \text{m}^3 = 28.32$ liters; $1\ \text{in}^3 = 16.39\ \text{cm}^3$

Velocity:

$1\ \text{cm/s} = 0.03281\ \text{ft/s};\ 1\ \text{ft/s} = 30.48\ \text{cm/s}$
1 statute mile/min $= 88\ \text{ft/s} = 60$ statute miles/hr

Acceleration:

$1\ \text{cm/s}^2 = 0.03281\ \text{ft/s}^2 = 0.01\ \text{m/s}^2$
$30.48\ \text{cm/s}^2 = 1\ \text{ft/s}^2 = 0.3048\ \text{m/s}^2$
$100\ \text{cm/s}^2 = 3.281\ \text{ft/s}^2 = 1\ \text{m/s}^2$

Force:

1 dyne = 1 gm cm/s^2; 1 newton (N) = 1 kg m/s^2; 1 lb f = 1 slug ft/s^2
1 dyne = 2.247×10^{-6} lb f = 10^{-5} N
1.383×10^4 dynes = 0.0311 lb f = 0.1383 N
4.45×10^5 dynes = 1 lb f = 4.45 N
10^5 dynes = 0.2247 lb f = 1 N
1 kilopond (kp) = 9.80665 N; 1 N = 3.5969 oz = 7.2330 poundals
1 poundal = 0.138255 N

(lb f = pounds force; lb m = pounds mass; N = newton)

Mass:

1 slug = 32.174 lb m
1 gm = 6.85×10^{-5} slug = 10^{-3} kg
453.6 gm = 0.0311 slug = 0.4536 kg
1.459×10^4 gm = 1 slug = 14.5939 kg
10^3 gm = 0.0685 slug = 1 kg
1 kg = 2.2046 lb; 1 lb = 0.4536 kg

Pressure:

1 atm = 14.696 lbf/in^2 = 1.013×10^6 dynes/cm^2 = 1.01325×10^5 N/m^2

Energy:

1 joule = 1 newton meter; 1 erg = 1 dyne cm
1 joule = 10^7 ergs = 0.239 cal; 1 cal = 4.18 joule

Temperature:

0 K = −273.15°C
0°R = −459.67°F
0°C = 32°F = 273.15 K; 100°C = 212°F

$\Theta[K] = \Theta[^\circ\mathrm{C}] + 273.15$
$\Theta[^\circ\mathrm{C}] = (Q[^\circ\mathrm{F}] - 32)(5/9)$
$\Theta[^\circ\mathrm{F}] = (9Q[^\circ\mathrm{C}]/5) + 32$

Magnitude of degrees: 1 deg = 1°C = 1 K = 9/5°F.

Index

Aberration, 104–106
Actuators, 144–149
Aerodynamic:
  center, 54
  coefficients, 59–60
  forces, 26
  moment, 55–57
  pitching moment, 62–63, 66, 69
  rolling moment, 62–64, 69
  yawing moment, 62–63, 66–67, 69
Aircraft sensor, 289
Airfoil, 71
Airframe characteristics, 77–80, 85
Air launched cruise missile, 521–534,
  error analysis, 543–551
Angular momentum, 25–26, 31, 33, 373
Aphelion, 591
Apoapsis, 591
Apogee, 377, 381, 591
Apsis, 591
Atmosphere, 607–608
  standard model, 605–606
Atmospheric reentry, 482–489
Augmented proportional navigation,
    225–228
Autopilot gain, 134, 137–138
Autopilots, 129–144
  adaptive, 134, 140–142
  pitch/yaw, 135–140
  roll, 132–135

Ballistic coefficient, 418, 504,
    515, 518–519
Ballistic dispersion, 271
Ballistic missile, 365, 389–392
  definition, 6
  error coefficients, 418–435
  free flight, 367–368
  powered flight, 366–367
  intercept, 504–515
  reentry, 368
Bank to turn, 92
Barrage fire, 271–272
Beam rider, 164
Bias, 272
Bomb steering, 344–350

Canard, 78
Center of gravity, 54, 68, 81
Center of pressure, 54, 81
Circular error probable (CEP),
    273, 277, 313, 322, 327,
    360–363, 543
Clutter, 118–119
Command guidance, 162–164, 206–207
Compressible fluid, 44
Conic sections, 368–370
Control surfaces, 67, 144–149
Coordinate systems, 15–16, 36
  body, 53, 57, 70, 72–74
  Earth fixed, 20
  Inertial, 20
  launch centered inertial, 20
  north-east-down (NED), 20–22, 39
  transformations, 18–22, 548–549
Coriolis, 30, 319, 324–325
Correlated velocity, 395, 443–445, 453
Covariance analysis, 320–322

Cruise missiles, 521–527
  navigation system, 534–543
  system description, 527–532

Daisy cutter, 249
D'Alembert's principle, 45–46
Delivery accuracy, 273–274
Delta guidance, 470–471
Direction cosine matrix (DCM), 18–19, 40, 43
Drag coefficient, 55
Drag polar, 59
Dynamic pressure, 40, 54

Earth curvature, 351–353
Earth oblateness effects, 399–403, 503, 516
Earth rotation effects, 440–443
Eccentric anomaly, 385–386, 579
Eccentricity, 368–370, 654
Electronic countermeasures (ECM), 122
End game, 256–257
English bias, 136, 151–153, 181, 205
Epoch, 379
Error analysis, 326–327, 543–547
Error ellipse, 537
Error sensitivity, 294–297
Euler:
  angles, 18–19, 34
  equations, 33
Euler-Lagrange equations, 49
Explicit guidance, 466–469

Fire control computer (FCC), 292–293
Forces, 26
  axial, 71, 83
  normal, 65–66, 84
  side, 55–56, 60
Free flight, 367–368
Free stream velocity, 68

Glint, 114–116
Glitter point, 258–260
Global Hawk, 619–620
Global positioning system (GPS), 168, 576–583
Global positioning system/inertial navigation integration, 168, 583–586
Gravitation models, 400, 503
Gravity, 342–343
  drop, 275
  turn, 460, 462–463, 466, 494–498
Great circle, 549, 592
Guidance, 85, 173
  active, 155
  beam rider, 164
  collision course interception, 165–166, 187–188
  command, 162–164, 206–207
  delta, 470–471
  deviated pursuit, 165
  explicit, 466–469
  homing, 158
  hyperbolic, 166
  implicit, 469–470
  laws, 162
  passive, 155, 160
  semi-active, 155, 159
  three point, 166
Guided missile definition, 5
Gyrocompassing, 9

Hamilton's principle, 49
Hit equation, 392–395, 397
Holonomic system, 46
Homing-on-jam, 122–124
Hour circle, 592

Imaging infrared (IIR), 111
Implicit guidance (see also guidance), 8–9
Incompressible fluid, 44
Inertial frame, 20
In-plane error coefficients, 421–430
Infrared seeker, 111–112, 125–129
Infrared tracking, 125–129
Irdome, 110, 125–129

Jamming, 122–124
Jerk model, 232–233

Kalman filter, 236–237, 517–518, 575–576
  continuous, 237–240
  discrete, 240–242
  suboptimal, 242
Keplerian motion, 371, 373
  ellipse, 370

Kepler's first law, 378–379
third law, 379
Kinetic energy, 48, 387, 409

Lagrange's equations, 46–49, 324
LAIRCM, 129
Lambert's theorem, 382–388
Laser systems, 167, 298
Lift, 55–57, 60
coefficient, 41, 55–57, 60
Linear quadratic regulator, 235, 242–245, 330
Load factor, 92, 94–95

Mach number, 23, 325
Mass 23, 36
MATLAB, 36
Matrix Riccati equation, 238–245
Maximum principle, 330
Mean anomaly, 387
motion, 386
Minimum:
energy, 247
energy trajectory, 397, 403, 407–409, 415, 429
fuel, 247
principle, 330
time, 246
Miss distance, 100–101, 105, 308–309
Missile:
classification, 611–615
control system, 457–461
guidance equations, 174–175, 181–194
launch envelope, 275, 353–354
mathematical model, 91–95
seeker, 102–104
Moments, 62
inertia, 32
pitching, 62–63
rolling, 62–64, 69
yawing, 62–63, 66–67, 69
Multipath, 118–119

Navier-Stokes equation, 44–45
Navigation, 290, 471–472, 534–539
inertial, 8–9, 532, 543–551
Newton's equations, 22, 47, 49
second law, 25, 29
Noise, 113
glint, 114–116
range-independent, 115
scintillation, 115–117
thermal, 118–119
white, 117, 237–238

Oblateness effects of the Earth, 399–400
Orbital period, 378
Out-of-plane error coefficients, 430–435

Parasitic attitude loop, 79, 101–102, 105, 142–143
Particle beam, 262
Perigee, 377, 381, 593
Pitching moment, 62–63, 66, 69
Powered flight, 366–367
Predator, 618–619
Probability of kill, 171, 263–265
Proportional navigation, 161, 166, 194–218, 236
augmented, 225–228
biased, 195–196, 213
effective ratio, 194, 202–204
generalized, 196
ideal, 196
ratio, 194
three-dimensional, 228–235
true, 196

Q-guidance, 445–446, 451–452, 471
-matrix, 445–450
Quaternions, 19, 40, 42–43

Radar, 110–113, 297–298
cross-section, 116, 121
frequency bands, 659
Radial error probable (REP), 277
Radome, 104–107, 110–111
slope error, 106–108
Ramjet, 88, 150
Reentry, 368
Refraction, 104–106
Relative wind, 54–55
Reynold's number, 53, 63, 325
Rigid body, 22–23
Rolling moment, 62–64, 69
Runge-Kutta method, 117, 178–179, 498–500

Scintillation noise (see “noise”)
Scramjet, 88, 150
Seekers, 102–104
  infrared, 111–112, 125–129
  radar, 111–113
Semi-latus rectum, 369
Sidereal day, 593
Sidereal hour angle, 593
Sideslip angle, 44, 61–63
Signal-to-noise ratio (SNR), 113–114, 122
Skid-to-turn, 53, 56, 91
Situational awareness/Situation assessment (SA/SA), 333–336
Speedgate, 151
Spherical hit equation (see “Hit equation”)
Standard atmosphere (see “atmosphere”)

Target offset, 279
Targeting systems, 336–338
Tensors, 17–18
Terrain aided navigation (TAN), 574–575
Terrain contour matching (TERCOM), 551–555
  position updates, 571–574
  roughness characteristics, 568–570
  system errors, 570–571
Terrain profile matching (TERPROM), 554
True anomaly, 369, 378
Two-body problem, 366–382

Unmanned aerial vehicle (UAV), 618–620
Unmanned combat aerial vehicle(UCAV), 620–623
Unpowered precision guided munitions, 644–646

V-1, V-2 rockets, 2–5
Vectors, 15
  transformation properties, 15–17
Velocity-to-be-gained, 443–447, 449–454
Velocity:
  angular, 26–27
  required, 395, 411–413, 416
Virtual work, 45
Vis viva equation, 388

Warheads, 85, 262–263
Weapon delivery, 269–284
White noise, 117, 237–238
Wind axes, 57–59

Z-velocity steering, 459–460